Industrial Applications of Batteries

From Cars to Aerospace and Energy Storage

Edited by

M. Broussely & G. Pistoia

Industrial Applications of Batteries

From Cars to Aerospace and Energy Storage

This page intentionally left blank

Industrial Applications of Batteries

From Cars to Aerospace and Energy Storage

Edited by

M. Broussely
SAFT
Speciality Battery Group
Poitiers, France

and

G. Pistoia
Rome, Italy

ELSEVIER

Amsterdam – Boston – Heidelberg – London – New York – Oxford – Paris
San Diego – San Francisco – Singapore – Sydney – Tokyo

Elsevier
Radarweg 29, PO Box 211, 1000 AE Amsterdam, The Netherlands
The Boulevard, Langford Lane, Kidlington, Oxford OX5 1GB, UK

First edition 2007

Copyright © 2007 Elsevier B.V. All rights reserved

No part of this publication may be reproduced, stored in a retrieval system
or transmitted in any form or by any means electronic, mechanical, photocopying,
recording or otherwise without the prior written permission of the publisher

Permissions may be sought directly from Elsevier's Science & Technology Rights
Department in Oxford, UK: phone (+44) (0) 1865 843830; fax (+44) (0) 1865 853333;
email: permissions@elsevier.com. Alternatively you can submit your request online by
visiting the Elsevier web site at http://elsevier.com/locate/permissions, and selecting
Obtaining permission to use Elsevier material

Notice
No responsibility is assumed by the publisher for any injury and/or damage to persons
or property as a matter of products liability, negligence or otherwise, or from any use
or operation of any methods, products, instructions or ideas contained in the material
herein. Because of rapid advances in the medical sciences, in particular, independent
verification of diagnoses and drug dosages should be made

Library of Congress Cataloging-in-Publication Data
A catalog record for this book is available from the Library of Congress

British Library Cataloguing in Publication Data
A catalogue record for this book is available from the British Library

ISBN-13: 978-0-444-52160-6
ISBN-10: 0-444-52160-7

For information on all Elsevier publications
visit our website at books.elsevier.com

Printed and bound in The Netherlands

07 08 09 10 11 10 9 8 7 6 5 4 3 2 1

Working together to grow
libraries in developing countries

www.elsevier.com | www.bookaid.org | www.sabre.org

ELSEVIER BOOK AID International Sabre Foundation

Preface

This book aims at updating the list of battery-powered industrial applications and the improvements made in their batteries in terms of materials and technological advances.

Actually, applications and batteries are interrelated: new or improved applications stimulate the realization of new or improved batteries and vice versa. In some cases, electrochemical systems with new electrode materials or electrolytes have been produced, while in some others the improvements come from better battery engineering. Electrolytes standing extreme temperatures (Chapters 1, 6 and 12) or modified electrodes, *e.g.* lithiated Ni-Co oxide as a positive for Lithium Ion batteries (Chapters 4 and 5), are examples of improved active materials. New casings or new separators or management systems are examples of technological improvements (Chapters 3, 4 and 13).

The number of electrochemical systems used is still fairly high. From Chapter 1, we may count ten nonaqueous batteries (with liquid, polymeric or molten salt electrolytes), and, in Chapter 2, the same number of aqueous batteries used in the main applications are reported.

It is remarkable that, among these systems, the oldest one, Lead Acid, and the youngest one, Lithium Ion, have the largest shares of the secondary battery market (in terms of value, including consumer market). Lead Acid, dating back to 1859, has benefited from the automotive market, but is still widely used (in some cases almost exclusively) in various segments, *e.g.* energy storage, telecommunications and UPS (Chapter 7-9). Lithium Ion, born in the early 1990s, owes its success to consumer electronics, but is now being used in a number of industrial applications, *e.g.* power tools, aerospace, asset tracking and load leveling (Chapters 5, 6, 8, 11,12), and is appearing in hybrid electric vehicles (Chapter 4).

Battery energy and power are continuously increasing, although, as is obvious, at a different pace for the various chemistries. Simultaneously, the battery safety is also increasing, as imposed by strict regulations and severe tests. Especially at the industrial level, many systems are endowed with battery management systems ensuring a high level of control (Chapter 13). It is remarkable that, at the same time, our safety may receive in several instances a benefit from the use of batteries. Examples are provided throughout this book: power back up, car accessories, alarms, rescue systems, portable medical equipment, *etc.* (Chapters 10-12).

What is the fate of this huge battery production? Will it be a further contribution to our planet's pollution or may we avoid this and even exploit the materials of spent batteries? Collection and recycling is now mandatory in many countries with definite rules, as detailed in Chapter 14.

It is now commonplace that we live in a world that would be very different, and certainly less comfortable, if consumer and industrial batteries would not exist. We shall take advantage from their use at a growing rate in the future (Chapter 15). For this reason, gratitude should be expressed to any person, scientist or technician, who has given through the years a contribution to the advancements in this field.

Michel Broussely Gianfranco Pistoia

Contents

Chapter 1. Nonaqueous Batteries Used in Industrial Applications

G. Pistoia

1.1. Introduction 1
1.2. Primary Lithium Batteries 1
1.2.1. Lithium/Sulfur Dioxide Batteries 2
1.2.1.1. Cell Construction and Performance 3
1.2.2. Lithium/Thionyl Chloride Batteries 5
1.2.2.1. Cell Construction and Performance 6
1.2.3. Lithium/Manganese Dioxide Batteries 10
1.2.3.1. Cell Construction and Performance 11
1.2.4. Lithium/Carbon Monofluoride Batteries 14
1.2.4.1. Materials, Electrode Reactions, Cell Types and Performance 15
1.2.5. Basic Parameters of Primary Li Batteries 17
1.3. Rechargeable Batteries 17
1.3.1. Lithium-Ion Batteries 17
1.3.1.1. Carbons 18
1.3.1.2. Positive Electrodes 21
1.3.1.3. Liquid Electrolytes 22
1.3.1.4. Cell Construction and Performance (with Liquid Electrolytes) 23
1.3.1.5. Li-Ion Batteries with Polymeric Electrolytes 29
1.3.1.6. Examples of Applications 30
1.3.2. Batteries with a Lithium Electrode 32
1.3.2.1. Lithium/Sulfur Batteries 32
1.3.2.2. Li-Metal-Polymer Batteries 32
1.3.2.3. Li-Al/Iron Sulfide Batteries 38
1.3.3. Batteries with a Sodium Electrode 41
1.3.3.1. Sodium/Sulfur Batteries 42
1.3.3.2. Sodium/Nickel Chloride (Zebra) Batteries 46
1.3.4. Basic Parameters of Secondary Nonaqueous Batteries 49

Chapter 2. Aqueous Batteries Used in Industrial Applications

G. Pistoia

2.1. Introduction 53
2.2. Lead/Acid Batteries 53
2.2.1. Electrodes 53
2.2.2. Grids 55
2.2.3. Plate Designs 55

2.2.4. Electrolyte and Separators 57
2.2.5. Charge/Discharge Reactions 57
2.2.6. Design Features and Applications 59
2.2.7. Discharge Characteristics, Peukert Equation and Self-Discharge 63
2.2.8. Charging Methods 65
2.3. Nickel/Cadmium Batteries 66
2.3.1. Introduction 66
2.3.2. Types of Ni/Cd Batteries 66
2.3.3. Charge/Discharge Reactions 69
2.3.4. Discharge Characteristics, Memory Effect and Self-Discharge 71
2.3.5. Charging Techniques 73
2.3.6. Cycle Life 74
2.3.7. Applications 76
2.4. Nickel/Metal Hydride Batteries 77
2.4.1. Materials and Electrode Reactions 77
2.4.2. Cell Construction and Performance 80
2.4.3. Charging the Ni/MH Battery 83
2.4.4. Cycle and Battery Life 86
2.4.5. Applications 86
2.5. Nickel/Hydrogen Batteries 89
2.6. Nickel/Iron Batteries 91
2.7. Nickel/Zinc Batteries 94
2.8. Zinc/Air Batteries 97
2.9. Silver/Zinc Batteries 101
2.10. Zinc/Bromine Batteries 103
2.11. Vanadium Redox-Flow Batteries 106
2.12. Alkaline Primary Batteries 108
2.12.1. Electrode Materials and Processes 109
2.12.2. Cell Construction 110
2.12.3. Cell Performance and Applications 111
2.13. Basic Parameters of Aqueous Secondary Batteries 114

Chapter 3. Characterization of Batteries by Electrochemical and Non-Electrochemical Techniques

D. Aurbach

3.1. Introduction 119
3.2. Categories of Battery Materials 120
3.2.1. Electrode Materials 120
3.2.1.1. General Features 120
3.2.1.2. Negative Electrodes 122
3.2.1.3. Positive Electrodes 124
3.2.2. Electrolyte Systems 126

3.2.2.1. Aqueous Solutions 126
3.2.2.2. Nonaqueous Solutions 126
3.2.2.3. Solid Electrolyte Systems 127
3.2.3. Supporting Elements 127
3.2.3.1. Current Collectors 127
3.2.3.2. Separators and Membranes 128
3.3. Stages and Levels in Battery Characterization 129
3.3.1. Introduction 129
3.3.2. Non-Destructive Studies of Full Cells 129
3.3.3. Post-Mortem Analysis of Full Cells 129
3.3.4. Half Cell Testing 130
3.3.5. Solution Studies 130
3.3.6. Electrode Studies – Bulk 131
3.4. A Brief Summary of Available Techniques Related to the Characterization of Batteries 132
3.4.1. Glove Box Operations 132
3.4.2. Bulk Analytical Tools 133
3.4.2.1. Basics of Mass Spectrometry 133
3.4.2.2. Mössbauer Spectroscopy 134
3.4.2.3. Nuclear Magnetic Resonance 135
3.4.2.4. IR, UV-Vis, Raman 136
3.4.2.5. Inductively Coupled Plasma 139
3.4.2.6. Diffraction Techniques (X-Ray and Neutron Diffraction) 140
3.4.2.7. X-Ray Techniques: EXAFS and XANES 141
3.4.3. Microscopy 142
3.4.3.1. Electron Microscopy and Related Techniques 142
3.4.3.2. Atomic Force Microscopy 144
3.4.4. Analysis of Surface Area by Gas Adsorption Processes 146
3.4.5. Thermal Analysis 147
3.4.5.1. DTA, DSC and TGA 147
3.4.5.2. Accelerating Rate Calorimetry 148
3.4.6. Surface Analysis 149
3.4.6.1. General Remarks 149
3.4.6.2. FTIR and Raman Spectroscopies 149
3.4.6.3. XPS and AES 152
3.4.7. Electrochemical Techniques 155
3.4.7.1. Introduction 155
3.4.7.2. Fine Electroanalytical Techniques 155
3.4.8. Some Miscellaneous Techniques 160
3.4.9. *In Situ* Measurements 162
3.5. Typical Studies of Electrolyte Solutions and Solid Electrolytes 167
3.5.1. Evaluation of Solvents Parameters and Solutions Conductivity 167
3.5.2. Electrochemical Windows of Electrolyte Solutions 169
3.5.3. Thermal Studies 171
3.6. Typical Studies of Electrodes and Electrode Materials 173
3.6.1. The Scheme of Material Research 173

3.6.2. On the Electrochemical Characterization of Battery Electrodes 175
3.6.2.1. Metallic Electrodes 175
3.6.2.2. Electrodes for Flow Batteries (*e.g.* Air Batteries) and Batteries with Liquid Cathodes 176
3.6.2.3. Composite Electrodes 177
3.6.3. On the Surface Characterization of Battery Electrodes 184
3.7. Measurements of Complicated Batteries 186
3.7.1. Introduction – General Aspects 186
3.7.2. Examples of Standard Electrochemical Performance Tests for Commercial and Prototype Batteries 187
3.7.3. Measurements of Prototype Batteries, Impedance Measurements and the Study of Failure Mechanisms 189
3.7.4. Safety Features and Safety Tests 192
3.8. Theoretical Aspects of Battery Characterization 192
3.9. Concluding Remarks 193

Chapter 4. Traction Batteries. EV and HEV

M. Broussely

4.1. Introduction 203
4.2. The Different Types of Electric Vehicles 204
4.2.1. Electric Vehicles (EV) 204
4.2.2. Hybrid Electric Vehicles (HEV) 208
4.2.2.1. Micro Hybrids “Stop and Start” 210
4.2.2.2. Soft Hybrids “Stop and Go” 211
4.2.2.3. Mild Hybrids 212
4.2.2.4. Full Hybrids or “Power Assist” 212
4.2.2.5. Plug-in Hybrids (PHEV) 213
4.2.2.6. Fuel Cell Hybrid EV 213
4.2.2.7. Large Hybrid Vehicles: Transit Buses, Light Trucks and Tramways 214
4.3. Battery Technology for Traction 214
4.3.1. Lead Acid 215
4.3.1.1. Lead Acid Batteries for Micro Hybrids 218
4.3.2. Nickel Cadmium 221
4.3.2.1. Nickel Cadmium for EVs 222
4.3.3. Nickel Metal Hydride 228
4.3.3.1. NiMH Batteries for EVs 229
4.3.3.2. NiMH Batteries for HEVs 231
4.3.4. Lithium Ion 242
4.3.4.1. Lithium Ion Technology 246
4.3.4.2. Lithium Ion Batteries for EVs 247
4.3.4.3. Lithium Ion Batteries for HEVs 256
4.3.5. Lithium Polymer Batteries 262
4.3.5.1. Battery Chemistry and Technology 263

4.3.5.2. Integration in Vehicle 263
4.3.6. Sodium Nickel Chloride Battery 265
4.3.6.1. Battery Chemistry and Technology 265
4.3.6.2. Bench Tests 267
4.3.6.3. On board Testing 268
4.4. Conclusion 268

Chapter 5. Aerospace Applications. I. Satellites, Launchers, Aircraft

Y. Borthomieu and N. Thomas

5.1. Introduction 273
5.2. Satellite Batteries 273
5.2.1. Satellite Requirements 274
5.2.1.1. GEO Satellites (Geostationary Earth Orbit) 274
5.2.1.2. LEO Satellites (Low Earth Orbit) 277
5.2.1.3. MEO and HEO Satellites (Medium Earth Orbit and High Earth Orbit) 279
5.2.2. Satellite Battery Technologies 280
5.2.2.1. NiCd Batteries 281
5.2.2.2. NiH_2 Batteries 288
5.2.2.3. Li-Ion Batteries 297
5.3. Launcher Batteries 308
5.3.1. Rechargeable Batteries 309
5.3.2. Primary Batteries 311
5.3.2.1. Silver-Zinc Batteries 311
5.3.2.2. Lithium Batteries 312
5.3.3. Thermal Batteries 314
5.4. Aircraft Batteries 314
5.4.1. Batteries on Board Aircraft 314
5.4.2. Role of the Main Aircraft Battery 314
5.4.3. Defining the Aircraft Environment 315
5.4.4. Current Technology 317
5.4.5. Future Trends 323

Chapter 6. Aerospace Applications. II. Planetary Exploration Missions (Orbiters, Landers, Rovers and Probes)

B. V. Ratnakumar and M. C. Smart

6.1. Introduction 327
6.2. General Characteristics of Space Batteries 328
6.3. Planetary and Space Exploration Missions 329
6.3.1. Robotic Space Exploration 330

6.3.1.1. Orbiters 330
6.3.1.2. Fly-by and Sample-Return Missions 332
6.3.1.3. Landed Missions – Lander 332
6.3.1.4. Landed Missions – Rovers 333
6.3.1.5. Landed Missions – Probes 334
6.3.1.6. Impactors and Penetrators 335
6.3.1.7. Miscellaneous Science Missions 336
6.3.2. Human Exploration Missions 336
6.3.2.1. Space Shuttle 336
6.3.2.2. Crew Exploration Vehicles 336
6.3.2.3. Planetary Ascent Stage and Descent Stage Modules 337
6.3.2.4. Extra-Vehicular Activities (EVA) 338
6.3.2.5. NASA's Future Surface Exploration Missions 338
6.4. Past and Current Planetary Missions 339
6.4.1. Lunar Missions (Apollo) 339
6.4.2. Missions to Mars and Other Planets 339
6.4.3. Other Missions 354
6.5. Future Mars Missions 356
6.6. Aerospace Battery Technologies 357
6.6.1. Primary Batteries 357
6.6.1.1. Silver-Zinc 357
6.6.1.2. Lithium-Sulfur Dioxide 359
6.6.1.3. Lithium-Thionyl Chloride 361
6.6.1.4. Lithium Carbon Monofluoride 361
6.6.1.5. Comparative Assessment of Primary Batteries 362
6.6.2. Thermal Batteries 363
6.6.3. Rechargeable Batteries 365
6.6.3.1. Silver-Zinc 365
6.6.3.2. Nickel-Cadmium 365
6.6.3.3. Nickel-Hydrogen 368
6.6.3.4. Nickel-Metal Hydride 373
6.6.3.5. Lithium-Ion 374
6.7. Unique Performance Attributes of Aerospace Li-Ion Batteries 380
6.7.1. Low Temperature Performance of Li-Ion Batteries 381
6.7.2. Radiation Tolerance 382
6.7.3. Calendar Life 384
6.8. Lithium Batteries – Advanced Systems 384
6.9. Concluding Remarks on Rechargeable Batteries 387

Chapter 7. Stationary Applications. I. Lead-Acid Batteries for Telecommunications and UPS

R. Wagner

7.1. Introduction 395

7.2. The Lead-Acid Battery Technology 396
7.3. Large Batteries 402
7.4. Improvement of Power Performance 409
7.5. Features of VRLA Technology 417
7.6. Gel Batteries 430
7.7. AGM Batteries 435
7.8. Future Trends 442
7.9. Conclusions 451

Chapter 8. Stationary Applications. II. Load Levelling

J. Kondoh

8.1. Signification of Stationary Application 455
8.1.1. Electric Power Systems 455
8.1.2. Load Curves and Allocation for Power Plants 456
8.1.3. Load Levelling 457
8.1.4. Load Frequency Control 458
8.1.5. Other Applications 458
8.1.6. Present Conditions 458
8.1.7. Future Prospects 459
8.2. Sodium-Sulfur Battery Systems 460
8.2.1. Battery Chemistry and Components 460
8.2.2. Practical System 462
8.2.3. Capital Cost 468
8.3. Vanadium Redox Flow Battery Systems 468
8.3.1. Battery Chemistry and Components 468
8.3.2. Practical System 470
8.4. Other Secondary Battery Systems 475
8.4.1. Lead-Acid Battery Systems 475
8.4.2. Nickel-Metal Hydride Battery Systems 475
8.4.3. Lithium-Ion Battery Systems 477
8.5. Other Electric Energy Storage Systems 478
8.5.1. Pumped Hydroelectric Energy Storage Systems 479
8.5.2. Compressed Air Energy Storage Systems 479
8.5.3. Superconducting Magnetic Energy Storage Systems 482
8.5.4. Electric Double Layer Capacitors 484
8.5.5. Flywheel Energy Storage System 485
8.6. Comparison 486
8.6.1. Existing Systems 486
8.6.2. Lifetime and Capital Cost 486
8.6.3. Output Power and Stored Energy Densities 489
8.6.4. Cycle Efficiency 492

Chapter 9. Stationary Applications. III. Lead-Acid Batteries for Solar and Wind Energy Storage

R. Wagner

9.1. Introduction 497
9.2. Energy Storage for Solar and Wind Systems 498
9.3. Flooded Batteries 502
9.4. Large Batteries 505
9.5. Small Systems with VRLA Batteries 512
9.6. Large Systems with Gel Batteries 524
9.7. Further Developments 537
9.8. Conclusions 543

Chapter 10. Stationary Applications. IV. The Role of Nickel-Cadmium Batteries.

A. Green

10.1. Introduction 547
10.2. History 547
10.3. Chemistry 548
10.3.1. Memory Effect 549
10.4. Construction Features of Nickel-Cadmium Cells 550
10.4.1. Plate Technology 550
10.4.2. Active Materials 551
10.4.3. Separators 552
10.4.4. Electrolyte 552
10.4.5. Range of Products Available 552
10.5. Electrical and Mechanical Characteristics 552
10.5.1. Performance at High and Low Temperatures 553
10.5.2. Lifetime at High Temperatures 554
10.5.3. Cycling Behaviour 554
10.5.4. Charge Characteristics 555
10.6. Cost and Reliability Considerations 556
10.7. A Large Battery in an Energy Storage Application 558
10.7.1. Introduction 558
10.7.2. Defining the BESS 558
10.7.3. The BESS Design 559
10.7.3.1. The Battery 559
10.7.3.2. The Electrical System 560
10.7.4. Operating Results 561
10.7.5. Awards 561
10.7.6. Final Considerations 562

10.8. Small Batteries in Telecommunication Applications 562
10.9. Lifetime and Reliability: The Case of an Old Battery 564
10.10. Nickel-Cadmium Applications Summary 566

Chapter 11. Miscellaneous Applications. I. Metering, Power Tools, Alarm/Security, Medical Equipments, *etc.*

M. Grimm

11.1. The Power Sources 573
11.1.1. The Different Electrochemical Systems 573
11.1.2. How to Select the Right Power Source? 577
11.2. Metering Systems 578
11.2.1. Heat Meters and HCA (Heat Cost Allocators) 580
11.2.2. Power (Electricity) Meters 581
11.2.3. Gas Meters 582
11.2.4. Water Meters 583
11.2.5. Data Loggers with RF Transmission 583
11.2.6. Data Loggers with GSM or GPRS Transmission 584
11.2.7. AMR (Automatic Meter Readers) 585
11.2.8. Others 586
11.3. Remote Mobile Monitoring 587
11.3.1. ID Tags 587
11.3.2. Bar Code Portable Readers 589
11.3.3. GPS (Global Positioning Systems) 590
11.3.4. GSM (Global System for Mobile Phones) Modules 591
11.4. Automatic Assistance Systems 592
11.4.1. SARSAT/COSPAS Beacons 592
11.4.2. Safety Lights 594
11.5. Alarm and Security Systems 594
11.5.1. Emergency Light Units (ELUs) 595
11.5.2. Wireless Alarm Sensors 596
11.5.3. Wireless Alarm Central Units 597
11.5.4. Alarm Sirens 597
11.5.5. ZigBee 598
11.5.6. Access Control Systems 599
11.5.7. Remote Level Control Systems 600
11.5.8. Telematics Systems 601
11.5.9. Power Line Surveillance 601
11.5.10. PIGs 601
11.6. Memory Back Up (MBU) – Real Time Clocks (RTC) 602
11.7. Professional Cordless Tools 603
11.7.1. Drills 604
11.7.2. Drills and Screw Drivers-Wrenches 605
11.7.3. Screw Drivers 605

11.7.4. Grinders and Sanders 605
11.7.5. Planers 606
11.7.6. Saws (Circular, Jig, Sabre, Diamond, *etc.*) 606
11.7.7. Mini Tools 606
11.7.8. Irrigation Systems 607
11.7.9. Hedge Trimmers, Chain Saws, Pruning Shears 607
11.8. Professional Appliances 608
11.8.1. Handheld Terminals 608
11.8.2. Professional A/V (Audio/Video) Equipments 609
11.9. Ambulatory Medical Equipments 610
11.9.1. Portable Defibrillator Systems 610
11.9.2. Inter-Cardial Pump Systems 611
11.9.3. Ventricular Assist Pump Systems 612
11.9.4. Emergency Portable Medical Fluid Warmers 612
11.9.5. Powered Respirators 613
11.9.6. Special Medical Tools 614
11.10. Conclusion 614

Chapter 12. Miscellaneous Applications. II. Tracking Systems, Toll Collection, Oil Drilling, Car Accessories, Oceanography

H. Yamin, M. Shlepakov and C. Menachem

12.1. Introduction 617
12.2. Tyre Pressure Monitoring System (TPMS) 617
12.2.1. Direct, Indirect and Battery-Less TPMS 618
12.2.2. Power Consumption 619
12.2.3. Power Sources for TPMS 619
12.3. Electronic Toll Collection 620
12.3.1. Toll Collection Systems 621
12.3.2. Power Sources 621
12.4. Automatic Crash Notification (ACN) 622
12.4.1. Electrical Requirements and Power Sources 623
12.5. Tracking 624
12.5.1. Tracking Methods 624
12.5.1.1. RFID (Radio Frequency Identification) 624
12.5.1.2. GPS (Global Positioning System) 625
12.5.2. GPS Transmitters 626
12.5.3. Power Sources 628
12.5.4. Advantages and Disadvantages of Available Batteries 631
12.6. Oil Drilling 632
12.6.1. Applications 633
12.6.2. Power Requirements 634
12.6.3. Criteria of Battery Choice 636
12.6.4. Battery Chemistry 638

12.6.5. Future Developments 640
12.7. Oceanography 641
12.7.1. Applications 642
12.7.2. Power Requirements 642
12.7.3. Criteria of Battery Choice 643

Chapter 13. Battery Management and Life Prediction

B. Y. Liaw and D.D. Friel

13.1. Definitions 649
13.1.1. Battery Management 649
13.1.2. Battery Life Prediction 650
13.2. Monitoring & Measuring 652
13.2.1. Cell Monitoring 652
13.2.2. Cell Measurement 655
13.2.3. Battery Monitoring 656
13.2.4. Battery Measurement 657
13.3. Battery Management Functions 657
13.3.1. Charge Management 658
13.3.1.1. Charge Management with Temperature 659
13.3.1.2. Charge Management with Voltage 660
13.3.1.3. Charge Management with Other Means 661
13.3.2. Discharge Management 663
13.3.2.1. Discharge Management with Voltage 664
13.3.2.2. Discharge Management with Temperature and Current 666
13.3.2.3. Discharge Management with State-of-Charge 668
13.3.3. Safety Management 670
13.3.4. "Smart Battery System" – A Specific Battery Management Example 671
13.4. Life Prediction 673
13.4.1. Performance Prediction: Stage One Developments 675
13.4.2. Life Prediction with Laboratory Evaluations: Stage Two Development 679
13.4.3. Life Prediction in Practical Use: Stage Three Developments 683
13.4.4. Future Directions 686

Chapter 14. Battery Collection and Recycling

D. Cheret

14.1. Introduction 691
14.2. Eco-efficiency Study on Recycling Techniques 692

14.3. Trans-Boundary Movement of Batteries within the OECD Member States 696
14.4. Battery Collection Schemes 699
14.4.1. The Particular European Situation 699
14.4.2. Financing the Schemes 700
14.4.3. A Closed Loop Concept to Reduce the Exposure to Metal Price Fluctuation 703
14.5. The Particular Example of a Battery Producer: SAFT 704
14.6. Recycling Rate: What Does It Mean? 705
14.7. Battery Recycling: The Existing Technologies 707
14.7.1. The Recycling of Mixed Batteries 709
14.7.2. The Recycling of Batteries Containing Mercury 711
14.7.3. The Recycling of Zinc-Carbon and Alkaline-Manganese Primary Batteries 714
14.7.4. The Recycling of Lithium Primary Batteries 718
14.7.5. The Recycling of Lead-Acid Batteries 719
14.7.6. The Recycling of NiCd Batteries 722
14.7.7. The Recycling of NiMH Batteries 727
14.7.8. The Recycling of Li-ion and Li-Polymer Batteries 730
14.8. Conclusion 736

Chapter 15. World Market for Industrial Batteries

D. Saxman

15.1. Scope & Analysis Assumption 737
15.1.1. Definition of Industrial Battery 737
15.1.2. Definitions of Industrial Battery Market Sectors 738
15.1.3. Other Analysis Assumptions 740
15.2. Driving Forces Used to Predict World Market Value 740
15.3. Industrial Energy Storage Systems 742
15.3.1. Battery Characteristics by Type 743
15.3.2. Competing Fuel Cell Systems 746
15.3.3. Competing Exotic Energy Storage Systems 748
15.4. Industrial Battery Configurations 748
15.4.1. Lifecycle Configurations 749
15.4.2. Technical Configurations 749
15.5. Driving Forces by Market Sector 750
15.5.1. Computing Batteries 750
15.5.2. Communications Batteries 751
15.5.3. Portable Tools Batteries 753
15.5.4. Other Portable Product Batteries 754
15.5.5. Medical Batteries 755
15.5.6. Computer Memory Batteries 756
15.5.7. UPS/Stationary Batteries 756

15.5.8. Military/Aerospace Batteries 757
15.5.9. Industrial EV Batteries 759
15.5.10. HEV/EV Batteries 760
15.5.11. Auto SLI Batteries 761
15.6. Historic and Predicted World Market Summary for Industrial Batteries 762

Subject Index 767

This page intentionally left blank

List of Contributors

Doron Aurbach, *Department of Chemistry, Bar-Ilan University, Ramat-Gan 52900, Israel* (aurbach@mail.biu.ac.il)

Yannick Borthomieu, *SAFT, Rue G.Leclanché, BP1039, 86060 Poitiers Cedex 9, France (yannick.borthomieu@saftbatteries.com)*

Michel Broussely, *Saft / SBG, rue Georges Leclanché, BP1039, 86060 Poitiers, France (michel.broussely@saftbatteries.com)*

Daniel Cheret, *Umicore Recycling Solutions, Umicore Group, 2250 Olen, Belgium* (daniel.cheret@umicore.com)

Daniel D. Friel, *Honeywell Batteries, Global Technology Systems, Inc., One Apple Hill Drive PMB 8007, Natick, MA 01760-2012, USA* (present address) (DFriel@HoneywellBatteries.com)

Anthony Green, *Consultant, Redditch, Worcestershire, United Kingdom* (ag.info@btinternet.com)

Michel Grimm, *SAFT LBD, rue Georges Leclanché, 86060 Poitiers, France* (michel.grimm@saftbatteries.com)

Junji Kondoh, *National Institute of Advanced Industrial Science and Technology (AIST), AIST Central 2, 1-1-1, Umezono, Tsukuba, Ibaraki, 305-8568 Japan* (j.kondoh@aist.go.jp)

Bor Yann Liaw, *Hawaii Natural Energy Institute, University of Hawaii, Honolulu, HI 96822, USA* (bliaw@hawaii.edu)

Chen Menachem, *Tadiran Batteries Ltd., P.O. Box 1 K. Ekron, 70500 Israel*

Gianfranco Pistoia, *Consultant, Via G. Scalia 10, 00136 Rome, Italy* (gianfranco.pistoia0@alice.it)

B. V. Ratnakumar, *Jet Propulsion Laboratory, California Institute of Technology, 4800 Oak Grove Drive, Pasadena, California 91109, USA* (ratnakumar.v.bugga-103068@jpl.nasa.gov)

Donald Saxman, *BCC Research, 15402 Winterhaven, Tomball, TX 77377, USA* (donsaxman@aol.com)

Michael Shlepakov, *Tadiran Batteries Ltd., P.O. Box 1 K. Ekron, 70500 Israel*

Marshall C. Smart, *Jet Propulsion Laboratory, California Institute of Technology, 4800 Oak Grove Drive, Pasadena, California 91109, USA*

Nigel Thomas, *SAFT, 12 Rue S.Carnot, 92170 Bagnolet, France*

Rainer Wagner, *EXIDE Technologies, Deutsche EXIDE GmbH, Odertal 35, D-37431 Bad Lauterberg, Germany* (rainer.wagner@exide.de)

Herzel Yamin, *Tadiran Batteries Ltd., P.O. Box 1, Kiryat Ekron 70500, Israel* (h_yamin@tadiran-batt.com)

Industrial Applications of Batteries. From Cars to Aerospace and Energy Storage
M. Broussely and G. Pistoia Eds.,
© 2007 Elsevier B.V.

Chapter 1

NONAQUEOUS BATTERIES USED IN INDUSTRIAL APPLICATIONS

Gianfranco Pistoia

Consultant, Via G. Scalia 10, Rome, Italy

1.1. Introduction

In this chapter, and in the following one, fundamental aspects of batteries used in industrial applications will be presented, *e.g.* materials, electrode reactions, construction, storage characteristics, energy and power outputs. Their applications will be briefly dealt with, but more information can be found in the chapters dealing with specific applications.

1.2. Primary Lithium Batteries

This section includes batteries with Li metal as an anode. They feature the highest energies (both on a weight and volume basis) among all primary batteries.

The research on these batteries started in the 1960s and the first commercial products were marketed in the 1970s. At the beginning, only niche applications, such as military and medical, took advantage of these new systems. In a few years, they were widely used both in portable and stationary applications; however, because of cost and safety issues, their market share has been inferior to that of aqueous primary batteries. Yet, in some applications, *i.e.* those requiring long operation/storage times, extreme temperatures or high power, these are the batteries of choice.

The basic characteristics making primary Li batteries suitable for many applications are:

- High energy (over 200 Wh/kg and 400 Wh/L)
- High and flat potential
- High power (in spirally wound configurations)

- Long shelf-life, with capacity losses of ~1%/year at room temperature
- Wide temperature range: cells with soluble cathodes may be used between -60°C (-80°C in special cells) and 150°C
- Construction in several form factors (coin, cylindrical, prismatic and very thin batteries) and with capacities ranging from few mAh to several Ah.

In this section, Li/SO_2, Li/$SOCl_2$ and Li/MnO_2 batteries are described, as they are the most used in industrial applications. The first two are examples of soluble-cathode batteries: carbon electrodes support their reduction reactions.

1.2.1. Lithium/Sulfur Dioxide Batteries

Li/SO_2 cells, the first lithium cells to be commercialized, have remarkable advantages over aqueous primary batteries. In summary, they have:

- High specific energies and energy densities (~275 Wh/kg and ~450 Wh/L)
- High pulse power density (~650 W/kg)
- Wide temperature range (-55/-60°C to +70°C)
- Long shelf life (more than 10 years at room temperature and one year at 70°C).

These cells are available in spirally wound configurations (Figure 1.1).

The anode is Li foil, while the cathode is Teflon-bonded acetylene black. The solvent is CH_3CN in which LiBr and SO_2 are dissolved. The reactions are:

Anode: $2Li \rightarrow 2Li^+ + 2e$

Cathode: $2SO_2 + 2e \rightarrow S_2O_4^{2-}$

Overall: $2Li + 2SO_2 \rightarrow Li_2S_2O_4$ (1)

$Li_2S_2O_4$ (Li dithionite) precipitates into the pores of the carbon cathode. The stability of this cell (and of other cells with a soluble cathode) is connected with the formation of a passivating film on the Li surface as soon as Li is exposed to the electrolyte. SO_2 passivates the anode through a reaction that has long been identified with reaction (1). Actually, the film is heterogeneous in nature, being composed of Li_2S, Li_2SO_3, $Li_2S_2O_5$, $Li_2S_nO_6$ (with $n \geq 3$) and $Li_2S_2O_4$ [1]. The film growth rate increases during storage of partially discharged cells. It can be noted that $Li_2S_2O_5$ and $Li_2S_nO_6$ have been identified as minor discharge products at high rates and/or elevated temperatures [1].

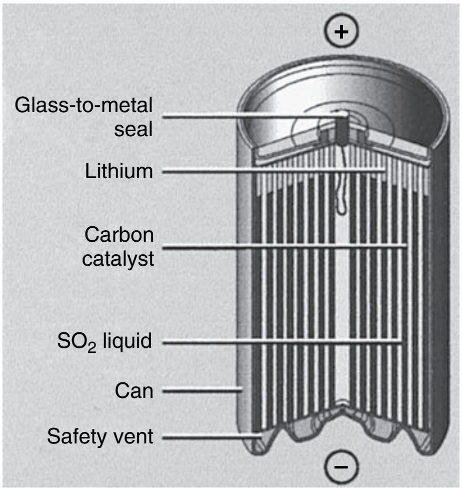

Figure 1.1. Cross-section of a Li/SO_2 cell. (*Courtesy of SAFT*)

1.2.1.1. Cell Construction and Performance

The presence of SO_2 requires a special construction: previous crimp-sealed cells have been replaced by the hermetically sealed ones to avoid SO_2 loss through the seal. The electrolyte is kept in the liquid state by maintaining a pressure of 2 atmospheres within the cell. A safety vent is incorporated (see Figure 1.1) to cope with pressure values exceeding certain limits (*e.g.* 24 atm). The acetylene black-Teflon mix is supported on an Al screen and is characterized by high values of conductivity, surface area and porosity. The last feature ensures that $Li_2S_2O_4$ precipitating on the cathode does not cause its clogging since the early reaction stages.

The electrolyte contains 70% SO_2 and has a conductivity (specific conductance) of $5 \cdot 10^{-2}$ $ohm^{-1}cm^{-1}$ at 20°C and $2.2 \cdot 10^{-2}$ $ohm^{-1}cm^{-1}$ at -50°C. The very high conductivity even at low temperatures affords the use of this system in applications (space, oceanography, cold areas) prohibited to other chemistries. A typical low-temperature performance is shown in Figure 1.2: below 0°C, significant percentages of the room-temperature capacity are recovered. The curves at -20/-40°C evidence the typical voltage delay effect connected with the passivating film on Li [2].

The cylindrical cells have capacities in the range ~1 Ah to ~11 Ah; however, cells of up to 25 Ah are also available. The 11-Ah cell can accept continuous currents of 8 A and pulse currents of 60 A. These cells can maintain a high proportion of their capacity even at the 1-hour discharge rate, whereas the capacity of aqueous batteries with a Zn anode starts declining at

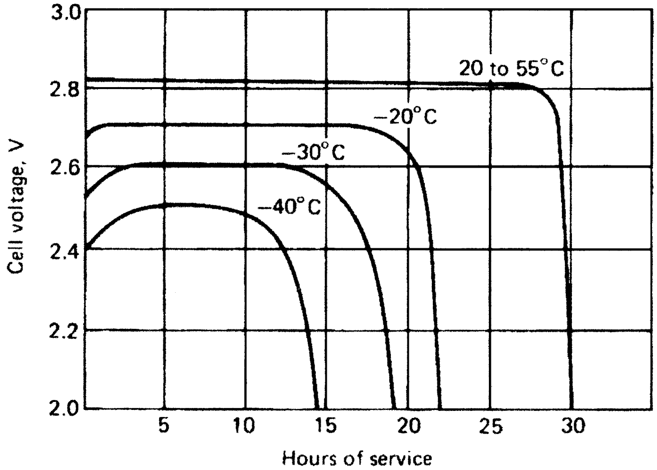

Figure 1.2. Discharge curves of Li/SO_2 cells at the C/30 rate and different temperatures. (*From Ref. 2*)

the 20 to 50-hour rates.

Long storage is possible even at temperatures as high as 70°C. At higher temperatures, the following reaction occurs:

$$4LiBr + 4SO_2 \rightarrow 2Li_2SO_4 + S_2Br_2 + Br_2$$

With this reaction, LiBr and SO_2 are removed from the electrolyte, this reducing the cell capacity; furthermore, the formation of Br_2 leads to corrosion of normally stable components.

Early-design cells had a Li/SO_2 ratio as high as 1.5:1. However, it was ascertained that this ratio greatly impaired the cell safety. Indeed, in deeply discharged cells, when the SO_2 concentration is below 5% and the passivating film removed, the reaction of Li with CH_3CN occurs [1]:

$$2Li + 4CH_3CN \rightarrow LiCN + CH_4 + CH_3C(NH)_2{=}CHCN + LiCH_2CN$$

Cell venting in these conditions causes burning of CH_4 if the cells are hot enough. Therefore, cells with a Li/SO_2 ratio close to one are now preferred: in these balanced cells, Li remains passivated as there is a sufficient amount of SO_2. At present, only cells for special applications, such as sonobuoys, use a Li excess [3]; in these cases, a high pulse capability is required, which can only be obtained in unbalanced cells.

Studies on the over-discharge-related safety concern of the Li/SO_2 system have evidenced the occurrence of the exothermal reaction [1]:

$$10Li + Li_2S_2O_4 \rightarrow 2Li_2S + 4Li_2O \ (\Delta H = -400 \text{ Kcal})$$

Furthermore, if the cell reaches a temperature of ~180°C, $Li_2S_2O_4$ undergoes a decomposition reaction leading to SO_2, S and Li_2SO_3 (and, perhaps, other decomposition products) [1].

The cell safety is enhanced by the use of microporous polypropylene separators that allow electrolyte flow in their 200-nm channels, while blocking carbon particles that might reach the anode and short the cell.

If the cell is to deliver high currents, a fuse is necessary to ensure safety; if there is any possibility of cell (or battery) charging, a diode is also needed.

Li/SO_2 cells are used in a number of military and civilian applications. A list of civilian applications includes the following:

- Security Alarms
- Automotive electronics
- Professional electronics
- Radio communications
- Emergency location buoys
- Meteorology – Space
- Toll-gate systems
- Utility metering – AMR (not recommended but possible)

1.2.2. Lithium/Thionyl Chloride Batteries

The energies of $Li/SOCl_2$ cells are among the highest of all systems: for instance, an AA bobbin-type cell has a specific energy of 475 Wh/kg and an energy density of 1000 Wh/L [2]. Furthermore, these cells can long be stored (with capacity losses of ~1-2%/year at room temperature) and can be operated in an exceptionally wide temperature range (-80°C [with a special electrolyte] to 150°C).

Low-rate $Li/SOCl_2$ cells are in the bobbin-type configuration and used mainly for memory back-up, while moderately high-power cells are built in the spirally wound configuration and used in several electric and electronic devices.

Li metal foil is the anode, porous carbon is the cathode support, and $SOCl_2$ is both the active cathode material and the solvent for the electrolyte salt (usually $LiAlCl_4$).

The overall cell reaction can be written as:

$$4Li + 2SOCl_2 \rightarrow 4LiCl + S + SO_2$$

LiCl precipitates on the carbon surface and stops cell operation when pore clogging occurs in cathode-limited cells. SO_2 is soluble in the electrolyte, while S is soluble up to ~1 mol/L and can precipitate on the cathode towards the end of discharge. LiCl is also the main component of the passivating film formed on the Li anode.

The cell capacity could be improved by adding excess $AlCl_3$ to the electrolyte. In this case, the cathode reaction can be written as:

$$4AlCl_3 + 2SOCl_2 + 4e \rightarrow 4AlCl_4^- + S + SO_2$$

Soluble $LiAlCl_4$ is formed instead of LiCl, so that no pore clogging occurs. However, $AlCl_3$ dissolves the LiCl passivating film on Li, thus favoring its corrosion. For this reason, excess $AlCl_3$ is only used in high-rate reserve cells [2].

1.2.2.1. Cell Construction and Performance

Industrial cells for low-rate applications are essentially constructed with the bobbin-type configuration shown in Figure 1.3.

Li is swaged against a stainless or nickel-plated steel can. The porous cathode, Teflon(10%)-bonded acetylene black, occupies most of the can volume and includes a metallic cylinder as a current collector for larger cells (see figure) or a pin for smaller cells (*i.e.* AA-size). Bobbin-type cells are cathode- limited, as this is considered safer than the anode-limited type [2]. No hazards have been observed when submitting these cells to short circuits, over-discharge or over-charge. Their capacities range from 0.36 Ah to an impressive 38 Ah for a DD cell.

In Figure 1.4, the low-rate discharges of AA cells at various currents and at two temperatures are presented. The flat discharge voltage and the moderate performance loss at -40°C are remarkable.

The spirally wound configuration of Figure 1.5 allows using the $Li/SOCl_2$ couple in applications requiring medium to moderately high rates. Safety devices, such as a vent and a fuse (see figure) are incorporated to prevent accidents stemming from overpressures or short circuits.

Both cathode- and anode-limited cells show moderate increases of the internal temperature and pressure during normal discharge. Indeed, for a C-size

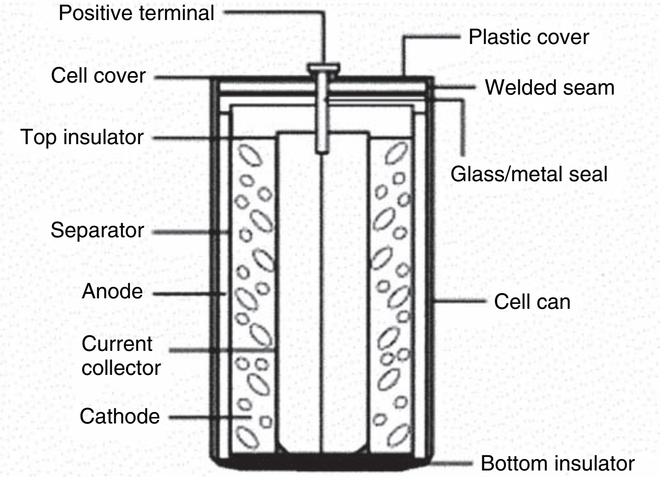

Figure 1.3. Cross-section of a bobbin-type Li/SOCl$_2$ cell. (*Courtesy of Tadiran*)

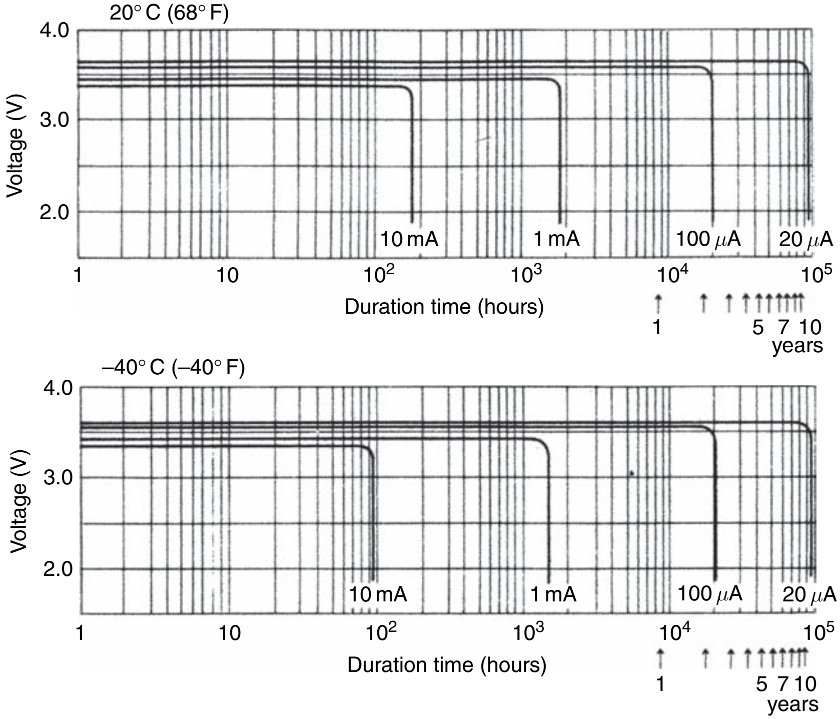

Figure 1.4. Discharge curves of an AA bobbin-type Li/SOCl$_2$ cell at different rates and at two temperatures. (*Courtesy of Maxell*)

cell discharged to 0 V at 2 A, these values remain below 50°C and 25 psig, respectively. Conversely, during over-discharge the temperature may reach 115°C and the pressure 140 psig in cathode-limited cells [1].

The pressure attained in normal discharge is lower than expected on the basis of the SO_2 formed. A complexation of the latter with $LiAlCl_4$ provides the rationale for this behavior [1]:

$$LiAlCl_4 + 2SOCl_2 \rightleftharpoons Li^+(OSCl_2)_2AlCl_4^- \overset{SO_2}{\rightleftharpoons} Li^+(OSCl_2)(SO_2)AlCl_4^- + SOCl_2$$

$$Li^+(OSCl_2)(SO_2)AlCl_4^- \overset{2SO_2}{\rightleftharpoons} Li^+(SO_2)_3AlCl_4^- + SOCl_2$$

The vapor pressure of the last complex is less than 1 atm at room temperature. SO_2 can also be absorbed by the porous carbon.

Higher capacity and lower cathode polarization may be obtained if catalytic substances are added to the cathode. A number of such catalysts have been proposed. Among them, metallomacrocycles (porphyrins, phtalocyanines and tetraazaannulenes) seem preferable [1].

Improvement of the performance of $Li/SOCl_2$ cells is also possible with the use of interhalogen compounds, *i.e.* BrCl (BCX cells). With this additive, the OCV rises from 3.65 to 3.90 V, and enhancements are observed in terms of capacity, low-temperature performance and safety [1,2]. These nice features are counterbalanced by the reduced storage capability shown by cells discharged beyond a certain DOD. For instance, a 13-Ah cell discharged to 3 Ah, and left on storage one year at room temperature, showed a severe voltage depression and a considerable capacity loss [1].

The low-temperature performance may also be improved by using $LiGaAl_4$ instead of $LiAlCl_4$. With this salt, a working temperature of -80°C is attainable, as demonstrated, for instance, by the cells used in the Mars Microprobe Mission [2].

The rate capability of $Li/SOCl_2$ cells is not sufficient for some applications, *i.e.* buoys, GPS, automatic meter readings (AMR), *etc.* In these cases, some alternative types of $Li/SOCl_2$ cells can be used. In an approach proposed by Tadiran, a bobbin-type cell is coupled to a hybrid layer capacitor (see also Chapter 12). The cell manages ordinary loads, while the capacitor can sustain the high current pulses (up to several amperes) required from time to time [4]. In another approach, illustrated for sonobuoy applications, thin components are arranged in a bipolar configuration. Large multicell stacks are capable of delivering pulse powers of ~4 kW/kg [5].

The voltage delay effect, more noticeable at high rates and low temperatures, may be reduced in $Li/SOCl_2$ (and Li/SO_2) cells by applying a conductive polymeric film on the Li anode. A very attractive polymer is the

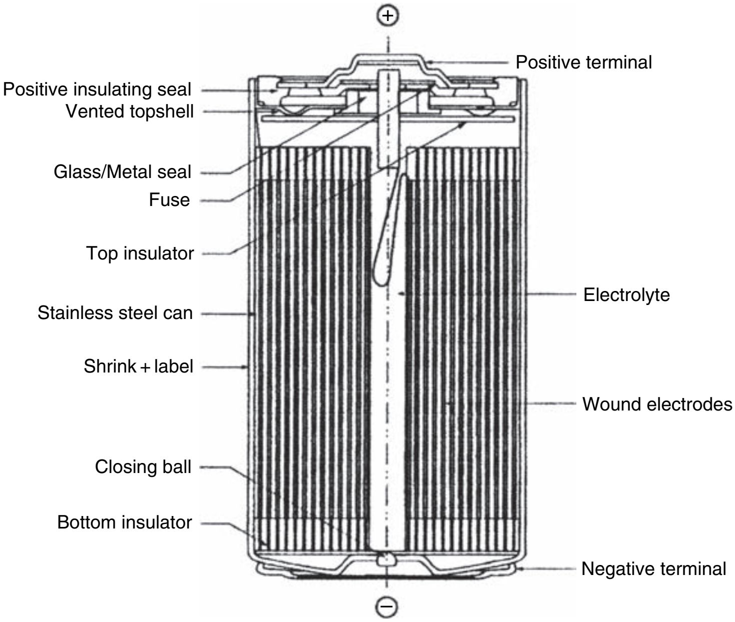

Figure 1.5. Cross-section of a spirally wound Li/$SOCl_2$ cell. (*From Ref.2*)

one formed by the complex of a Li salt with poly[bis-(methoxyethoxy-ethoxide)phosphazene] (MEEP) [1]. For instance an electrolyte based on MEEP$(LiClO_4)_{0.25}$ has a conductivity of $1.7 \cdot 10^{-5}$ $ohm^{-1}cm^{-1}$ and, so, is 10^3 times more conductive than LiCl. In Figure 1.6, the difference between a coated and an uncoated Li anode during storage is shown. The double-layer film on uncoated Li has a porous layer whose thickness increases with storage, while the thickness of the conductive polymer film remains constant [1].

Ordinary bobbin-type cells (-55 to 85°C) can be used in:

- Memory back-up
- Automatic meter readings
- Alarm systems
- Automotive electronics
- Lighting

High temperature cells (-50 to 150°C) can be used in:

- Measurements while drilling (MWD)
- Downhole pressure measurements
- Tyre pressure monitoring systems (TPMS)
- Geothermal applications

Spirally wound high-power cells can be used in:

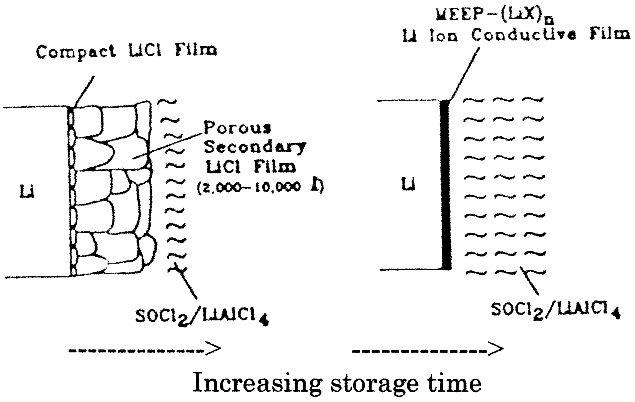

Figure 1.6. Left: LiCl film on the Li surface of a Li/$SOCl_2$ cell; it consists of a compact, protective section and a porous section whose thickness increases with storage time. *Right*: Li coated with MEEP-$(LiX)_n$ electrolyte. (*From Ref. 1*)

- Automatic meter readings
- Security –Alarms
- Radio communications
- GPS
- Automotive electronics
- Several types of buoys

1.2.3. Lithium/Manganese Dioxide Batteries

The Li/MnO_2 system was one of the first investigated and its initial performance was rather poor. Especially the cathode properties had to be substantially modified to have the cells available today. Commercialized since 1975, this primary Li battery is by far the most widely used, as it owns several nice features: high voltage, high energy (both on a gravimetric and a volumetric basis), wide operating temperature range, good power (in some designs), long shelf-life, safety, and low cost. The Li/MnO_2 battery is produced by several manufacturers in coin, cylindrical or prismatic forms (the last one including thin cells) and can be used in a variety of applications.

The fundamental step towards an efficient system was made when Sanyo's researchers realized that moderate heating of electrochemically active MnO_2 could modify its crystallographic and physico-chemical properties, so to make it an ideal solid cathode for primary Li cells [6,7]. Further studies have allowed pinpointing the nature of the changes brought about by heating [8].

The original structure of the MnO_2 used, the γ form, undergoes a minor transformation into the γ–β form upon heating at 350-400°C. Both forms are based on octahedra sharing corners and edges, so to create 1x1 and 2x2 tunnels [8,9]. Heating also produces: 1) a gradual loss of both adsorbed and structural H_2O (with an incomplete H_2O release even around 450°C); 2) a two-order of magnitude increase of the conductivity; 3) a large reduction of the surface area; 4) an oxidation of Mn^{3+}, always present in this oxide, to Mn^{4+} [8].

All these changes favor Li^+ insertion within the tunnels of γ–β MnO_2, so that a good portion of its theoretical capacity (0.31 Ah/g) can be exploited at an operating voltage near 3 V. The overall reaction may be represented as:

$$x\text{Li} + \text{MnO}_2 \rightarrow \text{Li}_x\text{MnO}_2$$

The formula Li_xMnO_2, with $0<x<1$, best explains the gradual accommodation of Li^+ ions into the host structure.

Li foil is used as the anode, heat-treated MnO_2 (with a residual H_2O content of ~1%) as the cathode, and a preferred solution is $LiClO_4$-PC-DME (PC=propylene carbonate, DME=dimethoxyethane; room temperature conductivity: $\sim 12 \cdot 10^{-3}$ $ohm^{-1}cm^{-1}$).

1.2.3.1. Cell Construction and Performance

Li/MnO_2 cells for industrial uses are mainly manufactured with the

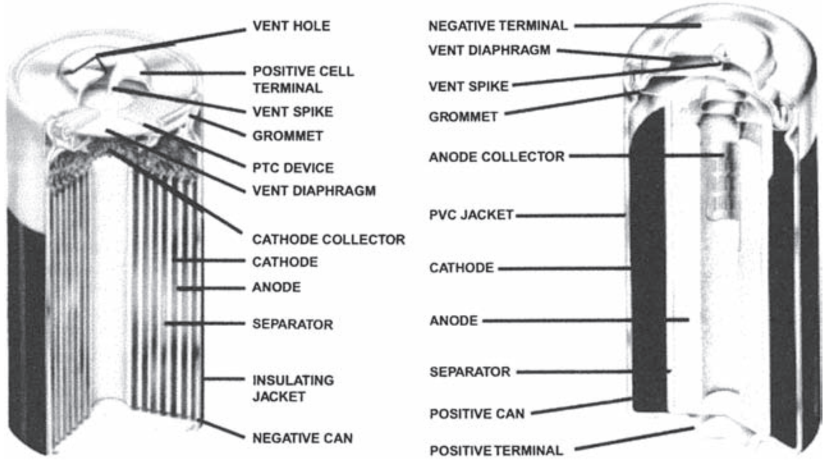

Figure 1.7. Cross-sectional views of spirally wound, crimp-sealed (*left*) and bobbin, laser-sealed (*right*) Li/MnO_2 cells. (*Courtesy of Duracell*)

following designs: spirally wound cylindrical, bobbin type cylindrical, 9-V prismatic and thin cells. The first two designs are most widely used and are illustrated in Figure 1.7. Details on the other form factors can be found in Ref. [2]. The bobbin cells have a laser seal, while the spirally wound ones may have a crimp or a laser-welded seal. The differences are shown in Figure 1.8. The laser sealing technology ensures a cell life of 10 years at r.t., and a wider temperature range. Indeed, these cells can be operated in the range -40 to 85°C, while for those with crimp seals the range is: -20 to 60°C.

The cell cans are made of stainless steel and the separator is polypropylene. Bobbin and spirally wound cells are endowed with safety vents, and the latter, meant for high power applications, have a PTC (positive temperature coefficient) device for additional safety. Other differences may be appreciated in Figure 1.7. High-power cells can also have relatively high capacities, *e.g.* more than 10 Ah in the D size [10].

Typical discharge curves of cylindrical cells are shown in Figure 1.9(a,b). The excellent performance of the spirally wound cell at low and high temperatures is particularly noticeable. The wide liquid range of the electrolyte and the thermal stability of all cell components permit this performance. This cell can sustain a maximum pulse current of 2.5 A. As anticipated, the Li/MnO_2 system has excellent storage characteristics. This is confirmed in Figure 1.9(c) for a bobbin cell at several temperatures.

The applications are different for bobbin and spirally wound cells and are summarized in Table 1.1 [11]. An interesting new application is in a system that monitors sensors around a car and automatically sends an emergency message with car location in case of road accident [10]. (See also Chapter 12 on this subject).

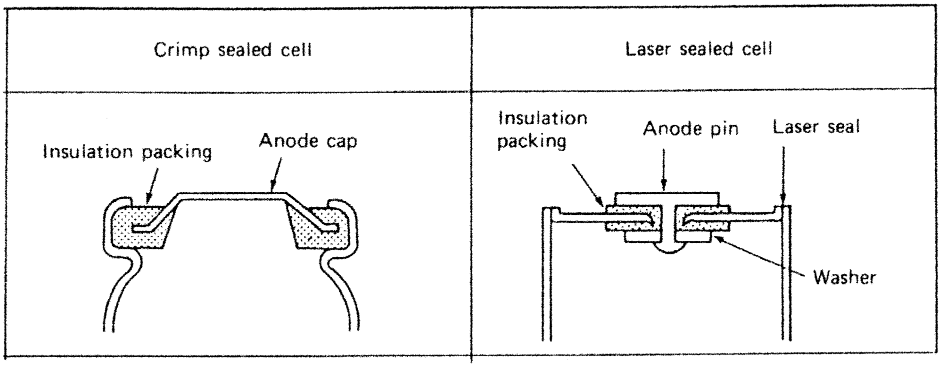

Figure 1.8. Basic differences of crimp- and laser-sealing in Li/MnO_2 cylindrical cells. (*From Ref. 2*)

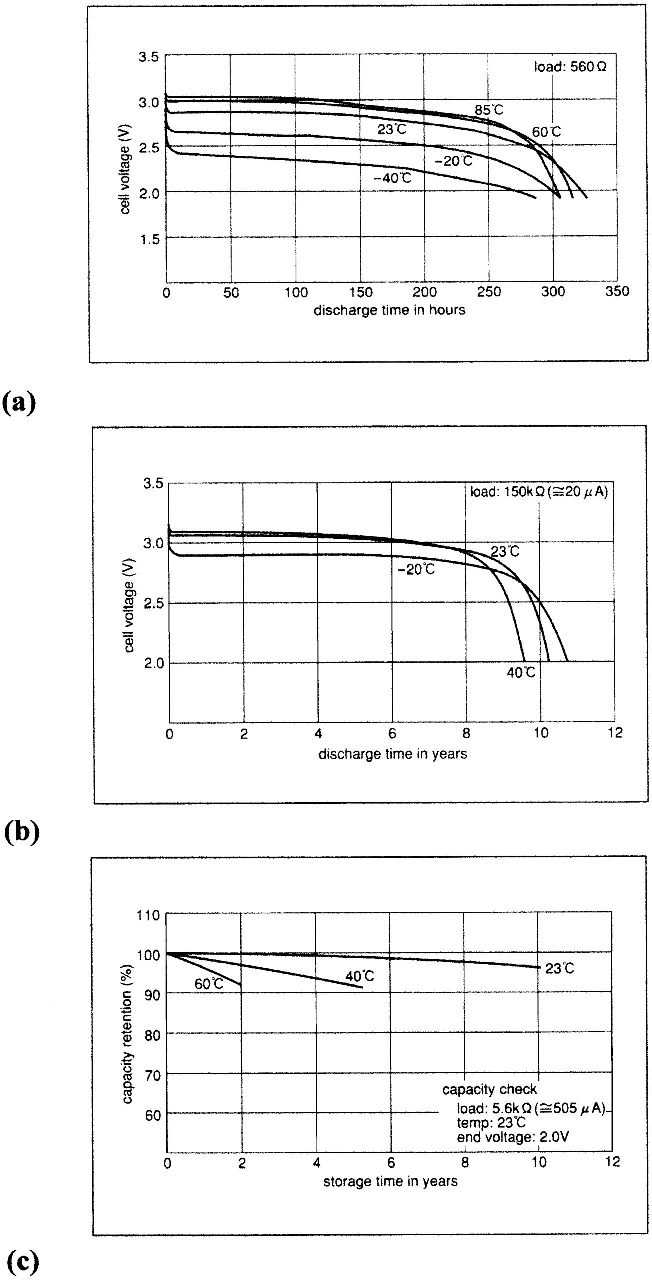

Figure 1.9. (*a*) Temperature characteristics of a spirally wound Li/MnO$_2$ cell (1500 mAh, ~5 mA); (*b*) low-rate discharge *vs.* temperature for a bobbin-type cell (1800 mAh, ~20μA); (*c*) storage characteristics of the cell in (*b*). (*Courtesy of Sanyo*)

Table1.1. Applications of Li/MnO_2 cells as a function of cell sizes and characteristics. (*Adapted from Ref. 11*)

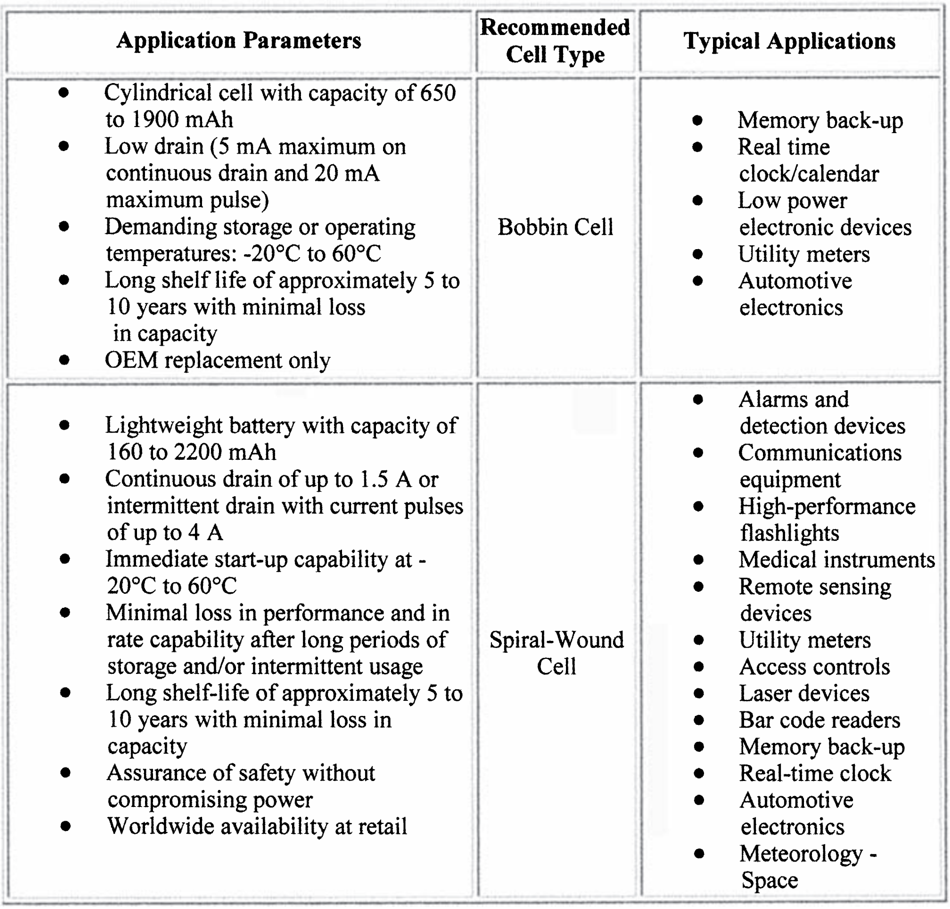

Application Parameters	Recommended Cell Type	Typical Applications
• Cylindrical cell with capacity of 650 to 1900 mAh • Low drain (5 mA maximum on continuous drain and 20 mA maximum pulse) • Demanding storage or operating temperatures: -20°C to 60°C • Long shelf life of approximately 5 to 10 years with minimal loss in capacity • OEM replacement only	Bobbin Cell	• Memory back-up • Real time clock/calendar • Low power electronic devices • Utility meters • Automotive electronics
• Lightweight battery with capacity of 160 to 2200 mAh • Continuous drain of up to 1.5 A or intermittent drain with current pulses of up to 4 A • Immediate start-up capability at -20°C to 60°C • Minimal loss in performance and in rate capability after long periods of storage and/or intermittent usage • Long shelf-life of approximately 5 to 10 years with minimal loss in capacity • Assurance of safety without compromising power • Worldwide availability at retail	Spiral-Wound Cell	• Alarms and detection devices • Communications equipment • High-performance flashlights • Medical instruments • Remote sensing devices • Utility meters • Access controls • Laser devices • Bar code readers • Memory back-up • Real-time clock • Automotive electronics • Meteorology - Space

1.2.4. Lithium/Carbon Monofluoride Batteries

Another interesting primary battery is the one using poly(carbon monofluoride), $(CF_x)_n$, as a cathode. This compound is synthesized by direct fluorination of carbon, in the form of graphite or coke, with fluorine gas at temperatures of 300°C to over 600°C. Covalent C-F bonds are formed in a structure resembling that of the initial carbonaceous material. The value of x ranges from 0.9 to 1.2, and useful cathode material have $x \geq 1$. In the following, this cathode material will simply be written as CF_x (where x is normally equal to 1).

This system was one of the first to be commercialized, especially for its high energy content, even at high temperatures, and flat voltage.

1.2.4.1. Materials, Electrode Reactions, Cell Types and Performance

The reactions are:

Anode: $Li \rightarrow Li^+ + e$

Cathode, (assuming x=1): $CF + e \rightarrow C + F^-$

Overall: $Li + CF \rightarrow LiF + C$

Typical electrolytes useful for this system are: $LiAsF_6$ in BL or $LiBF_4$ in PC-DME [2].

The Li/CF_x system has a number of pleasant features: flat and high operating voltage (~2.8 V), quite high capacity and energy at low-moderate drains, wide useful temperature range (-40°C to +85°C, and up to 125°C for some cells), and substantially lower self-discharge rate compared to other primary cells. On the other hand, the power capability is low.

A comparison of the storage characteristics of different cells is shown in Figure 1.10: the capacity loss of the Li/CF_x system after one year of storage at room temperature is barely appreciable, and that at 90°C is ~2%/year.

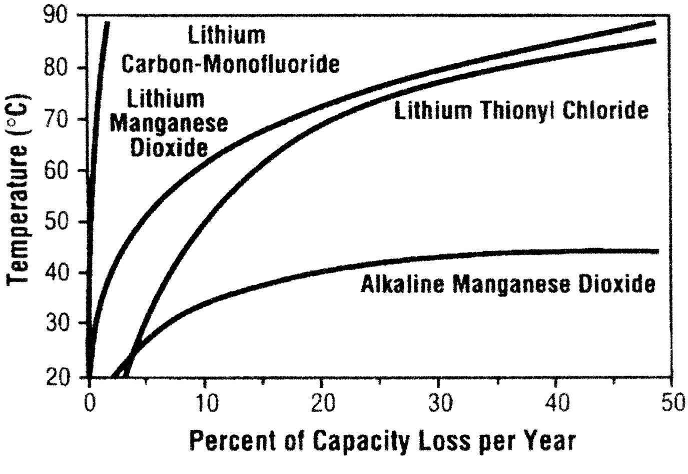

Figure 1.10. Self-discharge *vs.* temperature for different primary cells. (*Courtesy of Rayovac*)

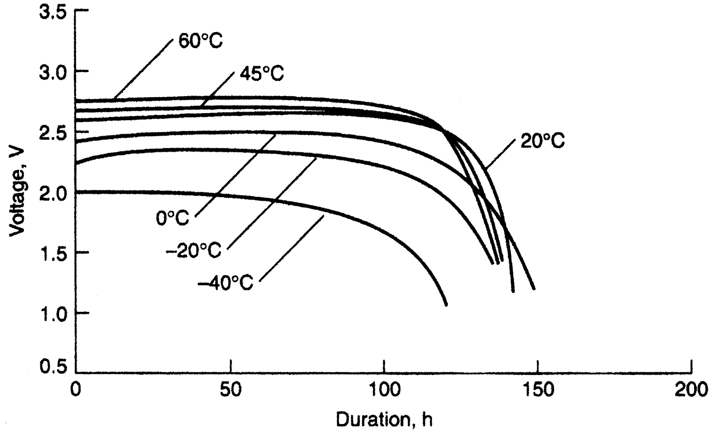

Figure1.11. Discharge curves of a cylindrical 2/3A Li/CF$_x$ cell (1200 mAh) at various temperatures. Load: 300 ohms. (*Courtesy of Panasonic*)

Storage tests run for a period of 10 years at 70°C have evidenced losses <4%. This is attributed to the inherent thermal and chemical stability of the C-F covalent bond in CF$_x$ and to the use of stable electrolytes.

Commercial pin, coin, cylindrical and prismatic cells are available, with capacities ranging from 25 mAh to 5 Ah. Large prismatic cells with a capacity of 40 Ah are available for biomedical and space applications [2]. The pin-type cells use the inside-out design with a cylindrical cathode and a central Li anode. Coin-type cells have a Li foil rolled onto a Cu net, while the cathode, also containing Teflon and acetylene black, is supported on a Ni net. The cylindrical cells mainly use the spirally wound configuration (see Figure 1.7) [2].

In Figure 1.11, discharge curves as a function of temperature are shown for a cylindrical Li/CF$_x$ cell. The performance at 60°C is excellent and a good proportion of the capacity is maintained at low temperatures, but at -40°C a remarkable voltage drop has to be taken into account. The formation of carbon on discharge enhances the electronic conductivity of the cathode.

The applications of these cells depend on their design (the pin-type ones are used for consumer applications).

- Coin type: low-power consuming cordless appliances, memory backup
- High temperature coin type: automotive electronic systems, toll way transponders, RFID (radio frequency identification)
- Cylindrical type: utility meters, emergency signal lights, electric locks, electronic measurement equipment
- Prismatic type: biomedical and space systems.

1.2.5. Basic Parameters of Primary Li Batteries

The basic parameters of the batteries dealt with in the previous sections are compared in Table 1.2. They offer a range of potential, energy, power and operating temperature that can satisfy many industrial applications.

1.3. Rechargeable Batteries

1.3.1. Lithium-Ion Batteries

These batteries possess a number of favorable characteristics:

- High specific energy and energy density
- Low self-discharge
- Long cycle life
- No maintenance
- No memory effect
- Fairly wide operating temperature
- Fairly high rate capability
- Possibility of special form factors

On the other hand, some weak points must be mentioned:

- Relatively high initial cost

Table1.2. Characteristics of primary Li batteries.

Attribute/Cell	**Li/SO_2**	**$Li/SOCl_2$**	**Li/MnO_2**	**Li/CF_x**
Average Voltage (V)	2.7-2.9	3.4-3.6	2.8-3.0	2.6-2.8
Specific Energy (Wh/kg)	260-280	450-600 (bobbin) 200-450 (spiral)	250-300 (bobbin) 150-230 (spiral)	200-250 (small) 530-600 (large)
Energy Density (Wh/L)	400-450	700-1100 (bobbin) 400-850 (spiral)	580-650 (bobbin) 400-520 (spiral)	580-635 (small) 900-1050(large)
Power Density	high	low/medium (bobbin) medium/high (spiral)	low/medium (bobbin) medium/high (spiral)	low
Temp. Range (°C)	-55÷70	-55÷85 (standard) -50÷150 (h.t.)	-40÷85 (laser) -20÷60 (crimp)	-40÷85 -40÷125 (h.t.)
Shelf-Life (years at r.t.)	10	10-15	10	15
Relative Market	5	15	100	1
Relative Cost (per kWh)	0.9	1.5	1	2

- Need of a protection circuit to avoid overcharge, overdischarge and excessive temperature rise
- Degradation at high temperature and capacity fade
- Moderate power

However, it is to be stressed that some of the above drawbacks are being progressively reduced: the cost is steadily decreasing, some Li-ion batteries (especially the polymeric ones) can work with simplified protection elements, the capacity fade is being reduced, and the power output has been greatly improved in some models thanks to proper battery engineering.

At present, the majority of commercial Li-ion cells for industrial applications has C (especially graphite) as a negative, $LiCoO_2$, $LiNi_{1-x-y}Co_xM_yO_2$ or $LiMn_2O_4$ as a positive (some other cathodes, such as $LiFePO_4$, are emerging), and an organic liquid electrolyte. Polymeric electrolytes, now widely used in small batteries for consumer applications, are also receiving close attention.

1.3.1.1. Carbons

Carbons capable of Li^+ intercalation can be roughly classified as graphitic and non-graphitic. Pure graphite has a layered structure with a perfect stacking of the graphene layers, *i.e.* is the basal planes formed by the hexagonal network of C atoms, and is highly crystalline. Graphitic carbons have a layered structure characterized by some structural defects. Some carbons may have a relatively high content of such defects or turbostratic disorder.

Non-graphitic carbons are characterized by amorphous areas together with more crystalline (graphitic) ones. These carbons may be divided into two classes: graphitizing (soft) carbons, *i.e.* those developing a graphitic structure by heating at temperatures as high as 3000°C, and non-graphitizing (hard) carbons, *i.e.* those unable to assume a graphitic structure. In Figure 1.12, a schematic view of the C layers arrangement in graphite, soft carbon, and hard carbon is shown. All these carbons have received attention as candidates for Li-ion batteries. The initial choice of a soft carbon (coke), made by Sony for their first-generation batteries, later gave way to the use of graphite. Therefore, this type of carbon will be dealt with in more detail.

In pure graphite, the layers are prevalently stacked as shown in Figure 1.13: hexagonal graphite. A different ordering may less frequently occur: rhombohedral graphite [12]. Up to 1 Li^+ can be intercalated per 6 C atoms, *i.e.* the limiting composition is LiC_6. The Li^+ intercalation/de-intercalation reaction at the negative electrode can be described as:

$$Li_xC \rightleftharpoons C + xLi^+ + xe$$

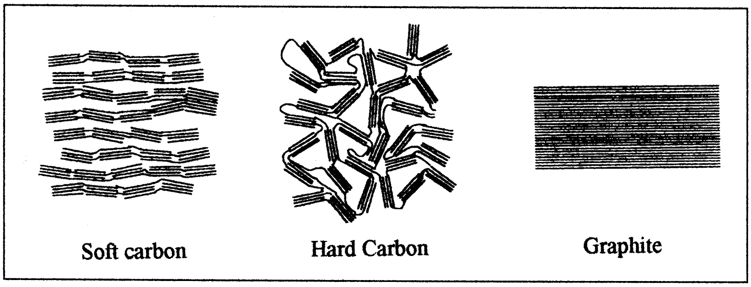

Figure 1.12. Carbon types showing different stacking of the graphene layers.

Full Li^+ intercalation into the graphite layers (charge) shifts the interlayer distance from 0.335 nm to 0.372 mm, and this expansion is fully reversed upon de-intercalation (discharge). In the long run, expansion/ contraction cycles may be deleterious for the cyclability. However, optimization of the cell structure allows compensating for the electrode deformation.

In the first charge, electrolyte decomposition and formation of a solid electrolyte interface (SEI) on C occur. Such a process is necessary as the behavior of the C electrode depends on the characteristics of this layer. The 1st cycle (charge-discharge) of a graphite electrode is shown in Figure 1.14. The initial voltage *vs.* Li/Li^+ reference electrode is above 3 V but drops suddenly to

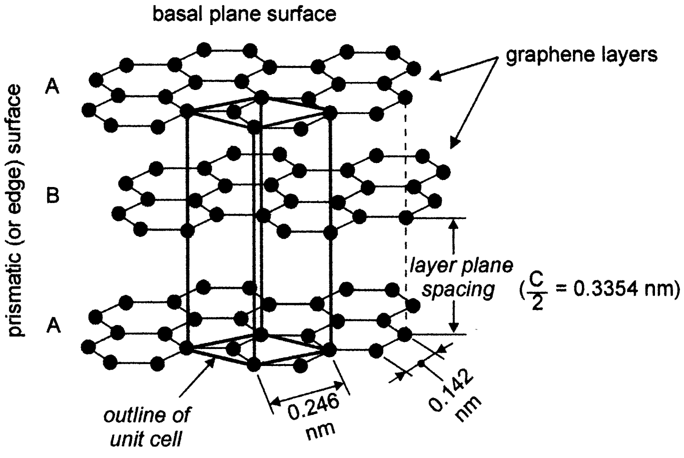

Figure1.13. Crystal structure of hexagonal graphite showing the layer stacking sequence, the unit cell, and the interlayer space. (*From Ref.12*)

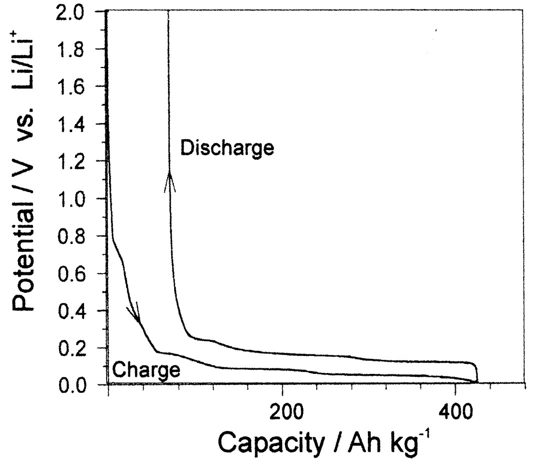

Figure 1.14. Typical 1st cycle characteristics of a graphite electrode. (*From Ref.12*)

~0.8 V, where electrolyte decomposition starts. The SEI formation continues down to ~0.2 V; at this potential Li^+ intercalation begins. When the voltage approaches 0 V, the charge is stopped to avoid Li deposition. Because of the SEI formation, the 1st-charge capacity exceeds the 1st-discharge capacity. The difference (irreversible capacity) should be minimized to reduce excess of the Li^+ source (the positive electrode) in a real battery. The irreversible capacity largely depends on the surface area of the carbon material: a high surface area causes large electrolyte decomposition, and should be therefore below ~5 m^2/g. Indeed, at 5 m^2/g the irreversible capacity is ~50 mAh/g, that is 13% of the theoretical specific capacity of graphite (372 mAh/g). In last-generation cells, the irreversible capacity is kept below 10%, and surface treatment of graphite can reduce the loss to 7%.

In a practical cell, the positive electrode is in excess, but, considering the amount of Li^+ used to form the SEI, the graphite capacity is not fully exploited. This prevents reaching 0 V on charge (see Figure 1.14), which would cause the unwanted Li plating on C. From the second cycle on, the capacity of the carbon electrode exceeds that of the positive electrode by ~10%.

The use of a negative electrode not based on carbon is now receiving renewed attention. Several inorganic materials, including oxides, silicides, phosphides and nitrides are being investigated with the aim of finding negative electrodes with higher capacities (*e.g.* 800 mAh/g for a compound of formula $Li_{2.6}Co_{0.4}N$) and lower initial irreversible capacity [13].

1.3.1.2. Positive Electrodes

The positives used are derived from layered materials, such as $LiCoO_2$ and $LiNiO_2$, or from a tridimensional material, such as $LiMn_2O_4$. In Figure 1.15, the structure of $LiCoO_2$, equivalent to that of $LiNiO_2$, is depicted. It can be described as a hexagonal structure in which the CoO_2^- slabs are separated by Li^+ layers. Li^+ can be removed from this structure, with a maximum practical delithiation of ~60%, this corresponding to a capacity of ~160 mAh/g. More Li^+ can be deintercalated from $LiNiO_2$, so that a capacity of about 200 Ah/g may be obtained. However, this material is difficult to synthesize, has a remarkable capacity loss on cycling, and a limited thermal stability. Much better performance is obtained by partly substituting Ni with Co and another metal (preferably Al). $LiNi_{1-x-y}Co_xAl_yO_2$ (with $Ni>0.75$, $Co+Al<0.25$) is a stable material capable of sustaining hundreds of cycles, and large Li-ion cells can be built with it.

The Li^+ intercalation/de-intercalation reaction in a layered $LiMO_2$ material (M= Co or Ni or their mixtures) can be described as:

$$Li_{1-x}MO_2 + xLi^+ + xe \rightleftharpoons LiMO_2$$

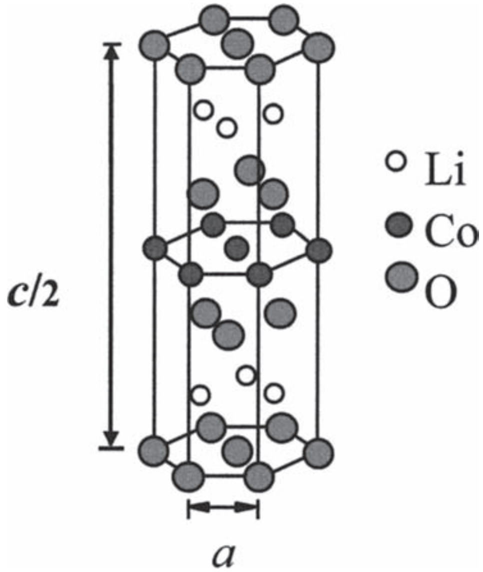

Figure 1.15. Crystal structure of $LiCoO_2$ showing the alternating layers of Li, Co and O. (*From Ref. 14*)

Combining this reaction with that of graphite (page 18), one obtains the overall reversible process in a C/$LiMO_2$ cell:

$$Li_{1-x}MO_2 + Li_xC \rightleftharpoons C + LiMO_2$$

The spinel-type structure of $LiMn_2O_4$ is depicted in Figure 1.16. This tridimensional structure can accept Li^+ in its tunnels. In comparison with $LiMO_2$, advantages of this material are: flatter and higher voltage profile, higher thermal stability, and lower cost. Negative points are: lower charge/discharge efficiency in the 1st cycle, lower discharge capacity (110-120 mAh/g *vs.* ~150 mAh/g), and lower cycling stability especially at elevated temperatures.

Apart from the above materials, $LiFePO_4$ also appears of interest for its high theoretical capacity (170 mAh/g), flat voltage at ~3.4 V, low cost and safety. However, concern has been recently raised on its low volumetric energy density, which may affect the possibility of practical applications [15]. Attention are also receiving layered Mn-containing materials, such as $Li[Ni_{1/3}Co_{1/3}Mn_{1/3}]O_2$ [16]. $LiMn_2O_4$, $LiFePO_4$ and $Li[Ni_{1/3}Co_{1/3}Mn_{1/3}]O_2$ are regarded as prospective cathodes for high-rate applications [16].

1.3.1.3. Liquid Electrolytes

Among the pre-requisites of organic liquid electrolytes to be used in Li-ion batteries, two are of particular importance due to the specific nature of the electrode materials in Li-ion systems. First, the electrolyte has to grant a stable and efficient SEI on graphite, capable of limiting self-discharge (Li^+ de-

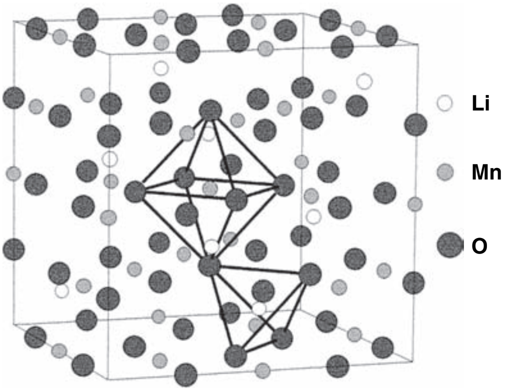

Figure 1.16. Crystal structure of spinel $LiMn_2O_4$. (*From Ref. 14*)

intercalation) while allowing fast reversible Li^+ transport. Secondly, the electrochemical window of the electrolyte has to range from 0 V to at least 4.3 V *vs.* Li/Li^+.

Electrolytes commonly used in Li-ion batteries are based on $LiPF_6$ and a binary solvent mixture, EC-DMC or EC-DEC. Their r.t. conductivities are in the range $7\text{-}10\cdot10^{-3}$ $ohm^{-1}cm^{-1}$ for 1 molar concentration of the salt, while at the upper usable limit of 60°C the conductivities are in the range $14\text{-}20\cdot10^{-3}$ $ohm^{-1}cm^{-1}$. Solutions of $LiPF_6$ in EC-DMC and EC-DEC are either solid or liquid with a very low conductivity at -40°C. For instance, a 1 M $LiPF_6$ solution in EC-DEC has a conductivity of only $0.7\cdot10^{-3}$ $ohm^{-1}cm^{-1}$ at -40°C. Better values have been found with ternary or quaternary mixtures of carbonates (see, *e.g.*, Chapter 6). Low conductivity has been taken for quite some time as the only responsible of the poor performance of Li-ion cells at low temperatures. However, it has been found out that the graphite electrode plays a role in this performance [17]. Indeed, in these conditions, Li^+ diffusivity within the graphene layers is slow and the graphite capacity is limited.

At the other extreme, temperatures above 60°C are problematic for Li-ion cells operation [18]. While at the positive electrode parasitic reactions with the electrolyte are fastened, the SEI on the C surface becomes unstable. It can reform, but irreversible losses have been observed. Additives to improve the SEI are vinylene carbonate, used by SAFT and Sanyo, and methyl cinnamate, used by NEC.

One of the greatest concerns with liquid electrolytes is their flammability, which becomes a source of risk in case of cell venting. Additives that may lower the flammability (fire retardants) include trimethyl and triethyl phosphate, and other P-containing organic compounds [18].

Other additives may be used to avoid problems created by overcharging. A current interrupting device may be activated if during overcharge a gas is generated. Additives of this type include: cyclohexylbenzene (Asahi), biphenyl (NEC) and pyrocarbonate (Sony) [18].

Liquid electrolytes need to be supported by microporous separators. Poly-ethylene and -propylene are most widely used. They can also act as a thermal fuse. Indeed, the former melts at 135°C and the latter at 165°C. If the cell temperature reaches these values, melting of the polyolefin films shuts their pores and no current flow is further allowed.

1.3.1.4. Cell Construction and Performance (with Liquid Electrolytes)

Commercial Li-ion cells are mainly available in cylindrical or prismatic form factors, where strips of electrodes and separator are wound (Figure 1.17). Some cells with flat plates are also available. The negative electrode is

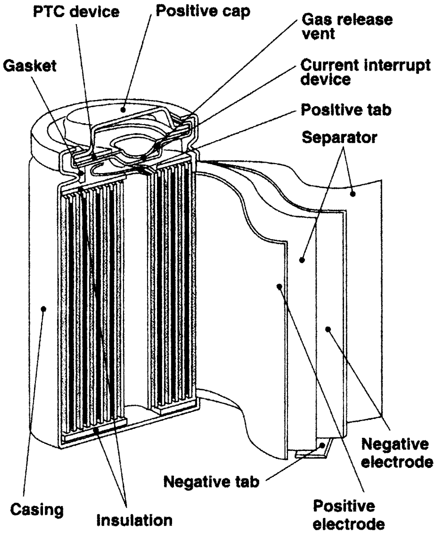

Figure 1.17. Construction of a Li-ion cylindrical cell. Note the PTC device and the vent. (*Courtesy of Sanyo*)

supported on a Cu foil, while the positive electrode is supported on an Al foil. The case is normally the positive electrode and is made of Ni-plated steel or Al. The cell cap often contains a PTC device and a safety vent (Figure 1.17). Sizes are standardized for consumer cells, but not for those of industrial interest. In the latter case, modules and stacks are often used. Recent Sony's data show that the popular 18650 cylindrical cell, which forms the basis of several modules, has reached a capacity of 2.5 Ah [19]. However, cells of much higher capacities and energies have been described, especially for energy storage, *e.g.* up to 270 Wh or ~70 Ah [20].

Examples of Li-ion cells used in industrial applications, *e.g.* for electric traction, are presented in Chapter 4 and Ref. [21]. Data for high-power cells are reported in Figure 1.18, while in Table 1.3 the characteristics of some modules used in stationary applications are listed.

The results of tests on large cylindrical cells are shown in the following figures. In Figure 1.19, a 27-Ah cell, intermediate between a high-energy and a high-power cell, shows its ability to sustain high continuous rates [22]. In Figure 1.20, the variation of the specific energy during long cycling is shown. In Figure 1.21, the power evolution as a function of cycle number is shown at two DODs for a high-energy 45-Ah cell. In Figure 1.22, the energy retention at full charge during storage at 40°C is reported for the same cell. This figure shows that in last-generation Li-ion cells a minor fraction of their energy is lost

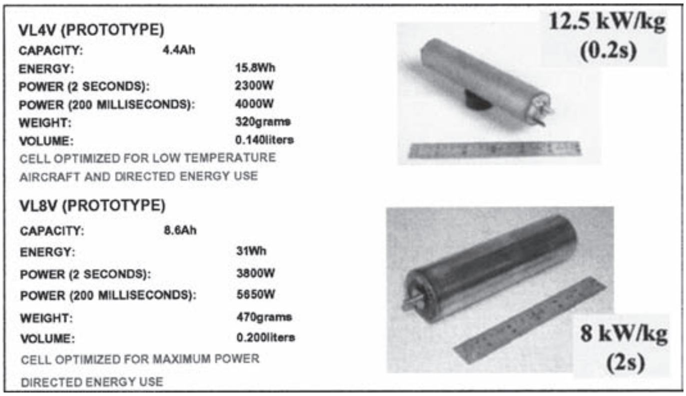

VL4V (PROTOTYPE)
CAPACITY: 4.4Ah
ENERGY: 15.8Wh
POWER (2 SECONDS): 2300W
POWER (200 MILLISECONDS): 4000W
WEIGHT: 320grams
VOLUME: 0.140liters
CELL OPTIMIZED FOR LOW TEMPERATURE
AIRCRAFT AND DIRECTED ENERGY USE

VL8V (PROTOTYPE)
CAPACITY: 8.6Ah
ENERGY: 31Wh
POWER (2 SECONDS): 3800W
POWER (200 MILLISECONDS): 5650W
WEIGHT: 470grams
VOLUME: 0.200liters
CELL OPTIMIZED FOR MAXIMUM POWER
DIRECTED ENERGY USE

Figure 1.18. High-power Li-ion cells. (*From Ref. 21*)

Table 1.3. Performance of stationary Li-ion modules (8 series-connected single cells). 8-hr discharge rate. (*From Ref. 23*)

Item	Target*	Ni-Co positive[a]	Mn positive[b]
Battery Energy (kWh)	2	2.3	2.5
Specific Energy (Wh/kg)	120	128	122
Energy Density (Wh/L)	240	197 (285)[c]	255 (295)[c]
Energy Efficiency (%)	90	98	96
Cycle life (cycles)	3500	(900)[c]	(1200)[c]

*As set by the Japanese national project for energy storage; a. $LiNi_{0.7}Co_{0.3}O_2$; b. Li-rich $LiMn_2O_4$; c. numbers in parentheses refer to single cells

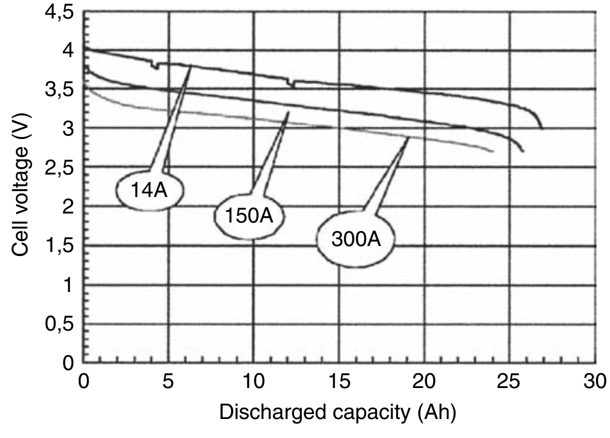

Figure 1.19. Discharge curves of a 27-Ah, 120 Wh/kg cell ($C/LiNi_{1-x-y}Co_xAl_yO_2$) at various rates. (*From Ref. 22*)

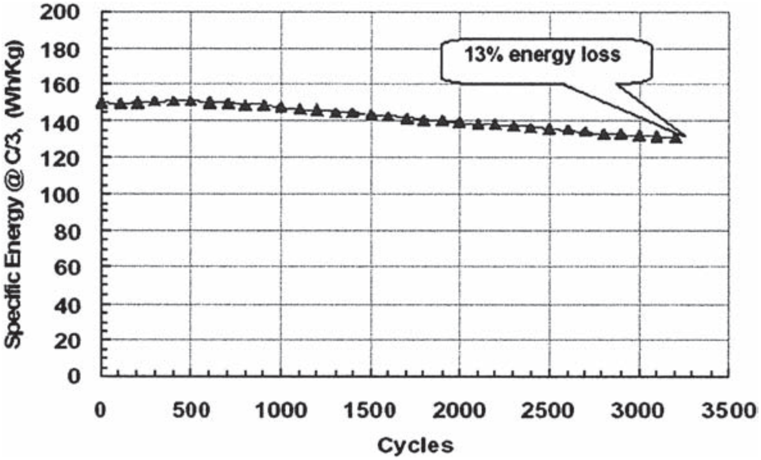

Figure 1.20. Specific energy *vs*. cycle number for a 45-Ah cell; C/3; DST (Dynamic Stress Test) cycling at 80% DOD. (*From Ref. 21*)

upon storage. The loss is ~2%/year, a remarkable result in comparison with the losses of other rechargeable systems, especially the Ni-Cd and Ni-MH cells.

For applications demanding very high energy and power output, cells are connected to give modules. Their energies may be well above 2 kWh, as shown in Tables 1.3 and 1.4 [23]. Stationary modules are meant, for example, for load leveling with a final target of 10 kWh-class batteries. The data of Table 1.3 indicate that these modules can attain the energy performance expected,

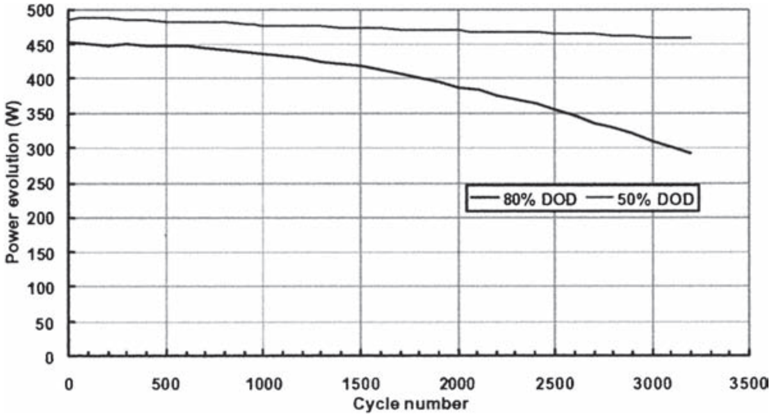

Figure 1.21. Power *vs*. cycle number for a 45-Ah cell at 50% and 80% DOD. Power measured from a 150 A, 2s pulse (20°C). (*From Ref. 21*)

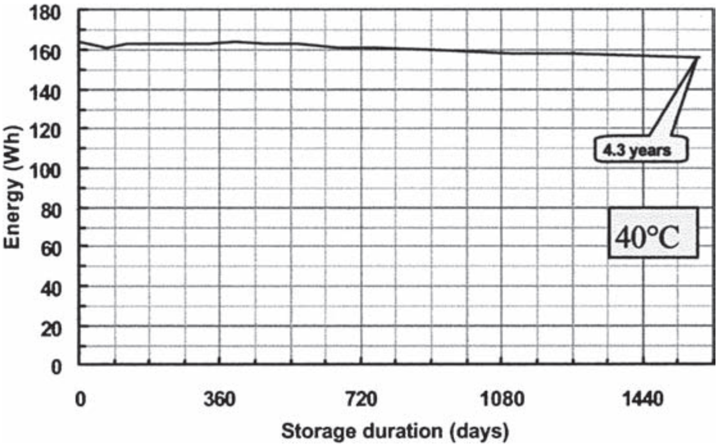

Figure 1.22. Energy retention on storage for a 45-Ah cell. Storage at 100% SOC, 40°C. Discharge at C/3 to 2.7 V, 20°C. (*From Ref. 21*)

but the present cycle number is unsatisfactory. The energy density of the module with a Ni-Co positive is low because the cylindrical form factor of the single cells leaves too much dead space in the module. The 3-kWh EV modules need to be improved in terms of energy density (these cells too are cylindrical) and, again, cycle life.

All modules have to include a battery management system (BMS) that controls both single cells and the battery. In general, single-cell supervising includes:

- Voltage measurements to prevent over-charge or –discharge
- Cell voltage balancing
- Data transmission to the battery controller

Battery management includes:

- Temperature, voltage and current measurements
- Charge/discharge control
- Predictions of state of charge (SOC), state of health (SOH) and power
- Monitoring of power devices (fuses, contactors, *etc.*)
- Emergency signals
- Interface and communication with the application

Li-ion batteries are normally charged with a double-step process: in the first, a constant current (CC) is applied until the voltage reaches a prefixed value (usually 4.2 V per cell); in the second, the cell is maintained at the constant voltage (CV) reached at the end of the previous step, while the current

Table 1.4. Performance of EV Li-ion modules (8 series-connected single cells). 5-hr discharge rate. (*From Ref. 23*)

Item	Target	Ni-Co positive[a]	Mn positive[b]
Battery Energy (kWh)	3	3.8	4.1
Specific Energy (Wh/kg)	150	150	155
Energy Density (Wh/L)	300	252 (341)[c]	244 (376)[c]
Specific Power (W/kg)	400	490	440
Energy Efficiency (%)	85	97	96
Cycle life (cycles)	1000	570 (800)[c]	580 (750)[c]

a. $LiNi_{1-x-y}Co_xMn_yO_2$; b. Cr-doped $LiMn_2O_4$; c. numbers in parentheses refer to single cells

decays. The charge is terminated when the current reaches values of C/10-C/30. A correct charge is done under control, and the end of charge is signaled by both the current value and the total time: a too long charge reveals some problems and is automatically stopped. The CC step has a current limit to avoid excessive cell heating. The charge has to be done in a precise temperature range, *e.g.* 0-45°C. The total charge time is 2-3 hours and typical charge currents are 0.7-1.0C.

Usually, Li-ion cells with $LiMO_2$ positive electrodes have long cycle lives even at high rates and in a relatively wide temperature range. Investigations on the causes of capacity fade for Li-ion cells have shown that the main responsible is the positive. Indeed, its interfacial resistance grows remarkably with cycling, as ascertained with impedance tests, because of oxidation phenomena. On the other hand, the carbon loses more capacity at high rates, *e.g.* 2C or 3C,

The rapid capacity fade of the $C/LiMn_2O_4$ system has been the subject of numerous studies. In this case, too, the positive electrode was responsible for the fade. However, optimized cells designed for HEV applications have proven able to limit capacity losses also at relatively high temperatures [24].

Other factors determining capacity loss upon cycling are DOD, discharge rate, and voltage limit on charge.

The SEI formed on the carbon electrode (see Sub-section 1.3.1.1) greatly limits further reaction with the electrolyte, so that capacity loss from this electrode is normally not very important. However, this is true if metal impurities are not present in the SEI. Indeed, if metal ions coming, for instance, from dissolution of the positive (*e.g.* Mn spinel) reach the interface, they are reduced to the metallic state and favor electron hopping and, so, Li corrosion (capacity loss) [25,26].

Most of the capacity and power loss on storage is attributable to the positive electrode. On standing, an organic layer (not necessarily an SEI) is formed on it, with a gradual increase of the interfacial impedance. Experiments on laboratory cells with a reference electrode have confirmed this, by separating the electrodes contributions. As shown in Figure 1.23, the area specific impedance (ASI) of the carbon electrode increases much less than that of the positive electrode ($LiNi_{0.8}Co_{0.2}O_2$) after a 2-week storage at 70°C [27].

1.3.1.5. Li-Ion Batteries with Polymeric Electrolytes

The use of polymeric electrolytes for Li-ion batteries had several false starts until 1999, when finally the first batteries were commercialized. Cells with polymeric electrolytes can offer some advantages over the conventional ones, *e.g.* no leakage, flexibility and very thin form factors. The use of the so-called gel polymer electrolytes has resulted in commercial products for consumer applications with performance characteristics comparable to those of liquid-electrolyte cells. The following information is based on small cells, as they are better developed, but scaling up to larger cells should occur without major modifications.

A gel polymer electrolyte (GPE) is formed by immobilizing a liquid electrolyte in a polymeric matrix. Various polymers have been proposed for this purpose, *e.g.* poly(methyl methacrylate) (PMMA), poly(vinylidene fluoride) (PVDF), poly(ethylene oxide) (PEO) and poly(acrylonitrile) (PAN). There are two approaches to make a GPE: in the first, the liquid electrolyte is added to the

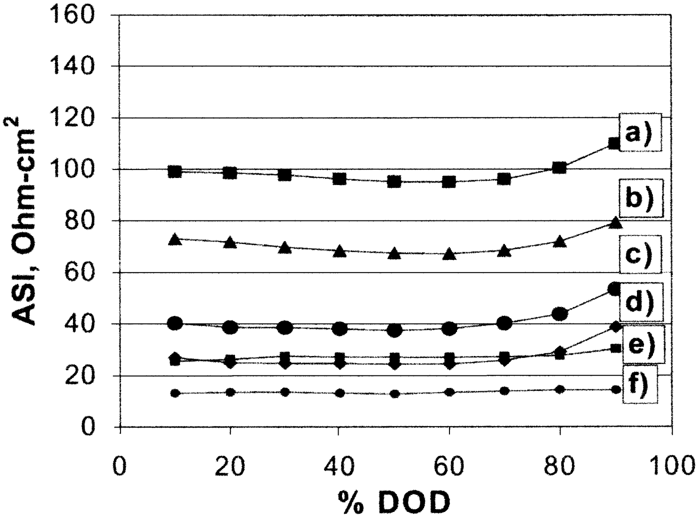

Figure 1.23. Specific impedance of : a) aged cell; b) aged positive; c) fresh cell; d) fresh positive; e) aged negative; f) fresh negative. Aging: 2 weeks at 70°C. (*From Ref. 27*) V

polymer matrix, which immobilizes it within its pores; in the second, polymer and electrolyte form a homogeneous phase. This latter condition may be obtained either by mixing polymer powder and electrolyte in a common solvent (which is then evaporated), or by adding to the electrolyte a polymer precursor and forming the polymer *in-situ.*

Whatever the approach, desirable features of a gel electrolyte are:

- Solvent confinement within the polymer structure, *e.g.* no free solvent available that may cause leakage
- Low vapor pressure of the solvent
- High conductivity at room temperature and below
- Good adhesion to the electrodes

The *in-situ* polymerization technique is exploited by Sanyo in their commercial Li-ion polymer cells. The cell is formed according to the usual technique for liquid electrolytes and, in the final step, a polymer precursor is added and heating is applied to polymerize [28]. The electrolyte is $LiN(SO_2C_2F_5)_2$ in EC-DEC and the polymer is cross-linked PEO.

In Sony's approach, the gel electrolyte is formed separately. They have chosen a copolymer of PVDF and poly(hexafluoropropylene) (PHFP) and an electrolyte formed by $LiPF_6$ in PC-EC [28]. The PHFP content in the copolymer is kept low (3-7.5% by weight) to maintain the mechanical strength typical of crystalline PVDF. PHFP grants good electrolyte absorption. The presence of PC in a cell with graphite electrode may be surprising as PC is decomposed while graphite is exfoliated. In Sony's cells, the graphite is coated with amorphous carbon, so to avoid decomposition; indeed, the irreversible capacity of the 1st charge is lower than 10%. The conductivity of this gel electrolyte, $9{\cdot}10^{-3}$ $ohm^{-1}cm^{-1}$ at 25°C, is comparable to those of liquid electrolytes and represents a remarkable improvement over 1st-generation electrolytes, as shown in Figure 1.24. This was made possible by optimization of salt concentration, PC/EC ratio, VDF/HPF ratio and molecular weight of the copolymer [28].

1.3.1.6. Examples of Applications

The evolution of Li-ion batteries has been remarkable in these years. Today, their maximum specific energies are approaching 200 Wh/kg and their energy densities 520 Wh/L. These values are very near to the limits: a calculation has set to 550 Wh/L the maximum energy density. Applications only thought possible for aqueous batteries are now at hand for Li-ion systems too. In aerospace applications, where price is not the main issue, these batteries are already used, *e.g.* in GEO and LEO satellites [29] and in rovers for planetary missions, such as the Mars Exploration Rover [30]. Forthcoming applications

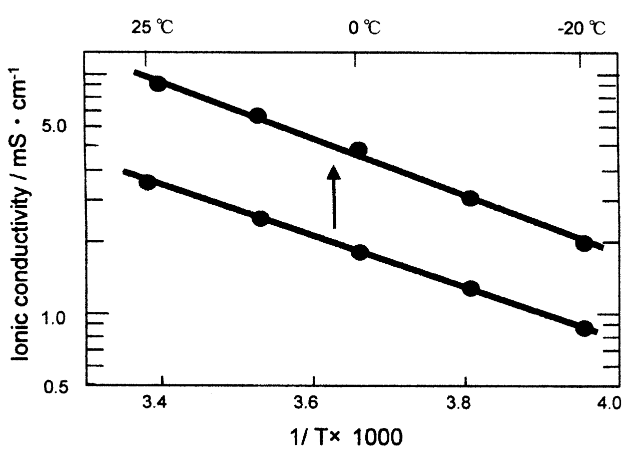

Figure1.24. Conductivities of first-generation (*lower line*) and second-generation (*upper line*) electrolytes used in Sony's Li-ion polymer cells. (*From Ref. 28)*

seem to be: traction (advanced prototypes are available) [31], UPS (Uninterruptible Power Supply) and BESS (Battery Energy Storage Systems) [32]. Relatively smaller batteries are reported to be usable in cleaners, motor assisted bicycles and power tools.

It can be remarked that the safety of large batteries has now reached satisfactory levels. An example is provided by the tests on an EV battery reported in Table 1.5.

For consumer and industrial applications, the combination of high-power Li-ion cells and high-energy fuel cells has been considered possible, but

Table 1.5. Safety tests of an EV battery (including the protection elements) at 100% SOC. (*From Ref. 21*)

TEST	Results
External short circuit (* §4.1)	No Event
Crash **	No event (liquid leakage)
Overcharge (* §4.3)	No Event
Overdischarge (* §4.4)	No Event
Water Immersion (* § 2.5)	No Event
Fuel Fire	Flames Low rate combustion

* §X : performed according to USABC Test Procedure Manual SAND 99-04-97

** : according to car manufacturer spec: 54km/h on 150 mm post.

further optimization of fuel cells is needed [33]. An interesting new couple formed by a primary Li cell, *e.g.* Li/$SOCl_2$, for high energy and a Li-ion cell for high power has also been proposed. This couple is already available [33].

1.3.2. Batteries with a Lithium Electrode

1.3.2.1. Lithium/Sulfur Batteries

An emerging system is based on the Li/S couple with a liquid electrolyte. Sulfur can provide a specific capacity of 1675 Ah/kg and a specific energy of 2600 Wh/kg in a Li/S cell, thus looking as a very appealing material. In recent years, efforts to exploit its potentialities have been renewed and interesting results reported. Sulfur is reduced in two steps. During the first, at ~2.4 V, soluble Li polysulfides are formed, which diffuse to the Li electrode where they are further reduced. The reduced forms may diffuse back to the positive where they are re-oxidized. This electrochemical shuttle prevents full recharge of the Li/S battery. Development of Li anode protection from polysulfide attack leads to a shuttle reduction of 3 orders of magnitude and to a limited self-discharge. If anode protection is coupled with an improved electrolyte, 100% charge efficiency is achieved [34]. As a result, total sulfur utilization can reach 75% or 1256 Ah/kg. Addition of a catalyst to enhance the kinetics of the second step, where insoluble and nonconductive short-chain polysulfides are formed, can afford 90% sulfur utilization, *e.g.* >1450 Ah/kg. This battery has been particularly developed in the U.S.A. by Sion Power for electronic devices [34]. 2.5-Ah cells have specific energies of up to 350 Wh/kg, and catalyst optimization allows foreseeing even higher energies. A scaling-up to large-capacity cells seems possible.

1.3.2.2. Li-Metal-Polymer Batteries

The prospects for batteries based on Li metal and polymeric electrolytes (LMP) are getting brighter. In this case, solvent-free polymers are preferred to limit Li reactions with the electrolytes and consequent occurrence of dendritic Li deposits and low charge-discharge efficiencies. The commonest polymeric electrolyte is obtained by dissolving a Li salt in polyethylene oxide (PEO). Dissolution is possible as Li^+ ions form electrostatic bonds with ether oxygen. The number of oxygen atoms bound to Li^+ may vary in a dynamic fashion, this giving rise to Li^+ movement along the polymer chains. The conductivity is due to segmental motion of the chains and is greatly enhanced in the amorphous regions, while is much slower in the crystalline ones. Li salts-PEO solutions are semi-crystalline and manifest appreciable conductivities only above their melting point. Therefore, to prevent crystallization, the basic architecture of the polymer has to be modified by addition of co-monomers and/or grafting and crosslinking the linear chains [35]. A convenient co-polymer is PEO-PPO (polypropylene oxide), which is much more amorphous than pure PEO and has a lower melting point. The conductivity of a solution having LiTFSI (Libis(trifluoromethylsulfonyl)imide) as a salt in PEO-PPO is higher than that of the classical $LiClO_4$-PEO solution in a wide temperature range [36]. However, below 40°C even the former electrolyte has a conductivity lower than $1 \cdot 10^{-4}$ $ohm^{-1}cm^{-1}$, the minimum value for a satisfactory battery performance. Therefore, the operating temperature of a battery with this electrolyte is kept above 40°C. A higher temperature is obviously necessary if pure PEO is used. For instance, a bipolar Li/FeS_2 battery with this electrolyte has been reported to cycle well for 500 cycles (100% DOD) at the temperature of 135°C [37,38]. This is a laboratory prototype.

An interesting system is the one based on Li metal as a negative and vanadium oxide as a positive in an electrolyte based on the PEO-PPO copolymer [36]. This battery is now commercialized by Avestor, a partnership of Hydro-Quebec (Canada) and Kerr-McGee (USA), for standby applications, *e.g.* telecommunications [39], and is receiving attention for use in electric cars.

Its building block is schematically shown in Figure 1.25. An ultra-thin Li foil is attached to an Al current collector; the polymeric electrolyte acts as a separator between positive and negative electrode; the positive mix contains vanadium oxide, carbon and polymer electrolyte, which binds the particles while providing a path for ionic conduction. The preferred vanadium oxide is LiV_3O_8, a layered material that may reversibly intercalate/de-intercalate more than 2 Li^+/mol, according to the reaction [40]:

$$y\mathrm{Li} + \mathrm{Li}_{1+x}\mathrm{V}_3\mathrm{O}_8 \rightleftharpoons \mathrm{Li}_{1+x+y}\mathrm{V}_3\mathrm{O}_8$$

In the battery commercially available, the composite laminate of Figure 1.25 has a thickness under 100 microns (including an insulating layer), a very low value if compared, for instance, with that of Li-ion batteries, *i.e.* 250 microns [41]. In actual manufacture, two cells are laminated back-to-back on the Al collector (bipolar configuration), with the insulating layer completely encapsulating the active cell layers. The laminates are assembled as rectangular plates into prismatic batteries, such as that shown in Figure 1.26 [42].

Different subsystems are needed for proper battery functioning. The heating element layers interspersed in the cell stack ensure a temperature range (normally 40- 60°C) that is maintained whatever the external temperature thanks to the insulation surrounding the stack. The cells are connected by a bus bar, so to create voltages of 24 or 48 V, typical of telecom applications. The pressure

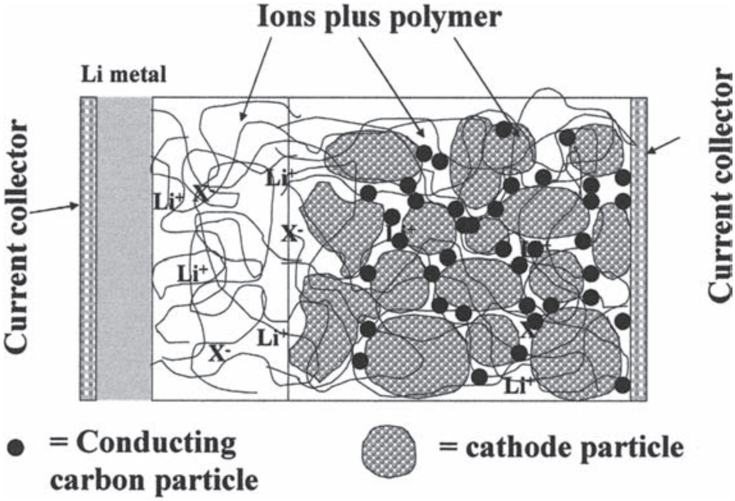

Figure 1.25. Scheme of a Li metal-polymer-metal oxide battery (*from Ref. 35*).

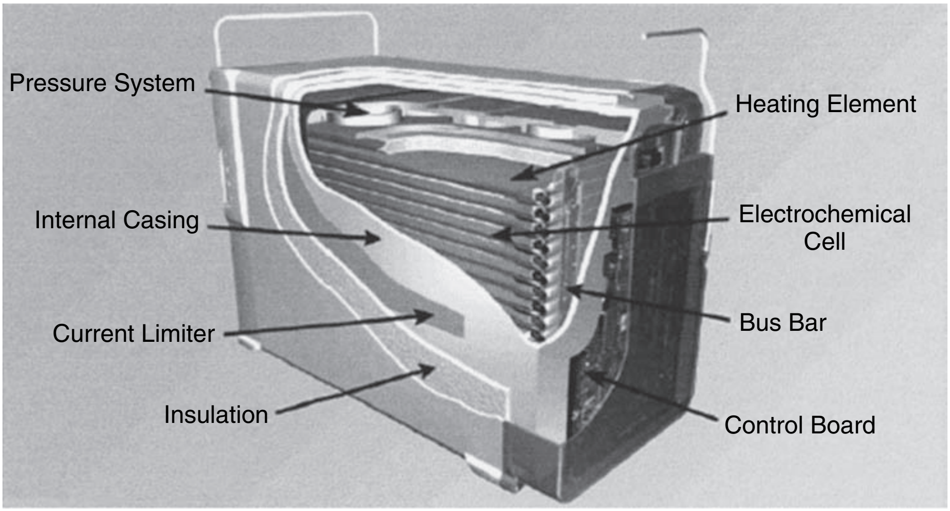

Figure 1.26. Cutaway view of a Li-metal-polymer battery construction. (*From Ref. 42*). The SE48S80 battery commercialized by Avestor for telecommunications has the basic characteristics: 48 V, 80 Ah minimum (25°C), 3.8 kWh (at C/8, 25°C), 20 A maximum current, 27.5 kg. (*From Ref. 39*)

system is a spring load structure ensuring a uniform pressure over the stacked cells. This is particularly important to have smooth Li plating during charge, as was demonstrated in the 1980s by the small Li cell commercialized by Moli Energy (Canada). Li reaction with a dry polymeric electrolyte is less important than that with a liquid solution, but still does not allow obtaining dendrite-free deposits. Therefore, a pressure system providing strong polymer adhesion to the Li metal is needed. The current limiter avoids over-currents during charge. Finally, the control board monitors battery voltage, current, temperature, and operating status and optimizes the battery conditions.

A typical voltage profile of the 48-V battery used for back-up in telecom applications is presented in Figure 1.27. The battery is based on 18 single cells. The reversible range of each cell is 3.1-2.0, as outside this range a rapid capacity fade is observed. In the practice, a cell is not discharged below 2.35 V, this corresponding to 42 V for the battery, as shown in the figure [36]. The battery management system (BMS) can perform several disconnect actions, as also shown in the figure, to ensure the longest battery life. The temperature is kept by the BMS at 40°C during stand-by and short discharges (less than 30 minutes), while it is raised to 60°C for longer discharges. Indeed, the capacity is higher at the latter temperature, as shown in Figure 1.28. The BMS automatically switches the temperature from 40°C to 60°C as the voltage of a single cell drops below 2.75 V [42].

The Li-metal-polymer battery has long life characteristics. On storage at room temperature and up to 60°C, the Avestor battery looses only 1%/year of its capacity, so that more than 10 years of shelf-life are expected. Tests carried out in operating conditions, *i.e.* during float and back-up periods, have shown that the battery can be operated for at least 12 years, as shown in Figure 1.29 [42].

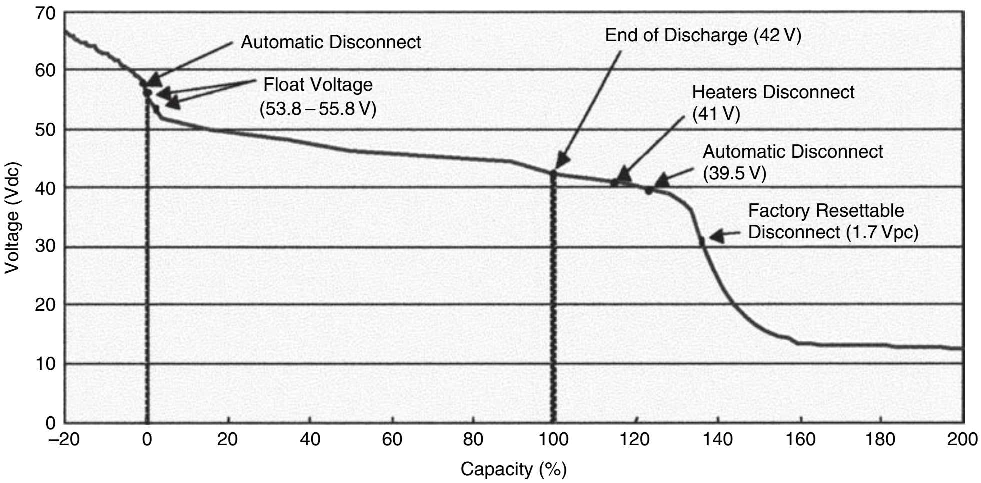

Figure 1.27. Discharge curve at 40°C of the 48-V Avestor battery. (*From Ref. 36*)

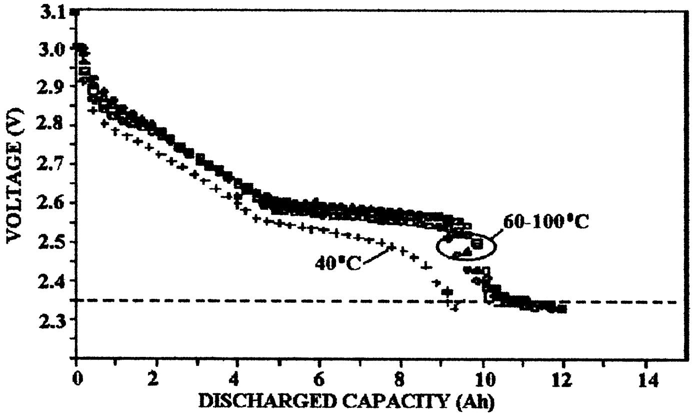

Figure 1.28. Discharge curves as a function of temperature. (*From Ref. 42*)

The float percentages represent the time the battery is on float with respect to the total operating time. A floating rate of 99.4% is actually similar to that recorded for telecommunications in the U.S.A. (99.6%), so a real life of 25 years can be reasonably expected.

Thanks to its thermal control and insulation, the battery can operate in a wide range of external temperatures, *i.e.* -40°C to 65°C. On storage, the upper limit can be extended to 75°C. It is remarkable that only 15% of the rated capacity is lost at -40°C [43]. A commercial battery module of 48 V is reported to deliver 140 Wh/kg and 174 Wh/L at 25°C [39].

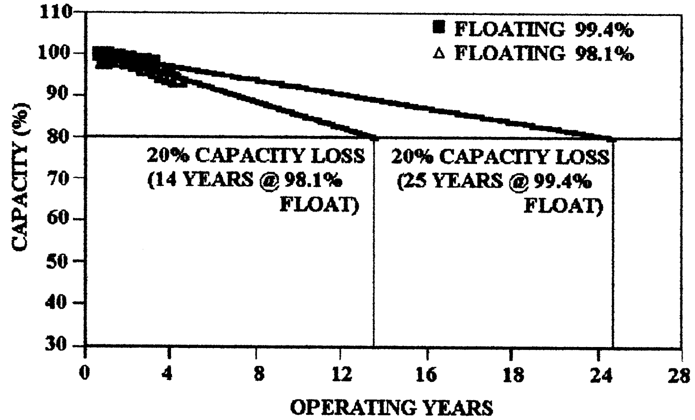

Figure 1.29. Operating life of a 24-V module at 60°C. (*From Ref. 42*)

The lithium-metal-polymer battery has also received attention for use in EV and HEV applications [41,44-46]. Avestor's basic cell is formed by laminating together the same materials mentioned for the stationary battery. Very long laminates are then wound into prismatic shapes that are assembled in the battery. A typical EV battery module, working in the temperature range 60-80°C, has a specific energy of 120 Wh/kg, a specific power of 260 W/kg and can sustain 600 cycles. For HEV applications, the modules have an energy of 850 Wh, a power of 20.5 kW and a specific power of 1.4 kW/kg (10 sec pulses at 80% DOD) [44]. Tests of EV modules have given performances very near to the USABC's criteria for mid-term (commercialization) batteries. The cycle life of a cell and a module for EV is shown in Figure 1.30 [41]. The capacities remain constant with cycle number. An extension of the cycle life to 800-1000 cycles is thought possible.

LMP batteries have been tested with good results in experimental cars. For instance, Avestor's batteries have powered such cars as the Ford Think City, Honda Insight and Cleanova. However, in 2005 Avestor stopped its production of prototypes for EV. Batscap's (Bolloré) LMP batteries have been used in the Bluecar. Operating ranges of about 200 km are reported for both batteries [45,46]. (See Chapter 4 for more details on these types of vehicles).

A comparison of the performance of different chemistries in EV modules is made in Table 1.6. The presently used Ni-MH battery is challenged by Li-metal-polymer and Li-ion batteries. The last one, in particular, would be superior in all respects, if the cycle life could be further increased.

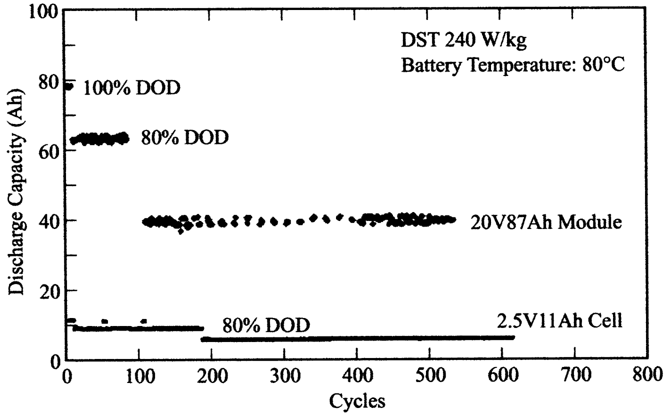

Figure 1.30. Cycle life of an 11-Ah cell and a 20-V, 87-Ah module at 50% DOD (where not indicated) and 240 W/kg DST (as proposed by the USABC). (*From Ref. 41*)

Table 1.6. Comparison of the characteristics of different EV modules. (*Adapted from Ref. 46*)

Technology	Specific Energy (Wh/kg)	Energy Density (Wh/L)	Specific Power (W/kg)	Cycle Life (Cycles)
BatScap LMP	110	110	320	
Avestor prototype LMP	120	140	240	300
Avestor Projected LMP	120	160		800
Li-ion	140	210	430	550
Ni-MH	65	150	200	800
Ni-Cd	50	90	120	800
Lead-Acid	35	85	180	600

1.3.2.2. Li-Al/Iron Sulfide Batteries

Batteries containing lithium alloy as the negative and iron sulfide as the positive electrode in molten salt electrolytes have been studied since the early 1970s especially at the Argonne National Laboratory in the U.S.A. [47]. The alloy is multiphase, $(\alpha+\beta)$Li-Al and $Li_5Al_5Fe_2$, this granting overcharge tolerance in a bipolar configuration, while both FeS and FeS_2 could be used as a cathode. The electrolyte is a low-impedance LiCl-LiBr-KBr mixture (LiCl-rich), allowing high specific powers in the 400-425°C temperature range. Using a dense FeS_2 cathode in this electrolyte, more than 1000 cycles have been obtained. Fabrication of electrolyte-starved, bipolar cells or stacks is made possible by the use of chalcogenide ceramic sealants. These materials produce strong bonds between a variety of metals and ceramics. A separator made of pressed MgO powder is normally used.

The electrochemical reactions for FeS and FeS_2 (upper plateau only) can be described as:

$$2\text{Li-Al} + \text{FeS} \rightleftharpoons \text{Li}_2\text{S} + \text{Fe} + 2\text{Al}$$

$$2\text{Li-Al} + \text{FeS}_2 \rightleftharpoons \text{Li}_2\text{FeS}_2 + 2\text{Al}$$

The first reaction occurs at 1.33 V with a theoretical specific energy of 460 Wh/kg, while the second occurs at 1.73 V (490 Wh/kg). In the discharge reaction of FeS, the intermediate Li_2FeS_2 is formed. The reaction of FeS_2 is more complex and three stages are involved in the upper plateau: $Li_3Fe_2S_4$, $Li_2Fe_{1-x}S_2$ + $Fe_{1-x}S$, and Li_2FeS_2 [48]. Full discharge of FeS_2 would result in a lower plateau with the formation of Li_2S. Stopping the discharge at the end of the upper plateau enhances the reversibility of FeS_2 and prolongs its cycle life

[48]. Indeed, in this case, the overpotential for recharge to FeS_2 is only 20 mV and no soluble species are formed, this favoring cyclability.

FeS_2 has a higher sulfur activity than FeS, hence a higher voltage, but poses corrosion problems. The former material is also a better electronic conductor, this allowing the use of thicker electrodes.

Positive electrodes are fabricated by compressing a mixture of FeS_x and

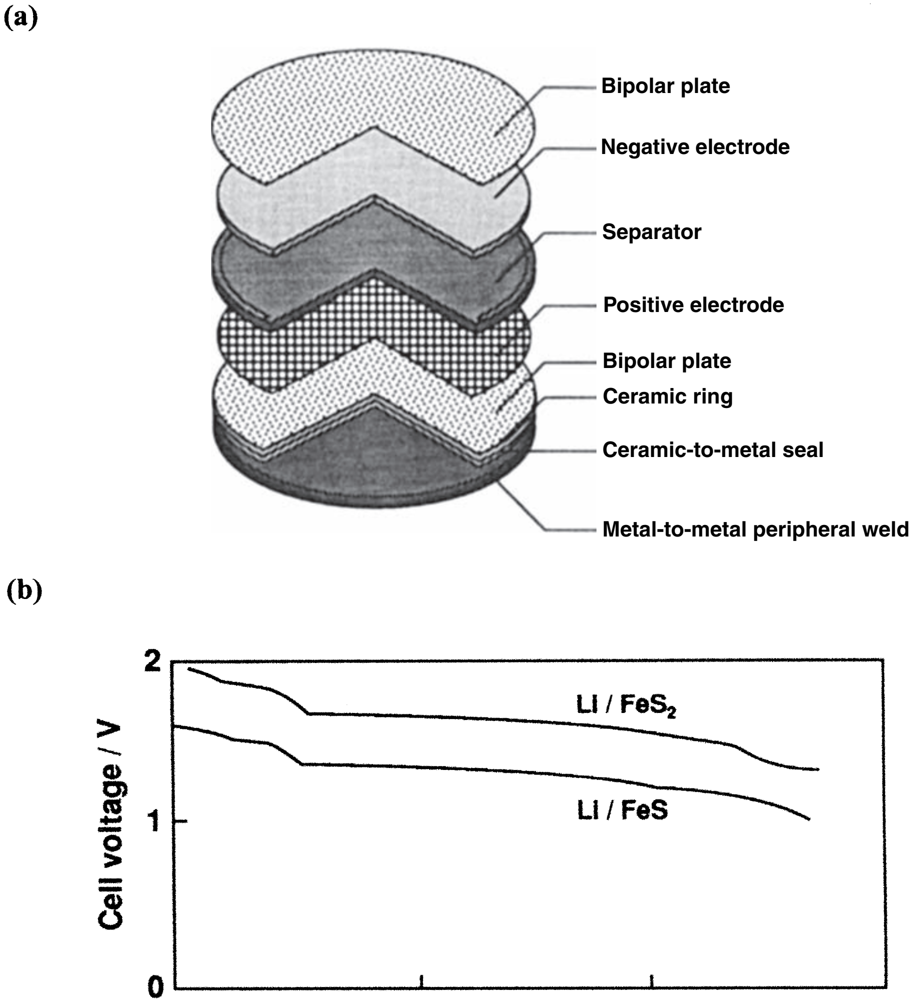

Figure 1.31. (*a*) Exploded view of a four-cell bipolar Li-Al/FeS_x stack; (*b*) Discharge curves of prototype bipolar Li-Al/FeS_2 and Li-Al/FeS cells at 425°C. (*From Ref. 49*)

electrolyte onto a current collector or loading the material into a honeycomb matrix [48]. Graphite may be included and, sometimes, CoS_2 and NiS_2 are also added.

The bipolar cell configuration is preferable over the monopolar one. An exploded view is shown in Figure 1.31(a). The electrodes are of high surface area and the cell design is compact, also thanks to the use of starved electrolyte and MgO separator, this resulting in a higher power output. The presence of the two-phase alloy at the negative electrode ensures tolerance to overcharge, so that the state of charge of all cells can be equalized. Indeed, the alloy (LiAl+ $Li_5Al_5Fe_2$) has a sufficiently high Li activity towards the end of charge to cause solubilization of Li metal in the molten-salt electrolyte; Li can be reoxidized at the positive, thus giving rise to a shuttle mechanism [48].

The design criteria to be met for an efficient bipolar stack are [48]:

1. Provision for an equalized state of charge of the cells in series, as mentioned above.
2. The use of a starved-electrolyte regime and a MgO separator. This is made possible by using the Li-rich LiCl-LiBr-KBr electrolyte that has a conductivity, in the starved configuration, equivalent to that of the LiCl-LiBr eutectic in the flooded configuration. Furthermore, in these conditions the corrosion is limited.
3. The use of effective seals. Bipolar cells are more difficult to seal than monopolar cells. This problem was solved by introducing the chalcogenide seal mentioned above. For cells with FeS_2 cathodes, a steel-ceramic-molibdenum seal was found adequate.

Several prototypes of bipolar Li-Al/FeS_x batteries were manufactured in the early 1990s. Such cells (diameter: 130 mm, weight: 250 g) could deliver 25 Ah at the C/5 rate, as shown in Figure 1.31(b). The specific energy and power values of cells (not batteries) are presented in Table 1.7 [49]. In terms of energy, both cells meet the mid-term USABC's target (80-100 Wh/kg) and the Li/FeS_2 cell approaches the long-term target (200 Wh/kg). However, it has to be noted that the above targets refer to fully engineered batteries. The specific power of the Li/FeS_2 cell is very interesting. Indeed, the mid- and long-term values set by the USABC are 150-200 W/kg and 400 W/kg, respectively. Other positive

Table 1.7. Performance characteristics of bipolar Li-Al/FeS_x cells. The data do not include thermal enclosure. (*From Ref. 49*)

Cell Type	**Specific Energy (Wh/kg)**	**Specific Power at 80% DOD (W/kg)**
Li-Al/FeS_2	180 at 30 W/kg	400
Li-Al/FeS	130 at 25 W/kg	240

features of this system are: good cyclability (in excess of 1000 cycles), tolerance to overcharge and overdischarge and to freeze-thaw cycles.

Sealed modules with a nominal voltage of 25 V and a capacity of 60 Ah have been fabricated from prismatic bipolar cells [49]. They have a specific energy of 75 Wh/kg and an energy density of over 200 Wh/L, and can be cycled for many hundreds of deep discharge cycles. It is noteworthy that failure of these modules occurs via short circuits when they reach the end of life. However, series stacks remain operational after the loss of one or more cells: the loss of energy, in this case, is limited to the energy content of the failed cell(s) [50].

The advantages of the Li-Al/FeS_x system can be summarized as:

- Simple modular design and construction
- High energy - at least twice that of lead-acid batteries
- High power
- Long cycle life
- Heat management not requiring auxiliary heating or cooling during use
- Safe, even under severe abuses

The Li-Al/FeS_x system shows an improved safety over sodium/sulfur (see Sub-section 1.3.3.1), while with respect to sodium/nickel chloride (see Sub-section 1.3.3.2) it has a higher specific power (but less safety). On the other hand, a couple of disadvantages are evident: a) as any other thermal battery, stored energy is consumed to keep the cell warm during standby periods, and b) the bipolar design is likely to have manufacturing problems and high costs.

The remarkable advancements made with this systems suggested to the USABC to select it as the long-term battery to be developed for electric vehicles. However, in the mid-1990s the R&D efforts were discontinued also in view of the new technologies based on Li-ion and Li-polymer batteries. Indeed, these technologies have power and energy outputs similar to that the Li-Al/FeS_2 battery, but can operate at much lower temperatures. This system remains a viable candidate for stationary energy storage [50].

Development of the Li/iron sulfide system is continuing, but molten salts electrolytes have been replaced by polymeric electrolytes. An example, with a composite electrolyte based on PEO, has already been mentioned (see Refs. [37,38]).

1.3.3. Batteries with a Sodium Electrode

High-temperature batteries based on sodium as a negative electrode, sulfur or $NiCl_2$ as a positive, and β''-Al_2O_3 as a Na^+-conducting solid electrolyte are now used for energy storage applications and are receiving attention for EV and space applications. The theoretical specific energies of the Na/S system (760 Wh/kg) and Na/NiCl$_2$ system (796 Wh/kg) are much higher than those of the aqueous systems (Pb/Acid and Ni/Cd) thus far used for energy storage.

1.3.3.1. Sodium/Sulfur Batteries

Investigations on this battery date back to the early 1970s and were oriented for several years to motive applications. However, technical and economic issues have suggested switching to large battery packs for stationary applications. Indeed, the Na/S battery has distinct advantages over other technologies, such as high energy and good power density, high cycle life, high energy efficiency, independence from external temperature, and moderate cost.

The operating temperature of this system is between 310 and 350°C. In this temperature range, both Na and S are liquid, while the solid electrolyte has a high Na$^+$ conductivity, thus ensuring good kinetics.

During discharge, Na$^+$ migrates from Na to S and forms polysulfides, as indicated in Figure 1.32. The first plateau corresponds to the coexistence of two immiscible liquids, S and Na$_2$S$_5$; in the single-phase sloping section, the sulfur content of the polysulfide decreases down to Na$_2$S$_{2.7}$; the second plateau corresponds to the formation of Na$_2$S$_2$ [51], but is never reached in practical cells. Indeed, formation of Na$_2$S$_3$, at 1.78 V, is taken as the discharge limit. Complete discharge would cause corrosion and local overdischarge due to non-uniformities in temperature and DOD. At the C/3 rate, the average voltage is 1.9 V.

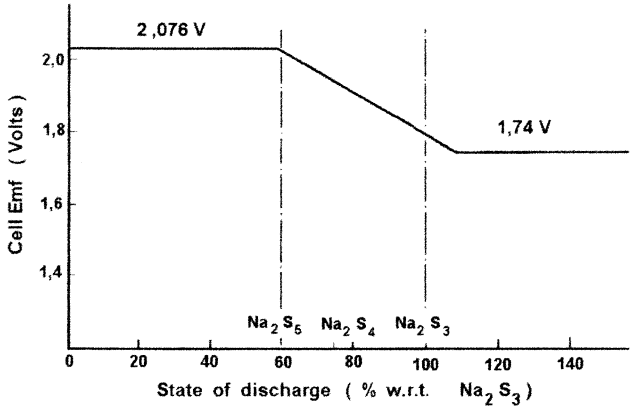

Figure 1.32. OCV of a Na/S cell at 350°C. (*From Ref. 51*)

During charge, the reactions described above are reversed and in the final stages there is a marked resistance increase due to the insulating character of sulfur. Therefore, the charge has to be stopped before complete Na recovery, and subsequent discharges provide 85-90% of the theoretical capacity [52].

As already mentioned, this system has a high cyclability (up to 5000-6000 cycles). This is mainly due to the liquid state of reactants and products: the aging mechanism based on morphological changes of the electrodes is not operating here.

A scheme of a Na/S cell is shown in Figure 1.33 for the common configuration with the central sodium electrode. An essential pre-requisite for this electrode is high purity, *i.e.* other metals and Na compounds are not allowed. Contaminants tend to concentrate at the interface with the electrolyte, reducing the electrode active area or even causing its failure [48].

In order to minimize cell resistance, molten sodium has to properly wet the electrolyte surface. This requires a smooth surface, a proper temperature range (300-350°C) and the absence of impurities. The sodium electrode is contained in a metal (safety) can that restricts, through the metering hole, the flow of sodium to the electrolyte, thus reducing the amount of Na that may come into direct contact with S in case of tube failure.

The sulfur electrode is impregnated into a layer of carbon or graphite felt. The carbon fibers ensure a good electronic conductivity, as sulfur is an

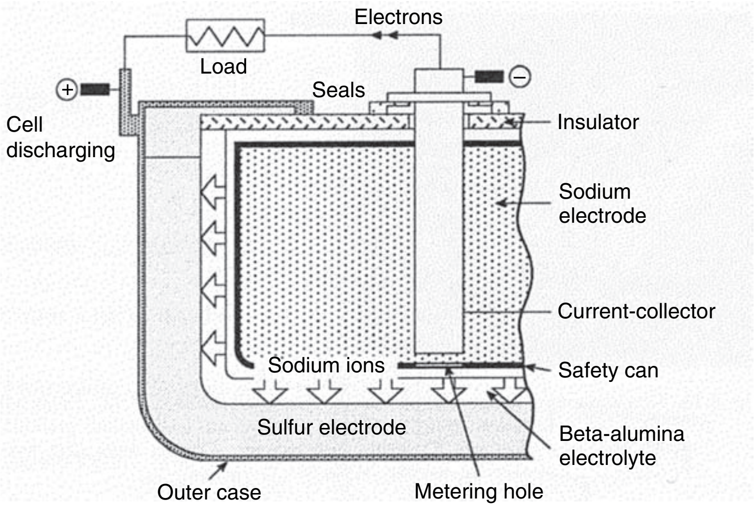

Figure 1.33. Schematic of cross-section of the Na/S cell. (*From Ref. 48*)

insulator for both electrons and ions. Fortunately, Na polysulfides are good ionic conductors.

The electrolyte is β''-Al_2O_3, which has a negligible electronic conductivity and is impermeable to molten Na and S. Its basic structural unity is a spinel-like slab formed by 4 layers of close-packed oxygen ions in a cubic stacking. The slabs are separated from each other by oxygen bridges. The sodium ions move in the space between these slabs. The idealized composition of β''-Al_2O_3 is $Na_2O{\cdot}5.33Al_2O_3$ or $Na_6Al_{32}[Vac]_{Al}^{3+}O_{51}$, with a vacancy of Al^{3+} in the spinel block that is balanced by 3 Na^+ in the conduction plane. This results in high conductivity. Pure β''-Al_2O_3 is not easy to prepare, so it has to be stabilized with Mg or Li ions that substitute for Al ions. Typical compositions contain 4.0 wt% MgO or 0.7 wt% Li_2O.

The conductivity of this electrolyte is ~0.5 $ohm^{-1}cm^{-1}$ at 350°C for the polycrystalline form. However, β''-Al_2O_3 is rather sensitive to moisture, this favoring deterioration of its mechanical properties. Therefore, some β-Al_2O_3 (idealized formula, $Na_2O{\cdot}11Al_2O_3$) is enclosed in the mixture, in spite of its lower conductivity, as it is less hygroscopic. A conductivity of ~0.2 $ohm^{-1}cm^{-1}$ is regarded as acceptable for practical electrolytes [48].

Production of Na/S batteries for stationary applications is particularly active in Japan. Table 1.8 presents the basic characteristics of some cells.

In Figure 1.34, three single cells and the module constructed with the largest one are shown [53]. Different modules are presented in Table 1.9, for applications connected with energy networks (see footnote). Very large energy-storage systems can be built with these modules: their storage capacity may be as high as 57.6 MWh (see Figure 1.35) [54]. A comparison of different energy storage systems, including various batteries, pumped hydro storage, compressed

Table 1.8. Characteristics of stationary Na/S cells (*From Ref. 52*)

Manufacturer	**NGK**	**NGK**	**NGK**	**Yuasa**	**Hitachi**
Cell Designation	T4.1	T4.2	T5		
Capacity, Ah	160	248	632	176	280
Diameter, mm	62	68	91	64	75
Lenght, mm	375	390	515	430	400
Weight, kg	2	2.4	5.4	2.7	4
Energy Density, Wh/L	285	340	370	240	300
Specific Energy, Wh/kg	160	202	226	120	133
Power Density, W/L	36	43	46	60	

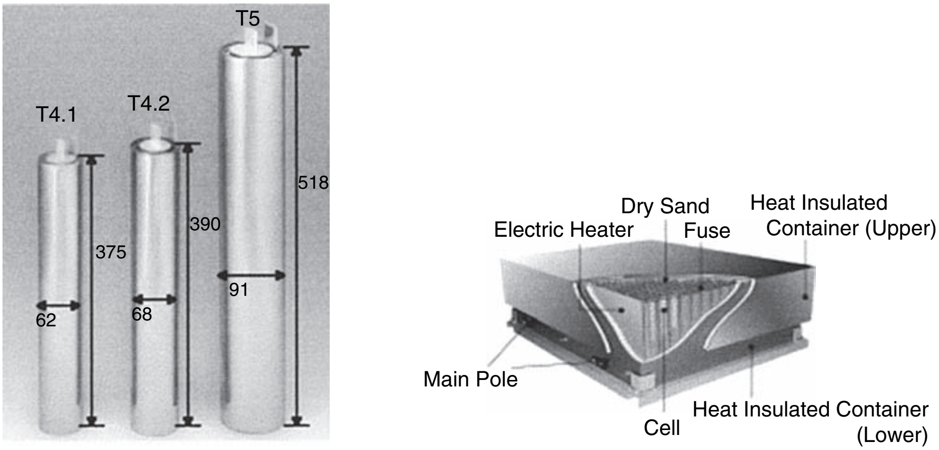

Figure 1.34. Na/S cells (*left*) and module (*right*). The module is built with 384 T5 cells and has an energy of 421 kWh (energy density, 170 Wh/L) and a power of 52.6 kW. (*From Ref. 53*)

Table 1.9. Na/S modules for stationary applications. (*From Ref. 52*)

Manufacturer	**NGK**	**NGK**	**NGK**	**Yuasa**	**Hitachi**
Battery Designation	12.5 kW	25 kW	52 kW	25 kW	12.5 kW
Prime Application*	LL;PS;PQ	LL;PS;PQ	LL;PS;PQ	LL	Renew
Number of Cells	336	480	384	320	216
Capacity, Ah	2280	2272	3624	1408	290
Energy, kWh	105	211	421	100	100
Voltage, V	48	96	128	80	144
Volume, L	941	1448	2481	1086	2592
Weight, kg	1400	2000	3620	1700	1900
Specific Energy, Wh/kg	75	105	116	59	53
Energy Density, Wh/L	112	145	170	92	40

* LL: utility-based load leveling; PS: peak shaving; PQ: power quality; Renew: renewable energy hybrid

air storage, and superconducting magnetic storage, has shown that the Na/S batteries have the highest energy densities [55]. They can live in this application for up to 15 years providing thousands of cycles. (See also Chapter 8).

All development of Na/S batteries for EV applications was stopped by

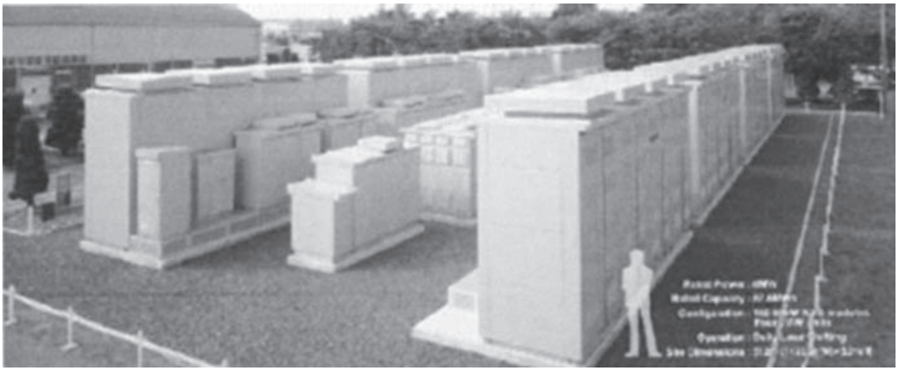

Figure 1.35. 57.6 MWh (8 MW) battery installed in Japan for load levelling by NGK. (*From Ref. 54*)

mid-1990s. Two companies (Asea Brown Bovery in Germany and Silent Power in the U.S.A.) were especially involved in this field. The properties of the cells developed by these companies are compared in Table 1.10 with those of an Na/NiCl$_2$ cell developed by the Swiss company MES-DEA.

1.3.3.2. Sodium/Nickel Chloride (Zebra) Batteries

This battery bears some analogies with the Na/S battery. The negative electrode and the electrolyte are the same, but a metal chloride is used instead of

Table 1.10. Comparison of cells with Na as a negative electrode for EV applications. (*From Ref. 52*)

Manufacturer	**Asea Brown Boveri**	**Silent Power Ltd**	**MES-DEA**
Cell Designation	A04	PB	ML3
Chemistry	Na/S	Na/S	Na/NiCl$_2$
Capacity, Ah	38	10.5	32
Electrolyte Shape	cylindrical	cylindrical	cruciform
Diameter, mm	35	44	36.5
Lenght, mm	220	45	232
Weight, g	410	120	715
Resistance, ohm	6	32	6-20
Specific Energy, Wh/kg	176	178	116
Specific Peak Power, W/kg*	390	250	260

* At 2/3 OCV and 80% DOD

sulfur as a positive electrode. As the initial research was carried out in South Africa for EV applications, the acronym Zebra (Zero Emission Battery Research Activity) is often used [52].

Preferred material for the positive electrode is $NiCl_2$, but $FeCl_2$ has also been studied. During normal discharge, Ni and NaCl are formed, as shown by the scheme of Figure 1.36. The voltage, 2.58 V, is higher than that of Na/S, 2.06−1.78 V (see Figure 1.32). Other differences will be remarked in the following description.

A schematic of this cell (Figure 1.37) shows that liquid Na is placed in the outer part, while in practical Na/S cells it is in the central part. Furthermore, Na is not initially included in the cell assembly, but produced *in situ* during charge, as the cell is assembled in the discharged state. The positive electrode is solid and this would pose problems, as the solid-solid interface with the electrolyte would not allow high currents. Therefore, a second electrolyte, $NaAlCl_4$, which is liquid at the operating temperatures, is added. Inside the β''-Al_2O_3 tube, a compact mix of Ni metal and NaCl is inserted, and molten $NaAlCl_4$ is then poured to form a narrow annulus between the positive electrode and the electrolyte. The presence of the second electrolyte lowers the specific energy of the ZEBRA battery by ~10% [56].

The tolerance to over-charge and over-discharge is outstanding by virtue of the reversible reactions occurring in these segments (see Figure 1.36). On over-charge, $NaAlCl_4$ further chlorinates the Ni matrix, while on over-discharge excess Na reacts with the liquid electrolyte. This feature has a practical implication: it is possible to connect in series several cells, without parallel connections, as cell imbalances are leveled out by the above reactions.

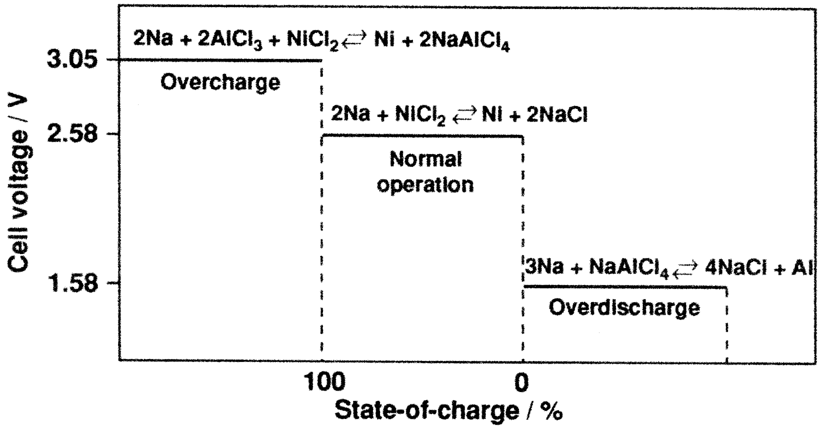

Figure 1.36. Equilibrium voltage *vs.* state of charge of $Na/NiCl_2$ cell at 250°C. (*From Ref. 48*)

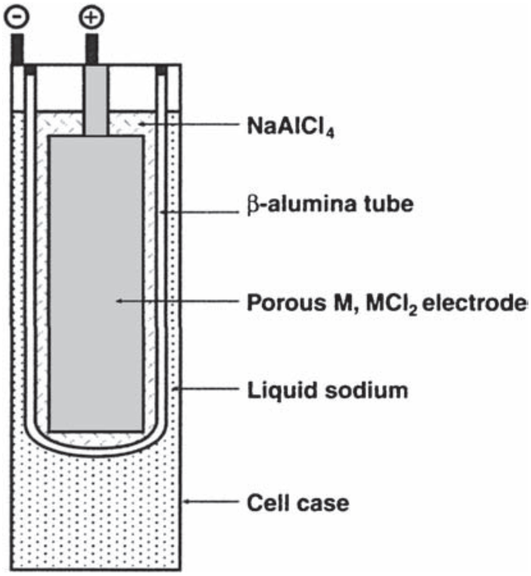

Figure 1.37. Schematic of sodium/nickel chloride cell. (*From Ref. 48*)

Another advantage of this battery, with respect to the Na/S system, is represented by its enhanced safety. If the electrolyte tube cracks, molten Na reacts first with $NaAlCl_4$, according to the reaction of Figure 1.36. The resulting Al metal shorts the cell, while NaCl tends to plug the crack. Therefore, in a battery with a series of cells, the shorted cell does not cause failure of the all

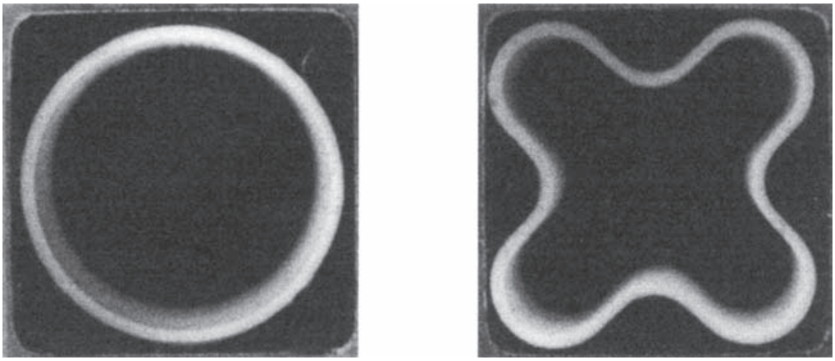

Figure 1.38. Cross-section of a conventional ZEBRA cell (*left*) and a high-power cell (*right*). (*From Ref. 48*)

battery [56].

As a further advantage, the Zebra cell can work in a wider temperature range, *i.e.* 220-450°C, although the practical range has to be restricted to 270-350°C.

To improve the battery capacity and energy, cells with a square section may be constructed, as this greatly reduces the dead space typical of batteries assembled from cylindrical cells. Specific energies of 120-130 Wh/kg are possible.

A limitation of the conventional design is the increasing resistance with DOD, this lowering the power capability. A convenient way to overcome this limitation is designing the ceramic electrolyte with the cruciform shape of Figure 1.38. The tube so obtained, termed a "monolith", allows the construction of thinner and less resistive positive electrodes. To further decrease the resistance, Fe-doped $NiCl_2$ is used. As a result, the cell's specific power may reach 260 W/Kg at 80% DOD (Table 1.10), and batteries with a specific power of 150 W/kg (the USABC's mid-term target for EV) have recently been built.

The Zebra system is specifically intended for EV applications. As shown in Table 1.10, it has lower specific energies (but the gap is reduced on a volumetric basis) and powers than Na/S cells. However, it is preferred for EV applications thanks to such factors as safety, easiness of construction, cyclability (more than 1000 cycles), low corrosion, *etc.*

Some specific applications have recently been proposed: in photovoltaic systems, for instrumentation packs in oil exploration, and in hybrid cars also containing a PEM fuel cells. In this latter application, two 40-kW $Na/NiCl_2$ batteries are coupled to a 6-kW fuel cell. Using this hybrid architecture allows doubling the EV range from 120 km to 240 km [57].

1.3.4. Basic Parameters of Secondary Nonaqueous Batteries

In Table 1.11, relevant data of the secondary batteries dealt with in this chapter are summarized. Due to the continuous evolution of these batteries, especially Li-ion and Li-polymer, the data have to be considered with some caution. Caution is also necessary in view of differences in battery size/configuration and test conditions.

Table 1.11. Characteristics of non-aqueous secondary batteries.

System	Voltage Range (V)	Operating Temperature (°C)	Cycle Life (cycles)	Specific Energy (Wh/kg)	Energy Density (Wh/L)	Specific Power (W/kg)^a	Ref.
Li-ion^b, stationary ($LiNi_{0.7}Co_{0.3}O_2$)	4.0-2.8	-20÷60	900^1	128	197		23,58
Li-ion^b, EV ($LiNi_{1-x-y}Co_xMn_yO_2$)	4.0-2.8	-20÷50	570	150	252	490	23,58
Li-ion^b, stationary ($Li_{1+x}Mn_2O_4$)	4.0-3.0	-20÷60	1200^1	122	255		23,58
Li-ion^b, EV ($LiCr_xMn_{2-x}O_4$)	4.0-3.0	-20÷50	580	155	244	440	23,58
Li metal-polymer^b	3.0-2.0	40÷60^2 60÷80^3	800	140^2 120^3	174^2 160^3	260	39,42 41,46
Li/FeS^c	1.7-1.0	375÷500	1000	130	220	240	2,50,58
Li/FeS$_2$^{c}	2.0-1.5	375÷450	1000	180	350	400	2,50,58
Na/S^c	2.0-1.8	300÷350	6000	155^2 175^3	300^2 350^3	250^3	2,52 2,52
Na/NiCl$_2$^{c}	2.1-1.7	250÷300	2500	115	190	260	2,58

a. pulse discharge, b. battery; c. cell

1. single cells; 2. stationary applications; 3. EV

References

1. K.M. Abraham, *J. Power Sources* 34 (1991) 81.
2. D. Linden and T.B. Reddy, in "*Handbook of Batteries*" (Chapter 14), D. Linden and T.B. Reddy, Eds., McGraw-Hill, New York, 2002.
3. T.B. Reddy, in "*Modern Battery Technology*", C.D.S. Tuck Ed., Ellis Horwood, Chichester (U.K), 1991.
4. www.powertech.co.nz/tadspecs
5. P.G. Russel and F. Goebel, *J. Power Sources* 54 (1995) 180.
6. H. Ikeda, T. Saito and H. Tamura, in "*1st International Symposium on Manganese Dioxide*", Cleveland, Ohio, 1975, p. 384.
7. H. Ikeda, M. Hara and S. Narukawa, U.S. Patent 4,133,856 (1979).
8. M.M. Thackeray, in "*Handbook of Battery Materials*", J.O. Besenhard, Ed., Wiley-VCH, Weinstein, 1999.
9. G. Pistoia, *J. Electrochem. Soc.*, 129 (1982) 1861.
10. Ultralife Batteries – Products, www.ulbi.com
11. Duracell: Technical OEM, Lithium/Manganese Dioxide, www.duracell.com
12. M. Winter, K.-C. Moeller and J.O. Besenhard, in "*Lithium Batteries - Science and Technology*", G. A. Nazri and G. Pistoia, Eds., Kluwer Academic Pub., Boston, 2004.
13. (a) L.F. Nazar and O. Crosnier, (b) G.G. Amatucci and N. Pereira, in "*Lithium Batteries - Science and Technology*", G. A. Nazri and G. Pistoia, Eds., Kluwer Academic Pub., Boston, 2004.
14. A. Manthiram, in "*Lithium Batteries - Science and Technology*", G. A. Nazri and G. Pistoia, Eds., Kluwer Academic Pub., Boston, 2004.
15. (a) S. Yang, Y. Song, K. Ngala, P. Y. Zavaliy and M. S. Whittingham, *J. Power Sources* 119-121 (2003) 239; (b) M. S. Whittingham, *Chem. Rev.* 104 (2004) 4271; (c) M. S. Whittingham, *IBA-HBC Meeting*, Waikoloa, Hawaii, January 2006.
16. (a) G. Pistoia, in "*Lithium Batteries - Science and Technology*", G. A. Nazri and G. Pistoia, Eds., Kluwer Academic Pub., Boston, 2004; (b) M.-H. Yang, H.-C. Wu, D.-T. Shieh, C.-Y. Su and Z.Z. Guo, *IBA-HBC Meeting*, Waikoloa, Hawaii, January 2006.
17. C.-K. Huang, J.S. Sakamoto, J. Wolfenstine and S. Surampudi, *J. Electrochem. Soc.* 147 (2000) 2893.
18. G.E. Blomgren, *J. Power Sources* 119-121 (2003) 326.
19. Sony Global – Press Release, www.sony.net/Sony Info/News/Press/
20. K. Imasaka *et al*, *12th IMLB Meeting,* Abs. 418, Nara, Japan, June 2004.
21. M. Broussely, *22nd International Seminar on Primary/Secondary Batteries*, Fort Lauderdale (FL, USA), March 2005.
22. M. Broussely, Ph. Blanchard, Ph. Biensan, J.P. Planchat, K. Nechev and R.J. Staniewicz, *J. Power Sources* 119-121 (2003) 859.
23. K. Takei, K. Ishihara, K. Kumai, T. Iwahori, K. Miyake, T. Nakatsu, N. Terada and N. Arai, *J. Power Sources* 119-121 (2003) 887.
24. C. Amemiya, J. Kurihara, M. Yonezawa, *NEC R§D* 42 (2001) 241
25. M. Broussely, in "*Advances in Lithium-Ion Batteries*", W. van Schalkwijk and B. Scrosati, Eds., Kluwer Academic Pub. Boston 2002.
26. M. Broussely, *1st International Symposium on Large Lithium Ion Battery Technology and Applications*, Honolulu, Hawaii, June 2005.
27. K. Amine, C.H. Chen, J. Liu, M. Hammond, A. Jansen, D. Dees, I. Bloom, D. Vissers and G. Henriksen, *J. Power Sources* 97-98 (2001) 684.
28. Y. Nishi, in "*Advances in Lithium-Ion Batteries*", W. van Schalkwijk and B. Scrosati, Eds., Kluwer Academic Pub. Boston 2002.

29. M. Broussely in "*Lithium Batteries - Science and Technology*", G. A. Nazri and G. Pistoia, Eds., Kluwer Academic Pub., Boston, 2003.
30. B.V. Ratnakumar *et al*, *12th IMLB Meeting*, Abs. 424, Nara, Japan, June 2004.
31. T. Horiba *et al*, *12th IMLB Meeting*, Abs. 49, Nara, Japan, June 2004.
32. N.H. Clark and D.H. Doughty, *12th IMLB Meeting*, Abs. 420, Nara, Japan, June 2004.
33. M. Broussely and G. Archdale, *J. Power Sources* 136 (2004) 386.
34. (a) Y.V. Mikhaylik and J.R. Akridge, *12th IMLB Meeting*, Abs. 190, Nara, Japan, June 2004; (b) Y.V. Mikhaylik, *IBA-HBC Meeting*, Waikoloa, Hawaii, January 2006.
35. J.B. Kerr in "*Lithium Batteries - Science and Technology*", G. A. Nazri and G. Pistoia, Eds., Kluwer Academic Pub., Boston, 2004.
36. V. Dorval, C. St-Pierre and A. Vallée, "Lithium-Metal-Polymer Batteries: From the Electrochemical Cell to the Integrated Energy Storage System" (www.avestor.com/rtecontent/document/Battcon), 2004.
37. E. Peled, D. Golodnitsky, E. Strauss, J. Lang and Y. Lavi, *Electrochim. Acta* 43 (1998) 1593.
38. E. Strauss, D. Golodnitsky and E. Peled, *Electrochim. Acta* 45 (2000) 1519.
39. www.avestor.com/se48s80.ch2
40. G. Pistoia, S. Panero, M. Tocci, R.V. Moshtev and V. Manev, *Solid State Ionics* 13 (1984) 311.
41. C. Létourneau, D. Geoffroy, P. St-Germain, A. Bélanger and R. Atanasoski, "Progress in Lithium-Metal-Polymer Battery System for Electric Vehicles", (www.avestor.com/rtecontent/document/evs15)
42. C. St-Pierre, T. Gauthier, M. Hamel, M. Leclair, M. Parent and M.S. Davis, , "Avestor Lithium-Metal-Polymer Batteries Proven Reliability Based on Customer Field Trials", (www.avestor.com/rtecontent/document/AVESTOR_WhitePaper_Battcon2003)
43. C. Robillard, A. Vallée and H. Wilkinson, "The Impact of Lithium-Metal-Polymer Battery Characteristics on Telecom Power System Design", (www.avestor.com/ rtecontent/ document/AVESTOR_Intelec_paper_2004)
44. C. St-Pierre, R. Rouillard, A. Bélanger, B. Kapfer, M. Simoneau, Y. Choquette, L. Gastonguay, R. Heiti and C. Behun, "Lithium-Metal-Polymer Battery for Electric Vehicle and Hybrid Electric Vehicle Applications", (www.avestor.com/rtecontent/document/evs16)
45. www.greencarcongress.com/2005/03/bolloreacute_gr
46. www.avestor.com/automotiveev.ch2
47. G.L. Henriksen and D.R. Vissers, *J. Power Sources* 51 (1994) 115.
48. D.A.J. Rand, R. Woods and R.M. Dell, "*Batteries for Electric Vehicles*", Research Study Press, Taunton, U.K., 1998.
49. T.D. Kaun, P.A. Nelson, L. Redey, D.R. Vissers and G.L. Hendriksen, *Electrochim. Acta* 38 (1993) 1269.
50. G.L. Henricksen and A.N. Jansen, in "*Handbook of Batteries*" (Chapter 41), D. Linden and T.B. Reddy, Eds., McGraw-Hill, New York, 2002.
51. H. Bohm, in "*Handbook of Battery Materials*", J.O. Besenhard, Ed., Wiley-VCH, Weinstein, 1999.
52. J.W. Braithwaite and W.L. Auxer, in "*Handbook of Batteries*" (Chapter 40), D. Linden and T.B. Reddy, Eds., McGraw-Hill, New York, 2002.
53. www.electricitystorage.org/pubs/2001/IEEE_PES_Winter2001/wm01nas
54. www.electricitystorage.org/pubs/2004/Newsletter_Oct_2004
55. J. Kondoh, I. Ishii, H. Yamaguchi, A. Murata, K. Otani, K. Sakuta, N. Higuchi, S. Sekine and M. Kamimoto, *Energy Convers. Manag.* 41 (2000) 1863.
56. R.M. Dell and D.A.J. Rand, "Understanding Batteries", RSC, Cambridge, U.K., 2001.
57. www.greencarcongress.com/2005/05/zestful
58. P.C. Symons and P.C. Butler, in "*Handbook of Batteries*" (Chapter 37), D. Linden and T.B. Reddy, Eds., McGraw-Hill, New York, 2002.

Industrial Applications of Batteries. From Cars to Aerospace and Energy Storage
M. Broussely and G. Pistoia Eds.,
© 2007 Elsevier B.V.

Chapter 2

AQUEOUS BATTERIES USED IN INDUSTRIAL APPLICATIONS

Gianfranco Pistoia

Consultant, Via G. Scalia 10, Rome, Italy

2.1. Introduction

In this chapter, a description will be made of both traditional and advanced rechargeable batteries with aqueous electrolytes. Primary aqueous batteries will not be extensively treated here; however, basic information on alkaline batteries, still utilized in some industrial applications, will be provided.

2.2. Lead/Acid Batteries

The first practical Pb/Acid battery was developed in 1859. After 150 years, this system still has an extraordinary commercial success, also by virtue of continuous performance improvements. Its advantages can be summarized as: low cost, high-rate capability, moderately good performance at low and high temperatures, good float service, and availability of maintenance-free designs. Its main disadvantages are: limited specific energy (normally <30-40 Wh/kg) and energy density (normally <70-80 Wh/L), relatively low cycle life, poor charge retention and storability in the discharged state (electrode sulfation).

2.2.1. Electrodes

Here, the preparation of the commonest electrode, the pasted type used for both the negative and the positive, is described in some detail. In Section 2.2.3, two additional designs for the positive, Planté and tubular, will be described.

To prepare both the positive and the negative electrode, a mixture of Pb (~25%) and PbO (predominantly α-PbO, ~75%) is first produced in a ball mill or by oxidation of molten Pb in the so-called Barton pot process [1,2]. This leady oxide is then mixed and pasted with H_2SO_4 and H_2O. Plastic fibers are often added, especially to the paste for the positive, in order to enhance the mechanical strength. Such additives as $BaSO_4$, carbon black and organic lignins or lignosulfonates are also added to the paste used for the negative. $BaSO_4$, isomorphous with $PbSO_4$, forms the base for nucleating the latter, thus preventing the build up of large crystals difficult to reduce to Pb on charge. During pasting, a significant proportion of PbO is converted to basic lead sulfates, namely the mono-, tri- and tetra-basic varieties (xPbO·$PbSO_4$, with x=1,3 or 4). The amount of H_2O and H_2SO_4 has to be controlled in order to provide the paste with the required thixotropic properties [2]. By properly adjusting the humidity, temperature and time values during this process, it is possible to have a paste with a limited amount of mono-basic sulfate, which is detrimental to battery performance, and with a high proportion of tribasic sulfate [2].

The paste is applied to a grid (see Section 2.2.2) and the resulting plate is then passed through a high-temperature tunnel oven to remove the surface moisture, while the interstitial one is totally maintained. Afterwards, the curing process is applied to provide the material with the necessary cohesion and adhesion characteristics. During this process, the basic changes occurring in the active material are: 1) growth of basic Pb sulfate crystals; 2) development of basic Pb carbonates; 3) conversion of Pb particles to α-PbO; 4) corrosive attack of the metal alloy grid, to establish a good contact between grid and Pb oxides or sulfates. In the final stage of the curing process, the electrode is thoroughly dried to remove adsorbed and interstitial H_2O.

The plate so obtained is ready for the formation process, *e.g.* the electrochemical conversion, in an H_2SO_4 solution, to Pb sponge (negative electrode) and PbO_2 (positive electrode). For the latter, it can be noted that the crystals of tetrabasic sulfate (4BS) are much coarser than their tribasic counterparts (3 BS) and, so, more difficult to oxidize to PbO_2. This means that several formation cycles are needed for 4BS-rich plates, unless a curing technique able to reduce the crystal size is applied [2]. Studies of the crystalline structure of PbO_2 resulting from the formation process have revealed that the β form predominates in the outer layers, whereas the α form resides in the inner ones. Some nice features of the latter *vs.* the former, *i.e.* more compact morphology, greater mechanical strength and higher electrical conductivity, are counterbalanced by a lower discharge capacity [2].

At the end of the formation process, the negative electrode has a surface area of ~0.5 m^2/g and a porosity of ~60%; the positive one has the same porosity and a larger area: ~4 m^2/g [1].

2.2.2. Grids

Good mechanical strength and corrosion resistance require the use of grids based on Pb alloys, such as Pb/As/Sb or Pb/Ca/Sn.

In the first alloy, Sb has a fundamental role as it improves metal fluidity during manufacture, hardness, strength, creep resistance and corrosion resistance [2]. Sb strengthens Pb by forming, at the grain boundaries, a eutectic phase whose structure is based on fine platelets of both elements. Strengthening is increased by the precipitation of fine particles of Sb and As, this inhibiting the movement of imperfections, both in the crystals and in the grain boundaries, which would weaken the alloy [2]. These mechanical characteristics enable the grid to resist deformations due to corrosion or volume changes while cycling.

A disadvantage in the use of Sb is represented by its dissolution from the positive grid during charge and subsequent plating on the negative electrode. This results in a lowering of the overpotential for hydrogen evolution and, consequently, in gassing, water loss and self-discharge. Today, low-antimony alloys (with ~2% Sb) are widely used in flooded batteries. Casting problems, such as cracking, have been overcome with As or other agents, *e.g.* Cu, Se, S and Te, which enhance hardness and tensile strength of the alloy.

Pb/Ca or Pb/Ca/Sn alloys are now increasingly used. They have hydrogen overpotential higher than that of the Sb-containing alloys, higher conductivity, and are sufficiently malleable to allow easy grid fabrication. The Ca content is important in determining the alloy properties. The tensile strength has a maximum at 0.07% Ca, and the rate of corrosion accelerates above this percentage. This type of alloy is used not only in flooded batteries but also in valve regulated lead-acid batteries (VRLA). Sn enhances the mechanical properties, increases the conductivity at the grid/paste interface, and the corrosion resistance [2].

Examples of grid shapes will be presented in the next sub-section.

2.2.3. Plate Designs

Three designs are possible for the positive plate: flat pasted (Faure), Planté and tubular. The negative plate is only constructed with the pasted-type configuration.

The grids supporting the pasted-type electrodes may have different shapes. Two examples are depicted in Figure 2.1(a).

The Planté version, used in flooded batteries for stand-by service, is obtained by casting a plate of pure Pb with numerous vertical grooves, to increase the surface area. The active material, PbO_2, is formed through a series of charge/discharge cycles in an $H_2SO_4/HClO_4$ mixture.

The tubular plate consists of a row of tubes containing coaxial Pb alloy rods (spines) surrounded by active material (Figure 2.1[b]). Two types of multitubes (gauntlets) may be used: single braided glass-fiber or woven polyester-fiber. The gauntlets are made by converting a one-piece section into tubes by stitching. After filling with a mixture of leady oxide and red Pb, the tubes are soaked in H_2SO_4 to obtain $PbSO_4$, which is converted to the active material during formation. These plates are used both in stand-by and motive applications [2].

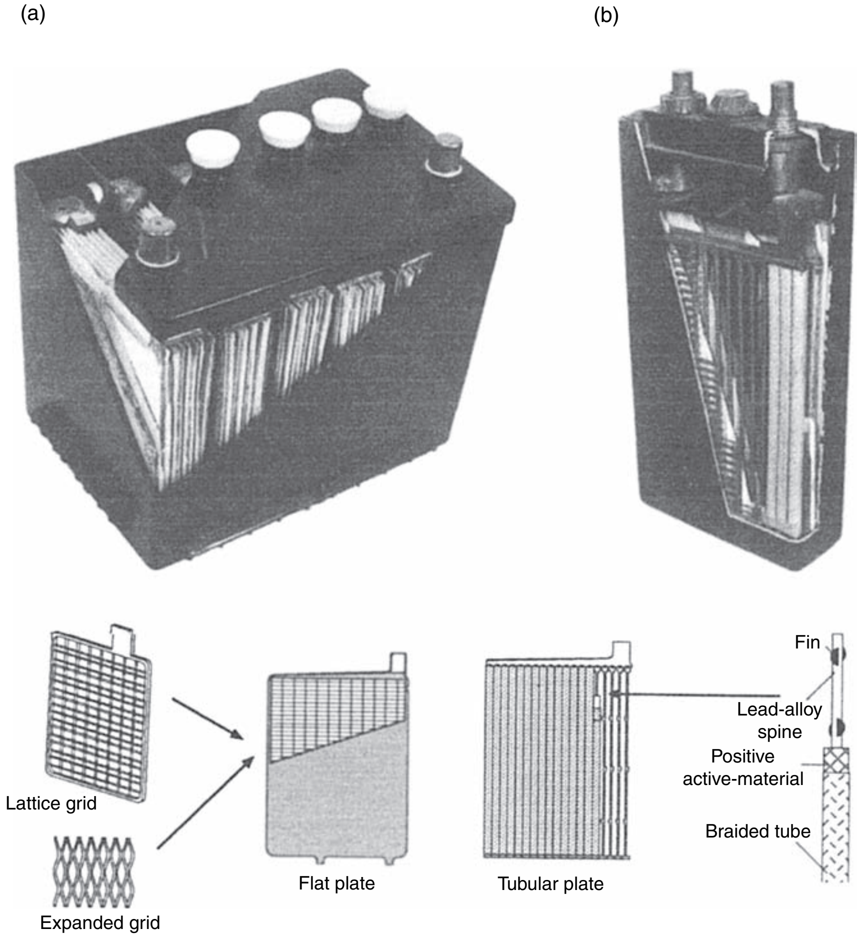

Figure 2.1. Pb/Acid batteries: (a) flat plates; (b) tubular plates. (*From Ref. 2*)

2.2.4. Electrolyte and Separators

In most industrial batteries, the cell stack is flooded with high-purity, aqueous H_2SO_4 at the 30-40% concentration (density: 1.27-1.30 g/cm^3). The resistivity is minimal in this concentration range: 1.5 ohm·cm at 25°C. Traction batteries use more concentrated solutions to increase the energy density.

The separators are basically non-conductive, microporous structures with good wettability, small and uniform pore-size, good strength and flexibility, low electrical resistance [2]. They can be made of: rubber, cellulose, PVC, PE, glass fiber or microglass [3]. Their porosities range from 40% for PVC to 90% for microglass, while the average pore sizes range from <0.1 μm for PE to 80 μm for glass fiber. In recent years, the traditional leaf separators have often been replaced by envelope separators, which can prevent dendritic growth and improve retention of active material.

VRLA batteries use a limited amount of immobilized electrolyte. The aqueous H_2SO_4 solution can either be soaked into an absorbent glass mat (AGM) or gelled by addition of fumed SiO_2. The glass mat is based on microfibers having diameters in the range 0.25 to 4 μm.

In VRLA batteries, the electrolyte cannot move, this resulting in some distinct advantages: a) the battery can be operated in any position; b) acid stratification is hindered or eliminated; c) there is enough free space inside the cell to allow for the diffusion of O_2, produced on overcharge, back to the negative electrode (oxygen cycle – see later).

2.2.5. Charge/Discharge Reactions

An unusual feature of this battery is that the primary reactions at both electrodes involve the same elements:

Negative electrode: $Pb \rightleftharpoons Pb^{2+} + 2e$

$Pb^{2+} + SO_4^{2-} \rightleftharpoons PbSO_4$

Positive electrode: $PbO_2 + 4H^+ + 2e \rightleftharpoons Pb^{2+} + 2H_2O$

$Pb^{2+} + SO_4^{2-} \rightleftharpoons PbSO_4$

(Due to the high acid concentration, HSO_4^- is also present)

Overall reaction: $Pb + PbO_2 + 2H_2SO_4 \rightleftharpoons 2PbSO_4 + 2H_2O$

The nominal equilibrium voltage is 2.0 V.

As is evident from the above reactions, the processes at both electrodes occur by a dissolution/precipitation mechanism and not a solid-state ion transport or film formation mechanism [3,4]. $PbSO_4$ is sparingly soluble in the acidic solution, so that its migration during discharge/charge is not significant. Therefore, the electrodes basically maintain their structure throughout the battery life.

Secondary reactions occur at both electrodes within the battery operating voltage. At the positive electrode, O_2 is formed through the reaction:

$$2H_2O \rightarrow O_2 + 4H^+ + 4e$$

At the negative electrode there is H_2 evolution:

$$4H^+ + 4e \rightarrow 2H_2$$

The net reaction is just H_2O electrolysis at the equilibrium voltage of 1.23 V. At lower potentials, the reversal of O_2 formation is possible:

$$O_2 + 4H^+ + 4e \rightarrow 2H_2O$$

This means that O_2 reduction can always be expected at the negative [5].

Furthermore, at the high potential of the positive electrode, Pb can be oxidized to PbO_2, which forms a protecting layer. This is not very stable and some corrosion still occurs.

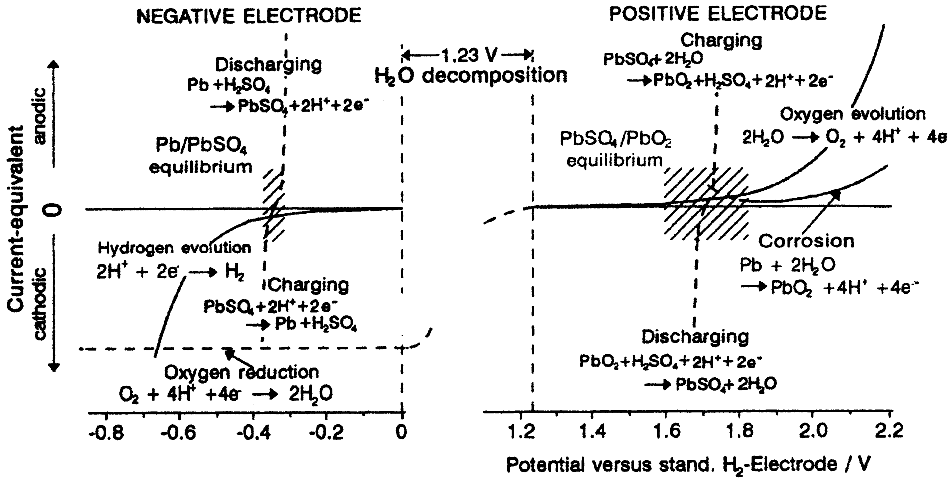

Figure 2.2. Reactions occurring in Pb/Acid batteries represented as I *vs.* V curves. (*From Ref. 5*)

All the above reactions are illustrated in Figure 2.2 [5]. The two hatched columns represent the equilibrium potentials of the negative and positive electrode, and their width reflects the dependence on acid concentration. The primary charge and discharge reactions are represented by steep curves indicating high rate capabilities even for voltage values not far from those of equilibrium.

H_2 and O_2 evolution already occurs in OCV conditions and increases gradually as long as the electrode polarization is limited. Conversely, the current steeply increases at higher polarizations. The rate of O_2 reduction is mainly determined by the transport characteristics and does not depend on the potential of the negative (Figure 2.2). It is characterized by a limiting current, which, in flooded batteries, is very small, as the diffusion of dissolved O_2 is very slow [5].

Conversely, in a VRLA cell, O_2 can diffuse in the gaseous phase at a speed that is more than 10^5 times greater than in the dissolved state. Diffusion occurs in the pores of the AGM not filled with electrolyte or in cracks of the gelled electrolyte. This determines the main characteristics of VRLA batteries, *i.e.* the internal O_2 cycle. The O_2 reduction at the negative is fast and allows recovering of O_2 generated at the positive, thus maintaining practically unchanged the H_2O amount in the electrolyte. In the VRLA battery, in addition to O_2 recovery, there is little H_2 evolution, which escapes the cell through the vent or though the plastic container itself. However, if the cell is overcharged at high rates (>C/3), the internal pressure caused by excess gas is released through the valve and the recombination process is partial. Therefore, overcharging at these rates has to be avoided.

2.2.6. Design Features and Applications

The applications of Pb/Acid batteries can be grouped into three main categories: a) SLI (starting, lighting, ignition) or automotive; b) traction (deep-cycle); c) stationary. In Table 2.1, specifications are given on their design features and operating duty.

SLI Batteries. These batteries should possess to a satisfactory level the requisites of power density, energy density, cycle life, float service life and cost [3]. Power is required to start an internal combustion engine (cranking). As the engine runs, the battery is maintained on float, *i.e.* at full charge. To maximize the cranking ability, SLI batteries must have grids with very low resistance, thin plates, and concentrated acidic solutions.

A major advance has been represented by maintenance-free batteries. They do not require H_2O additions, have a better capacity retention and very low corrosion of the electrode terminals. Charge control is needed to avoid H_2O

Table 2.1. Lead/Acid battery applications related to the electrode design features.

Application	Duty Type	Design Features
SLI (cars, motor cycles, trucks, aircrafts, ships)	High power discharge performance over wide temperature range. Shallow cycling duty with service life > 3 years	Thin plate, mostly 12 V, maintenance-free
Traction (electric trucks, road vehicles, golf carts, *etc.*)	Deep-cycle discharges (1 to 5 h rates). Service life of 500 to 2000 cycles	Tubular or flat plate designs, 24/96 V assemblies
Stationary (telecom, UPS, emergency lighting, energy storage)	Reliability over extended periods. Discharge duty: 1 to 6 h rates. Service life: 5-25 years on continuous charge. Limited cycling ability	Variety of designs including Planté, tubular, flat plate, VRLA cells

loss. On the other hand, as these batteries use low-Sb or Sb-free grids (*e.g.* Ca-Pb), the rate of H_2O loss on overcharge is reduced [3].

Heavy-duty SLI batteries for buses, trucks and other large vehicles use heavy and thick plates with high-density paste, high-quality separators (often glass mats), and rubber cases for a longer life.

Traction Batteries. These batteries must be able to withstand long cycling, while featuring high energy density and low cost. They are constructed with thick plates supporting high-density pastes, electrochemically formed in low-density acid solutions. Glass-fiber mats are needed to keep the active material in the positive plate [3].

Deep-cycling traction batteries are based on the flat-pasted type of positive electrode (especially in the U.S.A.) or the tubular type (in the rest of the world). Both types of batteries have positive-plate capacities in the range 45-170 Ah at the 6-h rate. The tubular type has longer life and lower grid corrosion and material shedding. Flat-pasted plates are arranged in such a way that they can be repaired or substituted in case of failure of one, or a few, plate(s).

The duty requirements of EV batteries demand overcoming the performance of the Pb/Acid battery, even in its advanced versions. The technical challenges can be summarized as: a) greater specific energy; b) higher specific power; c) longer service life (at deep discharge); d) faster recharge time [2].

A greater energy can be obtained by minimizing the weight of the inert components (normally ~30%) and by improving the active material utilization. VRLA batteries used in EV have specific energies of 30-40 Wh/kg and energy densities of 80-90 Wh/L [6]. It has been calculated that with bipolar or quasi-bipolar designs the specific energy could reach 50 Wh/kg [3]. The last figure is the target set by the ALABC (Advanced Lead/Acid Battery Consortium) [7]. On the other hand, the USABC (United States Advanced Battery Consortium) has

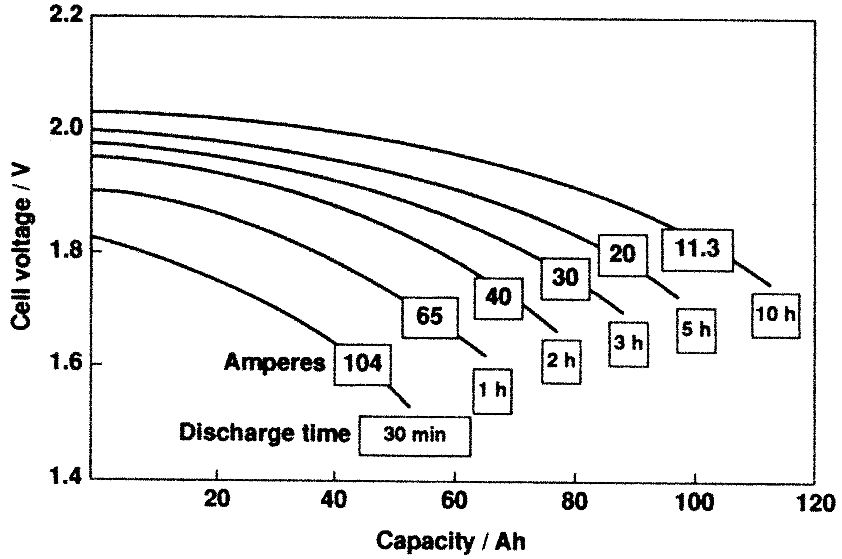

Figure 2.3. Discharge characteristics of a conventional 100-Ah (at the C/5 rate) Pb/Acid EV battery. (*From Ref. 9*)

set to 80-100 Wh/kg the values for mid-term EV batteries. In Figure 2.3, the capacity variation of a conventional EV battery as a function of discharge rate is shown. At short discharge times, the electrode reaction only occurs at the plate surface, and the $PbSO_4$ formed tends to clog the pores. Thus, the capacity is greatly reduced at high rates.

Present values of specific power for EV Pb/Acid batteries are around 190 W/kg. Advanced bipolar designs are claimed to bring the power to 800 W/kg at 70% DOD, and 400 W/kg at 90% DOD [8].

According to the ALABC, an improved battery life should correspond to 3 years over 500 cycles of the simplified urban driving schedule (SFUDS) with less than 20% capacity loss. An improved rapid charging is set as: 100% in 4 h; 80% in 15 min; 50% in 5 min [2].

Stationary Batteries. Heavy, thick plates (of the Planté, Faure or tubular design for the positive) with high paste density are used [3]. All batteries are of the flooded type and are positive-limited. High energy and power are not requested, but the capability of long living on float or moderate overcharge is a must. Non-antimonial grids are normally used to limit H_2O loss and subsequent watering. Overcharge causes expansion of the positive grid: a 10% growth is allowed before the plates touch the container walls.

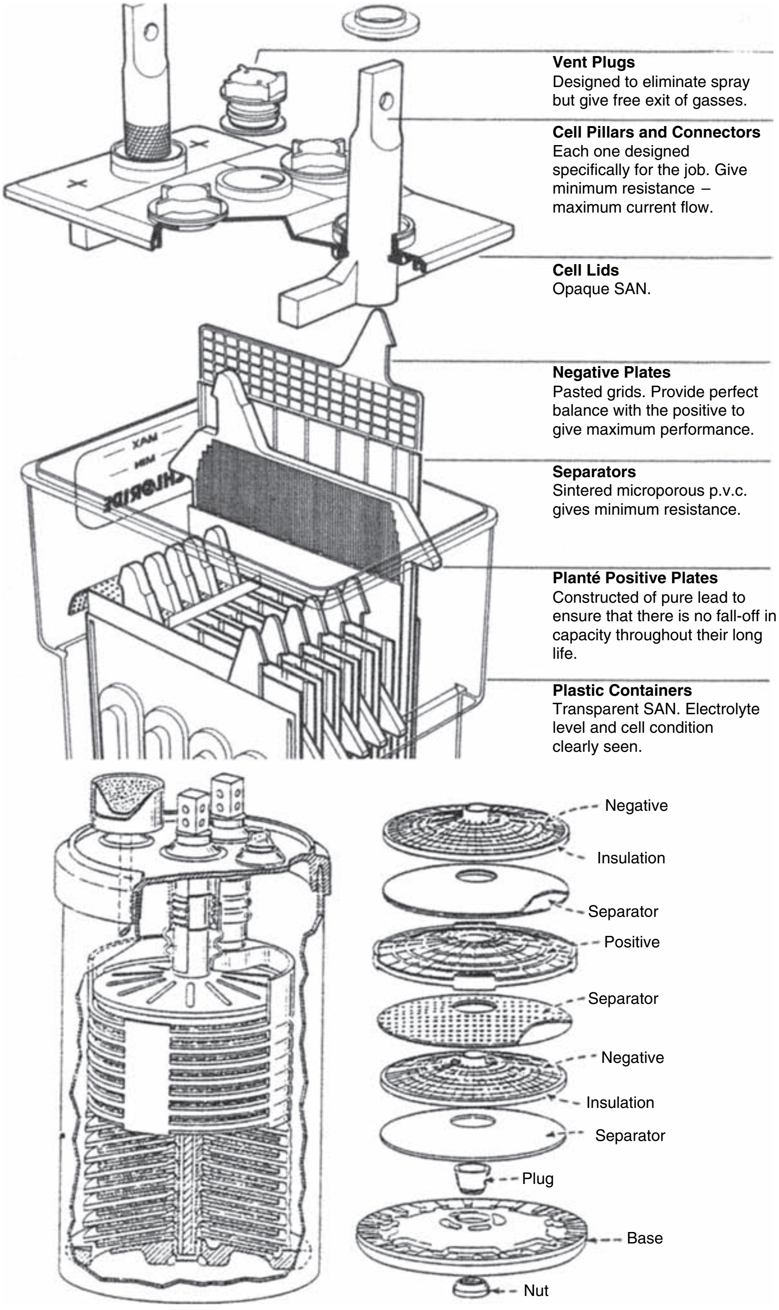
Vent Plugs
Designed to eliminate spray but give free exit of gasses.
Cell Pillars and Connectors
Each one designed specifically for the job. Give minimum resistance – maximum current flow.
Cell Lids
Opaque SAN.
Negative Plates
Pasted grids. Provide perfect balance with the positive to give maximum performance.
Separators
Sintered microporous p.v.c. gives minimum resistance.
Planté Positive Plates
Constructed of pure lead to ensure that there is no fall-off in capacity throughout their long life.
Plastic Containers
Transparent SAN. Electrolyte level and cell condition clearly seen.
MAX
MIN
CHLORIDE
Negative
Insulation
Separator
Positive
Separator
Negative
Insulation
Separator
Plug
Base
Nut

Figure 2.4. (*up*) Planté cell (Chloride Industrial Batteries) (SAN stands for styrene-acrylonitrile copolymer); (*down*) Bell System cell (Lucent Technologies). (*From Ref. 1*)

A significantly different design of stationary battery is the cylindrical one developed at the Bell Laboratories [2,3]. Traditional batteries for telecommunication networks have lifetimes of 5-20 years. To extend this term, a cylindrical battery has been built with circular, saucer-shaped pure Pb grids and horizontally stacked plates. Tetrabasic $PbSO_4$ fills the grids and is converted to PbO_2 in a prolonged formation process. The resulting structure shows good resistance to shedding. The traditional Planté design and the Bell System design are represented in Figure 2.4. The latter's life was initially predicted to be 30 years or more. Data based on long-term corrosion investigations have allowed extending the life prediction to 68 years [3]. VRLA batteries are also increasingly used, especially in telecom and UPS applications.

A comparison of flooded and VRLA batteries is schematically done in Table 2.2 [10]. In recent years, considerable effort has been done, especially on VRLA batteries, to improve their power output for EV and UPS applications [11,12]. Details on the numerous types and sizes of Pb/Acid batteries can be found in Ref. [3].

2.2.7. Discharge Characteristics, Peukert Equation and Self-Discharge

The dependence of capacity on discharge current, graphically shown in Figure 2.3, can also be expressed by the so-called Peukert equation [13]:

$$I^{n} \cdot t = K$$

where K and n are constants determined from discharge data. An n value of 1.36 and a K value of 300 can be derived from Figure 2.3. Using these data, the discharge time can be pre-determined at any current.

Major limitation of the Peukert equations are: the temperature effect is neglected, and the accuracy is greatly reduced at low and high discharge rates.

Accounting for the temperature effect is rather difficult, because the capacity also depends on a number of factors: design, method of manufacture, storage, service history and, obviously, current density [2]. However, in a limited temperature range around 30°C, the International Electrochemical Commission has recognized the validity of the equation:

$$C_T = C_{30}\,(1+0.008[T-30])$$

As for the effects of low and high rates, it has been calculated that n tends to 2 at very high currents, and to 1 at very low currents [1].

Self-discharge in Pb/Acid batteries occurs not only because of the

Table 2.2. Advantages/disadvantages of VRLA batteries with respect to the flooded ones. (*From Ref. 10*)

Advantages	**Disadvantages**
No H_2O addition	Careful charging required
No acid spillage	Thermal management more critical, especially for AGM types
Negligible acid fumes	Significant variation of top-off charge voltage
Easy transportation	Increase in overcharge required at elevated temperatures
No special ventilation requirements	Deep-cycle life often inferior under optimum operating conditions
Can be operated horizontally	Electrolyte density cannot be measured
Smaller footprint (batteries can be multi-stacked	Not available in dry-charged state
Negligible acid stratification (gel type)	Maximum shelf-life: two years
Less overcharge required at room temperature	
Good high-rate discharge capacity (AGM type)	

inherent instability of Pb and PbO_2 in concentrated H_2SO_4, but also by virtue of the reactions indicated in the following [4].

Self-discharge reactions at the positive electrode:

(1) O_2 evolution: $PbO_2 + H_2SO_4 \rightarrow PbSO_4 + H_2O + \frac{1}{2}O_2$

(2) oxidation of organics: $2PbO_2 + R + 2H_2SO_4 \rightarrow 2PbSO_4 + 2H_2O + CO_2 + R'$

(3) sulfation of residual PbO: $PbO + H_2SO_4 \rightarrow PbSO_4 + H_2O$

(4) corrosion of Pb current collector: $Pb + PbO_2 + 2H_2SO_4 \rightarrow 2PbSO_4 + 2H_2O$

(5) oxidation of an alloying metal (*e.g.* Sb): $5PbO_2 + 2Sb + 6H_2SO_4 \rightarrow 5PbSO_4 + (SbO_2)_2SO_4 + 6H_2O$

Self-discharge reactions at the negative electrode:

(1) H_2 evolution: $Pb + H_2SO_4 \rightarrow PbSO_4 + H_2$

(2) O_2 recombination: $Pb + H_2SO_4 + 1/2O_2 \rightarrow PbSO_4 + H_2O$

The rates of O_2 and H_2 evolution are primarily determined by the acid concentration. Grid corrosion (point 4) can also occur with the cell in the discharged state, as the protecting PbO_2 layer is destabilized. This explains the slight minimum in the corresponding curve of Figure 2.2 [5].

The overall rate of self-discharge at the positive is slow: typically 0.2%/day at 25°C for fresh, fully charged cells, and decreases as the reactions proceed. Indeed, $PbSO_4$ grants a certain level of passivation, although with the penalty of increased resistance. Conversely, the rate of self-discharge is fast at the negative. In particular, H_2 evolution is enhanced when the positive plate contains Sb in the grid: indeed, Sb can dissolve during charge and diffuse to the negative where it is plated, thus reducing the H_2 overpotential of the electrode. This problem could be alleviated with low-Sb grids, or could be eliminated with pure Pb or Pb/Ca grids. On the other hand, pure Pb grids have inferior strength, while Pb/Ca grids have reduced cycle lives on deep discharge [2]. Fresh batteries with Sb-containing grids lose capacity at the rate of ~1%/day at 25°C, but this rate increases by a factor of 2 to 5 as the batteries age. For Sb-free grids, the capacity loss is below 0.5% and independent on battery age.

The self-discharge of Pb/Acid batteries with Sb-containing grids increases esponentially with temperature, so that storing should be made between 5 and 15°C to minimize self-discharge [3]. Finally, it has to be stressed that prolonged storing in the discharged state results in a permanent capacity loss. Indeed, $PbSO_4$ tends to grow into large crystals (hard sulfate) which cannot be converted back to the active materials on charge.

2.2.8. Charging Methods

General rules for correct charging, applying to all types of Pb/Acid batteries, are:

1. The initially high charging current has to be limited to keep the cell voltage below 2.39 V (gassing voltage).
2. To shorten recharge times, the current can be set at values corresponding to voltages just below 2.39 V.
3. When full charge has been restored, the current decays to a low value, normally C/20. Any further current applied to counterbalance self-discharge should be lower than this.

The most popular charging methods may be summarized as: a) constant current; b) constant potential; c) constant current-constant potential; d) taper; e) pulse; f) trickle; g) float; h) rapid.

In several industrial applications, including EV and stand-by, modified constant-potential (CP) charging is used. An initial constant current (CC) step is applied until the potential reaches a pre-determined value that is maintained up to charge completion. A finishing, low-rate CC step may be applied to cope with self-discharge.

Taper charging is a low-cost variation of the modified CP charging. Basically, the battery receives charge at high rate for low states of charge, and at low rate as full charge is approached.

In pulse charging, especially used for traction batteries, the charger is periodically isolated from the battery and the OCV measured. Only for OCV below a pre-set value, CC pulses are continued. Short pulses are used to maintain the battery at full charge.

Trickle and float charging are low-rate CC and CP methods, respectively, to keep the battery fully charged, as is requested, for instance, in stand-by applications.

Rapid charging is used for applications demanding recharge within one hour. In this case, an intelligent semiconductor-based charger able to control all relevant parameters is needed.

2.3. Nickel/Cadmium Batteries

2.3.1. Introduction

Ni/Cd batteries belong to a group of five rechargeable batteries, *e.g.* Ni/Cd, Ni/MH, Ni/H_2, Ni/Zn, Ni/Fe, having in common a Ni-based positive electrode and an alkaline solution. Even though some known drawbacks can be associated with the Ni/Cd battery, especially low energy density and environmental impact, still it can advantageously be used in a number of industrial applications. Its positive features will be mentioned as a function of the specific construction type.

Cd is used as a negative electrode and β-NiOOH as a positive. The electrolyte is a solution of KOH (22%, d=1.2 g/cm^3) containing some LiOH (8-20 g/L). The latter improves cycle life and high-temperature performance.

2.3.2. Types of Ni/Cd Batteries

Ni/Cd batteries can be assigned to two broad categories: vented and sealed. Vented batteries can use any of the four electrode constructions listed in the following.

Pocket plate. The vented battery using this type of electrode is the oldest one, dating back to the early Jungner's work at the end of the nineteenth century. Both electrodes have flat pockets of Ni-plated, perforated steel strips holding in place the active materials [14]. Two methods of inserting the materials into the strips are used. Once the upper and the lower strips are formed into channels, a loose powder is added to fill the lower channel, or, for heavier electrodes, tablet of active material are formed and subsequently inserted into the channel [15]. These folded strips are interlocked with each other to form long electrode strips (5-10 m), which are then cut into plates to be used in a battery. The negative plate is always thinner than the positive. The stages in pocket plate manufacture are illustrated in Figure 2.5.

The positive electrode is formed from a mixture containing $Ni(OH)_2$

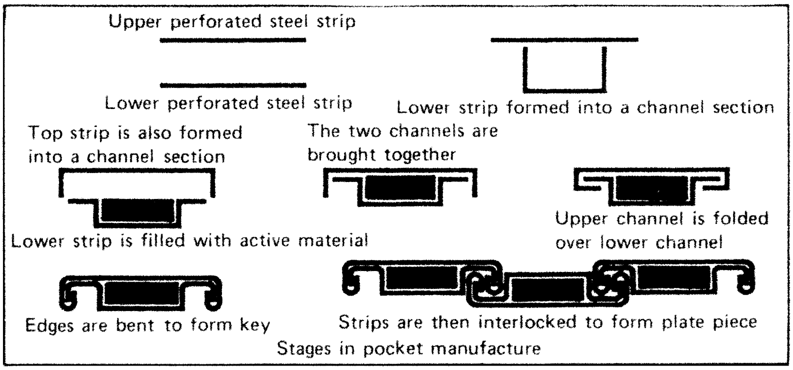
Upper perforated steel strip
Lower perforated steel strip
Lower strip formed into a channel section
Top strip is also formed into a channel section
The two channels are brought together
Lower strip is filled with active material
Upper channel is folded over lower channel
Edges are bent to form key
Strips are then interlocked to form plate piece
Stages in pocket manufacture

Figure 2.5. Stages in pocket plate manufacture for Ni/Cd batteries. (*From Ref. 15*)

(80%), $Co(OH)_2$ (2%) and graphite (18%), while the mixture for the negative contains $Cd(OH)_2$ (78%), Fe (18%) and small amounts of Ni and graphite [14].

Sintered plate. The sintered electrode was developed in order to increase the energy output of the Ni/Cd battery. Indeed, with this electrode, the energy density is up to 50% greater than that of the pocket plate. Furthermore, the sintered electrode can be much thinner, so that the battery has a higher rate capability. Other favorable features include flat discharge profile, good capacity retention and low-temperature performance. On the other hand, the sintered electrode is expensive, requires careful temperature control on charging and manifests the memory effect.

Vented Ni/Cd batteries with sintered electrodes are especially used when high power is required, *e.g.* aircraft turbine engine and diesel engine starting. In many applications, these batteries allow a reduction in size, weight and maintenance [14].

The preparation of the sintered electrode can be made in different ways according to: a) nature of the substrate; b) method of sintering; c) impregnation process; d) plate formation [16].

Two types of substrate can be used, *e.g.* perforated strips or woven screens (in both cases, made of pure Ni or Ni-plated steel). The sintered structure formed before impregnation with the active materials (plaque) has a porosity of 80-85% and a thickness of 0.4-1.0 mm. It is obtained by filling the substrate with a slurry or a dry powder. In both cases, battery grade carbonyl Ni is used. Sintering is done in a reducing atmosphere at 800-1000°C. Then, the sintered structure for the positive electrode is impregnated with a solution of $Ni(NO_3)_2$, while for the negative a solution of $Cd(NO_3)_2$ is used. The nitrates are converted into the respective hydroxides by chemical or electrochemical precipitation in an alkaline solution [17,18]. In the former procedure, more widely used, the plate filled with the nitrate is cathodically polarized in NaOH solution, rinsed, dried and weighed. The process is repeated until the pre-fixed weight (capacity) is obtained. Formation is done by charging/discharging the electrodes at high current against inert counter-electrodes; at the end of it, the electrodes are ready to deliver their full electrochemical capacity.

FNC (Fiber Nickel Cadmium). These batteries use fiber-structured electrodes: a mat of synthetic fibers is nickel-plated and subsequently sintered in a H_2 atmosphere at 800°C. The final step is impregnation with the active mass. This method allows the production of electrodes with a thickness ranging from 0.6 to 10 mm without changing the ratio between the current conducting substrates and the active mass [19]. The substrate is very porous (90%) and allows excellent utilization of the active material. No conductive additive is needed. The active materials, $Ni(OH)_2$ for the positive plate and $Cd(OH)_2$ for the negative, are mechanically embedded directly into the fiber plates [14]. Depending on the electrode thickness, batteries with low to very high power output can be constructed [20]. The improved charging efficiency of these batteries results in a lower amount of gas and, therefore, watering of vented cells is less frequent. In sealed cells, maintenance is not necessary, operating and shelf-life are longer than in vented cells, and the O_2 recombination at the Cd electrode is rapid and complete.

Plastic-bonded plate. This recent design, mainly used for the negative electrode, has afforded improved performance. The active material is mixed in a solvent with a polymer, normally PTFE, to produce an isotropic paste. The paste is extruded, rolled or pasted onto a current collector - normally Ni-plated perforated steel [14]. The plastic-bonded negative electrode, used in conjunction with a sintered positive electrode, results in reduced battery weight and volume (about 20%), and lower overcharge current that leads to reduced water consumption.

The operation of sealed batteries is based on the O_2 cycle, similar to that of VRLA batteries. The Cd electrode has a greater capacity than the positive (ratio: 1.5-2 to 1) so that, on charge, the latter reaches the fully charged state earlier and starts to evolve O_2. Oxygen migrates to the negative through a permeable separator, and undergoes a reduction reaction leading to $Cd(OH)_2$ (see later).

Three types of positive electrodes can be used for the sealed batteries: a) sintered; b) fiber; c) foam. The first two types are basically as previously described. The nickel foam electrode is obtained by Ni plating porous polyurethane or acrylic fibers, followed by pyrolisis. The frame so obtained has a porosity of 90%, so that the amount of active material that can be stored in it is larger than in sintered electrodes. This improves the capacity and energy density of the electrode in spite of a poorer utilization of the active material.

Typical sintered electrodes have capacities of ~450 mAh/cm^3, while foam electrodes can reach 700 mAh/cm^3 [21].

The negative electrode in sealed Ni/Cd batteries can be of the sintered or non-sintered type. The construction of the former has already been described, while the latter is obtained by coating a Ni-plated steel grid with a CdO-based paste [22]. With the non-sintered type, a volumetric capacity increase of ~30% has been obtained [21].

Felts usually made from nylon or polypropylene are used to immobilize the small volume of alkaline solution [23].

Sealed batteries are used not only in portable devices but also in a number of stationary applications (emergency lighting, communication equipment, *etc.*) with capacities as high as 25 Ah [23].

2.3.3. Charge/Discharge Reactions

The reactions determining the battery capacity are:

Negative electrode: $Cd + 2OH^- \rightleftharpoons Cd(OH)_2 + 2e$

Positive electrode: $\beta\text{-}NiOOH + H_2O + e \rightleftharpoons \beta\text{-}Ni(OH)_2 + OH^-$

At the negative electrode, a dissolution-precipitation mechanism is operating, with the formation of such soluble intermediates as $Cd(OH)_3^-$ or $Cd(OH)_4^{2-}$.

The reversible reduction of NiOOH to $Ni(OH)_2$ involves the intercalation of a hydrogen ion into the layered structure of the former, this corresponding to a solid-state mechanism.

The overall reaction is:

$$Cd + 2\beta\text{-}NiOOH + 2H_2O \rightleftharpoons 2\beta\text{-}Ni(OH)_2 + Cd(OH)_2 \quad (E_{cell}=1.30\ V)$$

During charge, H_2O electrolysis is in competition with the primary reactions. In vented cells, H_2 and O_2 are released through the vent; in sealed cells, O_2 evolves as the capacity-limiting positive electrode enters overcharge, according to the reaction:

$$4OH^- \rightarrow 2H_2O + O_2 + 4e$$

At the negative electrode, formation of Cd occurs:

$$2Cd(OH)_2 + 4e \rightarrow 2Cd + 4OH^-$$

The overall electrochemical reaction in these conditions is:

$$2Cd(OH)_2 \rightarrow 2Cd + 2H_2O + O_2$$

O_2 evolved at the positive travels through the permeable separator and reacts chemically with Cd:

$$2Cd + O_2 + H_2O \rightarrow 2Cd(OH)_2$$

The net sum of the overall electrochemical and chemical reactions on overcharge is zero, *i.e.* no chemical change occurs. This means that electricity is just converted into heat: indeed, the overcharge reaction is exothermic [14]. The mechanism of O_2 recombination is visually shown in Figure 2.6.

The O_2 recombination in sealed cells makes the final stages of the charge process quite different with respect to those of vented cells, as also illustrated in Figure 2.7. In vented cells, as full recharge is approached, H_2O

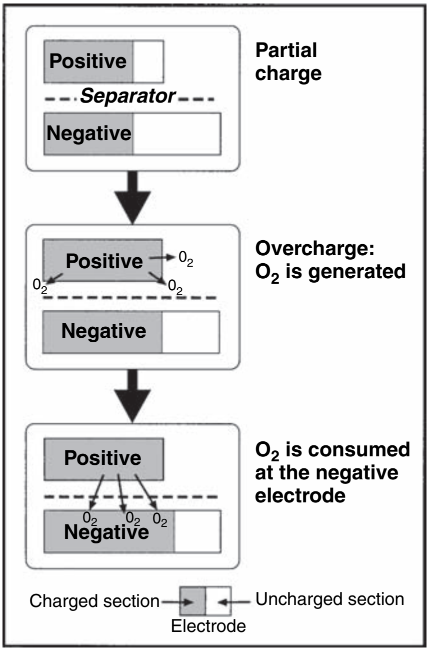

Figure 2.6. Mechanism of recombination of O_2 generated at the positive electrode of the sealed Ni-Cd battery on overcharge. *(From Ref. 23)*

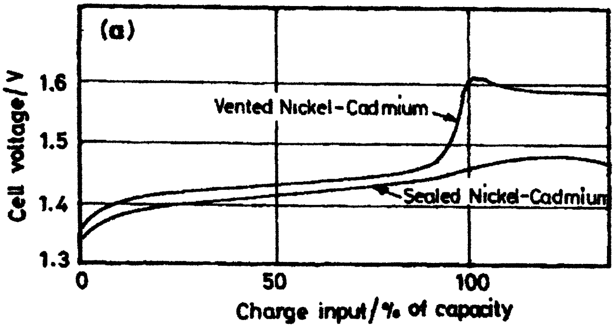

Figure 2.7. Charging profiles of vented and sealed Ni/Cd cells at the C/10 rate. (*From Ref. 18*)

electrolysis causes a steep voltage rise. Conversely, the gas recombination mechanism limits the voltage rise in sealed cells and a certain degree of overcharge is allowed.

2.3.4. Discharge Characteristics, Memory Effect and Self-Discharge

The ability to sustain high discharge rates is generally good, but with a marked dependence on cell construction. This is stressed in Table 2.3, where a comparison is made among the different types presented in Section 2.3.2.

The pocket-plate cell has the lowest rate capability. It is noteworthy that, from this point of view, the sintered electrode performs better in sealed than in vented cells. Indeed, thin, rolled electrodes can be used in the cylindrical design preferred for the former, while flat plates are used in prismatic vented cells. Finally, fiber electrodes may manifest an outstanding rate capability and cells featuring ultra high rates can be constructed. For example, a 47-Ah, high-rate cell can be discharged for 60 sec with currents in the range 1-2.5 kAmp [25].

Voltage curves at various discharge rates are shown in Figure 2.8 for a sealed cell. The voltage regulation is good even at high rates, with a psudo-plateau at ~1.2 V. However, the curve profile may be appreciably altered in the presence of the so-called memory effect (voltage depression), especially noted in sealed cells. This occurs in case of repetitive shallow discharges. After recharge, the cell may not be able to give its full capacity at a given cut-off voltage, as if remembering the previous shallow discharges (Figure 2.9). This is due to the voltage decrease (some 100 mV) accompanying the effect. Full capacity may be regained with some deep discharges followed by complete charges. However, as shown in the figure, this may not be possible after a high number of shallow discharges.

Table 2.3. Comparison of the capacities of different types of Ni/Cd batteries at various rates.

Rate (C)	**Capacity (%)**			
	Vented Pocket Plate[1]	**Vented Sintered Plate**[2]	**FNC**[3]	**Sealed Sintered Plate**[4]
0.1	102			
0.2	100		106	113
0.5	92		102	
1	82	100	99	103
2	76			
3	67	83		
4				92
5	58	77	98	
8				83
10		63	88	

1) From Ref. 14; 2) From Ref. 24; 3) From Ref. 20; 4) From Sanyo's Catalog: "Cadnica"

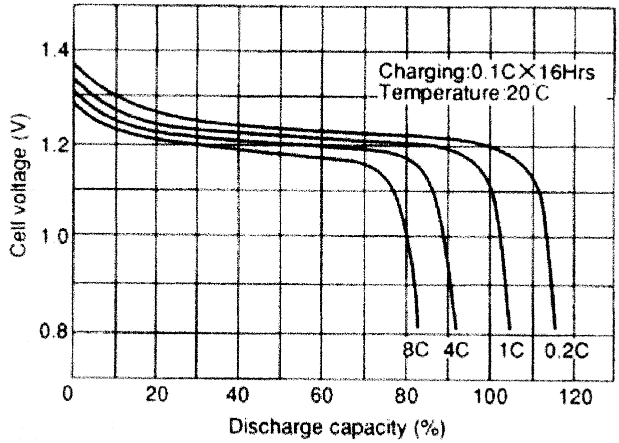

Figure 2.8. Discharge curves at various rates of standard sealed Ni/Cd batteries. (*From Ref. 26*)

A similar effect can be observed with long-term overcharge, especially at high temperatures [18]. The rationale for the memory effect has long been debated. Its presence, although not to the same extent, in Ni/MH cells allows excluding the Cd electrode. According to some authors, the positive electrode is responsible as, in the conditions described above, β-NiOOH changes into γ-NiOOH [27].

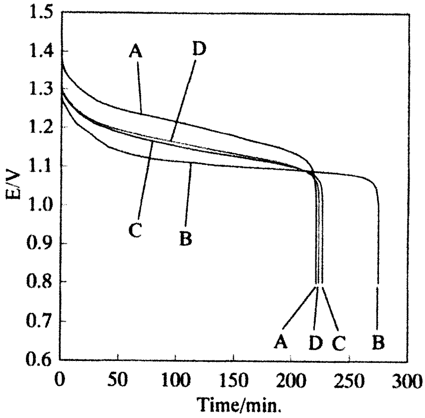

Figure 2.9. Memory effect (voltage depression) in an experimental Ni/Cd cell submitted to 100 shallow discharge cycles. A: discharge curve at normal state; B: 1st discharge after 100 shallow cycles; C) 2nd discharge; D: 3rd discharge. (*From Ref. 27*)

Most Ni-Cd batteries can be stored in the temperature range -30/-40°C to 50/60°C without significant performance deterioration. Some batteries have been stored for up to 10 years and could still deliver, after recharge, almost 100% of their original capacity. The rate of capacity loss is related, at a given temperature, to the electrode structure. Pocket-plate electrodes lose 3-5% per month of their capacity at room temperature. Sintered-plate and fiber electrodes lose, at the same temperature, 10-15%/month. The faster self-discharge of these electrodes is connected with their higher surface area: this favors chemical reactions rapidly bringing the battery to a discharged state, especially above ~30°C.

2.3.5. Charging Techniques

Ni/Cd batteries may be charged with CC or CV methods or their modifications. However, CC charging is normally preferred for all types. In all cases, a final step consisting in a float or trickle charge may be applied to: 1) counterbalance self-discharge of stand-by batteries that have to maintain their full state of charge; 2) completing a (relatively) fast charge. In vented batteries, overcharging has to be limited to 101-105% to avoid excessive gas generation and frequent water replenishing. Conversely, sealed batteries can afford a higher degree of overcharge by virtue of the gas recombination mechanism. These batteries use end-point detecting techniques, which may either be based on the

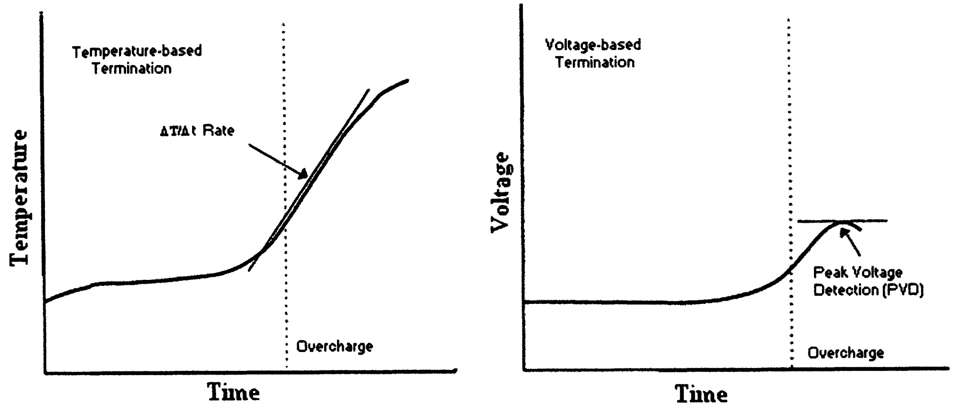

Figure 2.10. ΔT/Δt detection (*left*) and peak voltage detection (*right*) for charge termination of sealed Ni-Cd cells. (*From Ref. 28*)

temperature rise when full charge is approached, or on the typical voltage peak appearing on overcharge. These methods are illustrated in Figure 2.10

The maximum in the voltage, which is typical of this system and of the Ni-MH system, signals the end of the $Ni^{II} \rightarrow Ni^{III}$ oxidation at the positive electrode. Peak detection becomes less defined as the charging rate decreases, and if the temperature approaches or exceeds 40°C. In these cases, the rate of temperature increase (ΔT/Δt) gives more reliable results; however, with the latter method, the battery could be subjected to more overcharge, this shortening its life. Fast charge is possible if the rate is not higher than that of O_2 recombination or heat dissipation: in this case, internal pressure and temperature remain low throughout the charging process. This is made possible by properly designed electrode structures and electrolyte distribution.

The effect of charging rate on voltage, pressure and temperature is shown in Figure 2.11 for standard batteries [18]. A rate greater than C/3 is not recommended, due to the rapid temperature and pressure increase. Normal rate charging (7-10 h) should be performed in the temperature range 0-45°C, while in fast charging (1h) the lower limit has to be raised to 15°C [29].

2.3.6. Cycle Life

Ni/Cd batteries are capable of long cycling even at high DODs. Cycle numbers in the range 500-5000 are possible. If Ni/Cd and Pb/Acid batteries are compared, the former show a longer cycle life, especially when a deep discharge is requested. This is shown in Figure 2.12: the Pb/Acid battery can deliver about 1000 cycles at DODs< 30%, but the cycle number dramatically

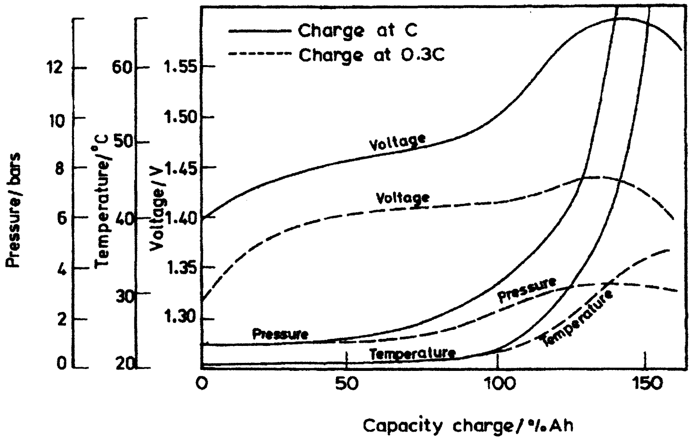

Figure 2.11. Shapes of the charging curves of standard sealed Ni-Cd batteries at two rates. (*From Ref. 18*)

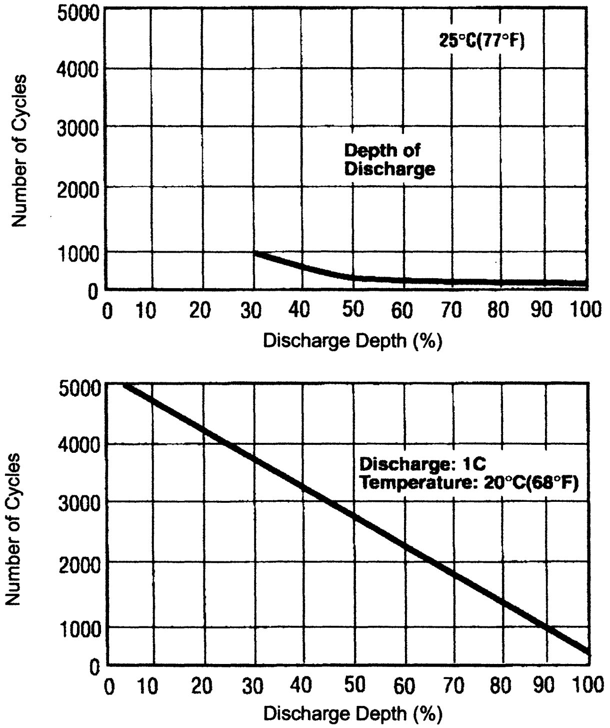

Figure 2.12. Cycle life *vs.* DOD for a sealed 6.5-Ah Pb/Acid battery (*up*) and a sealed 4-Ah Ni/Cd battery (*down*). (*From Ref. 30*)

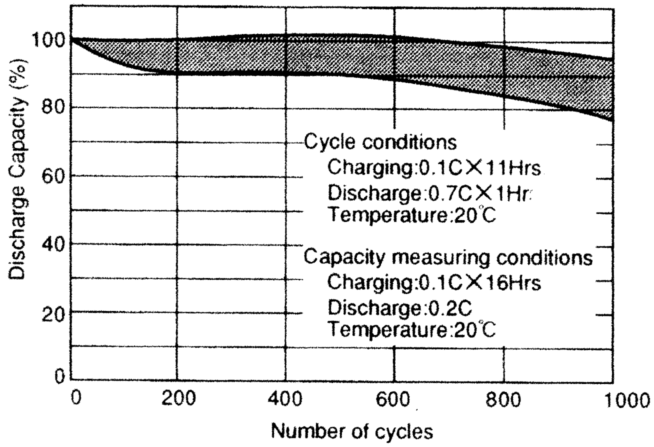

Figure 2.13. Cycling characteristics of a sealed 1.2-Ah Ni/Cd battery. (*From Ref. 26*)

decreases on deeper discharges. The Ni/Cd battery has instead a linear trend *vs.* DOD and can still deliver some 1400 cycles at 80% DOD.

The capability of maintaining an almost stable capacity upon extended cycling is shown in Figure 2.13, and can be referred to the very limited variation of the internal resistance. This is normally low (some millihoms for a sintered-plate electrode) and has been found to remain practically constant as a function of SOC and after long cycling [23,31].

2.3.7. Applications

Major applications for industrial Ni/Cd batteries include [14,32]:

- Conventional power stations
- Solar power stations
- UPS plants
- Train lighting and air conditioning
- Marine batteries
- Alarms
- Aircrafts
- Traction
- Telecommunications systems
- Signal equipment
- Emergency lighting
- Broadcasting stations
- Switchgear
- Signalling
- Satellites
- Starting (diesel engines, *etc.*)

Pocket-plate vented batteries are the largest ones, with capacities of up to 1450 Ah. Fiber-plate and plastic-bonded plate batteries can reach capacities of 450-500 Ah [14], while the maximum capacity of sintered plate batteries is 100 Ah [23]. Finally, the largest sealed battery (M size) has a capacity of 25 Ah [21]. Stationary applications of Ni/Cd batteries are described in Chapter 10.

2.4. Nickel/Metal Hydride Batteries

2.4.1. Materials and Electrode Reactions

The negative Cd electrode is replaced by a hydrogen storage alloy in the Ni/MH system, while the positive electrode is the same. During charge, a hydrogen atom, formed by H_2O reduction, deposits on the surface of the alloy and then diffuses into it to form a metal hydride (MH). The reaction at the positive electrode is the same of the Ni/Cd battery. The electrolyte solution (aqueous KOH) is also the same.

The reversible reactions can be written as:

Negative electrode: $MH + OH^- \rightleftharpoons M + H_2O + e$

Positive electrode: $\beta\text{–NiOOH} + H_2O + e \rightleftharpoons \beta\text{–Ni(OH)}_2 + OH^-$

Overall reaction: $\beta\text{–NiOOH} + MH \rightleftharpoons \beta\text{–Ni(OH)}_2 + M \quad (E_{cell}=1.32\ V)$

The overall process consists in the reversible transfer of a proton from an electrode to the other. The proton released from the storage alloy during discharge is first taken by OH^- groups to form H_2O and, then, transferred to NiOOH to form $Ni(OH)_2$. This process is reversed upon charge. Therefore, at both electrodes a homogeneous solid-state process is operating. This eliminates problems occurring in electrodes where a dissolution-precipitation mechanism is present, *i.e.* variations in crystallography, mechanical integrity, surface morphology and electrical conductivity [18,33].

Furthermore, at variance with the overall reaction of the Ni/Cd system, where H_2O is consumed on discharge and reformed on charge, here there is no net reaction involving H_2O, so that the concentration and conductivity of the solution does not change.

The Ni/MH battery can be subjected to overcharge and overdischarge with well identified reactions, as reported in the scheme of Figure 2.14 [18]. The cell capacity is limited by the positive electrode, with a negative to positive ratio of 1.5-2 to 1. During overcharge, O_2 is evolved at the positive and diffuses to the negative to form H_2O by reaction with MH. The net sum of the two overcharge reactions at the negative is just the reversal of the reaction at the positive. During overdischarge, H_2 is evolved at the positive and again gives rise to H_2O at the negative. Therefore, at variance with the Ni/Cd battery, both H_2 and O_2 recombine to form H_2O, thus assuring sealed operation of a Ni/MH battery.

The alloys currently used are of the AB_5 or AB_2 type. An example of the

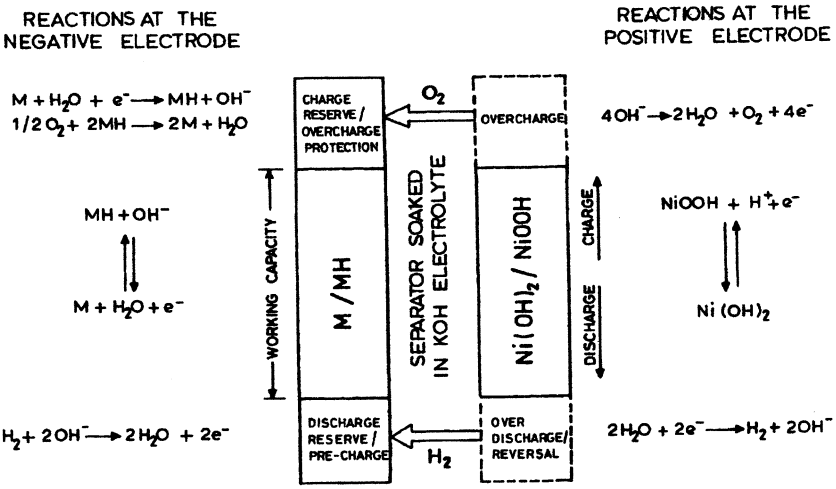

Figure 2.14. Scheme of all reactions occurring in a sealed Ni/MH cell. (*From Ref. 18*)

former is $LaNi_5$, whereas ZrV_2 exemplifies the latter. Both types of alloys have undergone over the years important developments to improve their characteristics, which can be summarized as: wide operating temperature range, high capacity and energy, long cycle life, high electrochemical activity, high hydrogen diffusion velocity, low cost, environmental friendliness [34]. The scheme of Figure 2.15 presents the various optimization steps for the $LaNi_5$ alloy [22]. Mm stands for misch metal, *i.e.* a naturally occurring mixture of rare earth elements: La, Nd, Pr, Ce. Using this mixture instead of pure La enhances the resistance of the alloy to alkali and reduces cost. A typical composition is: 25% La, 50% Ce, 7% Pr, 18% Nd [18]. Partial Ni substitution with Co prevents alloy pulverization, Mn increases the capacity, and Al improves the resistance to oxidation during the manufacture [22]. Finally, it was found that a composition. $Mm(Ni\text{-}Co\text{-}Mn\text{-}Al)_{4.76}$ gives a discharge capacity of 330 mAh/g, that is 10% higher than AB_5.

AB_2-type alloys (A: V,Ti; B: Zr,Ni plus minor amounts of Cr,Co, Mn, Sn) have higher capacities, *e.g.* 385-450 mAh/g [35]. However, at low and high temperatures and demanding discharge rates, the AB_5 alloy works better. This alloy is also less prone to self-discharge and, as it is also cheaper and easier to use, is still preferred.

A larger capacity is expected from new alloys under study. The *bcc* type (example: V_3Ti) has twice the capacity of AB_5, and the Mg-Ni type (example: Mg_2Ni+2Ni) has 1.5 times the capacity of AB_5. However, these new alloys share non-secondary drawbacks: poor corrosion resistance, shorter cycle life, initial activation and lower operating voltage (in comparison with AB_5). Capacities of 700-1000 mAh/g are thought possible in the future [36].

The positive electrode is basically the same of Ni/Cd batteries. High density, spherical $Ni(OH)_2$ also contains Co and Zn [35,37]. Addition of CoO results in the formation of β-$Co(OH)_2$, which is oxidized on charge to the highly conductive β-CoOOH. Its presence is important as β-$Ni(OH)_2$ has a very low conductivity (five orders of magnitude less than that of β-NiOOH). Both Co and Zn greatly limit on overcharge the formation of γ-NiOOH, which is taken as responsible of the memory effect [27] and causes morphological changes in the electrode [37]. Furthermore, these additives improve the charge acceptance and retention at high temperatures (up to 45°C).

It has been found, in different samples of $Ni(OH)_2$, that the uptake/ release of protons is enhanced by crystal imperfections. Materials with an increasing degree of disorder in the stacking of the basal planes have higher specific capacities [21].

O_2 evolved at the positive on overcharge may oxidize the separator. Therefore, a chemically stable separator is needed as, for instance, sulfonated polypropylene.

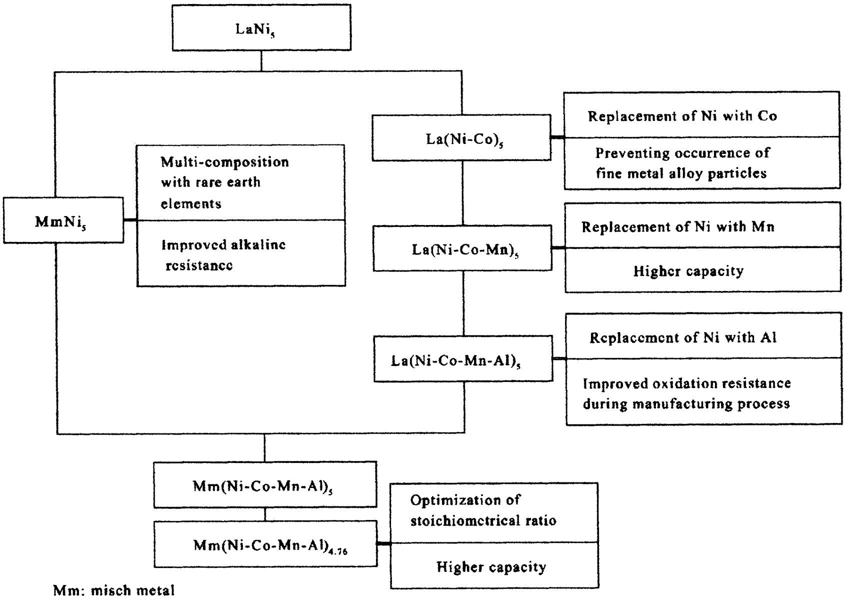

$LaNi_5$
$La(Ni\text{-}Co)_5$
Replacement of Ni with Co
Preventing occurrence of fine metal alloy particles
Multi-composition with rare earth elements
Improved alkaline resistance
$MmNi_5$
$La(Ni\text{-}Co\text{-}Mn)_5$
Replacement of Ni with Mn
Higher capacity
$La(Ni\text{-}Co\text{-}Mn\text{-}Al)_5$
Replacement of Ni with Al
Improved oxidation resistance during manufacturing process
$Mm(Ni\text{-}Co\text{-}Mn\text{-}Al)_5$
$Mm(Ni\text{-}Co\text{-}Mn\text{-}Al)_{4.76}$
Optimization of stoichiometrical ratio
Higher capacity
Mm: misch metal

Figure 2.15. Progressive optimization of the AB_5 hydrogen storage alloy for the negative electrode of a sealed Ni/MH battery. (*From Ref. 22*)

2.4.2. Cell Construction and Performance

Small cells (e.g. for electronics)

Ni/MH batteries are constructed with the same designs of the Ni/Cd ones. The electrodes have a high surface area so to stand high current rates. In the cylindrical configuration (the most common one), the positive electrode has generally a felt or foam substrate, into which the active material is impregnated or pasted. The negative electrode has also a porous structure (perforated Ni foil or grid) supporting the plastic-bonded hydrogen storage alloy. The electrodes are spirally wound, as in the analogous Ni/Cd batteries, and contained into a Ni-plated steel can. The cell top contains, in this case too, a releasable safety vent, which operates at around 27 atmospheres.

Prismatic batteries are able to deliver up to 20% more capacity. The electrodes are flat and rectangular, other things being the same as in the cylindrical design.

Large cells

The metal alloy is supported by a perforated (or expanded) Ni foil or Ni foam. The positive active material is commonly supported by a Ni foam, but Ni fibers or sintered Ni fibers may also be used, especially for operation at high rates and low temperatures [20,35].

Both cylindrical and prismatic configurations can be used, the former being preferred for capacities below 10 Ah. Cylindrical cells are of the jelly roll type, with long electrode strips coil wound: this is the same configuration used in other systems. However, as the Ni/MH cells are often operated at very high rates, the edge current collector has to be welded in several points of each electrode to ensure a very low internal resistance (1-2 mΩ) [35]. Cylindrical cells of more than 20 Ah are difficult to construct, so the prismatic form factor prevails in this case. Prismatic cells use the conventional flat electrode stacks with intermediate separators. The ratio of active to inactive materials is dictated by the power to energy trade-off for a given application.

Practically all Ni/MH batteries are sealed and use a limited amount of electrolyte (6 M KOH plus LiOH as an additive) to allow for fast gas diffusion and recombination.

Cylindrical cells only use metal cases. The metal hydride electrode is connected to the can, which serves as the negative terminal. Furthermore, high internal pressures deriving from O_2 evolution on fast charge demand a metallic case. Large prismatic batteries may use both metal and plastic cases. The latter ones have an advantage in cost and electrical isolation, this being of prime importance in large packs for EV.

In Figure 2.16, discharge curves of a cylindrical Ni/MH cell are shown at different rates. The cell loses little capacity by increasing the rate, although at the expenses of the mean voltage. At variance with the exothermic nature of the discharge reaction of Ni/Cd batteries, in these ones the discharge is endothermic. Therefore, heating due to current flowing in the cell is partly balanced. Although a Ni/MH battery is capable of sustaining relatively high discharge currents, repeated discharges at these currents reduce the battery's cycle life. Best results are achieved with rates of 0.2C to 0.5C. At the 0.2C rate, the Ni/MH battery delivers 40% more capacity than the Ni/Cd one, and a correspondingly higher energy density. In optimized cells, specific energies approaching 100 Wh/kg and energy densities above 300 Wh/L are now available. In comparison with Ni/Cd cells, however, the rate capability is generally lower, self-discharge is faster and tolerance to overcharge lesser.

The battery sensitivity to temperature is evident in both operating and storage conditions. Capacity loss is rather fast on storage at high temperatures, as shown in Figure 2.17. If one compares Ni-Cd and Ni/MH batteries, the faster self-discharge of the latter above room temperature is evident: at 45°C, a Ni/Cd battery can still retain 60-70% of its capacity after one month, while a Ni/MH one delivers 20-40% only. Room temperature storage does not cause a permanent capacity loss, as full capacity is recovered upon charge. However, long term storage at high temperatures produces permanent damages to seals and separator, and should be avoided. Some tests have shown that continuous exposure to 45°C reduces the cycle life by ~60% [38].

A study has been performed on the mechanism of self-discharge in an 85-Ah traction battery with AB_2-based negative electrode [39]. Careful evaluation of the OCV decay as a function of time allows to detect three distinct periods of voltage decay, each giving a linear slope in the OCV *vs*. ln(t) curve. The first stage covers a short time, 10 – 100 sec; the second, intermediate stage corresponds to the range 10 min – 25 h; the third stage starts from ~2 days of storage and continues for months. The predominant self-discharge mechanism for each stage can be written as:

1. $6NiOOH + 2H_2O + H_2 \rightleftharpoons 6Ni(OH)_2 + O_2$
2. $2NiOOH + H_2 \rightleftharpoons 2Ni(OH)_2$
3. $NiOOH + MH \rightleftharpoons Ni(OH)_2 + M$

Due to the short time span of the first stage, the proposed mechanism has to be taken with some care. All three stages involve reaction of hydrogen gas at the positive electrode. In particular, the last reaction is caused by H_2 released from the alloy through a mechanism of the type: $MH_{abs} \rightarrow MH_{ads} \rightarrow M + 1/2H_2$. In this respect, it has to be observed that the AB_2 alloy has a higher H_2 partial pressure in comparison with AB_5.O_2 recombination also contributes to self-discharge, but only in the first 4 h after full charge. Subsequently, oxidation of H_2 at the positive is the main reaction. The charge retention for this battery is shown in Figure 2.18. After 72 days of storage, only 43% of the original capacity is left [39].

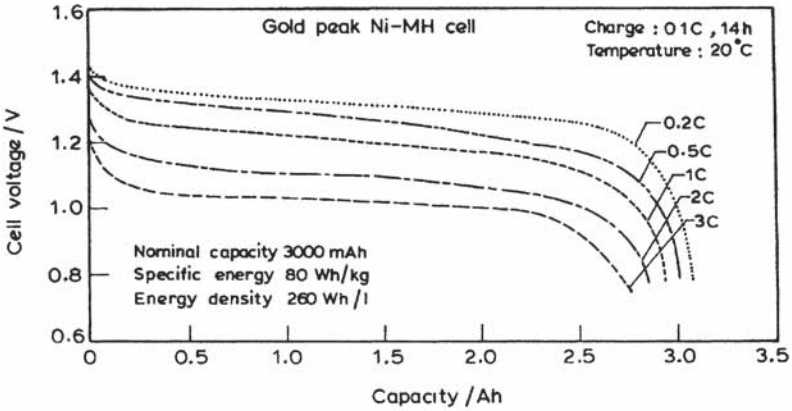

Figure 2.16. Discharge curves at various rates of a cylindrical 3-Ah Ni/MH cell. (*From Ref. 18*)

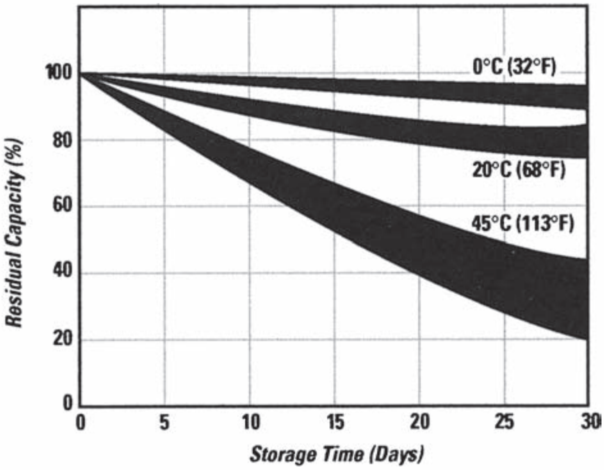

Figure 2.17. Storage characteristics of Ni/MH batteries at various temperatures. Charge at 0.3C for 5 hours; discharge at 0.2C to 1.0 V (room temperature). (*Courtesy of Duracell*)

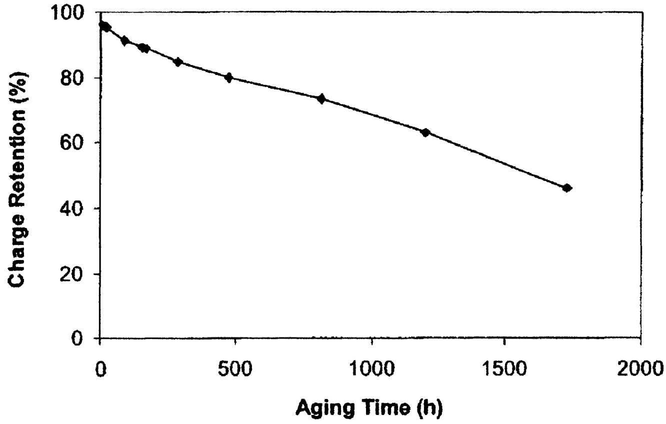

Figure 2.18. Charge retention of a prismatic 85-Ah Ni/MH battery over 72 days of storage at room temperature. (*From Ref. 39*)

2.4.3. Charging the Ni/MH Battery

Charge is a critical step in determining the performance and overall life of Ni/MH batteries, due to their sensitivity to the charging conditions. Choosing the appropriate charging rate, the temperature range and the most effective techniques indicating end-of-charge is of the utmost importance.

Ni/MH batteries are commonly charged at constant current, which has to be limited to avoid overheating and incomplete O_2 recombination. Shapes of the charge curves at different rates are presented in Figure 2.19 together with the corresponding temperatures. The voltage raises more sharply around 80% charge, due to a more significant O_2 evolution, and tends to level off, or to a maximum value, at medium-high rates. In comparison with the charge of Ni-Cd batteries (Figure 2.11), the voltage drop, when present, is not so evident.

The charge process is exothermic in Ni/MH, while it is endothermic in Ni/Cd. Therefore, the temperature of the former, for the same charge input, is higher than that of the latter. After about 80% charge, simultaneously with the O_2 evolution, the temperature of both batteries significantly increases due to the exothermic O_2 recombination reaction. This increase in temperature causes the voltage to drop (or level off) as the battery reaches full charge and enters the overcharge zone [40].

On the basis of the above considerations, the charge temperature has to be controlled to obtain high discharge capacities and should not overcome 30°C, as an increasing O_2 evolution takes places at high temperatures.

On the other hand, it has been ascertained that the charge efficiency is very good in the range 10-30°C, so temperatures below 10°C should also be

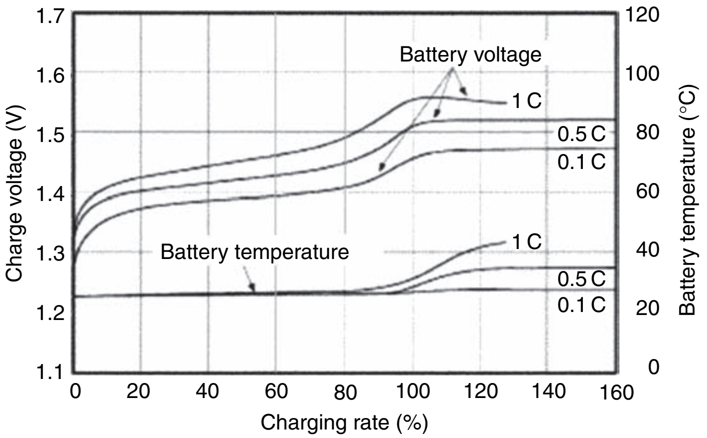

Figure 2.19. Voltage and temperature profiles of Ni/MH batteries charged at various rates. (*From Ref. 22)*

avoided.

Voltage drop and temperature rise, in addition to calculation of the charge input (Ah), can be taken as indicators of the end of charge, but, as can be inferred from the above discussion, the choice of the method greatly depends on the conditions of a specific charge. The need of a charge control is especially evident in fast charges, where temperature and pressure may reach exceedingly high values with possible cell venting.

Hereafter, the methods for charge control are summarized.

Charge input. From current and time, the amount of charge is calculated. This method can be applied only to slow charges (<0.3C) to avoid overcharges that could occur in incompletely discharged cells.

Voltage drop (-ΔV). This method, obviously applicable if the drop is present, *i.e.* at high rates (and low temperatures), should stop charging at potentials of 5 to 10 mV past the peak. It is shown in Figure 2.10.

Voltage plateau. This is applicable to low-rate charges where the voltage levels-off (see charge at 0.1C in Figure 2.19). A top-up charge, *i.e.* a time- and current-limited charge, may follow to ensure full charge.

Temperature cut-off (TCO). This method stops charging when the temperature reaches a pre-set limit indicating overcharging. It is usually used as a backup of other methods, in case of their failure.

Delta temperature cut-off (ΔTCO). This method measures the temperature increase with respect to the starting value. The limit temperature depends on several factors and, in particular, should be determined for each battery type. At the 1C rate, a typical ΔTCO could be 15°C.

Rate of temperature increase ($\Delta T/\Delta t$). This measures the rate of temperature rise *vs.* time (Figure 2.10) and stops the charge when a predetermined value, *e.g.* 1°C/min, is reached. This is the preferred method to stop high-rate charges, as it can sense starting of overcharge earlier than the $-\Delta V$ method, thus ensuring longer cycle lives. This confirms that the Ni/MH battery suffers if repeatedly overcharged.

In terms of charge rates, appropriate termination methods are described in Table 2.4. In general, one of these procedures can accomplish charging the Ni/MH battery.

Low-rate charge (12 hours). If there is no need to charge a battery in a short time, a 12-hour charge at 0.1C may be adequate. A 120% charge input is ideally suited to ensure a long cycle life. The temperature range is 0-40°C, preferably 15-30°C.

Quick charge (4 hours). This requires charge control to avoid overheating and exceeding the O_2 recombination rate. A convenient rate may be 0.3C and termination may be controlled with $\Delta V = -10$ mV. Termination backup methods: charge input of 120% and TCO of 60°C. The temperature range is 10-45°C. A top-up charge is not necessary.

Fast charge (1 hour). For obtaining the highest capacity in a fast charge, the following three-step procedure is recommended:

1. Charging at 1C with $\Delta T/\Delta t$ termination (1°C/min) in the preferred temperature range 10-35°C.
2. Applying a top-up charge at 0.1C for half an hour.
3. Applying a maintenance (or trickle) charge at C/300 with no time limits.

The last step counterbalances self-discharge and is only required in applications with batteries in a fully charged state.

An investigation on the charge efficiency at different rates for the 85-Ah traction battery described above has been carried out [41]. At slow charge rates (below C/4), the battery can be charged with an efficiency of 98% (a small degree of overcharge [1-2%] is applied). At rates above C/4, and setting the

Table 2.4. Recommended charge termination methods for Ni/MH batteries as a function of charge rate. (*From Ref. 42*)

Charge Rate	Termination Method
1C to 0.5C	Voltage or temperature based
0.5C to 0.33C	Voltage based
0.33C to 0.1C	Not recommended
0.1C or below	Time limit

pressure of the release valve at 6.8 atm, the battery can be recharged with an efficiency of 93% at C/2, and 85% at 1C. O_2 recombination is already active at low rates (less than C/2), whereas at high rates (1C or above) another recombination mechanism occurs: excess H_2 at the hydride electrode recombines at the NiOOH electrode, thus forming $Ni(OH)_2$. This reaction contributes to the voltage drop ($-\Delta V$) in the final charge stages at high rates (Figure 2.19).

In addition to the charging techniques reported above, and considering that the Ni/MH battery is largely used in EV and HEV applications, one has to mention charging by regenerative breaking. The energy lost during breaking is used to charge the battery at very high power, 500 W/kg. Not all batteries can accept charge in these conditions, but the Ni/MH one can do so over a wide state of charge and temperature range [35].

2.4.4. Cycle and Battery Life

The main factors determining the battery life, *i.e.* temperature, current, storage, charge termination method, over-charging and -discharging, have been discussed above. Under mild conditions, *i.e.* charge/discharge at 0.2C, 20°C, limited overcharge, the Ni/MH battery can deliver in excess of 500 cycles (up to ~1000-1200) before its capacity drops to 80% of the initial value. In HEV applications, where high-current pulses are applied and the SOC varies between 2 and 10%, more than 100,000 cycles are possible.

The DOD is also very important. Cycling at moderate rates and 100% DOD can still allow obtaining ~500 cycles. However, on repeated deep cycles at high currents, the performance starts to deteriorate after 200-300 cycles. Shallow rather than deep discharge cycling should be applied at these currents.

2.4.5. Applications

The vast majority of circulating EV and HEV vehicles use Ni/MH batteries, as they are those best approaching the mid-term USABC goals [35].

The second-generation module and pack used in the Toyota Prius are shown in Figure 2.20. Their characteristics have been improved in recent years: the third-generation module has a power of 1300 W/kg, as compared to 1000 W/kg of the previous one; on the other hand, the specific energy has maintained the value of 46 Wh/kg. The pack is made up of 28 modules (*vs.* 38 of the previous generation), this corresponding to 201.6 V [43]. The Prius has a computer that is solely dedicated to keeping the battery at the optimum temperature and charge level. (See Chapter 4 for more data on this subject).

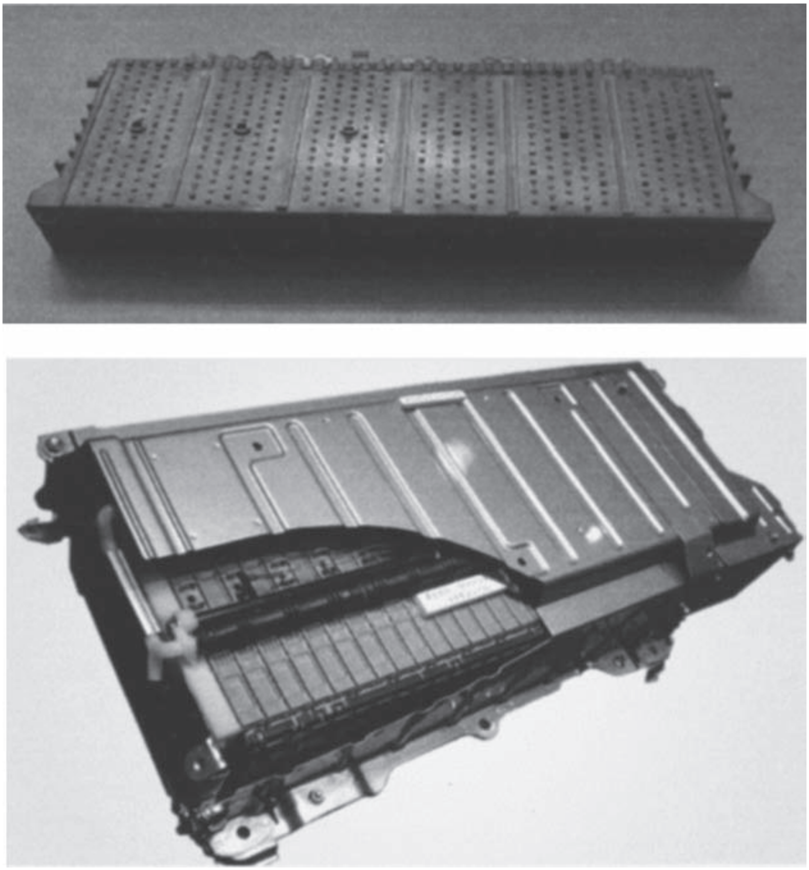

Figure 2.20. Ni/MH battery module (*up*) and pack (*down*) for second-generation Toyota Prius. (*Courtesy of Panasonic*)

According to Toyota' data, the battery can do 290,000 km of normal driving with absolutely no degradation of the battery's performance [44].

Standby power systems are also an area of application for the larger Ni/MH batteries. They have a variety of advantages over the traditional Pb/Acid batteries employed in these applications. The advantages include [45]:

- Small Footprint
- Low Maintenance
- Light Weight
- Long Life Cycle Characteristics
- High Power
- Safety

On the other hand, they are more expensive than Pb/Acid and Ni/Cd, another system used in stand-by applications. Furthermore, Ni/Cd is more resistant to aging than Ni/MH and has a longer cycle life. Therefore, the use of Ni/MH in these applications will probably be limited.

Other applications are in aircraft, satellites, in connections with fuel cells in hybrid vehicles, and in SLI systems with 36-42 V, as compared to the usual 12 V systems based on Pb/Acid batteries [35]. In this last application, the Ni/MH battery has inherent advantages, *i.e.* higher energy and longer cycle life, especially at high DOD.

Ni/MH batteries used in portable, EV and HEV applications have typical specific energies of 70-90, 65-75, and 45-60 Wh/kg, respectively.

Ni/MH batteries have been introduced in the early 1990s. Since then, they have experienced significant improvements in their characteristics. In Figure 2.21, the energy and power progress in different applications is shown.

The gain in specific power is especially remarkable. It has long been thought that Ni/MH batteries could never reach the performance of analogous Ni/Cd batteries. Some technological advancements, *i.e.* low resistance current collectors, highly catalytic metal hydrides and fiber-structured Ni electrodes [21,35], make now possible using special Ni/MH batteries in a variety of high-power applications.

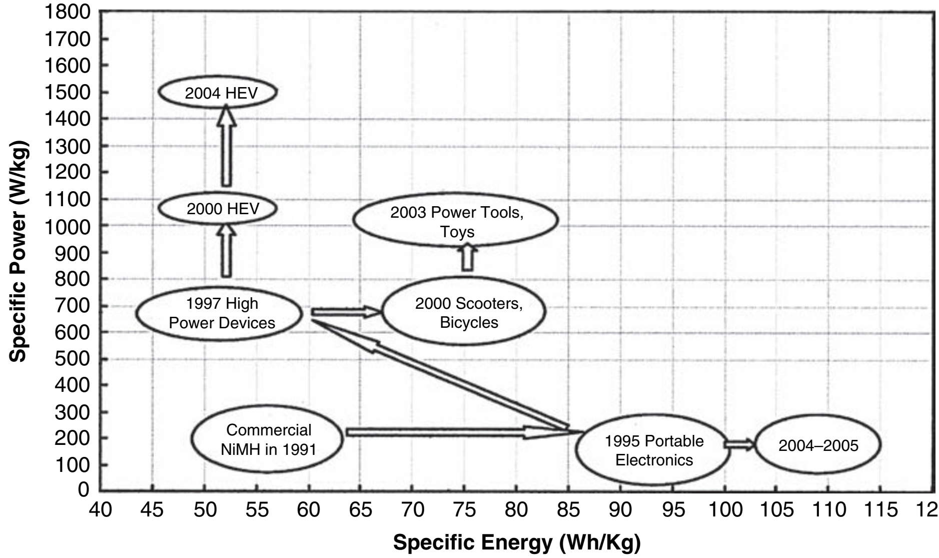

Figure 2.21. Evolution of the specific energy and power of Ni/MH batteries for various applications during 1991-2005. (*From Ref. 46*)

2.5. Nickel/Hydrogen Batteries

The Ni/H_2 cell utilizes the positive electrode already described in the previous sections and a lightweight H_2 electrode as a negative electrode. This system has specifically been developed for aerospace applications and has been in continuous development since the early 1970s. The first launch of a Ni/H_2 battery dates back to 1977 aboard an experimental satellite [47].

During normal operation, when the cell is cycled between voltage limits preventing overcharge or polarity reversal, the reactions are:

Positive electrode: $NiOOH + H_2O + e \rightleftharpoons Ni(OH)_2 + OH^-$

Negative electrode: $1/2H_2 + OH^- \rightleftharpoons H_2O + e$

Overall reaction: $1/2H_2 + NiOOH \rightleftharpoons Ni(OH)_2$ (E_{cell}=1.32 V)

The net reaction shows no change in electrolyte concentration or H_2O consumption.

One of the major advantages of this system is its ability to tolerate overcharge and reversal. On overcharge (and in the final charge stages), O_2 is evolved at the Ni electrode and recombines at the H_2 electrode to form H_2O. State-of-the-art cells are negative-limited, so during reversal NiOOH is reduced to $Ni(OH)_2$ at the nickel electrode and O_2 is evolved at the H_2 electrode [18]. Therefore, the net reaction on reversal is:

$$2NiOOH + H_2O \rightleftharpoons Ni(OH)_2 + 1/2O_2$$

O_2 so generated is consumed during recharge. In positive-limited cells, *i.e.* all cells manufactured till the mid-1980s, H_2 is generated at the positive during reversal and consumed at the negative with the same rate [18,48].

The preferred Ni electrode consists of a porous sintered Ni powder substrate, supported by a Ni screen, electrochemically impregnated with $Ni(OH)_2$.

The H_2 electrode consists of a thin-film of Pt black catalyst supported on a photo-etched Ni foil substrate, backed by a gas diffusion membrane [47].

The separator is a thin and porous ZrO_2 ceramic cloth. If features excellent electrolyte retention and high ionic conductivity, but is fragile and susceptible to breaking [48]. The electrolyte is a concentrated KOH solution (*e.g.* 31%).

The electrodes can be stacked with two configurations: a) back to back, in which electrodes of the same polarity face each other; b) recirculating design, in which positive electrode, separator, negative electrode and gas membrane are stacked in sequence (electrodes of different polarity face each other) [18].

The electrode stack is contained in a pressure vessel made of Inconel 718 alloy. The vessel is cylindrical with hemispherical ends and can stand operating pressures of 40-80 atm. Ni/H_2 cells are manufactured in various configurations. The individual pressure vessel (IPV) cell contains an electrode stack (single or double) in a pressure vessel (voltage, 1.25 V); in the common pressure vessel (CPV) cell, two stacks are in series in a vessel (voltage, 2.5 V); in the single pressure vessel (SPV) battery, a number of cells (typically 22 [47]) are connected in series and placed in a single vessel.

Cell of this type are typically used in geosynchronous earth-orbit (GEO) satellites and in low earth-orbit (LEO) satellites. The requirements of the two applications are different. LEO satellites require batteries lasting 3-6 years and capable of, typically, 18,000-36,000 cycles; GEO satellites demand longer lives, *e.g.* 15-20 years, and 1500-2000 cycles [48]. In both types, the primary power source is represented by solar panels. When the orbit brings the satellite to the earth shadow (eclipse period), the battery starts to deliver energy. The solar panel will subsequently recharge the battery during sunlit periods.

Figure 2.22 shows the interior of a dual-stack CPV cell, and the 28 V, 16-Ah battery obtained by connecting in series 11 such cells. This battery has been used in a LEO satellite [49].

The cycling characteristics of a 350-Ah IPV cell, tested in a standard LEO regime (charge at 0.43C, discharge at 0.64C to 40% DOD), are presented in Figure 2.23. Practically no change is visible in the voltage profile after 2075 cycles, as compared with the 5th cycle [47].

To achieve long life, a Ni/H_2 battery has to work in a limited temperature range, preferably -10°C to +15°C. Therefore, an accurate

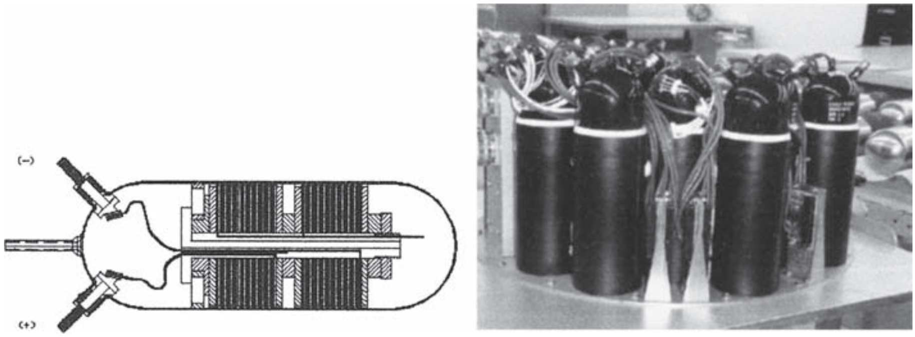

Figure 2.22. Dual-stack CPV Ni/H_2 cell (*left*); 28 V, 16-Ah, 11-cell battery for a LEO satellite (*right*). (*Courtesy of EaglePicherTechnology*)

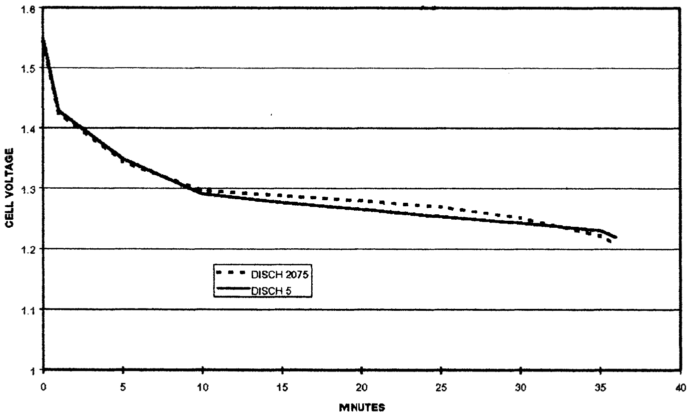

Figure 2.23. Discharge profile during cycling of a 350-Ah, dual stack, IPV cell at 5°C. Continuous line: 5th cycle, dashed line: 2075th cycle. (*From Ref. 47*)

temperature control is needed [48]. Self-discharge for this battery is rather fast even at +10°C, *e.g.* 10% capacity loss after 3 days. This is one major drawback together with low volumetric energy, high cost, high thermal dissipation at high rates, and safety hazards.

The specific energy of Ni/H_2 cells depends on their design and normally follows the order IPV<CPV<SPV (range: 43-55 Wh/kg). The energy density is low compared to the specific energy: 65-80 Wh/L.

A popular LEO is the Hubble Space Telescope, launched in 1990 and still in operation at the end of 2006. In this LEO, the solar arrays charge 6 Ni/H_2 batteries that provide power for about 25 min per orbit [50]. These batteries have also been used in several planetary missions, especially to Mars. The Mars Global Surveyor, launched in 1996, uses 20-Ah, 28 V batteries; the 2001 Mars Odissey combines two types of cells: 11 CPV (2 cells each) plus one IPV, for a total of 23 cells (16 Ah); the Mars Reconnaissance Orbiter, launched in 2005, is powered by a 50-Ah, 11-cell CPV. More information on Ni/H_2 batteries for satellites and planetary missions can be found in Chapter 5 and 6.

Terrestrial applications are mainly in stand-alone photovoltaic systems and stand-by power for emergency or remote sites [48]. The number of these applications is limited, due to the high initial cost of these batteries.

2.6. Nickel/Iron Batteries

The Ni/Fe battery was developed and commercialized at the beginning of the last century by Jungner in Europe and Edison in the U.S.A. It is based on

Fe as a negative electrode and NiOOH as a positive, with the following main total reaction:

$$Fe + 2NiOOH + 2H_2O \rightleftharpoons 2Ni(OH)_2 + Fe(OH)_2 \quad (E_{cell}=1.37\ V)$$

Under deep discharge, a negative-limited cell shows a second discharge step:

$$NiOOH + Fe(OH)_2 \rightleftharpoons Ni(OH)_2 + FeOOH \quad (E_{cell}=1.05\ V)$$

These reactions are highly reversible in the alkaline electrolyte (30% KOH plus ~50 g/L LiOH), particularly for the first step [18]. As the Fe→$Fe(OH)_2$ reduction proceeds through the formation of a the dissolved intermediate ion, $HFeO_2^-$, the mechanism is heterogeneous (both solid and liquid phases involved). FeOOH obtained on deep discharge has the δ structure, and is formed by insertion of a proton into the $Fe(OH)_2$ structure [18].

The electrode materials fill Ni-plated perforated steel tubes or pockets, hence tubular or pocket plate cells are available [51]. The negative electrode is made by dissolving pure Fe in 20-25% H_2SO_4; the $FeSO_4$ so obtained undergoes several treatments until a powder containing Fe and Fe_3O_4 is produced, to which small amounts of additives (S, FeS and HgO) are finally added to reduce gas evolution and improve conductivity [51]. The positive material is made by spraying a $NiSO_4$ solution into hot NaOH, and the resulting precipitate is treated to obtain particles in the range 0.07-0.5 mm. The positive support is filled with alternate layers of $Ni(OH)_2$ and Ni flakes, the latter providing a conductive matrix [2].

Even under abuse conditions, such as shocks and vibrations, overcharge/overdischarge, and storage in a fully charged or discharged state, the Ni/Fe battery can undergo ~3000 deep-discharge cycles with a calendar life of about 20 years. A better cycle life is obtained with positive-limited cells.

Two important corrosion reactions occur in these cells. Fe is thermodynamically unstable in the alkaline solution, so that H_2 is evolved. On the other hand, dissolved O_2 can also be reduced at the negative electrode. Because of these reactions, a high self-discharge occurs, *i.e.* 1-2%/day at 25°C. As H_2 is also evolved on charge, the charge/discharge efficiency is reduced, ranging from 30% for commercially pure Fe to 60% for high-purity Fe [18]. High self-discharge and low coulombic efficiency are not the only drawbacks of this battery: poor energy and power density, poor low-temperature performance, higher cost than Pb/Acid may be added. On the other hand, the extreme ruggedness, resistance to any abuse (see above), and the long cycle life are points in favor of this old system, which has recently been re-proposed in

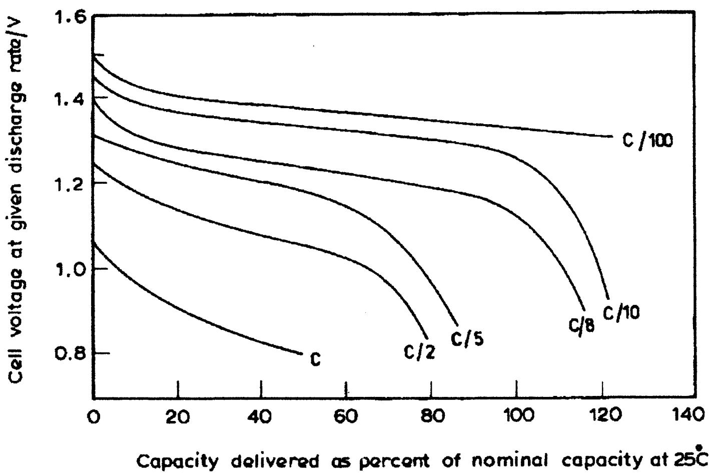

Figure 2.24. Discharge curves of a Ni/Fe cell at various rates at 25°C. (*From Ref. 18*)

advanced configurations.

In Figure 2.24, discharge curves at various rates are presented [18]. The poor rate capability is evident, and the battery nominal voltage, 1.37 V, decreases to 0.85 V at the 1C rate. The combined influence of temperature and rate on battery capacity is presented in Figure 2.25. The poor low-temperature performance is attributable to several factors: besides slower kinetics of the positive electrode and higher electrolyte resistivity, the Fe electrode is more

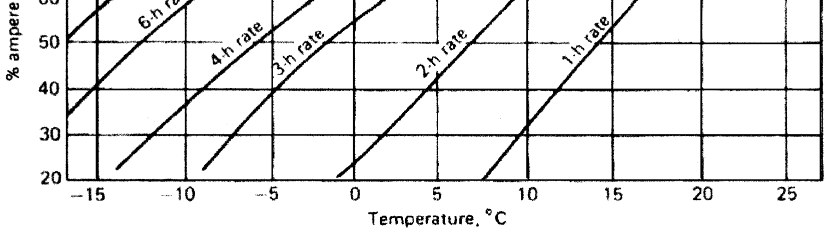

Figure 2.25. Effect of temperature and rate on the capacity of a Ni/Fe cell. (*From Ref. 51*)

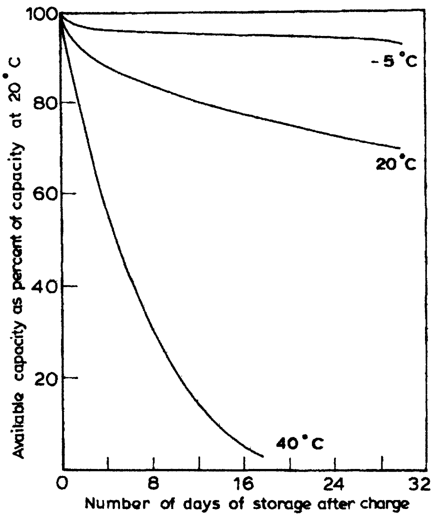

Figure 2.26. Storage characteristics of a Ni/Fe cell at three temperatures. (*From Ref. 18*)

passivated and the intermediate ion $HFeO_2^-$ is less soluble [51]. Using the battery below -15°C even at moderate rates (C/6 or lower) is not allowed. On the other hand, high temperatures are also not recommended in view of the high self-discharge rates. As shown in Figure 2.26, a self-discharge of 8-10%/day can be measured at 40°C [18].

Conventional Ni/Fe batteries have a specific energy of ~30 Wh/kg, an energy density of ~60 Wh/L and a specific power of ~25 W/kg. Advanced batteries have been produced in the last 20 years by several companies. By way of comparison, the characteristics of the SAFT's battery may be mentioned: specific energy: 60 Wh/kg; energy density: 120 Wh/l; specific power: 170 W/kg [2]. These values have been confirmed in actual EV operation, which is one of the possible applications of this battery. Other uses may be in material handling and stationary applications.

2.7. Nickel/Zinc Batteries

In the charged state, a Ni/Zn battery has NiOOH as a positive and Zn as a negative electrode. The latter has a higher specific energy than the Cd electrode, so that the specific energy of this battery, 372 Wh/kg, is higher than that of the Ni/Cd system, 244 Wh/kg. Other pleasant features are: no environmental problems, relatively low cost, good rate capability, and good cycle life. However, problems connected with the use of the Zn anode have so far impaired exploitation of the potentialities of this system. In recent years, a number of solutions have been proposed to favor its commercialization.

The reaction at the positive electrode has been already described. At the negative electrode, the reaction occurs through a first dissolution step:

$$Zn + 4OH^- \rightleftharpoons Zn(OH)_4^{2-} + 2e$$

followed by a precipitation step:

$$Zn(OH)_4^{2-} \rightleftharpoons ZnO + 2OH^- + H_2O$$

Therefore, the overall reaction is:

$$Zn + 2NiOOH + H_2O \rightleftharpoons ZnO + 2Ni(OH)_2 \quad (E_{cell}=1.73\ V)$$

During overcharge, O_2 is evolved at the positive and, in sealed cells, easily recombines at the Zn electrode.

The electrolyte is usually a 31-35% KOH solution, with 1% LiOH to enhance the charge acceptance of NiOOH [18,52]. However, it has been recently ascertained that a KOH concentration in the range 20-25% increases the cycle life, as Zn solubility and migration are reduced. ZnO is even more soluble than Zn in KOH, whereby formation of the zincate takes place.

The problems connected with the use of a Zn electrode in a concentrated alkaline solution can be summarized as [53]:

Dendrite growth. During charge, Zn deposits at points of high current density, with formation of dendrites that can pierce the separator and short the cell.

Zn Corrosion. Zn in KOH is corroded to produce zincate and H_2. This reaction obviously results in a relatively fast self-discharge.

Shape change. On repeated cycling, there is a relocation of Zn from the edges to the centre of the electrode plate. This process (densification) reduces the surface area of the electrode and is a consequence of Zn replating from solution.

Zn Poisoning of the Ni Electrode. On cycling, especially at high DOD, zincate ions reprecipitate as ZnO onto the Ni electrode, this blocking its pores and causing capacity loss.

All these drawbacks could be tackled by reducing the Zn and ZnO solubility. To this end, in addition to the use of a less concentrated KOH solution, approaches based on electrode additives have proven effective. $Ca(OH)_2$ is especially useful when coupled to a ZnO electrode (the cells are normally assembled in the discharged state). Formation of Ca zincate through the reaction:

$$Ca(OH)_2 + 2ZnO + 4H_2O \rightleftharpoons Ca[Zn(OH)_3]_2 \cdot 2H_2O$$

takes place [52]. The zincate is thermodynamically stable and insoluble in alkali. It forms a passivating film at the electrode/electrolyte interface that greatly limits dissolution of Zn formed on charge. On the other hand, the poor electronic conductivity of the film creates concern in terms of rate capability. This can be mitigated by adding conductive metallic oxides, such as PbO or Bi_2O_3.

There are two ways of preparing the Ca zincate electrode. $Ca(OH)_2$ can be directly mixed with ZnO and, during the formation process, the zincate is formed *in situ*. Alternatively, the zincate is formed separately and the electrode is prepared with it. The Ni electrode may be of the sintered or non-sintered type [52,53].

A microporous polypropylene separator is commonly used, as it is chemically stable in concentrated alkaline solution and proves an excellent barrier to zinc migration [52].

Typical characteristics of the Ni/Zn battery are: specific energy, 50-60 Wh/kg; energy density, 80-120 Wh/L; specific power, 280 W/kg; cycle life (100% DOD), ~500 cycles. The capacity loss on standing is ~20%/month at 25°C.

In Figure 2.27, the dependence of the capacity of a 30-Ah battery on rate and temperature is presented. It may be appreciated that the capacity

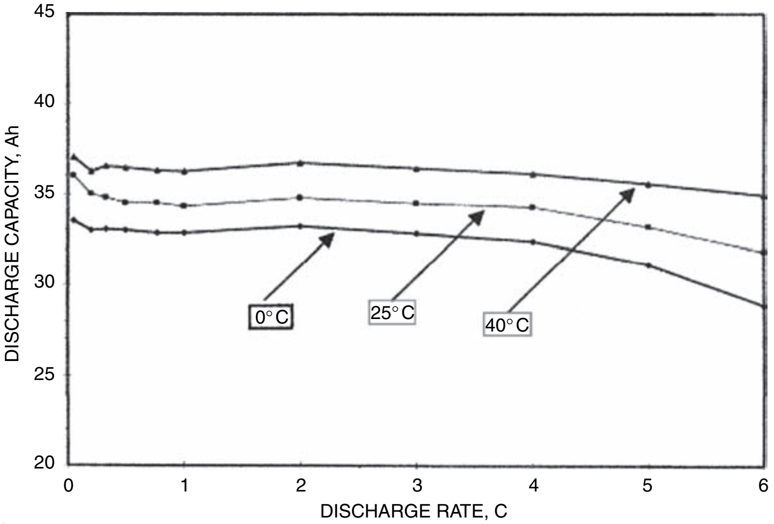

Figure 2.27. Capacity of a 30-Ah Ni/Zn cell as a function of temperature and rate. (*Courtesy of Evercel*)

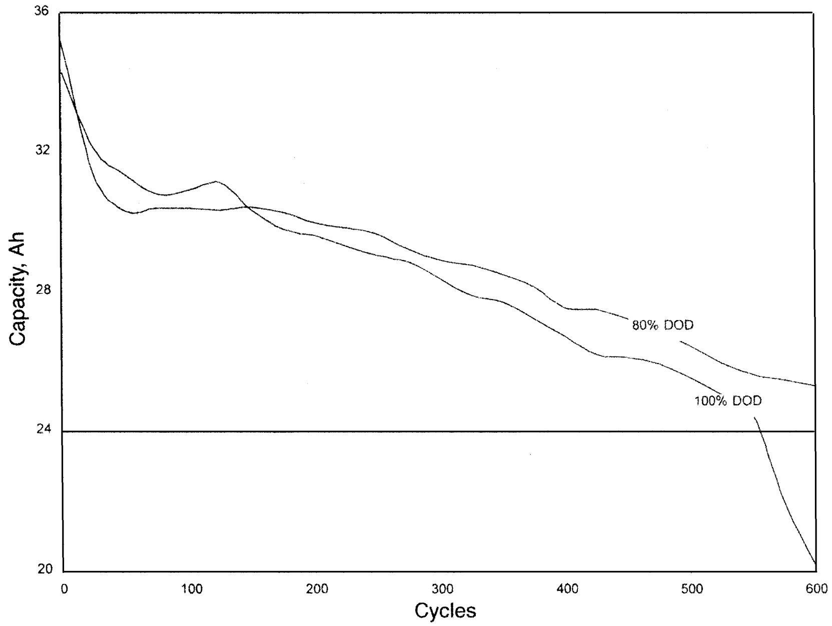

Figure 2.28. Cycle life of 30-Ah Ni/Zn batteries. Discharge at 0.2C. (*Courtesy of Evercel*)

moderately decreases as the rate increases up to 6C. The decrease is obviously more marked at 0°C, but the performance is still satisfactory at all rates.

In Figure 2.28, the cycle life characteristics are shown. The battery can give 600 cycles at 80% DOD while retaining more than 80% of its rated capacity. At 100% DOD, the battery achieves 550 cycles.

The Ni/Zn battery has been used in motive applications, such as scooters and EV. EV batteries are claimed to have a performance similar to that of the Ni/MH ones, but at a much lower cost. 288-V packs mounted on two-passenger or utility vehicles are reported to provide an effective range of up to 240 km, and a top speed of 130 km/h. A hybrid all-electric car, equipped with a high-energy Zn/Air battery and a high-power Ni/Zn battery (for acceleration), recently proved able to run for 525 km on a single charge, which is the best performance of all times for an EV [54]. However, the limited cyclability of the Ni/Zn system does not allow foreseeing a bright future in this application.

2.8 Zinc/Air Batteries

The Zn/Air battery uses Zn metal as a negative electrode and O_2 from the air as a positive electrode. O_2 diffuses through the electrode support and after reaching the interface with the alkaline electrolyte, is catalytically reduced. In this respect, the positive of a Zn/Air cell resembles the one of a fuel cell. Since one active electrode material (O_2) is outside the cell, the other (Zn) occupy most of the cell volume. As the energy of the cell only depends on that of Zn, which is rather high (1300 Wh/kg), the theoretical energy of the Zn/air cell is also high. (1350 Wh/kg). Problems with the use of a Zn electrode in an alkaline solution have been mentioned (see the Ni/Zn battery). Other problems arise with the use of the O_2 electrode, this justifying the limited commercial success of this system. For industrial applications, both primary and secondary batteries can be used.

At the negative electrode, the reaction in the alkaline solution occurs through the dissolution/ precipitation steps described in the previous section:

$$Zn + 4OH^- \rightleftharpoons Zn(OH)_4^{2-} + 2e; \quad Zn(OH)_4^{2-} \rightleftharpoons ZnO + 2OH^- + H_2O$$

At the positive electrode, the reaction is:

$$1/2O_2 + H_2O + 2e \rightleftharpoons 2OH^-$$

Therefore, the overall reaction is just Zn oxidation:

$$Zn + 1/2O_2 \rightleftharpoons ZnO \qquad (E_{cell}=1.6\ V)$$

The Zn electrode can be manufactured with different techniques. In primary cells, it is a high-purity foil containing small amounts of metals (*e.g.* Pb and In) to decrease H_2 evolution. In secondary cells, several types of electrode structure have been studied: 1) ZnO powder combined with binders and a current collector: during the formation cycle, a porous, high-surface area matrix is obtained [55]; 2) Zn powder combined with electrolyte and a gelling agent, with particles sizes in the range 20 to 820 µm (this is the most used type) [55]; 3) Zn foil (see above); 4) Zn bed formed by Zn and/or Zn-coated particles [56].

In rechargeable cells, Zn is the capacity limiting electrode, but not the life limiting factor, and can be cycled to nearly 100% of its theoretical capacity.

The air electrode has carbon as the primary structural component. In a typical battery configuration, such as that with two air electrodes of Figure 2.29, the electrode is made as follows. Carbon black is mixed with a binder; the current collector is expanded Ni metal; a hydrophobic gas diffusion layer is on the air side and a hydrophilic catalyst layer is on the electrolyte side. A number of catalysts have been proposed, such as metals, metal organic macrocycles, and transition metal oxides, *e.g.* pyrochlores, perovskites or spinels [55]. The first two categories are mainly used in primary cells, while metal oxides have demonstrated bifunctional activity, *i.e.* they can catalyze both O_2 reduction and formation.

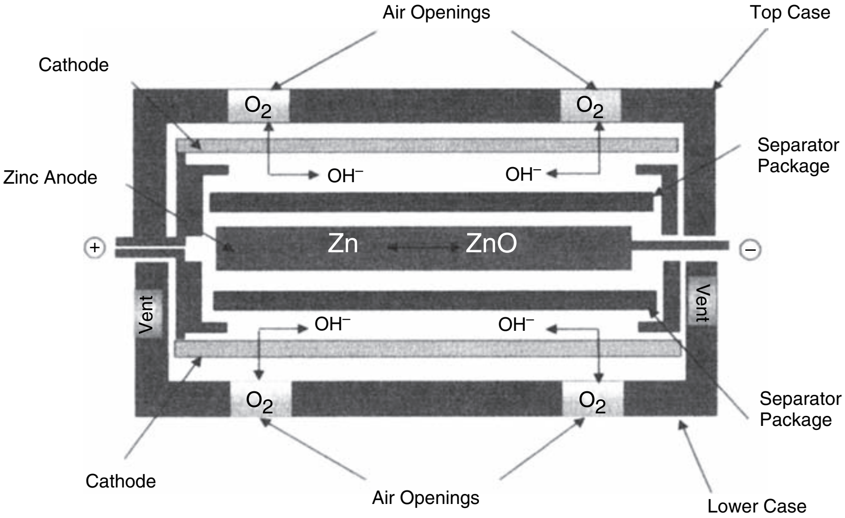

Figure 2.29. Cross-section of a Zn/Air cell with a dual air electrode. (*From Ref. 55*)

Primary Zn/Air batteries are usually very large (more than 1000 Ah) and have been used for many years in such applications as railroad signaling, seismic telemetry, buoys, and remote installations [56]. Reserve, water-activated batteries or pre-activated batteries (in some versions, with gelled electrolyte) are available. A typical Zn/Air primary battery is the so-called Edison Carbonaire, formed by two or three cells in series or parallel, with capacities ranging from 1100 to 3300 Ah. An 1100-Ah battery can provide its nominal capacity at the maximum rate of 1.25 A [56].

Secondary Zn/Air batteries can be quite different according to the recharge procedure, which can be electrical or mechanical. In turn, the latter may involve replacement of the entire Zn compartment or the Zn powder only.

Electrically rechargeable batteries are based on the bifunctional O_2 electrode, while the negative can be Zn foil, high-porosity Zn or a Zn paste [55,56]. Large batteries, *e.g.* for traction purposes, prefer the last type of negative electrode. Cycle life may largely vary according to the DOD and is generally short at high DOD, as shown in Figure 2.30 [55]. The steady capacity fade has not to be related to the Zn electrode, but to electrolyte carbonation and H_2O loss. Therefore, cells of this type have to provide means for removing CO_2 while allowing a certain humidity level in the incoming air. Other drawbacks are the limited rate capability and the short separator life.

Batteries proposed for electric traction are based upon a mechanical substitution of the exhausted Zn electrodes. Such batteries have been tested on the road, especially in buses and vans. A typical module has 47 cells, an

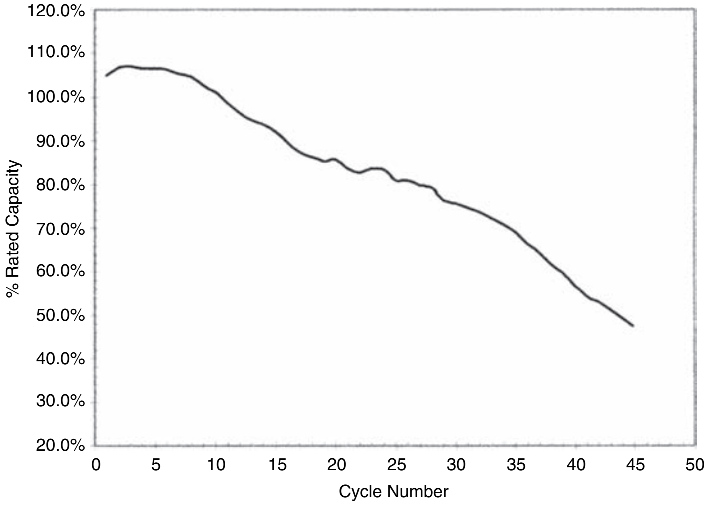

Figure 2.30. Typical cycling profile of an electrically rechargeable Zn/Air cell (100% DOD). (*From Ref. 55*)

operating voltage range of 57-40 V, a capacity of 325 Ah, a specific energy of 200 Wh/kg, and an energy density of 220 Wh/L (total energy, 17.4 kWh) [57]. A transit bus is powered by 3 trays of 6 modules each, for a total of 312 kWh. Depleted modules are substituted by new ones at servicing stations. The former are sent to a regeneration plant, where the zinc anodes are regenerated by submitting the ZnO formed on discharge to electrowinning. This procedure, illustrated in Figure 2.31, raises obvious concern for logistic and cost reasons.

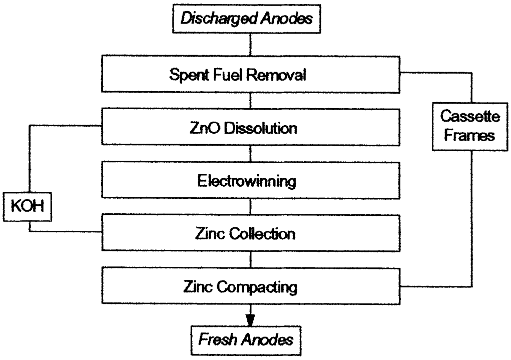

Figure 2.31. Scheme of anode regeneration for a mechanically rechargeable Zn/Air battery. (*From Ref. 57*)

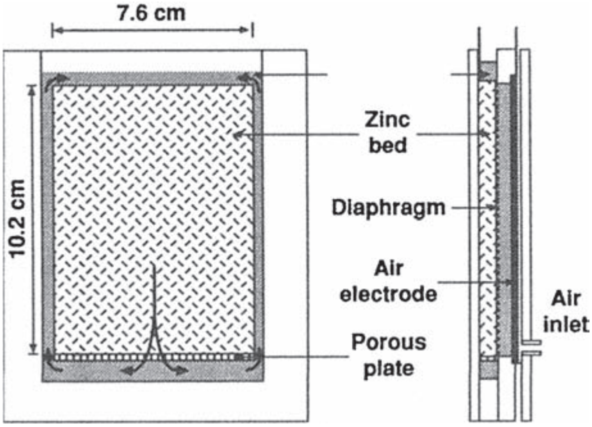

Figure 2.32. Schematic of the packed-bed Zn/Air cell developed at the Lawrence Berkeley Laboratory. (*From Ref. 58*)

Zn/Air cells may be formed with the so-called packed bed of Zn powder, as shown in Figure 2.32. Metallic Zn particles, or seed particles onto which Zn is deposited, form a bed and natural convection is used for electrolyte circulation through it. Laboratory cells of this type, designed for optimum capacity, provide specific energies of 200 Wh/kg in urban driving cycle, which increase to 290 Wh/kg at 55°C [2]. Spent electrolyte and particles are suctioned from the cell and replaced with fresh slurry obtained with an electrowinning process.

2. 9. Silver/Zinc Batteries

Silver/Zinc batteries are attractive by virtue of their high specific energy and energy density, proven reliability and safety, and the highest power output per unit weight and volume of all commercially available batteries [59]. They can be even discharged at the 20C rate. However, notable disadvantages, *i.e.* low cycle life (50-100 cycles), poor performance at low temperature and high cost, have limited their use to some specific applications [60].

The characteristics of the negative Zn electrode in an alkaline solution (35-45% KOH) have already been mentioned. Its discharge product is ZnO. The positive electrode may be either the peroxide AgO or the monoxide Ag_2O, whose reduction reactions are:

$$2AgO + H_2O + 2e \rightleftharpoons Ag_2O + 2OH^- \; ; \; Ag_2O + H_2O + 2e \rightleftharpoons 2Ag + 2OH^-$$

The Zn/AgO couple has an OCV of 1.86 V, whereas the Zn/Ag_2O couple has an OCV of 1.60 V. AgO has nearly twice the capacity of Ag_2O, 0.43 Ah/g *vs.* 0.23 Ah/g, so it is certainly desirable to use the former as a positive. However, AgO is unstable both in dry charged batteries (reserve batteries) and in activated batteries, at it tends to react with Ag support to give Ag_2O. Therefore, Ag_2O may preferentially be used, in spite of its lower capacity, also in view of these advantages: the voltage of its plateau is more stable at high rates and the separator is not damaged by this material, so that a longer wet life and cycle life is obtained [61].

Many Zn/AgO batteries have positives formed from sintered Ag anodized in KOH solution. Typically, the electroformed electrodes contain Ag, AgO and Ag_2O along with some impurities (especially Ag_2CO_3). If chemically prepared AgO is used, the secondary reaction between AgO and Ag can be minimized [62]. The Zn electrodes are made by dry pressing, by a slurry method or by electrodeposition. They contain small amounts of metal oxides to limit corrosion in the alkaline solution [60]. Self-discharge amounts to ~5%/month at 20°C.

Silver/Zinc batteries are especially produced as prismatic batteries with flat electrodes wrapped with multiple layers of separator (up to three different separators may be used) [60]. Typical discharge curves are shown in Figure 2.33. At high rates, the plateau of the AgO→Ag_2O step is not visible. As mentioned above, this system is especially notable for its high specific power: conventional high rate cells may give 1.5-1.8 kW/kg, which may become 3.7-4.3 kW/kg, by using thin electrodes and thin separators, or even 5.5 kW/kg in batteries with bipolar electrodes [61]. These unusually high power characteristics are especially exploited in space applications. An example is

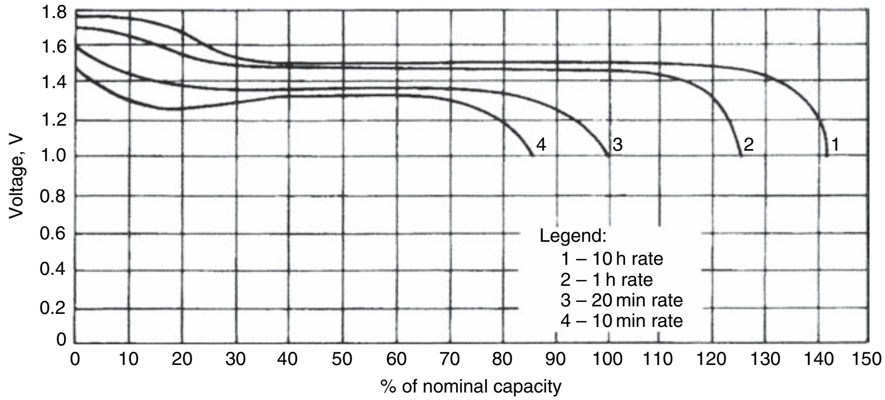

Figure 2.33. Discharge curves of a Zn/AgO battery at various rates (20°C). (*From Ref. 60*)

provided by the 150 Ah, 28 V battery for the Atlas V launch vehicle used for the Mars Reconnaissance Orbiter (August 2005) [63]. The Silver/Zinc battery has also been used by the astronauts of several missions in all their extravehicular activities [59,60].

2.10. Zinc/Bromine Batteries

The concept of Zn/Br_2 battery is rather old, but its development was long thwarted by: 1) the Zn plating in dendritic form that could short-circuit the cell; 2) the solubility of Br_2 in the $ZnBr_2$ solution that accelerates self-discharge. Only by resorting to a complex system with electrolyte circulation, during battery operation, and its confinement in reservoirs, during stand-by, development could be fulfilled. A schematic of this system is shown in Figure 2.34. Its basic components are: 1) a stack of bipolar electrodes; 2) a micro-porous separator; 3) a reservoir for the electrolyte circulating at the negative electrode, also including a heat exchanger (not shown); 4) another reservoir for the electrolyte circulating at the positive, which includes a smaller reservoir for the bromine complex; 5) pumps and manifolds.

The negative electrode is obtained by plating Zn on one side of the bipolar support, whereas the positive electrode is Br_2 obtained by oxidation of

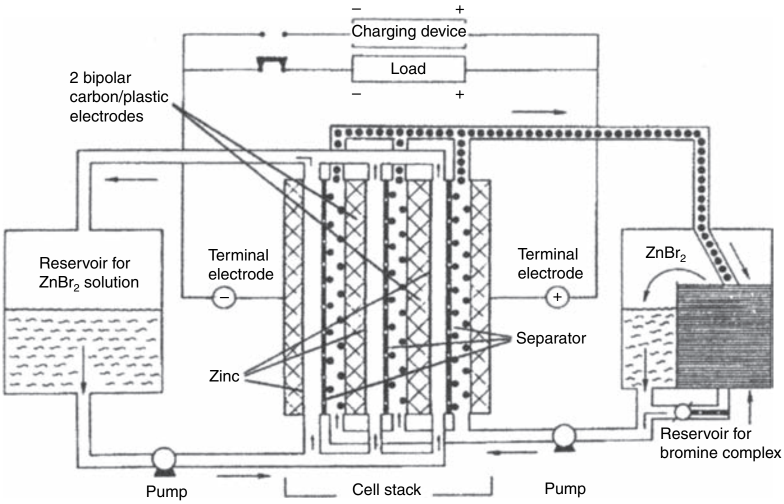

Figure 2.34. Schematic of a Zn/Br_2 battery with the cell stack based on bipolar electrodes. (*From Ref. 64*)

Br^- at the other side of the support. The total reaction may be written in the simple form:

$$Zn + Br_2 \rightleftharpoons ZnBr_2 \qquad (E_{cell} = 1.85\ V)$$

Diffusion of Br_2 towards the Zn deposit is largely impeded by the microporous separator. However, to keep to a low level the concentration of the corrosive Br_2, a complexing agent is used. This is an alkylammonium salt, *e.g.* N-methyl-N-ethylmorpholinium bromide, which associates with the polybromide ions resulting from the reaction of Br_2 and Br^-, thus forming a low-solubility second liquid phase [65]. This complex is stored in the reservoir shown in Figure 2.34, where it settles by gravity.

The bipolar electrode is a composite of carbon, high-density polyethylene and glass reinforcement. The separator is made from silica-filled polyethylene [66]. Pumps, reservoirs and tubing are all made from plastic materials to avoid attack from Br_2. The heat exchanger needed for thermal management is also made from plastics. The solution pH is adjusted around 3, as higher values cause Zn plating in an undesirable mossy form, whereas lower values result in increased Zn corrosion [65].

A battery with non-flowing electrolyte has also been projected. This concept is only applied to relatively small batteries (few kWh) to be used in small vehicles [66].

A typical charge/discharge cycle of a Zn/Br_2 battery is shown in Figure

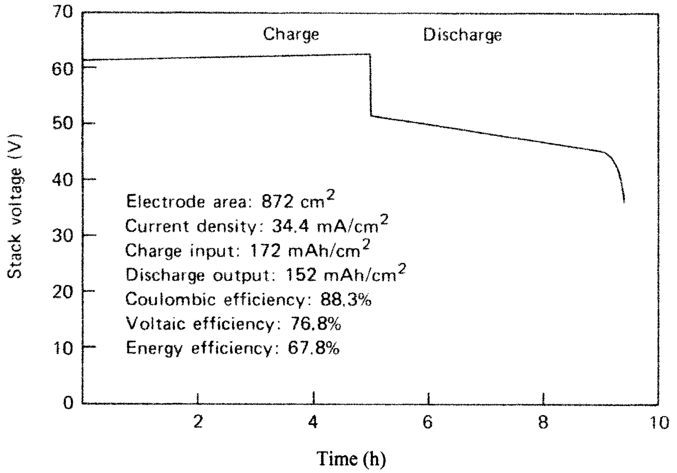

Figure 2.35. Charge/discharge cycle of a 30-cell, 1.4 kW Zn/Br_2 battery. (*From Ref. 68*)

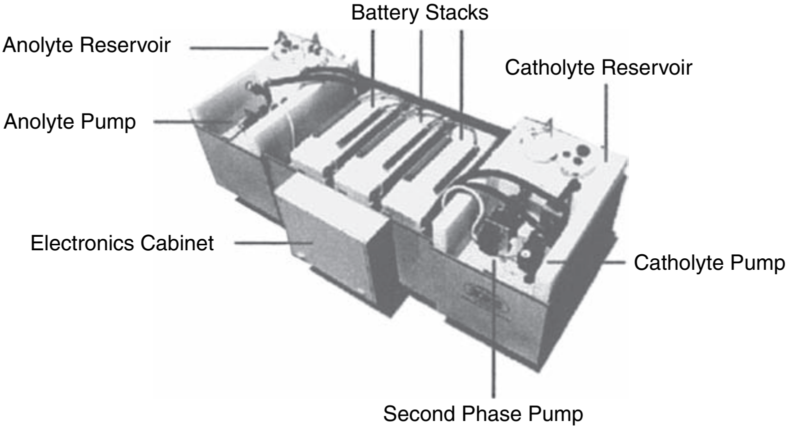

Figure 2.36. 50-kWh Zn/Br_2 module: it consists of three battery stacks connected in parallel. Each stack contains 60 cells. (*By ZBB Energy Corp., from Ref. 68*)

2.35 [67]. The battery performance is good at all rates and can be summarized in the following points: high specific energy (65–85 Wh/kg as compared to around 35 Wh/kg for Pb/Acid); tolerance to deep discharge: the battery can be discharged to 100% DOD without damage; long cycle life: the battery can exceed 2000 full charge/discharge cycles during its operating lifetime [66].

Two factors may negatively affect the battery performance: shunt current and the portion of energy requested by the auxiliary systems. The former factor (a self-discharge) occurs because the voltage difference between cells in the stack may create parasitic currents through the electrolyte flowing in the common channels. Therefore, the channels are made long and thin to increase the resistance in the shunt circuit [67]. The shunt current can also be reduced by building stacks with a high number of cells: a 60-cell stack is reported to loose 1% only of its capacity because of this current [65].

Figure 2.36 shows a 50-kWh module made by connecting in parallel three 60-cell stacks [68]. The stacks are flanked by the electrolyte tanks and the pumping systems. The electronics cabinet allows a correct battery management. A stationary battery can be formed with 10 modules arranged in two strings of five modules in series (540 V). The two strings are not connected in parallel and operate as separate batteries. A continuous discharge can be made at 600 A, thus giving the maximum power (250 kW) for two hours (500 kWh) [69].

The Zn/Br_2 battery is especially intended for stationary applications: utility load management, solar and wind energy storage, emergency back-up power and UPS [66]. These systems may have capacities as high as 2 MWh.

Traction batteries, with energies in the range 5-45 kWh, have been tested in small cars and buses [65].

2.11. Vanadium Redox-Flow Batteries

The flowing electrolyte concept of the Zn/Br_2 cell has also been exploited in the redox-flow batteries, characterized by the fact that all reactants are ionic species. The most developed battery of this type is the vanadium redox-flow battery (VRB), whose electrode reactions involve different oxidation states of vanadium. Absence of solid phases and electrolyte circulation confer to this battery an exceptionally high power capability. Other pleasant features are: 1) the capacity can be increased by just increasing the electrolyte volume; 2) full discharge is possible without detrimental effects; 3) the solution can be used for an indefinite time; 4) self-discharge is negligible; 5) the battery response is instantaneous (<1 msec).

The electrolyte flowing in the negative compartment contains the redox couple V^{2+}/V^{3+} as $VSO_4/V_2(SO_4)_3$, while the positive compartment contains the couple VO^{2+}/VO_2^+ as $VOSO_4/(VO_2)_2SO_4$ (V^{4+}/V^{5+}). The electrode reactions at are:

Negative electrode: $V^{2+} \rightleftharpoons V^{3+} + e$ ($E_o = -0.26$ V)

Positive electrode: $VO_2^+ + 2H^+ + e \rightleftharpoons VO^{2+} + H_2O$ ($E_o = 1.00$ V)

The total reaction is (discharge from left to right):

$$V^{2+} + VO^{2+} + 2H^+ \rightleftharpoons V^{3+} + VO_2^+ + H_2O$$

At the 1 M concentration for each vanadium species and at 25°C, the

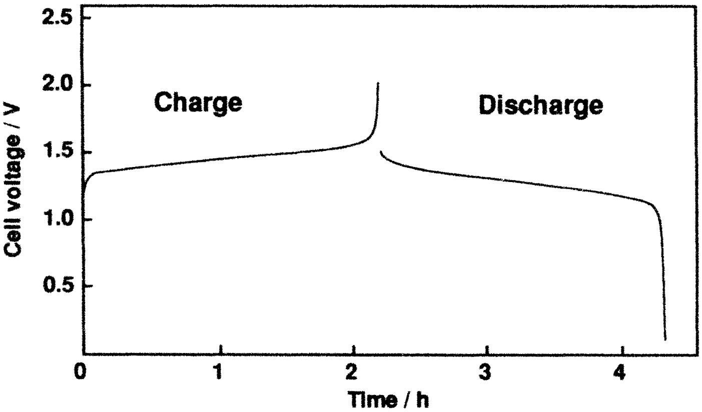

Figure 2.37. Charge/discharge curve for a VRB at 30 mA/cm^2 (35°C). (*From Ref. 70*)

standard potential is 1.26 V. In practical batteries, the vanadium concentration is around 2 M in 2-4 M H_2SO_4. So, the actual OCV for a charged cell is ~1.6 V. In Figure 2.37, the charge/discharge profile of a VRB is shown. The operating voltage is in the range 1.5-1.0 V and the energy efficiency is ~85%.

The cell scheme is similar to that of the Zn/Br_2 battery, with stacks of bipolar electrodes and electrolyte tanks, as shown in Figure 2.38. The bipolar electrodes are made of graphite-polyethylene plates onto which graphite felt is bonded. The felt acts as a substrate for electron transfer and as a flow-through electrode with a large surface area [2]. The end electrodes have felt on one side and plated Cu on the other side to minimize ohmic losses. These electrodes have now reached resistivities as low as 0.6 ohm cm^2 (0.8 ohm cm^2 for the end electrodes). A cation-exchange membrane acts as an efficient separator: mixing of the electrolytes would correspond to a self-discharge. Microporous separators of much lower cost are also under investigation.

The VRB can be used in several stationary applications, *e.g.* load levelling, momentary voltage sag suppression, emergency power supply, wind/solar power generation stabilization, power demand and supply control [71,72]. Studies on traction applications have been carried out [2].

The positive features of the VRB are counterbalanced by rather low specific energies and energy densities. For a battery to be used in electrical energy storage (4 stacks in series of 80 cells each, for a total energy of 444 kWh), a specific energy of 20 Wh/kg and an energy density of 30 Wh/L have been calculated [73]. By increasing the vanadium concentration to 3 M (in 5 M

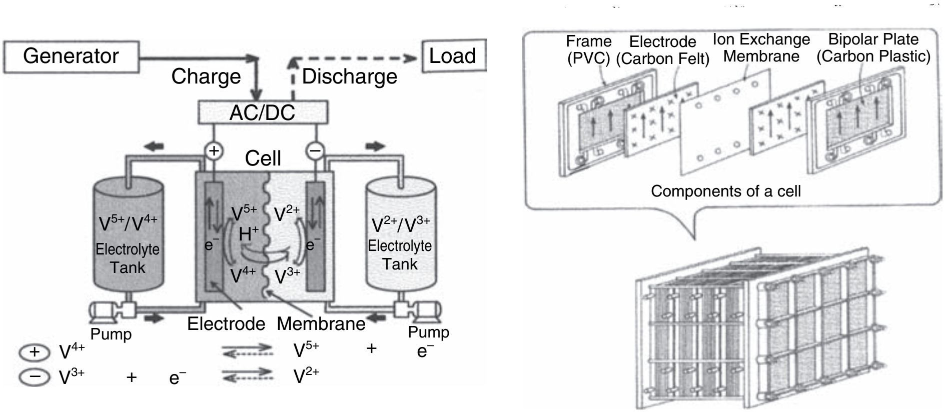

Figure 2.38. Schematic of the VRB (*left*) and construction of the cell stack (*right*). (*From Ref. 71*)

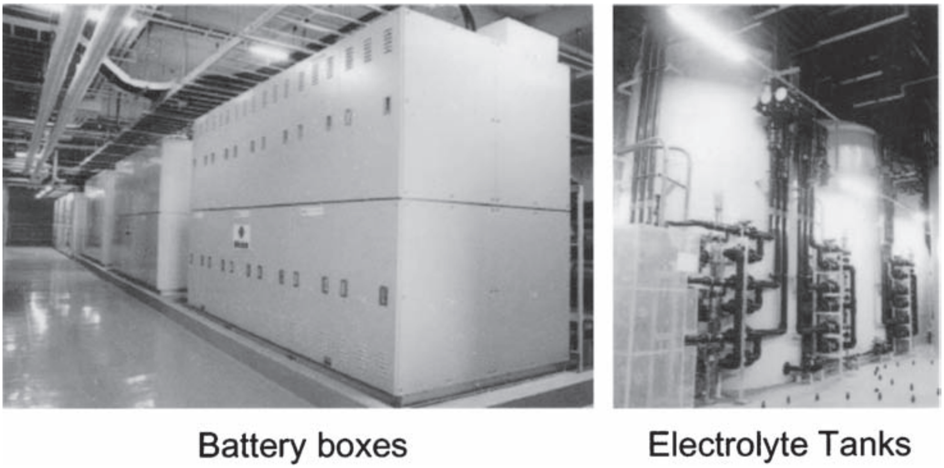

Battery boxes

Electrolyte Tanks

Figure 2.39. VRB battery for load levelling (AC 1500 kWx1h) and voltage sag protection (AC 3000 kWx1.5 sec) (*From Ref. 71*)

H_2SO_4), the energies could become 28 Wh/kg and 47 Wh/L, respectively, but high concentrations have been found to favor precipitation of V^{5+} as V_2O_5 [74]. The above battery could give more than 3000 cycles in the operating temperature range 10-45°C [73].

An example of large VRB used for load levelling and voltage sag protection is shown in Figure 2.39. The battery cubicle and the electrolyte tank form separate units. Under normal conditions, load levelling operation is conducted, but in case of instantaneous voltage sag the battery can provide at once the very high power necessary to avoid interruptions. In general, the power output of a VRB may be raised by increasing the electrolyte flow rate or the number of cells in the stack. At the current stage of development, the stack membrane is the component more prone to deterioration and has to be replaced every five years [73].

2.12. Alkaline Primary Batteries

Alkaline batteries are the only primary aqueous batteries of interest in industrial applications (except primary Ag-Zn for space). Their rechargeable analogues, RAM batteries (rechargeable alkaline manganese), are not used at the industrial level because of their limited rate capability and rechargeability.

In the early 1960s, alkaline Zn/MnO_2 batteries were introduced and widely accepted for some benefits with respect to other primary aqueous batteries:

- Long service life at continuous, high drain discharge
- No need for "rest periods"
- Low internal resistance
- Rugged, shock-resistant construction
- Cost-effective on a cost-per-hour-of-service basis
- Acceptable low temperature performance
- Excellent leakage resistance
- Long shelf-life at ambient temperature

Nowadays, the use of these batteries in industrial applications is decreasing. Li primary batteries or different rechargeable batteries are generally preferred whenever cost is not the main factor.

2.12.1. Electrode Materials and Processes

The anode of alkaline Zn/MnO_2 is essentially high-purity Zn powder. Its high surface area can affords relatively high discharge rates, while the electrolyte is uniformly distributed. Furthermore, the combination of a porous anode and a conductive electrolyte reduces the extent of accumulation of reaction products near the electrode, this resulting in lower polarization. The practice of adding Hg, Pb or other heavy metals as gassing suppressors has been eliminated or greatly reduced. This has been made possible by a substantial reduction of the impurity level in the zinc powder, with particular reference to iron. A gelling agent is instead necessary for immobilizing the electrolyte contained in the anode and for improving its processibility. To this end, starch, cellulose derivatives or polyacrylates are often used. The electrolyte is an aqueous KOH solution (35-52%), featuring higher conductivity and reduced gassing (Zn corrosion) in comparison with the acidic solutions used in Zn-Carbon cells.

The cathode is based on electrolytic MnO_2 (EMD), as only this form can grant high power and long shelf life. EMD contains ~92% MnO_2, ~4.5% H_2O and several ionic impurities. The electronic conductor is carbon in the form of graphite, although some acetylene black may also be used to enhance the surface area.

The separator, which has to be chemically stable in the concentrated alkaline solution, is normally a nonwoven fabric, as cellulose, vinyl polymer, polyolefin, or their combination.

The high porosity of cathode, anode and separator allows their saturation with the electrolyte. The homogeneous distribution and the high conductivity of the electrolyte afford high discharge rates also on continuous drains.

The electrochemical reactions occurring at the electrodes may be described as follows.

Anode: $Zn + 2\ OH^- \rightarrow Zn(OH)_2 + 2e$

Due to the limited amount of water present at the anode, $Zn(OH)_2$ slowly looses H_2O [$Zn(OH)_2 \rightarrow ZnO + H_2O$].

Cathode: $MnO_2 + H_2O + e \rightarrow MnOOH + OH^-$

In this process, Mn^{IV} is reduced to Mn^{III} through the insertion of H^+ into the structure of electrolytic MnO_2. The overall reaction, in a discharge limited to the formation of MnOOH, is:

$$Zn + 2\ MnO_2 + 2\ H_2O \rightarrow 2\ MnOOH + Zn(OH)_2$$

In a prolonged discharge, the reduction of MnO_2 proceeds to the formation of Mn_3O_4. However, this reaction, to which a flat voltage-time curve corresponds, is usually not exploited.

Zn powder is obviously quite reactive and can decompose H_2O with the production of hydrogen. The latter can in turn cause MnO_2 self-discharge, not to mention the overpressure it generates in the battery. As mentioned above, reducing the impurity level in the Zn powder greatly limits gassing. Otherwise, additives for the anode are necessary, such as ZnO (or other oxides) or organic inhibitors (polyethylene oxide compounds).

2.12.2. Cell Construction

Cylindrical cells

A cylindrical alkaline cell is shown in Figure 2.40. The can is not an active material, but is made of steel or nickel-plated steel and acts as the cathode current collector. The cathode is pressed against the steel can by one of two processes: applying a high pressure to the powder when in contact with the can, or forming annular pellets, which are then inserted into the can. The Zn powder is allocated in the central cavity, around a brass current collector welded to the cell bottom (negative cap).

The anode cap is separated from the positive cell can by an insulator. A plastic grommet, sealed to the cell can, ensures that the cell is leak-proof. The grommet incorporates a membrane vent for relieving overpressure in case of short circuits or cell abuse.

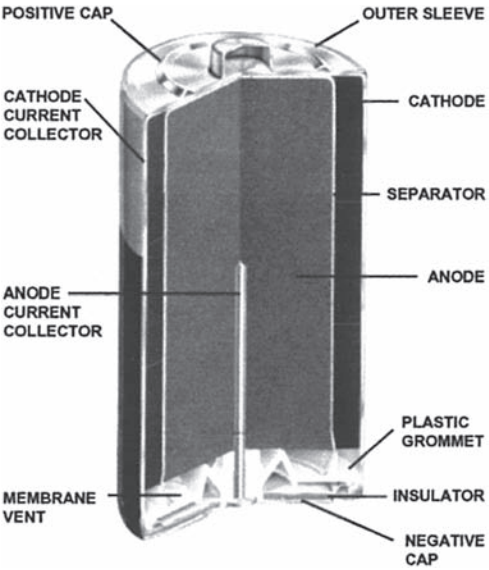

Figure 2.40. Cross section of a cylindrical alkaline cell. *(Courtesy of Duracell)*

Cylindrical cells can be manufactured in standard sizes and can reach high nominal capacities. For instance D cells (34x61 mm) have capacities of 14-18 Ah, and F cells (33x91 mm) of 22 Ah.

Prismatic batteries

Multicell prismatic batteries have voltages in the range 4.5-9 V. Their capacities range from <1 Ah to 44 Ah for a 6-V battery.

2.12.3. Cell Performance and Applications

In Figure 2.41, typical discharge curves at room temperature of an AA cell are shown at different rates. The nominal capacity, 2.8 Ah, is delivered at low rate (C/140), while 2.1 Ah can be drawn at the C/10 rate. This capacity retention can be judged as satisfactory, but lags behind that of spirally wound primary Li cells, as Li/MnO_2 and Li/$SOCl_2$, designed for high-rate applications [79]. In 1999, premium alkaline cells have been commercialized. They are capable of a better performance at high discharge rates than the standard models. This has been made possible by a further reduction of the cell resistance through: coatings applied to both the negative and positive current collector; using a finer graphite grade; and, packing more MnO_2 into the space available for the

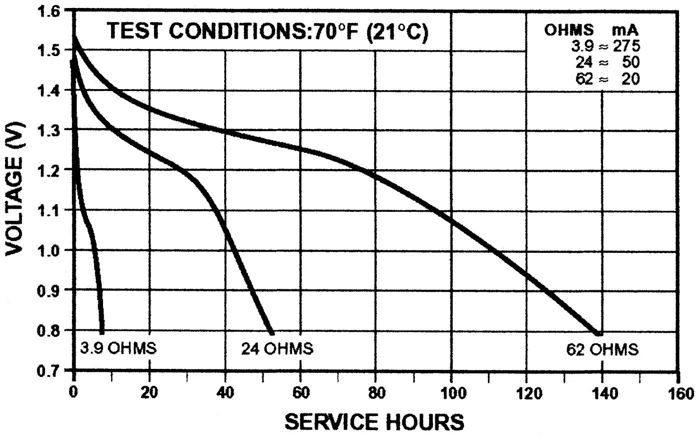

Figure 2.41. Discharge curves at 21°C of an AA-size alkaline cell. Based on a nominal capacity of 2.8 Ah, the rates are: C/140 at 62 Ω, C/56 at 24 Ω and C/10 at 3.9 Ω. (*Courtesy of Duracell*)

cathode. Coating reduces the build up of corrosion products on the current collectors, while a finer graphite powder improves the electronic conductivity.

In Figure 2.42, the behavior of alkaline batteries as a function of

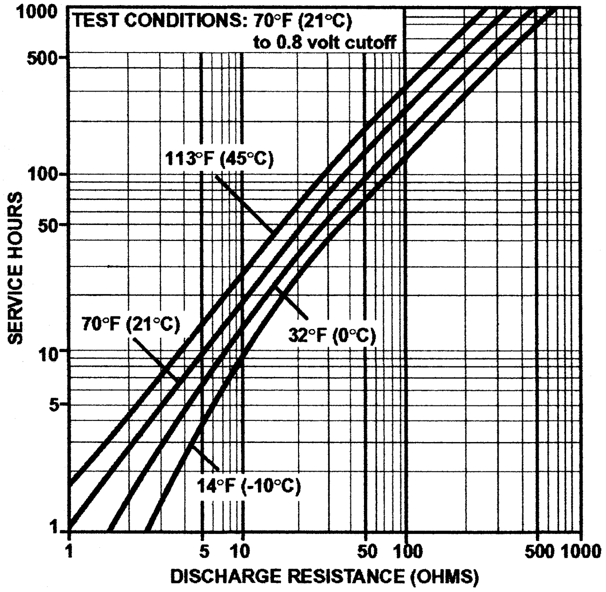

Figure 2.42. Discharge curves of a D-size alkaline cell at various temperatures. (*Courtesy of Duracell*)

Table 2.5. Characteristics of Pb/Acid and Ni/Cd batteries. (*From Refs. 2, 75-78*)

System	Voltage Range (V)	Operating Temperature (°C)	Cycle Life (cycles)^b	Specific Energy (Wh/kg)	Energy Density (Wh/L)	Specific Power ^{c}	Self-Discharge (%/month)
Pb/Acid^a							
SLI	2.0-1.8	-40÷55	200-500	35	70	H	3
Traction	“	-20÷40	1500	25-30	80	MH	4-6
Stationary	“	-10÷40	400	20-30	50-70	MH	2
Ni/Cd^a							
Vented Pocket Plate	1.35-1.1	-20÷45	500-2000	15-35	35-45	H	5
Vented Sintered Plate	“	-40÷40	“	30-40	60-100	H	10
FNC	1.35-1.0	-50÷60	500-3000+	10-40	15-80	L to VH	10-15
Sealed	“	-40÷45	300-700	15-35	50-120	M to H	15-20

a. cell level; b. dependent on DOD; c. pulse discharge (L=low, M=moderate, H=high, MH=moderately high, VH=very high)

Table 2.6. Characteristics of aqueous secondary batteries (except Pb/Acid and Ni/Cd). (*From Refs. 75-78*)

System	V Range (V)	Operating Temperature (°C)	Cycle Life (cycles)^c	Specific Energy (Wh/kg)	Energy Density (Wh/L)	Specific Power ^{d}	Self-Discharge (%/month)
Ni/MH^a	1.4-1.2	-30÷65	800-1200	60-80	200-270	M to H	25-30
Ni/H$_2^a$	1.5-1.2	-10÷30	>2000	45-55	65-80	M	60
Ni/Fe^a	“	-10÷60	2000-3000	30	60	L to M	25-30
Ni/Zn^b	1-9-1.5	-20÷50	300-600	60	100-120	H	15-20
Zn/Air^b	1.2-1.0	0÷45	20-30	150-200	160-220	L to M	
Zn/AgO^a	1.8-1.5	-20÷60	50-80	90-100	180	VH	5
Zn/Br$_2^b$	1.9-1.6	10÷50	>500	65-70	60-70	L to M	12-15
VRB^b	1.5-1.1	10÷50	3000	10-30	10-30	M to H	5-10

a. cell; b. battery; c. dependent on DOD; d. pulse discharge (L=low, M=moderate, H=high, MH=moderately high, VH=very high) temperature is reported. These batteries can nominally be used in the temperature range -20 to 55°C. The lower limit can be extended to -30°C for low-rate discharges; however, as can be seen from the figure, the battery performance severely decreases at low temperatures. In comparison, the low-temperature behavior of primary Li cells is more satisfactory [79], as also pointed out in Chapter 12.

Alkaline cells loose ~3% of their capacity after 1 year of storage at 20°C; the loss becomes ~12% at 40°C, and ~35% at 60°C.

Applications include the following (see also Chapters 11 and 12):

- Heavy Duty Lighting
- Hand held terminals
- Ambulatory medical equipment
- Transceivers
- Tracking
- Oceanography
- Portable GPS
- Memory back up
- Strobes
- Access control systems
- Remote controllers
- Electronic door locks
- Oil drilling
- Gas meters
- Wireless alarm sensors
- Real time clock

2.13. Basic Parameters of Aqueous Secondary Batteries

The main characteristics of the secondary batteries described in this chapter are reported in Tables 2.5 and 2.6. The values are averaged from several sources. They have to be treated with some care as the experimental conditions are not exactly the same and the batteries may differ in size and construction. A comparison can be made with Table 1.11 of Chapter 1, reporting the characteristics of nonaqueous secondary batteries. As for the primary alkaline battery, its basic parameters are reported in Chapters 11 and 12.

References

1. K. Peters, in "*Modern Battery Technology*", C.D.S. Tuck Ed., Ellis Horwood, Chichester (U.K), 1991.
2. D.A.J. Rand, R. Woods and R.M. Dell, "*Batteries for Electric Vehicles*", Research Study Press, Taunton, U.K., 1998.
3. A.J. Salkind, A.G. Cannone and F.A. Trumbore, in "*Handbook of Batteries*" (Chapter 23), D. Linden and T.B. Reddy, Eds., McGraw-Hill, New York, 2002.
4. K.R. Bullock, *J. Power Sources* 51 (1994) 1.
5. D. Berndt, *J. Power Sources* 100 (2001) 29.
6. R.G. Jungst, in "*Used Battery Collection and Recycling*", G. Pistoia, J.-P. Wiaux and S.P. Wolsky, Eds., Elsevier, Amsterdam, 2001.
7. J.F. Cole, *J. Power Sources* 40 (1992) 1.

8. T. Juergens and R.F. Nelson, *J. Power Sources* 53 (1995) 201.
9. J. Tuphorn, *J. Power Sources* 31 (1990) 57.
10. R.H. Newnham, *J. Power Sources* 52 (1994) 149.
11. J.R. Pierson, J.P. Zagrodnik, R.T. Johnson, *J. Power Sources* 67 (1997) 7.
12. M.L. Soria, J. Valenciano, A. Ojeda, *J. Power Sources* 136 (2004) 376.
13. W. Peukert, *Elektrotech. Z.* 18 (1897) 287.
14. A.O. Nilsson and C.A. Baker, in "*Handbook of Batteries*" (Chapter 26), D. Linden and T.B. Reddy, Eds., McGraw-Hill, New York, 2002.
15. C.P. Albon and J. Parker, in "*Modern Battery Technology*", C.D.S. Tuck, Ed., Ellis Horwood, Chichester (U.K), 1991.
16. G. Halpert, *J. Power Sources* 12 (1984) 117.
17. A. Fleischer, *J. Electrochem. Soc.* 94 (1948) 289.
18. A.K. Shukla, S. Venugopalan and B. Hariprakash, *J. Power Sources* 100 (2001) 125.
19. Varta, Development of the Battery, http://micro.magnet.fsu.edu/electromag/ electricity/ batteries/sinteredplate.html
20. D. Ohms, M. Kohlhase, G. Benczur-Urmossy, G. Schadlich, *J. Power Sources* 105 (2002) 127.
21. U. Kohler, C. Antonius and P. Bauerlein, *J. Power Sources* 127 (2004) 45.
22. Y. Morioka, S. Narukawa and T. Itou, *J. Power Sources* 100 (2001) 107.
23. J. Carcone, in "*Handbook of Batteries*" (Chapter 28), D. Linden and T.B. Reddy, Eds., McGraw-Hill, New York, 2002.
24. J.M. Evjen and A.J. Catotti, in "*Handbook of Batteries*" (Chapter 27), D. Linden and T.B. Reddy, Eds., McGraw-Hill, New York, 2002.
25. Acme Electric Co., www.acmeelec.com/aerospace/batteries.htm
26. K. Nishio and N. Furukawa, in "*Handbook of Battery Materials*", J.O. Besenhard, Ed., Wiley-VCH, Weinstein, 1999.
27. Y. Sato, S. Takeuchi and K. Kobayakawa, *J. Power Sources* 93 (2001) 20.
28. M. Beheshti, Chemistry-Independent Charge Management, *PowerPulse.Net* 2003, www.powerpulse.net
29. Energizer/Eveready, Nickel-Cadmium Batteries, www.data.energizer.com
30. Isco, Ni/Cd and Pb/Acid Battery Comparison, www.isco.com/WebProductFiles/ Applications/ 201/Nicad_vs_LeadAcidBatteries
31. www.batteryuniversity.com/parttwo-36.htm
32. H. Franke, in "*Battery Technology Handbook*", H.A. Kiehne, Ed., Marcel Dekker, New York, 2003.
33. G. Pistoia, *"Batteries for Portable Devices"*, Elsevier, Amsterdam, 2005.
34. M. Suzuki and M. Wada, in "*Energy Storage Systems for Electronics*", T. Osaka and M. Datta, Eds., Gordon&Breach Science Pub., The Netherlands, 2000.
35. M. Fetcenko, in "*Handbook of Batteries*" (Chapter 30), D. Linden and T.B. Reddy, Eds., McGraw-Hill, New York, 2002.
36. T. Kohno, M. Yamamoto, M. Kanda, *J. Alloys Comp.* 193 (1999) 643.
37. J. McBreen, in "*Handbook of Battery Materials*", J.O. Besenhard, Ed., Wiley-VCH, Weinstein, 1999.
38. Motorola, Rechargeable Battery Cycle Life Issues, www.motorola.com
39. X.-G. Yang and B.Y. Liaw, *J. Electrochem.Soc.* 151 (2004) A137.
40. D. Linden and D. Magnusen, in "*Handbook of Batteries*" (Chapter 29), D. Linden and T.B. Reddy, Eds., McGraw-Hill, New York, 2002.
41. X.-G. Yang and B.Y. Liaw, *J. Electrochem.Soc.* 148 (2001) A1023.
42. Duracell, Technical/OEM, Ni-MH Rechargeable Batteries, www.duracell.com
43. User : Rjf/Prius Battery Specs, www.seattleeva.org/wiki/User:Rjf/Prius_Battery_Specs
44. Toyota Prius Battery Pack, www.cleangreencar.co.nz/page/prius-battery-pack

45. Introduction to NiMH Battery Technology, www.cobasys.com/pdf/tutorial/InsideNimhBattery
46. M. Fetcenko, *22nd International Seminar & Exhibit on Primary and Secondary batteries*, Fort Lauderdale (FL, USA), March 2005.
47. D. Coates, D. Caldwell and R. Hudson, "5.5 Inch Diameter Nickel-Hydrogen Cell Development Update", www.eaglepicher.com/NR/rdonlyres/ E21D0154-5A9A-4438-A276-C104FA592AEA/0/PS_2611a_paper1
48. J.D. Dunlop, J.N. Brill and R. Erisman, in "*Handbook of Batteries*" (Chapter 32), D. Linden and T.B. Reddy, Eds., McGraw-Hill, New York, 2002.
49. W.D. Cook and W. Studyvin, "C/NOFS Battery and Magnetic Properties", www.eaglepicher.com/NR/rdonlyres/ 305D0202-B2C0-4965-B340-015BF39BBE3F/0/PS_2611a_paper5
50. ESA, www.esa.int/esaSC/SEM106WO4HD
51. J.J. Jackovitz and G.A. Bayles, in "*Handbook of Batteries*" (Chapter 25), D. Linden and T.B. Reddy, Eds., McGraw-Hill, New York, 2002.
52. D. Coates and A. Charkey, in "*Handbook of Batteries*" (Chapter 31), D. Linden and T.B. Reddy, Eds., McGraw-Hill, New York, 2002.
53. A. Duffield, in "*Modern Battery Technology*", C.D.S. Tuck, Ed., Ellis Horwood, Chichester (U.K), 1991.
54. Earthtoys Alternative Energy Library – Emagazine, www.earthtoys.com/emagazine.php?issue_number=04.02.01&article=evionyx; Universal Electric Vehicle – UEV Products, www.universalelectricvehicle.com
55. L.A. Tinker and K.A. Striebel, in "*Energy Storage Systems for Electronics*", T. Osaka and M. Datta, Eds., Gordon&Breach Science Pub., The Netherlands, 2000.
56. R.P. Hamlen and T.B. Atwater, in "*Handbook of Batteries*" (Chapter 38), D. Linden and T.B. Reddy, Eds., McGraw-Hill, New York, 2002.
57. Electric Fuel Technical Brochure, www.electric-fuel.com/evpro/EF-bus-brochure
58. J.C. Salas-Morales and J.W. Evans, *J Appl. Electrochem.* 24 (1994) 858.
59. A.P. Karpinski, B. Makotevski, S.J. Russel, J.R. Serenyi and D.C. Williams, *J. Power Sources* 80 (1999) 53.
60. A.P. Karpinski, S.F. Schiffer and P.A. Karpinski, in "*Handbook of Batteries*" (Chapter 33), D. Linden and T.B. Reddy, Eds., McGraw-Hill, New York, 2002.
61. A.P. Karpinski, S.J. Russell, J.R. Serenyi and J.P. Murphy, *J.Power Sources* 91 (2000) 77.
62. D.F. Smith and C. Brown, *J. Power Sources* 96 (2001) 121.
63. Army Technology-Eagle Picher, www.army- technology.com/contractors/electrical/ eagle/press7.
64. C. Fabian and K. Kordesch, *Dechema Monographs*, Vol. 109, Dechema, 1987, p. 355.
65. 66. P.C. Butler, P.A. Eidler, P.A. Grimes, S.E. Klassen and R.C. Miles, in "*Handbook of Batteries*" (Chapter 39), D. Linden and T.B. Reddy, Eds., McGraw-Hill, New York, 2002.
66. M.H. Thomas, "Persistence and Progress - The Zinc Bromine Battery in Renewable Energy Systems", *Rega Forum 2003*, Yarra Valley, Victoria, Australia, June 2003.
67. A. Leo, in "*Modern Battery Technology*", C.D.S. Tuck, Ed., Ellis Horwood, Chichester (U.K), 1991.
68. Inventions&Innovations: Deep-Discharge Zn/Br_2 Battery, www.eere.energy.gov/inventions/pdfs/zbbenrg
69. ZBB Energy Corporation, The Zinc/Bromine Battery, www.zbbenergy.com/brochures/utility
70. M. Skyllas-Kazakos, D. Kasherman and M. Kazakos, in "*New Developments in Electrode Materials and Their Applications*", L. Wood and A.J. Jones, Eds., Canberra, Australia, 1990.
71. Sumitomo Electric Industries, www.sei.co.jp/sn/2001/05/feature_article
72. Redox Flow battery [KEPCO], www.kepco.co.jp.english/rd/solution/solution_2
73. C.J. Rydh, *J. Power Sources* 80 (1999) 21.
74. L. Joerissen, J. Garche, Ch. Fabjan and G. Tomazic, *J. Power Sources* 127 (2004) 98.

75. D. Linden and T.B. Reddy, in "*Handbook of Batteries*" (Chapter 22), D. Linden and T.B. Reddy, Eds., McGraw-Hill, New York, 2002.
76. www.thermoanalytics.com/support/publications/batterytypesdoc
77. *Modern Battery Technology*" (Appendix A), C.D.S. Tuck, Ed., Ellis Horwood, Chichester (U.K), 1991.
78. P.C. Symons and P.C. Butler, in "*Handbook of Batteries*" (Chapter 37), D. Linden and T.B. Reddy, Eds., McGraw-Hill, New York, 2002.
79. D. Linden and T.B. Reddy, in "*Handbook of Batteries*" (Chapter 14), D. Linden and T.B. Reddy, Eds., McGraw-Hill, New York, 2002.

This page intentionally left blank

Industrial Applications of Batteries. From Cars to Aerospace and Energy Storage
M. Broussely and G. Pistoia Eds.,
© 2007 Elsevier B.V.

Chapter 3

CHARACTERIZATION OF BATTERIES BY ELECTROCHEMICAL AND NON-ELECTROCHEMICAL TECHNIQUES

Doron Aurbach

Department of Chemistry, Bar-Ilan University, 52900 Ramat-Gan, Israel

3.1. Introduction

While batteries are usually simple for use, transport and even manufacturing, they are very complicated electrochemical devices in which three bulks: positive and negative electrodes and an in-between electrolyte phase, and two electrode-electrolyte interfaces have to work simultaneously. The chemistry of many battery systems may be very complicated, including, in addition to the main electrochemical reactions (that are the heart of their energy storage mechanisms), side reactions and passivation phenomena. The science behind batteries involves, in addition to electrochemistry, materials and surface chemistry, physics, and transport phenomena (diffusion processes in both solid and liquid phases) and multiphase charge transfer by ions and electrons through bulks and interfaces. Having superior battery chemistry is never sufficient for practical commercial success. The engineering side is critical for success, as is the proper choice of materials (in terms of purity and morphology), current collectors, separators, cases, and safety features. Therefore, it is impossible to develop battery systems based on trial and error work. The engineering of battery systems has to be based on solid scientific work in which the major chemistry, the transport phenomena, the side reactions, and the thermal behavior are fully understood. Maintaining a high level of scientific research in the field of batteries is extremely important for thinking ahead about all the possible failure mechanisms and safety problems. This is critically important for products such as batteries that are mass-produced and widely distributed. A recall of batteries from the market due to unexpected safety or operational problems may be fatal for battery manufacturers.

The science behind batteries, their quality testing, the prediction of their limits of use, safety features, and calendar and cycle life, all require the establishment of well defined and high level techniques and procedures. Below we list the most important aspects relevant to the characterization of batteries.

a) The characterization of new materials during the course of R&D – metals, transition metal oxides and sulfides, carbonaceous and ceramic materials, polymeric matrices, electrolyte solutions, salts, and solvents.

b) Quality control of bulk produced, selected materials coming from specifically chosen manufacturers. Quality control also includes the development of efficient *in situ* characterization methods, as well as judicious post-mortem analysis when needed.

c) The correct measurement of the electronic properties of the various components, impedance and overall electrochemical performance in terms of capacity, voltage, rates, energy and power density, and cycle life for rechargeable systems.

d) Understanding the temperature-dependence behavior, the relevant temperature window for operation, thermal stability and related safety limitations.

e) Understanding aging processes, capacity-fading mechanisms, and the reasonable prediction of shelf and calendar life.

f) Understanding as well as possible all safety limitations, and setting well-defined safety regulations and instructions.

g) A good understanding of environmental aspects, establishing suitable waste management, and suggesting suitable recycling processes when relevant.

3.2. Categories of Battery Materials

In Chapters 1 and 2 of this book, the most relevant battery systems have been categorized. In this section, the active and non-active battery materials will be presented in detail.

3.2.1. Electrode Materials

3.2.1.1. General Features

Battery electrodes may be divided into four categories:

1) Metallic materials (usually the negative, see Sub-section 3.2.1.2)

2) Composite structures, which include the active mass, conducting additives, binder and current collector (the most commonly used in battery systems).

3) Catalytic materials, which include supporting porous material and dispersed catalyst particles, embedded in the supporting matrix (usually carbonaceous materials).

4) Monolithic materials, thin film of the active mass sputtered/deposited on a current collector. Such electrodes are used in microbatteries, where the amount of active mass being used is small (usually solid-state systems).

Major parameters of interest are theoretical capacity (mAh/g), potential and rate capability. The latter parameter can be expressed in capacity *vs.* current density (A/g) or *vs.* C-rates: xC or C/x (xC means x times the full capacity discharged during 1 hr, and C/x means discharging the full capacity during x hrs). For rechargeable systems, stability, cycle life and capacity-fading (*e.g.*, % capacity loss per cycle) are also important parameters. The shape of the voltage profile during galvanostatic discharge (or charge) is also important. For instance, when the electrode processes are metal dissolution or intercalation via phase transition, the potential profile is flat (plateau), while when solid solutions or concentration gradients are formed (in the electrode and/or in solution), the potential profile is sloping. The most commonly used electrodes in batteries have a composite structure (No. 2 above), as illustrated in Figure 3.1. The active mass is a powder that has to be spread on a metallic/inert current collector, bound with a polymeric binder that keeps the system integral. The uniform electrical contact with composite electrodes is maintained by electrically conductive additives, usually carbon particles. In most cases, the percentage of active mass, binder and conductive additives in composite electrodes is 85-80%, 5-10%, 5-10%, respectively (by weight). Relevant technical aspects and questions related to composite electrodes are listed below.

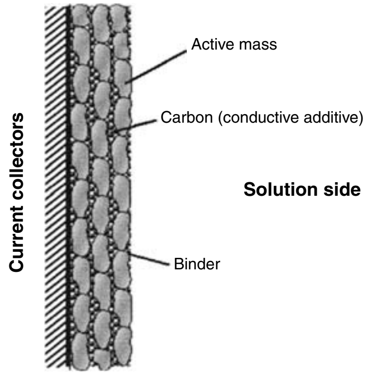

Figure 3.1. A scheme of a composite electrode.

a. The particle size and surface area are very important. There are two main processes that can be rate determining: interfacial charge transfer and bulk transport (*e.g.*, solid-state diffusion in intercalation processes). Hence, the smaller the particles, the higher is their surface area and the smaller is their diffusion length. Therefore, the kinetics of their electrochemical reaction should be faster. However, too small particles means problems with inter-particle electrical contact, and a high surface area means a better chance for side reactions. Thereby, the particle size of the active mass in composite electrodes has to be optimized.

b. The electrode's thickness is important and has to be optimized to the relevant needs. A thick active mass means a higher capacity per unit area, but also sluggish kinetics due to a limited contact between the entire active mass and solution. For high rates, thin electrodes should be better, although resulting in a lower practical capacity.

c. The porosity of composite electrodes is important. High porosity enables good contact between the active mass and solution at the expense of good inter-particle contact. Hence, the average practical density of pressure to be applied during their fabrication in order to compress the active mass is a matter of optimization.

d. The electrodes active mass in many battery systems, especially when the solutions are nonaqueous (Li, Li-ion batteries), may react spontaneously with solution species, thus forming surface films that cover the particles. Hence, in many battery electrodes, the general charge transfer process includes the necessary step of ion migration through surface films (as is the case for most of the electrodes for Li and Li-ion batteries).

e. The contact between the active mass and solution is critical. Thus, the properties of both electrodes and solutions have to be optimized to obtain the sufficient wetting of the active mass. In the case of gel, polymeric and other solid-state systems, the electrodes should also contain the electrolyte system, built in, as part of the composite structure.

3.2.1.2. Negative Electrodes

The negative electrodes for batteries are classified as follows.

a. Active metals in aqueous batteries: Cd (Ni-Cd), Pb (Lead-Acid), Zn (Zinc-Air alkaline Zn-MnO_2), Al (Al-Air), Mg (reserve batteries). The discharge reactions here are the active metal dissolution: $M \rightarrow M^{Z+} + ze^-$.(1-9)

b. Active metals in nonaqueous batteries: Li in primary and secondary Li batteries. For the latter systems, the relevant electrolyte systems seem to be gel, polymeric or ceramic.(10) We can also mention magnesium in rechargeable magnesium batteries (still in the R&D stage). The discharge reaction here is again the active metal dissolution.(11)

c. Metallic compounds for Ni-MH batteries. These include the AB_5 type (A=La, B=Ni as major components, which can also include Ce, Nd, Pr, Gd, Y and Cr), and the AB_2 type (A=Ti, Zn; B=Ni as major components, which can also include V, Al and Cr). These compounds can store hydrogen in a hydride form. Hence, the electrode's reaction is: $MH+OH^- \leftrightarrows M+H_2O+e^-$ ($E^o = 0.83$ V *vs.* SHE). These electrodes have to be porous, comprising sintered particles, in order to facilitate the above heterogeneous reaction.(12)

d. Carbonaceous electrodes for Li-ion batteries. These are composite electrodes comprising micron-size carbon particles with a polymeric binder (90:10% by weight).(13) The most commonly used active mass is graphite, which inserts lithium according to the reaction: $Li^+ + C_6 + e^- \leftrightarrows LiC_6$ (specific capacity: 372 mAh/g). There are several types of graphite particles: synthetic flakes, natural flakes, chopped graphite fibers, and round-shaped particles such as mesocarbon microbeads, MCMB.

The first process of a Li-ion battery has to be charging, which lithiates the graphite, thus forming LiC_6 (at a potential close to that of 0 V *vs.* Li/Li^+). The polarization of graphite in solution to low potentials leads to a rich surface chemistry-reduction of solution species, possible co-intercalation of solvent molecules with Li-ions, and the precipitation of passivation surface films (comprising insoluble Li compounds formed by the reduction of solution species in the presence of Li-ions).(14) In general, the surface chemistry of graphite electrodes may be similar to that of Li metal.(15) Both LiC_6 and Li metal, which are highly reactive towards all relevant polar aprotic solvents, are apparently stable due to the precipitation of protecting surface films, and hence, their kinetics is controlled by Li-ion migration through Li-ion conducting surface films, (*i.e.*, they behave according to the SEI model).(16) Li insertion into graphite occurs via a series of phase transitions between LiC_n stages, and thus, the potential profile of these processes includes several major steps (plateaus) between 0.3-0 V *vs.* Li/Li^+).(14) The reactions between the pristine graphite and solution species during its first polarization in the batteries, consume irreversible charge. This irreversible capacity and the stability upon cycling depend on the morphology of the particles, the solution composition, the first polarization rate, and the ratio between the electrodes and solution mass.(17,18) Since the irreversible capacity has to be compensated by an excess of cathode material (which is usually the heaviest and the most expensive active element in the cell), it is very important in practical systems to reduce the irreversible capacity to a minimum. Hence, the percentage of irreversible capacity from the reversible one is a critical parameter in these systems. We should mention that there are also non-graphitic carbons such as disordered and hard carbons, which are used as negative electrode materials in Li-ion batteries. Their advantage over graphite may be higher capacity and better stability upon cycling.(19)

e. Other anodes for Li batteries: Efforts are underway to develop Li alloys and intermetallic compounds as substitutes for the highly reactive Li metal electrodes. These include Li-Sn, Li-Si, Li-Si/SnM1M2 (M1M2 are metals such as Cu, Ni, B). Li can form alloys with Sn and Si up to a stoichiometry of $Li_{4.4}Sn$ or $Li_{4.4}Si$, *i.e.* capacities of 900 and 4000 mAh/g, respectively.(20) The latter systems may suffer from instability due to the huge volume increase during the lithiation of Sn or Si. There are innovative approaches as to how to stabilize these systems (beyond the scope of this chapter), and the use of intermetallic compounds, namely, Li-Sn/SiM1M2, *etc.*, as one of these approaches.(21) There are also ideas of using low potential, lithiated transition metal oxides as negative electrodes for Li-ion batteries. A good example is the spinel structure of $Li_4Ti_5O_{12}$ (1.5 V *vs.* Li/Li^+, 120 mAh/g), which shows prolonged cycleability at high rates.(22)

3.2.1.3. Positive Electrodes

In general, the positive electrodes have to be electrochemically active at relatively high redox potentials. The most relevant ones are classified in Tables 3.1 and 3.2.

The cathode materials for Li-ion batteries are lithiated transition metal oxides. All of them are reactive with alkyl carbonates/$LiPF_6$ solutions and develop surface films. Hence, their electrochemical behavior and stability are largely influenced by their surface chemistry.(23,24)

Over the years, there have been attempts to develop redox polymers, including electronically conducting polymers, such as polypyrrole, polythiophene and polyaniline. The special use of such polymers was suggested for full plastic Li rechargeable batteries.(55) However, these systems suffer from limited kinetics and stability.

Liquid cathodes used in some primary Li batteries (*e.g.*, Li-$SOCl_2$) were mentioned in Chapter 1 of this book. Catalytic electrodes used, for instance, in Zn-Air batteries were mentioned in Chapter 2. These electrodes do not contain any active mass, but rather serve as a catalytic surface for the relevant battery reactions. The most commonly used matrices for such electrodes are porous carbons on which the specific catalyst particles (usually of submicronic or nanometric size) are embedded.

Table 3.1. Metal oxides and sulfides, used as cathode materials for batteries. (*Excluding cathodes for Li ion batteries presented in Table 3.2*).

Compound	Battery System	Relevant Potential	Relevant Spec. Cap., mAh/g	References
MnO_2	Rechargeable alkaline	1.5V *vs.* Zn/Zn^{2+}	>200	25
MnO_2	Primary alkaline	1.5V *vs.* Zn/Zn^{2+}	>200	26
MnO_2	Primary Mg	1.7V *vs.* Mg	270	27
MnO_2	Primary Li	3V *vs.* Li/Li^+	>250	28
CuO	Primary Li	1.5V *vs.* Li/Li^+	>400	29
Ag_2O	Primary	1.6V *vs.* Zn/Zn^{2+}	180	30
AgO	Rechargeable Zn	1.5V *vs.* Zn/Zn^{2+}	280	30
AgO	Rechargeable Cd	1.1V *vs.* Cd/Cd^{2+}	230	30
PbO_2	Rechargeable	2V	120	31
V_2O_5	Rechargeable Li	3.5-2V *vs.* Li/Li^+	>250	32,33
NiOOH	Ni-metal hydride rechargeable	1.2V	180	34
$Li_{0.3}MnO_2$	Rechargeable Li	3V *vs.* Li/Li^+	≈250	35
TiS_2	Rechargeable Li	2.5V *vs.* Li/Li^+	>200	36
MoS_2	Rechargeable Li	2.5V *vs.* Li/Li^+	>200	37
Mo_6S_8 chevrel	Rechargeable Mg	1.1-1.3V *vs.* Mg/Mg^{2+}	>100	38
FeS_2	Thermal Li	1.5V *vs.* Li/Li^+	>200	39

Table 3.2. Typical lithiated transition metal oxide cathodes for Li-ion batteries.

Name of compound	Status	Major lithiation process	Relevant Potentials, V *vs.* Li/Li^+	Relevant Spec. Cap, mAh/g	References
$LiCoO_2$	Commonly used	Phase transition	3.5 – 4.2	160	40,41
$LiNiO_2$	R&D	Phase transition	3.5 – 4.2	200	42,43
$LiMn_2O_4$	Some uses	Two-phase transitions	3.5 – 4.2	140	44,45
$LiCo_{0.2}Ni_{0.8}O_2$	Some uses	Solid solution	3.5 – 4.2	200	46,47
$LiMn_{1.5}Ni_{0.5}O_4$	R&D	Two-phase transition	4.5 – 5.0	150	48
$LiFePO_4$	Final; R&D	Phase transition	3.2 – 3.7	150	49
$LiNi_{0.5}Mn_{0.5}O_2$	R&D	Solid solution	4.0 – 4.7	200	50,51
$LiCo_{1/3}Ni_{1/3}Mn_{1/3}O_2$	R&D	Solid solution	4.0 – 4.7	200	52,53
LiV_3O_8	R&D	Several phase trans.	2.0 – 3.3	200	54

3.2.2. Electrolyte Systems

3.2.2.1. Aqueous Solutions

These solutions are used in several important systems, including Zn-MnO_2, Zn-Air, Ni-Cd, Ni-MH, and Pb-Acid. Except for the last system, in which the electrolyte is H_2SO_4, for all the other batteries the solutions are alkaline, using KOH as the electrolyte. In general, the thermodynamic electrochemical window of water is 1.229 V. However, the high over voltage for H_2 formation on Pb electrodes enables operation of Pb-Acid batteries at 2.2 V in acidic solutions. In the case of alkaline systems, their high pH enables working with low potential anodes such as Cd, Zn or $LaNi_5$-H. The conductivity of acidic or alkaline aqueous solutions is sufficiently high, and hence, the electrolyte systems in these batteries do not play a major role in determining their internal resistance. The low temperature performance of the aqueous systems is limited by the freezing point of their solutions.

3.2.2.2. Nonaqueous Solutions

These solutions are relevant mostly to Li and Li-ion batteries. Commonly used polar aprotic solvents include: ethylene and propylene carbonate, dimethyl and diethyl carbonate, sulfolane, dimethyl sulfoxide, tetrahydrofuran, diethyl ether, *etc*. Salts for lithium batteries include: $LiClO_4$, LiBr, LiI, $LiAsF_6$, $LiPF_6$, $LiAlCl_4$, $LiBF_4$, $LiCF_3SO_3$, $LiN(SO_2CF_3)_2$, $LiC(SO_2CF_3)_3$, *etc*.

Over the last four decades, and to some extent in parallel to the accelerated development of Li batteries, intensive efforts have been devoted to the characterization of polar aprotic solutions.(56,57) Critical aspects are:

a) How to monitor purity; what are the unavoidable contaminants?

b) How to define polarity and to what extent can the chosen definitions be correlated with properties such as ionic conductivity and with thermodynamic and kinetic reactions?

c) Mechanisms of electrolyte dissolution, ion separation and electrical conductivity.

d) Electrochemical stability, potential windows.

e) Major reduction and oxidation reactions/products at the limits of the electrochemical windows.

f) Limits of chemical stability, especially with radical ions formed by electrochemical reactions.

g) Possible reactions with active materials, *e.g.* active metals, transition metal oxides, and related passivation phenomena.

h) How properties can be improved by additives: apparent stability by passivation, inflammability, overcharge protection, and ionic association.

Another class of nonaqueous systems that has become important over the past years is that of ionic liquids, *i.e.* room temperature molten salts.(58)

3.2.2.3. Solid Electrolyte Systems

Four classes of solid electrolytes for batteries can be mentioned:

a) Gel electrolytes: solid polymeric matrices that are soaked with liquid electrolyte solutions; the solvent present dissolves the electrolyte.(59)

b) Solvent-free polymeric electrolytes: the polymeric chains can dissolve Li salts. This is relevant mostly to polyethers and their derivatives.(60)

c) Composites comprising polymer, ceramic materials and electrolyte systems: in these systems, preferred ceramic materials are nano-powders, *e.g.* SiO_2, Al_2O_3, dispersed within the polymeric matrices and providing additional conducting mechanisms of ions via migration on their high surface area. The use of such composite systems is relevant to both gel- and solvent-free polymeric matrices.(61)

d) Ceramic materials and solid state electrolytes.(62)

In general, gel electrolyte systems can function at ambient temperatures, while the other three classes are relevant mostly to high temperatures.

3.2.3. Supporting Elements

3.2.3.1. Current Collectors

Current collectors should have the following properties:

a) Excellent bulk electrical conductivity.

b) Minimal thickness/weight, yet the appropriate strength to support the active mass.

c) Electrochemically and chemically inert in the potential range of the relevant electrode.

d) Excellent surface conductivity as well, no electrically insulating surface films.

e) Cheap.

In general, carbonaceous materials have the widest chemical window. However, their mechanical properties are not suitable for many applications. In Li and Li-ion batteries, copper foils/grids are the appropriate material for negative electrodes. Both bulk and surface conductivity of this metal are sufficiently high, and it is chemically and electrochemically inert in nonaqueous solutions in the 0-3 V *vs.* Li/Li$^+$ potential range, which is relevant to all the possible anodes in Li batteries. However, carbon fibers and cloth that are strong, flexible and electronically conductive are commercially available and can be used as current collectors for battery electrodes. As an example regarding the problems and choice of current collectors, the case of Li and Li-ion batteries is dealt with below.

For the positive electrodes in Li/Li-ion batteries, there is a problem of anodic stability of most metals, including nickel, copper, silver, and even stainless steel. Aluminum, which is an active metal (E^0 = -1.2 V *vs.* SHE), may be the most suitable material for current collectors of positive metals due to its unique electrical properties and passivation phenomena. In solutions containing salts that liberate active fluoride anions such as $LiPF_6$, $LiBF_4$, and $LiAsF_6$, Al is passivated by a protective AlF_3 layer, which is thin enough to allow electron transport from the Al foil or grid to the active mass.(63)

3.2.3.2. Separators and Membranes

The role of separators/membranes in batteries is critical, and it affects internal resistance, rates, stability, cycle life, temperature range, and safety features. In most of the battery systems, the active mass is contained in solid electrodes, and the same ions in solution react with both electrodes. This is the case for all alkaline stationary batteries, Pb-acid systems, and nonaqueous Li, Li-ion and Mg batteries. In such cases, what are needed between the electrodes are separators that maintain the mechanical stability of the systems. In Ni-Cd, Ni-MH, and Pb-Acid systems, the aqueous solutions are involved in the electrochemical reactions. Thus, they have to be thick enough to contain the appropriate amount of solution. For batteries in which the solution serves only as an ion conductor, the separator should be as thin as possible, porous, but yet strong enough to maintain the mechanical and electrical separation between two rough composite electrodes. For instance, porous polypropylene or polyethylene films (a few tens of microns thick) are used for Li-ion batteries. In Li metal batteries, one has the problem of dendrite formation during charging (Li deposition). Separators containing ceramic particles may be useful for preventing dendrite growth and penetration through the separator. The design of separators is a special art in this field: there is a compromise between the degree of porosity and mechanical strength. In addition, the wettability of the pores is important: separators may contain ceramic particles that facilitate their wetting by the solution.(64)

In flow batteries, including systems such as $Zn\text{-}Br_2$, $V^{2+}/V^{3+}\text{-}V^{4+}/V^{5+}$ and metal-air batteries, the separators have to act as selective membranes that prevent the flow of active species in solutions from side to side. A discussion on membrane design for such batteries is beyond the scope of this chapter, because each flow battery requires a special design of its separator/membrane.

3.3. Stages and Levels in Battery Characterization

3.3.1. Introduction

There are several levels of battery characterization according to which the various techniques should be classified (all the various techniques mentioned below are described in detail in Section 3.4).

3.3.2. Non-Destructive Studies of Full Cells

In general, full cells can be studied *in situ* by electrochemical and X-ray techniques. The most relevant electrochemical techniques are chronopotentiometry, namely, V *vs.* t/capacity response at constant current operation, and impedance spectroscopy. Measuring V or I *vs.* t during discharge at a constant load, *i.e.* external resistance, may also provide some insight. Full cells can be photographed by X-ray, thus obtaining a general picture of rough changes in the electrodes' morphology/layout. By using synchrotron radiation, it is possible to produce *in situ* analysis by X-ray absorption and diffraction, if there is no interference or masking effect, and thus the response of the electrode of interest can be clearly recorded. Some thermal aspects of batteries can also be studied *in situ* by calorimetery. For instance, the heat evolution during charge and discharge can be precisely measured by isothermal calorimetric measurements. Changes in the battery volume during charge and discharge and/or during storage can be measured, and provide critical information about their stability and possible failure trends.

3.3.3. Post-Mortem Analysis of Full Cells

A highly important tool in the R&D process of new battery systems and in the understanding of failure mechanisms of batteries is post-mortem analysis. The first stage in this analysis is the opening of the battery case in a non-destructive and safe manner, so that the active material is not damaged and the operation does not cause a dangerous short circuit. When high energy density systems such as lithium batteries are involved, a short circuit may lead to a thermal runaway and explosion. Therefore, it may be important to design an operation (case cutting) with remote control (see Refs. 65 and 66, for example). The second stage is the examination of the active mass, the electrolyte solution, separator, and electrodes. In many cases, especially when cycled rechargeable batteries are explored, the residual solution, which contains useful information, is trapped in the separator and in the porous electrodes. Hence, its extraction by an inert solution may be an important preliminary stage. The different components can be studied by bulk analytical techniques, surface analysis, and microscopy, while the separated electrodes can be studied electrochemically if they are appropriately shaped. Such analyses may be very important in determining which part/component of the batteries is responsible for failure, capacity fading, *etc.*(65,66)

3.3.4. Half Cell Testing

In many cases, especially in the R&D stages, it is not advisable to work on full cells that comprise two problematic electrodes, but rather to concentrate on a specific electrode. Therefore, it may be useful to construct cells comprising the working electrode of interest and a counter electrode whose electrochemical response is simple, and easy to separate from that of the working electrode. In the field of Li-ion batteries, there are extensive studies on new electrodes in half cells. The best counter electrode for the study of new working electrodes for Li-ion batteries is Li metal. The electrochemical response of Li is simple, and includes only Li deposition or dissolution. The exchange currents of these processes is high (*i.e.* fast kinetics), and the impedance of Li electrodes is usually lower than that of Li insertion electrodes. Counter electrodes made of metal do not contaminate most of the nonaqueous solutions because they are fully passivated. In any event, even when working with relatively simple half cells with Li counter electrodes, it is always recommended to use 3-electrode cells that contain reference electrodes. In this way, the electrochemical response of the cell reflects the working electrode only. For nonaqueous systems containing Li salts, Li wire is a suitable reference electrode. For aqueous systems, it is possible to use pseudo reference electrodes such as Ag wire, Ag/AgCl, or the M/M^{z+} couple of the suitable metal, *e.g.* Zn, Cd, or Pb. The most relevant techniques for half cell testing are, of course, all the fine electrochemical techniques and analytical methods for the components (*in situ* methods and post-mortem analysis, see Section 3.4).

3.3.5. Solution Studies

There are five major aspects of solution studies.

1) Chemical composition, ion structure, purity, contamination level, and the use of bulk analytical techniques such as ICP, GCMS, NMR, Raman, FTIR.

2) Conductivity measurements by standard electrochemical means, including temperature effects.

3) Electrochemical windows/stability using voltammetry.

4) Thermal stability using a variety of methods, including DSC, ARC, DTA. (67-69) These studies may include both pure solutions and a mixture of solutions and electrode materials.

5) Unique reduction and oxidation products, when important, *e.g.* for understanding the surface chemistry of battery electrodes. Such studies may include polarization by electrochemical techniques, followed by analytical studies of solution phase and surface chemistry (*e.g.* surface films) developed on noble metal electrodes.

For surface studies of films on noble metal electrodes, FTIR and XPS are the most useful. Over the years, aqueous and nonaqueous solutions were also studied successfully by *in situ* FTIR spectroscopy, using noble metal electrodes.(70-72) Such studies enable the more complicated surface chemistry of lithium and lithium-carbon electrodes to be deciphered.

3.3.6. Electrode Studies – Bulk and Surface Analysis

The major aspects of electrode studies include the following topics.

a) Electrochemical studies. These are carried out in half-cell testing, as mentioned above. Major electroanalytical tools of interest are chronopotentiometry (V *vs.* t in constant current operation), voltammetry (fast and slow scan rates), transients – especially the various titration techniques, PITT and GITT, and impedance spectroscopy.(73-75)

b) Structural analysis. Major tools for this are X-ray powder diffraction, neutron diffraction (for more complicated structures), EXAFS,(76) XANES,(77) and electron diffraction, which is a by-product of electron microscopy. HRTEM(78) is also a useful tool for structural analysis. Solid-state NMR has also become an important technique.(79)

c) Morphological analysis. Major tools are electron microscopy (TEM, SEM, HRSEM) and scanning probe microscopy, mostly AFM.(80) Electron microscopy also provides local element analysis by analyzing the X-ray radiation emitted by the interaction between the electron beam and the solid matter (known as the EDS or EDAX technique).(81)

d) Surface area measurements. These are techniques that use gas adsorption measurements, *e.g.* N_2 at low temperatures, followed by analysis based on adsorption, *e.g.* the BET method.(82)

e) Surface analysis. Major tools for this are FTIR, Raman and photoelectron spectroscopies, which provide information on functioning groups and oxidation states of elements on the surface (XPS). Depth profiling with XPS also provides 3D chemical analysis near the surface.(83)

f) Thermal studies. The high temperature behavior of materials can be studied by several techniques, including DSC, ARC,(84) DTA, and TGA.(85) This last technique enables gravimetric changes as a function of temperature to be followed, due to desorption and decomposition processes. TGA coupled with MS provide specific analysis of thermal reaction products.

3.4. A Brief Summary of Available Techniques Related to the Characterization of Batteries

3.4.1. Glove Box Operations

a) Introductory remarks. Nonaqueous systems are highly sensitive to atmospheric components, *e.g.* H_2O, O_2, CO_2, and even N_2. Elimination of atmospheric contaminants is, therefore, a first and mandatory condition for carrying out work with nonaqueous systems. Several modes of operation may be applicable.

1. Use of Vacuum Systems

There are several reports in the literature on electrochemical studies in vacuum systems. These reports include studies by Yeager *et al.*(83) Of special importance are recent reports on electrochemical measurements in ultrahigh vacuum systems by Scherson *et al.*(86)

2. Use of Dry Rooms

The Li battery industry uses dry rooms in which the humidity is maintained at 1-2%. For certain applications, especially for mass production, dry room can provide an appropriate atmosphere. However, for most of the rigorous studies with nonaqueous solutions, dry rooms are definitely inadequate.

3. Glove Boxes

Glove box operation is the most common way to enable a comfortable and continuous study under inert atmosphere.

b) Basic features of a good glove box system. The basic working station is a box constructed of metal or plastic. The best materials for constructing the box are aluminum or stainless steel. Polycarbonate is the best material for the window.

The entire system should contain the following elements.

1. Vacuum chambers attached to the box through which items are introduced into the glove box. The vacuum chamber should be equipped with the appropriate hermetically closed doors, valves, and a vacuum pump.

2. H_2O and O_2 absorbers (molecular sieves and other active materials) through which the glove box atmosphere is continuously circulated.
3. H_2O and O_2 analyzers that are capable of monitoring these contaminants at the ppm level.
4. A trapping system for the vapors of organic solvents and CO_2. These systems are based on the massive circulation of the glove box atmosphere through a cooled trap outside the glove box.
5. Electrically-controlled connections to the inert gas supply and the vacuum pump line, which are capable of maintaining any desirable pressure inside the box.
6. High voltage electrical outlets for the operation of electrical instruments inside the box.
7. Low impedance connectors for electrochemical measurements taken with equipment that is located outside the glove box. High impedance, or the bad shielding of these electrical lines, may introduce artifacts.

3.4.2. Bulk Analytical Tools

3.4.2.1. Basics of Mass Spectrometry(87)

The physics behind mass spectrometry is that a charged particle passing through a magnetic or electrostatic field is deflected along a circular path on a radius that is proportional to the mass to charge ratio, m/z. The universal ability to analyze almost all substances that can be ionized has made this technology very popular. In the past decades, mass spectrometry has found its way into many analytical laboratories due to the development of the coupling technologies, GC/MS and LC/MS, which use mass spectrometers as online detectors for chromatographic separation technologies. Below are the various techniques to measure atomic mass.

a) Electron ionization or electron impact (EI). Electron ionization is achieved through the interaction of a compound with an energetic electron beam that results in the loss of an electron from the compound and the production of a radical cation.

b) Chemical ionization (CI) evolved as a means to ionize compounds to energetically labile state for traditional EI analysis. CI can be thought of as EI performed in the presence of a large excess of a reagent gas.

c) Fast atom bombardment (FAB). In the FAB experiment, a sample that has been dissolved in a suitable matrix is inserted into the mass spectrometer and bombarded with heavy atoms.

d) The use of a liquid matrix yields more intense and longer-lived analyte signals than those generated by solid state, secondary ion mass spectrometry (SIMS).

e) Matrix-assisted laser desorption ionization (MALDI). This desorption technique is very similar to FAB, but it utilizes photons instead of particles to desorb analyte molecular ions from a crystalline matrix.

f) Thermo-spray ionization source (TSP), which is capable of producing ions from an aqueous solution that had been sprayed directly into the mass spectrometer. TSP ionization is achieved by passing a pressurized solution through a heated tube, which partially vaporizes the effluent to generate a spray prior to entering the ion source.

g) Electro-spray ionization (ESI). This liquid-introduction technique uses a high electric field to produce a fine mist of highly charged droplets. This high potential has the unique advantage of being able to generate multiply charged ions.

f) GEMS and LCMS are major tools for bulk solution studies in their reaction products, impurities, *etc.*

h) SIMS is one of the most sensitive and helpful surface sensitive techniques. It allows the analysis of surface species at sub-micronic lateral resolution and, combined with a sputtering capability, enables the depth profiling of surfaces, *i.e.* 3D analysis of thin media. This technique requires UHV ($<10^{-11}$ torr), and hence, highly sensitive samples can be measured (if the appropriate sample transfer procedures are used).

3.4.2.2. Mössbauer Spectroscopy

Mössbauer spectroscopy is a spectroscopic technique based on the Mössbauer effect.(88) In its most common form, Mössbauer absorption spectroscopy, a solid sample is exposed to a beam of gamma radiation, and a detector measures the intensity of the beam that is transmitted through the sample. The gamma-ray energy is varied by accelerating the gamma-ray source through a range of velocities with a linear mirror. The relative motion between the source and the sample results in an energy shift due to the Doppler effect.(89)

In the resulting spectra, the intensity of the gamma radiation is plotted as a function of the source velocity. At velocities corresponding to the resonant energy levels of the sample, some of the gamma rays are absorbed, resulting in a drop in the measured intensity and a corresponding dip in the spectrum. The number, positions, and intensities of the dips (peaks) provide information about the chemical environment of the absorbing nuclei and can be used to characterize the sample.

In order for Mössbauer absorption of gamma rays to occur, the gamma ray must be of the appropriate energy for the nuclear transitions of the atoms being probed. Also, the gamma-ray energy should be relatively low, otherwise the system will have a low recoil-free fraction resulting in a poor signal-to-noise ratio. Only a handful of elemental isotopes exist for which these criteria are met, so Mössbauer spectroscopy can only be applied to a relatively small group of atom isotopes including ^{57}Co, ^{57}Fe, ^{134}I, ^{124}Sn, and ^{126}Sb. Of these, ^{57}Fe is by far the most common element studied, using this technique.

Mössbauer spectroscopy is used primarily to study the electron structure of materials. This resonant absorption is observed best in isotopes having long-lived, low-lying excited nuclear energy states. Among all the elements, the largest recoil-free resonant cross-section occurs for the isotope Iron 57. The resonant energies are extremely narrow (~1 part in 10^{12}). This extreme resolution allows the observation of the hyperfine interactions between the nucleus and the surrounding electrons. This link between the Mössbauer spectrum and the electron structure of the sample can be exploited in the study of many types of materials. Fields in which Mössbauer spectroscopy has been applied include solid-state physics, surface physics, metallurgy, chemistry, biochemistry, geology, and recently, battery research.(90)

3.4.2.3. Nuclear Magnetic Resonance(87)

Nuclear Magnetic Resonance (NMR) spectroscopy is based on the fact that many common nuclei align themselves relative to an external magnetic field, and that energy transitions can be induced by exposing the sample to electromagnetic radiation of the appropriate energy (usually in the radiofrequency range). Since then, the scope of this technique has tremendously expanded.

NMR has become the most informative, and therefore the most popular spectroscopy, to the point that it would be inconceivable nowadays to think of a Chemistry Department that does not have at least one instrument dedicated to NMR. A more recent development of the original idea is Magnetic Resonance Imaging (MRI), which is widely used in the medical field.

Most NMR experiments are performed by dissolving the substance of interest in an appropriate solvent. In the liquid phase, one tends to obtain sharp lines, and from these a wealth of information that often leads to structure determination. However, this leaves out several cases in which the sample cannot be dissolved (*e.g.* polymers), or in which the properties of the solid state are by themselves of interest. Part of the problem is that the lack of mobility and anisotropic environment of the molecules in a solid sample introduces other interactions that usually enormously broaden the NMR lines. One solution is a technique called magic angle spinning (MAS), in which the sample is rapidly rotated (typically at speeds of the order of 10^4 Hz) at an angle of exactly 54° 44′ 8″ to the (usually vertical) magnetic field. This is technically demanding, but results in a drastic sharpening of the lines and produces spectra with resolutions almost up to liquid standards.

MAS-NMR has thus become in the last few years a crucially important technique for researchers interested in bulk solids. The technique is also ideal for the study of mesophases such as gels, mobile coatings of small solid particles, liposomes, and other microstructured samples which are not quite solids but are not really liquids either. MAS-NMR is applied for the characterization of battery materials.(91)

Multinuclei NMR was widely used in solution studies, *e.g.* the extensive use of this technique was done, within the framework of R&D of rechargeable magnesium batteries, in studies of the relevant electrolyte solutions (ethers/MgR_2 – $AlCl_{3-n}$ solutions).(92) In recent years, solid state NMR became highly important for the structural analysis of materials for Li batteries:

1. Studies of polymeric electrolytes.(93)
2. Studies of the lithiation of carbonaceous materials.(94)
3. Structural analysis of $LiM^1_xM^2_yM^3_zO_2$ Li insertion materials ($M^{1\text{-}3}$ = transition metal).(95)
4. Distinguishing among various locations of Li ions (surface films, lithium in layers, transition metal layers) in new cathode materials for Li batteries.(96)

3.4.2.4. IR, UV-Vis, Raman

a. Infrared Spectroscopy.(87) Infrared (IR) spectroscopy is a chemical analytical technique that measures the intensity of IR transmittance or absorbance *vs.* the wavelength (or wavenumber) of the incident-absorbed light. In terms of wavenumber, infrared light can be divided into far infrared (4 ~ 400 cm^{-1}), mid infrared (200 ~ 4,000 cm^{-1}) and near infrared (4,000 ~ 14,000 cm^{-1}). Mid infrared light is suitable for exciting molecular vibrations. Thereby, the spectral response at this range is characteristic of specific types of chemical bonds and enables the identification of molecules by type of bonds and functional groups. The absorption, $A = -\log I/I_0$ (A- absorption, I – intensity of the output beam, I_0 – intensity of the input beam), is displayed *vs.* wavenumber and is almost linearly dependent on the concentration of the absorbing material by the Beer's law: $A = \varepsilon bc$, where A is the absorbance, ε is the absorbance coefficient, b is the length of the sample, and c is the concentration of the sample (which is, in fact, linear to the area of the peaks and nearly proportional to their height). Two different types of spectrometers are used for IR measurements:

(i) **Dispersive IR**. This spectrometer is a double beam one, in which the incident beam is divided: one passes through the sample and the other passes through a reference environment. Then, the beams are directed to a monochromator that is usually constructed of a grating or a prism and a slit. The grating separates the IR wavelengths. The moving slit directs each wavelength separately to the detector. The wavelengths are measured one after the other, with the slit monitoring the spectral bandwidth, and thus, the resolution of the spectrum. This type of IR spectrometer suffers from several drawbacks: the sensitivity and resolution of the spectra are limited by the grating and the slit; in addition, improved signal to noise ratio can be obtained only by very prolonged measurements.

(ii) **Fourier Transform IR (FT-IR).**(97) The FT-IR is based on the Michelson's interferometer, in which the IR beam source is directed to a beamsplitter that divides the beam into two parts. One part is directed to a fixed mirror and the other one to a moving mirror that moves backwards and forwards on an optical bench at a constant velocity. The beams are reflected from the two mirrors and recombine at the beamsplitter. Since the two beams travel different optical ways, their combination produces interference patterns. The degree of constructive or destructive interference of the two beams depends on the wavelength. The output signal of the interferometer is called interferogram: intensity *vs.* time, which includes the simultaneous contribution of all the wavelengths. A computerized Fourier transform of the interferogram is needed in order to obtain a "normal" intensity *vs.* a wavelength spectrum. The major advantage of FTIR is the very short time needed for the collection of each spectrum, which enables the repetitive collection of spectra that improve the SNR, and therefore, the sensitivity of the measurements. The spectral resolution depends on the moving mirror velocity. Based on improvements in sensitivity and resolution by this technique, several novel techniques that enable the analysis of surface chemistry and powders were developed:

i. Attenuated Total Reflection (ATR). Attenuated total reflection is a method for analyzing surfaces. The IR beam is directed into an optical crystal with a high refractive index (*e.g.* Si, Ge, ZnSe) at a critical angle that sets off conditions for total internal reflection. The radiation is reflected several times within the ATR element. The analyzed surfaces are closely connected to the surface of the ATR crystal. The beam reflected through the crystal penetrates a finite depth into the sample with each reflection by the so-called "evanescent" wave. The beam is directed from the crystal to the detector.

ii. IR Reflectance Absorbance Spectroscopy (IRRAS).(98) Reflectance absorbance spectroscopy is a method for analyzing thin films on reflecting surfaces. It is highly sensitive and enables the analysis of monolayers. The IR beam is directed to the analyzed reflective surface and is partially absorbed by the surface films, and is then directed from the surface to the detector. The IRRAS is dependent on the optical constants of the thin film and the substrate, the angle of incidence, as well as the polarization state of the incident IR beam. The angle of the incident that is mostly sensitive to the surface is 80-87^0 and is known as a grazing angle. The radiation is a combination of *p*-polarized light that is parallel to the surface vectors and *s*-polarized light that is perpendicular to the surface vectors. Usually, the *p*-component of the beam interacts with the adsorbed species whose dipoles are perpendicular to the surface. Hence, there are the so-called "surface selection rules" for IRRAS, which can be used to study the molecular orientation of thin films or monolayers deposited on reflective surface such as metals.

iii. Diffuse Reflectance Spectroscopy (DRIFTS).(99) Diffuse reflectance spectroscopy is a technique that collects the scattered IR radiation reflected from rough solids, and hence can be used for the analysis of fine particles and powders, as well as rough surfaces. When an IR beam is directed to such samples, part of the radiation penetrates the particles and some of it is reflected from the particles' surface. The portion that penetrates the sample undergoes scattering. A fraction of this radiation can be collected, concentrated, and directed to the detector. The Kubelka-Munk model(100) and its co-ordinates are suitable for presenting diffuse reflectance spectra..

b. Raman Spectroscopy.(101) Raman spectroscopy is a complementary technique to infrared spectroscopy and is based on the Raman effect. When radiation is scattered from matter, most of the light is scattered with the same energy (wavelength) as the incident light. A small fraction of the light is scattered at a different energy (usually lower). The process leading to this inelastic scattering is called the Raman effect, which is derived from changes in the vibration, rotation or electronic energy levels of the scattering medium. For practical Raman spectroscopy, only the changes related to vibrational levels are considered. Hence, the difference in energy between the incident light and the scattered light is equal to the energy of vibrations of the scattering molecules. Not all the molecular vibrations are necessarily Raman active. Only vibrations that relate to changes in the polarizability of the molecule are active. A plot of intensity of the scattered light *vs.* energy difference expressed in wavenumber (cm^{-1}) is a Raman spectrum, which is, in fact, a vibrational spectrum parallel to the IR spectrum of a molecule. The interpretation of Raman spectra is very similar to that of infrared spectra. The main difference between the two techniques is their selection rules. In infrared spectroscopy, the active vibrations are those that lead to changes in the permanent dipole moment of the molecule during vibration, while the analogue Raman selection rule relates to changes in polarizability during vibration. Therefore, Raman spectroscopy, may offer complementary data on vibration modes that are inactive in infrared spectroscopy. Due to the relatively low intensity of Raman scattering, a very intense light source is needed, and thus, all the Raman instrumentation uses laser beams as the source of light. This raises the problem of possible damage to surfaces measured by this technique.

It is possible to obtain intense Raman signals by surface enhanced Raman scattering (SERS) phenomena,(102) which are mostly used to study monolayers adsorbed on metals, including electrodes. This application of Raman spectroscopy is based on the pronounced enhancement obtained when a spectrum is measured from an absorbed species on rough metallic surfaces. This surface-enhanced Raman scattering is strongest on rough silver, but is observed with rough gold and copper surfaces as well.

c. Ultraviolet/Visible Spectroscopy (UV/VIS):(87) UV/VIS spectroscopy is useful for characterizing the absorption, transmission, and reflectance of a variety of materials related to their electronic levels. The light in the UV/VIS range of the spectrum (200-400nm, 400-800nm) is energetic enough to probe the electronic transitions of molecules. Conjugated systems, aromatic materials, heteroatomic organic systems, and transition metal ions in solutions absorb visible or UV light. Therefore, UV/VIS spectroscopy is applicable for a wide range of materials. The UV/VIS spectra have broad features because vibrational and rotational contributions are superimposed on top of the electronic response. Therefore, the use of this spectroscopy for a rigorous identification of materials is very limited. However, UV/VIS is very valuable for quantitative measurements because the intensity of the absorbance in UV-VIS depends linearly on the concentration of the absorbing species (Beer's law).

3.4.2.5. Inductively Coupled Plasma (ICP)(103)

ICP is an analytical atomic spectrometery. It can identify most of the elements (except for H,N,O,C,F) and quantify their concentrations in ppm units (mg/liter). The analysis is performed in aqueous homogeneous media. The media may be also dilute acids or alkalis (up to 10%). Organic polar solvents are suitable for analysis only if they can be diluted with water without causing precipitation. In fact, it is possible to analyze all media, after treatments that form water-soluble compounds.

The principle of the ICP instrumental technique: ICP measures the energy lost by an atom passing from an excited state to a lower energy state.

The energy is released in the form of light, and each element has its characteristic wavelengths. The intensity of the emitted light is proportional to the number of atoms in the emitting sample. The sample is atomized in the instrument in the following way: the liquid sample is converted to a wet spray (nebulization), after which the water is driven off and the remaining solid and liquid portions are converted to gases and plasma comprising inert gas, usually argon, maintained at high temperature (600°K-1000°K).

An ICP-AES instrument consists of a sample delivery system (or "sample introduction system"), Inductively Coupled (IC) plasma to generate the signal, one or more optical spectrometers to measure the signal, and a computer for controlling the analysis.

The most common sample delivery system consists of a peristaltic pump and capillary tube to deliver a constant flow of the analyte liquid into a nebulizer. The largest droplets fall out into a drain at the bottom of a spray chamber and the finest droplets are carried by gas into the IC plasma. Hence, this technique is suitable for analyzing both electrolyte solutions and electrode materials (that can be dissolved in water by suitable treatment).

3.4.2.6. Diffraction Techniques (X-Ray and Neutron Diffraction)

Electrodes and solid electrolytes are usually crystalline materials with a regular atomic structure that determines their electrochemical behavior. For instance, the ionic transport in solid electrolytes or insertion electrodes is possible only due to a special atomic arrangement in these materials.(104) The only way to learn about the crystal structure of materials is through diffraction techniques such as X-ray, electron and neutron diffractions, which are suitable for all crystalline materials.(104) X-ray diffraction (XRD) is the most common, because it does not need any special material preparation for analysis, as for electron diffraction, or special radiation sources, as for neutron diffraction. The most powerful modern techniques are X-ray and neutron diffraction (ND) that use monochromatic, high intensive synchrotron sources. Crystalline materials irradiated by any of these beams give diffraction patterns, *i.e.* a number of reflections that can be transformed into the atomic arrangement.(105) All commonly used, modern diffraction techniques allow structural analysis for powder samples.

The positions (angles) and intensities of the reflections in the diffraction patterns are typical (fingerprint) for each compound.(104-105) As a result, the X-ray powder diffraction patterns are widely used to identify the type of material (phase identification) by comparison with the standard patterns of the International Powder Diffraction File (PDF) database.(106) By this method, qualitative and quantitative analyses of complex poly-phase materials can be made.

The phase identification is especially important for insertion electrodes. In this case, the electrochemical curves can be regarded as some kind of phase diagrams for the hosts and the insertion ions.(107) Thus, the electrochemical process reflects the phase transitions that take place in the host upon ion insertion. The study of such processes by phase analysis can be done for the electrodes taken out from the solution at the characteristic points of the electrochemical curve (*ex situ* experiments), but it can also be performed simultaneously with the electrode's polarization in the electrochemical cell (*in situ* experiments).

3.4.2.7. X-Ray Techniques: EXAFS and XANES(108-110)

Of the bulk X-ray chemical analyses, the most powerful ones for material characterizations are EXAFS and XANES. These techniques necessitate intense monochromatic X-ray beam sources, available only in adjacent to giant particle accelerators, and are thus less accessible for the common researcher.

EXAFS stands for Extended X-ray Absorption Fine Structure. In this technique, the sample is illuminated by an intense monochromatic X-ray beam, generated by the accelerator. The analysis is made by gradually increasing the photon energy until it reaches the edge, for absorption by one of the sample atoms. Since the energy is just slightly above the absorption edge, the ejected electron can be backscattered by neighboring atoms. The probability for backscattering is dependent on the electron's energy, which in turn is dependent on the beam's energy, as well as on the scatterers. Backscattering results in changes in the absorption probability. The net picture, then, is oscillation in the absorption magnitude beyond the edge. The mathematical analysis of these oscillations can yield information regarding the scatterers, their number, their distance, and their arrangement. EXAFS can become surface sensitive by directing the beam at the grazing angle.

XANES (X-ray Absorption Near Edge Structure) is a complementary technique to EXAFS that concentrates on the absorption structure in the *ca.* 40 eV region beyond the edge. The edge position gives information regarding the atom oxidation state, while the analysis of the oscillations can provide information on vacant orbitals, on the atom's site symmetry, and on its electronic configuration. The data interpretation is not always straightforward, and is usually done by comparing experimental data to modelistic semi-empirical calculations.

3.4.3. Microscopy

3.4.3.1. Electron Microscopy and Related Techniques(111)

Electron microscopes use a beam of highly energetic electrons to examine objects on a very fine scale. The following information can be obtained.

- Topography. The surface features of an object or "how it looks", its texture; direct relation between these features and materials' properties (hardness, reflectivity, *etc.*).
- Morphology. The shape and size of the particles making up the object; direct relation between these structures and materials' properties (ductility, strength, reactivity, *etc.*).
- Composition. The elements and compounds that the object is composed of and their relative amounts; direct relationship between composition and materials' properties (melting point, reactivity, hardness, *etc.*).
- Crystallographic information. How the atoms are arranged in the object; direct relation between these arrangements and materials' properties (conductivity, electrical properties, strength, *etc.*).

Electron microscopes were developed due to the limitations of light microscopes, which are limited by the physics of light to 500-1000x magnification and a resolution of 0.2 micrometers. In the 1920s, it was discovered that accelerated electrons behave in vacuum just like light. They travel in straight lines and have a wavelength about 100,000 times smaller than that of light. Furthermore, it was found that electric and magnetic fields have the same effect on electrons that glass lenses and mirrors have on visible light.

Electron microscopes (EMs) function exactly like their optical counterparts except that they use a focused beam of electrons instead of light to "image" the specimen and gain information on its structure and composition. Below are the basic steps involved in all EMs.

1. A stream of electrons is formed (by the electron source, *e.g.* a filament) and accelerated towards the specimen using a positive electrical potential.
2. This stream is confined and focused using metal apertures and a magnetic lens into a thin, focused, monochromatic beam.
3. This beam is focused onto the sample using a magnetic lens.
4. Interactions occur inside the irradiated sample, affecting the electron beam.

These interactions and effects are detected and transformed into an image. The above steps are carried out in all EMs regardless of type.

Today, electron microscopy comprises a wide range of different methods that use the various signals arising from the interaction of the electron beam with the sample to obtain information about structure, morphology and composition. The energetic electrons in the microscope strike the sample and two different types of interactions appear. In *elastic* interactions, no energy is transferred from the electron to the sample. The electron either passes without any interaction (direct beam) or is scattered by the positive potential inside the electron cloud. These signals are mainly exploited in TEM and ED (electron diffraction). There are also *inelastic* interactions in which energy is transferred from the incident electrons to the sample: secondary electrons, phonons, UV quanta- or cathodo-luminescence are produced; shooting out inner shell electrons leads to the emission of X-rays or Auger electrons. These signals are used in analytical electron microscopy.

Critical parts in EMs are:

- Objective lens: generates the first intermediate image, the quality of which determines the resolution of the final image.
- Diffraction/intermediate lens: switching between imaging and diffraction mode.
- Projective lenses: further magnification of second intermediate image (image or diffraction pattern, respectively).
- Image observation: images and diffraction pattern can be directly observed on the viewing screen in the projection chamber or via a TV camera mounted below the microscope column. Images can be recorded on negative films, on slow-scan CCD cameras or on imaging plates.
- Vacuum system: because of the strong interactions of electron with matter, gas particles must be absent in the column. The required high vacuum is maintained by a vacuum system typically comprising a rotary pump (pre-vacuum pump), a diffusion pump, and one or more ion getter pumps.

Electron microscopy methods include the following.

TEM -Transmission Electron Microscopy

- Bright Field (BF)/Dark Field (DF) mode, which detects crystalline areas, defects and grain boundaries, phase analysis, and particle size.
- High Resolution Transmission Electron Microscopy (HRTEM), which is the direct visualization of structures and defects at a resolution of 0.1 nm.
- Electron Diffraction (ED), which determines lattice parameters and crystal symmetry, crystal orientation, and enables phase analysis. Electron diffraction is a collective elastic scattering phenomenon with electrons being scattered by atoms in a regular array (crystal). The incoming plane electron wave interacts with the atoms, and secondary waves are generated which interfere with each other. This occurs either constructively (reinforcement at certain scattering angles generating diffracted beams) or destructively (extinguishing of beams). As in XRD, the scattering event can be described as a reflection of the beams at planes of atoms (lattice planes). The Bragg law gives the relation between interplanar distance d and diffraction angle Θ: $n\lambda = 2d\sin\Theta$.

  Since the wavelength λ of the electrons is known, d can be calculated from ED patterns. Furthermore, information about crystal symmetry can be obtained.

- Energy Dispersive X-ray Microanalysis (EDX), which is a quantitative elemental analysis (fixed-point, time-resolved, mapping) with sensitivity down to a few atomic percent. EDX is a micro analytical technique that uses the characteristic spectrum of X-rays emitted by the specimen after excitation by high-energy electrons to obtain information about its elemental composition. EDX is a relatively simple technique, generally better suited to detecting elements of high atomic number, and provides rapid qualitative microanalysis of the specimen. The spatial resolution is determined by the probe size, beam broadening within the specimen, and the effect of backscattered electrons on the specimen around the point of analysis.

A main advantageous characteristic of a transmission electron microscope is the possibility to obtain information in real space (imaging mode) and reciprocal space (diffraction mode) almost simultaneously.

STEM - Scanning Transmission Electron Microscopy. This mode utilizes elastically scattered electrons - direct and diffracted beams. In STEM, a tiny, convergent electron beam is scanned over a defined area of the sample. At each spot, the generated signal is simultaneously recorded by selected detectors, building up an image. Furthermore, such a convergent beam is used to gain a highly localized signal from the specimen in analytical TEM (*e.g.* EDX) and thus the combination of STEM with analytical methods is a main application in practical work.

SEM - Scanning Electron Microscopy. This technique uses back scattered and secondary electrons. In a scanning electron microscope, a tiny electron beam is scanned across the sample. Simultaneously, the generated signals are being recorded, and an image is formed pixel by pixel. In SEM, the signals are observed on the same specimen site as the incoming electron beam (*cf.* STEM, using transmitted electrons). In contrast to TEM methods needing very thin samples, compact samples can thus be investigated by SEM. Valuable information about morphology; surface topology and composition can be obtained. High-resolution SEM microscopes achieving resolutions below 1 nm are now commercially available.

The use of SEM for the study of sensitive electrodes may need the use of special transfer systems.(112)

3.4.3.2. Atomic Force Microscopy (AFM)(113)

An atomic force microscope (AFM) is an instrument used for studying surface properties of materials at the micron to atomic level. It is used in electronic, telecommunications, biological, chemical, automotive, aerospace, and energy industries. The AFM can be used to investigate a variety of materials, which include thin and thick film coatings, ceramics, composites, glass, synthetic and biological membranes, metals, polymers and semiconductors. It may be used to image surfaces at atomic resolution, as well as to measure forces at the nano-Newton scale.

AFM consists of a cantilever spring with a sharp tip at its end, typically composed of silicon or silicon nitride with tip sizes in the order of nanometers. The tip is brought into the close proximity of a sample surface. The Van der Waals forces between the tip and the sample lead to a deflection of the cantilever according to Hook's law, where the spring constant of the cantilever is known. Typically, the deflection is measured using a laser beam reflected from the top of the cantilever into an array of photodiode detectors. Images are taken by scanning the sample relative to the probing tip and measuring the deflection of the cantilever as a function of its lateral position.

In essence, the instrument can also record the vertical movement of the apparatus, which is required in order to keep the cantilever deflection constant. This provides the same topography information as before, but gives the instrument a greater dynamic operating range. The most common way to sense the cantilever deflection in AFM instruments is by a laser beam, which is typical for AFM; however, other sensory-feedback techniques can also be used. Typical spring constants are between 0.001 to 100 N/m, and motions from microns to ~ 0.1Å are measured by the deflection sensor. Typical forces between tip and sample range from 10^{-11} to 10^{-6} N. For comparison, the interaction between two covalently bonded atoms is of the order of 10^{-9} N at separations of ~1Å. Therefore, this technique is essentially non-destructive.

The atomic force microscope was developed to overcome a basic drawback of STM, *i.e.* that it can only image conducting or semiconducting surfaces. The AFM can image almost any type of surface, including polymers, ceramics, composites, glass, and biological samples. Besides imaging, it is also one of the foremost tools for the manipulation of matter at the nanoscale.

Contact Mode (C-AFM)

In C-AFM, the tip makes physical contact with the sample. As the tip is moved across the sample, the contact force causes the cantilever to bend according to changes in topography.

Non-contact Mode (NC-AFM)

In NC-AFM, the cantilever is vibrated near the surface of the sample. The distance between the tip and the sample is of the order of tens of thousands of angstroms. NC-AFM is advantageous because the tip has little or no contact with the sample.

Intermittent Mode (IC-AFM)

IC-AFM ("tapping") is very similar to NC-AFM. In IC-AFM, the vibrating cantilever tip is drawn closer to the sample surface and the tip just barely hits, or "taps" the sample. It is also: a) less likely to damage the surface than C-AFM; b) able to eliminate lateral forces between the tip and the sample; c) more effective than NC-AFM for imaging larger scan sizes that may include larger variations in topography.

Phase Imaging

Phase imaging is used to map properties such as visco-elasticity, adhesion, and friction. Phase imaging can be produced simultaneously while operating in NC-AFM or IC-AFM. It provides nanometer-scale information about surface structures often not seen by other AFM modes.

Phase imaging monitors the phase lag between the signal that oscillates the cantilever and cantilever oscillation output signal. Changes in the phase lag reflect changes in the mechanical properties of the sample surface.

AFM has been adopted by many electrochemistry groups as an *in situ* morphology-electrochemical technique. It was successfully used for the study of Li electrodes, Li deposition-dissolution process and Li intercalation processes into carbonaceous materials.(114) For the above studies, special work stations were built that included glove box systems. See detailed descriptions in Ref. [115]. All studies relating to Li batteries and descriptions of the relevant workstations are well documented in the literature.(116,117)

3.4.4. Analysis of Surface Area by Gas Adsorption Processes

There are commercial instruments that operate by measuring the quantity of gas adsorbed onto, or desorbed from, a solid surface at some equilibrium vapor pressure by the *static volumetric method.* The data are obtained by admitting or removing a known quantity of adsorbate gas in/out of a cell containing the solid adsorbent maintained at a constant temperature below the critical temperature of the adsorbate. As adsorption or desorption occurs, the pressure in the sample's cell changes until equilibrium is established. The quantity of gas adsorbed or desorbed at the equilibrium pressure is the difference between the amount of gas admitted or removed and the amount required to fill the space around the adsorbent (void space).

These instruments have the capability of measuring adsorbed or desorbed volumes of nitrogen at relative pressures at a range where the lower limit extended from $1x10^{-6}$ to slightly under 1.0 torr. This volume-pressure data can be reduced by an appropriate software into BET surface area (single and/or multipoint), Langmuir surface area, adsorption and/or desorption isotherms, pore size and surface area distribution, micropore volume, and surface area, using an extensive set of built-in data reduction procedures.

Before performing gas sorption experiments, solid surfaces must be free of contaminants such as water and other adsorbed species. Surfaces' cleaning (degassing) is carried out by placing a sample of a solid in a glass cell and heating it under vacuum. Once clean, the sample is brought to a constant temperature of the adsorption process (by means of an external bath). For instance, in the case of nitrogen adsorption isotherm measurements, the temperature of liquid nitrogen (boiling point is 77.35 K) is used.

The standard method for measuring a specific surface area is based on the physical adsorption of nitrogen on a solid surface, using the BET (Brunauer, Emmet and Teller) method with the equation:(118)

$$\frac{1}{V((P_0/P)-1)} = \frac{1}{V_m C} + \frac{C-1}{V_m C}\left(\frac{P}{P_0}\right),$$

in which V is the volume of gas adsorbed at a relative pressure, P/P_0, and V_m is the volume of gas adsorbed when the entire adsorbent surface is covered with a complete unimolecular layer. The term C (the BET C constant) relates to the energy of adsorption in the first adsorbed layer, and consequently its value is an indication of the magnitude of the adsorbent/adsorbate interactions. From calculations of V_m, it is possible to estimate the surface area of the porous materials (obtained by the instrument's software).

3.4.5. Thermal Analysis

3.4.5.1. DTA, DSC and TGA

These techniques provide information about the heat of reactions or free energy/enthalpies as a function of temperature. Differential thermal analysis (DTA) measures temperature differences between a sample and a reference, as the temperature is increased at a known and constant rate (0.1 to 160°C/min), or held at isothermal conditions up to 1500°C. Differential scanning calorimetery (DSC) measures reaction enthalpies as the sample is heated at a known and constant rate (0.1 to 320°C/min), or held at isothermal conditions up to 750°C.

DTA and DSC are versatile methods providing important information on the physical and chemical behavior of processes using very small sample quantities. These methods provide qualitative and quantitative information about whether a reaction is endothermic or exothermic. They also provide insight into reaction onset temperatures and can be used to screen reactive systems that may be risky when used. DSC and DTA measurements can be used to obtain fundamental kinetic data, either using non-isothermal methods or by studying reaction rates at different isothermal temperatures. In addition, DSC can be used to measure heat capacities.

Thermal Gravimetric Analysis (TGA) complements DTA and DSC. TGA measures mass changes as a sample is heated at a known and constant rate

(0.1 to 160°C/min) or at isothermal conditions. Mass changes as a function of temperature can be used to determine reaction mechanisms, particularly when coupled with gas analysis. When coupled with DTA and DSC, TGA results are used to identify the temperature ranges of interest for DSC or TGA measurements, in order to determine precisely free energy/enthalpy values of the studied reactions.

The possibility of analyzing the gases evolved during TGA/DTA analyses using mass spectrometry (MS) or infrared spectroscopy (IR) enables key insights to be gained about thermal reactions.

3.4.5.2. Accelerating Rate Calorimetry

The accelerating rate calorimetry (ARC) technique has been used to evaluate thermal hazards associated with battery materials.(119)

ARC measures temperature changes due to thermal (exothermal) reactions at adiabatic conditions. It was originally designed to assess the hazards of potentially reactive systems with respect to processes. ARC is programmed to monitor heat (temperature) changes at adiabatic conditions as follows: the system gradually heats the sample, and if the instrument does not detect any temperature changes, it then heats the sample to the next operator-selected temperature and again searches for temperature changes in the sample. Once an exothermal reaction is ignited and heat is dissipated, the system detects a change in temperature due to thermal reaction and follows the temperatures that are developed by exothermal reactions at adiabatic conditions, up to 400°C. This approach allows the samples to self-heat, and thus undergo a thermal runaway reaction when relevant. In addition to its obvious application for characterizing the thermal reactivity risk of materials, ARC can be used to measure reaction enthalpies and determine kinetic parameters. It can be especially useful when both temperature and pressure changes are monitored.

The major raw data from which both kinetic and thermodynamic information can be obtained are T and P *vs.* t, $\frac{dT}{dt}$ and $\frac{dP}{dt}$ *vs.* t, and $\frac{dT}{dt}$ and $\frac{dP}{dt}$ *vs.* T.

ARC is an ideal tool for the study of the thermal runaway processes of electrolyte solutions and electrode-electrolyte solution systems. A combination of ARC and DSC, especially when it is possible to measure both pressure and temperature changes with the former technique, provides a complete analysis of the high temperature behavior of battery materials and sub-systems.(120)

3.4.6. Surface Analysis

3.4.6.1 General Remarks

Several of the techniques mentioned above can be considered as surface analytical tools, including SEM, EDS, AFM, small angle XRD, Raman and FTIR spectroscopies. In many cases (especially relevant to the field of Li and Li-ion batteries) the surface films on electrodes and side products formed in battery systems may be very sensitive to atmospheric gases, mostly trace water, O_2 and CO_2. Thereby, spectroscopic and microscopic measurements should be carried out under strict atmospheric control. Hence, FTIR and Raman spectrometers should operate in glove boxes if the main focus of the spectroscopic studies is active materials. In addition, the application of techniques such as XPS or electron microscopy for measuring highly reactive materials requires the use of transfer systems from glove boxes or dry rooms to the instruments. See Figure 3.2 for examples.

3.4.6.2. FTIR and Raman Spectroscopies

The use of Raman spectroscopy for surface analysis is not trivial since Raman signals are relatively weak. The application of surface-enhanced Raman spectroscopy (SERS, see Sub-section 3.4.2.4.) in battery research may only be relevant for studying the reduction/oxidation products of selected electrolyte solutions, using noble metal working electrodes. The analysis of such reactions sheds light on side reactions of the solutions as well as on passivation phenomena. Note, however, that the laser beam used for this technique can burn the surface studied, due to the intensity of the light. Hence, Raman spectroscopy of surfaces can provide misleading results due to the destructive impact of the laser beam. In any event, micro Raman systems available today enable the use of this technique for mapping electrodes' surfaces at the microscopic level and to monitor aging of composite electrodes.(121) FTIR spectroscopy provides parallel information on surface functional groups (through the vibrational response), while not being destructive at all. FTIR spectroscopy can be applied for battery research through the following approaches (see also Sub-section 3.4.2.4 above), schematically described in Figure 3.3.

a) Transmittance mode. Pristine, powdered active mass, as well as particles scraped from polarized/aged/cycled electrodes, can be ground with KBr (the usual medium for IR spectroscopy of pellets) and then pelletized to transparent pellets that can be measured by transmittance mode. IR signals of surface species formed on the particles, as well as the IR response of the particles, can be obtained. Major drawback: loss of information and low

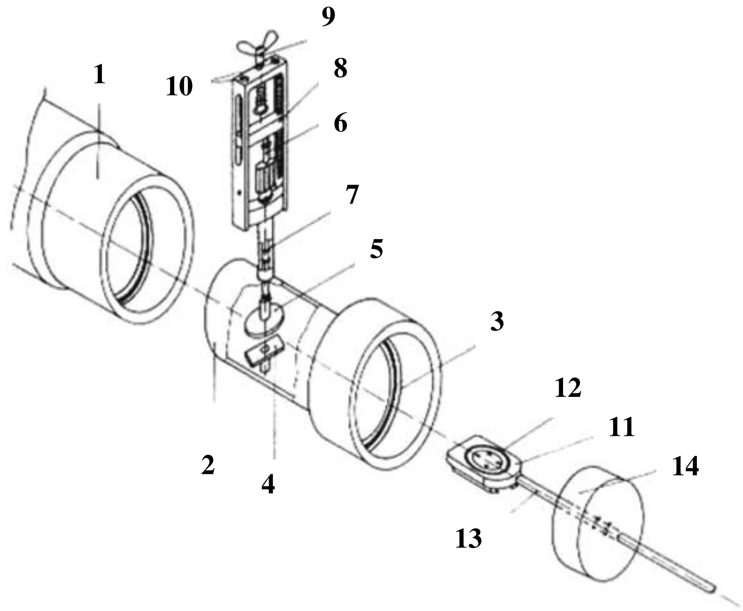

A transfer system for lithium samples from glove boxes to scanning electron microscope. **1.** Microscope inlet. **2.** Brass cylinder system body. **3.** Rubber ring. **4**. A fixed tray. **5.** A brass disc (hermetically closed the samples on the sample tray). **6.** A brass shaft. **7.** A brass cylinder with two rubber rings that welded to the body. **8.** A bridge attached to the edge of the shaft. **9.** A bolts that press down the bridge to the shaft. **10.** Bolts that release the tray from the bridge. **11.** The samples tray. **12.** A rubber ring. **13.** Manipulator. **14.** A Perspex leader to the manipulator.

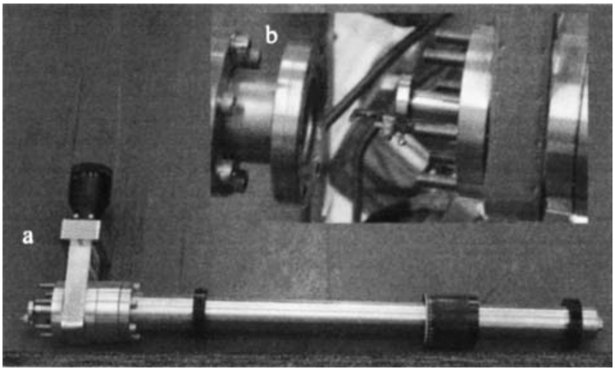

Figure 3.2. Examples of transfer systems from glove box to microscopy and spectroscopy. *Top*: a transfer system developed to transfer sensitive samples from an inert atmosphere (glove box) to a scanning electron microscope (*Ref. 112*). *Bottom*: (a) a picture of a transfer system from glove boxes to XPS/AES systems, which includes a gate valve and a magnetic sample manipulator. In (b), there is a picture of the port in the spectrometer, to which the transfer system is mounted.

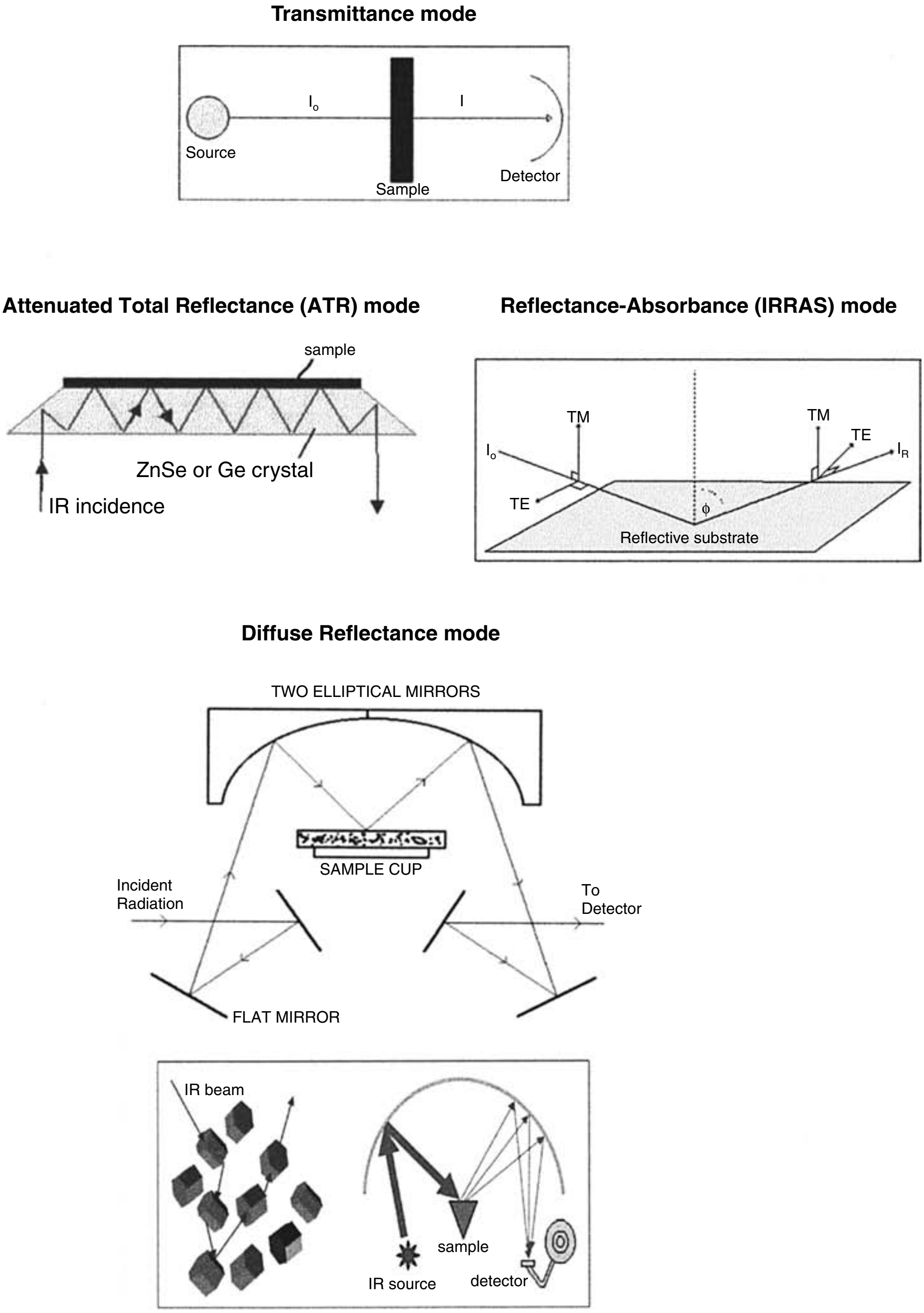

Figure 3.3. Different modes for surface and bulk analysis by infrared spectroscopy (*Ref. 97*, www.nuance.northwestern.edu).

resolution spectra, because most of the relevant powders (active mass of interest) are not transparent, and hence, there is significant interference by optical artifacts.

b) Attenuated total reflectance (ATR) mode. The sample, that can be an aged composite electrode, is pressed on a facet of a paralleloid crystal made of IR transparent material of a high refractive index. Suitable materials are ZnSe, Ge and Si especially prepared for these techniques. The IR beam enters the crystal and is reflected internally from the interface between the crystal and the sample. The beam has a penetration depth of about ½ λ, and hence is absorbed by surface species on the sample. This technique is very suitable for IR measurements of both solid and liquid matter.

c) Flat reflective electrodes. Metallic surfaces covered by surface films can be measured by reflectance mode, using commercially available accessories. The best response from surface species on reflective surfaces can be obtained using reflectance-absorbance mode (IRRAS) with grazing angle incidence of the IR beam (using a grazing angle attachment). Adding a polarizer to the accessory, which allows only P polarized light to pass through, may increase the signal to noise ratio of adsorbed species, whose moment dipoles are perpendicular to the reflective surface (on which they are adsorbed).

d) Diffuse reflectance mode. This is the most effective mode for measuring surface species on particles (powders can be measured directly). Commercial accessories containing parabolic mirrors focus the IR beam on the powder sample, collect the light scattered from the sample, and direct it to the detector. The IR spectra obtained by this mode may be distorted, and hence, should be presented after their modification by the Kubeka-Munk transformation (see Sub-section 3.4.2.3). Such a presentation is available by all software programs of modern FTIR spectrometers.

It is important to note that both Raman and FTIR spectroscopies can be applied to reactive electrochemical systems as *in situ*, surface sensitive, spectro-electrochemical techniques. Hence, the surface chemistry can be analyzed in solutions, under potential control. By these modes, many problems related to reactions with atmospheric components, washing out surface products, and irreversible changes due to removal from the electrochemical cell, can be overcome. In fact, the application of *in situ* measurements enables the confirmation of the results obtained from the easier *ex situ* measurements. Some *in situ* techniques are discussed in Section 3.4.8.

3.4.6.3. XPS and AES(122)

XPS. Of all the X-ray chemical analyses, the most powerful ones for surface characterizations are XPS and AES. In the last two decades, XPS gained popularity in the battery characterization field, both because it is a technique that matured to the point that many institutions can afford to purchase it and because the spectral interpretation became much more reliable. In XPS, solid samples (that are compatible with the required high vacuum) are irradiated with a soft X-ray beam, usually around 1.5 KeV. As a result, due to the photoelectric effect, electrons are ejected from the sample atoms. The electrons are, in general, ejected from the orbitals according to the X-ray beam's energy, although the probability of each level to eject the electron differs. Thus, although many elements give quite a rich spectrum, the "analytical" emissions are usually the strongest ones, or the ones with the characteristic narrowest band. Basically, three types of electrons are counted in the XPS spectrometer: core electrons, valence electrons and X-ray-induced auger electrons. Each of them carries some information that can be valuable for the sample characterization. Core electrons, the main body of the XPS analyses, can be used to gain information on both the relative elemental surface concentration and the oxidation state of the various elements detected.

The quantitative information, although subjected many times to gross errors and, hence, more of a semi-quantitative type, is calculated from the relative peak areas with an empirical normalization value, of which the peak of fluorine F 1*s* is the RSF (relative sensitivity factor) convention. It is crucial to remember that the quantitative analysis is based on logarithmic equations, which were derived for both lateral and depth homogeneous samples. Unfortunately, most "real" samples are not chemically homogeneous, and thus, the quantification should be taken with caution. Moreover, even relatively homogeneous samples are always covered with adventitious adsorbed layers of carbonaceous materials, and possibly oxides and water that might adversely affect the quantitative analysis due to the surface sensitivity of the XPS analysis. Qualitative information is frequently extracted from the exact position of the emission peak by the NMR analogue to "chemical shift". In simple cases (neglecting charging, relaxation, and other quantum effects), the ejected electron kinetic energy is related to the chemical nature of the atom from which it was released through the equation $E_k^F = H_n\text{-BE}$, in which E_k^F is the ejected electron kinetic energy, H_n represents the X-ray source beam energy, and BE is the electron's binding energy. All atoms possess a particular set of electrons; each held in orbital around the nucleus by a distinct force, its binding energy. The BE is influenced by the distance of the relevant electron from the atom's nucleus, the shielding of the other electrons, and the existence of excess positive or negative charge. Thus, if a particular atom in the sample exists as a positive ion, *e.g.* due to interaction with oxygen (*e.g.* FeO), then the deficiency of one electron causes the rest of the electrons to bind more strongly to the nucleus, and hence to show a characteristic positive shift in the emitted BE electrons. A similar effect is registered with anions, but then the XPS spectrum will be characterized by a negative shift in the BE for this particular atom. Interestingly, there is no need for a complete electron transfer, as in ionic materials, to register chemical shifts, and in many cases it is sufficient that the analyzed atom interacts with a neighbor atom with a strong electron withdrawing or donating character in order to see a pronounced chemical shift in the binding energy. It is important to bear in mind that in many cases the collapse of simple rules and post-emission effects, as well as charging and other complex effects, might lead to unpredictable chemical shifts, which are extremely hard to interpret. Apart from the basic quantitative and qualitative information, core electrons frequently carry additional chemical information, manifested as additional satellite peaks. All core electrons, except the *s* ones, exist as doublets due to spin-orbit coupling, whose magnitude can be extracted from the peak separation. Multiplet splitting, shake-up, and shake-off, as well as surface and bulk plasmons, are all important features in XPS analysis from which intricate information can be attained, such as spin state, existence of conduction bands, pi-system, *etc*.

The XPS valence band is usually used as fingerprint mode material identification, or as a powerful analytical tool to study the Fermi-level and conduction-band structures. This region, which lies in the low-BE side of the spectrum, is identified by high kinetic energy electrons, and suffers from low resolution, as compared to UPS, a complementary technique that uses an ultraviolet source instead of an X-ray one.

The XP Auger electrons are seldom used in XPS analysis, although, as they are not source dependent, they are utilized occasionally to discriminate between hard to determine cases.

As was mentioned above, XPS is surface sensitive. This is because it relies on ejected electrons, which have limited mobility within matter. As a rule of thumb, the analysis depth is said to be some 70-100 Å, although using angle-resolved XPS can improve the surface sensitivity.

AES, Auger electron spectroscopy, is another UHV-based, surface sensitive chemical analysis technique. This technique is complementary to XPS. In AES, the sample is irradiated with an electron beam that knocks electrons off the sample's atomic orbitals. The resulting cations, frequently missing an electron from core orbitals, relax by various mechanisms, including electron rearrangement in which electrons form higher shells that fill the core void. This in turn is accompanied by the ejection of other electrons, according to the energy conservation rule. In AES, just like in XPS, the Auger electrons are collected through electron optics and analyzed for their kinetic energy and relative flux.

Each atom in the periodic table, except for hydrogen, has a set of known Auger emissions, dominated by the electronic structure of the element and by quantum mechanical rules. The measurement of AES allows both the qualitative chemical analyses of solid samples, *e.g.* electrodes, and semi-quantitative information as to the relative abundance of each element in the sample. Similarly to XPS, chemical shifts in the Auger electron emissions allow chemical information to be extracted regarding the atom's interaction. AES can be made more surface sensitive than XPS by tuning the impinging e-beam to lower energies. AES, like all the other techniques, does not come without shortcomings. First, the data interpretation is often not straightforward. The analysis requires sophisticated and costly UHV systems. The AE emission is statistically weak, and is more applicable for lighter elements. In addition, one of the greatest problems with AES is the danger of e-beam damage, especially to organic layers and even to some oxides. Ref. [123] provides comprehensive examples for the use of these techniques for the characterization of battery materials.

3.4.7. Electrochemical Techniques

3.4.7.1. Introduction

Naturally, electrochemical techniques are the most important tools for the characterization of batteries and their components. The electrochemical response may be much more sensitive to surface and bulk structures and changes than most of the commonly used spectroscopic and diffraction techniques. Today, there is an impressive collection of computerized, multichannel electrochemical analyzers, operated by developed software, that enables the simultaneous application of all electrochemical techniques of interest to hundreds of cells, as well as the analysis of the response. Table 3.3 lists the most important electrochemical techniques relevant for battery characterization, and summarizes in brief their main properties and output. Table 3.4 lists typical types of equipment from leading companies useful for the electrochemical characterization of batteries and their components.

3.4.7.2. Fine Electroanalytical Techniques

The combined application of conventional electro-analytical techniques such as chronopotentiometry, slow scan rate cycling voltammetry (SSCV) and a variety of small-amplitude relaxation techniques (potentiostatic intermittent titration [PITT], galvanostatic intermittent titration [GITT] and electrochemical impedance spectroscopy [EIS] for equilibrium [thermodynamic]), and the kinetic characterization of intercalation processes in ion-insertion electrodes

Table 3.3. List of electrochemical techniques and their characteristic time parameters. (*Refs.124-129*).

Technique	Input	Output	**Time Parameter(s)** (or special response)
Cyclic voltammetry (fast and slow) CV	Voltage $E_0 = E_0 + \nu t$	Current i(E)	RT/Fν (ν = potential scanning rate)
Chronopotentiometry, zero-current potentiometry	none	Voltage, E_{ocv} *vs.* t	Open circuit conditions, long t
Chronoamperometry	Voltage E *vs.* t	Current, i *vs.* t	Linear i *vs.* $\frac{1}{\sqrt{t}}$
Chronocoulometry	Voltage E *vs.* t	Charge *vs.* t $Q = \int_0^t I dt$	τ end of reaction
Electrochemical impedance spectroscopy EIS	Small-amplitude *ac* voltage	Small-amplitude *ac* current	Z" *vs.* Z' or log $\lvert Z \rvert$ and phase angle *vs.* log ω (ω = 2πf)
Rotating disk electrode voltammetry	Voltage E *vs.* t, Rotation rate	Current i *vs.* t	At high overpotential $i_L \propto \sqrt{\omega}$ i reaches ω=2πf
Polarography Dropping Hg electrode	Voltage E *vs.* t	Current i *vs.* E	t_{max} (drop time)
Chronopotentiometry	Current programming i *vs.* t	Voltage profile V *vs.* t	τ $C_{active\ species}$ becomes zero at the E. surface
Electrochemical quartz-crystal microbalance	Voltage as in CV	Current, mass I, Δm *vs.* E	RT/Fν or τ as in cyclic voltammetry or chronopotentiometry, depending on the type of time dependence of voltage

Table 3.4. Typical companies producing electrochemical instrumentation.

Company name	Location	Type of equipment
Arbin	USA	Fully programmable, automated multichannel testing systems for energy storage/conversion devices (batteries, capacitors).
Maccor	USA	Fully programmable automated multiple station secondary and primary cell testing systems, programmable electronics to sink and source current, frequency response analyzers, cell formation equipment.
EG&G - Princeton Applied Research (PAR)	USA	All kinds of electrochemical instrumentation. Potentiostat-galvanostat systems, multichannel analyzers, impedance spectroscopy, EQCM.
EcoChemie	The Netherland	Autolab Modular Electrochemical Instruments systems and Autolab SPR Instrumentation for all electrochemical techniques.
Bitrode	USA	Electrochemical instrumentation for industry and R&D laboratories: batteries and fuel cells testing.
A&H Battery services	Singapore	Equipment for batteries testing.
Storage battery systems (SBS)	USA	Testing instrumentation for batteries and fuel cells.
Bekal Hikmat Sdn Bhd	Malaysia	Electrical circuits and batteries testing equipment.
Solartron Analytical	UK	Instrumentation and software for electrical and electrochemical measurements, including single and multi channel systems, electrochemical impedance spectroscopy (EIS) and modeling, for the fields of corrosion, batteries and fuel cells.

presents many advantages compared to the case when they are used separately.(124) When characterizing new electrode materials, the application of the above techniques in a certain sequence helps to achieve a faster and deeper comprehension of the nature of the intercalation processes under study.

SSCV is the preferable tool for starting the experimental characterization of ion-insertion electrodes since cycling voltammetry is, in essence, a kind of large-amplitude voltage spectroscopy that provides information on the number of insertion steps and their formal redox-potentials. It also helps in estimating the related equilibrium charge and discharge capacities, along with qualitative information on the nature of phase transitions and their kinetics. In order to determine more precisely the characteristic charge-discharge capacities, chronopotentiometry with a small-applied current density should preferably follow the SSCV study. Analysis of the slope of the chronopotentiometric curves of intercalation electrodes at low current densities, in combination with the simultaneous (or in parallel) *in situ* XRD analysis, may provide additional information on the character of the insertion process, distinguishing between two different intercalation paths, *i.e.* via a solid solution or, alternatively, via a two-phase coexistence. Cyclic voltammetry, when used at different scan rates, may also be useful for the separation between the above alternative paths. However, an adequate modeling of the measured CV curves is required in this case.(124-128)

One of the most common rate-determining steps (RDS) of the entire ion-insertion process is solid-state diffusion within a thin-layer electrode or a powdery electrode composed of individual particles. The above large-amplitude technique provides only qualitative information on the possible involvement of solid-state diffusion as a RDS, since these techniques reflect mainly long-time domains of the responses. Practically, an increase in the slope of chronopotentiometric curves and broadening SSCV peaks may indicate the diffusion as RDS. However, similar trends are also characteristic of large ohmic drops. More precise information on the diffusion time constants τ_d, and, hence, the chemical diffusion coefficient, D, can be obtained by the application of small-amplitude techniques, PITT, GITT and EIS. The selection of the small amplitude of perturbation from equilibrium, in addition to a sufficiently long durability of the perturbation, leads to the determination of D, which is highly resolved with respect to the electrode potential, E (note that D is usually a sharp function of E in the case of two-phase reactions, and thus experimental skill is required to reliably probe the diffusion domain of these reactions).(124,126,128,130)

One of the most fruitful ideas of the classical electrochemistry of solution redox species is the concept of time windows and accessible rate constants of different electroanalytical techniques.(129) This approach was recently extended to studying finite-space diffusion within the intercalation particles by a combination of various electroanalytical techniques.(124,126,128,130)

When τ_d is the characteristic diffusion time constant of the intercalation process, it should not, of course, be dependent on the small-amplitude technique chosen, provided that the thickness of the film electrode is constant, or all the particles of the composite electrode have the same diameter.

We can state that τ_d (and hence D) can be conveniently represented as a simple function of the time invariant kinetic parameter Φ (characteristic of the technique used), and the equilibrium characteristic of the electrode, namely, differential intercalation capacitance, C_{dif}:

$$\tau_d = l^2/D = f(\Phi, C_{dif}) \tag{1}$$

where l denotes the characteristic diffusion length.

Explicit expressions for Φ and C_{dif} are presented in columns 4 and 5 of Table 3.5 for each technique considered. The perturbed parameter, as well as the measured quantities, are indicated in columns 2 and 3, respectively (note that ν and I_p are the potential scan rates and the peak currents in SSCV experiments, respectively; A_w is the Warburg slope, $-Z''(\omega)$ and $Z'(\omega)$ are the imaginary and real parts of the impedance presented as a function of the angular frequency ω).

Perturbation in PITT and GITT is attained by the application of small potential steps or pulses of current, respectively, from the equilibrium potentials of the electrode attained during the preceding titration step, so that the entire titration consists of a reasonable number of sequential small-amplitude steps of sufficient durability, and covers the entire potential range of the intercalation reaction.

Conventional equations for the chemical diffusion coefficient, D, derived for small-amplitude techniques, are presented in Eqs. 2-4.

$$\text{PITT:} \quad D = [\pi^{1/2} l \, (It^{1/2}/\Delta E)/ C_{dif}]^2 \tag{2}$$

$$\text{GITT:} \quad D = (4l^2 I^2/\pi)[C_{dif}(dE/dt^{1/2})]^{-2} \tag{3}$$

$$\text{EIS:} \quad D = 0.5\, l^2\, [C_{dif} A_w]^{-2} \tag{4}$$

The combination of Eqs. 2 and 4 allows the direct interrelation of the characteristic kinetic parameters Φ of PITT and EIS:

Table 3.5. Fine electro-analytical techniques and their relevant parameters: the type of perturbation, response, characteristic time invariant parameter and the relevant formula for the electrode's differential capacitance (*Refs. 124-132*).

Technique	Perturbed parameter	Measured quantities	Φ	C_{dif}
SSCV	ν	I *vs.* E	$I_p \nu^{1/2}$	I/ν
PITT	ΔE	I *vs.* t	$(It^{1/2}/\Delta E)$	$\Delta Q/\Delta E$
GITT	ΔI	E *vs.* t	$dE/dt^{1/2}$	$I\Delta t/\Delta E$
EIS	ω	$-Z''(\omega)$ *vs.* $Z'(\omega)$	A_w	$-1/\omega\, Z''_{\omega\to 0}$

$$A_w\,(It^{1/2})/\Delta E = (2\pi)^{-1/2} \tag{5}$$

From Eq. 5, it can be seen that the reciprocal of their product is simply equal to the square root of the fundamental constant 2π. A similar operation can be carried out with Eqs. 2 and 3:

$$(dE/dt^{1/2})(It^{1/2}/\Delta E)=2l/\pi, \tag{6}$$

showing the intrinsic link between the kinetic parameters of PITT and GITT.

Thus, if the intercalation electrode under consideration is uniform (in the sense defined above), the same value of D should be returned by either of the small-amplitude techniques used. We, however, extended the application of these techniques for two important practical cases of non-uniform electrodes, *e.g.* (i) when the electrode is composed of particles of different size, but with the same effective thickness of the porous electrode layer, and (ii) when the porous layer itself is geometrically non-uniform, possessing a distribution of different thicknesses (particles may have the same or different size).(131) When the electronic bulk conductivity of the electrode and the ionic conductivity of solution in the pores of the electrode are high enough, a sensitive indicator for such non-uniformity was shown to be the PITT method, with a particular presentation of the measured chronoamperometric curves in a specific form: $d\log|I|/d\log t$ *vs.* t/τ_d.(132) The distribution of the diffusion time constants in particles of different size becomes most spectacular using this plot (note that D remains constant since the distribution of τ_d is caused only by the related distribution of l!). In cases when the electronic conductivity of the electrode host and the ionic conductivity of the solution are not high enough, the most convenient technique was shown to be EIS.(131) Geometrical non-uniformity may result in a certain combination of parameters to the appearance of a large low-frequency semicircle specific to this kind of electrode non-uniformity.

Summarizing our approach to the electroanalytical characterization of practical ion-insertion electrodes, the following features should be emphasized: (i) a certain sequence in the application of electroanalytical tools facilitates the characterization of intercalation processes in new prospective electrode materials for rechargeable batteries; (ii) three basic, small-amplitude relaxation techniques (PITT, GITT and EIS) return the same D value only for uniform electrodes and when solid-state diffusion is the single RDS (a simple method for refining D values in cases of mixed kinetics is proposed in Ref. [133]; (iii) PITT and EIS can be extremely useful in distinguishing between the different types of non-uniformity of practical insertion electrodes for battery application.

3.4.8. Some Miscellaneous Techniques

There are techniques that are used in basic electrochemical studies, but their implications for the characterization of batteries and battery compounds are of secondary importance. Below we list some techniques with short descriptions and references for further reading.

a) Moving electrodes(134)

The famous dropping mercury electrodes and rotating disc and rotating ring-disc electrodes are widely used in electroanalytical chemistry. Polarography is the technique that uses the former electrode and its modifications: normal pulse and differential pulse polarography enables the detection of trace electroactive species in solutions down to a concentration of ppb. Hence, the major applications of polarography are analytical. For further reading see Ref. [135]. The rotating disc electrodes are useful for mechanistic studies in electrochemistry. Their use can be relevant to the battery field for the characterization of reactions in solution phase. For instance, the mechanistic studies of the reduction of $SOCl_2$ (in primary Li batteries) used rotating disc electrodes.(136)

b) Electrochemical quartz crystal microbalance (EQCM)(137-139)

In this technique, thin metallic electrodes deposited on thin quartz crystal (*e.g.* 10 μm thick) are used. The resonance frequency of the crystal depends on the weight of the species deposited on it, and there is a linear dependence between ΔF (frequency changes due to weight) and m (mass of deposits). Hence, it is possible to use the thin metallic electrodes on the quartz crystal for electrochemical measurements, and measure simultaneously the weight accumulated and depleted from the electrodes due to the electrochemical processes, by measuring changes in the quartz crystal frequency. By measuring charge and mass changes simultaneously, it is possible to estimate the equivalent weight of surface species deposited during electrochemical processes. This technique was used for analyzing the behavior of Li and Mg electrodes for rechargeable batteries (see details in references 138, 139).

c) Scanning tunneling microscopy (STM)(140)

In this technique, very small currents that are conducted by tunneling electrons flowing from an atomically sharp tip and conducting surface (due to controlled potential difference) are analyzed. Since their current intensity depends strongly on the distance between the tip and the surface, it is possible to translate changes in tunneling currents to topography on an atomic scale (a few Å). The use of the appropriate piezoelectric devices in 3D, enables the topographic/morphological analysis of surfaces at atomic resolution. This method can be used for *in situ* electrochemical measurements, since tunneling currents can flow from sharp tips and electrodes in solution phase as well (provided that there is no Faradaic electrochemical process possible at the potential difference applied). Note that this technique is not applicable for isolating surfaces, *e.g.* electrodes covered by passivating surface films. This method was found to be relevant for the study of reversible magnesium electrodes for rechargeable Mg batteries in complex ethereal solutions in which Mg electrodes are not passivated.(141) In addition, this method is highly useful for *in situ* studies of corrosion processes.(142)

d) Ellipsometry(143)

In this technique, changes in polarized visible light reflected from surfaces are measured and analyzed as a function of frequency and state of the surface. Factors that influence the polarization of the reflected light are: refractive indices of the reflective surface and the surface species on it, roughness of the surface, films thickness and the multilayer structure of surface films. This technique can be used *in situ* for the analysis of deposition processes and surface films formation on electrodes. The analysis of the polarization parameters of the reflected beam requires the use of a model for the surface structure, and hence information on the refractive indices of the surface species formed is needed. This technique was used for the analysis of both lithium and carbon electrodes in nonaqueous solutions relevant to the field of Li batteries.(144) These electrodes are covered by multilayered surface films: *in situ* ellipsometric measurements could provide useful information on the structure and dynamics of formation of these films.(145)

e) UHV characterization

In recent years, several groups established the capability of measuring highly reactive surfaces at UHV conditions. At pressures below 10^{-10} torr, the level of atmospheric contaminants is sufficiently low to allow very reliable measurements of active metal surfaces. It was possible to evaporate Li metal and deposit a very clean and smooth layer on the UHV system. Solvent layers of interest could then be condensed on the Li surface (from the gas phase). The reactions products could be analyzed by a variety of surface sensitive techniques, including XPS and FTIR.(146,147) There are also reports on the study of Li batteries containing polymeric electrolytes in a UHV condition, thus providing information on the surface chemistry and morphology of lithium electrodes by *in situ* observation.(148)

3.4.9. *In Situ* Measurements

The use of *in situ* measurements, namely, the combination of spectroscopic or microscopic techniques in conjunction with electrochemical control, for the study of electrode-solution systems is very elegant. *In situ* measurements may provide highly reliable and authentic data, especially when the products of electrochemical reactions are unstable or highly reactive with atmospheric components. Below we list the most important techniques for which there are reports on successful and meaningful *in situ* measurements, relevant to the field of batteries.

a) FTIR spectroscopy

Over the years, *in situ* FTIR measurements were used for the identification of surface films formed on lithium electrodes and non-active metals polarized to low potentials in the same solutions,(149) and for the study of oxidation and reduction processes of solutions of interest for Li and Li-ion batteries.(150) Several cells (and approaches for conducting *in situ* FTIR measurements relating to Li batteries) are illustrated in Figure 3.4.

b) Raman spectroscopy

The application of Raman spectroscopy to electrochemical systems is easier than FTIR because it usually requires visible light, and hence, relatively simple glass optical windows are used (for FTIR, the optical windows have to be constructed from IR transparent materials, most of which are fragile, hygroscopic and expensive, *e.g.* KBr, ZnSe, Ge, Si). *In situ* Raman can be useful for solution studies and bulk changes in composite electrodes. Surfaces studied by Raman are very problematic because of the weak signals and possible destructive impact of the laser beam to the surface. There have been impressive *in situ* studies by Raman spectroscopy on single particles of graphite and transition metal oxides that undergo reversible intercalation with lithium. It was possible to follow by Raman spectroscopy as a *bulk technique*, the dynamics of Li insertion processes into graphite(151) and $LiMn_2O_4$.(152)

c) XRD

In recent years, there have been many reports on *in situ* XRD measurements of Li battery electrodes. It is possible to use either transmittance or reflectance modes. A scheme of a suitable cell is provided in Figure 3.5, as well as a typical response of such experiments.(153) Appropriate window materials can be berillium metal or mylar (plastic, polymeric material). *In situ* XRD measurements can analyze, in the clearest way possible, the nature of intercalation processes, thus identifying phase transitions, the formation of solid solutions, *etc.*(154) Such experiments can be especially effective when using a high intensity X-ray beam, *e.g.* by synchrotron facilities.(155)

d) EXAFS, XANES

As already reported, it was possible to analyze electrodes in full cell testing using both techniques. The use of the high intensity X-ray beam needed for these techniques (using synchrotron facilities) enables the design of relatively simple electrochemical cells.(156,157)

e) Scanning probe microscopes: AFM, STM

Both techniques are very suitable for *in situ* measurements since the experiments can be carried out in solution phase (see an example of the cell in Figure 3.6). Special cells have to be designed for such measurements. Most of the commercial companies that produce AFM and STM systems (usually as

Spectroelectrochemical cell for ATR spectroscopy

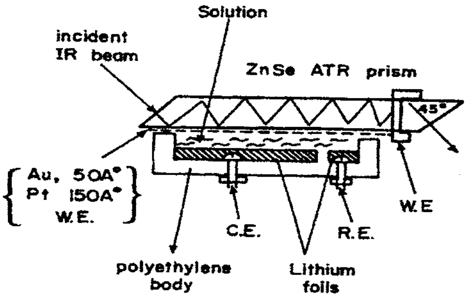

Spectroelectrochemical cell for singe internal reflection spectroscopy

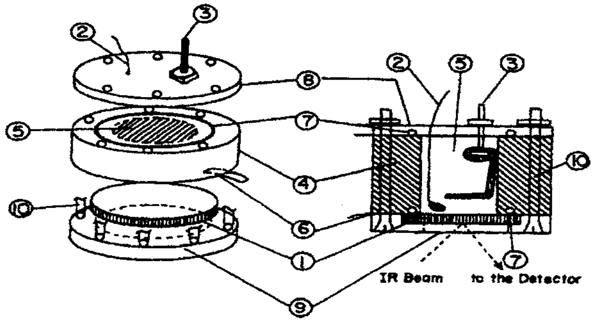

1. Working electrode - thin film of inert metal on optical NaCl window. **2.** Li wire reference electrode. **3.** Li foil counter electrode. **4.** Polyethylene cell. **5.** Space for solution. **6.** Electric contact. **7.** O ring. **8.** Upper cover. **9.** Holder for the optical window. **10.** Bolts.

Spectroelectrochemical cell for specular reflection spectroscopy

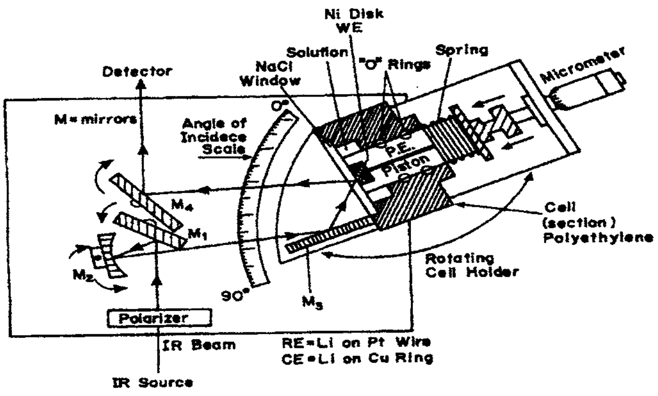

Figure 3.4. Different cells for *in situ* FTIR measurements (*Refs. 70,71*).

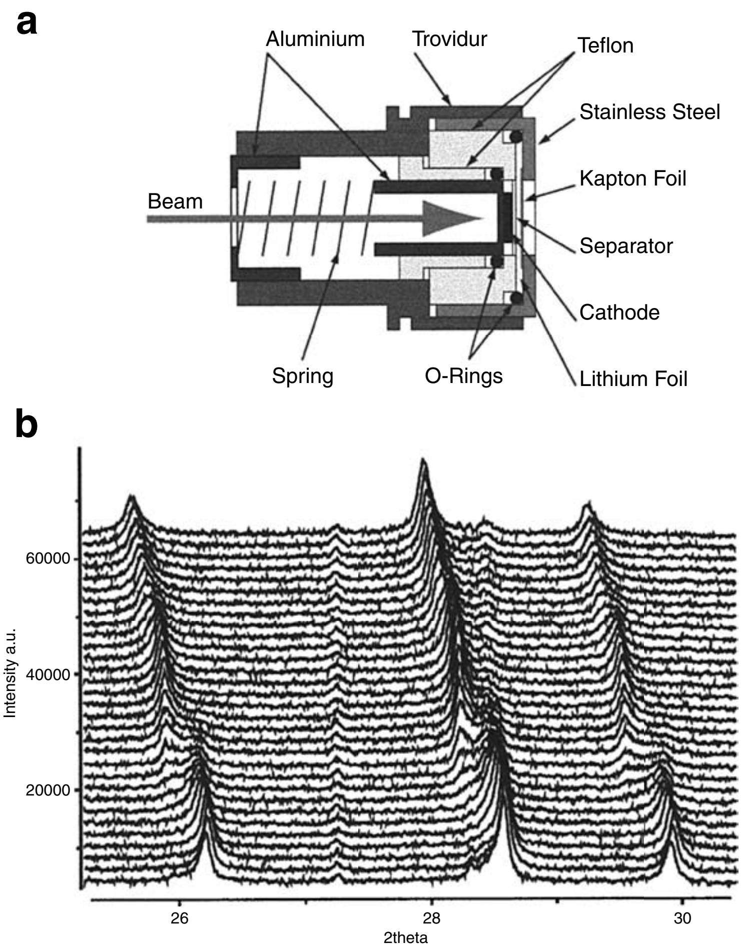

Figure 3.5. (a) A typical cell for *in-situ* XRD experiments in transmission mode and (b) the evolution of the XRD patterns of spinel $Li_xMn_2O_4$. Bottom: $x = 0$, top: $x = 1$. (*Ref. 153*).

one instrument having both functions), also provide electrochemical cells for *in situ* measurements. However, these cells may need further modification for working with highly reactive electrochemical systems. The valuable analysis of Li and Li-graphite electrodes by *in situ* AFM measurements(158) and the *in situ* analysis of Mg electrodes by STM(159) was demonstrated in recent years. It should be noted that modern SPM instrumentation allows the use of important modifications of these techniques, such as local electrical conductivity and the magnetic response of surfaces, at a nanometric resolution.(160)

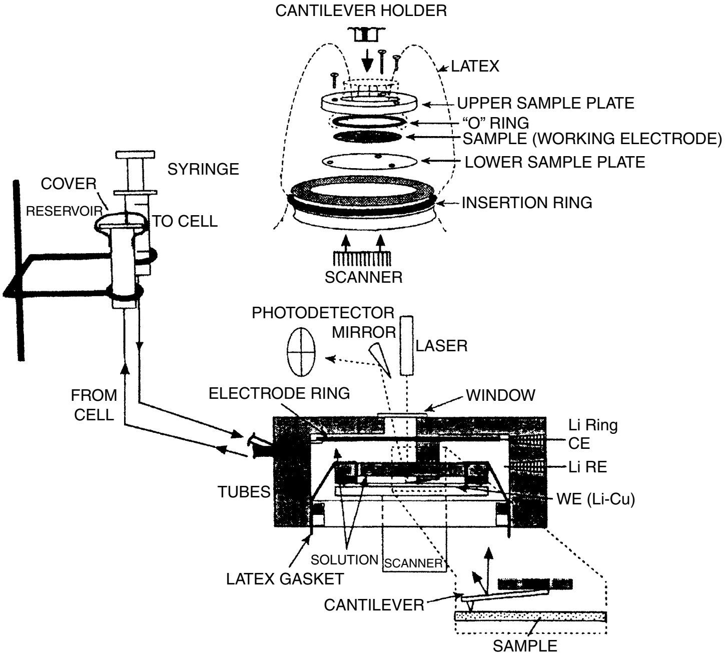

Figure 3.6. A scheme of an electrochemical cell for in-situ AFM measurements, for highly sensitive electrochemical systems (*Refs. 114,115*).

f) Mass spectroscopy

Over the years, the ability to conduct electrochemical measurements, while detecting mass spectra, was developed.(161,162) By using the appropriate membrane to separate the liquid phase in the electrochemical cell and the vacuum chamber of the spectrometer, it was possible to analyze gaseous, and even volatile, products of electrochemical reactions. This technique enables the analysis of both reduction and oxidation products of important solutions for Li and Li-ion batteries, and hence, can help in understanding basic electrode reactions in Li-ion batteries.(163)

g) Mössbauer spectroscopy

Mössbauer spectroscopy can be applied in conjunction with electrochemical measurements. There are important battery materials that contain transition metals, *e.g.* Fe, Ni, Mn and Sn, which provide strong signals. As this spectroscopy usually requires thick electrodes, *in situ* Mössbauer spectroscopic experiments have to be designed to low rates. This technique was found to be useful for studying Sn- and Fe-containing battery electrodes.(164, 165)

3.5. Typical Studies of Electrolyte Solutions and Solid Electrolytes

3.5.1. Evaluation of Solvents Parameters and Solutions Conductivity

It is important to find criteria for the solvent classification that can be correlated not only to salt solubility and apparent conductivity, but also to the impact of the solvents on the thermodynamics and kinetics of the electrochemical reactions. There are several approaches to defining solvent properties that can be correlated to the thermodynamics and kinetics of reactions conducted in its solutions (*i.e.* a linear free-energy relationship). A comprehensive review of this topic has been made by Reichardt,(166)

Especially interesting are the parameters: donor number (DN)(167) and acceptor number (AN).(167)

The donor properties of solvents are defined as the numerical value of the heat of adduct formation between the donor molecule and the reference acceptor $SbCl_5$ in a diluted 1,2-dichloroethane solution.

$SbCl_5$ + solvent → [$SbCl_5$ solvent] in 1,2-dichloroethane.

The values range between zero and about 60 kcal/mole. The acceptor number (AN) of a solvent (S) is defined by ^{31}P NMR measurements of Et_3PO in a solvent (S), in hexane and the adduct $SbCl_5 \cdot Et_3PO$ in di-chloro-ethane according to the following equation:

$$AN = \frac{\delta\ (Et_3PO \text{ in solvent S}) - \delta\ (Et_3PO \text{ in hexane})}{\delta\ (SbCl_5 \cdot Et_3PO \text{ in } C_2H_4Cl_2)}$$

(δ = the shift of the ^{31}P NMR signal)

The importance of solvent parameters such as DN and AN and the advantage of their use over physical-electrostatic parameters was demonstrated by Mayer.(168)

The conductivity of electrolyte systems (solutions, polymeric matrices, solids) and its temperature dependence is a critical parameter for batteries, as it determines, together with the interfacial parameters, the internal resistance of battery systems. The resistance determines the actual voltage of working systems, energy losses and heat dissipation.

The most common and important conduction mechanism for electrolyte solutions relates to the motion of separated ions in the liquid medium, retarded by friction (solvent-solute and ion-ion interactions).

The mobility of ions in solutions is proportional (at constant temperature) to their diffusion coefficient (Einstein equation(169)). Basic properties of solutions are their specific (χ) and molar ($\Lambda = \chi/c$, c = concentration of the electrolyte) conductivity, resulting from the sum of the contributions of the various ions). The molar conductivity of solutions with strong electrolytes depends slightly on the concentration ($\alpha\sqrt{C}$(169,170)). When there is no full dissociation of the electrolytes in solutions, either in cases of weak electrolytes or solvents of low polarity, we observe a variety of complicated phenomena, including the formation of ion pairs, triple ions, *etc.*

An important approach to forming conductive nonaqueous solutions is the use of solvent mixtures. There are many important highly polar aprotic solvents whose polarity leads to strong, intermolecular interactions, and thus to high viscosity. Hence, the advantage of the high electrolyte dissociation due to the high polarity is balanced by the high viscosity, which leads to the relatively low conductivity, since the latter property depends inversely on the solvent viscosity.(169,170) Combining such solvents with solvents of low dielectric constant and low viscosity may form mixtures of higher conductivity, compared with the single solvent systems. In fact, high conductivity at low temperatures can be obtained by using ternary and quaternary solvent systems, as demonstrated by a recent review.(171) The concentration of the salts should be optimized as well. Conductivity *vs.* salt concentration is a function with a maximum (at too high concentrations, the mobility of the ions decreases due to various types of electrostatic interactions).

Conductometry is usually simple and should be measured in parallel plate cells using low amplitude alternating voltage current at sufficiently high frequency (in order to avoid the influence of charge transfer and ion diffusion limitations). The specific conductivity χ ($\Omega^{-1}\bullet\mathrm{cm}^{-1}$) is equal to $\frac{1}{\rho}=\frac{l}{R\bullet A}$ (ρ = specific resistance, R = resistance measured, l = distance between the plates, and A = their area). Reliable, easy to use conductometers (including cells) are commercially available. It should be noted that there are well established theories that calculate the effect of salt concentration and temperatures on the specific conductivity of polar aprotic electrolyte solutions(172-175).

Extensive work has been devoted to electrolyte systems based on polymeric matrices. The major directions towards improving ionic conductivity of polymeric electrolytes are:

1) The use of gels. The polymeric matrix contains polar aprotic solvents that dissolve the salt and separate the ions.(176)
2) The use of branched polymers that prevent crystallinity. The organization of the polymer-salt matrix thus facilitates the free movement of the ions.(177)
3) The use of composites, *i.e.* polymeric matrices containing ceramic nanomaterials.(178)

Key factors to be measured with polymeric electrolytes are the temperature dependence of their conductivity and the transference number of the ions.

An ideal situation is when the transference number equals 1 for the interacting ions *e.g.* Li ions in lithium batteries. A transference number <1, especially in polymeric matrices of slow relaxation, causes concentration gradients near the electrodes. In the design of novel polymeric matrices, this constraint is taken into account. Elegant methods for measuring transference numbers in polymeric electrolyte matrices were demonstrated.(179)

3.5.2. Electrochemical Windows of Electrolyte Solutions

In order to discuss briefly the electrochemical stability of electrolyte solutions, the classification of the electrode types used is very important. The relevant electrodes may be divided into the following categories.

a) Noble metal electrodes and special carbons

Noble metal electrodes are metals whose redox couple M/M^{z+} is not involved in direct electrochemical reactions in all aqueous and nonaqueous systems of interest. Typical examples that are the most important are gold, platinum, and glassy carbon.

b) Reactive metal electrodes

Reactive electrodes refer mostly to metals from the alkaline and the alkaline earth groups. These metals may react spontaneously with most of the nonaqueous polar solvents, salt anions containing elements in a high oxidation state (*e.g.* ClO_4^- and PF_6^-) and atmospheric components (O_2, CO_2, H_2O, N_2). Note that all the polar solvents have groups that may contain C-O, C-S, C-N, C-Cl, C-F, S-O, S-Cl, *etc.* These bonds can be attacked by active metals to form ionic species, and thus the electrode-solution reactions may produce reduction products that are more stable thermodynamically than the mother solution components. Consequently, active metals in nonaqueous systems are always covered by surface films.(180)

When introduced into the solutions, active metals are usually already covered by 'native' films (formed by reactions with atmospheric species), and then these initial layers are replaced by surface species formed by the reduction of solution components.(181) In most of these cases, the open circuit potentials of these metals reflect the potential of the $M/MX/M^{z+}$ half-cell, where MX refers to the metal oxide/hydroxide/salts which compose the surface films. The potential of these half-cells may be close to that of the M/M^{z+} couple.

At potentials positive to the OCV, the electrochemical window may be very limited because dissolution of the active metal takes place either via migration of M^{z+} ions through the surface films or by the breakdown of the surface films, exposing the active metal to the solution and enabling a 'direct' dissolution process (182). At potentials lower than the OCV, the situation is more complicated. Since there is no possibility of a cathodic breakdown mechanism of the surface films, the possibility of obtaining active metal deposition depends either on the feasibility of migration of the M^{z+} ion through the surface films, or on electron tunneling though them to form metal deposits outside the surface layer. In the case of alkaline metals such as lithium, the electrochemical window is very narrow because Li dissolution and deposition take place above and below the OCV at very low overpotentials, as Li ions migrate through the surface films that cover Li electrodes.(183)

c) Non-active/slightly reactive metal electrodes

Nonactive/slightly reactive electrode materials include metals whose reactivity towards the solution components is much lower as compared with active metals, and thus, there are no spontaneous reactions between them and the solution species. On the other hand, they are not noble, and therefore their anodic dissolution may be the positive limit of the electrochemical windows of many nonaqueous solutions. Typical examples are Hg,, Ag, Ni, Cu, *etc*. It is possible to add to this list both Al and Fe, which may react spontaneously by themselves with nonaqueous solvent molecules or salt anions containing central atoms of high oxidation states.(184) However, they are not reactive due to the passivation phenomena. Hence, the electrochemical window of nonaqueous solutions with electrodes such as Al or stainless steel may be determined by the electrochemical reaction of the solution components.(185)

Indeed, Al is used as a current collector for positive electrodes in lithium batteries. The stability of Al in many Li salt solutions at potentials as high as 4.5 V *vs.* Li/Li^+ is due to the formation of highly insoluble Al-halides on its surface, which remain stable and thus protect it from corrosion.(186)

d) Intercalation electrodes

Intercalation electrodes may include either carbon or transition metal oxide and sulfide, which intercalate with solution components such as metal cations. The most important example is the intercalation of Li^+ into many types of carbonaceous materials at low potentials (0-1.5V *vs.* Li/Li^+)(187) and transition metal oxides and sulfides at high potentials (2.5-5 V *vs.* Li/Li^+).(188)

e) Redox electrodes

Redox electrode materials mostly include electronically-conducting polymers such as polypyrrole, polythiophene, or polyaniline that may undergo reversible oxidation-reduction reactions accompanied by doping of the polymer with the counterion that balances the charge.(189)

In general, this topic, namely, electrochemical windows of electrolyte solutions, has been extensively studied over the years. The cathodic and anodic reactions of most of the electrolyte solutions relevant to the battery field were investigated and understood. Intensive discussions on the possible reactions of all commonly-used nonaqueous solutions, including those important for batteries, appear in Ref. [171]. A brief summary is provided below.

1) The order of cathodic stability: ethers>esters>alkyl carbonates ≈ imidazolium-based ionic liquids (IL). The nature of the cation is very important. With tetralkylammonium, no electrode passivation occurs, and hence, the intrinsic cathodic stability of the solvent is reflected by the electrochemical measurements. When metallic cations are present, passivation processes take place because reduction of solution species in the presence of metallic cations forms insoluble species. For instance, the cathodic limit of all the above solvents in the presence of Li salt is around 0-0.5 V (Li/Li^+).(190)

2) The order of anodic stability: 5.5 V (Li/Li^+) ILs>alkyl carbonates (4.5-5 V *vs.* Li/Li^+) >esters>ethers (≈ 4 V *vs.* Li/Li^+). The anodic stability of the above systems is determined by the solvents and is not dependent on the salt (neither anions nor cations). Apparently, alkyl carbonates seem to be stable up to 5 V. However, their small-scale oxidation on noble metals (no passivation or inhibition) can occur at potentials >3/5 V. See discussion in Ref. [150].

3) The electrochemical window of solvent-free polymeric electrolytes, which are in fact derivatives of polyethers, is very similar to that of ethers (≈0-4 V *vs.* Li/Li^+).

4) The most useful study of the stability of electrolyte solutions is the application of cyclic voltammetry to systems comprising glassy carbon, platinum or gold working electrodes, and well-separated (*e.g.* U-type cells) counter electrodes from the same materials. As reference electrode in active metal salt solutions (*e.g.* Li, Mg salt solutions), an active metal wire is suitable. Silver wire can also be used as a stable pseudo reference electrode in both nonaqueous and aqueous solutions. Figure 3.7 shows the results of typical studies of electrochemical windows of electrolyte solutions of interest, thus demonstrating several of the above points.

3.5.3. Thermal Studies

There are two levels of thermal studies related to electrolyte solutions:

a) investigation of electrolyte solutions; this includes the study of the high temperature behavior of the solvents, salts and their combination (solution phase).

b) investigation of solutions in contact with electrode materials.

Nonaqueous solutions for Li batteries are in fact redox couples in which the salt anion (*e.g.* PF_6^-) is an oxidizer and the solvent molecules are reducing agents. At elevated temperatures, very exothermic reactions between solvents such as alkyl carbonates and salts such as $LiPF_6$ can be ignited.(120) It is important to explore such high temperature reactions and their products, in

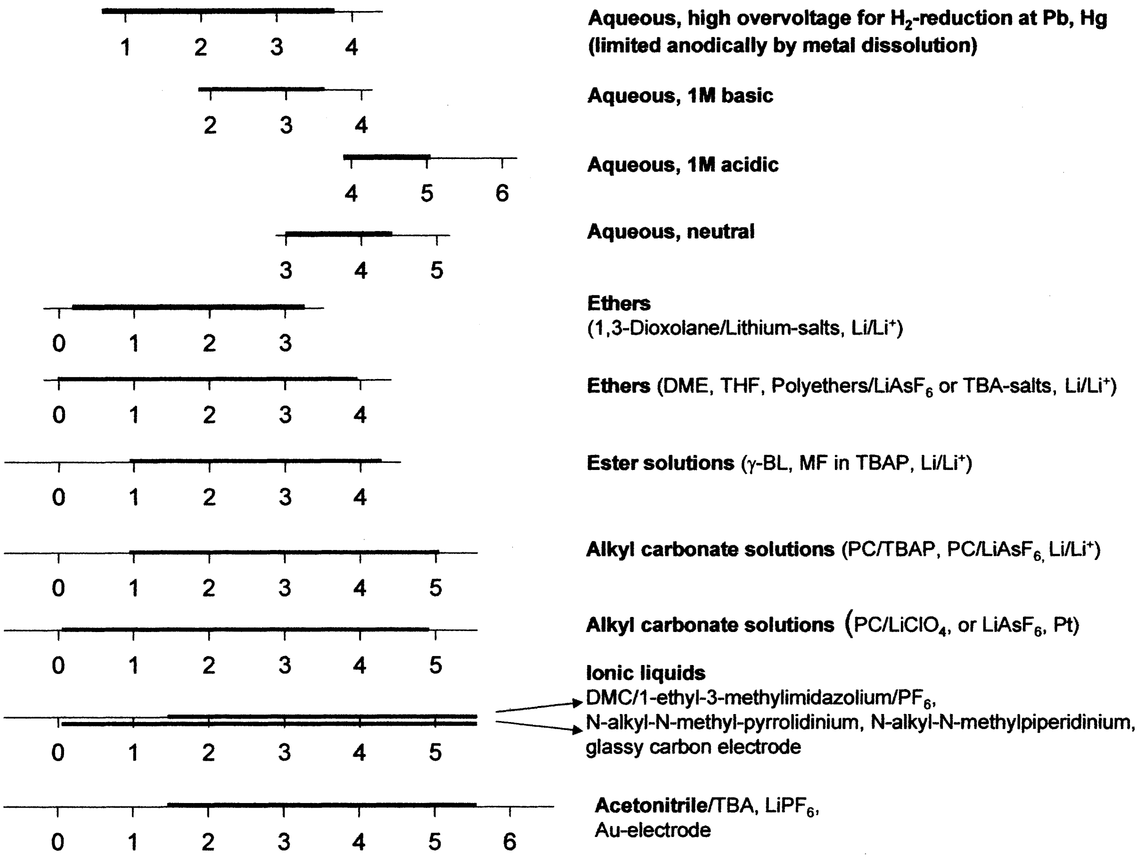

Figure 3.7. Electrochemical windows of several aqueous and non-aqueous solutions. The potentials (V) are referred to Li/Li^+.

order to understand safety features and limitations of batteries.

A useful study should include both DSC and ARC measurements. It is important to establish an option of pressure control in ARC measurements, because monitoring both temperature and pressure allows the analysis of all possible thermal reactions, including endothermic reactions. In addition, it is important to modify the ARC system so that the thermal reaction products (gas, liquid, solid) can be collected and analyzed. Hence, complete studies of the thermal behavior of electrolyte solutions should include the following stages:

a) Scanning calorimetry (DSC, heat flow *vs.*T) of the salt and solvent alone, and then the study of the solutions.

b) Parallel ARC measurements (solvent, salt, solution) in which T and P *vs.* T and $\frac{dT}{dt}$ and $\frac{dP}{dt}$ *vs.* T are measured simultaneously.

c) Stopping the experiments at different high temperatures, followed by product analysis.

d) Data analysis to map all thermal reactions and the relevant heat of reactions.

Figure 3.8 demonstrates typical thermal studies of EC-DEC/$LiPF_6$ solutions.(120)

After the thermal behavior of the electrolyte solutions is known, it is important to study the thermal behavior of solutions in contact with battery materials. The most intensive studies of this kind were carried out by Dahn's group.(191,192) Thermal studies of solutions in contact with lithiated graphite, in which several types of reactions were analyzed (active Li^+ solution, reaction of surface species with the solution, and further reactions between the surface species and reactive Li) can also be mentioned.(193) Highly important were studies of transition metal oxides (positive electrodes) at different degrees of Li content, with solutions.(194) Exothermic reactions between solution species and oxide decomposition products, *e.g.* molecular oxygen and solution species, were analyzed. Systematic studies enabled the thermal stability of a variety of important cathode materials to be mapped. (191-194)

3.6. Typical Studies of Electrodes and Electrode Materials

3.6.1. The Scheme of Material Research

In this section, the characterization of new electrodes will be dealt with in detail. Analysis of electrode materials should include the following measurements:

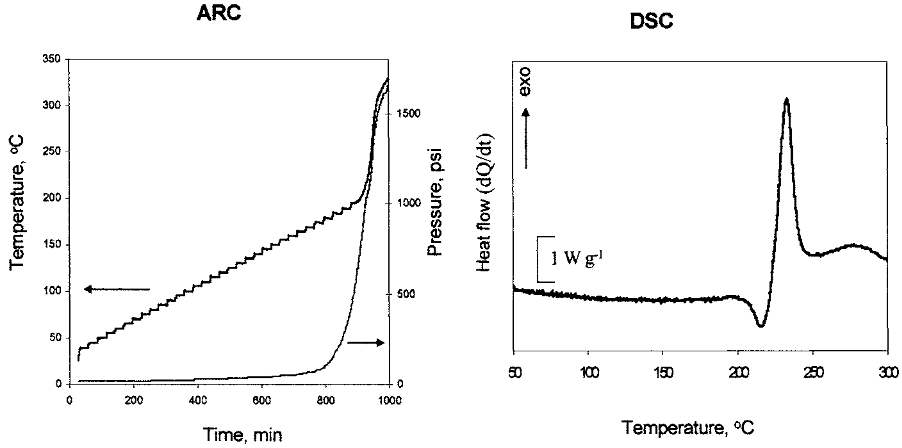

Liquid Decomposition Products			
140°C	180°C	220°C	350°C
$F_2PO_2^-$	ethanol, methanol, CH_3CH_2F, CH_3F (small amount), traces of P containing polymer, 25% of initial product decomposed	methanol, ethanol H_3O^+, EG, Polymer, FCH_2CH_2X,CH_3CH_2F	complete decomposition, traces of polymer containing CF_3
Gas Phase			
		methanol, DMC, H_2O, EG,CH_3CH_2F, $OHCH_2CH_2F$, CH_3F	methanol, DMC, H_2O, CH_3CH_2F, CH_3F After the complete gas evacuation at 220°C and following heating: $OHCH_2CH_2F$, CH_3CH_2F, CH_3F

Figure 3.8. Results of typical thermal studies of Li ion battery electrolyte solutions: EC-DMC-DEC/1M $LiPF_6$ studied by ARC (*left*) and DSC (*right*). In the ARC measurements, both temperature rise (T *vs.* t) and pressure changes (P *vs.* t) were monitored. Studies by DSC provided information on both endothermal and exothermal reactions (minimum and maximum in dQ/dt *vs.* T, respectively). The ARC is arranged to allow collection of gas, liquid and solid reaction products (which can be studied by bulk analytical techniques). The table provides results of products analysis (*Ref. 120*).

a) Chemical analysis: element analysis by conventional methods, *e.g.* ICP of solutions in which the material is dissolved, for instance by the use of strong acids and/or oxidizers. Raman spectroscopy complements the chemical analysis.

b) Structural analysis by XRD: when the exact structure is important, ND, Solid-State NMR, Mössbauer and EXAFS can complement the XRD measurements.

c) Morphological studies by electron microscopy: high resolution TEM may be highly useful for the completion of the structural and chemical analyses (electron diffraction and element analysis by EDS). The particles' size and shape are imaged.

d) The surface area should be obtained by gas adsorption techniques.

e) Surface films can be analyzed by FTIR and XPS.

The recent literature of electrochemistry and materials science includes thousands of papers that describe the complete development of new battery materials from design and synthesis to a completed analysis. The fabrication of electrodes and electrochemical measurements should not be carried out before the composition bulk structure, particle size, morphology, surface area, and surface structure of the material are well established.

3.6.2. On the Electrochemical Characterization of Battery Electrodes

3.6.2.1. Metallic Electrodes

Metallic electrodes are always the negative side of the batteries. The study of metallic electrodes is the simplest because such electrodes are usually monolithic, easy to construct and measure. The parameters of interest depend on the type of batteries. For primary batteries, the most important_parameters are voltage and rates, *i.e.* how the current density influences the working potential. The measurements of interest are thus V *vs.* t at constant current or I *vs.* t at constant voltage. It is also useful adding morphological microscopy studies to such measurements, in order to realize uniform morphology upon discharge. For rechargeable systems, a very important parameter is the cycling efficiency of the electrode as a function of conditions: solution composition, rates, temperature, and depth of discharge. In order to measure cycling efficiency, it *is not useful* to study foils of the relevant material. The experiments that can provide significant information should include electrochemical metal deposition from the solution of interest onto an inert substrate, usually a metallic current collector, followed by controlled, repeated dissolution. Such experiments can be carried out in 2-electrode cells, using a counter electrode made of the same active metal. Two types of experiments are relevant:

a) Repeated deposition-dissolution, thus measuring cycling efficiency as

Q_{diss}/Q_{dep}.

b) Deposition of a certain amount of the active material on a substrate, followed by repeated cycling of 20-30% of the deposited metal. After repeated cycling, the residual metal is dissolved. The average cycling efficiency is calculated as

$$\mathrm{CE}\,(\%) = 100\ \left\{ Q_{cyc.} - \left[\frac{Q_{in} - Q_{final}}{n}\right] \right\} / Q_{cyc}$$

(Q_{in}, Q_{final}, and Q_{cyc} are the charges involved in the initial, final, and cycling deposition processes). R&D of rechargeable Li batteries involve extensive studies of the cycling efficiency of Li electrodes in a wide variety of electrolyte solutions and conditions.(195,196) Such studies should also include morphological analysis, using electron microscopy. The morphology of metallic electrodes in secondary batteries is critical to their performance, and should be as uniform as possible.

3.6.2.2. Electrodes for Flow Batteries (*e.g.* Air Batteries) and Batteries with Liquid Cathodes

These electrodes do not contain the active mass, but rather serve as a catalytic surface for the active material that is forced to pass through/on it. Depending on the electrochemical reaction and its products, these electrodes can be combined with a membrane that should block transport of the active mass and its reaction products to the counter electrode. Hence, these electrodes should also include, in addition to the current collector, a carrier matrix, *e.g.* porous carbon, on which the catalyst is embedded. Such electrodes need special engineering that allows a constant and efficient flow of the active mass (*e.g.* air in Zn metal-air batteries, electrolyte in Zn-Br_2 batteries) and good contact with the catalyst. Table 3.6 describes several types of catalytic electrodes for flow batteries.

In general, the important parameters for such batteries are: I, V, t behavior as a function of flow rates, concentration of the active mass in the effluent, optimal load of the catalyst and porosity of the matrix. (1-4)

In this category we also include liquid cathodes. The most important systems of this type are Li-$SOCl_2$ and Li-SO_2 batteries. Here, the electrodes are in fact current collectors on which the cathodic reactions take place (see Table 3.6). The important parameters related to these electrodes are: I, V, t behavior as a function of the electrode's area, and liquid cathode volume (with an attempt to keep the electrode's weight as minimal as possible). The natural

Table 3.6. Typical electrodes for flow systems and batteries with liquid cathodes. (*Refs. 1-5,9*)

Battery system	**Type of active material**	**Reaction**	**Catalyst/matrix**
Zinc-Air	Flowing gas (oxygen)	$Zn + 1/2\ O_2 + H_2O \rightarrow Zn(OH)_2$	PTFE laminated carbon/catalyst
Aluminum-Air	Flowing gas (oxygen)	$Al + 3/4\ O_2 + 3/2H_2O \rightarrow Al(OH)_3$	PTFE laminated carbon/catalyst
Vanadium redox	Flowing solution with red-ox species	$V^{5+} + V^{2+} \rightarrow V^{+4} + V^{3+}$	Mono or bipolar carbon felt
Li-Thionyl chloride	Liquid cathode material	$4Li + 2SOCl_2 \rightarrow 4LiCl + SO_2 + S$	Porous carbon electrode
Li-Sulfur dioxide	Liquid cathode material	$2Li + 2SO_2 \rightarrow 2Li_2S_2O_4$	Porous carbon electrode
Zinc-Bromine	Flowing solution with red-ox species	$Zn + Br_2 \rightarrow ZnBr_2$	Carbon – polyethylene composite

candidates for electrode materials in these cases are porous carbons. (See Refs. [1-4] for more descriptions and discussion).

3.6.2.3. Composite Electrodes

Composite electrodes are widely used in all kinds of stationary batteries, because in most cases it is impossible to use a monolithic active mass (except for metallic anodes, as discussed in Sub-section 3.6.2.1), but rather powdery materials. Hence, the electrodes should have a composite structure, including current collector (usually metallic foil or grid), a powdery active mass, polymeric binder, and additives that improve the electrical conductivity of the composite structure (usually carbon powder). The first issues to be dealt with relate to the composite structure:

a) The morphology of the active mass: microparticles or nanoparticles? As the particle size is smaller, the diffusion length for solid-state processes in the bulk is shorter, hence faster kinetics, and the surface area is higher, hence faster charge transfer and lower overall interfacial impedance per unit volume or weight of the active mass. However, a smaller size and a higher surface area also mean a more problematic contact of the entire active mass and the possibility of side reactions.

b) The choice of materials for current collector and binder depends on their chemical and electrochemical stability. Both components should not be involved in any pronounced side reactions.

c) The engineering parameters, including the percentage of the active mass, binder and additives, thickness, method of preparation (aqueous or nonaqueous slurry, spreading techniques and machinery, drying procedure) and porosity (depending on external pressure application during preparation).

It should be noted that while the above issues are relevant, they are very specific to many battery systems, and thereby, a detailed discussion about these parameters is beyond the scope of this chapter, but rather relates to discussions on specific battery systems. The electrochemical response of composite electrodes is very strongly dependent on their structure (percentage of active mass, electrical conductivity, porosity, thickness, and the intensity of the interparticle electrical contact). In an ideal composite electrode, the electrolyte phase is in contact with all the particles, and all the particles interact simultaneously with the current collector (electron transfer) and with the solution phase (ion transfer). A complete study of composite electrodes should include a study of single particle electrodes, thin electrodes and practical thick electrodes in the relevant solution. Comparing the electrochemical response of the three systems mentioned above enables the evaluation of the rate-determining steps (RDS). It can be ascertained whether the primary electrochemical reaction is the RDS or the interparticle contact and impeded ion transport in solution phase within the composite structure become the limiting factor. Studies on single microparticles can be found in Refs. [151, 152, 197], while studies on thin electrodes and a comparison with the behavior of thick electrodes can be found in Refs. [124-126], [130-133] and [198-200]. In Figure 3.9, SSCV and EIS spectra for a thin and a thick electrode are shown.

For the elucidation of solid-state diffusion behavior and the dependence of the diffusion coefficient on the degree of intercalation and potential, CV is not suitable. Small amplitude titration techniques such as PITT or GITT should calculate the diffusion coefficient of ions in the host (during intercalation-deintercalation) as a function of potential (and degree of ion insertion).

The impedance spectroscopy of battery electrodes, especially those related to Li and Li ion batteries, deserves further attention because impedance spectra reflect all the relevant time constants of electrochemical processes. Figure 3.10 compares typical impedance spectra of: 1) noble metal electrodes polarized cathodically to low potentials in polar aprotic Li salt solutions, 2) Li electrodes and 3) lithiated graphite electrodes. The common denominator in all three systems is the formation of multilayered surface films that are Li ion conducting (the SEI model) and hence, the high frequency part of the spectra reflect Li ion migration through multilayered surface films that can be simulated by a 'Voight' type analog – C||R circuits in series.(199,203) The medium-low frequency part of the spectra is different in the case of noble metal electrodes: it reflects a huge transfer resistance (to reduction of solution species). In the case of Li electrodes, the low frequency part is degenerated and is not significant because the impedance relates mostly to Li ion migration through the surface films (the R_{CT} of Li ions across the various interfaces is small).(203)

In the case of graphite electrodes, the low frequency part of the spectra reflects the charge transfer of Li ions from the surface films to intercalation sites, solid-state diffusion, and accumulation of lithium (capacitive behavior at very low frequencies). Hence, the impedance spectra of Li graphite electrodes contain a pronounced 'Warburg' type element that reflects the solid state diffusion of Li ions in the host.(199) In fact, all Li insertion electrodes (including $LiMO_x$ cathode materials) behave in a similar manner to graphite electrodes. The Li ion insertion processes include ion migration through surface films (formed on cathode materials as well), interfacial charge transfer, solid-state Li ion diffusion, and the accumulation of Li ions in the host (capacitive behavior). Therefore, impedance spectra of many Li insertion electrodes are similar, as demonstrated in Figure 3.11.

With the results from SSCV and PITT or GITT, it is possible to understand the impedance spectra and to separate various time constants. Note that at very low frequencies the applied ω (or f) → 0, and the imaginary component of the spectra (Z") reflects the electrode's differential capacity: $C' = \frac{1}{\omega Z''}$ ($\omega = 2\pi f$). Hence, C' *vs.* E calculated from EIS should be similar to C' calculated from SSCV ($C' = \frac{i}{\upsilon}$), where i = current density and ν = potential scanning rate.(124, 125, 201) Such studies have been carried out for different electrodes, including Li_xC_6 (Li graphite), $Li_xV_2O_5$ and Li_xCoO_2.(124-126,128,130-133,199-,201) In all these cases, Li insertion into the host involves phase transitions. Figure 3.12 shows SSCV, D and EIS for a $LiCoO_2$ electrode. The minimum in D *vs.* E, which appears at the peak potential of C' *vs.* E (obtained from CV, PITT or ITS), reflects attractive interactions among the intercalation sites, *i.e.* the inserted ions and their electronic environment due to the lattice structure.(124,199,200) These attractive interactions (well understood in terms of lattice gas models), in fact drive the segregation and separation of phases as ion insertion and electron transfer proceed. (See detailed discussions in Refs. [124-127,129-133, 199-200]).

After the basic electrochemical response of the active mass is understood, it is possible to analyze properly the more complicated response of thick composite electrodes. It is possible to use techniques such as EIS to evaluate the impact of different types of non-uniformity in the electrodes' structure (*e.g.* non-uniform thickness, non-uniform particle size, blocked

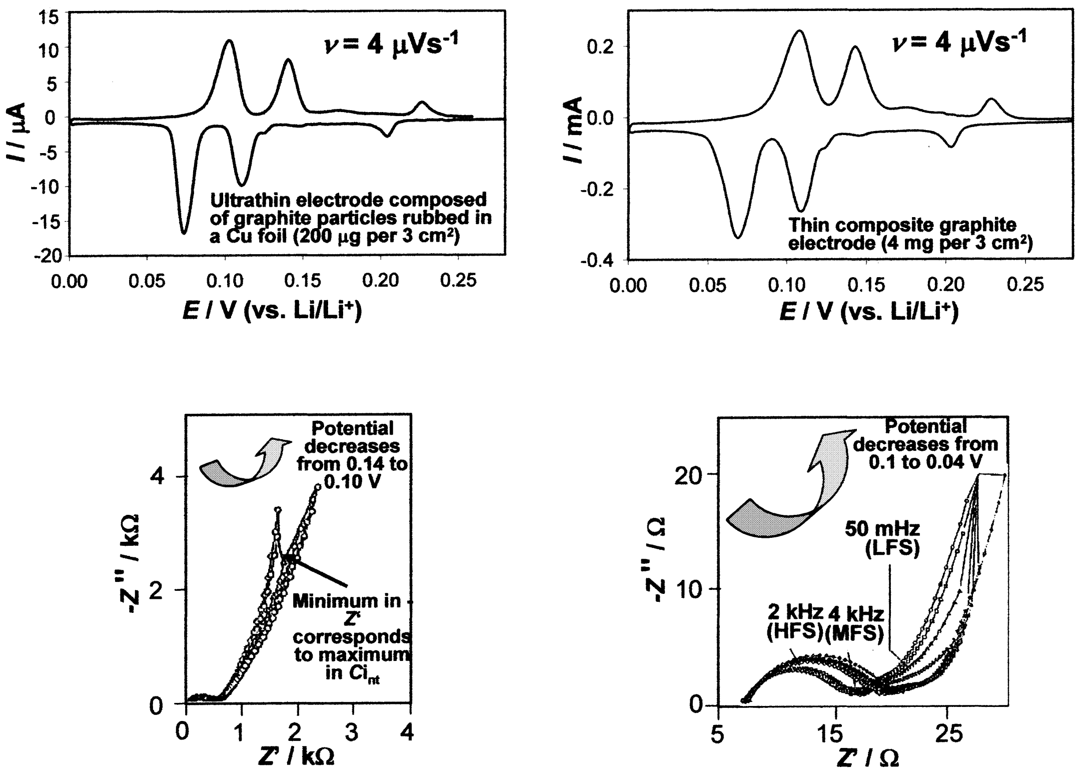

Figure 3.9. Comparison of SSCV and impedance spectra of a very thin (1 μm) electrode (*left*) and thick (10 μm) electrode (*right*) on the way for analysis of practical thick electrodes (*Refs. 196, 200*). The behavior of ion intercalation electrodes (relevant to all kinds of Li batteries, Zn-MnO_2 and alkaline batteries with nickel oxide cathodes) is complicated and its understanding requires the simultaneous application of several electroanalytical techniques. The general electrochemical behavior, staging phase transitions, or formation of solid solutions, can be visualized using SSCV and chronopotentiometry.

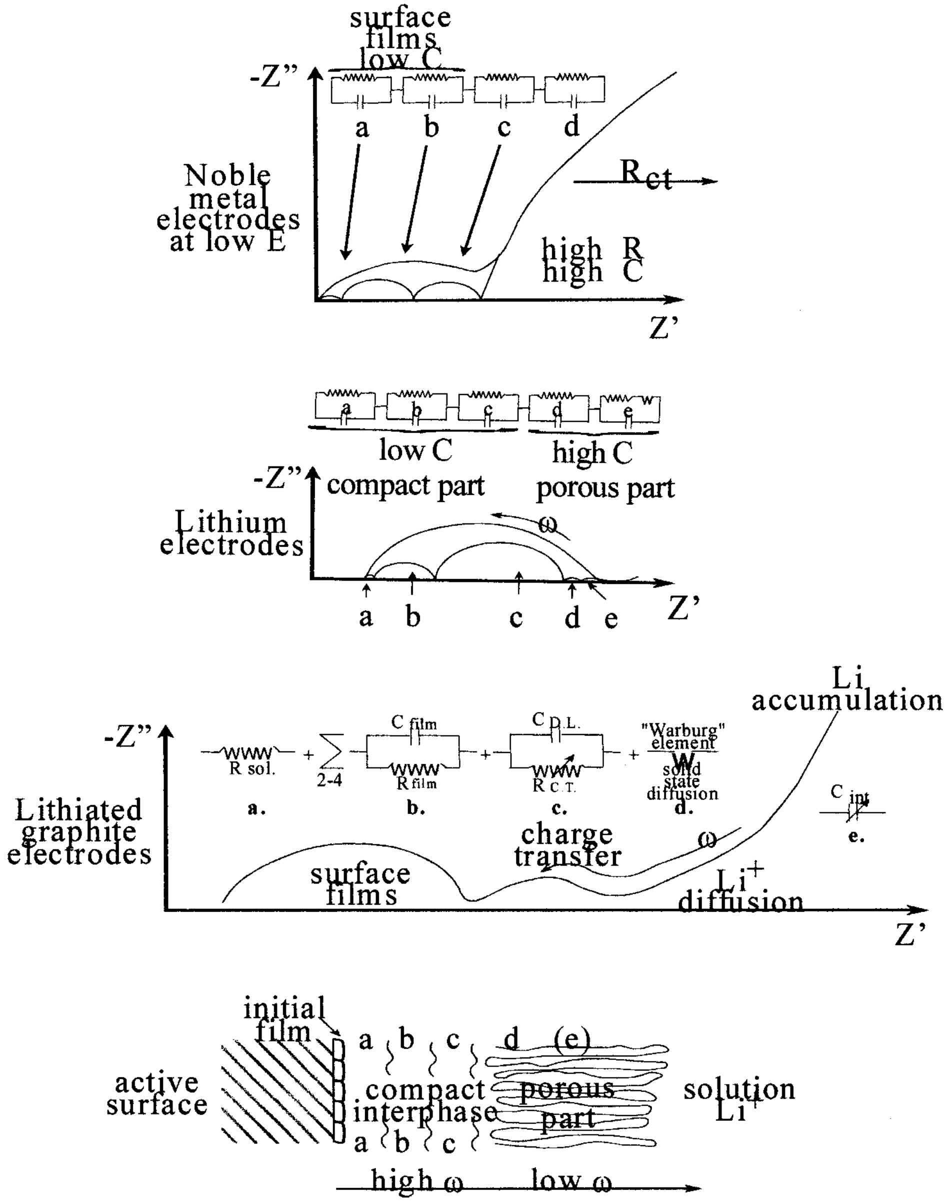

Figure 3.10. A comparison of representative impedance spectra of noble metal electrode polarized to low potentials, Li and Li-graphite electrodes. Common denominator: formation of multilayer surface films, see the scheme at the bottom. In all three cases, the high frequency domain reflects impedance of Li ions migration through surface films, thus the response is similar. The low frequency domains are different (*Refs. 201-203*).

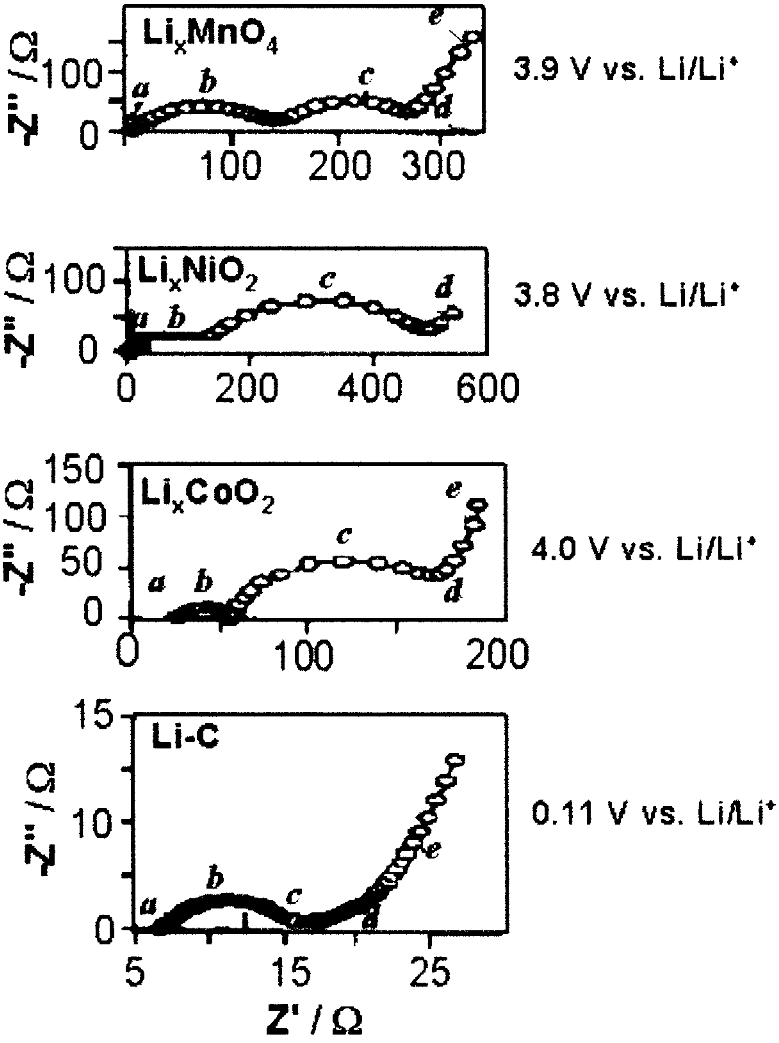

Figure 3.11. Typical impedance spectra of Li insertion electrodes which reflect similarity. Electrodes and potentials are indicated. EC-DMC/$LiAsF_6$ solutions. (*Ref. 201*)

systems and limitations resulting from different types of contact problems, both electrical-interparticle and electrochemical – not all the active mass is in contact with the solutions).

Refs. [130-133] discuss and demonstrate the above approach and related studies. Electrochemical studies of composite electrodes can be useful and comprehensive if they are carried out in conjunction with other bulk and

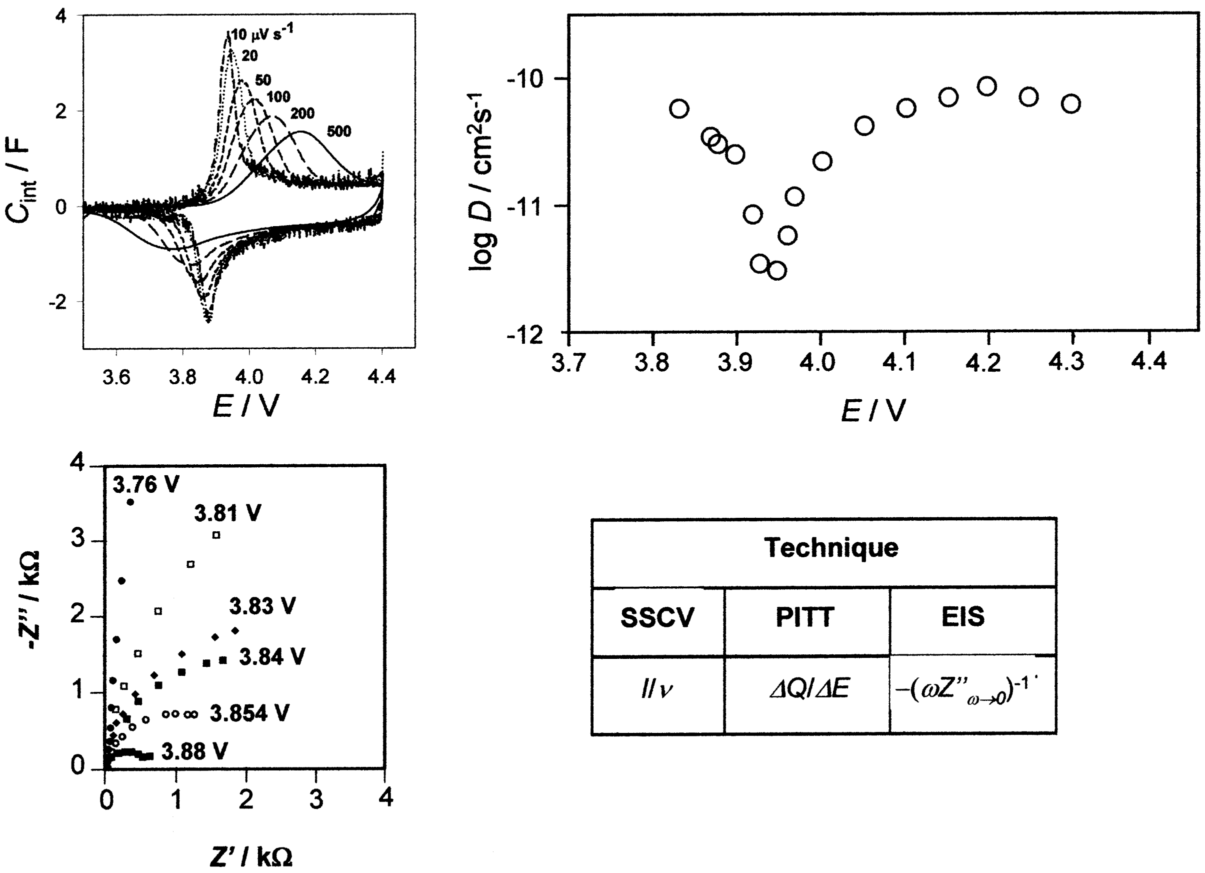

Technique		
SSCV	PITT	EIS
I/v	$\Delta Q/\Delta E$	$-(\omega Z''_{\omega\rightarrow 0})^{-1}$

Fig 3.12. Complete studies of a $LiCoO_2$ electrode (EC-DMC/$LiAsF_6$ solution). SSCV, D *vs.* E obtained from PITT, and EIS. The Z" at ω→0 enables to calculate precisely C_{int} *vs.* E from EIS. The table provides the formulae for calculating differential capacity *vs.* E from the various techniques. (*Refs 199-201*)

surface characterization techniques. Morphological studies of aged electrodes by electron microscopy may be useful, showing changes in the active mass. *Ex situ* and *in situ* XRD measurements clearly reflect possible changes in the bulk active mass upon aging and cycling. Aging tests should also include solution studies. It is important to analyze solution phase after aging by a technique such as ICP (see Section 3.4) in order to discover possible dissolution of ions from the electrodes as part of their aging processes. For instance, upon aging of cathodes comprising Li_xCoO_2 ,$Li_xMn_2O_4$ or Li_xFePO_4 at elevated temperatures, transition metal ions (Co^{2+}, Mn^{2+}, Fe^{2+}) dissolve from the active mass to the solution phase, processes that are accompanied by pronounced changes in the lattice structure of cathode materials and the formation of non-active phases (see Ref. [204] for example). Very important are surface studies of electrodes. In fact, in many cases, batteries fail because of surface phenomena such as passivation processes, an increase in the electrode's impedance due to detrimental surface chemistry, and loss of electrical contact of the active mass due to its isolation by passivating surface films. Such studies are dealt with in the next section.

3.6.3. On the Surface Characterization of Battery Electrodes

Because of the central role of surface chemistry, surface films and passivation phenomena in the performance of many battery electrodes, intensive attention has been focused on surface studies of battery systems. Hence, it is impossible to cover these topics in a single book chapter. In this section, we summarize several important guidelines, with the appropriate referencing to surface studies of battery electrodes. The most challenging studies in recent years related, of course, to lithium and lithium-ion battery systems. Negative electrodes in lithium batteries, whose surface chemistry is the most important, are also the most sensitive to atmospheric contaminants. Therefore, as already mentioned, their study requires the development of special transfer methods from electrochemical cells to spectrometers and microscopes, and special modifications to *in situ* techniques (FTIR,(70,71,205) Raman,(206) XRD, (154,207) AFM,(115) STM(159)) were specially developed, thus preventing complications and loss of authentic information. Several important points related to the surface studies of reactive battery electrodes are listed below.

a. It should be noted that some of the surface techniques may be detrimental to reactive surface species. The X-rays in XPS and AES may induce further reduction of surface species on lithium or Li-C surfaces. The laser beam needed for Raman measurements also has a destructive impact on reactive surfaces. FTIR spectroscopy is never destructive, but is limited to surface groups whose FTIR spectra are well resolved and comprise intense peaks. The application of FTIR and photoelectron spectroscopy in the same study may be synergistic and helpful.

b. For the study of active electrodes such as lithium, it may be useful to add surface studies of non-active electrodes, *e.g.* Ni, Ag, Pt, Au mirrors, polarized to low potentials in the same solutions of interest. Similar surface species may be formed and can be studied more easily and at a better resolution, compared to Li or Li-C electrodes.(202)

c. It is possible to study very efficiently reflective Li electrodes by FTIR spectroscopy using an internal reflectance mode at a grazing angle, while the active surfaces are protected by IR transparent windows (KBr and NaCl are suitable). These studies are very efficient because the actual spectra could be compared to a library of FTIR spectra of a large variety of compounds (organic and inorganic Li salts) that can be formed on Li surfaces in all the commonly-used electrolyte solutions.(208)

d. Over the years, several approaches and cells for *in situ* FTIR studies of Li electrodes were developed, including both external and internal reflectance modes. The relevant details were published, and hence, the relevant experimental experience was clearly shown and can be used. These methods could also be applied for the study of other reactive systems such as magnesium electrodes in nonaqueous solutions.(70,71, 149, 209)

e. For the study of composite reactive electrodes such as lithiated carbon, it is better to study the electrodes after Li deintercalation. Most of the surface species formed at low potentials remain stable on the carbon surface after lithium deintercalation. The most appropriate technique for particulate materials is diffuse reflectance. However, the atmosphere of the spectrometer should be strictly controlled (it has to be H_2O- and CO_2-free).

f. Surface studies of composite electrodes are very complicated by their porous structure, which traps solution species, and the presence of a binder. Hence, efficient washing and evacuation before *ex situ* measurements are important. For spectral analysis, it is important to have for comparison spectra of the pristine electrodes, its separate components, *e.g.* active mass, binder, additives, and the relevant solution species (solvents, salt, solution). (204,210)

g. It is possible to prepare reference surface compounds by some unique experiments, including lithiation of the nanopowder of CoO or CuO(211) and the electrolysis of alkyl carbonates and esters on non-active metal electrodes, in their tetraalkyl ammonium salt solutions (reduction under non-passivation conditions).(190) Complicated FTIR surface spectra measured by diffuse reflectance mode from lithiated carbonaceous material can be compared to much better resolved spectra measured from reference compounds, lithium, and non-active electrodes polarized to low potentials in the same solutions.(212)

In conclusion, the study of the surface chemistry of composite electrodes can be conclusive by the use of several techniques (combining *in situ* and *ex situ* techniques if possible), and the availability of as wide as possible a library of spectra of reference compounds (FTIR, Raman, XPS, *etc.*), to which the electrodes' spectra can be compared.

3.7. Measurements of Complicated Batteries

3.7.1. Introduction – General Aspects

The characterization of full cells has to cover several aspects, including:

a. Determination of the right set of tests that provide a true and sufficient reflection of the battery performance.

b. Understanding possible failure and capacity fading mechanisms: which components are problematic and how the electrodes influence each other.

c. Designing short tests of failure mechanisms and capacity fading that simulate prolonged storage/cycling.

d. Guidelines for upscaling the batteries.

e. Guidelines for connecting batteries in parallel and in series in accumulators, and the choice of appropriate control of multicell systems.

f. Determination of the safety features, study of the thermal behavior, choice and application of the correct safety tests.

f. Setting the correct operation guidelines for different applications.

There are, of course, different requirements for rechargeable cells and each battery chemistry means very specific electrochemical and thermal behavior, and hence, deserves specific characterization and quality control guidelines. Hence, this section can provide only general information. An important distinction has to be made between discussions on commercial, mass produced systems, and batteries that are in their R&D process. Another point of distinction relates to the battery's first process. In the case of primary batteries, the first process is obviously the only one, namely, discharge. Regarding secondary batteries, there are systems in which the batteries are fabricated in their charged state, such as Li batteries. Other systems such as Li-ion, Ni-MH, and Pb-Acid are fabricated in a discharged state, and hence, the first process has to be charging at an optimal regime, determined by the battery chemistry, possible side reactions, the importance of passivation processes, *etc.* (to be optimized by the producers, based on the R&D process and an understanding of the science behind the system). Therefore, standard measurements of such batteries should be started after the first process is completed successfully. (See Refs. [1-4] for many examples).

3.7.2. Examples of Standard Electrochemical Performance Tests for Commercial and Prototype Batteries(1-4)

Major performance tests for batteries are listed below.

a. Typical discharging-charging behavior at ambient temperatures and at the highest rates at which the maximal capacity can be reached. Classical tests provide V *vs.* t (or capacity) curves, measured at constant current

b. Rate capability tests in which the capacity is measured as a function of current (V *vs.* t at different constant currents). In these tests, a decision has to be made as to how the capacity is defined, depending on the cut-off voltage for discharge and charge processes. From the capacity and potential measured, the practical energy density is calculated (gravimetric in Wh/Kg and volumetric in Wh/L).

c. The maximal power density is calculated from V *vs.* t curves. Based on these tests, it is possible to calculate energy density *vs.* power density (Ragone plots).

d. The low temperature limitations are very important. V *vs.* t curves at constant current should be measured as a function of temperature. A capacity decline is expected at low temperatures.

e. Pulse behavior, namely, the response of the voltage and current to transients (fast changes) in the load, should be measured.

f. Phenomena such as voltage delay (*i.e.* initial minimum in voltage obtained upon discharge due to passivation phenomena) and/or memory effect (*i.e.* dependence of the V *vs.* t behavior on depth of discharge) should be characterized.

g. Cycling behavior should be measured in repeated discharge-charge cycling. The discharge capacity is plotted *vs.* cycle number. The cycling behavior should be measured as a function of temperature and rates. Note that such tests can be very prolonged.

h. Shelf-life tests are important: to what extents do charged batteries retain their capacity after prolonged storage? It is possible to simulate prolonged storage conditions at ambient temperature by tests carried out at elevated temperatures. For each type of batteries, the specific correspondence between storage at high and low temperatures should be determined, based on rigorous preliminary studies.

i. Short circuit over charge and over discharge tests is important for determining the safety features of the batteries.

Figure 3.13 shows a set of tests related to rechargeable AA, Li(metal)-$Li_{0.3}MnO_2$ batteries, developed and commercialized by Tadiran Inc. a decade ago.(214,215) The charts in this figure demonstrate a complete set of standard measurements whose results justified commercialization and mass production.

It should be mentioned that these batteries possessed a unique internal safety mechanism based on the fast polymerization of the solvent (1-3 dioxolane) upon short circuit or over charging, which shuts down the battery

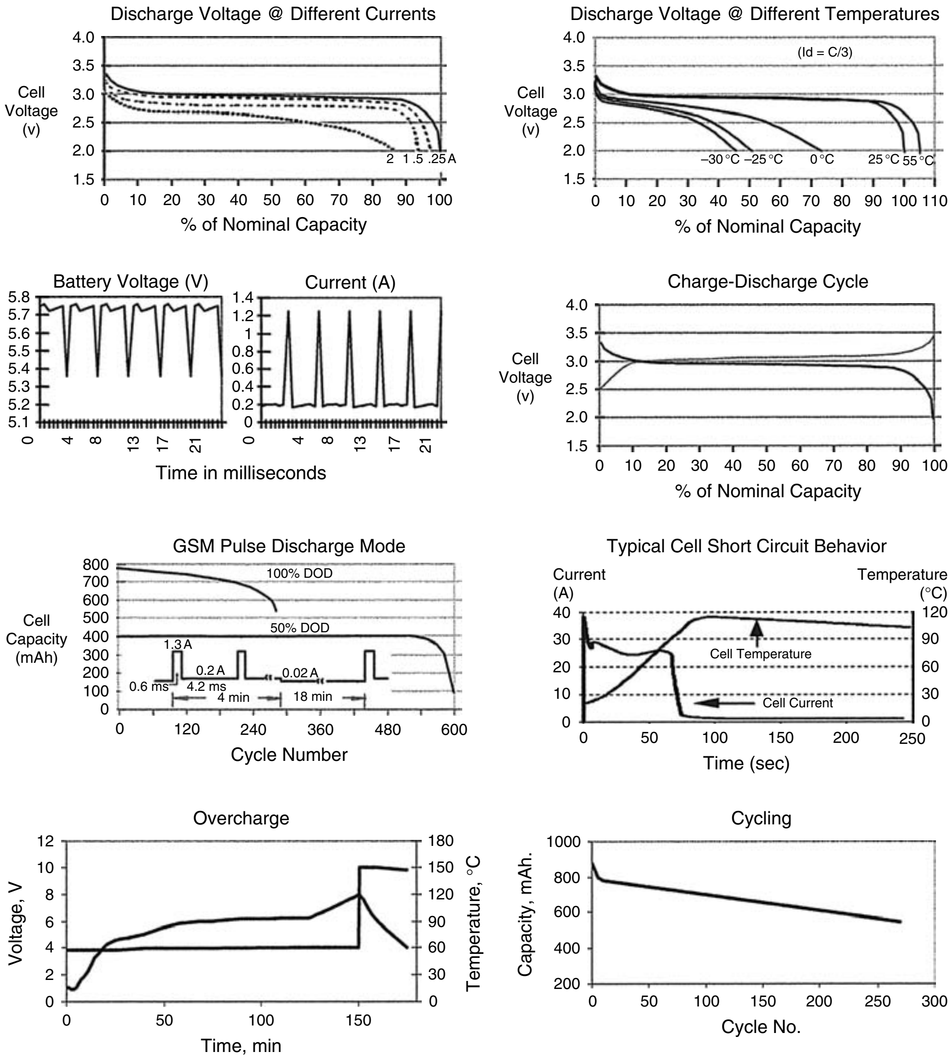

Figure 3.13. Typical required tests for rechargeable batteries: Tadiran Li-Li$_{0.3}$MnO$_2$ Incharge^{TM} (AA batteries) Cell Performance (*Refs. 214,215*).

in abuse cases and prevents its thermal runaway.(214,215) (See the relevant tests in the figure).

3.7.3. Measurements of Prototype Batteries, Impedance Measurements and the Study of Failure Mechanisms

During the course of R&D, full cells are characterized as prototype systems whose basic features, including electrochemical performance, safety limitations and failure limitations, are determined. In this section, some aspects related to final R&D states of batteries and the study of prototype cells are dealt with.

a. It is important to separate the contribution of each electrode in the battery to the overall response in terms of potential profile, impedance capacity, rate capability, and capacity fading. Hence, it is important to develop methodology for that (specific to each battery system). Note that obvious previous stages in the R&D process, in which sub systems were developed and studied (*i.e.* electrolyte solution, single electrodes) cannot provide sufficient information, because in the full cell the electrodes influence each other (*e.g.* dissolution-deposition of products of side reactions), and the geometry and compactness are designed to obtain the maximal energy density. Hence, it is important to use prototype cells with a reference electrode in which potential profile and impedance response of both electrodes can be measured simultaneously.

Figure 3.14 demonstrates a scheme of prototype coin-type cells with reference electrodes. In these cells, the geometry spacing, electrode thickness, and ratio between the electrodes' active mass and the solution content may be quite similar to that in practical prismatic or spirally wound cells. Figure 3.15 presents results from testing Li-ion battery prototypes (coin-type cells with a reference electrode) comprising MCMB graphite (negative) and $LiCoO_2$ (positive) at elevated temperatures.(216) The fact that the capacity fading of this system at elevated temperatures is caused by the anode side is clearly demonstrated. It should be noted that while impedance spectroscopy may be a very powerful tool for the analysis of electrochemical systems, it might usually provide ambiguous information. Hence, it is useless to measure impedance spectra of full cells as a characteristic tool, without the separation of the response of the various electrodes. However, the impedance measurements of full cells at high frequencies may be a direct measurement of the solution resistance in the cell.

b. In order to understand failure mechanisms, and measure the capacity fading behavior of reasonably short experiments, it is recommended that the

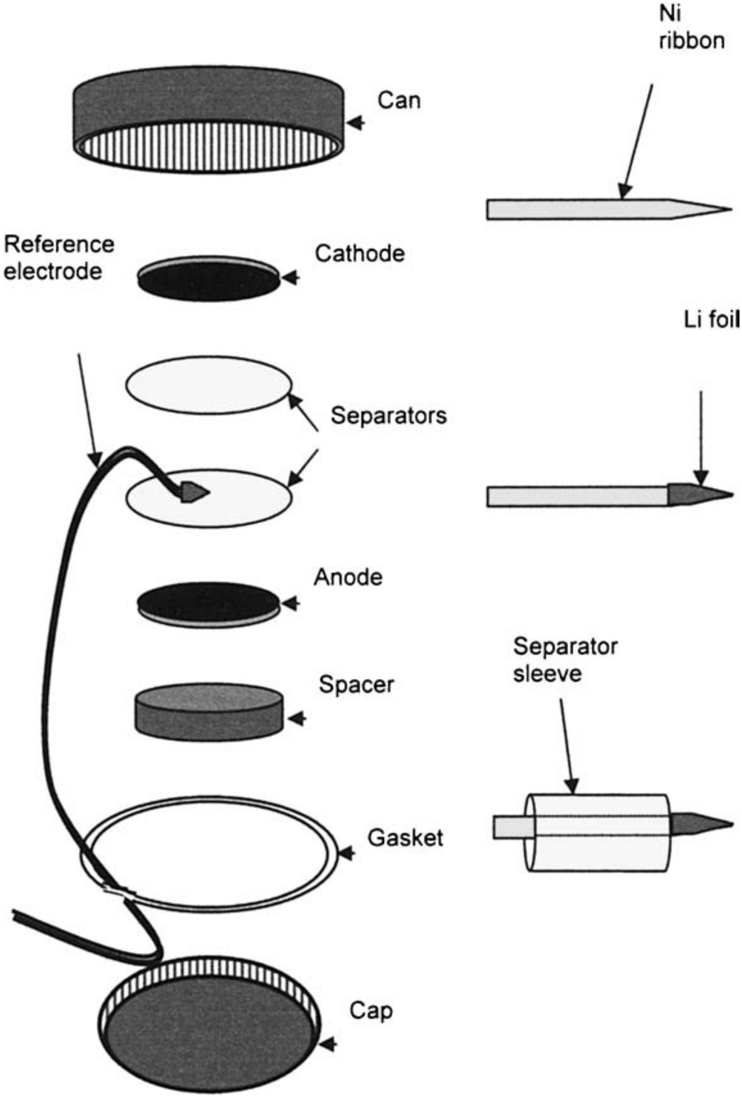

Figure 3.14. A scheme of three-electrode coin-type cell for fine electroanalytical measurements of prototype batteries (on the right-hand side, the preparation of the reference electrode is described).

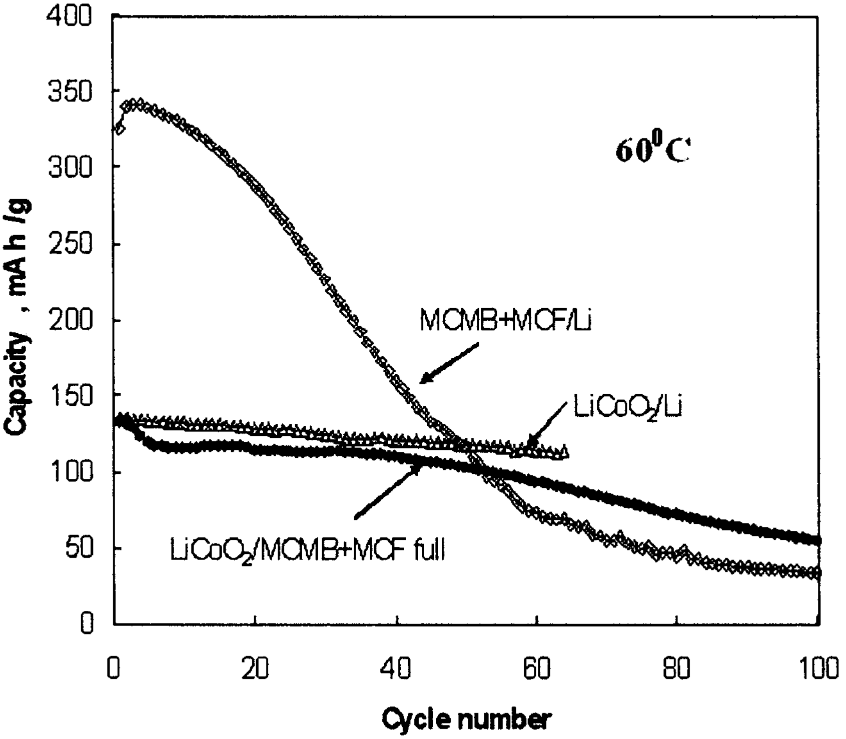

Figure 3.15. A typical study of capacity fading of $LiCoO_2$/MCMB+MCF full cells and two half cells: MCMB+MCF/Li and $LiCoO_2$/Li at elevated temperatures. Electrolyte solution: 1M $LiPF_6$ in EC/EMC 1:2. This study demonstrates that the cells failure is due to the negative electrode (MCMB = meso carbon micro beads, MCF = meso carbon fibers). (*Ref. 216*)

behavior of batteries at elevated temperatures be explored. Side reactions, dissolution of ions from electrodes to the solution phase, and the breakdown of passivation, are all accelerated at high temperatures, and hence, can provide good insight into the expected failure during prolonged time at ambient temperatures.(217-218)

c. Understanding capacity fading and the failure mechanisms of batteries cannot be completed without the post-mortem analysis of failed batteries. Therefore, each R&D process of batteries should include this analysis, including the safe opening of the case without short circuit, separation of the active components under a non-reactive atmosphere (mostly relevant to nonaqueous systems), and access to all the necessary analytical tools (solution phase, morphological, structural and surface analyses).(219)

3.7.4. Safety Features and Safety Tests

The characterization of batteries has to include rigorous safety tests. Several such tests may be dangerous and lead to explosions; hence, they have to be carried out with remote control in appropriate chambers.

Several elementary safety tests are listed below:

a. A short circuit test in which the battery poles are directly connected followed by current and temperature measurements (see Figure 3.13). For rechargeable batteries, short circuit tests should be carried out for cycled batteries at several stages in terms of state of charge and number of cycles.

b. Over-discharging and over-charging tests.

c. Storage at elevated temperature, setting the maximal temperature that the batteries can tolerate.

d. Studies of possible thermal runaway of the batteries and analysis of the thermal reaction products, in order to set environmental limitations.

e. Observing the reactions to nail penetration, crashing, mechanical shocks.

f. Environmental tests for corrosion resistance of the battery case.

The chemical composition of pristine and used batteries, and the products of possible thermal reactions of the battery components, dictate the waste regulations of the batteries and their environmental compatibility and risks.

3.8. Theoretical Aspects of Battery Characterization

In parallel to the extensive experimental work carried out on research, development and production of batteries, there is also impressive theoretical work in the field that covers the following aspects:

a. Theoretical studies of transport phenomena in different kinds of electrolytic media (solutions, polymer matrices, solids), in solid electrode materials (solid-state diffusion processes, ion intercalation) and across interfaces.(220)

b. *Ab initio* calculations of battery materials, elucidation of phase diagrams for electrode materials that undergo phase transition during the course of their redox reactions. In recent years, most of the important Li insertion materials were theoretically analyzed by *ab initio* calculations, and their expected structural changes during the course of Li insertion-deinsertion were calculated, achieving an excellent match with the experimental results. Hence, the theoretical study of electrode materials has reached a high level of reliability.(221-223)

c. *Ab initio* calculations of surface reactions. For Li batteries, the surface chemistry and surface film formation on the electrodes play a central role in their operation and performance. Moreover, since only a few solvents and salts are suitable for Li-ion batteries, the improvement of these systems in terms of better passivation, reducing side reactions, and high temperature stability, can be obtained by the use of additives. The theoretical calculation of the energies of surface reactions and selected compounds with active electrode surfaces, can assist in the judicious search of suitable additives.(224-226)

d. Prediction of the performance of battery systems in terms of I,V,t behavior, impedance, rates, and power and energy density based on a good understanding of the physical situation (interfacial aspects, resistive elements in the systems such as surface films, composite electrode structure, and the transport phenomena related to the electrolyte system). Over the years, batteries with both liquid and solid electrolyte systems were theoretically analyzed. These studies could help to improve the engineering of batteries, address processes with problematic heat dissipation, map temperatures reached at high rates, and optimize properties of components in order to achieve high rates and low voltage drops due to internal resistance.(227-229)

e. Based on the understanding of passivation phenomena and side reactions in batteries, it was possible to develop models for the calendar life of batteries and successfully predict the effect of prolonged storage on the practical capacity of batteries. Impressive work of this kind was attributed to lithium batteries.(230-231)

3.9. Concluding Remarks

The field of battery characterization is very wide because it includes many aspects of electrochemical, surface and materials science, physics (transport phenomena), organic and inorganic chemistry, solid-state chemistry, and extensive engineering considerations. Moreover, each battery system is in itself a world of chemical, physical and engineering challenges, problems, and unique properties. Hence, this chapter could only briefly cover several fundamental and practical aspects of this wide topic. However, for more in-depth studies, the chapter provides references for each subject in which detailed experimental work is described and discussed.

Acknowledgements

The author thank Professors Mikhail Levi and Elena Levi, Drs. Orit Chusid, Yossi Gofer, Elena Markevich, Boris Markovsky, Ella Zinigrad, and Gregory Salitra, Mrs. Liraz Asraf, Mr. Yossi Tal-Yosef and Mr. Maxim Koltypin (Ph.D. students) and

Mrs. Louise Braverman from Bar-Ilan University for their assistance in the preparation of this chapter.

References

1. D. Linden, in "*Handbook of Batteries*", second edition, McGraw-Hill, Inc. (NY), 1994.
2. R.M Dell and D.A.J. Rand, in "*Understanding Batteries*", The Royal Society of Chemistry, Cambridge, (UK) 2001.
3. T.R. Crompton, in "*Battery Reference Book*", 3rd Ed, Newnes, Oxford, (UK) 2000.
4. "*Handbook of Battery Materials*", J. O. Besenhard, Ed., Wiley-VCH Weinheim, (NY) 1999.
5. E. Peled and H. Yamin, *Israel J. Chem.* 18 (1979) 131.
6. M. Gaberscek and P. Stane, *J. Electrochem. Soc.* 146 (1999) 933.
7. D. Aurbach and I. Weissman, in "*Nonaqueous Electrochemistry*", Marcel Dekker, Inc. D. Aurbach Ed. ,New York,(1999) CH. 1.
8. J. O'M Bockris and A.K.N Reddy, in "*Modern Electrochemistry: Electrodics in Chemistry, Engineering, Biology and Environmental Science*", Kluwer Academic, New York, (NY) Ch. 13, 2000.
9. S.C. Singhal and K. Kendall, in "*High-Temperature Solid Oxide Fuel Cells: Fundamentals, Design and Applications*", Elsevier., Oxford, (UK) 2003; G. Hoogers, in "*Hoogers Fuel Cell Technology Handbook*", CRC Press, Florida, (USA) 2003.
10. P. Novak, K. Muller and O. Haas, *Chem. Rev.* 97 (1997) 207.
11. D. Aurbach, I. Weissman, Y. Gofer and E. Levi, *Chem. Record* 3 (2003) 61.
12. W.K. Hu, X.P. Gao, M.M. Geng and D. Noreus, *Electrochem. Solid State Lett.* 7 (2004) A439.
13. R. Yazami, *J. Power Sources* 97-98 (2001) 33.
14. K. Nakajima and Y. Nishi in " *New Trends in Electrochemistry: Energy Storage Systems for Electronics*", T. Osaka and M. Datta Eds., Gordon and Breach Science Publishers, (Australia, Canada, Japan, India and Switzerland) 2000 Ch. 5.
15. D. Aurbach, O. Youngman Chusid, Y. Carmeli, M. Babai and Y. Ein-Eli, *J. Power Sources* 43 (1993) 47; D. Aurbach, Y. Ein-Eli, O. Chusid, M. Babai, Y. Carmeli, and H. Yamin, *J. Electrochem. Soc.* 141 (1994) 603.
16. E. Peled, in "*Lithium Batteries*", J.P. Gabano Ed., Academic Press, London, (NY. and Paris), 1983, Ch. 3.
17. D. Aurbach, M. Koltypin and H. Teller, *Langmuir* 18 (2002) 9000.
18. D. Aurbach, H. Teller and E. Levi, *J. Electrochem. Soc.* 149 (2002) A1255.
19. E. Buiel and J.R. Dahn, *Electrochim. Acta* 45 (1999) 121.
20. K.E. Aifantis, J.P. Dempsey and S.A. Hackney, *Rev. Adv. Mater. Sci.*, 10 (2005) 408: W.R. Liu , Z.Z. Guo, W.S.Young D.T. Shieh ,C.H. Wu , M. H. Yang and N.L. Wu , *J. Power Sources* 140 (2005)139.
21. M. Tillard, C. Belin, L. Spina and Y.Z. Jia, *Solid State Sci.* 7 (9) (2005) 1125-1134. E. Ronnebro , J.T Yin , A Kitano , M Wada , S Tanase and T. Sakai *J. Electrochem. Soc.* 151 (2004) A1738: E. Ronnebro , J.T Yin , A Kitano , M Wada and T. Sakai , *Solid State Ionics* 176 (2005) 2749.
22. K. Mukai, K. Ariyoshi and T. Ohzuku, *J. Power Sources* 146 (2005) 213
23. D. Aurbach, M.D. Levi, E. Levi, H. Teller, B. Markovsky, G. Salitra, L. Heider and U. Heider, *J. Electrochem. Soc.* 145 (1998) 3024; D. Aurbach, K. Gamolsky, B. Markovsky, G. Salitra, and Y. Gofer, *J. Electrochem. Soc.* 147 (2000) 1322.
24. D. Aurbach, B. Markovsky, M.D. Levi, E. Levi, A. Schechter. M. Moshkovich and Y. Cohen, *J. Power Sources* 81-82 (1999) 95.

25. J. Daniel-Ivad, K. Kordesch and E. Daniel-Ivad, *Proc. 39th Power Sources Conf.*, Cherry Hill, N.J., 330, 2000.
26. D.M. Holton, W.C. Maskell and F.L. Tye, *Proc. 14th International Power Sources Symp.* (Brighton), Pergamon, New York, 1984.
27. J.L. Robinson, in *"Magnesium Cells"*, N.C. Cahoon and G. W. Heise Eds., *The Primary Battery*, Vol. 2, Wiley-Interscience, New York, Chap.2. (1976).
28. J. Gabano in *"Lithium Batteries"*, Academic, London, 1983.
29. T. Iijima, Y. Toyoguchi, J. Nishimura and H. Ogawa, *J. Power Sources* 5 (1980) 99
30. A. Fleischer and J. Lander Eds., in *"Zinc-Silver Oxide Batteries"*, Wiley, (NY), 1971.
31. H. Bode, in *"Lead-Acid Batteries"*, Wiley, (NY), 1977.
32. E. Shembel, R. Apostolova, V. Nagirny, D. Aurbach and B. Markovsky, *J. Power Sources* 80 (1999) 90.
33. E. Andrukaitis, P.W.M. Jacobs and J.W. Lorimer, *Solid State Ionics* 27 (1988) 19.
34. J.K. Erbacher, in *"Nickel-Metal Hydride Technology Evaluation"*, Final Report Wright Laboratories WL-TR—96-2069, Fairborn, OH, 1996.
35. E. Levi, E. Zinigrad, H. Teller, M.D. Levi, and D. Aurbach. *J. Electrochem. Soc.* 145 (1998) 3440.
36. K.M. Abraham, G.M. Holleck, T. Neguyen, D.M. Pasquariello and D.A. Schwartz, *J. Power Sources* 26 (1989) 313
37. K. Kumai, T. Ikeya, K. Ishihara, T. Iwahori, N. Imanishi, Y. Takeda, and O. Ymamamoto, *J. Power Sources* 70 (1998) 235.
38. M.D. Levi, E. Lancry, H. Gizbar, Y. Gofer, E. Levi and D. Aurbach, *Electrochim. Acta* 49 (2004) 3201.
39. Y. Shao-Horn and Q.C. Horn, *Electrochim. Acta, 46* (2001) 2613.
40. T. Ohzuku, A. Veda, M. Nagayama, Y. Iwakoshi and H. Komori, *Electrochim. Acta* 38 (1993) 1159.
41. M. Winter, J.O. Besenhard, M.E. Spahr and P. Novak, *Adv. Mater.* 10 (1998) 725.
42. M.G.S.R. Thomas, W.I.F. David, J.B. Goodenough and P. Groves, *Mater. Res. Bull.* 20 (1985) 1137.
43. T. Ohzuku, H. Komori, M. Nagayama, K. Sawai and T. Hirai, *Chem. Express* 6 (1991) 621.
44. G.G. Amatucci, C.N. Schmutz, A. Blyr, C. Sigala, A.S. Gozdz, D. Larcher and J.M. Tarascon, *J. Power Sources* 69 (1997) 11.
45. Y. Xia, Y. Zhou and M. Yoshio, *J. Electrochem. Soc.* 144 (1997) 2593.
46. Z. Wang, C. Wu, L. Liu, F, Wu, L. Chen and X. Huang, *J. Electrochem. Soc.* 149 (2002) A466.
47. J. Cho, Y.J. Kim, T.-J. Kim and B. Park, *Angew. Chem. Int. Ed.* 40 (2001) 3367.
48. K. Dokko, M. Mohamedi, N. Anzue, T. Itoh and I. Uchida, J. *Mater. Chem.* 12 (2002) 3688.
49. A.K. Padhi, K.S. Nanjundaswamy and J.B. Goodenough, *J. Electrochem. Soc.* 144 (1997) 1188.
50. M.E. Spahr, P. Novak, B. Schnyder, O. Haas and R. Nesper, *J. Electrochem. Soc.* 145 (1998) 1113.
51. Z. Lu, D.D. MacNeil and J.R. Dahn, *Electrochem. Solid State Letters* 4 (2001) A191.
52. T. Ohzuku and Y. Makimura, *Chem. Lett.* 1 (2001) 642.
53. D.C. Li, T. Muta, L.Q. Zhang, M. Yoshio and H. Noguchi, *J. Power Sources* 132 (2004) 150.
54. G.Q. Liu, C.L. Zeng and K. Yang, *Electrochim. Acta* 47 (2002) 3239.
55. Y. Gofer, H. Sarker, J.G. Killian, J. Giaccai, T.O. Poehler and P.C. Searson, *Biomedical Instrumentation & Technology, Association for the Advancement of Medical Instrumentation* 32(1) (1998) 33.
56. G. Blomgren, in *"Lithium Batteries"* J.P. Gabano Ed., Academic Press, (London, N.Y. and Paris), 1983, Ch. 2.

57. M. Nazri, in *"Lithium Batteries, Science and Technology"*, G.A. Nazri and G. Pistoia Eds., Kluwer Academic Publishers, Boston, (N.Y. and London), 2004, Ch. 17.
58. M. Buzzeo, R. Evans and R. Compton, *Chem. Phys. Chem.* 5 (2004) 1107
59. T. Osaka, T. Momma, H. Ito and B. Scrosati, *J. Power Sources* (1997) 392.
60. X.-G. Sun and J. B Kerr, *Macromol.* 39(1) (2006) 362.
61. M. Wachtler, D. Ostrovskii, P. Jacobsson and B Scrosati, *Electrochim. Acta*, 50(2-3) (2004) 357.
62. K. Shahi, J.B. Wagner and B.B. Owens, in *"Lithium Batteries"*, J.P. Gabano Ed., Academic Press, (London, NY and Paris), 1983 Ch. 15.
63. A.H. Whitehead and M. Schreiber, *J. Electrochem. Soc.* 152 (2005) A2105.
64. P. Arora and Zh. Zhang, *Chem. Rev.* 104 (2004) 4419.
65. D. Aurbach, E. Zinigrad, H. Teller, and P. Dan, *J. Electrochem. Soc.* 147 (2000) 2486.
66. D. Aurbach, B. Markovsky, A. Rodkin, M. Cojocaru, E. Levi and H.J. Kim *Electrochim. Acta* 47 (2002) 1899.
67. D.H. Doughty, E.P Roth, C.C. Crafts, G. Nagasubramanian, G. Henriksen and K. Amine, *J. Power Sources* 146 (1-2) (2005) 116.
68. M. Herstedt, H. Rensmo, H. Siegbahn and K. Edstrom, *Electrochim. Acta* 49 (2004) 2351.
69. R. Yamaguchi H. Ikuta and M. Wakihara, *J. Thermal Anal. Calorim.* 57 (3) (1999) 797.
70. E. Goren, O. Chusid and D. Aurbach, *J. Electrochem. Soc.* 138 (1991) L6.
71. D. Aurbach and O. Chusid, *J. Electrochem Soc.* 140 (1993) L155.
72. W. Kautek, A. Conradi, Ch. Fabjan and G. Bauer, *Electrochim. Acta* 47 (2001) 815; G.L.J Trettenhahn, G.E. Nauer, and A. Neckel, *J.Power Sources* 42 (1993) 137.
73. J.Y. Go, S.-I. Pyun and S.-I. Cho, *Electrochim. Acta* 50 (2005) 5435.
74. M.D. Levi, R. Demadrille, A. Pron, M.A. Vorotyntsev and D. Aurbach, *J. Electrochem. Soc.* 152 (2005) E61.
75. M.D. Levi and D. Aurbach, *J. Phys. Chem. B* 109 (7) (2005) 2763.
76. W. Wen, B. Kumarasamy, S. Mukerjee, M. Auinat and Y. Ein-Eli,. *J. Electrochem. Soc.* 152(9) (2005 A1902.
77. M. Holzapfel, O Proux, P. Strobel, C. Darie, M. Borowski and M. Morcrette, J. *Mater. Chem.* 14 (2004) 102.
78. Y.I. Jang, N. Dudney, D. Blom and L. Allard, *J. Power Sources* 119-121 (2003) 295.
79. C. Grey and S. Greenbaum, *Bull. Mater. Res. Soc.* 27 (2002) 613.
80. D. Aurbach and Yaron Cohen, *J. Phys. Chem. B* 104 (2000) 12282.
81. K. Amine, J. Liu and I. Belharouak, *Electrochem. Comm.* 7 (2005) 669.
82. J.B.Hudson in "*Surface Science: An Introduction*", Wiley-IEEE, (NY) p. 183, 1998
83. D. Aurbach. M. Daroux, G. McDougal and E.B. Yeager, *J. Electroanal. Chem.* 358 (1993) 63.
84. J. Jiang and J.R. Dahn, *Electrochim. Acta* 49 (2004) 2661.
85. Y.Z. Jin, Y.J. Kim, C, Gao, Y.Q. Zhu, A. Huczko, M. Endo and H.W Kroto, *Carbon* 44 (2006) 724.
86. Y. Gofer, R. Barbour, Y. Luo, D.A. Tryk, J. Jayne, G. Chottiner and D.A. Scherson, *J. Phys. Chem.* 99 (1995) 11797.
87. R.M. Silverstein and F.X. Webster, in *"Spectroscopic Identification of Organic Compounds"*, 6th edition, Wiley (NY) 1963.
88. J.R. Haskins, *Am. J. Phys.* 33 (1965) 646.
89. J.S. Winans, *J. Opt. Soc. America* 61 (1971) 1585.
90. RA Dunlap, D.A. Small, D.D. MacNeil and J. Dahn, *J. Alloys Comp.* 289 (1999)135.
91. C. Grey and Y. Lee, *Solid State Sci.* 5 (2003).
92. H. Gizbar, Y. Viestfrid, O. Chusid, Y. Gofer, H. E. Gottlieb, V. Marks and D. Aurbach, *Organometallics* 23 (2004) 3826.
93. I. Cheung, K. Chin, E. Greene, M. Smart, S. Abbrent, S. Greenbaum, G. Prakash and S. Surampudi, *Electrochim. Acta* 48 (2003) 2149.

94. F. Chevallier, M. Letellier, M. Morcrette, J. M. Tarascon, E. Frackowiak, J.N. Rouzaud and F. Be′guin, *Electrochem. Solid-State Lett.* 6 (2003) A225.
95. C.P. Grey and N. Dupre, *Chem. Rev.* 104 (2004) 4493.
96. Y. Wang, V. Yufit, X. Guo, E. Peled and S. Greenbaum, *J. Power Sources* 94 (2001) 230.
97. B.H. Stuart, in "*Infrared Spectroscopy: Fundamentals and Applications*", John Wiley and Sons, (NY) 2004.
98. W.J. Tornquist and G.L. Griffin, *J. Vacuum Sci. Technol., A: Vacuum, Surfaces and Films* 4 (1986) 1437.
99. B. C Smith, in "*Fundamentals of Fourier Transform Infrared Spectroscopy*", CRC Press, (NY) 1995.
100. K. Nishikida, in "*Selected Applications of Modern Ft-Ir Techniques*", Taylor & Francis, 1996.
101. E. Smith and G. Dent, in "*Modern Raman Spectroscopy: A Practical Approach*", John Wiley and Sons (UK) 2005.
102. E.R. Menzel and M.R. Menzel, in "*Laser Spectroscopy: Techniques and Applications*", Marcel Dekker (NY) 1994.
103. A. Montaser, in "*Inductively Coupled Plasma Mass Spectrometry*", Wiley-VCH, (NY) 1998.
104. A.R. West in "*Basic Solid State Chemistry*", Wiley-VCH, (Chichester and NY), 1998 chapters and references therein.
105. P.W. Atkins and J.D. Paula, in "*Physical Chemistry*", 7th edition, Oxford University Press, (England), Ch. 23, 2002.
106. R. Jenkins and R. Snyder in "*Introduction to X-ray Powder Diffractometry*", Wiley, (NY), 1996 chapters and references therein.
107. R. Schollhorn, *Angew. Chem. Int. Ed. Engl.* 19 (1980) 983.
108. Y. Iwasawa, in "*X-ray Absorption Fine Structure*", World Scientific Publishing Co. Pte., Ltd., MA, (USA) 1996.
109. J. McBreen, in "*Handbook of Solid State Batteries and Capacitors*", P.S.S. Prasad Ed., World Scientific Publishing Co. Pte., Ltd., (Singapore), p. 60-78, 1996
110. A.R. Gerson, P.J. Halfpenny, N.S. Pizzini, R. Ristic, K.J. Roberts, D.B. Sheen and J.N. Sherwood, in "*X-ray Characterization of Materials*", E. Lifshin Ed., Wiley-VCH, Weinheim, (Germany), pp. 105-170, 1999
111. I. Rom, M. Wachtler, I. Papst, M. Schmied, J.O. Besenhard, F. Hofer and M. Winter, *Solid State Ionics* 143 (2001) 329.
112. D. Aurbach, Y. Gofer and Y. Langzam, *J. Electrochem. Soc.* 136 (1989) 3198.
113. O. Marti, B. Drake, S. Gould and P.K. Hansma, *J. Vacuum Sci. Technol., A:Vacuum, Surfaces and Films* 6 (1988) 287.
114. D. Aurbach and Y. Cohen, *J. Electrochem. Soc.* 143 (1996) 3525 .
115. Y. Cohen and D. Aurbach, *Rev. Scient. Instrum.* 70 (1999) 4668.
116. Z. Ogumi and S.K. Leong, *Electrochem.* 71 (2003) 1011.
117. F.P. Campana, R. Kotz, J. Vetter, P. Novak and H. Siegenthaler, *Electrochem. Comm.* 7 (2005) 107.
118. S. Brunaur, H.R. Emmet and H. Teller, *J. Am. Chem. Soc.* 66 (1938) 309.
119. J. Jiang and J.R. Dahn, *Electrochem. Comm.* 6 (2004) 39.
120. J. S. Gnanaraj, E. Zinigrad, L. Asraf, H. E. Gottlieb, M. Sprecher, M. Schmidt, W. Geissler and D. Aurbach. *J. Electrochem. Soc.* 150 A, (2003) 1533.
121. R. Kostecki and F. McLarnon, *J. Power Sources* 119-121 (2003) 550.
122. D. Briggs and J.T. Grant in "*Surface Analysis by Auger and X-ray Photoelectron Spectroscopy*", IM Publications, Chichester and Surface Spectra Manchester (UK) 2003.
123. T. Matsushita, K. Dokko and K. Kanamura, *J. Electrochem. Soc.* 152 (2005) A2229; K. Kanamura, S. Shiraishi, H. Takezawa and Z. Takehara, *Chem. Mater.* 9 (1997) 1797; S. Shiraishi, K. Kanamura and Z. Takehara *J. Appl. Electrochem.* 29 (1999) 869.
124. M.D. Levi and D. Aurbach, *Electrochim. Acta* 45 (1999) 167.

125. M.D. Levi and D. Aurbach, *J. Electroanal. Chem.* 421 (1997) 79.
126. M. D. Levi, G. Salitra, B. Markovsky, H. Teller, D. Aurbach, U. Heider and L. Heider, *J. Electrochem. Soc.* 146 (1999) 1279.
127. W.R. McKinnon and R.R. Haering, in "*Modern Aspects in Electrochemistry*", Plenum Press, (New York) Vol. 15, p. 235, 1987.
128. M.D. Levi, K. Gamolsky, D. Aurbach, U. Heider and R. Oesten, *J. Electroanal. Chem.* 477 (1999) 32.
129. A.J. Bard and L.R. Faulkner, in "*Electrochemical Methods. Fundamentals and Applications*", John Wiley & Son, (New York), p.434, 1980
130. E. Markevich, M.D. Levi and D. Aurbach, *J. Electroanal. Chem.* 580 (2005) 231.
131. M.D. Levi and D. Aurbach, *J. Phys. Chem. B* 108 (2004) 11693.
132. M.D. Levi, C. Wang and D. Aurbach, *J. Electroanal. Chem.* 561 (2004) 1.
133. M. D. Levi, E. Markevich and D. Aurbach, *J. Phys. Chem. B* 109 (2005) 7420.
134. J. Albery, in "*Electrode Kinetic*", Clarendon Press, Oxford (UK) 1975.
135. C.H. Hamann, A. Hamnett and W. Vielstich in "*Electrochemistry*" Wiley-VCH, (NY) p. 388, 1999
136. M. Sakai, J. Osteryoung and R.A. Osteryoung, *J. Electrochem. Soc.* 135 (1988) 3001.
137. S. Bruckenstein, A. Fensore, Z. Li and A.R. Hillman, *J. Electroanal. Chem.* 370 (1994) 189
138. D. Aurbach and M. Moshkovich, *J. Electrochem. Soc.* 145 (1998) 2629.
139. D. Aurbach, M. Moshkovich, A. Schechter and R. Turgeman, *Electrochem. Solid State Lett.* 3 (2000) 31.
140. G. Binning and H. Rohrer, *Physica B & C* 127 (1984) 37.
141. D. Aurbach, Y. Cohen and M. Moshkovich, *Electrochem.Solid State Letts.* 4 (2001) A113.
142. D.S. Kong, L.J. Wan and S.H Chen, *Progr. Chem.* 16 (2004) 204.
143. R E White, B. E. Conway and J.O. Bockris in "*Modern Aspects of Electrochemistry*" Springer (NY) p. 123, 1992
144. J. Lei, L. Li, R. Kostecki, R. Muller and F. McLarnon, *J. Electrochem. Soc.* 152 (2005) A774-A777.
145. F. Kong, R. Kostecki, G. Nadeau, X. Song, K. Zaghib, K. Kinoshita and F. McLarnon, *J. Power Sources* 97 (2001) 58.
146. D. Scherson, in "*Nonaqueous Electrochemistry*", D. Aurbach Ed. Marcel Dekker, (NY) Ch. 5, p. 213, 1999.
147. G. Zhuang and P.N. Ross, *J. Power Sources* 89 (2000) 143.
148. G. Zhuang, K. Wang, G. Chottiner, R. Barbour, Y. Luo, I.T. Bae, D. Tryk and D.A. Scherson, *J. Power Sources* 54 (1995) 20.
149. D. Aurbach, R. Turgeman, O. Chusid and Y. Gofer, *Electrochem. Comm.* 3 (2001) 252.
150. M. Moshkovich, M. Cojocaru, H.E. Gottlieb and D. Aurbach, *J. Electroanal. Chem.* 497 (2001) 84.
151. Y. Luo, W.B. Cai, X.K. Xing and D.A. Scherson, *Electrochem. Solid State Lett.* 7 (2004) E1.
152. Q. Shi, Y. Takahashi, J. Akimoto, I.C. Stefan and D.A. Scherson, *Electrochem. Solid State Lett.* 8 (2005) A521.
153. T. Baehtz, N.N. Buhrmester, K. Bramnik, K. Nikolski and H. Herenberg, *Solid State Ionics* 176 (2005) 1647.
154. D. Aurbach and Y. Ein-Eli, *J. Electrochem. Soc.* 142 (1995) 1746.
155. M.R. Palacin, F. Le Cras, L. Sequin, M. Anne, Y, Chabre, J.M. Tarascon, G. Amatucci, G. Vaughan and P. Strobel, *J. Solid State Chem.* 144 (1999) 36.
156. A.J. Kropf, H. Tostmann, C.S. Johnson, J.T. Vaughey and M.M. Thackeray, *Electrochem. Comm.* 3 (2001) 244.
157. Y.W. Tsai, B.J. Hwang, G. Ceder, H.S. Sheu, D.G. Liu and J.F. Lee, *Chem. Mater.* 17 (2005) 3191.
158. M. Koltypin, Yaron Cohen, Yair Cohen, B. Markovsky and D. Aurbach, *Electrochem. Comm.* 4 (2002) 17.

159. D. Aurbach, A. Schechter, M. Moshkovich and Y. Cohen, *J. Electrochem. Soc.* 148 (2001) *A*1004.
160. A. Wadas, *J. Magnetism Magnetic Mater.* 78 (1989) 263.
161. R. Imhof and P. Novak, *J. Electrochem. Soc.* 145 (1998) 1081.
162. J. Ufheil, A. Wurzig, O.D. Schneider and P. Novak, *Electrochem. Comm.* 7 (2005) 1380.
163. M.E. Spahr, H. Buqa, A. Wurzig, D. Goers, L. Hardwick, P. Novak, F. Krumeich, J. Dentzer and C. Vix-Guterl, *J. Power Sources* 153 (2006) 300.
164. I. Novik, R.H. Herber, M. Koltypin, D. Aurbach and S. Licht, *J. Phys. Chem. Solids* 66 (2005) 1307.
165. I. A. Courtney, R. A. Dunlap and J. R. Dahn, *Electrochim. Acta* 45 (1999) 51.
166. C. Reichard, *Angew. Chem. Int. Ed. Engl.* 18 (1979) 87.
167. U. Mayer, in *"Proceedings of the Workshop on Lithium Nonaqueous Battery Electrochemistry"*, E.B. Yeager, B. Schumm, Jr., G. Blomgren, D.R. Blankenship, V. Leger and J. Akridge, Eds., The Electrochemical Society, Inc., softbound series PV 80-7 p. 13 1980.
168. U. Mayer, *Monatsch. Chem.* 108 (1977) 1479.
169. P.W. Atkins and J.D. Paula, *Physical Chemistry*, 7th ed. Oxford University Press, Oxford, (Melbourne and Tokyo) Ch. 24, 2002
170. S.H. Maron and J.B. Lando in *"Fundamentals of Physical Chemistry"*, Macmillan, (New York; Collier Macmillan, London) Ch. 13, 1974
171. K. Xu, *Chem. Rev.* 104 (2004) 4303.
172. G. Blomgren, in *"Nonaqueous Electrochemistry"*, D. Aurbach, Ed., Marcel Dekker, (NJ), Ch. 2, 1999
173. J.F. Casteel and E.A. Amis, *J. Chem. Eng. Data* 17 (1972) 55.
174. C.A. Angell and J C. Tucker, *J. Phys. Chem.* 78 (1974) 278.
175. J. Barthel, H.G. Gores, P.Carlier, F. Feuerlein and M. Utz, *Ber. Bunsenges. Phys. Chem.* 87 (1983) 436.
176. G.B. Appetecchi, F. Croce, P. Romagnoli, B. Scrosati,, U. Heider and R. Oesten, *Electrochem. Comm.* 1 (1999) 83.
177. H.R. Allcock, N.J. Sunderland, R. Ravikiran and J.M. Nelson, *Macromol.* 31 (1998) 8026.
178. F. Croce, L. Persi, B. Scrosati, F. Serraino-Fiory, E. Plichta and M.A. Hendrickson, *Electrochim. Acta* 46 (2001) 2457.
179. D. Golodnitsky, G. Ardel and E. Peled, *Solid State Ionics* 147 (2002) 141.
180. D. Aurbach and Y. Gofer, in *"Nonaqueous Electrochemistry"*, D. Aurbach, Ed., Marcel Dekker, (N.Y), Ch. 4, 1999.
181. D. Aurbach, R. Skaletsky and Y. Gofer, *J. Electrochem. Soc.* 138 (1991) 3536.
182. Z. Lu, A. Schechter, M. Moshkovich and D. Aurbach, *J. Electroanal. Chem.*, 466 (1999) 203.
183. K. Kanamura, S. Toriyama, S. Shiraishi and Z. Takehara, *J. Electrochem. Soc.* 143 (1996) 2548.
184. D.A. Shifler, P.J. Moran and J. Kruger, *Electrochim. Acta* 42 (1997) 567.
185. K. Kanamura, *J. Power Sources* 81-82 (1999) 123.
186. M. Morita, T. Shibata, N, Yoshimoto and M. Ishikawa, *Electrochim. Acta* 47 (2002) 2787.
187. J.R. Dahn, A.K. Sleigh, H. Shi, B.M. Way, W.J. Weydanz, J.N. Reimers, Q. Zhong and U. von Sacken, in *"Lithium Batteries – New Materials, Developments and Perspectives"*, G. Pistoia, Ed., Elsevier-North Holland, (Amsterdam), 1992.
188. T. Ohzuku, A. Veda, M. Nagayama, Y. Iwakoshi and H. Komori, *Electrochim. Acta* 38 (1993) 1159.
189. M. Gazard, in *"Handbook of Conducting Polymers"*, Vol. 1, T.A. Skotheim, Ed., Marcel Dekker, (New York) Ch. 19, 1988.
190. D. Aurbach and H. Gottlieb, *Electrochim. Acta* 34 (1989) 141.
191. J. Jiang and J.R. Dahn, *Electrochim. Acta* 50 (2005) 4778.

192. J. Jiang, K.W. Eberman, L.J. Krause and J.R. Dahn, *J. Electrochem. Soc.* 152 (2005) A1879.
193. M. N. Richard and J.R. Dahn, *J. Electrochem. Soc.* 146 (1999) 2068.
194. D.D. MacNeil and J.R. Dahn, *J. Electrochem. Soc.* 49 (2002) A912.
195. D. Aurbach, in "*Nonaqueous Batteries*", D. Aurbach Ed., Marcel Dekker, (NY) Ch. 6 1999.
196. J.O. Besenhard and G. Eichinger, *J. Electroanal. Chem.* 60 (1976) 1.
197. M. Umeda, K. Dokko, Y. Fujita, M. Mohamedi, I. Uchida and J. E. Selman, *Electrochim. Acta* 47 (2001) 885.
198. D. Aurbach, J. S. Gnanaraj, M. D. Levi, E. Levi, G. Salitra, J. F. Fischer and A. Claye, *J. Electrochem. Soc.*148 (2001) A525.
199. D. Aurbach and M.D. Levi, *J. Phys. Chem.* B. 101 (1997) 4630.
200. D. Aurbach, M.D. Levi and M. Vorotyntsev, *Cond. Matt. Phys.* 5 (2002) 1.
201. D. Aurbach in "*Advances in Lithium Ion Batteries*", W.V. Schalkwijk and B. Scrosati Eds., Kluwer Academic/Plenum Publishers Inc. Chapter 1 (NY) 2002.
202. D. Aurbach and A. Zaban. *J. Electrochem Society* 141 (1994) 1808.
203. D. Aurbach, E. Zinigrad and A. Zaban, *J. Phys. Chem. 100*, (1996) 3089.
204. D. Aurbach, *J. Power Sources* 146 (2005) 71; E. Markevich, G. Salitra and D. Aurbach, *Electrochem. Comm.* 7 (2005) 1298.
205. D. Aurbach, *J. Electrochem. Soc.* 136 (1989) 906.
206. D.E. Irish, Z. Deng and M. Odziemkowski, *J. Power Sources* 54 (1995) 28.
207. G. Nazri and R.H. Muller, *J. Electrochem. Soc.* 132 (1985) 1385.
208. D. Aurbach and E. Granot. *Electrochim. Acta* 42 (1997) 697.
209. P. Novak, D. Goers, L. Hardwick, M. Holzapfel, W. Scheifele, J. Ufhiel and A. Wursig, *J. Power Sources* 146 (2005) 15.
210. D. Aurbach, B. Markovsky, A. Rodkin, E. Levi, Y.S. Cohen, H-J. Kim and M. Schmidt, *Electrochim. Acta* 47 (2002) 4291.
211. R. Dedryvere, L. Gireaud, S. Grugeon, S. Laruelle, J.M. Tarascon and D. Gonbeau, *J. Phys. Chem. B* 109 (2005) 15868.
212. D. Aurbach, B. Markovsky, K. Gamolsky, E. Levi and Y. Ein-Eli, *Electrochim. Acta* 45 (1999) 67.
213. D. Aurbach, O. Chusid, Y. Gofer, M. Watanabe, T. Momma and T. Osaka, *J. Power Sources* 97 (2001) 632.
214. P. Dan, E. Mengeritsky, Y. Geronov, D. Aurbach and I. Weissman, *J. Power Sources* 54 (1995) 143.
215. D. Aurbach, I. Weissman, A. Zaban, Y. Ein-Eli, E. Mengeritsky and P. Dan, *J. Electrochem. Soc.* 143 (1996) 2110.
216. E. Markevich, G. Salitra, B. Markovsky and D. Aurbach, "High Temperature Performance of Li-ion Battery Systems on Failure Mechanisms and Stabilization". (2006). In preparation.
217. D. Zhang, B.S. Haran, A. Durairajan, R.E. White, Y. Podrazhansky and B.N. Popov, *J. Power Sources* 91 (2000) 122.
218. P. Ramadass, B. Haran, R. White and B.N. Popov, *Journal Power Sources* 112 (2002) 606.
219. J.P. Peres, F. Perton, C. Audry, Ph. Biensan, A. de Guibert, G. Blanc and M. Broussely, *J. Power Sources* 97 (2001) 702.
220. J. Maier *Nature Mater.* 4 (2005) 805.
221. M.K. Aydinol and G. Ceder, *J. Electrochem. Soc.* 144 (1997) 3832.
222. M. K. Aydinol, A. F. Kohan and G. Ceder, *J. Power Sources* 68 (1997) 664.
223. G. Ceder, Y.-M Chiang, D. R Sadoway, M. K Aydinol, Y.-I. Jang and B. Huang, *Nature* (London) 392 (1998) 694.
224. Y. Zhang, Y. Wang, L.G. Scanlon and P.B. Balbuena, *J. Electrochem. Soc.* 152 (2005) A1955.
225. Y. Wang, S. Nakamura, K. Tasaki and P.B. Balbuena, *J. Am. Chem. Soc.* 124 (2002) 440.
226. Y. Wang and P.B. Balbuena, in "*Li Ion Batteries: Solid Electrolyte Interphase*", P.B. Balbuena and Y. Wang Eds., Imperial College Press, (UK) Ch. 5, 2004

227. J. Christensen, V. Srinivasan and J. Newman, *J. Electrochem. Soc.* 153 (2006) A560.
228. J. Christensen and J Newman, *J. Electrochem. Soc.* 151 (2004) A1977.
229. G. Ning, and B.N. Popov, *J. Electrochem. Soc.* 151 (2004) A1584.
230. M. Broussely, P. Biensan, F. Bonhomme, P. Blanchard, S. Herreyre, K. Nechev and R.J. Staniewicz, *J. Power Sources* 146 (2005) 90-96.
231. C. Pouillerie, F. Perton, P. Biensan, J.P. Peres, M. Broussely and C. Delmas, *J. Power Sources* 96 (2001) 293.

This page intentionally left blank

Industrial Applications of Batteries. From Cars to Aerospace and Energy Storage
M. Broussely and G. Pistoia Eds.,
© 2007 Elsevier B.V.

Chapter 4

Traction Batteries. EV and HEV

Michel Broussely

Saft / SBG, RueGeorges Leclanché, BP1039, 86060 Poitiers, France

4.1. Introduction

At the end of the 19th century, electric cars seemed to be destined for a great future. The energy storage onboard was possible thanks to the lead acid battery, invented in 1859 by Gaston Planté, and battery engineers were optimistic about continuing improvements to solve the weaknesses (poor energy and power density, short life...), giving confidence in a better future service.

The first electric vehicle in Europe seems to be attributed in 1881 to the French Gustave Trouvé who equipped a tricycle with an electric motor powered by two batteries. The electric car story started soon after and in 1899, 1575 electric vehicles were sold in the USA[1], compared to 1681 steam cars, and 936 gasoline cars. Amazing performance could be achieved: for example, the Belgian engineer Jenatzy was able to reach the automobile speed record of 100 km/h with his electric car "Jamais Contente" (never satisfied) produced in 1899.

However, in the following years gasoline car development progressed at a much higher rate. While sales of electric vehicles more than doubled in the USA from 1899 to 1909 (about 4000), the sales of gasoline cars increased more than 120 times (about 120000). The same situation also occurred in Europe.

There were several causes for this "defeat", but poor performance of the battery, leading to short range and low power, and higher selling price were the main ones. At the same time, mass production of gasoline cars reduced their cost drastically.

One century later, as both technologies considerably improved, vehicle range and cost of EVs, in which batteries play a major role, are still the main challenges for their widespread success.

Energy storage is indeed the key technology that governs the development of electric vehicles. Until fuel cells can be adopted in this application, regularly predicted and postponed but surely progressing, batteries are the sole electric energy storage technology available today.

Pure EVs are still not widely commercialized, despite the many prototypes produced over the years. However, the introduction a few years ago of commercially available hybrid cars is completely changing the picture. Very large market developments are now anticipated in the short term, for which the battery is a key component.

The purpose of this chapter is to review the main requirements of batteries as energy storage for motive power. From these requirements, the possible solutions existing today, or soon to exist, will be discussed.

There are many types of vehicles using electric power, from very large, such as tramways and hybrid buses, to "small," such as forklift trucks, golf carts, *etc*, all needing batteries at different level. The choice has been made to focus on full electric and hybrid cars, because they are facing challenges today and have a big stake in the future: how to move in a sustainable manner, saving fossil energy, and reducing emissions of CO_2 and other pollutants. In this challenge, batteries play a major role as a critical component in many respects, such as energy and power capability, life, safe use and cost.

In the first part, specific features of the different types of electric vehicles are described, and the main general requirements for the power source are discussed.

In the second part, properties of the different battery technologies that were, are or will be used in these applications are presented. Examples of applications are described, discussing which of the battery systems provides or will provide the best fit to the requirements of each of these vehicles.

4.2. The Different Types of Electric Vehicles

4.2.1. Electric Vehicles (EV)

In this category, the battery is the sole source of energy in the vehicle, powering electric motors through appropriate power management interfaces. They are also called "ZEV" for zero emission vehicle.

Before use, the battery should be recharged from an external power source. To challenge conventional cars, the battery has to store an amount of energy insuring a sufficient driving range, and has to be recharged in a relatively short period.

The latter property can be compared to the refueling of a combustion engine car. Unfortunately, a high-energy battery cannot be recharged within a few minutes because the power capability of the battery is not high enough to accept such a very high charging rate. This might be possible with a battery designed for high power, but the battery energy would then be reduced to an unacceptable level, giving too short a driving range. Indeed, battery design is always a trade-off between energy and power. High power battery design necessitates more inactive materials such as current collectors, separator and electrolyte. To put some numbers to this, a typical battery size for a medium EV car is about 30 kWh. Fully charging this battery in five minutes would therefore need 360 kW. Should the battery accept this high rate charge, providing such a power everywhere (eventually to several vehicles at the same time) would obviously create severe infrastructure problems and costs. This is why typically the battery is recharged overnight at home from the grid, within five to eight hours. Additional partial recharges at medium rate can be made in various public areas during the day when the car is parked, but that necessitates lower power levels, easier to distribute.

As a consequence, the driving range with a full charge becomes the crucial parameter, which is directly dependent on the size of the battery. While the volume of the battery is important for the car design and utilization, as it limits the available useful space, its weight is more critical and is limited by obvious physical considerations. There is a maximum weight for a complete car of a given size that cannot be exceeded otherwise it cannot be safely driven.

In addition, energy is needed to move the battery; therefore, the car range is not proportional to the energy of the battery. Therefore, the weight of the battery itself, which is an important fraction of the total weight, is consuming part of the available energy. This case is illustrated in Figure 4.1, which describes the maximum car range of a vehicle as a function of energy of batteries delivering 28 Wh/kg (the average for a lead acid battery). The 800 kg vehicle (without the battery) is assumed to consume 135 Wh/ton/km. As the energy is increased, the weight of the battery quickly becomes intolerable for the vehicle. Figure 4.2 displays the corresponding weights of several batteries of different specific energy. From this picture, it can be seen that a minimum of about 100 Wh/kg is mandatory to exceed a 200 km range. As it will be

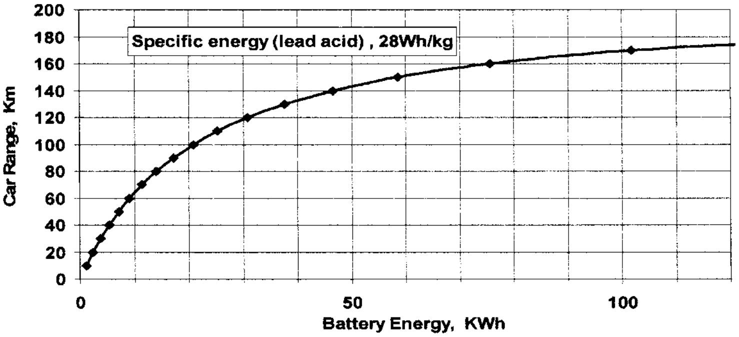

Figure 4. 1. Example of a calculated mid-size EV range as a function of battery energy.

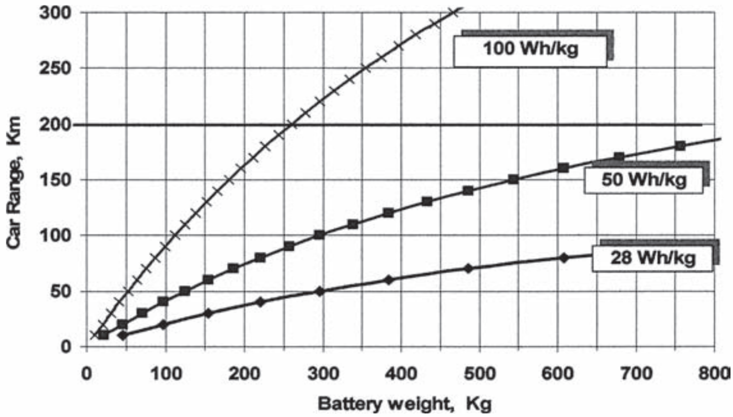

Figure 4.2. Calculated car range as a function of battery weight for several specific energies.

discussed further, only lithium-based batteries can achieve this goal today.

The most important parameters are therefore the maximum amount of energy that can be stored in a minimum volume and weight; *i.e.* the energy density (Wh/L) and the specific energy (Wh/kg) of the battery.

As the energy required is large, the battery cost becomes a very sensitive issue. The battery life has to match the vehicle life, *i.e.* at least 10 years. (The new US Advanced Battery Consortium goal is 15 years). A cycle life of much more than 1000 cycles is therefore expected from the battery. In addition, to be cost effective, the battery will be sized at a minimum, and it will deliver a significant part of its total energy in daily use. In terms of cycling conditions, that means deep Depth of Discharge (DOD) cycling, usually about 80%.

The batteries for EVs need to meet the stringent requirements of the components of vehicles operating on the roads. They must not present safety hazards for the people inside the vehicle or for the vehicle environment, even in abuse conditions. The potential hazards are proportional to the amount of energy stored, and quantity of chemicals inside the battery. These considerations, in addition to the requirement for low cost, show that EV utilization is probably one of the most demanding applications for a battery system.

Lead acid has long been the sole battery system used in EVs, but the limited car range, typically about 60 km, the considerable maintenance requirements and poor cycle life, have severely limited its development. For about 20 years, NiCd has been used in Europe, especially in France, extending the range to about 80 km, and with better life. Although the number is limited (in the thousands), this is the most commonly used battery in electric cars today.

NiMH has been developed for several demonstration programs, improving the energy density and car range (100+km) with no battery maintenance, but has never actually been commercialized, partly due to high manufacturing cost. The new high energy density battery technologies based on lithium, especially Li Ion, have been studied for this application for more than 10 years, leading to demonstration fleets. They are now close to the commercialization phase, bringing the EV to a possible range of 200 km or more.

Table 4.1 and Table 4.2 summarize examples of comparative characteristics of different batteries weighing 250 kg or having a volume of 200 liters, respectively, to power a typical mid-size car[2]. These technologies and application examples will be described further in this chapter.

Table 4.1. Comparison of different technologies of EV batteries for a typical size of 250 kg.

Technology	Pb Acid	NiCd	NiMH	Li Ion
Vehicle curb weight	1200 kg			
Battery weight allocation (typ.)	250 kg			
Battery structure, cooling *etc.*	55 kg			
Module weight allocation	195 kg			
Energy density (module)	33 Wh/kg	45 Wh/kg	70 Wh/kg	120 Wh/kg
Onboard energy	6.4 kWh	8.8 kWh	13.0 kWh	23.4 kWh
Calc. range @120Wh/ton/km	53 km	73 km	114 km	195 km

Table 4.2. Comparison of different technologies of EV batteries for a typical size of 200 liters.

Technology	Pb Acid	NiCd	NiMH	Li Ion
Battery volume allocation (typ.)	200 L			
Battery structure, cooling *etc.*	70 L			
Module volume allocation	130 L			
Volumetric Energy (module)	75 Wh/L	80 Wh/L	160 Wh/L	190 Wh/L
Onboard energy	9.8 kWh	10.4 kWh	20.8 kWh	24.7 kWh
Range @120Wh/ton/km	81 km	87 km	173 km	206 km

Table 4.3. Power characteristics comparison for a 250 kg battery using different chemistries.

Technology	Pb Acid	NiCd	NiMH	Li Ion
Vehicle curb weight	1200 kg			
Battery weight allocation (typ.)	250 kg			
Battery structure, cooling *etc.*	55 kg			
Module weight allocation	195 kg			
Power density (module)	75 W/kg	120 W/kg	170 W/kg	370 W/kg
Battery Power	15 kW	24 kW	33 kW	72 kW

The vehicle's ability to accelerate and climb hills depends on the battery power, if it is not limited by the electric motor power. Here again, Li Ion exhibits superiority over the traditional chemistries, as shown in Table 4.3.

The car range can be increased by a small combustion engine able to recharge the battery during driving or not; this car is called EV with range extender. The low-power combustion engine can be used either on demand by the driver or when the battery charge level is below a certain value.

The battery is the same as for a pure EV of the same size, and has to fulfill the same requirements. This is an elegant means to extend the range of a car to meet exceptional needs. This car can also be considered as a series hybrid vehicle.

4.2.2. Hybrid Electric Vehicles (HEV)

In an HEV, both combustion engine and electric motors are used. The electric energy is used to provide car starting and power peaks, when the conventional Internal Combustion Engine (ICE) would otherwise consume a large amount of fuel. The goal is to have a vehicle with the same range capability as the ICE cars, with lower fuel consumption and possibly ZEV mode. The first consequence for the battery is that the size is much smaller than in the EV, but the power has to be about the same. Therefore, the most important property is the power density.

Many ways have been and are considered by the car manufacturers to achieve this aim. The usual way to describe hybrid car technology is to discriminate between "series" and "parallel" hybrids. In the "series" hybrid, energy provided by the combustion engine is converted to electricity, which is used to propel the vehicle or is stored in the battery.

The EV with range extender is typically a "series" hybrid configuration. In the "parallel" hybrid, the combustion engine is the primary means of driving the car forward. Electric motor(s) is (are) added to provide power during phases when the combustion engine has a poor efficiency. The battery is maintained at a constant state of charge using energy from the combustion engine and kinetic energy during deceleration and braking. A usual way to summarize the different configurations is presented in Figure 4.3.

In fact, there is a continuum of variations that can exist in these configurations, depending on the goal pursued:

- to reduce fuel consumption and CO_2 emissions as much as possible while maintaining the driving performance and comfort of a conventional car (power, acceleration, *etc.*);
- to improve driving performance and comfort *vs.* conventional cars, with some fuel consumption reduction;

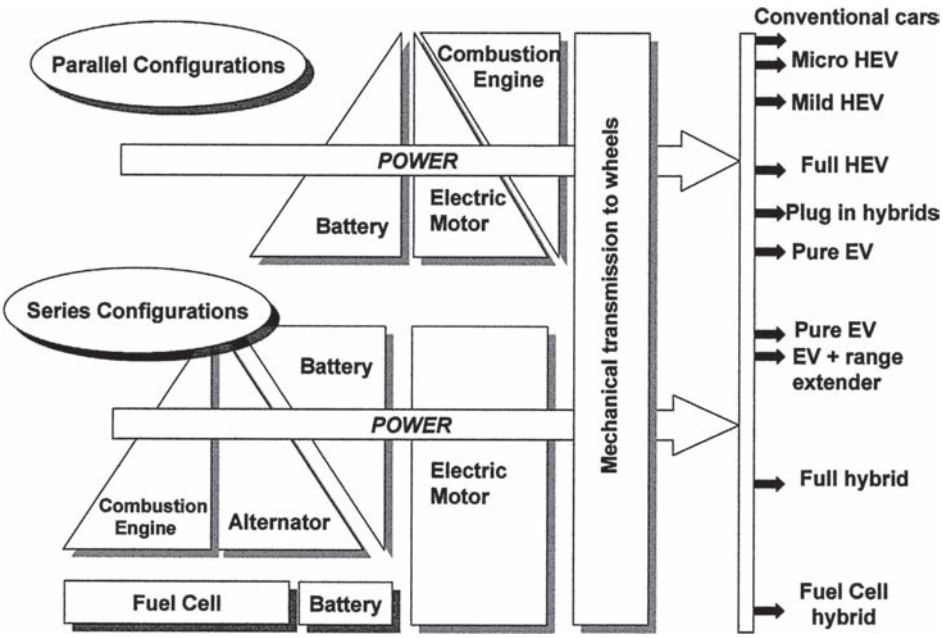

Figure 4.3. Summarized description of electric vehicle architecture.

- to maximize the car performance with the same level of fuel consumption.

Depending on these goals, a large variety of hybrid cars can be designed. The different categories are divided into several main "families". They are described below, and their requirements for battery systems are summarized in Table 4.4 and illustrated in Figure 4.4, which include EVs. It should be emphasized that these approximate values are given for comparative purposes. They may vary significantly in each category depending on vehicle size, from small cars to vans or SUVs.

Table 4.4. The different types of EVs/HEVs and approximate energy/power requirements.

EV type	Power range kW	Energy range kWh	Voltage range, Volts
Micro hybrids	2.5-5	0.5	12 - 36
Mild HEV	15-20	1	120 - 160
Full HEV	30-50	2-3	200-350
FCHEV	25-30	1-2	220
Plug-in HEV	30 to 100 (Van)	5 - 15	200-350
EV	35 to 70 (Van)	25 - 40	200-350

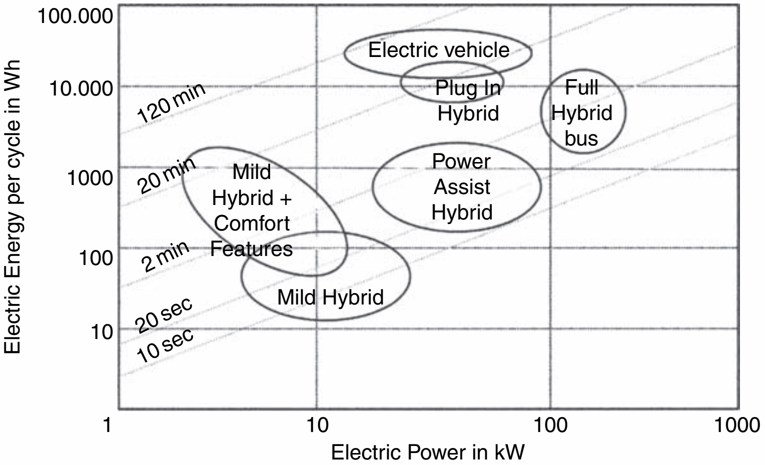

Figure 4.4. Description of the power/energy characteristics required from the battery by different types of electric vehicles.

These quite different needs in electrical power and energy between the different solutions have of course a strong influence on the choice of a battery, and its size. Each of the main battery systems (Pb Acid, NiMH, Li Ion) may find an outlet, as will be described further. Lead acid in micro-hybrids, and NiMH in mild and full hybrids are presently considered to be the options working satisfactorily in commercial cars. Li Ion is considered as the best future solution for hybrids, when fully optimized. These technologies and application examples are described in the last section of this chapter.

4.2.2.1. Micro Hybrids "Stop and Start"

The specific feature of these types of cars is that they can use the existing ICE cars platforms. This is a "non intrusive" technology, as it only adds elements to existing architecture of combustion engine cars. Generally, a simple electric machine Starter-Alternator Reversible System is put in the power chain via a belt, powered by a suitable battery and electronic inverter.

In these cars, the combustion engine is stopped as soon as the car stops. The starter-alternator is only used to start the engine; there is no regenerative energy recovered from braking. Power required is in the order of 2.5 kW, with energy of few hundred Wh. Therefore, 12 V SLI lead acid batteries of the largest size can supply the required power. The same battery provides the energy for on board equipment and starting. AGM technology (see battery

Table 4.5. Typical idling stop rate description in city drive (Kyoto). (*From Ref. 3*)

Driving course		Kyoto city
Driving time/day	min	140
Driving distance/day	km	30
Average discharge current	A	22
Number of stops	times	38
Accumulated stops duration	min	35.2
Total idling stop rate	%	25.1

description in the next section) is the most appropriate and offers the best cost/performance ratio. The battery is usually maintained at full SOC, but much more frequently discharged than the conventional SLI. Battery aging is the challenge, the projected lifetime being generally about one to two years less than SLI batteries in conventional cars. Because of the relatively low cost of this battery, the replacement cost may be compensated by increased fuel economy. This fuel consumption reduction is obviously very dependent on the driving mode. In true urban configuration, with many stops, fuel saving can be more than 15%.

Table 4.5 describes a typical utilization in urban conditions[3], recorded in Kyoto.

4.2.2.2. Soft Hybrids "Stop and Go"

Similar to stop and start, this technique can be applied to existing ICE cars. In this case, the main difference is that some energy is saved by regenerative electric power produced on braking, (50 to 60% braking energy is converted to electricity) and more electric energy is used on starting, because the car starts in an electric mode, while the ICE is being started. Compared to "stop and start", the gain in fuel consumption can be almost doubled in the same driving conditions (from 5 to 25%). It is expected that such vehicle will be rapidly expanding, and several developments are on the way, with the aim of series production by about 2008.

There is a strong impact on the energy storage system that must be able to sustain high charge peak power, and provide more power and energy during the starting phase. The average power required during car start, and average regeneration power is about 6 KW. The lead acid battery provides the energy required during start, and all on board electric energy needs. Because the battery provides more energy, the SOC will vary more than in the "stop and start", and typical depth of cycling range is 20% DOD, between 100 and 80% SOC, for a battery of similar size to the "Stop and start" hybrid. The conventional lead acid battery design with flat plates is not well suited for this working mode, and lifetime would be reduced. The solution would be to increase the battery size, but volume and weight is then a burden. A better technical solution is the advanced high power lead acid technology of spirally wound design. The other solution considered today is an association of conventional SLI lead acid battery and supercapacitors. The role of the capacitors is to accommodate and store the high peak of regenerative power and help on starting, while the battery provides energy. Advanced lead acid solutions are better fitting when high energy level is required in upper class cars, causing deeper DOD cycling.

High power Li Ion batteries can fulfill both power and energy requirements and can be considered as a future optimized solution as soon as the cost become compatible.

4.2.2.3. Mild Hybrids

With "Mild Hybrids", the technology becomes more "intrusive" in the conventional car design than the previous hybrids. The drive train must be completely redesigned, and manufacturing this type of car supposes a much deeper change in design and technology than the previous configurations. An electric motor is inserted in the drive axle, and the electric driving mode grows a step further. After starting, the car can stay in EV mode up to a speed of about 10 to 20 km/h before the ICE starts. On driving, a mild power "boost" is provided during accelerations, which allows some ICE downsizing. Therefore, more power is required from the battery, which is more frequently and deeply discharged.

4.2.2.4. Full Hybrids or "Power Assist"

This is a typical parallel configuration. Both the combustion engine and electric motor contribute to powering the car, with electric power being used for starting and acceleration. A limited range of a few kilometers in pure EV-mode may be possible. From the battery side, the energy required is still small; therefore, the power density has to be higher. The battery is permanently either on discharge or charge, and the state of charge has to be maintained at an intermediate level in such a way that it can deliver peak power to the drive train, and accept power from the engine or regenerative braking. The main requirement of the battery is therefore its ability to sustain a very large number of high drain and shallow cycles, and store this energy efficiently. NiMH batteries are presently used in soft and full hybrids, and are already commercialized.

4.2.2.5. Plug-in Hybrids (PHEV)

Unlike other hybrid cars, the battery of a plug-in hybrid can be recharged from outside, connected to the electricity network.

This is a sort of intermediate between EV with range extender and full HEV. The car can run in pure electric mode (ZEV), as long as the state of charge of the battery is sufficient, and the speed of the car below a certain limit. The potential range in electric mode is smaller than the pure EV car (30 to 50 km). If higher speed is required, the combustion engine starts to operate. During this phase, the state of charge of the battery is depleting, from the starting point supposed to be at full charge. When the battery has reached a minimum state of charge (for example 30%), the car runs in full hybrid mode, and the state of charge of the battery is maintained.

The battery size is about 1/3 to 1/2 that of a pure EV. The battery is recharged (plug-in) from an external source of electricity when the car is not used. Both energy density and power density are important. The required cycle life is more demanding, as strong cycling capability at deep DOD is needed. A cycle life requirement comparison is described in Table 4.6[4], for an expected 10-year life. PHEV is assumed to be driven 4000 miles/year in EV mode, and 9500 miles/year in HEV mode.

Before the longer-term commercialization of fuel cell powered vehicles, this type of car seems to be destined to a good future, with the expected permanent increases in the price of oil. It is the best compromise between using as much electrical energy as possible from the grid, reducing pollution in urban areas, and still offering long-range utilization with fuel.

4.2.2.6. Fuel Cell Hybrid EV

Fuel cell vehicles can also be considered as HEVs. The hybridization

Table 4.6. Cycle life requirements for EDV batteries, over a 10-year life. (*From Ref. 4*)

EDV type	Deep cycles		Shallow cycles	
	Cycles @80%DoD	Cumulative energy (MWh)	Cycles @50Wh	Cumulative Energy (MWh)
Full HEV	n.a	n.a	200k	10
PHEV- 20	2400	12	120k	6
EV	1000	32	n.a	n.a

does not come from two different types of energy (thermal and electric), but from primary (refuelable) and secondary (rechargeable) electrochemical power sources. A rechargeable battery is required to provide the energy and power for vehicle starting and for the fuel cell auxiliary equipment (also called BOP, Balance of Plant), and to provide the peak power necessary during acceleration. Energy is provided by the fuel cell at a more constant power level, closer to the average. That permits downsizing of the fuel cell stack, which is a very important contributor in fuel cell cost. The battery operates in similar conditions to present full hybrid cars. Because of the longer time expected before production of this type of car, Li Ion chemistry is the most studied for this application.

4.2.2.7. Large Hybrid Vehicles: Transit Buses, Light Trucks and Tramways

Public urban transportation and urban delivery light trucks are a very interesting field for application of hybrid propulsion, aiming for both improvement of fuel economy and better environmental conditions. The typical driving pattern includes very frequent stops (for example an average of every 300 m in European cities), leading to needs for electric launch of the vehicle and regenerative storage of braking energy. Hybrid electric bus technologies have been demonstrated in several cities in Europe in recent years.

In hybrid tramways or trolley buses power is all electric, the "cordless" battery operation allows catenaries to be avoided in some parts of the lines, for example historical centers of cities, and allows more flexibility and simplification of infrastructure.

Many battery systems have been experimented, using Pb Acid, NiCd or NiMH. Practical experience shows that NiMH, in spite of its higher cost, is the most suitable system in terms of endurance and reliability. The performance requirements are basically the same as for all hybrids, with higher energy and power. Typical needs are summarized in Table 4.7[5].

4.3. Battery Technologies for Traction

The aim of this section is not to present in detail the electrochemistry of the different technologies, described in the first two chapters of this book, but to summarize the general characteristics and describe the specific features of the main battery types suitable for traction, either already manufactured and commercialized, or being developed as prototypes. Examples of vehicles in which they are or have been used are also described.

Table 4.7. Typical needs of large hybrid public transportation vehicles. (*From Ref. 5*)

	Hybrid bus (ICE or FC)	Hybrid dual mode bus	Hybrid trolley bus	Hybrid tramway
km/cycle in autonomous electric mode	Power assist / no autonomous operation	5 to 20	1 to 5	0.4 to 1
Cycles/hour	20 to 100	1 or 2	1 to 3	1 to 3
Cycles/year	100,000 to 500,000	5,000 to 10,000	5,000 to 15,000	5,000 to 15,000
kWh/cycle	< 0.5	1 to 5	1 to 7	2 to 10
kW	50 to 100	50 to 100	50 to 100	50 to 150
Allowable DOD from battery	1 to 5%	5 to 20%	5 to 20%	5 to 20%

4.3.1. Lead Acid

Since their invention by Gaston Planté in 1859 and basic development in the 19th century, lead acid batteries have become increasingly specialised. The main application areas are: SLI (Starting-Lighting-Ignition) for automobiles; motive power for forklift trucks, golf carts and other vehicles; and standby power for a variety of stationary applications. The low initial cost of lead acid batteries is unmatched by other technologies, and consequently lead acid is the most widely manufactured and used of all industrial batteries worldwide.

Lead acid cells are typically characterized by their positive plate construction, the lead alloy used in their plates, or whether they are of vented (flooded) or valve-regulated (sealed) design.

The vented design, in which electrolyte is abundant, allows the emission of gas at the end of charge when water is electrolyzed. Regular water topping-up is therefore required, the frequency depending on the cycling conditions, temperature, *etc.*

The Valve Regulated Lead Acid (VRLA) design allows water recombination at the end of charge. Oxygen is released at the positive electrode, moves to the negative through the electrolyte, and is recombined on the negative electrode. As the consequence, maintenance for water addition is no longer required. To facilitate the recombination, the electrolyte is immobilized and specific electrodes and separator design had to be developed.

VRLA designs are therefore further subdivided by the method used to immobilize the acid electrolyte. These are called absorbed glass mat (AGM) or gel types.

In the AGM design, the electrolyte is absorbed in a glass mat separator. To promote recombination, the electrolyte amount must also be reduced. The mat is a non-woven mixture of glass fibers to absorb electrolyte and facilitate the oxygen gas transfer, and organic fibers to insure sufficient mechanical strength.

Cells with pasted or flat positive plates are frequently used in traction applications, particularly in North America, where they are prevalent. Although pasted-plate SLI designs are used in many low-end traction applications for reasons of cost and/or energy density, they do not perform well in deep-cycling operation. This is because they have very thin plates that are close-packed to optimise starting performance. Thin plates do not retain their active material very well during cycling as the active material expands and contracts during discharge and charge, respectively. Furthermore, the close-packed plates do not allow free circulation of electrolyte, so the acid tends to stratify (forming layers of varying concentration).

Pasted-plate cells that are designed for traction applications typically have thicker plates with high paste density. Positives are wrapped with one or more layers of glass fiber, which helps to retain the active material. Plate spacing is larger than in SLI designs, to promote electrolyte mixing.

There are also intermediate designs that are essentially SLI batteries, modified for enhanced cycling performance. These include so-called 'deep-cycle marine' and golf cart battery designs.

Traction batteries in Europe are more typically based on tubular positive plates. (A few designs in North America also have tubular positives). While these plates generally cost more than pasted types, cells with tubular plates exhibit minimized corrosion rates and better active material retention.

Positive grid alloys play a major role in cycling performance. Until the middle of the 20th century, cells with pasted or tubular plates used antimonial alloys containing between 4% and 11% antimony, regardless of their intended application. While such alloys allow good cycling performance, there is also a penalty to be paid in terms of steadily increasing maintenance requirements throughout life. This is due to antimony being oxidised from the positive plate during charging and plated onto the negative, where local action causes the negative to self discharge at an increasing rate. Under IU charging conditions, this self discharge causes the current to increase, resulting in greater water loss from electrolysis. This so-called 'antimonial poisoning' led researchers to explore alternative alloys that would result in reduced maintenance needs.

A significant move away from antimonial alloys was started in 1935 with the first research paper on lead-calcium alloys[6]. It was not until around 1950, however, that the position of lead-calcium was firmly established in the USA when the Bell System announced plans to use this technology in its large central office batteries. Cells with lead-calcium alloys exhibited very low and stable float currents and minimal water consumption; unfortunately, they also had very poor deep-cycle performance, providing no more than 50-100 deep discharges. In later developments, it was found that the addition of 0.25 to 2.0% tin to calcium alloys would improve their cycling capability, but even so, calcium-based alloys are not used extensively in traction applications.

Research efforts in Europe concentrated on retaining the beneficial aspects of antimonial alloys while eliminating antimonial poisoning. In the late 1970s it was found that so-called lead-selenium alloys gave favourable results. These alloys had much lower levels of antimony, typically less than 2%, but with a small amount of selenium producing a fine grain structure. A report by Varta in 1980 documented cycling tests in which cells without antimony failed after about 200 cycles, while those with 6% antimony gave 1400 cycles. This higher cycling level was nearly matched by cells using an alloy with 1.6% antimony, stabilised with 0.02% selenium, giving just over 1000 cycles[7].

Another type of low-antimony alloy is used by the GNB division of Exide Technologies in its "Absolyte" VRLA AGM cells. This alloy contains 1.5% antimony and 1.5% cadmium and is used in the positive plates only (the negative alloy is a lead-calcium type). This design is one of the few AGM-type VRLA batteries that is commonly used for deep-cycling applications.

With the exception of this battery, virtually all VRLA batteries use lead-calcium-tin or lead-tin alloys. AGM-type batteries generally cycle better than their vented counterparts do because their plate groups are maintained under compression, and the glass mat separator acts as an effective retainer for the active material. The overall cycling capability of these cells still falls well short of that of vented cells with antimonial alloys, however. Gel-type VRLA batteries may perform somewhat better in this regard if phosphoric acid is added to their electrolyte. Phosphoric acid helps to reduce the formation of poorly conducting sulphate layers that can occur in cells with lead-calcium alloys. The use of phosphoric acid in gel-type cells was originally patented by Sonnenschein[8].

One area in which VRLA batteries can out-perform their vented cousins is in partial-state-of-charge (PSOC) cycling. The negative electrode of lead acid cells generally recharges with greater efficiency than the positive, particularly at high states of charge (SOC). In a vented cell the positive starts to release oxygen gas (in an amount represented by the charging inefficiency) while the negative continues to charge with high efficiency. If charging is discontinued before the positive is completely charged, there will be an imbalance between the electrodes that will worsen on successive cycles. This gives rise to a need for relatively frequent high-rate charges to restore balance to the cells. In VRLA batteries, on the other hand, the oxygen released from the positive will pass through to the negative plate and discharge it, thus counteracting the ongoing charging of that electrode and preventing an imbalance between the plates. In

PSOC operation, then, VRLA batteries need far fewer equalize charges than do vented batteries.

There are, however, limits to this PSOC operation of VRLA batteries, and these limits become dominant in HEV applications. The high rates of charge and discharge inherent in HEV operation, and corresponding voltage drops across the width and height of the plates, result in uneven utilization of the active material. The underutilized material exhibits growth of large, hard sulphate crystals, principally on the negative electrode, ultimately leading to cell failure. The difficulty of today's lead acid batteries to support PSOC operation is one of the primary factors limiting the widespread introduction of 42-volt 'mild' hybrids. The International Lead-Zinc Research Organization (ILZRO) and the Advanced Lead Acid Battery Consortium (ALABC), along with the US Department of Energy, have been funding research aimed at solving this problem and have published some proposals[9]. The ease of manufacture of the proposed batteries remains in question, however.

4.3.1.1. Lead Acid Batteries for Micro Hybrids

The "micro-hybrid" cars are the best opportunity today for lead acid to be introduced in the new electric vehicles, beside such applications as forklift trucks, golf carts and other specific vehicles where they have long been used. Improved products adapted to this application that should strongly expand in a near future are being developed by all the main lead acid battery manufacturers, such as Exide[11], JCI, and GS Yuasa[12].

Figure 4.5 describes an automotive AGM VRLA battery that can be used in the "Stop and Start" application, such as the recently launched Citroën C3 car from PSA in France in 2005[10]. It uses a battery of 55 Ah with improved cranking power. The decrease of fuel consumption is about 10% in urban mode

Table 4.8. Typical cycle life test for Stop and Start application[11].

Sequences	
1	Charge during 20 h at 14.4 V + 4 h at $I_{20} \cdot 0.5$ (100%SOC)
2	10,000 cycles @40°C, 1.3% DOD Charge: 3 min at 14 V (max current 50 A) Discharge 1 min@ $I_{20} \cdot 16$
3	Recharge during 20 h at 14.4 V + 4 h at $I_{20} \cdot 0.5$
4	Capacity test: Discharge at C/20 @25°C to 10.5 V (>10 h)
5	Recharge during 20 h at 14.4 V + 4 h at $I_{20} \cdot 0.5$
6	Cold cranking test: High rate 10 sec pulse @ -18°C to 7.2V
7	Back to 1

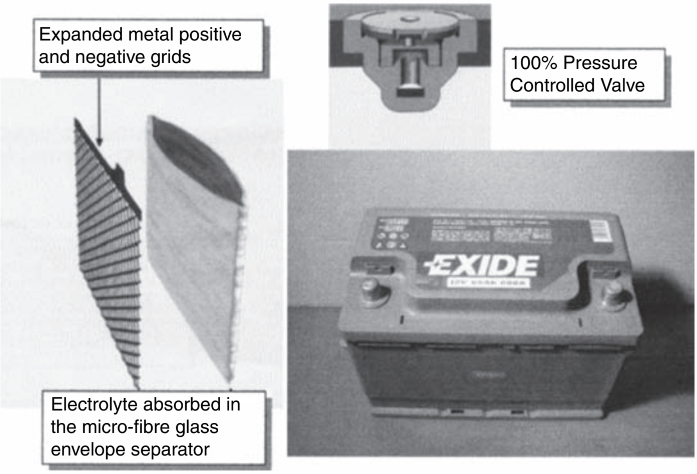
Expanded metal positive and negative grids
100% Pressure Controlled Valve
EXIDE
Electrolyte absorbed in the micro-fibre glass envelope separator

Figure 4.5. Example of VRLA AGM battery for automotive application. (*Courtesy of Exide Technologies*)

(5.7 l/100km), equivalent to 14 g of CO_2/km.

Table 4.8 describes a typical cycle life test sequence for the "Stop and Start" application. Cycling is made at 100% SOC, 1.3% DOD, at 40°C. Figure 4.6 describes an example of capacity evolution[11] during this cycling test with AGM VRLA batteries compared to a flooded standard design. Figure 4.7 describes the cold cranking power during the same test.

This utilization is very demanding compared to SLI, and shows new failure modes of cell aging: positive grid corrosion, increased by the high

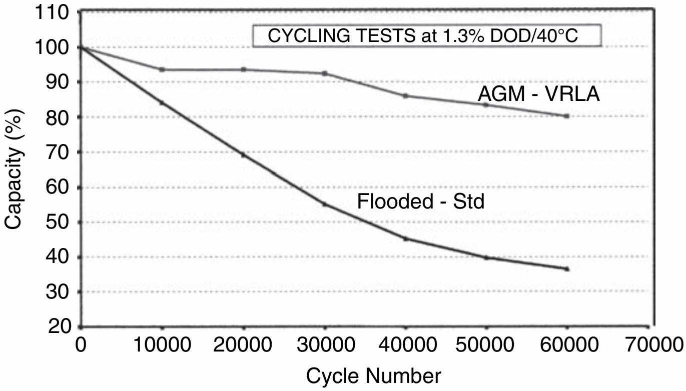

Figure 4.6. Capacity evolution of AGM VRLA cell during Start and Stop cycling test, compared to conventional flooded lead acid. (*From Ref. 11*)

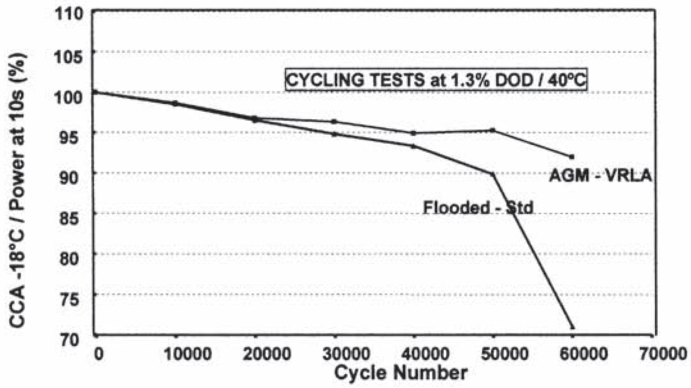

Figure 4.7. Evolution of cold cranking power at -18°C of AGM VRLA cell during Start and Stop cycling test, compared to conventional flooded lead acid. (*From Ref. 11*)

temperature of the engine compartment, and negative plate sulfation at the bottom, which leads to about 3 to 5 years life expectation. Strong efforts of R&D are devoted to improve this behavior, to fulfill the requirements of longer life required by the customers[12].

When more power and better cycle life are required, a spiral wound cell configuration with thin electrodes is more appropriate. Such a design, which has been developed by most of the lead acid battery manufacturers[13], provides better cycling at deep DOD, higher cranking power and charge acceptance.

This type is more suited for the "stop and go" or soft hybrid application, requiring acceptance of regenerative power on braking. Some characteristics of this type of battery are detailed in Table 4.9 and pictures of examples are displayed in Figure 4.8. Higher voltage batteries (36 V) can also be designed. Typical power density of these batteries (cranking and regenerative power) is up to 500 W/kg on discharge and 200 W/kg on charge.

A challenging operating condition is overcharging during regenerative braking, creating drying out of the battery. Improvement can be obtained by increasing valve pressure or saturation of the separator[14]. For better charge acceptance, association of advanced lead acid batteries with double layer capacitors or advanced supercapacitors is a solution being considered to improve the system life. The cost of this energy storage system is however much higher and is challenged by emerging new technologies such as Li Ion, for which the performance for both peak power and long-term cycling ability are suitable, providing a lighter and smaller system. As production volume increases, it is anticipated that it may become a cost effective solution.

Table 4.9. Example of spirally wound lead acid cells OPTIMA ™ characteristics. (*From Ref.14*)

MODEL NUMBER	D34/78	D75/25	D51 & D51R
PERFORMANCE			
Voltage	12 V	12 V	12 V
Cold Cranking Amps @ -18°C	750	650	500
Cranking Amps @ 0°C	870	810	625
Capacity (C/20 Rate) (Ah)	55	48	41
Internal Resistance (ohms)	.0028	.0030	.0046
PHYSICAL SPECS			
Length (cm)	25.4	23.6	23.6
Width (cm)	17.5	17.3	12.8
Height (cm)	19.8	19.4	22.7
Mimimum Weight (kg)	19.7	17.2	11.8

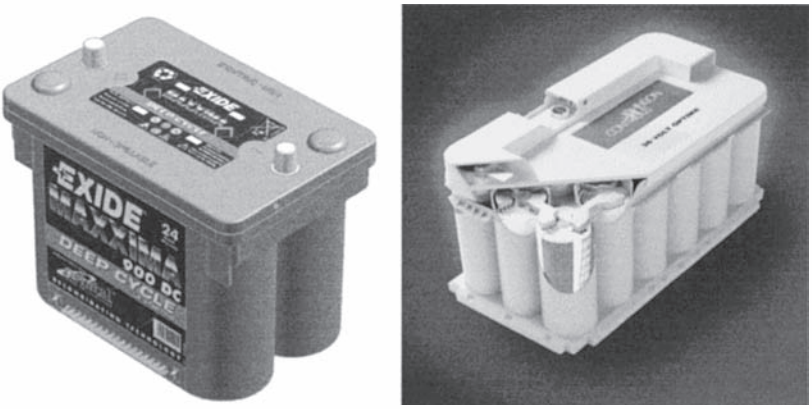

Figure 4.8. Examples of advanced spiral lead acid batteries (12 or 36 V). (*Courtesy of Exide and Johnson Controls*)

4.3.2. Nickel Cadmium

The nickel cadmium battery was invented in 1899 by Jüngner in Sweden. This was the first system to seriously challenge the lead acid batteries. They provide higher specific energy (up to about 55 Wh/kg), or higher specific power in high power designs (up to about 800 W/kg), but their main breakthrough compared to lead acid is a much longer deep cycling life and more "robust" behavior, more tolerant to abusive conditions, electrical or temperature extremes. Specifically, they do not suffer from corrosion failure mechanisms, drastically improving the reliability and life.

As in lead acid technology, two main families exist in the NiCd batteries: vented and sealed. The main difference is the ability of the sealed system to "recombine" totally the reaction products and reform water that is electrolyzed at the end of charge. In the vented technology, this recombination is not 100% efficient, and the gas produced is expelled through appropriate vents. The consequence is water consumption during cycling, necessitating some battery maintenance. The small NiCd batteries used in portable applications are sealed, while large batteries in industrial applications are vented. The main uses of these large batteries are for standby back up power sources, railways and aviation.

While the small portable nickel cadmium cells are of cylindrical shape with spirally wound electrodes, the large cells for industrial application are prismatic, using flat plate electrodes.

The electrode technologies have been varying over the years, from the original tubular plates to sintered nickel porous plates, plastic bonded, or nickel foam or fiber structures. Interestingly, all these technologies still coexist (except the tubular replaced by prismatic shape pocket plates) in very different sizes and applications.

4.3.2.1. Nickel Cadmium for EVs

Technology

The use of NiCd in pure EVs has been developed by Saft in the 1980s and 1990s, replacing lead acid, especially for cars manufactured in Europe. The specifically designed battery for this application is a vented "low maintenance" technology, with reduced water consumption.

The 6 V battery module described in Figure 4.9 consists of 5 cells in series assembled in a single polypropylene "monobloc" casing. The cells are series connected by a specific connection through each cell wall, without outside intermediate terminals. Temperature control of the battery is provided via liquid circulating in the cooling chambers on each side of the large surfaces of the battery casing. The same size exists with an air-cooled casing.

The positive electrode is manufactured by chemical impregnation of nickel hydroxide and additives into a sintered nickel structure, placed onto a perforated nickel-plated steel strip. The "plastic bonded" negative electrode is obtained by pasting cadmium oxide and a polymer binder additive onto a perforated nickel-plated steel strip. The separator is a multilayer non-woven polypropylene, selected to ensure the main properties: good ionic conductivity

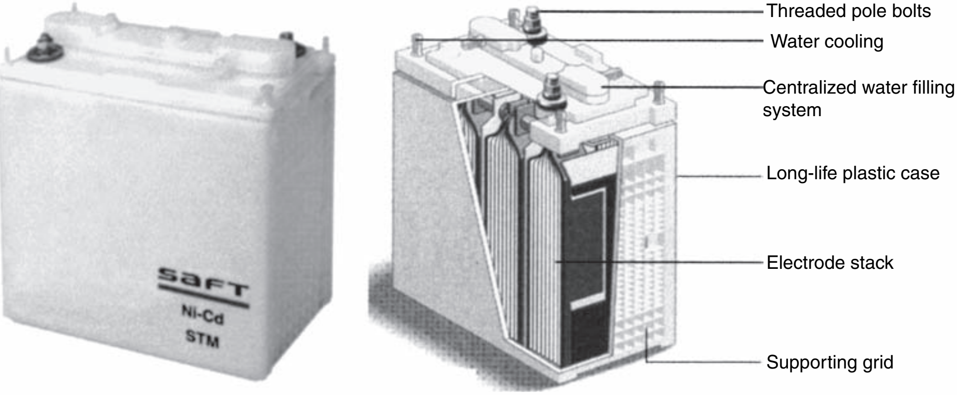

Figure 4.9. Nickel Cadmium 6 V, 100 Ah "monobloc" module for EV battery system, manufactured by Saft.

of the electrolyte while maintaining strong mechanical and electronic insulation between electrodes, and good oxygen diffusion towards the negative electrode during charge to facilitate recombination.

The electrolyte is a solution of potassium hydroxide, with lithium or sodium hydroxide additive. Its density remains mostly unchanged with the state of charge. It varies slightly as water is consumed during cycling.

Performances

Its typical mechanical and electrical characteristics are described in Table 4.10, and discharge curves at several rates are shown in Figure 4.10.

One of the advantages of these NiCd batteries is the excellent cycle life, as shown in Figure 4.11 that describes the capacity evolution during cycling with a C/2 charge and C discharge rate. The specific power as a function of state of charge is described in Figure 4.12.

Table 4.10. Typical characteristics of a 100 Ah 6 V nickel cadmium module for EV battery (Saft).

Module	STM 5-100 MR
Capacity, Ah	100
Voltage, V	6
Weight, kg	12.9
Dimensions (mm)	248 *120 *260
Volume, dm^3	7.74
Typical specific energy Wh/kg, (C/3)	55
Typical energy density, Wh/L, (C/3)	88
Typical specific power (at 80%DOD), W/kg	122

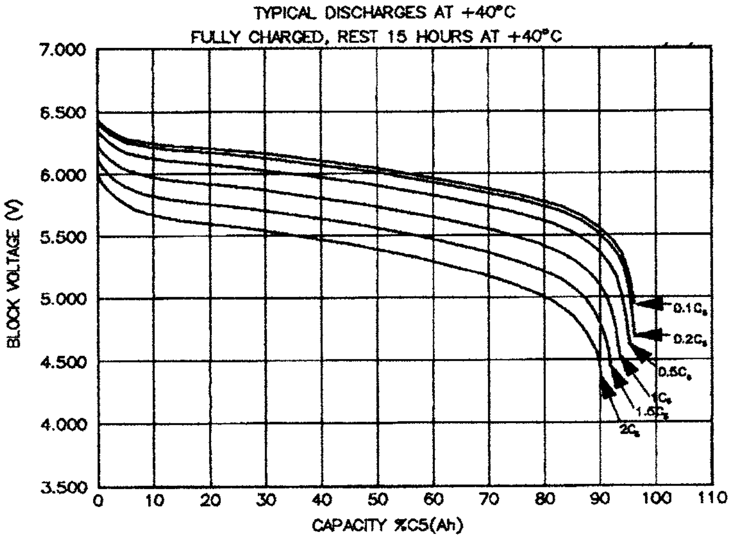

Figure 4.10. Discharge curves of 100 Ah monobloc NiCd Saft battery at several rates (40°C).

A weak point of the NiCd system is its relatively high self discharge rate, which greatly depends on cell design. The charge retention of the 100 Ah battery during storage at ambient and 40°C is shown in Figure 4.13.

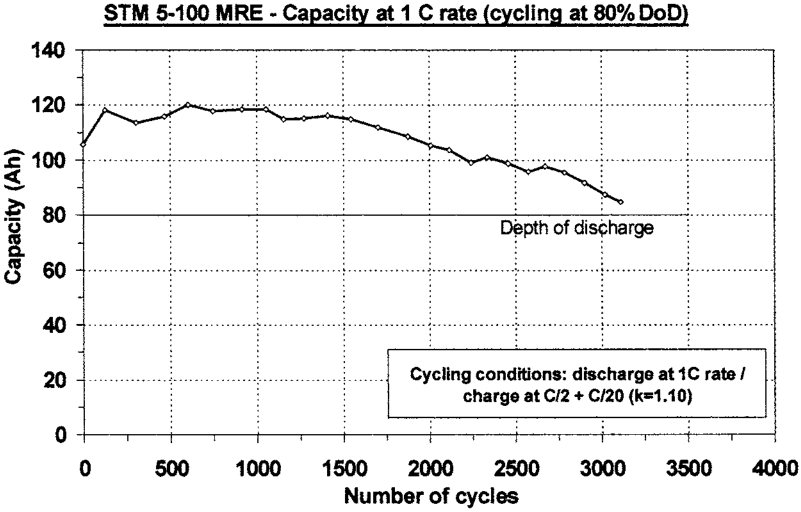

Figure 4.11. Capacity evolution during cycling of a 100 Ah 6 V NiCd module (Saft).

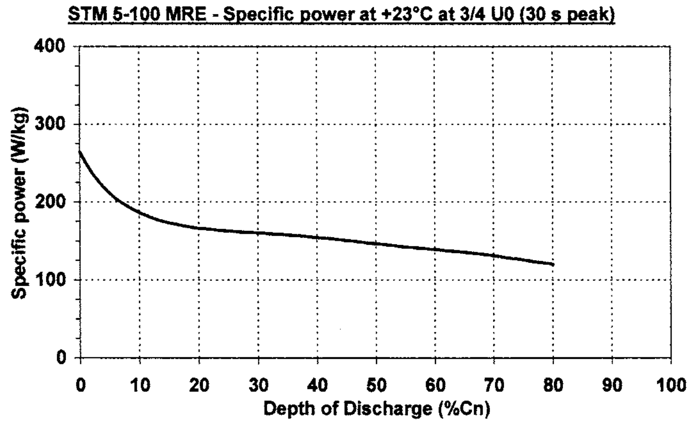

Figure 4.12. Specific power of a 100 Ah 6 V NiCd module (Saft) as a function of state of charge.

Recycling

As all other car components, batteries must be recycled. This is particularly the case for those containing metals like lead and cadmium. In most parts of the word, specifically in Europe, battery collection after use is to become mandatory, but large nickel cadmium batteries have already been collected for many years. At the end of their life, the batteries are transported to a national collection point, then sent to recycling companies for recycling and component reclamation. The recycled cadmium is reused to manufacture new electrodes. More than 99% of cadmium is recycled. The other metals used,

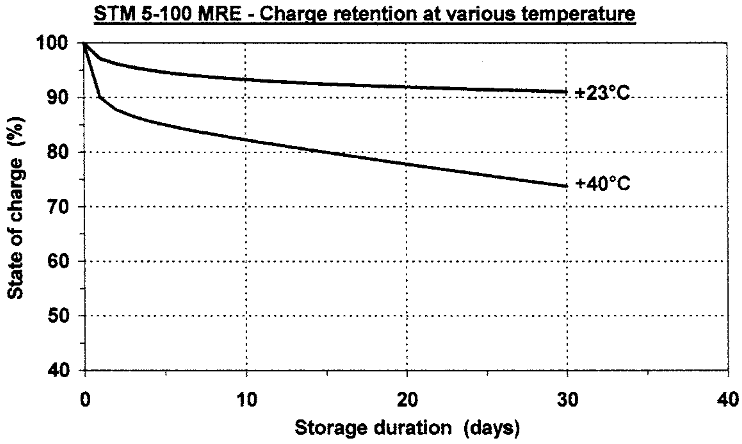

Figure 4.13. Charge retention of a 100 Ah 6V NiCd module (Saft) during storage.

particularly nickel and iron, are also recovered and reused to produce stainless steel. (See also Chapter 14 on this subject).

According to trade agreements between recycling companies and accumulator manufacturers, all the recovered cadmium is re-used solely for the manufacture of new nickel cadmium accumulators. In the same way as for battery manufacture, emissions into the atmosphere and water from recycling plants are continuously monitored, and monthly reports on these are sent to the local authorities. These emissions all comply with current legislation and are audited yearly by an independent laboratory.

Battery assembly

Modules are connected in series to build a high-voltage battery system for EV. An example of such a battery assembly is described in Figure 4.14. Made of two separate boxes (14 and 8 modules) placed under the chassis, the total voltage of the system is 132 V, and its weight 312 kg. A water filling system connects the "monoblocs" in series, through which topping-up is performed when necessary. The design avoids any risk of electrolyte contact with the next cell that would create leakage currents.

Like all electrochemical systems, NiCd batteries generate heat during operation (charge and discharge).Therefore, as a general rule, the temperature must be monitored, and heat dissipated. In the case of a liquid cooling system, generally requested by most of the car manufacturers, the cooling chambers of monoblocs are series/parallel connected. When a forced air cooling system is preferred, 10 to 20 mm of space between rows is allowed on the large side of the modules to insure airflow produced by fans.

In the particular case of charge, as in VRLA, extra heat is produced due to water recombination. The cooling system must be optimized for the type of car, battery size and type, *etc.*

On board experience

Tens of thousands of these batteries have been manufactured during the last 10 years for the major French car manufacturers for commercialized electric vehicles. Typical car range is about 80 km in urban drive. An example of such a car and its battery is described in Figure 4.15 and Table 4.11.

Unfortunately, the market did not expand and most of these cars are no longer produced. Batteries are still manufactured for replacement market, and some other small specific cars. The reasons are a relatively low maximum car range that makes the car little attractive for general use, and a dissuasive selling price. Increasing cost of gas, and strongest environmental regulations on pollution in city centers may change the situation in the future. Availability of higher energy density batteries (see in further sections) can extend the range about more than two times.

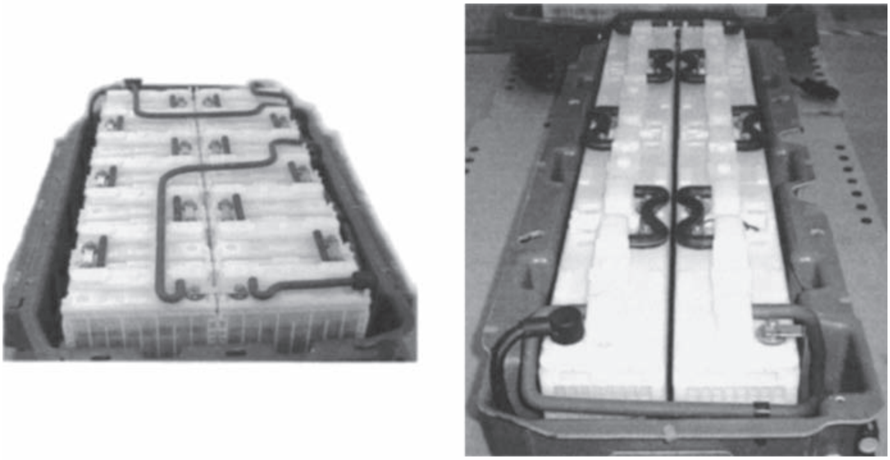

Figure 4.14. Picture of a complete battery system made of 132 V 100 Ah NiCd modules; air cooling (for Renault Kangoo).

Mass:
Mass on the road: 1087 kg
Charge: 315 kg
Performances:
Maximum speed: 91 km/h
Acceleration to 50 km/h: 8.3 s
Range in city driving: 80 km
Energy usage: 0.2 kWh/km
Recharge time: 6 hours max,
or +20 km in almost 1 h

Figure 4.15. General characteristics description of 106 Peugot EV.

Table 4.11. Battery and electric motor characteristics of Peugeot 106 EV.

Battery type / brand	Nickel Cadmium / Saft
Nominal voltage	120 V
Capacity	100 Ah
Total weight	255 kg
Number of modules	20
Battery life	1500 cycles
Cooling	Liquid
Electric motor type / brand	DC / Leroy Somer
Nominal power	11 kW
Maximum power	20 kW

4.3.3. Nickel Metal Hydride

Studied in the 1980s, this system is an evolution of the NiCd technology, using hydrogen inserted in metallic alloys instead of cadmium at the negative electrode. The composition of these alloys based on $LaNi_5$ + many other metallic additives have been extensively studied over 20 years. This is the key point of the technology, to insure long life on cycling and storage.

For different reasons, including the fact that water does not participate to the electrochemical reaction as it does in NiCd, the resulting feature is a much higher energy density (up to about 250 Wh/L) and, to a lesser extent, a higher specific energy (about 70 Wh/kg) compared to NiCd.

The battery has of course to be sealed, to prevent hydrogen loss, although the average pressure in the cell is low (typically 0.5 bars at 40°C). As in sealed NiCd, 100% water recombination takes place at the end of charge. This recombination mechanism, common to sealed aqueous battery systems, limits the battery state of charge even when charging current is still applied, thus providing self balancing of cells in series at the end of charge. Meanwhile, the energy that is not stored electrochemically is released as heat, which necessitates a strong temperature control especially for high rate charging. These batteries are maintenance free (no water addition).

The electrodes are spirally wound in cylindrical cells or flat and stacked in prismatic shape for small sizes (up to about 10 Ah). They are always stacked in prismatic design for large sizes.

Because of their high energy density, these batteries were vigorously developed in small portable format at the beginning of the 1990s for the emerging markets of portable electronics, *i.e.* cameras, mobile phones, *etc.*, but were very soon progressively replaced by the newly developed Li Ion.

Less used than NiCd in large industrial batteries, mostly because the cost is significantly higher, NiMH was however considered as a replacement for NiCd batteries for EV applications because of the significant improvement in energy density. A lot of R&D effort, supported by funded programs by the United States Advanced Battery Consortium (USABC), was devoted by several companies to this application in the 1990s, and many car prototypes have been successfully built, although never commercialized. It is now considered that the performance is insufficient to justify the much higher cost and these projects were abandoned in favour of new technologies such as Li Ion, with energy density that allows a major step forward.

When the hybrid car concept was developed into a commercial product in the late 1990s, NiMH was the advanced battery technology selected to build the high power energy storage system required. Mass produced for several years, this battery system is presently the only one used on commercially available full hybrid cars.

The main manufacturers of NiMH batteries for HEV or EV are PEVE (a joint venture of Panasonic/Toyota), SANYO in Japan, JCS Advanced Power Solutions (a joint venture of Johnson Controls Inc/Saft) in USA/Europe and Cobasys in the USA.

Both cylindrical and prismatic shapes exist in this application and are adopted in commercialized vehicles. Each cell shape has advantages and disadvantages. The electrical characteristics (energy density, power density) are essentially the same. The choice of a specific design is mostly oriented by geometrical constraints on the complete battery system, heat control systems, *etc*. Ultimately, cost can be the selection criterion.

4.3.3.1. NiMH Batteries for EVs

Large NiMH prismatic batteries have been developed in the 1990s, particularly with support of USABC programs. Although they have only been used to power prototypes or limited production cars, their technology reached a mature level on industrial pilot lines. In 1996, a large NiMH battery system from US manufacturer Ovonic (now Cobasys) was designed to power the GM EV1 car. About 1000 batteries were produced, enabling these cars to have a real world range of 250 km. In another electric vehicle project, the Chevy S10 Pick-up Truck achieved a range of 110 to 130 km with a full payload. The GM EV1 battery is shown in Figure 4.16.

In the same period, Saft produced a battery for the Chrysler EPIC Minivan, with characteristics described in Figure 4.17.

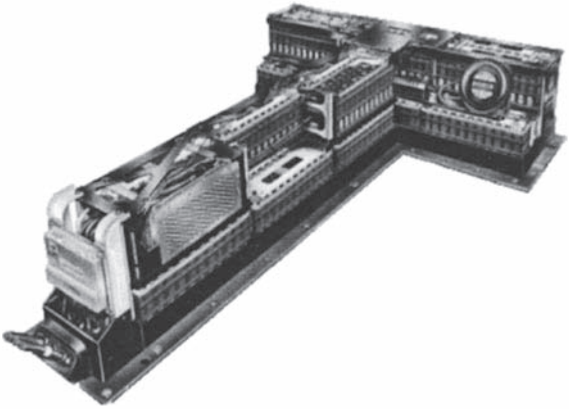

Figure 4.16. NiMH battery for the GM EV1 car (Cobasys).

Dimensions and mass:
4733×1950×1740 mm
Mass on the road: 2681 kg
Charge: 350 kg
Seats: 5

Performances:
Max speed: 100 km/h
Acceleration to 50 km/h: 6 seconds
Range in urban driving: 110km

Electric Motor
Type: AC – induction
Brand: Northrop.Grumman
Nominal power: 56 kW
Maximum power: 75 kW

Battery:
Type: Nickel-metal hydride
Brand: Saft
Cycle life: 1000 cycles
Nominal Voltage: 360 V
Capacity: 100 Ah
Total weight: 592 kg
No of modules (24 V): 15

Figure 4.17. General characteristics description of Chrysler EPIC electric minivan.

Technology

The battery system was built with 24 V series-connected modules that were themselves made by the association of two 12 V monoblocs, similar to

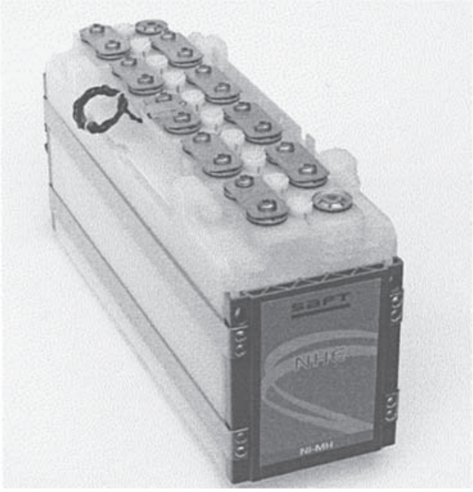

Figure 4.18. High energy 12 V NiMH battery modules (Saft).

Table 4.12. Main characteristics of the 12 V module NiMH NH12.3 (Saft).

Voltage	12 V
Capacity, C/3	100 Ah
Power @ 80% DOD, 30s @ +25°C	2800 W
Dimensions (L / W / H)	390 / 120 / 195 mm
Weight	19 kg
Specific energy	66 Wh/kg
Energy density	137 Wh/L
Specific power	150 W/kg
Power density	310 W/L

those described in Figure 4.18 and Table 4.12. Positive electrodes are made from a slurry of nickel hydroxide and a binder pasted onto a nickel foam structure. Negative electrodes are made in a similar fashion to the plastic bonded cadmium electrode, by pasting metal hydride powder and a polymer binder additive onto a perforated nickel plated steel strip.

Performance

These batteries can provide the required cycle life, as demonstrated for example in Figure 4.19 and Figure 4.20 describing evolution of capacity and power during a continuous cycling test. The main aging mechanism is due to the metal hydride powder evolution during cycling. Division in small particles, corrosion to form hydroxides, and electrolyte consumption lead to a progressive loss of power at the end of life.

Although the energy density and specific power of complete battery systems were significantly improved versus NiCd and VRLA, the significantly higher cost/kWh, even in large production quantities prevented the spread of this technology in EVs, and the market remains small today. Higher energy density batteries based on lithium electrochemistry are today the challengers to address and develop this market.

4.3.3.2. NiMH batteries for HEVs

Full hybrid

NiMH batteries are presently "on the road" with several

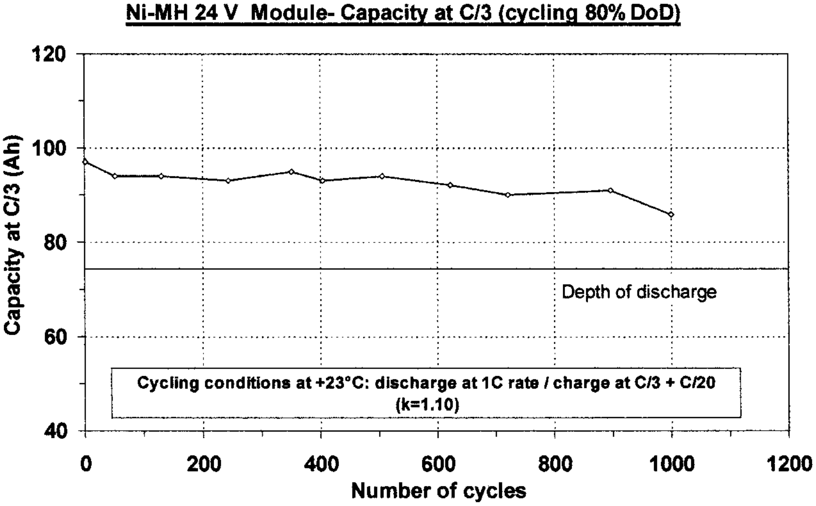

Figure 4.19. Capacity evolution during cycling of NiMH 24 V modules for EV battery (Saft).

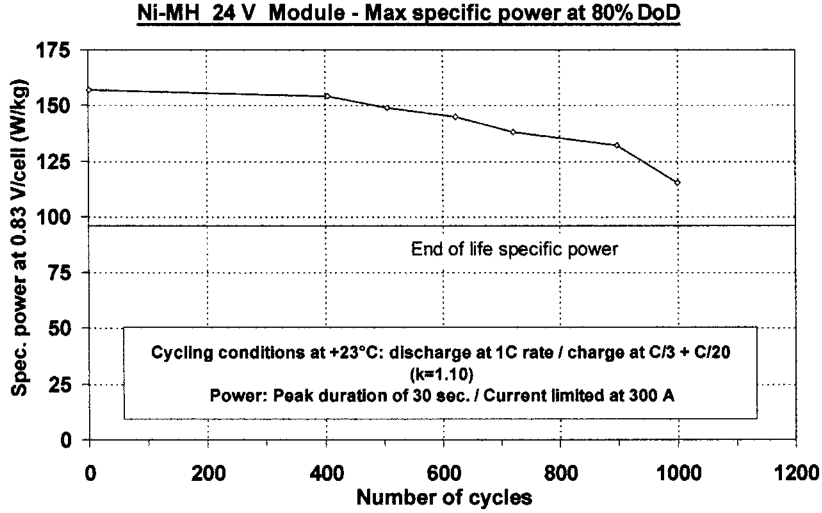

Figure 4.20. Power evolution during cycling of NiMH 24 V modules for EV battery (Saft).

commercialized hybrid cars, *e.g.* Toyota Prius, Honda Civic and Accord, Ford Escape, *etc.* As of April 2006, about 8 hybrid cars are presently commercially available [15] in the USA, and many more announced within 2 years. Many programs of future HEVs are underway, for which unfortunately little or no detailed information is available.

First on the market, the most famous Toyota Prius full hybrid car (Figure 4.21) uses a NiMH battery manufactured by PEVE.

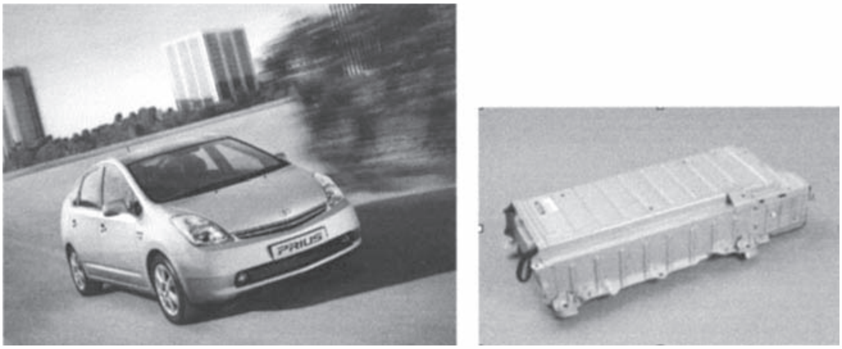

Figure 4.21. Toyota Prius hybrid car, using a NiMH battery pack (PEVE).

Gasoline Engine	1.5 liters (1497 cc) Aluminum double overhead cam (DOHC) 16-valve VVT-i 4-cylinder Power output: 76 hp (57 kW) @ 5000 rpm
Electric Motor	Permanent magnet AC synchronous motor Power output 67 hp (50 kW) @ 1200-1540 rpm Voltage: 500V maximum
Battery	Sealed NiMH Power output 28 kW; Voltage: 201.6V Expected life based on lab testing: 150.000 miles
Hybrid System Net Power	110 hp (82 kW)

Figure 4.22. Main specifications of the Prius (2006) hybrid car [16].

Table 4.13. Main Characteristics of PEVE NiMH high power modules for HEVs[17].

	1st Gen Cylindrical	Prismatic Gen1	Prismatic Gen2	New model
Nominal Voltage	7.2 V	7.2 V	7.2 V	7.2 V
Nominal capacity	6 Ah	6.5 Ah	6.5 Ah	6.5 Ah
Output power (6-cell module)	872 W	1050 W	1352 W	1352 W
Mass, g	1090	1050	1040	1197
Dimension mm	19.6 (W) 106 (H) 285 (L)	19.6 106 285	19.6 106 271.5	18.4 96 279
Battery pack height, mm		174	176	142

Technical specifications of the Prius hybrid car are reported in Figure 4.22.

Cell Design

Introduced by Toyota in 1997, the first generation car used a battery system made with cylindrical cells, while the new car generations are using a prismatic design. The unit cell characteristics of the different generations are described in Table 4.13. The main property is of course the cell power, and all parameters that can lead to a reduction in cell resistance must be carefully studied. In the latest design, the PEVE module provides a 55% power increase *vs.* the first configuration, in addition to a 20% volume reduction. This is in particular obtained through a specific cell-to-cell connection, as described below.

The prismatic cells of Gen1 and 2 include a polymer casing. A new model was recently described[18] using a metallic casing. Improvements in heat transfer capability have lead to an improvement of 14% in cell volume, and 26% at pack level. The present Gen2 module design consists of 6 cells attached side by side. The new cell design, with terminals on the cell side as described in Figure 4.23, allows a large reduction in module height. Because of the power increase, the number of modules in the battery system could be reduced from 38 to 28 and the energy reduced from 1.8 to 1.3 kWh[19].

Unlike the current design, which allows a 6-cell module only, the new

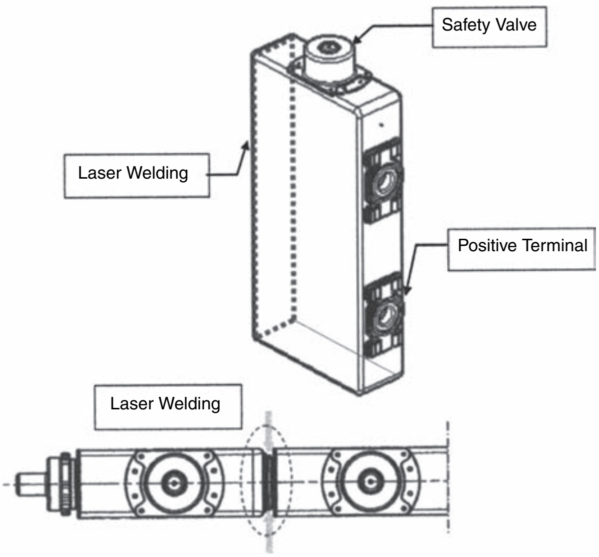

Figure 4.23. New PEVE NiMH cell structure for HEV[18].

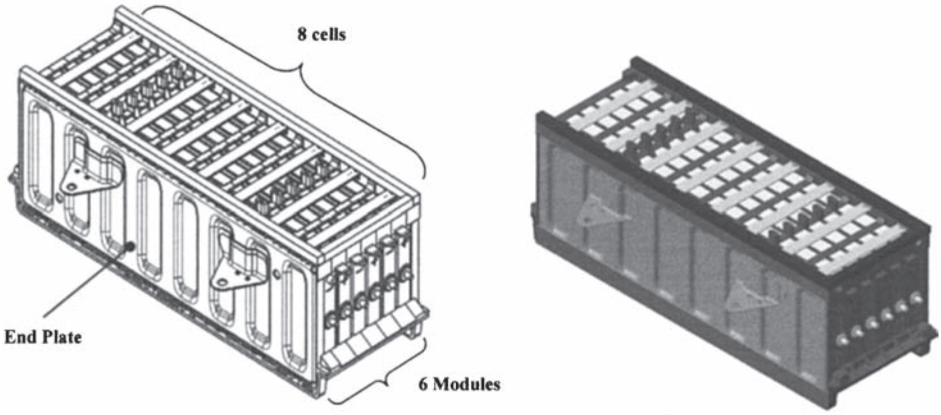

Figure 4.24. Example of a new NiMH battery pack for HEV (PEVE)[17].

concept allows a variation in the number of cells for module construction, giving more flexibility for the complete battery design, and better fitting capability to the vehicle. An example of a battery pack containing 6 modules of 8 cells is shown in Figure 4.24. This type of pack is used to build the battery of the Toyota Lexus RX400H SUV.

The specific power of the battery module exceeds 1000 W/kg, as described in Figure 4.25, measured during 2s and 10s pulses as a function of

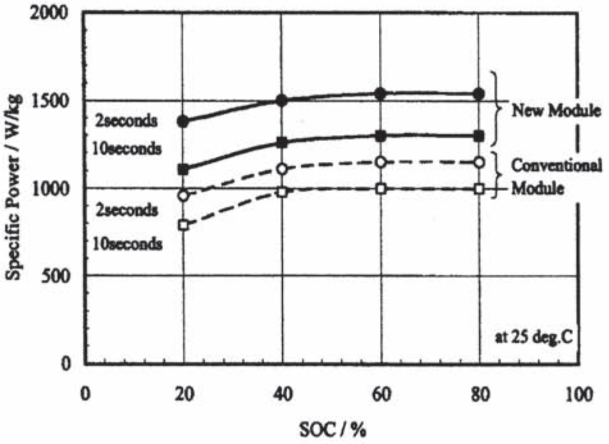

Figure 4.25. Specific power variation of a NiMH module for HEV battery as a function of SOC, at 25°C. (*From Ref. 20*)

state of charge[20]. As with all electrochemical systems, low temperature results in a significant decrease in power capability, as shown in Figure 4.26 for 10s pulses at 60% SOC[20]. Pre-heating of the battery by the thermal management system is necessary to get the minimum required power when the temperature is below 0°C. Self heating of the battery due to polarization will then bring the temperature rapidly to an adequate level.

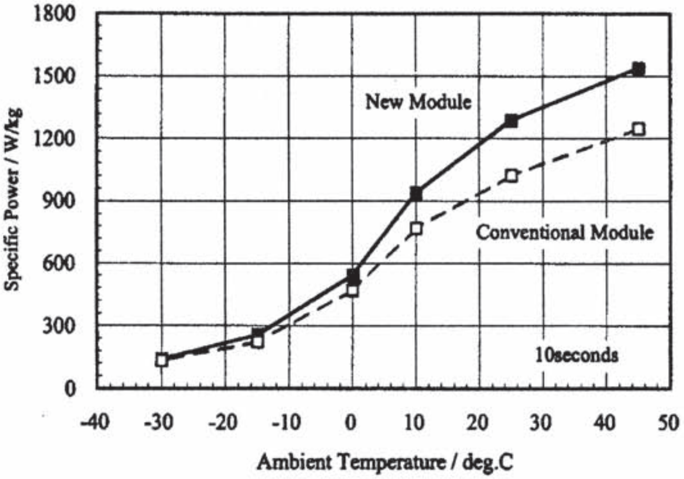

Figure 4.26. Specific power variation of a NiMH module for HEV battery as a function of temperature at 60%SOC (*From Ref. 20*)

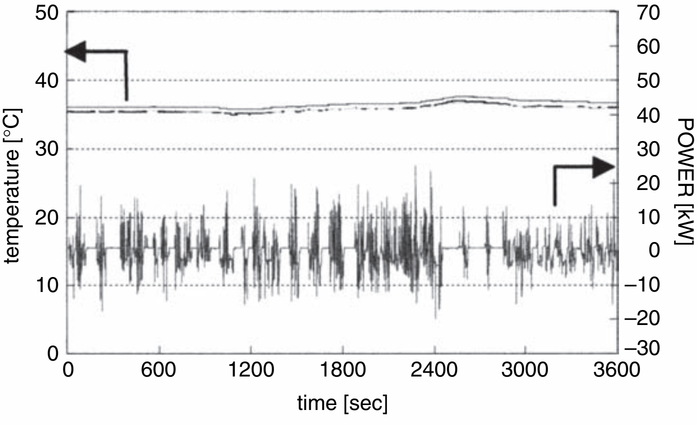

Figure 4.27. Peak power and temperature variation of several battery modules during Prius HEV urban driving. (*From Ref. 19*)

Thermal management is a very important feature of the battery designs. Channels are provided to allow air cooling by forced air produced by fans. The cell metallic casing, although heavier than the polymeric, provides much easier heat transfer. Heat is produced due to cell polarization when providing peak power on discharge and charge. Excess heat is also produced because the charge efficiency is less than 100%. Since the temperature strongly accelerates aging, it

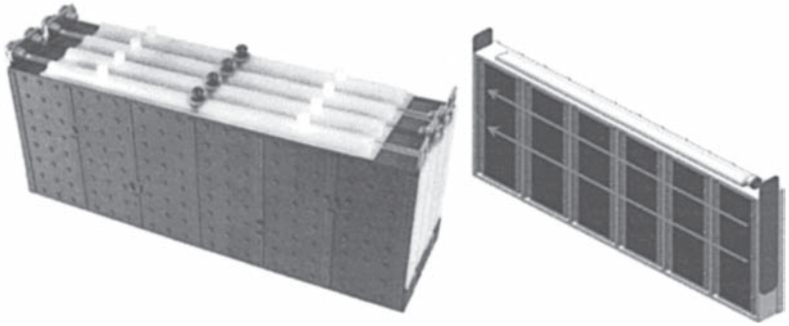

Figure 4.28. NiMH module of prismatic cells, 1350 W/kg, 2550 W/L (Johnson Controls-Saft Advanced Power Solutions)

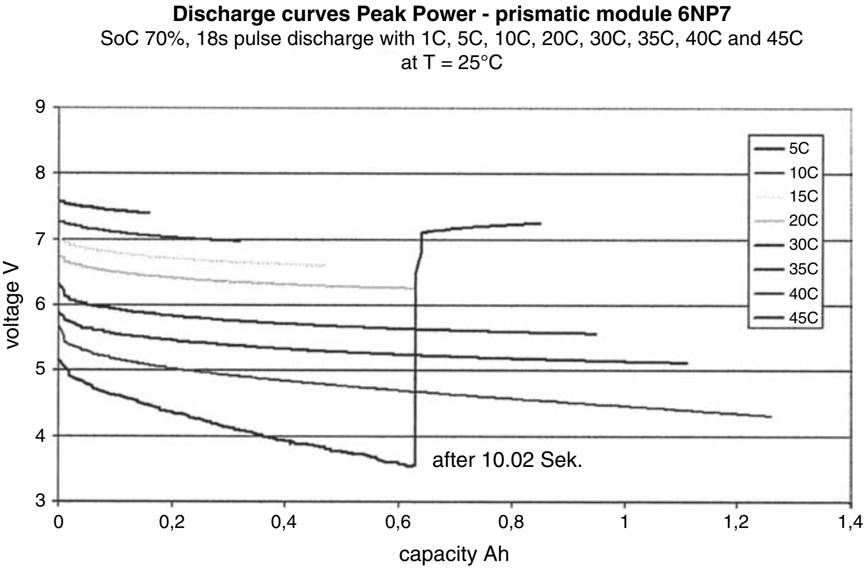

Figure 4.29. Peak power discharge of prismatic NiMH modules, at 70% SOC. (Johnson Controls-Saft, *Ref.21*)

must be reduced as much as possible, and be evenly distributed throughout the system to maintain battery life. The average temperature during use is usually about 35°C, as shown in Figure 4.27.

Other battery manufacturers also produce prismatic designs, as shown for example in Figure 4.28 for Johnson Controls-Saft Advanced Power Solutions and Figure 4.30 for Cobasys. The power characteristics of the former module are shown in Figure 4.29.

While Toyota and PEVE chose the prismatic design NiMH battery, the Honda Accord and Honda Civic were launched with NiMH batteries using cylindrical cells[22]. These cells are based on the same design as normal consumer products based on spirally wound configuration. The characteristics of such a cell manufactured by Sanyo[23] are described in Table 4.14.

Figure 4.31 represents a D size 6 Ah cell, manufactured by Johnson Controls-Saft Advanced Power Solutions. Cells are assembled, as shown in the picture, to make series connected groups, which are themselves assembled in series to make high voltage battery systems. Current collection is of course very

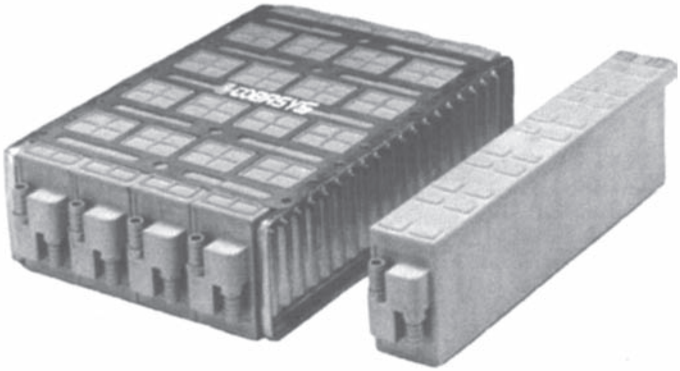

Figure 4.30. NiMH module 21000 series, 2400 W, 12 V (Cobasys)[24].

Table 4.14. Characteristics of Sanyo's NiMH battery for HEVs: HR-DP. (*From Ref. 23*)

Capacity	6.0 Ah
Weight	180 g
Discharge power (SOC 50% , to 0.9V) @25°C	190 W
Charge power (SOC 50%, to 0.9 V) @25°C	155 W
Charge efficiency @ 55°C	96 %
Capacity retention on storage, 1 week @45°C	87%
Life	10 years

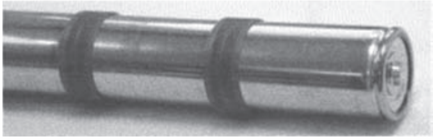

Capacity	6 Ah
Power (10s, 35%SOC)	170 W
Specific power	1100
Power density	3800

Figure 4.31. High power D size 6 Ah cells for HEV applications. (*Courtesy of Johnson Controls-Saft Advanced Power Solutions*)

important to provide the required low resistance.

The usually mentioned disadvantage of the cylindrical design is the larger volume loss in battery assembly due to the round shape. In addition, a smaller surface area compared to prismatic cells of the same capacity reduces the heat transfer surface for temperature control. However, the necessary volume to be provided for airflow in the battery structure for heat management, and the use of a metallic case mitigates this drawback. Some advantages such as easier manufacturability with high-speed machines, or easier size (height) modification when at the industrial stage can be credited to cylindrical cells.

Cycle life.

The typical characteristic of the Full Hybrid application is a large number of shallow cycles at small DOD. During driving, the battery is continuously charged and discharged, but the average state of charge must be maintained at a specified value. A battery management system monitors the SOC using measurements of current, voltage and temperature. It also checks for abnormalities in the system, and transmits information to the vehicle control system. Figure 4.32 illustrates the power output/input variation during actual use, and corresponding state of charge variation[19].

Figure 4.33 describes the power evolution during a cycling test of two battery generations at 40°C, showing that the cell resistance remains stable up to an equivalent driving distance of at least 300,000 km, demonstrating the excellent cycle life of the NiMH system.

Soft Hybrids

NiMH cells can also be used to build low voltage batteries for "soft hybrids". Saft and Valeo designed a demonstrator of an integrated 42 V starter-generator and battery system[25], based on high power cylindrical 4/5F size cells. The 10 kW – 620 Wh battery composed of 36 cells was used in a demonstration vehicle based on Opel Astra. CO_2 and fuel consumption reduction of up to 25% were reported compared to the original Astra, with the same car weight,

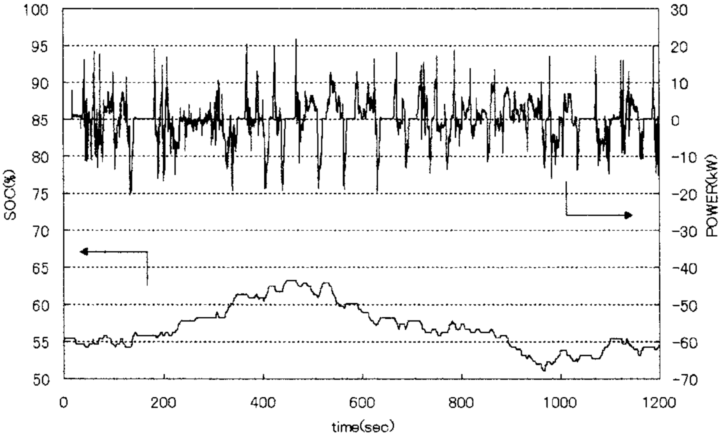

Figure 4.32. Example of power and SOC variation during Prius HEV urban driving. (*From.Ref. 19*)

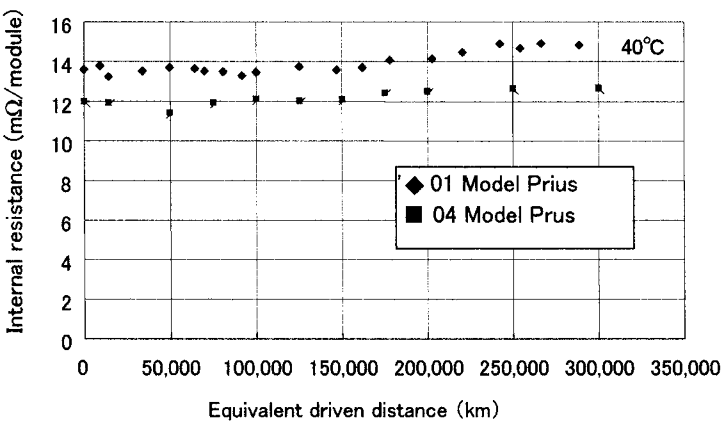

Figure 4.33. Cycle life characteristics of NiMH PEVE batteries for HEV: internal resistance variation versus equivalent driven distance. (*From Ref. 19*)

maximum speed and power capability.

Large HEVs

NiMH batteries are also used for large hybrid vehicles, buses and tramways. Because larger capacities and power are required, the cell is generally of prismatic design. Figure 4.34 displays a picture of a 4.2 kW module used in high power batteries for hybrid buses or tramways.

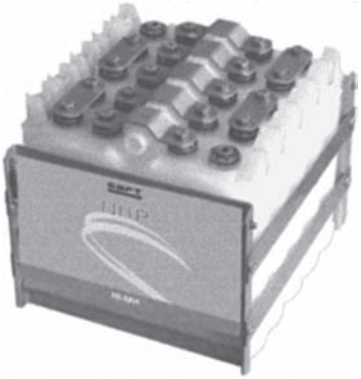

Module type	NHP 340	NHP 680
Nominal Voltage	12 V	6 V
Rated capacity @ C/3	34 Ah	68 Ah
Typical power @ 25°C @ 50% SOC, 10s	4200 W	
Weight	8.6 kg	
Dimensions, mm	165x168x165	
Specific energy	50 Wh/kg	
Energy density	91 Wh/L	
Specific power	520 W/kg	
Power density	970 W/L	

Figure 4.34. NiMH NHP module for high power (Saft).

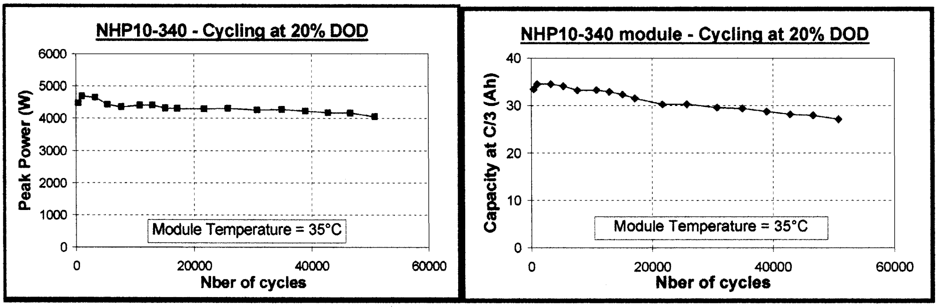

Figure 4.35. Capacity and power retention during cycling @ 20% DOD of a high power NiMH module (Saft).

The module case is made of high performance plastic material sustaining a wide temperature range (-30 to 65°C). A water-jacket design allows for efficient thermal management. A cycle life bench test is reported in Figure 4.35, performed on the NHP 340 module, simulating operation of a hybrid bus. The maximum discharge rate is 150 A, and maximum charge rate 120 A. After 40,000 cycles at an average temperature of 35°C, the power capability is close to the original value, while capacity has decreased by less than 20%. This performance represents a total capacity discharge of 8000 times the rated capacity, corresponding to a 6-year life on a typical hybrid bus.

Battery system typical specifications for Hybrid Tramways

Hybrid light rail vehicles are increasingly selected for urban transport, especially in historic cities where overhead lines and other external power delivery systems are no longer desirable. As with conventional systems, a hybrid tramway will draw its power from the catenaries for most of its journey, and then switch to an onboard battery system for city squares and historical areas for distances of up to 1 km. This requires a high power battery capable of delivering sufficient autonomous power until the hybrid vehicle next connects to the external supply. Here, some characteristics are listed.

- Typical Hybrid Tramway weight: 30 to 60 tons.
- Driving distance in autonomous mode: 200 to 800 m.
- Overall run time without catenaries: 100 to 200 s.
- Number of starts in autonomous mode (with possible traffic jams): 2 to 5.
- Power needed during the start of the trams: 80 to 200 kW for few seconds (up to 30 seconds).
- Typical voltage of the hybrid system: 500 to 900 V.
- Average energy needed for the autonomous drive corresponds to a DOD between 5 and 20%.

Ni-MH batteries have already been designed for this application. Table 4.15 describes for example the characteristics of such NiMH high power batteries.

4.3.4. Lithium Ion

The term "Li Ion batteries" actually encompasses a whole family of batteries using various active materials to build several electrochemical systems that are used or being studied for many different applications.

Introduced at the beginning of the 1990s, as the first non aqueous rechargeable system to be widely manufactured, Li Ion can be considered as a

Table 4.15. Example of typical NiMH battery specifications for hybrid tramways (Saft).

Battery	44 to 68 NHP 10-340
Nominal Voltage	530 to 820 V
Battery System Weight	800 to 1100 kg
Battery energy	18 to 28 kWh
Battery Power	90 to 200 kW
Depth of discharge	8 to 20%
Life duration	40,000 to 60,000 cycles
Life duration	6 to 8 years

revolution in battery technology. Although recent, it is the result of decades of research work on lithium batteries. A decisive step was reached when the use of carbon as an insertion structure for lithium was proposed to replace the lithium metal electrode, whose bad cycling efficiency in non aqueous electrolytes has never been satisfactorily improved.

The main general feature of Li Ion batteries is firstly a remarkable high specific energy and high energy density, surpassing all existing systems. Using highly energetic materials, lithium in the negative and high oxidation state metal ions in the positive, produces a high unit cell voltage, in the range of 3 to 4 V (mostly depending on the nature of the positive electrode chosen), *i.e.* more than twice that of conventional aqueous systems. This has two significant benefits: 1) use of a single cell in such applications for which 3 V minimum is required (example: portable phone) or 2) fewer cells to build a high voltage battery as is the case for large batteries, for example about 300 V for an EV.

The second feature is that Li ion electrochemistry can also be used to build very high power batteries. This is a paradoxical property for a non aqueous battery, using organic electrolyte of generally low conductivity. This is made possible because the electrolyte does not participate in the electrochemical reactions, and side reactions causing self discharge are very limited. Very thin separators and electrodes can therefore be used, allowing a large surface area.

A general comparison of different battery systems in a pseudo-Ragone plot of W/kg versus Wh/kg is displayed in Figure 4.36.

Materials

The most common electrochemistry used today is the $LiCoO_2$/graphite system in small portable applications, where it is likely to persist for a long time. Its main drawback is the high and variable cost of cobalt, which makes it impractical for most large industrial battery applications.

Other chemistries are either commercialized in smaller volume or being developed, mainly differing by the nature of positive materials.

$LiMn_2O_4$ and derived materials have lower expected cost, but suffer from short life due to the slight solubility of manganese that destroys the long-term stability of the negative electrode, especially at high temperature.

$LiNi_xM_yO_2$ materials, where M can be several metal ions, so called Ni-based, have similar structure to $LiCoO_2$, but lower potential cost because they use less cobalt. One of these, $LiNi_xCo_yAl_zO_2$, also called "NCA", has been studied and commercialized by Saft in industrial batteries for several years. It exhibits excellent cycling and calendar life properties, with the best figures that Li Ion chemistries can show today[26]. Nickel/Cobalt/Manganese oxides "NMC" are also studied, with the aim of replacing $LiCoO_2$ at lower cost.

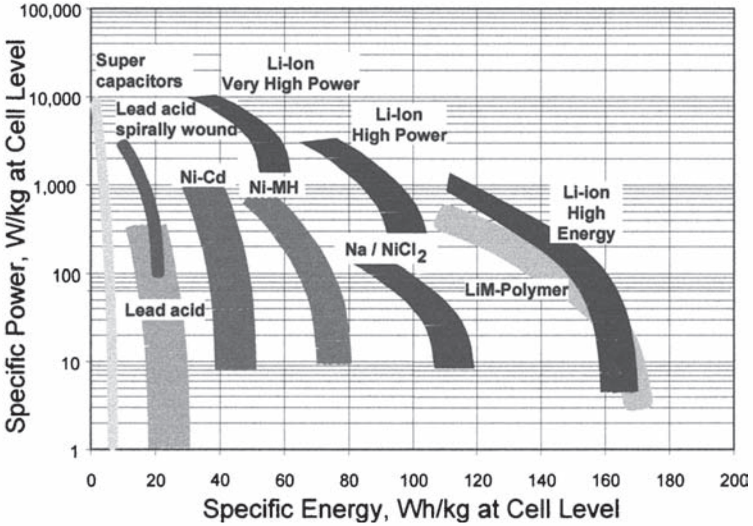

Figure 4.36. General comparison of main rechargeable systems used in industrial batteries. Pseudo-Ragone diagram (W/kg / Wh/kg).

$LiFePO_4$ has been more recently introduced[27]. Its main feature is an improved stability on overcharge (increased safety), and it has the potential for low cost due to the use of iron. Energy density is however significantly reduced, and it may be more suitable for high power applications rather than high energy.

The negative active material consists of carbon powder, in which lithium ions are inserted during charge, together with the corresponding number of electrons. The initial carbon material when Li Ion was first introduced was a disordered carbon (hard carbon), which is still used in some cases. Most Li Ion designs now use higher capacity density and lower voltage graphitized carbons.

Most of the electrochemical systems (except the one based on $LiFePO_4$/graphite) exhibit a continuous variation of voltage, decreasing as a function of state of charge. This is a very interesting feature for two reasons: 1) easy state of charge indication and 2) self balancing of cells in parallel, making direct parallel connection possible to provide the required capacity from smaller single cells. An example of voltage profile is given in Figure 4.37. This is a very important property to build high capacity batteries, with cells in parallel being maintained at the same state of charge and ensuring good distribution of current density, which is of paramount importance for long life.

Electrolyte

Typical electrolytes are made of solutions of $LiPF_6$ salt in mixtures of liquid linear or cyclic carbonate solvents (*e.g.* PC, EC, DMC, DEC, EMC). The

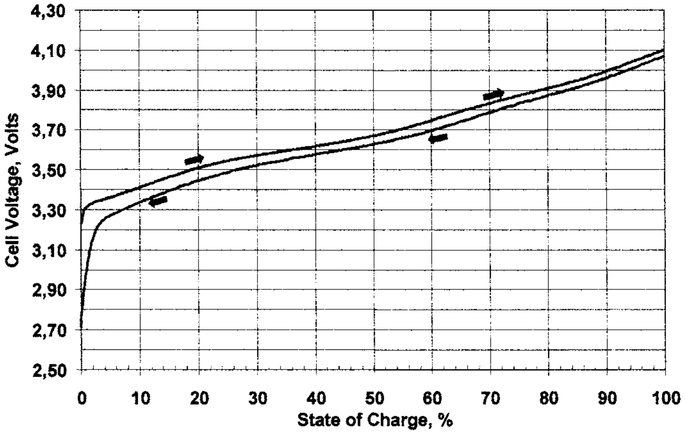

Figure 4.37. Typical Li Ion voltage profile (LiNi$_x$Co$_y$Al$_z$O$_2$/graphite system). Charge/discharge curves at low rate.

exact composition differs between manufacturers, and is generally customized to the application's requirements. Up to now LiPF$_6$ is the only lithium salt found to be suitable for the electrolyte of Li Ion batteries. Its high manufacturing cost accounts for a significant part of the total cell cost, although a significant price reduction occurred in the last 10 years with the increasing production volume of Li Ion batteries.

Although not participating directly to the electrochemical oxidation-reduction reactions during use, the electrolyte is not neutral with respect to electrode reactivity. It actually forms, at least on the negative electrode, a passivating layer that efficiently protects against corrosion of inserted lithium and gives the system its chemical stability. The nature of this layer, also called Solid Electrolyte Interface (SEI, see also Chapters 1 and 3) is the key to Li Ion long life, cycling and storage. Additives to the solvents have been extensively studied to improve the property of this layer. Among them, vinylene carbonate (VC) has been found to be the most effective[28,29].

Because electrolyte recombination or consumption is not involved as in aqueous systems, the energy efficiency on cycling is much better. From a coulombic standpoint, 100% of electricity put in is recovered, the only energy loss being due to polarization effects. This is a very attractive property for any application where saving energy is critical, *i.e.* most industrial applications, including EV and especially HEV. Beside the energy saving, less heat is produced on charge, allowing a simpler heat exchange system to control temperature.

A good selection of chemistry (which of course includes electrolyte and possibly additives) may provide outstanding chemical stability, providing the battery with a very long life expectancy. In this aspect, the nickel based system

$LiNi_xCo_yAl_zO_2$/graphite exhibits excellent performance. This feature will be described later in this chapter when discussing application examples, and in the following chapters addressing batteries for space vessels where battery life and reliability are of prime importance.

4.3.4.1. Lithium Ion Technology

Electrodes

The normal technology is a thin coating of a slurry of powdered materials with binder and solvent, onto metallic foils, aluminum for positive and copper for negative. The binder solution is generally PVDF dissolved in N-methyl pyrrolidone. The electrode manufacturing process is a key point of the Li Ion technology. The electrode thickness is very low, generally less than 100 µm, and the loading precision (weight of active material per unit surface area) must be closely monitored to ensure the proper balance between the positive and negative facing each other. Maintaining a precise constant thickness ensures good homogeneity of current density in the electrode stack.

Separator

Almost exclusively, the separator used in Li Ion batteries is a very thin (10 to 25 µm) sheet of microporous polymer material (polyethylene and/or polypropylene). This kind of material has also been widely used for many years in primary lithium batteries. It exhibits good mechanical properties, with the low thickness needed to provide the required power. However, it accounts for a significant part of the cost, especially when large surface areas are involved to make high power cells. Being mostly governed by manufacturing costs, high production volumes contribute significantly to cost reduction.

Cell design

Two main cell designs exist for electrode assembly: spirally wound electrodes or flat electrode stacks. Spiralled assemblies are found either in cylindrical or prismatic designs (with flat coils), while flat electrode stacks are mostly used in thin prismatic batteries. This latter design is generally improperly called “Li-Ion polymer”, when the cell case is made of plastic material (aluminum/polymer composite). This confusion comes from the fact that the separator – or part of it – is composed of a binding polymeric material to bond the electrodes to each other. In fact, these Li Ion cells contain as much liquid electrolyte as the conventional type. In some cases, the liquid electrolyte can be jellified with a monomer additive.

Metallic cases, mostly used in large cells, can be nickel-plated steel, stainless steel, or aluminum depending on polarity. Hermetic sealing is mandatory, to prevent electrolyte leakage or water intrusion.

Most of these technologies are presently considered, at different development stages, to build the cells for EV or HEV batteries.

Battery assembly and monitoring systems

A significant difference from conventional aqueous batteries for the user is the absence of electrochemical reactions involving water from the electrolyte, notably at the end of charge or on overcharge. This absence necessitates accurate end of charge monitoring to prevent overcharge, which would destroy the electrochemical properties of the materials, and in extreme cases would produce overheating and create safety issues. Fortunately, overcharge is always associated with over-voltage, which makes monitoring easy by voltage control. Monitoring through electronic circuits is therefore mandatory whenever several cells are assembled in series to constitute a battery system.

Other main functions of the Battery Management System (BMS) are state of charge (SOC) indication and monitoring, and capacity equilibration between cells as necessary over battery life ("balancing"). When the OCV depends on the SOC, these functions can be easily accomplished. That is not the case when the OCV remains constant whatever the SOC, as for example the case of the $LiFePO_4$/graphite electrochemistry.

Although such a BMS is always necessary, even with aqueous systems, using Li Ion cells makes it more complicated and is a contribution to the higher global cost of such technology. On the other hand, these systems allow better control of complex battery assemblies, easier monitoring, diagnostics, state of health knowledge, state of charge, *etc.*, all parameters that can be transferred to the monitoring system of the application (vehicle). A description of BMS functions is detailed in the next section.

4.3.4.2. Lithium Ion Batteries for EVs

Because of its high energy density and specific energy, Li ion is a very attractive system for powering EV. In parallel with the development of portable Li Ion, some very important R&D programs started in the early 1990s aiming at demonstrating the feasibility of such batteries in electric vehicles. These programs were supported by a strong financial effort all over the world. European commission and French government organizations in Europe, DOE/ USABC in USA, CRIEPI/LIBES in Japan (initially addressing stationary batteries for individual home power sources).

Sony, the first to launch the Li Ion concept for portable appliances, also built the first prototype of an EV battery for Nissan in Japan, using $LiCoO_2$ as a positive material[30] . Saft was one of the few companies involved and chose from the beginning a nickel-based positive material [31], because of the high and variable price of cobalt. The first prototype car using this battery was built in the frame of the "Vedelic" program in France, which fully demonstrated the battery capabilities[32]. The manganese spinel $LiMn_2O_4$ material, which offers a potentially lower cost, has also been largely studied for this application, especially in Japan[33]. However, the drawback of poor battery life due to a tendency of Mn^{2+} ions to dissolve in the electrolyte was never satisfactorily overcome, and new mixed nickel/manganese/cobalt oxides (NMC) are replacing it.

Cell design

All battery makers have selected the wound coil technology that is the optimum industrial solution to achieve a low process cost. These coils are then inserted into cylindrical or round-edge prismatic metallic cans. The can material may be nickel-plated steel or aluminum depending on which of the coil polarities is connected to the cell structure. A pressure release valve prevents cell bursting in case of overpressure.

For pure EV applications, the battery manufacturers have developed ranges of cells with individual capacities between 25 and 100 Ah. As an example, the main characteristics of the high-energy cell range manufactured by Johnson Controls-Saft Advanced Power Solutions (Joint venture between JCI and Saft) are described in Table 4.16.

Battery design

The size of an EV battery design is of course dependent on the vehicle size. Typically, battery energy is in the range of 10 to 30 kWh, with a voltage of 300 V or more. The batteries are built from modules, each comprising a number of cells with total energy in the range of 1 to 2 kWh. An example of an EV

Table 4.16. Main characteristics of high-energy cells (Johnson Control-Saft Advanced Power Solution).

Cells		VL 45 E	VL 41 M	VL 27 M
Nominal Voltage	V	3.55	3.55	3.55
Rated Capacity at C/3	Ah	45	41	27
Typical Power	W	710	850	760
Dimensions (Ø / h)	mm	54 / 222	54 / 222	54 / 163
Typical Weight	kg	1.07	1.07	0.77
Specific Energy	Wh/kg	150	135	130
Energy Density	Wh/L	310	285	275

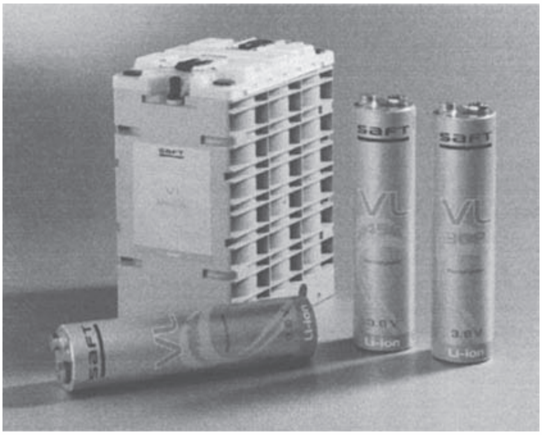

Figure 4.38. View of EV Li Ion module and cells (Johnson Controls-Saft Advanced Power Solution).

module comprising 6 cells that may be configured in any series or parallel combination is shown in Figure 4.38. The module includes an electronic board that consolidates cell measurements and transmits data (voltage, temperature) to the battery controller. The module is also designed to manage cell temperature. The Li Ion chemistry has a very low entropy coefficient, and the temperature gradient inside a battery is not as critical as it is for some aqueous battery systems (NiMH for instance).

There is no extra heat on charge, and heat generation during a drive cycle is low. Air or liquid cooling can be used, the selection being left to the automotive manufacturer. Air-cooling is lighter and cheaper but tends to be noisy and does not allow for battery heating during cold temperature operation. Liquid cooling using the car infrastructure is more compact and quieter but heavier and more expensive. It allows for battery heating for cold temperature operation.

The modules are then assembled in batteries, to reach the size required by the customer. A standard battery system is composed of:

- An assembly of modules electrically connected in series.
- A cooling system that may be limited to fans in the case of air cooling, or a pump, hydraulic manifolds, a thermal regulation valve and a liquid-to-air heat exchanger in the case of liquid cooling.
- A fuse to protect the battery against external short circuit.
- A contactor to insulate the battery from the vehicle when parked. This contactor may also be connected to a vehicle impact detector to insulate the battery in case of an accident.
- A ground fault detector, which is mandatory for high voltage batteries.

Most of these subsystems are managed by a battery controller that collects data coming from the module electronic boards, runs the various battery algorithms (*e.g.* charge, capacity gauge, protection against abuse) and communicates with the vehicle.

Figure 4.39 represents an example of a battery design that was used for a DaimlerChrysler EPIC van prototype[34]. The battery characteristics are: 38.5 kWh, 315 V average voltage, >80 kW, 330 kg (excluding battery tray), 212 dm^3. It provides EPIC with a 200+ km range.

A more recent example of a 25 kWh battery configuration, using two separate trays, is represented in Figure 4.40.

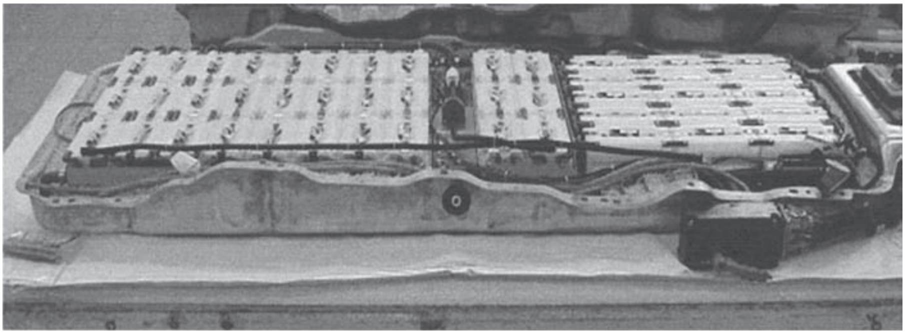

Figure 4.39. Open view of the Saft Li Ion battery for EPIC DaimlerChrysler van.

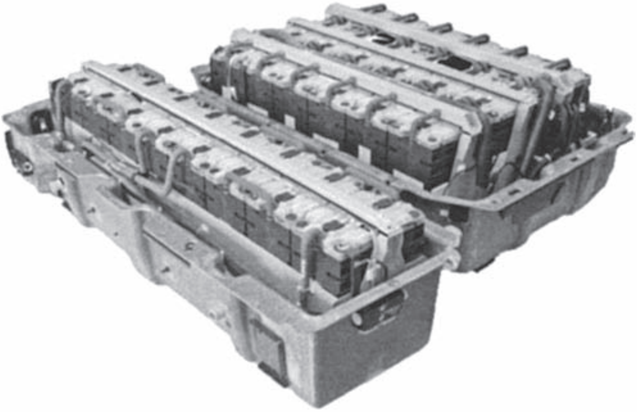

Figure 4.40. Open view of a 25 kWh Li Ion battery for EV (Johnson Controls-Saft Advanced Power Solutions).

Battery Management System

All EV batteries made by connecting many cells in series need management principles to ensure good operating behavior of the whole system. Because of their specific electrochemical properties, new battery technologies need more sophisticated management, for example monitoring charge and discharge conditions to avoid overcharge and overdischarge, which is a general rule for all Li Ion batteries. Therefore, the BMS must manage the system in its nominal function range over the entire operating environment of the electric vehicle, and has to ensure the following functions:

- Collecting information from sensors in the battery: current, voltage, temperatures, *etc*. The information is sent to the BMS to process in order to ensure correct management of the battery.
- Controlling the charger to ensure proper charge of the battery. The charger can be an onboard charger or an external one. The control is designed to react to data (cell voltage, temperatures, *etc.*) from the sensors associated with each module (telemetry boards) and respond according to parameters or special algorithms in the computer. The control of the charger is normally accomplished via the vehicle communication bus, which allows dialogue with other on-board equipment.
- Managing cell balance to ensure optimum performance of the battery. Balancing is necessary between all battery cells. The weakest cell limits the global performance of the battery. The BMS controls the balancing electronics devices integrated on each telemetry board according to a predetermined strategy or algorithm.
- Safety device: suppresses risks of overcharge or overdischarge or other major anomalies that can occur in case of failure of the battery, support equipment, or the surrounding environment. The action of the electronic system can be physical (emergency shut down of the battery) or informational (reporting trouble to the user).
- Reporting the battery state: communication of information (alarms, gauge, *etc.*) to the user and to other on-board equipment via the communication bus.
- Thermal management of the battery: the BMS monitors the temperature of the cells in all modes of operation (drive, charge, *etc.*) and controls the pump, fans, and heater to manage the temperature of the battery.
- Communication with the vehicle: sending and receiving data and commands between the vehicle computer and the BMS via the communication bus (CAN 2.0B). This bus is a standard of the automotive field.
- Maintenance via the BMS: users will have the ability to connect maintenance and diagnostic tools to undertake necessary operations for the maintenance of the battery.

- Monitor the battery: use of a laptop PC to monitor and store the battery measurement data collected by the BMS, allowing the capability to examine the results using normal software tools such as spreadsheets.

Similar functions are ensured by the BMS for other HEVs.

Typical performances in bench tests

The automotive industry considers that an EV battery reaches its end of life when it has lost 20% of its capacity/energy content or 20% of its power capability. Figure 4.41 shows the performance of high-energy cells under cycling down to 80% DOD in a "DST" (dynamic stress test) profile, which includes charge (regeneration) and discharge peaks at various rates, corresponding to an average rate of about C/3. The available energy and power were monitored during diagnostic tests made every 50 cycles. Energy was checked by a full discharge at C/3, and power was measured using a 300 A pulse (6.7C) at 80% DOD. As can be seen, the energy remains remarkably stable during more than 2000 cycles, as does the power ability. For an electric vehicle capable of 150 km at each of these cycles, this corresponds to more than 300,000 km, exceeding the life usually achieved by conventional vehicles. These results illustrate the good behavior of this selected electrochemistry, which is much better than the usual performance of commercial Li Ion cells for portable applications.

The life of the battery also depends on its ability to be stored during extended periods without degradation. The stability of the passivation layer on

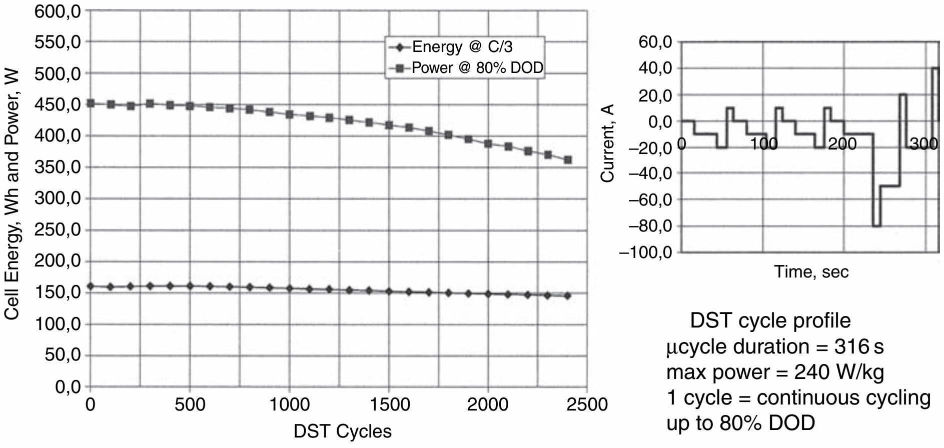

DST cycle profile
µcycle duration = 316 s
max power = 240 W/kg
1 cycle = continuous cycling
up to 80% DOD

Figure 4.41. Energy and power evolution of Saft "VL45E" cells during cycling at 80% DOD DST cycle. Every 50 cycles, energy measured at 100% DOD - C/3, power measured at 80% DOD, 300 A – 5 min pulse

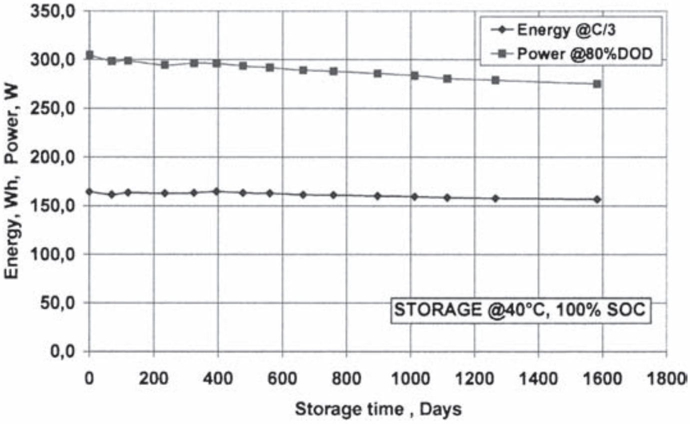

Figure 4.42. High energy Saft "VL45E" cells: power and energy retention during storage @ 4.0V (100% SOC) and 40°C.

the carbon electrode is an important parameter to ensure a good shelf life of Li Ion batteries. The chemistry selected by Saft, including the choice of electrolyte composition, graphite negative and $LiNi_xCo_yAl_zO_2$ positive, ensures an excellent calendar life as illustrated for example in Figure 4.42. High energy cells were maintained at full charge at a constant float voltage of 4.0 V, at 40°C to accelerate aging. After more than 4 years in these conditions, both energy and power remain stable.

Abuse tolerance

The main safety concern for a Li Ion battery comes from the fact that the active components are highly energetic and the electrolyte is flammable. Cell overheating may ultimately lead to battery ignition in the worst case, through active material decomposition. Therefore better intrinsic cell stability would come from the discovery of a non- or less-flammable electrolyte, which is presently an important research task for Li Ion throughout the world.

There are, however, means to prevent abusive situations at all levels, from cell to complete battery assembly. They usually include shutdown separators internal to the cell, fuses to avoid heavy short circuits, and voltage and temperature monitoring to shut down power in case of overvoltage or overheating. Ultimately, no explosion should ever occur, thanks to the case and safety vent design. Considering the worst case, should an individual cell ignite, the fire must be contained and/or extinguished, and not propagate to the whole battery. These considerations are taken into account for battery design on a case-by-case basis.

Complete EV batteries have been subjected to abuse tests by carmakers in the frame of joint development programs. As for example, a severe crash test was applied to the EPIC battery[34], simulating an accident where the battery hits a tree or a telegraph pole. The impact speed of the battery was 52 km/h. Sparks during the crash resulted in a fire, burning electrolyte. It was allowed to burn for about 15 min, then was extinguished without any problem.

The observations were stated as follows: "There was no explosion, the fire was not dramatic, and could have been easily extinguished in a short time, there was a very slow transition to other modules". At the end of the experiment, only the battery modules in the crash zone were destroyed. It must be emphasized that the crash with the battery system only was really a worst case. It is much worse than for a real crash with the same battery integrated properly in a vehicle. From this behavior, the carmaker considered that the risk is acceptable and allows continuation of the development of this technology for this application.

Onboard vehicle experimentation

At the time this text was written, no EVs with Li Ion batteries were commercially available to customers. Real life experience with EV Li Ion batteries is limited to fleet operations. Hitachi Vehicle Energy Ltd in Japan has been producing such batteries, based on manganese material, as have a few Chinese companies. Most European car manufacturers have been experimenting with batteries from Saft (now Johnson Controls-Saft Advanced Power Solutions) for more than 5 years with very good performance stability. Among all the vehicles running with these Li Ion batteries, no problem linked to the cells has been reported. See for example the field experience reported by Fiat Research Center and Saft on Fiat Seicento Elettra cars[35].

The most recent vehicle launched in Europe, "Cleanova" shown in Figure 4.43, is manufactured by Société des Véhicules Electriques (SVE) in France, using a 25 kWh Li Ion battery from Johnson Controls-Saft Advanced Power Solutions. This vehicle has a "range extender option" with a small combustion engine. The range extender can recharge 80% of the battery capacity in 2h. Typical charge is made overnight, and 70% of battery energy can be fast-charged in ½ hour from a 35 kW-150 A electric supply. The driving range performance is described in Table 4.17.

Cost

This is certainly a key point to consider when speculating about the probability of having a large deployment of EVs. At present, the prices of large Li Ion EV batteries correspond to prototypes and small production volumes. Beyond the basic product cost, they often include R&D activities. They are still much greater than the targeted volume prices, which are about $150/kWh for

Figure 4.43. Recently launched Cleanova II EV (2005), using a Li ion battery. (*Courtesy of SVE*)

Table 4.17. Range performances of Cleanova II car using a Li ion battery. *(From SVE)*

	Cleanova II	Cleanova II + range extender
Energy on board	25 kWh	22 kWh+ 20 l fuel
European urban use	210 km	530 km
European suburban use	150 km	390 km
Mix urban / suburban	170 km	450 km

high energy and \$35/kW for high power types.

Cost reduction is a permanent subject in development programs. Li Ion is still a new technology, and a very substantial cost decrease occurred in the portable battery business during the last 5 years. The OEM selling price in large quantities is presently in the order of \$0.3/Wh[36] and is expected to continue going down with competition, leading in turn to significant reductions in the cost of large batteries.

The battery assembly cost may vary significantly with the level of sophistication of the management system (thermal, electronics). The added cost is generally assessed to be in the range of 15 to 20% of the total cost.

The onboard EV experimentation also demonstrates that Li Ion technology exhibits the lowest operating cost per kilometer among the four main competitive technologies. The reasons are indicated in the following.

The energy efficiency (ratio between the discharged energy and the charged energy) of Li Ion is better than 90 % while the energy efficiencies of aqueous batteries are in the 70-80% range. Therefore, for the same available energy stored in the battery, less energy will be drained from the charging network.

For the same onboard energy, a vehicle fitted with Li Ion has a longer range thanks to the lighter weight of the battery.

Comparing two identical vehicles, one fitted with a Li Ion battery, and the other with a lead acid battery of the same energy, the lead acid powered vehicle consumes from the charging network twice the energy needed by the Li Ion vehicle to achieve the same driving range. Assuming an acceptable purchasing price, and taking in account zero maintenance costs and long operating life, Li Ion can be a very efficient technology based on life cycle cost.

4.3.4.3. Li Ion Batteries for HEVs

With appropriate electrode thickness and bussing, Li Ion batteries can provide very high power, and are therefore a good candidate for HEV batteries. Their high voltage, low weight, small volume and potentially long life make them very attractive. With decreasing cost as production volume increases, they are considered to be economically competitive to replace the presently used NiMH in the medium term[37]. This property of Li Ion for HEV was recognized early[38], notably through the PNGV program that started in the USA in 1995 and is now sponsored by DOE in the framework of the FreedomCar program[39] and presently the subject of considerable development work throughout the world. In Japan, NEDO has promoted a 5-year program, started in 2002, on "R&D on Lithium Batteries for FCV and HEV"[40]. No HEV using Li Ion is yet available to customers, but this is expected to happen within the next few years.

Several chemistries have been considered. Some manufacturers in Japan investigated $LiMn_2O_4$, especially Shin Kobé[41] (now Hitachi Vehicle Energy Ltd), Japan Storage Batteries[42] (now GS Yuasa), and NGK Insulators[43]. With its lower energy density being less important in this high power application, this material was studied to bring better safety, and potentially lower cost. Unfortunately, the shelf life problems due to Mn dissolution are still not overcome. A new improved manganese-based material of undisclosed type is now used by Hitachi Vehicle Energy in Gen2 cells[44, 45]. At the same time, Saft selected the Ni-based positive material $LiNi_xCo_yAl_zO_2$ already studied for energy cells[46]. More recently, Toyota Motors selected the same material to build the battery used in the Intelligent "Idling Stop" System, tested on Toyota "Vitz" car[47]. Matsushita Battery Ind. Co., Ltd recently published[48] the development of a high power Li Ion battery module using $LiNi_{0.53}Co_{0.3}Al_{0.17}O_2$ in the framework of the NEDO project. The more recently developed $LiFePO_4$ material is also proposed as a potential candidate for a high power Li Ion battery for HEV[49].

Cell design

Similar to the energy cells developed for EV, high-power Li Ion cells mainly differ by having thinner electrodes to improve the electrochemical kinetics and increase the working surface area. Power loss in current collection is minimized by appropriate internal and external bussing to decrease the cell resistance, as for any battery system.

Different cell designs are considered by the battery manufacturers. The spirally wound design is mostly used, either in a cylindrical or prismatic shape. An example of cylindrical cell characteristics and design are described in Table 4.18 and Figure 4.44.

A prismatic cell with spiralled coil is used in the Toyota Vitz[50], and other designs are being studied by other manufacturers, such as a "laminated" thin flat prismatic in a "pouch" case made of polymer/aluminum composite[51,52]. The large footprint of this latter design allows a better heat transfer.

Performance

Table 4.19 lists most of the important requirements for HEV, as initially defined for the PNGV program[53].

The HEV battery must provide high power on demand, normally manifested in short bursts of a few seconds, but must also accept fast charging from regenerative braking. Typical test profiles therefore include discharge and charge pulses as defined by the car manufacturers.

Because of this, the battery of a full HEV works around 50% SOC, at the so-called "sweet spot". As the Li Ion cell voltage depends on SOC, the power capability on charge and discharge varies. Figure 4.45 shows typical profiles of charge/discharge power as a function of DOD and pulse duration. This property, which could appear as a weakness, is in fact very useful to

Table 4.18. Characteristics of some high power Li Ion cells.

	VL30P (*)	VL20P (*)	VL7P (*)	VL8V (**)	VL4V (**)
Capacity (Ah)	30	20	7	8.6	4.4
Max cont. curr. (A)	300	250	100	520	260
Peak current (A)	500	500	250		
Energy (Wh) (C/3)	107	71	25	30	16
Power (W)	1250	1130	670	1880	1150
Diameter (mm)	54	54	41	41	34
Length (mm)	222	163	145	152	152
Weight (kg)	1.1	0.80	0.37	0.47	0.32

*Johnson Controls-Saft Advanced Power Solutions
** Saft prototypes

Figure 4.44. VL7P 7Ah cell.

Table 4.19. Technical requirements of Power Assist HEV battery.

Characteristics	**Units**	**Requirement**
Pulse discharge power	kW	25 (18 sec)
Peak regenerative pulse power	kW	30 (2 sec)
Total available energy	kWh	0.3 (at C/1 rate)
Minimum roundtrip efficiency	%	90
Cold cranking power at –30°C	kW	5
Cycle life at 25 Wh cycle energy	cycles	300,000
Calendar life	years	15
Maximum weight/volume	kg/L	40/32
Operating voltage limits	V dc	$V_{MAX} \le 440$ / $V_{MIN} \ge 0.5*V_{MAX}$
Maximum allowable self discharge	Wh/day	50
Temperature range		
Operation	°C	-30 to +52
Survival		-46 to +66

monitor the state of charge of the battery during the shallow cycling of actual use.

Specific power of about 2 to 3 kW/kg are typically obtained from Li Ion cells for HEV, but this is not the limit that can be provided, depending on the required energy density. For example, 12 kW/kg can be obtained during 0.2s pulses from the VL4V cell prototype described in Table 4.18.

Low temperature operation is also required. Some power reduction is observed, resulting from slower kinetics, especially in the ionic mobility of

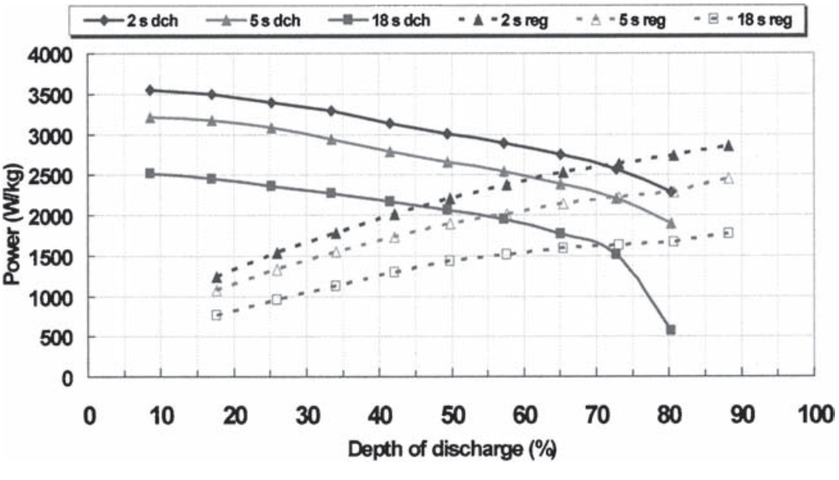

Figure 4.45. Specific power during discharge (dch) and charge (reg) pulses. VL7P Cell (Johnson Controls-Saft Advanced Power Solutions). (*From Ref. 37*)

electrolytes. The typical power capability of a VL7P cell is described in Figure 4.46 as a function of SOC, at different temperatures. In actual operation in HEV, the battery temperature normally exceeds 25°C due to the heat produced by polarization. A thermal management system is required at the battery level.

Calendar and cycle life

As for EV, longevity of an HEV battery is critical and must be compatible with the car life. From the PNGV requirements[53], 15 years life including 300,000 shallow DOD cycles should be obtained with less than 20% power loss. This is a key point to be demonstrated by any Li Ion chemistry to be validated in a HEV application. This can be obtained, as shown in Figure 4.47, through proper design and good chemistry. This is a strength of the $LiNi_xCo_yAl_zO_2$/graphite chemistry, as described earlier in this chapter. The storage capability of this system is also excellent, as shown in Figure 4.48 in accelerated high temperature aging conditions. From all accumulated data on this technology in different designs, the goal of a battery life equal to, or exceeding, the car life can be reached[54].

That is not the case with $LiMn_2O_4$ based cells, which exhibit capacity and power loss on cycling and high temperature storage. To overcome this behavior, Hitachi Vehicle Energy Ltd reported recent improvements through an undisclosed new manganese-based positive material[44]. Figure 4.49 describes the capacity and resistance variation of the new generation cell compared to the Gen1 containing spinel $LiMn_2O_4$.

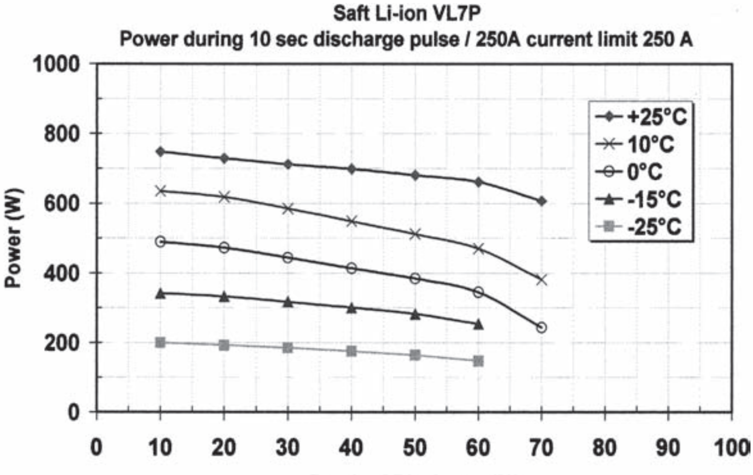

Figure 4.46. Typical power capability of a VL7P cell ((Johnson Controls-Saft Advanced Power Solutions) during 10sec pulses as a function of DOD, at different temperatures. (*From Ref. 37*)

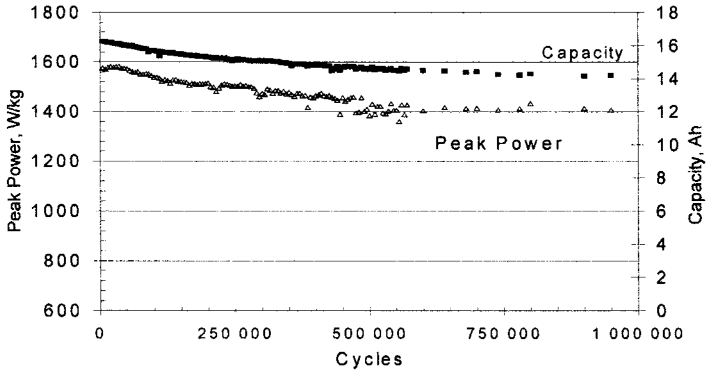

Figure 4.47. Shallow cycling of high power Li Ion cell under HEV load profile (Saft cell, periodic 100% DOD diagnostic). (*From Ref. 2)*

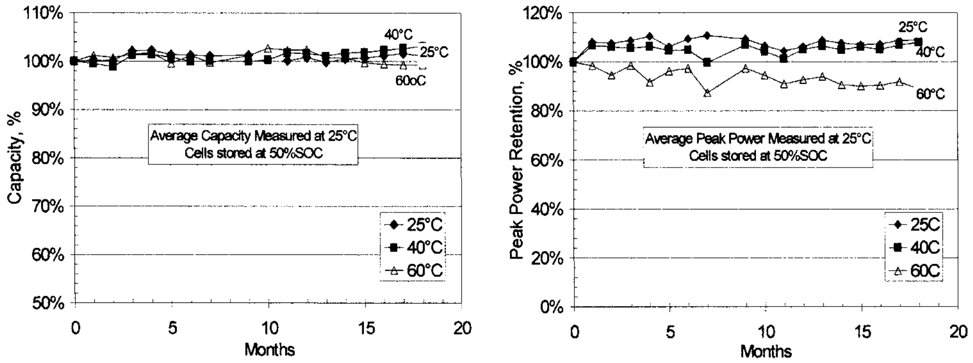

Figure 4.48. Capacity and power evolution of cells (by SAFT) stored at 50% SOC, at various temperatures. (*From Ref. 2)*

Abuse tolerance

The same comments as for EV batteries can be made (see previous section). However, high power cells are safer in abuse conditions because the energy density is lower, decreasing the amount of heat that can be generated. The VL7P cell described above using a Ni-based positive electrode material can pass all the abuse testing prescribed by automakers, as illustrated in Table 4.20. These tests were applied to the bare cell, without additional protection. In battery configuration, no event occurred in case of electrical abuse, due to the operation of protective devices.

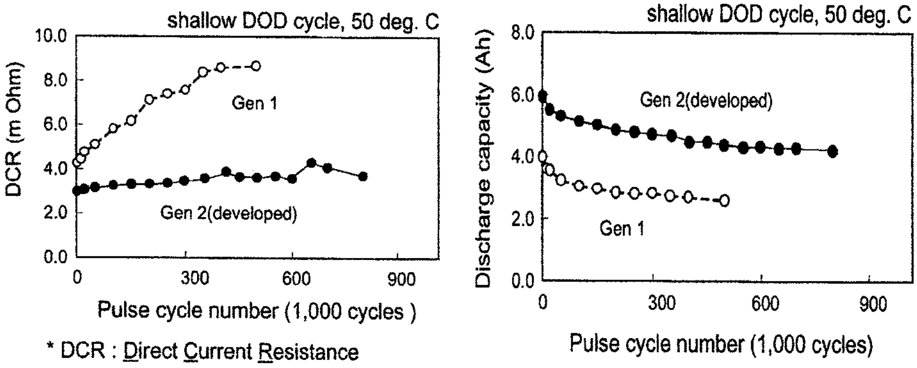

Figure 4.49. Resistance and capacity evolution of high power Li ion cell for HEV, using $LiMn_2O_4$ (Gen1) and new material and electrolyte (Gen2) by Hitachi Vehicle Energy. (*From Ref. 44*).

Battery assembly design

The association of cells in series to obtain the required high voltage must comply with the same principles as described for EV cells. Battery design generally includes:

- cells incorporated into module hardware;
- electronic Battery Management System;
- active thermal management with air or water cooling options;
- power and safety devices.

On board experimentation

Being more recently developed than EV batteries, there has been less experimentation on board vehicles (fleets) up to now, but this situation is going to change very quickly. A large number of car prototypes are being tested with different technologies, but with very little public data available today. The largest fleet test is probably the Toyota Vitz car, in a "stop and start"

Table 4.20. VL7P cell behavior under abuse tests. (*From Ref. 54*)

Test	Result
Overcharge at 3 C rate	Cell venting + light smoke
External short circuit on fully charged cell	No event
Spike test on fully charged cell	Cell venting and smoke
Overheat on fully charged cell	Cell venting and smoke
Crush on fully charged cell	No event
Over discharge	No event
Immersion in salt water on fully charged cell	No event

configuration, including some regenerative braking. No conclusions have been published so far.

Li Ion for Plug-in Hybrids

Li Ion batteries are well adapted to the requirements of Plug-in Hybrids (see Sub-section 4.2.2.5). Because the battery has to provide more energy, the much larger energy density and specific energy of Li Ion is a benefit compared to nickel metal hydride. A medium size battery, intermediate between EV and HEV can provide both the pure EV mode up to a certain speed limit for a predetermined range, and the full HEV mode in other conditions. The good accuracy of SOC determination and good charge efficiency are additional advantages over NiMH in this application.

In the USA, the Electric Power Research Institute (EPRI) [55] is conducting a program in collaboration with DaimlerChrysler on PHEV based on the Sprinter van. The prototypes are testing two different battery systems: NiMH and Li Ion, associated with two liquid fuels: diesel and gasoline.

Cost

As for EV batteries, cost reduction of Li Ion batteries is the key for fast introduction to the market. It is considered that they can compete with NiMH and provide a more economic solution over the long term as production volume increases.

4.3.5. Lithium Polymer Batteries

The specific property of true lithium polymer batteries (as opposed to Li Ion polymer) is the use of a polymeric electrolyte, based on polyethylene oxide, instead of a liquid electrolyte. Invented by Armand and Duclot [56] at the end of the 1980s, this concept has been applied by Hydro-Quebec in Canada to develop lithium batteries. This battery system was studied by Argotech[57] (a joint venture of Hydro-Quebec and 3M) to build batteries for EVs under the USABC program in the 1990s, then followed by Avestor (a joint venture of Hydro-Quebec and Kerr-McGee) in Canada. Battery prototypes were built and integrated on demonstration vehicles. Avestor decided recently (2005) to stop the EV program to concentrate on standby telecom batteries of the same concept. The French company Bolloré started developing this type of batteries for EV in 1998 under a French government program (PREDIT)[58].

Avestor only has released information on the chemistry and technology of this battery type; therefore, the information reported in the next sub-section is based on their know-how.

4.3.5.1. Battery Chemistry and Technology

The polymer electrolyte is obtained by dissolution of a lithium salt, $Li(CFSO_2)_2N$ (LiTFSI) in a polyethylene oxide-propylene oxide (PEO-PPO) matrix[57]. Because the conductivity of the polymer electrolyte is very low at room temperature, the battery must be operated at a temperature of, typically, 60-80°C. For the same reason, the electrodes have to be very thin. Although the reversibility of the lithium metal electrode is better than in a liquid organic electrolyte, the formation of lithium dendrites is not completely suppressed and an excess of lithium has to be provided in the cell design to achieve the minimum number of cycles required, *i.e.* about 600. The positive electrode is made of lithiated vanadium oxide $Li_{1+x}V_3O_8$, providing an operating voltage window of about 3 to 2 V. Higher voltage material such as used in lithium ion cells is not compatible with the polyethylene oxide voltage window stability. The high reversible specific capacity of this material (above 200 Ah/kg) allows a specific energy at the cell level of ~150 Wh/kg, similar to that of Li Ion.

Battery modules are made by series connected flat prismatic stacks placed in a single stainless steel box. Several flat heater devices are placed between the cells to heat the battery and maintain the appropriate working temperature. The battery module is also thermally insulated. A battery management system maintains the temperature between 60°C and 80°C. Depending on operating conditions, it may be required to cool or heat the battery.

As any other non aqueous battery, cell voltages must be monitored with an appropriate battery management system.

4.3.5.2. Integration in Vehicle

Under the USABC program, Avestor integrated prototypes inside a Ford TH!NK *city* car[59]. The main vehicle specifications are described in Table 4.21.

Table 4.21. Main LMP TH!NK city specifications. (*From Ref. 59*)

Vehicle name	TH!NK *city* (Demo)
Dimensions (L,W,H), m	2.9, 1.6, 1.98
Seat capacity	2 passengers
Curb weight, kg	870.9
Battery	LMP (Lithium-Metal-Polymer)
Configuration	7 modules (143 V,80 Ah,11.5 kWh)
Electric motor	27 kW

Table 4.22. LMP battery pack specifications. (*From Ref. 59*)

Energy (kWh)	11.5
Power 30 sec @ 80%DOD (kW)	29
Capacity (Ah)	80
Nominal Voltage (V)	143
Dimensions (W,L,H), mm	755, 945, 270
Weight (kg)	160

The LMP battery pack was made of seven series connected modules, each module being made of 8 cells in parallel and 8 cells in series to achieve 20 V and 80 Ah. The main specifications are described in Table 4.22. Being placed in the volume of the original NiCd battery, the LMP modules do not fill the whole battery compartment, and more energy could be provided with specifically designed modules. A liquid cooling circuit and heat exchanger are part of the battery management system. The total weight is about 871kg, compared to 941.2 kg of the NiCd batteries.

The top speed recorded at 100% SOC was 89 km/h with a minimum payload of 77.1kg, essentially the same as with the NiCd battery, but acceleration from 0 to 48.3 km/h was 4.6 sec compared to 7 seconds for the standard vehicle. The range obtained in this urban loop at 36.4 km/h average speed was 96.5 km (to 90% DOD) compared to 85.3 km specified with NiCd batteries.

With the exception of another demonstration prototype with Honda Insight, no other demonstration vehicle fleet has been recently reported, and the use of LMP batteries in EV is no longer considered by Avestor.

The French company Bolloré has announced the manufacturing of a LMP battery, soon to be integrated in a new EV. No precise information is available on the battery design. The characteristics of the LMP module[58] are reported in Table 4.23.

Table 4.23. Lithium polymer projected characteristics of 2.8 kWh module. (*From Ref. 58*)

Weight, kg	23
Volume, L	25.2
Nominal capacity, Ah	90
Nominal Voltage, V	30.6
Dimensions, cm	18x34x40
Specific energy, Wh/kg	120
Energy density, Wh/L	110
Specific power @80%DOD, W/kg	>200

Because its power capability is lower than Li Ion, the use of LMP in HEVs is not anticipated, and would be limited to pure EVs. This might be a handicap for reducing the cost by large mass production. In terms of technical specifications, the challenge of LMP batteries is to match the proven long cycle life of Li Ion batteries with high reliability. Because it does not contain flammable liquid organic solvent, its behavior under abuse conditions is reported to be safer. However, the large amount of lithium metal may still create serious safety concerns beyond the melting point of lithium, 180°C, where it might start burning violently.

4.3.6. Sodium Nickel Chloride Battery

This high temperature battery system known as "ZEBRA" has been studied since mid eighties as an improvement of the sodium sulfur battery. The main features are the use of a solid electrolyte, β alumina, a liquid salt electrolyte $NaAlCl_4$ and an operating temperature of about 300°C. ZEBRA batteries are now manufactured by the Swiss company MES-DEA. This system has reached a mature development and has been manufactured in several battery configurations to power different types of vehicles, from EV to buses, although not yet on commercially available cars.

4.3.6.1. Battery Chemistry and Technology

Based on the high-energy $Na/NiCl_2$ couple, the battery must be maintained in the range 270-350°C to operate, were both sodium and electrolyte salt $NaAlCl_4$ are molten. The cell voltage is 2.58V @ 270°C. Sodium ions move during charge/discharge through the beta alumina solid electrolyte separator, which has a tubular shape.

The hermetically sealed cells are built in the discharged state and sodium is formed *in situ* during the first charge. A critical point of the cell design is the alumina tube sealing to the cell can and to the insulating alumina ring of the negative terminal. This is achieved by a type of glass having appropriate sealing and thermal expansion properties[60].

The power density, which is a limitation of this battery system, has been continuously improved, from the 50 W/kg of the first prototypes[61] at the cell level to more than 200 W/kg. This was particularly obtained through shape modification from round to clover cross section of the tubular β'' alumina separator, and adding iron to the nickel as secondary active material. This additive allows increasing the power at deep DOD.

Table 4.24. ML/8 ZEBRA cell specifications. (*From MES-DEA data sheet*)

Cell type	ML/8
Capacity, Ah	25
Weight, kg	0.45
Dimensions, mm	36.5x36.5x146.4
OCV, V	2.58
Max regen voltage, V	3.1
Min discharge voltage, V	1.72
Max discharge current, A	80
Specific energy, Wh/kg	143
Peak power, W	102
Specific power, W/kg	240

Table 4.25. B1 ZEBRA battery specification. (*From MES-DEA data sheet*)

Battery type	Z21
Cell type / number	ML/8, 240 cells
Rated energy, kWh	15.5
Weight with BMI, kg	134
Dimensions (WxLxH), mm	444x962x206
OCV, V	310
Max regen voltage, V	372
Min discharge voltage, V	206
Max discharge current, A	175
Specific energy, Wh/kg	115
Peak Power, kW	24
Specific power, W/kg	180
Thermal loss, W	< 90
Cooling	Air
Heating time, h	24 @ 230 Vac
Ambient temperature, °C	-40 to +50

Recently published[62] performance of cells and batteries are reported in Table 4.24 and Table 4.25. The lower height of the new cell and battery was designed for better integration in small passenger cars under the floor pan.

A picture of a standard 17.8 kWh Z5C ZEBRA battery is shown in Figure 4.50.

The battery should be maintained during rest at its operating temperature by electric resistance heaters, while during discharge the temperature is mainly maintained by the energy generated by ohmic losses and polarization. For high power applications, a cooling system is also necessary to keep the temperature within the operating range when high power is required. The heat loss of a battery type Z5 is less than 100W @ 270°C, which represents a maximum of 12.5 days storage capability without external power source for a 30 kWh battery. Although cooling down to ambient and re-heating is not convenient, it was demonstrated that more than 40 freeze/thaw cycles had no detrimental effect on the performance [63].

4.3.6.2. Bench Tests

Capacity retention is excellent as shown for example in Figure 4.51. The full nameplate capacity (80% of the total 40 Ah reversible capacity) was maintained during 7000 cycles (3000 nameplate cycles) over 4 years of typical driving cycles as specified by the car manufacturer. The actual aging

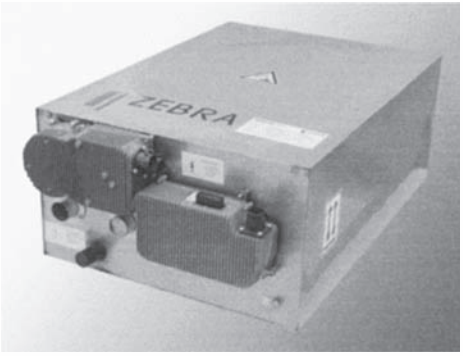

Figure 4.50. 17.8 kWh Z5C ZEBRA battery for EV. (*Courtesy of MES-DEA*)

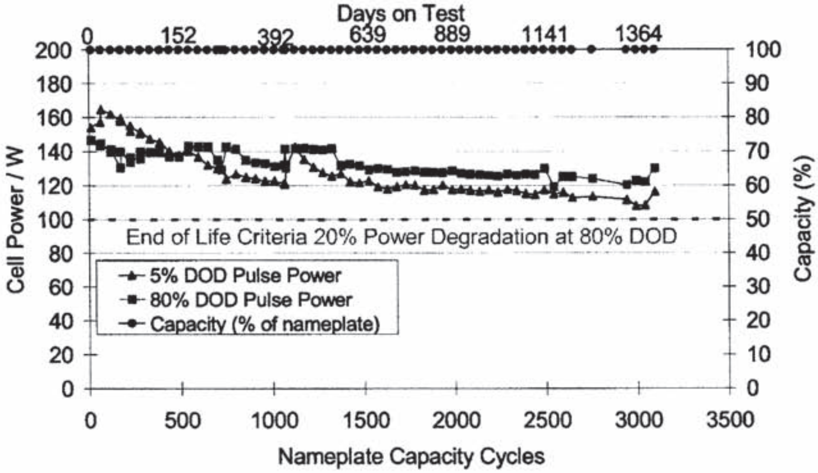

Figure 4.51. Cycle history for ZEBRA ML/4 cell module running in excess of 3000 nameplate cycles. (*From Ref. 62*)

phenomenon is related to resistance increase and power fading, but still shows adequate behavior compared to specifications.

4.3.6.3. On Board Testing

ZEBRA batteries have been tested onboard many vehicles for more than 15 years. In 1997, Daimler-Benz reported[63] more than 1 million cumulated km of ZEBRA battery testing in road trials, starting from 1988 in a Mercedes 190, then in the C-Class. An A-Class prototype was then equipped with a Z12 30 kWh battery system. The main characteristics are: 298 V, 104 Ah, 58 kW peak, 370 kg, 220 L, 81 Wh/kg, 155 W/kg up to 80% DOD. The 4-person, 1730 kg car exhibited a range up to 200 km (SAE J1634) without air conditioning, with a maximum speed of 130 km/h.

Recently published data[64] on a fleet test by the municipality of Mendrisio in Switzerland demonstrated the utilization of ZEBRA batteries in Renault Twingo cars, by comparison to 15 Peugeot 106, a similar size car, equipped with reference NiCd batteries. The first phase of the program, aiming at promoting the use of electric cars in cities, was completed in 2001 with NiCd batteries. In the second phase, Twingo cars with ZEBRA batteries were also introduced. The battery energy was 21.2 kWh, compared to 14 kWh of NiCd, giving respectively 120 and 80 km range to the vehicles, whose total weights were 1230 and 1350 kg, respectively. One of the purposes was to evaluate the average energy consumption of the vehicles, which ultimately was fairly comparable. The average consumption over about 200,000 cumulated km for several vehicles was 25.8 kWh/100 km for the Peugeot 106 with NiCd, and 23.2 kWh/100 km for the Renault Twingo with ZEBRA battery. The energy loss to maintain the battery temperature was compensated by the 100% faradic (Ah) charge efficiency of the $Na/NiCl_2$ system, compared to an average measured 76% energy for the NiCd.

4.4. Conclusion

After more than a century of periodic interest, electric traction has probably reached a decisive step of its history with the increasing interest in hybrid cars. The concern about fossil energy shortage and recognition of the CO_2 emission harmfulness will definitely confirm this trend. Because there are various type of hybrid cars, several battery systems may take benefit of this opportunity for growth. Today, improved lead acid batteries are employed in "micro-hybrids" because of their low cost and large availability, while nickel metal hydride batteries are largely deployed in "full" and "soft" hybrid cars because of their technical performance and availability at industrial scale. The new Li Ion technology, already widely spread in a multitude of portable equipments, offers performance advantages that make it the best challenger to become in a medium term the most used power source. Cost decrease projections with large manufactured quantities would make them cheaper than NiMH, and competitive with lead acid on a life cycle cost basis. The increasing success of hybrid cars should also benefit to the development of pure electric or "plug in" hybrids vehicles, where new technologies can bring the required high level of energy density performance.

Acknowledgments

The author wish to express many thanks to all engineers and scientists from several companies who contributed on helping to this chapter by providing data and information, and more specially Claude Adès (CEREVEH), Jim McDowall, Philippe Ulrich, Christophe Morin, Claude Chanson, Jean Michel Dauchier, Marc Bariand, Georges Caillon (Saft), Jean Louis Liska, Francois Barsacq, Uwe Khöler (Johnson Controls - Saft Advanced Power Solutions).

References

[1] R. Cowan and S. Hulten, *Technology Forecasting and Social Change*, Report, 1996.
[2] M. Broussely, in "*Lithium Batteries - Science and Technology*", G.A.Nazri and G.Pistoia, Eds., Kluwer Academic Publishers, Boston, USA, 2004.
[3] T. Kameda, *Proceedings of AABC Conference*, Hawaii, USA, 2005.
[4] F. Kalhammer, *Extended Abstracts, 46th Battery Symposium in Japan*, Nagoya, Japan, 2005.
[5] P. Ulrich and J.L. Liska, *Proceedings of 20th Electric Vehicle Symposium (EVS20)*, Long Beach, USA, 2003.
[6] H.E. Haring and U.B. Thomas, *Trans. Electrochem. Soc.* 68 (1935) 293.
[7] D. Berndt, "Stationary Lead-Acid Batteries With Selenium Alloys", *Varta Spezial Report* 1/1980.
[8] German Patent 16 71 693 (Accumulatorenfabrik Sonnenschein GmbH, Büdingen, 1.12.67).
[9] P. Moseley, "The Design of VRLA Batteries for Successful Operation in a High-rate, Partial-state-of-charge Regime", *Electrical Energy Storage Applications and Technologies (EESAT)*, 2005.
[10] J. Pessis, *Proceedings of 21th Electric Vehicle Symposium (EVS21),* Di 2 - A2, Monaco, France, 2005.
[11] F. Trinitad, C. Hernandez, M. Lacadena, B. Jacq, G. Fossati and R. Johnson, *Proceedings of AABC Conference*, Hawaii, USA, 2005.
[12] T. Kameda, M. Kiribayashi, K. Sawai, T. Ohmae and S.Osumi, *Abstracts of the 46th Battery Symposium*, Nagoya, Japan, 2005.
[13] F. Trinitad, M. Lacadena, A. Sanchez and J. Valenciano, *Abstracts of the 46th Battery Symposium*, Nagoya, Japan, 2005.

[14] Website: http://www.optimabatteries.com (Johnson Controls).
[15] Web site http://www.hybridcars.com/cars.html
[16] From Toyota Website: http://www.toyota.com/prius/specs.html
[17] H. Miyamoto, T. Asahina, T. Matsuura, S. Hamada and T. Eto, *Proceedings of 21th Electric Vehicle Symposium (EVS21)*, Monaco, France, 2005.
[18] S. Hamada, T. Asahina, T. Matsuura, H. Myiamoto and T. Eto, *Proceedings of AABC conference*, Hawaii,USA, 2005.
[19] S. Nagata, H. Umeyama, Y. Kikuchi and H. Yamashita, *Proceedings of 20th Electric Vehicle Symposium (EVS20)*, Long Beach, USA, 2003.
[20] K. Ito and M. Ohnishi, *Proceedings of 20th Electric Vehicle Symposium (EVS20), Long Beach*, USA, 2003.
[21] C. A. Rosenkranz and U. Köhler, *Abstracts of the 46th Battery Symposium*, Nagoya, Japan, 2005.
[22] M. Mitsumori, K. Inoue and T. Matsuda, *Abstracts of the 46th Battery Symposium*, Nagoya, Japan, 2005.
[23] I. Yonezu, K. Shinyama, Y. Magari, H. Nakamura, K. Kitaoka, M. Takee and K. Ishiwa, *Abstracts of the 46th Battery Symposium*, Nagoya, Japan, 2005.
[24] From Cobasys website http://www.cobasys.com.
[25] C. Chanson and D. Thiercery, *Proceedings of 3rd AABC conference*, Nice, France, 2003.
[26] M. Broussely, *Proceedings of the 1rst International Symposium on Large Lithium ion Battery Technology and Application (LLIBTA)*, Honolulu, USA, 2005.
[27] J.B. Goodenough, A. Phadi, K.S. Nanjundaswamy and C. Masquelier, WO9740541 Patent, University of Texas, 1997.
[28] B. Simon, J.P. Boeuve, B. Spigai and M. Broussely, *ECS Meeting Abstracts Vol.97-2*, 184, Paris, 1997.
[29] B. Simon and J.P. Boeuve, SAFT Patents, FR 94 04889 (1994), EP 0683537, US 5,626,981.
[30] T. Miyamoto, M. Touda and K. Katayama, *Proceedings of EVS13 symposium,* Vol 1, 37-44, Osaka, Japan, 1996.
[31] M. Broussely, G. Rigobert, J.P. Planchat and G. Sarre, *Proceedings of EVS13 symposium Vol* 1, Osaka, Japan, 1996.
[32] J. Beretta and D. Porcelatto, *Proceedings of 20th ElectricVehicle Symposium (EVS20*), Long Beach, USA, 2003.
[33] K. Nakai, T. Aiba, K. Hironaka, T. Matsumura and T.Horiba, *Abstract 41th Battery Symposium in Japan*, Nagoya, Japan, 2000.
[34] O. Bitsche, G. Gutmann, A. Schmloz and L. d'Ussel, *Proceedings of 18th ElectricVehicle Symposium (EVS18)*, Berlin, Germany, 2001.
[35] G. Sarre, P. Laflaquière, C. Borello, P. Ceres and P. Rena, *Proceedings of 3rd AABC Conference*, Nice, France, 2003.
[36] H. Takeshita, *23rd International Seminar on Primary and Secondary Batteries*, Fort Lauderdale, USA, 2006.
[37] M. Broussely, P. Blanchard, P. Biensan, G. Rigobert, J.L. Liska, P. Genin and F. Barsacq, *Abstracts of the 46th Battery Symposium*, 3E, Nagoya, Japan, 2005.
[38] K. Nechev, M. Saft, G. Chagnon and A.Romero, *Proceedings of 2nd AABC Conference*, Las Vegas, USA, 2001.
[39] J.A. Barnes, T.Q. Duong and D. Howell, *Abstracts of the 46th Battery Symposium*, 3E, Nagoya, Japan, 2005.
[40] T. Ikeya, H. Miyazaki, H. Kuriyama and Y. Sato, *Proceedings of 21th Electric Vehicle Symposium (EVS21)*, A1, Monaco, France, 2005.
[41] T. Horiba, K. Hironaka, T. Matsumura, T. Kai and M. Koseki, *J. Power Sources* 119-121 (2003) 893.

[42] T. Inoue, T. Iwamoto, N. Imamura, H. Yoshida and K.Kamada, *Proceedings of 5th AABC Conference*, Hawaii, USA, 2005.

[43] K. Kitoh and H. Nemoto, *J. Power Sources* 81-82 (1999) 887.

[44] T. Horiba, T. Maeshima, T. Matsumura, M. Koseki, J. Arai and Y. Muranaka, *J. Power Sources* 146 (2005) 107.

[45] J. Arai, T. Yamaki, S. Yamauchi, T. Yuasa, T. Maeshima, T. Sakai, M. Koseki and T. Horiba, *J. Power Sources* 146 (2005) 788.

[46] M. Broussely, K. Nechev, G. Chagnon, J.P. Planchat, G. Rigobert and G. Sarre, *43rd Battery Symposium, Abstracts*, Kyushu, Japan, 2002.

[47] T. Tsuchiya, Y. Nakayama, M. Motono, K. Toki and T. Matsuura, *Proceedings of 20th Electric Vehicle Symposium (EVS20)*, Long Beach, USA, 2003.

[48] K. Haraguchi, M. Nagatami and Y. Ozaki, *Abstracts of the 46th Battery Symposium*, Nagoya, Japan, 2005.

[49] R. Fulop, *23rd International Battery Seminar and Exhibit,* Fort Lauderdale,USA, 2006.

[50] T. Sekimori, *Proceedings of 3rd AABC Conference*, Nice, France, 2003.

[51] O. Shimamura, T. Abe, T. Saito, T. Itou, T. Kinoshita, K. Watanabe, H. Horie, H. Sugawara, N. Hirata and T. Miyamoto, *Proceedings of 21th Electric Vehicle Symposium (EVS21)* A2, Monaco, France, 2005.

[52] S.W. Kim, J.S. Yu, D.Y. Jung and M.H. Kim, *Proceedings of 21th Electric Vehicle Symposium (EVS21)*, Dil- B1, Monaco, France, 2005.

[53] *PNGV Battery Test Manual*, Rev. 3, February 2001.

[54] J.L. Liska, B. Lacout and P. Genin, *Proceedings of 21th Electric Vehicle Symposium (EVS21),* A1, Monaco, France, 2005.

[55] *EPRI Journal*, Fall 2005. Available on : http://my.epri.com

[56] M. Armand and M. Duclot, French Patent FR 7832976 (1978).

[57] C. Letourneau, M. Gauthier, A. Belanger, D. Kuller and J. Hoffman, *Proceedings of 14th Electric Vehicle Symposium (EVS14)*, Orlando, USA, 1997.

[58] F. Huglo, S. Lascaud and P. Angot, *Proceedings of 18th Electric Vehicle Symposium (EVS18),* Berlin, 2001.

[59] C. St-Pierre, C. Carignan, D. Pomerleau, P. St-Germain and E. Ridell, *Proceedings of 18th Electric Vehicle Symposium (EVS18),* Berlin, 2001.

[60] R.N. Bull, W.G. Bugden, S.D. Brook, R.C. Galloway and W.A. Holmes, *Proceedings of 15th Electric Vehicle Symposium (EVS15)*, Bruxelles, 1998.

[61] C.-H. Dustmann, *Proceedings of 14th Electric Vehicle Symposium (EVS14*), Orlando, USA, 1997.

[62] R.N. Bull and A.R.Tilley, *Proceedings of 18th Electric Vehicle Symposium (EVS18),* Berlin, 2001.

[63] J. Gaub and A.van Zyl, *Proceedings of 14th Electric Vehicle Symposium (EVS14),* Orlando, USA, 1997.

[64] R. Domeniconi, N. Mona, C.-H. Dustmann, R. Manzoni, M. Pulfer, *Proceedings of 21th Electric Vehicle Symposium (EVS21)*, Monaco, France, 2005.

This page intentionally left blank

Industrial Applications of Batteries. From Cars to Aerospace and Energy Storage
M. Broussely and G. Pistoia Eds.,
© 2007 Elsevier B.V.

Chapter 5

AEROSPACE APPLICATIONS. I. Satellites, Launchers, Aircraft

Yannick Borthomieu[a] and Nigel Thomas[b]

[a]SAFT, Rue G.Leclanché, BP1039, 86060 Poitiers Cedex 9, France
[b]SAFT, 12 Rue S.Carnot, 92170 Bagnolet, France

5.1. Introduction

Beside the widely distributed portable applications for NiCd, NiMH and Li Ion batteries, utilization of these high energy density power sources in high demanding applications, such as aerospace, requires a very long life, typically more than 10 years, sometimes in difficult environmental conditions. In addition, these types of battery require high reliability figures for the mission durations. Performances and cycle life must therefore demonstrate margins of use. Specific qualifications are conducted in order to demonstrate the ability of the product to sustain the requirements, which are energy or power focused.

Considering the range of aerospace applications, this chapter describes the battery products and configurations used for satellites, launchers and aircraft.

5.2. Satellite Batteries

This paragraph describes the different types of battery used on board satellites. In fact, as satellite battery designs and configurations are entirely dependant on the satellite orbits, the different types of missions and applications must be considered.

Why are there batteries on board satellites? To answer this question, it is necessary to describe the satellite configuration. A satellite is an assembly of a payload and a platform. The payload comprises all the equipment that delivers the service to the user (for example, transponders and antennae for a geostationary telecommunication satellite); the purpose of the platform is to supply all the services to the payload. The electric power is also supplied by the platform. This power supply is based on a system including solar panels, batteries and a Power Control Unit (PCU). When the satellite is in sunlight (orbit day), the solar panels provide the power to the satellite through the PCU. In addition to supplying power to the payload, the solar panels allow recharge of the batteries during daylight. When the satellite enters in the earth shadow (eclipse), as the solar panels are no longer efficient, the batteries supply power to platform and payload. Therefore, the batteries are discharged during the eclipse and recharged during the next sunlight period. This constitutes a "cycle". The number of cycles for a mission is directly dependant on the type of orbit where the satellite is located.

5.2.1. Satellite Requirements

Considering the battery constraints, three main satellite families can be considered based on the different orbits.

5.2.1.1. GEO Satellites (Geostationary Earth Orbit)

Geostationary orbits are circular orbits orientated in the plane of the earth's equator. In a geostationary orbit, the satellite appears stationary, *i.e.* in a fixed position, to an observer on earth. More technically, a geostationary orbit is a circular prograde orbit in the equatorial plane with an orbital period equal to that of the earth; this is achieved with an orbital height of 35,786 km. In practice, the orbit has small non-zero values for inclination and eccentricity, causing the satellite to trace out a small figure of eight in the sky. The footprint, or service area, of a geostationary satellite covers almost 1/3 of the earth's surface (from about 75 degrees south to about 75 degrees north latitude), so that near-global coverage can be achieved with a minimum of three satellites in orbit. By placing the satellite at an altitude where its orbital period exactly matches the rotation of the earth, the satellite thus appears to 'hover' over one spot on the earth's equator and thus appears to stay stationary over the same point.

A geostationary satellite completes one revolution in circular orbit (Figure 5.1) round the earth, every 24 hours. These satellites, however, do not see the poles at all, while geosynchronous satellites in an orbit sufficiently inclined with respect to the equatorial plane can do this. The orbital location of geostationary satellites is called the Clarke Belt in honor of Arthur C. Clarke who first published the theory of locating geosynchronous satellites in earth's equatorial plane for use in fixed communications purposes [1]. The term

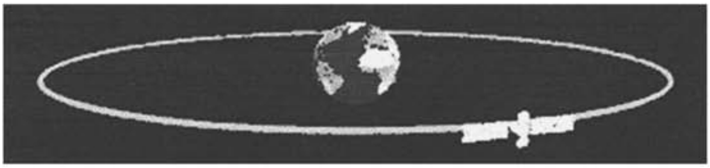

Figure 5.1. GEO satellite's orbit.

'geostationary satellite' is often shortened to 'GEO satellite'. The main disadvantage of a GEO satellite in a voice communication system is the round-trip delay of approximately 250 milliseconds due to the huge earth-satellite distance.

Due to their main characteristics (fixed position over one point on the earth), these satellites are used for telecommunications by operators that have assembled fleets covering the earth (*e.g.* direct home TV broadcasting, voice and internet: Intelsat, Eutelsat, Astra satellites). It is also important to remember that GEO satellites are used for earth observation purposes (remote sensing) in addition to communication applications: meteorological satellites are also positioned in geostationary orbits (Meteosat and NOAA: National Oceanic and Atmospheric Administration satellites).

The characteristics of this satellite can be summarized as follows:

- As the satellite rotation speed is identical to the earth's, the GEO satellite orbit duration is 24 hours.
- As a GEO satellite's position is far from the earth, and due to the inclination of the earth pole axis to the ecliptic plane, the satellite goes through the earth's shadow cone only once a day during the equinox period (2 times 45 days per year). The equinox periods (also called season) are centered on the equinox days: the 21st of March and the 23rd of September (Figure 5.2). Therefore, the number of eclipses seen by a GEO satellite per year is 90.
- The eclipse duration is not constant but increases during the first 22 days up to 72 minutes maximum (1.2 hours) and then decreases the last 22 days of the eclipse period, as seen in Figure 5.2.
- Depending on the application, the lifetime is from 12 to 18 years. This corresponds for the battery to 1,080-1,620 cycles (charge/discharge).
- Until a recent past, the GEO satellites were repositioned (to compensate the Coriolis force that makes the satellite move on to his orbit to the East) using small thrusters. The system including the gas reserve was heavy. The new repositioning system uses a new principle based on rare gas (Ar or Xe) thrusters. Using the electric power, this gas is transformed into plasma, which delivers the energy to reposition the satellite. As the repositioning

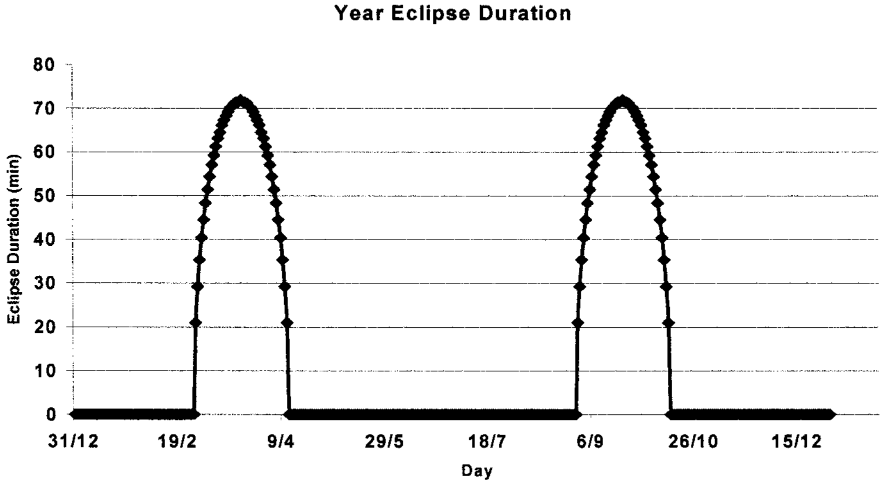

Figure 5.2. GEO eclipses duration.

could be done once or twice a day, power is consumed (including that of the battery). This system allows the weight of the gas container to be reduced compared to standard propulsion systems, but leads to an additional number of cycles for the battery.

In the last few years, thanks to the communication demands (TV mainly) the GEO satellite power has increased from 5 to 18 kW inducing an increasing size of the satellite and the battery system. Based on the power demand, the maximum depth of discharge (DOD) of such battery system is from 60 to 80%.

The key parameters for the batteries to be used in GEO missions are:

- Life duration up to 18 years.
- Maximum 1,620 charge and discharge cycles.
- Due to the available recharge time (at least 24 hours minus 1.2 hours), the charge rate is C/10.
- Due to the power and the number of cycles, the DOD for GEO satellites is from 50 to 80%.
- Discharge current, which is directly dependant on the DOD, is from C/2 to C/1.5.
- Temperature from -20 to +40°C depending on the technology.
- Use of the battery at low DOD during the solstice period for electric thrusters positioning system (once to twice a day).
- High vibrations levels in relation with launcher characteristics.
- High specific energy to reduce the weight as the battery represents a big part of satellite weight (from 10 to 20% depending on the technologies).

- High reliability.

In summary, for GEO application the battery must be designed to deliver very high energy and be cycled less than 2,000 times at high DOD for a long time (>15 years).

5.2.1.2. LEO Satellites (Low Earth Orbit)

The LEO satellites (Low Earth Orbit) use either elliptical or (more usually) circular orbits at a height from 400 to 2,000 km above the surface of the earth (Figure 5.3). The orbit period at these altitudes varies between ninety minutes and two hours. As the altitude of the LEO satellites is low, their velocity is very high (>25,000 km per hour).The maximum time during which a satellite in LEO orbit is above the local horizon for an observer on the earth is up to 20 minutes. A global communications system using this type of orbit (mainly due to low propagation delay of 20-30 ms), requires a large number of satellites, in different inclined orbits.

Satellites in LEO are affected by atmospheric drag, which causes the orbit to deteriorate gradually, and the typical life of a LEO satellite is 5-8 years. However, launches into low earth orbit are much less costly than into GEO orbit, due to the shorter distance and their much lighter weight. Moreover, multiple LEO satellites can be launched at one time whereas only two GEO satellites can be launched at one time with today's best heavy rocket.

Most of the LEO satellites (except the constellations which are used for direct telecommunication systems: Iridium™ and Globalstar™) are used for earth or space observation. The best examples of LEO satellites are the Space Telescope Hubble, the Spot family (earth imaging and survey) and military

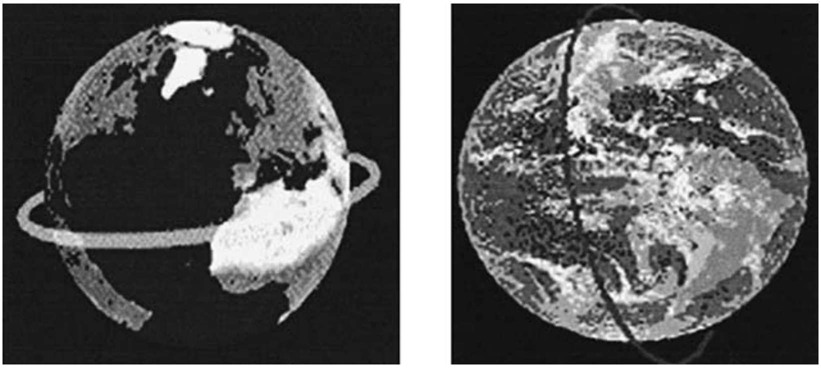

Figure 5.3. LEO satellites. On the left: equatorial orbit; on the right: polar orbit.

observation satellites.

LEO satellites can have orbits that are inclined from 0 to 90 degrees from the equatorial plane. A specific orbit, called "polar orbit", is inclined at about 90 degrees to the equatorial plane, covering both poles. The orbit is fixed in space, and the earth rotates underneath. Therefore, a single satellite in a polar orbit provides in principle coverage to the entire globe, although there are long periods during which the satellite is out of view of a particular ground station. This may be acceptable for a store-and-forward type of communication system. Accessibility can of course be improved by deploying more than one satellite in different orbital planes. Most small LEO systems employ polar, or near-polar, orbits. A particular example of a system that uses this type of orbit is the COSPAS-SARSAT Maritime Search and Rescue system. This system uses 8 satellites in 8 near-polar orbits.

The key parameters for such type of satellites are:

- The orbit duration from 90 to 120 minutes, depending on the orbit inclination.
- The number of eclipses per year from 4,500 to 5,500, depending on the satellite altitude.
- The eclipse duration from 20 to 35 minutes.
- The life time from 5 to 8 years (2 to 3 years for "small" LEO).
- Satellite power from 10 to 3,000 W.

Two main LEO satellite families can be distinguished: the "small" LEO (sometimes called nano- or micro- satellites) and normal LEO. Nano- and micro-satellites are used for scientific short-term missions and are manufactured by small companies or universities. They are the way to access space at low cost. The standard LEO satellites are more often used for earth or space observation for civil, governmental or military purposes. These satellites can have multiple detection systems such as visible and infrared cameras, X-ray detectors, *etc.*

On the battery side, the large number of charge/discharge cycles is the key point for LEO applications.

The main parameters for the batteries to be used in LEO missions are:

- Life duration from 2 to 10 years.
- Roughly 5,000 charge and discharge cycles per year; 50,000 cycles for a 10-year LEO mission.
- Charge rate close to C/3.
- Discharge rate from C/2 to C/1.5.
- Temperature range from 0 to +40°C.
- DOD from 10 to 40% depending on the mission duration and the battery technology.
- High vibration levels in relation with launcher characteristics.

It is to be noted that the battery weight is not a key factor compared to the GEO satellites, as the launch price per kg is less for LEO due to the lower altitude.

To summarize, the LEO battery application is characterized by a huge number of cycles (>25,000) with a low DOD (<30%) for a mission duration up to 10 years with an average close to 5 years.

5.2.1.3. MEO and HEO Satellites (Medium Earth Orbit and High Earth Orbit)

MEO satellites (Figure 5.4) use circular/elliptic orbits at an altitude of around 10,000 km. Their orbit period measures about 6 hours. The maximum time during which a satellite in LEO orbit is above the local horizon, for an observer on the earth, is of the order of a few hours. A global communications system using this type of orbit requires a modest number of satellites in 2 to 3 orbital planes to achieve global coverage.

MEO satellites are operated in a similar way to LEO systems. However, compared to the latter, hand-over is less frequent, and propagation delay and free space loss are greater.

One well-known example of MEO satellite application is the ICO constellation, which is composed of 10 plus 2 satellites in 2 inclined planes at 10,355 km.

HEO satellites (Figure 5.4) typically have a perigee at about 500 km above the surface of the earth and an apogee as high as 50,000 km. The orbits are inclined at 63.4 degrees in order to provide communications services to locations at high northern latitudes. The particular inclination value is selected in order to avoid rotation of the apses, *i.e.* the intersection of a line from earth centre to apogee, and the earth surface will always occur at a latitude of 63.4 degrees North. Orbit period varies from 8 to 24 hours. Owing to the high eccentricity of the orbit, a satellite will spend about two thirds of the orbital period near apogee, and during that time it appears to be almost stationary for an observer on the earth (this is referred to as apogee dwell). After this period, a switchover needs to occur to another satellite in the same orbit in order to avoid loss of communications. Free space loss and propagation delay for this type of orbit is comparable to that of geostationary satellites. However, due to the relatively large movement of a satellite in HEO with respect to an observer on the earth, satellite systems using this type of orbit must cope with large Doppler shifts.

An example of HEO is the Russian Molniya system, which employs 3 satellites in three 12-h orbits separated by 120 degrees around the earth, with apogee distance at 39,354 km and perigee at 1,000 km. (Note: for battery

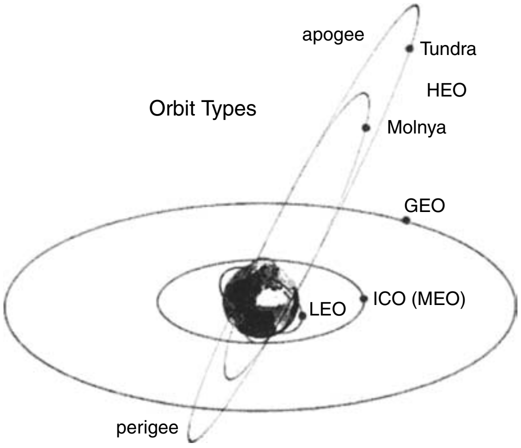

Figure 5.4. MEO and HEO orbits.

requirements [*e.g.* number of cycles, life time, DOD], MEO and HEO missions are covered by GEO products).

5.2.2. Satellite Battery Technologies

All satellites, probes and space vehicles include electrochemical generators. In most of the case (except nuclear sources used for long-term space exploration probes and the Shuttle that uses fuel cells), these systems are equipped with rechargeable batteries.

Three rechargeable systems have been qualified for space use:

- Nickel-Cadmium (NiCd)
- Nickel-Hydrogen (NiH_2)
- Lithium-ion (Li Ion)

Space applications are extremely demanding in terms of performance and reliability. Regarding performance, some of the main criteria are listed below:

- energy density
- power capability
- cycle and calendar life capability
- thermal dissipation during charge and discharge (no convection in space)
- hermeticity (in order not to contaminate the optic and electronic components)
- mechanical strength (to sustain the launch vibrations).

Reliability of the battery is mandatory, as no repair is possible, and its failure would result in a huge cost. Needless to say, developing a new cell, not to mention a new technology, and demonstrating its performance and reliability is also extremely lengthy and expensive.

5.2.2.1. NiCd Batteries

The majority of spacecraft launched since the beginning of the space era included energy storage systems composed of NiCd batteries. The reason for this can be found in the high cycle-life capability, the robustness and the relatively simple charge-control requirements of this electrochemical system. Because the reliability of the system is also good, NiCd batteries have been used for extended unmanned missions (satellites), as well as for manned missions. For satellite applications, mission length has increased up to 15 years in the last 40 years [2,3].

A large part of this success is linked to the availability of hermetically sealed cells. Originally developed for commercial purposes (mainly industrial systems for trains, subways, stationary applications, *etc.*), the earliest NiCd cells were not suitable for aerospace applications. Therefore, developments were performed by the main suppliers in order to improve the electrochemistry (to sustain long life), the processes, the cell hermeticity (to guarantee the seal reliability), the capacity ranges, and the thermal designs. By the late 1970s, cell reliability was improved based on the work performed on:

- Determination of the common failure causes.
- Understanding of the management parameters effect on the cycle-life performance (such as temperature, charge method, *etc*).
- Determination of the key manufacturing parameters, such as plate thicknesses, loadings, precharge, positive to negative ratio, separator types, *etc.*
- Establishment of the manufacturing and control procedures.

This extensive work, performed by government agencies, satellite manufacturers and cell suppliers, led to the qualification of NiCd cells fabricated with nylon separators and chemically impregnated plates. Batteries based on these cells are still in use today.

In the late 1980s, "super" NiCd cells were qualified using significant changes from the manufacturing processes point of view. The main change was the use of electrochemical impregnation for electrode manufacturing. However, this design did not encounter the same customer demand compared to the previous design.

In addition, up to end of the 1980s, NiCd batteries were the only type of battery used on board satellites as the main power source. Since then, NiCd was progressively replaced by NiH_2 technology mainly for geostationary satellites. The main reason was the low specific energy of the NiCd compared to NiH_2 and the higher DOD used.

However, NiCd has been used continuously up to now for LEO applications thanks to its robustness and cycle life: some satellites have been in operation for more than 15 years in low earth orbit with these batteries.

NiCd electrochemistry

Basic information on the electrochemistry of NiCd batteries has been given in Chapter 2. Here, complementary information of specific interest for the applications of this chapter will be provided.

Concerning the electrode manufacture, the majority of aerospace cells flown on US and European satellites have been made using the process developed by Saft to produce sintered electrodes. The plate fabrication process starts with a roll (spiral) of perforated nickel-plated steel sheet that serves as the current collector (the substrate). The steel sheet is passed through a nickel slurry and sintered in a high-temperature furnace to produce a high-porosity (>80%) nickel plaque. Several spirals are stacked on a "post" and placed in a tank in which the high-porosity plaque is chemically impregnated with nickel nitrate to form the positive plates and with cadmium nitrate to form the negative plates. Impregnation is done with a vacuum process and usually requires several cycles to obtain the desired plaque loading levels.

The impregnation is followed by a conversion of the nitrates to form hydroxides in an alkaline solution. The final step – formation – is done by charging/discharging the electrodes at high current against inert counter-electrodes.

Plate manufacturing may also be done with a dry method that uses a nickel mesh or screen for the substrate, and a dry powder sintering process. This technique uses a support to hold the powder while running through a sintering furnace. This process is less automated and does not lend itself to high volume production. Impregnation is done in small batches using processes similar to those described above.

A non-woven polyamide felt, porous to retain electrolyte and to allow permeability to OH^- and oxygen, is used as a separator. Various types of separators have been extensively studied and analyzed. Mainly the sensitivity to hydrolysis reaction in the KOH solution has been determined on different separator types such as Pellon and Karl Freudenberg products [4].

The electrolyte used in space NiCd cells is a pure solution of KOH in water at a 31% weight concentration. This concentration allows good ionic conductivity in the temperature range 0 - 40°C, typical for batteries operating in orbit.

The space “sealed” cell has an "electrolyte-starved" design and is characterized by a capacity always limited by the positive electrode.

During charge, some of the current is utilized in the generation of O_2, which is related to positive plate efficiency. On overcharge, all the current is used at the positive plate to produce O_2.

During both charge and overcharge, oxygen is recombined at the negative electrode and there is a pressure stabilization, the kinetics of which depend on charge rate and temperature [5,6]. The cell pressure increases to a level that is dependent on the recombination rate of oxygen at the negative electrode, the rate of diffusion of the oxygen through the separator, the amount of electrolyte in the cell, and the cell free volume.

Approximately 60% of the "excess" negative capacity remains when the positive plates are fully charged. This uncharged material is referred to as "overcharge protection" and is required to prevent the negative plates from becoming fully charged and generating hydrogen gas.

The remainder of the excess negative is in the charged state when the cell is completely discharged and is for over-discharge protection. This excess charged Cd is referred to as precharge [5].

Key design parameters for a “good” space NiCd cell are:

- The positive and negative electrode manufacturing, including thickness, loading, porosity.
- The electrode capacity ratio, which ensures overcharge protection and precharge level.
- The inter-electrode distance that ensures plate insulation, available quantity of electrolyte, ability of gas transfer for recombination.
- The separator composition that ensures performance for a lifetime, such as inter-electrode distance, electrolyte retention, stability in KOH.
- The seal type, which ensures perfect hermeticity of the cell over 10 years in the space environment.

NiCd cell degradation modes and lifetime reduction

The performance degradation of flight cells can be readily measured in terms of decreased discharge voltage, capacity loss, and increased overcharge voltage. The rate of degradation of these parameters is dependent on the specific application and the environment. In addition, it can be correlated to changes in, or degradation of, the positive plates, negative plates, separator, and electrolyte. Degradation processes such as separator breakdown, Cd migration and positive plate expansion are irreversible. Changes such as electrolyte redistribution and Cd crystal size may be reversible.

It is generally accepted that the rate of an electrochemical reaction in a NiCd cell doubles for every 10°C rise in temperature. Years of testing performed for NASA at the US Naval Surface Warfare Center (NSWC) at Crane, Indiana, and at ESA (European Space Agency) have characterized the effects of temperature on performance and cycle life of NiCd cells [7,8]. The generally accepted temperature for optimum battery performance is 5°C.

This temperature reflects a compromise between the low (<-5°C) temperature effects on plate charge acceptance and the high temperature effects on plate charge efficiency and nylon separator degradation [9,10].

All cell components are affected by elevated temperatures. The most readily observed effect is the decrease in charge efficiency, which is evident as a decrease in storable capacity that becomes significant above 20°C. The decrease in charge efficiency as temperature increases is generally attributed to the positive electrode. Various additives such as Co and Cd have been used in attempts to increase the charge efficiency in these conditions, with various degrees of success.

Of all the NiCd cell failure mechanisms, the degradation of the cadmium plate is the least understood. The environment is known to cause profound changes in the negative plate crystal morphology. The growth of large crystals is one of the most important factors in capacity fading and contributes to the conversion of the cadmium material - from active to inactive - with cycling. The change in crystal morphology is also thought to cause the generation and persistence of the cadmiate ion that is responsible for Cd migration.

In general, conditions that promote the formation of small crystals in the negative plates are good, and those that promote large crystals are bad. Some conditions known to promote the formation of large crystals include open circuit stand, low discharge rates, and high temperature. Conversely, conditions that promote small crystals are prolonged low charge rates, high discharge rates, and low temperature.

Other factors influencing Cd migration are the mechanical compression introduced into the plate stack during cell assembly, compression used in the fabrication of most batteries, and expansion of positive plates with cycling. A well-designed cell will have a minimum permissible inter-electrode spacing.

The other degradation mechanism which occurs with nickel electrodes is the so called "memory effect". This effect is encountered during cycling at constant DOD (mainly in LEO application): a voltage drop (up to 50 mV) appears when the DOD is limited [11,12].

NiCd cell technology

At the start of the satellite era, the first NiCd batteries used low capacity cylindrical cells. These cells have been modified, with respect to the standard consumer use design, at the can and terminal levels. The need to increase the capacity has led to the development of prismatic NiCd cells. [6]

The sealed prismatic NiCd cell is constructed of positive plates (nickel oxi-hydroxide electrodes), negative plates (cadmium electrodes) and a separator material. Figure 5.5 details the design of a space cell. The plates are connected to the respective cell terminals, which are attached to a cell cover and inserted in a steel case and welded shut. The electrolyte is added through the "fill tube". The stainless steel case is equipped with two insulated feed-through terminals made with fully hermetic systems using in most cases metal welded ceramic materials.

NiCd battery designs

It is hard to give a detailed state of the art of the NiCd battery designs, as each battery is custom made in accordance with the satellite requirements. Since the 1960s, battery designs have evolved mainly from the capacity point of view: at the start of the space era, NiCd capacities were close to 5 Ah, but increased up to 50 Ah in the 1990s.

In fact, the battery must fit the satellite specification. The main points are:

- The mission type (satellite orbit) determines the use of the battery in terms of number of cycles and DOD. For example, as described previously, 25,000 LEO cycles (5 years) lead to a maximum DOD close to 20%, whereas a 10-year GEO mission corresponds to 50% DOD.
- The satellite bus voltage determines the number of cells placed in series within the battery. The selected power system used at satellite levels (unregulated voltage bus, limited voltage bus and regulated voltage bus) acts directly on the required voltage range of the battery.
- The orbit and eclipse durations allow calculating the charge energy, given by the solar panels, and the discharge energy taking into account the eclipse duration and the average power needed by the satellite (payload and platform). The energy need determines the cell capacity taking into account the DOD.
- The position of the battery within the satellite with respect to its centre of mass is critical, as the battery is one of the heaviest items of the spacecraft. This imposes a specific volume (footprint) and weight. The mass limitation represents a constraint particularly for GEO satellites. In addition, relatively few locations are available for the radiators that are required to control that the temperature is in the range ensuring the mission life (just above 0°C). The heater circuits are directly linked to the power capability and the thermal environment.
- The charge method has to be properly chosen among different possibilities:

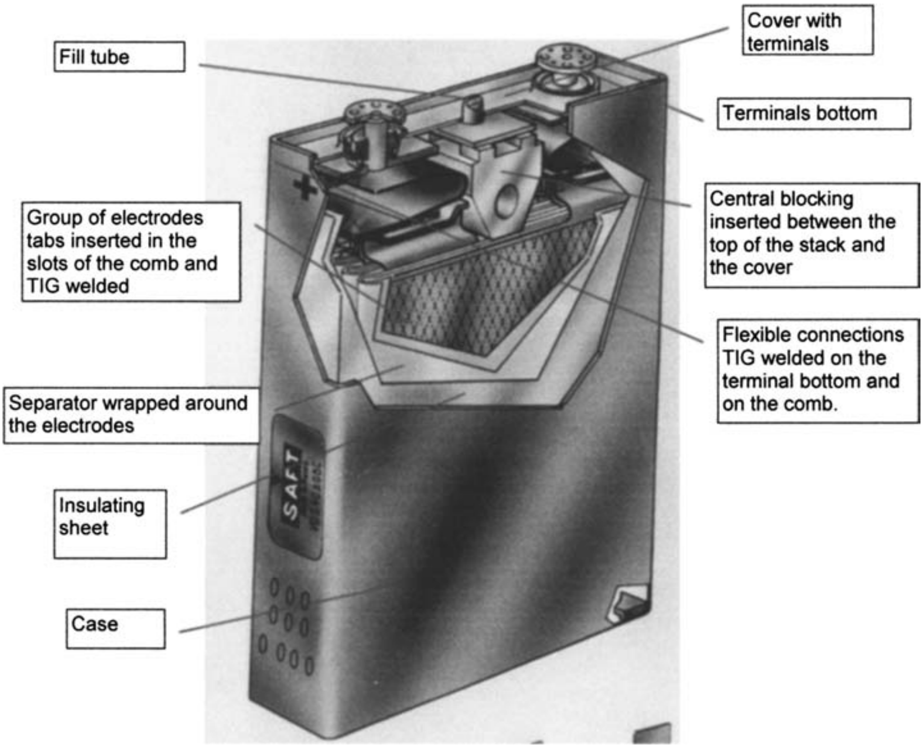
Fill tube
Cover with terminals
Terminals bottom
Group of electrodes tabs inserted in the slots of the comb and TIG welded
Central blocking inserted between the top of the stack and the cover
Flexible connections TIG welded on the terminal bottom and on the comb.
Separator wrapped around the electrodes
Insulating sheet
Case
SAFT
+

Figure 5.5. Prismatic NiCd cell (Saft).

semi-constant current, timer-control, temperature detection, -ΔV detection, trickle charge, *etc.* (see also Chapter 2).

- The mechanical constraints linked to the launcher type, satellite design, the battery position and the vibration spectrum.
- The failure modes and protection requirements.

Designed in the 1990s, the NiCd battery presented hereafter as an example is based on a battery concept developed by Saft, widely used for geosynchronous missions up to the 1990s and still used for low-earth orbit application. This battery is a standard 24 VOS40 used on the Spot 4 satellite family. It is composed of 40-Ah space NiCd cells (VOS) connected redundantly in series with tin soldered connectors (Figure 5.6). The cells are arranged in two rows of 12 cells each, separated by thermal collectors, and are maintained between two rigid end plates, which are secured with four tie rods (Figure 5.7). The connectors are attached to one end plate. The thermal collectors transfer excess of heat generated by the cells to the radiator base-plate.

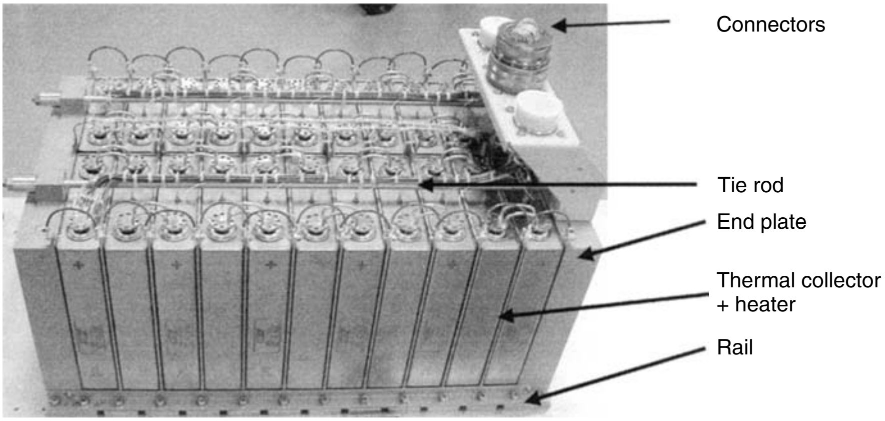

Figure 5.6. 24 VOS40 battery (Saft). rit e centrare

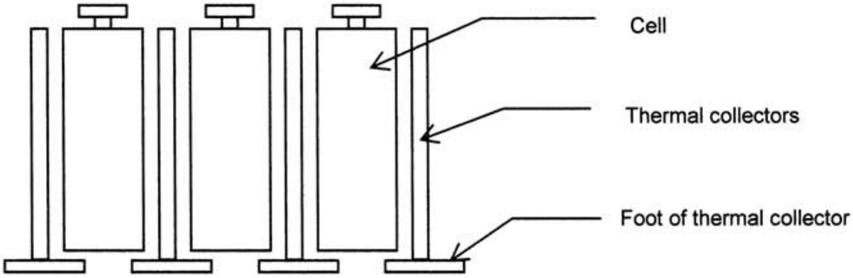

Figure 5.7. Thermal design for the battery of Figure 5.6.

The series production battery 24 VOS40 AGBC is equipped with heaters split in two groups of 11 and 13. Battery temperature is monitored by one thermal sensor located on the cover of a central cell.

In order to ensure electrical insulation, a Kapton sheet is glued on each thermal collector, between collector and cell.

This design leads to the following battery characteristics for LEO applications:

- voltage range: 24 to 36 V with 28 V average
- capacity: 46 Ah
- specific energy: 30 Wh/kg
- dimensions: 464 x 260 x 260 mm
- weight: 47 kg.

This type of battery has already demonstrated more than 10 years of operation in LEO applications.

NiCd technology advantages

NiCd has been used since the beginning of the space industry. Even though the specific energy is low, other performances are outstanding and the cell can be made extremely reliable mainly in LEO. NiCd is extremely rugged, operating in a wide temperature range. The cell management is simple and can be easily done at satellite level. The reliability is very high and the technology enjoys an incomparable heritage highly praised by the space industry. NiCd is still used in LEO and has already been selected on ATV programs up to 2012 and more.

5.2.2.2. NiH_2 Batteries

The majority of spacecraft launched in GEO since the mid-1980s included energy storage systems composed of Nickel-Hydrogen batteries [13].

This technology was discovered in the 1950s in the USSR, but real developments were initiated in the USA by Comsat/Intelsat only in the early 1970s [14]. The first western satellite that used NiH_2 was a LEO NTS-2 launched in June 1977. Ford Aerospace agreed to replace NiCd batteries with NiH_2 batteries on Intelsat V [15]. Launched in 1983, Intelsat V was the first commercial communication satellite to use NiH_2 batteries. Since then, more than 300 GEO satellites have been launched with this battery. The main reason of the technology change is linked to the increase of the specific energy: 50-55 Wh/kg, about twice that of NiCd. In addition, it has been demonstrated that the DOD can be increased up to 70-80 % compared to a limit of 50 % for NiCd. The weight saving on the battery has been the main reason for the technology change mainly for GEO applications for which the launch cost on a weight basis is roughly two to three times that in LEO.

It can be outlined that during the 1970s and 1980s, more than four US companies were supported by Comsat and Air Force to develop this new technology: Eagle Picher Technology, Hughes Aircraft Company, Yardney and Gates Aerospace Batteries. Later in Europe (since the early 1980s), at least three battery companies started NiH_2 cell development: Saft, BAE and Daimler. In Japan, Toshiba also tried to develop this technology. In Russia, it seems that two battery companies developed and qualified this technology: Istochnick and Saturn. Most of the Russian satellites used batteries from these two suppliers.

In the middle of the 1990s, only three suppliers remained in this market: Eagle Picher, Saft and Saturn. All the others have disappeared mainly due to profitability figures, except Hughes Aircraft Company (now Boeing Satellite

System), which continues the manufacturing of NiH_2 only for its own satellites. Saft acquired Gates Aerospace Batteries and Yardney stopped this activity due to technical problems. The others stopped also as they could not get a sufficient "flight experience" to stay in the market.

NiH_2 electrochemistry

The NiH_2 cell utilizes a NiOOH positive electrode and a lightweight H_2 electrode as a negative electrode. More details will be given here with respect to the description of Chapter 2.

Positive electrode

The sintered positive electrode is obtained by impregnation of a porous sintered nickel plaque with the active material: nickel hydroxide. Two methods are used to fabricate the sintered plaques:

- dry powder: a sandwich is made with some nickel power put on both side of a pure nickel wire mesh screen. This sandwich, positioned on a mould, is transferred into the sintering furnace using a mesh belt. The temperature in the sintering zone is 800 to 1000 °C in reducing atmosphere (H_2 and N_2) to avoid nickel oxidation;
- wet slurry as per NiCd.

The main difference *vs.* the NiCd cell is the process used to fill this porous structure. While NiCd uses a chemical impregnation process (CI) deposition, here the nickel hydroxide is deposited using an Electrochemical Impregnation process (ECI). The ECI process leads to a more uniform filling of the sinter as the impregnation takes place from the middle to the surface, the opposite of the chemical process that fills the sinter from the surface to the middle. The loadings are accurately controlled and more uniform with ECI. In addition, the sintered nickel corrosion that occurs during the CI process is reduced with ECI as the sintered plaques are cathodically polarized. Therefore, the ECI electrode performance is better than that of CI because of:

- Higher specific capacity, due to higher utilization of the active material.
- Less swelling in lifetime as the rate of plaque expansion with cycling is four times higher with CI plaques compared to ECI plaques.

Two types of ECI have been used:

- Aqueous process (Bell Laboratories process): the impregnation bath uses an aqueous-based nickel nitrate solution [16].
- Alcoholic process (Air Force process): the impregnation bath uses an alcohol-based nickel nitrate solution [17].

The electrode shape is pineapple slice in order to fit the cylindrical container. It can be noted that some electrode structures are also made with Ni foam or fiber.

The electrochemical reaction at the positive is the same as in NiCd.

Negative electrode

The negative electrode is the product of fuel cell technology. It consists of a Teflon-bonded platinum black catalyst supported on a photo-etched Ni substrate grid. A hydrophobic Teflon backing is added to the Pt electrode to stop H_2O or electrolyte loss from the back of it during charge or overcharge, while allowing diffusion of H_2 and O_2 [18].

It uses the principle of the hydrogen electrode that oxidizes hydrogen to water in discharge and reforms gas during charge. The hydrogen is stored in a container supporting high pressures.

Separator

Two types of separators materials are used for NiH_2 cells:

- Asbestos: fuel-cell grade nonwoven asbestos has been used on the first generation of NiH_2 cells in the USA. This type of separator is still in use in Russia, but US manufacturers stopped using it due to health safety concern.
- Zircar: Zircar fibrous ceramic separator is available in textile forms composed of zirconium fibers stabilized with yttrium. This type of material has good chemical resistance, excellent mechanical properties in compression and a low oxygen bubble-through pressure. The Zircar separator has been used in one or two layers; today, the two-layer configuration is the standard.

Stack design

Two basic types of electrode stack designs have been used [18,19]:

- The still used back to back design (see Figure 5.8): two positive electrodes are positioned back to back. Two separator layers are placed on either side of this pair of electrodes. Two negative electrodes are also placed back to back (the Goretex membrane face to face) with a plastic gas diffusion screen positioned in between. This pair is then placed on the separator layers. This assembly constitutes one module of the electrode stack.
- The re-circulating design: one module consists of a gas screen, a negative electrode, a separator layer and a positive electrode, as shown in Figure 5.9.

It is recognized that the re-circulating design is more sensitive to popping phenomena, which occur at end of charge. Popping is a non-controlled oxygen recombination reaction that leads to a micro-explosion. Therefore, the selection of the back to back design is now preferred.

Electrolyte

The standard electrolyte is a pure solution of KOH in H_2O at a 31%

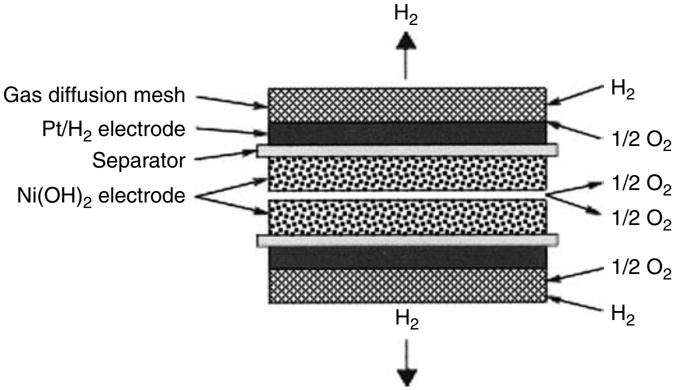

Figure 5.8. NiH_2 cell: back to back design.

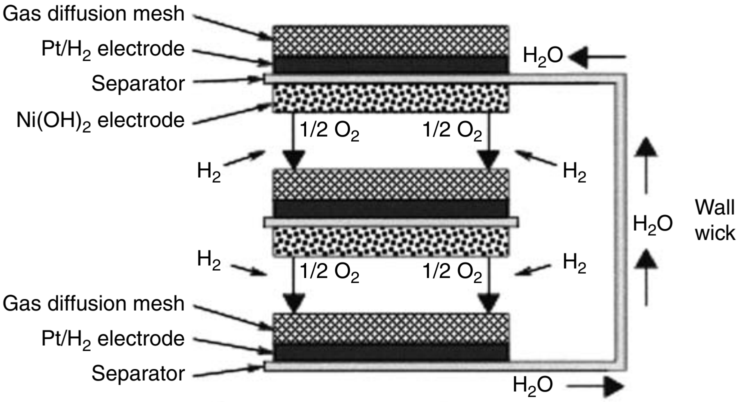

Figure 5.9. NiH_2 cell: re-circulating design.

weight concentration. For some LEO applications, the concentration has been lowered to 26 % to ensure long LEO lifetime.

NiH_2 cell designs

All NiH_2 cells are pressure vessels as they contain H_2 at high pressure [20]. The H_2 produced in charge is stored in a sealed container. So as not to oversize this container, the envelope or pressure vessel is designed to resist high pressures, up to 70 bars. Inconel 718 material is used to avoid too heavy a container. The Inconel wall is 0.6 to 0.8 mm thick. The structure can be constructed with:

- one or two hydro-formed spherical or hemi-spherical domes
- one cylinder only or one cylinder with dome.

In fact, depending on the design, the dome and the cylinder can be one mechanical part. So, one TIG (Tungsten Inert Gas) weld around the circumference is done to assemble the cylinders with spherical end with the dome or two TIG welds are done to assemble the two domes on the cylinder. Figure 5.10 shows a design with two domes and two circumferential welds. Terminal locations are positioned at both ends of the cell (axial design) or on the same dome (rabbit ear design, as shown in the figure).

The circumferential weld includes a weld ring supporting the stack of electrodes. With two welds, the stack is maintained at both ends by two end plates, also manufactured with Inconel, for reasons of stiffness, or with polysulfone. The electrode stack components (positive, negative electrodes, separators and gas screens) are assembled onto a polysulfone central core attached to the end plates. This core provides electrode alignment during assembly, position of the stack within the pressure vessel, structural support and conduits for the positive and negative electrical tabs. Belleville washers provide a constant force on the electrode stack by accommodating the positive electrode swelling during the lifetime.

The inside walls of the pressure vessel are plasma sprayed with zirconium oxide to form a wall wick that is in contact with the Zircar separators. This junction allows the electrolyte to be exchanged between the other pairs of electrodes.

Two types of terminals have been used:

- a compression seal with a formed Teflon bushing compressed between the dome-cylinder seal area and the terminal boss with the ceramic washers
- a ceramic seal with a brazed ceramic-to-metal system, which is similar to the one used in NiCd cells.

The first cell designs were qualified using a 3.5 inches (88.9 mm) diameter [21]. Capacity has been adapted by changing the number of electrode pairs. For example, the first Intelsat V cells used 24 electrodes for each polarity and delivered 30 Ah. The 3.5 inches capacity range is from 30 to 110 Ah. Other diameters have been qualified afterwards: 2.5 inches (63.5 mm) cells for low earth orbit applications, 4.5 inches (114.3 mm) to provide the range 100-220 Ah and finally 5.5 inches (139.7 mm) cells to cover the range from 250 to 350 Ah. All these cell designs are named IPV (Individual Pressure Vessel).

Some CPV (Common pressure vessel) or DPV (Dependant Pressure Vessel) designs have been used in orbit [22,23]. CPV includes 2 separate stacks of electrodes using "common" hydrogen. That leads to a 2-cell battery which

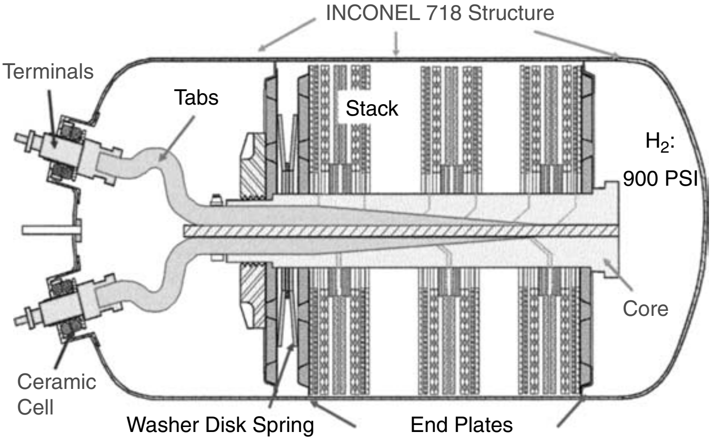

Figure 5.10. Saft NiH_2 cell.

delivers a mid–discharge voltage close to 2.5 V instead of 1.25 V for the IPV. The DPV uses the same principle with 20 to 24 separate stacks of electrodes (enclosed in plastic bags equipped with gas exchange valves): it replaces a full battery. The container diameter is higher than 25.4 cm (10 inches). The key point for these systems is to avoid stack electrolyte exchange with some physical barrier while having the same hydrogen content.

During charge, oxyhydroxide is formed at the positive electrode and hydrogen is produced at the negative (see reactions in Chapter 2). As H_2 is produced in a sealed container, the internal pressure increases to 65-70 bars. It should be mentioned that the cell structure sustains the end-of-charge pressure with a safety factor from 2.5 to 3. During cell manufacturing, burst tests are performed to demonstrate the safety factor.

As in NiCd cells, during overcharge, when the positive electrode is fully charged, O_2 only is formed at the positive. During both charge and overcharge, oxygen is recombined at the negative electrode: there is a pressure stabilization, whose kinetics depends mainly on the charge rate and temperature.

The recombination reaction leads to heat production and can lead to popping, *e.g.* a micro-explosion due to the spontaneous reaction of oxygen and hydrogen when concentrations reach the combustible range. This explosion can destroy the electrodes and lead to short circuit. To avoid such phenomena, oxygen diffusion through separators must be high enough to prevent oxygen bubble formation.

Two precharge types can be set-up in NiH_2 cells:

- Negative precharge: a hydrogen precharge cell is in fact a positive-limited cell. The positive electrode is fully discharged when the cell voltage reaches 0 V. On reversal, hydrogen is produced at the positive electrode and consumed at the negative electrode following the normal operation. The cell can continuously operate in the reversal mode without pressure build up.
- Positive precharge: a positive precharge cell corresponds to a negative-limited cell. When the cell is fully discharged, no more hydrogen is available. During the reversal of a positive precharge cell, oxygen is produced at the negative electrode until the positive is fully discharged. This oxygen is consumed when the cell is recharged. It is not recommended to push a positive precharge cell into reversal because oxygen can react with platinum, which can dissolve.

NiH_2 cell degradation modes and life reduction

The performance degradation of flight cells can be readily measured in terms of decreased discharge voltage, capacity loss, and increased overcharge voltage. The rate of degradation of these parameters is dependent on the specific application and the environment, and it can be correlated to changes in, or degradation of, the cell behavior. The following degradation or failure modes at cell level can be listed [24,25].

Positive electrode

Capacity reduction of the positive electrode can be linked to a second plateau appearance. This is often due to bad storage conditions (high temperature and/or low voltage). Cobalt, present in the positive as a conductor, may dissolve leading to cobalt segregation in the electrode [26]. As the cobalt concentration is more reduced at the interface, the insulating layer formed there induces a high voltage drop before complete discharge. So, part of the capacity is recovered at low voltage (close to 0.8 V).

The positive electrode can affect the cell performance due to the electrode thickness increase. The structural changes that occur in the active material during charge (mainly γ phase formation, instead of β) and discharge lead to a permanent electrode structure increase. High loading, bad hydroxide distribution and low stiffness sinter can lead to high growth. The change of thickness leads to porosity changes that can modify the electrolyte distribution leading to dry-out phenomena. Internal impedance increase and capacity reduction are the consequences of the dry-out. High impedance leads to mid-discharge voltage and end-of-discharge voltage reduction, which may have an impact at the satellite power system level.

The third type of degradation seen at the positive electrode is a corrosion that occurs with the time. Nickel from the collector reacts with KOH and is transformed into nickel hydroxide. Therefore, the total active material increases. However, as this active material is exclusively formed by pure

$Ni(OH)_2$, part of the additional capacity is recovered at low voltage by increasing of the second plateau capacity.

Negative electrode

The negative electrode can be degraded by the above-mentioned popping phenomena, which always occurs during cell activation, when porosity is created within the separator by expelling the excess electrolyte with the oxygen gas flow. Popping damage leads to a small amount of localized combustion holes in the negative electrodes. Normally, after the activation process, the popping stops. Some huge popping events have been reported linked to bad electrolyte distribution, which can induce electrode fracture. In most cases, a hard short circuit is formed due to the contact of broken pieces of the two electrodes.

Stack

Concerning the performance degradation, the electrolyte quantity and distribution act as key factors. The large free volumes and the distances between the electrode stack and the vessel walls can induce a high temperature gradient. With an internal gradient of 5-7°C, evaporation/condensation phenomena can occur. Therefore, some water is found outside the stack (most often in the domes) and the electrolyte concentration increases, leading to positive electrode ageing and internal impedance increasing. To avoid or reduce this phenomenon, some ZrO_2 wall wicks have been used to provide a return path for the lost water or electrolyte to the stack.

Container

NiH_2 cells are designed to operate at high pressures when fully charged: as already mentioned, the end-of-charge pressure (EOCP) can reach 60 to 70 bars. All of the cells are proof-tested to 1.5 times the MOP (maximum operating pressure) and a burst test is performed on two Inconel structures. However, the long-term mission operation can lead to hydrogen leakage, which can occur in the circumferential weld area and/or the terminal weld zone. H_2 leakage leads to a pressure decrease, but also to a capacity reduction.

NiH_2 battery designs

NiH_2 battery design is directly linked to the satellite platform, the power requirements and mission type. The maximum DOD is specified for GEO and LEO applications:

- GEO: 10 to 15 years for discharges at 50 to 80% DOD
- LEO: 3 to 7 years for discharges at 20 to 40% DOD.

The satellite power control unit determines the number of cells depending on the voltage range. In addition, the platform type gives the allowable volume for the batteries [27].

NiH_2 batteries utilize a base-plate with holes/alveolus to position the cells. The base-plate is made from anodized aluminum. The cells are supported with cylindrical aluminum or graphite/epoxy (for weight saving) mounting sleeves. A layer made from RTV or Kapton sheet and adhesive (solithane) allows the cell to be mechanically restrained during the launch vibration, to be electrically insulated from the battery structure, and to conduct the heat generated by the cell to the base-plate. Key parameters are the layer conductivity, the thickness and the interface characteristics. The sleeve design must withstand the stress resulting from the pressure vessel expansion, as the pressure increases when the cell is charged.

The sleeves are fixed onto the base-plate using screws or specific adhesive. Figure 5.11 shows the Saft battery design. The sleeve mounting design ensures two electrical insulation barriers from the cell to the base-plate. The electrical connections are made with Cu or Al wires or bus bars. The connections are attached to the terminal studs. A power connector allows the battery to be charged and discharged.

The electrical design also includes individual cell voltage wires for checking the battery health by telemetry. A few cells are equipped with

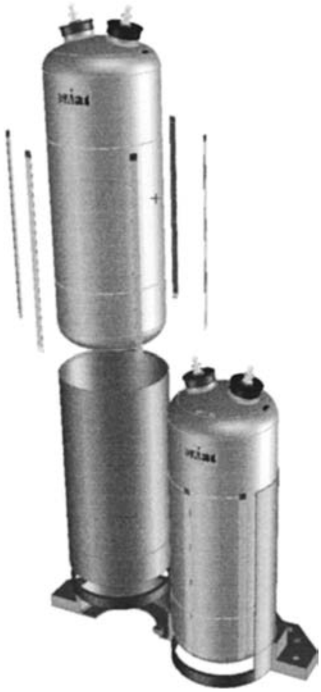

Figure 5.11. Saft NiH_2 battery design.

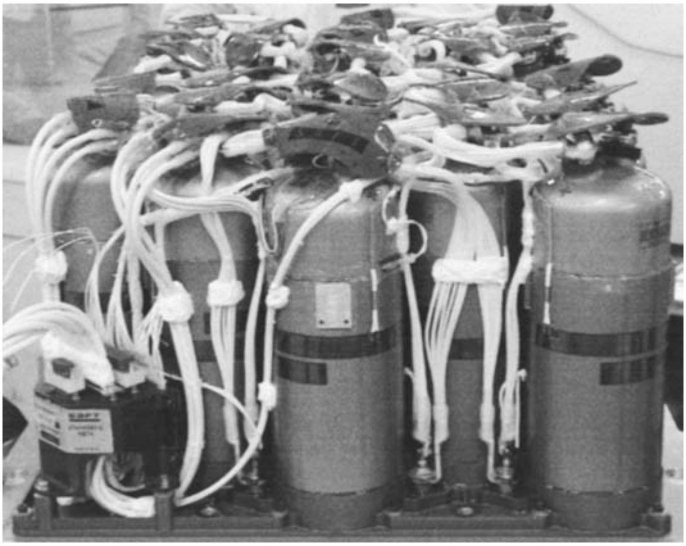

Figure 5.12. NiH_2 battery (Saft) with the auxiliary parts.

thermocouples for temperature management performed with heaters positioned on each cell. The pressure is monitored with temperature compensated strain-gauge bridges mounted on the dome of 3 to 4 cells. Specific connectors for telemetry signals are used.

Each cell is equipped with a by-pass circuit to avoid open circuit failure, which can occur in case of H_2 leakage. The charge protection is provided by three silicon diodes in series (u=2.3 V) and the discharge protection is provided by one or two Shottky diodes (u= -0.7 V).

Figure 5.12 is a photograph of a battery showing the diodes, connectors, sleeves, wires and heater circuit.

5.2.2.3. Li Ion Batteries

Until the recent past, geostationary communication satellites used the current NiH_2 technology. The size of these satellites, and consequently the power demand during eclipses has been continuously growing since the 1980s. By the early 1990s, the average satellite weight was 2 tons for a power demand in the range of 2 to 3 kW. Today the average weight is at least 5 tons for a 10-kW power demand or more.

The satellite manufacturers have planned to build 15-30 kW satellites for 2006-2007. An example is Alphabus, the next generation satellite that is under development in Europe (up to 25 kW).

A NiH_2 battery for a 20-kW satellite weighs at least 700 kg. The complete battery will soon reach the critical weight. Considering the launch price per kilogram into GEO orbit, the battery is a strategic and key component. Moreover, the use of NiH_2 batteries is limited to the range 14-16 kW due to the high thermal dissipation.

The overall work done with CNES/ESA/Alcatel Alenia Space and EADS-Astrium in the frame of the Stentor project, started in 1996, demonstrated the usefulness of Lithium-ion for GEO satellites (a Saft battery was used).

The commercial satellites WA3 and Amazonas, launched in 2004, were really the start of the new battery technology era for GEO communication satellites.

For LEO, the approach has been to use micro satellites. Indeed, ABSL technology (previously AEA) provided low power batteries for short-term mission satellites: STRV and Proba 1.

Li Ion can be considered the best battery technology for this application, due to its numerous advantages compared to the two other space technologies, NiCd and NiH_2. The main advantage is the weight reduction of the battery system due to a specific energy higher than 125 Wh/kg, whereas the maximum achieved with NiH_2 is 60 Wh/kg. At battery level, the weight reduction is more than 40%. More than 350 kg weight saving is expected on a 20-kW satellite.

The second advantage is a further weight saving linked to the lower thermal dissipation and higher faradic efficiency of Li Ion compared to NiH_2. These characteristics impact on the solar panel and radiator sizes: at least, an additional 5-10% of the weight can be saved.

Self discharge of Li Ion is very low compared to NiH_2: 0.03%/day *vs.* 10%/day. Therefore, management of the state of charge on satellite during integration, launch pad operations and solstice period is easier. The lower self discharge allows launch operations to be simplified by avoiding battery recharge when the satellite is installed on the launcher. The high NiH_2 self discharge imposes recharge of the battery up to the final countdown: this operation is a critical phase of the launch mainly because of the thermal management of the battery.

In addition, the memory effect observed in NiCd and NiH_2, which affects the cycling performance of such batteries, does not exist in Li Ion. So, in-orbit management can be simplified as the reconditioning operation necessary for NiH_2 can be cut out by using Li Ion.

Table 5.1 summarizes the advantages and drawbacks of the Li Ion technology versus the two current ones.

Table 5.1. Advantages and drawbacks of the Li Ion technology *vs.* NiCd and NiH_2.

	NiCd	NiH_2	Li Ion	System Impact
Specific energy (Wh/kg)	30	60	125	Weight saving
Energy efficiency (%)	72	70	96	Reduction of charge power: solar panel
Thermal power (scale: 1-10)	8	10	3	Reduction of radiator, heat pipes sizes
Self discharge (%/month)	10	80	1	No trickle and simple management at launch pad
Temp. range (°C)	0 - 40	-15 - 20	10 - 35	Management at ambient
Memory effect	Yes	Yes	No	No reconditioning
Energy Gauge/ Monitor	No	Pressure	Voltage	Better observability of SOC
Charge management	CC	CC	CC CV + balancing	Balancing system needed
Modularity	No	No	Yes	One cell design, ability to put cells in parallel

The impacts at satellite level are visually presented in Figure 5.13.

Another major advantage of Li Ion is the direct relationship between SOC and OCV. This characteristic induces two specificities:

- The voltage is used as a precise energy gauge that allows the state of charge of the battery to be known exactly at any time of the mission. In NiH_2, strain gauges are used (as the cell pressure increases with charge) to give a rough order of the state of charge.
- The cells can be directly assembled in parallel giving high battery modularity.

The only drawback of the Li Ion is the need of a more sophisticated electronic system for battery management.

The numerous advantages of Li Ion compared to the two current Nickel technologies lead to an increasing number of satellite projects adopting Li Ion batteries as baseline power source. All satellites manufacturers have already adapted their platforms to the characteristics of this new electrochemical couple.

Li Ion electrochemistry

The electrochemical properties of the Li Ion system are described in detail in Chapter 1. Some properties of special interest for space applications, particularly satellites, are discussed here.

There is indeed a variety of electrochemical systems in the Li Ion concept, which have quite different properties and may, or may not, fulfill the specific requirements of these highly demanding applications. The systems

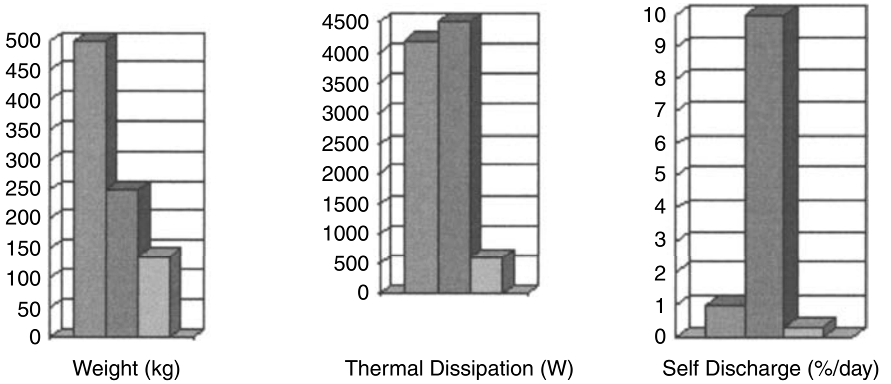

50% weight saving vs. NiH_2 Radiator size reduction Simplified launch operation

Figure 5.13. Comparison of the three satellite battery technologies (for 8 kW satellite power). *Left bar*: NiCd; *center*: NiH_2; *right*: Li Ion. The advantages of Li Ion are outlined.

dedicated to satellites are based, at present, either on $LiCoO_2$ positive material, associated with graphite or hard carbon, or a mixed Ni-based oxide, $LiNi_xCo_yAl_zO_2$, associated with graphite.

Positive materials

$LiCoO_2$ is used in cells built in France, Japan and USA. Thanks to the material's ability to release ~0.5 Li per mole, and oxidize half of the cobalt to the tetravalent state, the resulting specific capacity is ~140 Ah/kg, and the capacity density is ~690 Ah/L. However, for very long life applications, this material suffers from some dissolution and degradation at temperatures higher than 30°C, causing capacity loss on storage. This type of material is therefore more suitable for short missions.

$LiNiO_2$ has a higher specific capacity (up to 200 Ah/kg). It has been investigated at Saft since the early days of Li Ion for space use in the context of the Stentor project (European technological satellite) [28]. Cheaper than cobalt, it is a better candidate for large batteries. However, this material was much more difficult to synthesize, and had some drawbacks: less stable in overcharge conditions, which increases the potential hazards on abuse, and with a lower voltage. Research work in the past years has been focused to mixed oxides and $LiNi_xCo_yAl_zO_2$, has been selected for the present definition of Saft's space Li Ion batteries, and is now available in large industrial quantities [29].

The amount of Li that can be extracted from the Ni-based oxide is larger than from $LiCoO_2$, producing larger capacities. However, the efficiency during the first charge is less than 100%, and an excess of Li is created, stored in the carbon of the negative electrode. As Li loss from the negative due to oxidation by the electrolyte is one of the aging phenomena during cell life, this excess, of about 12%, is extremely useful to extend the battery life.

Negative materials

Several types of materials (coke, hard carbon, graphite) either well crystallized or amorphous have proved to be able to insert lithium, thus being candidates as negative electrodes in Li Ion cells. Graphite, whose specific capacity is higher, is used in most space applications. The surface characteristics are very important, as they govern the properties of the passivation layer that builds at the interface between electrolyte and carbon. This layer, which protects the negative against further oxidation, is a key point of the technology. When materials are properly selected, an outstanding long life can be obtained, on both cycling and storage. Saft has discovered the very positive properties of an additive to electrolyte, vinylene carbonate (VC), able to improve the properties of the passivation layer [30,31].

Electrolyte

The electrolyte in Li Ion for space cells does not differ from that used in other applications. Each manufacturer has its own specific formulation, which may be adapted to the nature of the active materials. As an example, Saft electrolyte in Ni-based cells for space consists of a PC/EC/DMC 1M $LiPF_6$ solution, with VC additive. The composition of the electrolyte and its purity are key factors to ensure long battery life.

Electrode design

Because of the lower ion mobility in the organic electrolyte media, Li Ion cell technology requires relatively thin electrodes (less than 0.2 mm). They are made by coating with a slurry a thin metallic sheet, which serves as a current collector and electrode support. The slurry is made of a mix of active material powder, appropriate binder, and an additional conductive powder. Most of the batteries are simply made by winding the two electrodes together, separated by a thin separator made of microporous polypropylene or polyethylene (~25 microns thick).

In spite of the fact that these cells are not pressurized, a sufficient mechanical strength is desirable, therefore a cylindrical design is more suitable for large cells.

A high power design will necessitate thinner electrodes of larger surface, *i.e.* more separator, electrolyte, and current collector. Appropriate tabbing ensures current collection with minimum power loss. On the other hand, maximum energy density will be obtained with thicker electrodes, thus reducing the amount of non-active materials in the same volume.

Satellite Li Ion cell designs

The Li Ion cells used onboard satellites have capacities ranging from 1.5 to 100 Ah. In fact, true space cells have been specifically developed and qualified taking into account space requirements. This is what has been done by Saft, JSB and Yardney. Even though the designs are quite different, the development phases were similar. Existing industrial designs have been adapted to space requirements: specific terminal designs have been qualified, specific tabs, cans, welds have been studied.

Two types of cell shapes have been evaluated:

- the generic cylindrical cell
- the prismatic or elliptic prismatic cell.

Key points for space cells are:

- the terminals, which must ensure a total hermeticity for the mission duration
- the stack support in the container to withstand the vibration levels (during the launch phase).

Two examples of different space cell structures are described hereafter.

The Stentor GEO program was the first opportunity for Saft to fly a Li Ion battery as the main power source of a satellite (Figure 5.14). This experimental program, funded by the French Space Agency CNES, was dedicated to validating new technologies. The Stentor battery used the cell developed in France for electric vehicles and adapted to space applications. The VES140 delivers 140 Wh (40 Ah) with a specific energy close to 125 Wh/kg. $LiNi_xCo_yAl_zO_2$ is the positive and graphite is the negative electrode. The container comprises a cylinder with two welded covers that support the terminal. This cell has been extensively ground tested from the mechanical, thermal, electrical, radiation and cycling point of view. It has been launched for

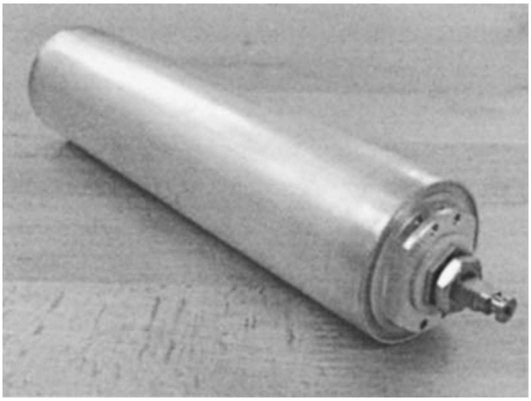

Figure 5.14. The VES140 Li Ion cell (Saft).

the first time on board an ESA satellite (SMART1), in September 2003, and is the base-line for the main GEO platforms.

The second type of space cell has been developed by GS Yuasa Technology (formerly JSB, Japan Storage Battery) and sold by Melco. This is an elliptic prismatic cell of 360 Wh (100 Ah) with a specific energy close to 140 Wh/kg (Figure 5.15). This cell uses $LiCoO_2$ as positive and graphite as a negative electrode; the case is made with an aluminum alloy. It has been launched for the first time in 2003 on board SERVIS1, a Japanese experimental satellite; in 2005, it was on board the IPSTAR satellite manufactured by Space System Loral.

These high-capacity cells are mainly built for GEO satellites needing high power.

It should be mentioned that commercial cells have also been used for satellite applications. The work done by ABSL (previously AEA) is a typical example. ABSL supplies large batches of small capacity (1.5 Ah) cells in the 18650 format manufactured by Sony ($LiCoO_2$ positive material with a hard carbon negative). Batteries made with these cells are mainly for low power LEO satellites (micro- and mini-satellites).

Li Ion cell degradation modes and life reduction

As mentioned before, battery life is of paramount importance in space application. Knowledge of degradation mechanisms is therefore mandatory to assess the service duration [32].

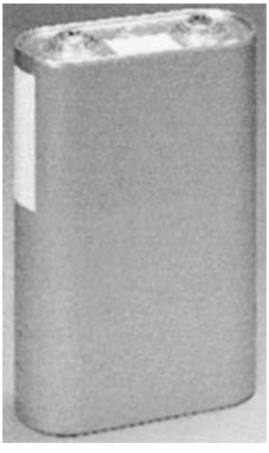

Figure 5.15. GYT 100 Ah Li Ion cell.

The life of a Li Ion battery in a space mission is a succession of storage periods and cycling periods. If we consider GEO, it is obvious that storage periods occur during the solstices and cycling periods occur during the equinoxes. For the LEO mission, the storage period must be considered before the launch and continuous cycling right after.

The negative electrode behavior on storage has been analyzed in detail, and degradation is attributed to insoluble SEI layer growth, the rate of which is assumed to be limited by the electron tunneling through the crystal defect of the layer [33]. Indeed, the layer growth consumes part of the lithium inserted in the carbon, so reducing the cell capacity, and the rate decreases as long as the thickness increases. This lithium corrosion effect of the negative electrode through the passivating layer accounts for a significant and predictable capacity loss, as a function of time and temperature.

Positive capacity reduction can appear in storage with $LiCoO_2$ as Co ions may dissolve in the electrolyte and migrate to the negative. The reduction of metallic ions favors Li corrosion within the negative. On the other hand, the presence of Al in the Ni-based positive ($LiNi_xCo_yAl_zO_2$) allows the oxide to be stabilized in storage avoiding any loss of capacity. As discussed previously, this oxide induces a lithium excess within the negative electrode, this providing an important life extension. All these features give the $LiNi_xCo_yAl_zO_2/C$ system, developed by Saft for industrial applications, outstanding properties both for cycling and calendar life [34].

Li Ion battery designs

Because of the large variety of possible applications, many types of battery assembly can be designed. These are greatly facilitated by two properties: the voltage dependence on SOC, which allows direct parallel connection to obtain the required capacity without any electronic component, and the cell ability to work in any position. On the other hand, as no overcharge shuttle mechanism exists in batteries with organic electrolyte, the end of charge and discharge voltages must be monitored for each cell or parallel grouping, this requiring specific battery management features, especially when high voltages are involved, sometimes close to 100 V.

Progress in high power electronics makes this achievable, however, ensuring very precise and stable battery characteristics, much better than could be expected from a chemical shuttle inside the cell, as in aqueous systems. Battery management systems may include sophisticated intelligent functions, which can communicate with the application. The most used information is the battery 'fuel' gauge, giving a real time read out of the state of charge.

The balancing system is a key point of Li Ion space batteries. Contrary to NiCd and NiH_2 cells, Li Ion does not exhibit overcharge and recombination phenomena that can equilibrate the end of charge state. Therefore, in case of a state of charge disequilibrium (due to cell/battery or telemetry external leakage current) within a serial branch of the battery, there is no way to rebalance the cells as performed in NiCd/NiH$_2$ batteries. Generally, all Li Ion batteries necessitate electronic devices to perform balancing. In the case of space batteries, specific electronic components with redundancy must be used. The balancing system uses a resistor to by-pass a small current to rebalance the highest SOC cells versus the lowest ones. In fact, the active balancing is performed by the on board computer (OBC) that determines the cell voltage spread thanks to individual cell telemetry. When the voltage spread is too high, the PCU sends a command to the relay to connect the relays of the cells with the highest state of charge. Thereby, the resistor induces an external leakage current that equalizes the state of charge of the cells that have manifested higher voltages to that of the other cells.

Two opposite battery configurations exist:

- The *s-p* topology is characterized by serial strings of cells in parallel. The number of cells within each string gives the battery output voltage; the energy/capacity is adapted for the power need. This topology is mainly used for low power batteries using low capacity cells. The *s-p* configuration is adequate for unregulated satellite buses that cannot afford a voltage loss. By using multiple strings, the battery can withstand cell failures without voltage decay. Individual cell protection for short-circuit events is in this case mandatory. The main disadvantage of the *s-p* topology comes form the need of an *s*$*$*p* balancing (individual cell) system. This is the same situation as for the voltage telemetry. As described hereafter, this system is mandatory to avoid any unbalanced state of charge with time (linked to the spread of leakage current). Figure 5.16 shows the cell arrangement for the *s-p* topology.
- The *p-s* topology is better adapted to high capacity cells. This configuration is adopted mainly for non-regulated satellite bus. Cells in parallel constitute one module that defines the battery capacity; modules are connected in series to deliver the battery voltage. The number of modules must be compatible with the satellite voltage range, especially in case of cell failure. Indeed, in this case, the module could be lost inducing a 3.6 V voltage drop at battery level. However, the capacity of the battery remains the same.

This topology is well adapted for high power batteries such as in GEO communication satellites. Moreover, the number of electronic systems needed with *p-s* topology is only *s*. Considering the cost of space electronics, reducing the number of balancing systems gives a tremendous advantage. As all the cells within the same module have the same SOC and same voltage, the number of telemetry lines is also reduced to *s*. Figure 5.17 gives a schematic view of the *p-s* topology. The modules of this topology in a space battery can be equipped with a by-pass system to protect the battery from open circuit failure and the

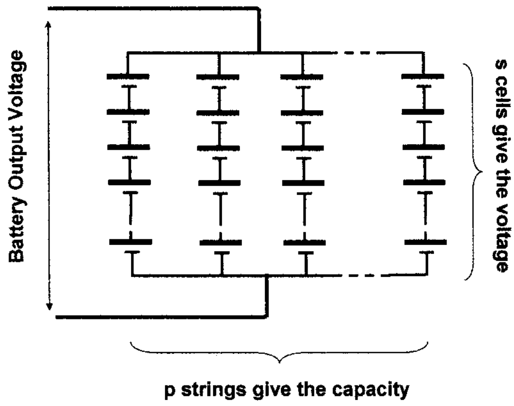

Figure 5.16. The *s-p* Li Ion topology.

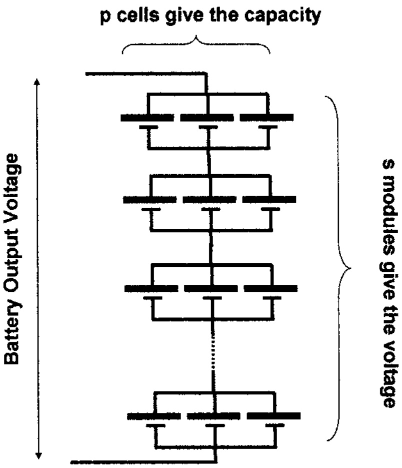

Figure 5.17. The *p-s* Li Ion topology.

module from overcharge.

As for NiCd and NiH_2 batteries, space Li Ion batteries are specific to each satellite. The designs are dependant on the cell configuration, as detailed in the following.

The first space battery qualified by Saft in the context of the STENTOR satellite was composed of two battery sets of 2P11S (11 serial cell package of 2 cells mounted in parallel) as shown at Figure 5.18. This battery included balancing electronic system, individual module by-pass, heaters and connectors to meet GEO requirements.

As GEO commercial satellites require higher power than that obtainable from Stentor, a range of modules of different sizes has been set. Module designs from 3P to 12P allow the range of LEO and GEO satellite power from 1 to 30 kW to be covered. These modules are equipped with cell by-pass (activated device), connectors, balancing electronics and heaters.

The GEO batteries are made of 10 to 12 modules (10 to 12 S) in series ("50 volts" bus) or 20 to 24 modules (20 to 24 S for a "100 volts" bus). The module type depends on the power need. For example, a 6P module delivers 23.4 kW with a "100 V " bus and two times less with a "50 V " bus. A capacity of more than 105 Wh/kg is achieved for the module type over 8P.

The elliptic cylindrical 100 Ah Li Ion cell developed by GS Yuasa Technology Ltd. and Melco (Mitsubishi Electronic Corp.), reported in Figure 5.15, forms the basis for another satellite battery. The battery design is close to Saft's and is equipped with [35,36]:

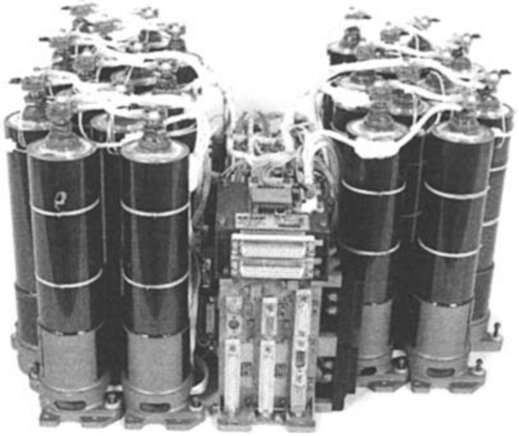

Figure 5.18. Stentor battery set.

- paralleled cells mounted in series (*p-s* architecture)
- by-pass system per package
- electronics for balancing.

Figure 5.19 shows a 100 Ah battery module, using 10 cells in series. Rated at 1 kW, 3.6 kWh, this 35.9 kg module delivers 100 Wh/kg.

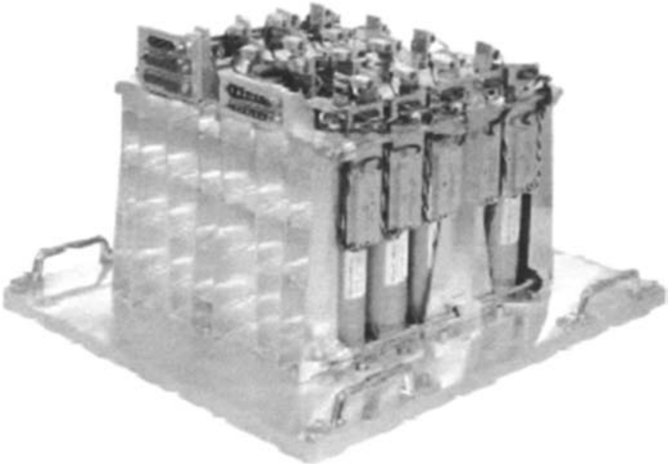

Figure 5.19. Melco 10 S 1 kW battery. (*From Melco internet web site*)

For micro and small LEO satellites, ABSL/AEA Technology has made the choice of using specially selected small commercial cylindrical 1.5 Ah cells (18650HC manufactured by Sony) [37]. Cells are connected in series strings to match the required voltage and these strings are assembled in parallel to achieve the required capacity. No electronics is required at the cell level as it is assumed that the cell properties are uniform and well matched due to the large manufacturing. This cell, originally designed for a multipurpose use, includes a safety current breaker to prevent individual cell overcharge. There is no balancing, considering that the failure of one cell when overcharged within a string should simply lead to the loss of one string. The number of strings is sized taking into account the failure probability, to ensure the required battery life.

Thanks to the small capacity increments, this configuration fits the various needs for small spacecraft and ABSL batteries have been selected for a number of microsat scientific projects. For example, a 3 x (6s-11p) 1.07 kWh construction is designed for the ESA Rosetta platform, launched at the beginning of 2003 towards the Comet Churyumov-Gerasimenko. Extension of this concept to larger battery configurations is being tested, in order to demonstrate its reliability.

Saft also proposes low-capacity batteries based on MP176065 (Medium Prismatic cell), which delivers 5.8 Ah for LEO micro satellites. The Proba2 battery uses an *s-p* technology with 8S3P, with individual cell balancing resistors (automatic balancing circuit).

Conclusion on space Li Ion batteries

Thanks to the good in-orbit performances of the first Li Ion batteries on board the first satellites, operators, satellite integrators, insurers are now convinced that Li Ion technology is ready to fly on board satellites.

All European and US satellite manufacturers have designed their future LEO and GEO satellites platforms with a power system using Li Ion. Thanks to its numerous advantages, Li Ion is replacing the existing satellite battery technologies, similarly to what happened in the past with the replacement of NiCd by NiH_2.

5.3. Launcher Batteries

Launchers are used to bring to space satellites, stations, instruments or astronauts. They need power sources with high specific energy for one-time missions, whose duration may range from few minutes to few months.

The following technologies, rechargeable or primary, are currently used or considered for launcher power systems.

Rechargeable:

- Nickel-Cadmium
- Lithium-ion

Primary :

- Lithium-Thionyl chloride (LTC)
- Lithium-Sulfur dioxide (LSDO)
- Silver oxide-Zinc
- Silver oxide-Aluminum,
- Silver chloride-Magnesium
- Thermal batteries (TB)

Fuel cells (FC) can also be used.

Their characteristics are detailed below. All these batteries must have a common feature: a resistance to vibrations even higher than that requested to satellite batteries.

5.3.1. Rechargeable Batteries

The main purpose of having a rechargeable system on a launcher is:

- to make tests before the launch and to have a proved and reliable system to ensure the behavior of the equipment for the whole mission
- to avoid changing the battery in case of launch delay.

NiCd was the only secondary battery technology used for many years on board launchers.

Saft has been providing all the Ariane batteries since the beginning of life of this launcher. NiCd batteries have been specifically designed and qualified for this need. They are dedicated to supplying power to electronic equipment (functional battery), activation of pyrotechnics devices, safety and telemetry. Typically, the NiCd battery is made of an association of cylindrical cells designed to sustain vibration levels and to be fully hermetic. Figure 5.20 shows an Ariane V battery used for safety. US and Russian launchers also use specific NiCd products for launchers. On the other hand, China uses commercial NiCd cells (for consumer applications).

The main features of NiCd batteries are:

- average voltage: 1.2 V
- specific energy: 30 Wh/kg
- good specific power.

The main advantages of the NiCd technology for launchers are:

- space qualified launchers (Ariane, *etc.*) ;
- re-usable (>500 times): capacity checks can be done prior to launch to ensure the performance of the batteries

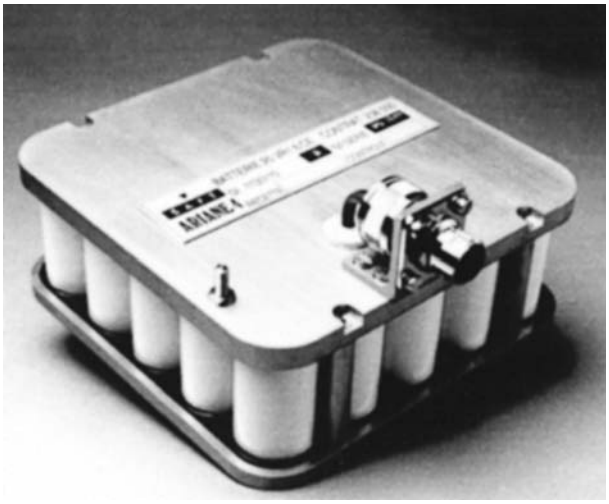

Figure 5.20. Ariane NiCd 25VR1.6 battery.

- hermetic (welded can) system.

The drawbacks are:

- storage life: 2 to 3 years
- maintenance needed
- poor specific energy
- launch pad wait: high self discharge.

The new generation of Li Ion batteries has also been considered. The main features of this type of batteries for launchers are:

- average voltage: 3.6 V
- specific energy: 125 Wh/kg
- very high specific power.

The main advantages of the Li Ion technology for launchers are:

- space qualified launchers (Vega, *etc.*)
- re-usable (see NiCd)
- storage life (>5 years)
- low self discharge
- hermetic (welded can) system
- OCV can be used as an energy gauge.

The drawbacks are:

- flammable materials
- maintenance needed
- large range of voltage.

The first example was the use of a power Li Ion battery for the Korean launcher Kari, shown in Figure 5.21. This type of battery, using 10S VES140

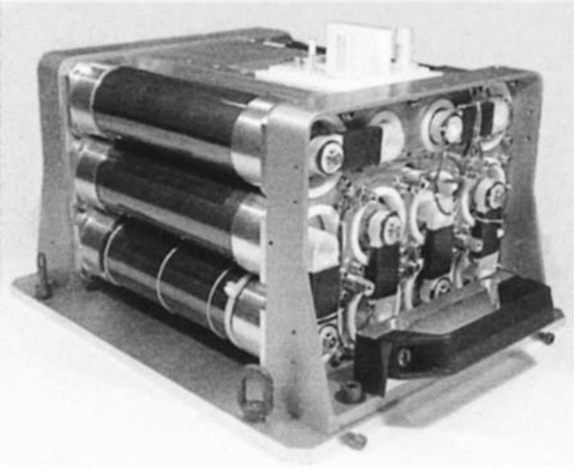

Figure 5.21. Kari launcher battery.

(40 Ah) cells, is designed to deliver power pulses up to 600 Amps (15C) for 100 ms and 340 Amps (8C) for 5 minutes.

In addition, the European launcher Vega has base-lined a high power Li Ion battery for the TVC (Thruster Vector Control) which is achieved with 8-Ah high power cells. The flight electrical profile uses 200 Amps current charge and discharge corresponding to 25C rate.

So, due to their specific energy and power capability, Li Ion batteries should be considered more and more for launcher applications.

5.3.2. Primary Batteries

Launchers are the biggest users of these batteries, as high discharge rate and specific energy are the most important factors. Much larger primary batteries will be needed when the expected switch from hydraulic to electrical actuators will occur.

5.3.2.1. Silver-Zinc batteries

For many years, the main primary battery system used was silver-zinc (see Chapter 2 for the basic features of this chemistry). Whilst it has a high specific energy (~100 Wh/kg) and excellent rate capability, its storage life is short once the electrolyte has been added. This is acceptable for launchers, although the need to replace batteries in case of long launch delays is an inconvenience. Figure 5.22 shows a silver-zinc space battery for the Ariane program and for various shuttle and science missions.

The main features of this type of battery are:

- average voltage: 1.5 V
- specific energy: 100 Wh/kg
- high specific power.

The main advantages of the silver-zinc technology for launchers are:

- space qualified launchers (*e.g.* Ariane, NASA)
- maintenance free during dry storage (2 to 3 years).

The drawbacks are:

- cell activation prior to launch
- storage life limitation after activation (1 month)
- non hermetic cells.

5.3.2.2. Lithium Batteries

Large Li/thionyl chloride cells have been developed by Saft for the US Centaur upper stage (Figure 5.23) and for the Hermes Shuttle project. These batteries have flown on a large number of European and US programs and have been selected for the ATV (Automated Transfer Vehicle).

The main characteristics of primary lithium technologies for this application are given in Table 5.2.

Manned vehicles require the largest primary batteries in terms of watt-

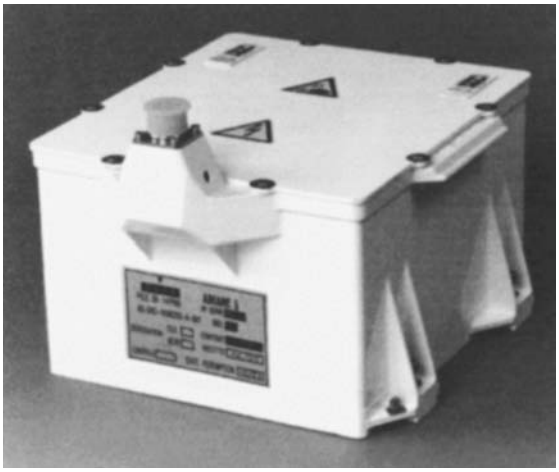

Figure 5.22. Saft's silver-zinc battery 39 x 14 PNS.

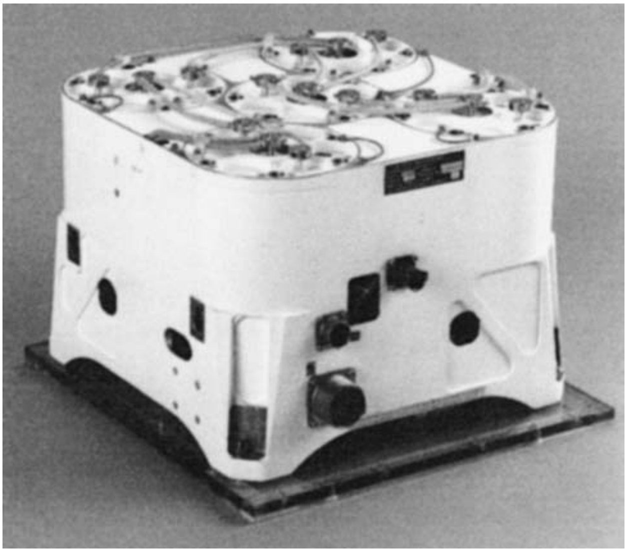

Figure 5.23. Titan 4 Centaur Li/$SOCl_2$ 250 Ah battery (Saft).

hours. For long manned vehicle missions (shuttle), maximum specific energy is mandatory, this favoring the use of fuel cells. For expendable transport (ATV) and crew emergency rescue (CRV) vehicles, specific energy is less critical compared with long shelf life, resulting in a preference for primary lithium batteries.

For scientific applications requiring long storage life, Li/sulfur dioxide and Li/thionyl chloride batteries should be used. Whilst having excellent

Table 5.2. Characteristics of primary Li batteries for launchers.

	Li/$SOCl_2$	Li/SO_2	Li/MnO_2
Average Voltage (V)	3.5	2.9	3.0
Specific Energy (Wh/kg)	500	260	275
Specific Power	Very Low	Medium	Low
Advantages	Storage life >10 years	Storage life >10 years	Storage life >10 years
	Maintenance free	Maintenance free	Maintenance free
	Very low self discharge	Very low self discharge	Very low self discharge
	Hermetic cells	Hermetic cells	Hermetic cells
			Low passivation
Drawbacks	High passivation	Medium passivation	Flammable materials
	Low power		

specific energies, they can suffer from "voltage delay" when first used after a long period of storage. In addition, very high-energy, bobbin-type Li/$SOCl_2$ batteries have poor rate capability.

5.3.3. Thermal Batteries

Some thermal batteries are also used on launchers. Their main characteristics are:

- average voltage: 1.2 V
- specific energy: 120 Wh/kg
- high specific power.

The main advantages of the thermal battery technology for launchers are :

- space qualified launchers (*e.g.* Ariane, NASA)
- storage life >20 years
- maintenance free
- very low self discharge
- hermetic cells.

The drawbacks are:

- activation command needed
- no test possible prior to launch
- activated life >2 hours.

5.4. Aircraft Batteries

5.4.1. Batteries on Board Aircraft

There is a long list of aircraft equipment powered by batteries (either on an on-off basis or as back-up in case of the failure of the main supply). It includes emergency lighting units, avionics equipment, emergency escape deployment and emergency medical equipment. Most important is the "main" or "emergency" battery, which is the subject of this section.

5.4.2. Role of the Main Aircraft Battery

In the pioneering days of transatlantic flight, the on board equipment was similar to that of the automobile. The battery ensured easy starting of the petrol engine, but most importantly supplied the aircraft electrical system and the communications system. As equipment became more complex and its tolerance to wide voltage variation decreased, the constant voltage system with a battery connected to the distribution busbar came to be adopted. In general this was a 28 VDC circuit for nominally 24 VDC equipment, and 28 VDC remains the standard for most modern aircraft today.

The main battery in today's aircraft plays several roles, similar to those of the earliest. The principle one is to provide the emergency electrical energy necessary, in the case of main electrical generation failure, to assure the return to ground of the aircraft during a period of 30 or 60 minutes. A second but hardly less important role is engine or auxiliary power unit (APU) starting, that demands high peak power capability for a short duration of typically 15 to 30 seconds. High power is also a characteristic required for switching and transfer when the battery may supply the switches or contactors, and supports essential loads during the process. In a shorter timeframe, the battery can act as a capacitive filter helping to regulate the aircraft's DC network, reducing the effect of transients and spikes and superimposed AC that may arise from the generating source. Main battery energy is also used on the ground during refueling and checks.

5.4.3. Defining the Aircraft Environment

General

Aircraft equipment and systems are subject to the requirements of the regulatory authorities, such as FAA in the USA or EASA in Europe. They are mainly concerned to assure that the batteries do not present a hazard to aircraft safety. Of course, the battery choice has to be based on an analysis carried out by the aircraft system designer in accordance with FAA/EASA regulations, taking into account de-rating factors (end-of-life performance, temperature, state of charge, *etc.*) that can have an impact on battery performance.

In order to ensure airworthiness, procedures have to be established for their demonstration at the qualification test stage and throughout life. Continued airworthiness including safety of operation when installed and ability to perform the required functions, especially in emergency conditions, is confirmed by maintenance checks even for 'maintenance free' batteries.

There exist several specific aircraft battery standards principally aimed at defining common performance and safety test methods based on the aircraft environment. These include EN2570, IEC60952 and RTCA DO 293. These standards provide design guidelines and standardized formats, while facilitating performance comparisons.

Standards also exist, such as EN2270, Mil Std 704 that define the quality of the aircraft network to which the battery may be connected. For the

DC network, this includes the permitted voltage limits under normal, abnormal and emergency conditions as well as the level of spikes and transients.

The aircraft environment itself is rather well established according to the widely used standard Eurocae/RTCA DO160 and various military standards (such as US Mil 810). The environment can be generally characterized according to aircraft type (*e.g.* large transport, helicopter, trainer), location in the aircraft (*e.g.* uncontrolled, partially temperature controlled, pressurized), engine type (*e.g.* piston, jet, turboprop), proximity to vibration sources, *etc.* Each factor will influence the temperature, altitude, acceleration, shock and vibration to which the battery will be exposed. In addition, other exposure requirements may apply such as humidity, salt fog, and resistance to contaminants such as cleaning agents, fuel and lubricants.

The electrochemical heart of main aircraft batteries is not a source of electromagnetic interference to the aircraft electrical system. In the same way, it is considered immune to the effects of external electromagnetic disturbance such as may be induced by a lightning strike on the aircraft. Of course, if it is equipped with electronic components and their resistance to the electromagnetic environment has to be demonstrated.

It may take from three months to two years to develop a new battery and a similar lapse of time may be necessary to complete the qualification process. The timescale is shortest for mature technologies like NiCd and for designs that are close to an existing product.

Temperature

Temperature requirements are typically:

- ground survival (limited duration)
- temperature variation: -55°C to +85°C (thermal shock transition < 5 min)
- operation: -40°C to +70°C.

However, acknowledging the limitations of the available chemistries, limitations have to be accepted at the extremes of temperature. For example, -20°C is normally the practical limit for starting duty on commercial aircraft.

Altitude

Equipment in unpressurized zones has to withstand altitudes in the range of 1,300 ft up to 60,000 ft. The equivalent altitude in pressurized zones is typically 8,000 ft, but in that case the effects of rapid decompression must also be accounted for.

Mechanical

Vibration requirements are normally represented by sweeping a random vibration spectrum having an intensity varying between 0.0001 g^2/Hz and 0.2 g^2/Hz for frequencies between 10 Hz and 2000 Hz. The severity represented by these spectra is a function of the distance of the equipment from the vibration source and the type of source, the major component of which is the engine. In the particular case of turboprops and rotary wing aircraft, peaks related to the rotation rate are superimposed to the random vibration spectrum at discrete frequencies.

Shock and acceleration requirements are imposed at two levels: a 'normal' operational level and a higher 'crash' level. In the former case, the battery has to function normally while in the latter case it merely has to remain intact. Operational levels depend on the aircraft type and relate to such effects as aerodynamic buffeting but are inevitably higher for military aircraft undergoing acrobatic maneuvers.

Typical requirements are:

- operational shock (saw tooth): 6g/11ms (civil) up to 10g/11ms (military)
- crash shock (saw tooth): 20g/11ms (civil) up to 30g/11ms (military)
- operational acceleration (sustained): 5g (civil) up to 10g (military)
- crash acceleration (sustained): 9g (civil) up to 15g (military).

As well as the normal shock, vibration and acceleration tests, resistance to short-term events, such as the loss of a fan blade or a tyre burst that can induce a series of severe shocks, may also need to be demonstrated.

5.4.4. Current Technology

General

Two principal chemistries are in use on aircraft today: NiCd and Lead-Acid. Silver-Zinc offers higher performance capabilities and in the past found widespread use in Eastern Europe, but its relatively short cycle life has largely led to its replacement by NiCd.

Vented Lead-Acid and NiCd batteries have been used since the very earliest days of flying. The former continue to be used in light aircraft or general aviation but the introduction of valve regulated Lead-Acid (VRLA) batteries has provided strong competition. On the other hand, vented NiCd batteries dominate the larger aircraft (Figure 5.24) and helicopter applications, while some overlap with Lead-Acid technology is found in smaller aircraft such as business jets.

Valve regulated NiCd aircraft batteries exist but have not found widespread application for aircraft, mainly because of the need for a dedicated on board charger and limitations imposed by thermal management. Similar constraints, as well as low temperature performance limitations, have also prevented the widespread adoption of the Nickel Metal Hydride technology.

Today, the most attractive technology for aircraft use is Li Ion. It potentially offers large weight savings compared with current technology and

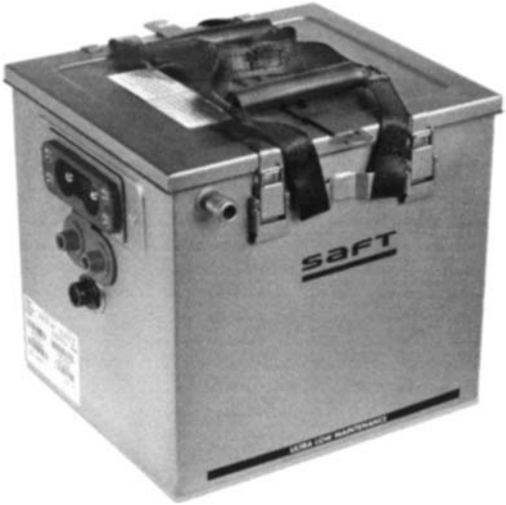

Figure 5.24. 50-Ah NiCd battery for Airbus A380.

has already been adopted for the most advanced military programs. Since Li Ion batteries require closer control than traditional technologies, much effort is going into system development.

Battery construction

Vented NiCd aviation batteries generally consist of individual cells connected externally in series and housed in metal containers equipped with a power connector and ventilation tubes. An auxiliary connector may be provided for temperature or voltage sensors and, sometimes, a heater circuit.

The cells contain interleaved electrodes connected to an internal current collector linked to a terminal that passes through the cell cover. The positive electrodes are usually formed by the deposition of the active materials onto a highly porous nickel substrate deposited by 'sintering' nickel powder on a nickel plated mild steel perforated substrate. The negative electrodes may be formed in the same way or by a direct pasting process. Alternatives to nickel powder include the use of fibrous nickel and pre-prepared nickel foam.

The separator is typically non-woven polyamide felt. An oxygen barrier is included in the separator assembly to reduce the transfer of O_2, generated during overcharge at the positive electrode, to the negative electrode, where it would recombine, generating heat and increasing overcharge current.

The cell stack is immersed in electrolyte consisting principally of potassium hydroxide to which a small proportion of lithium and sodium hydroxide may be added to enhance high temperature chargeability.

The individual cells are housed in cases (usually plastic) fitted with closures that prevent spillage but allow generated gases to be released through low-pressure valves; the closures are removable to allow water replenishment.

Vented Lead-Acid batteries generally use a single plastic container into which the individual cell containers are formed. Cell connection is usually made through the cell wall in order to reduce weight. The active materials are pasted onto lead alloy (lead-calcium, lead-tin) grids, which are then welded to the current collector for ultimate connection to the battery power connector. Inter-electrode separation is assured by the use of polymeric or glass fiber mats that maintain the sulfuric acid electrolyte in contact with the active surface.

VRLA batteries use similar construction methods but the individual cells are fitted with higher pressure valves designed only to relieve internal pressure under abusive conditions. Unlike vented systems, the separator is constructed to promote oxygen transfer to maximize oxygen recombination. In this way, water loss and drying out is greatly reduced.

Valve regulated (VR) NiCd batteries are constructed in a similar way to vented NiCd batteries but employ higher venting pressures and auxiliary electrodes to enhance gas recombination.

Discharge characteristics

Main 24 V aircraft batteries are available with capacities between 15 and 60 Ah (at the C rate). Actual performance depends on the design trade off between energy and power.

To illustrate the impact of discharge rate and temperature, Figure 5.25 shows the energy density of different batteries related to that of a NiCd battery (discharges at 1C and 8C, at 23°C and -18°C). The data are taken from manufacturers' information for 24 V batteries with capacities of 40-50 Ah.

Figure 5.26 shows the power density of the same batteries related to that of NiCd at 23°C and -18°C.

The number of batteries installed in the aircraft depends on the system architecture. When more than one battery is required, it is often specified for logistic reasons (reduced number of parts, interchangeability, *etc.*) that they must be of the same type.

In smaller aircraft, there are commonly two batteries. One is used for starting and, in order to maximize power availability, its voltage may be allowed to fall to 12 – 14 V. During the start, the second battery supports loads imposed by essential equipment that would be disrupted if the supply voltage fell below 18 – 20 V. During emergency conditions, the batteries are connected in parallel to provide the necessary energy. Examples of this are the Embraer regional jets ERJ145 which uses two 24 V, 44 Ah NiCd batteries weighing a total of about 75 kg, and the ERJ170 which uses two 22.8 V, 27 Ah NiCd

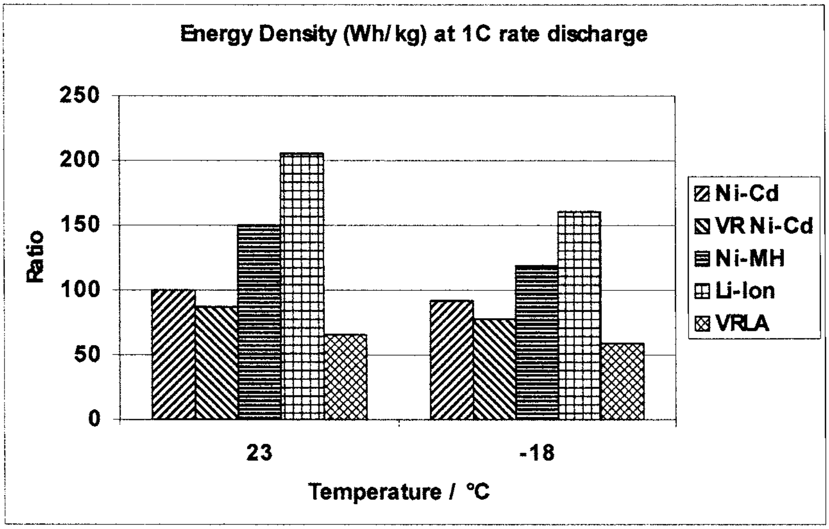

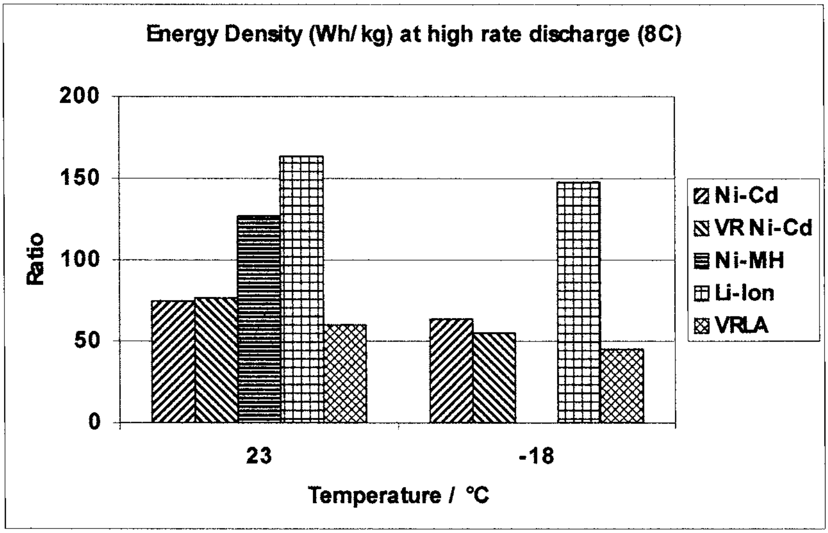

Figure 5.25. Ratio of the energy density of different batteries *vs.* that of NiCd, at 23°C and -18°C, 1C and 8C.

batteries weighing a total of ~50 kg. The difference in battery sizes arises from the different starting and emergency requirements and the different charging systems.

At the other end of the spectrum, the Airbus A380 has a complex architecture designed to allow the network to be reconfigured and power transfers to be carried out without a break. Three 24 V, 50 Ah NiCd batteries

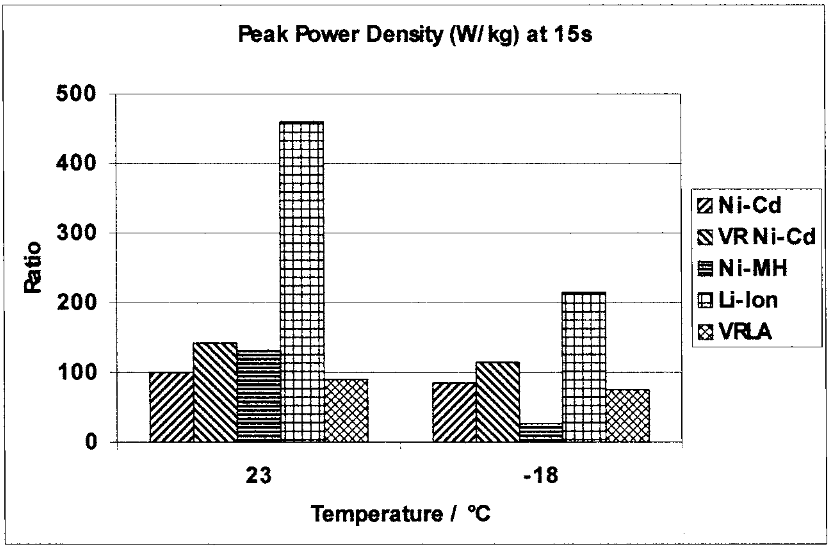

Figure 5.26. Ratio of the peak power density of different batteries *vs.* that of NiCd, at 23°C and -18°C

are installed to assure this function. A fourth 50 Ah battery is dedicated to APU starting. The total weight of the batteries is about 210 kg. The impact on battery weight of the different requirements is striking.

On board charge

Many batteries are charged by direct connection to the DC network, which is itself powered by a DC generator or by an alternator and transformer. Since the charging voltage cannot easily, if at all, be changed, there is little scope for optimizing the battery charge with such systems.

Some aircraft systems use dedicated battery chargers that may also play a part in regulating the DC network. Such chargers generally modify the charge current and voltage as a function of battery temperature and time of charge in order to maximize the SOC in the shortest possible time, whilst minimizing the overcharge that contributes to ageing and, for vented systems, leads to water consumption. Dedicated charge control functions, whether external or inside the battery, are considered particularly important for the Li Ion technology, since uncontrolled overcharge can lead to battery destruction.

The phenomenon of thermal runaway has long been of concern to the regulatory authorities. When the rate of heat generation in a battery exceeds the rate of heat dissipation, the battery temperature rises. Heat generated during discharge or overcharge is dissipated principally by natural convection although some specific battery designs permit enhanced or forced convection. Under normal constant voltage charge, the heat generation is balanced by the heat dissipation, so that a stable condition is established. However, in some circumstances, thermal instability can occur.

At a given charging voltage, the overcharging current depends on the battery temperature. In this case, if the temperature rises, the overcharge current rises, thus leading to more heat generation and further temperature rise, and so on. In this way, a vicious circle can be established leading to a rapid temperature rising.

Causes of instability include: too high charging voltage in relation to high ambient temperature; specific operating sequences, *e.g.* frequent starts in high temperature conditions leading to accumulated heat build up; incorrect maintenance failing to detect the signs of ageing.

Duty cycle

The duty cycle experienced by an aircraft battery depends on its role within the aircraft system architecture and the operating profile of the aircraft. It is therefore difficult to define a 'normal' duty cycle relating to depth of discharge and charge duration. The latter depends largely on the duration of the flight and ground operations. Even here, the ratio of operating to flying hours may vary between 1.3 and 2.0 according to whether the aircraft is used for commuter or long haul operations.

A start may consume between 10% and 20% of the battery capacity. Sometimes more than one start attempt may be necessary, although this is usually limited to three in order to avoid damage to the engine or APU. However, the dedicated starting battery may be used before every take off or only when there is no ground power supply available. It may also be used for APU starting in association with the on board generation during final landing approach. The emergency battery may never be significantly discharged and could spend the majority of its life floating on the DC bus.

On the other hand, either battery may be discharged on the ground when ground power is disconnected and no on board generation is available due to loads applied for example during system start up and shut down, flight preparation, and re-fuelling. Further loads may be applied during maintenance or cleaning and, while it may be possible to disconnect some of them, they are a frequent cause of unscheduled removal due to 'battery flat'. There are also some low level loads, for example supplying memory devices or clocks connected to a 'hot' bus, that are never disconnected: although only of the order of hundreds of milliamperes, they can cause deep discharge if the aircraft is unused for several days.

Battery life

The life duration of a battery depends on various factors such as number of operating hours, ambient temperature, start frequency and on board charge.

It is therefore difficult to determine in advance how long the expected life of a cell will be in the real situation. Typically, the life of NiCd vented batteries on long-range transport jets is 6 to 9 years, while in commuter aircraft is 5 to 7 years. On the other hand, in military trainers and fighters it is typically 4 to 6 years. By comparison, the life of Lead-Acid batteries is half to one third that of NiCd.

There are three principal failure mechanisms, all of them progressive, which occur in a vented NiCd battery: oxygen barrier failure (leading potentially to thermal runaway), separator failure (leading to short circuit within one or more cells), and irreversible capacity loss due to degradation of active materials. Failure on open circuit is almost unknown. Preventive maintenance procedures detect impending failures, before they can occur on board the aircraft, with a high degree of reliability.

The principal failure mechanisms of Lead-Acid batteries are: capacity loss due to active material degradation, isolation of the active material from the current collecting structure leading to high internal resistance, and corrosion of the collecting structure. While capacity loss is progressive, active material isolation can be rapidly provoked by deep discharge such as may occur during ground operation. More problematic for aircraft applications, where permanent availability even in degraded operation is normally required, is corrosion that can lead to battery failure on open circuit without warning.

5.4.5. Future Trends

Since weight reduction leads to reduced fuel burn and/or increased payload, the aircraft manufacturer will continue to seek to reduce the aircraft weight to the minimum and this applies to the equipment as well, such as batteries and their supporting structures. Significant weight reduction is unlikely to be available from traditional battery technologies, so the solution should come from Li Ion.

Most importantly, increasing amounts of equipment are leading to a growth in power generation requirements. Today's aircraft have four sources of power generation: mechanical, hydraulic, pneumatic and electric. For reasons of weight saving, maintainability, reliability and efficiency, aircraft manufacturers are seeking to shift more of this generation towards the electric, for example by replacing hydraulic circuits and actuators with electrical ones. Going further into the future, fuel cells offer the possibility of replacing the present internal combustion auxiliary power unit machines. They are nonetheless likely to require battery support for certain phases of their operation.

These developments are leading to a reconsideration of the aircraft electrical systems, for example the doubling of the voltage (115 V) of AC and DC networks or even moving to a 270 VDC network to which the battery would be directly connected. It again seems likely that a technology like Li Ion will be best suited to respond to the needs of such 'more electric aircraft' systems, because of its lower weight and reduced number of cells required to support a given voltage.

List of Acronyms

AC: Alternating Current
BOL: Beginning of Life
C/n: current rate equal to nominal capacity divided by n
CI: Chemical Impregnation
CPV: Common Pressure Vessel
DC: Direct Current
DOD: Depth of Discharge
DPV: Dependant Pressure Vessel
ECI: Electrochemical Impregnation
EOC: End of Charge
EOCP: End of Charge Pressure
EOCP: End of Discharge Pressure
EOCV: End of Charge Voltage
EODV: End of Discharge voltage
EOD: End of Discharge
EOL: End of Life
GEO: Geostationary Earth Orbit
HEO: High Earth Orbit
IPV: Individual Pressure Vessel
LEO: Low Earth Orbit
LSDO: Lithium Sulfur Dioxide
LTC: Lithium Thionyl Chloride
MEO: Medium Earth Orbit
MOP: Maximum Operating Pressure
NiCd: Nickel Cadmium
NiH_2: Nickel Hydrogen
NiMH: Nickel Metal Hydride
OBC: On Board Computer
P: Parallel
PCU: Power Control Unit

S: Serial
SOC: State of Charge
TB: Thermal Batteries
TIG : Tungsten Inert Gas
TVC: Thruster Vector Control
VRLA: Valve Regulated Lead Acid

References

1. A. C. Clarke, "Extra Terrestrial Relays", *Wireless World,* 1945.
2. W.R.C. Scott and D.W. Rusta, "Sealed-Cell Nickel Cadmium Battery Application Manual", *Nasa Reference Publication 1052,* Dec. 1979.
3. F. E. Ford, G.M. Rao and T.Y. Yi, "*Handbook for Handling and Storage of Nickel Cadmium Batteries: Lessons Learned*", Nasa Reference Publication 1326, Feb. 1994.
4. H.S. Lim *et al*, "Studies of the Stability of Nylon Separator Materials", *Proc.27th Power Sources Symposium,* Atlantic City, NJ, A77-28126, 83-85, 1976.
5. A.K. Shukla, S. Venugopalan and B. Hariprakash, *J. Power Sources* 100 (2001) 125.
6. G.Halpert, *J. Power Sources* 15 (1985) 119.
7. P.R. Voyentzie, G. Rampel and W.N. Carson, "Characterization of Recombination and Control for Spacecraft Nickel Cadmium Cells, Final Report", *Nasa* Contract 5-11547, 1970.
8. Naval Weapons Support Center, "Evaluation Program for Secondary Spacecraft Cells", *25th Annual report of cycle life test,* Contract S4166D, WQEC/C 85-52, 1985.
9. W.R. Scott, "A study of Degradation of Plates for Nickel Cadmium Spacecraft Cells", *TRW Report* N°24118-6002-RU 00, 1974.
10. G.W. Morrow, "Nickel-Cadmium Cell Design Variable Program Data Analysis", 1984 Goddard Space Flight Center Battery Workshop, *NASA Conference Publication* 2382, 208-227, 1984.
11. Y. Sato, S.Takeuchi and K. Kobayakawa, *J. Power Sources* 93 (2001) 20.
12. J. Carcone, in "*Handbook of Batteries*" (Chapter 28), D. Linden and T.B. Reddy, Eds., McGraw-Hill, New York, 2002.
13. J.D. Dunlop, G.M. Rao and T.Y. Yi, "NASA Handbook for Nickel Hydrogen Batteries", *Nasa Reference Publication 1314,* 1993.
14. J.D. Dunlop, G. Van Ommering and J. Stockel, "Nickel Hydrogen Cells" US Patent 3,867,199, 1975.
15. L. Miller, "The NiH_2 Battery System: A Space Application Summary" *Proc. 23 IECEC,* Denver, Colorado, 489-492, 1988.
16. R.L. Beauchamp, "Positive Electrode for Use in Nickel Cadmium Cells and the Method for Producing Same and Product Utilizing Same", US Patent 3,653,967, 1972.
17. D.F. Pickett, H.H. Rogers, L.A. Tiker, C. Bleser, J.M. Hill and J. Meador, "Establishment of Parameters for Production of Long Life Nickel Oxide Electrodes for Nickel-Hydrogen Cells" *Proc IECEC,* Seattle WA, 1918, 1980.
18. J. D. Dunlop, J.N. Brill and R. Erisman, in "*Handbook of Batteries*" (Chapter 32), D. Linden and T.B. Reddy, Eds., McGraw-Hill, New York, 2002.
19. H.H. Rogers, S.J. Krause and E. Levy," Design of Long Life Nickel Hydrogen Cells", *Proc. 28th Power Sources Conference,* 1978.
20. J.D. Dunlop and J.F. Stockel, " Status of Comsat/Intelsat Nickel Hydrogen battery technology", *Proc 15th IECEC,* Seattle, WA, 1878, 1980.

21. G. Van Ommering, C.W. Koehler and D.C Briggs, "Nickel Hydrogen Batteries for Intelsat V", *Proc 15th IECEC*, Seattle, WA, 1885, 1980.
22. J.P. Zagrodnik and K. Jones, "Development of Common Pressure Vessel Nickel Hydrogen Batteries", *25th IECEC*, Reno, Nevada, 1990.
23. J.C. Garner," A Nickel-Hydrogen Common Pressure Vessel Space Flight Experiment", *Proc. 27th IECEC*, 6-115, 1992.
24. M. Earl, "Intelsat VII. A NiH_2 Cell Evaluation", COMSAT Laboratories, Private Communication, 1993.
25. "Nickel Hydrogen Storage/Capacity Fade Session" 1992, *NASA Aerospace Battery Workshop, Nasa Conference publication 3192,* 1992.
26. H. Vaidyanathan, *J. Power Sources* 22 (1988) 221.
27. D.E. Nawrocki and J.D. Armantrout, "The Hubble Space Telescope Nickel Hydrogen Battery Design", *25th IECEC*, Reno, Nevada, 1990.
28. Y. Borthomieu, M. Broussely and J.P. Planchat, *Proceedings Sixth European Space Power Conference*, p. 679, May 2002.
29. G. Dudley, J.P. Planchat and P. Willmann, *Proceedings Sixth European Space Power Conference*, p. 673, May 2002.
30. B. Simon, J.P. Boeuve, B. Spigai and M. Broussely, *ECS Meeting,* Abstracts Vol. 97-2, 184, Paris, 1997.
31. B. Simon and J.P. Boeuve, SAFT Patents, FR 94 04889 (1994), EP 0683537, US 5,626,981.
32. M. Broussely, in "*Advances in Lithium Ion Batteries*", W. A. van Schalkwijk and B.Scrosati, Eds., Kluwer Editors Academic/Plenum Publishers, Ch. 13, 2002.
33. M. Broussely, S. Herreyre, P. Biensan, P. Kasztejna, K. Nechev and R.J. Staniewicz, *J. Power Sources* 97-98 (2001) 13.
34. M. Broussely, Ph. Biensan, F. Bonhomme, Ph. Blanchard, S. Herreyre, K. Nechev and R.J.Staniewicz, *J. Power Sources* 146 (2005) 90.
35. T. Gonai, T. Okamura and M. Goto, *Proceedings 19th International Communications Satellite Systems Conference*, Toulouse, p. 147, April 2001.
36. T. Inoue, N. Imamura, H. Yoshida, M. Mizutani and M. Goto, *Proceedings 19th International Communications Satellite Systems Conference*, Toulouse, p. 186, April 2001.
37. R. Spurrett, C. Thwaite, M. Slimm and D. Lizius, *Proceedings Sixth European Space Power Conference*, Porto, p. 476, May 2002

Industrial Applications of Batteries. From Cars to Aerospace and Energy Storage
M. Broussely and G. Pistoia Eds.,
© 2007 Elsevier B.V.

Chapter 6

AEROSPACE APPLICATIONS. II. Planetary Exploration Missions (Orbiters, Landers, Rovers and Probes)

B. V. Ratnakumar and Marshall C. Smart

Jet Propulsion Laboratory, California Institute of Technology,
4800 Oak Grove Drive, Pasadena, California 91109, USA

6.1. Introduction

Batteries are essential components of the spacecraft and provide the heartbeat either alone or in conjunction with an energy source, such as photovoltaic or nuclear radioisotope power sources. Solar arrays are usually preferred for inner and near planets or planetary objects, where sufficient solar intensity is available for many missions. For missions to farther planets, with little solar intensity, nuclear power sources may be adopted, as exemplified by NASA's premier missions in the 1980s, Voyager to the outer planets and Galileo to Jupiter. The choice of power generation source influences the requirements for energy storage, which in turn dictates the selection of the battery system. For solar powered missions, rechargeable battery systems with adequate cycle life are desirable to provide power during eclipse periods. For some radioisotope powered missions, on the other hand, battery systems with high power and long calendar life are essential. In Chapter 5, a detailed discussion has been provided on the batteries employed for satellite applications, such as the Low Earth Orbit and Geostationary Earth Orbit satellites; in addition, a discussion of various systems being employed for launchers and aircraft has been included. This chapter therefore exclusively deals with the batteries used in planetary exploration missions. There have been a number of reviews in the past that describe in detail different aspects of aerospace batteries, which are only in part within the scope of this chapter.[1-5]

Three different types of batteries have been used routinely in the planetary exploration missions: primary, secondary and thermal batteries. Primary batteries are used to i) supply power during launch and post-launch operations prior to the deployment of solar panels, ii) supply high power for short durations, typically less than 30 mS, for firing a pyro device that results in a mechanical action, or firing a rocket motor for mid-course correction, and iii) alternately, supply very low power for extended periods for clocks and computer memory. It is to be expected that primary batteries are preferred to rechargeable batteries in one-shot applications, owing to their higher specific energies, especially where there is no provision for recharge or no energy source available.

Rechargeable batteries are used in the spacecraft to provide power i) during launch and post-launch until the deployment of solar panels; ii) for firing pyros and rockets for attitude control; iii) during cruise anomalies or trajectory control maneuvers; iii) to the spacecraft, its equipment and payload during sun eclipse periods; iv) for nighttime or eclipse-time experimentation; v) for communicating and data transmission; vi) to keep the electronics warm, and vii) for clocks.

Thermal batteries are typically used to support series of short duration high-power pulses for firing pyros. For example, thermal batteries assist in the operation of separating a lander or a rover from the main spacecraft or during the entry, descent and landing (EDL) phase of the mission. Specific operations during EDL include events such as a) parachute deployment, b) separation from the heat shield, and 3) firing of retrorockets (TIRS and RAD). Thermal batteries are activated just before these events, due to their short life of 5-30 minutes subsequent to activation. These batteries have characteristically high power capability owing to the use of molten salt electrolytes, albeit with low specific energies.

6.2. General Characteristics of Space Batteries

Aerospace batteries have unique characteristics, owing much to the fact that they are developed to meet stringent requirements and environments. The unique characteristics of these specialty batteries are their extreme reliability, robustness and safety. It is readily understood why there is such a large focus upon high reliability and safety, given the high cost of space exploration and the need to ensure the safety of any humans involved. This invariably imposes significant constraints on the chemistry and design of the battery systems. In addition to safety and reliability, space batteries are characterized by the following features:

i) Ability to operate under vacuum, as encountered in space, without the out-gassing of any undesirable material that would contaminate the spacecraft instruments or compromise the spacecraft. This is ensured by prior tests under simulated conditions of temperature and vacuum, termed as thermal vacuum cycling.

ii) Ability to operate under extreme temperatures. Missions exploring inner planets require high temperature batteries, *e.g.*, Venus missions would need batteries to survive 475°C, whereas Mars and outer planetary mission would be greatly benefited by low temperature batteries, as Mars surface temperature is around -120°C.

iii) Ability to survive high intensity radiations: Jupiter, for example, has high levels of radiation, ~4 Mrad, which can potentially degrade polymeric materials.

iv) Ability to operate in any orientation and in microgravity.

v) Ability to survive high levels of vibration and acceleration environments during a) launch, b) shocks during pyro events, and c) shock levels during planetary landing.

vi) Negligible contamination to the instruments as well as minimal microbial contamination (planetary protection) to the planetary environments.

Beyond these generic requirements, it is imperative that aerospace batteries meet the 'form fit and functionality' needs of the particular mission. The energy storage needs of the planetary missions are diverse, as described below.

6.3. Planetary and Space Exploration Missions

Space exploration missions may be broadly classified into two categories: robotic and human. In addition, there are several science missions, *e.g.* deploying telescopes in space, which would require batteries. Planetary missions under robotic exploration have different categories, including i) Orbiters, ii) Fly-by and sample return missions ii) Landers, iii) Rovers, iv) Probes, v) Penetrators or Impactors and vi) Miscellaneous science missions. The human exploration missions, on the other hand, include: i) the Crew Exploration Vehicle (CEV), a proposed replacement for the Space Shuttle, ii) the International Space Station, iii) (Lunar) ascent and descent modules, iv) Extra-vehicular Activities (EVA), v) Surface exploration missions and vi) Miscellaneous science missions. To provide further details, the extra-vehicular activities consist of i) field science (*i.e.*, observations, geologic sample collection and geophysical profiling, drilling, or trenching), ii) emplacement science (geophysical monitoring [*e.g.*, seismicity], space physics monitoring [*e.g.*, radiation], and astronomical instruments), and iii) technology demonstrations, such as *in situ* resource utilization, excavation and processing, surface mobility/transportation, astronaut suit, human-carrying rovers. Each of these missions is briefly described here, especially in terms of the desired attributes for the energy storage device (Table 6.1).

Table 6.1. Attributes of the batteries used in various robotic and human planetary missions. (XX: high; X: moderate).

Category	Mission Type	Energy Source	Specific Energy	Energy density	Wide Op. Temp	Cycle Life	Calendar Life	Power Density	Radiation Tolerance	Safety
Robotic	Rovers/Landers	Solar	XX	XX	XX	X	X	X	–	X
		Nuclear	X	X	XX	XX	XX	XX	XX	X
	Sensors		XX	XX	XX	X	X	X	XX	X
	Scouts		XX	XX	XX	X	X	X	XX	X
	Probes		XX	XX	XX	N/A	X	X	XX	X
	Impactors		XX	XX	–	XX	X	X	XX	X
	Orbiters	Solar				XX	XX	X	X	X
		Nuclear	X	X	–	XX	XX	XX	XX	XX
Human	Space Station		X	X	–	XX	XX	X	XX	XX
	Crew Exploration Vehicle		X	X	–	X	X	XX	XX	XX
	Crew Launch Vehicle		X	X	–	X	X	XX	XX	X
	Planetary Ascent Module		X	X	X	X	X	XX	XX	XX
	Planetary Descent Module		X	X	X	X	X	XX	XX	XX
	Outpost-Hybrid		X	X	–	–	XX	XX	XX	XX
	Astronaut Tools		XX	XX	X	X	X	XX	XX	XX
	Extra Vehicular Activities		XX	XX	X	X	X	X	XX	XX

6.3.1. Robotic Space Exploration

Robotic exploration is generally the more desirable approach of space exploration, especially to planetary objects that are too distant from the Earth and too hostile for human visitation. Owing to advances in robotics, communication and power technologies, NASA has achieved significant success in the recent past in exploring various planetary objects in our solar system. The characteristics of such robotic missions are described here.

6.3.1.1. Orbiters

Orbiters are typically deployed for mapping surfaces of planetary objects, to assist in understanding their atmosphere, and to monitor daily global weather. Further, they often serve as a communication link between the Earth and the planetary surface mission, which may involve either a rover or a lander. Historically, the planetary orbiters, especially lunar and Mars orbiters, have used solar energy as their primary power source and require secondary batteries to provide power during eclipse periods. On the other hand, orbital missions to outer planets (*i.e.*, Jupiter, Saturn and Neptune as well as their satellites) may preferentially use nuclear power sources, either with capacitor or long-life rechargeable batteries for load-levelling purposes. The two recent major outer planetary orbital missions that used nuclear power source are Galileo around Jupiter and the on-going Cassini around Saturn. In contrast, there have been several major Mars missions recently, *i.e.,* Global Surveyor, Odyssey, Express and Reconnaissance Orbiter, performing continuous monitoring of Mars.

Orbiters revolve around the planets multiple times, *e.g.,* 12 times per day around Mars for the Mars Global Surveyor, from pole to pole for several years. The rechargeable batteries for these missions are therefore required to have excellent cycle life (~ 5000 cycles/year) combined with good active or wet life (5-10 years). The batteries undergo rapid cycling with such a cycling regime, *i.e.*, discharge for about 30 minutes followed by charge within the next sixty minutes to the original state of charge. No battery system can provide such large number of cycles of ~ 30,000 under deep-discharge conditions. However, at partial depths of discharge, the cycle life improves significantly, increasing non-linearly with decreasing depth of discharge,[6-10] such that some battery systems, *e.g.*, nickel-cadmium and nickel-hydrogen, have shown impressive ability to provide thousands of cycles. High specific energy and energy density are desirable from the batteries, but not as critical as longevity. With the energy available from the solar arrays, the batteries are maintained above sub-zero temperatures, such that their low temperature performance is not a factor. Orbiters to outer planets, especially Jupiter, encounter high intensities of radiation and the batteries are required to withstand such high levels, in the absence of any further attenuation. Typical requirements of batteries for orbital missions are illustrated in Figure 6.1 and listed in Table 6.1.

Nickel rechargeable battery systems, especially nickel-cadmium and nickel-hydrogen, have been the preferred choices for this application, owing to their excellent cycle life characteristics. Detailed performance characteristics of various designs of Ni-Cd and Ni-H_2 batteries are presented in the subsequent sections. Silver-zinc batteries cannot fulfill the cycle life requirement, while nickel-metal hydride batteries have never achieved the status of aerospace batteries. Recently, lithium-ion batteries have shown impressive cycle life performance, combined with reduction in mass and volume, and are well poised to replace the nickel systems in future orbital missions.

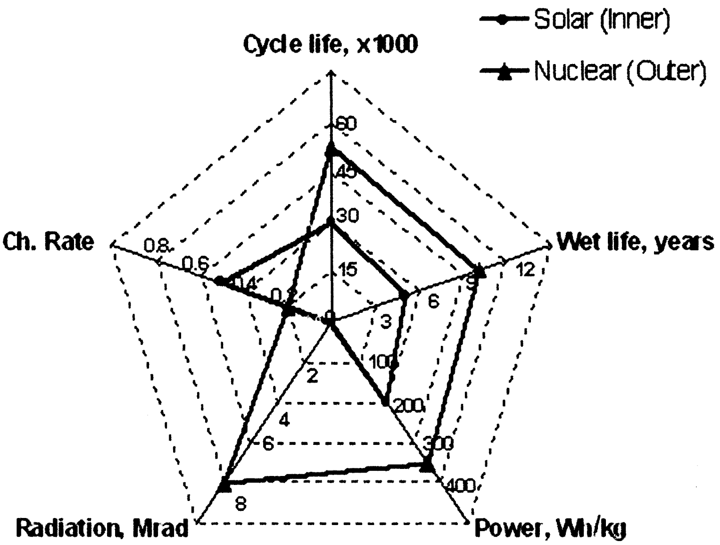

Figure 6.1. Performance requirements of batteries for planetary orbiters.

6.3.1.2. Fly-by and Sample-Return Missions

Fly-by missions are another class of missions, where the spacecraft approaches near enough to perform studies of the planetary object. A fly-by is a flight maneuver in which an aircraft or spacecraft passes close enough to a specified target to make detailed observations without orbiting or landing. The fly-by missions may have science instruments for *in situ* analyses or may be equipped with a sample-return capsule to bring samples back to Earth.

6.3.1.3 Landed Missions – Lander

The primary scientific objectives of the lander mission are to study the biology, chemical composition (organic and inorganic), meteorology, seismology, magnetic properties, appearance, and physical properties of the planetary surface and atmosphere. This class of missions requires energy storage technologies that are mass and volume efficient. Cycle life requirements depend on the mission duration and the power source of the lander. Solar powered missions require rechargeable energy storage with low-to-moderate cycle life capability. Missions that would use Radioisotope Power System (RPS) would require a secondary power source, preferably a rechargeable battery with high power density and long calendar life, for augmenting the RPS power levels.

The landed spacecraft generally experiences extreme temperatures corresponding to the surface temperatures of the planetary body, for example temperature swings as wide as -120°C to + 30°C on Mars, while Moon surface temperatures range from -120 to 90°C. Therefore, it is desirable to have batteries able to work in a wide temperature range. The difficulty of landing on the surface of Mars imposes constraints on mass and volume, due to the scaling impacts on the entry descent and landing system. In particular, entry aero-shell volume is constrained, and the capability of parachutes, propulsive landing systems and landing shock attenuation systems (such as airbags) is entirely driven by the landed mass. Additionally, the volume of the battery is equally critical in accommodating sufficient science equipment on the lander. Reductions in the mass and volume of battery and hence power system will significantly enhance missions, by allowing bigger payload and/or to reduce the mission risk by lowering impact loads.

Governed by the needs of high specific energy and energy density, silver-zinc batteries were used in the past for the planetary landers.[11] However, their limited cycle life became a significant disadvantage. Further, the advent of lithium-ion batteries, which have superior cycle life and calendar life characteristics, with comparable specific energy and energy density, marked the end of silver-zinc batteries for this type of missions.

6.3.1.4. Landed Missions – Rovers

Rovers perform similar scientific exploration studies of the planetary surfaces, such as imaging and performing *in situ* analyses of the surface rocks and understanding the biology and geology of the planetary surface. Unlike landers, rovers are equipped with an additional capability to rove or move around on the surface as commanded, and perform exploration at different sites. Energy storage needs of rovers are similar to those of landers, but are generally even more constrained in mass and volume. Energy storage requirements also depend on whether the rovers are solar or radioisotope powered. Solar powered rovers require rechargeable energy storage with low-to-moderate cycle life capability. Rovers using Radioisotope Power System (RPS) may require a secondary power source, preferably a rechargeable battery with high power density and long calendar life, for augmenting the RPS power levels. Rovers also need energy storage devices that are operational at, and tolerant to, wide temperatures, at least in the range of -30°C to + 40°C. Typical requirements of the batteries for lander and rover orbital missions are schematically represented in Figure 6.2 and listed in Table 6.1.

High energy primary batteries, specifically lithium-thyonil chloride,

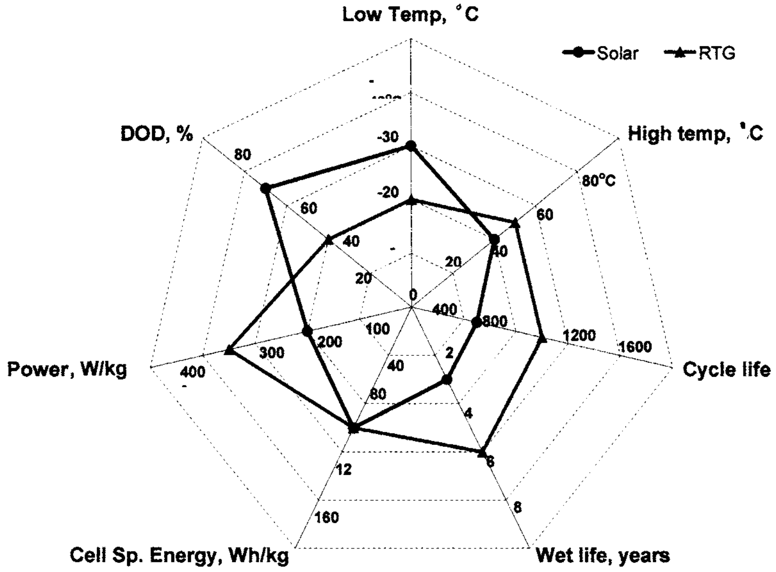

Figure 6.2. Performance requirements of batteries for planetary landers and rovers.

were used in the first planetary rover mission with a limited life.[12] Li-ion batteries have replaced the primary ones in subsequent rover missions and contributed to an extended mission life.

6.3.1.5. Landed Missions - Probes

Another class of planetary *in situ* missions includes planetary probes, such as the Galileo or Cassini-Huygens probe, or planetary penetrators such as Mars Deep Space 2. These missions are equipped with relatively small payload containing science instruments to probe the atmosphere and/or the surface of the planetary object. Being small, they are not equipped with any energy sources, except small batteries. Being constrained by size and mass, the specific energy and energy density are important criteria. Primary battery is often the energy source for these missions, unless the discharge conditions favor rechargeable systems in terms of specific energy and energy density. Also, it is desirable to have the batteries operational at the extreme surface temperatures of the planets, as low as -80°C, because of limitations on thermal insulation. Another unique requirement of the batteries for the penetrators is their tolerance to high levels of impact, as high as 80,000 g, due to severe g-forces during landing. Figure 6.3 and Table 6.1 illustrates the typical requirements of batteries for planetary probe and penetrator missions.

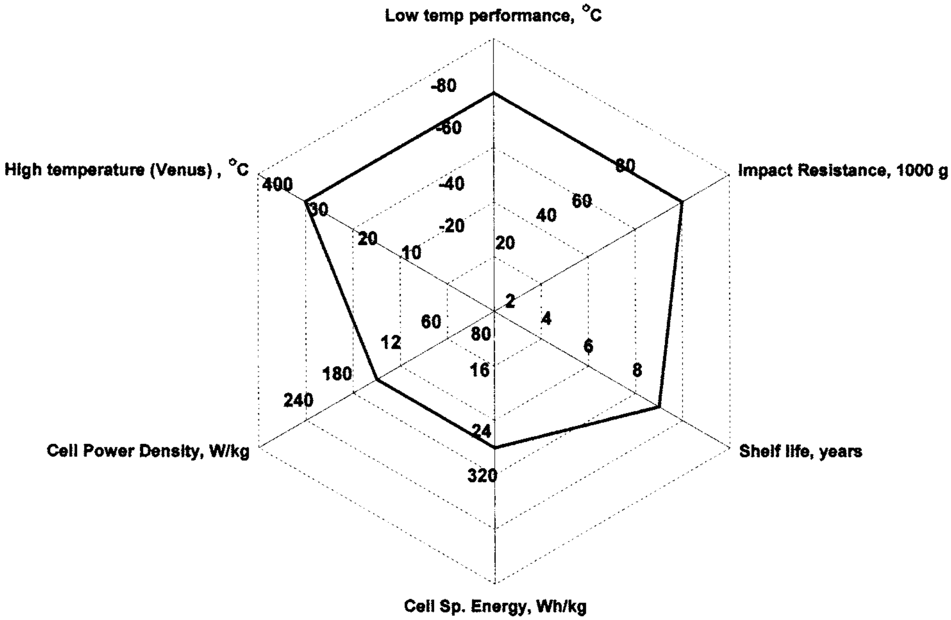

Figure 6.3. Performance requirements of batteries for planetary probes to inner and outer planets.

High specific energy lithium primary systems, especially with liquid cathodes, are the obvious choice for this application, also because of their impressive shelf life. The Li-SO_2 system was adopted for planetary probes, while for microprobe missions requiring ultra-low temperature performance and high impact resistance, modified Li-$SOCl_2$ batteries were developed.[13]

6.3.1.6. Impactors and Penetrators

In these missions, the spacecraft examines the surface of planetary objects more closely, but not in a passive manner. An impactor of large mass, for example of 370 kg in the case of the recent Deep Impact mission, is made to impact with the planetary object. Consequently, a crater is expected to be produced, with the surface layers ejected from the crater revealing fresh material beneath. Likewise, the penetrator is expected to penetrate deep into the planetary surface to probe the compositions underneath. More useful information, neither available from the orbiter images, nor from the rover/lander surface studies, is thus expected from these missions probing the inner layers of the planetary surfaces. In terms of energy needs, the impactor and penetrator missions require primary battery systems, while the mother spacecraft may be powered by a solar array or an RPS and a long-life rechargeable battery, for example Ni-H_2 battery in the Deep Impact mission.

6.3.1.7. Miscellaneous Science Missions

These missions include various science missions that involve optical or spectroscopic studies outside the Earth atmosphere for reduced interference from our atmosphere and enhanced resolution. The spacecraft are stationed in an orbit around the Earth, for example, about 3500 miles away for the Hubble Space Telescope. Since these missions are expected to perform scientific measurements over a few years, the power subsystem typically contains a solar array and a long-life rechargeable battery. Hubble Space Telescope has a Ni-H_2 battery,[14] while upcoming NASA missions, such as Kepler, will utilize the Li-ion battery technology for mass and volume savings.[15]

6.3.2. Human Exploration Missions

Human exploration missions were undertaken in the late 1960s under the Apollo program, which involved human landing on moon. Recent human exploration missions have been focused on Space Station. Various such past and future human exploration missions are briefly described here. Their energy requirements are listed in Table 6.2.

6.3.2.1. Space Shuttle

The shuttle has been used to transport cargo into near Earth orbit, about 100 to 217 nautical miles above the Earth, to the International Space Station. The cargo or payload would be carried in a bay, about 4.65 m in diameter and 18.6 m long. The orbiter would carry a flight crew of up to eight persons for a mission duration of seven days in space. Every U.S. manned space mission during the past four decades has used fuel cell power plants, specifically alkaline fuel cells. The shuttle would contain three fuel cells, each of 12 kW. Cryogenic hydrogen and oxygen tanks would be installed under the payload bay, just aft of the crew compartment.

6.3.2.2. Crew Exploration Vehicles

The Crew Exploration Vehicle and Crew Launch Vehicle missions are

Table 6.2. Energy requirements of human exploration missions.

Mission Element	Missions/ Applications	Energy System	Battery Performance Drivers
Crew Exploration Vehicle (CEV)	Command Module (CM) Service Module (SM)	• 5-10 KWh • 4.5 kW Ave. • 3 x 28 V bus	• Human-rated (Safety) • High energy density • Long life, high power • High temp. resilience
	Crew Launch Vehicle (CLV)		
Surface Ascent Module (PSAM)	Ascent Stage	• 13.5 kWh • 3 x 28 V bus	• Human-rated (Safety) • High energy density • Long life, high power • High temp. resilience
	Descent Stage	• 4.5 kW Ave. • 1 x 28 V bus	
Surface Missions			
Sorties	EVA	• 0.1 – 1 kW	• Human-rated (Safety) • High energy density • Long life, high power • Low and high temp. perform.
	Un-pressurized Rovers/landers	• 1 kW	• Low & high temp perform. • High energy density • Long life, high power • Safety
Outpost missions	Un-pressurized Rovers/landers	• 1 kW	
	Pressurized Rovers/landers	• 1-5 kW	• Human-rated (Safety) • High energy density • Long life, high power • Low and high temp. perform.
	Fuel cell/ battery hybrid power Station	• 10-100 kW	• Human-rated (Safety) • High energy density • Long life, high power

the next-generation shuttles in NASA's future exploration missions to Moon, Mars and beyond. The crew exploration vehicles would be powered by rechargeable Li-ion batteries, of about 5-10 kWh and with an average power of 4.5 kW. The most critical driver for this application is the human-rated characteristic or safety. In addition, the battery system will be required to have high specific energy and energy density. Long cycle life and calendar life are desirable but not critical. As well, the low temperature operation is not mandatory for this application, though the ability to survive relatively high temperatures is requested.

6.3.2.3. Planetary Ascent Stage and Descent Stage Modules

These Lunar Ascent Stage and Descent Modules are intended to facilitate human exploration of lunar surface in the near future and of Mars surface in later years. The estimated average power for these modules would be 4.5 kW and the energy storage is expected to be about 13.5 kWh, both coming mainly from Li-ion batteries. The most critical need for this application is also the human-rated characteristics or safety. Other desirable attributes will be high specific energy, high temperature resilience and long calendar and cycle life.

6.3.2.4. Extra-Vehicular Activities (EVA)

The extra-vehicular activities may be classified as the following:

- Field science (requires surface mobility for each crew member), which includes a) Field observations, b) Geologic sample collection, c) Geophysical profiling, drilling, or trenching
- Emplacement science (require long-duration power), which includes a) Geophysical monitoring (*e.g.*, seismicity), b) Space physics monitoring (*e.g.*, radiation) and c) Astronomical instruments
- Technology demonstrations, which consist of ISRU (*In Situ* Resource Utilization) excavation and processing, surface mobility/transportation and astronaut suit and human-carrying rovers.

The energy needs for these various applications would be different and are expected to be less than 1 KWh. In addition to safety, there is a greater need for high specific energy and wide operating temperature range for the batteries in this category.

6.3.2.5. NASA's Future Surface Exploration Missions

Surface exploration missions may be broadly classified as a) (Lunar) sorties, with limited, four-days of surface exploration and b) Outpost missions, with long-term operations. The sortie missions, which are robotic, may include: 1) EVA, 2) Small unpressurized rovers and landers, 3) Science equipment, and 4) ISRU demonstration (*e.g.*, polar volatile extraction rover). The outpost missions will include: 1) Lunar habitat, 2) Pressurized rover, 3) Science Equipment, 4) Resource excavation (excavation, transportation), and 5) ISRU pilot plant (volatile or regolith resources).

The energy storage systems for the surface exploration will cover a broad range in terms of size and needs. The robotic mobile systems or unpressurized rovers, for example, require power in the range of hundreds of watts, while the pressurized or human-piloted rovers would need several kilowatts. Apart from the usual attributes of high specific energy, long life and safety, one unique performance criterion for the surface missions is the batteries' ability to operate at extreme temperatures. Specifically, these systems require operations at low temperatures of -40 to -60°C, coupled with the ability to survive in high temperatures (<60°C). The outposts and habitat applications require power in the range of kilowatts to several tens of kilowatts for several days. This application requires a rechargeable energy storage system with several tens/hundreds of kilowatt-hours of energy storage capacity, and ability to meet both normal and peak loads. Hybrid systems comprising fuel cells for the base load and rechargeable batteries for peak loads may be the preferred choice.

6.4. Past and Current Planetary Missions

Various planetary and space missions from NASA, the U.S. National Aeronautics and Space Administration, the European Space Agency (ESA) and other space agencies are briefly described below in the same classifications as described above. Details on the missions and their batteries can be found in Tables 6.3–6.5.

6.4.1. Lunar Missions (Apollo)

A series of five, highly maneuverable, Moon-orbiting NASA spacecraft were launched in 1966-67. The Lunar Orbiters' primary mission was to obtain topographic data in the lunar equatorial region to help in the selection of suitable landing sites for the unmanned Surveyor and manned Apollo missions. With this objective achieved by Lunar Orbiter 3, the remaining two flights were able to carry out further photographing of lunar surface features for purely scientific purposes. Altogether, 99% of the Moon was photographed with a resolution of 60 m or better. The Lunar Orbiters also collected data on radiation and micrometeoroids in the circumlunar region.

The power subsystem for these orbiters consisted of four solar panels, to provide power levels of 375 W, and 12-Ah Ni-Cd batteries. The batteries were used during brief periods of eclipse, when no solar power was available.

6.4.2. Missions to Mars and Other Planets

Mariner Missions

Between 1962 and 1973, NASA's Jet Propulsion Laboratory designed and built ten spacecraft named Mariner to explore the inner solar system, visiting the planets Venus, Mars and Mercury for the first time, and returning to Venus and Mars for additional close observations. The Mariners were all relatively small robotic explorers, each weighing less than half a ton.

The power system on the Mariner 2 consisted of two solar cell wings, which powered the craft directly or recharged a 1000-Wh sealed silver-zinc battery, which was used before the panels were deployed, when the panels were not illuminated by the sun, and when loads were heavy.

Power for mariners 3 and 4 was supplied by 28,224 solar cells contained in the four solar panels, which could provide 310 W at Mars. In addition, a rechargeable 1200-Wh silver-zinc battery was used for maneuvers and backup.

Mariner 9 (the first spacecraft to orbit another planet) was able to map 70% of the Martian surface and to study temporal changes in the Martian atmosphere and on the Martian surface. It was powered by four solar panels with a total area of 7.7 square meters and containing 14,742 solar cells. The solar panels could produce 800 W at Earth and 500 W at Mars. Power was stored in a 20-Ah Ni-Cd battery. Mariner 9 arrived at Mars on November 1971 after a 167-day flight. The spacecraft gathered data on the atmospheric composition, density, pressure, and temperature and also the surface composition, temperature, gravity, and topography. Mariner 9 was left in an orbit which should not decay for at least 50 years, after which the spacecraft will enter the Martian atmosphere.

Viking Program (1975)

Viking program consisted of two unmanned space missions to Mars, Viking 1 and Viking 2. Each mission had a satellite designed to photograph the surface of Mars from orbit, and to act as a communication relay for the Viking lander that each mission carried. The orbiters continued imaging and other scientific operations from orbit while the landers deployed instruments on the surface. The power for the orbiter was provided by eight 1.57 × 1.23 m solar panels, two on each wing. The solar panels were made up of 34,800 solar cells and produced 620 W of power at Mars. Power was also stored in two 30-Ah Ni-Cd batteries. Power for the landers was provided by two radioisotope thermoelectric generators (RTG) units containing plutonium-238, providing 30 W of continuous power at 4.4 volts. Four sealed Ni-Cd batteries (8 Ah, 28 V) were also onboard to handle peak power loads. Viking 1 orbiter and its lander continued Martian exploration for about four and six years, respectively, while Viking 2 orbiter and lander survived for about two and 3.5 years, respectively

Mars Observer (1992)

Mars Observer was the first U.S. spacecraft sent to the red planet after the 1976 Viking missions. It was designed to study the geoscience and climate of Mars, specifically the global elemental and mineralogical character of the surface material, and to understand its gravitational and magnetic fields.

However, it turned out to be one of the unsuccessful missions for NASA after it lost contact three days prior to scheduled orbit insertion. Power was provided through a six-panel solar array. During the cruise phase, however, only four panels were deployed (due to the proximity of the spacecraft to the sun) to reduce the amount of power generated. During periods when the spacecraft was in Mars' shadow, energy was to be provided by two Ni-Cd batteries, each with a capacity of 43 Ah.

Mars Global Surveyor (1996)

NASA's Mars Global Surveyor orbiter is the oldest Mars spacecraft still in operation after about ten years, gathering scientific data on topography, gravity, magnetic fields, thermal properties, surface composition, and atmosphere, more than all other Mars missions combined. It was the first successful U.S. mission launched to Mars since the Viking mission in 1976. Aided by its laser altimeter it provided scientists with their first 3-D views of the striking topography of Mars. In its extended phase, this mission's goals have included continued monitoring of Mars until Mars Reconnaissance Orbiter has got into action, imaging possible landing sites for the Phoenix 2007 Mars Scout lander and 2009 Mars Science Laboratory rover.

The power subsystem on the MGS consists of four solar array panels (2 GaAs, 2 SI) providing 980 W of power to the spacecraft at 28 V DC, combined with two 20-Ah Ni-H_2 batteries. Each battery contains eight two-cell common pressure vessels (CPVs), with a total of sixteen cells per battery, as shown in Figure 6.4. A DC-DC voltage converter allows getting the desired voltage of 28 V. The batteries are equipped with usual two strain gauges and two temperature sensors per battery. The telemetry measures battery voltage, half battery voltage and thermally compensated voltages (V_T) for charge control, cell pressures and coulombic integration.[16]

Mars Surveyor Program: Mars Climate Orbiter and Mars Polar Lander (1998)

The Mars Surveyor '98 program was comprised of two spacecraft launched separately, the MCO (Mars Climate Orbiter, formerly the Mars Surveyor '98 Orbiter) and the Mars Polar Lander (formerly the Mars Surveyor '98 Lander). The two missions were to study the Martian weather, climate, and water and carbon dioxide. The orbiter was also to serve as a data relay satellite for the Mars Polar Lander and other future NASA and international lander missions to Mars. The Mars Climate Orbiter was destroyed when a navigation error caused it to miss its target altitude at Mars by 80 to 90 km, instead entering the Martian atmosphere at an altitude of 57 km during the orbit insertion maneuver.[17] The spacecraft power was provided by three panels of GaAs/Ge

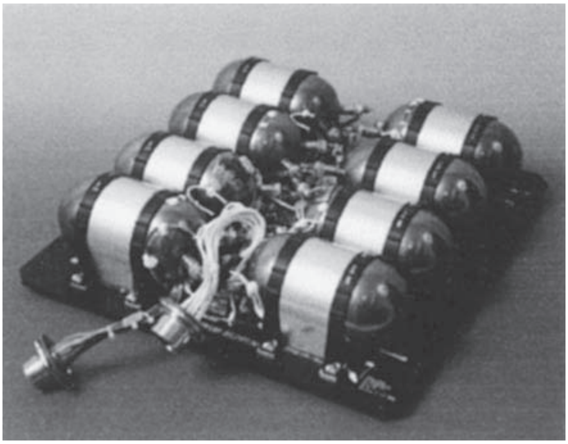

Figure 6.4. $Ni\text{-}H_2$ battery (20 V, 20 Ah) for Mars Global Surveyor.

solar cells on the single-wing solar array, which would provide 1000 W of power at Earth and 500 W at Mars. Augmenting this power source was a $Ni\text{-}H_2$ common pressure vessel battery.

Launched in 1999 with the two Mars Deep Space 2 probes attached, the Mars Polar Lander was scheduled to arrive at Mars in December 1999. After a direct atmospheric entry, the lander was to be slowed by a Mars Pathfinder-heritage aeroshell and parachute. Power would be generated using two GaAs solar array wings deployed from the lander after touchdown on the Martian surface. Two $Ni\text{-}H_2$ batteries were to assist low solar insolation periods and during peak power operations. The failure of the Mars polar lander was attributed to the generation of spurious signals when the lander legs were deployed during descent. The spurious signals gave a false indication that the spacecraft had landed, resulting in a premature shutdown of the engines and the destruction of the lander when it crashed on Mars.

Mars Odyssey (2001)

The core architecture of the 2001 Mars Odyssey electrical power subsystem is direct energy transfer and contains a solar array and a $Ni\text{-}H_2$ battery. The solar array is electrically divided into six segments each consisting of 12 strings of cells. The battery is a single $Ni\text{-}H_2$ cell stack, containing eleven 16-Ah two-cell common pressure vessels mounted to an aluminum baseplate. The energy transfer is performed by the charge control unit, which controls the solar array strings required for the battery charge voltage, according to 16 selectable voltage-temperature (V_T) curves.

Mars Express (2003) and Beagle-2 Lander

In its first planetary mission, the European Space Agency launched Mars Express orbiter and its lander, Beagle 2, to provide remote sensing of the atmosphere, ground and up to 5 km below the Martian surface, to a degree of accuracy never before achieved. Mars Express has since successfully completed its nominal mission lifetime of one Martian year or 687 Earth days. Recently, it was decided to extend the mission by an additional Martian year.

The power system on the Mars Express is comprised of solar panels, which, even when Mars is at its maximum distance from the sun (aphelion), are capable of delivering 650 Watts, more than the mission's maximum requirement of 500 Watts.[18] Augmenting this solar array is a Li-ion battery (67.5 Ah) to provide power during solar eclipse. The unique feature of this Li-ion battery fabricated by AEA/ABSL is that it contains several 18650 (1.5 Ah) Li-ion cells made by Sony corporation with hard carbon anode, lithiated cobalt oxide cathode and with built-in safety attributes in a high volume production environment. These cells were screened by judicious matching criteria to get cells similar in their electrical characteristics, such that there would be no need for any sophisticated electronics to control the charging of the batteries.

Six days before its arrival to Mars, Mars Express ejected the Beagle 2 lander, which was to have made its own way to the correct landing site on the surface, aided by parachute and air-bags. Unfortunately, Beagle 2 was declared lost after it failed to make contact with orbiting spacecraft and ground-based radio telescopes.

Mars Reconnaissance Orbiter (2005)

Taking advantage of Earth's once-in-twenty-six-months close encounter with Mars, NASA launched the 2005 Mars Reconnaissance Orbiter to make a more comprehensive inspection of Mars than any previous mission, with the powerful telescopic camera ever sent to orbit a foreign planet.[19] Some of its penetrating radars will scan underground layers for water and ice, identify small patches of surface minerals to determine their composition and origins, track changes in atmospheric water and dust, and check global weather every day. It is also expected to stream home its pictures and other information using the widest dish antenna and highest power level ever operated at Mars. Further, it will scout the landing sites and provide a critical transmission relay for the surface missions. Mars Reconnaissance Orbiter gets all of its electrical power at 32 V from two solar panels, each with an area of approximately 100 m^2 and containing 3,744 high-efficiency triple-junction solar cells. At Mars, the two panels together produce 1000 watts of power. Mars Reconnaissance Orbiter also uses two Ni-H_2 batteries (Eagle Picher Technologies), as a power source when the solar panels are not facing the sun (such as during launch, orbital insertion and aerobraking) or when Mars blocks out the sun during a period in each orbit.

Each battery consists of eleven RNH-50-71 CPV (Common Pressure Vessel) cell units of 50 Ah, connected in series side-by-side as shown in Figure 6.5. The battery's dimensions are approximately 34.3x118.1 cm with a height of ~10 cm and mass of ~41 kg. The battery is equipped with five temperature sensors and three strain gages. The design features of the CPV cell include an Inconel pressure vessel (diameter: 3.5", 8.9 cm), two-layer Zircar separator, 35-mil slurry plaques, dual stack design of 64 electrode plates, rabbit ear terminal, maximum end pressure of 1200 psi and an overall mass of 2.7 kg. In a typical discharge, ~40% of the battery capacity is used.

In 2006, Mars Reconnaissance Orbiter has successfully entered Martian orbit and has started sending impressive images of Mars. It is currently in the process of adjusting its orbit from elliptical to circular around Mars, by a process termed 'aerobraking'.

Galileo (1989)

Galileo represented a highly successful orbiter mission around Jupiter. It had sophisticated instruments to measure magnetic fields and charged particles, and slowly rotated in order to optimize their measurements. Galileo also carried a descent probe designed to drop into Jupiter's turbulent atmosphere. Galileo discovered strong evidence that Jupiter's moon Europa has a melted saltwater ocean under an ice layer on its surface. The spacecraft also found indications that two other moons, Ganymede and Callisto, have layers of liquid saltwater as well. The power source on the main spacecraft consisted of two radioisotope thermoelectric generators (RTGs), *i.e.*, a combination of fission reactor, using plutonium-238, and thermoelectric devices. The parachute-assisted probe collected 58 minutes of data on Jupiter's weather, as it descended through 150 kilometers of the top layers of the atmosphere. The probe was successfully powered by Li-SO_2 batteries, which provided a nominal power output of ~580 W with an estimated capacity of ~21 Ah on arrival at Jupiter, after 7 years in the cruise.[20]

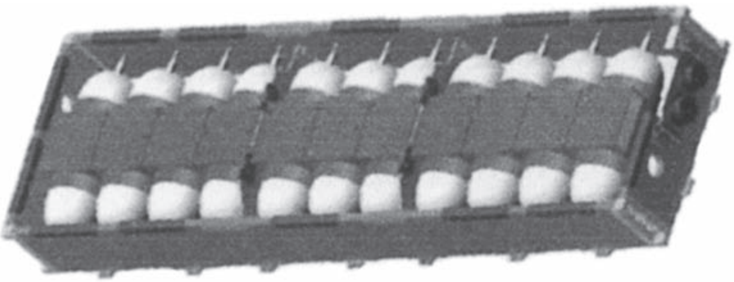

Figure 6.5. Ni-H_2 battery (28 V, 50 Ah) for Mars Reconnaissance Orbiter.

Mars Pathfinder Lander and Sojourner Rover (1995)

Mars Pathfinder represented one of most successful Mars surface exploration missions for JPL and NASA in mid-1990s, and is also the first mission with a planetary robotic rover. It served as a demonstrator mission of a new low-cost landing method - parachutes and airbags - instead of the conventional rocket-powered landing, as in the previous Viking landers. Mars Pathfinder mission enriched our understanding of Mars by returning 2.3 billion bits of information, over 16,500 images from the lander and 550 images from the rover, and more than 15 chemical analyses of rocks and soil and extensive data on winds and other weather factors. Both the lander and the Sojourner rover outlived their design lives - the lander by nearly three times, and the rover by twelve times. The finds suggest that Mars was at one time in its past warm and wet, with water existing in liquid phase and a thicker atmosphere.

Augmenting solar arrays, the energy storage systems in the Pathfinder mission consisted of Ag-Zn rechargeable and Li-$SOCl_2$ primary batteries on the lander and rover, respectively.[21] Both these systems were chosen for their high gravimetric and volumetric energy densities. The challenging requirements for the Ag-Zn battery included: 1) inverted launch, 2) 40 operational cycles, 3) 14 months of total wet stand, and 4) no electrolyte leakage.

In retrospect, a Li-ion battery, if available, would have probably been a better choice. The MPF Ag-Zn battery (27 V and 40 Ah, see Figure 6.6) from BST had unique design features such as 1) robust separator system, 2) minimal

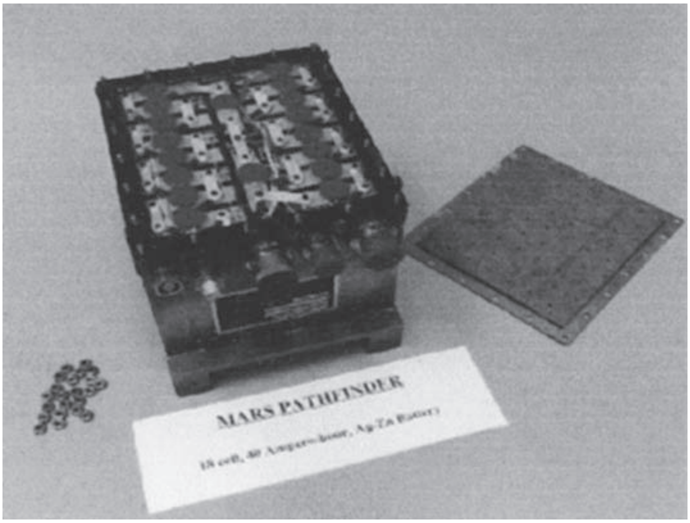

Figure 6.6. Silver Zinc battery (27 V, 40 Ah) for Mars Pathfinder Lander.

free electrolyte, 3) special vent valves and 4) titanium battery case and cover. The battery showed a capacity of 55 Ah in the pre-launch discharge. During the cruise period, it was held under open circuit at ~ 80% state-of-charge and at -5 to 0°C. The MPF lander battery performed satisfactorily and met the mission needs during pre-launch, cruise, entry, descent and landing (EDL), and primary mission (sol 1 - sol 30, sol being the Martian day). In addition, it also supported an extended mission from sol 31 to sol 84. The primary mission required thirty charge/discharge cycles, with discharge at ~C/40 for 16 hours and charge at ~ C/12 for 6-8 hours. After successful completion of the primary mission, the mission was effectively extended, due to prolonged battery life through 84 Martian days, albeit at reduced loads. In addition to the Ag-Zn battery, a Li-FeS_2 thermal battery was also used in the Pathfinder missions to support high pulse loads for pyro events during the EDL sequence.

Sojourner is a small, six-wheel robot, weighing about 11.5 kg. It was designed to land on Mars aboard the Pathfinder, egress and traverse the Martian terrain, performing science and technology experiments, and transmit images and data back to the Lander spacecraft. Even though the primary mission was completed in four days, the rover was designed to survive several cold Martian nights through a warm electronics box heated by radioisotope heater units (RHUs). The power system contained solar panels made up of an "array" of over 200 photovoltaic cells to provide 16 W of power. Additionally, it contained high

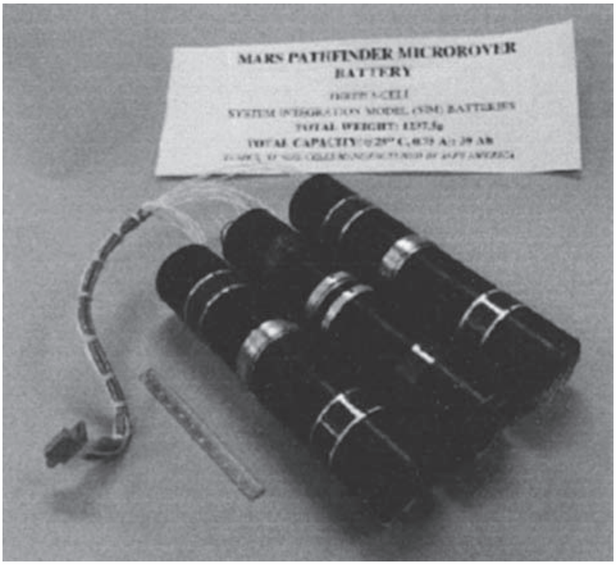

Figure 6.7. Lithium Thionyl Chloride battery (12 V, 39 Ah) for the Sojourner Rover.

specific energy primary batteries for night time experiments and communications. It thus had three Li-$SOCl_2$ batteries of 12 V and 39 Ah (3S3P configuration, see Figure 6.7), which powered the rover through 83 days.

Mars Microprobe-Deep Space 2 (1998)

The 1998 Mars Surveyor Lander mission employed two experimental high technology probes termed as Deep Space 2 Mars Microprobes. Upon arrival at Mars, these probes were to separate from the spacecraft, descend through the atmosphere, and penetrate into the surface of Mars in a pre-selected location. During penetration, the probe was designed to separate into two sections; a surface (aftbody) module, and a subsurface (forebody) module, intended to penetrate one foot into the Martian surface for analysis (see Figure 6.8). The probes contained several instruments for scientific measurements and transmitters for relaying the data to Earth via the 1996 Mars Global Surveyor (MGS) Orbiter. Unfortunately, these missions as well as the primary Mars Surveyor Lander mission did not meet with the anticipated success, but

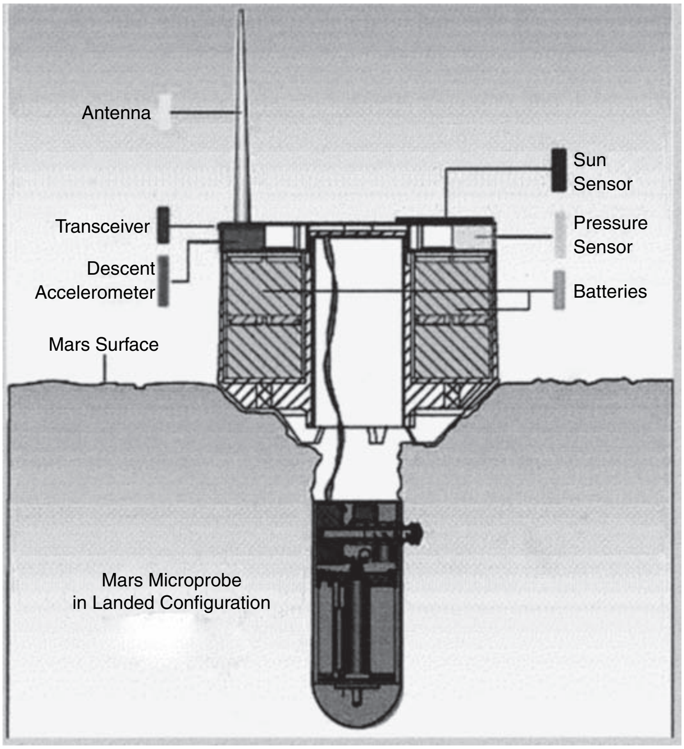

Figure 6.8. Deep Space 2 Mars Microprobe. Forebody: below surface; Aftbody: above surface.

there was notable advancement in the battery technology.

$Li\text{-}SOCl_2$ batteries powered the instruments and communications devices that operate during descent and after penetration into the surface. Due to high impact the probes were to encounter during landing and penetration and the ultra-low temperature the aftbodies were to experience, the batteries had unusual requirements to meet, *i.e.,* tolerance to high impacts of ~80,000g and ability to operate at temperatures of -80 to -60°C, combined with a good shelf life of at least two years.

$Li\text{-}SOCl_2$ battery is the most amenable to such low temperatures,[22] and its performance was further improved by a) the use of $LiGaCl_4$ instead of the conventional $LiAlCl_4$, specifically for reduced passivation and voltage delay at low temperatures, and b) the decrease of salt concentration from 1.0 M to 0.5 M, to reduce electrolyte viscosity, and enhance ionic conduction, among other things.[23] Likewise, the impact tolerance, especially in the axial direction was improved with a pan cake electrode design in half-D size cell hardware (Figure 6.9). Each probe contained two $Li\text{-}SOCl_2$ batteries (Yardney Technical Products), each battery containing four cells to provide a battery voltage of 6-14 V. The battery capacity was 2 Ah at 25°C and 550 mAh at -80°C at C/50 to C/100 discharge rate, with a projected shelf life of 2.5 years and impact tolerance to 80,000g shock. The shelf life was confirmed by microcalorimetric measurements and post-mission performance tests, and the shock resistance

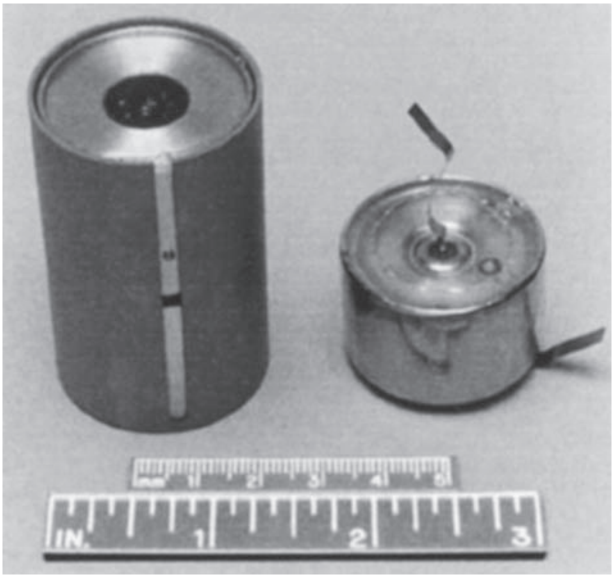

Figure 6.9. Lithium Thionyl Chloride battery (2 Ah) for DS 2 Mars Microprobe.

demonstrated by air-gun tests by JPL during battery qualification.

Mars Surveyor Program (MSP01) Lander (2001)

The rechargeable battery system on the MSP 01 Lander was intended to be Li-ion, which would have been the first of its type in the planetary exploration.[24] The spacecraft was designed to have two batteries in parallel, for redundancy purpose, each with eight 25-Ah Li-ion cells in series. Lockheed Martin designed and fabricated a cell balancing unit, with a complete cell by-pass, once the cells attained the set charge voltages. To facilitate this, individual cell voltages would be monitored, as well as full and half battery voltages and temperatures at five different locations: the baseplate, three cell locations and one for ground testing. Three different chemistries were evaluated for this application, which include Li-ion cells from 1) Yardney Technical Products (currently Lithion), 2) Bluestar Technology (currently part of Eagle Picher), both types containing liquid electrolytes and 3) Alliant Tech. Systems, with a gel polymer electrolyte. Each of these technologies provided good credence to the use of Li-ion chemistry for this application[25] and had distinct advantages, though Yardney battery was eventually down-selected. This battery contained sixteen prismatic Li-ion cells (nameplate capacity: 25 Ah) arranged in 8s2p configuration (Figure 6.10).

These cells contained the first-generation low temperature electrolyte, 1 M $LiPF_6$ in equi-proportion mixture of ethylene carbonate (EC), diethyl carbonate (DEC) and dimethyl carbonate (DMC), developed at JPL.[26] NASA decided to abort this mission mid-way through the spacecraft built. Several subsystems, including batteries were fully developed and fabricated by this time. Many of these components would be used later in the Phoenix lander, a resurrected MSP 01 lander mission. The prototype battery assemblies thus made available were split into individual eight-cell batteries and were subjected to performance tests relevant to both Mars Lander and Mars Orbiter applications.[27] The battery showed impressive performance with little decay in the end of discharge voltage (EODV) after ~1400 cycles over a period of ~5 years. A similar battery tested for the orbiter application has exhibited over 13,000 cycles thus far, once again with little decrease in the EODV and about 9% loss in capacity.[28]

Mars Exploration Rovers (2003)

The 2003 Mars Exploration Rover missions, both Spirit and Opportunity, illustrate the benefits of a Li-ion rechargeable battery system in planetary surface missions, as compared to the conventional aqueous systems.[29] There are several unique features associated with the Li-ion battery system, such that any other battery system would not have resulted in as much success with the mission. For example, the RHU-heated warm electronics box (WEB) of the

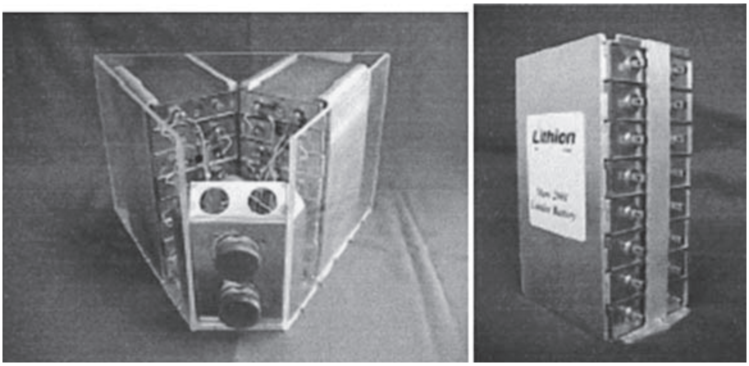

Figure 6.10. Li-ion battery (28 V, 60 Ah [actual capacity]) for Mars Surveyor Lander.

rovers, wherein batteries resided under a controlled thermal environment, imposed severe restrictions on the mass and size of the batteries. A Ni-H_2 battery would have been unacceptably bulky and heavy, so to provide 20-25% only of the desired energy in the available mass and volume. Ag-Zn, while far less bulky, was still twice as massive and provided inadequate lifetime, *i.e.* a mission life of <90 days. A primary battery, as in Sojouner, would have grossly limited the lifetime of the mission.

Spirit and Opportunity constitute two of the most successful space exploration missions in the history of planetary exploration. These two 'robotic geologists' were aimed at examining the surface of Mars and analyzing the core of its rocks to detect the presence of water and, thus, any evidence of life. In addition, they were aimed at providing invaluable information on the geological conditions prevailing on Mars, which will have a bearing on our understanding of its origin.[30,31] Since their exciting landing on Mars at the beginning of 2005, these rovers have successfully completed the primary phase of the missions, which includes about 90 days of operation, and are well into their extended phases, with about 800 Martian sols completed thus far. Several astounding scientific contributions have already been made by both these rovers, including detection of past water at both the landing sites, located at opposite sides of Mars.

The energy conversion system on the rovers is comprised of deployable solar arrays with triple-junction GaInP/GaAs/Ge cells. The BOL (beginning of life) energy of the solar array is about 1000 Wh per sol. Over the course of 500 cycles and 18 months of operation, there have been decreases in their energy levels, partly due to Martian dust accumulation on the array; at that point, the arrays were partly cleaned by localized winds, thus restoring their energy levels (Figure 6.11). The energy storage system on these rovers is comprised of Li-ion batteries, used for the first time in such planetary exploration missions of

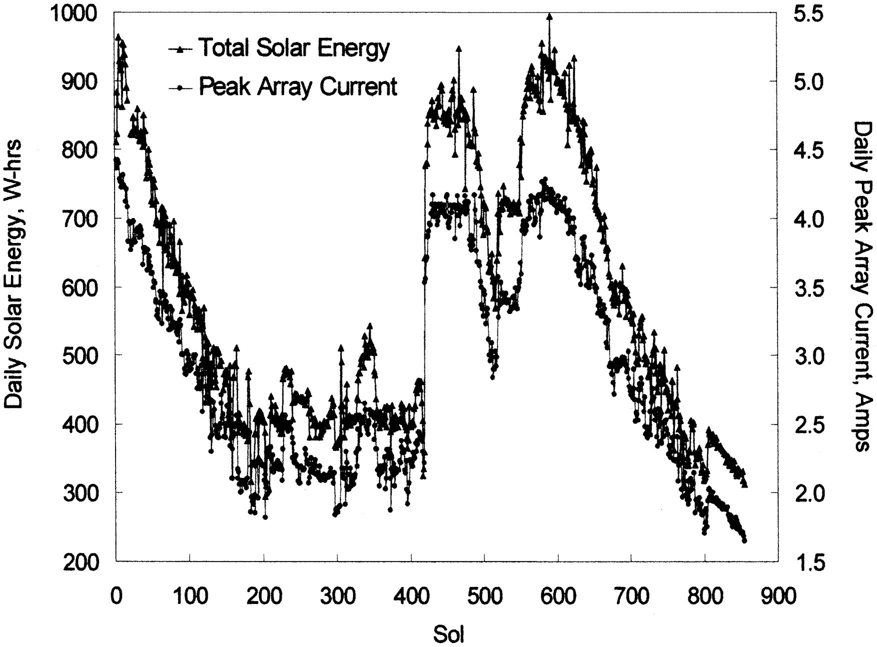

Figure 6.11. Total energy (*upper curve*) and peak current (*lower curve*) of the solar array on-board Spirit rover.

NASA.[29,32,33] A distinct feature of the MER Li-ion batteries is their ability to operate over wide range of temperatures, being enabled by a JPL-developed low temperature electrolyte. Specifically, the batteries could operate down to –30°C as well as at ambient temperatures (30°C), which reduces the thermal management mass and size. They were designed to provide about 200 Wh during launch, about 160 Wh during cruise for supporting anomalies during trajectory control maneuvers (TCM), about 280 Wh for surface operations, and to provide energy to fire three simultaneous pyros (each with a load of 7 A), multiple times during the Entry, Descent and Landing (EDL) sequence. Both Spirit and Opportunity rovers have two parallel Li-ion batteries, each with eight 10-Ah cells in series. The 28 V, 20 Ah batteries were fabricated by Yardney (Lithion), using the same chemistry that was developed earlier for MSP01 Lander mission. This chemistry utilized our first generation low-temperature electrolyte, *i.e.*, 1 M $LiPF_6$ in EC-DEC-DMC. In addition to good low temperature performance, this chemistry showed excellent calendar and cycle life, much more than required by the rover missions, and a wide operating temperature range of –30 to +40°C.

Each of these batteries is electronically-independent on the other, with individual Battery Control Boards (BCBs) to control the battery charges and discharges within specified voltage limits. These BCBs were designed and fabricated at JPL to monitor and control individual cell voltages in each of the batteries and thus to prevent overcharge or overdischarge of any cell. The cell balancing during charge was accomplished via individual cell bypass through a 120-ohm resistor. Several battery parameters were followed via telemetry during the mission. Measurements were obtained for all individual cell and battery voltages, for the current passing through each battery, and for the battery temperature. The four temperature probes (PRTs) are located on two end cells, one on the middle cell and one on the battery casing.

Subsequent to the launch, the batteries were brought down to ~80% of the initial capacity, and the temperature reduced eventually to –10°C during cruise to minimize permanent capacity losses.[32,34] During launch, the lowest cell voltage was 3.82 V; during cruise, the cells were periodically balanced, once the cell divergence increased beyond 140 mV.[32,34] On the surface of Mars, Spirit and Opportunity have thus far completed over 800 sols, with healthy EOD voltages of ~28 V for each battery (Figures 6.12 and 6.13 report data for the first 550 sols).

Despite a software-related anomaly around sol 20 for the Spirit, which led to a complete discharge below 24 V, the batteries recovered well. The maximum and minimum daily temperatures showed continuous decrease to 0°C

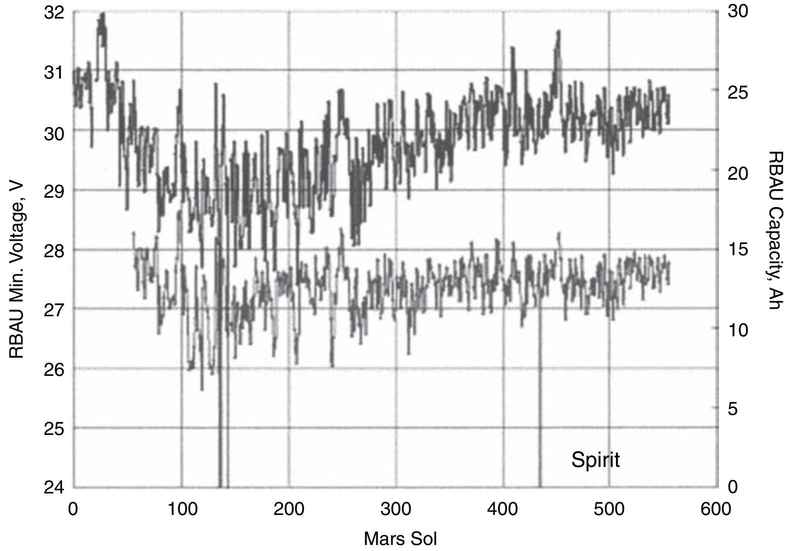

Figure 6.12. EOD voltage (*upper curve*) and capacity (*lower curve*) of the RBAU (Rechargeable Battery Assembly Unit) on Spirit.

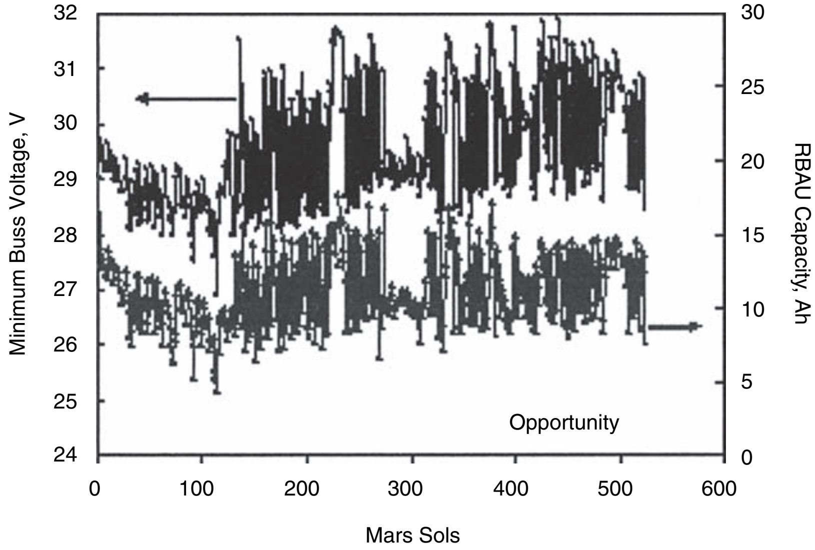

Figure 6.13. Minimum buss voltage (*upper curve*) and capacity (*lower curve*) of the RBAU on Opportunity.

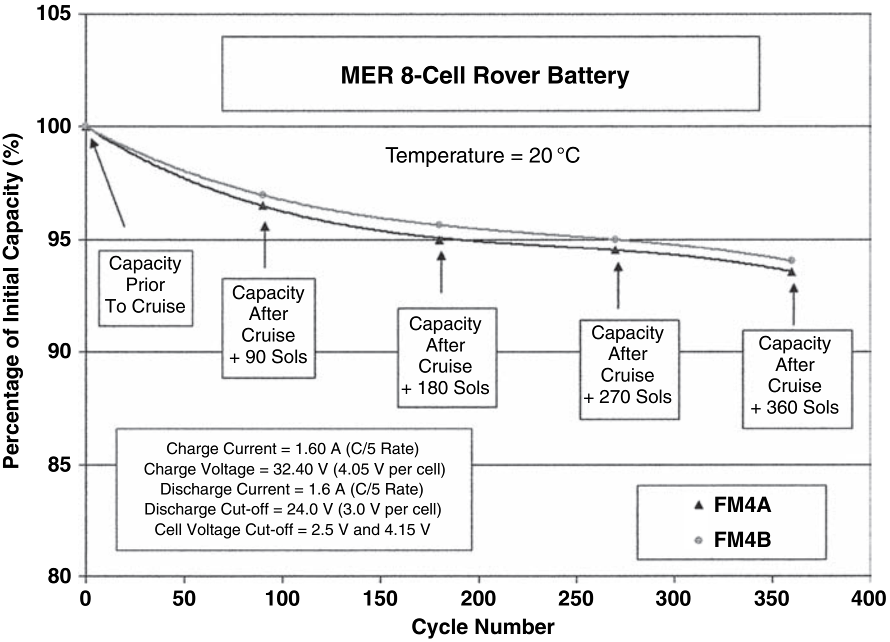

Figure 6.14. Ground experiment simulation of the MER capacity decrease.

and -15°C around sol 200 followed by an increase back to the initial values of 23 and 10°C, respectively.

With the solar arrays doing well and the Li-ion batteries losing less than 10% of their initial capacity during over 800 sols of surface exploration, as also demonstrated in the ground, mission-simulation test (Figure 6.14),[35] the rovers are well poised to continue their Martian studies for another couple of years.

6.4.3. Other Missions

Hubble Space Telescope (1990)

In addition to the solar array (SA3) providing 176 Amps for battery charging and load support, the power system of the Hubble Space Telescope (HST) still relays on the original six batteries. These are connected in parallel through three interconnected busses, with diode isolation, and contain two modules each of three 88-Ah Ni-H_2 batteries. Each of the IPV batteries, manufactured by Eagle Picher /Lockheed Martin, comprises 23 cells in series, but only 22 cells are electrically connected. The cells are based on dry sintered nickel positive electrodes stacked with the platinum negative electrodes, zirconium oxide cloth separators and gas screens on a polysulfone core. The battery's performance has been impressive through over 16 years in flight.[36-38]

International Space Station

NASA and the 15 international station partners marked the fifth anniversary of continuous crewed operations in November 2005. Led by the United States, the International Space Station (ISS) draws upon the scientific and technological resources of 16 nations: Canada, Japan, Russia, 11 nations of the European Space Agency and Brazil. NASA scientists have gathered vital information on the station that will help with future long-duration missions, as the station has a unique microgravity environment that cannot be duplicated on Earth. ISS, the largest and most complex international scientific project in history, has been in an orbit with an altitude of 250 statute miles with an inclination of 51.6 degrees. This orbit allows the station to be reached by the launch vehicles of all the international partners to provide a robust capability for the delivery of crews and supplies. The orbit also provides excellent Earth observations with coverage of 85 percent of the globe and flight over 95 percent of the population. More than four times as large as the Russian Mir space station, ISS has a mass of 183 tons and habitable volume of 424 m^3.

In addition to the 100-kW solar arrays, the ISS electrical power system has a NiH_2 battery. 38 IPV Ni-H_2 cells, are series-connected and packaged in an Orbital Replacement Unit (ORU, see Figure 6.15)[39]. Two ORUs are series-connected utilizing a total of 76 cells. The cells are of the RNH-81-EPI type,

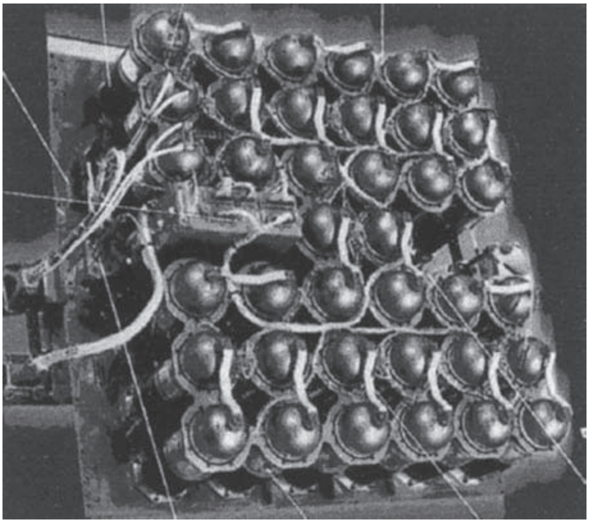

Figure 6.15. Nickel Hydrogen battery unit on board the International Space Station.

each with a capacity of 81 Ah.[39] The ORU has a voltage of 62.3-38 V, an energy of 4 kW, a weight of ~820 kg, and dimensions of 94x104x48 cm. It has been designed for about 38,000 LEO cycles over a period of 6.5 years. The batteries should cycle at 35% DOD, but currently operate at approximately 15-25% DOD. The power subsystem has been successfully maintaining power for all on-board loads, thus meeting or exceeding all ISS requirements. Over a period of 6.5 years, the batteries lost little capacity, such that their replacement is being delayed.[40] There have been proposals by Boeing to replace Ni-H_2 batteries with Li-ion in 2004, but were not approved by NASA for lack of sufficient long-term test data on Li-ion chemistry at that time.

Stardust (1999)

Stardust is the first U.S. space mission dedicated solely to the exploration of a comet, and the first robotic mission designed to return extraterrestrial material from outside the orbit of the Moon. The Stardust spacecraft was launched on February 1999, with the primary goal to collect the dust from Wild-2 Comet, using the lightest aerogel material available. Comets are believed to be the oldest, most primitive bodies in the solar system, possibly comprised of some of the basic building blocks of life. They contain the remains of materials used in the formation of stars and planets, holding volatile, carbon-based rich elements that are likely to provide clues about the nature of the building blocks of our solar system. Stardust spacecraft had a rendezvous with the Comet in January 2004, after nearly four years of space travel.

Recently, in January 2006, the Sample Return Capsule (SRC) of Stardust successfully returned to Earth, bringing the Comet dust for further detailed analysis.

Two non-gimballed solar arrays were deployed immediately after launch. They provided 6.6 m^2 of solar energy to power the Stardust spacecraft, even when it was nearly three times farther from the sun than is the Earth. One $Ni\text{-}H_2$ battery containing eleven 16-Ah CPV cell pairs provided power during eclipses and for peak power operations.[41] The Sample Return Capsule was aided by $Li\text{-}SO_2$ batteries during its re-entry and parachute-supported landing. Two batteries with four cells each (LO26 SHX by SAFT America) were connected in parallel for redundancy purpose. The batteries exhibited an impressive shelf life of ~7 years during this mission.

Genesis (2001)

The science objective of the Genesis mission was to send a spacecraft beyond the influence of Earth to collect pristine material from the solar wind for a period of two years, and then return the samples to Earth for analysis of its elemental and isotopic abundances in state-of-the-art laboratories. These studies will enrich our understanding of the birth and evolution of the planets, their satellites, and all other bodies in our solar system. With the mission being a sample return mission as the Stardust mission, it had considerable heritage from the latter, especially in the power subsystem consisting of solar array and batteries. Indeed, it used the same battery chemistries, *i.e.*, $Ni\text{-}H_2$ for the main spacecraft and $Li\text{-}SO_2$ for the Sample Return Capsule. The batteries went through successful depassivation, about three years after launch, during re-entry, but the improperly-installed g-switches failed to activate the timer subsequently, resulting in a hard landing of the SRC. A majority of the mission's science objectives were achieved, however, through collection and analysis of samples contained in the SRC.

6.5. Future Mars Missions

Phoenix Lander (2007)

The Phoenix Mars Mission, scheduled for launch in August 2007, is the first in NASA's "Scout Program." Scouts are designed to be highly innovative and relatively low-cost complements to major missions being planned as part of the agency's Mars Exploration Program. Phoenix is specifically designed to measure volatile molecules (especially water) and complex organic molecules in the arctic plains of Mars, where the Mars Odyssey orbiter has discovered evidence of ice-rich soil very near the surface. Similar to its namesake, Phoenix "raises from the ashes" a spacecraft and instruments from two previous unsuccessful attempts to explore Mars. The 2001 Mars Surveyor Lander, administratively mothballed in 2000, is being resurrected for the Phoenix Mission. Similarly, many of the mission's scientific instruments have already been built, requiring little or no modification for flight to Mars. Phoenix is a fixed lander, using a robotic arm to dig the ice layer and to analyze samples with a suite of sophisticated on-deck scientific instruments.

Mars Science Laboratory (2009)

The proposed Mars Science Laboratory (MSL) Rover mission (in planning for launch in 2009) has adopted RPS power of about 110 W as the baseline. It would contain a secondary battery, which would be a Li-ion battery, with long-life and wide operating temperatures, for load-leveling purposes. The rover contains a suite of instruments, about ten, to carry out *in situ* analytical studies on Martian rocks, and is expected to traverse over 6000 m during its two years of surface exploration. Due to the planned increases in capability and lifetime of the MSL Rover compared to the MER Rovers, the energy density, specific power, and lifetime of the energy storage systems are important to the MSL mission design. Substantial mass and volume savings are likely if advanced secondary energy storage technology is used. It is likely that the MSL mission would achieve a landed mass saving of ~40 kg from use of Li-Ion batteries, and an even greater reduction in launch mass, compared to the aqueous systems. The required life of 860 Sols and calendar life of three years for Li-ion batteries have already been demonstrated in space by the Mars Exploration Rovers.

6.6. Aerospace Battery Technologies

As mentioned above, different battery technologies, including primary, rechargeable and thermal batteries, were used depending on the needs of the missions and the available technology options, as summarized in Table 6.3, which lists the various primary and secondary batteries used in different NASA missions. A more detailed discussion is presented below on the typical performance characteristics of these energy technologies from this perspective.

6.6.1. Primary Batteries

6.6.1.1. Silver-Zinc

Primary silver-zinc batteries have been used mainly in launch vehicles

Table 6.3. Significant robotic and human exploration missions and their battery systems.

Exploration	Mission type	Mission	Purpose	Year	Energy Storage	Battery system	Mission Life
Robotic	Orbiter/Fly-by	Lunar Orbiter	Earth's Moon	1967	Rechargeable	Ni-Cd	
		Mariner-2	Venus Fly-by	1962	Rechargeable	Ag-Zn	
		Mariner-4	Mars Imaging	1962	Rechargeable	Ag-Zn	Three Years
		Mariner-5	Venus atmosphere	1962	Rechargeable	Ag-Zn	
		Mariner-9	Mars mapping	1972	Rechargeable	Ni-Cd	1st planetary orbiters- 11 m
		Viking-1	Mars mapping	1975	Rechargeable	Ni-Cd	Four Years
		Viking-2	Mars mapping	1975	Rechargeable	Ni-Cd	Two years
		Mars Observer	Mars Orbiter	1996	Rechargeable	Ni-Cd	Unsuccessful
		Mars Global Surveyor	Mars mapping	1996	Rechargeable	Ni-H_2	> 10 years; on-going
		Mars Climate Orbiter	Mars mapping	1998	Rechargeable	Ni-H_2	Unsuccessful
		Mars Odyssey	Mars mapping	2001	Rechargeable	Ni-H_2	> 5 years; on-going
		Mars Express	Mars mapping	2003	Rechargeable	Li-Ion	> 3 years
		Mars Reconnaissance Orbiter	Mars mapping	2005	Rechargeable	Li-Ion	> 3 months; on-going
	Lander	Viking-1	Mars Surface Exploration	1975	Rechargeable	Ni-Cd	Four Years
		Viking-2	Mars Surface Exploration	1975	Rechargeable	Ni-Cd	3.5 Years
		Mars Pathfinder	Mars Surface Exploration	1995	Rechargeable	Ag-Zn	84 days
		Mars Polar Lander	Mars Surface Exploration		Rechargeable	Ni-H_2	Unsuccessful
		Mars Surveyor Program lander	Mars Surface Exploration	2001	Rechargeable	Li-Ion	Mission suspended
		Beagle-2 lander	Mars Surface Exploration	2003	Rechargeable	Li-Ion	Unsuccessful
		Phoenix lander	Mars Surface Exploration	2007	Rechargeable	Li-Ion	90 days design
	Rover	Mars Sojourner	Mars Surface Exploration	1995	Primary	Li-$SOCl_2$	84 days
		Mars Exploration rovers	Mars Surface Exploration	2003	Rechargeable	Li-Ion	> 1000 days; on-going
		Mars Science Laboratory	Mars Surface Exploration	2009	Rechargeable	Li-Ion	680 days design
	Probe	Galileo	Jupiter Environment	1992	Primary	Li-SO2	> 8 years (cruise)
		Cassini-Huygens	Saturn Environment	2004	Primary	Li-SO2	> 8 years (cruise)
		Mars Microprobe-DS2	Mars Sub-surface	1998	Primary	Li-$SOCl_2$	Unsuccessful
	Sample Return	Stardust	Comet Wild-2	1998	Primary	Li-SO2	> 3 years (cruise)
		Genesis	Solar particles	2000	Primary	Li-SO2	> 8 years (cruise)
		Deep Impact	Comet	2002	Primary	Li-$SOCl_2$	> 3 years (cruise)
	Other	Hubble Space telescope	Space Telescope	1990	Rechargeable	Ni-H_2	> 14 years; on-going
Human exploration	Human Lander	Apollo	Lunar Surface				
	Other	International Space Station		1998	Rechargeable	Ni-H_2	> 8 years; on-going
	Exploration Missions	Crew Exploration Vehicle	Transport astronauts to Space/Lunar station	2012	Rechargeable	Li-Ion	N/A
		Crew Launch Vehicle		2012	Rechargeable	Li-Ion	N/A
		EVA	Astronaut suit and tools	2012	Rechargeable	Li-Ion	N/A

to power pyro devices and onboard electronics guidance and control systems. They were also used in a number of military applications such as missiles and aircraft because of their attractive high specific energy, high power density and high energy density (see Table 6.4).

The Ag-Zn cell utilizes a powdered zinc anode, a silver oxide cathode, and an aqueous alkaline electrolyte comprised of potassium hydroxide (40-45%) with dissolved zincate. The most popular configuration is parallel-plate prismatic for sizes from a few Ah to hundreds of Ah. Ag-Zn prismatic cells contain alternate silver oxide and zinc plates separated by layers of polymeric separator. Aerospace Ag-Zn batteries are available from Yardney Technical Products, Eagle Picher Industries & BST Systems Inc.[42]

The nominal cell operating voltage is 1.5 V. The specific energy of a cylindrical cell is 200 Wh/kg and the energy density is >500 Wh/L, with a very high specific power. The battery parameters are generally 50% of the cell values depending on structure, wiring, connectors and sensors. This system has the highest rate capability compared to other primary battery systems. The major limitations of this battery are short storage life (some months) due to dissolution of the active materials, reduced performance at low temperature (70% of capacity at 0°C and 35% at –20°C), limited operating temperature range as for all aqueous systems, and orientation sensitivity. Life is also diminished sharply at elevated temperatures. This battery system has limited applicability to planetary missions primarily because of its limited shelf life.

6.6.1.2. Lithium–Sulfur Dioxide

NASA has used Li-SO_2 cells and batteries in planetary probes (Galileo, Cassini-Huygens probe), sample return capsules (Genesis, Stardust) and the lander of the Mars Exploration Rover (See Table 6.3). The chemistry underlying this system involves metallic Li as an anode, and sulfur dioxide dissolved in the electrolyte as a cathode, whose reduction occurs at the carbon current collector.[43] The electrolyte is formed by 1 M LiBr dissolved in acetonitrile. Other details may be found in Chapter 1. While Honeywell made the batteries for both the Galileo and Cassini-Huygens probe missions, SAFT America fabricated batteries for the Stardust, Genesis and Mars Exploration Missions. Currently, only one U.S. manufacturer, SAFT America, produces Li-SO_2 cells for space and DoD applications.

Li-SO_2 cells have high specific energy (>225 Wh/kg) and high energy density (~375 Wh/L). Deliverable battery outputs depend on the battery design and construction and vary from 50 to 80% of cell values in actual applications. The cell has the highest specific power of lithium primary cells, and can operate between -40°C and 60°C. When the load is applied, this cell exhibits a short

Table 6.4. Performance characteristics of aerospace primary battery systems.

System	Application	OCV	Ah	Configuration	Wh/kg	Wh/L	W/kg	Operating Temp, °C	Self-disch., %/y	Mission life	Manufacturer
Ag-Zn	Prismatic Cell	1.6			200	550	1100	0 to 55	60		YTP, EPI,BST
	Launch Vehicle	28			119	283	118	5 to 40	60	3m	EPI
$Li-SO_2$	Cylindrical Cell	3			238	375	682	-40 to 70	<2.5		
	Galileo Probe	30	21	13S3P	91	147	261	-15 to 60	<2.5	9y	Alliant Tech
	Genesis SRC	24	14	8S2P	142	127	402	-20 to 30	<2.5	6y	SAFT
	MER	30	35	12S5P	136	388	390	0 to 60	<2.5	5y	SAFT
	Stardust	12	20	4S2P	116	182	400	-26 to 50	<2.5	10y	SAFT
$Li-SOCl_2$	Cylindrical Cell	3.65			390	878	139	-30 to 60	<1		SAFT,WG,EPI
	Sojourner	11	36	3S3P	245	514	102	-20 to 30	<1	5y	SAFT
	Deep Impact	33	250	9S24P	221	380	106	-20 to 30	<1	5y	SAFT
	DS-2	14	2	4S2P	128	339	64	-60 to 30	<1	5y	Yardney
	Centaur Launch	30	250	9S	200	517	83	-20 to 30	<1	5y	Yardney
Li- BCX	Cylindrical Cell	3.8			414	933	148	-40 to 70	<2		Wilson GB
	Astronaut Equip	7.6	12	2S	185	211	115	-50 to 72	<2	3y	Wilson GB
$Li-CF_x$	Cylindrical Cell	3.0			614	1051	15	-20 to 60	<1		EPI
	Range Safety	39	24	13S	167	149	14	-20 to 60	<1	10y	EPI

delay, termed as voltage delay or delayed action, in reaching full voltage due to passivation of the lithium electrode.[44] Application of a conditioning discharge or pre-discharge prior to actual use minimizes or reduces this problem. The other limitations of this battery system for space science missions are reduced capacity at low temperatures, uncertain radiation tolerance, and uncertain life capabilities beyond ten years. Some actual mission experience with these batteries is provided in Table 6.4.

This system will be an excellent candidate for planetary exploration missions and applications that require good power densities and moderate specific energy, and operation between –40°C and 60°C.

6.6.1.3. Lithium-Thionyl Chloride

Lithium-thionyl chloride batteries have been used on the Mars Pathfinder Rover – Sojourner (Figure 6.7), New Millennium Deep Space 2, astronaut equipment, and in the Deep Impact mission. Li is the anode material, while the cathode material is liquid thionyl chloride ($SOCl_2$). The electrolyte consists of $LiAlCl_4$ dissolved in $SOCl_2$. In some cells, the use of $LiGaCl_4$ allows cell operation down to -80°C. Preferred Li-$SOCl_2$ cells for space applications have the spirally wound, cylindrical configuration.

A few variants of this basic chemistry have been used. In some cells (Li-BCX) Bromine Chloride (BrCl) is added to the electrolyte to improve safety and performance. BrCl functions as a liquid cathode and provides a higher OCV[45]. Li-$SOCl_2$ are available from SAFT (France), SAFT America Inc., Eagle Picher Industries and Wilson-Greatbatch Ltd., this last company also manufacturing Li-BCX cells.

Li-$SOCl_2$ and Li-BCX cells have higher specific energy (390 - 410 Wh/kg) and energy density (875 – 925 Wh/L) than Li-SO_2 cells (Table 6.4). Deliverable battery outputs vary from 30 to 60% of cell values in actual applications, depending on design and construction. The major limitations of these batteries are low specific power (<100 W/kg), limited performance capability at low temperatures (-40°C), and significant voltage delay especially after storage, due to Li passivation. Use of a conditioning discharge regime prior to use minimizes the voltage delay associated with this system.

6.6.1.4. Lithium-Carbon Monofluoride

Li-CF_x batteries have had limited use in space applications because of their limited rate capability and safety concerns (see Table 6.4). Li-CF_x cells employ Li as the anode material, solid CF_x as the cathode material together with conducting carbon powder, and a liquid organic electrolyte (*e.g.* $LiBF_4$ in PC/DME or $LiAsF_6$ in BL [butyrolactone]).[46] The cells and batteries, made in cylindrical configurations, are available mainly from Eagle Picher Industries, though non-specialty cells are being made by Rayovac and Panasonic.

The Li-CF_x cell exhibits an operating voltage of 2.5-2.7 V and has the highest specific energy (400-600 Wh/kg) and energy density (up to 1000 Wh/L) of the lithium systems (Table 6.4). The major limitations of this battery system are limited performance at low temperatures and very low specific power (~15 W/kg). The last feature is mainly due to low electronic conductivity of carbon monofluoride cathode. Other influencing factors include low conductivity of the electrolyte and low surface area of existing cells with thick electrodes. Developments have been underway recently in all these categories. The electronic conductivity of carbon fluorides may be improved by the use of partially fluorinated carbons, with the fluorination done at low temperatures and with suitable catalysts.[47] The use of such sub-fluorides results in enhanced rate capability and improved low temperature performance.[48] Similarly, electrolytes based on low-viscosity co-solvents, such as fluorinated propylene carbonate and fluorinated ethers, contribute to further enhancement of low-temperature performance.[49] The viscosity is also reduced by the use of low salt concentrations. A novel approach to improve the rate capability would be adding anion receptors to the electrolyte, *e.g.* tris (hexafluoroisopropyl) borate, that would complex with the fluoride ions formed upon discharge, thus preventing the cathode passivation due to precipitation of LiF.

While these improvements to the chemistry appear promising, Eagle Picher undertook the development of high rate and low temperature Li-CF_x cells, by using thin electrodes. Experimental 'D-size' cells thus developed have impressive rate capability. At the discharge of 2 A, which corresponds to ~C/8, the cells delivered about 15.5 Ah, with a cathode specific capacity of 720 mAh/g. This amounts to a specific energy of 463 Wh/kg and an energy density of 860 Wh/L compared to 260 Wh/kg and 440 Wh/L for Li-SO_2 and 260 Wh/kg and 630 Wh/L for Li-MnO_2, respectively. This cell delivers about 11.5 Ah at -29°C and C/15, which corresponds to a cathode specific capacity of 590 mAh/g.

These recent advances make the Li-CF_x system highly appealing for planetary missions requiring primary batteries.[50]

6.6.1.5. Comparative Assessment of Primary Batteries

For a selection of appropriate primary battery systems for a planetary mission, the following is a brief comparison of the currently available systems:

a) Li-SO_2 and Li-$SOCl_2$ batteries provide high energy, moderate to high short-term power capability, and operation within the temperature limits of –40 to

+70°C. The performance at low temperatures, however, declines significantly in terms of both power and energy, and operation above 70°C would create safety problems due to the enhanced internal pressure. Both systems, especially Li-SO_2 have demonstrated impressive shelf life of about ten years at ambient or sub-ambient storage temperatures, as also evident from successful missions, such as Galileo, Stardust and Mars Exploration Rovers, and have abundant flight heritage.

b) Li-BCX batteries have slightly higher energies and comparable temperature limits and performance compared to the Li-$SOCl_2$ system. However, lifetime beyond a few years is uncertain.

c) The radiation tolerance of the primary battery systems is relatively unknown, except for the reportedly good tolerance of Galileo's Li-SO_2 batteries to a cumulative radiation dosage of 600 krad.[51] Also, all the above primary batteries typically meet shock levels of about 5,000g, beyond which not many tests have been carried out, except for the specially designed Li-$SOCl_2$ cells for DS2 (Deep Space 2) that could survive high shock levels of 80,000g.

d) Li-CF_x batteries yield perhaps the highest energy, in a potentially long life, but very low power capability within temperature limits of –40 to +70°C, mainly due to low electronic conductivity and the typically large thicknesses of the cathode.

6.6.2. Thermal Batteries

Thermal batteries are typically used in planetary missions to support high current pulses that are required to perform various pyro events, *e.g.*, during the critical entry descent and landing sequence that lasts for only a few minutes. Such operations include spacecraft separation, parachute opening, firing of retro rockets, *etc.* A thermal battery uses a molten salt electrolyte with high ionic conductivities to permit such high power densities.[52] The electrolyte is in solid form before activation, which combined with a hermetic seal of the battery enclosure, minimizes parasitic losses within the battery and thus provides indefinite storage without degradation of performance. The electrochemical system used for most thermal batteries is formed by a Li alloy anode and an iron disulfide cathode in a molten eutectic mixture of alkali halides. The eutectic electrolyte is the basis for many of a thermal battery's desirable characteristics. The material is completely inert and nonconductive until the battery is activated, at which time it becomes molten and highly conductive and allows the cathode to interact with the anode. The thermal source will be a mixture of Fe powder and $KClO_4$. Ignition of the thermal source supplies the energy to melt the electrolyte and allows the battery to become active. Ignition is generally accomplished by a pulse, from the solar array or battery of the mother spacecraft, to an electrical initiator or by mechanically striking a percussion primer. The advantages of thermal batteries include substantial power density, low and uniform internal impedance while active, minimal noise, and adaptability to a broad spectrum of environments. The configuration of a thermal battery is dictated by mechanical and thermal considerations and is generally a right circular cylinder. Mechanically, since the cell stack components are rigid and brittle, the stack is sealed under mechanical pressure for dynamic environment considerations such as shock, vibration, and acceleration. Thermally, the configuration must be an efficient retainer of heat. The right circular cylinder provides the optimum ratio of internal volume to surface area and the best heat retentive properties, and therefore a cylindrical configuration is utilized if possible.

The various cell components, in the form of pellets, are stacked sequentially, as shown in the single cell of Figure 6.16.[53]

As power density and volume requirements dictate, a thermal battery may consist of a single series stack of cells or of two or more parallel stacks of series cells. The stacks, insulated as thoroughly as possible, are placed in a hermetically sealed stainless steel container. Electrical connections are provided through standard glass to metal seals. Once activated, the battery will continue to function until a critical active material is exhausted or until the battery cools below the melting point of the electrolyte. It is therefore important that the battery be well insulated. The activated battery is somewhat more sensitive to environments; however, it will still function efficiently under substantial shock, vibration and acceleration. Once activated, the battery will climb rapidly (within a couple of seconds) to a peak voltage, which will decline gradually during the remainder of the active life.

The thermal battery that has been repeatedly used in several planetary missions is EAP 12137 (fabricated by Eagle Picher Technologies) with a mass

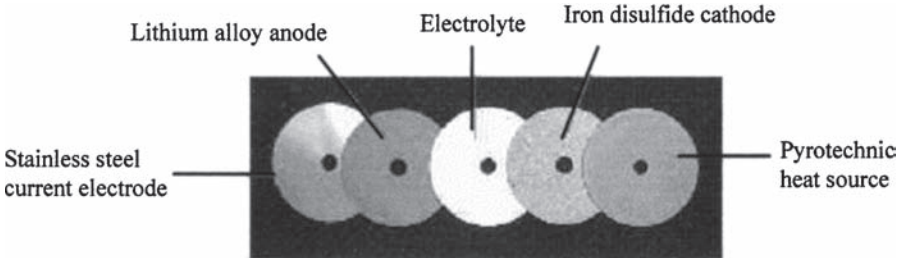

Figure 6.16. Cell components of a typical thermal battery manufactured by Eagle Picher.

of 680 g, diameter of 6.8 cm and height of 5.6 cm, and a typical life time of 650 seconds. This battery successfully supported pulses of 30-50 A even at low activation temperatures of -40°C, in several missions, such as Mars Pathfinder, Mars Odyssey and Mars Exploration Rovers.

6.6.3. Rechargeable Batteries

The rechargeable battery systems that have been so far utilized in planetary exploration missions include aqueous systems, such as Ag-Zn, Ni-Cd, and Ni-H_2, and the non-aqueous system Li-ion. Their characteristics are listed in Table 6.5 and described briefly below.

6.6.3.1. Silver-Zinc

Ag-Zn batteries have been used in a number of NASA applications as rechargeable batteries with limited cycle life. As mentioned earlier, these batteries were used on the Mars Pathfinder Lander to provide ground station power during launch and for supporting nighttime experimentation and communications, including the relayed data from the Sojourner rover to the ground station and then back to Earth for about three months on Mars.[40]

Rechargeable Ag-Zn batteries are similar to the primary Ag-Zn cells and batteries. The major differences are the use of improved separator materials to extend cycle life, and alternate electrode designs. The nominal cell operating voltage is 1.5 V. The cell has specific energy of >100 Wh/kg and energy density ~250 Wh/L. The Pathfinder battery, on the other hand, displayed ~65 Wh/kg at the system level. This system has high rate capabilities compared to other rechargeable alkaline electrolyte cells. The major drawbacks are limited shelf and operating life, limited operating temperature range and orientation sensitivity. Ag-Zn batteries are available from Yardney Technical Products, Eagle Picher Industries and BST Systems Inc. Their use in the future space science missions will be reduced primarily because of their limited cycle life and shelf life (Table 6.5).

6.6.3.2. Nickel–Cadmium

From the 1960s through the early 1990s, Ni-Cd batteries were the workhorses for space missions. Explorer 6 (launched in 1959) was the first spacecraft that used a Ni-Cd battery and was followed closely by the first of a series of successful long-term weather satellites (TIROS). From that time on,

Table 6.5. Performance characteristics of aerospace rechargeable battery systems.

System	Application	Configuration	Capacity		Operating Voltage	Specific Energy, Wh/kg	Energy Density, Wh/L	Operating Temp. Range, oC	Design Life, Years	Cycle Life to Date	Manufacturer
			Rated	Actual							
Ag-Zn	Cell	1	40	51	1.5	128	248	-20 to 25			BST
	Pathfinder Lander	22S	40	51	27	100	191	-20 to 25	2	100	Yardney
Ni-Cd	Standard 50 AH	1	50	62	1.25	37	111	-20 to 25	3		Gates
	Landsat	22S3P	50	60	22-36	34	53	-20 to 26	3	25K	MDAC
	TOPEX	22S3P	50	60	22-36	34	53		3-5	40K	MDAC
Super Ni-Cd	9 Ah Cell	1	9	12	1.25	31	93	-20 to 30	15		EPI
	50 AH Cell	1	50	63	1.25	32	100	-20 to 30	15		EPI
	Sampex Battery	22S	9	12	28	28	72	-20 to 30	5	58K	EPI
	Image	22S	21	24	28	33	71	-20 to 30	5	14K	
IPV Ni-H_2	IPV Cell	1	83	98	1.25	48	71	-20 to 30			EPI
	Space Station	76S6P	81	93	48	24	8.5	-20 to 30	6.5	11K	Boeing
	HST	22S6P	80	85	28	8	4	-20 to 30	5	65K	EPI
	Landsat 7	17S2P	50	62	24			-20 to 30	5	>50K	LMAC
CPV Ni-H_2	CPV Cell	2	16	18	2.50	43.4	77				EPI
	MIDEX MAP	11S	16	18	28	36	21				
	Odyssey	22S2P	16	18	28	36	21.1	-3 to 8	10 to 14	1K	LMAC
	Mars 98	11S	16	18	29	37	41	5 to 10	3		LMAC
	MGS	16S2P	20	23	20	35	25	5 to 10	1 Mars Yr	50K	LMAC
	EOS Terra	54S2P	50	55	67			-5 to 10	5		
	Stardust	11S	16	18	28	36	21	-5 to 11	7	1135 days	LMAC
SPV Ni-H_2	SAR 10065	12S	50	60	28	54.6	59.3				EPI
	Clementine	22S	15	18	28	54.8	78		200 cycles	200 cycles	JCI/NRL
	Iridium	22S	60	70	28	53.4	67.7	-20 to 30			
Li-Ion	2001 Mars Lander	8S2P	50	62	28	105	240	-20 to 30	90 d	1300 (ground)	Yardney
	2003 Mars Rovers	8S2P	16	20	28	92	240	-20 to 30	90d	860	Yardney
	Mars Express	8S45P	68	68	28	90	200	0 to 20	1	10000	ABSL

Ni-Cd cells and batteries became a dominant source of energy storage for NASA spacecraft. The NASA 'Standard Battery', containing NASA 'Standard Cells' (developed in the 1970s), was used successfully in many LEO missions (LANDSAT, TOPEX),[54] GEO missions, and early Mars orbital missions (Mars Observer, Magellan, *etc*). Recently, missions utilized 'Super' Ni-Cd batteries, as standard Ni-Cds were not readily available. Some of the important characteristics of the state of practice Ni-Cd batteries are given in Table 6.5.

Ni-Cd cells have a sintered NiOOH positive electrode. Other details can be found, *e.g.*, in Chapter 2 and Ref. [55]. Prismatic cells replaced the cylindrical ones to extend technology to large capacity cells and for efficient battery packaging. Space quality Ni-Cd cells are significantly different from commercial cells in electrode construction, separator system, and types of seals. The charge control is provided either from the charge/discharge capacity ratio or from charging at constant current, followed by taper current at constant voltage, which is thermally compensated. This thermal compensation (V_T charging, *i.e.* the constant voltage is lowered as the temperature increases) is applied to avoid a possible thermal runaway.

Space Ni-Cd batteries are available in two versions: a) NASA standard Ni-Cd and b) super Ni-Cd. NASA standard Ni-Cd batteries contain electrodes prepared by chemical impregnation methods and employ nylon separators. Super Ni-Cd batteries contain electrodes produced by electrochemical impregnation methods[56] and an inorganic separator material, zirconium oxide (zircar). Standard Ni-Cd batteries are not in production presently in the USA and only super Ni-Cd batteries are available from Electro Energy Mobile Products (formerly Eagle-Picher Ind., Colorado Springs, CO, USA). The availability of these super Ni-Cd batteries is also uncertain due to shift in manufacturing emphasis to other battery systems. However, Ni-Cd cells may be available from Japan or SAFT, France.

Ni-Cd batteries have demonstrated very long cycle life capability and reliability, as evident from their successful and widespread use in several planetary missions, prior to the advent of Ni-H_2. These batteries achieved more than 30,000 LEO cycles at 20-30% DOD, and more than 1000 GEO cycles at a DOD of 50% and even higher. The cells have a specific energy of only 30-35 Wh/kg and an energy density of 60-90 Wh/L; these values decrease by 10-20% in batteries, based on design and construction (Table 6.5).

Super Ni-Cd batteries were found to have outstanding radiation tolerance because of the absence of a polymeric separator. Their Zircar separator was projected to have little degradation from exposure to radiation. The other inorganic cell components including aqueous electrolyte, metallic oxide electrodes, stainless steel cell case and ceramic seals were also projected to be radiation-tolerant. These projections were later confirmed from JPL studies,[57] wherein 37-Ah Super Ni-Cd cells (by Eagle Picher) for Mars

Observer, stored for ten years in refrigerated conditions, were subjected to various cumulative radiation levels using a Cobalt-60 source and exhibit impressive tolerance to 29 Mrads.

The major limitations regarding these batteries are that they are heavy, bulky, have limited operating temperature range, high self-discharge and exhibit a memory effect. On the positive side, they display excellent cycling behavior (several thousands of cycles at partial depths of discharge), impressive calendar life and built-in overcharge tolerance in the form of oxygen recombination.[55] Despite these advantages, the increasing mass and volume constraints and temperature needs of the planetary missions make these batteries unsuitable for future surface missions, such as landers and rovers, especially with the maturation of aerospace Li-ion cells. However, these batteries can be considered for orbital missions, especially where the long cycle life and calendar life are critical. Even for these applications, their applicability is being challenged by the higher specific energy of Li-ion cells, with reportedly continuous improvements in cycle and calendar life.

6.6.3.3. Nickel-Hydrogen

For many space applications, such as planetary orbiters and satellites, the expected cycle life of the batteries may exceed thousands of cycles and the life of the missions extend beyond several years. The Ni-H_2 battery stands out as the preferred choice for orbital and other long-life missions, especially for multiple years of operation.[58] Some of the notable NASA space missions powered by Ni-H_2 batteries include various Mars Orbiters, such as Mars Global Surveyor, Mars Odyssey, and Mars Reconnaissance Orbiter, other long-life missions, such as Hubble Space Telescope (HST), International Space Station, Stardust, Genesis, and several other LEO and GEO satellites. Indeed, the number of cumulative years this system has been in service thus far exceeds that of any battery system, even though it has been in use only for less than two decades.

The first functional Ni-H_2 cell was developed in Russia and the first patent was granted in 1964. In 1970 INTELSAT (COMSAT & Tyco Laboratories) initiated the first aerospace Ni-H_2 cell development for GEO satellites.[59,60] In 1972, the US Air Force and Hughes Aircraft began cell development for LEO satellite applications. These developments were motivated by the fact that Ni-H_2 cells demonstrated a higher specific energy and cycle life than Ni-Cd. An in-depth description of this battery technology as related to various NASA applications is provided in Ref. [61], while the basic chemistry is described in Chapters 2 and 5.

The H_2 electrode consists of a thin-film of Pt black catalyst supported on a photo-etched Ni foil substrate, backed by a gas diffusion membrane. The nickel oxyhydroxide electrode is normally obtained impregnating with $Ni(OH)_2$ a porous sintered Ni powder supported by a Ni screen. The hydrogen formed upon charge increases the internal pressure, which is often used as a state of charge indicator for the cell and for charge control. As the hydrogen pressure can reach ~1000 psi towards the end of charge, the cell pack is to be contained in a pressure vessel with hemispherical caps (typically constructed of Inconel 718 alloy) on both ends to form a hermetically sealed unit, as shown in Figure 6.17.

The Inconel material is especially resistant to hydrogen embrittlement. There exist two design variations in terms of electrode ratios: a) hydrogen precharge, *i.e.*, excess hydrogen compared to the capacity of positive electrode and b) positive precharge, where part of the hydrogen formed during initial charging is vented out. The positive precharge design seems to provide longer cycle life. The negative precharge design, on the other hand, provides a complete protection against deep discharge, with the oxygen evolving from the positive electrode combining with the remaining hydrogen. Two levels of electrolyte concentrations have been widely tested: 31 wt% or 26 wt% KOH solution. Higher electrolyte concentration is believed to maximize the capacity, whereas the lower concentration is reported to extend the life. The current practice has been to use a 31% solution for almost all of the space

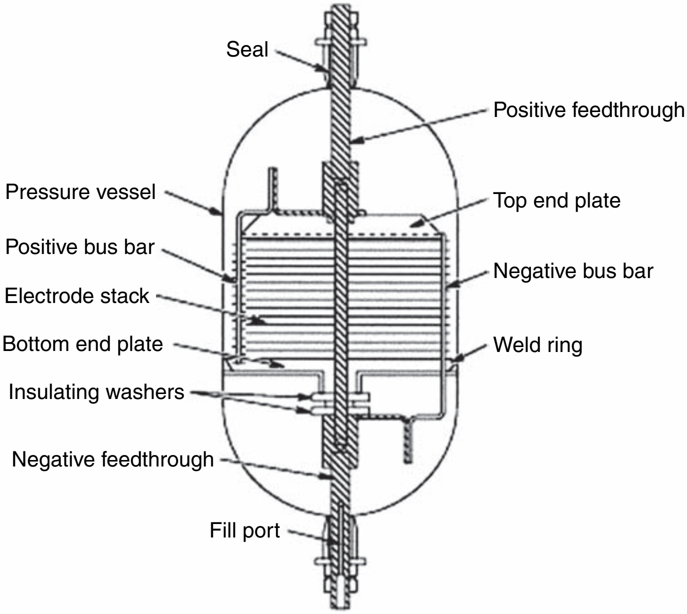

Figure 6.17. Cross-sectional view of the COMSAT/EPI NTS Ni-H_2 cell.

missions. Similarly, there are three variations with respect to pressure vessel: 1) Individual Pressure Vessel (IPV), where each cell is encased in its own vessel, 2) Common Pressure Vessel (CPV), where multiple cells, typically two, share the vessel and 3) Single Pressure Vessel (SPV) where all the cells required for the battery are housed in a single vessel.

Two basic types of electrode stack designs are used for aerospace cells: the back-to-back design of Comsat and the recirculating design developed by a USAF team working with the Hughes Company.[62] In the back-to-back design shown in Figure 5.8 of Chapter 5, two positive electrodes are positioned back-to-back. On either side of the positive electrode are placed separators, followed by negative electrodes (with platinum side facing the positive electrode), and gas screens. These components constitute one module of the electrode stack and several such modules are housed in the pressure vessel, depending on the desired capacity. In the recirculating design (see Figure 5.9 of Chapter 5), there are several modules, each consisting of a gas screen, negative electrode, separator and positive electrode, with the last stage containing a hydrogen electrode and separator. Again, there are two variations for the electrode configuration. In the first configuration, the bus bars are located on the outside of the electrode stack (Comsat design, Figure 6.17), on opposite sides for the positive and negative electrodes. In the second configuration, the electrodes are in the shape of pineapple slice (*i.e.*, in the Air Force/Hughes design) with a large central hole for the tabs, which can be in opposite directions or in the same direction depending on the terminal configuration. In recent years, a modified design known as the "ManTech" design has combined the Comsat stacking arrangement with the pineapple-slice geometry and other features of the Air Force design. This configuration has an improved negative electrode to facilitate gas diffusion, and thermal management. After welding the pressure vessel shells to the weld ring, the vessel is sealed by compression seals. The electrolyte fill tube is a part of the negative terminal and is welded after electrolyte filling. The cell pressure is monitored using a strain-gauge bridge mounted on the dome of the cell.

Multiple cells, typically twenty-two IPV cells or eleven 2-cell CPVs connected in series for a 30 V battery, are mounted on a base plate either horizontally or vertically. In the latter design, which is more common, the cells are mounted using aluminum sleeves, which serve two purposes, *i.e.*, to support the cells on the base plate under launch loads and to provide thermal management by mainly dissipating heat evolved from battery during discharge. A flexible silicone rubber adhesive is used to relieve the shear stress between the cells and the sleeve that develops because of the pressure vessel expansion during charge.

The Ni-H_2 battery is currently being used, for example, in the International Space Station, as illustrated in Figure 6.15. The overall specific energy and energy density of this battery (weight and volume of the assembly included) are 24 Wh/kg and 9 Wh/L.

In the early stages of Ni-H_2 technology, there were many competitive manufacturers and alternative designs. Eventually, it became clear that the ManTech design was superior and that Eagle Picher Technologies had become the dominant producer. A joint NASA/USAF LEO life test study revealed that the Eagle Picher battery was clearly the best for aerospace applications. Significant contributions were made at the NASA Glenn Research Center (Cleveland, OH, USA) to this technology relative to electrolyte concentration, wall-wicks, and standardization of manufacturing processes. After the 1986 Shuttle/Challenger disaster, a joint-services team dedicated itself to applying Ni-H_2 technology to the Hubble Space Telescope (HST). The original five batteries manufactured in 1990 are still supporting the mission. The impact of this was huge in terms of infusing this technology for several later space missions as well as DoD applications. The Ni-H_2 business in the USA peaked at approximately 6,000 cells/year (or $90 M/year) normalized to 50 Ah, with HST, ISS and Defence programs accounting for the bulk of this market. Eagle Picher has supplied about 90% of the Ni-H_2 cells and batteries for the various national and international space programs.

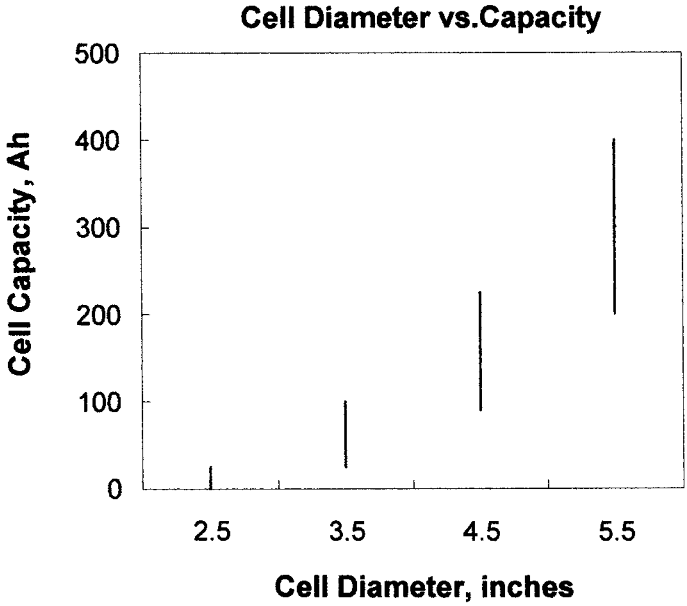

Figure 6.18. Variation of the Nickel Hydrogen cell capacity *vs.* cell diameter.

Over the years, several Ni-H_2 cell designs have evolved. The most common design is the IPV cell. This cell has a voltage under load between 1.20 and 1.27 volts. Pressure vessel diameters range from 6.3 cm (2.5 in) to 14.0 cm (5.5 in). Cell capacities range from 20 to 350 Ah, depending on the diameter of the cell (Figure 6.18).[63]

Because this cell requires a pressure vessel, the volume is large compared with the Ni-Cd and the energy densities are relatively low, about 60 Wh/L. The specific energy, on the other hand, is higher than that of Ni-Cd; the IPV Ni-H_2 cell has a demonstrated specific energy of 50 Wh/kg. Use of a common pressure vessel (CPV) or a single pressure vessel (SPV) battery can further enhance specific energy and reduce the volume. The SPV design, which consists of 22 cells in a single case, is more efficient from a battery structure point of view. Batteries using these cells typically contain between 16 and 76 cells. SPV Ni-H_2 batteries have been manufactured and flown in the Clementine and Iridium programs. The capacities for these batteries are lower than the batteries using IPV cells. For example, cells for commercial IPV batteries can be as high as 350 Ah, while the largest SPV battery flown (on the Iridium Program) to date is 50 Ah.

Typical performance characteristics of these batteries are listed in Table 6.5 and some of the notable NASA's missions utilizing Ni-H_2 batteries are listed in Table 6.3. Apart from a higher specific energy compared with Ni-Cd cells, Ni-H_2 cells offer longer life at a higher DOD. Cells designed for the ISS, for example, are expected to reach 30% DOD compared with Ni-Cd cells that are typically designed for 10-25% DOD and often operate at lower DOD. Ni-H_2 cells cycled at 50–75% DOD have far exceeded the performance of Ni-Cd cells. Cells in GEO orbit have been designed to meet a requirement of 75% DOD at its maximum eclipse period compared with the 50-60% for Ni-Cd cells. Additional benefits for Ni-H_2 cells include: a) simple state of charge indication from internal pressure, b) potential cell reversal without damage to the cell, c) greater tolerance to overcharge than Ni-Cd cells. The disadvantages, on the other hand, include: a) heat generation on overcharge and possible internal shorts caused by "popping" (the uncontrolled recombination of oxygen with hydrogen on the catalyzed surface of the negative electrode); b) possible pressure vessel punctures/leaks/rupture; c) high loss of capacity on storage; and d) higher cell cost.

Ni-H_2 batteries have been used in several Earth and planetary orbiting missions since the first commercial flight by INTELSAT V in 1983. Because of its demonstrated long life in GEO, this battery has been the workhorse for commercial communications satellites over the past 20 years. NASA first utilized Ni-H_2 batteries in a LEO orbit when it launched the HST mission. These batteries, operating at a low DOD (10%), have performed flawlessly since 1990.

In addition to DOD, a correct temperature range is crucial for the battery's life. The usual operating range for Ni-H_2 cells is -10°C to +30°C. The temperature of the battery structure or base plate needs to be controlled in a spacecraft and this may be done in either a passive or an active manner.

One method to optimize battery life in a LEO application is to use a temperature-compensated voltage control (V_T), *i.e.*, a temperature-dependent charge voltage, when the cells reach a point at which gassing occurs. This method, already mentioned for the NiCd cell, consists in drawing a high constant current from the solar arrays until the battery reaches a pre-set voltage limit. The charge process is highly efficient during this period. When the battery reaches the preset voltage, a taper current passes for the rest of the charge duration. The charge voltage is adjusted with temperature, specifically reduced as the temperature increases, to avoid uncontrollable overcharge. In addition, the charge control system will account for unexpected high depths of discharge and/or imbalance between cells and/or batteries. This approach for charge control contributes to the long life achieved in many missions and is particularly relevant to orbital missions. In a GEO orbit, when the cells are in the sun, a trickle charge is applied to minimize the current and the heat generated during the long charge process. During the eclipse season, the battery is charged at higher rates to return the energy provided. Then the charge current is reduced using a V_T control or, in the Ni-H_2 case, signals from pressure transducers indicating that the cells have reached a point of near full charge. The current is then reduced to minimize the overcharge current.

6.6.3.4. Nickel-Metal Hydride

For the chemistry of this system, see Chapter 2. Ni-MH batteries had an impressive start during the 1990s when they were introduced in the portable electronics market to replace Ni-Cd batteries.[64,65] They provide a remarkable improvement in energy, compared to Ni-Cd, with almost identical performance characteristics otherwise. There are uncertainties relative to the cycle life of Ni-MH cells, especially at partial depths of discharges, where Ni-Cd batteries have well-established cycle lives of over 30,000 cycles. Ergenics (Ringwood, NJ, USA) has developed a battery that might be attractive for aerospace applications, as it combines the energy storage capability of metal hydride alloys with the excellent cycle life and discharge rate capability of the Ni-H_2 battery. As soon as H_2 is formed on charge, it is allowed to flow through a valve towards a metal alloy where it is stored. The alloy is in a separate compartment and is not immersed in corrosive electrolyte, this resulting in indefinite alloy life. Increased cycle life of the battery comes from the separation of the electrode materials when the battery is on open circuit. Upon discharge, H_2 is released again through the valve and can reach the "electrochemical section" of the battery. Compared to a conventional Ni-MH battery, this system possesses a clear advantage not only in cycle life, but also in rate performance. Indeed, the alloy is not required to store H_2 and be, at the same time, the support for the electrochemical reaction, which instead takes place on an electrode favoring a fast redox process.

Before the Ni-MH chemistry was thoroughly evaluated for space needs, the interest in developing Ni-MH batteries faded quickly, especially within the aerospace community, with the advent of Li-ion batteries that provide almost a two-fold benefit over Ni-MH batteries in specific energy. In fact, it is highly likely that Li-ion batteries will gradually replace Ni-H_2 for many future space applications.

6.6.3.5. Lithium-Ion

The Li-ion battery system is a relatively newcomer to aerospace applications. However, it is rapidly becoming the preferred choice for a number of missions, especially with demanding mass and volume requirements and moderate cycle life requirements. Rapid technological advancements were made on this battery system over the last several years, mainly prompted by the portable device market. Most of these devices are powered by small capacity (1-2 Ah) Li-ion batteries that were employed in the space shuttle to power camcorders and other tools used by the astronauts. While some of the European missions, for example Mars Express and Proba, and other applications such as astronaut tools in shuttle have also been powered by these small-capacity cells, particularly those made by Sony, larger cells have started emerging in prismatic, cylindrical and wound-prismatic configurations for aerospace needs. Such developments in the USA may be attributed to a successful NASA-DoD consortium[66] set up to develop the manufacturability of Li-ion cells of 5-200 Ah with various specific requirements, *e.g.*, low temperature operation, high capacity, long cycle life and good calendar life.

Advantages and Disadvantages. A survey of the characteristics of Li-ion cells can be found, *e.g.*, in Chapter 1. The most significant advantages of these cells are their high specific energy and energy density. These batteries allow three to four times mass and volume savings compared to the state of practice aerospace systems, *i.e.*, Ni-Cd and Ni-H_2, which results in reduced launch and landing costs, increased payloads and enhanced mission science activities. Further, this system has no parasitic losses and hence has high coulombic efficiency, close to 100% compared to ~75% for the aqueous systems, which in turn results in reduced solar array sizing as well as smaller radiators for heat rejection.

Such advantages are also significant at low operating temperatures, due to the inherent capability of Li-ion cells to function better at sub-zero temperatures, by virtue of their non-aqueous electrolyte solutions. This characteristic is especially beneficial in planetary exploration missions, often considerably enhancing, if not enabling, the missions. The higher cell voltage, about three times that of aqueous systems, translates into fewer cells and interconnects. Further, the self-discharge rate is significantly lower, about three to five times lower than that of Ni-Cd cells and about ten to fifteen times lower than that of $Ni\text{-}H_2$ cells, which implies reduced maintenance. Two minor deterrent factors for the use of Li-ion batteries, on the other hand, include: a) the absence of overcharge-limiting reactions, which necessitates sophisticated electronics to avoid cell overcharge, which could be a potential safety hazard and b) limited demonstrated cycle life, inferior to that of $Ni\text{-}H_2$, at all depths of discharge, as shown in Figure 6.19.

The research to further improve the performance of these cells is focused, as far as the electrolytes is concerned, mainly on enhancing the low temperature performance as well as improving the high temperature resilience.[67-72] In other words, extending the operating range of Li-ion batteries is of great benefit to the planetary surface missions, especially in terms of thermal management. As for the cell design, the improvements include replacement of stainless steel cases with aluminum or pouch cases. Apart from these developments in the cell components, several aerospace laboratories have been engaged in establishing or demonstrating the capabilities of the Li-ion technology for various space applications, such as orbiters, satellites, landers and rovers. These studies include performance tests under various conditions, *i.e.*, cycling at different DODs and temperatures.

Aerospace Li-ion batteries are being manufactured or developed by few manufacturers across the world. These include: 1) In the USA, Yardney Technical Products, SAFT America, NRO/DoD, NASA, AFRL, and to a small extent Eagle Picher Industries, 2) In Japan, the Japanese Space Agency and Japan Storage Battery Company, and 3) In Europe, the European Space Agency, SAFT Battery Company in France, and AEA (currently ABSL) in the UK. All these manufacturers make large capacity cells of different sizes, while ABSL make aerospace Li-ion-batteries with 18650 cells made by Sony Corporation.

Current Li-ion cells have a specific energy of 100 to 150 Wh/kg and an energy density of 250 to 350 Wh/L, depending on cell size and chemistry/vendor. These values are typically 20-30% lower when calculated at the battery level. Expectedly, the derating of energy values at the battery level is less than with $Ni\text{-}H_2$ batteries, due to relatively simpler battery designs. The typical cycle life exhibited by state of art aerospace Li-ion cells is over 1000 cycles at 100% DOD with a fade rate of 0.015-0.03% per cycle. The demonstrated operating temperature range is from –20 to 40°C, with capacities

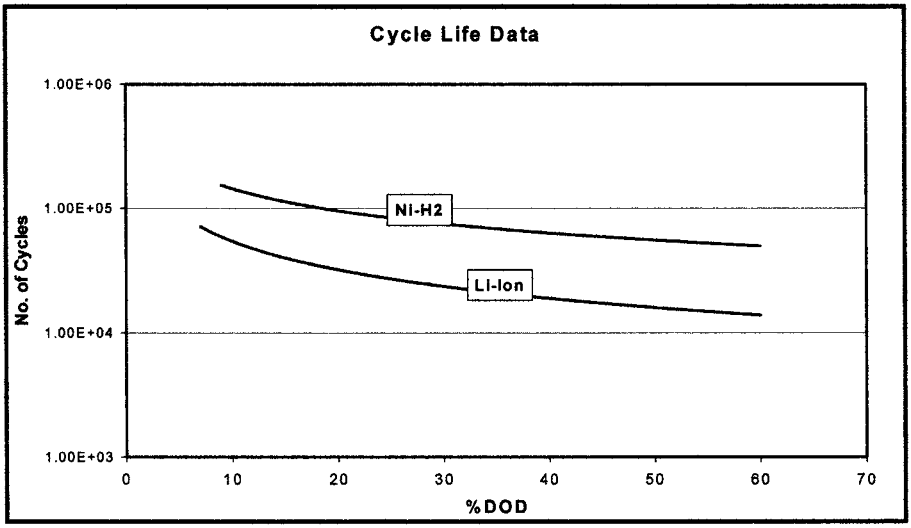

Figure 6.19. Expected lifetimes of Ni-H_2 and Li-ion batteries at different DODs.

Table 6.6. Performance characteristics of aerospace Li ion cells from various sources.

	Yardney	EPI	SAFT-USA	MSA	JSB	ABSL
Chemistry	MCMB, $LiNiCoO_2$	MCMB, $LiCoO_2$	C, $LiNiCoO_2$	MCMB, $LiCoO_2$	C, $LiCoO_2$	MCMB, $LiCoO_2$
Amp-Hrs	5, 10,25,55	6,25	4,8,44,115	10,50	50,100,175	
Cycle Life (GEO)						1350
Cycle Life (DOD %)	18,000 (30%)	8000 (30%)	18,000 (30%)	>10,000 (40%)	> 10,000	11,000 (30%)
Cycle Life-100%DOD	>1000	>1000	>1000		>1000	>1000
Sp. Energy* (Wh/kg)	130-145 (C) 110 (B)	110-130	130-150 (C)	98-123	136-146	104 (B)
En. Dens. (Wh/L)	260-300	240-260	277-315	256-315	254-300	

* C=cell; B=battery

as high as 70% of room temperature values been realized during cycling at -20°C at the C/5 rate. The performance characteristics of aerospace Li-ion cells are summarized in Table 6.6. (Note: The partial DOD cycle life values expressed here represent the number of cycles demonstrated to date and do not necessarily represent the respective technology's capability).

MSA cells under NRO/DoD (National Reconnaissance Office/Department of Defence) program.

The NRO/DoD program in the USA is focused on developing Li-ion cells/batteries required for LEO applications, and the program is aimed at developing 10-50 Ah prismatic cells with >30,000 cycles at 30% DOD. The chemistry of this cell is similar to that used by Sony. The technical approaches being pursued to improve the cycle life performance include: a) establishment of stringent process controls, b) optimization of operational regimes (DOD, charge voltage selection and temperature of operation), c) minor modifications in cell chemistry in terms of electrolytes and electrode additives, and d) the use of lightweight cell components and Ziegler terminal seals. Experimental cells have been fabricated and the cycle life performance assessment of these cells is in progress at a number of institutions.

Yardney (Lithion) Li-Ion Batteries.

Yarndey Technical Products, or its subsidiary Lithion, produces Li-ion cells and batteries mainly for aerospace and defense applications. The cells are truly prismatic, with several flat plates of cathode and anode connected in parallel to get the desired capacity. One such early cell, the 20-Ah cell developed for the Mars Surveyor Lander, is shown in Figure 6.20. The case is isolated from the terminals with glass to metal seals. The electrolyte in many of the aerospace applications consists of 1M $LiPF_6$ dissolved in an equi-proportion mixture of EC/DEC/DMC, an early formulation developed at JPL for enhanced low

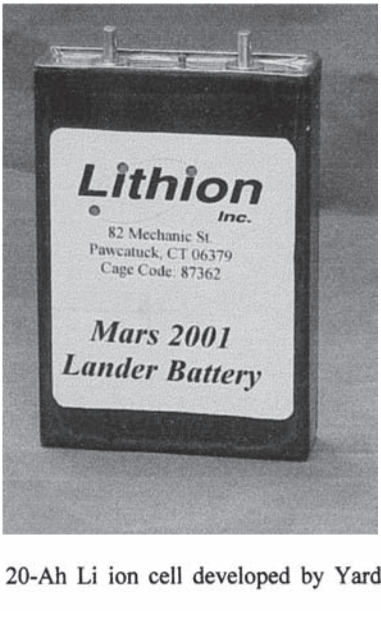

Figure 6.20. True prismatic 20-Ah Li ion cell developed by Yardney in 1996 for NASA/DoD Consortium.

temperature performance.

Table 6.7 lists various Li-ion cells made by Lithion. The aerospace cells range from 7 to 55 Ah, with specific energies of 120-145 Wh/kg in the high energy versions. The high-rate versions, on the other hand, can operate at 10C (continuous), albeit with a lower specific energy, 105 Wh/kg.

Specific examples of aerospace cells include NCP-8 for Mars Exploration rover, NCP-12 and NCP-43 used for the X-37 (unmanned vehicle to test technologies), NCP-25 for Mars Landers and the NCP-55 examined for EAPU (Electric Auxiliary Power Unit) needs.

SAFT

At SAFT, a mixed Ni-Co oxide as cathode and graphitic carbon as anode are used. The cells are cylindrical, initially with a stainless steel negative case, and later with an aluminum positive case. Cell capacities of 4 Ah (D-size), 9 Ah (DD size), 40 Ah and 100 Ah are available. In addition, high rate designs of ~15 Ah were developed for specific applications. DD cells have been evaluated for planetary rover applications, while 40-Ah cells are used for satellites, space shuttle, and DoE hybrid vehicles. Details on the high-capacity SAFT cells can be found in Chapter 4.

AEA (ABSL)

AEA, currently ABSL Power Solutions, claim to have the tools and capability to design and manufacture batteries for demanding environments, where vibration, thermal cycling and electromagnetic compatibility become key issues. High reliability batteries and chargers have been designed for spacecraft, aircraft, balloons, and unmanned airborne vehicles (UAVs). Batteries can be sized precisely and with confidence for long missions attested by the vast amount of data, over 40 million hours of life test data.

The approach adopted by AEA/ABSL is different from other aerospace Li-ion battery manufacturers. Instead of designing batteries with cells of the desired capacity, ABSL utilizes multiples of small 18650 cells in the desired series-parallel configuration. With a cell capacity of ~1.5 Ah, an 8 cell string (8S) will have a voltage of 30 V. Several such strings are connected in parallel to produce the required capacity. For example, a 20-Ah and 30 V battery qualified for GEO applications and being used on NASA's Kepler mission has 16 such strings (8S16P). The batteries are thus modular and meet the needs of redundancy even with the failure of one or two strings. Another distinct advantage, as claimed by ABSL, is the lack of necessity for electronic cell charge control. The cells, being made rather uniformly in well-controlled and fully automated operations, and subsequently well matched in terms of impedance and self-discharge, will have little divergence in the course of cycling or storage. Accordingly, battery charging may be controlled based on

Table 6.7. Standard Li-ion cells produced by Yardney (Lithion).

Model	Capacity (Ah)^1	V	Discharge Rate (A)		Discharge Temp Degrees C	Width^3 (mm)	Thickness^3 ((mm)	Height^3 (mm)	Weight (kg)	Energy Density Wh/l	Specific Energy Wh/kg
			Continuous^1	Pulse^{1,2}							
NCP0.05-1	.05	3.6	0.25	0.5	-20 to +60	14	4	25	0.004	175	60
NCP7-X*	7	3.6	Up to 140	*	-40 to +60	52	25	77	Varies by Cell Type		
NCP8-1	8	3.6	40	80	-40 to +60	78	25	64	0.305	320	130
NCP9-1	8.5	3.6	16	24	-40 to +60	54	19	100	0.246	289	121
NCP12-1	12	3.6	60	120	-20 to +50	71	25	102	0.420	305	125
NCP12-2	12	3.6	120	600	-40 to +60	71	25	102	0.422	237	102
NCP25-1	30	3.6	125	250	-20 to +50	95	28	152	0.890	335	145
NCP25-2	25	3.6	250	1250	-40 to +60	95	28	152	0.908	250	105
NCP43-1	43	3.6	86	344	-20 to +50	107	31	166	1.270	340	142
NCP55-1	50	3.6	200	400	-40 to +70	138	34	145	1.600	265	112.5
NCP55-2	55	3.6	100	300	-20 to +50	138	34	145	1.582	291	125.16

1. Room temperature. 2. 0.1 seconds. 3. External dimensions, without terminals.

* This family includes several types

string voltage rather individual cell voltages, which is also enabled by built-in safety features within the cells.

Japan Storage Batteries

Japan Storage Battery (JSB) Company is developing cells of 50-190 Ah for GEO and LEO and has distributed several cells to U.S. aerospace companies for evaluation. The performance characteristics of these cells are listed in Table 6.8. The number of cycles achievable at low DOD (<40%) is impressive: the cycle life of Li-ion cells and batteries improves considerably as the DOD is reduced, similarly to the behavior of nickel systems. JSB cells are shown in Figure 6.21. These cells are built in wound-prismatic configuration to take advantages of the ease in fabrication for a wound cell and packaging for a prismatic geometry.

6.7. Unique Performance Attributes of Aerospace Li-Ion Batteries

Apart from the general performance characteristics, aerospace Li-ion batteries have unique performance attributes, such as good low temperature performance, long cycle life at partial DODs for orbital or LEO satellite applications; and long calendar life for outer planetary or GEO satellite missions. The current status in these areas and the on-going studies to demonstrate or improve these characteristics are briefly described below.

Table 6.8. Performance characteristics of JSB aerospace Li-ion cells.

Cell Type	DOD%	Cells on Test	Cycles to Date	Start Date	Estimated Cycles to Failure	Cycling Conditions	Temp (°C)	Testing at
LSE 100	7 avg.	2	80,000	May-98	250,000	Charge: 0.5C Discharge: 1C 5 cycles per 99min.	15	JSB
LSE 100	12 avg.	3	49,000	May-99	100,000	Charge: 0.25C Discharge: 1C 5 cycles per 99min.	15	JSB
LSE 100	20	2	24,000	Mar-01	100,000	Charge: 0.5C, 30min Discharge: 1C, 12min	15	JSB
LSE 100	25	5	25,000	Apr-99	115,000	Charge: 0.3C, 60min Discharge: 0.5C, 30min	15	JAXA
LSE 100	30	3	23,000	May-99	35,000	Charge: 0.25C, 85min Discharge: 0.6C, 30min	20	ESTEC
LSE 100	40	5	24,000	Apr-99	42,000	Charge: 0.5C, 60min Discharge: 0.8C, 30min	15	JAXA

JAXA: Japan Aerospace Exploration Agency; ESTEC: European Space Research and Technology Center

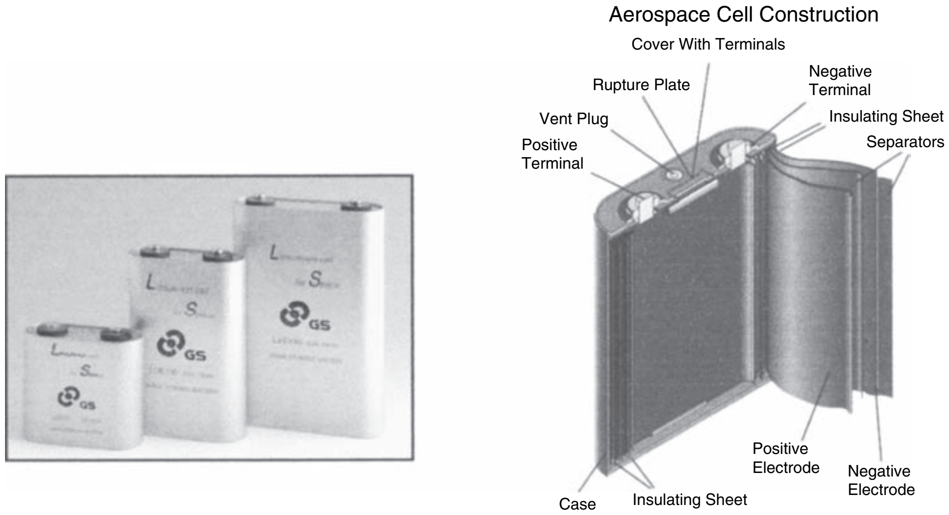

Figure 6.21. Wound prismatic Li ion batteries produced by Japan Storage Batteries.

6.7.1. Low Temperature Performance of Li-Ion Batteries

Factors affecting the low temperature performance of Li-ion batteries are:

- Cell design features
  - Separator material properties
  - Current collection
  - Cell size and thermal properties
- Electrolyte properties
  - Electrolyte conductivity
  - Electrode passivation
- Electrode properties
  - Active material loading
  - Bulk Li$^+$ diffusion
  - Li$^+$ kinetics (diffusion in SEI)

Several laboratories have been working on improving the low temperature behavior for a variety of applications. In particular, NASA and its industrial partners have focused on aerospace applications and planetary missions.

In the late 1990s, JPL had developed a Li-ion cell that can function at -20°C and this technology was transferred to Yardney and SAFT for manufacturing. Li-ion batteries made by Yardney with one such electrolyte are presently in use on the MER rovers (Spirit and Opportunity) and have the best low temperature performance of any state of practice rechargeable battery.

Subsequent to the ternary system for the Mars rovers, JPL has continued its studies and identified several new electrolytes, with novel mixtures containing low-viscosity solvents, which permit effective operation of Li-ion cells at temperatures as low as –60°C.[71-73] Experimental cells fabricated by Lithion and SAFT using this electrolyte showed more than 50% higher capacity at –40°C compared to state-of-practice Li-ion cells. Figure 6.22 illustrates the relative performance of experimental Li-ion cells with some of these advanced low-temperature electrolytes. These electrolytes are also being successfully utilized in several aircraft applications by the DoD. In addition to advances made at JPL, other groups have developed electrolyte formulations with good low temperature performance, including Army Research Laboratory[74], Covalent Associates[75], and Saft America.[76] However these solutions have not been utilized for space applications.

6.7.2. Radiation Tolerance

Li-ion cells contain organic electrolytes and polymeric separators that

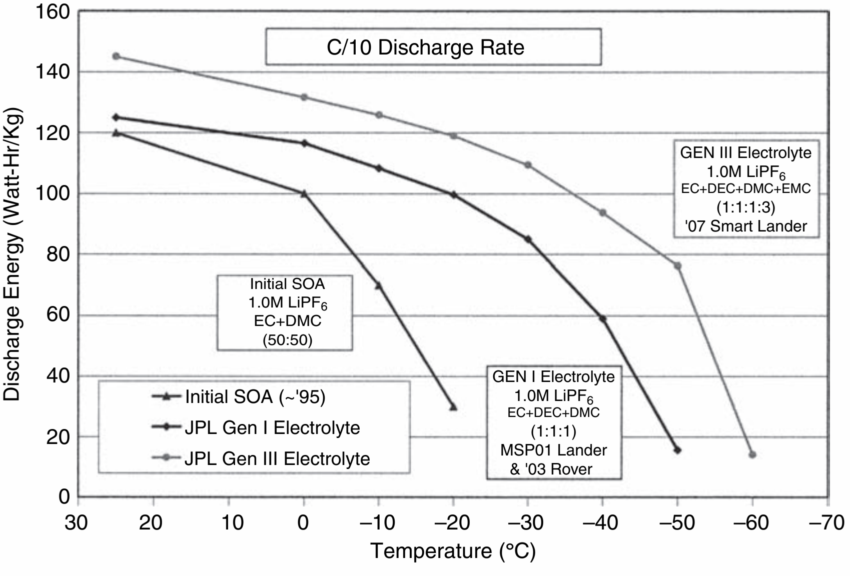

Figure 6.22. Performance of Li-ion cells with advanced low-temperature electrolytes.

could be affected by high levels of radiation. A detailed experimental evaluation was therefore undertaken by JPL to determine the performance of these cells after exposure to various levels of cumulative radiation, up to about 25 Mrad. Prototype cells were obtained from three different sources: a) SAFT, b) Yardney and c) Sony/ABSL. Typical materials and components in SAFT and Yardney cells included graphite anodes, mixed nickel cobalt oxide cathodes, electrolytes with 1M $LiPF_6$ dissolved in mixtures containing cyclic and linear organic carbonates, copper anode and aluminum cathode substrates, fluoropolymer binders, polypropylene/polyethylene separators, glass to metal seals, and molybdenum pins and stainless steel cases. Sony's cells are not much different. The cells were incrementally exposed to gamma radiation, using a ^{60}Co source both at high dosage rates of 30 rads/sec (corresponding to 1.5 Mrad over 14 hours) and at low dosage level of 1.24 rad/sec (1.5 Mrad over two weeks). After each irradiation, the cell capacities were measured both at ambient and low temperatures. The fade rates were established from charge-discharge cycles. This study revealed that Li-ion cells are tolerant to radiation levels as high as 18 Mrad and exhibit a loss of less than 5% upon such high levels of radiation exposure. Furthermore, a portion of this 5% loss can be attributed to the cycling or storage during this incremental radiation exposure. Figure 6.23 shows the performance characteristics of the three chemistries upon radiation exposure.[77-78] In general, all the three chemistries showed impressive and adequate tolerance to

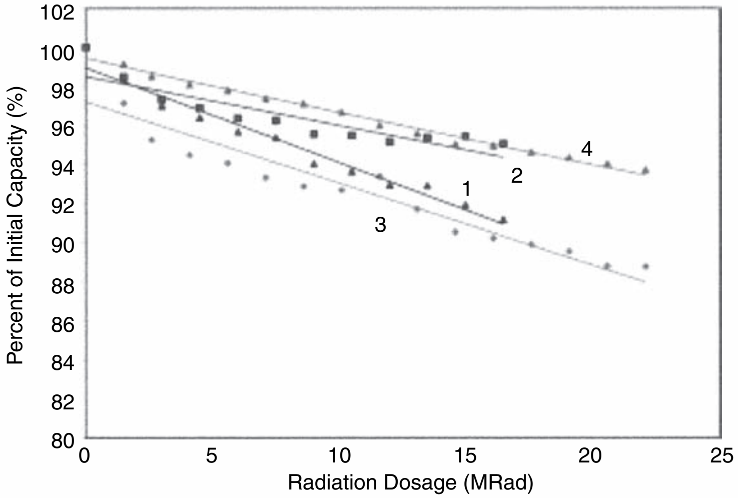

Figure 6.23. Capacity retention of (1) Sony/AEA 18650, 2) Sony/AEA control cells, 3) Lithion prismatic 7 Ah cells, and 4) SAFT DD Li ion cells, during exposure to various cumulative level of γ-radiation.

radiation, with their small differences attributable to the differences in the chemistry or the degree of attenuation. Further studies are warranted to understand the effects of the radiation in terms of individual components and to assess the radiation effects after extended storage, as encountered in outer planetary missions.

6.7.3. Calendar Life

Calendar life is another characteristic that is most critical to aerospace application. Some of the planetary explorations missions, particularly those to outer planets, such as Jupiter and Saturn would require battery lives as long as 6-12 years. Aerospace Li-ion chemistry is still relatively new and evolving to exhibit such a long demonstrated life. Few studies, both accelerated and real-time are on going at JPL[79] and elsewhere[80,81] on the calendar life of Li-ion cells/batteries. Two chemistries, 7 Ah prismatic cells from Lithion and 9 Ah cylindrical DD cells from SAFT America, have been under evaluation at JPL on storage for the last five years, at a floating charge voltage of 3.65 V/cell, corresponding to ~50% state of charge, and at different temperatures: 55°C, 40°C, 23°C, 10°C, 0°C, and -20°C. These cells have been subjected to capacity checks, both at ambient and low temperatures, as well as AC impedance (EIS) measurements. The results on the capacity retention observed thus far are quite encouraging, and the projected capacity losses based on these accelerated storage tests make the Li-ion technology promising for long-lasting missions, as shown by Figure 6.24. There are two models to understand the capacity loss sustained by Li-ion cells during storage and/or cycling. One model involves a growth of the solid electrolyte interphase (SEI) on the carbon[80] and the other relates to the loss of electronic conductivity on the positive electrode,[81] due to morphological rearrangements related to volume changes upon intercalation/ deintercalation.

6.8. Lithium Batteries –Advanced Systems

Lithium or lithium-ion cells may assume unusual shapes by replacing the liquid electrolyte either with polymeric electrolytes or, in limited applications, solid electrolytes. The former category includes gel polymers (a liquid electrolyte is added as a plasticizer to an inert polymer matrix) or “dry” polymers sustaining Li^+ mobility through their segmental motion above a given temperature. These systems show promise of enhanced performance compared to the state-of-art Li-ion cells as well as conventional Ni systems (Ni-Cd or Ni-H_2). The Li-solid inorganic electrolyte system has the intrinsic capability of

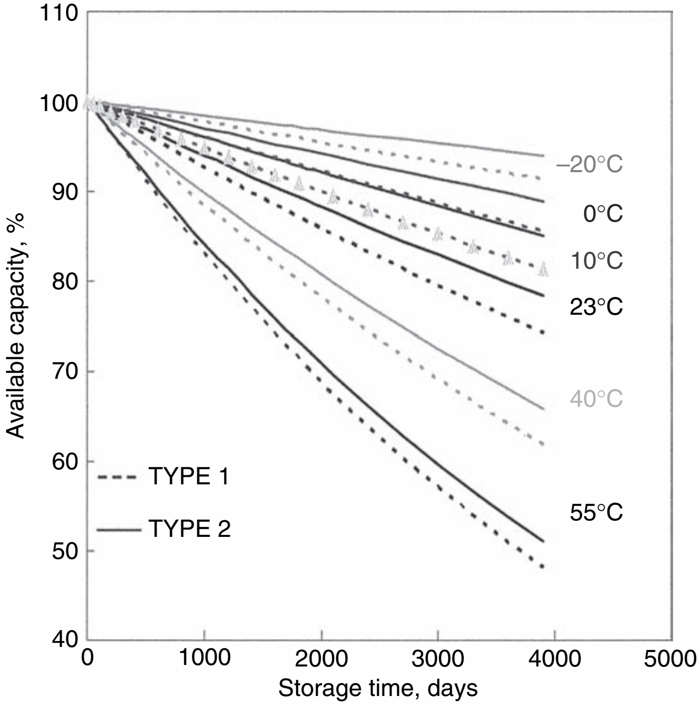

Figure 6 24. Projected retained capacities during storage on bus at 3.65 V (50% SOC) at different temperatures.

providing very long shelf and operational life compared to the other lithium systems. However, both these technologies are in their early stages of development, with a Technology Readiness Level (TRL) of 1-3.

The characteristics of gel polymer electrolytes (GPE) Li-ion cells are closer to that of liquid electrolyte lithium-ion cells, with advantages only in terms of packaging efficiency (90-95%) and form factor. Gel polymer Li-ion cells normally use light cases (*e.g.* pouch cells), so there is the need to incorporate them into hermetically sealed housing in order to be applicable for use in deep space vacuum.

Recently, Li-ion polymer cells, manufactured by Compact Power, an US subsidiary of LG Chem, have been tested at JPL. The cycle life capability and low temperature performance of these cells, the latter data representing cells activated with JPL low temperature electrolytes, are illustrated in Figures 6.25 and 6.26, respectively.[82]

Li metal-solid polymer electrolyte batteries offer potential performance advantages over Li-ion batteries. Since the polymer systems are solvent-free,

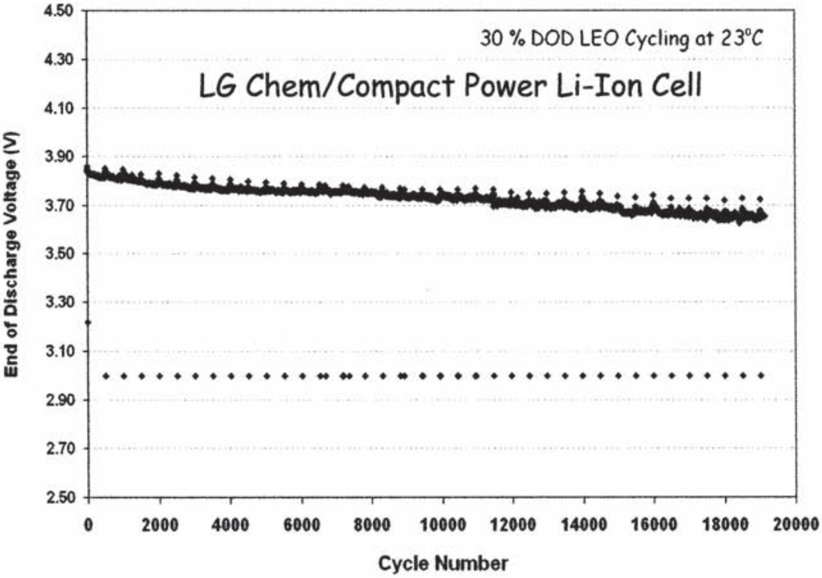

Figure 6.25. LEO cycle life performance (30% DOD) of LG Chem/Compact Power cells at 23°C.

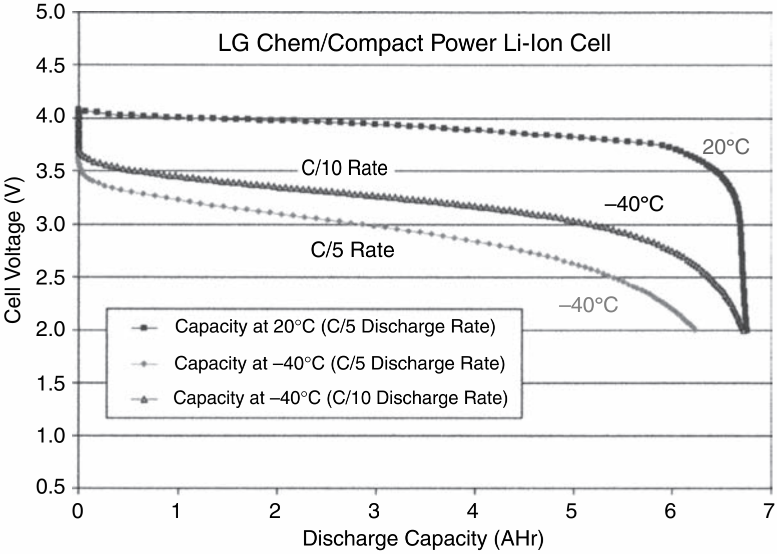

Figure 6.26. Low temperature performance LG Chem/Compact Power cells with JPL electrolyte.

lithium metal can be used as the anode material, instead of carbon, this affording higher energies. In addition, due to the lack of volatile components, dry polymer electrolyte-based cells have the potential to dramatically decrease internal cell pressure, thus enabling the use of lighter aluminum/resin-laminated films (~100 μm in thickness) as casings. Therefore, the projected specific energy may exceed 200 Wh/kg. Commercial Li-polymer batteries with energies of 140 Wh/kg and 174 Wh/L are already available for stationary applications.

Improved cycle life, shelf life, and self-discharge characteristics are expected, due to the absence of reactive solvents (that are primarily responsible for impedance increase and capacity loss). Another potential advantage of cells with polymer-based electrolytes is their flexible shape that may aid in their integration into spacecraft structures.

The technical challenges involved in developing practical Li-SPE cells and batteries for space include development of:

- Large-scale membrane fabrication processes yielding large, uniform films with predictable performance
- Cell fabrication techniques and appropriate cell designs that will result in aerospace quality cells (5-50 Ah size).

6.9. Concluding Remarks on Rechargeable Batteries

Among the available options for rechargeable batteries, Ag-Zn batteries, although having the highest specific energy and energy density of the aqueous systems, are suitable only for short-term applications, *e.g.*, launch vehicles. This system is unsuitable for many other planetary missions because of its limited cycle and shelf life. Ni-Cd batteries, on the other hand, have good cycle life and calendar life characteristics, and demonstrated many years of operation in LEO and GEO satellites and in orbiters, within a temperature range of –10°C to 20°C. Additionally, super Ni-Cd batteries have outstanding radiation resistance. However, the Ni-Cd chemistry is not attractive for planetary surface missions that require reduced mass and volume, *e.g.*, landers, rovers and probes. Like Ni-Cd, Ni-H_2 batteries have demonstrated impressive cycle life performance (>50,000 cycles at 30-40% DOD) and calendar life (>15 years of GEO operational life), superior to any other rechargeable battery system. However, their unfavorable energy densities and specific energies make them suitable only for orbital missions, where cycle life is the main factor.

The use of Li-ion batteries in planetary mission has just begun and is rapidly increasing, mainly due to their higher gravimetric and volumetric energy and good low-temperature behavior compared to the nickel systems. These advantages are particularly significant in planetary surface missions. The on going improvements and demonstrations in both cycle life and calendar life will

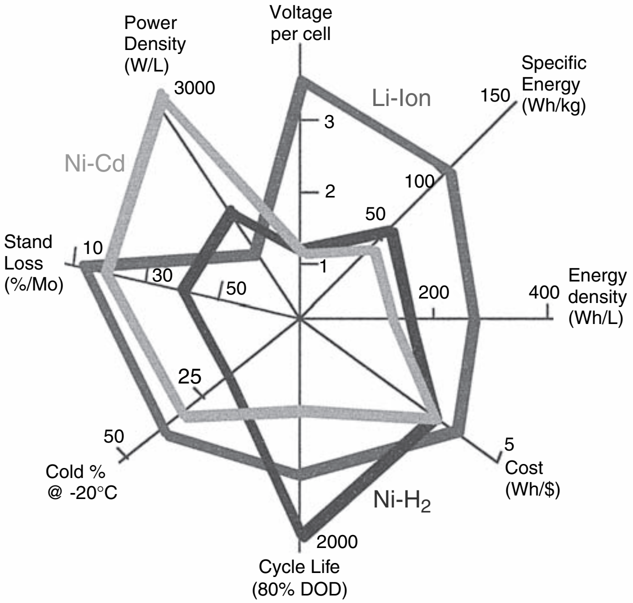

Figure 6.27. Comparison of Li-ion cells with standard rechargeable cells. The stand loss for Li-ion is in %/year.

result in their use in orbital applications as well. Figure 6.27 gives a snapshot of the relative performance of aerospace rechargeable batteries.

Acknowledgements

Some portions of the work described here was carried out at the Jet Propulsion Laboratory, California Institute of Technology under contract with the National Aeronautics and Space Administration and was supported by various battery programs. We also acknowledge the data provided through personal correspondence from technologists, often beyond what is available in published literature.

References

1. G. Dakermanji and R. Sullivan, "Space Power Systems", in "*Fundamentals of Space Systems*" 2nd Edition, Vincent L. Pisacane, Ed., Oxford University Press, New York, 2005.
2. A. K. Hyder, R. L. Wiley, G. Halpert, D. J. Flood and S. Sabripour, "*Spacecraft Power Technologies*", Imperial College Press, London, 2000.
3. C. A. Hill, "Satellite Battery Technology: A Tutorial and Overview, *IEEE Aerospace and Electronic Systems Magazine*, 153-158, 1998.

4. L. D. Massie, "Future Trends in Space Power Technology", *IEEE AES Systems Magazine,* November 1991.
5. S. Ginter, G. Gisler and J. Hanks, "Spacecraft Energy Storage Systems", *IEEE AES Systems Magazine,* May 1998.
6. *"Handbook of Batteries"*, D. Linden and T.B. Reddy, Eds., McGraw-Hill, New York, 2002.
7. P. J. Johnson, S. W. Donley and D. C. Verrier, *J. Power Sources* 76 (1998) 210.
8. D. K. Coates, C. L. Fox, *J. Propulsion Power* 12 (1996) 879.
9. S. W. Hall, 27th Annual Report of Cycle Life Test, EDD-96-109, Department of the Navy Crane Division, NSWC Cabd, Indiana, 1996.
10. R. M. Sullivan, C. G. Hoffman and G. M. Rao, *J. Power Sources* 69 (1997) 27.
11. (a) S. Surampudi, B. Otzinger, D. Perone, R. Ewell, D. Burger, M. Shirbacheh and P. Bankston, "Mars Pathfinder Lander Battery and Solar Array Performance", *36th Aerospace Sciences Meeting and Exhibit,* Reno, NV Jan 12-15, 1998, and (b) D. E. Perrone, M. Klekotka and S. DiStephano, "The effect of cell design and storage conditions on the cycle life performance of silver-zinc cells", *Proceedings of the 31th Intersociety Energy Conversion Engineering Conference*, Aug 11-16, 1996, p. 416-420.
12. B. V. Ratnakumar, M. C. Smart, R. C. Ewell, L. D. Whitcanack, A. Kindler, S. R. Narayanan and S. Surampudi, "Lithium-Sulfur Dioxide Batteries on Mars Rovers", *Proceedings of the 2nd International Energy Conversion Engineering Conference*, Providence, Rhode Island, August 15-18, 2004.
13. P. G. Russell, D. Carmen, C. Marsh, T. B. Reddy, R. Bugga, F. Deligiannis and H. A. Frank, "Development of a Lithium/Thionyl Chloride Battery for the Mars Microprobe Program", *Proceedings of the 13th Annual Battery Conference on Applications and Advances*, Long Beach, CA, Jan. 13-16, 1998, p. 341-346.
14. G. M. Rao and H, Wajsgras, "Hubble Space Telescope On-Orbit NiH_2 Battery Capacity Performance (1990 to 2002), *Proceeding of the 37th Intersociety Energy Conversion Engineering Conference*, July 29-31, 2004, p. 295.
15. D. Koch, *et al.*, "Overview and Status of the Kepler Mission", *Optical, Infrared, and Millimeter Space Telescopes, SPIE Conference 5487*, Glasgow, 2004.
16. S. DiStefano, D. Perrone and B. V. Ratnakumar, "Characterization of Nickel-Hydrogen 2-Cell Common Pressure Vessels for NASA Missions", *Proceedings of the 32nd Energy Conversion Engineering Conference*, Honolulu, HI, July 27-Aug. 1, 1997, pp. 145-158.
17. D. T. Lyons, J. G. Beerer, P. Esposito and M. D. Johnston, "Mars Global Surveryor: Aerobraking Mission Overview", *J. Spacecraft and Rockets*, 36/3, 1999.
18. R. Ferretti, M. Denis, A. Moorhouse, E. Rabenau, O. Page and E. Escale, "Mars Express Power Subsystem In-Flight Experience", *SpaceOps 2006 Conference*, Rome, Italy, June 19-23, 2006.
19. J. E. Graf, M. D. Johnston, R. W. Zurek, R. P. De Paula, H. J. Eisen and B. Jai, "The Mars Reconnaissance Orbiter Mission", *54th International Astronautical Congress of the International Astronautical Federation*, Bremen, Germany, Sept. 29-Oct. 3, 2003.
20. B. P. Dagarin, R. K. Taenaka and E. J. Stofel, "Galileo Probe Battery Systems", *Proceedings of the 31st International Energy Conversion Engineering Conference*, Washington, DC, Aug. 11-16, 1996, pp. 427-432.
21. S. Surampudi, B. Otzinger, D. Perrone, R. Ewell, D. Burger, M. Shirbacheh and P. Bankston, "Mars Pathfinder Lander Battery and Solar Array Performance", *Proceedings of the 36th Aerospace Sciences Meeting and Exhibit,* Reno, NV, Jan. 12-15, 1998.
22. B. V. Ratnakumar, H. Frank, A. Kindler, F. Deligiannis, E. Davies, J. Blakevoort and S. Surampudi, *NASA Battery Workshop*, Huntsville, AL, Oct. 27, 1998.
23. H. Frank, F. Deligiannis, E. Davies, B. V. Ratnakumar, S. Surampudi, P. G. Russel and T. B. Reddy, *NASA Battery Workshop*, Huntsville, AL, Oct. 27, 1998.

24. M. C. Smart, B. V. Ratnakumar, L. Whitcanack, S. Surampudi, J. Byers and R. Marsh, "Performance Characteristics of Lithium-Ion Cells for NASA's Mars 2001 Lander Application", *IEEE Aerospace and Electronic Systems Magazine* 14 (1999) 36.
25. R. A. Marsh, S. Vukson, S. Surampudi, B. V. Ratnakumar, M. C. Smart, M. Manzo and P. J. Dalton, *J. Power Sources* 97-98 (2001) 25.
26. M.C. Smart, B.V. Ratnakumar and S. Surampudi, *J. Electrochem.Soc.* 146 (1999) 486.
27. M.C. Smart, B.V. Ratnakumar, L. D. Whitcanack, K. B. Chin, S. Surampudi, R. Gitzendanner and F. Puglia, Performance Testing of Lithion 8-Cell, 25 Ah Lithium-Ion Batteries for Future Aerospace Applications", *1st International Energy Conversion Engineering Conference (IECEC)*, Portsmouth, Virginia, Aug. 17-21, 2003.
28. C. M. Reid, M. C. Smart, R. V. Bugga, M. A. Manzo, T. B. Miller and R. Gitzendanner, "Performance and Comparison of Lithium-ion Batteries Under Low-Earth-Orbit Mission Profiles", *4th International Energy Conversion Engineering Conference (IECEC)*, San Diego, CA, June 26-29, 2006.
29. B. V. Ratnakumar, M. C. Smart, A. Kindler, H. Frank, R. Ewell and S. Surampudi, *J. Power Sources* 119 (2003) 906.
30. S. W. Squires *et al.*, *Science* 305 (2004) 794.
31. S. W. Squires *et al.*, *Science*, 306 (2004) 1698.
32. B. V. Ratnakumar, M. C. Smart, R. C. Ewell, L. D. Whitcanack, K. B. Chin and Surampudi, S., "Lithium-ion Rechargeable Batteries on Mars Rovers", *2nd International Energy Conversion Engineering Conference (IECEC)*, Providence, Rhode Island, 18 Aug. 2004.
33. B. V. Ratnakumar, M. C. Smart, R. C. Ewell, L. D. Whitcanack, K. B. Chin and S. Surampudi., "Lithium-ion Rechargeable Batteries on Mars Rovers", *NASA Battery Workshop*, Huntsville, AL, Nov. 2003.
34. B. V. Ratnakumar, M. C. Smart, L. D. Whitcanack, K. B. Chin, R. C. Ewell, S. Surampudi, F. Puglia and R. Gitzendanner, "An Update on the Performance of Lithium-Ion Rechargeable Batteries on Mars Rovers", *4th International Energy Conversion Engineering Conference (IECEC)*, San Diego, CA, June 26-29, 2006.
35. M. C. Smart, B.V. Ratnakumar, R. C. Ewell, L. D. Whitcanack, S. Surampudi, F. Puglia and R. Gitzendanner, "An update on the Ground Testing of the Li-ion Batteries in Support of JPL's 2003 Mars Exploration Rover Mission", *4th International Energy Conversion Engineering Conference (IECEC)*, San Diego, CA, June 26-29, 2006.
36. D. E. Nawrocki, J. R. Driscoll, J. D. Armantrout, R. C. Baker and H. Waisgras, *Proceedings of the 1992 NASA Aerospace Battery Workshop, NASA-CP-3192,* Huntsville, AL, USA, 1992, p. 293.
37. Hollandsworth and J. D. Armantrout, "Hubble Space Telescope Battery Capacity Trend Studies", *Proceedings of the 2003 NASA Aerospace Battery Workshop*, Huntsville, AL, USA, 2003.
38. S. J. Krol and G. M. Rao, "Hubble Performance On-Orbit", *IEEE Aerospace and Electronic Systems Magazine* 18 (2003) 13.
39. F. Cohen and P. Dalton, "International Space Station Nickel-Hydrogen Battery Start-Up and Initial Performance", *Proceedings of the 36th Intersociety Energy Conversion Engineering Conference (IECEC),* Savannah, GA, July 29-August 2, 2001.
40. P. Dalton and F. Cohen, "International Space Station Nickel-Hydrogen Battery On-Orbit Performance", *Proceedings of the 37th Intersociety Energy Conversion Engineering Conference (IECEC)*, Washington DC, July 28-August 2, 2002.
41. C. P. Bankston, "Progress in Spacecraft Electric Power System Technologies for Deep Space Missions", *Proceedings of the 35th Aerospace Sciences Meeting and Exhibit,* Reno, NV, Jan. 6-9, 1997.
42. R. Serenyi and J. Skelton, "Silver-Zinc-Battery Technology Improvement Program, *Proceedings of the 41st Power Sources Conference*, Philadelphia, PA, June 14-17, 2004,

paper 28.1.

43. D. Linden and B. McDonald, *J. Power Sources* 5 (1980) 35.
44. B. V. Ratnakumar, M. C. Smart, R. C. Ewell, L. D. Whitcanack, A. Kindler, S. R. Narayanan and S. Surampudi, "Lithium-Sulfur Dioxide Batteries on Mars Rovers", *Proceedings of the 2nd International Energy Conversion Engineering Conference,* Providence, Rhode Island, August 15-18, 2004.
45. C. C. Liang, P. W. Krehl and D. A. Danner, *J. Appl. Electrochem.* 11 (1981) 563.
46. (a) R. L. Higgins and L. R. Erisman, "Applications of the Lithium/Carbon Monofluoride Battery", *Proc. 28th Power Sources Symp., Electrochemical Society,* Pennington, NJ, June 1978 and (b) E. S. Takeuchi and S. A. Smesko, "Performance Aspects of Low Rate Lithium/CFx Cells", *Proc. 7th Annual Battery Conf.*, Long Beach, CA, 1992.
47. K. Guerin, J. P. Pinheiro, M. Dubois, Z. Fawal, F. Masin, R. Yazami and A. Hamwi, *Chem. Mater.* 16 (2004) 1786.
48. (a) Jay Whitacre, R. Yazami, A. Hamwi, M. C. Smart, W. Bennett, G. K. S. Prakash, T. Miller and R. Bugga, "Low Temperature Li-CF_x Batteries Based on Sub-Fluorinated Graphitic Materials", *209th Meeting of the Electrochemical Society,* Denver, CO, May 7-12, 2006. (b) Ratnakumar Bugga, J. Whitacre, M. C. Smart, R. Yazami, G. K. S. Praksh, W. Bennett and T. Miller, Recent Advances in Li-CF_x Battery Technology for High-Rate and Low-Temperature Applications, *2005 Space Power Workshop,* Manhattan Beach, CA, April 27, 2006.
49. M. C. Smart, J. F. Whitacre, B. V. Ratnakumar, G. K. S. Prakash, P. Bhalla and K. Smith, "Development of Electrolytes for High Specific Energy Li-CF_x Batteries Capable of Operation over a Wide Temperature Range", *IBA/JPL Workshop on Carbon Fluorides for Lithium Batteries,* Pasadena, CA, Feb 21, 2006.
50. W. C. West and J. F. Whitacre, *IBA/JPL Workshop on Carbon Fluorides for Lithium Batteries,* Pasadena, CA, Feb 21, 2006.
51. D. L. Bindshadler, E. E. Theilig, K. A. Schimmels and N. Vandermey, "Project Galileo: Final Mission Status", *54th International Astronautical Congress of the International Astronautical Federation*, Bremen, Germany, Sept. 29-Oct. 3, 2003.
52. B. H. van Domelan and R. D. Wehrle, "A Review of Thermal Battery Technology", *Intersoc. Energy Convers. Conf.*, 1974.
53. F. Tepper, "A Survey of Thermal Battery Designs and Their Performance Characteristics", *Intersoc. Energy Convers. Conf.*, 1974.
54. F. Deligiannis, R. Sherwood, D. Perrone and S. Di Stefano, "TOPEX/Poseidon NiCd Battery Performance-Comparison of Flight and Ground Test Results", *Proceedings of the 29th Intersociety Energy Conversion Engineering Conference*, Monterey, CA, Aug 7-11, 1994.
55. J. Carcone, in "*Handbook of Batteries*" (Chapter 28), D. Linden and T.B. Reddy, Eds., McGraw-Hill, New York, 2002.
56. B. Abrams-Blakemore and T. A. Edgar, "Performance Evaluation of Nickel-Cadmium and Nickel-Hydrogen Aerospace Cells with Electrochemically Deposited Nickel Electrodes", *Proceeding of the 9th Annual Battery Conference on Applications and Advances*, Long Beach, CA, January 11-13, 1994, pp. 70-73.
57. P. Timmerman, L. Whitcanack, E. Davies and F. Deligiannis, "Ultra-Radiation Hard Aerospace Batteries", *Proceeding of the 16th Annual Battery Conference on Applications and Advances*, Long Beach, CA, January 2001.
58. D. K. Coates, C. L Fox and L. E. Miller, *Int. J. Hydrogen Energy* 19 (1994) 743.
59. J. Dunlop, J. Giner, G. van Ommering and J. Stockel, U. S. Patent 3,867,199 (1975)
60. J. D. Dunlop, G. M. Rao and T. Y. Yi, *NASA Handbook for Nickel-Hydrogen Batteries, NASA Reference Publication 1314,* Sept. 1993.
61. J.D. Dunlop, J.N. Brill and R. Erisman, in "*Handbook of Batteries*" (Chapter 32), D. Linden and T.B. Reddy, Eds., McGraw-Hill, New York, 2002.

62. (a) H. H. Rodgers, S. J. Krause and E. Levy, Jr., "Design of Long Life Nickel-Hydrogen Cells", *Proc. 28th Power Sources Conf.*, June 1978. (b) G. L. Holleck, M. J. Turchan and D. DeBiccari, "Improvement and Cycle Testing of Ni/H_2 Cells", *Proc. Proc. 28th Power Sources Conf.*, June 1978, and (c) G. Holleck, "Failure Mechanisms in Nickel-Hydrogen Cells", *Proc. 1976 Goddard Space Flight Center Battery Workshop*, pp. 279-315.
63. L. Miller, *J. Power Sources* 18 (1986) 279.
64. H. F. Gibbard, "Nickel Metal Hydride Battery Applications", *Proceedings of the 9th Annual Battery Conference on Applications and Advances*, Long Beach, CA, Jan. 11-13, 1994, pp. 65-70
65. (a) H. S. Lim, D. F. Pickett, J. F. Stockel and J. J. Smithrick, "Advanced Nickel-Metal Hydride Cell Development at Hughes: A Joint Work with US Government" *Proceedings of the 10th Annual Battery Conference on Applications and Advances*, Long Beach, CA, Jan. 10-13, 1995, pp. 65-70, and (b) J. Chen, D. H. Bradhurst, S. X. Dou, H. K. Liu, Y. S. Zhang and D. Y. Song, "Development of High Energy Nickel-Metal Hydride Cells" *Proceedings of the 13th Annual Battery Conference on Applications and Advances*, Long Beach, CA, Jan. 13-16, 1998, pp. 405-409.
66. R. A. Marsh, S. Vukson, S. Surampudi, B. V. Ratnakumar, M. C. Smart, M. Manzo and P. J. Dalton, *J. Power Sources* 97-98 (2001) 25.
67. M.C. Smart, B.V. Ratnakumar and S. Surampudi, *J. Electrochem.Soc.* 146 (1999) 486.
68. M. C. Smart, B. V. Ratnakumar, L. Whitcanack, K. Chin, S. Surampudi, H. Croft, D. Tice and R. Staniewicz, *J. Power Sources* 119 (2003) 349.
69. W. Li and B. L. Lucht, *J. Electrochem. Soc.* 153 (2006) A1617.
70. M. C. Smart, B. V. Ratnakumar, J. F. Whitacre, L. D. Whitcanack, K. B. Chin, M. D. Rodriquez, D. Zhao, S. G. Greenbaum and S. Surampudi, *J. Electrochem. Soc.* 152 (2005) A1096.
71. M. C. Smart, B. V. Ratnakumar and S. Surampudi, *J. Electrochem. Soc.* 149 (2002) A361.
72. M. C. Smart, B. V. Ratnakumar, K. B. Chin and S. R. Narayanan, "Ester-Based Electrolytes that Enable Lithium-Ion Cell Operation at Very Low Temperatures (-40 to –70°C)", *206th Meeting of the Electrochemical Society*, Honolulu, Hawaii, Oct. 3-8, 2004.
73. M. C. Smart, B. V. Ratnakumar, L.D. Whitcanack, Ji-Sang Yu and M. Alamgir, Low Temperature Ester-Based Electrolytes and their Demonstration in High Power, Gel Polymer Electrolyte Lithium-ion Cells, *207th Meeting of the Electrochemical Society*, Quebec City, Canada, May 19, 2005.
74. E.J. Plichta and W.K. Behl, *Proceedings of the 38th Power Sources Conference*, Cherry Hill, NJ, p. 444, June 1998.
75. Y. Ein-Eli, S.R. Thomas, V. Koch, D. Aurbach, B. Markovsky and A. Schechter, *J. Electrochem. Soc.* 142 (1996) L273.
76. S. Herreyre, O. Huchet, S. Barusseau, F. Perton, J. M. Bodet and Ph. Biensan, *J. Power Sources* 97-98 (2001) 576.
77. B. V. Ratanakumar, M. C, Smart, L. D. Whitcanack, E. D. Davies, K. B. Chin, F. Deligiannis and S. Surampudi, *J. Electrochem. Soc.* 151 (2004) A652.
78. B. V. Ratnakumar, M. C, Smart, L. D. Whitcanack, E. D. Davies, K. B. Chin, F. Deligiannis and S. Surampudi, *J. Electrochem. Soc.* 152 (2005) A357.
79. B. V. Ratnakumar, M. C. Smart, K. B. Chin , L. D. Whitcanack, S. R. Narayanan and S. Surampudi, "Storage Characteristics of Li-Ion Batteries for NASA's Missions", *206th Meeting of the Electrochemical Society*, Honolulu, Hawaii, Oct. 3-8, 2004.
80. M. Broussely, S. Herreyre, P. Biensan, P. Kasztejna, K. Nechev and R. J. Staniewicz, *J. Power Sources* 97-98 (2001) 13.
81. T. Inoue, H. Yoshida, M. Mizutani and M. Goto, "Qualification Test Results of 100 AH Lithium Ion Cells for Space Applications", *18th AIAA International Communications Satellite Systems Conference*, Oakland, CA, Apr. 10-14, 2000.

82. M. C. Smart, B. V. Ratnakumar, A. Behar, L.D. Whitcanack, J.-S. Yu and M. Alamgir, "Gel Polymer Electrolyte Lithium-Ion Cells with Improved Low Temperature Performance", *IBC-HBA 2006,* Waikoloa, Hawaii, 9-12 January 2006.

This page intentionally left blank

Industrial Applications of Batteries. From Cars to Aerospace and Energy Storage
M. Broussely and G. Pistoia Eds.,
© 2007 Elsevier B.V.

Chapter 7

STATIONARY APPLICATIONS. I. LEAD-ACID BATTERIES FOR TELECOMMUNICATIONS AND UPS

Rainer Wagner

EXIDE Technologies, Deutsche EXIDE GmbH, Odertal 35, D-37431 Bad Lauterberg, Germany

7.1. Introduction

Lead-acid batteries have been used for more than 130 years in many different applications including automotive and various traction duties as well as in telecommunication systems and uninterruptible power supplies (UPS). The last two groups constitute the major part of the so-called stationary battery sector, and the lead-acid battery has proved to be a very reliable system for these applications.

Although the lead-acid battery has a relatively low specific energy in comparison with alternative electrochemical storage systems it remains the world's most important secondary power source. This is due to the fact that it is not sufficient to consider specific energy alone. In the final analysis, it is the combination of specific energy, life, and cost that is usually decisive in battery selection for industrial use. Further, attributes such as specific power, reliability, availability of raw materials, and the possibility of recycling are also important. Considering all these factors, the lead-acid battery provides a good compromise and, therefore, is expected to remain the most important electrochemical storage system for a long time. This is especially true for stationary applications where the high weight of lead is not so important. For such applications, the volumetric energy density has a higher priority than gravimetric energy density (specific energy) and, therefore, the lead-acid battery is a suitable choice.

The nickel-cadmium system also used, although to a lower extent, in the applications described in this chapter will be dealt with in Chapter 10.

This chapter presents the different types of lead-acid batteries for stationary applications, focusing especially on valve-regulated lead-acid

(VRLA) designs. Batteries with capacities of up to 200 Ah usually have flat positive plates; for higher capacities, tubular designs are also used.

Lead-acid batteries were first used in stationary, stand-by applications more than 130 years ago [1]. For a long period, there were only flooded batteries; nowadays, UPS and telecommunications applications use valve-regulated designs. Large, utility-scale applications such as load leveling continue to use flooded batteries, but it seems that, increasingly, valve-regulated batteries are chosen even for these applications.

During stand-by service, the battery should be maintained in a completely charged state by applying a float voltage that is slightly higher than the battery open-circuit voltage and that provides the energy for all the side reactions in the battery. These reactions are, in general, grid corrosion and oxygen evolution on the positive plate and hydrogen evolution and, in case of valve-regulated batteries, recombination of oxygen at the negative plate. The choice of the optimum float voltage at different temperatures is an important factor in maintaining valve-regulated batteries in a healthy state. This issue is discussed in more detail in a subsequent section.

In the past decades, the specific power of stationary lead-acid batteries has been raised steadily. These developments have also given a much better charge acceptance. An overview is given of the progress made in the development of high power lead-acid batteries.

There are two ways to improve the power performance of lead-acid batteries, namely: (i) reduction of the electrical resistance of the current collector parts, for example, the grids, (ii) optimization of the active materials and the cell design. For applications where cost and long service-life have lower priority, an extremely high power density has been achieved. In general, measures that improve power give lower cycling performance, and vice versa. Thus, compromises must be made. Recent developments have shown, however, that very high power can be combined with excellent cycle life, through the adoption of novel cell design.

7.2. The Lead-Acid Battery Technology

The lead-acid battery system has PbO_2 as the positive active material and Pb as the negative active material. Both active materials are used with a rather high porosity of more than 50%. The electrolyte is dilute H_2SO_4. The open circuit voltage (OCV) of this electrochemical cell depends on the concentration of sulfuric acid. In general, the acid concentration is measured as an acid density (specific gravity) because this parameter can be determined rather easily. For example, an acid density of 1.26 g/cm^3 at room temperature is equivalent to a weight concentration of sulfuric acid of about 35%. A specific gravity of 1.26 g/cm^3 gives then an OCV of about 2.10 V per cell. For the relation between specific gravity and OCV a good approximation can be used by the formula that the specific gravity plus 0.84 gives the OCV.

When the lead-acid battery is discharged, lead and lead dioxide are converted into $PbSO_4$ and H_2O. The discharge reaction of the lead–acid system is:

$$Pb + PbO_2 + 2H_2SO_4 \rightarrow 2PbSO_4 + 2H_2O \qquad (1)$$

During the discharge, sulfuric acid is consumed and the specific gravity of the electrolyte decreases. This reduction of the sulfuric acid concentration can therefore be used to determine the depth-of-discharge (DoD) of the battery.

When the battery is charged, reaction (1) is reversed:

$$2PbSO_4 + 2H_2O \rightarrow Pb + PbO_2 + 2H_2SO_4 \qquad (2)$$

From the cell reaction (1), the theoretical specific energy (gravimetric energy density) can be calculated and results in 161 Wh/kg. However, this figure can by far not be achieved in practice because it is reduced by several unavoidable factors as illustrated in Figure 7.1. The practical energy density has

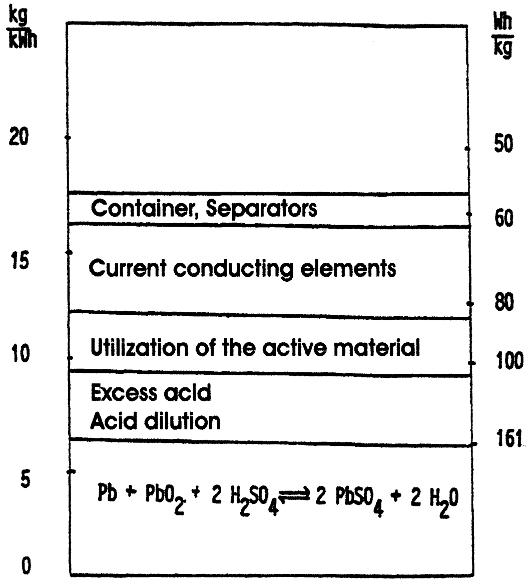

Figure 7.1. Energy density of lead-acid batteries.

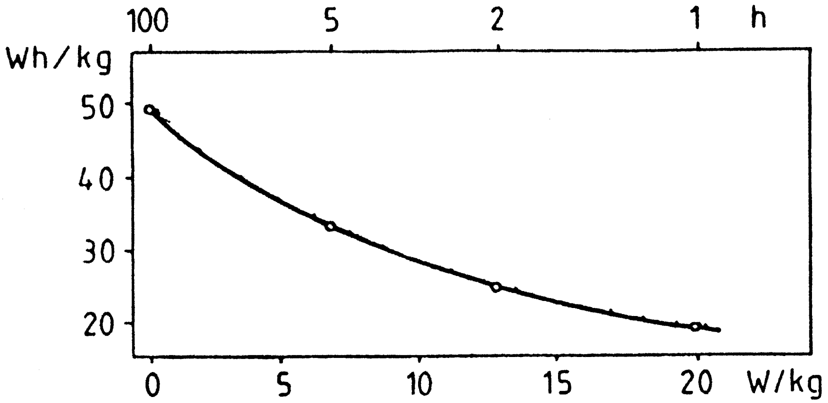

Figure 7.2. Energy density as a function of the discharge rate.

been improved steadily over the decades and is nowadays around 35 Wh/kg at the 5 h discharge rate and up to about 55 Wh/kg at the 100 h discharge rate. These are relatively high figures in comparison to the theoretical 161 Wh/kg and are a result of much development activities over a long period of time.

The lead-acid system requires an excess of sulfuric acid, since otherwise the discharge reaction would lead to pure water with a lack of conductivity. Some sulfuric acid in the discharged state is also needed to avoid unwanted reactions. Moreover, diluted acid must be used since concentrated acid has no conductivity and would convert the active material rather quickly into lead sulfate.

An excess of the active materials, lead and lead dioxide, is also needed because the active materials cannot be utilized completely. Additionally, some more components are required. This includes the separators, the container and the current-conducting elements like the grids, the top bars and the terminals. All these factors give a significant reduction in the energy density. Especially the active mass utilization depends much on the discharge rate and is reduced significantly at higher discharge rates (shorter discharge times).

The decrease of the energy density with higher discharge rates is shown in Figure 7.2 for discharge times between 1 h and 100 h. At even higher discharge rates, *i.e.* less than 1 h discharge time, the available energy density is even lower. The causes of this decrease are discussed in more detail in a subsequent section.

Although VRLA batteries have been used steadily more for stationary applications, there are still some ranges in use of the flooded design. Batteries with small or medium capacities of up to about 500 Ah often have flat positive plates. Such types (OGi) are available in two ranges:

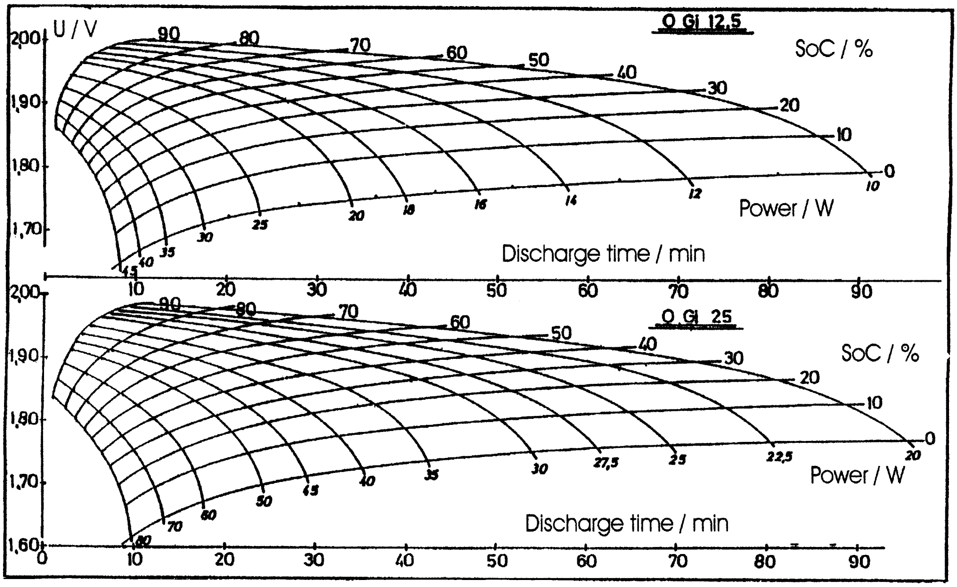

Figure 7.3. Discharge curves of OGi 12.5 Ah and OGi 25 Ah plates at different constant power discharge rates.

1) 6 V modules with capacities between 12.5 Ah and 200 Ah.

2) 2 V cells with capacities between 200 Ah and 475 Ah.

For these ranges, two plate sizes are used with a capacity of either 12.5 Ah or 25 Ah per plate. The use of a relatively small plate size with max. 25 Ah has much advantage to get to a high power discharge performance. Figure 7.3 gives for a 12.5 Ah and a 25 Ah plate couple (one positive and one negative plate) the voltage for different discharge periods and different constant power discharge rates. For UPS applications, constant power discharge rates are more important than constant current discharge rates, because in practice such applications require constant power and not constant current supply from the battery.

The curves in Figure 7.3 are useful to find the appropriate number of plate couples for a given application. From the required power and discharge time as well as from the minimal acceptable discharge voltage, the diagram gives the number of plate couples to be used in the cell and, therefore, the size of the module. The curves do not start from the very beginning of discharge but at 10% depth of discharge (DoD). This is due to the fact that in the beginning of a discharge the voltage depends on the history of the battery. It depends on the kind of charge and discharge that the battery had before. There is especially the so-called 'coup de fouet' which can appear very soon after the beginning of a discharge. It is an additional voltage drop over a few seconds.

This phenomenon comes from a crystallization overvoltage which is caused be a delay of lead sulfate deposition due to a lack of seat crystals in the active material in the beginning of a discharge. This gives an oversaturation of lead ions in the electrolyte and results in a lower discharge voltage of about 30 mV per cell. It appears just on the positive side because the negative active mass has some barium sulfate as an additive, which can act as seat crystals for the lead sulfate deposition. On the positive side however, such an additive cannot be used and consequently this voltage drop typically appears at this electrode if the discharge starts from a fully charged battery. For most battery applications, this voltage drop is not important at all. For some stand-by operations, however, where a rather stable discharge voltage is required such a 'coup de fouet' can be the lowest voltage during discharge and has to be considered for the decision about the appropriate size of the battery.

The normal way to recharge UPS batteries is a voltage limited constant current charging (IU) by using, as a voltage limit, the floating voltage (in general 2.23 V per cell). This procedure has the disadvantage that a rather long time is needed for a complete recharge of the battery. The use of a higher initial charge current can slightly reduce the total charge time.

A more effective way, however, is to use an automatic system which, after a discharge, switches to a higher charge voltage, *i.e.* 2.40 V per cell, for a certain period of time. Afterwards, the system returns to the floating voltage. This charge regime results in a significantly shorter recharge time and there is virtually no reduction in service life since that higher charge voltage is used for a period of a few hours, which is rather short in comparison to the total time the battery is on float voltage.

The OGi battery range was designed for a service life of at least 10 years at an operation temperature of 20°C. The field experience has shown that there is no problem at all to achieve 10 years. Actually, 12 years was found as a typical service life of this battery type.

The open circuit voltage (OCV) of a lead-acid battery depends from the concentration of sulfuric acid used as electrolyte. However, it is important to realize that, after charge or discharge, some time is needed before the OCV gives the rest potential of the battery. Especially the VRLA batteries need a certain time before all the overvoltages after current flow have been decreased, due to the much slower diffusion for the equalization of the electrolyte in such batteries. From an electrochemical point of view, the OCV is the difference between the potential of the positive and negative electrode. The electrode potential can be calculated from the standard electrode potential and the concentrations or more exactly the activities of all components of the electrode reaction, according to Nernst's equation.

Due to some polarization when current is flowing, the charging voltage must be markedly higher than the OCV. The decision about the optimal charge voltage is influenced by many parameters as, for example, the time that is available for a complete recharge after a discharge. This is especially true for cycling applications where an overvoltage (the difference between the OCV and the charge voltage) of up to 600 mV per cell is used at the end of charging. At stand-by operation, most of the time the batteries are in a completely charged stage by keeping them on a so-called float voltage. This float voltage gives a relatively small charge current, which causes side reactions at the electrodes: mainly grid corrosion and oxygen evolution at the positive plate and hydrogen evolution at the negative plate. In case of VRLA, the recombination of oxygen at the negative plate is an additional reaction. The float voltage must be so high that the current covers all these side reactions, otherwise the battery would be slowly discharged. Another important point is to consider that the charge voltage should be on a level that the corrosion rate at the positive grid is as low as possible. The minimum of corrosion rate of the positive grid is not at the open circuit potential of the positive plate but at a slightly higher potential, *i.e.* at a polarization of about 70 mV. This point is discussed in more detail in one of the following sections on VRLA batteries.

Considering a flooded cell with an acid density of 1.24 g/cm^3 and a floating voltage of 2.23 V per cell, the overvoltage is about 140 mV, which is to be divided into two parts, one for the negative and one for the positive plate. The overpotential (polarization) of the negative plate depends strongly on the amount of other metals apart from lead at the electrode surface of the negative active mass, as virtually all other metals reduce the hydrogen overvoltage of the negative plate resulting in a greater hydrogen evolution.

If there is a surface extremely clean with only very few other metals, most of the overvoltage will be on the negative side. In practice, however, there are some other metals at the surface and thus, overvoltage is on both the positive and the negative side. Assuming that the overvoltage is approximately divided into two similar parts for the negative and positive electrode there would be about half of 140 mV, *i.e.* 70 mV on the positive plate and this is close to the minimum of positive grid corrosion. This overvoltage of the positive plate is not only favorable for minimizing the corrosion rate, but is also high enough to keep the positive plate in a completely charged condition.

In a flooded battery, grid alloys are used which have only a rather low content of antimony. In fact, for stand-by operation, today often lead-calcium alloys without any antimony are used and then the hydrogen overvoltage can be more shifted to the negative side resulting in a relatively low overvoltage of the positive plate. If the float voltage is relatively low, it might come to the point that the potential at the positive electrode is too low resulting in a higher corrosion rate and insufficient state of charge of the positive plate. For such unfavorable situations, it is convenient to add a small quantity of impurities to the electrolyte in order to reduce hydrogen overvoltage. The situation becomes more complicated in case of valve-regulated batteries. This is discussed later in one of the following sections.

7.3. Large Batteries

Stationary lead-acid batteries with capacities up to some thousands of ampere-hours are commercially available as 2 V units. On the positive side such cells have tubular plates, which are very robust, resulting in a rather long service life of the battery. This type is called OPzS and cells are available in the range from 200 Ah to 3000 Ah in transparent containers and for even higher capacities up to 12000 Ah in hard rubber containers. The floating voltage is, in general, the same as for OGi (2.23 V per cell).

Batteries with such high capacities often have tall plates. A general rule is that, the taller the plates, the greater is the ratio of grid electrical resistance to the total, internal resistance of the cell. As a result, plates taller than about 50 cm undergo a lower depth-of-discharge at the bottom of the cell. The large voltage drop down the grid reduces the available energy of the battery and also increases heat generation in the cell. In order to improve this situation, a novel

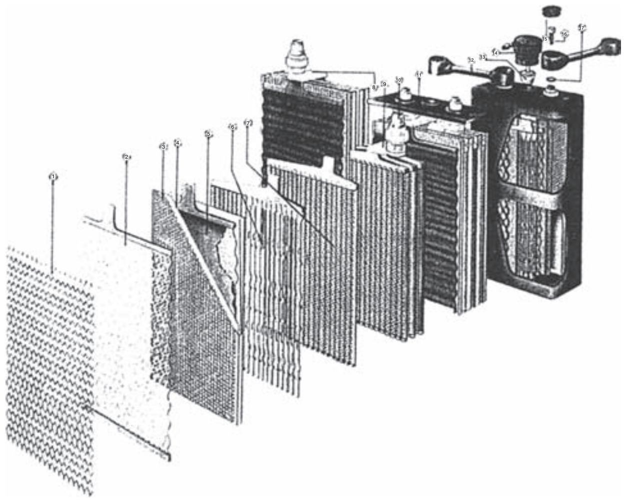

Figure 7.4. Constructive details of a CSM cell. The copper-stretch-metal grid can be seen on the very left side of this picture.

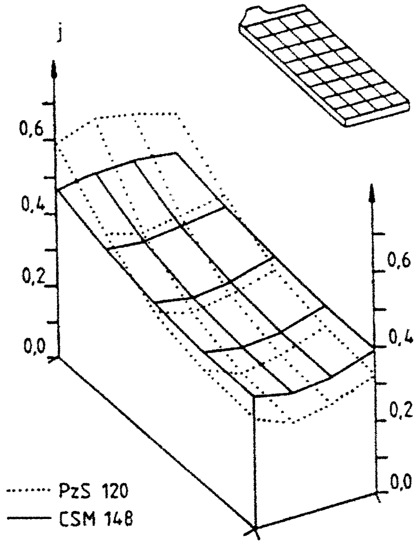

Figure 7.5. Local current density distribution of PzS and CSM with the same plate height at a discharge rate of 2 x I_5.

cell with a 'Copper-Stretch-Metal' (CSM) grid design was developed and placed on the market more than two decades ago [2-4].

The constructive details of such a CSM cell are demonstrated in Figure 7.4. The copper-stretch-metal grid can be seen on the very left side of this picture. CSM cells have the same weight and volume as standard cells, but copper is used instead of lead as the negative grid material. Actually, the grid is an expanded copper structure covered with a thin layer of lead. On the positive side of the cell, tubular plates are used. The influence of copper as the grid material of the negative plate on the discharge and charge behavior of the cell has been estimated by using a theoretical model developed in earlier papers [5,6]. In this model, the cell is considered as a network of vertical and horizontal resistances. A comparison of cells with plates of the same height (555 mm) shows the CSM cell internal resistance to be about 17% lower than that of the standard cell. Due to the lower resistance of the negative plate, the CSM design displays a markedly more uniform current distribution between the top and the bottom of the cell [7]. Experimental investigations of the current distribution in CSM and standard cells have confirmed the prediction obtained from the theoretical model.

The local current–density distribution in standard and CSM cells with the same plate height (555 mm) are illustrated in Figure 7.5 at the beginning of

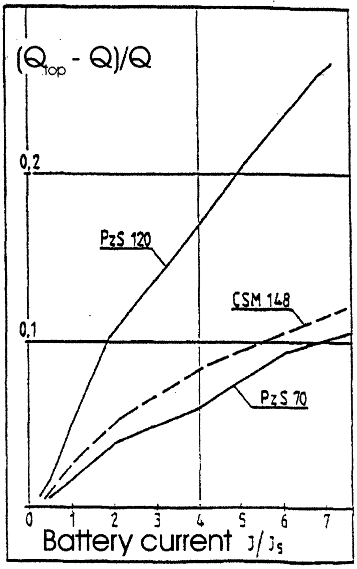

Figure 7.6. Relative deviation of the local DoD at the top of the plate to the DoD in average $(Q_{top} - Q) / Q$ for different discharge rates of PzS and CSM with a plate height of 555 mm and PzS with a plate height of 315 mm.

a 2 x I_5 discharge, where I_5 is the current at the 5 h rate. At the top of the plates, there is a much higher current density with the standard cell than with CSM. Conversely, near the bottom of the plates, the CSM cell has a higher current density than the standard cell. This means the current distribution is more uniform in CSM plates. The difference in local current density also means a difference in the local DoD of the plate.

Figure 7.6 presents the relative deviation of the local DoD at the top of the plate to the DOD in average $(Q_{top} - Q)/Q$ for different discharge rates between 0.5 x I_5 and 7 x I_5. In addition to PzS 120 and CSM 148, both with a height of 555 mm, there is also a PzS 70 plate with a height of 315 mm. It can be seen that the CSM plate displays similar behavior to the much shorter PzS cell. The relative deviation of the local DoD is a measure for the unbalanced mass utilization. PzS 120, with a plate height of 555 mm, has a significantly different mass utilization between the top and the bottom areas, especially at high discharge rates. This means that the mass utilization at the top is relatively high, while at the bottom there are mass reserves that cannot be used.

As the electrical conductivity of copper is much higher than that of lead, less grid material is required in CSM cells. This provides an option of having more active mass and electrolyte in the cell which, in turn, results in an increase in both volumetric energy density and power density. It is important to realize that the use of copper instead of lead for the negative grid is not only a benefit during discharge, but also provides a greatly improved charge acceptance with better energy efficiency. CSM cells (for traction applications) and OCSM cells (for stationary applications) should be used whenever cells with tall plates are required, to provide medium or high discharge power and high energy efficiency [2-4].

OCSM cells with tubular positive plates and copper negative grids have been used successfully for various stationary applications. In 1986, for example, a 17 MW/14 MWh battery was installed at BEWAG in Berlin. At that time, the battery was the largest in the world [8,9]. Designed to strengthen Berlin's 'island-utility' system, it was used from the beginning of 1987 for frequency regulation and spinning reserve.

A schematic of the BEWAG battery storage system is presented in Figure 7.7. There were 12 battery strings in parallel and each string had 590 cells in series with a capacity of 1000 Ah. This provided, in total, an 1180 V, 12000 Ah battery that, via converters and transformers, was connected directly to the 30 kV grid of BEWAG in Berlin.

A typical current flow in one string of the BEWAG battery over 42 h during frequency regulation is given in Figure 7.8. The current was limited to +/-700 A per string, this corresponding to a maximum power of +/-8.5 MW,

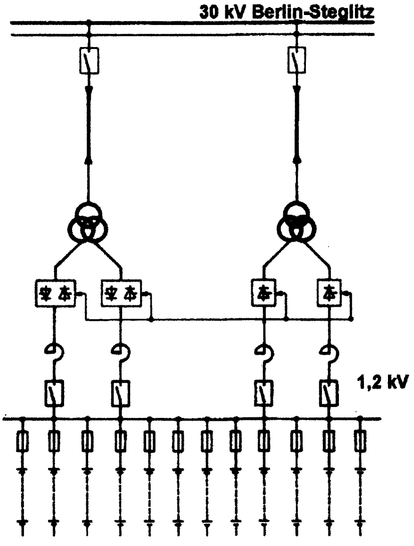

Figure 7.7. Schematic of the BEWAG battery storage system.

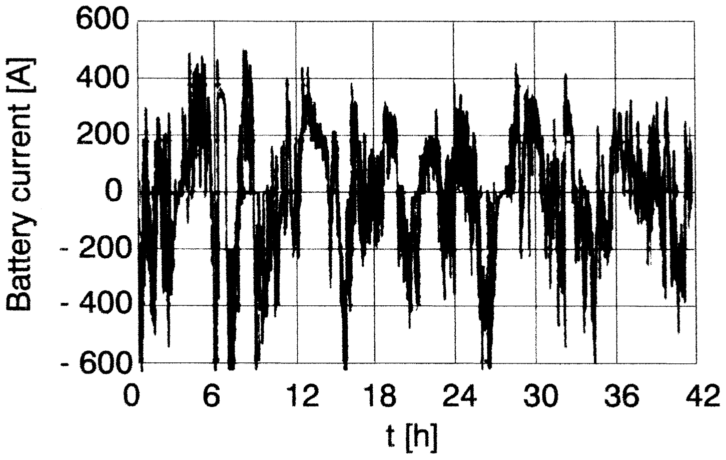

Figure 7.8. Typical current flow of one battery string during frequency regulation at BEWAG.

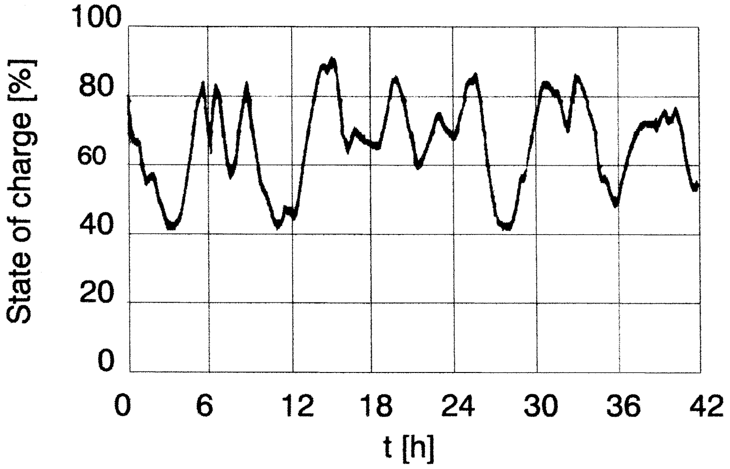

Figure 7.9. SoC of the battery during frequency regulation at BEWAG.

which was sufficient to keep the frequency always at 50 Hz with a maximum deviation of +/-0.2 Hz. When spinning reserve was needed, the limit of the discharge current was changed to 1400 A per string so that 17 MW were then available.

The state-of-charge (SoC) of the battery during the same time period over 42 h is presented in Figure 7.9. The SoC was kept to around 70% with a deviation of +/-20% so that there was always good charge acceptance and a certain reserve of capacity. Even the minimal SoC of 50% made it possible to have a spinning reserve of 17 MW maximum for at least 30 min. After two days of frequency regulation duty, the cells were charged over 4 h by an IU charging procedure. Every week, there was also a complete recharge over 14 h.

For such application, batteries with high power and good charge acceptance, as well as good cycle life, are needed. An important target was to have a total energy efficiency of more than 80%. Therefore, it was decided to use HAGEN CSM design with negative copper grids and positive tubular plates. From 1981 to 1986, there were some preliminary tests in order to evaluate all the information required for the use of such lead-acid batteries in frequency regulation and to obtain some basic data about the service life and the energy efficiency. The results were very promising and strongly influenced the decision to install the 14 MWh battery at the BEWAG plant in Steglitz [10].

In order to get high power and an energy efficiency of more than 80%, 10 V block batteries were used, rather than a single-cell design. In order to minimize the resistance of the intercell connector, there was a direct connection through the partition, a well-proven technique for starter batteries. The 5-cell block container was made of polypropylene and the HAGEN patentpole was used with copper inserts. There was an automatic water refilling system for each cell so that the maintenance work could be kept to a relatively low level. As the plate height was 800 mm and the charge voltage had to be limited to 2.4 V per cell, problems with acid stratification were expected. To overcome these problems, an electrolyte stirring system was installed. In the beginning, it was estimated that the maximum turnover would be 2.2 times the nominal capacity per day. In fact, it turned out that the daily turnover was much higher (up to 3.3). Plastic pipe heat-exchangers were used to avoid extreme temperature differences within the whole battery.

In 1987, when the 14 MWh battery commenced operation at the Steglitz plant, BEWAG placed some 48 V, 1000 Ah batteries in their test facilities in order to investigate in more detail the behavior of batteries under the operating conditions of the Steglitz plant [11]. These investigations included some comparative tests of different battery types. The main targets were to develop an optimal operating regime for battery storage systems used for frequency regulation and spinning reserve, and to collect more data on the energy efficiency and the service life [12].

In December 1993, Berlin was connected to the West European electricity grid. Therefore, frequency regulation was no longer a serious problem. From that time on, there were only small frequency deviations and the capacity turnover became rather small. Nevertheless, the battery continued in service as a spinning reserve for nearly a further two years.

In 1995, the BEWAG battery reached the end of its service life. During its time in service, the 14 MWh battery storage system operated successfully with virtually no problems [13,14]. This was a very remarkable result, as the operation conditions were severe. The battery had a capacity turnover of some 7000 times the nominal capacity, and the total energy turnover was about 100 GWh.

Originally, BEWAG planned to install four more battery storage systems of the same size in the Berlin electricity grid. Due to political changes in Eastern Europe, however, Berlin ceased to be an 'island utility', and plans for further battery storage systems were abandoned. It should be noted, however, that a battery design such as that used at BEWAG could be of considerable interest for other 'island systems' around the world.

Although in large inter-connected grid systems such as the European grid, frequency regulation is not a serious problem, there are still other areas in which large batteries can be very useful. For example, it has been pointed out that there can be a marked economical benefit when batteries are used for primary and secondary control [14]. Such an application could become a very interesting market for lead-acid batteries.

For special stationary applications where very high power over a time period of just a few minutes is needed, a new battery type was developed that is based on the OCSM design. The new type, called OCSM peak power, has negative copper grids but, on the positive side, the tubular plate is replaced by a flat plate that is significantly thinner in comparison to the tubular plate design. This makes it possible to use more plate couples in the same cell volume resulting in a better high power discharge performance. Figure 7.10 gives the discharge currents *vs.* time of an OCSM peak power cell (negative copper

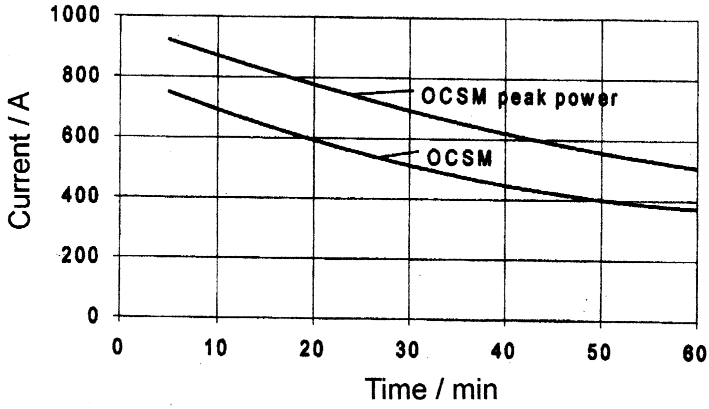

Figure 7.10. Discharge currents at different discharge times (between 5 and 60 minutes) of an OCSM peak power cell (negative copper grid, positive flat plate design) and, for comparison, of an OCSM cell (negative copper grid, positive tubular plate design) with the same container size.

grid, positive flat plate design) and, for comparison, an OCSM cell (negative copper grid, positive tubular plate design) with the same container size. The much better discharge performance of OCSM peak power is clear.

In summary, it seems that there is a rapidly increasing market for large batteries in a variety of utility applications. So far, this has mainly been a market for flooded batteries, but it is likely that the valve-regulated battery can replace the flooded type in utility applications in the same way that it has replaced them in UPS and telecommunications applications.

7.4. Improvement of Power Performance

The power P supplied from a battery can be expressed by the product of the discharge current I and the battery voltage U. The voltage U is the difference between the open-circuit voltage, U_0, and the product IR_i, where R_i is the internal electrical resistance of the battery, *i.e.*

$$P = (U_0 - IR_{i,}) \cdot I \qquad (3)$$

The maximum current is the short-circuit current, I_s, *i.e.*

$$I_s = U_0 / R_i \qquad (4)$$

The maximum Power P_{max} can be supplied at $U = 1/2U_0$, *i.e.*

$$P_{max} = U_0^2 / 4R_i \qquad (5)$$

Therefore, the maximum power can be raised by an increase of OCV and/or by a reduction in the internal electrical resistance.

The OCV is given mainly by the electrode couple. In case of a lead-acid battery, the OCV is around 2.1 V per cell. The exact figure depends, as already discussed in a previous section, on the concentration of sulfuric acid.

The internal electrical resistance is rather complex and does not just include a couple of ohmic resistances, but also some overpotential terms ('polarizations'). If just the specific resistance ρ of the electrolyte is considered, a power factor P_f can be calculated [15], *i.e.*

$$P_f = U_0^2 / \rho \qquad (6)$$

Calculation of such a power factor for various battery types gives the best result for the lead-acid system. The reason is that the lead-acid battery has a relatively high U_0 (2.1 V) and a rather low specific resistance of sulfuric acid (1.1 Ωcm). The alkaline nickel batteries (Ni-Cd or Ni-MH) have a markedly lower OCV (1.3 V) and additionally, a higher specific resistance of the electrolyte (1.8 Ωcm). Lithium-ion batteries are significantly higher in OCV (3.6 V); this is a clear advantage because the square of U_0 is taken in the power factor calculation. Organic electrolytes are used however, and have a specific resistance that is 50 times or more above that of sulfuric acid.

Double-layer capacitors, also called supercapacitors or ultracapacitors, have either aqueous electrolytes with low specific resistance, but then, U_0 cannot be much above 1 V, or organic electrolytes, where a markedly higher U_0 is possible, but then, there is a much higher specific resistance of the electrolyte.

Of course, the internal electrical resistance of a battery system is not just given by the electrolyte resistance. If systems have a rather small distance between the electrodes, the effect of high specific electrolyte resistance can be compensated. The polarization effects have also to be taken into account. Supercapacitors have an extremely high electrode surface area of more than 1000 m^2g^{-1} and this feature can reduce markedly any polarization. It has also to be realized that sulfuric acid is a part of the electrochemical process in a lead-acid battery and is consumed during discharge, which results in increase of the specific resistance of the electrolyte. Nevertheless, the lead-acid battery has a high power capability and, in spite of the weight of lead, is a suitable system for a high power supply. In addition, lead-acid has a significant cost advantage. Thus, there are numerous high power applications where lead-acid batteries have been used.

If a bipolar design with very thin layers of positive and negative mass is used, the internal resistance will be dominated by the electrolyte resistance and then, extremely high power can be supplied but only for short periods. The lifetime will also be markedly reduced. Prototypes of such batteries have given about 4 $kWkg^{-1}$ over 10 s; this is rather impressive [15].

Most of the improvements in power capability were achieved by reduction of the internal electrical resistance. For VRLA design with antimony-free grid alloys, the OCV has been raised to a slightly higher level over the years by an increase in sulfuric acid concentration from a relative density of 1.26 or 1.28 to about 1.30 or even slightly higher, but there are certain limits for any further increase.

The internal resistance has been reduced significantly over the past decades and there appears to be room for further reduction. As already pointed out, the internal resistance of a battery is rather complex: there is the ohmic resistance from all the current-collector parts and the electrolyte but there are also some polarization effects. The latter include charge-transfer reactions, diffusion and crystallization. All these are non-ohmic and depend significantly on the current and the time of current flow, as well as on the state-of-charge, and whether the battery is on charge or discharge.

In the beginning of a high power discharge, the voltage drop mainly arises from all the ohmic resistances and the charge-transfer reactions. Very soon, other effects (diffusion, change of active mass surface) exert an influence and result in a higher voltage loss, which reduces the power capability of the battery. Thus, if very short high-power discharge pulses are required, then the polarization is less important in comparison with a longer period of high power discharge.

The ohmic resistance of the electric current conductor parts makes a significant contribution to the internal resistance of the battery. It includes the grids, top bars, intercell connections, and the terminals. For high–power applications, there have been attempts to reduce the resistance by improved grid designs [16,17]. This can be calculated quite readily and with high accuracy by using computers with the result that it is indeed possible to produce grid structures with markedly lower resistance. Unfortunately, it is not so easy to cast well grids that have minimal electrical resistance, and this can result in higher corrosion rates. Pasting can also be more difficult. Therefore, changes in the grid structure have to be performed carefully by considering possible casting and pasting problems [18]. A way to avoid any restrictions from grid casting was proposed recently [19]. It is a novel grid production method with an electro-deposition process, which minimizes grid weight and optimizes grid structure for low electrical resistance. This method is discussed in more detail in a subsequent section.

Another way to improve the high power performance is the use of copper as the negative grid material for lead-acid batteries with high capacities and rather tall plates as already discussed in a previous section.

An alternative to negative copper grids is the use of a second lug (or 'tab') at the bottom of the plate as a current take-off tab in order to improve the current-collection function of the grid [20-22]. The benefits, especially at high discharge rates, are similar to the use of negative copper grids, namely: less voltage drop along the grid, less heat, and better and more uniform mass utilization at the bottom of the plate. Again, charge acceptance will also be much better. The dual-tab concept has been used to develop a spiral-wound VRLA design for high-power applications.

As discussed above, a bipolar design is the best approach to minimize the electrical resistance of the conductor parts. There are some reports of theoretical calculations, and about testing of prototypes made as a bipolar or a semi-bipolar version [23-27]. For short lifetime requirements in special applications, it has been quite successful. Whenever a longer life has been needed, however, such batteries have suffered from many problems as corrosion and leakage. Thus, up to now, none of these bipolar concepts has been successfully placed in the market.

Polarization is much influenced by the surface area of the active mass. During discharge, some active mass is consumed and lead sulfate covers part of the surface. Therefore, with proceeding discharge, the available surface area is reduced significantly and this results in a steadily increasing polarization. This effect could be compensated, at least to some extent, by using an active mass surface structure with higher surface area. At present, however, this parameter is already on a rather high level (for the positive mass it is about 5 m^2g^{-1}) and a further increase would give a significant reduction in lifetime, especially in cycling applications. If lifetime is not a high priority, increase in surface area is a way to reduce polarization effects. It has to be realized that, during cycling, there is a marked reduction in the surface area. This ageing effect gives a decrease in the high current performance of the battery.

A good mass adhesion to the grid is important to avoid problems at the grid/mass interface. Any appearance of barrier layers results in significant increase in resistance in this part of the battery [28-30]. The use of a proper alloy, especially with a sufficient high tin content (often about 1 wt% or more), is important to avoid such problems [18,31-33]. A good plate processing, especially the curing, is also helpful.

Both active materials (lead dioxide and lead) act as electrical conductors from the points of the electrode process to the nearest grid member. However, the porous structure of the active material and the lower conductivity of lead dioxide have to be considered. As discharge goes on, steadily more non-conductive lead sulfate is formed. Therefore, the pellet size has an impact on the electrical resistance inside the active mass.

There has been an investigation [34] about the use of polymer-structured electrodes, where the grids were made from a polymer, coated with thin layers of copper and lead. These PNS (polymeric network structure) grids had significantly lower weights and much smaller mesh sizes in comparison with standard lead grids. There were some variants between 1x1 mm and 3 x3 mm mesh size. The rather small mesh size gave a much better discharge performance due to the shorter current paths within the active ass. Although prototypes gave promising results, the rather high cost is a disadvantage of such electrodes.

During discharge, sulfuric acid inside the pores of the active mass is used first. Very soon, diffusion starts where sulfuric acid is transferred from the space between the plates into the pores of the active mass. At high discharge rates there can be a limitation by diffusion. This results in a lack of electrolyte inside the plate, where the electrode reaction nearly stops, although there is still sufficient active mass available. A cross–section through a positive tubular

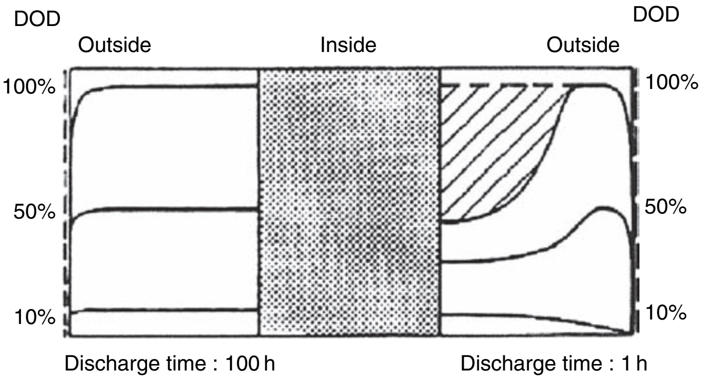

Figure 7.11. Cross section through a positive tubular plate showing diffusion limitation of thick plates at high discharge rates.

plate is shown in Figure 7.11. It can be seen that a 100-h discharge rate gives the same discharge level in the inner and outer parts of the plate. With a 1-h rate the inner part is just 50% discharged in comparison with the outer part due to the diffusion limitation of thick plates.

The diffusion problem can be reduced by using thinner plates. This has been a successful way in the past decades to improve automotive starter and UPS batteries. Present plates are rather thin. For certain applications, they have sometimes a thickness of just 1 mm. An alternative to a thin plate design would be an electrolyte flow through the plates. Although a reduction of the diffusion problem could be found on tests of such prototypes, there are other disadvantages and, thus, it has not been used so far in the field.

The use of very thin electrodes has been reported as the TMF (thin metal foil) concept [35-37]. Spiral wound, thin metal sheet electrodes and absorptive glass mat (AGM) separators offered extremely high power and excellent chargeability. The grids were rolled sheets of only about 0.6 mm thickness and had an active-mass layer thickness of about the same dimensions. The battery was developed for use in power tools, automobile starting and other applications where high power and rapid recharge capability is required. This development to novel design features is a good demonstration to show the extremely high power performance of the lead-acid system. It has been rather difficult however, to achieve reliability and a sufficiently long life. Another approach has been proposed recently, namely, the UHP (ultra high power) design with thin flat plates and thin microglass mats or special microporous polyethylene membranes as the separator [38]. Prototypes were tested and gave the expected improvement in power performance. Such a design is especially interesting for UPS applications.

Part of the electrolyte resistance comes from the separator. Indeed, at high discharge rates there is a significant contribution of the separator to the total voltage losses in the battery. Much progress has been made in the past decades to improve the separator with regards to many parameters that include a low electrical resistance [39,40]. Today, polyethylene separators are often used, and are made from a blend of ultrahigh-molecular-weight polyethylene pellets with a mixture of silica and oil. Such separators have a high porosity and a rather low electrical resistance. They are very useful for starter batteries where high cold cranking performance is needed. An even lower electrical resistance can be achieved with AGM separators. This is discussed in more detail in one of the next sections.

The effects of reduced surface area of the active mass and lack of electrolyte during longer discharge periods with high power is much influenced by the crystalline structure (porosity and crystal size) of the active mass. There is an impact from the paste recipe and density, but the manufacturing process can also exert a strong influence. This includes pasting, curing/drying, soaking, and formation. Many studies on these subjects have been published in recent years; some examples are given in Refs [41-45]. Positive plates were made by using paste densities between 3.8 gcm^{-3} and 4.3 gcm^{-3} in combination with low, medium, and high curing temperatures, which resulted in a tribasic (3BS) or tetrabasic (4BS) lead sulfate structure of the cured mass or a mix of both [43,44]. The investigations also involved various soaking and formation programs with pulse technique and discharge steps. In the end, there were rather different crystalline structures of the formed positive mass with different initial performance data and cycle life results.

The above studies also included an accelerated cycle test of single positive plates with an excess of electrolyte and negative mass. Different plate types were used, made from a paste density between 3.8 gcm^{-3} and 4.3 gcm^{-3} and with cured crystalline structure of 3BS, 4BS or a mix of both. The mass structure after formation was investigated by SEM. Positive mass formed from 4BS had still the typical network structure of tetrabasic lead sulfate with rather large crystals that act like a skeleton for the positive active mass. The pictures of positive mass formed from 3BS show a well formed mass with the typical structure of β-PbO_2 forming a network of agglomerates of rather small PbO_2 particles.

The positive plate was put between two negative counter plates in sulfuric acid with a relative density of 1.30. The discharge current was 11 A down to 1.5 V and the charge current was 2.8 A up to 2.4 V, followed by an additional charge with 0.7 A over 6 h. After 70 cycles, the test was terminated. Afterwards, the weight loss of the positive plate was measured in order to determine the amount of shed material. The test results are presented in Figure 7.12. Plates prepared from 4BS gave less shedding than those based on 3BS.

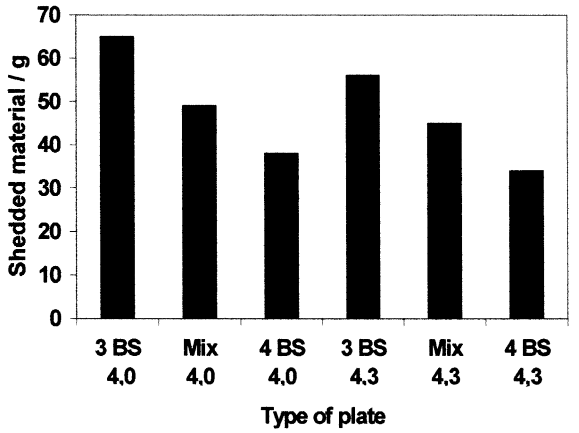

Figure 7.12. Amount of positive shed material after accelerated cycle tests in a flooded system with excess of sulfuric acid and negative mass.

The mix of 3BS and 4BS lies in between. There is also an influence of paste density. More shedded material was found with 4.0 in comparison with 4.3 gcm^{-3}. The accelerated cycle test with an excess of electrolyte and a high discharge rate gave comparable results with tests that employed lower discharge currents or other special cycle programs. Those tests showed that without any support of the positive active mass, *e.g.* by gauntlets, as in case of tubular plates or by tight separator design, the lower porosity/higher density with more contact area between the mass particles and the better crystal network of tetrabasic lead sulfate slowed down the shedding process.

Thus, further increase of active mass porosity and surface area, as well as plate thickness reduction, has certain limits with respect to the life of the battery, especially if some cycling performance is needed. On the other hand, the use of an AGM design with high pressure of the glass mats on the plates gives additional options. Test with the same plates used in flooded or AGM design clearly demonstrated that AGM allows much better cycle life and less influence of the cured mass structure and porosity in comparison with a flooded design. This means that with an AGM design and high pressure by glass mats, a more porous active mass and a higher surface area can be used and can result in better power capability without incurring a dramatic loss of cycling performance.

To investigate the effect of an AGM design, the same plates as those used in the accelerated cycle tests of Figure 7.12 are taken to make 2 V AGM cells with a nominal capacity of 24 Ah at the 5-h discharge rate. These cells had 3 positive plates enveloped by glass mat separators with a thickness of 1.7 mm

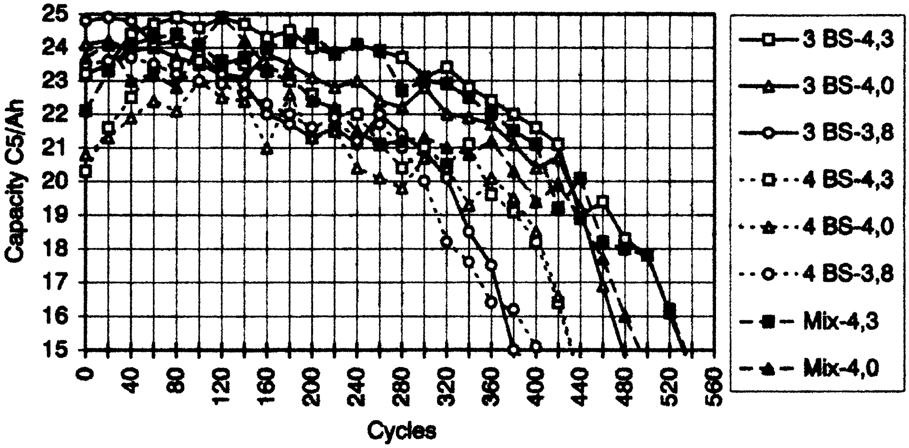

Figure 7.13. Accelerated cycle test of 2 V AGM cells after 2 h soaking and constant current formation.

in the compressed stage (about 35% fine fibers and 25% compression) and 4 standard negative plates. For the container Perplex was used together with a pressure release valve with an opening pressure between 120 and 150 mbar. The electrolyte was filled by gravity within about 8 minutes using a volume to get a saturation of 95%. For the accelerated cycle tests the discharge current was 34 A down to 1.5 V. The cell was charged with IU by using 10 A up to 2.4 V and the total charge time was 7 h (at 30°C). This is a quite hard test method and there is the experience from former tests that with such a test regime, differences with regard to cycle life can be seen easily. Normally a better cycle life in this test means also a better cycle life under real conditions in practice.

Figure 7.13 gives the results of the cycle tests with AGM cells. First, the results show that there is indeed a quite different behavior of AGM cells in comparison to the flooded design. The cycle life was much better with AGM and there was not really a benefit of 4BS in AGM cells as it had been found with the same type of plates in the first test series in flooded cells. Actually, 4BS is worse whereas the 3BS/4BS mix and 3BS behave markedly better. There was also a better cycle life with higher paste density. The best results were found with 4.3 gcm^{-3} paste density in combination with 3BS or a 3BS/4BS mix whereas 3.8 gcm^{-3} paste density gave the worst results both for 3BS and 4BS. It is remarkable that the generally held believe that 4BS is always the best choice for getting a good cycle life is not valid for AGM batteries. Actually, the difference is even worse than the direct comparison of the achieved number of cycles. As 4BS gave lower capacity from the beginning, the difference in the achieved total capacity turnover is even bigger.

These investigations have shown clearly that it is possible to get a good cycle life with AGM design even at high discharge rates. Using the same type of plates, AGM gave a much better cycle life in comparison to the flooded design. The failure mode was in all cases softening of the positive active mass. For AGM design, 4BS is not necessary to get a good cycle life, 3BS is even better and so it is possible to get AGM batteries with a high capacity and performance from the beginning by using a relatively short formation time. This result is contrary to that of the tests with flooded design where 3BS was markedly worse than 4BS. The main difference between flooded and AGM design is that the latter provides a starved electrolyte situation and a very good support of the positive mass by glass mats with relatively high compression. Besides, there was a marked influence of paste density and 4.3 gcm^{-3} gave the best and 3.8 gcm^{-3} the worst results.

7.5. Features of VRLA Technology

Among the many advances in lead-acid battery technology, (*e.g.* increase in energy density and cycle-life, reduction of self discharge, automation of manufacture leading to reduced production costs, *etc.*), the development and introduction of the gas-recombination technology is probably one of the most important. These gas-recombination batteries, *i.e.* valve-regulated lead-acid (VRLA) batteries, make it possible the use of lead-acid batteries in applications where flooded batteries cannot be used due to risk of acid spillage.

There are additional advantages with recombination batteries. For example, topping up with water is not necessary over the whole life of the battery, and the battery can be designed to survive a 30-days short circuit test and, after recharge, have virtually the same capacity as before the test. Due to a marked reduction in water decomposition, there is only a small release of hydrogen gas and a low rate of self discharge. Many studies of VRLA batteries have been published in recent years; some examples are presented in Refs [18,46-58].

In VRLA batteries, the electrolyte is immobilized by an absorptive glass-mat (AGM batteries) or by a gelling agent (gel batteries). Immobilization of the electrolyte makes the recombination process possible; oxygen produced at the positive plate, especially during charging, can migrate to the negative plate where it reacts (recombines) to form water. As this reaction reduces the amount of hydrogen gas evolved at the negative plate, there is a marked reduction in the amounts of hydrogen and oxygen that leave the cell. Nevertheless, the amount of gas released is not exactly zero and the term 'sealed battery', which is sometimes used, should not lead to the assumption that there cannot release gas at all.

The two technologies, gel and AGM, have many similarities, but there are also some differences. For example, it is well known that for tall cells in a vertical position, only gel cells can be used; otherwise, acid stratification cannot be avoided. There are some fairly tall AGM cells on the market, but these are intended for use only in a horizontal position in order to avoid the acid stratification problem. For short cells, both gel and AGM designs are possible without restriction on cell orientation. Often, AGM is used when high power is requested whereas gel is especially useful to achieve a long lifetime.

In general, VRLA batteries use lead alloys that are virtually free of antimony. This is because antimony is released from the positive grid by corrosion and migrates to the negative plate where it lowers the hydrogen overvoltage. As a result, there is an increase in hydrogen evolution and, consequently, higher self discharge and more water loss.

Nowadays, most battery manufacturers prefer to use lead-calcium alloys. Calcium acts as a grid-hardening agent. There is also some tin (up to 1%, sometimes more) in the alloy. This improves the casting process and helps to avoid problems at the grid/active material interface of the positive plate.

There is a substantial difference between the corrosion behavior of lead-calcium-tin and lead-antimony alloys. Tests reveal that antimony-containing alloys generally exhibit a higher corrosion rate, and that the rate decreases with decreasing antimony content. This type of corrosion, which is typical for antimony alloys, is an intragranular process with a quite regular corrosion front over the whole area. In the case of lead-calcium alloys, well-cast samples undergo low corrosion rates, but, if the grids are not properly cast, there can be heavy intergranular corrosion. This type of corrosion is not uniform but penetrates deeply into some parts of the grid and causes tremendous grid growth.

Sometimes this growth is so heavy that it produces a bending of the lid. In the case of grid growth, it is not the total oxidation of the grid lead to lead dioxide that limits the life of the battery. More often, failure results where the grown grid comes into contact with the negative top-bar to create an internal short-circuit.

During stand-by duty with very few discharges, another consequence of grid growth can be that the active material is not able to follow the grown grid and, therefore, contact between grid and material is lost. Figure 7.14 shows a positive plate of a battery that has been used in floating service and has developed a grown lead-calcium-tin grid. Due to poor grid casting, the battery failed after 3 years. During cycling, however, the active mass can maintain contact with the grid so that the whole positive plate, including the active

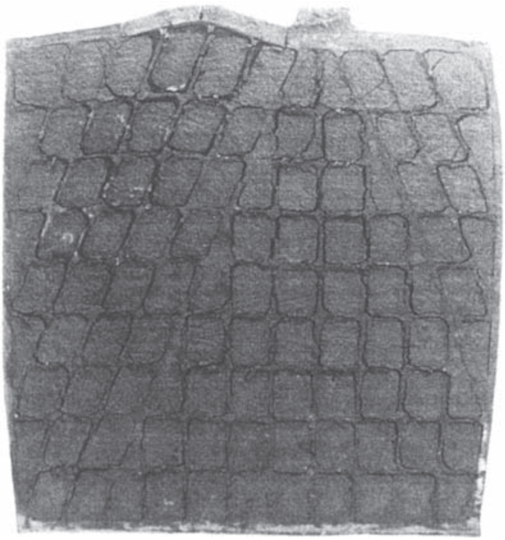

Figure 7.14. Positive plate with a grown lead-calcium-tin grid of poor cast quality after 3 years of usage in floating experiments.

material, grows and then an internal short-circuit between the positive grid and the negative top-bar can limit the life of the battery.

As positive grid corrosion has an important influence on the expected lifetime of stand-by batteries, there have been many investigations of the parameters affecting the corrosion rate. Grid corrosion and growth depend on: (i) alloy composition; (ii) grid design; (iii) casting conditions; (iv) positive active material; (v) impurities that accelerate corrosion; (vi) battery temperature; and (vii) potential of the positive plate.

The influence of alloy composition on the corrosion stability of positive grids in VRLA batteries has been reported in Refs [59-70]. In practice, it has been found that lowering the calcium content reduces the corrosion rate. Unfortunately, since lower calcium content results in slower grid hardening, a compromise is often necessary. A calcium content is used that is sufficiently high to allow handling of the grids during plate processing but sufficiently low (often, well below 0.1%) to avoid severe corrosion. In general, this compromise imposes a rather small acceptable range of calcium content.

Of course, the influence of the other variables mentioned above has also to be taken into consideration. It turns out that a relatively high calcium content (up to about 0.09%) can be tolerated if all other conditions are favorable. Conversely, unfavorable variables (items (ii) to (vii) above) can cause high corrosion rates even with much lower calcium content.

The influence of the grid design on the casting process and on corrosion behavior is often underestimated. Particularly for applications where high discharge currents are needed, there has been a tendency to modify the grid structure to reduce its electrical resistance. As already discussed in a previous section, such changes in grid structure have to be performed carefully with due consideration of possible casting and corrosion problems.

The casting process involves many variables that influence the quality of the grids and, therefore, the corrosion behavior. These variables include for example, the grid/mould design, the temperature of the pot of molten alloy and the mould, the speed of casting, the cooling rate, and the pressure in the case of pressure casting. In general, pressure casting is used for tubular plates and, if all other variables are reasonably favorable, produces lead-calcium-tin grids with very low corrosion rates. Even after several years in use, the spines of grids produced in this way exhibit only a very thin corrosion layer. Corrosion of lead-calcium-tin tubular grids has seldom been the cause of the failure of VRLA batteries.

Gravity casting of grids is usually employed for the manufacture of flat positive plates. Flat positive lead-calcium-tin grids are more sensitive and more prone to corrosion than tubular grids. Nevertheless, it must be pointed out that even for batteries with flat positive plates, corrosion has been only one of the limiting factors during stand-by applications.

An example of the influence of alloy composition and casting conditions on grid corrosion is given in Figure 7.15. During this accelerated corrosion test of gravity-cast, lead-calcium-tin grids in sulfuric acid, the grids were taken out of the electrolyte every 3 weeks. They were washed and dried without removal of the corrosion layer, and their weight was determined. In all experiments, there were small increases in weight during the first weeks due to oxidation of some of the grid material. The decreases in weight during the following weeks can be explained by the shedding of oxidized material during progressive oxidation.

Normally, good corrosion stability gives only a small increase of weight in the beginning of cycling, and shedding starts quite late, whereas poor corrosion stability gives a higher increase of weight in the beginning followed by a more rapid decrease of weight due to shedding. It can be seen from Figure 7.15 that an improvement of the alloy with respect to calcium and tin contents gives slightly better corrosion stability, but the influence of casting conditions is more pronounced.

The addition of copper as a grain-refining material can improve markedly the corrosion resistance of the positive grids. Figure 7.16 gives the results of an accelerated test on gel, A400 monoblock batteries by overcharge

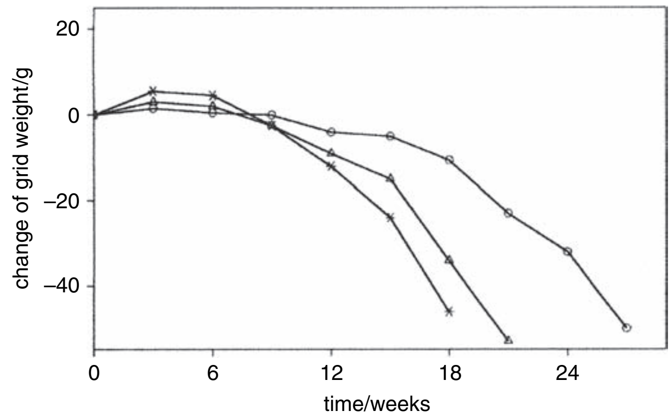

Figure 7.15. Accelerated corrosion test of gravity cast, lead-calcium-tin grids in sulfuric acid (60°C, 1.26 g cm^{-3} specific gravity, 1.85 V constant potential against SHE). Change of grid weight measured every 3 weeks without removal of corrosion layer: (*) standard alloy/standard casting; (△) improved (in terms of calcium and tin content) alloy/standard casting; (○) improved (in terms of calcium and tin content) alloy/improved casting.

with 2.40 V per cell at 45°C. The battery without grain refiner had a marked capacity loss after 12 test cycles, and a tear-down analysis showed significant positive grid corrosion.

Conversely, the battery with copper addition to the positive alloy behaved much better, with capacity stable and still above 100% after 12 test cycles. Tear-down analysis of this battery showed a much lower corrosion rate.

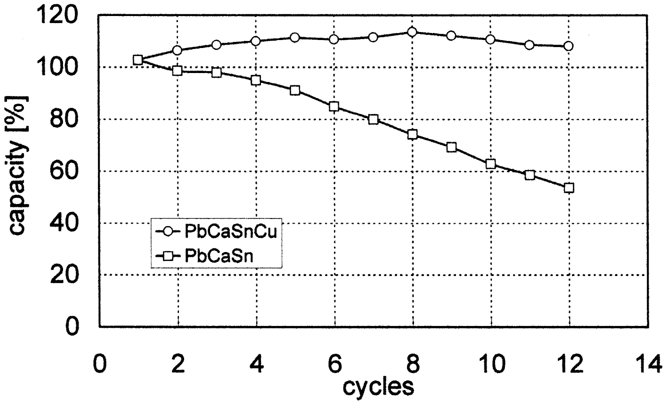

Figure 7.16. Accelerated overcharge test of gel batteries (A400 type) with and without copper as a grain refiner for the positive alloy.

It is not easy to understand completely the influence of the positive active mass on grid corrosion, although much has been published about this subject [71-74]. There must be an influence, however, because the results of corrosion tests are different for bare and pasted grids. The influence of the mass may be due to an increase in the pH near the grid surface at the end of discharge, connected, in turn, to a limited diffusion capability of the electrolyte in the pores of the mass. Another factor may be the stress on the grid due to volume changes of the mass during charge and discharge. It must also be considered that some parts of the grid are in very close contact with the mass such that no electrolyte can reach these parts. The active mass can accelerate or slow down grid corrosion, but in either case it must not be ignored. Thus, the results of corrosion tests with well-prepared lead samples in the laboratory can be quite different from the results obtained with batteries.

Impurities that accelerate the grid corrosion rate (*e.g.* organic acids or chlorine components) are well known, and there is, in general, no difference between the behavior witnessed in flooded cells and in valve-regulated cells. Normally, impurities can be excluded rather easily. By comparison with flooded cells, valve-regulated cells have the advantage that topping up of water is not required and, therefore, impurities cannot be introduced into the cell during use. Battery manufacturers, of course, must avoid introducing contamination or impurities during fabrication. This is important because of accelerated corrosion of grids and because there is a marked influence of some impurities on both self discharge and hydrogen evolution.

The features discussed so far are, in general, the responsibility of battery manufacturers. Beyond these, incorrect use or abuse of valve-regulated batteries is also an important determinant of grid corrosion. The most pertinent factors are temperature and charging voltage or, more precisely, the potential of the positive plate. The influence of temperature is often described by the general rule that a higher temperature results in a higher corrosion rate. This is valid for both flooded and VRLA batteries. For stand-by service, the expected lifetime is often specified for a temperature of 20°C, which implies a recommendation to keep the battery around 20°C in order to obtain maximum endurance.

Although reasonably self-evident, it is emphasized here that battery temperature and not the temperature of the environment is the relevant factor. If battery temperatures appreciably above 20°C cannot be avoided, then it is necessary to adjust the charging voltage, according to the instructions of the battery manufacturer, in order to avoid a serious reduction in service-life. Regulation of charging voltage may also be necessary if the battery temperature is appreciably below 20°C.

A typical malpractice is to place batteries as close together as possible in order to save space. As batteries produce some heat, even on float, tight packing of batteries can produce a situation whereby the heat emission (a combination of heat radiation and heat transportation by air convection around the battery) is smaller than the heat produced so that the battery temperature increases. Ignoring the heat produced by batteries can give a marked reduction in service life due to accelerated grid corrosion, even if the temperature does not reach a level such that drying out or thermal runaway takes place. Although this is also valid for flooded cells, the situation described can be more dangerous for valve-regulated batteries because, during float, nearly all the electrical energy input is used for the oxygen recombination process and is completely transformed into heat.

The influence of charging voltage on the corrosion of positive grids has been reported widely. A discussion about the special situation in valve-regulated batteries can be found in Refs [50,75-77]. The corrosion rate does not depend only on the charging voltage but also on the oxygen recombination efficiency. The latter influences the charging current and, therefore, the potential of the positive plate, which is the determining factor for corrosion.

The polarization of the positive electrode at different cell voltages for flooded, gel and AGM cells is shown in Figure 7.17. For a flooded cell, it is assumed that the overvoltage of the positive and the negative plate is nearly the same. In the case of AGM cells, one example is given of high and one of low oxygen recombination efficiency. It is emphasized that this is only a schematic representation of the behavior. In reality, the situation may be more complicated [50]. Adapting the charging voltage to acid density, and vice versa, is very important [77].

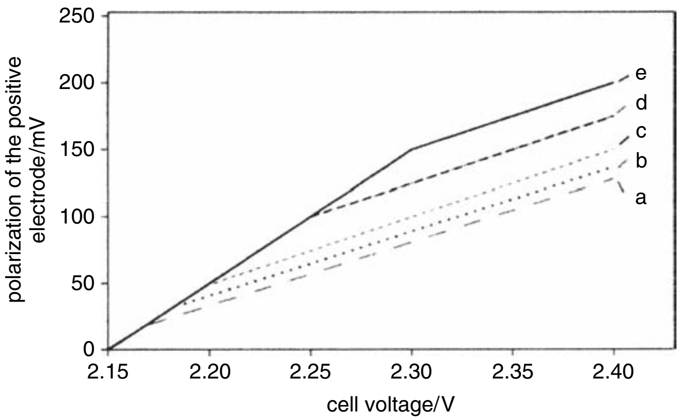

Figure 7.17. Schematic of positive electrode polarization of flooded, gel and AGM cells (assumed specific gravity: 1.30 gcm^{-3}). (a) flooded cell; (b) gel, new cell; (c) AGM, low recombination efficiency; (d) gel, after prolonged periods of use; (e) AGM, high recombination efficiency.

Drying out is mostly connected with a too severe charging regime, often in combination with high cell temperature. The best way to circumvent this problem is to prevent extreme situations in battery operation. This means, for example, the avoidance of charging at too high rate, especially after deep discharge and at high battery temperatures. In cases where very high temperatures are a potential threat, the use of special cooling systems might be required. In general, drying out reduces the capacity of the cell and, finally, limits its life. Drying out also increases the oxygen recombination efficiency, and this can be a severe problem in UPS applications where excessive recombination efficiency can increase the temperature of the battery dramatically. The so-called 'thermal runaway' effect, which can be exhibited by VRLA batteries in UPS service, arises as a consequence of these phenomena.

The best way to avoid dry out and runaway is to remember that, during float charging, the battery produces some heat and, therefore, avoid packing batteries closely together. It is much better to provide a spacing of at least 10 mm between adjacent batteries. Keeping batteries at such a distance normally allows effective heat dissipation.

As discussed in more detail below, a high charging voltage is helpful for reducing charging time and avoiding sulfation. Nevertheless, it must be remembered that, under this conditions, a higher current flows through the cell, which promotes the risk of thermal runaway and dry out. Therefore, a higher charging voltage should only be allowed for a restricted period after discharge. A charger that automatically reduces the charging voltage to the float voltage after a given period of time would be an appropriate way to circumvent this problem.

The best way to avoid thermal runaway is to monitor battery temperature and to change the float voltage or current automatically, according to the measured temperature. It is strongly recommended that the measured battery temperature, and not the room temperature, be used for controlling the float voltage or the float current. In the case of AGM batteries, it is also important to have a good control of the degree of saturation of the separator. It is well known that a too low level of saturation will result in very high oxygen recombination efficiency and in high currents, even at quite moderate float voltages.

The fact that, with the same float voltage, quite dissimilar currents can flow through an AGM cell, as determined by the oxygen recombination efficiency, has been discussed previously [50]. The situation in a gel battery is different at the beginning of life when the recombination efficiency is always rather low. After some water loss, however, the recombination efficiency in these batteries will increase also. If too much water is lost (dry out), the recombination efficiency of gel batteries can be quite high.

Papers published over the past few years have described the benefits of gas recombination catalysts in VRLA cells [78-80]. The insertion of a catalyst into the headspace of a cell can assist the recombination of a significant amount of hydrogen that would otherwise escape and constitute water loss. It is claimed that such catalysts not only reduce water loss but can also balance float charging of VRLA batteries. There remains some uncertainty, however, about the reliability and service life of such catalysts.

A pressure-release valve with a high opening pressure could be helpful in reducing water loss, but the benefit of such a device is not sufficient to offset other problems that must be faced with high pressure in the cell. In general, a pressure between 100 and 200 mbar seems to be a good compromise to avoid excessive loss of water.

The behavior of valve-regulated batteries during float operation is influenced by many parameters and is rather complex [55]. A mathematical model has been developed [81] that describes the effects of kinetic cell parameters, float voltage/current, and temperature on electrode potentials and rates of electrode reactions. In flooded batteries, the main side reactions are grid corrosion and oxygen evolution on the positive side and hydrogen evolution on the negative side. In valve-regulated batteries, the recombination process, *i.e.* oxygen reduction at the negative plate, must also be considered. The mathematical model, in combination with experimentation, has shown clearly that discharge of the active material can occur under unfavorable conditions during float duty.

When recombination efficiency is high, oxygen evolution will be virtually balanced by oxygen reduction, and it follows that the hydrogen evolution current at the negative plate must be approximately equal to the grid corrosion current at the positive plate in order to avoid any discharge of the electrodes. If the grid corrosion rate is too high in comparison with the hydrogen evolution rate, the positive plate will be slowly discharged, resulting in some sulfation. On the other hand, if the hydrogen evolution rate is too high in comparison with the grid corrosion, the negative plate will be slowly discharged and sulfated. Therefore, the choice of a proper float voltage and the right temperature compensation has a significant influence on maintaining the positive and negative plates in a completely charged state. In particular, too high a reduction of float voltage at higher temperature can result in sulfation problems of the battery.

An improved temperature compensation of the float-charge voltage for gel batteries has recently been proposed [82]. Important elements of this scheme are that, in comparison with past practice, the float voltage is reduced less at higher temperatures, and there is a range of temperatures within which no compensation of the float voltage is necessary. For a type A400, gel battery,

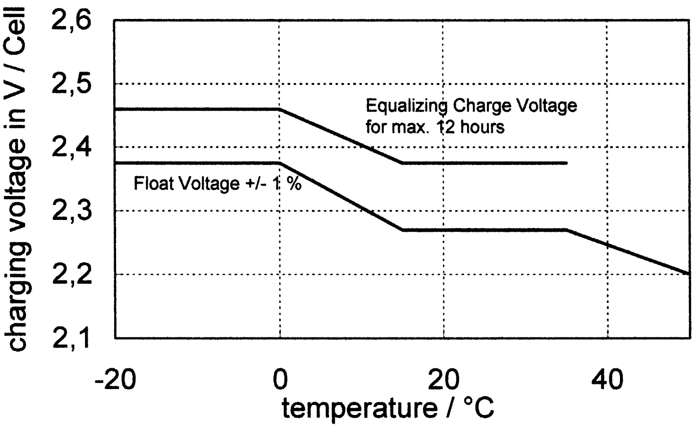

Figure 7.18. Float and equalization charge voltage at different temperatures for type A400, gel batteries.

Figure 7.18 shows how the float and equalization-charge voltages should be changed for different temperatures. The equalization charge is used to bring all the cells of a string to a complete state-of-charge. This higher voltage charge, however, should be limited to a period of no more than 12 h.

In some cases, AGM batteries used under float operation suffer from sulfation of the negative plate. It has been established that, in order to avoid sulfation of the negative plates, impurities that reduce the hydrogen overvoltage must be kept to a sufficiently low level [83]. The worst situation with regard to the health of the negative plate is a very corrosion-resistant positive grid and a

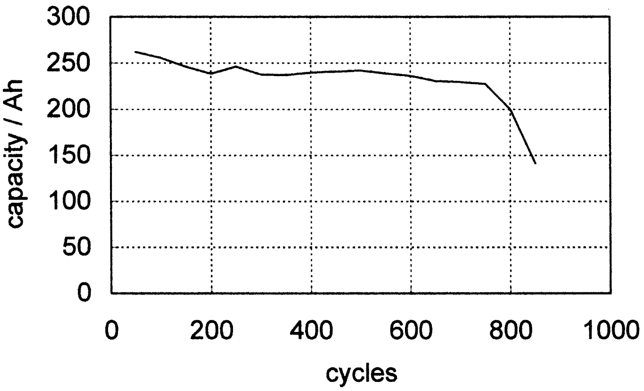

Figure 7.19. Cycle test (cycling to 80% DoD) with a 6 V, 240 Ah gel battery. Capacity test every 50 cycles.

high concentration of deleterious impurities in the battery.

Float operation with an occasional discharge is the standard service of stand-by batteries. In some cases, however, the application includes more discharges than usual, and this means that some cycling performance is also needed. The result of an 80% DoD cycle test with 6 V, 240 Ah gel batteries is shown in Figure 7.19. Every 50 cycles there was a capacity test. It can be seen that there is a rather long period where the capacity is rather stable around 100%. After about 600 cycles, the capacity decreased steadily, reaching the 80% level after 800 cycles. This result is typical for gel batteries with flat positive plates. In general, gel batteries have a rather good cycle-life.

The cycle performance of AGM batteries has been improved significantly in recent years [18,53]. At the beginning of the development of these batteries for cycling applications, there were severe problems with acid stratification. By improving the design of such batteries, it has become possible to avoid this phenomenon almost completely. A key factor was to impose a sufficiently high stack pressure and to choose the right degree of saturation of the separator. For tall-plate AGM design, however, acid stratification can only be overcome by placing the cells in a horizontal position.

Some decades ago, when lead-acid batteries with positive lead-calcium grids without antimony were first placed on the market, there was a major disaster in terms of very poor cycle-life. Investigation of the phenomena revealed that the cause of the failure was the formation of a barrier layer of lead sulfate between the positive grid and the active material [28-30]. Since this occurred more easily when antimony was excluded from the battery, it was called the 'antimony-free effect'. Following this unfortunate experience with the early lead-calcium batteries, the antimony-free effect and the influence of grid alloy composition on the behavior of the positive plate during charging and discharging has been the subject of many investigations and much research activity [56,57,84-88].

An important result of these studies was the discovery that a lack of antimony has not only an effect on the grid/positive-material interface, but also on the whole crystalline structure of the positive active mass [84] and on the so-called mass softening process. Nowadays deleterious effects that are promoted by using grids without antimony are collectively termed 'premature capacity loss' (PCL). There has been much research effort worldwide to overcome the PCL problem [89].

It appears that softening of the positive material is a more severe problem than the development of barrier layers. As a result of the research activity (*e.g.* improvement of the curing process, the paste formulation and the alloy composition, especially the tin content and the use of additives), it seems that barrier layers no longer have a marked effect on the life of valve-regulated batteries, even when the battery is used for applications which include some cycling. This findings conflicts with the original idea that lead-acid batteries without antimony fail principally through formation of lead sulfate barrier layers at the positive grid/mass interface.

Softening of the positive material can easily be distinguished from sulfation, as the former failure does not produce any reduction of acid density in the cell. This is because the soft mass consists predominantly of lead dioxide, and the content of lead sulfate is generally quite low. Softening of the mass occurs because PbO_2 particles lose contact with each other, so that parts of the active mass become electrically isolated and cannot participate any longer in the discharge process. Therefore, batteries with softening of the positive mass have the nominal open-circuit voltage (OCV), but a lower available capacity. Softening always starts from the outer part of the plate and subsequently progresses into the inner parts as the cycle number increases. It has been shown that the decrease in capacity during the last stages of cycling is directly associated with increasing amounts of softened material [18].

The cause of softening of the positive mass has been the subject of many investigations during the last few years. In some papers, the so-called 'Kugelhaufen' theory has been formulated to provide an explanation for the degradation [84,90-93]. This theory uses a model in which the positive active mass is considered a network of agglomerates of spherical particles with narrow contact zones. This is a good approach towards describing the changes in the crystalline structure of the positive mass taking place during charge and discharge. For a complete understanding of the softening phenomenon, however, there might be the problem that, in reality, the active mass consists not only of spherical particles with smooth surfaces, but there is also a marked microstructure on the surface of the particles and much of the material can take the form of needle-shaped crystallites.

A second theory considers the active mass as a mixture of crystalline and gel parts [86,94-96]. It is assumed that there is a significant portion of hydrogen in the mass of the gel zones, and that changes in these zones during cycling could be the cause of the contact loss between the particles of lead dioxide. The influence of hydrated zones and of the so-called X-ray 'amorphous' material on the behavior of the positive active mass during cycling has been discussed [96-101]. Recently there was a detailed investigation of the change of the microstructure of lead dioxide during charge-discharge cycling [102].

Although both theories allow a better understanding of the degradation of the positive active mass during cycling, even today it is not completely clear which parameters are the most important in avoiding softening, or at least in slowing down the softening process. Often it is found that softening is promoted by high discharge rates, but the effect sometimes happens even when rather small discharge currents are used. In general, however, it is true that high discharge pulses accelerate the softening process. Several parameters strongly influence the speed of softening. These parameters include the design of the battery, the plate processing, the type of application, and the charge regime. There have been studies of the influence of different charge regimes [91,92,103]. The influence of paste density and processing, focusing especially on curing and formation, has also been investigated in detail [43,44].

Sulfation of the positive mass is often caused by a charge regime that does not match well the application of the battery. Often there is only a small margin between overcharging, which results in water loss and eventually dry out, and undercharging which produces sulfation of the positive mass [18,50,104].

Figure 7.20 shows the result of a cycle test with batteries that were charged with three different charging regimes. It can be seen that the use of a higher charging voltage was helpful in keeping the battery in a good condition for a long time. The water loss was always very small even with a charging voltage of 14.4 V.

Some battery applications require an intermediate duty between stand-by service, with only a few discharges during the whole life of the battery, and heavy cycling with an extensive discharge every day. Between these extremes, there are, for example, solar power applications (see also Chapter 9), load leveling duties or stand-by operations with rather frequent discharges. Due to the problem that a high charging voltage promotes grid corrosion and drying out, whereas a low charging voltage can encourage sulfation, there is often a good compromise to use a charger that automatically switches the charging voltage to a lower value after the battery has been charged for a given time period at the higher level. For example, the charging voltage can be changed from 2.4 to 2.3 V per cell after 12 h of charging. This procedure is also useful for flooded batteries as discussed in a previous section. The charging time and initial charging currents at a charge voltage of 2.40 V per cell to return an AGM battery (drysafe type) to 100% of the discharged capacity after discharge to different depth-of-discharge (DoD) are given in Figure 7.21.

The operational characteristics of valve-regulated batteries configured in parallel strings have been studied. Data, presented some years ago, have shown that parallel-configured battery strings can be satisfactorily operated under a wide range of discharge and recharge conditions [105]. Parallel strings share the current required by the load on discharge and recover the energy delivered on recharge in proportion to the nominal capacity available in each of the battery strings.

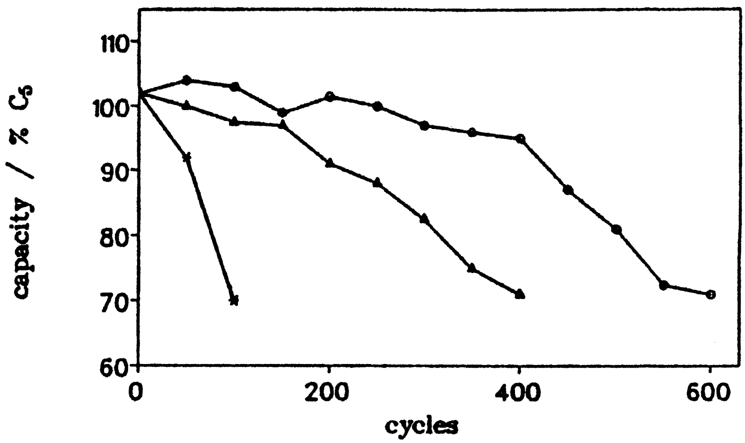

Figure 7.20. Influence of charging voltage on cycle life of an AGM battery (Drysafe Compact Plus, 12 V, 25 Ah). 25°C, capacity test every 50 cycles, discharge: 5 A down to 10.20 V; charge: IU, 15 h, I = 2 x I_5, U = (*) 13.80 V, (△) 14.10 V, (○) 14.40 V.

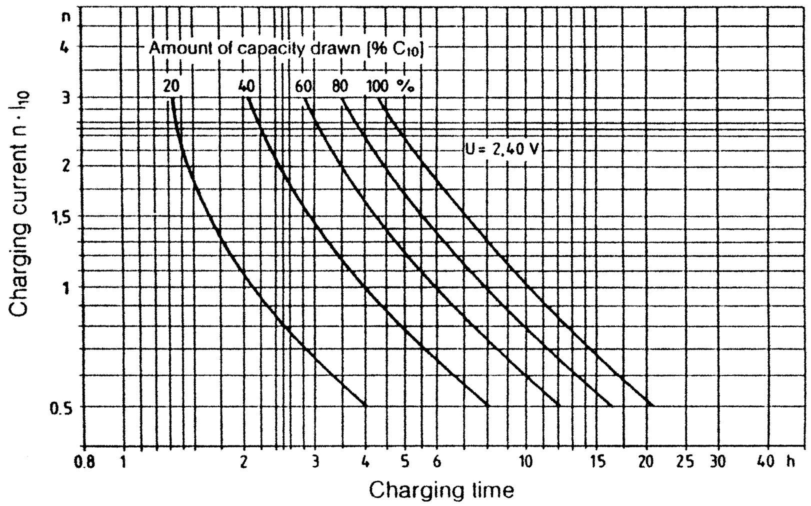

Figure 7.21. Charging time and initial charging current to return an AGM battery (Drysafe Compact Plus) to 100% of discharged capacity after different depths of discharge.

7.6. Gel Batteries

Gelling is a way to immobilize the electrolyte. The gelling agent is, in general, silica with a very high surface area of 200 m^2g^{-1} or more. The primary particles are extremely small but, in the cell, they form a three-dimensional

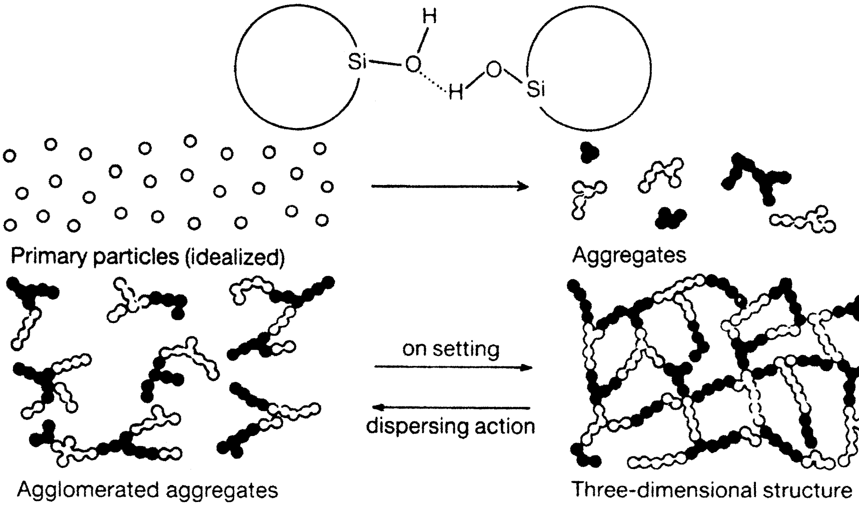

Figure 7.22. Illustration of gel-structure development.

network structure. The gel structure and the different stages of the gelling process are illustrated in Figure 7.22. Before filling, the gel is a highly dispersed mixture of electrolyte with silica, and it is possible to maintain it at a low level of viscosity by stirring. The primary particles, which had already been transformed into small aggregates during the production of the silica, form agglomerated aggregates, but the mixture still behaves as a liquid system, which can be filled into the cell quite easily. Afterwards, when there is no longer any dispersing action, the silica forms a three-dimensional structure, and the mixture stiffens to form a firm gel. A more detailed discussion about the silica structure and the gel ageing effects is given in Ref. [106].

It is an important feature of this gel structure that acid stratification can be avoided even in the case of large cells with tall plates standing in the vertical position. Acid stratification is a well known problem for flooded batteries where either some overcharge, resulting in strong gassing, or an electrolyte stirring system must be used to re-mix the electrolyte. Gel batteries do not suffer from acid stratification to any significant degree.

For gel batteries, both tubular and flat positive plates are used. Gel cells with tall plates often have the tubular positives design although there are some with flat positives. Gel cells with small plates, in general, have flat positives; however, a few exceptions will have tubular positives. In comparison with the AGM design, gel batteries have a markedly higher internal electric resistance. This is a clear disadvantage for all high-power applications.

The advantages of the gel design are that it provides a very long service life and has an extremely high reliability, even under extreme conditions (for example, higher temperatures or deep discharge periods). Another advantage is that gel batteries can be stored for a rather long time (up to two years) at room temperature without any charging. This is due to the very low rate of self discharge and to the excellent recharge behavior. It is well known that, normally, recharging batteries after a two-year storage is rather difficult; with gel batteries, this is not a problem.

Gel batteries are sometimes produced with phosphoric acid added to the electrolyte and sometimes without. Phosphoric acid is not generally used for stand-by applications; it is mainly used for applications that include some cycling. Investigations of the effect of phosphoric acid, especially with regard to an improvement in cycle-life, can be found in the literature [107-113]. According to the results of these investigations, there is an adsorption of phosphoric acid on to the lead dioxide surface, which modifies crystal growth. It has also been pointed out that phosphoric acid hinders the formation of an insulating film between the positive active mass and the grid.

The most important application of gel technology is in the telecommunications market. As already discussed, this is mainly due to the very high reliability of gel batteries. In addition, the float current of gel batteries is, in general, relatively low and does not increase too much with temperature, which is very helpful for avoiding the risk of a thermal runaway. Gel batteries are also used when the standby operation includes a significant amount of discharge-recharge cycling.

Sonnenschein was the first company to introduce gel battery technology to the market successfully. They started in 1958 with rather small batteries for flashlights. Since that time, this technology has steadily replaced the conventional, flooded lead-acid battery in various applications [82,114,115]. Phosphoric acid addition for cycling was introduced in 1965. Larger gel batteries with tubular positive plates were developed for stationary applications in 1978. More recently, gel batteries have been produced for starter and traction applications, and thick, flat positive plates were added for telecommunications applications.

Gel batteries with higher capacities normally have tubular plates. For such batteries, the capacity range is generally between 200 and 3000 Ah. These batteries are characterized by extremely high reliability and very long service life. Kramm and Kretzschmar [114,116] investigated the use of gel batteries for standby applications, and especially the influence of temperature and charge voltage on the endurance of the batteries. The results of these investigations show clearly that a remarkably long life can be achieved with standard gel batteries of the OPzV design. The expected life of one type of gel battery during float operation is shown as a function of temperature in Figure 7.23. As this

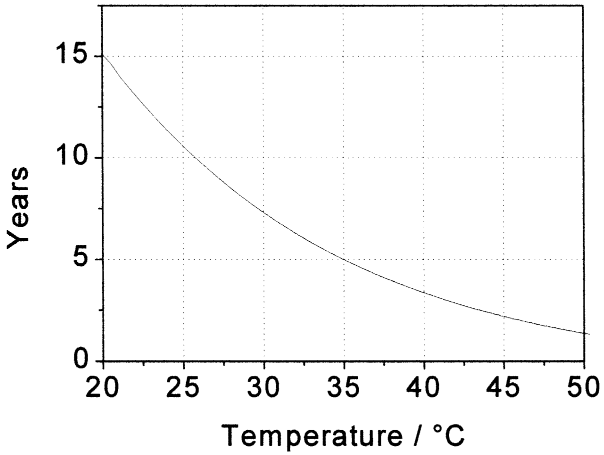

Figure 7.23. Life of stationary, gel batteries (OpzV, A600 type) during float operation at different temperatures.

type of battery has been on the market for some decades, there is much experience available from the field proving that the real service-life at around 20°C is between 15 and 18 years.

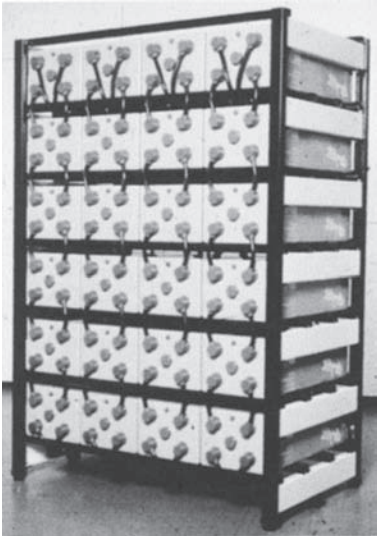

Figure 7.24. Stationary, 48 V, 1000 Ah battery with OPzV, A600 type gel cells for telecommunications applications in a horizontal position.

Since the electrolyte is immobilized as a gel, the cells can also be placed in the horizontal position without any risk of acid leakage. A 48 V, 1000 Ah, lead-acid battery with gel cells, positioned horizontally for a telecommunications application, is shown in Figure 7.24.

Gel batteries are also produced in 6 V and 12 V monoblocks with capacities between 5 and 180 Ah. These are also mainly used for telecommunications applications. They have flat positive plates, and provide a

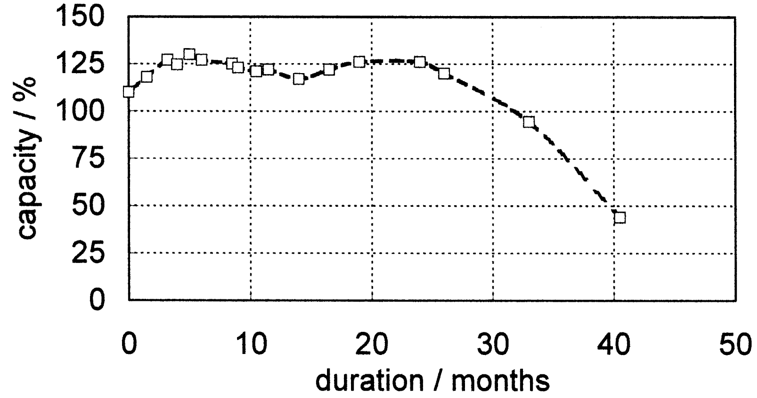

Figure 7.25. Accelerated lifetime test at 40°C of gel batteries (A400 type) with a float voltage of 2.22 V per cell.

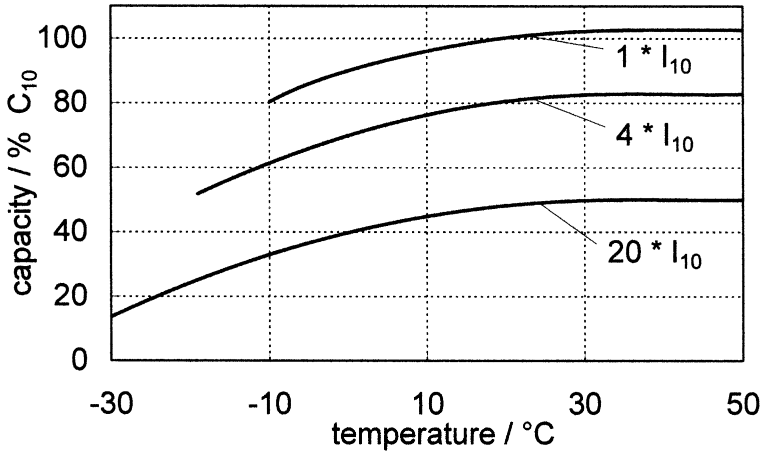

Figure 7.26. Capacity of a dryfit battery (A400 type) at different discharge rates and temperatures. I_{10} is the discharge current for a uniform, 10 h discharge.

service life of more than 12 years. The results of an accelerated life test of 12 V, 16 Ah batteries at 40°C and a float voltage of 2.22 V per cell are shown in Figure 7.25. It can be seen that the capacity decreased below the 80% level after about 35 months and reached 50% after about 40 months. This corresponds to an expected life of more than 12 years at 20°C.

The influence of discharge rate and temperature on the available capacity is shown in Figure 7.26. Most of the applications of this battery type require discharge currents between 1 and 4 times the 10 h discharge rate. Therefore, this battery type has been optimized to a high energy density for discharge times between 10 and 2 h.

There are some applications where, after a discharge, only a short time interval is available to bring the battery back to a relatively high state-of-charge. It is well known that lead-acid batteries, in general, can be charged quite fast after a discharge, as long as the SoC is below about 70-80%. Beyond this point, however, charging becomes steadily more difficult, and, for the last few percent, a much longer time is needed. This is true for flooded, gel, and AGM batteries.

The recharge time of a gel battery to different states-of-charge (50, 70, and 90%) after a complete discharge (100% DoD), for different initial charge currents and a voltage limit of 2.40 V per cell, is shown in Figure 7.27. It can be seen that, with an initial charge current of 10 times the 20 h discharge rate, a state-of-charge of 70% can be reached after about 2h, and after 4h the state-of-charge is 90%. Although high-power AGM batteries can be recharged even faster, Figure 7.27 shows clearly that, for gel batteries too, fast charging is possible.

It must be realized, however, that the charge voltage limit of 2.40 V per cell is significantly higher than the float voltage. This is possible for gel batteries as well as for AGM without any service life reduction, as long as the time period for that higher charge voltage is limited and the charge voltage returns to the float level soon. Therefore, it is important to adhere to the maximum voltage and time period specified by the battery manufacturer for such fast charging procedures.

7.7. AGM Batteries

In AGM batteries, the electrolyte is immobilized in glass-mat separators with a very high porosity of more than 90%; a typical value is 93%. The glass fibers are rather fine and, therefore, the absorption capability is high. The glass-mat has a medium pore size of a few microns. A picture of a typical glass-mat

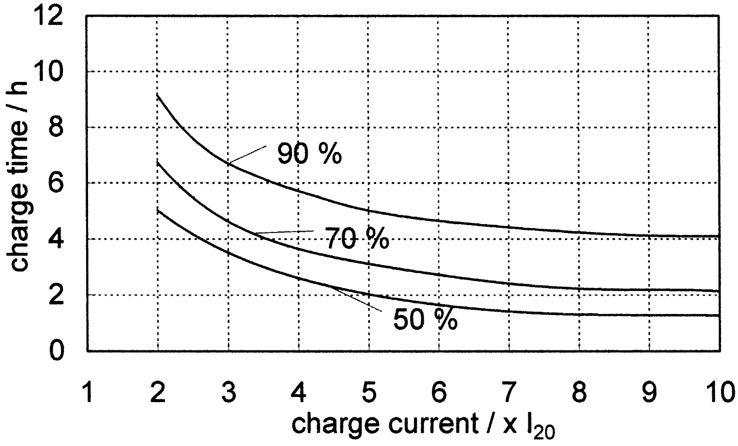

Figure 7.27. Charging time of a dryfit battery (A500 type) to return to a certain SoC after a complete discharge (100% DoD), at a charge voltage limit of 2.40 V per cell for different initial currents. (I_{20} is the discharge current for a uniform 20 h discharge).

separator with fine and coarse fibers is shown in Figure 7.28. The interweaving glass fibers can be seen clearly.

As fine fibers are much more expensive than coarser ones, a compromise is often adopted in which a blend of, for example, one-third fine and two-thirds coarse fibers is used. The decision about this proportion is much influenced by the mechanical properties the separator should have as well as by other parameters, *e.g.* wicking ability and mean pore size. Investigations of batteries with different amounts of fine fibers in the separator have shown that a higher portion of the fine ones is helpful in reducing acid stratification and extending service life. Glass mats with 100% fine fibers are seldom used due to the high cost of such material. For extreme conditions where a standard blend of fine and coarse fibers is inadequate, however, the use of 100% fine fibers, or of a blend with a high proportion of them, is a good option.

In recent years, the AGM separator has become the focus of much attention, and attributes such as compressibility and resilience have been thoroughly investigated [117,118]. For AGM batteries, in general, glass-mat separators are used which are made from 100% glass fibers. Some synthetic fiber reinforcement can be employed in order to improve the strength of the separator [119]. Although the 100% glass fiber version has some advantages, the mechanical properties are relatively poor, and this can be a disadvantage during plate group processing and for avoiding short circuits inside the battery. As a compromise, sometimes a few percent of organic fibers are added to

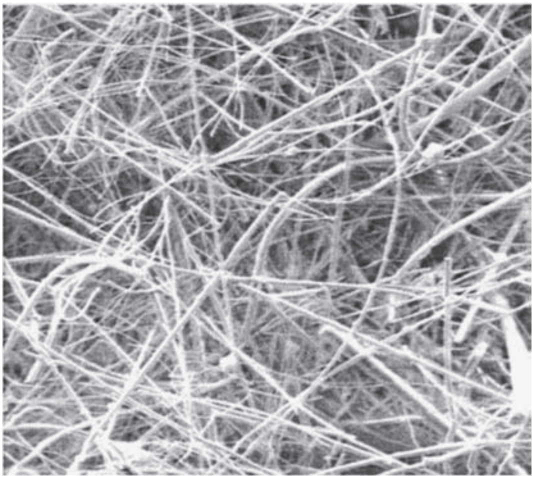

Figure 7.28. SEM picture of an AGM separator; magnification: 500. (Fibers range in diameter between approximately 0.5 and 5 microns).

achieve an AGM separator with better mechanical behavior without loosing too much of the performance of the 100% pure glass version.

For AGM batteries, in general, flat positive plates are used. The high porosity and the pore structure of the separator result in an extremely low electrical resistance, which makes AGM most suitable at high discharge rates. Indeed, tests with AGM and gel batteries have shown clearly that the higher the discharge rate the better is AGM in comparison with gel. Thus, for most of the applications where high power performance is needed, AGM is used rather than the gel design. However, for applications at extreme conditions, such as high temperature or deep discharges, gel can be a better choice even if the power demand is high.

AGM batteries can be optimized either for life and energy density or for power. The discharge curves of a long-life, 12 V, 80 Ah AGM battery with an expected lifetime of 12 years at 20°C are shown in Figure 7.29. It can be seen that, even with a current of 120 A, the discharge capacity is about 35 Ah. The discharge time is more than 17 min and the voltage is at a relatively high level for quite a long time. This is a typical characteristic of high-power, AGM batteries.

This battery type is available as 6 or 12 V monoblocks with a capacity range between 30 and 180 Ah at the 10 h discharge rate, and as 2 V cells with capacities between 200 and 500 Ah. It is used for telecommunications systems as well as for all applications where long service life, high energy density, and medium to high discharge power are needed.

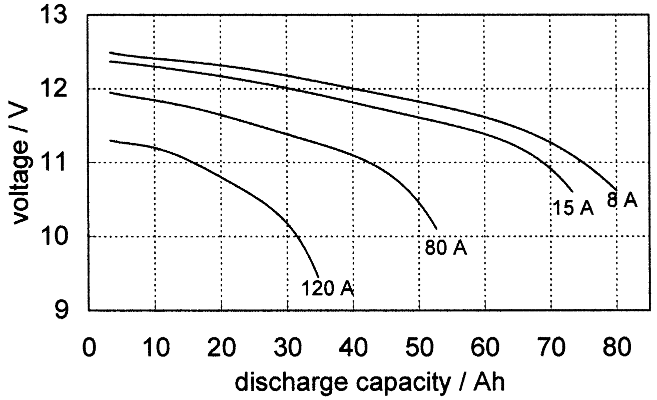

Figure 7.29. Discharge curves of a 12 V, 80 Ah AGM battery (Marathon type) at 20°C.

The discharge behavior at different temperatures between -20°C and 40°C can be seen in Figure 7.30. At lower temperatures, especially below 0°C, there is a marked decrease of the capacity. This means that a too low temperature should be avoided if the full performance of the battery is needed. On the other hand, there is an increase of capacity with increasing battery temperature but, although this is a benefit with regard to the available energy, higher temperatures should be avoided because there is a significant increase of corrosion rate resulting in a reduction of service life of the battery.

A special group of batteries has an unusual front terminal design. These are long-length, short-width batteries with both terminals at the front of the

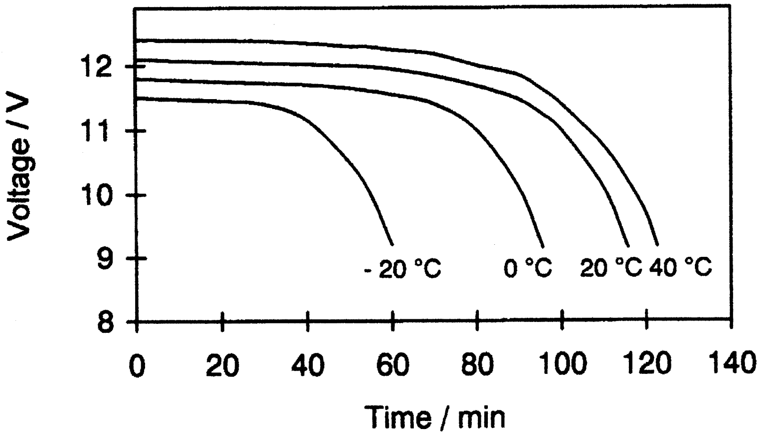

Figure 7.30. Discharge curves at 30 A of a 12 V, 60 Ah AGM battery (drysafe type) at different temperatures.

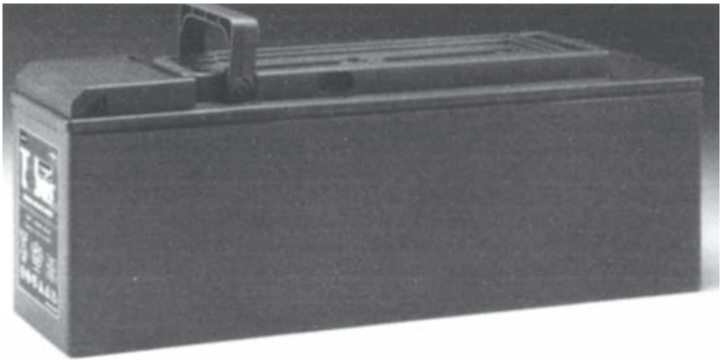

Figure 7.31. 12 V, 100 Ah AGM battery (Marathon type) with front terminal for telecommunications applications.

battery rather than one at each end. This makes the installation of the battery, and especially the connection of the individual monoblocks in racks or cabinets for telecommunications applications, much easier. A picture of such a front-terminal, 12 V, 100 Ah battery is shown in Figure 7.31. Such batteries are used nowadays in telecommunications systems.

An accelerated lifetime test, at a temperature of 55°C and a float voltage of 2.27 V per cell on 12 V, 50 Ah, front-terminal AGM batteries, confirms the expected life of 12 years at 20°C. At intervals of about two months, capacity was checked at the 10 h discharge rate, and the test results are

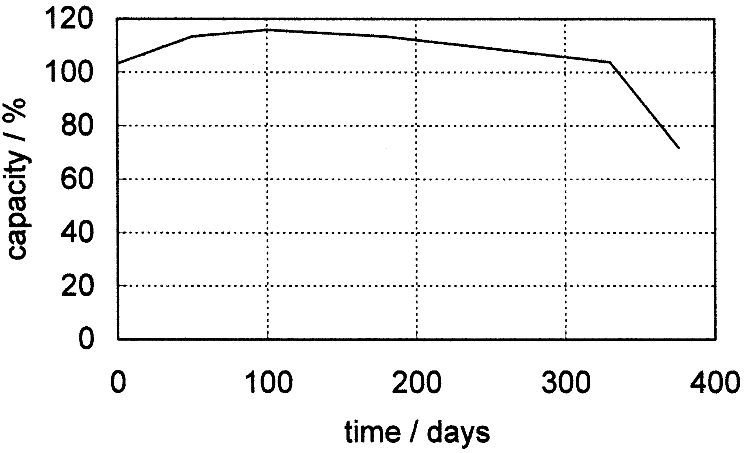

Figure 7.32. Accelerated lifetime test of 12 V, 50 Ah front terminal batteries (Marathon type) at 55°C with a float voltage of 2.27 V per cell.

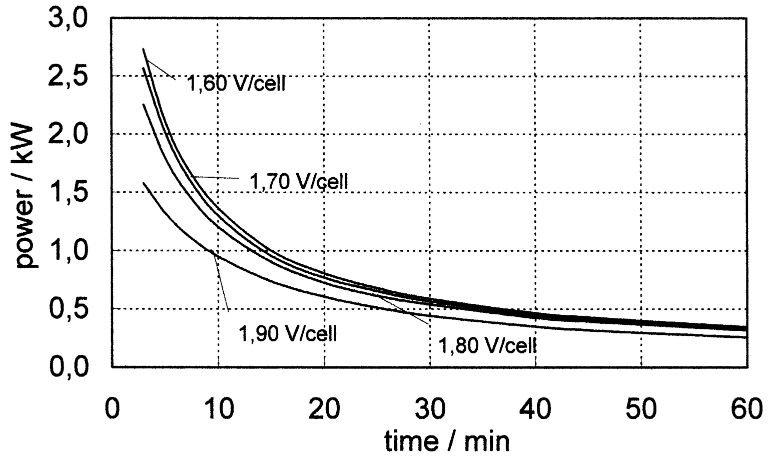

Figure 7.33. Discharge power per cell of a 40 Ah, AGM battery (Sprinter-type) for discharge time periods between 3 and 60 min at different cut-off voltages between 1.60 and 1.90 V per cell.

shown in Figure 7.32. During more than 300 days the capacity remained at a high level and rather stable. Afterwards, the capacity decreased significantly, and the test was stopped after 380 days when the capacity had dropped to 70% of the nominal value. The float life at 55°C is, therefore, 1 year, this corresponding to a life of 12 years for a floating operation at 20°C.

AGM batteries designed to provide very high power (180 WL^{-1} at the 15 min discharge rate) may offer a life of 10 years and are produced as 6 and 12 V units with capacities between 60 and 180 Ah. Such batteries are often used for applications with discharge times below 1 h and down to about 5 min. The power per cell of one of these batteries with a nominal capacity of 40 Ah at the 10 h rate, is shown in Figure 7.33 for discharge time periods between 3 and 60 min at different cut-off voltages between 1.60 and 1.90 V per cell. It can be seen that the power available from one cell is more than 2000 W for a discharge time of 5 min.

A second group of very high power batteries includes 12 V units with capacities between 5 and 85 Ah. These batteries have been optimized to a power density of 200 WL^{-1} at the 15 min discharge rate. The typical application is UPS. Due to the optimization towards extremely high power, however, the expected life is significantly shorter than for the 10-year battery.

All the AGM batteries discussed here are designed to accommodate a short circuit. This means that they can survive a 30-day short circuit and, after recharge, have virtually the same capacity as before the test. This is also true for the gel battery types described earlier.

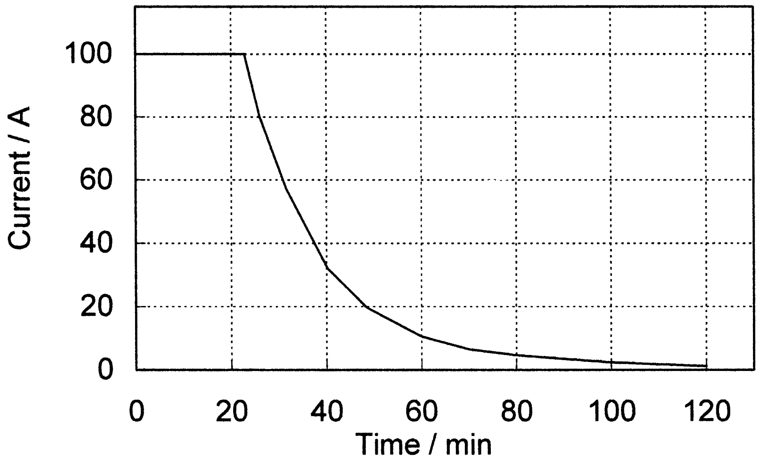

Figure 7.34. Fast-charging characteristics of a 12 V, 65 Ah AGM battery with current limit of 100 A and voltage of 14.40 V.

In addition to high power performance, AGM batteries also have good charge acceptance. The charge behavior of a 12 V, 60 Ah, AGM battery during current-limited, constant-voltage charging (14.4 V, limited to 100 A) is shown in Figure 7.34. The battery was initially discharged to 100% DoD. It can be seen that the battery accepted the 100 A for more than 20 min. More than 50% of the total capacity was recharged during this time. After 1 h, the charge current had reduced markedly, and the battery was recharged to about 90% of capacity. It is important to realize that high-power AGM batteries can be recharged very quickly to about 50% SoC, then relatively fast to 80-90% SoC. For the last few percent of charge restoration, however, a significantly longer time is needed.

The charge behavior shown in Figure 7.34 was measured with AGM batteries with medium plate thickness. The trend is to reduce the plate thickness in order to achieve even higher power performance. This will further improve the charge acceptance of the battery.

The temperature inside an AGM battery increases during fast charging [120,121]. Tests have shown a significant increase in the temperature although, normally, this increase remains within tolerable limits. Thus, fast charging is an acceptable way to restore the battery quickly after a discharge. Under certain conditions, however, charge-control based on the battery temperature is needed. When both temperature and charge voltage are controlled, the life of AGM batteries will not be reduced by fast charging [53].

Experience with a large (1.4 MWh) AGM battery in a stationary application was reported recently [122,123]. The battery was installed in the island village of Metlakatla, Alaska, in 1997 in order to stabilize the island's power grid by supplying instantaneous power to the grid and absorbing excess power from it. The battery consists of 2 V, 3600 Ah, AGM modules; each module consists of 3 individual cells connected in parallel. The cells are operating in a horizontal position to avoid any problem with acid stratification.

7.8. Future Trends

For UPS application, there has been a clear trend to shorter discharge times and higher discharge rates. The discharge time required is often between 5 and 15 min, and a high power supply during this time interim is the only discharge performance the customer expects from the battery. Currently, available lead-acid battery technology provides 200 WL^{-1} at the 15 min rate; however, 220 WL^{-1} is a realistic target, and batteries to achieve it have already been produced. Thinner positive and negative plates have to be used in order to pack more couples into a given cell volume. This implies the use of thinner grids. In order to maintain the service life of the battery in this application, the corrosion rate must be sufficiently low.

For telecommunications applications, there is also a trend to higher energy and power densities. In this application, however, the most important discharge time is around a few hours. In future, this application will also require high reliability and a long service life, sometimes under extreme conditions. This has to be achieved with a reduced grid thickness, when higher energy and power densities are also needed. In the case of telecommunications applications, there is also an increasing demand for batteries with the front-terminal design.

Thus, the general trend towards higher volumetric power and energy densities, in combination with a long service life, requires thinner grids with low corrosion rates. This can be achieved with the conventional batteries by improving positive grid alloys and other parameters that influence the corrosion behavior. There are more options, however, when advanced battery designs are used.

There was the development of a completely new material and manufacturing process for lead-acid battery grids [19]. The novel processing route includes production of battery grids by electro-codeposition of lead with dispersed particles. The grid thickness and design can be chosen within a wide range. This permits to minimize grid weight and to optimize grid design for current distribution. There is a galvanic deposition instead of grid casting and this allows improving the grid design beyond the limitation existing for gravity cast and expanded grids.

Lead is deposited electrochemically onto a cathode, which is pre-structured with conducting lines according to a desired grid shape, and the lead deposit is stripped after a predetermined thickness is reached. Such a process makes it possible to produce grids that are thinner and lighter than cast grids. The strength, required for the battery manufacturing process, can be provided by adding to the electrolyte constituents insoluble in lead such as copper or TiO_2 particles with very small size which are co-deposited with the lead and give rise to dispersion strengthening. The process to deposit electroformed Pb-based grids uses a fluoroborate electrolyte containing phosphate and soothing additives and operates at about 40°C. The cathode onto which the grids are deposited is a printed circuit board with a copper pattern that is the reproduction of the grid design. Typical diameter (average) of the dispersoid particles are 10 to 100 nm. A volume fraction of just a few tenth of percentage is sufficient to achieve a significant increase in hardness.

An additional advantage of this method is that composite grids are possible, which consists of a Pb-dispersoid core and a Pb-Sn alloy as a coating around. Tin is most beneficial in the outer part of the grid, as already discussed in a previous section. In comparison to the conventional cast grid, the new method allows to have tin just where is needed.

The typical thickness of such grids is around 0.5 mm. This is significantly thinner than standard cast grids. The grid properties were investigated thoroughly. The hardness can be adjusted in a wide range by choosing particle size and volume fraction of the dispersoid. The creep resistance is excellent.

Corrosion tests indicated that grid corrosion is similar to, or better than, that of cast Pb-Ca-Sn grids. Such grids were used to make some hundred battery plates (positive and negative) in order to test them electrically. The investigations include some life tests. The result of such accelerated life tests showed that there was virtually no difference between well cast Pb-Ca-Sn grid samples (20 week units) and samples with electrodeposited grids (18 week units). This is a very good result because the amount of grid material was markedly higher for the standard cast version (55 g) than for the electrodeposited grids (33 g). Moreover, there appears to be room for optimization of the grid production process with regard to further improvement of the corrosion resistance.

There is a good chance that, in the end, the corrosion stability can be superior to that of standard cast grids even if thinner and lighter grids are used. There were also some investigations on batteries made from electrodeposited grids. At high discharge rates there were better results with the electrodeposited grids in comparison to batteries with standard cast grids by using the same amount of positive and negative active material.

These promising results have shown that the new grid type is an interesting candidate for high power batteries. The process is also suitable for the production of lead alloy foil for alternative battery designs. The new manufacturing process can be combined with a hydrometallurgical process for the recycling of battery grids and paste, such that it is possible to have a fully integrated processing route from the treatment of battery scraps to the production of new battery grids.

For standby batteries, the standard grid manufacturing technology has been book-mould casting for flat plates and pressure casting for tubular plates. The production of starter batteries, however, has already moved to more advanced grid production technique, such as expanded-metal or continuous casting. These techniques have made it possible to manufacture plates continuously with an automated process line. A view of part of an expanded-metal grid ribbon, such as it is used for plate production for starter batteries, is shown in Figure 7.35. Due to the positive experience gained with this technology, it can be expected that it will progressively replace the traditional grid casting in starter battery plants.

At the beginning of the development of the expanded-metal technology, there were severe problems with the corrosion rate of the positive grids. By using improved alloys and a special rolling process for the strip, however, this problem has been effectively eliminated. Expanded positive grids with lead-calcium-tin alloys no longer suffer from the corrosion problems that formerly reduced the expected life of batteries under typical automotive applications [124]. Initially, expanded-metal grids were used with the flooded battery design; however, there was already a development of an AGM battery with expanded positive and negative grids for automotive applications [125].

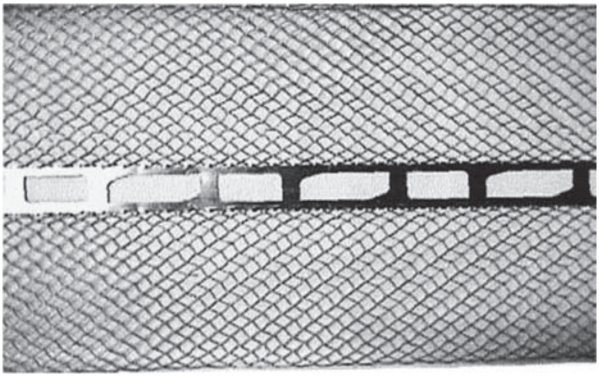

Figure 7.35. Expanded-metal grid ribbon used for continuous plate production for automotive batteries.

There is no reason, in principle, why continuous plate processing, such as the expanded-grid technology, cannot be used also for stand-by batteries. Of course, the stand-by application is significantly different from automobile duty, and battery life expectation is also different. The main issues are corrosion and possible growth of the positive grids, bonding of the positive active mass to the grid and avoidance of short circuits.

Further improvements of the alloys and the grid manufacturing techniques, as well as of the complete plate fabrication process, could make it possible to extend the life of batteries with expanded-metal grids so much that they would be a good alternative to the traditional book-mould cast grids, at least for some standby applications. A detailed discussion of the metallurgy and performance of cast and rolled lead alloys for battery grids is given by Prengaman [88,126-128].

Another alternative route to continuous plate processing is the continuous grid casting process where the molten lead or lead alloy is fed to a casting shoe sliding on a rotating drum. The method is restricted to rather thin grids because, otherwise, the amount of lead in the cavities of the rotating drum surface cannot be cooled fast enough. If the so-called 'Concast' process is used with lead-calcium-tin alloys for negative grid production, in general no problems occur. The positive grids, however, suffer significantly from corrosion and growth.

A way to overcome this problem is to use a special rolling process just after the continuous casting. By using such a 'Conroll' process, the problem of grid corrosion seems to disappear completely. Mass adhesion is another issue, however, and this is much influenced by the special, two-dimensional structure of such grids, which is significantly different from the three-dimensional structure of book-mould cast or expanded-metal grids. There has been some investigation about how to overcome the mass-adhesion problem by special plate processing, but up to now it is not clear whether lead-calcium-tin 'Conroll' grids can be a practical alternative to the standard grid technologies.

A second way to overcome the corrosion problems of 'Concast' positive grids is the use of either pure lead or a lead-tin alloy. The disadvantage is the well-known fact that such grids, without any calcium, are very soft. Therefore, significant problems can occur during plate processing as well as during assembling of the battery. The corrosion rate of the positive grids can be much reduced. Besides some handling difficulty, however, there is still the problem of achieving a sufficient positive mass adhesion, and this makes good plate processing a necessity.

Another way to produce grids continuously is punching of lead sheets. This brings the disadvantage that a relatively large proportion of the original lead sheet forms scrap and has to be remelted. This method, however, does allow the production of relatively thin grids from pure lead and these have a

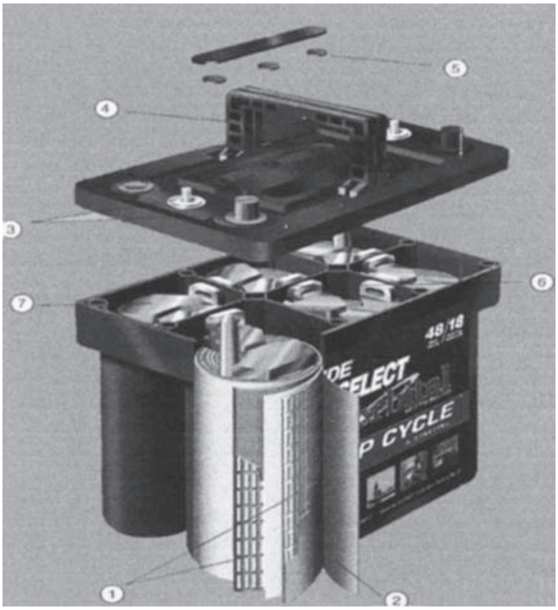

Figure 7.36. AGM spiral battery for automotive applications.

very low corrosion rate. There is, again, a handling problem due to the softness of the calcium-free grids, but the good corrosion resistance makes the punching technique quite attractive for high power, standby batteries with thin plates.

Apart from the traditional design of AGM batteries with flat plates, there is also the option to make cylindrical cells with spiral electrodes and AGM separators. A key point is that the spiral design and the tightly wound layers of a lead-tin grid make it possible to keep the separator under high compression. This is very useful in helping to achieve a long life and a good performance of the battery. The thin electrode design provides an active mass surface that is significantly larger than in conventional, flat plate, batteries. This reduces the internal electrical resistance and provides exceptionally high power [129-131]. A photograph of a 12 V spiral battery with a capacity of 50 Ah – the orbital design – that was developed some years ago as a starter version, is given in Figure 7.36.

There have been many investigations of the power capability and charge acceptance of Orbital batteries at different temperatures and SoCs [132]. The average power supplied at 10 V over 10 s by a 12 V, 50 Ah Orbital battery at different temperatures and SoCs is shown in Figure 7.37. At 40°C and a SoC of 80% or higher, more than 6 kW is provided by the battery. Nevertheless, at

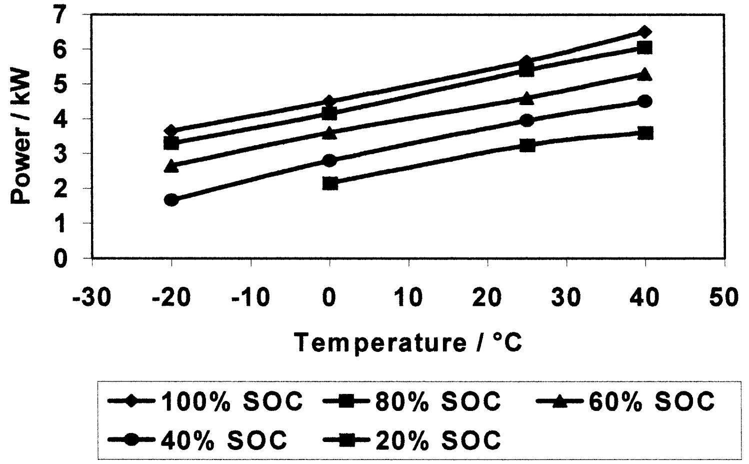

Figure 7.37. Discharge power of Orbital battery (12 V, 50 Ah) at different temperatures and SoCs.

all temperatures there is a significant reduction in power capability with decreasing SoC. At 0°C and 20% SoC, as well as at -20°C and 40% SoC, the supplied power is about 2 kW, which is just one-third of that at 40°C and 80% SoC. Both temperature and low SoC have a significant impact on power capability. For applications that include the use of the battery at very low temperatures, the SoC should be kept at a relatively high level.

The average charge acceptance at 15 V over 5 s at different

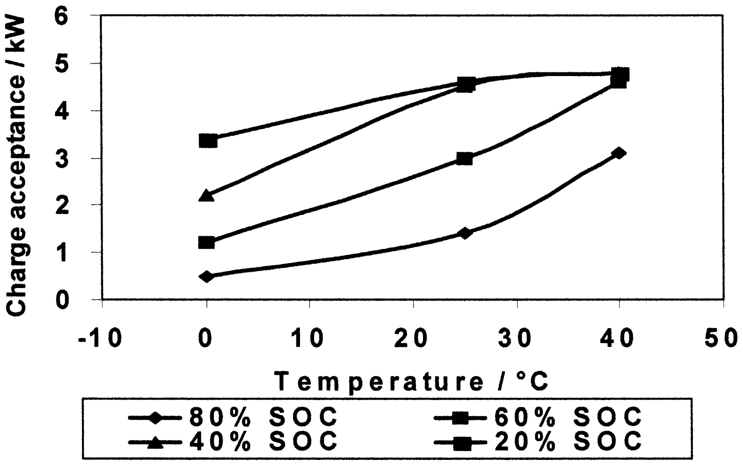

Figure 7.38. Charge acceptance of Orbital battery (12 V, 50 Ah) at different temperatures and SoCs.

temperatures and SoCs of the same 12 V, 50 Ah Orbital battery can be seen in Figure 7.38. At favorable conditions (high temperatures and low SoC), the charge acceptance is not limited by the battery, but by the power supply equipment. Close to 100% SoC, the charge acceptance is very poor at all temperatures and is not shown in the diagram. At 0°C, the charge acceptance is low unless the battery is nearly fully discharged. At temperatures below 0°C, it is even more difficult to bring a significant amount of power back into the battery.

The exceptional high power capability of Orbital technology can also be seen from the internal resistance that was measured on a 12 V, 50 Ah Orbital battery at different temperatures and SoCs [132]. Data obtained for a discharge after 1 s are presented in Figure 7.39. The battery has just about 3 mΩ at 40°C and even under the unfavorable conditions of -20°C and 40% SoC, the internal resistance is still below 5 mΩ.

When the resistance was measured at charge after 1 s, the results, as expected, reflected the well known experience that the lead-acid system can be discharged with much more power than is possible on recharge. Again, there was no measurement at 100% SoC because of the poor charge acceptance of a fully charged battery. There is a significant increase in the electrical resistance at lower temperature or higher SoC, and especially for a combination of both parameters (lower temperature than 20°C and higher SoC than 60%), as shown in Figure 7.40.

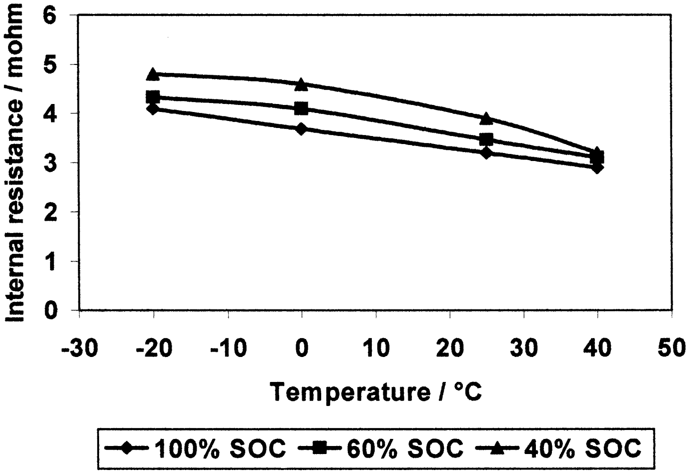

Figure 7.39. Internal electrical resistance at discharge of Orbital battery (12 V, 50 Ah) at different SoCs in the temperature range -20°C to 40°C.

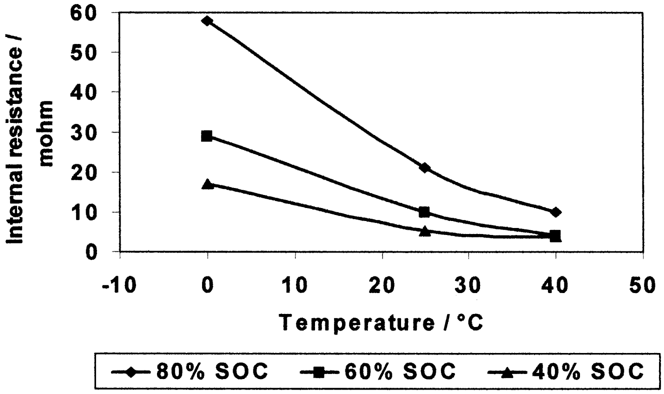

Figure 7.40. Internal electrical resistance at charge of Orbital battery (12 V, 50 Ah) at different SoCs in the temperature range 0 – 40°C.

During service life, ageing effects increase the internal resistance, this reducing the high-power performance. The regular measurement of resistance and OCV is therefore a good way to determine and control the state-of-health of a battery.

Orbital batteries have an excellent cycling performance. There were some tests where the battery was discharged to 60% SoC and, then, subjected to continuous cycling with a rather small change of DoD (1.25%). About 300000 cycles could be achieved under these conditions [133,134].

It should be realized that the results on Orbital 12 V, 50 Ah modules were achieved with a version optimized for a very good cycle life. A second version has been developed as a power-optimized design with even better results in terms of discharge power and charge acceptance. Cycle life was slightly worse in comparison with the optimized version, however, although still much better than with conventional flat plate AGM technology. For applications where high power has a high priority, this version would be the best choice.

This design was developed recently as an automotive starter battery. It has very high gravimetric energy and power densities, both of which are important factor for automotive applications. Related to the volume, the energy and power densities are lower due to the cylindrical shape of the cells, which results in some volume that cannot be used for the electrochemical elements. As the volumetric energy and power densities are more important than the weight of the battery for many of the stand-by applications, this might not be the best approach for stand-by service. As this design has a relatively high specific energy, however, even though not all the volume is used, it could be an interesting alternative for at least some standby applications in the future.

A clear disadvantage of the AGM separator is that it does not provide sufficient restraint to prevent positive active mass expansion. This is due to the fact that the glass-mat is compressible. The use of a very high stack pressure is limited by the mechanical properties of the glass fibers, which cannot withstand high pressures. There can also be a lack of resilience of the glass-mat. Therefore, positive active mass expansion, which may occur during discharge-charge cycling, cannot be avoided completely with the AGM design.

A material with similar properties to a glass-mat separator, but which is much less compressible, would be a good alternative. Recently, an acid jellifying separator (AJS) that consisted of an ultrahigh molecular weight polyethylene with a certain amount of silica inside the pores was tested [135,136]. The mean pore size of the AJS was 0.2 µm and, therefore, was much smaller than that of AGM, which is typically a few µm. The porosity of the AJS was above 80%, but is lower than that of glass-mat separators, which is above 90%. The porosity of the AJS seems to be high enough, however, to absorb a sufficient amount of electrolyte between the plates so that this design could be used in a valve-regulated battery.

Indeed, an AJS has a behavior between that of gel and AGM separators and might become a third way to immobilize the electrolyte in valve-regulated batteries. The compressibility of the material is much lower than that of a glass-mat. The thickness reduction in an AJS and an AGM separator with increasing stack pressure is shown in Figure 7.41. Also included is a similar curve for an

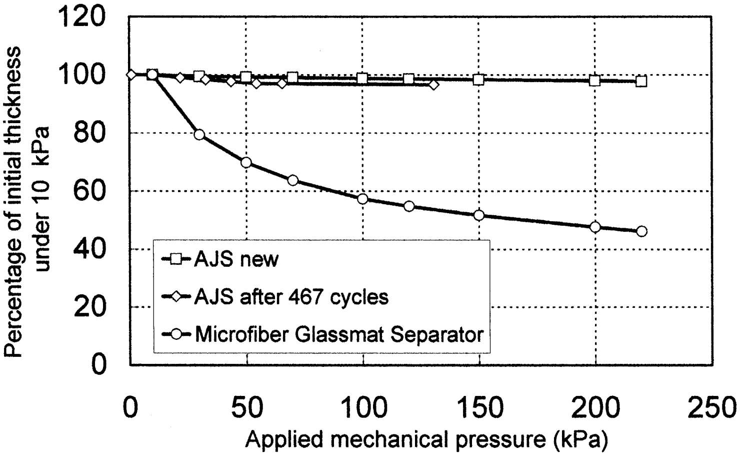

Figure 7.41. Reduction of AJS and AGM separator thickness with increasing stack pressure.

AJS separator after 467 cycles in a battery. As the AJS is nearly incompressible, active mass expansion is precluded, and this can be a clear advantage for some applications, especially those that include cycling. Although the main application seems to be related to cycling, such a material could also be suitable for certain standby applications.

7.9. Conclusions

Lead-acid batteries will continue to have, by far, the major share of the standby battery market, due to their outstanding specific energy, life and cost characteristics. It is expected that there will be a significant growth of the standby battery market during the next few years. Most standby batteries already have the valve-regulated design. For UPS applications, there is a clear tendency to a higher power requirement with a discharge time of only a few minutes. Therefore, improvement of the high-power performance, without a reduction of life and/or reliability, has become the most important objective of battery development for standby applications.

References

1. H. Bode, *Lead/acid Batteries*, Wiley-Interscience, New York, 1977
2. R. Kießling, *J. Power Sources* 19 (1987) 147
3. R. Wagner, in H. Kahlen (ed.) *Batterien*, Vulkan, Essen, Germany, 1992
4. R. Wagner, *VDI Berichte* 1058 (1993) 131
5. J. Euler, W. Nonnenmacher, *Electrochim. Acta* 2 (1960) 268
6. J. Euler, L. Horn, *Electrochim. Acta* 10 (1965) 1057
7. J. Meiwes, *Electrotech. Zeitung* 8 (1986) 3
8. H. Dominik, G.K. Krämer, B. Voigt, *Proc. 21th IECEC*, San Diego, CA, USA, 1986
9. R. Kießling, *J. Power Sources* 19 (1987) 227
10. C. Böhle, K.G. Krämer, *Electrotech. Zeitung* 14 (1987) 652
11. K.G. Krämer, R. Saupe, H. Staroske, *Proc. 4th Int. Conf. Batteries for Energy Storage*, Berlin, Germany, 1993
12. K.D. Aust, Henschel, K.G. Krämer, *Proc. Int. Conf. Batteries for Utility Energy Storage*, Berlin, Germany, 1987
13. K.D. Aust, *Proc. 5th Int. Conf. Batteries for Energy Storage*, Puerto Rico, 1995
14. K.G. Krämer, *Proc. 5th Int. Conf. Batteries for Energy Storage*, Puerto Rico, 1995
15. A.I. Attia, D.E. Perrone, *ILZRO-Seminar*, Orlando, Fl, USA, 1989
16. E.M. Valeriote, *J. Power Sources* 28 (1989) 93
17. E. Meissner, *J. Power Sources* 42 (1993) 103
18. R. Wagner, *J. Power Sources* 53 (1995) 153
19. G. Barkleit, A. Grahl, M. Maccagni, M. Olper, P. Scharf, R. Wagner, H. Warlimont, *J. Power Sources* 78 (1999) 73
20. L.T. Lam, R.H. Newnham, H. Ozgun, F.A. Fleming, *J. Power Sources* 88 (2000) 92

21. M.J. Kellaway, P. Jennings, D. Stone, E. Crowe, A. Cooper, *J. Power Sources* 116 (2003) 110
22. A. Cooper, L.T. Lam, P.T. Mosely, D.A.J. Rand, in D.A.J. Rand, P.T. Mosely, J. Garche, C.D. Parker (eds.), *Valve-regulated Lead-Acid Batteries*, Elsevier, Amsterdam, Netherland, 2004
23. K. Wen-Hong, *J. Power Sources* 36 (1991) 155
24. Z. Mao, R.E. White, *J. Electrochem. Soc.* 138 (1991) 1615
25. M. Saakes, D. Schellevis, D. van Trier, M. Wollersheim, *J. Power Sources* 67 (1997) 33
26. M. Saakes, E. Kluiters, D. Schmal, S. Mourad, P. ten Have, *J. Power Sources* 78 (1999) 199
27. M. Saakes, C. Kleijnen, D. Schmal, P. ten Have, *J. Power Sources* 95 (2001) 68
28. J. Burbank, *J. Electrochem. Soc.* 111 (1964) 1112
29. H. Giess, in K.R. Bullock and D. Pavlov (eds.), *Advances in Lead-Acid Batteries*, The Electrochemical Society, Pennington, NJ, USA, 1984
30. T.G. Chang, in K.R. Bullock and D. Pavlov (eds.), *Advances in Lead-Acid Batteries*, The Electrochemical Society, Pennington, NJ, USA, 1984
31. R. Miraglio, L. Albert, A. El Ghachcham, J. Steinmetz, J.P. Hilger, *J. Power Sources* 53 (1995) 53
32. N. Bui, P. Mattesco, P. Simon, J. Steinmetz, E. Rocca, *J. Power Sources* 67 (1997) 61
33. R.D. Prengaman, *J. Power Sources* 78 (1999) 123
34. M.L. Soria, J. Fullea, F. Saez, F. Trinidad, *J. Power Sources* 78 (1999) 220
35. T. Juergens, R.F. Nelson, *J. Power Sources* 53 (1995) 201
36. J.R. Pierson, J. Zagrodnik, R.J. Johnson, *J. Power Sources* 67 (1997) 7
37. R.C. Bhardwaj, *J. Power Sources* 78 (1999) 130
38. M.L. Soria, J. Valenciano, A. Ojeda, G. Raybaut, K. Ihmels, J. Deiters, N. Clement, J. Morales, L. Sanchez, *J. Power Sources* 116 (2003) 61
39. J.K. Whear, W. Böhnstedt, *J. Power Sources* 116 (2003) 141
40. K. Ihmels, W. Böhnstedt, in D.A.J. Rand, P.T. Mosely, J. Garche, C.D. Parker (eds.), *Valve-regulated Lead-Acid Batteries*, Elsevier, Amsterdam, Netherland, 2004
41. D. Pavlov, *J. Power Sources* 53 (1995) 9
42. N.E. Bagshaw, *J. Power Sources* 67 (1997) 105
43. R. Wagner, P. Scharf, *Proc. 30th Int. Symp. Automotive Technology and Automation*, Florence, Italy, 1997
44. I. Dreier, F. Saez, P. Scharf, R. Wagner, *J. Power Sources* 85 (2000) 117
45. D. Pavlov, in D.A.J. Rand, P.T. Mosely, J. Garche, C.D. Parker (eds.), *Valve-regulated Lead-Acid Batteries*, Elsevier, Amsterdam, Netherland, 2004
46. R.F. Nelson, *J. Power Sources* 31 (1990) 3
47. H. Tuphorn, *J. Power Sources* 31 (1990) 57
48. D. Berndt, *Maintenance-Free Batteries*, Research Studies Press, Taunton, Somerset, UK, 1993
49. G. Baudo, *Proc. 11th Int. Lead Conf.*, Venice, Italy, 1993
50. R. Wagner, *Proc. 11th Int. Lead Conf.*, Venice, Italy, 1993
51. B. Culpin, *J. Power Sources* 53 (1995) 127
52. K. Takahashi H. Yasuda, H. Hasegawa, S. Horie, K. Kanetsuki, *J. Power Sources* 53 (1995) 137
53. R. Wagner, W. Bögel, J.-P. Büchel, *Proc. 29th Int. Symp. Automotive Technology and Automation*, Florence, Italy, 1996
54. F.A. Fleming, P. Shumard, B. Dickinson, *J. Power Sources* 78 (1999) 237
55. D. Berndt, *J. Power Sources* 95 (2001) 2
56. R. Wagner, in D.A.J. Rand, P.T. Mosely, J. Garche, C.D. Parker (eds.), *Valve-regulated Lead-Acid Batteries*, Elsevier, Amsterdam, Netherland, 2004
57. P.T. Moseley, D.A.J. Rand, in D.A.J. Rand, P.T. Mosely, J. Garche, C.D. Parker (eds.), *Valve-regulated Lead-Acid Batteries*, Elsevier, Amsterdam, Netherland, 2004

58. R. Wagner, *J. Power Sources* 144 (2005) 494
59. A.M. Howart, E.Willinganz, *Electrochem. Technol.* 6 (1968) 370
60. W. Sharfenberger, S. Henkel, *Z. Metallk.* 64 (1973) 478
61. G.W. Mao, J.G. Larson, P. Rao, *J. Electrochem. Soc.* 120 (1973) 11
62. M.V. Rose, J.A. Young, *Proc. 5th Int. Lead Conf.*, Paris, France, 1974
63. J. Perkins, G.R. Edwards, *J. Mat. Sci.* 10 (1975) 136
64. R.D. Prengaman, *Proc. Electrochemical Society, Fall Meet.*, Las Vegas, NV, USA, 1976
65. E.M.L. Valeriote, *J. Electrochem. Soc.* 128 (1981) 1423
66. N.E. Bagshaw, *J. Power Sources* 12 (1989) 113
67. R.D. Prengaman, *J. Power Sources* 33 (1991) 13
68. H. Giess, *J. Power Sources* 53 (1995) 31
69. L. Albert, A. Goguelin, E. Jullian, *J. Power Sources* 78 (1999) 23
70. S. Fouache, A. Chabrol, G. Fossati, M. Bassini, M.J. Sainz, L. Atkins, *J. Power Sources* 78 (1999) 12
71. A.C. Simon, S.M.Caulder, *J. Electrochem. Soc.* 121 (1974) 531
72. S. Feliu, E. Otero, J.A. Gonzalez, *J. Power Sources* 3 (1978) 145
73. G. Papazov, T. Rogachew, D. Pavlov, J. Garche, K. Wiesener, *J. Power Sources* 6 (1981) 15
74. J. Garche, *J. Power Sources* 53 (1995) 85
75. W.B. Brecht, D.O.Feder, J.M. McAndrews, A.J. Williamson, *INTELEC 1988, Conf. Proc.*, San Diego, CA, USA
76. M.E. Fiorino, F.J. Vaccaro, R.E. Landwehrle, *INTELEC 1988, Conf. Proc.*, San Diego, CA, USA
77. W.B. Brecht, N.F. O'Leary, *INTELEC 1988, Conf. Proc.*, San Diego, CA, USA
78. W.E. Jones, D.O. Feder, *INTELEC 1996, Conf. Proc.*, Boston, MA, USA
79. D. Berndt, W.E. Jones, *INTELEC 1998, Conf. Proc.*, San Francisco, CA, USA
80. S.S. Misra, T.M. Noveske, S.L. Mraz, A.J. Williamson, *J. Power Sources* 95 (2001) 162
81. D. Berndt, U. Teutsch, *J. Electrochem. Soc.* 143 (1996) 790
82. F. Kramm, *INTELEC 1998, Conf. Proc.*, San Francisco, CA, USA
83. F.A. Fleming, *INTELEC 1999, Conf. Proc.*, Copenhagen, Denmark
84. A. Winsel, E. Voss, U. Hullmeine, *J. Power Sources* 30 (1990) 209
85. A.F. Hollenkamp, *J. Power Sources* 36 (1991) 567
86. D. Pavlov, A. Dakhouche, T. Rogachev, *J. Power Sources* 42 (1993) 71
87. M. Kosai, S. Yasukawa, S. Osumi, M. Tsubota, *J. Power Sources* 67 (1997) 43
88. R.D. Prengaman, in D.A.J. Rand, P.T. Mosely, J. Garche, C.D. Parker (eds.), *Valve-regulated Lead-Acid Batteries*, Elsevier, Amsterdam, Netherland, 2004
89. P.T. Moseley, *J. Power Sources* 88 (2000) 71
90. U. Hullmeine, A. Winsel, E. Voss, *J. Power Sources* 25 (1989) 27
91. E. Meissner, E. Voss, *J. Power Sources* 33 (1991) 231
92. E. Meissner, *J. Power Sources* 46 (1993) 231
93. E. Bashtavelova, A. Winsel, *J. Power Sources* 46 (1993) 219
94. D. Pavlov, I. Balkanov, T. Halachev, P. Rachev, *J. Electrochem. Soc.* 136 (1989) 3189
95. D. Pavlov, *J. Electrochem. Soc.* 139 (1992) 3075
96. D. Pavlov, in D.A.J. Rand, P.T. Mosely, J. Garche, C.D. Parker (eds.), *Valve-regulated Lead-Acid Batteries*, Elsevier, Amsterdam, Netherland, 2004
97. S.M. Caulder, J.S. Murday, A.C. Simon, *J. Electrochem. Soc.* 120 (1973) 1515
98. A.C. Simon, S.M. Caulder, in D.H. Collins (ed.), *Power Sources* 5, Academic Press, London, UK, 1975
99. J.P. Pohl, H.Rickert, in D.H. Collins (ed.), *Power Sources* 5, Academic Press, London, UK, 1975
100. K. Harris, R.J. Hill, D.A.J. Rand, *J. Electrochem. Soc.* 131 (1984) 474
101. J. Yamashita, Y. Matsumaru, *J. Appl. Electrochem.* 18 (1988) 595
102. I.M. Steele, J.J. Pluth, J.W. Richardson, *J. Power Sources* 95 (2001) 79

103. R.F. Nelson, in D.A.J. Rand, P.T. Mosely, J. Garche, C.D. Parker (eds.), *Valve-regulated Lead-Acid Batteries*, Elsevier, Amsterdam, Netherland, 2004
104. R. Wagner, D.U. Sauer, *J. Power Sources* 95 (2001) 141
105. B.A. Cole, R.J. Schmitt, J. Szymborski, *INTELEC 1998, Conf. Proc.*, San Francisco, CA, USA
106. F. Kramm, H. Niepraschk, *INTELEC 1999, Conf. Proc.*, Copenhagen, Denmark
107. K. Eberts,in D.H. Collins (ed.), *Power Sources* 2, Pergamon Press, Oxford, UK, 1970
108. S. Sternberg, A.Mateescu, V. Branzoi, L. Apatenau, *Electrochim. Acta* 32 (1967) 349
109. K. Bullock, D.H. McClelland, *J. Electrochem. Soc.* 124 (1977) 1478
110. K. Bullock, *J. Electrochem. Soc.* 126 (1979) 360
111. K. Bullock, *J. Electrochem. Soc.* 126 (1979) 1848
112. G.A. Morris, P.J. Mitchell, N.A. Hampson, D.I. Dyson, *Power Sources*, 12 International Power Sources Symposium Committee, Leatherhead, UK, 1989
113. E. Meissner, *J. Power Sources* 67 (1997) 135
114. F. Kramm, H.Kretzschmar, *INTELEC 1996, Conf. Proc.*, Boston, MA, USA
115. R. Wagner, *J. Power Sources* 67 (1997) 163
116. F. Kramm, *INTELEC 1997, Conf. Proc.*, Melbourne, Australia
117. G.C. Zguris, *J. Power Sources* 67 (1997) 307
118. C. Pendry, *J. Power Sources* 78 (1999) 54
119. R. Simarro, *J. Power Sources* 78 (1999) 65
120. H. Giess, *INTELEC 2000, Conf. Proc.*, Phoenix, AZ, USA
121. P. Häring, H.Giess, *J. Power Sources* 95 (2001) 153
122. J. Szymborski, G. Hunt, A. Tsagalis, *INTELEC 2000, Conf. Proc.*, Phoenix, AZ, USA
123. C.D. Parker, J. Garche, in D.A.J. Rand, P.T. Mosely, J. Garche, C.D. Parker (eds.), *Valve-regulated Lead-Acid Batteries*, Elsevier, Amsterdam, Netherland, 2004
124. M.D. Achtermann, M.E. Greenle, *J. Power Sources* 33 (1991) 87
125. S. Fouache, J.P. Douady, G. Fossati, C. Pascon, *J. Power Sources* 67 (1997) 15
126. R.D. Prengaman, *J. Power Sources* 67 (1997) 267
127. R.D. Prengaman, *J. Power Sources* 78 (1999) 123
128. R.D. Prengaman, *J. Power Sources* 95 (2001) 224
129. F. Trinidad, F.Saez, J. Valenciano, *J. Power Sources* 95 (2001) 24
130. F. Trinidad, C. Gimeno, J. Gutierrez, R. Ruiz, J. Sainz, J. Valenciano, *J. Power Sources* 116 (2003) 128
131. J. Valenciano, F. Trinidad, M. Fernandez, *J. Power Sources* 113 (2003) 318
132. J. Valenciano, *Internal EXIDE Report*, 2004
133. J. Valenciano, F. Trinidad, *Proc. 2nd Europ. Conf., Alternative energy sources for automobiles*, Poitiers, France, 2004
134. M.L. Soria, J. Sainz, J. Valenciano, F. Trinidad, *Proc. STORE Conf., Storage for Renewable Energies*, Aix-en-Provence, France, 2003
135. W. Böhnstedt, *J. Power Sources* 78 (1999) 35
136. M. Perrin, H. Döring, K. Ihmels, A. Weiss, E. Vogel, R. Wagner, *J. Power Sources* 95 (2001) 85

Industrial Applications of Batteries. From Cars to Aerospace and Energy Storage
M. Broussely and G. Pistoia Eds.,
© 2007 Elsevier B.V.

Chapter 8

STATIONARY APPLICATIONS. II. LOAD LEVELLING

Junji Kondoh

Energy Technology Research Institute, National Institute of Advanced Industrial Science and Technology (AIST)
AIST Central 2, 1-1-1, Umezono, Tsukuba, Ibaraki, 305-8568 Japan

Section 8.1 summarizes the significance of the stationary applications of secondary battery systems. Sections 8.2 and 8.3 describe advanced commercial battery systems while referring to practical systems installed in AIST Tsukuba. Sections 8.4 and 8.5 explain other secondary battery systems and energy storage systems that use different storage methods, respectively. Finally, a comparison is made among the energy storage systems in Section 8.6.

8.1. Signification of Stationary Applications

8.1.1. Electric Power Systems

During the initial stage of the electric utility industry (about a century ago), almost all consumers were within several kilometers of the central power stations that supplied them with electricity, and the electrified areas were independent. Later, electrical islands linked with each other and spread, and finally resulted into the huge power systems established in developed countries.

Figure 8.1 is a schematic diagram of typical electric power systems. Multiple central power plants generate electric power and supply it to transmission systems. The transmission systems transfer large amounts of electric power to distribution systems. The distribution systems supply it to loads in consumers at appropriate voltage levels. In recent years, it has become popular to install dispersed generators with renewable energy resources and combine heat and power generation in the distribution systems. Interconnection ties are constructed between regions and countries.

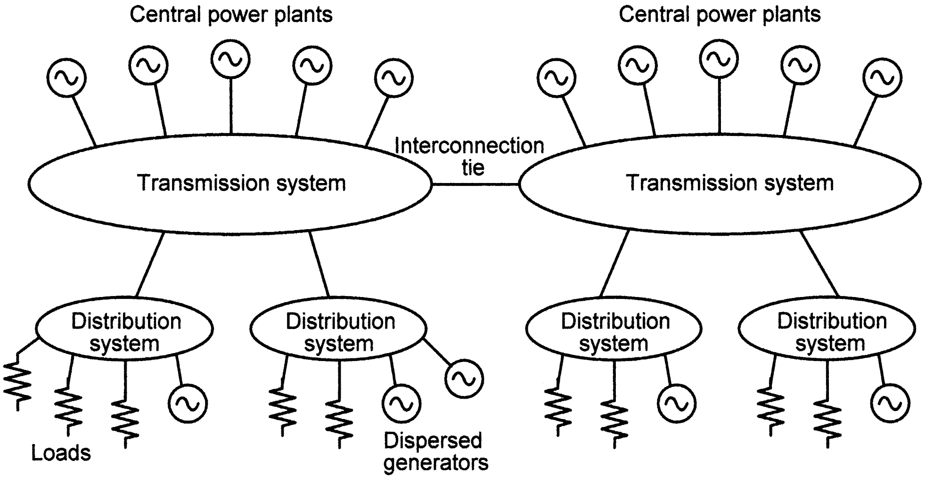

Figure 8.1. Typical electric power systems.

Some of the reasons for the growth of power systems are as follows: scale merits, location conditions of power plants, and so on. The reduction in the fluctuating proportion of the total demand is also one of the prominent advantages, as indicated in the next section.

8.1.2. Load Curves and Allocation for Power Plants

In general, electrical machinery and apparatuses require fluctuating power consumption in accordance with their operation states. It is difficult for local generators to efficiently supply such fluctuating power with one-to-one correspondence, although in order to maintain stable frequency and voltage, it is necessary that the supply balance with the demand at every moment in electric power systems.

If such fluctuating local demands are combined by connecting to power systems, the proportion of the non-correlative fluctuating elements in the total demand can be reduced by following the statistical law of large numbers. Thus, in huge electric power systems, only daily and seasonal variations remain mainly in demand, which are easy to forecast for economic rationalized dispatch planning.

Figure 8.2a shows a typical daily load curve and supply power allocation in an electric power system. Large scale power plants with low operating costs and insufficient follow-up abilities supply base load under optimized operating conditions; middle scale power plants adjust their power

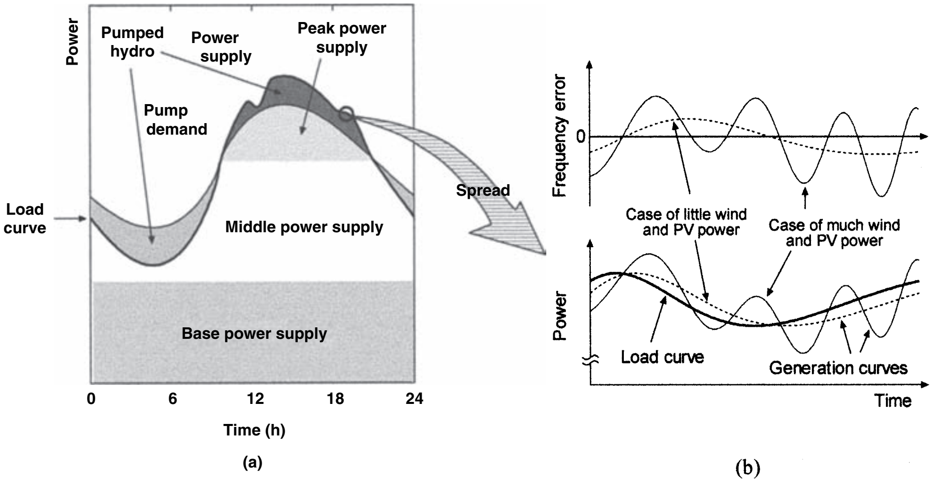

Figure 8.2. Typical daily load curve and supply power allocation.

generation for intermediate load; and small scale power plants with high operating costs are used for peak load. Pumped hydroelectric power stations are the electric energy storage systems explained later in Section 8.5.1.

8.1.3. Load Levelling

Daily and seasonal load levelling, which is peak demand curtailment and/or bottom demand increase, results in better economical operation of the electric power systems. Furthermore, the peak demand curtailment is important to restrict excessive equipment investment, because some plants are reserved in order to operate for only several hours in a year to meet the peak demand.

The seasonal load variation is managed by time consideration in the periodic inspection plan of power plants and application of reservoir type hydro power stations. The daily load levelling is effective for improving the economic and energy efficiencies, since it directly affects the arrangement and operation of electric power systems.

One solution for the daily load levelling problem is managing the demand by shifting the energy consumption periods of time-deferrable loads, such as electric water heaters, into night time with discounted off-peak prices, but such applications are limited. Another solution is the installation of electric energy storage systems.

8.1.4. Load Frequency Control

A characteristic of electric power systems is that the frequency fluctuates with a slight imbalance between the demand and supply as shown in Figure 8.2b. It is then essential to restrict the frequency deviation at a low level in order to ensure both stable system operation and high-quality supply. The imbalance is compensated by follow-up control, which is also referred to as load frequency control, of spinning reserve in hydro and oil-fuelled power plants. The spinning reserve is expensive and its reserve capacity is very limited.

In recent years, the installation and addition of renewable energy resources, especially wind and solar energy, to electric power systems have been increasing rapidly. The initial motivation for these installations was governmental subsidies due to environmental consideration, but the capital costs of these systems have reduced to commercially competitive levels. However, their generated power is uncontrollable and fluctuates according to climatic conditions. Thus, large amounts of their installation require additional spinning reserve, and the sharing of the increased expenses is now a controversial issue between electric utilities and wind energy suppliers, especially in Japan. One solution of this problem is to level the fluctuating output by using electric energy storage systems, whose experimental demonstrations are underway at wind farms.

8.1.5. Other Applications

Stationary electric energy storage systems in consumer sites are available as uninterruptible power supply (UPS) for emergency power use during blackouts, and/or voltage sag. They are also available to avoid an expensive distribution upgrade. This application is considered in residential photovoltaic power generation systems for high-density connections in Japan. Furthermore, they are able to act as a reactive power source for local voltage regulation on feeder lines since they are connected via self-commutated inverters or synchronous machines.

Table 8.1 summarizes the applications of stationary electrical energy storage systems. The daily cycle application is not only suitable for electric utilities but also for consumers due to the reduction in the electric charge derived from contract demand reduction and off-peak power utilization.

8.1.6. Present Conditions

Currently, large pumped hydroelectric power stations are the dominant

Table 8.1. Applications of stationary electrical energy storage systems.

Application / User	Long duration (a day)	Short duration (seconds to tens minutes)
Electric utility	Daily load leveling Network upgrade avoidance	Load frequency control
Consumer	Contract demand reduction Off-peak price utilization	Uninterruptible power supply
Wind and solar power supplier	Network upgrade avoidance	Output power regulation Voltage regulation

electric energy storage systems for daily load levelling and load frequency control. In addition, a few 100-MW class gas turbine power plants with compressed air energy storage (CAES) have been operating in the world, and smaller scale secondary battery energy storage systems have been installed for applications ranging from a few seconds up to a few hours. The total delivered electric power cycled through storage systems is approximately 15%, 10%, and 2.5% in Japan, Europe and U.S., respectively [1]. The high percentages in Japan and Europe are due to attractive pumped hydro sites, and particularly in Japan, low utility load factor (average load / peak load).

8.1.7. Future Prospect

The number of geographically suitable sites for pumped hydroelectric power stations has been decreasing in recent years, and the number of suitable geological sites for CAES is very limited. In addition, the peak power demand is expected to increase with the demand for electricity. On the other hand, advanced battery systems are under vigorous development and some of them have been already commercialized. These battery systems are promising candidates for future energy storage systems in stationary applications while optimally utilizing the advantages of dispersed-type storage systems. The breakeven cost of dispersed storage systems in distribution systems for load levelling was estimated to be almost twice when compared with pumped hydro plants in Japan; this is because they do not require reinforcement in the transmission and distribution systems [2].

In stationary applications, the specific energy density is considered when electric energy storage systems are installed in urban areas; however, it is not very crucial when compared with transportable applications in general. On the other hand, items related to the economy play an important role since the capacity and scale are so large. Therefore, systems with low capital costs and high overall efficiency, which results in low operation costs, and longer lifetime are suitable under the condition of adequate performances and reliability.

8.2. Sodium-Sulfur Battery Systems

8.2.1. Battery Chemistry and Components

Figure 8.3a shows internal constitution of a cell. The cell has a molten-sodium negative electrode and a molten-sulfur positive electrode. The electrodes are separated by the β"-Al_2O_3 solid electrolyte. The cells must be operated at a sufficiently high temperature (270 to 350°C) to keep the active electrode materials (sodium and sulfur) in a molten state and to ensure adequate ionic conductivity through the β"-Al_2O_3 electrolyte. The two half-cell and full-cell chemical reactions are as follows:

Negative electrode: $2\text{Na} \underset{\text{charge}}{\overset{\text{discharge}}{\rightleftharpoons}} 2\text{Na}^+ + 2\text{e}^-$

Positive electrode: $x\text{S} + 2\text{e}^- \underset{\text{charge}}{\overset{\text{discharge}}{\rightleftharpoons}} \text{S}_x^{-2}$

Overall cell: $2\text{Na} + x\text{S} \underset{\text{charge}}{\overset{\text{discharge}}{\rightleftharpoons}} \text{Na}_2\text{S}_x \quad (x = 5 \text{ to } 3) \quad E_{\text{ocv}} = 2.076 \text{ to } 1.78\text{ V}$

The open-circuit voltage E_{ocv} is constant at 2.076 V for ~60% of the discharge when the two-phase mixture of sulfur and Na_2S_5 is present. The voltage then decreases linearly in the single-phase Na_2S_x region to the selected discharge end point [4].

Figure 8.3b shows internal constitution of a module. The module packs hundreds of cells with sand filler in an adiabatic enclosure. The chemical reactions of the cells are exothermic in the discharge state and endothermic in the charge state. The cells are then heated due to their ohmic resistance in both the discharge and charge states. The temperature in the module depends on the thermal balance among the electrode reactions, the ohmic heating in the cells,

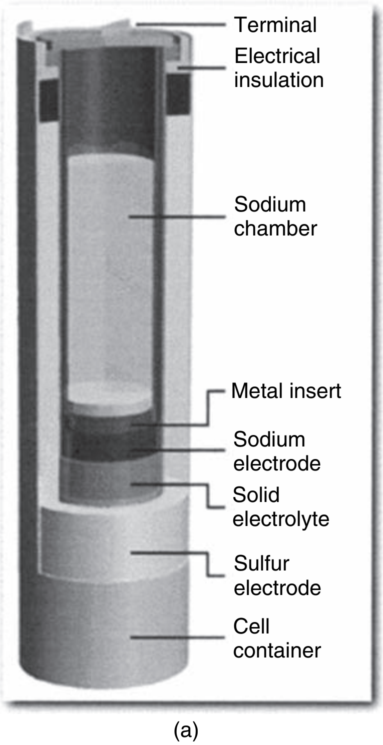

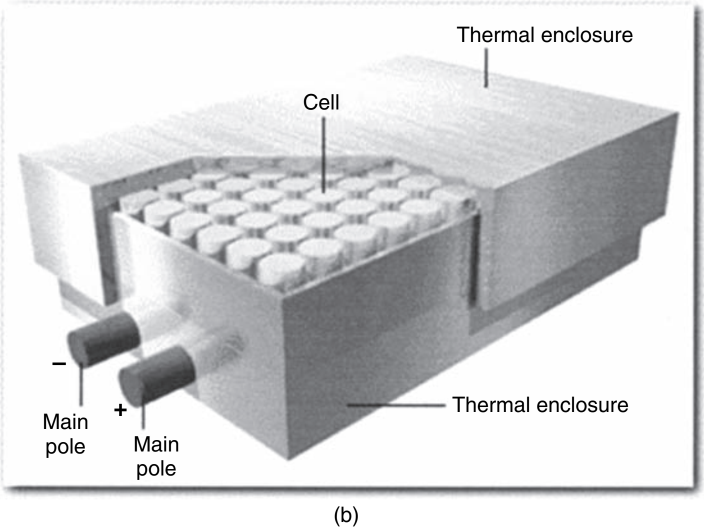

Figure 8.3. Constitution of sodium sulfur battery. (*From Ref. 3, Courtesy of NGK Insulators, Ltd.*)

heat radiation from the module enclosure, and the ohmic heating by the electric heaters. Electric heaters are used to adjust the temperature in the module between 300°C and 350°C. The typical time variations of the operating temperature are shown in Refs. [5,6]. The heater power decreases the overall efficiency of the sodium-sulfur (NaS) battery systems.

NGK Insulators, Ltd., the vendor of NaS batteries, provides some types of modules, for daily load levelling and/or for fast discharge and charge. In the module for daily load levelling, the cells are connected both in series and in parallel. However, in the module for fast discharge and charge, all the cells are connected in series, and the module is designed to reduce the radiant heat in order to minimize the energy dissipation in electric heaters. This is because the periods in the standby state are so long in the practical use for this application. The module is designed to deliver 500% power for 30 seconds against the continuous rated power [5]. This means that NaS batteries are available not only for daily load levelling but also for short-duration peak load shaving; however, the operational pattern needs to be determined before the module type is selected.

The storage capacity of the NaS battery decreases gradually and irreversibly along with the accumulation of the discharge and charge cycles, and deep discharges steeply decrease the cycle life [5]. The initial storage capacity is designed to have an extra capacity of 13%, and in this case the storage capacity decreases to the rated capacity after a 15-year operation utilizing 150 cycles of rated depth of discharge per year. The cyclic efficiency decreases by a few percent due to the increase in the internal resistance of the cells with the aged deterioration.

The sealing design at 300°C limits the prescribed lifetime of NaS battery systems to 15 years. The heat cycles between the ambient temperature and operation temperatures have an insignificant influence on the storage capacity; but they are not desirable due to the application of heat stress on the ceramic electrolyte. It is prescribed that the heat cycles should be restricted within ten times during the lifetime.

A package comprises some modules as per the required capacity and suitable voltage for a power conversion system (an AC-DC converter and a transformer). The system connects with bus lines of electric power systems. The discharge and charge power is adjusted by controlling the AC-DC converter.

8.2.2. Practical System

In order to reduce the consumed power and its expense and demonstrate the validity of the most up-to-date technique developed in national R&D projects, distributed photovoltaic power generation systems with 1-MW total, a

2000-kW NaS battery system, and a 170-kW vanadium redox flow (VRF) battery system were installed at AIST Tsukuba in Japan. The NaS battery has high specific energy density and high discharge and charge efficiency. On the other hand, the VRF battery has the advantages of fast discharge and charge and for short-durations a high overload up to more than three times compared with the continuous discharge rate. In order to make good use of these characteristics, the NaS battery system is applied on daily load levelling for the purpose of displacing the more expensive peak energy prices with the less expensive off-peak energy prices, and the VRF battery system is applied for peak demand curtailment and solar power smoothing [7]. The NaS battery system is described in this section and the VRF battery system is described in Section 8.3.

A 2000-kW$_{ac}$, 7.2-h NaS battery system was installed at a site in AIST Tsukuba in 2004. Figures 8.4 and 8.5 show a photograph and a ground plan of the NaS battery system, respectively. There are two packages (10.3 m (W) × 2.3 m (D) × 5.2 m (H), 86 tons each) for a 1-MW NaS battery and a package (9.2 m (W) × 3.3 m (D) × 4 m (H), 31 tons) for transformers and a 2400-kVA AC-DC converter. Each 1-MW NaS battery comprises twenty 50-kW modules (52.6 kW$_{dc}$ output/57 kW$_{dc}$ input) in series. Each module consists of 384 cells (12 parallel and 32 series connections of 2-V, 1.5-kW cells). Since the electrode materials (sodium and sulfur) are listed as hazardous materials, the fire

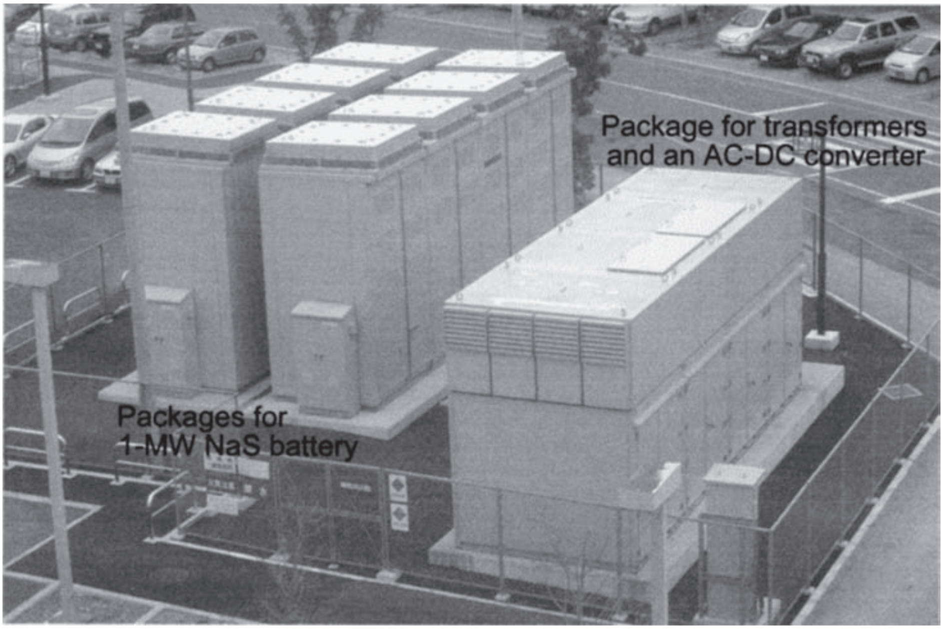
Package for transformers and an AC-DC converter
Packages for 1-MW NaS battery

Figure 8.4. Photograph of the 2 MW$_{ac}$, 7.2 h NaS battery system at a site in AIST Tsukuba.

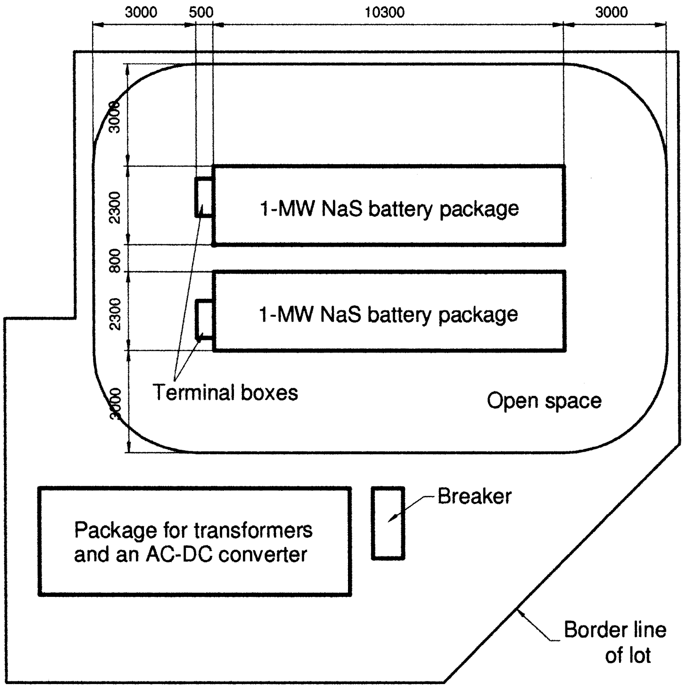

Figure 8.5. Ground plan of the 2 MW_{ac}, 7.2 h NaS battery system.

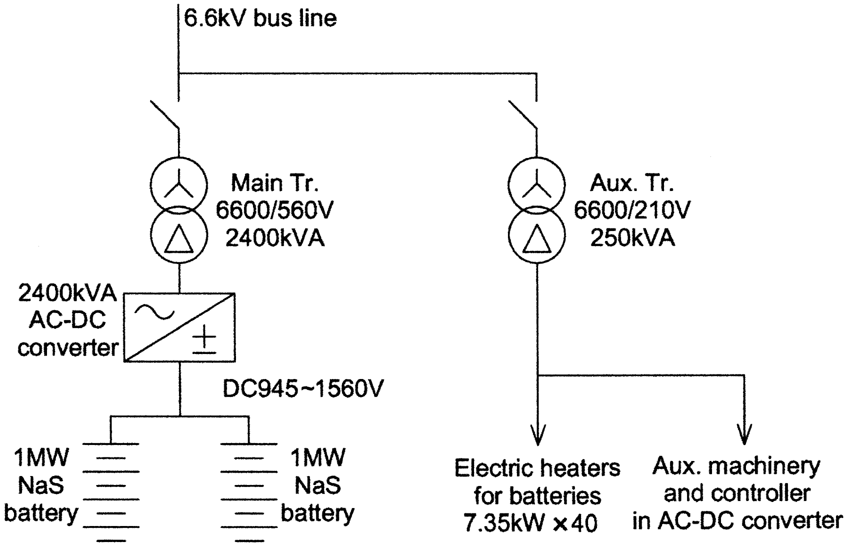

Figure 8.6. Single-line diagram of 2 MW_{ac}, 7.2 h NaS battery system.

protection law in Japan requires an open space of 3 m surrounding the battery packages.

Figure 8.6 shows a single-line diagram of the NaS battery system. The NaS batteries are connected to a 2400-kVA main transformer via the AC-DC converter. In the case of this system, the AC-DC converter is always operated with a power factor of 1.0, and the system supplies no reactive power to the connecting feeders. In addition to the main transformer, a 250-kVA auxiliary transformer was installed to supply the electric heaters and auxiliary machinery in the AC-DC converter. The electric heaters with a total power of 7.35 kW for each module are attached on the bottom and side faces of the module enclosure.

Figure 8.7 shows the operation curves for sampling at intervals of 10 min on a summer day. The State of Charge (SoC) is calculated by using current and time values, and the full charge state is indicated by the voltage. The heater power in Figure 8.7 also includes the power dissipated by the auxiliary machinery and the controller in the AC-DC converter; however, the heater power is dominant. The heater power is high in the charge state in order to compensate for the chemically endothermic reaction in the cells.

The discharge and charge pattern of the NaS batteries is scheduled by hand in advance of the operation while considering the load curve, which is predicted empirically, in the site. The schedule is set to discharge at daytime to reduce the peak load, and to charge the low-price electric energy to the utmost limit at night. The charge power depends on either the rated power (2400 kW_{ac}) in the battery system or the gross contract demand (8300 kW) of loads plus the battery systems on the site. Therefore, the depth of discharge also depends on the loads during the charge state (at night), and it is shallow in summer due to the high air-conditioning demands. Furthermore, the battery system does not discharge on Sundays and holidays. Therefore, the battery system has been experienced the operations with some different depths of discharge.

Figure 8.8 shows the average daily energy losses in the battery system, which were analyzed using the yearly operation data from December 2004. The cycle loss in the battery was calculated using the difference between the charged and the discharged energies. These energies were measured at the primary side of the main transformer. Therefore, the cycle loss in the battery at the AC terminal not only includes the loss in the battery but also the losses in the AC-DC converters and the main transformer. The heater loss was measured at the secondary side of the auxiliary transformer and it contains the power dissipated by the auxiliary machinery and the controller in the AC-DC converter. Figure 8.8 indicates that the cycle loss in the battery at the AC terminal increases with a deeper discharge, since the higher current flow causes high ohmic losses in the battery cells, the main transformer windings, and the AC-DC converter. On the other hand, the heater loss decreases with a deeper discharge because the ohmic losses in the battery cells also contribute to

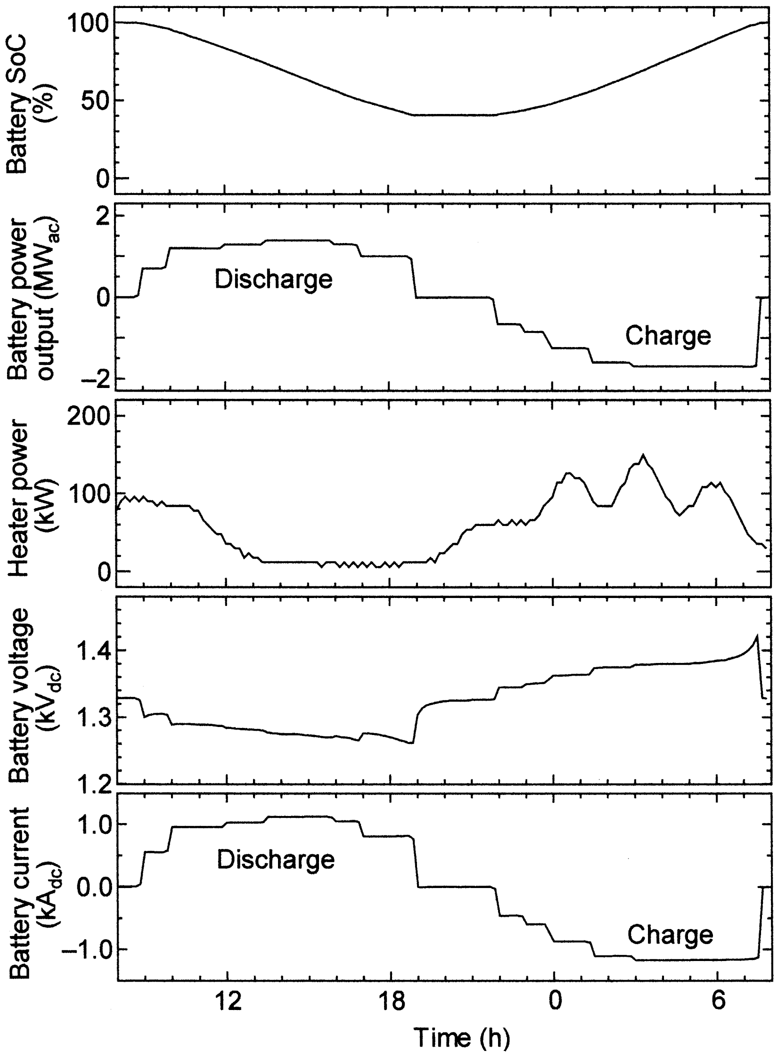

Figure 8.7. An example of the operation curves of 2 MW_{ac}, 7.2 h NaS battery system.

maintain the temperature in the battery modules.

Figure 8.9 shows the average daily efficiency in the battery system that is calculated from the data in Figure 8.8. The cycle efficiency of the battery was more than 85% at the AC terminal. However, the dissipated energy in the electric heaters decreased the overall efficiency, particularly in the case with shallow depth of discharge. The gross efficiency of the battery was 88% at the

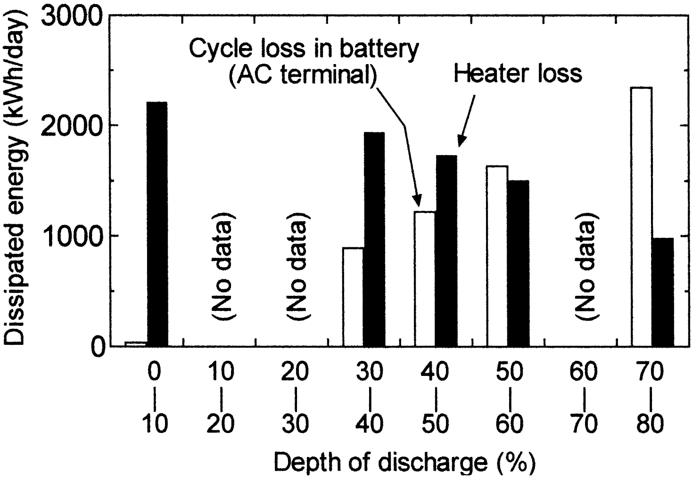

Figure 8.8. Daily energy losses in 2 MW_{ac}, 7.2 h NaS battery system.

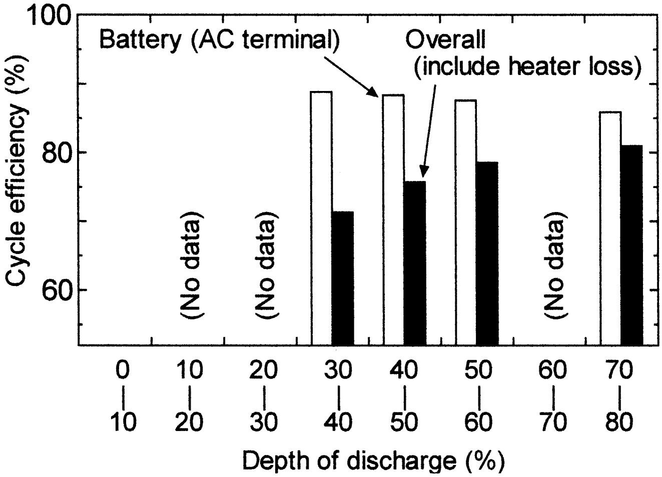

Figure 8.9. Daily efficiency in 2 MW_{ac}, 7.2 h battery system.

AC terminal, and the gross overall system efficiency was 75% during the year. The gross overall system efficiency at other 1000-kW NaS battery system in Meisei University was 77.6% during a year [8]. The efficiency increases by deeper discharge operation.

The data in the range 0–10% depth of discharge in Figure 8.8 pertain to days with no discharge and charge. There were 67 days with this condition

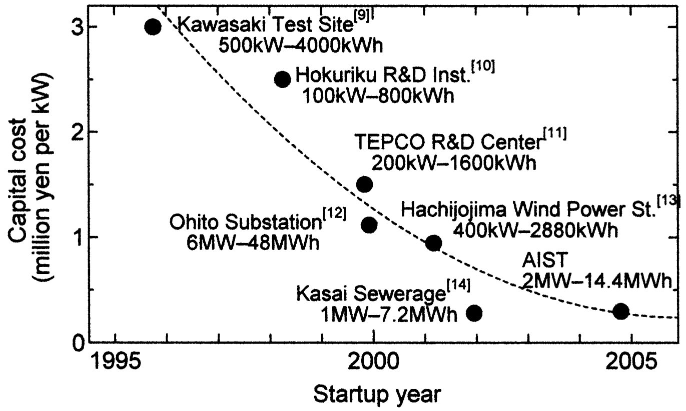

Figure 8.10. Change of capital costs for the NaS battery systems.

during the year. The average dissipated energy in the electric heaters on no-discharge days (2210 kWh) is equal to the radiant heat. Thus, the average heat loss from a module is calculated to be 2.3 kW.

8.2.3. Capital Cost

Figure 8.10 shows the relationship between the startup years and disclosed capital costs (some data include the maintenance expense) for the NaS battery systems in Japan. This figure indicates that the capital cost has been reduced drastically, because of research and development, and start of mass production. The current system price is about 240,000 yen per kW (1 U.S. dollar is about 110 yen), which is adequately competitive with those of pumped hydro storage power stations in Japan.

8.3. Vanadium Redox Flow Battery Systems

8.3.1. Battery Chemistry and Components

Figure 8.11 shows the constitution of a vanadium redox flow (VRF) battery. The cell of the VRF battery is based on the electron transfer between different ionic forms of vanadium. The electrolyte is sulfuric acid at approximately the same acidity level as that found in a lead-acid battery. It is stored in external tanks and pumped as required to the cells. The cell is divided into two half-cells by a proton exchange membrane. This membrane separates the two different vanadium-containing electrolyte solutions, and allows for the flow of ionic charges (H^+ ions) to complete the electric circuit [16]. The two half-cell and full-cell chemical reactions are as follows:

Positive electrode: $V^{5+} + e^- \underset{\text{charge}}{\overset{\text{discharge}}{\rightleftharpoons}} V^{4+}$

Negative electrode: $V^{2+} \underset{\text{charge}}{\overset{\text{discharge}}{\rightleftharpoons}} V^{3+} + e^-$

Overall cell: $V^{5+} + V^{2+} \underset{\text{charge}}{\overset{\text{discharge}}{\rightleftharpoons}} V^{4+} + V^{3+} \qquad E_{\text{ocv}} = 1.4 \text{ to } 0.9\ \text{V}$

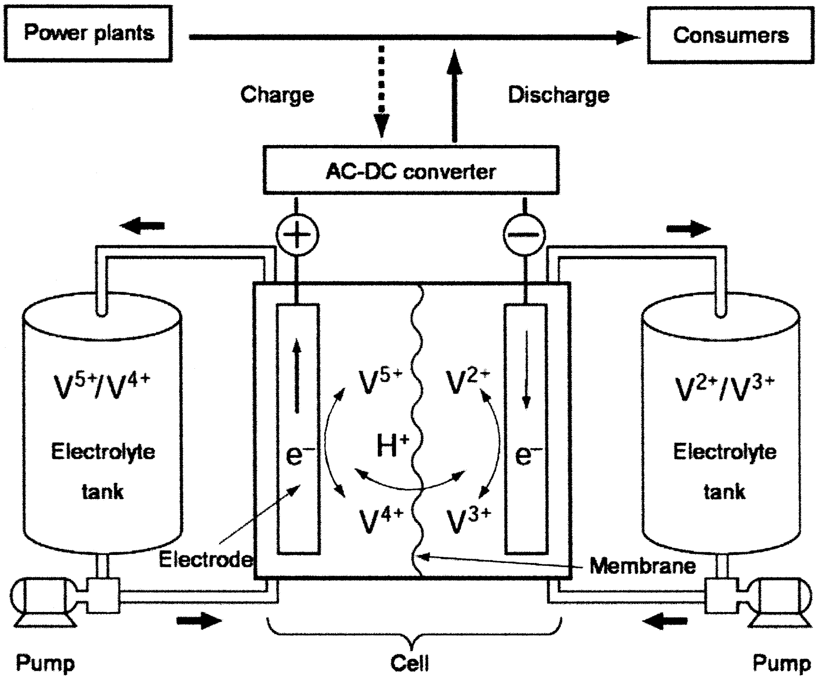

Figure 8.11. Principle of vanadium redox flow battery. (*From Ref. 15, Courtesy of Sumitomo Electric Industries, Ltd.*)

The rated power is determined by the cell stacks and the power conversion system (PCS) capacities, while the rated stored energy is determined by the quantity of electrolyte. Thus, these two system ratings are independent of each other in the VRF battery systems.

8.3.2. Practical System

As described in Section 8.2.2, a 170-kW$_{ac}$, 1360-kWh VRF battery system was installed at a site in AIST Tsukuba in 2004. Figures 8.12, 8.13 and 8.14 show a photograph, ground plan, and circulating system of the VRF battery system, respectively. The system has eight electrolyte tanks (diameter: 3 m, height 3.8 m), two packages for battery cell stacks, two packages for air-cooled heat exchangers, and a package for a power conversion system (transformers, an AC-DC converter, and switchgears), pumps, water-cooled heat exchangers, and an air-cooled chiller. The entire battery unit comprises four 48-kW battery cell stacks in series.

The heat in the cell stacks is removed by the electrolyte. Thus, the temperature of the stacks is regarded to be the same as the temperature of the electrolyte. When the system is operated daily, the temperature raises by 1-2°C per day. The tolerable temperature of the stacks is 40°C, and the system has the highest efficiency at a temperature of about 30°C. The value of ~30°C represents the intersection of the curves showing a decrease in the internal resistance and an increase in the self discharge with the temperature rise [17]. Therefore, the electrolyte is cooled by the air-cooled heat exchangers. When the cooling ability of the air-cooled heat exchangers is not sufficient in the summer, a water-cooled heat exchanger is used.

Figure 8.15 shows a single-line diagram of the VRF battery system. The VRF batteries are connected to a 300-kVA main transformer via a 300-kVA AC-DC converter. In this system, the AC-DC converter is always operated with a power factor of 1.0, and the system supplies no reactive power to the connecting feeders. In addition to the main transformer, a 75-kVA auxiliary transformer was installed for the auxiliary machinery (a chiller, pumps, cooling fans, and so on).

Figure 8.16 shows the operation curves for sampling at intervals of 30 s on a day in June. The data of the dissipated power in auxiliary machinery is rough because it was measured by using a watt-hour meter with a 1-kWh resolution. The dissipated power in the PCS was calculated by using the difference between the powers at the DC terminal and the primary side of the main transformer; it comprises losses in both the AC-DC converter and the main transformer. The VRF battery system has not yet been applied for peak demand curtailment and solar power smoothing; it has been

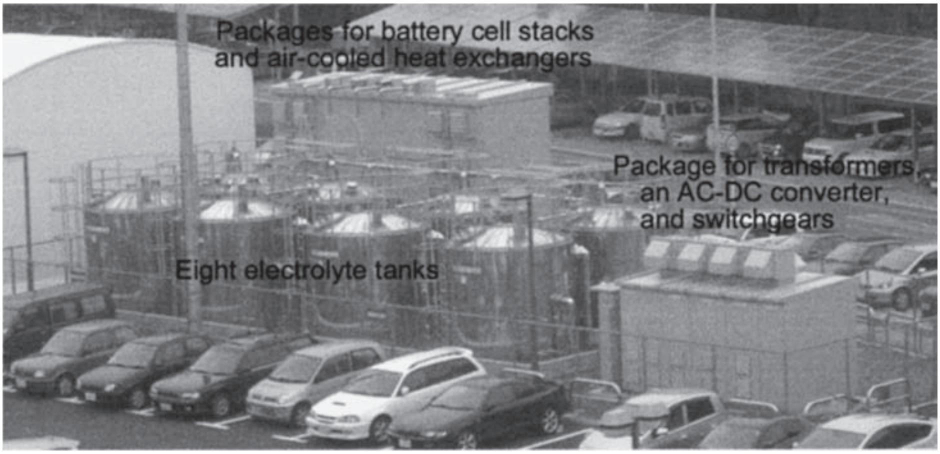
Packages for battery cell stacks and air-cooled heat exchangers
Package for transformers, an AC-DC converter, and switchgears
Eight electrolyte tanks

Figure 8.12. Photograph of the 170 kW_{ac}, 1360 kWh VRF battery system at a site in AIST Tsukuba.

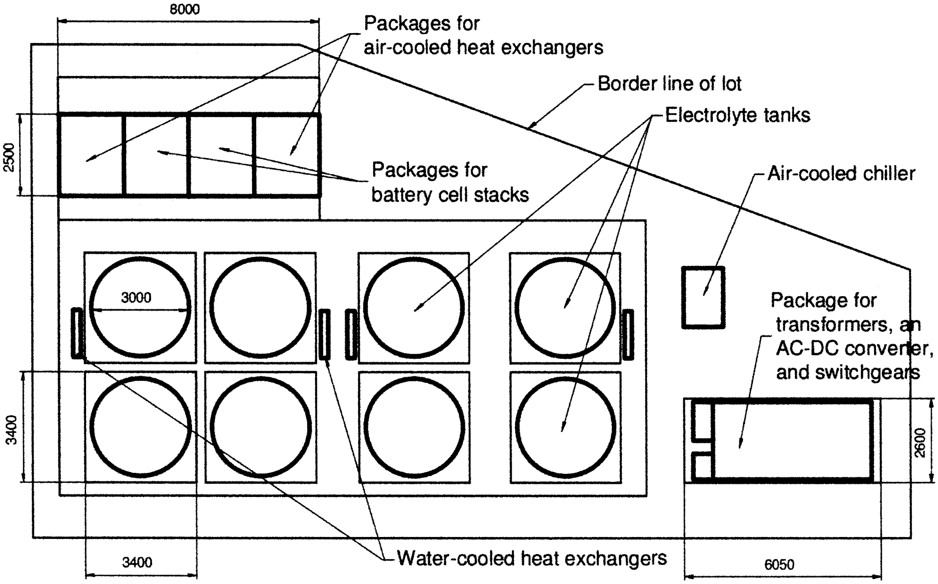
8000
Packages for air-cooled heat exchangers
Border line of lot
Electrolyte tanks
Air-cooled chiller
2500
Packages for battery cell stacks
3000
Package for transformers, an AC-DC converter, and switchgears
3400
2600
3400
Water-cooled heat exchangers
6050

Figure 8.13. Ground plan of the 170 kW_{ac}, 1360 kWh VRF battery system.

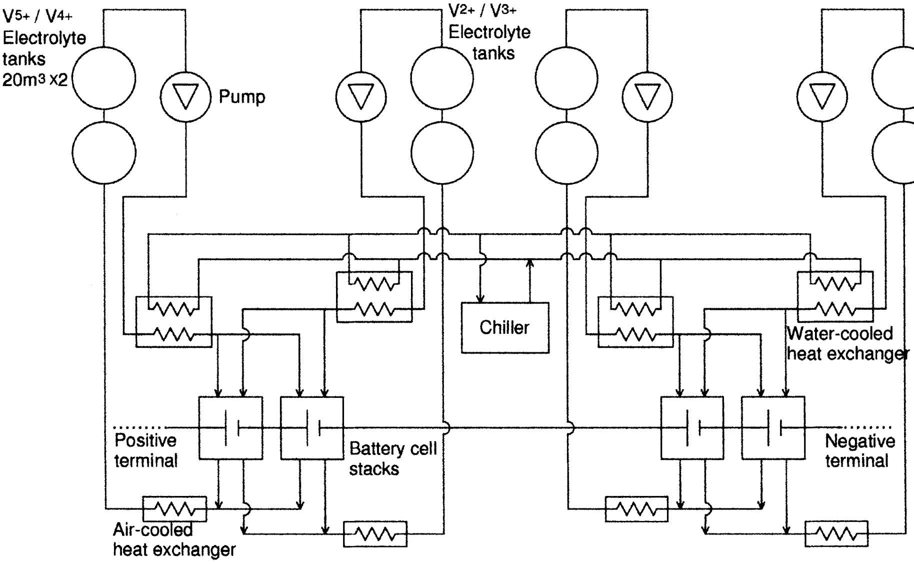
V5+ / V4+ Electrolyte tanks 20m3 x2
Pump
V2+ / V3+ Electrolyte tanks
Chiller
Water-cooled heat exchanger
Positive terminal
Battery cell stacks
Negative terminal
Air-cooled heat exchanger

Figure 8.14. Electrolyte circulating system of the 170 kW_{ac}, 1360 kWh VRF battery system.

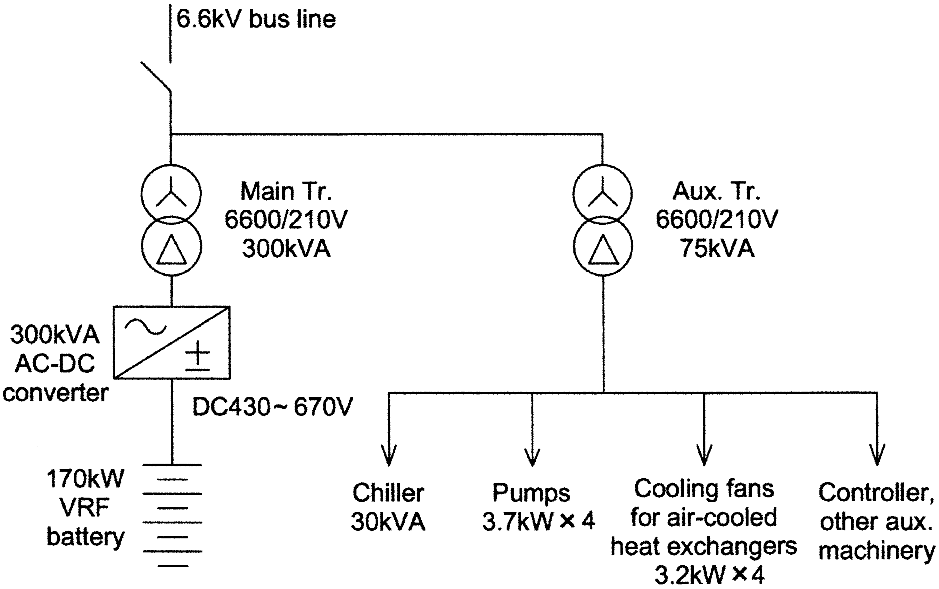

Figure 8.15. Single-line diagram of the $170kW_{ac}$, 1360 kWh VRF battery system.

used for load levelling on weekdays. In the charging state, the DC input power is maintained at 230 kW until the DC voltage first reaches 660 V. The DC voltage is then maintained at 660 V by decreasing the current. Finally, the full charge state is determined when the current reaches 220 A [17]. The stored energy is discharged with 170-kW$_{ac}$ power constantly for 8 h. The battery system is not discharged on Sundays and holidays. In this manner, the battery system has experienced both the operation with 100% depth of discharge and the one-day standby state.

The system operation was commenced in November 2004.

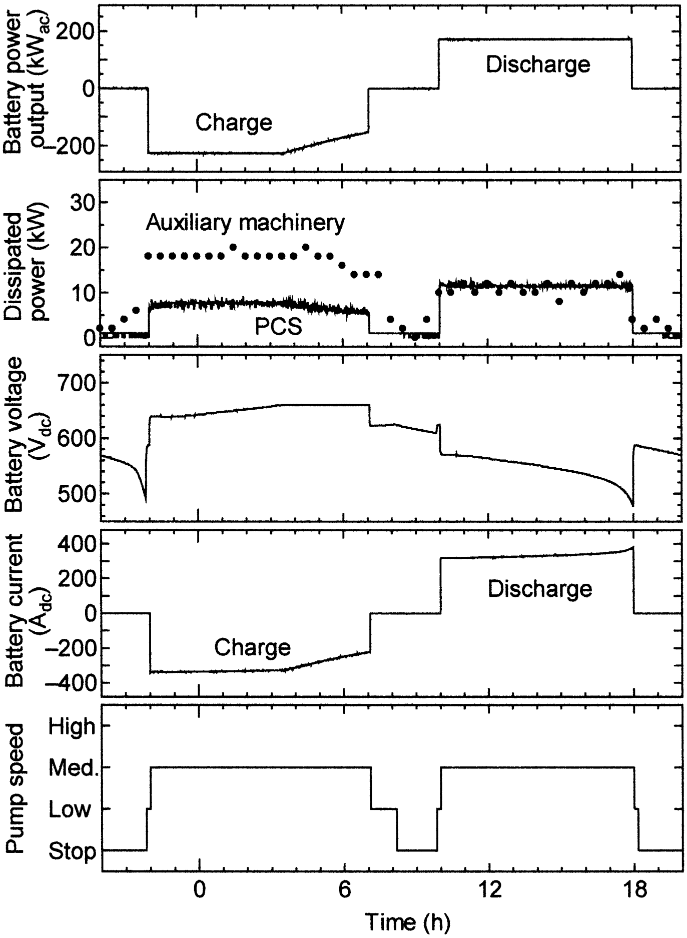

Figure 8.16. An example of the operation curves of 170 kW$_{ac}$, 1360 kWh VRF battery system.

Table 8.2. Daily energy losses and gross efficiency over two months.

DOD (%)	Number of days	E_{cyc} (kWh)	E_{pcs} (kWh)	E_{aux} (kWh)	η_{dc} (%)	η_{ac} (%)	η_{all} (%)
0	12	0	18	42	0	0	0
100	53	386	156	237	79	71	64
Gross		314	129	202	79	71	63

Unfortunately, the system stopped twice for long periods in the summer of 2005 and the following winter, due to the electrolyte leakage from the cell stacks. Furthermore, the measurement of the dissipated energy in the auxiliary machinery commenced in May 2005. Therefore, operation data for the whole battery system have been obtained for 2-month periods from May to June and from October to November in 2005.

Table 8.2 shows the average daily energy losses and gross efficiency in the battery system during the measured periods. The cycle loss E_{cyc} in the battery was calculated using the difference between the charged and discharged energies at the DC terminal. The power conversion system loss E_{pcs} was calculated using the difference in the transferred energies between that at the DC terminal and that at the primary side of the main transformer. The dissipated energy in the auxiliary machinery E_{aux} was measured at the secondary side of the auxiliary transformer. η_{dc} and η_{ac} are the efficiencies at the DC terminal and the primary side of the main transformer, respectively, and η_{all} is the overall system efficiency.

The overall system efficiency η_{all} at DOD = 100% was 64%, which is rather low; nevertheless, $\eta_{\mathrm{all}} > 70\%$ and $\eta_{\mathrm{dc}} > 80\%$ have already been achieved by other systems [18]. The reasons for this appears to be the following: high ohmic heating loss in the battery due to high-power and long-duration operation, slightly low efficiency in the PCS, need for high cooling power against solar radiation due to outdoor settlement. An improvement of the cells to decrease the pressure loss in the pumps is under development [19] and is expected to lead to greater system efficiency.

The average dissipated energy at no discharge days is low. This is an advantage of the VRF battery systems. The gross overall system efficiency η_{all} was 63%, which is almost the same as η_{all} at DOD = 100%.

8.4. Other Secondary Battery Systems

8.4.1. Lead-Acid Battery Systems

Although lead-acid batteries have many disadvantages such as low specific power and energy, short cycle life, high maintenance requirements, and environmental hazards associated with lead and sulfuric acid, they were accepted as the default choice for energy storage because of their low cost and ready availability. Continuous improvements in design and techniques have mitigated many of these disadvantages, and lead-acid batteries remain as the most popular energy storage system for most large-scale applications [20].

In 2001, a 200-kW$_{ac}$, 1320-kWh lead-acid battery system was installed in the Cape Tappi site for wind power fluctuation smoothing tests. The capital cost was 108 million yen [13].

Shin-Kobe Electric Machinery Co., Ltd. has developed newly designed VRLA (Valve Regulated Lead-Acid) batteries with a long cycle life. These batteries have excellent characteristics of 4500 cycles, 15-year lifetime with 70% depth of discharge and 87% cycle efficiency. Figure 8.17 shows a cycle life characteristic of a cell. A 2-V, 1000-Ah type cell has dimensions of 172 mm (W) × 303 mm (D) × 507 mm (H) and a weight of 72 kg. Demonstration tests are being conducted for several-hundreds-kW power storage systems [22]. Figure 8.18 shows a VRLA battery set of twelve 2-V, 1500-Ah type cells.

A 100-kW system was installed at a 40-m^2 area in Nabari Factory in 2002. The entire battery sets are 288 V, 2000 Ah, and 24 t, which comprise 288 cells of a previous type (3000 cycles, 67 kg) with metal frame structures. There are six battery sets with dimensions of 1.145 m (W) × 1.02 m (D) × 1.456 m (H) each. The 100-kW PCS has dimensions of 1.8 m (W) × 0.9 m (D) × 2.15 m (H) and a weight of 1.8 t.

8.4.2. Nickel-Metal Hydride Battery Systems

There are many types of batteries using a nickel electrode: nickel-iron, nickel-cadmium, nickel-zinc, nickel-hydrogen, and nickel-metal hydride. Nickel-cadmium (NiCd) batteries are the most commonly used batteries in the utility industry; they have a higher energy density, longer cycle life and require less maintenance than lead-acid batteries. The use of these batteries in stationary applications is dealt with in Chapter 10. Nickel-metal hydride (NiMH) batteries do not contain cadmium, which many users see as an environmental advantage, and generally have a higher energy density than the equivalent NiCd batteries. Further, NiMH batteries have a less pronounced tendency for reversible capacity loss due to memory effect and a

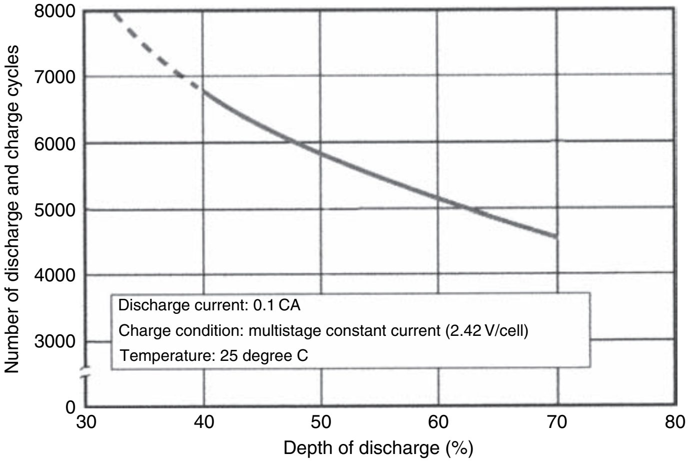

Figure 8.17. Discharge and charge cycle life of new VRLA batteries. (*From Ref. 21, Courtesy of Shin-Kobe Electric Machinery Co., Ltd.*)

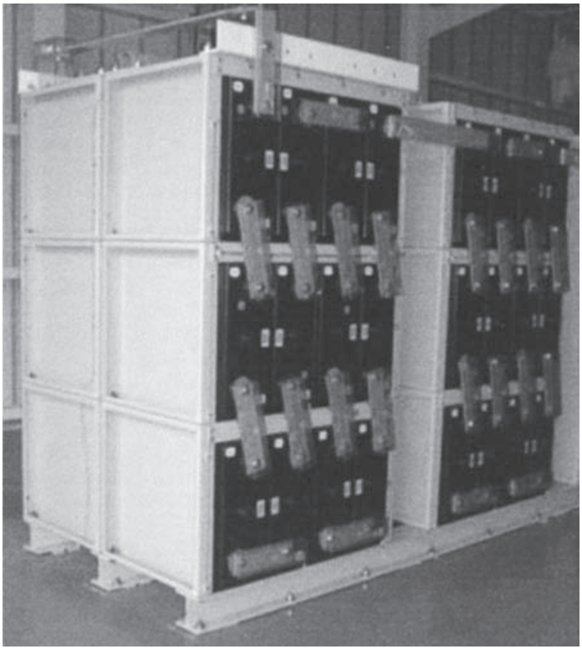

Figure 8.18. Set of the 2-A, 1500-Ah VRLA battery. (*From Ref. 22, Courtesy of Shin-Kobe Electric Machinery Co., Ltd.*)

somewhat better cycle life [23].

NiMH batteries are constructed as both cylindrical and prismatic types, and each type has advantages and disadvantages. The construction of the cylindrical type is extremely difficult and the prismatic configuration is the dominant type in applications above 20 Ah [24]. Although large-capacity NiMH batteries have been intensively developed for electric vehicle and hybrid electric vehicle applications, stationary applications are also promising.

Kawasaki Heavy Industries, Ltd. is developing NiMH batteries for stationary applications, and they installed twenty 2.3-kWh NiMH battery stacks in a microgrid demonstration site. A microgrid is a small-scale power supply network to provide energy for a small community by dispersed generators, where quick energy storage for demand and supply balance is required. Figures 8.19 and 8.20 show a constitution and a photograph of the NiMH battery. The 191 Ah × 12 V stack has dimensions of 1050 mm (W) × 160 mm (D) × 350 mm (H) and comprises 10 prismatic cells [25]. The battery is useful for high-rate (several *C*) applications.

8.4.3. Lithium-Ion Battery Systems

The major advantages of Li-ion batteries in comparison to other types of batteries are as follows: high specific energy (~150 Wh/kg) and energy density (~400 Wh/L) of commercial products, low self-discharge rate (2 to 8% per month), long cycle life (greater than 1000 cycles), broad temperature range of operation (charge at –20°C to 60°C and discharge at –40°C to 65°C), high cell voltage (2.5 to 4.2 V) and high-rate discharge capability [26]. Due to these

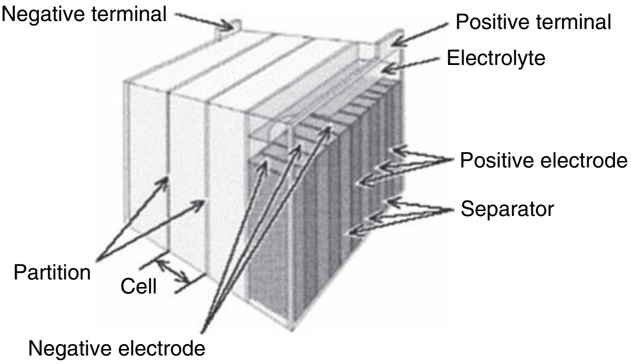

Figure 8.19. Structure of the nickel-metal hydride battery. (*Courtesy of Kawasaki Heavy Industries, Ltd.*)

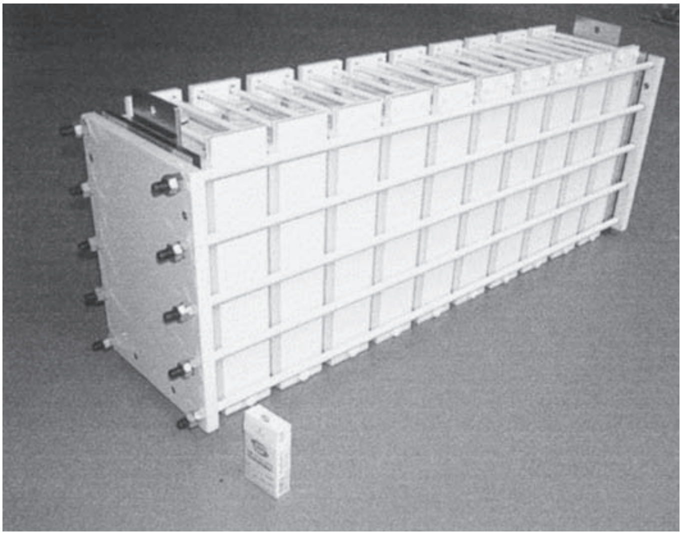

Figure 8.20. A 12-V, 440-Ah NiMH battery stack. (*Courtesy of Kawasaki Heavy Industries, Ltd.*)

advantages, Li-ion batteries have been widely applied in mobile devices such as cellular telephones and laptop computers; further, stationary applications are also promising.

Mitsubishi Heavy Industries, Ltd. and Kyushu Electric Power have been carrying out a collaborative 8-h charge and 8-h discharge test on 24-kWh lithium-ion battery energy-storage systems [27]. Table 8.3 shows the specifications of the system. Although the initial capacity is 432 Wh, the rated capacity of the cell is set to 270 Wh after considering the deterioration due to discharge and charge cycles. The system package includes a power conversion system (PCS). The lifetime of more than 3500 cycles (corresponding to 10 years) is expected with a 70% depth of discharge with regard to the rated capacity. In an operation cycle with 8-h charge and 2.3-kW, 10-h discharge, the overall cycle efficiency was 86% at the AC terminal. The rest was losses: a battery cycle loss of 3%, controller consumption of 5%, and PCS loss of 10.5% [28].

8.5. Other Electric Energy Storage Systems

In addition to secondary batteries, there are many other types of electric energy storage systems such as pumped hydros, compressed air energy storage systems (CAES), superconducting magnetic energy storage systems (SMES), electric double layer capacitors, and flywheels. Each storage system has a different application depending on its characteristics.

8.5.1. Pumped Hydroelectric Energy Storage Systems

Pumped hydroelectric storage represents the largest energy storage technology; it is commercially available. Conventional systems comprise reversible pump-turbine generator-motors and two large reservoirs—one located at a low level and the other situated at a higher elevation. Two reservoirs are connected to each other by water conduits via a pump-turbine. During off-peak periods at night, water is pumped from the lower to the upper reservoir where potential energy is stored. During peak hours at day time, the water is released back to the lower reservoir while generating electrical power.

Kazunogawa Power Station in Yamanashi, Japan commenced operations in 1999. It is a 1.6-GW, 8.2-h pumped hydroelectric power system with an upper reservoir of 11.47×10^6 m^3, a lower reservoir of 11.5×10^6 m^3, and an effective head of 714 m [29]. The total capital cost is about 380 billion yen.

8.5.2. Compressed Air Energy Storage Systems

Compressed air energy storage systems are used with gas turbine generators, which are referred to as CAES-G/T systems. Conventional gas turbine plants need compressed air for effective combustion, and they use about 2/3 of the total fuel consumption for compressing air to a high pressure. CAES-

Table 8.3. Specification of 24-kWh lithium-ion battery energy-storage system.

		270-Wh class cell	1.1-kWh class module (4 cells)	24-kWh system package (22 modules and PCS)
Weight (kg)		2.7	12.2	700
Size (mm)	Width	66.5	160	940
	Depth	116	262	550
	Height	175	238	2075
Nominal voltage (V)		3.8 (3.1-4.2)	15.1	AC 100/200 V DC 264-370 V
Rated capacity (kWh)		0.27	1.1	24
Initial capacity (kWh)		0.432	1.69	Rated power: 3 kW
Init. energy density	(Wh/kg)	160	139	
	(Wh/L)	320	169	

G/T systems compress the combustion air in the off-peak periods of power demand with excess electric energy using a motor-generator, which works as a motor, and store it in an underground storage cavern. The compressed air is then withdrawn from the cavern to the gas turbine as combustion air in peak periods; the motor-generator now acts as a generator to produce electricity. A 290-MW, 4-h system (Huntorf plant) has been in operation in Germany since 1978, and a 110-MW, 26-h system (McIntosh plant) has been in operation in the U.S. since 1991. The Huntorf plant has two salt caverns with a total area of 320,000 m^3 and it stores the compressed air from 5.5 to 7.5 MPa. The McIntosh plant has a 540,000-m^3 salt cavern and stores the compressed air from 4.4 to 7.3 MPa [30].

The energy dissipated to compress air is converted to heat, which is cooled down to ambient temperature for effective storage. Thus, internal energy is not thermodynamically stored in the compressed air; instead, the enthalpy is increased with a density of p_g (gauge pressure), and the storage is practically effective.

Figure 8.21 shows the energy flow from and to CAES-G/T systems. It is impossible to calculate the discharge and charge cycle efficiency for the CAES-G/T systems because they have fuel input (F) as well as electrical energy input (E_{in}) and output (E_{out}). Delivery efficiency and storage efficiency are utilized instead of the cycle efficiency.

$$\text{Delivery efficiency is: } \frac{\text{Electrical energy output}}{\text{Net fuel input}} = \frac{E_{out}}{F + E_{in} / \eta_n} \tag{8.1}$$

$$\text{Storage efficiency is: } \frac{\text{Electrical energy output from storage}}{\text{Electrical energy input for storage}} = \frac{E_{out} - \eta_d F}{E_{in}} \tag{8.2}$$

In Eq. (8.1), η_n is the thermal efficiency of power plants that supply electric energy to the CAES-G/T systems for air compression at night and E_{in}/η_n represents the fuel input in the power plants. In Eq. (8.2), η_d is the thermal

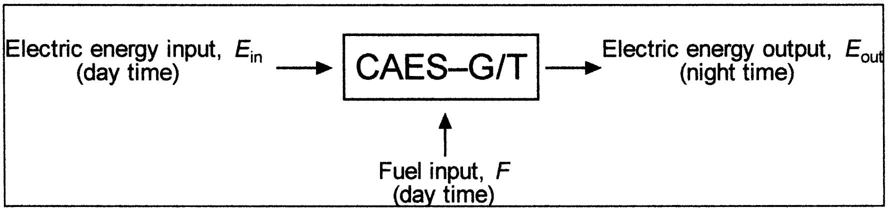
Electric energy input, E_{in} (day time)
CAES–G/T
Electric energy output, E_{out} (night time)
Fuel input, F (day time)

Figure 8.21. Energy flow in CAES-G/T systems.

efficiency of the power plants that are available instead of CAES-G/T systems during the day, and $\eta_d F$ represents the electric energy output that is generated if the fuel F is dissipated in the power plants. Thus, the efficiency of the CAES-G/T systems is estimated in relation to the efficiency of other thermal plants. On the other hand, when the cycle efficiency of other storage systems is η_s, their delivery efficiency is $\eta_s \eta_n$ and storage efficiency is η_s. For simplicity, the case of $\eta_p \equiv \eta_n = \eta_d$ is considered here.

Table 8.4 shows the efficiency of present CAES-G/T systems as compared to other storage systems. Parameters of $E_{in}/E_{out} = 0.83$ and $F/E_{out} = 1.612$ for the Huntorf plant and $E_{in}/E_{out} = 0.818$ and $F/E_{out} = 1.217$ for the McIntosh plant are used for the calculation [31]. The efficiency of the Huntorf plant is lower than that of the McIntosh plant since the former has no recuperator. The delivery efficiency is more important for the efficiency of the entire electric power system. In terms of the delivery efficiency, the Huntorf plant corresponds to a storage system with $\eta_s = 70\%$ when $\eta_p = 37\%$. In terms of the delivery efficiency, the McIntosh plant corresponds to a storage system with $\eta_s = 75\%$ and 70% for $\eta_p = 42\%$ and 50%, respectively. The reduction of the equivalent efficiency with an increase in η_p is derived from the thermal efficiency of the CAES-G/T systems as compared with other thermal plants.

Figure 8.22 shows the capital costs of the practical CAES-G/T systems

Table 8.4. Efficiency of the present CAES-G/T systems and other storage systems.

Plant		Delivery efficiency (%)	Storage efficiency (%)
Huntorf CAES-G/T (no recuperator)	η_p=0.37	25.9	52.5
	η_p=0.42	27.9	42.8
	η_p=0.50	30.6	33.1
McIntosh CAES-G/T (with recuperator)	η_p=0.37	29.2	70.2
	η_p=0.42	31.6	62.7
	η_p=0.50	35.1	55.3
Other storage (η_s=0.70)	η_p=0.37	25.9	70.0
	η_p=0.42	29.4	
	η_p=0.50	35.0	
Other storage (η_s=0.75)	η_p=0.37	27.8	75.0
	η_p=0.42	31.5	
	η_p=0.50	37.5	

[30], and 150-MW systems and 350-MW systems with a minimum 7-h storage capacity in salt caverns estimated in US dollars (for 1992) [32]. The capital costs are attractive, although they are very site-specific and may vary widely. Since suitable geological sites with salt stratum are limited, the development of low-cost storage methods is important for construction in the other sites.

8.5.3. Superconducting Magnetic Energy Storage Systems

The magnetic energy E_m that is stored in coils with an inductance L at a current I is equal to

$$E_\mathrm{m} = \frac{1}{2}LI^2 = \int \frac{B^2}{2\mu} dV_l \tag{8.3}$$

where B, μ, and V_l are the magnetic flux density, permeability, and volume, respectively. Eq. (8.3) indicates that the stored energy density is $B^2/(2\mu)$. If the normal conductor is wound for the coils, the stored energy is dissipated suddenly due to ohmic loss. Hence, superconducting coils are necessary for magnetic energy storage.

The superconducting state is maintained under the condition of lower temperature, lower current density, and lower magnetic flux density as compared to their respective critical values. These three critical values are related to each other. Thus, a superconducting coil must be placed in a cryostat and cooled down to the operational temperature by a liquid refrigerant or a

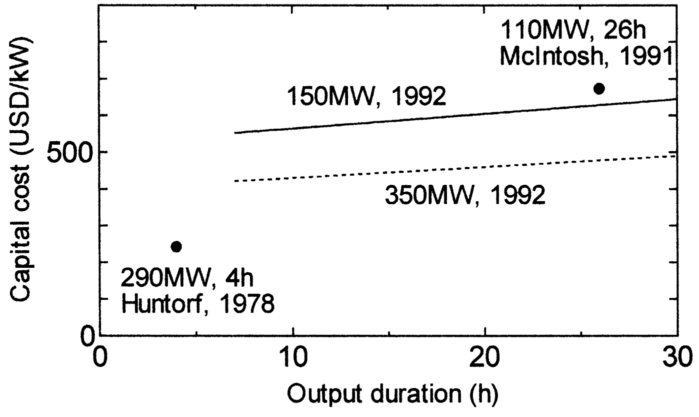

Figure 8.22. Capital cost of the CAES-G/T systems.

refrigerator. A power conversion system must then be used for the connection to an AC electric power system. Furthermore, a quench protection system, which comprises switches and resistors, for emergency discharge is also essential. These are the main components of superconducting magnetic energy storage (SMES) systems.

In principle, there are two configurations of superconducting coils for energy storage: dipole solenoid and toroid. The dipole solenoid stores larger energy with fewer winding conductors than the toroid, although the dipole solenoid generates a stray field in a wide space. It is necessary to reduce the stray field in an accessible area to less than 5 Gauss in order to avoid erroneous behavior in electronic devices.

Although the magnetic energy density in practical superconducting coils is much lower than energy density in secondary batteries, superconducting coil units for stationary applications have a high current (several kA) and high withstand voltage (several kV). Therefore, they are useful for short-duration high-power applications. The charging and discharging induce AC loss in the coil windings and eddy current loss at coil support materials. Furthermore, heat steadily leaks through the cryostat wall and current leads (connections with normal conductors at ambient temperature). These cause energy dissipation in refrigerating machinery.

A 1-MW, 1-kWh SMES system was installed for demonstration tests at the Imajuku substation in Fukuoka, Japan, in 1998, which is connected to a 6-kV commercial power line. Six D-shaped superconducting coils, with dimensions of about 0.75 m (W) × 0.2 m (D) × 1 m (H) each, have been used to obtain a toroid formation with a diameter of 2 m and a height of 1 m. The rated voltage, stored energy, and maximum flux density of the entire system are 500 V_{dc}, 3.6 MJ, and 5.5 T, respectively. The coils were wound with NbTi conductors and pool-cooled by 4.2-K liquid helium. The losses in the cryostat are 23 W in a standby state and 36 W in an operation state [33]. In order to eliminate these heat losses at 4.2 K, several hundreds times power is dissipated in the refrigerating machinery.

A 5-MVA, 1-s SMES system was installed for voltage sag compensation at a liquid crystal factory in Mie, Japan, in 2003. Four superconducting solenoids, with a diameter of 0.65 m and a height of 0.7 m each, are arranged in a four-pole system in order to reduce their stray field. The rated voltage, rated current, stored energy, available energy, and maximum flux density of the four-pole system are 2.5 kV_{dc}, 2657 A_{dc}, 7.34 MJ, 5.0 MJ, and 5.3 T, respectively. The coils were wound with NbTi conductors and pool-cooled by 4.2-K liquid helium. The SMES system was installed in a building with a layout space of 4.5 m × 18 m [34].

8.5.4. Electric Double Layer Capacitors

Electrostatic energy E_c that is stored in an electric double layer capacitor (EDLC) with capacitance C_{edlc} at voltage V is equal to

$$E_c = \frac{1}{2} C_{edlc} V^2 \tag{8.4}$$

Although the maximum voltage is as low as ~2.7 V, C_{edlc} is very large and the energy density of EDLC is several hundreds times higher than the electrolytic capacitors, although it is lower than the secondary batteries. EDLC is suitable for fast discharge and charge applications as compared to secondary batteries.

EDLC has a trade-off between the electric energy density and internal resistance. Thus, EDLCs with a low internal resistance and low energy density are used for short-duration pulse power applications, and those with high internal resistance and high energy density are used for long-duration applications. The EDLC module comprises capacitors connected in series and parallel in order to provide the required current and voltage, respectively.

Although the voltage of the EDLC modules varies with discharge and charge according to Eq. (8.4), a wide variation in the DC voltage supplied for voltage source inverters (typical AC-DC converters) is not desirable. Thus, it is essential to restrict wide variations of the DC voltage by using bi-directional DC-DC converters or change-over switches. The power loss in the bi-directional DC-DC converters results in lower discharge and charge cycle efficiency. The selection of change-over switches results in a slightly slow control ability.

Power Systems Co., Ltd. has developed a 100-V and 2-kW electric power storage system for a 2-h duration. The system stores 5.76 kWh but 4 kWh are available. The system has only change-over switches instead of DC-DC converters, and has achieved an overall discharge and charge cycle efficiency of more than 85% at AC terminal [35].

Chubu Electric power Co., Inc. and Meidensha Corporation have developed a 6.6-kV and 2000-kVA uninterruptible power supply (UPS) system for a 2-s duration. The system has dimensions of 13.5 m (W) × 2.8 m (D) × 3.4 m (H). The system uses capacitor banks having a total capacitance of 128 F and total voltage of 625 V. The capacitor banks use capacitor modules connected in series and parallel. Each capacitor module has a rating of 80 F and 125 V: dimensions of 362 mm (W) × 668 mm (D) × 431 mm (H) and a weight of about 100 kg [36]. The large stored energy ($0.5C_{edlc}V^2 = 25$ MJ) in the EDLC as compared with the available output energy ($P\Delta t = 4$ MJ) is due to the ohmic losses in the capacitors and converters, and available voltage range.

They have also developed a 210-V and 50-kVA UPS system for a 60-s duration. The system has dimensions of 2.6 m (W) × 0.8 mm (D) × 2.0 m (H). The stored energy ($0.5C_{\mathrm{edlc}}V^2$) in the capacitors is totally 5 MJ, while the available output energy ($P\Delta t$) is 3 MJ [37].

The capacitors in these systems have a lifetime of more than 15 years due to limited deterioration of the electrodes. These systems have undergone field tests and precisely compensated some voltage sags.

8.5.5. Flywheel Energy Storage Systems

The kinetic energy E_{r} that is stored in spinning flywheels with a moment of inertia J at angular frequency ω (rad/s) is equal to

$$E_{\mathrm{r}} = \frac{1}{2}J\omega^2 = \frac{1}{8}\left(GD^2\right)\omega^2 = \int \frac{1}{2}\rho(r\omega)^2\,dV_l \approx \int \frac{\sigma}{2}\,dV_l \qquad (8.5)$$

where GD^2, ρ, r, V_l, σ represent the flywheel effect, density of the rotating material, radius, volume, and circumferential tensile stress, respectively. $\sigma \approx \rho(r\omega)^2$ is obtained from the balance between centrifugal force and circumferential tension under the condition of no radial tension. The stored energy is discharged and charged through generator-motors. Flywheel energy storage systems are suitable for high-power applications.

A 215-MVA flywheel motor-generator was installed in 1985 as a pulsed power supply to magnetize the toroidal field coils in JT-60—an experimental device for a magnetically confined nuclear fusion reactor. The machine dimensions are a diameter of 11 m and a height of 12.2 m, with a rotor diameter of about 7 m. The maximum stored energy, available energy, and flywheel effect are 7.9 GJ, 4.0 GJ, and 16,000 ton-m^2, respectively. It is operated from 600 min^{-1} to 420 min^{-1} at intervals of 10 min and the operations are repeated. The range of the rotation speed was determined, considering the fatigue strength of the flywheel. The cycle life is 150,000 times at maximum rating operations and 450,000 times at 50% rating operations for start/stop of 3000 times [38]. The main losses at the rated rotating speed (600 min^{-1}) are a frictional loss of 2.2 MW on the bearings, a windage loss of 2.64 MW, and an iron loss of 0.7 MW [39].

Magnetic levitation is effective for the reduction in the frictional loss on the bearings. A 10 kWh-class flywheel energy storage system with superconducting magnetic bearing is under development. The entire system is installed in a vacuum vessel for windage loss reduction. The weight, diameter, rated rotation speed, and the moment of inertia in the CFRP rotor are 425 kg, 1 m, 15,860 min^{-1}, and 26.1 kg-m^2, respectively. 7,500-min^{-1} rotation with 2.24-kWh storage has been already achieved. The rotation energy losses with superconducting magnetic bearings and with active magnetic bearings for stabilization are 40 W and 58 W, respectively, at 7,500-min^{-1} rotation [40].

8.6. Comparison

This section provides a comparison between the characteristics of electric energy storage systems in terms of the scales of existing apparatuses, costs, power and stored energy density, and efficiencies, while revising a previous paper [41].

8.6.1. Existing Systems

The representative existing storage systems for stationary applications are shown in Table 8.5. Many storage systems in this table have already been described in this chapter. In this section, the storage systems are indicated by the symbols listed in this table.

The relationship between the output power and the output duration of the storage systems in Table 8.5 is shown in Figure 8.23. This figure shows that each storage system has a suitable range, and the storage systems can be distinguished into two types; daily load levelling and electric power quality improving types. Pumped hydro, CAES and batteries are suitable for levelling the daily load variation. SMES and flywheel with conventional bearings have a fast response and therefore can be utilized for the instantaneous voltage sag compensation, flicker mitigation and short duration UPS. Flywheels with levitation bearings and electric double layer capacitors (EDLC) are promising for durations of less than several hours and small capacities. NiMH batteries and Li-ion batteries may be also suitable for this time range.

8.6.2. Lifetime and Capital Cost

The lifetimes of the storage systems are shown in Table 8.6. Capacitance reduction of EDLC is estimated 9% after 20 years [35]. Although the lifetime for stationary applications is better than that for portable ones, the cycle durability of secondary batteries is still not high. The lifetime is limited to 10–15 years, which is approximately less than half that of other storage equipments.

The relationship between the output power per capital cost and the storage energy capacity per capital cost of the systems is shown in Figure 8.24. In the figure, one U.S. dollar is estimated to be equivalent to 110 yen. Here, the

Table 8.5. Installed electrical energy storage systems.

Symbol	Installed site	Year	Capacity
	<Sodium sulphur battery>		
S1	Kawasaki Test Site, Kanagawa, Japan	1995	500 kW, 8 h
S2	Hokuriku R&D Institute, Toyama, Japan	1998	100 kW, 8 h
S3	Tsunashima Substation, Kanagawa, Japan	1988	6000 kW, 8 h
S4	TEPCO R&D Center, Kanagawa, Japan	1999	200 kW, 8 h
S5	Ohito Substation, Shizuoka, Japan	1999	6000 kW, 8 h
S6	Hachijojima Wind Power Station, Tokyo, Japan	2001	400 kW, 7.2 h
S7	Kasai Sewerage, Tokyo, Japan	2001	1000 kW, 7.2 h
S8	Meisei Univ. Tokyo, Japan	2002	1000 kW, 7.2 h
S9	AIST, Ibaraki, Japan	2004	2000 kW, 7.2 h
	<Vanadium redox flow battery>		
R1	Tatsumi Substation, Osaka, Japan	1996	450 kW, 2 h
R2	Kashima-kita Electric Power Corp., Ibaraki, Japan	1997	200 kW, 4 h
R3	Horikappu Wind Power Station, Hokkaido, Japan	2001	170 kW, 6 h
R4	Liquid crystal factory, Tottori, Japan	2001	1500 kW, 1 h
R5	Kwansei Gakuin Univ., Hyogo, Japan	2001	500 kW, 10 h
R6	AIST, Ibaraki, Japan	2004	170 kW, 8 h
R7	Tomamae Wind Villa Power Plant, Hokkaido, Japan	2004	4000 kW, 1.5 h
	<Lead acid battery>		
P1	Tatsumi Substation, Osaka, Japan	1986	1000 kW, 4 h
P2	Tappi Wind Park, Aomori, Japan	2001	200 kW, 6.6 h
P3	Nabari Factory, Mie, Japan	2002	100 kW, 4 h
	<Nickel-metal hydride battery>		
N1	Microgrid demonstration, Tokyo Japan	2005	2.3 kWh
	<Lithium-ion battery>		
L1	Nagasaki R&D Center, Nagasaki, Japan	2004	3 kW, 8 h
	<Pumped hydroelectric power>		
H1	Kazunogawa Power Station, Yamanashi, Japan	1999	1600 MW, 8.2 h
	<CAES-G/T>		
A1	Huntorf Plant, Germany	1978	290 MW, 4 h
A2	McIntosh Plant, Alabama, U.S.	1991	110 MW, 26 h
	<SMES>		
M1	Imajuku Substation, Fukuoka, Japan	1998	1 MW, 1 kWh
M2	Liquid crystal factory, Mie, Japan	2003	5 MW, 1 s
	<Electric double layer capacitor>		
C1	Power Systems Co., Ltd., Kanagawa, Japan	1999	2 kW, 2 h
C2	Factory, Nagano, Japan	2002	50 kW, 60 s
C3	Factory, Nagano, Japan	2004	2000 kW, 2 s
	<Flywheel with conventional bearings>		
F1	JT-60, Ibaraki, Japan	1985	215 MVA, 1.12 MWh
F2	Chujowan Substation, Okinawa, Japan	1996	26.5 MVA, 58.4 kWh
	<Flywheel with levitation bearings>		
F3	Electric Power R&D Center, Aichi, Japan	1997	1 kWh
F4	Matsuyama FW Research Center, Ehime, Japan	1998	15 kW, 10 kWh

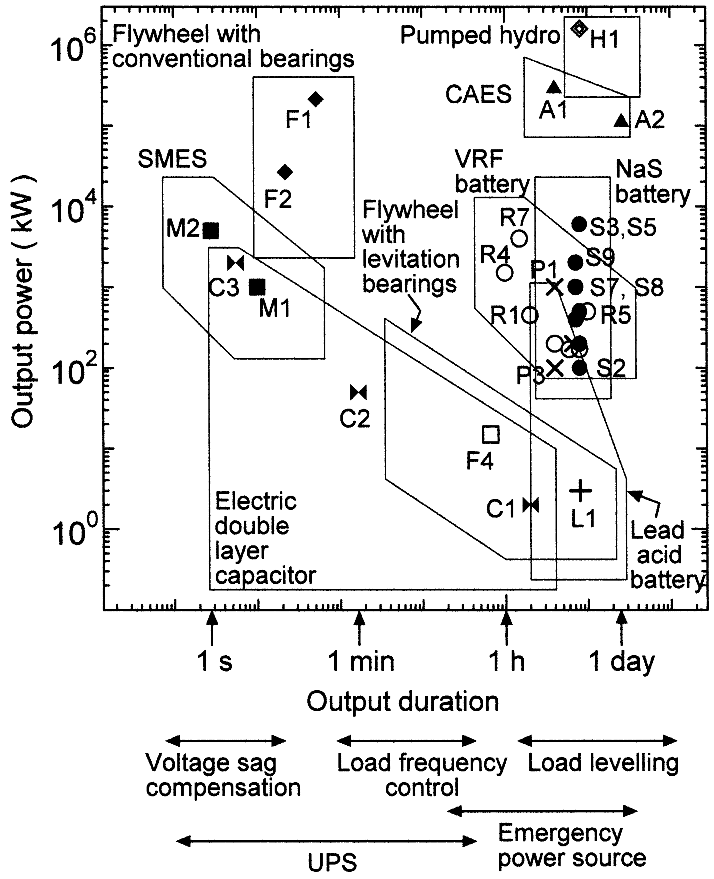

Figure 8.23. Output power and duration of electrical energy storage systems.

plots on the right-hand side indicate that the corresponding systems are suitable for storing a large amount of energy, and the plots on the upper side indicate that the corresponding systems are suitable for high power charge-discharge applications in terms of the capital costs. The distribution in this figure is slightly similar to that in Figure 8.23.

The capital costs of pumped hydroelectric energy storage systems have been increasing in general with the year of construction *x*. In Japan, the costs of systems constructed from 1970 to 1998 can approximately be indicated as 6.5(*x* – 1965) thousand yen/kW. The capital cost of the Kazunogawa power station (H1) is approximately 240 thousand yen/kW, which is roughly equal to the estimated value. The capital costs of CAES systems are reasonable at suitable geological sites. The capital costs of NaS battery systems have reduced

Table 8.6 Lifetime of energy storage systems.

	NaS	VRF[15]	Lead acid (P3)[22]	Li-ion (L1)[28]	Pumped hydro[42]	CAES[42]	EDLC (C1)[35]	Flywheel (F1)[38]
Years	15	>10	15	10	>40	>20	20	—
Cycles	2,250~4,500	>12,000	4,500	3,500	—	—	70,000	150,000

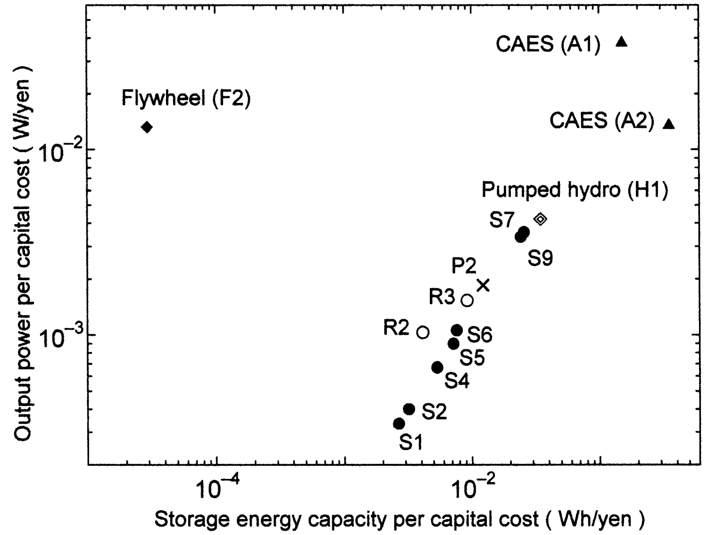

Figure 8.24. Output power and storage energy capacity per capital cost of the energy storage systems.

drastically as mentioned in Section 8.2.3. Although dispersed-type storage systems are advantageous as mentioned in Section 8.1.7, the disadvantage is their short lifetimes. After offsetting the disadvantage by the advantage, the NaS battery systems are now competitive with respect to the capital cost.

8.6.3. Output Power and Stored Energy Densities

The output power density p (W/m^3) and the stored energy density e (Wh/m^3) are described in this section. The output power density is defined as the rated output power divided by the volume of the storage device, and the stored energy density is the stored energy divided by the volume. Four types of volumes are considered for the calculation of these densities.

One type of volume is that of only the energy storing element—the battery cell and the flywheel; this type is indicated by subscript 1. The second type is the volume of the space for energy storage—a module of a battery or EDLC system, upper and lower reservoirs of a pumped hydro station, underground caverns of a CAES system and a rotor with a flywheel; this type is indicated by subscript 2. The third type is the volume of the units accompanying the energy storage equipment—battery packages, cryostat of an SMES system, a stator armature and supporting structures as well as rotating sections; this type is indicated by subscript 3. The last type is the volume of the entire energy storage system, which includes the power conversion systems and heat exchangers; this type is indicated by subscript 4. Furthermore, the theoretical energy density also needs to be considered; ρgh is obtained for pumped hydro stations, where ρ, is the water density, g is the gravitational acceleration and h is the effective head. The gauge pressure is obtained for CAES systems. $B_c^2/(2\mu)$ is obtained from Eq. (8.3) for SMES systems, where B_c is the critical magnetic field (11.5 T for NbTi wires at 4.2 K). For flywheel systems, $\sigma_c/2$ is obtained from Eq. (8.5), where σ_c is the tensile fatigue strength (~54 kg/mm^2 for steel and ~274 kg/mm^2 for CFRP under repeated load of 10^5 times). Theoretical density is indicated by subscript 0. As expected, the relationship between these densities is as follows: $p_1 > p_2 > p_3 > p_4$ and $e_0 > e_1 > e_2 > e_3 > e_4$.

The densities are shown in Figure 8.25. Data in Ref. [43] are applied for e_0 of secondary batteries. Unfortunately, all the data for the densities cannot be obtained. Figure 8.25a indicates that the output power densities of SMES, EDLC and flywheels are high. Figure 8.25b indicates that the secondary batteries exhibit higher energy densities than the others. Although the densities of the VRF battery [44] are slightly low, they rise by the increase of the vanadium ion concentration of the electrolyte [18].

For flywheel systems, the ratios e_1/e_0 and e_3/e_1 ($=p_3/p_1$) are considerably lower than those for the battery storage systems. These ratios increase as a result of the design optimization of the vessel. However, it is difficult to increase these ratios to the level of those for battery systems, since the supporting structure and stator armature, which store no energy, require greater space than the energy storing sections in the flywheel systems. Thus, the consideration of only the energy storing sections in flywheel systems for calculating practical densities may result in errors. Since a high rotation speed is possible under low friction losses, higher energy densities are obtained by using levitation bearings instead of conventional bearings by increasing the rotation speed of the CFRP flywheels, whose tolerable tensile strength is higher than that of steel flywheels. The difference is much more critical in respect of specific energy (Wh/kg).

Similarly, the ratio e_3/e_0 is low in the case of SMES systems since the required cryostat is extremely large when compared with the superconducting coils. In practice, SMES systems exhibit a low energy density. Solenoid-type

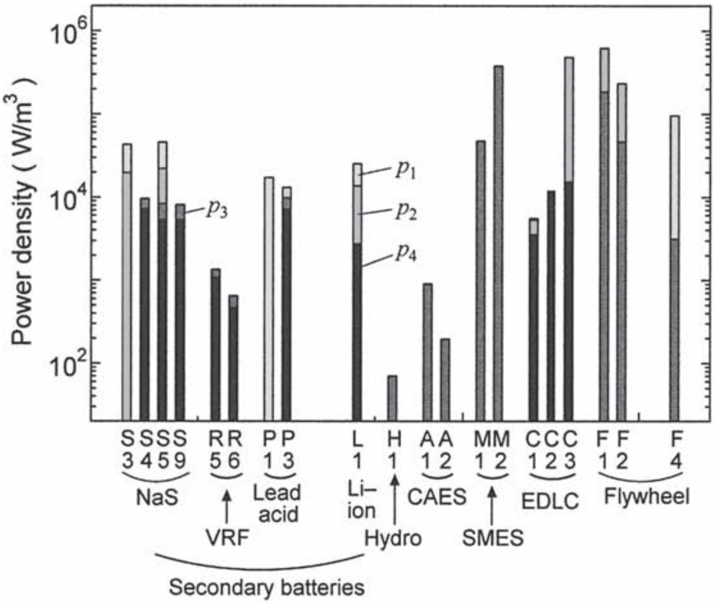

(a)

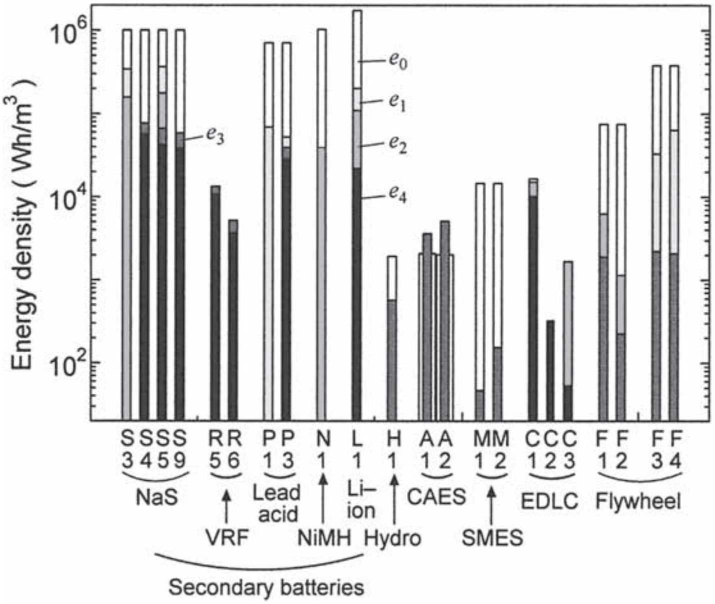

(b)

Figure 8.25. (a) Output power densities *p* and (b) storage energy densities.

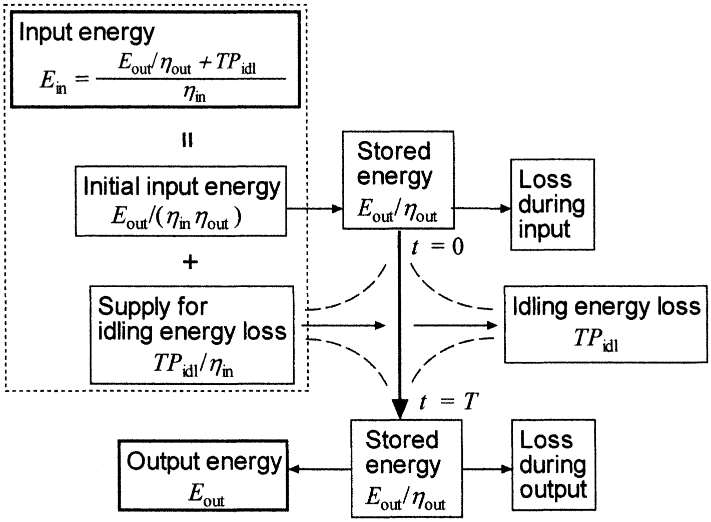

Figure 8.26. Energy flow during one charge-discharge cycle.

SMES systems can store energy more effectively since they produce magnetic fields on both their exterior and interior. However, their location must be selected such that stray external fields do not influence other equipment or living things.

e_0 of CAES is indicated by the thick white bar since e_2 is greater than e_0 as a result of fuel dissipation.

8.6.4. Cycle Efficiency

The energy flow during one charge-discharge cycle is illustrated in Figure 8.26. In this figure, T is the cyclic period; η_{in} is the conversion efficiency from the commercial AC side to the storage system side; η_{out} is the conversion efficiency from the storage system side to the AC side; P_{idl} is the loss when the rated energy E_s is stored. P_{idl} corresponds to self discharge in the cases of batteries and EDLC, idling loss in the case of flywheel. P_{idl}/η_{in} corresponds to the heater power in the case of NaS battery and refrigeration power in the case of SMES. Although P_{idl} is lower in a partial stored energy state during the charging or discharging phase as compared to the rated stored energy state, it is considered to be a constant for simplicity. From Figure 8.26, the AC terminal energy cycle efficiency η_e is expressed as follows:

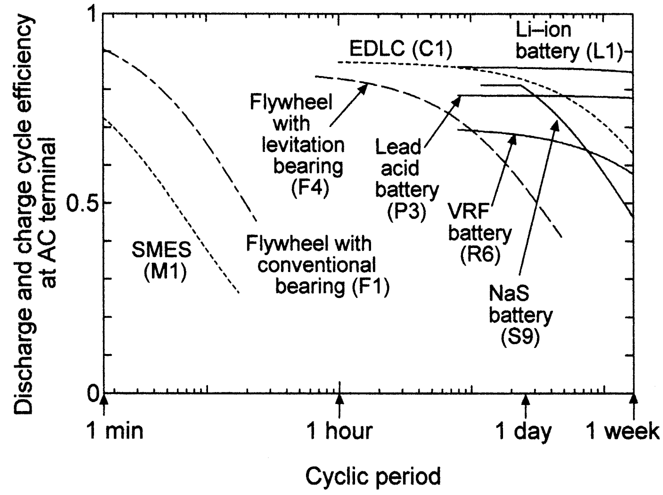

Figure 8.27. AC terminal efficiency *vs.* cyclic period.

$$\eta_e = \frac{E_{out}}{E_{in}} = \frac{\eta_{in}}{\dfrac{1}{\eta_{out}} + \dfrac{T}{\tau_s} \cdot \dfrac{E_s}{E_{out}}}, \quad \text{where } \tau_s = E_s/P_{idl} \qquad (8.6)$$

When T/τ_s is negligible, η_e can be approximated to $\eta_{in}\eta_{out}$. The relationship between η_e and T is shown in Figure 8.27. For the AC-DC converter, the conversion efficiencies from both DC to AC and AC to DC are both assumed to be 0.95. The influence of the discharge speed on the efficiency is neglected. In the calculation, general values are substituted for uncertain parameters in specific storage systems.

The efficiency of the VRF battery system (R6) is calculated under the assumption that power dissipation in the auxiliary machinery decreases by half due to an improvement in the cell structure, thereby decreasing the pressure loss in the pumps.

The refrigeration power of the SMES system (M1) is roughly calculated from the losses in the cryostat mentioned in Section 8.5.3 under the assumption that coefficient of performance (COP) is 1/500 at 4.2 K in the refrigerator. The SMES system is regarded as a test equipment, and the low efficiency of the SMES system is considered to be a special case. The heat-in-leak can be reduced, and the ratio relatively decreases for a greater size and capacity of the SMES system.

Although the efficiency of a pumped hydroelectric power station is not shown in Figure 8.27, it is approximately 75% in general. The efficiency of

CAES systems is also not described in Figure 8.27, since it has been mentioned in Section 8.5.2.

The efficiency of the NaS battery system becomes lower than that of other secondary batteries when the cyclic period is greater than a few days; this is because of the power dissipated in order to maintain the NaS battery system temperature above 300°C. However, the efficiency of the NaS battery system is sufficiently high for daily cyclic period operation. Further, the efficiency of the Li-ion battery system (L1) is extremely high.

The efficiency of a flywheel with conventional bearings (F1) sharply decreases with an increase in the cyclic period because of the large idling loss. The efficiency of EDLC drastically increased in comparison to its value reported in the previous paper [41] due to the improvement in the capacitor (reduction in the internal resistance and self discharge) and the use of change-over switches instead of DC-DC converters. The efficiency of a flywheel with levitation bearings also increased due to low bearing loss in a fully levitated flywheel.

Acknowledgment

The author would like to thank to Ms. K. Nibu who collected and arranged the information concerning battery systems and also drew the figures; Mr. M. Kounosu who offered useful insights and the operational data of battery systems; and all the people who worked to install and operate the battery systems and construct the remote measuring system in AIST Tsukuba.

References

1. H. Gotschall and D. Mears, in "*EPRI-DOE Handbook of Energy Storage for Transmission and Distribution Applications*" (Chapter 1, Introduction), No. 1001834, Electric Power Research Institute, 2003.
2. T. Shito, "Sodium sulfur (NaS) batteries", *OHM* 82 (1995) 32 (in Japanese).
3. Website for NGK Insulators, Ltd., http://www.ngk.co.jp/english/products/power/nas/index.html
4. J.W. Braithwaite and W.L. Auxer, in "*Handbook of Batteries*" (Chapter 40), D. Linden and T.B. Reddy, Eds., McGraw-Hill, New York, 2002.
5. H. Gotschall and D. Mears, in "*EPRI-DOE Handbook of Energy Storage for Transmission and Distribution Applications*" (Chapter 8, Sodium-Sulfur Batteries), No. 1001834, Electric Power Research Institute, 2003.
6. R. Ideta, K. Iba, "Data Analysis of Temperature and Auxiliary Power of NAS Battery", *2006 Annual Meeting Record*, IEE Japan, 6-116, p. 198 (in Japanese).
7. T. Kato, H. Tsuboi, M. Omori, "Distributed energy demonstration system in Tsukuba site", *AIST Today* 4 (2004) 15 (in Japanese).
8. S. Miyajima, T. Amemiya, "Present and future review of NAS battery", *OHM* 93 (2006) 36

(in Japanese).
9. Website for TEPCO, http://www.tepco.co.jp/cc/press/95082802-j.html (in Japanese).
10. Website for Hokuriku Electric Power Company, http://www.rikuden.co.jp/press/attach/denti.htm (in Japanese).
11. Website for TEPCO, http://www.tepco.co.jp/cc/press/99092901-j.html (in Japanese).
12. Website for TEPCO, http://www.tepco.co.jp/cc/press/99102701-j.html (in Japanese).
13. NEDO Investigation Report, "Introduction possibility investigation for wind power with storage battery", NEDO-NP-0004, p. 277, Feb 2002 (in Japanese).
14. Website for Sewerage in Tokyo, http://www.gesui.metro.tokyo.jp/oshi/img127pdf/info127_1.pdf (in Japanese).
15. N. Tokuda *et al.*, "Development of Redox Flow Batteries", *SEI Technical Review*, No. 156 (2000), p. 77 (in Japanese, English version is *SEI Technical Review*, No. 50 (2000), p. 88).
16. Ben Norris, in "*EPRI-DOE Handbook of Energy Storage for Transmission and Distribution Applications*" (Chapter 10, Vanadium Redox Batteries), No. 1001834, Electric Power Research Institute, 2003.
17. Communications with F. Sonoda, Sumitomo Electric Industries, Ltd., Feb-Mar 2006.
18. T. Itoh, T. Kanno, A. Ikeuchi, K. Kawai, T. Hara, N. Tokuda, "Development of Vanadium Redox Flow Battery System", *Proc. 34th IECEC* (1999).
19. M. Takao, "Technical development trend and application examples of redox flow battery", *OHM* 93 (2006) 42 (in Japanese).
20. H. Kamath, in "*EPRI-DOE Handbook of Energy Storage for Transmission and Distribution Applications*" (Chapter 6, Lead-Acid Batteries), No. 1001834, Electric Power Research Institute, 2003.
21. Website for NEDO, http://www.nedo.go.jp/kengyou/gyoumuka/tenjikai/h16/page/paneru/pa-ene/t_e-02-1.pdf
22. H. Takabayashi, I. Shimoura, K. Onoue, Y. Matsumura, S. Kondo, "Valve-Regulated Lead-Acid Batteries with a Long Cycle Life for Power Storage System", *Shin-Kobe Technical Report*, No. 15 (2005), p. 31 (in Japanese).
23. H. Kamath, in "*EPRI-DOE Handbook of Energy Storage for Transmission and Distribution Applications*" (Chapter 7, Nickel-Cadmium and Other Nickel Electrode Batteries), No. 1001834, Electric Power Research Institute, 2003.
24. M. Fetcenko, in "*Handbook of Batteries*" (Chapter 30), D. Linden and T.B. Reddy, Eds., McGraw-Hill, New York, 2002.
25. "Development for practical application of large capacity advanced nickel metal hydride battery systems", *Brochure of Kawasaki Heavy Industries, Ltd.* (in Japanese).
26. G.M. Ehrlich, in "*Handbook of Batteries*" (Chapter 35), D. Linden and T.B. Reddy, Eds., McGraw-Hill, New York, 2002.
27. Website for Mitsubishi Heavy Industries, Ltd., http://www.mhi.co.jp/power/e_power/topics/2004/nov_10.html
28. K. Hashizaki, H. Tajima, Y. Fujioka, T. Nishida, T. Hashimoto, Y. Mori, "Development of Power Storage System Applying Li-ion Batteries", *Mitsubishi Juko Giho* 41 (2004) 290 (in Japanese).
29. Kazunogawa Hydraulic Power Constructive Place in TEPCO, "Whole aspect of Kazunogawa Power Plant", *OHM* 87 (2000). 69 (in Japanese).
30. S. Kuroda, "Compressed Air Energy Storage Gas Turbine Power System (CAES-G/T) and a Pilot Plant", *Energy (Journal of the Japan Energy Association)*, No. 253 (1999) 21 (in Japanese).
31. Y. Uchiyama, M. Kadoyu, "Technical Assessment and Economic Study of Compressed Air Energy Storage in Japan", *CRIEPI Technical Report*, Y90002, 1990 (in Japanese).
32. R. B. Schainker, B. Mehta, R. Pollak, "Overview of CAES Technology", *Proc. 55th American Power Conference* (1993), p. 992, 1993.
33. H. Hayashi, T. Sannomiya, H. Kanetaka, K. Tsutsumi, F. Irie, M. Tezuka, K. Asano, S. Nose,

H. Yamamura, "Fabrication of a 1kWh/1MW Module Type SMES", *Advances in Superconductivity XI*, N. Koshizuka and S. Tajima, Eds., Springer, Tokyo, 1999, Vol. 2, p. 1401.

34. S. Nagaya, N. Hirano, M. Kondo, T. Tanaka, H. Nakabayashi, K. Shikimachi, S. Hanai, J. Inagaki, S. Ioka, S. Kawashima, "Development and Performance Results of 5 MVA SMES for Bridging Instantaneous Voltage Dips", *IEEE Trans. Applied Superconductivity* 14 (2004) 699.
35. NEDO, "Final report of demonstrated investigation for new load levelling technique", Mar 2000 (in Japanese).
36. S. Sugimoto, R. Hatano, N. Yamamoto, J. Shimomura, H. Zaitsu, H. Nara, M. Ohbe, "Development of High Voltage Large Capacity Uninterruptible Power Supply System", *2005 Annual Meeting Record*, IEE Japan, 4-027, p. 42 (in Japanese).
37. S. Sugimoto, R. Hatano, S. Ogawa, Y. Ando, H. Nara, "Development of Uninterruptible Power Supply System Utilizing Electric Double-Layer Capacitors", *Proc. 15th Annual Conference of Power & Energy Society*, IEE Japan (2004), 273, p. 25-9 (in Japanese).
38. T. Matsukawa, M. Kanke, R. Shimada, Y. Yoshida, K. Yamashita, T. Nakayama, "A 215 MVA flywheel motor-generator with 4 GJ discharge energy for JT-60 toroidal field coil power supply system", *IEEE Trans. Energy Conversion* 2 (1987) 262.
39. S. Ishizu *et al.*, "Energy Storage Systems for Industrial Applications", *Trans. IEE Japan*, 109-D (1989) 705 (in Japanese).
40. T. Ichihara *et al.*, "Fabrication and evaluation of superconducting magnetic bearing for 10 kWh-class flywheel energy storage system", *Physica C* 426-431 (2005) 752.
41. J. Kondoh *et al.*, "Electrical energy storage systems for energy networks", *Energy Conversion & Management* 41 (2000) 1863.
42. S. Hibino *et al.*, "Development of Fundamental Technology on Compressed Air Energy Storage", *CRIEPI Technical Report*, U28, 1994 (in Japanese).
43. Y. Sato, R. Shimada, "Electrical power system engineering", Maruzen, Tokyo, 2002 (in Japanese).
44. H. Morii, S. Miura, M. Minamiura, K. Motoi, "Application of Redox Flow Battery for Load Equalization", *Electrical Construction Engineering*, No. 587 (2001) 71 (in Japanese).

Industrial Applications of Batteries. From Cars to Aerospace and Energy Storage
M. Broussely and G. Pistoia Eds.,
© 2007 Elsevier B.V.

Chapter 9

STATIONARY APPLICATIONS. III. LEAD-ACID BATTERIES FOR SOLAR AND WIND ENERGY STORAGE

Rainer Wagner

EXIDE Technologies, Deutsche EXIDE GmbH, Odertal 35, D-37431 Bad Lauterberg, Germany

9.1. Introduction

There is an increasing use of solar and wind energy systems for the supply of electric energy in remote areas that are not connected to an electricity grid [1-3]. In some countries, even where mains grids have been established, the power supply is unreliable and of poor quality. The electric energy in such areas is needed for a wide variety of applications that include community dwellings and services, sign lighting, telecommunications systems, emergency lighting, water pumping, electric fences, lighting beacons, refrigerators, television/radio and many others. There is especially a demand for electric energy from sun and wind systems in developing countries. However, this is not the only application. In Europe, for example, the Alps are a typical area where solar and wind energy is used when there is no connection to an electricity grid.

In general, solar or wind systems which are used for such autonomic electric energy supply, need an additional energy source for those time periods when there is more energy demand than that produced by the solar or wind generator. Indeed, the electric energy produced by the generator is seldom equal to the energy demand of the consumer. This applies especially in climate zones where the solar energy is markedly different in summer and winter time. Either more electric energy is needed than produced or there is an excess of electric energy that cannot be used and would get lost if there were no storage system. Thus, an energy storage system and/or a diesel/gas generator are needed.

In most cases, the storage system is a lead-acid battery [2-4]. Less frequently other systems, like nickel-cadmium (Chapter 10) or nickel-iron, are used. Therefore, this chapter is focusing on lead-acid batteries for the energy storage in solar and wind autonomic systems.

The reasons for the decision to use the lead-acid system are the same as discussed in Chapter 7 for telecommunications and UPS applications. Lead-acid batteries have good characteristics in terms of life, cost, power, reliability, *etc.*

It is especially the rather low cost that makes lead-acid batteries so attractive. As already pointed out in chapter 7, the relatively high weight of lead is not so important for most of all the stationary applications where the volumetric energy density has a higher priority, and, therefore, the lead-acid battery is also a suitable choice for solar and wind energy storage.

9.2. Energy Storage for Solar and Wind Systems

A solar or photovoltaic (PV) system has a couple of components. The basic concept, shown in Figure 9.1, includes a solar generator, a charge controller, a battery and a set of consumer's appliances. Such a system is typically used for electric power supply to lightning, parking-fee systems, traffic signals, *etc.* If there are significant differences in sunshine between summer and winter time - this is typical, for example, for northern Europe - it is not common to use a battery size which allows energy storage for the complete winter time, otherwise the cost for such a storage system would be rather high in comparison to the solar generator. The cost-optimized design considers just a medium energy supply during the winter period [5]. The battery is then used to compensate the day/night changes and bad weather periods. In general, a sufficient energy supply from such systems is not always guaranteed.

The ratio between the available stored energy of the battery and the peak power capability of the solar generator varies mostly between 5 and 50 kWh/kWp [5]. It has to be realized that even with a relatively large battery, the basic concept cannot give a 100% guarantee for the energy supply. Systems with a ratio of less than 25 kWh/kWp often have a small diesel or gas engine to be used as an additional power source for extreme situations, *e.g.* longer bad weather periods or unusually high energy demands. Such a diesel or gas engine

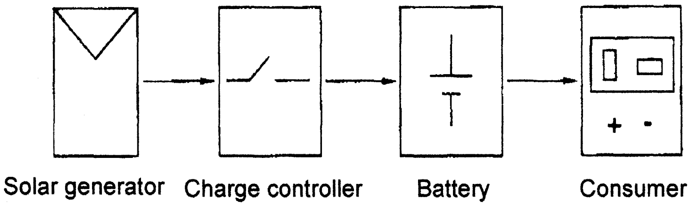

Figure 9.1. Schematic of a photovoltaic system without back up.

improves, in any case, the reliability of the system and, additionally, it can also mean a cost saving because it allows to reduce markedly the battery size.

A hybrid system is shown in Figure 9.2. This schematic gives an example for a combination of a solar generator and a gas engine. However, there are also hybrid systems using a wind generator or both a solar and a wind generator. The diesel or gas engine can either directly supply the energy to the consumer or it is connected via a charger/rectifier to the d.c. side, *i.e.* to the battery. A d.c./a.c. converter is used behind the battery if a.c. current supply is needed by the consumer.

Most of the components of a PV system have a rather long life expectation of up to 25 years. As the life of a battery is markedly shorter, a replacement of this component has to be considered in any calculation of the cost over a period such as 25 years. Therefore, it is obvious that any extension of the battery life is an important factor to reduce the overall cost of a photovoltaic system. This does not just mean an improvement of the battery design but there is also a significant effect from the application or in more detail from an appropriate charge/discharge strategy. Especially important are: the impact from the depth of discharge (DoD) of the battery and the voltage limit for charging [6,7]. This is discussed in detail in the next sections.

Maintenance of the battery, for example topping up with water, is another cost factor. There are certain costs if maintenance is performed properly and, if not, it can be even more expensive, because a lack of maintenance work has a markedly negative impact on the service life of the battery. The use of

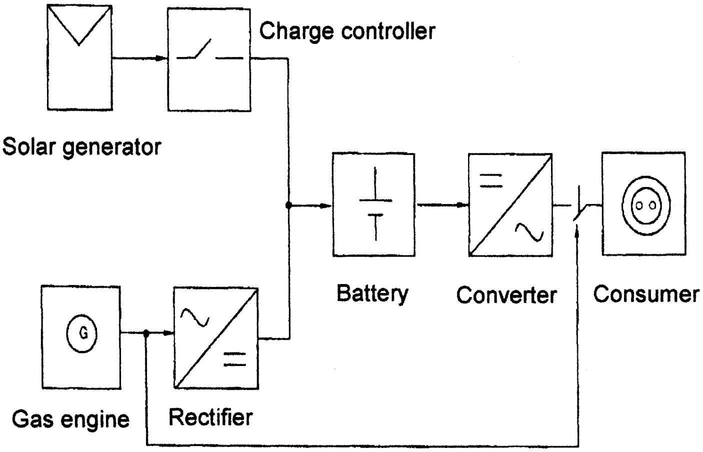

Figure 9.2. Schematic of a photovoltaic system with back up (gas generator) and converter for a.c. supply.

valve-regulated lead-acid batteries (VRLA), which are also called maintenance-free batteries, is an option to avoid that problem [7]. Such systems have steadily been more used in stationary applications (see also Chapter 7). VRLA batteries for solar and wind energy storage applications are discussed in detail in one of the following sections.

There are some papers about the use of lead-acid batteries in solar and wind power applications and about operating conditions [3,8-13]. The autonomic solar and wind power applications can be divided into two groups. The first one consists of rather smalls systems where the solar generator is the only energy source, as shown in Figure 9.1. The consumer is supplied with electric energy either directly by d.c. current or via a converter by a.c. current. Typical energy demand per day is around 0.25 kWh. The battery load includes discharge periods with relatively small currents and there is a rather shallow cycling. The state-of-charge (SoC) of the battery depends, often, from the time of the year: for example, the SoC is close to 100% in summer time and rather low in winter time.

The minimal SoC of the battery should be controlled by an automatic system, which disconnects the battery at a certain minimal discharge voltage. If not, the battery could be completely discharged, a situation to be avoided in order to keep the battery in a healthy condition. Such an automatic disconnection system is not complicated, as long as there is always approximately the same discharge current. If the discharge current varies in a wide range, the additional decrease of voltage by polarization at higher currents has to be taken also into consideration. The polarization effects of lead-acid batteries at higher discharge currents are discussed in detail in Chapter 7. Ways to overcome the problem of SoC determination, when there are significant discharge current variations, are shown in one of the following sections.

There is a relatively wide temperature range where the battery is used in such small systems. In many applications the battery temperature can vary between -10°C and +45°C; in some special applications, however, there are even more extreme temperatures. The temperature has much influence on many parameters, as the available performance of the battery (see Chapter 7). Thus, the temperature of the battery should be taken into consideration especially if it is significantly different from room temperature.

The second group of applications consists of larger systems where, besides a solar generator, also other energy sources (wind generator, diesel or gas engine, fuel cells) are used. Such so-called hybrid systems have often a daily energy turnover in the range 1 - 100 kWh. In general, hybrid systems should give 24 h per day a reliable energy supply with one- or three-phase a.c. current, which sometimes includes rather high power peak demands. In such applications the battery is used quite intensively: there is the experience that, in average, 2/3 of the energy is transferred via the battery [14]. This means around 100 full cycles or energy turnovers per year, and this is a significant load for the battery and requires battery types with good cycling performance; otherwise, there would be an insufficient service life. In comparison with many other stationary applications like telecommunication or UPS (see Chapter 7), the solar and wind power systems need more cycling performance of the battery. This has been taken into account for the development of solar lead-acid batteries.

More precisely, with respect to the operation of the battery, the group of hybrid systems can be divided into three subgroups [15,16]. One group includes applications with relatively small discharge currents but a high number of partial cycles at different SoCs. The temperature range is often between +5°C and +30°C. The second subgroup requires medium discharge currents and a high number of partial cycles, but SoC is always close to 100%: this means that normally there should be no deep discharge of the battery. These batteries are often installed in the house's cellar and work in the temperature range between +5°C and +20°C. The third subgroup requires rather high discharge currents and there are very deep discharge cycles, sometimes down to 20% SoC or even below. Such batteries normally work in rooms with a relatively constant and moderate temperature between +15°C and +25°C.

As already discussed above, the cut-off voltage for a deep discharge protection, where the battery is disconnected in order to stop a further discharge, has to be chosen carefully by taking into account that at low discharge rate the voltage is quite close to the open circuit voltage (OCV). Then, the voltage limit for disconnection should be on a relatively high level. For example, 1.90 V per cell could be too low at the 100-h discharge rate, as the limited polarization would keep the battery voltage just below the OCV value.

The efficiency of the complete system is an important factor for solar and wind power applications. The efficiency of the lead-acid battery is relatively high. The exact figure depends, of course, on the application. However, in many cases, the Ah efficiency is above 95%, typically 97%, and the Wh efficiency is above 90%, typically 91%. These figures are much better in comparison with those of other battery systems: for example, NiCd has ~90% Ah efficiency and ~80% Wh efficiency [17].

Although special lead-acid batteries have been developed for solar or wind power applications, sometimes in developing countries, for cost savings or a lack of availability of solar batteries, standard starter batteries are used with capacities in the range 50 – 150 Ah. Because starter batteries are optimized for high cold cranking power but not for the special requirements in solar and wind power applications, such batteries usually fail rather early and have to be frequently replaced. In general, due to this rather poor service life, such a strategy is, in the end, more expensive than to accept the higher cost of a solar battery having a much longer service life.

9.3. Flooded Batteries

A general overview of the lead-acid battery technology has been given in Chapter 7. The container size range of flooded lead-acid batteries for solar and wind power systems is the same as for the other stationary applications. On the positive side, there are either flat plates or, when high capacities are needed, tubular plates. The latter are used in 2 V cells of the OPzS type. The smaller types with flat positive plates are 6 or 12 V monoblocks. Contrary to the 10-h rate capacity given as the nominal performance of standby batteries, the solar battery versions have the 100-h rate capacity as the nominal performance. The difference in capacity between 10-h rate and 100-h rate capacity is about 20%. This means that, for example, a 360 Ah (100-h discharge rate) solar battery has the same container size of a 300 Ah (10-h discharge rate) standby battery.

Acid stratification is a serious problem of flooded batteries used in cycling applications [18-24]. Indeed, in typical cycling applications like traction duties, very soon a significant acid stratification can appear. However, with a strong overcharging, sometimes up to a charge/discharge factor of 1.2, *i.e.* 20% overcharging, there is a strong gassing inside the cell causing some movement of sulfuric acid and therefore, a remix of the electrolyte. Acid stratification is largely determined by the depth-of-discharge (DoD): the deeper the discharge the more intensive is the acid stratification.

Figure 9.3 shows the typical development of acid stratification in an OPzS cell over just a few cycles. In this example, cycling included a 100% DoD discharge in each cycle and not much overcharging. There was not much gassing and therefore, there was no possibility for a remix of the electrolyte. An alternative to overcharging is the use of an electrolyte circulation system, which periodically forces some movement of the electrolyte.

As already discussed, extension of service life of batteries used in solar and wind power applications is an important point with regard to the total cost of such systems. Increase of the positive grid corrosion resistance and improvement of the positive active mass cycling performance are key points.

There were a couple of investigations in the past years on how to improve these parameters and details about the achieved results are given in Chapter 7. Modern batteries have high corrosion resistant grids and a rather good cycling performance due to better active mass structures. Nowadays, the failure mode of the battery is not always connected to positive grid corrosion or positive active mass degradation, as active mass sulfation effects due to some undercharging of the battery also need to be considered.

Sulfation occurs when, after a discharge, the charging of the battery does not give a complete transformation of lead sulfate back to lead and lead dioxide. If this occurs during several discharge/charge cycles, an accumulation of lead

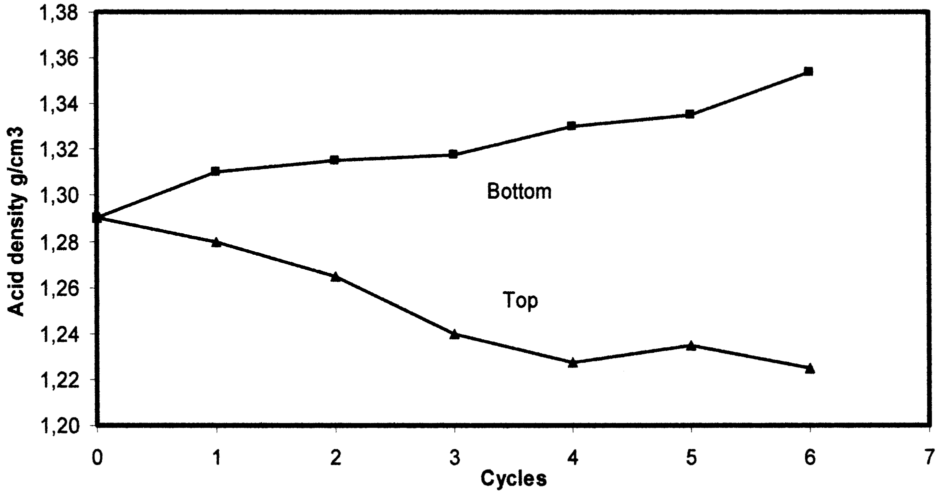

Figure 9.3. Example of acid stratification in flooded batteries used in cycling applications, when there is no overcharging with gassing and no electrolyte circulation system.

sulfate in the plates takes place. This reduces the concentration of sulfuric acid and results in a lower available capacity. Moreover, there is a second negative impact: the lead sulfate reduces the active mass surface area and decreases the diameters of the pores. This slows down the transport of sulfuric acid into the pores giving a further reduction of the available performance of the battery.

Actually, the situation is even worse. Lead sulfate deposits as a crystalline structure with very small crystals having a very high surface area, this resulting in dissolved lead sulfate during charge. However, if there is not a complete recharge very soon after the discharge, a re-crystallization of lead sulfate occurs with the effect that the very small crystal structure with a high surface area is changed into a structure with larger crystals and much lower surface area. Re-dissolution of this aged lead sulfate is more difficult and needs a significantly longer time. The longer lead sulfate remains in the plates the more difficult is to get the crystals solved and to recharge the battery completely: after a year or so, only relatively long charging periods or special charging techniques can really help to bring the plates with this aged lead sulfate back to a fully charged state. Thus, a complete recharge of the battery soon after a discharge is advisable.

Sulfation due to some undercharging can be an indication of an unbalance between energy demand of the consumer and energy supplied by the solar generator. The choice of an optimal charge voltage limit is also an important point: increasing this limit is helpful to reduce sulfation. However, a careful choice of the limit is needed because a higher charge voltage causes more corrosion and more water consumption.

It has also to be considered that discharged or strongly sulfated batteries have a rather low sulfuric acid concentration, this favoring freezing of the electrolyte if the battery is used at low temperatures. Figure 9.4 shows how the freezing point is influenced by the acid concentration.

A fully charged battery has, for example, an acid density of 1.26 gcm^{-3} or higher and this means, according to the diagram, a freezing point below -50°C. If the battery is partly discharged and the acid density is, for example, 1.20 gcm^{-3}, the freezing point will be about -30°C and this is still sufficiently low for most of the applications. However, at lower SoCs the freezing point approaches that of water (0°C). This is something to be avoided because it can result in battery damaging, *e.g.* the container can get cracked.

In order to know about the current SoC of the battery, sometimes state-of-charge indicators are used. Such systems are quite expensive especially if a certain precision and reliability is required; however, at least larger solar and wind power systems have today a state-of-charge indicator.

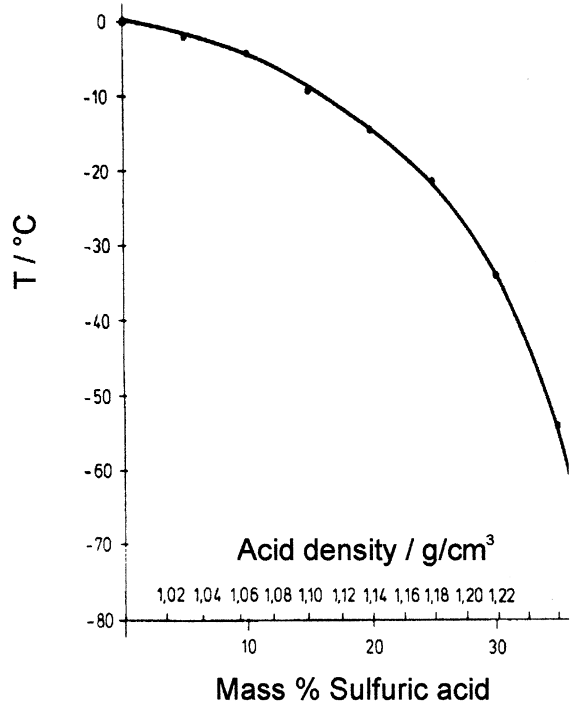

Figure 9.4. Freezing point of sulfuric acid solutions at different concentrations.

9.4. Large Batteries

For large solar or wind power plants, in general, rather large lead-acid batteries are needed with capacities of some thousands of Ah. Such batteries often consist of 2 V cells with tall plates. On the positive side, there are tubular plates that have proven to give a high reliability and a very long service life. The CSM technology with negative copper grids is suitable for a couple of solar and wind power applications where large batteries with tall plates are used. A detailed description of the CSM technology is given in Chapter 7.

Some years ago, the concept of a multifunctional energy storage system useful for improving the utilization of regenerative energy, has been evaluated [25]. This system includes three different functions: (i) uninterruptible power supply (UPS), (ii) improvement of power quality, and (iii) peak load assists via the use of regenerative power sources, with surplus energy from periods of low demand stored in a battery for peak-load periods.

Two multifunctional energy storage systems, each with a 1.2 MWh lead-acid battery, were installed in Germany. There is one system in combination with a solar power plant and another one in combination with a wind farm. The batteries consist of OCSM cells with a standard design, but modified according to the special demand of a multifunctional application. A schematic of one of these batteries is given in Figure 9.5: in total, it is a 544 V, 4140 Ah battery; there are three battery strings in parallel whereas each string has 272 cells in series with a capacity of 1380 Ah.

The battery consists of 2 V OCSM cells and has positive tubular plates and copper as the negative grid material. A low antimony grid alloy is used on the positive side. The cell container is made of transparent SAN and HAGEN patentpole is used with copper inserts. A special lid has been designed which has five holes, two for the cooling pipes, one for the electrolyte agitation system, one for the automatic water refilling system and one as an option to install an electrolyte level indicator. In 24 cells, this hole is used for temperature sensors.

There is an automatic water refilling system for each cell, so that maintenance work can be kept to a relatively low level. Actually, a battery filling system has been put on the cells and connected to a large 280 l water tank that serves as a water reservoir for the complete battery. This tank is automatically filled with water via an ion exchanger.

As discussed above, acid stratification is a well known problem especially in the case of large cells. A way to overcome this problem is to overcharge the battery significantly, resulting in a marked gassing that can re-mix up the electrolyte. Unfortunately, such a strategy gives a markedly worse charge efficiency. Moreover, it increases significantly water loss and heat generation in the cell. The use of an electrolyte agitation system can avoid all

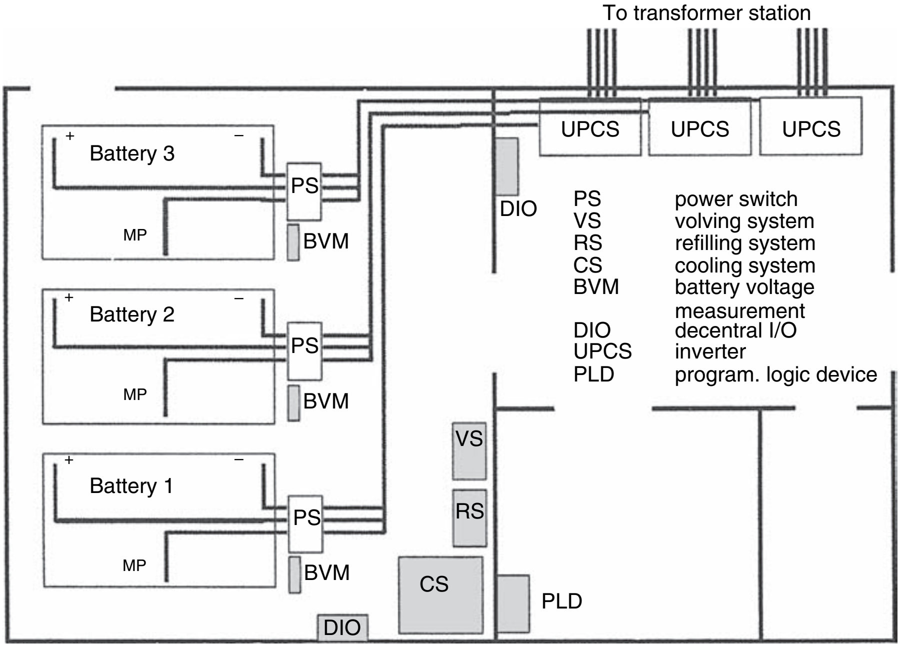

Figure 9.5. Schematic of the 1.2 MWh multifunctional lead-acid battery.

these disadvantages. The development of the multifunctional battery has included some work on the electrolyte agitation system. The same principle applied for the BEWAG battery (see Chapter 7) is used; however, the system has been slightly modified according to the demand of the 1.2 MWh battery. A central compressor supplies the air blown into all cells. For the complete battery, the amount of air is about 24 m^3/h. Every day, the electrolyte agitation system is in use for about 15 min, which is effective in equalizing the acid concentration.

The application as a multifunctional battery includes, at least occasionally, a rather extensive use of the battery with relatively high current. In order to avoid higher temperatures or marked temperature differences within the whole battery, a special cell design was developed which includes plastic pipe heat exchanger. Each cell has four windings of a plastic pipe with an inner diameter of 3 mm. In order to have enough space and to keep the windings completely within the electrolyte, a larger cell container with a height of 797 mm was used. This provides an increase of the electrolyte minimum level of about 40 mm.

Although the distance between the minimum and maximum levels was reduced markedly, which is possible in case of an automatic water refilling system, the terminals had to be extended too by about 20 mm. The cooling system has a power of 40 kW. For the battery in Herne, at the solar power plant, four cells are cooled in series in one circuit, whereas for the battery in Bocholt, at the wind farm, there are only two cells cooled in series. The cell separation is 10 mm and the battery temperature is measured by 24 PT100 sensors.

As the batteries supply rather high power and since slightly longer terminals are used, the terminals have copper inserts that have been extended from the top of the terminals down very close to the top bar in order to minimize the internal cell resistance. The cells have four terminals, two in parallel for each polarity. The voltage of groups with eight cells together is measured during use in order to control any deviation from balance within the battery. The cells are connected by flat copper bars each of 300 mm^2, which means, in total, a connection with 600 mm^2 as two terminals are used in parallel.

A group of six 1380 Ah OCMS cells were tested in the laboratory in order to confirm the expected performance of the battery. After the standard capacity investigations with different discharge currents, some high rate discharge tests were also carried out. Figure 9.6 gives the discharge curves for the 1380 Ah OCSM cells at constant power discharge of 1.47 kW and 2.94 kW per cell. It can be seen that the voltage of OCSM is at a relatively high level for a rather long

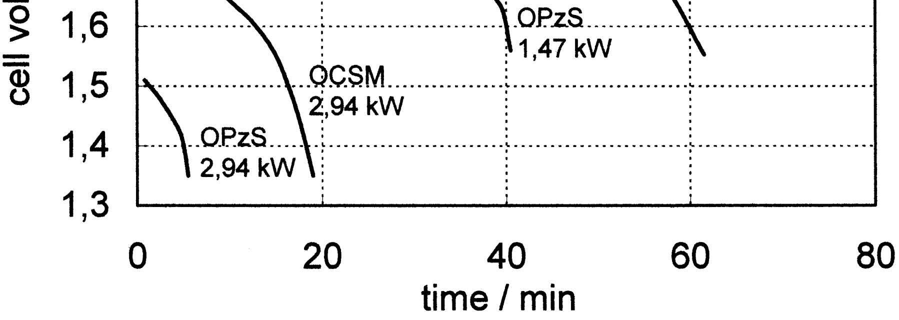

Figure 9.6. Discharge curves of the 1380 Ah OCSM cells in comparison to standard OPzS cells at high discharge rates with constant power of 1.47 kW and 2.94 kW, respectively.

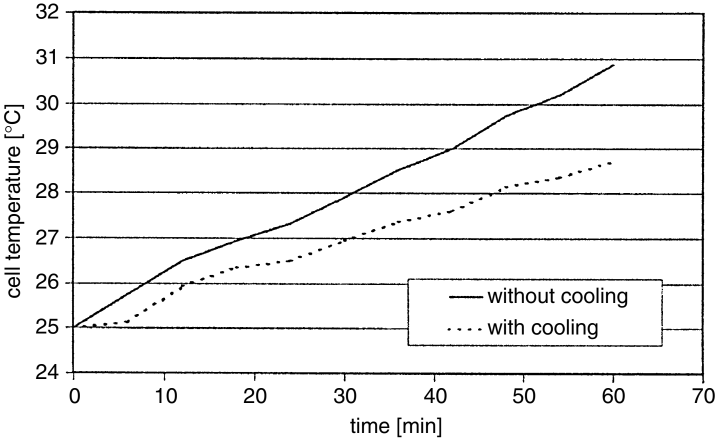

Figure 9.7. Change of electrolyte temperature of the 1380 Ah OCSM cells for the multifunctional battery during a 1-h discharge at 818 A with and without cooling.

part of the discharge even at the high rate of nearly 3 kW per cell. This is the typical behavior of a cell with copper as the negative grid material. The diagram shows also the discharge curves of standard OPzS cells with the same weight and size. The much better performance of the OCSM design can be seen clearly. In a test of charge acceptance, again the OCSM cells behaved markedly better in comparison to the standard OPzS design due to their much lower internal resistance.

There was also a test of all the other components, including electrolyte circulation, automatic water refilling and cooling system, and it turned out that they all worked properly. Figure 9.7 shows the result of a test on the cooling system during 1-h discharge at 818 A, where 3 cells out of 6 were cooled. The flow rate of the cooling water, with a temperature of 18°C, was 300 ml per minute. During the 1-h rate discharge, the electrolyte temperature increase was about 4°C with the cooling system and about 6°C without it. This result confirms the efficiency of the cooling system.

To achieve a large variety of functionality for the two batteries at Herne and Bocholt, a converter is used that can transfer active and reactive power from and to the electric grid. Moreover, to perform active filtering, the converter has a fast and intelligent control system. The three functions are:

- Substitution of peak-load power by stored solar/wind energy.

The use of a battery makes it possible to substitute the required peak-load power by stored power from renewable energy sources (solar or wind) with high efficiency. This smoothing of system load by the use of storage leads to an improved use of the existing system capacity and, thus, to delay in system extension measures. At the same time, the transmission losses in the system and the costs for the reserves are reduced. The cost advantages that are achieved by the reduction of the primary energy use and the optimal use of the power station and grid capacities result in attractive tariffs for the customers of utilities.

- Improvement of reliability of power supply.

Structural changes and steady modernization of production plants cause a growing use of high technology equipment (electronic control, microprocessors, *etc.*). These plants react to inevitable disturbances in electric grids by functional interruptions, malfunctions or failure leading to production interruptions and to process stops. In this connection, the energy storage represents an uninterruptible power supply for the time of failure.

- Improvement of quality of power supply.

On the consumers' side, the requirements regarding power quality are growing steadily. In the case of discontinuous production by renewable energy sources using power converters, the sinusoidal shape of the power is corrupted by harmonics that have disturbing effects on parallel operating, vulnerable consumers. The subject of system perturbation is discussed more and more intensively. In the future, a reduction of the permitted disturbance level may be expected for a secure operation of existing grids. In most cases, present disturbances may be compensated more economically if energy storage systems with suitable power converters are used instead of system extensions. The power converter used in Herne and Bocholt consists of a real-time control algorithm to compensate disturbances of load voltage by triggering the insulated gate bipolar transistors (IGBT) of the converter bridge.

For both the solar power plant in Herne and the wind farm in Bocholt, a Unified Power Conditioning System (UPCS) was used. Details about the development of this system are given in Refs. [26-28]. Figure 9.8 shows the

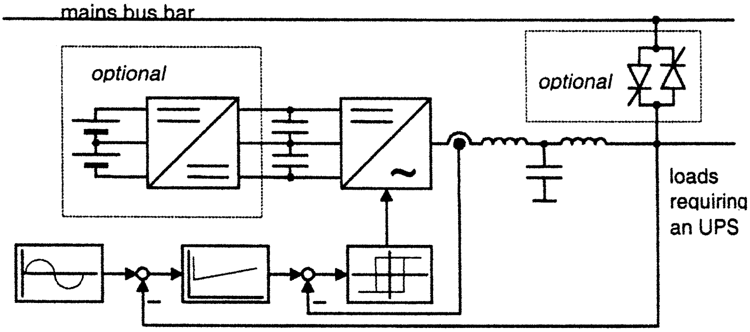

Figure 9.8. Instantaneous voltage control of the UPCS.

design concept of the UPCS. It consists of an optical static switch, an IGBT converter, a filter circuit and, optionally, a d.c./d.c. converter with a battery. The converter consists of three individually controlled IGBT half bridges. It is fed by a split d.c. link. The neutral is directly connected to the midpoint of the d.c. link. Each half bridge has an output filter to suppress the high frequency harmonics produced by the converter [27]. There is no output transformer needed to connect the UPCS to the low voltage busbar.

A test configuration was set up with a supply transformer, loads, a 100 kW-rated UPCS and a welding device with adjustable duration of operation and pause mode. The welding device was used in this test to produce voltage dips that can be measured as a voltage flicker. Figure 9.9 shows PCC voltage dips over refresh rate, which are reduced to a compatibility level by the use of the UPCS. In addition, the short-term flicker value P_{ST} is reduced significantly.

The energy storage system is divided into three modules, each consisting of a 400 kW-rated power converter and a battery string with a nominal voltage of 544 V and a 10-h rate capacity of 1380 Ah. These three storage modules are controlled by a process automation system.

This system is divided into a data acquisition and a data evaluation module. For an optimal battery operation, sufficient data describing the actual battery stage are necessary. Thus, a specific data acquisition system for the battery has been installed, which gathers information on charge and discharge currents, cell temperatures and cell voltages in groups of eight cells. In addition, the converters and auxiliaries are measured and controlled. The data

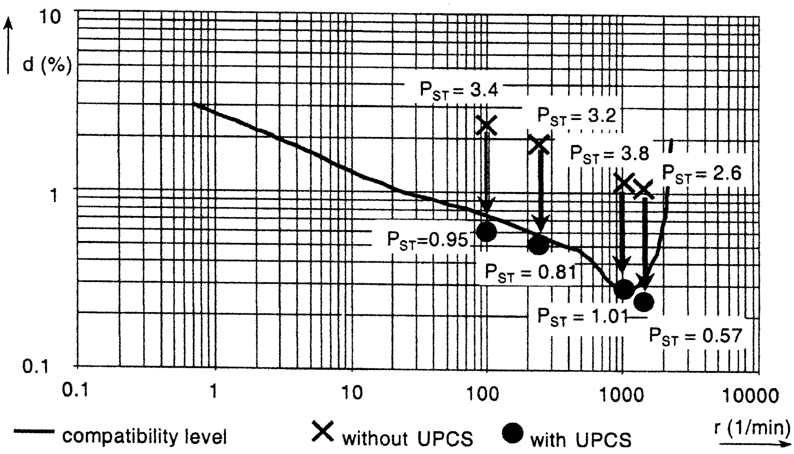

Figure 9.9. PCC voltage dips over refresh rate and short-term flicker caused by welding equipment with and without 100 kW-rated UPCS.

communication with the operator of the electrical grid is important for a correct operation of the energy storage system.

A major part of the automation system is the data evaluation unit that is generating commands for battery control. Highest priority is given to the safety relevant information, followed by measurement validation and generation of typical battery data from acquired data. Data validation is primarily the detection of possible measurement errors, which is done by range checking. Range checking gives also information on points in the system where the measured values cling to the upper or lower limit of the possible range of the equipment. Equipment malfunction can easily be detected as well. Methods for data evaluation are mainly data smoothing or offset correction: this is done to achieve high data quality and reliability.

Further validation concepts are used to get additional information on the data quality, especially in the case of measuring in wide ranges, *e.g.* measuring the battery current covering a range from a few amperes up to 1 kA. Battery specific data like discharged Ah describing the state of charge cannot be measured directly, so they have to be calculated. Calculated data form a base for estimating the reserve power of the battery and the necessary operating time on the grid. Comparing the two values leads to an optimized operation.

The relatively high d.c. voltage of the battery strings leads to problems with the data acquisition as far as galvanic separation is concerned. In order to avoid this problem, special modules are used to provide the necessary voltage separation ability. These modules need their own bus system, which can be connected to the general bus system by so-called bridges.

The general bus system is the main communication line. Transferred data are not only measured data but commands as well. Data evolution is responsible for creating decisions for the PLD (Programmable Logic Device) to give out signals to the converters and the other peripheral units. These commands influence the state and the mode of the energy storage modules, *i.e.* by activating or stopping the converters, setting desired values for power transmission, activating or stopping the auxiliaries, *etc.* While the process control is done by a PLD, an operator can interact through a visualization system. Moreover, the visualization system gives information on the process state and controls the database.

The two systems in Herne and Bocholt were installed in 1998 and are still working properly without any significant problems. The batteries too are still in good conditions. The experience gained in Herne and Bocholt have shown that such multifunctional battery energy storage systems can be used successfully to improve the utilization of renewable energy (solar and wind power) [29]. This is an example of how batteries are used together with solar and wind power systems when there is a connection to the electricity grid. In the future, there will be an increasing market for large lead-acid batteries, especially as there is a growing demand for high-quality power arising from the sensitivity of many operating systems to the perturbation of electric grids. Flooded batteries can be used for such utility applications, but the VRLA battery type is an option where floor-space is limited. A careful design, especially of large batteries, is necessary, however, in order to avoid potential difficulties such as temperature inhomogeneity. The next sections give a couple of application examples with VRLA. This includes both smaller and larger sized batteries of the gel and AGM type.

9.5. Small Systems with VRLA Batteries

VRLA batteries, *i.e.* maintenance-free batteries, have a couple of advantages in comparison to the conventional flooded types. For example, topping up with water is not necessary over the whole life of the battery, self discharge is very low and there is no risk of acid spillage. The features of the VRLA technology and a detailed description about the gel and AGM types used for standby applications are given in Chapter 7.

As for the batteries for telecommunication and UPS service, there has been also a clear tendency towards the VRLA design for solar and wind power applications. Contrary to the standby service, the solar and wind systems use often gel batteries rather than the AGM design. This is because there is not a high power requirement in many of these systems. However, in systems with high power requirements, AGM solar batteries are chosen.

Similar to the flooded batteries for solar and wind applications, there is often no difference in the container size between batteries used for standby and those used for solar/wind applications but, again, for solar batteries the capacity is related to the 100-h discharge rate rather than the 10-h rate used for standby batteries. This is valid for most of the VRLA solar batteries, small batteries with flat plate design as well as larger batteries with tubular design.

Stand-by duty, *e.g.* telecom and UPS, does often not include much cycling operations and, therefore, a moderate charge voltage is chosen in order to keep positive grid corrosion and water loss to a low level [30]. For solar or wind power operations, in many cases the application includes a significant cycling duty. In addition to a different cell design of batteries specially developed for such applications, there is also the need for a different charge strategy and charge voltage in order to keep the batteries healthy and in good conditions.

In general, for more intensive cycling, a significantly higher charge voltage is needed to avoid a reduction of service life of the battery due to undercharging and sulfation. On the other hand, a too high voltage gives unacceptably high grid corrosion and water loss, which can limit the battery life.

It appears that in solar and wind power applications the batteries suffer more from undercharging and sulfation than from grid corrosion and water loss. This means that often the charge voltage was not high enough to charge the battery properly. Especially gel batteries with taller plates and marked cycling duty require periodically a relatively high charge voltage to avoid sulfation of the positive plates. However, charge regimes with higher charge voltage have to be chosen carefully. A pressure-release valve with a higher opening pressure could be helpful in reducing water loss but the effect is not sufficient to justify other problems that must be faced with high gas pressure in the cell. In general, a pressure between 100 and 200 mbar seems to be a good compromise to avoid excessive loss of water.

Therefore, optimization of charge strategies is an important point in order to extend service life of gel and AGM batteries in solar and wind power applications [31,32]. Some years ago, a program to investigate and improve the charge strategies of VRLA batteries in such applications was developed. An investigation of the discharge strategies (for example, the maximum acceptable DoD) was also included. The most important results of these investigations are given below.

Part of the investigation was performed in Freiburg (Germany) at the 'Solarhaus Freiburg'. This house had already been used as a test field for solar power applications. The investigation was with both types of VRLA batteries, AGM and gel. The PV hybrid system was connected to the electricity grid and this connection was used as the back up system instead of a diesel or gas generator.

The 192 V battery had flat positive plate design. The PV hybrid system was divided into four part systems, each as a 48 V unit with a 48 V battery, a 1000 Wp solar generator, a charge controller and a rectifier for the back up by the electricity grid.

Figure 9.10 shows a schematic of the complete system. Three of the 48 V units consisted of gel monoblocks, each of 12 V and 155 Ah, whereas the fourth 48 V unit had AGM monoblocks, each of 6 V and 144 Ah. The capacity of the gel monoblocks was 185 Ah at the 100-h rate and 155 Ah at the 10-h rate. For the AGM design, the capacity was slightly lower, 170 Ah at the 100-h rate and 144 Ah at the 10-h rate. All monoblocks, *i.e.* the complete 192 V battery, were in one string so that for all cells the discharge load was the same.

The maximum charge current from the solar generator was 19 A, the charge current from the electricity grid as a back up was 20 A, and the maximum discharge current was 25 A. The temperature of the batteries depended on the time of the year and was in the range 12 - 25°C.

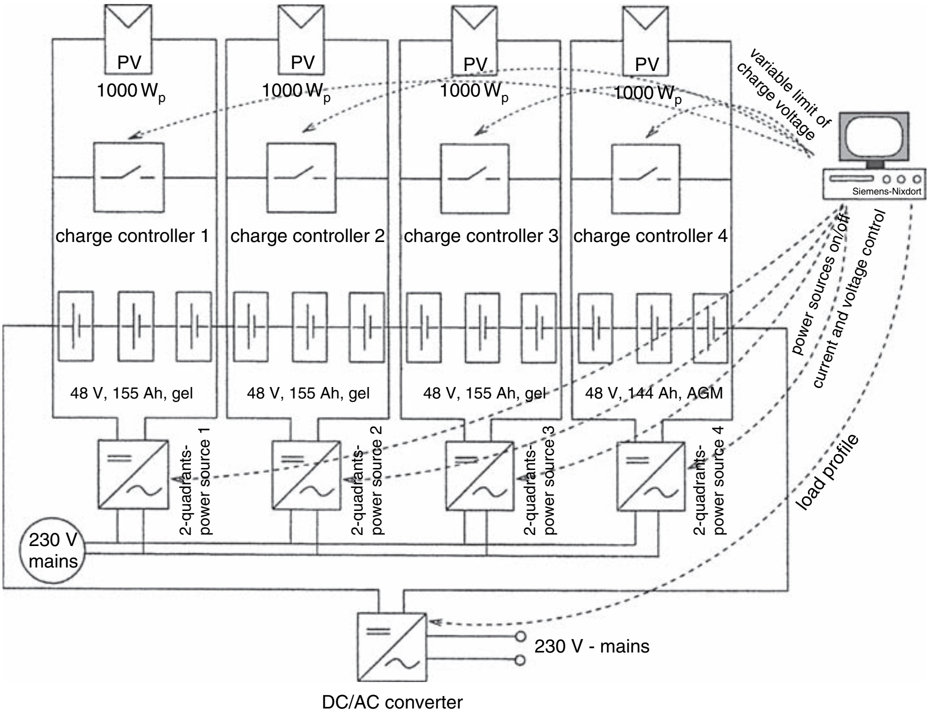

Figure 9.10. Schematic of the solar power system with a 192 V, 155 Ah battery with flat positive plates and four partial systems (three with the gel design and one with the AGM design) with a back up system at the Solarhaus Freiburg. Part systems 1-3: 12 V modules, 155 Ah (positive flat plates, gel); part system 4: 6 V modules, 144 Ah (positive flat plates, AGM)

The four partial systems could be charged individually both from the solar generator/charge controller and the electricity grid/rectifier. In turn, a computer controlled the charge controllers and the rectifiers. This computer was also used for the measurement and storage of all relevant data. This included the individual monoblock voltage and all currents flowing into, or out of, the battery, the solar generators, the rectifiers and the load. There were four different charge strategies where the limitation of the charge voltage was between 2.30 and 2.45 V per cell, as shown in Table 9.1.

At least every 30 days there was a 'solar full charge' of the battery according to the parameters given in Table 9.1 either by normal operation of the PV generator or by an extra charge operation of the back up charging unit. After such a 'solar full charge', the recharge was stopped and the DoD calculation (based on an Ah balance) was set to 0%.

Table 9.1. Differences in the charge/discharge strategy of the solar hybrid systems at 'Solarhaus Freiburg'.

	System 1	System 2	System 3	System 4
Battery type	Gel flat plate	Gel flat plate	Gel flat plate	AGM flat plate
Max. DoD (%)	70	70	70	70
Max. charge voltage (V/cell)	2.35 no time limit	2.45 max. 2 h per day then 2.35	2.30-2.45 depends on DoD	2.35 no time limit
Duration at maximum voltage until 'solar full charge' is assumed	5 h	2 h	depends on voltage	5 h

Every half a year the capacity of the batteries was tested by a discharge after a typical 'solar charge' regime followed by a second discharge after a rather intensive charge regime. This means that, before the first discharge, there was a charge according to the criteria given in Table 9.1. The intensive charge before the second discharge was a constant current/constant voltage/constant current IUI_a charge where, at the final stage, the battery voltage was significantly higher than during normal operation. The charge was terminated when 112% of the nominal capacity (or of the previous discharged capacity, if it was higher than the nominal capacity) had been recharged. The exact charge program for the IUI_a charge was: $I = I_{10}$, $U = 2.35$ V per cell, $I_a = 0.08 \times I_{10}$. After the second discharge, the battery was charged with the solar typical charge regime and could be used again in the solar power system.

The aim of this time-consuming procedure was to show the difference between the available capacity for the user (first discharge) and the state of health of the battery (second discharge). The differences are very important with respect to the available capacity of the system on one hand and, on the other hand, with respect to the guaranteed service life periods given by the battery manufacturer. As the results have shown, there were differences of up to 15% between the first and the second discharge.

This has also implication on the definition of the state of charge and the full state of charge. According to the definition given in Ref. [33], the 'solar charge' regime gives the 'practical full state of charge' ($FULL_p$) and the corresponding state of charge is the 'practical state of charge' (SOC_p). These definitions take into account that the user of the system has no access to the complete capacity of the battery because the charging conditions in PV systems do not allow a complete recharge of the battery. The second charge regime with the '112% charge' gives a 'full state of charge' (FULL) and this corresponds to

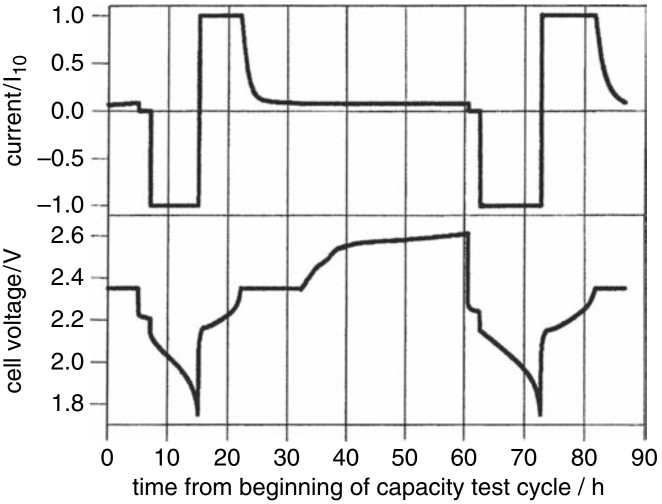

Figure 9.11. Typical current and voltage profile during the capacity test cycle with a solar charge, an I_{10} discharge, a 112% IUI_a charge (intensive charge) and a second I_{10} discharge. This test profile was used in all field tests.

the 'relative state of charge' (SOC_r). This is the capacity defined on the basis of the actual state of health of the battery. However, as mentioned above, this does not correspond to the available capacity for the user. A complete list of definitions on state-of-charge and related parameters under various operating conditions is given in Ref. [33].

Figure 9.11 shows a typical current and voltage profile of the capacity test cycles with the 'solar' IU charge (duration of I charging depends on state of charge of the battery at the beginning of the test), a first discharge (10-h rate), an IUI_a recharge to 112% of the previous discharged capacity or the nominal capacity (called the 'intensive' charge), a second 10-h rate discharge and an IU recharge to bring the battery into operation again.

Because of the capacity tests, the batteries got twice a year an intensive recharge. However, this is not available in the field with today's technology of PV systems.

Figure 9.12 gives the SoC of system 1 at the 'Solarhaus Freiburg' over a period of about 390,000 minutes (272 days). A capacity test in July after about 370,000 minutes can be seen from the deep discharge peaks. After about 260,000 minutes there were several days where the battery was fully charged (100% DoD), whereas most of the time the SoC was between 30% and 70%.

A study of the results of the investigations on the batteries at 'Solarhaus

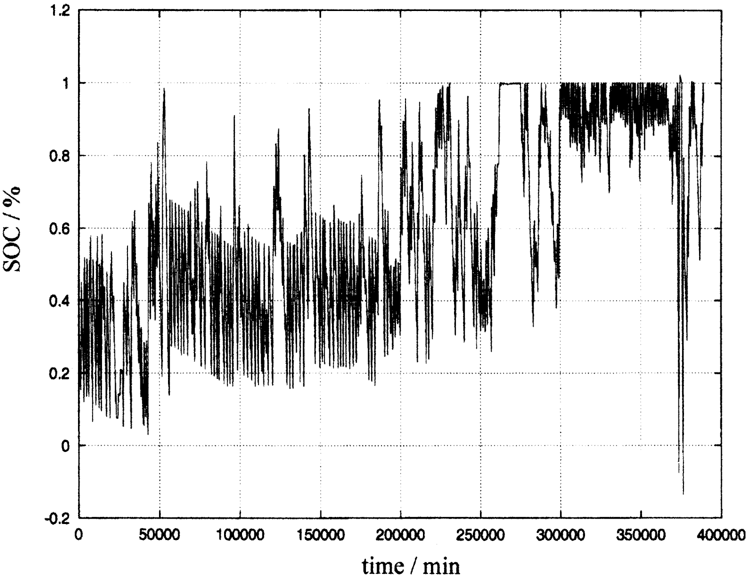

Figure 9.12. SoC of system 1 at the Solarhaus Freiburg over a period of about 390,000 minutes (272 days).

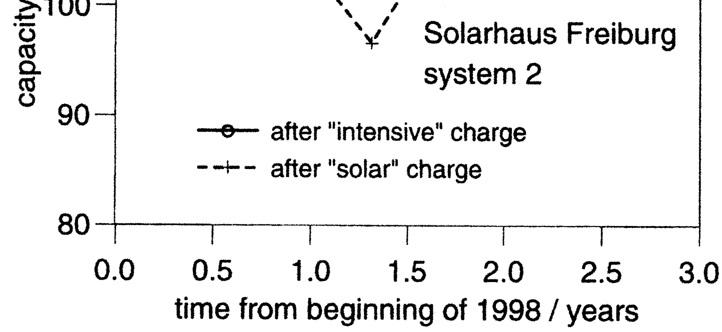

Figure 9.13. Development of the 10-h rate capacity of system 2 (gel, flat plate) at Solarhaus Freiburg, after 2 years of service, before and after an intensive charge.

Freiburg' after 2 years of service showed that there was indeed a difference in the capacities (5 - 15%) after the 'solar charge' and the 'intensive charge'. Figure 9.13 shows the results of these capacity tests. The deviation of the capacities of the individual gel monoblocks was quite low, whereas the deviation of the AGM monoblocks was more marked.

In the last stage of charge, the voltage of the individual monoblocks varied significantly, a phenomenon which is well known from other applications especially in the early stage of the battery life. It can be explained by some differences in the recombination behavior of VRLA batteries and, contrary to flooded cells, it does not indicate a battery failure. Figure 9.14 shows the voltage dispersion at the end of charge of one of the 48 V part systems with 6 V monoblocks of the AGM design. Some of the monoblocks had a relatively early increase of the charge voltage returning to lower values later, whereas other monoblocks had the voltage increase much later. This different behavior does not influence the capacity of the cells as it can be seen in Figure 9.15 from the results of the next 10-h rate discharge test of the same 8 AGM blocs.

The different charge regimes on the flat positive gel batteries are compared in Figure 9.16. There is not much difference with regard to the capacities after an intensive recharge but the capacity of the system with the highest charging voltage (2.45 V per cell in system 2) is significantly better than those of the other systems. All used charge regimes could not avoid

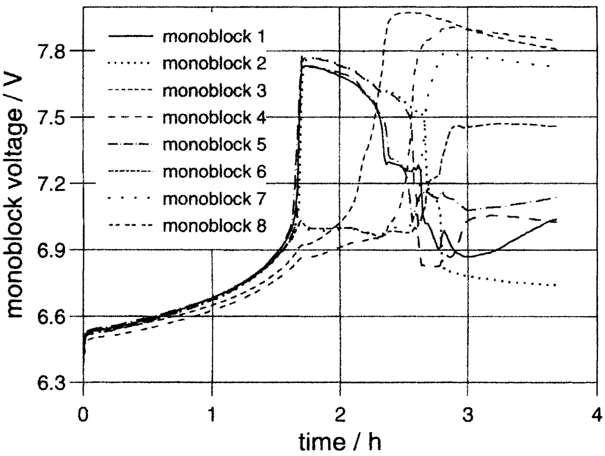

Figure 9.14. Voltage dispersion at the end of charge of system 4 at Solarhaus Freiburg with 6 V monoblocks of the AGM design.

completely some undercharging, but the capacity can be recovered by an extra charge with higher voltage.

These are the main results and the conclusions from the investigations at the 'Solarhaus Freiberg'. The total energy turnover per year of the battery was

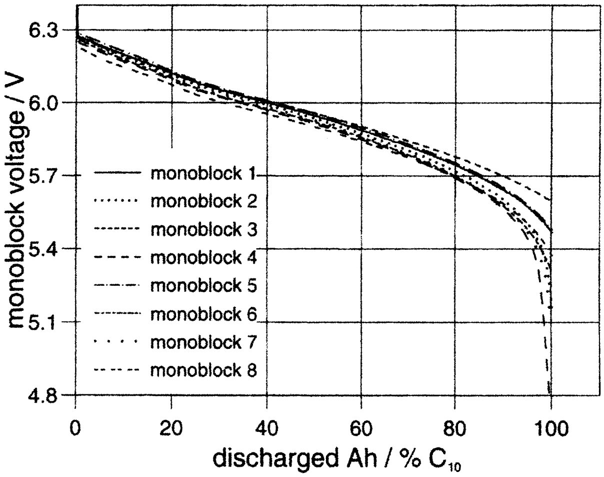

Figure 9.15. Discharge at the 10-h rate of the same 8 AGM blocs after the charge shown in Figure 9.14.

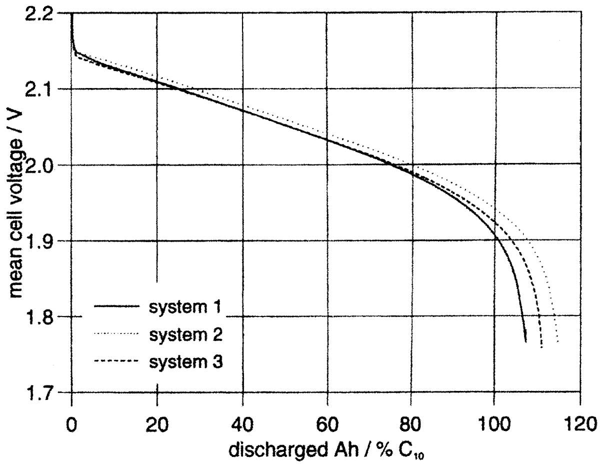

Figure 9.16. Influence of the different charge regimes on the flat positive plate gel batteries at the Solarhaus Freiburg after 2 years of service. The curves represent the average cell voltage during discharge with the 10-h rate after an intensive charge.

about 100 times the nominal capacity. The charge factor was very close to 1 in the beginning but there was a slight increase over the time to about 1.03 after 2 years. Due to this increase, the energy efficiency was slightly reduced but still around 90% after 2 years. The different charge strategies had not much impact on the discharge performance and service life of the batteries. Systems 2 and 3 had higher charge voltages but this had not significantly improved the capacity. All three systems with gel batteries had smaller deviations than the system with AGM batteries.

Another part of the investigations was performed with rather small systems with no back up. Again, both types of VRLA batteries (AGM and gel) were used. In total, the investigation included 16 systems, each with 28 V:

- 8 systems: 12 V modules, 41 Ah (positive flat plates, gel)
- 8 systems: 12 V modules, 45 Ah (positive flat plates, AGM)
- Load: 7 W per system
- Solar generator and no back up.

These systems were significantly different from those at 'Solarhaus Freiburg'. For the latter, the load could vary strongly and depended mainly on the decision of the people living in this house, whereas the load for the small

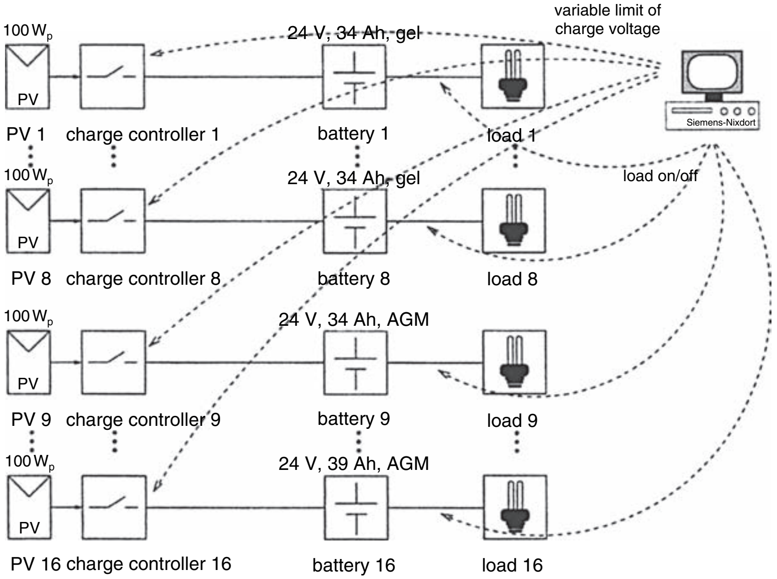

Figure 9.17. Schematic of 4 out of 16 small solar power systems, each with a 24 V battery with flat positive plates. Eight partial systems have the gel design (34 Ah) and the other eight have the AGM design (39 Ah).

systems was rather constant. There were in total 16 individual systems each with a 100 W_p solar generator, a charge controller, a light as a 7 W load and a 24 V VRLA battery. Eight systems had a gel battery with a capacity of 41 Ah at the 100-h rate and 34 Ah at the 10-h rate, and the other eight systems had an AGM battery with a capacity of 44 Ah at the 100-h rate and 39 Ah at the 10-h rate. All batteries consisted of 12 V monoblocks of the flat plate design.

Four of the partial systems are shown in Figure 9.17. The computer controlled the charge and disconnected the load when the voltage became too low. Additionally, the monoblocks voltage as well as all currents were measured and stored by this computer. The different charge/discharge strategies are shown in Table 9.2.

The load of 7 W could be supplied by the system over about 8 months of the year. In December, however, it was just 50%. The discharge current was ~0.25 A, this corresponding to ~150-h discharge rate. By reduction of the time of lightning, the discharged Ah could be reduced (different winter/summer operation modes). In general, during summer the load was all the time taking electrical energy whereas during winter the load was just connected over 16 h per day. The batteries were installed outside in a metallic box without any thermal isolation: the sun could shine directly on this box. This resulted in a wide temperature range (-15°C to +45°C) over the year. There was a deep discharge protection in all systems via voltage control and disconnection when a certain limit was reached. Again, different max DODs and charge strategies were tested.

Figure 9.18 gives the SoC of a small system (operating strategy 3, gel battery) over a period of ~380,000 minutes (264 days). In the beginning, in

Table 9.2. Differences in the charge/discharge strategy of the small systems.

Operating strategy	1	2	3	4
Number of test systems	4	4	4	4
Battery type	Gel/AGM flat plate	Gel/AGM flat plate	Gel/AGM flat plate	Gel/AGM flat plate
Max. DoD (%) (detected by voltage)	70	70	50	70
Max. charge voltage (V/cell)	2.35	2.40 max. 2 h per day, then 2.30	2.40 max. 2 h per day, then 2.30	2.40 max. 2 h per day, then 2.35
Max. charge voltage after load disconnect (V/cell) (24 h, accumulated)	2.35	2.45	2.45	2.45
Duration at maximum voltage until 'solar full charge' is assumed	5 h	2 h	2 h	2 h

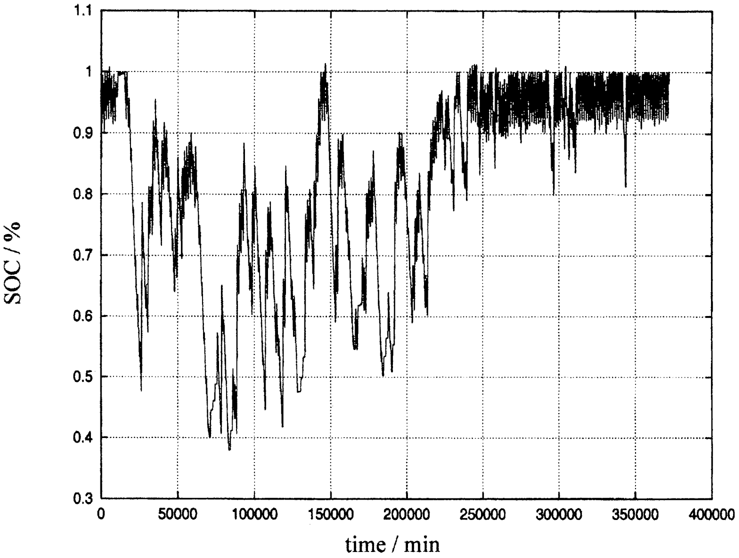

Figure 9.18. SoC of a small system (operating strategy 3, gel battery) over a period of about 380,000 minutes (264 days).

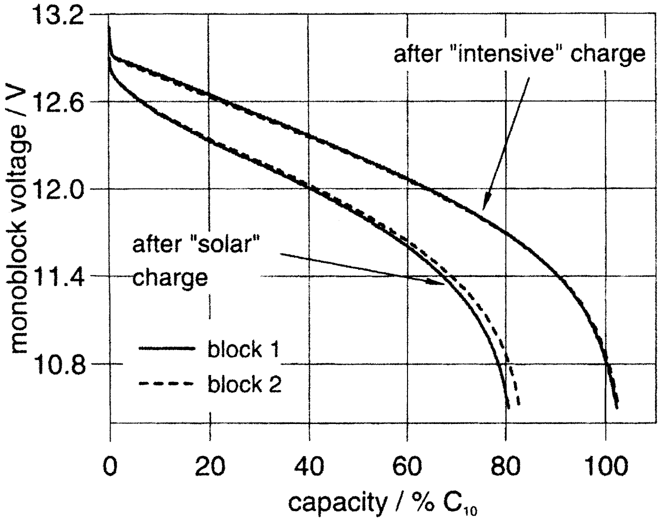

Figure 9.19. Discharge curves at 10-h rate of two 12 V gel monoblocks of small system 1, after one year of service before and after an intensive charge.

October, there was still a high SoC. Soon after, and over the whole winter time, the SOC was significantly below 100%. During the summer time, the daily discharge was about 8% DoD and every day 100% SoC could be achieved. During the winter, the load had to be reduced by about one third.

The differences between a solar typical recharge and an intensive recharge were rather high and in the range 10 - 20%. Figure 9.19 gives a typical example, by showing the discharge curves at 10-h rate of the two 12 V gel monoblocks in one of the small solar power systems with charge regime 2 after one year of service. The solar typical recharge afforded a capacity of about 80%, whereas the intensive recharge resulted in a capacity of more than 100%. The results with the other small systems were similar: there was always a difference of up to 20%, which shows that the small systems suffered even more from the undercharging under normal solar typical charge regimes than the systems at 'Solarhaus Freiburg'.

The capacity deviations of the individual gel monoblocks were quite low, whereas those within the AGM monoblocks were more marked. On the other hand, for AGM the difference between the capacity before and after an intensive charge was less in comparison with gel batteries. This could be explained by a better charge acceptance of the AGM batteries and suggests that probably the optimum charge strategies to avoid undercharging in solar power

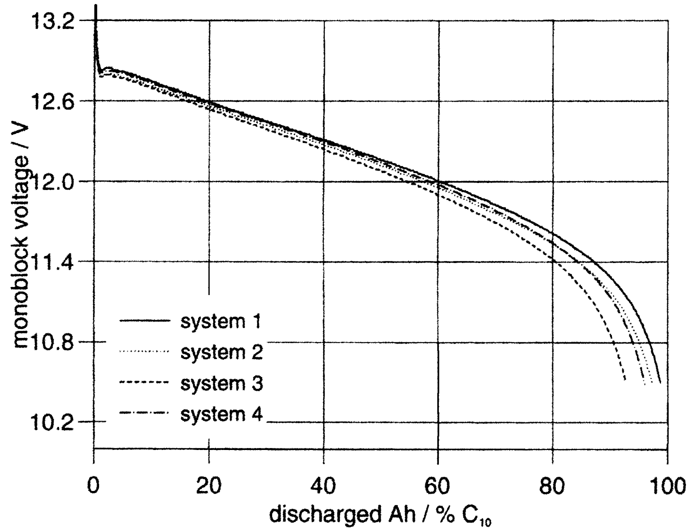

Figure 9.20. Influence of the different charge regimes on the flat positive gel batteries in the small solar power systems after 2 years of service. The curves represent the average monoblock voltage during discharge with the 10-h rate after an intensive charge.

applications should be different for gel and AGM designs.

The influence of the different charge regimes on the flat positive gel batteries in the small solar power systems is shown in Figure 9.20. It can be seen that there is not much difference between the different charge regimes after an intensive charge. However, it is remarkable that the operating strategy 3 gave the lowest capacity. System 3 has a similar charging strategy as system 2 but has a lower maximum DoD (50% instead of 70%).

It has to be realized that in the small systems the maximum charge voltage is reached almost every day between April and October, whereas in the hybrid systems the maximum charge voltage is reached much less frequently even during the summer.

The weights of the monoblocks were measured before each capacity test. The weight loss was found to be always rather low: water loss appears not to be a critical point.

These are the main results and the conclusions from the investigations of the small systems. The capacities of the batteries decreased markedly over the first 2.5 years, but then there was stabilization and no further decrease was found until the end of the test after in total 4 years of service time. The system with the lower maximum DoD (50% instead of 70%) showed the worse behavior. It seems that a restriction to a relatively low limit of the maximum DoD is not necessary and 70% DoD is acceptable without any disadvantage for the service life. There was more deviation in the performance of the AGM batteries in comparison with the gel batteries. Some of the AGM batteries had the same or an even better performance but others behaved worse, probably due to a manufacturing defect. The results confirm findings from other investigations, namely that both gel and AGM batteries can be used for such applications. However, it is rather impressive that all gel modules had very low deviations in performance in these investigations.

This was the first time that for solar power applications the influence of charge/discharge strategies on the life and performance of VRLA batteries was systematically investigated in the field. The outcome shows differences in the available capacity and deviations in the remaining capacity. Capacity tests after a solar typical charge regime reveals that the batteries could not be charged completely. However, after an intensive charge the batteries returned to full capacity.

9.6. Large Systems with Gel Batteries

Besides the smaller solar and wind power systems which require relatively small gel and AGM batteries, there are also applications where a

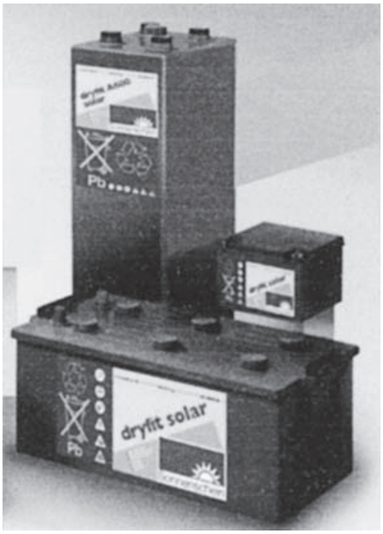

Figure 9.21. Picture of solar gel batteries. A 2 V OPzV cell with tubular plates on the left side at the back and two 12 V monoblocks with flat plates in the front and on the right side.

significant amount of stored energy is needed. In such a case, larger batteries with higher capacities are used. These batteries have often tubular positive plates. The flooded types (OPzS) have already been discussed in a previous section. There are also large VRLA solar batteries available with the same container size as the standby batteries. In most cases these are gel batteries (OPzV solar) because, with taller plates, AGM could not avoid the appearance of significant acid stratification (see also Chapter 7). Figure 9.21 shows some solar gel batteries.

In addition to the tests on smaller VRLA batteries at 'Solarhaus Freiburg', similar tests with OPzV cells were also carried out. Part of these investigations was performed at Talhof, in Germany, where there is a house not connected to the electricity grid but with an autonomic solar power system for the electric energy supply.

At Talhof, there is a PV hybrid system with a 1.8 kW_p solar generator, a gas engine with generator (5 kW) and a 48 V gel battery. The system is divided into four parts; each has a 12 V unit with a 12 V battery, a 450 W_p solar generator, a charge controller and a rectifier for the gas engine. A schematic of the complete system is given in Figure 9.22. Each of the 12 V units consists of 6 gel cells with tubular plates. The capacity is 360 Ah at the 100-h rate and 300 Ah at the 10 h rate. All cells are connected in series, *e.g.* the complete 48 V battery is one string so that for all cells the discharge load is the same. However, the four partial systems can be charged individually both from the solar

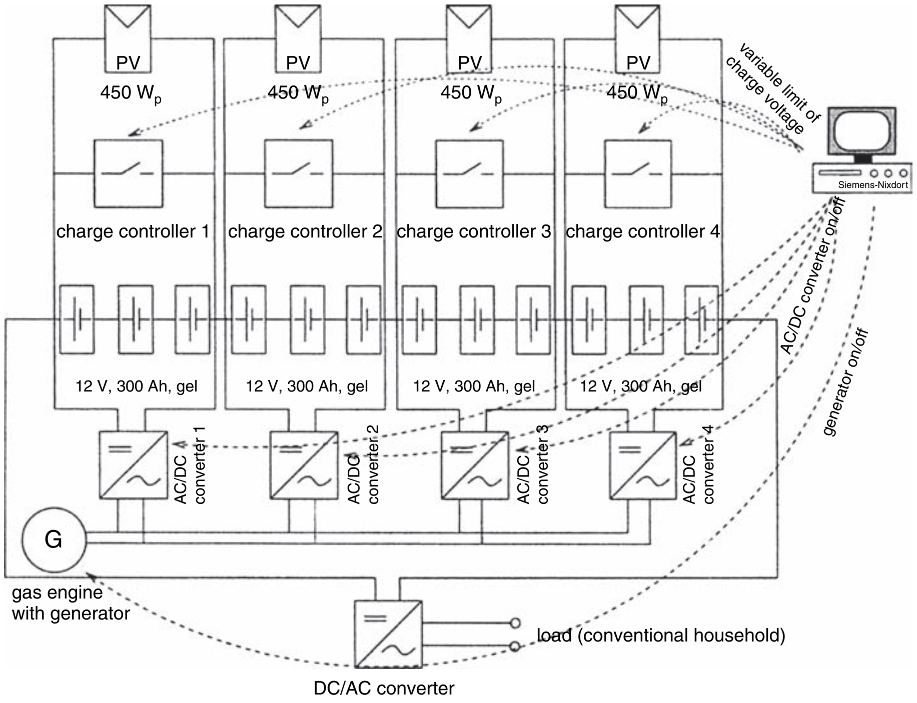

Figure 9.22. Schematic of the solar power system with a 48 V 300 Ah battery of the gel design with tubular plates and four partial systems with a back up system at Talhof.

generator/charge controller and the gas engine/rectifier.

The maximal charge current was 26 A from the solar generator and 59 A from the gas engine. The maximal discharge current was 75 A, but typical discharge currents were <10 A. The temperature of the batteries depended on the time of the year and was in the range 5 - 25°C. The intention was to use the gas engine as seldom as possible. Moreover, there was an additional restriction, *i.e.* there should be no operation of the gas engine during the night. Exceptions were only accepted in order to avoid a deep discharge (DoD > 80%) of the battery. The SoC of the battery was automatically checked in the evening and, by taking into account the expected energy consumption during the night, the battery was charged by the gas engine if necessary.

In order to avoid a very deep discharge, there was a complete stop of the discharge when DoD exceeded 90%; the control was by the battery voltage during current flow.

It should be realized that there was not a complete freedom to optimize the charge/discharge strategy just for the battery. Actually, the demands and expectance of the house dwellers had also to be taken into consideration (*e.g.* no gas engine running during the night, short gas engine running times, low gas consumption). It is much easier to develop an optimal charge/discharge strategy by neglecting such things, but in practice compromises are needed.

A computer controlled the charge controllers, the rectifiers and the gas engine. This computer was also used for the measurement and storage of all relevant data. This included the individual cell voltage, all currents flowing into, or out of, the battery, the solar generator, the gas engine and the load.

For the four partial systems, there were four different charge strategies. This means mainly the use of a different limitation of the charge voltage. The highest voltage was between 2.30 and 2.45 V per cell. The maximum DoD was 70% in three systems and 90% in one system. The different charge/discharge strategies are given in Table 9.3.

At least every 30 days there was a 'solar full charge' of the battery according to the parameters given in Table 9.3 either by normal operation of the solar generator or by an extra operation of the gas generator. After the 'solar full charge', charging was stopped and the DoD calculation (based on an Ah balance) was set to 0%.

Figure 9.23 gives, as an example, the discharge curves, after 2 years of service, of all cells of the partial system 1 after an intensive IUI_a charge. This charge procedure has already been described for the 'Solarhaus. All cells had still a capacity of more than 100%.

The influence of the different charge regimes can be seen in Figure 9.24. There is not much difference with regard to the capacities after an intensive recharge. Even the relatively high voltage limit of 2.45 V per cell could not avoid some undercharging. However, it was a reversible effect and the capacity could be recovered by an extra charge with higher voltage. It is also obvious that the relatively high voltage of 2.45 V, applied for a controlled time per day, did not harm the batteries at all.

Table 9.3. Differences in the charge/discharge strategy of the solar hybrid systems at Talhof.

	System 1	System 2	System 3	System 4
Battery type	Gel tubular	Gel tubular	Gel tubular	Gel tubular
Max. DoD (%)	70	70	70	90
Max. charge voltage (V/cell)	2.35 no time limit	2.45 max. 2 h per day, then 2.35	2.30-2.45 depends on DoD	2.35 no time limit
Duration at maximum voltage until 'solar full charge' is assumed	5 h	2 h	depends on voltage	5 h

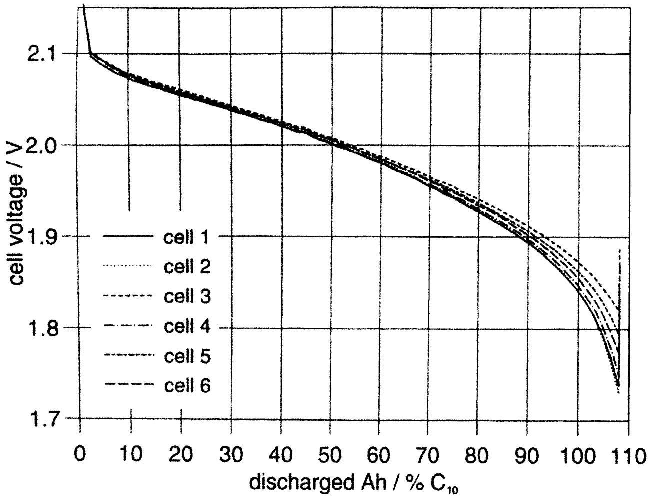

Figure 9.23. Discharge curves at 10-h rate of system 1 at Talhof, after 2 years of service with tubular plates gel cells after an intensive charge.

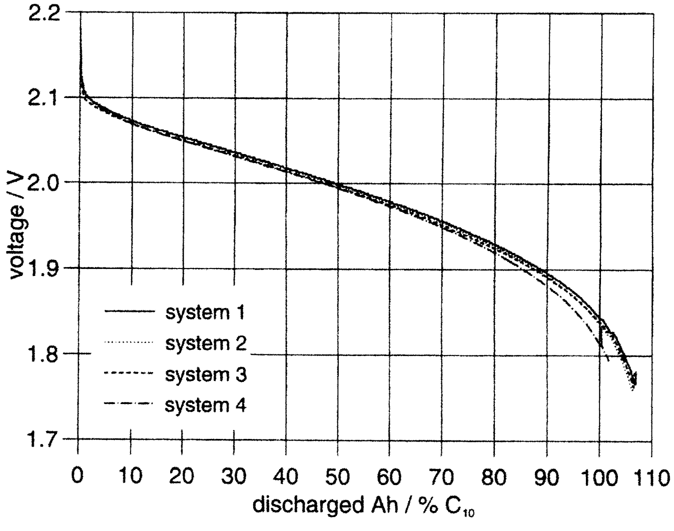

Figure 9.24. Influence of the different charge regimes on the tubular gel cells at Talhof after 2 years of service. The curves represent the average cell voltage during discharge at the 10-h rate after an intensive charge.

The energy turnover for the battery was about 100 times the nominal value per year, and the total energy consumption was 150 times the nominal value. This means that two-thirds of the energy consumption was stored firstly in the battery. The discharge/charge factor was rather close to 1 and this resulted in an energy efficiency of more than 90%, a very good value. The gas generator was used between 5 to 100 hours per month.

In total, the batteries were tested over a period of 3.5 years. Further capacity tests gave similar results as those shown in the figures above. Actually, after an intensive charge and after 3.5 years of service, the capacity was even higher than the initial one. This means that the batteries were in a very good condition and a much longer service life could be expected.

This also shows that gel cells with tubular plates are very robust and can achieve a long service life during operation in solar and wind power systems. Of course, there was every half a year an intensive charge to avoid sulfation. Indeed, the total charge/discharge factor including the intensive charge procedures was just slightly over 1. Without these intensive charges, this factor would have been even lower, and probably too low to avoid some undercharging. It can also be concluded that the different charge regimes as well as the different DoDs had not resulted in a significantly different performance of the batteries within the service time of 3.5 years.

There was another investigation about the best charge/discharge strategies at the ‘Rotwandhaus’ in the Alps, which has an autonomic electric energy system and is not connected to the electricity grid. This system had 2 parallel battery strings with 162 V. Again, OPzV gel cells were used.

At ‘Rotwandhaus’, there was a hybrid system including both a solar and a wind generator. There was also a diesel engine for back up. A 162 V gel battery was used with tubular plate design and a capacity of 720 Ah at the 100-h rate and 600 Ah at the 10-h rate. A schematic of the complete system is given in Figure 9.25. There were two strings in parallel, each with a capacity of 300 Ah at 10-h rate and 360 Ah at 100-h rate. The same 2 V cell type (OPzV) was used as for the Talhof system.

This time there was just one charge strategy and the only difference was the use of a charge equalizer (ChEq) in one string. This resulted in virtually the same voltage for all cells or cell groups in a string. More details about the ChEq system can be found in the literature [34-36].

The ChEq was included in this investigation program in order to find out whether such a system could give a higher energy turnover and a longer battery life. The charge strategy included a voltage limit of 2.35 V per cell and the DoD was restricted to 80%. As this charge/discharge strategy was the same for both strings, any difference in performance of one string could directly be related to the use of the ChEq. All important parameters were controlled, measured and stored by a computer system.

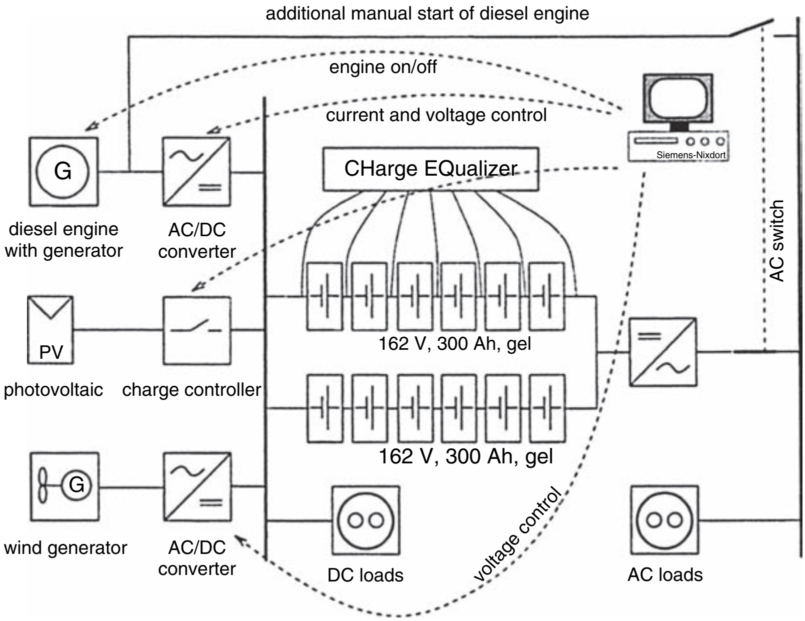

Figure 9.25. Schematic of the solar power system with a 162 V 600 Ah battery of the gel design with tubular plates at the Rotwandhaus in the Alps. There are two strings, one is equipped with a ChEq and the other is not.

Again, the running time of the diesel generator was kept as short as possible. However, the highest priority was to avoid a deep discharge of the battery. There was at least once a month a calibration of the SoC measurement unit after a recharge of the battery by the diesel generator.

One capacity test per year was run; each test included two discharges, one before and one after an intensive charge. Figure 9.26 shows the capacities of the string with a ChEq before and after an intensive 112% charge, while Figure 9.27 gives the same development of the capacities for the string without a ChEq. It can be seen that in both strings the capacity test after an intensive charge gave significantly better results. This means that, in this case too, there was some undercharging during the year with the standard charge/discharge strategy, but it could be compensated by the intensive charge.

A comparison of the results of both strings shows that the capacity was virtually the same and rather stable over about 1.5 years of service. Later, however, the string without the ChEq behaved much better and the capacity after 3.5 years service was even higher than the initial value. Conversely, the string with the ChEq had a significantly lower capacity at the end of the test: for solar and wind applications a charge equalizer is not useful.

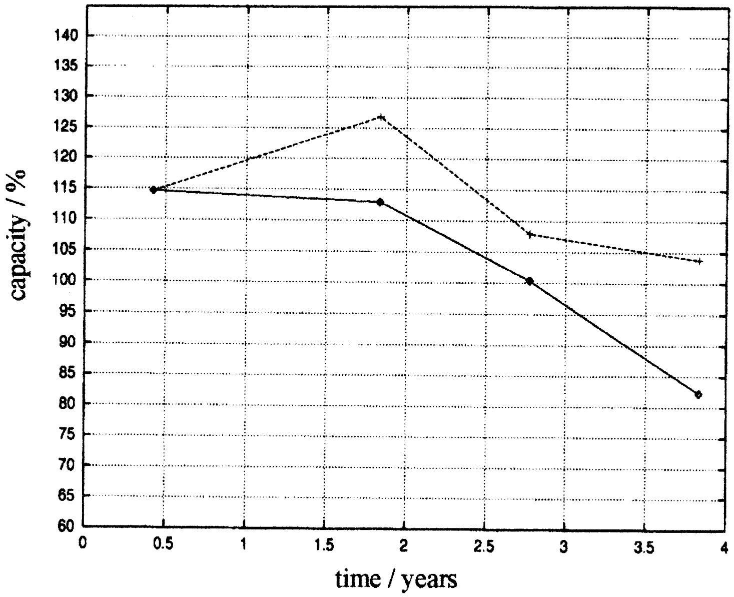

Figure 9.26. Development of the 10-h rate capacity of the string with a ChEq at the Rotwandhaus before and after an intensive charge. The upper curve represents the capacities after the intensive charge.

In a previous section and in Chapter 7, there is a detailed discussion about the use of negative copper grids in large batteries with tall plates, *i.e.* the CSM technology. The use of negative copper grids for large valve-regulated lead-acid batteries can result in high-power batteries, which have all the advantages of the valve-regulated design [37-39]. To date, copper negative grids have only been used in gel cells as copper is most useful with tall plates and, in such designs, gel is preferred over AGM [7]. An investigation of the combination of copper negative grids and gel technology established that this combination gives high-power, maintenance-free batteries without any risk of copper dissolution [40]. The results of this investigation agree well with field experience with this type of battery. During more than 15 years in different stationary applications, no noticeable amounts of copper have been found either in the electrolyte or on the negative active mass surface.

Besides higher power, such cells have also better charge acceptance [7,20,39] and this makes the CSM technology also interesting for solar and wind power applications, even if the discharge currents in such systems are, in general, not very high. The charging times for different initial charging currents to return a standard gel cell, OPzV (lead negative grid), and a gel cell with copper grids, OCSV, to 100% of the discharged capacity are shown in Figure

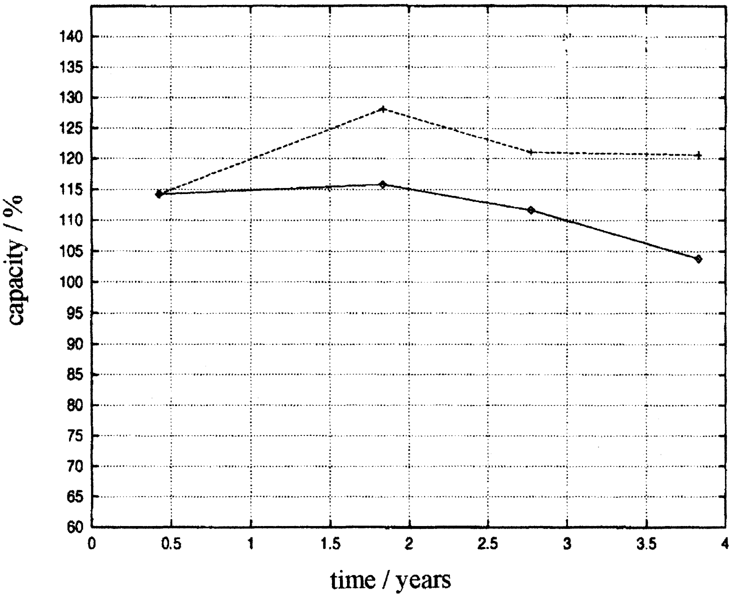

Figure 9.27. Development of the 10-h rate capacity of the string without a ChEq at the Rotwandhaus before and after an intensive charge. The upper curve represents the capacities after the intensive charge.

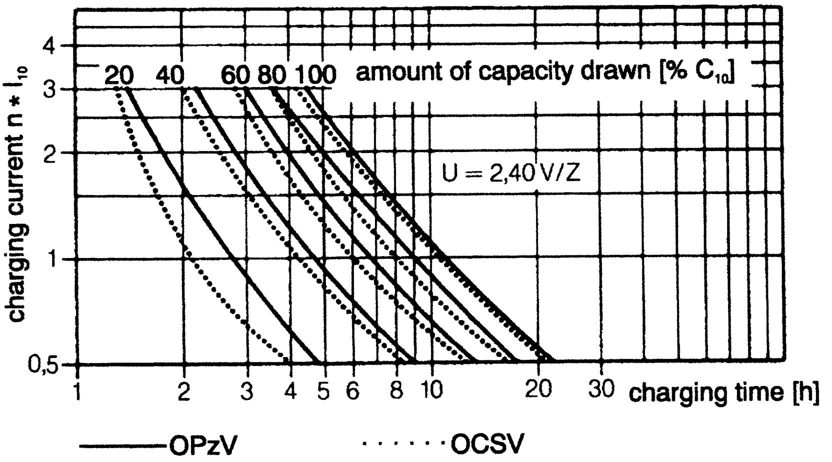

Figure 9.28. Charging time and initial charging current to return a standard (OPzV) and a CSM gel (OCSV) battery to 100% of discharged capacity after discharge to different depths-of-discharge.

9.28. It can be seen that the use of copper grids reduces markedly the charging time, due to the better charge acceptance of the OCSV cells.

Flanitzhütte is a small village in the south of Germany, where the maximum number of dwellers is about 70 in the summer time; its electric energy demand is about 40 MWh per year. This village, located in a forest and with the next village quite some distance away, is not connected to the electric grid. As the installation of a line would have been quite expensive, the utility in this area, Bayernwerke, decided to take the opportunity to gain some experience on the use of a solar power plant for electric energy 'island' systems. Accordingly, a solar power plant was installed there in collaboration with Siemens Solar, the supplier of the solar generator, and Hagen, the supplier of the battery. Since the summer of 1992, the supply of electric energy has been provided by the solar power plant [41-46].

A picture of this plant in Flanitzhütte is given in Figure 9.29. The solar generator and the house were the battery was installed are visible in the foreground. A schematic of the solar power plant is shown in Figure 9.30. This includes the most essential parts, *i.e.* the solar generator, the battery, the gas engine with generator and the converters. The solar generator consists of 360 m^2 silicon solar cells with a peak power of 40 kW. Via a d.c./d.c. converter and two three-phase d.c./a.c. converters (one 25 kW system for the basic demand, and a second one of 40 kW for peak power), there is three-phase a.c. available with the usual voltage and frequency for all houses.

On the d.c. side, there is a lead-acid battery that can supply some additional electric energy when the solar cells deliver less energy than needed by the consumer. The battery will be charged when the solar cells supply more energy than the actual demand. This means that overnight, and whenever the light intensity is rather low, the battery takes over in the main supply. On the other hand, during sunshine periods the solar cells provide all the needed energy to the consumer and the excess of energy is used for battery charging.

The 216 V and 2200 Ah lead-acid battery has positive tubular plates and gel electrolyte. Actually, the battery consists of 2 V OCSV cells with a capacity of 1100 Ah and there are two strings in parallel, each with 108 cells of 1100 Ah. In total, it is a 475 kWh battery and this size has been chosen in order to provide the village with an electrical autonomy for at least three days. Copper has been used as the negative grid material because, for such a high capacity, tall plates are needed and, although the discharge currents are rather small in case of solar power applications, copper grids give a much better charge efficiency. Figure 9.31 gives a picture of the battery room. The two strings with the OCSV cells, each installed on a rack by using two levels, can be seen clearly.

The ratio of solar energy to the total consumed energy of Flanitzhütte was about 65% over the whole year (about 98% during summer time and less than 50% during winter time). These contributions could have been increased

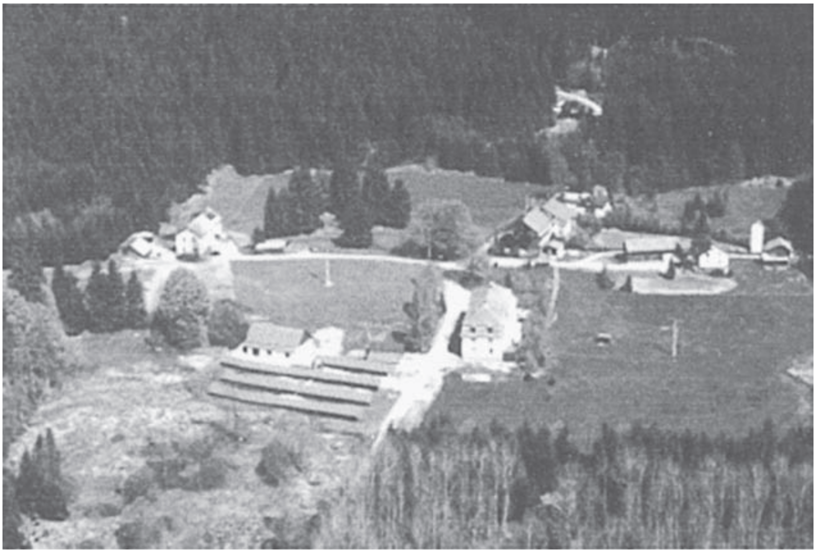

Figure 9.29. Picture of the solar power plant in Flanitzhütte.

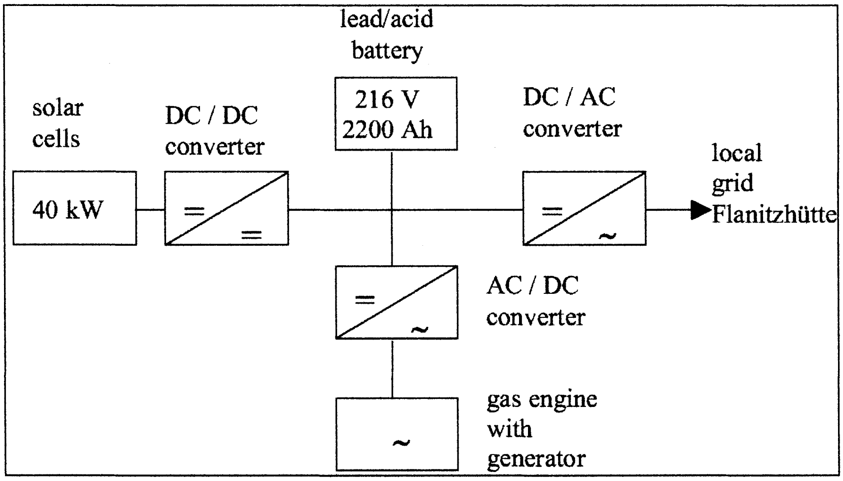

Figure 9.30. Schematic of the solar power plant in Flanitzhütte.

by installing a larger solar generator, but this would have caused higher costs, not to mention the marked excess of electric energy during summer time that could not be stored in the battery.

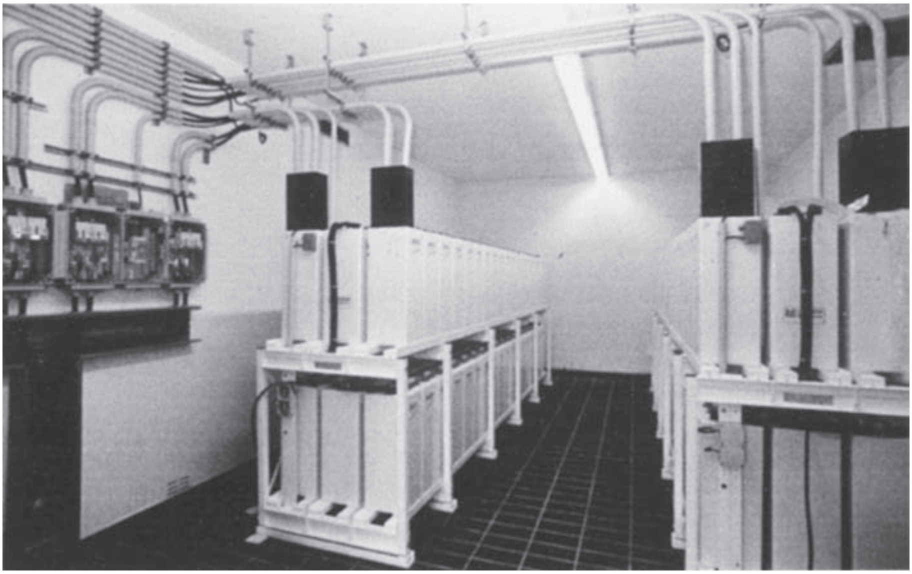

Figure 9.31. Picture of the battery room at the Flanitzhütte plant with the 216 V gel battery with two strings, each of 1100 Ah.

The difference between the consumed energy and the energy produced by the solar cells was supplied by a gas engine with a generator that was used for some hours whenever the SoC of the battery became too low. This happened seldom during summer, but much more frequently during winter, especially after longer rainy periods. In general, the gas engine started to work when the SoC of the battery was lower than 40% and stopped when the SoC had increased to 80%.

In fact, the algorithm for the use of the gas engine was more complex and was controlled by a computer program that addressed further conditions; for example, whether it was summer or winter, the time of day or night, and the SoC of the battery. The strategy was to avoid, as much as possible, an excess of solar energy that could not be stored due to a too high SoC of the battery. This means, for example, that a SoC of down to 30% was acceptable if it was achieved by the end of the night when it could be expected that the solar cells would quickly supply sufficient energy to restore the SoC of the battery.

There were some detailed investigations on how the SoC of the battery changed during summer and winter time. From the balance sheets of energy consumption and the energy supplied by the solar cells, this computer program had been improved to increase even further the portion of solar energy and to reduce as much as possible the use of the gas engine. As a consequence, the portion of solar energy increased from about 65% to more than 70%.

The SoC of the battery over 250 h during summer time is shown in Figure 9.32. The SoC was measured by Ah balance corrected by parameters such as battery temperature and voltage as well as charge/discharge currents. A complete recharge with an additional constant-current charging was given to the battery occasionally in order to recharge it completely and to set the SoC indicator to 100%. From the curve of Figure 9.32, it can be seen that the SoC was mostly between 90 and 40%.

A typical year profile (from October 1992 to September 1993) of the supplied energy from the solar cells, the energy consumption and the battery turnover can be seen in Figure 9.33. The most unfavourable period was between November and February because, during that time, there was the lowest amount of energy from the solar cells but rather high energy demand. The battery turnover per month was between 1.7 and 3.3 MWh to give, in total, nearly 30 MWh per year. The energy efficiency of the battery was found to be about 91%, which is a remarkably good value.

The OCSV battery at the solar power plant of Flanitzhütte was in use for more than 11 years and all the time the gel battery had operated successfully and without any problem worth mentioning. Then, the battery reached the end of its service life.

It seems that solar power application will become an interesting market for the lead-acid battery in future and probably a significant portion will be

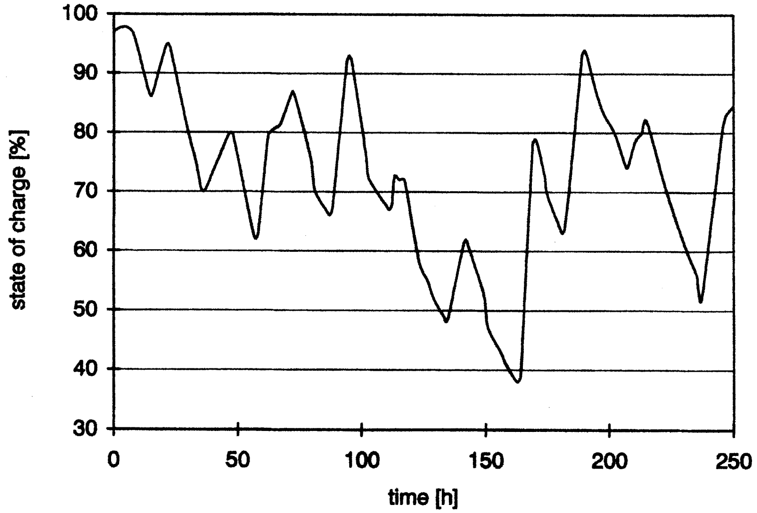

Figure 9.32. SoC of the battery over 250 h during summer time in Flanitzhütte.

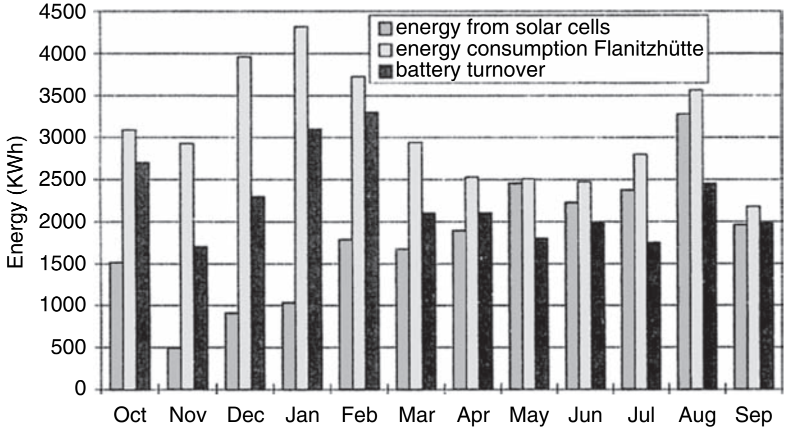

Figure 9.33. Typical year profile (from October 1992 to September 1993) of the energy supplied by the solar cells, the energy consumption of Flanitzhütte and the battery turnover.

valve-regulated batteries. The market is preferably in the developing countries, but there seems to be also a significant demand in Europe at places where there are electric 'island' situations. In such cases, it is often too expensive to make the connection to the electric grid so that a solar power plant including a battery can be an economical solution.

9.7. Further Developments

Summarizing all results from the investigations on solar batteries in the four different programs ('Solarhaus Freiburg', 'small systems', 'Talhof' and 'Rotwandhaus') the following conclusions can be made.

All tested charge regimes were not sufficient to charge the batteries completely: the capacity tests always showed some undercharging between 5% and 20%. By an intensive charge after the capacity tests, this undercharging could be recovered. It has to be realized, however, that during normal operation in solar and wind power applications such intensive charging is not used. It can be expected that without the intensive recharge the tested batteries would have performed worse.

The charge/discharge factor at Talhof and Solarhaus was just slightly above 1, which is also an indication of some undercharging. The small systems, however, had a higher charge/discharge factor because of the long full charge periods during the summer.

The OPzV batteries at Talhof and Rotwandhaus had the full capacity after nearly 4 years in service but only after an intensive recharge.

The flat plate gel batteries in the small systems had some decrease in capacity but stabilized at about 85 % of the nominal capacity after nearly 4 years of service. A 70% DoD limit was not a problem for the small systems batteries. On the contrary, it was better in comparison to a limit of just 50%.

The tubular plate gel batteries had also no problems with a 70% DoD limit and even slightly deeper discharges seem to be acceptable.

Thus, the common charge procedures in solar and wind power applications need to be optimized in order to reduce the problems with undercharging. An occasionally performed intensive charge could be a good way to overcome the problem. There is, however, also the need of further improvements of the current solar battery types. Some options for such improvements are given below.

In order to improve gel batteries for solar power applications, two types of batteries, one with positive flat plates and one with tubular plates, were modified with regard to the amount of electrolyte and to the amount of phosphoric acid as an additive. The ratio of electrolyte/active mass was increased by extending the plate distance resulting in a thicker plate group and by using a larger container. The amount of phosphoric acid was varied between no addition and the value normally used for hard cycling applications.

For the flat plate design, the plate distance was increased by 1 mm, this giving a 30% higher amount of electrolyte in the cell. For the tubular plate design, the distance increase was 1.5 mm, this resulting in 15% more electrolyte volume. Increasing the electrolyte volume affords a higher capacity and reduces freezing problems, as the discharged battery has a higher acid concentration.

The different variants of the flat plate design were:

- Standard electrolyte volume without phosphoric acid
- Standard electrolyte volume with phosphoric acid
- 30% more electrolyte volume without phosphoric acid
- 30% more electrolyte volume with phosphoric acid.

There was a cycle test with all four variants by using a discharge current of 6.1 A over period of 4 h. Every 10th cycle there was a complete discharge with 6.1 A and a cut-off voltage of 1.70 V per cell (100% DoD). The charge regime was IU with I = 5 A and U = 2.40 V per cell, the total charge time was 16 h.

Figure 9.34 gives the results of this test over 300 cycles. It can be seen that the use of phosphoric acid gave lower initial capacity. However, the capacities of these cells were rather stable with even a small increase during cycling. The batteries without phosphoric acid, however, were loosing soon some capacity and, after about 100 cycles, the batteries with phosphoric acid were already on a higher capacity level.

As expected, the capacity was markedly increased by the use of more

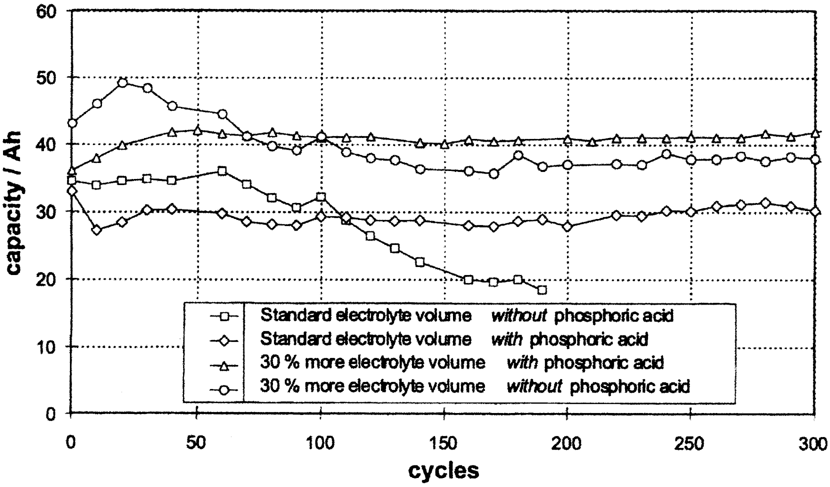

Figure 9.34. Cycle test of modified flat plate gel batteries with different amounts of electrolyte and phosphoric acid.

electrolyte. Both the behavior of the batteries with and without phosphoric acid and the influence of electrolyte volume on the capacity are known in principle and the results of this test confirm previous findings. There were especially a couple of detailed investigations on the impact of phosphoric acid on the performance of lead-acid batteries [47-53].

As the charging behavior of solar batteries is an important parameter for photovoltaic applications, the charge acceptance was investigated in laboratory tests. The charging time with a constant current of 5 A before reaching the voltage limit of 2.40 V per cell over 300 cycles is given by Figure 9.35. The discharge was made at 6.1 A over 4 h and was the same for all four battery variants.

It can be seen that there is a significant difference between the batteries with and without phosphoric acid, but there is virtually no influence of the electrolyte volume. The batteries with phosphoric acid accepted the 5 A charge current for a markedly longer time than those without phosphoric acid. Moreover, this time period was relatively constant (around 4.4 h) for batteries with phosphoric acid, whereas it was reduced from about 4.1 h in the beginning to around 3.8 h after 300 cycles for batteries without it. The charge/discharge factor before reaching 2.40 V per cell was ~84% without phosphoric acid and ~91% with phosphoric acid. There was a slight tendency to lower values with phosphoric acid during cycling.

From these results, it could be concluded that batteries with a higher

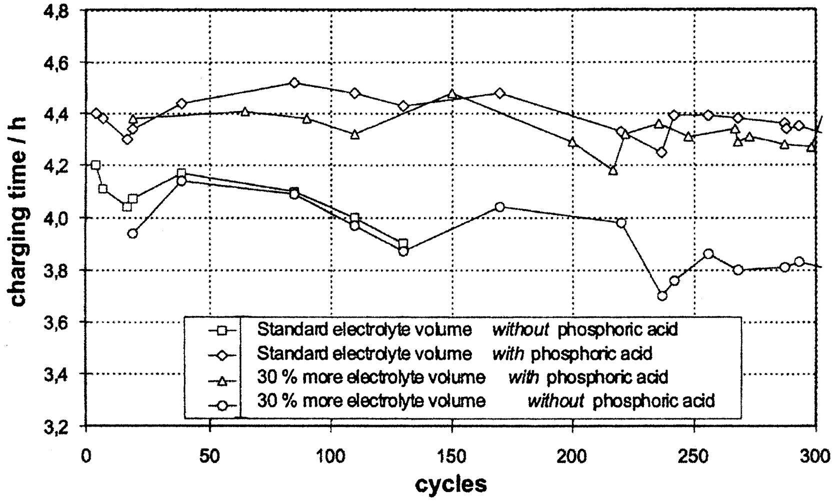

Figure 9.35. Charge acceptance of modified flat plate gel batteries with different amounts of electrolyte and phosphoric acid. The curves give the charging time with a constant current of 5 A before reaching the voltage limit of 2.40 V per cell.

electrolyte volume and with phosphoric acid are interesting candidates for solar and wind power applications. This combination gave good results on cycling and charge acceptance. However, as a laboratory test is different from the actual application in the field, all four variants were also tested in the 'Solarhaus Freiburg' in the same way as the standard batteries described in a previous section.

The results of these tests at the 'Solarhaus Freiburg' over a time period of two years were, however, different from the results achieved in the laboratory, because the variants without phosphoric acid were not worse but even slightly better than the variants with it. This shows again that laboratory tests do not always give the same results as field tests. The tests at the 'Solarhaus Freiburg' confirm also that the mechanism and the impact of phosphoric acid is rather complex and some more investigations are needed for a complete understanding of this phenomenon. The variants with more electrolyte volume, however, were running well at 'Solarhaus Freiburg' and confirmed the good results already achieved in laboratory tests.

The different variants of the tubular plate design were:

- Standard volume with the standard amount of phosphoric acid
- Standard volume with 25% of the standard amount of phosphoric acid
- Standard volume without phosphoric acid
- Standard volume with the standard amount of phosphoric acid but higher

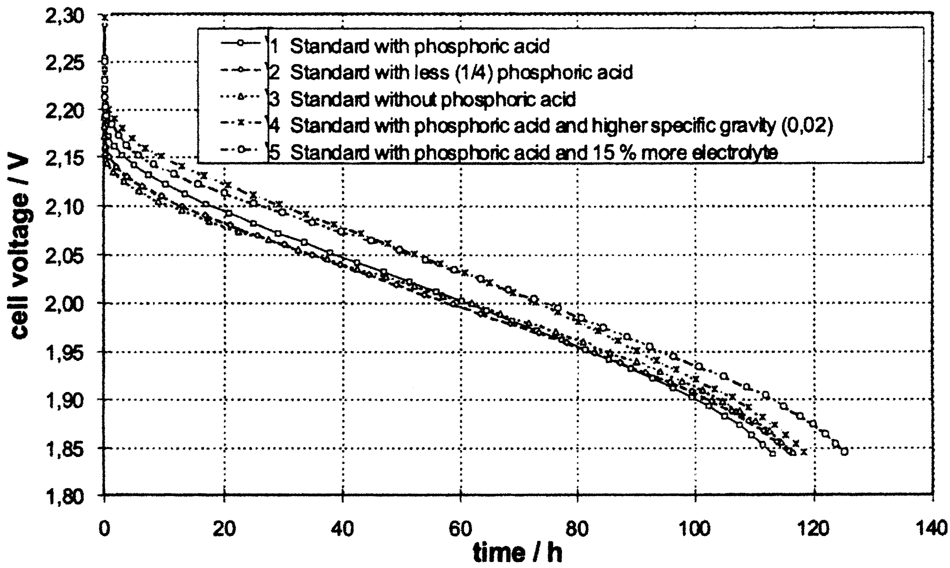

Figure 9.36. Discharge curves of modified tubular plate gel cells with different amounts of electrolyte and phosphoric acid.

specific gravity of the electrolyte (by 0.02 gcm^{-3})

- 15% more electrolyte volume with the standard amount of phosphoric acid.

The cells were discharged with 4.2 A by using a cut-off voltage of 1.85 V per cell. Figure 9.36 gives the discharge curves for all five variants in cells with modified tubular plates. The best result was achieved with 15% more electrolyte volume whereas the standard volume with phosphoric acid gave the worst discharge performance. There were also some differences of the voltage level during discharge. The initial performance data of the modified tubular batteries fit well to the results achieved with the modified flat plate batteries. Although the variant with phosphoric acid were worst in the initial performance, it could be expected that during cycling they would do better than the variant without phosphoric acid. Indeed, this was confirmed later by some cycling tests.

Besides the undercharging problem of batteries in solar and wind power applications, there can be also some failures of VRLA batteries due to an insufficient design or manufacturing process of the battery, which is completely in the responsibility of the battery manufacturer. Some typical failure modes are described below.

Special attention should be given to the pressure release-valve. If this valve is not in good condition, and does no longer close correctly after opening, serious problems will appear. In such a case, oxygen can enter the cell and oxidation of the negative mass causes sulfation of the negative plate during storage of the battery. To avoid this problem, the pressure-release valve has to be controlled carefully before fitting to the battery. This is also important with regard to the risk of drying out during battery use.

A corrosive attack of the lug top bar area is another problem that causes failure of the negative plates of valve-regulated batteries, especially if alloys with antimony are used for the top lead. This phenomenon has been discussed in several papers [20,54-56]. It is a type of corrosion that is similar to the so-called 'crevice corrosion' at the positive post of lead-acid batteries when there is a relatively tight covering around the metallic lead that leaves a crevice into which the sulfuric acid can penetrate. Under these conditions, there is only a thin electrolyte film on the lead, and when an electrochemical reaction takes place in this region, an ionic current flows along the thin film and causes voltage drops that shift the potential to a range where corrosion is accelerated.

The corrosion at the lug/top bar area can be so heavy that the connection is completely destroyed and there is no longer a contact between the plate and the top-bar. In order to avoid this latent danger, impurities in the top-bar that promote electrochemical reaction and enhance the ionic current along the thin film have to be excluded. Antimony is particularly deleterious in the top bar and, therefore, it is advisable to avoid its use in this critical area.

There is another important feature, namely, the use of a proper technique for welding or cast-on-strap (COS). It is well known that the welding of lead-calcium alloys is not easy and, therefore, special techniques have to be used to get a good bonding between the lug and the top bar. If COS is used, good cleaning of the surface of the lug (*i.e.* a proper fluxing process) is necessary to achieve a good bonding. Of course, this is valid for both positive and negative plate groups, since a poor connection also gives problems in the positive lug/top-bar sections. Therefore, the use of an appropriate alloy for the top-bar, together with a good top-bar/plate-group bonding, reduces markedly the risk of any corrosion in this part of the battery.

A short circuit inside the battery virtually always results in a failure. Avoidance of this is the responsibility of the battery manufacturer. Formerly, there were sometimes short circuits through the separator from the growth of lead needles, especially if the battery had been deep-discharged. Nowadays, this is no longer a severe problem, as with the addition of special ingredients to the electrolyte (in general, sulfate salts) the problem of growing lead needles can be completely overcome.

In order to increase the volume energy density, plate dimensions have been increasingly extended. Often, the plates are standing directly on the bottom of the case, because a mud space is no longer needed in valve-regulated batteries. If, for AGM batteries, glass mats are used as single sheets, there is always a latent danger of short circuits at the bottom of the cell. Enveloping of at least one of the two polarities of the plate (either the positives or the negatives) by glass-mats is a good way to overcome this problem. The use of enveloped plates has reduced failures by short circuits at the bottom of the cell virtually to zero. In order to increase the energy density even more, extreme values have been taken for both the width and the height of the plates. As the dimensions of the glass-mats cannot greatly exceed those of the plates, during assembly of the cell the glass-mats have to be adjusted carefully between the plates in order to avoid any short-circuits at the sides or the tops of the plates.

9.8. Conclusions

The majority of solar power applications do not include connection to the electricity grid. Then, in general, an energy storage system is needed and this is usually a lead-acid battery. There has been a significant growth of the autonomic solar power and wind power market and consequently the demand of batteries for such applications has been growing as well. It is expected that this trend will continue so that the solar battery market will become more interesting for the battery industry. There is also a clear trend to use VRLA batteries (often the gel design) rather than the flooded types. Undercharging and sulfation are the major failure modes of the battery. Thus, there is a need for improved charging strategies in such applications.

References

1. H. Gabler, in J. Garche, W. Höhe, G. Stadermann (eds.), *Elektrochemische Speichersysteme für regenerative Energieversorgungsanlagen,* Forschungsverbund Sonnenernergie, Berlin, Germany, 1999
2. R.H. Newnham, in D.A.J. Rand, P.T. Mosely, J. Garche, C.D. Parker (eds.), *Valve-regulated Lead-Acid Batteries,* Elsevier, Amsterdam, Netherland, 2004
3. A. Jossen, J. Garche, D.U. Sauer, *Solar Energy* 76 (2004) 759
4. J. Garche, in J. Garche, W. Höhe, G. Stadermann (eds.), *Elektrochemische Speichersysteme für regenerative Energieversorgungsanlagen*, Forschungsverbund Sonnenernergie, Berlin, Germany, 1999
5. J. Schmid, in J. Garche, (ed.), *Elektrochemische Speicher in regenerativen Energiesystemen,* Universitätsverlag, Ulm, Germany, 1994
6. R. Wagner, D.U. Sauer, *J. Power Sources* 95 (2001) 141
7. R. Wagner, in D.A.J. Rand, P.T. Mosely, J. Garche, C.D. Parker (eds.), *Valve-regulated Lead-Acid Batteries,* Elsevier, Amsterdam, Netherland, 2004
8. G. Bopp, M. Bächler, H. Gabler, W. Höhe, W. Mittermeier, D.U. Sauer, P. Sprau, B. Willer, M. Wollny, *Proc.13th E.C. Photovoltaic Solar Energy Conference*, Nice, France, 1995
9. J. Garche, *J. Power Sources* 53 (1995) 85
10. D.U. Sauer, G. Bopp, M. Bächler, W. Höhe, A. Jossen, P. Sprau, B. Willer, M. Wollny, *Proc.14th E.C. Photovoltaic Solar Energy Conference*, Barcelona, Spain, 1997
11. J. Garche, A. Jossen, H. Döring, *J. Power Sources* 67 (1997) 201

12. G. Bopp, H. Gabler, K. Kiefer, K. Preiser, E. Wiemken, *Proc. NORTH SUN*, Espoo, Finnland, 1997
13. D.U. Sauer, J. Garche, *J. Power Sources* 95 (2001) 130
14. H. Gabler, E. Wiemken, *Proc. 2nd World Conference on Photovoltaic Solar Energy Conversion,* Vienna, Austria, 1998
15. D.U. Sauer, M. Bächler, G. Bopp, W. Höhe, J. Mittermeier, P. Sprau, B. Willer, M. Wollny, *J. Power Sources* 64 (1997) 197
16. W. Höhe, A. Jossen, G. Bopp, D.U. Sauer, B. Willer, M. Wollny M. Bächler, P. Sprau, in J. Garche, W. Höhe, G. Stadermann (eds.), *Elektrochemische Speichersysteme für regenerative Energieversorgungsanlagen,* Forschungsverbund Sonnenernergie, Berlin, Germany, 1999
17. A. Jossen, H.-P. Hönes, H. Karl, G. Lehner, in J. Garche, (ed.), *Elektrochemische Speicher in regenerativen Energiesystemen,* Universitätsverlag, Ulm, Germany, 1994
18. S. McCarthy, A. Kovach, G.T. Wrixon, *Proc.9th European Photovoltaic Solar Energy Conference*, Freiburg, Germany, 1989
19. R. Wagner, in H. Kahlen (ed.) *Batterien,* Vulkan, Essen, Germany, 1992
20. R. Wagner, *J. Power Sources* 53 (1995) 153
21. H. Döring, A. Jossen, D. Köstner, J. Garche, *Proc.10th Symposium Photovoltaische Solarenergie*, Staffelstein, Germany, 1995
22. D.U. Sauer, *J. Power Sources* 64 (1997) 181
23. W. Rusch, in J. Garche, W. Höhe, G. Stadermann (eds.), *Elektrochemische Speichersysteme für regenerative Energieversorgungsanlagen,* Forschungsverbund Sonnenernergie, Berlin, Germany, 1999
24. D.U. Sauer, in A. Luque, S. Hegedus (eds.), *Handbook of Photovoltaic Science and Engineering*, Wiley & Sons, New York, USA, 2003
25. R. Wagner, M. Schroeder, T. Stephanblome, E. Handschin, *J. Power Sources* 78 (1999) 156
26. U. Kriegler, B. Ratering-Schnitzler, *Proc.4th European Power Quality Conference,* Nuernberg, Germany, 1997
27. R. Harke, U. Kriegler, B. Ratering-Schnitzler, M. Schroeder, T. Stephanblome, *J. Power Sources* 67 (1997) 173
28. U. Kriegler, B. Ratering-Schnitzler, *VDI Berichte* 1291 (1996) 73
29. R. Wagner, *Proc. Int. Symposium on Power Sources for stationary and distributed Power Systems*, Munich, Germany, 2003
30. R. Wagner, *Proc. 11th International Lead Conference*, Venice, Italy, 1993
31. R. Wagner, D.U. Sauer, in J. Garche, W. Höhe, G. Stadermann (eds.), *Elektrochemische Speichersysteme für regenerative Energieversorgungsanlagen*, Forschungsverbund Sonnenenergie, Berlin, Germany, 1999
32. R. Wagner, U. Theimann, G. Bopp, D.U. Sauer, *Proc. 15th Symposium Photovoltaische Solarenergie*, Staffelstein, Germany, 2000
33. D.U. Sauer, G. Bopp, A. Jossen, J. Garche, M. Rothert, M. Wollny, *INTELEC 1999, Conf. Proc.*, Copenhagen, Danmark, 1999
34. H. Schmidt, C. Siedle, L. Anton, *Proc.13th E.C. Photovoltaic Solar Energy Conference*, Nice, France, 1995
35. H. Schmidt, C. Siedle, L. Anton, H. Tuphorn, *Proc. 30th Int. Symp. Automotive technology and Automation,* Florence, Italy, 1997
36. H. Schmidt, L. Anton, *INTELEC 1999, Conf. Proc.*, Copenhagen, Danmark, 1999
37. R. Wagner, *VDI Berichte* 1641 (2001) 273
38. R. Wagner, *7. Kasseler Symposium Energie-Systemtechnik*, Kassel, Germany (2002) 60
39. R. Wagner, *J. Power Sources* 144 (2005) 494
40. R. Wagner, *J. Electrochem. Soc.* 143 (1996) 139
41. R. Wagner, *Elektrische Energietechnik.* 2 (1993) 6
42. R. Wagner, in J. Garche (Editor) *Elektrochemische Speicher in regenerativen Energiesystemen*, Universitätsverlag, Ulm, Germany, 1994

43. U. Kranz, in J. Garche, (ed.), *Elektrochemische Speicher in regenerativen Energiesystemen,* Universitätsverlag, Ulm, Germany, 1994
44. M. Eingartner, R. Knapp, U. Kranz, *Elektrizitätswirtschaft*, 21 (1995) 1376
45. R. Wagner, *J. Power Sources* 67 (1997) 163
46. R. Wagner, H.-U. Koch, *2.. Kasseler Symposium Energie-Systemtechnik*, Kassel, Germany (1997) 115
47. K. Eberts,in D.H. Collins (ed.), *Power Sources* 2, Pergamon Press, Oxford, UK, 1970
48. S. Sternberg, A.Mateescu, V. Branzoi, L. Apatenau, *Electrochim. Acta* 32 (1967) 349
49. K. Bullock, D.H. McClelland, *J. Electrochem. Soc.* 124 (1977) 1478
50. K. Bullock, *J. Electrochem. Soc.* 126 (1979) 360
51. K. Bullock, *J. Electrochem. Soc.* 126 (1979) 1848
52. G.A. Morris, P.J. Mitchell, N.A. Hampson, D.I. Dyson, *Power Sources,* 12 International Power Sources Symposium Committee, Leatherhead, UK, (1989)
53. E. Meissner, *J. Power Sources* 67 (1997) 135
54. G. Baudo, G.B. Cecchinato, *INTELEC 1989, Conf. Proc.*, Florence, Italy
55. R.D. Prengaman, *Proc. 4th Int. Lead-Acid Battery Seminar,* San Francisco, USA, 1990
56. D. Berndt, Maintenance-Free Batteries, Research Studies Press, Taunton, Somerset, UK, 1993

This page intentionally left blank

Industrial Applications of Batteries. From Cars to Aerospace and Energy Storage
M. Broussely and G. Pistoia Eds.,
© 2007 Elsevier B.V.

Chapter 10

STATIONARY APPLICATIONS. IV. THE ROLE OF NICKEL-CADMIUM BATTERIES

Anthony Green

Consultant, Redditch, Worcestershire, United Kingdom

10.1. Introduction

The nickel-cadmium (Ni-Cd) system is commonly found in its ‘sealed’ form as a rechargeable battery in portable equipment, where it can replace primary cells such as heavy duty or alkaline, and is available in many of the same sizes. In its ‘flooded’ form it is found in general industrial applications and this chapter concerns these larger capacity industrial Ni-Cd flooded batteries which have a specific niche market in application areas which are difficult for other battery technologies. Due to their beneficial technical characteristics as compared to lead-based technologies and good service lifetimes, they are especially used in critical stationary applications where a high level of security is required.

Nickel-cadmium cells have a nominal potential of 1.2 V. This is lower than the 1.5 V of popular primary cells, and much lower than the 2 V of the lead-acid battery. However, Ni-Cd batteries maintain a fairly constant voltage throughout their discharge, which helps to maintain the voltage level at the requirement for most electronic equipment. Despite their lower nominal voltage, these batteries are better suited for high current applications than lead-acid batteries. Due to a significantly lower internal resistance, they are capable of supplying very high surge currents. This makes them a favourable choice for engine starting and other high rate discharge operations.

10.2. History

In 1899, Waldemar Jungner of Sweden created the first nickel-cadmium battery. At this time, the only direct competitor was the lead-acid battery. The nickel-cadmium battery offered several advantages in certain applications. Early types were physically and chemically robust, and early modifications to the design increased the energy density to about half of that of primary batteries, significantly better than lead-acid.

In 1910, a company was formed to produce industrial nickel-cadmium batteries in Sweden. The batteries were "pocket plate type," constructed of nickel-plated steel pockets containing the nickel and cadmium active materials.

Improvements to the technology were achieved when German scientists Schlecht and Ackermann invented the sintered plate in 1932. This gave a much higher energy density than pocket plate types and made them particularly useful for aviation applications. Sintered plates are usually much thinner than the pockets of pocket type batteries, allowing more surface area per volume, in turn allowing higher currents for batteries of comparable size.

The major developments in the Ni-Cd technology were completed in 1947 when French scientist Neumann succeeded in completely closing the cell. Thus, sealed Ni-Cd became available and this was the predominant portable rechargeable battery until the arrival of nickel-metal hydride and, later, lithium ion batteries

10.3. Chemistry

Basic information on the chemistry of Ni-Cd batteries may be found in Chapter 2. Here, complementary information will be provided.

In the charged state, the positive plates consists of NiOOH and the negative plates consist of porous Cd, both plates being immersed in an electrolyte solution of KOH of specific gravity 1.2-1.3 gcm^{-3}, depending on the particular cell design. As the cell is discharged, the active materials consume H_2O, but not KOH, as shown by the electrochemical reaction:

$$2\,NiOOH + Cd + 2\,H_2O \leftrightarrow 2\,Ni(OH)_2 + Cd(OH)_2$$

There are a number of consequences arising from this:

- As water from the electrolyte is incorporated into the active materials during discharge, swelling occurs. The amount of water involved is a small proportion of the total and the effect on the specific gravity of the bulk electrolyte is negligible.
- There is little change in the electrolyte density during charge and discharge and this allows large reserves of electrolyte to be used without inconvenience to the electrochemistry of the couple.

- The structure of the positive active material NiOOH is complicated and exists in various crystallographic forms associated with different degrees of hydration.

Through its electrochemistry, the nickel-cadmium battery has a stable behaviour giving it a long life, good electrical and mechanical characteristics and a resistance against abusive conditions.

Another historically important modification to the basic nickel-cadmium cell was the addition of lithium hydroxide to the potassium hydroxide electrolyte. This has the effect of prolonging the service life by making the cell more resistant to electrical abuse.

In order to achieve a fully charged flooded cell it is necessary to carry out a certain level of overcharging and, in the case of the nickel-cadmium battery, there are two results from this practice. When the negative is overcharged, hydrogen gas is produced; and, when the positive is overcharged, oxygen gas is produced. Thus, in the normal functioning of the cell varying amounts of hydrogen and oxygen are emitted, depending on the nickel-cadmium technology used.

10.3.1. Memory Effect

It is sometimes claimed that nickel-cadmium batteries suffer from a so-called "memory effect" if they are recharged before they have been fully discharged. The apparent symptom is that the battery "remembers" the point in its charge cycle where recharging began and during subsequent use suffers a sudden drop in voltage at that point, as if the battery had been discharged. The capacity of the battery is not actually reduced substantially. Some electronics designed to be powered by nickel-cadmium batteries are able to withstand this reduced voltage long enough for the voltage to return to normal. However, if the device is unable to operate through this period of decreased voltage, the device will be unable to get as much energy out of the battery, and for all practical purposes, the battery has a reduced capacity.

There is confusion as to what actually constitutes ‘memory effect’ and any loss in capacity for whatever reason is often attributed to this phenomenon. However, it is generally agreed that in practice it is related to the small sealed sinter nickel-cadmium cells and is not experienced in industrial flooded cells. Therefore, it is not to be expected in stationary applications. For more details on this effect, see again Chapter 2 and specific references therein.

10.4. Construction Features of Nickel-Cadmium Cells

10.4.1. Plate Technology

The traditional design for the plates used in industrial NiCd batteries is the pocket construction. The active materials, either in powder form or compressed briquettes, are enclosed in perforated pockets produced from nickel-plated steel foil. This acts both as a mechanical support and as a current collector. Several pockets are then crimped or welded into a steel frame to form a rectangular plate. Pocket plates present a comparatively low area/volume ratio for the active material and are generally used in low to medium discharge rate applications. In Figure 10.1, a cutaway of a modern pocket plate cell is shown.

Sintered electrodes were developed to provide large area/volume profile, so giving improved high rate discharge characteristics. Carbonyl nickel powder, having a central backing foil of perforated nickel-plated steel, is sintered at about 1000°C in a reducing atmosphere, such as hydrogen, to avoid oxidation of the powder. Plaques are usually fabricated to between 0.5 to 1.0 mm thick and the process is completed by impregnation of a solution of the active material. Sintered substrates provide a high utilisation of the active material but are

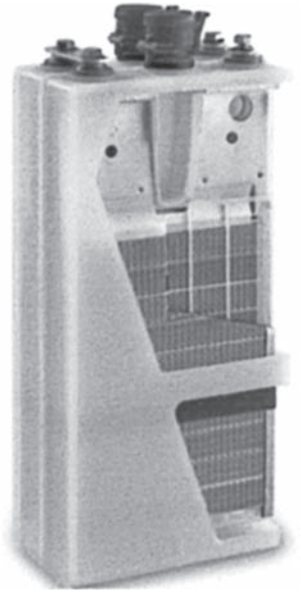

Figure 10.1. Cut-away of typical pocket plate cell.

expensive to manufacture.

In more recent years, fibre and plastic bonded electrodes have been developed. Fibre substrates are formed by coating organic or carbon fibres with nickel, the fibres then sometimes being removed by thermal decomposition. Advantages of this type of construction are that thicknesses of up to 10 mm are possible, providing a high specific capacity for low power applications. On the other hand, thin electrodes (~1 mm thick) can also be made for very high power applications. However, fibre electrodes are generally more expensive to produce than pocket plate in these application areas.

The plastic bonded electrode (PBE) construction follows a continuous process. The active material is mixed into a paste, blended with an organic thermal bonding agent, such as PTFE, and rolled onto a nickel-plated perforated steel substrate; it then passes through a continuous oven, has the tab material welded on and finally is stamped out to size. The PBE construction is only used in the manufacture of negative plates, as the positive active material has insufficient intrinsic strength to be used in this way and requires the mechanical support of a reinforcing substrate.

10.4.2. Active Materials

The active materials used in nickel-cadmium cells are produced in the discharged form. These are nickel and cadmium hydroxide for the positive and negative plate, respectively. To change them into nickel oxyhydroxide positive material and porous cadmium negative material, a formation process is used which involves charge and discharge cycles on the final cell plate stack.

The positive material for pocket and fibre plates is usually made by precipitation of $Ni(OH)_2$ from a solution of $NiSO_4$ by addition of NaOH. Cobalt in the form of $CoSO_4$, and sometimes $CdSO_4$, is also added to improve the high temperature performance and charge acceptance. In the case of pocket plate construction, the hydroxide powder used in the positive has graphite and/or nickel powder or flakes mixed in to improve electrical conductivity.

The active material for pocket, fibre and PBE (negatives) are prepared in solid or paste form, incorporating various additives which are introduced by mixing or co-precipitation. The $Cd(OH)_2$ negative material can be prepared by co-precipitation from solutions of cadmium and nickel sulphate and, in the case of material for negative pocket plates, iron sulphate. Although the addition of iron as an expander improves the performance of the negative active material, it does have a detrimental effect on the positive one. As an alternative to iron, various expanders, both organic and inorganic, can be added to the negative active material, but these are not as effective.

10.4.3. Separators

In pocket plate technology cells, vertical separating rods or bars made from polystyrene or polypropylene are used to prevent contact between adjacent positive and negative plates in the stack. In some low maintenance products, this type of separation is replaced by a fibrous polyamide separator which is used to enhance the recombination level and reduce water consumption. However, this is unsuitable for high rate performance pocket plate cells due to the increased internal resistance.

Woven and felted polyamide and polypropylene fabrics are also used as separators for sintered, PBE, foam and fibre plate constructions, usually in combination with a perforated backing piece of microporous PVC or gas barrier membrane-type separators.

10.4.4. Electrolyte

Normally, cells are filled with a potassium hydroxide solution having a density of 1.20-1.30 gcm^{-3}, depending on design and application. Pocket type cells tend to use weaker concentrations of 1.20-1.23 gcm^{-3}. Too low a concentration increases the internal resistance and results in a sluggish performance. High concentrations may reduce service life and degrade cell components, especially at elevated temperatures.

Lithium hydroxide is a common additive to the electrolyte, the amounts usually being 15 to 30 g per litre. Lithium appears to affect mainly the positive plates, improving the capacity and cycling ability of cells. High concentrations of lithium hydroxide reduce the ionic conductivity and cause some loss of high rate performance.

10.4.5. Range of Products Available

Nickel-cadmium products are available in a range of performances designed to match different applications and a typical spread of product types is shown in Table 10.1 [1-5]. For larger capacity requirements, batteries may be used in parallel strings.

10.5. Electrical and Mechanical Characteristics

The characteristics of the different industrial flooded nickel-cadmium

Table 10.1. Typical performance and capacity ranges.

Performance Type	Typical Discharge Regime	Typical Size Range (Ah)	Typical Applications
High rate discharge	Less than 30 mins	10 to 1000	Engine Starting Switch Closing Electricity Substations UPS Systems Electromagnets
Medium rate discharge	30 mins to 2 hours	10 to 1000	UPS Systems Power Supplies Electric Train Duties Gas Turbine Control General Mixed Loads
Low rate discharge	More than 2 hours	10 to 1500	Emergency Lighting Alarms Railway Signalling DC Instrumentation Telecom Systems Renewable Energy (Including Photovoltaic)

technologies discussed in this section are varying according to the technology type. Therefore, the characteristics that are general to all types will be described, with some notes where there are significant differences.

All technologies have a potential lifetime in excess of 20 years in normal floating applications at 20°C and are suitable for difficult environmental conditions.

10.5.1. Performance at High and Low Temperatures

Although high temperature has little effect on the performance of the product, low temperatures have a significant effect as illustrated in Figure 10.2.

The nickel-cadmium battery can be used over a very wide temperature range without damage. The effect of low temperatures on the performance of the sintered/plastic bonded product is less than the pocket plate product. Both cells, however, outperform the VRLA battery, whose performance markedly decreases below 0°C.

Clearly, it is possible to use any nickel-cadmium technology for all discharge regimes but the cost per Ah becomes a deciding factor. For this reason, nickel-cadmium cells are designed for different performance regimes.

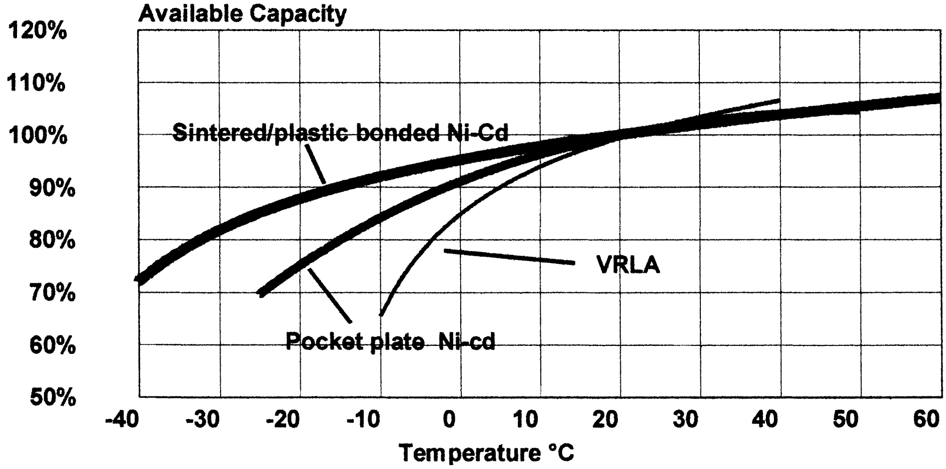

Figure 10.2. Effect of temperature on the performance of lead-acid and Ni-Cd cells.

10.5.2. Lifetime at High Temperatures

It is well known that the electrochemical activity of a battery increases with temperature and so the speed of natural ageing of the active material also increases. However, this does not affect the steel structural components of the electrode assembly of the nickel-cadmium cells, which manifest long life characteristics. The rate of ageing is about 20% reduction in life for 10°C increase in temperature. This compares to lead-acid batteries, where the rate of ageing is about 50% for each 10°C rise in temperature.

Thus a 20-year life (at normal temperature) nickel-cadmium cell when run at an average ambient temperature of 45°C would give 15 years and a 10-year life lead-acid product under the same conditions would be reduced to a little over 2 years life.

Thus, the nickel-cadmium battery is the preferred solution for an application where there is a high-temperature environment. Examples are: external cabinets for telecommunications (see Section 10.8), oil fields explorations, photovoltaic and wind energy storage applications, railroad trackside equipment. A temperature range of -20°C to 50°C is allowed and even extreme temperatures of -50°C or 70°C can be tolerated by special batteries.

10.5.3. Cycling Behaviour

The nickel-cadmium pocket plate cell is able to perform many deep discharge cycles, the number of cycles depending on the depth of discharge (DOD) of each cycle.

A pocket plate cell will perform in excess of 1000 cycles to a 70% depth of discharge and in excess of 10,000 cycles at a 15% depth of discharge (Figure 10.3). This makes it suitable for most cycling applications.

In the case of the sintered positive/plastic bonded negative technology battery, it is possible to perform in excess of 3,500 cycles to 70% DOD, and this has led to its use by the major electric vehicle manufacturers.

10.5.4. Charge Characteristics

Either two-level or single level constant voltage charging can be used, and the method chosen has an influence on the recharge time and the water consumption of the product.

The two-level charger is generally of the type that has a high voltage level charge for a fixed duration and then passes to a low permanent floating voltage level which is intended to maintain the state of charge of the cells. The first high voltage charge stage is initiated whenever the battery is discharged, *i.e.* the system is used, and quickly brings the battery back to a high level of charge. The advantage of this type of charge system is that the low floating voltage

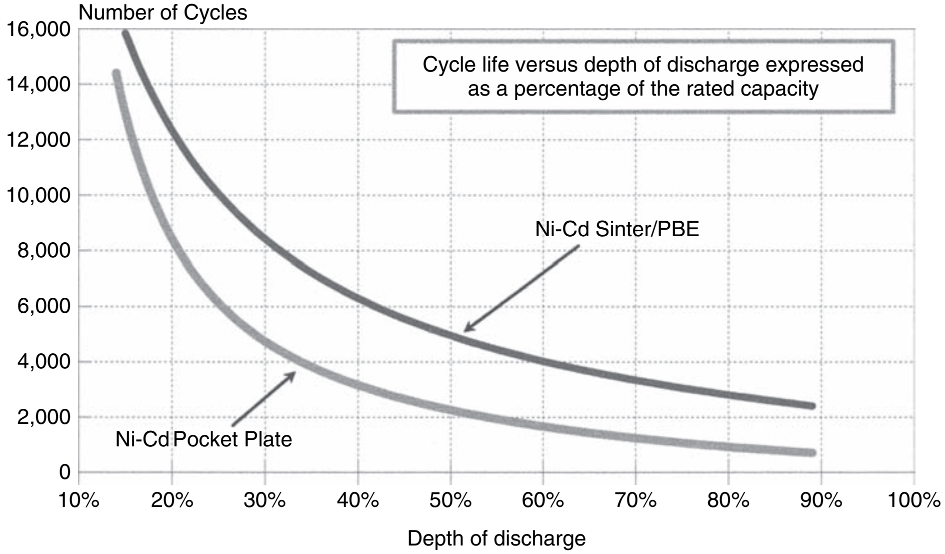

Figure 10.3. Cycle behaviour for nickel-cadmium cells.

generates a very small current in the cells and so the water usage is minimised and the high charge voltage, which only operates for a relatively short time, gives a rapid recharge of the battery. The technology used can accept these fast recharge times without deterioration.

At relatively low voltage charge rates, the sintered/PBE product can be fully charged in 24 hours from a completely discharged state. The pocket plate product does not achieve the same level but nevertheless can be recharged to 90% over the same period. After this stage, the batteries would then pass to a maintenance voltage that would be sufficient to maintain and slightly charge the battery.

The single level charge has only one voltage level which has to be a compromise between a voltage high enough to charge the battery relatively quickly and a voltage low enough that it does not consume excessive water. However, it does have the major advantage of simplicity and, hence, reliability.

Typical voltage levels per cell for the two types of charge are shown in Table 10.2 for the two technologies.

10.6. Cost and Reliability Considerations

The nickel-cadmium battery, because of its complex manufacturing requirements, is a more expensive product than the simpler lead-acid product. However, the cost of ownership of a battery is much higher than simply the initial purchase cost and the least expensive initial cost solution can easily become the most expensive solution over the life of the system. In practice, the cost of ownership of a battery system can be split into three sections as follows:

- The initial procurement cost includes the cost of the battery, the purchasing and administration costs and the installation labour.
- The annual maintenance costs include the battery inspection costs, which are often linked to national standards and, where appropriate, any battery watering required.
- The battery replacement costs include the new battery cost, the purchasing and administration costs, the installation labour and the disposal cost of the old battery.

Table 10.2. Typical charge voltages for nickel-cadmium cells.

	Single level (V)		**Two level (V)**		
Type	min	max	min	max	floating
Pocket	1.43	1.50	1.45	1.70	1.40-1.42
Sinter/PBE	1.40	1.43	1.45	1.55	1.39-1.41

These factors favour different battery types according to the application, and choices are made between valve regulated lead-acid, flooded lead-acid, flooded nickel-cadmium and low maintenance nickel-cadmium.

However, in any critical application the criteria are not just cost, even life cycle cost, but also reliability and the costs of producing reliable systems grow exponentially as reliability requirements are increased (Figure 10.4).

Reliability is based on the number of failure modes and their severity. The measure of reliability is related to battery performance under the actual operating conditions and a predictable failure mode is important for any controlled regime. If failure is regarded as the inability of the battery to meet the discharge specification, then it is very important for the battery to be 'fail-safe'. In other words, the battery should avoid any sudden failure while the user is expecting it to work.

For a battery involved in a critical application, it is important to evaluate a number of factors. Those related to cost are lifetime, maintenance and installed cost. Those related to reliability are a predictable failure mode, ability to cycle, behaviour under temperature extremes and tolerance to electrical system malfunction and mechanical disturbances.

The right balance between reliability and cost is not simple to achieve and requires careful analysis.

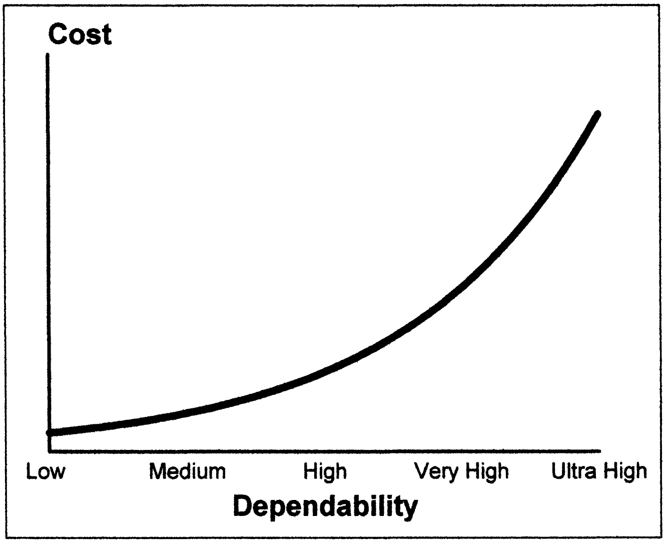

Figure 10.4. Increase in cost with reliability.

10.7. A Large Battery in an Energy Storage Application

10.7.1. Introduction

In terms of power supplies, Alaska is trying to behave as an "island", *i.e.* trying to be self sufficient without importing power from outside. This means that peaks or failures in the power have to be accommodated within the local power network. For this reason, an interest in a Battery Energy Storage System (BESS) was developed there. Its basic function would be covering the time from the tripping of a generator or transmission line to the diesel generators reaching generation speed (spinning reserve); in practice, it would also cover a number of different power schemes.

The Golden Valley Electrical Association (GVEA) is based in Fairbanks, Alaska and serves a population of 90,000 residents (40,000 customers) over a 5,700-km^2 area. In winter, the temperature may be as low as -60°F (-51°C). In summer, it may rise above 90°F (32°C). It has generation facilities of 25 MW coal-fired and 200 MW of diesel and oil-fired gas turbines and it controls 3,540 kilometres of distribution line and 540 kilometres of transmission line.

The construction of a 300-kilometer 138 kV Intertie in 1985, between the Anchorage utilities and the GVEA system, allowed GVEA to take advantage of low-cost natural gas and hydroelectric generation. However, this increased the need for GVEA to provide excess generating capacity above the current system load and increased the risk of generation outages and transmission line disturbances. In the early 1990s, a group representing the utilities which was examining stability issues concluded that the most effective solution would be the construction of a battery energy storage system.

10.7.2. Defining the BESS

The requirement for the BESS, based on the needs of other planned projects, was that it should be capable of providing 40 MW for 15 minutes and have enough residual energy for a controlled ramp-down at 4 MW/minute. The 40 MW was based partly on the anticipated output of the US Department of Energy-funded Healy Clean Coal Plant (HCCP), and was projected to eliminate 74% of the system outages historically experienced. The 15-minute run time would allow for alternative generation to be brought on line. Since the specification was based on performance, it allowed potential suppliers the ability to tailor their systems to their own particular abilities.

The BESS was required to have the possibility to operate in seven different modes: VAR support, spinning reserve, power system stabilizer, automatic scheduling, scheduled load increases, automatic generation control and charging.

It was a particular requirement that the cost should be based on a 20-year life for the installation and so a full life cycle cost analysis was required from each supplier in support of his proposal.

The project milestones for the ABB/Saft consortium covered a period of over 10 years and are summarised as follows:

- 1990: project conceived
- 1996: meeting with GVEA consultants
- 1996: ABB/Saft consortium formed
- 1998: technical proposal
- 2000: commercial proposal
- 2001 (May): ABB/Saft chosen for final negotiations
- 2001 (Aug): final proposal
- late 2001: decision

When GVEA signed the contract in 2001, the Healy Clean Coal Plant was not ready to enter service and so the performance requirement was reduced from 40 MW to 27 MW, with the possibility of increasing this at a later stage. However, even at this reduced level a decrease in outages of 68% was predicted.

10.7.3. The BESS Design

There are two primary components making up the BESS; these are:

- The nickel-cadmium battery, developed by Saft, which constitutes the energy storage medium.
- The converter, designed and supplied by ABB, which changes the battery's dc power into ac power, ready for transmission over the GVEA grid.

Although it is possible for the BESS to produce up to 46 MW for a short time, this is not the principal role. This, in fact, was to cover the 15-minute period between sudden loss of generation and start-up of back-up generation.

10.7.3.1. The Battery

The BESS battery consists of four parallel strings of 3,440 920-Ah high performance pocket plate cells. Hence the storage capacity was $4 \cdot 920$ Ah = 3,680 Ah and the total number of cells in the battery was $3{,}440 \cdot 4 = 13{,}760$. In order to simplify handling, the cells were built into 10-cell modules, which were mounted into an industrial racking system. An aisle between the racks allowed for service access for a swing-arm fork truck.

The complete battery weighs some 1,300 tons and the area in which it is located measures 120x26 m. The high-performance pocket plate construction was chosen to give the full 20-25 year life without any loss of the beneficial characteristics of Ni-Cd batteries. These pocket plate cells can deliver 80% of their rated capacity in 20 minutes and can withstand repeated deep discharges with little effect on battery life.

The use of 10-cell modules in the design allowed for easy installation, as the modules were prefabricated at the factory, gave a quick change out facility in the case of problems and allowed for simple water replenishment via a purpose built water filling system.

Although the battery was configured with four battery strings, it could be extended to six or eight strings as the utilities requirements increase.

10.7.3.2. The Electrical System

The voltage source converter at the heart of the electrical system

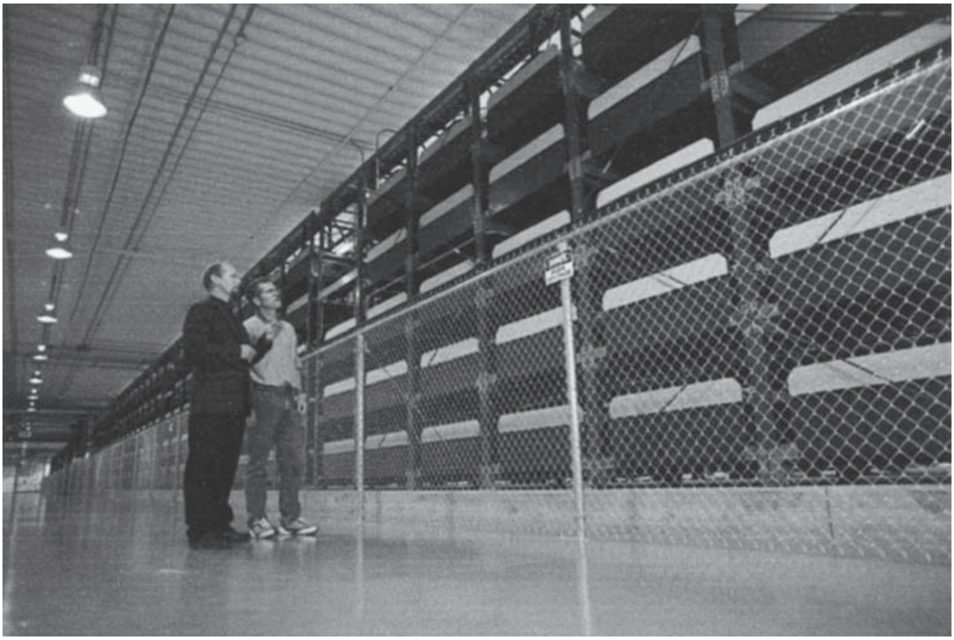

Figure 10.5. Part of BESS battery.

comprises standardized PEBBs (Power Electronic Building Blocks). One double-stack PEBB in NPC (Neutral Point Clamped) connection forms a single-phase H-bridge and four of these bridges are installed per phase. The stacks are cooled by deionised water. The use of proven, reliable components enhances the reliability and all components were made readily accessible to enhance serviceability.

10.7.4. Operating Results

The BESS was handed over for commercial operation on September 19, 2003 and saw its first 'real' discharge on November 11, saving approximately 2,500 customers from being disconnected.

In 2004, BESS operation was triggered 56 times, saving a total of nearly 290,000 customer disconnections and, for the period to date (mid 2006) the number of outages prevented is shown in Table 10.3 [5]. This is constantly updated on the GVEA BESS web site.

A GVEA requirement was that the system should be able to demonstrate at least 98% availability over the first 18 months, this not only including total system outages but also partial outages involving individual battery strings. Over the availability guarantee period, the system availability was slightly over 99%

10.7.5. Awards

It is quite unusual to mention awards when discussing battery based systems, but the Alaska BESS has become quite a celebrity in its field. ABB was awarded the Platts 2003 Global Energy Award for its design and

Table 10.3. Outages prevented to date by the Alaska's BESS.

Year	Total outages prevented	Total Outage Time	Number of Consumers	Total time of prevented outages per member	Avg. Number of prevented outages per member
2003	3	24 min	11,122	8 min	<1
2004	56	529 min	286,598	66 min	7
2005	34	416 min	226,052	48 min	5.6
2006 (to July)	36	334 min	117,897	27 min	2.9

development of the BESS converter, GVEA were awarded an EPRI technology award for the BESS project, and the BESS won a Guinness World Record certificate as the world's most powerful battery when it discharged 46 megawatts for five minutes in April 2005.

10.7.6. Final Considerations

In reducing power outages in the Fairbanks area, the GVEA BESS has given additional benefits in the areas of transmission and distribution, generation and strategic planning:

- In the area of transmission and distribution it has improved voltage regulation, first swing stability and loss reduction.
- In the generation area it provides spinning reserve, ramp-rate constraint relief, load following, black starts, load levelling, and a reduction in deferred turbine starts.
- Other factors arising from its use include improved power quality, reduced demand peaks, and enhanced service reliability through reduced power supply generated outages.

The BESS is an example of the use of reliable equipment in a critical application and the need to carry out a thorough assessment of the options available and the real costs involved before decisions are taken.

10.8. Small Batteries in Telecommunication Applications

In a traditional telecommunications environment the battery system is usually housed in a clean, well ventilated building with a controlled temperature range. This is not a difficult situation for a battery and, although they have not really met their life predictions, the VRLA (valve regulated lead-acid) batteries, which are compact and have simple maintenance, are an acceptable, and preferred, choice.

With the advent of cellular telephone systems, fibre to the curb and other developments, there is a requirement for reliable kerb-side and remote relay systems. These systems are often housed in units that have limited ventilation and can have interior temperatures well in excess of the outside temperature. Theses cabinets contain their own power back-up systems which are supported by a battery.

As these systems were developed, it was logical to continue with established technology which was well known in the industry and to use the

VRLA as the preferred energy storage system. Its compactness constitutes a major requirement for an outdoor cabinet.

However, this change of housing moved the VRLA battery to an extremely arduous environment and, soon, premature failures were occurring in the field. Therefore, a better battery technology was required.

Unfortunately, the compact nature of the VRLA battery meant that it was not possible to purchase an 'off-the-shelf' replacement and it was necessary to design and build a special nickel-cadmium battery block based on the experience of the sinter/PBE technology used in the electric vehicle market. Even then, it was not possible to meet the dimensions needed to match the smaller capacity VRLA batteries and equivalents were limited to sizes above 100 Ah.

Ni-Cd batteries are deployed in telecommunication applications throughout the world, and, in the past 5 years, thousands of strings of the sinter/PBE construction batteries have been put into service.

The operational history has been positive with very few failures and a technical evaluation of this was carried out on a number of 'in-service' batteries. The results of these tests were reported at Intelec in 2002 [3]. Some of the batteries chosen were taken from field trials, where the batteries had been monitored throughout their history, while others were from normal commercial installations.

All the batteries examined were in a typical telecom 48 V system and were made up of 38 cells, each with a nominal voltage of 1.2 V, and operated in a voltage window of 42 to 55 V. They were of the standard low maintenance design which, in the difficult high temperature situations found in outdoor cabinets (Figure 10.5), were planned to have a required watering interval of once every 5 years.

The batteries tested were taken from the southern areas of the USA, *i.e.* the warmest areas, stretching from California to Georgia.

The batteries evaluated had been in service for between 7 months and 4 years and, in most applications, the available capacity was about 95% of the nominal capacity. In two cases, the available capacity was only around 75% and this was attributed to failure to follow the 'rules' for extended storage before putting into service. However, the batteries at 75% capacity were still working: they had not 'failed' and were still capable of supporting the system, albeit with a shorter than desired back-up time.

It must be noted that the available capacity tested was in the application conditions and is connected to the state of charge of the battery, *i.e.* to the charging conditions applied. This does not give an indication of the end of life of the battery, as a full charge cycle would return the batteries to values near their full capacities.

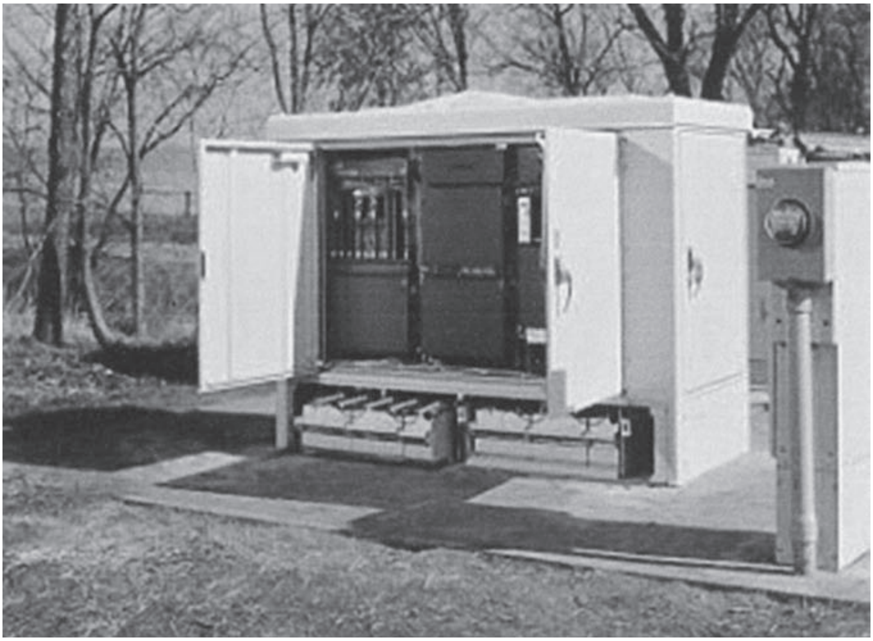

Figure 10.5. Typical outdoor cabinet installation.

The high temperature and lack of maintenance experienced in outdoor telecom cabinets is a very difficult environment for a battery. As mentioned above, experience with VRLA batteries have shown premature failure in service. The experience with the sinter/PBE nickel-cadmium batteries have shown that watering intervals were in the range of the predicted 5 years with lifetimes expected to achieve in excess of 15 years.

This could be predicted from the technology but field trials have verified this. These trials have demonstrated that careful attention to charging methods and preparation prior to installation are necessary to ensure that the batteries achieve the capability possible in such an environment.

This work emphasizes the advantage of the nickel-cadmium battery under high temperature conditions and outlines that under these conditions, provided the cost is evaluated in terms of life cycle, they can be a cost effective solution.

10.9. Lifetime and Reliability: The Case of an Old Battery

During the restoration work of giant steam engines at Kempton, near

Twickenham, England, an 84-cell battery, contained in 12 wooden crates, was discovered amongst the ancillary equipment. The nameplate revealed it as a nickel-cadmium 110 V battery with a capacity of 32.5 Ah, which had been produced by 'Nife Batteries' of Reddich (England). It is believed that the battery provided backup power for the instruments that monitored the chlorine house.

Analysis of the date code on the steel cells revealed that the batteries were manufactured in late 1960 and so went into service in late 1960 or early 1961 and were therefore 45 years old at the time that restoration began. As the engine house went out of service in 1980 it is believed that the batteries were used for a period of up to 20 years and then were left, without any service or maintenance, in a damp environment for 25 years before restoration.

The restoration work, sponsored by Saft, is now complete (Figure 10.6) and the cells have been brought as closely as possible to their original condition with some new components – the electrolyte in particular. The only changes that have been made have been to conform to modern safety requirements. After refurbishment, the cells achieved about 50% of their original capacity.

The whole system with its charger can now be seen very much as it was 45 years ago by visitors to the museum that has been built. The battery is to be used to provide back-up lighting for the engine house, where it is estimated that it will provide up to 3 hours lighting for the engineers. There is, of course, a modern emergency lighting system (using small sealed Ni-Cd batteries) to meet the legal requirements of safety for visitors.

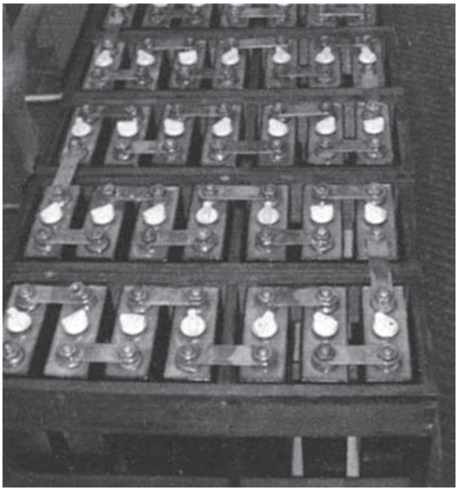

Figure 10.6. Kempton's old Ni-Cd battery after refurbishment.

This successful restoration further illustrates the durability of the nickel- cadmium cell and why it has gained its reputation of lifetime and reliability.

10.10. Nickel-Cadmium Applications Summary

Nickel-cadmium technology has been available for 100 years and, in that time, has created a niche market for its particular attributes. It is, in fact, available for all the areas where industrial batteries can be used and particular product types are designed to match specific application needs.

In particular, it has strengths in terms of lifetime, performance, cycling ability and ability to withstand extremes of temperature and other environmental conditions.

It is used in a widely diverse range of applications including engine starting, switchgear, UPS, process control, data and information, emergency lighting, security and fire alarms, switching and transmissions, signalling and renewable energy applications such as photovoltaic, wind and hybrid systems. It can be used in any industrial application where a battery system is required and each of these applications has different needs. Some of the above applications, of the stationary type, are briefly outlined below.

Engine starting

In critical applications, the nickel-cadmium product can be engineered for high power without compromising life. In the electricity industry, engine-starting batteries are required for auxiliary generators and fire extinguishers that have to be brought into action in case of failure in the main power supply. Typical starting cycle is 30 sec with high peak currents of 10C, to be repeated several times.

The battery must not fail due to short, and it must keep high power capability under any circumstances, even after ageing or at low SOC and at very low temperatures. Life expectancy is 15 to 20 years. In terms of cycles, the discharge is shallow, a few percent, and on this basis the nickel-cadmium cell can do hundreds or millions of cycles.

A typical engine starting battery (see Figure 10.7) is 24 V, 100 Ah; the full range is 12 to 36 V, 20 to 200 Ah.

UPS (uninterruptible power supplies)

These are applications which can have discharges from a few seconds to several hours. In this situation, it is simply a question of choosing the appropriate level of performance required from the nickel-cadmium cell to give the most cost effective solution. In terms of lifetime and resistance to failure, all

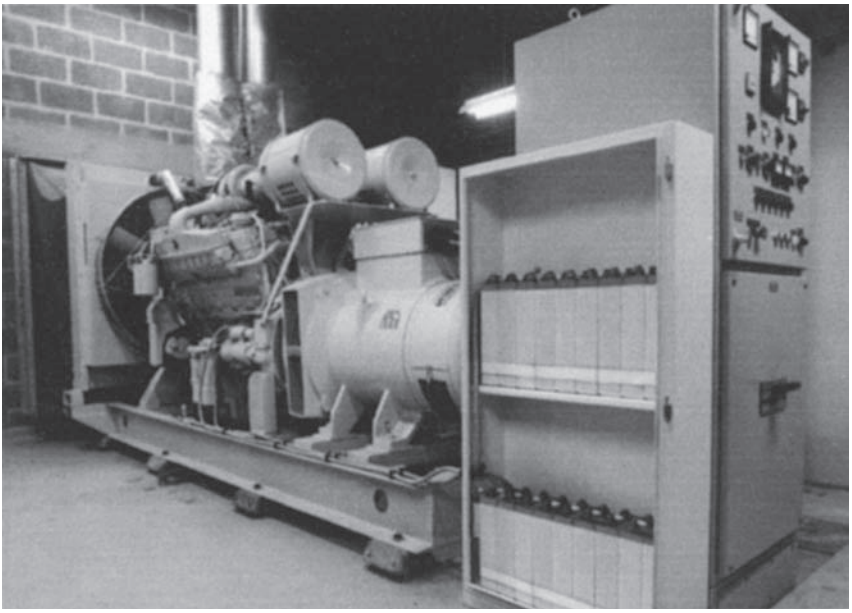

Figure 10.7. Engine starting system with NiCd battery.

levels of cell performance give the same level of security.

However, it is necessary to choose the optimised product from the low, medium and high discharge performance products, to find the best solution for a particular application. In recent years, fibre electrodes have also been used in UPS applications; different types can cover discharge times ranging from 0.5 to 600 min [6].

An UPS battery may be requested to operate for up to 8 hours, as is the case of the large Ni-Cd battery packs (>10,000 Ah) installed as a back up of the control and communication systems in a huge oil field exploration plant in the North Caspian sea [7].

Typical batteries for UPS applications are:

- Industrial UPS: 110 or 220 V, 100 to 200 Ah (but can reach 1500 Ah) for backup of 30 min to 1h, sometimes more;
- Data centers/banking: 400 V, ~100 Ah (but can reach 400 Ah), for 15 to 30 min backup time.

Figure 10.8 illustrates a very large battery system for multiple use with high power SPH Saft Ni-Cd batteries, installed in 1994 in an EDF power plant in France. It includes 230 V, 115 V and 24 V battery strings for UPS and a 230 V, 390 Ah back up power supply for engine starting (turbines greasing pump).

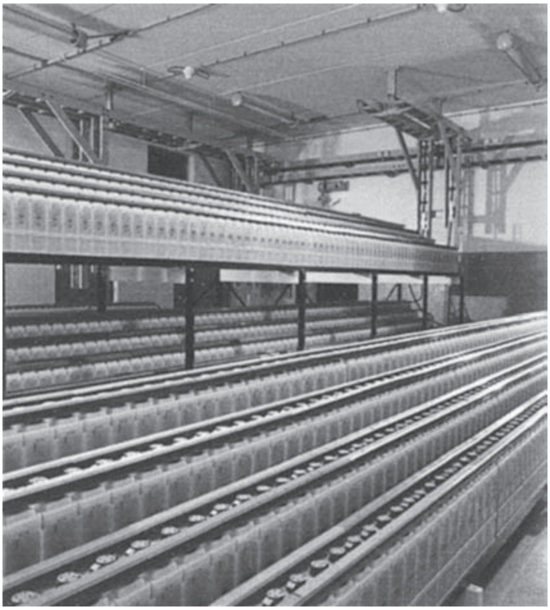

Figure 10.8. Example of a large industrial NiCd UPS battery. (*Courtesy of Saft*)

Electricity substations

These require good high-rate switching capability from (typically) medium-rate batteries. There should be a consistent high rate performance with no 'coup de fouet' phenomenon, experienced with lead-acid batteries, to compromise the application. The minimal fading of switching capability over life and long life at high temperatures in small substations in a distribution network are an important feature of the Ni-Cd battery in this situation.

Remote photovoltaic (PV) applications

The nickel-cadmium battery is ideally suited for these applications. It has good cycling capability; low maintenance in remote systems; lower weight for transport to remote sites and significant abuse resistance in terms of temperature and rough handling. Newer versions have been designed with extended maintenance intervals thanks to the use of enhanced recombination plate separators.

The batteries cycle at, typically, 5-30% DOD every day in the day/night cycle, but can be discharged much more deeply during wintertime. Ni-Cd batteries are particularly able to operate and cycle at low state of charge during the winter months with low illumination, when lead-acid batteries may suffer from sulfation as there is no possibility to boost charge them.

Typical uses are powering radio/telecom sites in remote areas, signalling along coastlines and on sea (lighthouses, beacons), electrification of oil platforms and pipelines.

An example is provided by the Ni-Cd battery connected to a combined PV-wind hybrid system in a remote island in the archipelago of Stockholm. The 48 V, 571 Ah, pocket plate battery, which has replaced a previously installed lead-acid, has been in service since 1983 and is expected to reach a lifetime of at least 20 years [8].

Batteries for this application are typically 12, 24 or 48 V, with capacities from 100 to 1000 Ah in a single string, with several strings being connected in some cases to give several thousands of Ah.

Figure 10.9 shows 6 V, 140 Ah and 45 Ah modules used to build batteries for photovoltaic energy storage.

Rail vehicles

Particular species of “standby” batteries can be found on board rail vehicles. Besides starter batteries for locomotives (see “engine starting”) NiCd batteries are installed on all kinds of rolling stock (except freight wagons): from electric locomotives (“e locos”) and EMUs (Electrical Multiple Units), to urban mass transit vehicles like metros and tramways, to long distance trains with either hauled passenger coaches or EMUs and high speed trains.

Batteries ensure energy to auxiliaries ranging from lights and ventilation only in passenger coaches, to door opening, braking, radio-communications, and air conditioning systems in most advanced train designs

Figure 10.9. NiCd Saft battery modules for photovoltaic energy storage.

Table 10.4. Characteristics of batteries used in rail vehicles.

Vehicle type	Voltage (V)	Capacity (Ah)	Discharge duration (h)
Passenger Coach	24	300-500	3-5
E locos and EMU	110	50-150	1
Metros	64, 72, 96 or 110 today	100-200	0.5-1
Tramways	24	100-200	0.5

in case of absence of main power or converter failure.

Sized for emergency cases, the batteries are very often subject to shallow cycling, as the converter or mains power is frequently interrupted in trains (changing sectors, manoeuvring, emergency stops, *etc.*)

Passenger coaches typically use 24 V, 300 to 500 Ah batteries for 3 to 5h discharges. E locos and EMU batteries are mostly 110 V today, providing 50 to 150 Ah during 1h discharge. Metros batteries are: 64 V, 72 V and mostly 96 V or 110 V today, providing 100 to 200 Ah in 0.5 to 1h. Batteries for tramways are mainly 24 V, 100 to 200 Ah, 30 min. In Table 10.4, the characteristics of batteries for these different vehicles are summarized.

Rail batteries are increasingly delivered as complete systems, with their mechanical housings and electro technical equipment allowing the rail OEM to install them directly into the train.

Figure 10.10 shows such a battery system using 74 MRX 80 Saft Ni-Cd cells providing a 96 V, 80 Ah power supply for 90-minute backup time.

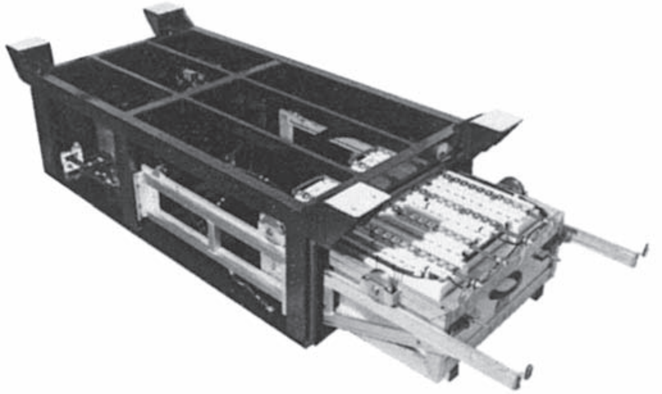

Figure 10.10. 96 V, 80 Ah battery system unit used to provide energy backup to railways vehicles. (*Courtesy of Saft*)

Nickel-cadmium batteries generally have a significantly higher initial cost than their lead-acid counterparts, and may not be the most cost effective choice in many applications. However, in specific conditions and where high reliability is critical, as in the examples provided above, the long-term cost of ownership of Ni-Cd, or life cycle cost, is frequently lower than for other battery options.

References

1. A. Green, Characteristics of the NiCd Battery related to Energy Storage in Renewable and Energy Storage Systems, *International Symposium on Power Sources for Stationary and Distributed Power Systems*, September 2003, Munich, Germany.
2. M. L. Whitehead, A Comparison of Nickel-Cadmium and Lead-Acid Industrial Batteries, *ERA Technology Ltd Report 98-0480,* May 1998.
3. S. Lansburg, J.M. Cocciantelli, O. Vigerstol, Performance of Ni-Cd Batteries After Five Years of Deployments in Telecom Networks Worldwide, *INTELEC,* Sept/Oct 2002, Montreal, Canada.
4. A. Green, Finding the Right Balance Between Reliability and Economics for Batteries Used in Critical Rail Trackside Applications, *Railway Engineering,* June 2005, London, UK.
5. J. McDowall, T. DeVries and N. Umbricht, Getting Results from the Most Powerful Battery System in the World, *PCIM,* June 2005, Nürnberg, Germany.
6. D. Ohms, M. Kohlhase, G. Benczur-Urmossy, G. Schadlich, *J. Power Sources* 105 (2002) 127.
7. www.engineeringtalk.com/news/sgt/sgt151.html
8. www.engineeringtalk.com/news/sgt/sgt114.html

This page intentionally left blank

Industrial Applications of Batteries. From Cars to Aerospace and Energy Storage
M. Broussely and G. Pistoia Eds.,
© 2007 Elsevier B.V.

Chapter 11

MISCELLANEOUS APPLICATIONS. I. Metering, Power Tools, Alarm/Security, Medical Equipments, *etc.*

Michel Grimm

SAFT LBD, rue Georges Leclanché, 86060 Poitiers, France

Listing all the industrial applications of batteries would be an endless exercise. For this reason, only a selection of technically challenging applications will be presented in this chapter:

- metering systems
- remote mobile monitoring
- automatic assistance systems
- alarm and security systems
- memory back-up and real time clocks
- professional cordless tools
- ambulatory medical equipments

Furthermore, even within the same market segment, the power source technical specifications may considerably differ. This is why it has not been possible to present precise parameter values to characterize the performances that are expected from the batteries in each application. Therefore, only "typical" or "general" data will be presented, knowing that more severe, or milder, specifications may exist in each of the applications presented below.

11.1. The Power Sources

11.1.1. The Different Electrochemical Systems

Compared to some other industrial applications, the ones that will be detailed in this chapter are characterized by the relatively small size of their power sources. In fact, the capacity of the battery packs will rarely exceed 20 Ah.

Another feature of these applications is the vast variety of the electrochemical systems they use. Apart from the popular 1.5 V alkaline cells (Zn/MnO_2), many primary lithium couples are available today, not all used to the same extent (see also Chapters 1 and 2):

- 1.8 V lithium/iron disulphide (Li/FeS_2)
- 3 V lithium/manganese dioxide (Li/MnO_2)
- 3 V lithium/carbon monofluoride (Li/CF_x)
- 3 V lithium/sulfur dioxide (Li/SO_2)
- 3.6 V lithium/thionyl chloride ($Li/SOCl_2$)

Among the secondary couples which co-exist today in the industrial application markets, the following are most widely used (see again Chapters 1 and 2):

- 2.0 V sealed or valve-regulated lead/acid couple (SLA or VRLA)
- 1.2 V nickel/cadmium (Ni/Cd)
- 1.2 V nickel/metal hydride (Ni/MH)
- 3.7 V lithium/ion (Li/Ion)

It is to be noticed, to make the selection process even more complicated, that, within each electrochemical system, several battery types may exist. The differences between the members of a system family may be due to the shape: some cells are cylindrical (by far the most widely spread geometry in industrial applications) but some others may be prismatic (rectangular) or coin shaped.

Furthermore, cells with the same electrochemistry and the same size may offer huge differences in terms of drain capabilities. This is because their internal design may be very different. For instance, the SAFT LS33600 is an R20 (or D) size $Li/SOCl_2$ cell, whose tubular positive electrode area is 42 cm^2; during an external short-circuit the current will not exceed 5.0 A. The SAFT LSH20 is also an R20 size $Li/SOCl_2$ cell, but the area of its spirally wound electrode is 328 cm^2; during an external short-circuit, the current could exceed 30 A.

The lithium/thionyl chloride system helps us illustrate this variety of shapes, sizes, internal designs and characteristics that a family of cells with the same chemistry can offer. Within this electrochemical system, the following cells can be found:

- low rate cylindrical cells: from small cells with a nominal capacity of less than 0.5 Ah up to DD size cells of more than 35 Ah
- low rate prismatic cells
- low rate wafer cells
- high rate cylindrical cells able to deliver pulses in excess of 50 A
- small, low rate cylindrical cells operating at temperatures of up to +150°C
- larger, high rate cylindrical cells able to operate at temperatures of up to

+200°C

- low rate cylindrical cells associated with an hybrid layer capacitor in parallel (see also Chapter 12)

Rechargeable systems also offer a wide variety of characteristics, as the Ni/Cd system may demonstrate: Ni/Cd cells may contain either the sinter/sinter technology (lower cost/lower performance) or the PBE one (plastic bonded electrode), or the high porosity nickel foam electrode type (higher cost/higher capacity).

So, the question is: how to choose among the many electrochemical systems offered to the device designers, or, in other words, how do these electrochemical systems compare?

Of course, some applications are so specific that the solution is obvious: for instance, the developers of down-hole logging tools operating at temperatures near 150°C do not have many options when selecting a power source for their equipments. However, most of the time, the designer has different power sources to utilize, and several ways to use them.

The applications mentioned in this chapter often contain equipments or devices that must be moved and/or handled. This means that weight and size will prove important for the selection of their power source. On the other hand, there are applications where a battery replacement is not an option, or it may be required that the replacement occurs as seldom as possible. In fact, the cost of replacing a cell may be very high (*e.g.* replacing a dead cell in a utility meter costs around 100 euro!). Consequently, a very long cell runtime is necessary: the amount of energy in the power source is a decisive factor too.

The operating environment conditions which, in case of outdoor applications may be very severe, will also contribute to orientate the choice: after all, there are not many batteries able to operate reliably between -40°C and + 70°C for more than 10 years, as expected from the cell powering the memory of an electronic electricity meter.

The cost is also a crucial factor that the engineer cannot ignore when making his choice. This is mainly due to the 12-month horizon of most purchasing departments. An approach based on costs is not always the right one, as the lower-priced solution may prove to be the most expensive in the long run.

To compare the different primary systems in light of the above mentioned characteristics, Table 11.1 may be useful (see also Chapters 1, 2 and 12).

Primary lithium cells, and their packs, are more expensive than packs made with alkaline cells for several reasons:

Table 11.1. Comparison of some primary electrochemical systems.

	Alkaline (C size)	**Li/MnO$_2$ (spiral C)**	**Li/CF$_x$ (spiral C)**	**Li/SO$_2$ (spiral C)**	**Li/SOCl$_2$ (spiral C)**
Voltage (V)	1.5	3.0	3.0	3.0	3.6
Capacity (Ah)	6.5	4.5	5.0	3.75	5.5
Typical operating temperature (°C)	-20/+60	-40/+70	-40/+85	-60/+70	-60/+85
Specific energy (Wh/kg)	140	280 bobbin: 355	360	280	390 bobbin: 610
Energy density (Wh/L)	370	510 bobbin: 720	565	425	750 bobbin:1155
Unit cost	low	high[1]	acceptable	acceptable	high[1]

1. Acceptable for low-rate bobbin cells

- some of them are equipped with a glass-to-metal seal. This sealing is definitively more costly than the plastic grommet used for alkaline cells
- Li cells have to be assembled in costly dry rooms while alkaline cells are manufactured in the open air
- often, lithium cells have to operate for many years, and sometimes in corrosive environments. The resistance to corrosion being a must, the use of more expensive stainless steel cans is a solution, but it costs more than the nickel-plated steel used to make the alkaline cell cans.

However, if lithium battery runtimes often reach 10 years (and even more in some meters or alarm sensors), the runtimes of alkaline cells do not exceed 4 to 5 years, and cautious users (or sensitive applications) may even require their replacement every year. Since, in some applications (*e.g.* utility metering) the replacement cost of one battery can be very high, the lower number of replacements allowed by the lithium solutions can lead to noticeable savings in the end.

In Table 11.2, a comparison of secondary batteries is presented (see also Chapters 1, 2 and 12).

The Li/Ion electrochemical system has been pioneered by battery manufacturers primarily to supply the huge consumer market of personal items, such as mobile telephones and laptop computers. However, over the last several years, lithium ion batteries have found use in an increasing number of industrial applications. The high energy density, wide operating temperature range, high cycle life, and low internal resistance have opened the scope of opportunities in diverse sectors. Li/Ion batteries are now replacing alkaline and other types of rechargeable batteries in many portable types of equipment as the price differential reduces and the technical benefits are realized. In addition, large lithium ion batteries are being introduced in applications where large alkaline batteries have been traditionally used.

Table 11.2. Comparison of some secondary electrochemical systems.

	SLA(*)	**Ni/Cd**	**Ni/MH**	**Li/Ion**
Voltage (V)	2.0	1.2	1.2	3.7
Specific energy (Wh/kg)	35	50	90	165
Energy density (Wh/L)	80	170	330	330
Number of cycles (100% DOD)	200	600/1000	300/500	500
Unit cost	low	moderate	acceptable	high

(*) Sealed Lead Acid

11.1.2. How to Select the Right Power Source?

Selecting the right power source to satisfy the specifications of a given industrial application, *i.e.* finding the battery which will satisfy the performance expectations of the device or equipment designer, may be a complex process, as illustrated below.

In fact, industrial projects are becoming more and more sophisticated and demanding, and the number of primary and secondary cells is very large. A possible approach to the right battery selection can be the following.

- First, it is necessary to have a comprehensive view of the project's technical specifications and of the economical expectations of the project leader. This may sound obvious, but knowing exactly what the performance of a power source should be is not always easy. For instance, how to describe, accurately enough, the operating temperature conditions of the cells used inside tollgate transponders, knowing that these devices are located behind the windshield of cars which can be driven either in Scandinavia or in Southern Europe?
- Then, a detailed analysis of the electrical requirements has to be carried out. The maximum and minimum acceptable voltage of the circuitry may immediately lead to the selection of a given electrochemical system and to the necessary number of cells in series.
- The highest peak currents will allow selecting high-, low- or moderate-rate cells. In the case of very low currents (a few mA maximum), coin cells may be selected. In the case of moderate currents (less than 500 mA), bobbin cells (with concentric electrodes) may be the solution. In the case of high pulses (more than 500 mA), either spirally wound cells or bobbin cells fitted with a capacitor in parallel will be used.
- The expected runtime of the battery will determine the size of the cells or the number of branches to be assembled in parallel in the battery pack.

Calculating the runtime of a battery in the conditions of a given application is a tricky process, whose details are considered industrial secrets and, as such, may not be revealed to the outside world.

- The environmental factors that may affect the battery performance must be studied. The knowledge of the storage and operating temperature extremes, or of the average temperature, will help selecting the proper cell chemistry, but this is not always sufficient: it is preferable to get a clear view of the temperatures histogram over a reasonable length of time.
- The mechanical constraints will have to be taken into account, more particularly when the cells will be assembled into a battery pack. Thermal shocks and cycling, mechanical shocks and drops, vibrations, accelerations, low and high pressures, corrosive atmospheres, fluid contaminations, potential abusive usages or situations: the list of harsh conditions that batteries may have to stand is limitless.
- The choice of a battery may simply be based on its maximum acceptable weight or size (*e.g.* when the battery compartment has been designed prior to the battery selection, which is not an exceptional case).
- The design of the battery pack often implies the selection of the proper material for the cell container, of a reliable connector (corrosive environments may lead to the adoption of gold-plated contacts when the batteries have to operate for many years), and protection components. The cell may be encapsulated into an epoxy resin for better protection or simply varnished.
- A review of all the norms and regulations to be satisfied by the power source will have to be made. The armed forces have issued many norms, and civil institutions have done the same. UN, IATA, IMO, ADR, CFR, IEC, UL, EN, RTCA, *etc.*, are familiar acronyms to battery users.
- The economic aspects of the projects will obviously have to be analyzed. Of course, the price of the cell or the battery pack will be considered, but other costs will affect the economic balance of the project, such as the battery development, the qualification tests, the tooling, and the replacement. The time required to develop a new battery pack may prove a decisive cost factor.

11.2. Metering Systems

Single users as well as industrial factories or administrative buildings use diversified "fluids", whose consumption needs to be quantified (metered). "Metering" implies several activities, such as counting, allocating, reading, transmitting, billing, valve actuation (*e.g.* in gas meters located in geographical areas where earthquakes can occur). To do so, utility companies rely upon different types of devices: meters, but also valves, gas volume correctors, cost allocators, meter readers, computer terminals, *etc.*, which may need autonomous power sources.

Formerly, mechanical and electromechanical types of meters were used, which were simple, robust and required limited maintenance. However, they presented a degrading accuracy over time and offered little possibility for innovation. To circumvent these limitations, not only have add-ons been fitted onto these old meters, but also electronic meters have been introduced in the early 1980s, which allowed for fraud or outage detection, multi-rate tariffs, time-of-use registration, prepayment possibilities, *etc.*

Four main functions are requested to the power sources for electronic meters:

- power the meter (*i.e.* the microprocessor which counts, the LCD display and, possibly, the prepayment unit) when no external power source is available
- provide a back up for the memory, the real time clock, or the LED display in case of mains outages
- power remote reading modules
- power meter accessories (*e.g.* valves) or auxiliary devices (gas correctors, data concentrators, meter reading repeaters, *etc.*)

All this translates into the following specifications:

- a few μA current during the sleep mode
- a few mA pulses during awakening and listening periods of time
- several mA pulses during reading receptions
- up to several Amps pulses during data transmissions
- minimum acceptable voltages between 2.0 V and 3.0 V
- wide operating temperature ranges: typically -40/+70°C
- runtimes of 5 to 10 years (with a recent tendency to stretch them towards 20 years)

Other capabilities are expected from the meter power sources:

- ability to long resist corrosive environments, since many types of meters are outdoor devices, which could be next to sea shores for instance
- capability to pass many qualification and safety-related test protocols, such as the Underwriters Laboratories recognition, the United Nation transportation regulation, the ATEX (intrinsic safety) norm, flame tests, *etc.*

In the vast majority of the metering devices, primary lithium batteries have been adopted. A review of the specifications of the major metering sub-segments, reported in the following, will explain why.

11.2.1. Heat Meters and HCA (Heat Cost Allocators)

Due to the rapid increase of the cost of oil, some European countries initiated a drastic energy saving program at the end of the 1970s. For instance, in Germany, the use of heat meters, destined to measure the consumption of hot water in each apartment, became compulsory.

If the flow measurement can be made mechanically with a rotating wheel, the temperature sensing and the heat consumption computing need some electronics. This is why heat meters are battery-operated.

To avoid germ proliferation, the water temperature in the pipes exceeds +70°C. Unless the meters are wall-mounted at some distance from the pipes, they (and their batteries) have a good chance to operate during very long periods at temperatures exceeding +45°C.

Heat cost allocators, also widespread in Northern Europe, need batteries for their electronics. Since each room within apartments or offices must be equipped, the market size is much larger and the competition is fiercer. As a result, manufacturers have worked hard to reduce the current consumption to make use of smaller and cheaper power sources, still capable of standing high temperatures, but during a part of the year only.

Technical specifications

- autonomous power source
- base currents: <20μA
- pulses: <50 mA
- cut-off voltage: 2.5 to 3.0 V
- operating temperature: +10/+80°C
- runtime: > 6 years (by law in Germany) to 12 years

Power sources

Taking into account these specifications, and because no other electrochemistry could stand high temperatures for so long, primary lithium

Table 11.3. Designations and dimensions of primary batteries mentioned in this chapter.

Common Designation	IEC Designation	Diameter (mm)	Height (mm)
1/2AA	1/2R6	14.5	25.2
AA	R6	14.5	50.5
C	R14	26.2	50.0
subC	subR14	23.0	43.0
D	R20	34.2	61.5
A		17.0	50.5
2/3A		17.0	33.3
9 V	6R61	47.5: 25.5:16.5 (H:L:W)[1]	

1. Prismatic battery

cells were immediately considered, both liquid-cathode and solid-cathode types: large 3 V Li/SO_2 and 1.5 V Li/CuO batteries in the early days, then 2.5 V Li/$Cu_4O(PO_4)_2$, 3 V Li/CF_x, 3 V Li/MnO_2 and 3.6 V Li/$SOCl_2$ cylindrical cells (*e.g.* R6 size cells, see Table 11.3 for all sizes mentioned in this chapter), and then, due to a sharp reduction of the current consumption, even 3 V coin cells have been used in HCA

Today, small (1/2R6) and large (R20) size Li/$SOCl_2$ cells are also widely marketed. This trend is due to the addition of more functions to the meters, such as data transmission to either nearby repeaters, inside buildings, or to remote meter readers. This trend is also due to the desire of the meter manufacturers to offer longer runtimes to their customers.

11.2.2. Power (Electricity) Meters

Electronic power meters appeared soon after the heat meters, on the US market, at the beginning of the 1980s. The utility companies' motivation was the sudden access to numerous functions such as multi-rate tariffs, energy management thanks to TOU (time-of-use) registration, remote reading, load switching, *etc.* These new kinds of meters contain, among other systems, a memory where power consumption data is stored. This memory being permanently powered from the mains, one of the major difficulties to be circumvented is the occurrence of brief power outages that can be responsible for the loss of information stored inside. The solution has been the adoption of primary lithium cells acting as a memory back up.

Technical specifications

- replaceable autonomous power source
- base currents: <20 μA
- pulses: less than a few mA
- cut-off voltage: 2.4 to 3.4 V
- operating temperature: -40/+70°C (sometimes +85°C)
- runtime: 10 to 20 years

Power sources

Under the leadership of a major US manufacturer, a 1/2R6 Li/$SOCl_2$ cell contained inside a plastic case became a *de-facto* standard on the North America market. The reasons for the early adoption of that solution were: the high operating voltage of the cell, its full hermeticity (it is fitted with a glass-to-metal seal) preventing any leakage, its ability to operate over a very wide temperature range (in the USA, power meters are outdoor devices located inside glass compartments), and its lower self discharge rates that allowed very long runtimes.

1/2R6 Li/SOCl$_2$ cells have also been used outside the USA. Over the years, other back up solutions have been introduced: Li/MnO$_2$ coin cells, and even super capacitors. Today, the 1/2R6 size cell is coming on strong again, with either the Li/MnO$_2$ system or, mostly, the Li/SOCl$_2$ version. The main reason for this new success is the fact that these Li/SOCl$_2$ small cells have demonstrated in the field (*e.g.* in alarm sensors) that a 20-year runtime is possible, removing the expensive replacement process.

11.2.3. Gas Meters

Electronic gas meters for industrial installations were first introduced in the middle of the 1980s. Then, in the early 1990s, partly due to the need of better accuracy, a British utility company has pioneered the fully electronic residential gas meter option. Since then, more than one million units have been installed in Great Britain. Other countries have followed (*e.g.* China) or, at least, have run field tests on a large scale (*e.g.* France).

The behavior of the meters (and their cells) has been satisfactory, but the cost of the electronic option (compared to the mechanical one) proved a definitive obstacle to its widespread adoption.

Technical specifications

- replaceable autonomous power source
- base currents: <100μA
- pulses: up to 250 mA (up to a few Amps in pre-payment meters where the gas delivery must be discontinued remotely in case of non-payment)
- cut-off voltage: 2.2 V to 3.0 V, typically
- operating temperature: -40/+70°C
- runtime: 10 years, typically (guarantees of 11 years have had to be given in a few cases).
- ATEX qualification (intrinsic safety) in Europe
- Flame test satisfaction

Power sources

The use of two Li/CF$_x$ R14 cells in parallel has been considered, but it is the R20 bobbin Li/SOCl$_2$ cell which has been initially adopted in the British meter and is often the solution of choice for this application today. This is because this solution offers a much higher energy density, and, therefore, a longer runtime that is necessary for the electronic option to draw upon the long lasting and cheaper mechanical version.

In more recent gas meters, smaller power sources have been adopted (*e.g.* R14 and two R6 in parallel).

In some cases, when high power is requested to open/close valves, alkaline cells, which are cheaper, easy to replace, and located on the outside of the meters, have been selected. The ATEX qualification (EN50020) has prevented the use of high rate, fuse protected $Li/SOCl_2$ cells, since during the test protocol the protecting fuse has to be removed.

11.2.4. Water Meters

It took a long time for the water meter manufacturers to come up with electronic devices. This is due to the fierce competition of low cost -and reliable- mechanical meters, onto which clip-on radio modules (AMR) can be fitted if remote reading is requested.

Today, electronic water meters, fitted with primary lithium batteries, do exist, but on a much smaller scale than initially expected.

Technical specifications

- replaceable autonomous power source
- base currents: <100 μA
- pulses: a few mA to 2A in case of GSM transmission or pre-payment function
- cut-off voltage: 2.5 V to 3.2 V in case of GSM transmission
- operating temperature: -20/+60°C
- runtime: 5 to 10 years (20 years required recently)

Power sources

Cylindrical $Li/SOCl_2$ cells (from R6 up to R20) are often the solution of choice for this application today, because of the high circuitry cut-off voltages and the need of high energy density cells. These cells may power a control unit and even a valve switch in pre-payment types of meters.

Both high-rate, large cells and low-rate versions fitted with a capacitor in parallel when high pulses are to be delivered (*e.g.* to actuate valves) are currently used. On a smaller scale, 2/3A Li/MnO_2 cells have been used.

11.2.5. Data Loggers with RF Transmission

In order to collect data, several communication techniques may be used, and radio frequency is one of them.

For instance, recently, a brand new system of wireless process data loggers has been launched. Using the open source norm WINA, supposedly more secure than WIFI or Bluetooth, a network of transmitters, each fitted with a radio module, transmit process data (*e.g.* pressure and temperature) to a base station. This system is of interest for remote equipments where the connection to the mains would prove too expensive.

Technical specifications

- autonomous power source
- base currents: <150 μA
- pulses: <100 mA
- cut-off voltage: 2.5 V to 3.2 V
- operating temperature: -20/+60°C in Europe, -40/+70°C in North America
- runtime: up to 10 years

Power sources

High energy density/low-rate cylindrical Li/$SOCl_2$ cells (from R6 up to R20) are often the solution of choice for this application today, because of their high operating voltages and their very long possible runtimes. Rechargeable power sources may also be used; for instance, the transmitters of the process data logger system are powered by Li/Ion batteries.

11.2.6. Data Loggers with GSM or GPRS Transmission

The introduction of the European mobile phone transmission system called GSM (Global System for Mobile communications) allowed the transmission not only of voice but also of data. This is why the GSM data system (9600 bps), and the more rapid GPRS (General Packet Radio Service) system (115000 bps) are currently being introduced to transmit all kinds of data. These systems are being often used in industrial out-door installations, so they need to rely upon autonomous power sources able to operate over a wide temperature range for a long time.

Technical specifications

- autonomous power source
- base currents: <100 μA
- pulses: up to 2 A (lasting 0.577 μsec, every 4.6 msec with the GSM)
- cut-off voltage: 2.5 V to 6.0 V, typically
- operating temperature: -20/+70°C
- runtime: 1 to 7 years (sometimes longer)

Power sources

Battery packs made with small Li/$SOCl_2$ cells (fitted with a capacitor, or a Li/Ion cell in parallel, because high pulses must be delivered) or with larger and more powerful cells (spiral R20 cells for instance) are often used for this application today. This is due to the high cut-off voltage of the GSM circuits.

11.2.7. AMR (Automatic Meter Readers)

Fully electronic meters are often disregarded due to their higher cost. Still, some of the functions they offer are very useful to the utility companies: for instance, remote reading, since the traditional visual inspection of meters has always been perceived as a problem.

The solution to this problem has been the Automatic Meter Reading (AMR), which, in fact, often means Remote Meter Reading (see, for example Figure 11.1). It consists in the adaptation, on the mechanical meter windows, of small electronic devices able to convert, for example, the displacement of an arrow into an electronic signal which can be transmitted in different ways (hand-held computer, radio system, telephone line, GSM, GPRS, ZigBee, *etc.*) to the utility company computers for billing purposes. These AMR devices appeared in the USA in the middle of the 1980s and are currently used all over the world.

Technical specifications

- autonomous power source
- base currents: <30 μA
- pulses: from 20 mA to 2 A in case of GSM transmission
- cut-off voltage: from 2.0 V to 3.2 V (GSM)
- operating temperature: -20/+70°C in Europe, -40/+80°C in the USA
- runtime: 10 to 20 years
- ATEX qualification (intrinsic safety) in case of AMRs for gas meters

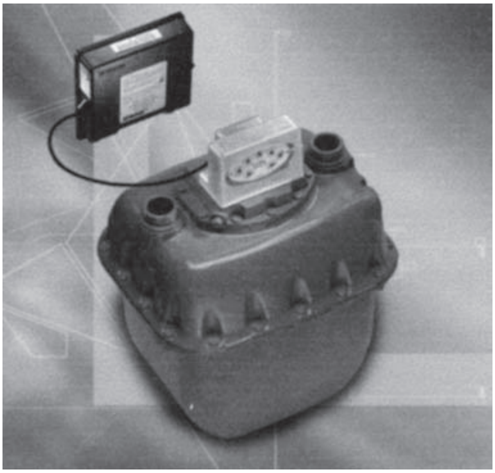

Figure 11.1. AMR with a gas meter.

Power sources

Small Li/$SOCl_2$ -mostly- and Li/MnO_2 cylindrical cells (R6 and A size) have been used since the AMR debut. Today, bigger (R14 or R20), high-rate Li/$SOCl_2$ cells are used when the GSM or GPRS transmission mode is involved. One of the key reasons for their adoption is the high cut-off voltage of the AMR circuitries as well as the need for the batteries to operate over a very wide temperature range for many years. This implies, for these cells, to manifest low self discharge rates and full hermeticity.

In the case of specifications requesting high pulses, two solutions are currently used:

- low-rate/high capacity cells, fitted with a capacitor in parallel. For instance, one battery vendor proposes a combination of a Li/$SOCl_2$ bobbin cell and an HLC (hybrid layer capacitor). In this combination, the cell offers its very high energy density and high operating voltage and the HLC its high drain capability. Runtimes between 10 and 20 years are achievable even in the case of widely fluctuating temperatures (see also Chapter 12).
- high-rate/low capacity cells (*e.g.* Li/$SOCl_2$ cells with spiral wound electrodes).

11.2.8. Others

Many types of meters (counters) exist (parking meters, taxi counters, gasoline pumps, thermometers, thermal regulators, handheld voting machines, industrial clocks, *etc.*) and, if many are powered by lower-cost alkaline cells, some can justify the use of more expensive primary lithium cells.

Technical specifications

- replaceable autonomous power source
- base currents: <20 μA
- pulses: <500 mA
- cut-off voltage: 2.5 V to 6.0 V. The cut-off may be lower than 3.0 V but a "low battery" indication may imply a high voltage
- operating temperature: -40/+85°C (+125°C in ovens)
- runtime: 2 to (sometimes more than) 10 years

Power sources

Due to the very wide range of specifications, these devices use many types of primary lithium cells, powerful or not, featuring long runtimes and wide operating temperature range. Rechargeable power sources may also be used.

11.3. Remote Mobile Monitoring

Getting information about the whereabouts of a specific mobile (object, animal, person), sometimes on a real time basis is more and more a modern world obligation. Instant communication is now considered as taken for granted.

Surveillance of transported parcels or luggage, study of animal migration, detection of machine failures, data collection on production lines (*e.g.* cars), location of trucks or salespersons, issues and returns system in public libraries, *etc.*: all these examples illustrate the fast growing interest in tracking travelling goods and persons, due to the noticeable productivity gains and service improvements that this machine-to-machine process brings.

Satellites, possibly combined with wireless communication networks, are among the tools used to this end. However, this monitoring could not work, especially when mobile assets are concerned, if dedicated communication terminals, powered by efficient power sources, were not available.

For a successful monitoring, several functions have to be carried out:

- identification of the mobile, thanks to transponders (RFID tags), code bars, *etc.*
- precise location, (mostly) using a satellite network or, sometimes, terrestrial base stations
- communication using either satellites, terrestrial cellular networks (GSM, GPRS) or, rarely, radio systems.
- messaging; with SMS or e-mails

This vast domain encompasses many applications and some of them will be described in Chapter 12 (*e.g.* tracking of assets, telematics systems). We shall focus on a few communication tools and technologies.

11.3.1. ID Tags

Identification (ID) consists in determining if an asset comes nearby an adequately positioned reader with scanning capability. It is based on dedicated short-range communication, most often by radio, and uses electronic devices linked to the asset.

ID tags are part of several market segments mentioned in this book, since they can be found not only in mobile monitoring systems but also in (anti-theft) alarm systems, and different tracking systems or access control systems.

The RFID technology is an identification system using radio frequencies: a smart tag located (or integrated) on the object contains all the necessary information while an emitting/receiving reader allows the collection of remote data, which will be then analyzed and treated by the information system. On this subject, see also Chapter 12.

RFID has the following objectives: identify, qualify and track products, components or persons.

In spite of their higher cost *vs.* other automatic identification technologies (*e.g.* bar coding), the many advantages offered by RFIDs (*e.g.* re-use and read/write possibilities, no need for the tags to be visible) afford limitless opportunities. In fact, these smart tags are already widely present today, *e.g.* in building access badges, car locking systems, highway toll systems, food tracking chains. For instance, an American transportation logistics provider is using a WI-FI-enabled RFID system to accurately locate, on a real-time basis, the many trailers moving through its large docking facilities. This system has contributed to a noticeable improvement of its operations, cutting yard management costs.

Pre-programmed RFID tags are not only used to start forklifts by their drivers, but also to manage the whole fleet by warehouse managers (number of hours of utilization, battery status, speed, *etc.*). Ultimately, it will be possible to control the location of all the forklifts inside a building, which will contribute to improve the traffic safety.

Identification using radio frequencies (RFID), the principle of which has been known since the World War II for the identification of aircraft, began to spread twenty years ago, thanks to its miniaturization. Very recently, a drug company decided to fit some of its drug boxes with RFID tags, in order to combat against the counterfeiting of these drugs. With this change, the drug authenticity can be assured all over the supply chain.

The invasion of the RFID technology is only just starting, even if its growth is still slowed down by many technical, commercial or social hurdles. The following examples may present a clue:

- in early 2006, an US company has implanted silicon chips in two of its employees. The purpose was to test a way of controlling access to a room where important documents were stored
- the Food and Drug Administration, in the USA, has approved chips to be implanted in human bodies for medical purposes

RFID tags may not contain a battery (passive tags) and present the advantage of a smaller size, but larger tags with a cell (active tags) are more versatile. For instance, they can incorporate sensors in order to relay interesting information, *e.g.* temperature changes when used to track food items, options when attached to the car frame during the assembly process, or security-related information when attached to sea containers.

Technical specifications of RFID tags

- autonomous power source
- base currents: <100 μA

- pulses: from a few mA to 250 mA, typically
- cut-off voltage: 2.5 V to 6.0 V
- operating temperature: -40 (or lower)/+85°C (or higher)
- runtime: from a few months to 10 years

Power sources

The above mentioned specifications explain why even the most efficient alkaline cells cannot come close to matching the primary lithium cells in RF ID tags.

If in many tags (*e.g.* anti-theft tags in stores), small 3 V coin cells can do the job, in some others, due to high cut-off voltages, or severe temperature conditions, small cylindrical (*e.g.* R6) Li/$SOCl_2$ cells have been widely adopted, because of their higher operating voltage, their ability to operate over very long periods of time, or the reliability of their glass-to-metal seals, which prevent any electrolyte leakage, even at temperatures near +100°C. As RFID tags migrate towards more power demanding designs, these cylindrical cells should increasingly be used.

When the temperature conditions are very severe (*e.g.* long exposure at very high operating temperatures), these Li/$SOCl_2$ cells may witness a noticeable increase in their internal impedance, which may become so high that their voltage may drop below the circuit cut-off voltages during peak currents. To circumvent this difficulty, the tag developers use either a high-rate cell or a low-rate cell fitted with a capacitor in parallel.

11.3.2. Bar Code Portable Readers

In spite of the introduction of the RFID solution, the bar code system remains the most widely used identification technique. This is due to its lower cost but also to the fact that the RFID system suffers from a lack of a common frequency. Although the International Standard Organization (ISO) has proposed a frequency of 13.56 MHz, many manufacturers of RFID tags keep on proposing systems operating with other frequencies, which handicaps a quicker adoption of the bar code competitor.

The bar code tags do not contain any power source, but their portable readers do.

These devices can be made truly hand-held and portable allowing operation throughout an eight-hour shift.

Technical specifications

- portable and rechargeable power source
- current: <0.2 A
- voltage: 3.6 V

- capacity: 1.2 Ah to 2.0 Ah
- operating temperature: from 0°C up to +40°C
- runtime: operation throughout an eight hour shift

Power sources

Because of their higher energy density, Li/Ion cells are now the power sources of choice for bar-code readers, with Ni/MH batteries still used in low cost devices.

11.3.3. GPS (Global Positioning Systems)

Initiated in 1973 by the US Department of Defence to guide long-range missiles, the satellite-based system called GPS (Global Positioning System) has found applications in numerous civil systems. The launches, in 1982, of the Russian GLONASS system and, in 1989, of the GALILEO system, emphasize the success of this concept. Not only can these systems locate any type of mobile, but they can help them in their movements, in which case they become genuine navigation, driving, flying and even mountaineering aids.

The GPS concept is used in several ways; for instance:

- GPS data loggers which collect and store location data (inside a "memory card") along with other data such as temperature, humidity or open/close status
- GPS mapping, where GPS receivers are part of a navigation aid system providing data about the location of the owner (*e.g.* a car driver). Most of the time, digitized street level maps stored on CD-ROM lead to an easy to read information using an on-board LCD screen.

GPS receivers can be split in two categories:

- stationary receivers which rely, for instance, on a car (or truck) lead-acid battery
- portable receivers which rely upon an autonomous power source

Technical specifications of portable GPS receivers (main power source)

- replaceable autonomous power source
- base currents: <100 μA generally, but a few mA sometimes
- pulses: 200 mA to 1 A (in case of backlighting) during several seconds
- cut-off voltage: 5 V to 10 V, typically
- operating temperature: -40/+80°C
- runtime: from some hours up to some years, or several hundreds of charge/discharge cycles
- handling: the batteries must be replaceable by non-trained people (in such a case, the Underwriters Laboratories User Replaceable recognition may then be required).

Power sources of portable receivers

A portable GPS receiver is fitted with two power sources: one for its internal clock and one for the main power.

The first one is often a 3 V lithium coin cell (some years ago, it had been a small 3.6 V $Li/SOCl_2$ cell too), the second one can make use of different battery chemistries. They may be either rechargeable (Ni/Cd, Ni/MH, Li/Ion) or primary (alkaline, lithium) depending upon the recharging or replacement possibilities. The choice will also depend upon the environmental operating conditions (temperature) or on the financial possibilities of the users.

This is why, large primary lithium battery packs, made with R20 Li/SO_2 or MnO_2 or $SOCl_2$, are used in military receivers, whereas small size lithium (rarely), alkaline and rechargeable cells are found in civil ones.

11.3.4. GSM (Global System for Mobile Phones) Modules

The GSM system has been introduced to transmit voice, but it has rapidly become a tool for the transmission of data too. However, today, the GPRS network seems to be gaining the favors of many tracking system users.

Several modules are available on the market and are used in different industrial equipments, from which data are retrieved remotely.

Technical specifications

- autonomous power source
- base current during stand-by: <100 μA
- base currents during communication: <300 mA
- pulses during communication: 1 to 2 A lasting 0.577 μsec every 4.6 msec
- cut-off voltage: 2.8 V to 10 V
- operating temperature: -25/+60°C (typically in Europe)
- runtime: 1 to 10 years

Power sources

They may be either rechargeable or not:

- rechargeable batteries: if, in consumer GSM phones, the Li/Ion system has the main market share, in industrial GSM modules Ni/Cd and Ni/MH are still used, along with Li/Ion
- non-rechargeable $Li/SOCl_2$ battery packs made with high-rate/lower capacity cells or with low-rate/higher capacity cells (supported by capacitors) are a solution when no charging possibility exists, or when severe environmental conditions prevail, or when size or weight are important.

11.4. Automatic Assistance Systems

Satellite communication is an integral part of the many automatic assistance systems that exist all over the world to protect travellers in distress.

The distress signals can be sent by:

- EPIRB (Emergency Position Indicating Radio Beacons); they are the marine safety devices which are actuated in case of problems at sea
- SPLB (Sub-marine Personal Locator Beacons)
- ELT (Emergency Locator Transmitters): for aircraft
- PLB (Personal Locator Beacons): for terrestrial use
- Telematics systems; they are currently under development for use in terrestrial vehicles for accident notification (see Chapter 12).

Among the many types of beacon (the transmission device used by the person in distress), the most famous are certainly the ARGOS and the SARSAT/COSPAS.

The ARGOS beacons are not occasionally activated but emit on a regular time basis, which allows a tracking. Although they are mainly utilized for environmental measurements (sea levels, stream speed and direction, volumes of fish, pollution, *etc.*), these thousands of beacons and a network of twenty satellites can prove useful to locate sailors in distress.

The SARSAT/COSPAS beacons, which can be transported anywhere on earth, sea, land or air, are activated only in rare occasions. As soon as a beacon is activated by a sailor in distress, it transmits signals that, thanks to a network of eleven satellites, are received by one of the forty-two terrestrial base stations. The position of the beacon is calculated and then it is automatically sent to one of the twenty control and rescue organizing sites located all over the world. More than 600,000 SARSAT-COSPAS beacons are used worldwide, most of them on-board boats.

It is to be noted that cellular phone networks are also used sometimes in case of emergency (for instance to locate stranded mountain trekkers) thanks to their location capability.

Not to be forgotten, among the rescue devices, are the safety lights that have been attached to life-jackets and life-rafts for decades.

11.4.1 SARSAT/COSPAS Beacons

The SARSAT/COSPAS system includes ELTs (121.5 and 406 MHz), EPIRBs (121.5 and 406 MHz), and PLBs (406 MHz). The SARSAT/COSPAS beacons are often referred to as the "406 MHz distress beacons" (Figure 11.2).

Figure 11.2. SARSAT/COSPAS beacon.

Technical specifications

- autonomous power source
- base current during the stand-by period: nil
- base current during the active mode: <100 mA
- pulses: 0.5 to 2 Amps
- cut-off voltage: 10.0 V to 20.0 V
- operating temperature: -20/+55°C (class 1) and -40/+55°C (class 2)
- runtime: 4 years of stand-by plus 48 hours of transmission
- safety: several approvals are required (*e.g.* SOLAS)

Power sources

The success of primary batteries in these devices is due to their superior ability to stand long storage episodes while remaining able to operate in a wide temperature range.

All the main lithium systems are used (Li/MnO_2, Li/SO_2, $Li/SOCl_2$), with R14 and R20 high-rate cells assembled in battery packs of different sizes (from 2 cells up to, sometimes, 10).

Li/MnO_2 offers the advantage of a better resistance to Li passivation, while Li/SO_2 cells offer higher drain capabilities at very low temperatures. The higher operating voltages of $Li/SOCl_2$ cells allow the use of only 4 cells in series to achieve a 10 V minimum cut-off, while 5 cells are required by the two previous chemistries. Smaller and lighter battery packs can thus be designed.

11.4.2. Safety Lights

These warning systems can be found on life jackets as well as on life rafts. Sea rescue flashlights and torches may be included in this segment.

Technical specifications

- replaceable autonomous power source
- base current during the stand-by period: nil
- operating currents: some mA to 500 mA
- cut-off voltage: 2.5 V to 5.5 V
- operating temperature: from -1/+30°C to -40/+75°C
- runtime: several years of stand-by plus several hours of operation
- Several approvals may be required (*e.g.* SOLAS, FAA)
- "Non-restricted-to-transport batteries" (*i.e.* batteries not assigned to the class 9, see Chapter 14) may be required

Power sources

Alkaline cells, which offer the advantage of easy accessibility and low costs, are used but their main drawback, in these devices, is their need for a frequent replacement.

Although still used today, 1.5 V sea-water activated batteries have gradually been replaced by higher energy density primary lithium cells, which also offer longer storage lives thanks to their lower self discharge rates. Low-rate cylindrical small cells as well as high-rate R20 size cells can be used in these devices.

It is to be noted that safety norms or regulations may influence the selection of a power source. For instance, recently an EPIRB manufacturer decided not to use a battery pack made with three Li/SO_2 cells, but to use instead a pack with six 2/3A size Li/MnO_2 cells, simply because the second solution would be declared "non-restricted to transport", *i.e.* not assigned to the class 9 transport category. In fact, the lithium contents of this pack was just 2 grams, which is the upper limit of the "non-restricted to transport" category of goods.

11.5. Alarm and Security Systems

Wireless home/building security devices appeared in France and in the

USA only by mid-1980s, but ELUs (Emergency Light Units) have long been installed in many public buildings. If the first market is the undisputed property of primary cells and batteries, the second one is dominated by rechargeable systems, mostly Ni/Cd.

The ELU market encompasses only one type of device (the luminaries), while the wireless market encompasses many:

- sensors detecting a presence or an event and transmitting this information
- sirens emitting noise signals
- keyboards where owners enter passwords
- central units that memorize (*e.g.* identification by sensors, chronology of previous events), supervise (*e.g.* the sensors, the radio network), activate (*e.g.* transmitters, sirens, telephones)
- phone transmitters that memorize and call
- emergency call personal alarms for elderly people

Just like in the previous section, only a narrow selection of applications will be presented here.

11.5.1. Emergency Light Units (ELUs)

Luminaries are part of the mandatory safety equipment of buildings in Europe, imposed by European directives such as: Safety in case of fire, and Building and Workplace directives, all translated into national laws. They must comply with the specific requirements of several standards: international (IEC 61951), Japanese (JISC 8705) and American (UL 924). They must satisfy the PSB audit and be qualified against ISO 9001.

Self-contained emergency lighting luminaries (*i.e.* lights drawing energy from batteries in the emergency mode), rely presently on batteries as power sources to comply with the safety requirements.

Technical specifications

- trickle chargeable power source (*i.e.* batteries able to stand a permanent overcharge), which must be ready to operate at any time
- permanent charge rate from C/20 to C/15. However, it is to be noted that luminary manufacturers are trying to lower the overall current consumption and to decrease the charging current down to C/30 or even C/50
- constant rapid recharge rate: C/10 maximum :
- cut-off voltage in charge: 1.55 V/cell (if temperature <0°C)
- cut-off voltage in discharge: 1.0 V/cell
- operating temperature: from -20°C to +60 °C
- lifetime: 4 years minimum in operating conditions (as stipulated in the International Luminaries Standard)

- runtime: the ELU must provide lighting during one to three hours, *i.e.* long enough for people to leave the building and for rescue teams to intervene

Power sources

More than 30 years of field experience in luminaries have demonstrated the reliability and reproducibility of Ni/Cd batteries. This explains why, today, these batteries are chosen for this application. Sintered positive electrode, plastic bonded negative electrode and, recently, plastic bonded nickel electrode technologies are used in the design of these cells.

The subR14 and R20 size cells (Table 11.3) are the most widely used in ELU battery packs, where, typically, the cells have a capacity of 0.6 to 7 Ah.

Ni/MH batteries have been tested for use in compact self-contained luminaries, in order to take advantage of their superior nominal capacity. This would have permitted the use of slimmer battery packs than those made with Ni/Cd cells. However, some current technical drawbacks have limited their use in the ELUs:

- in normal luminaries, the operating temperature conditions (+40°C and above) shorten the life of these batteries, due to the corrosion effects originating from the degradation of the negative metal hydride electrode
- the permanent over-charge situation, generally met in luminaries, results in a temperature increase that reduces the battery life
- the cost of the negative electrode (based on expensive alloys) is higher than that of Cd in Ni/Cd cells, this having a negative impact on the overall cell cost

However, in specific niche markets, for high–end applications requesting slimmest batteries, and when operating conditions are moderate, *i.e.* below +40°C, Ni/MH batteries are used. Today, they represent less than 1 to 2% of the ELU battery market.

The high cost of Li/Ion batteries, in comparison with the two previous ones, limits its use in this application, although their intrinsic performance could satisfy the Emergency Lighting Units requirements.

11.5.2. Wireless Alarm Sensors

Connected to the central units via radio communication, the sensors can detect several events: motion (of burglars), movement (of windows or doors), smoke or heat emission, leakage (of water or gas).

Sensors, fitted with a radio unit, have been installed in some production machines used in paper mills in order to monitor temperature and vibrations.

Technical specifications

- autonomous power source
- stand-by current: from 1 to 100 μA, typically
- operating current: from 20 to 150 mA, typically

- "low battery" indication voltage: 2.8 V to 8.4 V
- cut-off voltage: 2.0 V to 6.0 V
- operating temperature: from +5°C to +30°C for alarm systems installed inside buildings (up to +50°C inside factories); from -40°C to +70°C for out-door applications
- runtime: 1 to 20 years
- qualifications: UL technician or user replaceable component. When used inside an explosive environment, the ATEX certification (ATmosphere EXplosive), also known as EN50020, may be required too

Power sources

According to their price, these systems rely upon either alkaline or primary lithium cells. The 9 V size is predominant in the alkaline family, while the small cylindrical cells (1/2R6, R6, 2/3A, A) dominate the lithium systems, with 3 V Li/MnO_2 and 3.6 V $Li/SOCl_2$ prevailing. The low self discharge and the wide operating temperature range of lithium cells explain their success in an application where a 20-year life is becoming a must, in spite of possible very harsh temperatures (some sensors are affixed on window-panes or glass doors of department stores).

11.5.3. Wireless Alarm Central Units

They are the brain of the whole alarm system, receiving information and, then, initiating actions (*e.g.* phone calls, siren actuation) (Figure 11.3).

Technical specifications

- autonomous power source
- base currents: <150 µA
- pulses: from a few tens of mAmps to 2 A
- cut-off voltage: 3.0 V to 6.0 V
- operating temperature: 0/+50°C
- runtime: 1 to10 years

Power sources

Again, depending upon the price and performances of the system, alkaline or primary lithium cells (R14, R20) are used. However, if the alkaline solution is, by far, the preferred one for alarm systems for consumers, industrial customers generally prefer lithium.

11.5.4. Alarm Sirens

These alarms may be installed inside or outside the buildings (bank outlets, factories, shops, museums, *etc.*).

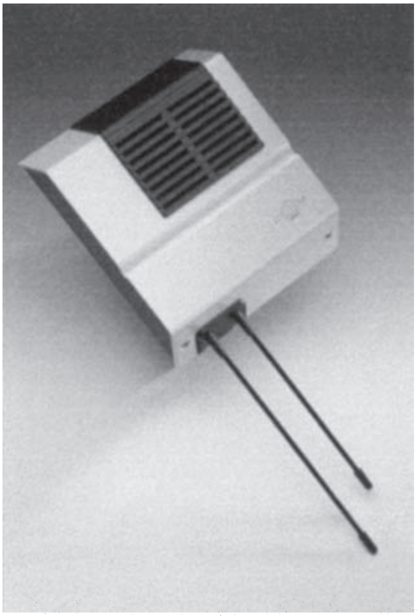

Figure 11.3. Central unit of wireless alarm system.

Technical specifications

- autonomous power source
- base currents: <150 µA
- pulses: up to a few Amps during 30 sec to several min
- cut-off voltage: from 3.0 V to 6.0 V
- operating temperature: -30/+70°C
- runtime: 5 to 10 years

Power sources

The requirements of a very long runtime and the delivery of high currents, in possible severe outdoor temperature conditions, have imposed the selection of high-rate primary lithium (*e.g.* two R20 size Li/SOCl$_2$ cells in series) in most alarm sirens used to protect commercial and industrial buildings. However, some wireless alarm system manufacturers claim a 5-year operating time for the alkaline battery packs they are producing.

11.5.5. ZigBee

Wireless radio interconnection can be implemented using several solutions: Bluetooth, WI-FI, WI-MAX, or ZigBee.

Like Bluetooth, but cheaper and simpler, ZigBee (also known as IEEE 802.15.4) is an emerging, cost-effective, wireless communication standard for short-range data transmissions.

Enabling machine-to-machine communication and networking, it is an excellent candidate for home control, remote lighting and heating control, as well as industrial and building automation. With ZigBee, a wide range of devices and appliances can be remotely controlled and used in a very flexible way. In order to facilitate the embedding of this technology in various consumer, commercial and industrial applications, the ZigBee Alliance has been created, which associates several companies promoting together this technology ZigBee relies upon low-power and cheap Radio Frequency 433 or 866 Mhz chips that need to be powered by batteries.

Technical specifications

- autonomous power source
- base currents: <200μA
- pulse magnitude: less than 200 mA
- cut-off voltage: from 2.2 V up to more than 3.0 V
- operating temperature: -20/+60°C in Europe
- runtime: 5 to 10 years

Power sources

In some current projects, small 1/2R6 Li/$SOCl_2$ cells are considered while, in some others, larger cells (*e.g.* R20) will prove necessary. High operating voltage and ability to operate for many years explain, here again, the selection of these types of cells.

11.5.6. Access Control Systems

Door locks, hotel safes, electronic keys, automatic blocking systems, ticketing equipment, *etc.*, are parts of the access control system. (The use of ID tags has been introduced in paragraph 10.3.1).

Automatic barriers, where Pb/Acid batteries are used in case of main power outages, are not included here, and neither are the electric door locking systems for cars.

Technical specifications

- autonomous power source
- base currents: 0 to a few μA (if memory back up is needed)
- pulses: up to 3 A (actuation of a lock)
- cut-off voltage: >2.5 V
- operating temperature: +5/+35°C (indoor) to -40/+70°C (outdoor)
- runtime: 1 to 10 years

Power sources

Alkaline cells are used when easy replacement is possible or when low prices are recommended.

3 V primary lithium coin cells are used for back-up memories (*e.g.* in safes).

A spirally wound 2/3A Li/MnO_2, or a low-rate small size Li/$SOCl_2$ cell (*e.g.* 1/2R6 or R6) fitted with a capacitor in parallel to deliver the pulses, actuate some locks.

9 V Li/MnO_2 cells are used in some digital locks.

11.5.7. Remote Level Control Systems

These systems can monitor the level of fluids or solid materials in reservoirs or tanks, *e.g.* gasoline in tanks and garbage in city bins.

To monitor the amount of fuel remaining in a tank, the system can be organized as indicated in the following. Pressure sensors are installed at the bottom of the fuel tank and transmit data to, for instance, a GSM box connected with a cable. This box transforms the data into SMS messages, which are received by a base station, where a computer estimates the quantity of fuel left. When the alert limit is reached, the tank is refilled.

In spite of their costs, these systems are of interest because, by allowing an optimization of the truck routing (for both deliveries and/or collections), they allow cost savings.

Technical specifications:

- replaceable autonomous power source
- base currents: up to a few hundreds of µA
- pulses: from a few tens of mAmps up to a few Amps
- cut-off voltage: 2.8 V to 8.0 V
- operating temperature: -40/+65°C
- runtime: 2 to 5 years (sometimes 10).
- qualification: ATEX in case of flammable product level controls (*e.g.* fuel oil or LPG)

Power sources

Older systems did not require high pulses and could use battery packs made with small, low rate, primary lithium cells (Li/MnO_2 and Li/$SOCl_2$). The more recent ones, which rely upon cellular networks (*e.g.* GSM) to transmit their alarm signals in outdoor temperature conditions, require the use of powerful packs made with the assembly of high-rate Li/$SOCl_2$ R20 cells or with their low-rate counterparts plus a capacitor in parallel. For cost saving reasons, packs made with alkaline cells are currently considered as well.

11.5.8. Telematics Systems

These alarm systems which are installed on-board cars, and which will become compulsory in brand new cars in some parts of the world, are described in the automotive applications of Chapter 12.

11.5.9. Power Line Surveillance

Power line outages can happen anywhere along the thousands of kilometres of power lines; this is why, when one occurs, it is necessary to detect rapidly its location. To do so, detectors fitted with flashing lights have been installed on power lines all over the national grid in several countries, such as France and Canada. Since these devices are to operate in case of power outages, they need to be fitted with an autonomous power source. Due to the severe environmental conditions, primary lithium batteries have been adopted in these equipments.

Technical specifications

- autonomous power source
- base currents: 0 to 500 μA in stand-by; <1 mA during the active phases
- pulses: <500 mA
- cut-off voltage: 2.0 V to 6.0 V
- operating temperature: -40/+70°C
- runtime: <1000 hours over 5 to 15 years

Power sources

The need for long operating lives in, sometimes, very severe outdoor conditions (*e.g.* in Canada) explains the universal use of 3.0 V or, preferably, 3.6 V primary lithium cells of the small or large size. When large usable capacities are needed, the low-rate R20 $Li/SOCl_2$ cell, assembled in series and/or parallel, is preferred because it has the highest capacity (up to 19 Ah). A capacitor in parallel with the battery pack is often used to deliver current peaks.

11.5.10. PIGs

Leakages may cause heavy financial losses to pipeline owners; this is why special tools, PIGs (Pipeline Inspection Gauges), designed to check the corrosion status of the tubes, are inserted inside pipelines.

Technical specifications

- autonomous power source
- base currents: less than a few Amps

- pulses: <10 A
- cut-off voltage: from 6.0 V up to 30 V
- operating temperature: -30/+90°C
- runtime: <200 hours

Power sources

Apart from some remote pipeline monitoring systems, which use the solar energy in hazardous areas, *i.e.* when the ATEX approval is required, big battery packs made with high-rate, low-energy R20 Li/$SOCl_2$ cells are the solution of choice for this application. Superior drain capability, high operating voltage and wide operating temperature range explain this choice.

11.6. Memory Back Up (MBU) - Real Time Clock (RTC)

Memories and real time clocks are found in a very large number of consumer and professional devices and, among the second family, we can mention the following:

- vending machines, gaming and gambling machines, coin dispensers, ABT (Automatic Bank Tellers)
- industrial tools such as PCs, PLCs (Programmable Logical Controllers), NC (Numerical Control) units, test machines, timers, welding machines, scales, *etc.*
- instruments and terminals of all kinds
- metering systems (*e.g.* electricity meters)
- controllers (*e.g.* contactless ticket readers)
- many types of office equipments (printers, PCs, mailing machines, copiers, telecom equipments, cash registers, smart keys, *etc.*)
- on-board instruments (aircraft, boats and terrestrial vehicles)
- (a few types of) memory cards

An interesting example can be found on the production floors of car manufacturers. In order that the many industrial robots used in automobile production plants can adopt the very same position and movements at start-up (otherwise they may damage each other), information concerning their position and movements are entered into their memory. At the end of the workday, or during holiday periods, the robot power is switched off, but the information contained in their memory must be preserved. This is why autonomous power, rechargeable or not, is needed to power the memory.

All these devices, which are fitted with a memory function (*e.g.* CMOS RAM) and, often, with a clock too, need a back up in case of main power outage or switch off. This is why they make use of an extra power source.

Technical specifications

- autonomous power source
- base currents: from less than 1 μA up to 1 mA
- pulses: up to a few tens of mAmps
- cut-off voltage: from 2.0 V to 7.0 V (with "low battery" indication above 8 V)
- operating temperature: -40 to +70°C (sometimes higher)
- runtime: from a few years up to 10 years

Power sources

The amount of energy needed is continuously decreasing, so EEPROMs or capacitors can do the work, but cells and batteries are still present in this market segment.

- Sometimes, a tiny or small-size battery is used. It can be a pack of alkaline coin cells, a 3.0 V or 3.6 V primary lithium coin cell or a small 3.0 V or 3.6 V cylindrical one, or a small rechargeable battery made with Ni/Cd button cells. The alkaline solution is adopted when price is the most important factor and the lithium solution is selected when the applications require operating lives in excess of five years, or when long exposures to high temperatures would alter the performances of other chemistries. 3.0 V Li/CF_x and Li/MnO_2 tiny coin cells have enjoyed a huge success in RAMified RTCs, or micro chips.
- Coin cells are generally fitted with a plastic grommet; electrolyte leakage through it leads to drying (and dying) of the cells after some years. To expand the lifetime of coin cells up to ten years, epoxy resin encapsulated cells have been proposed by some manufacturers.
- When the energy need is higher, small cylindrical primary lithium cells (*e.g.* R6) are used. Sometimes, it is so high (in industrial robots for instance), that packs made with several R14 (or even R20) primary 3.6 V lithium, or rechargeable 1.2 V Ni/Cd cells, are necessary.

11.7. Professional Cordless Tools

Maybe nowhere better than in professional cordless power tools, the progresses of the performance of Li/Ion cells can be appreciated. Indeed, these devices require, after a high energy density, power and fast charging and the recent technological advances in Li/Ion offer both. For instance, it is now possible to partially recharge these batteries in about 10 to 15 minutes.

Tool manufacturers recently introducing Li/Ion battery packs in their tools, claim in their commercial literature the following advantages:

- are 40% lighter

- deliver 40% to 50% more power or speed
- have 2 times more cycles than professional Ni/Cd batteries
- offer longer runtimes (according to a tool manufacturer, 28 V Li/Ion batteries offer twice the runtime of conventional 18 V Ni/Cd models).
- present a 5-times lower self discharge rate and, as a consequence, hold their charge longer (18 months according to a manufacturer producing some tools with a 28 V Li/Ion pack).
- manifest no memory effect
- can operate over a wider temperature range (-20/+70°C) than Ni/MH counterparts
- some universal chargers can work with both Li/Ion and Ni/Cd batteries

To be used in power tools, *i.e.* to operate at very high discharge currents (up to 10C or even higher), Li/Ion batteries have been modified, and higher-drain batteries offer lower usable capacities (the same situation is also met with other chemistries, *e.g.* $Li/SOCl_2$). For instance, a battery vendor offers, in the same format (18650), one version of 2.6 Ah at the 0.2C discharge rate and another one of 1.5 Ah at a 10C rate. To get higher drains without compromising safety, the battery vendors have replaced the cobalt-oxide cathode typically used in standard Li/Ion cells with other types of cathodes.

The nickel-metal hydride system is also improving drastically its performance to fit the requirements of this demanding market. For instance, it has been possible to increase the number of charge/discharge cycles from 500 to 1000. Also, thanks to the use of additives partially inhibiting the chemical reaction responsible for self discharge, the yearly capacity loss during storage at room temperature, has been reduced to 15-20% (85 to 80% of the initial capacity still retained after one year, 70 to 60% after two years) .

Cordless power tools represent one of the largest markets for rechargeable batteries. This family encompasses many tools used indoor and outdoor, in houses, factories or gardens. The technical requirements of a few types of cordless tools are presented below.

11.7.1. Drills

Technical specifications

- lightest possible portable power source
- voltage: 4.8, 7.2, 9.6, 12.0, 14.4, 18.0, 24 and even 36 V with recent Li/Ion battery packs
- capacity: from 1.2 to 3.0 Ah
- charge time: from 10 to 60 minute, but drills requiring 3-hour charges still exist

Power sources

Ni/Cd battery packs were the main power sources until some years ago and are still used in cheaper tools, but Ni/MH and, recently, Li/Ion batteries are now widely used. The energy density has been the obvious driving force behind that evolution, which is witnessed in most of the other cordless tools.

11.7.2. Drills and Screw Drivers-Wrenches

These tools can drill and screw.

Technical specifications

- lightest possible portable power source
- voltage: from 9.6 V up to 36 V (Li/Ion batteries)
- capacity: from 1.0 to 3.0 Ah
- charge time: from 10 to 60 minutes typically, but 3- to 5-hour charges are still mentioned in data sheets or operator's manuals

Power sources

This sub-segment witnesses the same evolutions as in drilling machines. Here too, Ni/Cd, Ni/MH and, recently, Li/Ion batteries share the market.

11.7.3. Screw Drivers

Technical specifications

- lightest possible portable power source
- voltage: two families exist here:
  - low voltages: from 2.4 V up to 4.8 V
  - high voltages: from 7.2 V up to 14.4 V
- capacity: 1.0 to 2.6 Ah, typically
- charge time: two families exist here too:
  - fast charges: from 15 to 60 minutes
  - slow charges: from 2 to 12 hours

Power sources

Ni/Cd and Ni/MH dominate this market, but Li/Ion battery packs have recently appeared in this application too. It is to be noted that alkaline battery packs (*e.g.* 4R6) are used to power a few units.

11.7.4. Grinders and Sanders

Technical specifications

- lightest possible portable power source

- voltage: 7.2 V to 18.0 V, typically
- capacity: 2.0 Ah
- charge time: typically 60 minutes

Power sources

Here, the Ni/Cd couple seems to maintain its supremacy, although Ni/MH in grinders, and Li/Ion batteries in sanders, are sometimes used too.

11.7.5. Planers

Technical specifications

- lightest possible portable power source
- voltage: 14.4 V and 18 V, typically
- capacity: from 2.0 to 3.0 Ah
- charge time: from 30 to 60 minutes

Power sources

Ni/Cd and Ni/MH battery packs equip these machines.

11.7.6. Saws (Circular, Jig, Sabre, Diamond, *etc.*)

Technical specifications

- lightest possible portable power source
- voltage: from 7.2 V to 24 V
- capacity: from 1.0 Ah to 3.0 Ah
- charge time: from 30 to 60 minutes, typically

Power sources

Ni/Cd and, mostly, Ni/MH battery packs equip these different types of sawing machines, but, here too, the Li/Ion system appeared recently.

11.7.7. Mini Tools

One may wonder if these tools are for the consumer or for the professional. Anyhow, due to their growing importance, they have been included in this paragraph.

Technical specifications

- lightest possible portable power source
- voltage: from 4.8 V up to 10.8 V (with a Li/Ion pack)
- capacity: from 1.0 Ah to 2.0 Ah, typically
- charge time: typically 3 hours

Power sources

In spite of their higher cost, their higher energy density has lead to the recent acceptance of Li/Ion batteries in cordless mini tools.

11.7.8. Irrigation Systems

Fields or gardens being located, sometimes, far from farms or houses, the electronic devices monitoring their watering systems cannot always be connected to the mains, and, consequently, autonomous power sources are required. Small cells may suffice to simply power a clock, but large and powerful batteries are to be used to activate more demanding functions, such as the closing and opening of automatic valves, in outdoor environmental conditions that are often rather harsh.

Technical specifications

- autonomous power source
- quiescent current: <150 μA
- peak currents: from 20 mA to 500 mA (in case of automatic valves)
- voltage: from 2.0 V to 3.0 V
- idling and operating temperature: between -20°C and +50°C
- runtime: 5 to 10 years

Power sources

Alkaline cells are used in consumer equipments, but the professional ones make use of primary lithium (often $Li/SOCl_2$) packs made with small (1/2R6) to large powerful cells (spiral R20).

11.7.9. Hedge Trimmers, Chain Saws, Pruning Shears

Although electrical or combustion-engine versions dominate the hedge trimmer market, a few cordless ones are offered today. The same is true for chain saws.

Technical specifications

- lightest possible portable power source
- voltage: from 9.6 V to 18.0 V (40 to 48 V for the pruning shears)
- peak currents: from 5 to 15 A for up to 1 second.
- capacity: from 1.5 Ah to 2.6 Ah, typically (up to 4.0 Ah for the pruning shears)
- charge time: 1 to 3 hours (even 10 hours for the pruning shears)
- operating time: typically a few hours with an obvious target of 8 hours, *i.e* a single working shift duration

Power sources

Even if these tools are mostly powered by Ni/Cd and Ni/MH battery packs, Li/Ion is penetrating this market too. The reasons are always the same: needs for lighter tools and longer working periods. For instance, during the grape harvest season, working times typically last 8 to 10 hours, and battery runtimes matching them would be welcome.

11.8. Professional Appliances

This vast family encompasses many devices: handheld terminals, professional notebook computers, gas monitors, audio/video equipments are only a few members of this family.

All the different types of autonomous power sources are used in these equipments: alkaline cells dominate among the primary batteries, while the secondary battery area sees the competition of three main systems, with Li/Ion gathering momentum.

11.8.1. Handheld Terminals

Hand held terminals are numerous and, therefore, we shall only present the specifications of the main power sources of wireless payment terminals, which are familiar representatives of this broad family.

Technical specification of the main power source

- portable power source
- current: 0.1 to 0.3 A with peaks of 2 to 4 A for up to 10 seconds (for the printing operation)
- voltage: 6.0 V to 7.2 V
- capacity: 0.8 Ah to 1.5 Ah
- charging time: 1 to 3 hours

Power sources

Primary and secondary chemistries are used in handheld terminals. For instance, gas detectors are currently powered by alkaline cells, Ni/MH or 12 V lead-acid battery packs

Payment terminals make use, principally, of Ni/MH R6 cells, but prismatic Li/Ion cells now appear in recent generations of terminals.

Sometimes, some of these devices make use of both types of power sources: a rechargeable one as the main source of energy and a small primary one (*e.g.* alkaline or Li/MnO$_2$ coin cells) for memory back up and real time clock.

11.8.2. Professional A/V (Audio/Video) Equipments

TV and movie professionals use different A/V equipments powered by autonomous power sources: stand-alone cameras, camcorders, lighting systems, audio recorders, *etc.*

Unlike consumer video cameras, professional versions are more power demanding for their electronics, and they are often required to supply power for an auxiliary lighting. These power requirements are satisfied through the use of battery packs contained inside belts or even small cases. Reliability is of key importance.

Technical specifications

- portable power source
- current: from a few Amps up to 5 A for the cameras, 4 to 10 A for the lighting systems
- voltage: 6 V to 14 V (typically 7.2 V) for the camera, 12 V up to 30 V for the lighting systems
- capacity: 4 to 9 Ah
- operating temperature: -30/+50°C
- charge time: 1 hour, typically
- discharge time: 2 to 3 hours, typically; sometimes 1 hour or 12 hours for not too sophisticated lighting systems
- weight: as small as possible in most cases

Power sources

Battery packs used to power professional A/V equipments are made with primary cells, or, more often, secondary batteries.

SLA batteries offer the advantage of a lower cost but are heavier.

Primary lithium cells (Li/SO_2, $Li/SOCl_2$) offer the advantage of allowing shooting in severe temperature conditions, but, of course, need to be replaced.

Ni/Cd batteries have long been the solution of choice for this application due to their ability to deliver the high drains required by the lighting systems, their 500+ charge/discharge cycles, and their good performance in most outdoor conditions. However, Li/Ion batteries, which offer a higher energy density, tend to occupy now an increasing percentage of this market. They are often coupled with solar panels for their charge (*e.g.* when used on-board boats or in isolated areas).

Ni/MH batteries can be found in these equipments too. For instance, 12 V Ni/MH battery packs are used to power cart-loaded audio recorders; they replace SLA and Ni/Zn batteries, which used to be the power sources of these equipments.

11.9. Ambulatory Medical Equipments

From devices implantable in the human body (*e.g.* pacemakers), to portable ones (*e.g.* holters) and ambulatory equipments, medical apparatuses are using all sorts of primary and secondary batteries.

Lithium iodine, lithium carbon monofluoride and lithium silver vanadium oxide cells power most implantable devices.

If alkaline cells (mostly 9V) have a firm grip on the portable ones, primary lithium cells can be found in a few of them (*e.g.* infusion pumps).

Rechargeable batteries power a large range of ambulatory equipments. Here again, the Li/Ion system is gaining a growing acceptance.

11.9.1. Portable Defibrillator Systems

This medical device is used to treat ventricular fibrillation (VF), a really dangerous malfunction. In VF, the heart quivers ineffectively and is unable to pump blood throughout the body; the defibrillators supply a powerful electrical shock, on the patient chest, that interrupts the VF and allows the heart's normal rhythm to regain control. Without this treatment, the patient would die within minutes.

Defibrillators can be either implanted in the human body or transportable (the latter is shown in Figure 11.4)

These systems include the defibrillators themselves and the monitors for follow-up. The use of portable defibrillators is becoming more widespread, hence, the demand for light-weight power sources has increased. These devices are now carried in police cars as well as in ambulances and on-board commercial aircraft.

Technical specifications

- portable power source
- base currents (during stand-by periods): a few μAmps
- base current (analysis phase): <500 mA lasting several minutes
- stroke pulse (defibrillation phase): 10 A typically for the defibrillators, for 5 to 10 seconds, while charging the capacitor, repeated every 15-20 seconds; about 2 A for the monitors
- output voltage: 8 to 20 V (12 V typically)
- operating temperature: from -20°C up to +60°C
- runtime: up to several hundreds discharges (even after 4 years of rest in aircraft)
- lifetime: up to 4 years in aircrafts, for instance
- sturdiness

Figure 11.4. Portable defibrillator.

- high energy density
- high reliability

Power sources

Ambulatory heart defibrillators have been using rechargeable battery packs for many years: preferably, Pb/Acid or Ni/Cd batteries. Today, some of them are powered by Li/Ion batteries.

However, a few years ago, it was decided that, by law, all the airline companies had to install one portable defibrillator on-board their commercial aircrafts. Since then, for weight reasons, lighter power sources have been needed and high-rate battery packs, made with powerful spirally wound primary Li/SO_2 or Li/MnO_2 cells (from 2/3A to R20 size) have been selected. A reliable detection of end of life has been another reason for the selection of these two primary lithium systems.

11.9.2. Inter-Cardial Pump Systems

Post operative temporary cardiac support is sometimes provided by an inter-cardial pump system. The batteries provide the power while the equipment is disconnected from mains, so the patient can be moved, and supply power during an emergency.

Technical specifications

- rechargeable power source
- current: up to 2.5 A for 1 hour
- voltage: 20 V
- operating temperature: room temperature
- high reliability

Power sources

Among the secondary batteries, the Li/Ion ones are occupying a growing place.

11.9.3. Ventricular Assist Pump Systems

These equipments have both internal and external blood pumps, which assist the heart as required. They can be used in permanent or post-operative situations. The power is provided by a rechargeable battery, either as the main source (to allow freedom of movement) or as the backup source, depending on the mode of use.

Technical specifications

- portable rechargeable power source
- current: 1 A for 2 hours
- voltage: 20 V, typically
- operating temperature: room temperature
- high reliability

Power sources

Here too, Li/Ion batteries are in increasing demand.

11.9.4. Emergency Portable Medical Fluid Warmers

Emergency blood and infusion supplies are stored at low temperatures, even sub-zero. However, before liquids can be used for an intravenous infusion or transfusion, their temperature needs to be raised to +37°C. In these life-critical missions, reliable control of the liquids' temperature is essential.

Technical specifications

- portable rechargeable power source
- current: 1 A for 2.5 hours
- voltage: 10 V, typically
- operating temperature: room temperature
- high reliability

Power sources

The battery weight being a concern, Li/Ion has allowed the use of batteries able to satisfy the above specification while weighing only ~200 g. An example is the 6.8 Ah prismatic battery shown in Figure 11.5.

11.9.5. Powered Respirators

The equipments to assist in breathing people suffering of chronic or acute respiratory failure used to be powered by the mains. However, recently, portable breathing-assistance equipments have been launched on the market. Up to 11 hours of autonomy can be obtained with one charge cycle.

Technical specifications

- portable rechargeable power source
- current: 0.5 A approximately
- voltage: from 4.8 V to, typically, 24 V
- capacity: 2 to 9 Ah
- operating temperature: room temperature
- charge time: 4 to 8 hours

Power sources

The battery weight being a concern, Li/Ion is the prime power source of these equipments, although some of them also use Ni/Cd packs. Another feature of the Li/Ion system proved of importance for its adoption: its clear end-of-life indication. Thanks to the use of a gas gauge, Li/Ion batteries enable the respirator users to see easily how much power remains.

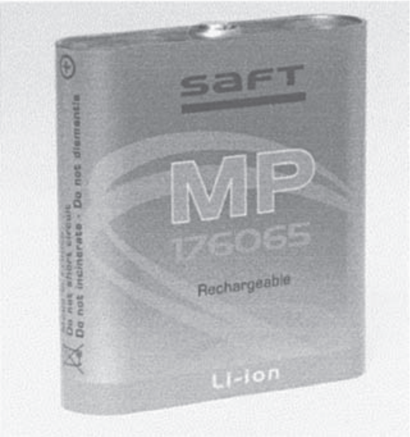

Figure 11.5. Saft Li/Ion prismatic size 6.8 Ah battery.

11.9.6. Special Medical Tools

Some surgical and laboratory tools have been powered by batteries for many years. Primary and secondary power sources are used here.

For instance, micropipettes have been powered by high-rate R14 $Li/SOCl_2$ cells for nearly 20 years; the high energy density and the drain capability of these cells have justified this choice.

One reason for using primary lithium cells in some surgical tools (*e.g.* planes, pointers) is the fact that only these cells can stand safely the accidental exposures to the very high temperature (+140°C) of the autoclaves used to clean these tools.

Technical specifications

- portable power source
- current: less than 200 mA
- voltage: 2.5 V to 3.0 V, typically
- operating temperature: room temperature usually, with possible accidental excursions up to very high values
- very high reliability
- runtime: from a few hours to a few years

A low magnetic signature of the power source has even been required, in some specific tools, so that the batteries cannot interfere with the electromagnetic signal produced by some other equipment. This requirement obliged the battery manufacturers who accepted this technical challenge to remove all the cell components containing nickel.

11.10. Conclusion

Both primary and secondary electrochemical systems have been able to find a notable place in industrial applications. When the specifications are not very severe (*e.g.* a runtime shorter than a few years, moderate operating temperatures), or when the cost of the power source is a prime concern, or if a recharge is not needed, the alkaline cells are widely used, as they represent the lower cost solution per unit (not always the lower overall operation cost).

Nearly 35 years after the birth of the first primary lithium cells (Li/I_2, Li/CuO, Li/Ag_2CrO_4), it is possible to assert that many of the industrial equipments that we are familiar with today owe their existence to the remarkable features of these lithium-based chemistries.

In fact, when very long runtimes or extreme temperatures are part of the technical requirements, primary lithium batteries are the only choice, in spite of their higher price (but not always their higher usage cost).

However, in many applications, a one-shot power source may represent an excessively costly solution and rechargeable batteries are then used. Here, the trend is clear and leads towards the growing use of the Li/Ion system, in spite of a few drawbacks:

- need to electronically control the charge and discharge voltages
- higher cost per Wh
- swelling of the prismatic cells (not the cylindrical ones) during the charge/discharge cycles

If its higher energy density and lower self discharge rate have already lured the developers of many cordless equipments, its recent performance improvements, like its expanded operating temperature range and its enhanced power capability, should attract a growing number of other users.

Acknowledgements

Thanks are due to Florence Auriol and Alain Jamard from SAFT RBS, and to Graham Archdale and Alain Kerouanton from SAFT LBD, for their contribution to this work.

This page intentionally left blank

Industrial Applications of Batteries. From Cars to Aerospace and Energy Storage
M. Broussely and G. Pistoia Eds.,
© 2007 Elsevier B.V.

Chapter 12

MISCELLANEOUS APPLICATIONS. II. Tracking Systems, Toll Collection, Oil Drilling, Car Accessories, Oceanography

Herzel Yamin, Michael Shlepakov and Chen Menachem

Tadiran Batteries Ltd., P.O. Box 1 K.Ekron, 70500 Israel

12.1. Introduction

This chapter is designed to give an overview of some industrial applications using batteries – mostly the nonaqueous ones. Specific topics presented here include: tire pressure monitoring system (TPMS), automatic collision notification (ACN), Electronic Toll Collections (ETC), tracking systems, oil drilling and oceanographic applications. For each of these applications, the typical load profile, the environmental requirements and the available power sources will be described in some detail.

12.2. Tire Pressure Monitoring System (TPMS)

Tire inflation pressure is an important factor for road safety, tire life and vehicle fuel consumption. In 2002, federal regulators at National Highway Traffic Safety Administration (NHTSA), in the U.S. Department of Transportation, issued a new rule mandating new light vehicles include tire pressure monitors as standard equipment. TPMS must warn drivers when tire pressure is 25% or more below the required level.

NHTSA reports that 23,000 crashes and more than 500 fatal crashes are annually caused by the blowout of tires. It is therefore estimated that the tire monitoring equipment will prevent more than 100,000 injuries and 70 deaths per year in the United States alone.

Several types of TPMS are currently available for light vehicles: the direct, indirect and battery-less TPMS. Each of these methods is here described.

12.2.1. Direct, Indirect and Battery-Less TPMS

There are two basic methods to monitor tire pressure: direct and indirect. The direct method uses pressure sensors to measure pressure in each of the four tires. These data are transmitted via wireless RF transmitters to an electronic central unit: if the pressure is too low or in the case of a sudden loss of pressure the system warns the driver by a display on the control panel. This system is called the direct measuring type because it involves the air-pressure monitor/transmitter attached directly to the tire wheel.

As the name indicates, the indirect method relies on measurement from a distance. There are various techniques available; the most advanced indirect TPMS works with the vehicle's anti lock brake system (ABS). The ABS employs the wheel speed sensors to measure the rotational speed of each of the four wheels. When a tire's pressure decreases, the rolling radius decreases: as a result, the rotational speed of the wheel increases correspondingly. The sensor detects the faster rotation and the system then alerts the driver.

The direct method can provide more accurate data than the indirect method, as it can detect a decrease in pressure as low as 1 psi and does not depend on changes in the outer diameter of the tire.

The battery-less TPMS concept replaces the central receiver with a transceiver that can receive and transmit signals, and a transponder as a passive component (replacing the active transmitter in the direct measurement system), which uses the energy of the signal received from the transceiver. This allows for the transmission of data from the tire pressure monitors located inside the tire without the need of a battery. In contrast to the direct measurement methods that have been widely used in mass production of tire monitoring systems, the battery-less TPMS is still in the development stage.

Several companies specialized in automobile equipments offer TPMS systems. Beru AG, Germany, one of the leading manufacturers of direct TPMS, offers the TSS (Tire Safety System). It consists of a system of electronics, mounted on the wheel, with pressure and temperature sensors that monitor the air pressure in the tire and transmit the data via a high-frequency antenna to an electronic control unit. Schrader Electronics, Ireland, also offers a direct TPMS. The basic operation of the system is by means of a valve sensor on each wheel that sends tire pressure information to the nearest wheel detector, which then signals the central receiver. TRW Automotive, U.S.A., can provide both direct and indirect types of tire pressure monitoring systems. ALPS Electric, Japan, developed the battery- less TPMS.

12.2.2. Power Consumption

Most automobile manufacturers require 7 to 10 years operational lifetime for TPMS. To meet this requirement, each component must have a very low stand-by current (at μA levels) while maintaining efficient measurements and transmitting as infrequently as possible. The life of the battery depends on several parameters: (a) pulse profile and peak current to drive the RF sensors: the stronger the pulse amplitude, the shorter the life of the battery; (b) average current consumption of the whole TPMS set: the lower the current, the longer the life of the battery. A typical TPMS requires 2-2.5 Volt minimum operational voltage, 1-5 μA stand-by current and several pulses per minute in the mA range, each a few milliseconds in length.

Since the battery in the "direct measurements" is located inside the tire, the weight, the volume and the shape of the battery are very important. A typical shape is wafer like with a height of a few millimeters. The environment inside the tire is relatively harsh with a possible temperature range of –40°C to 125°C and severe shocks and vibration frequencies.

12.2.3. Power Sources for TPMS

Several battery technologies are currently used in mass production TPMS: $Li/SOCl_2$, Li/MnO_2 and Li/CF_x. Each of these has its own advantages and disadvantages. The high energy density of the $Li/SOCl_2$ system, the low self discharge rate, the wide operating temperature range, –55°C to 150°C, and its hermetic sealing make it the system of choice for this application.

Figure 12.1 describes temperature cycling imitating the operating temperature range of TPMS applications.

Two coin-type $Li/SOCl_2$ cells are produced by Tadiran Batteries for these applications (Table 12.1). The cells consist of lithium anode as the negative material, $SOCl_2$ as the positive active material and inorganic electrolyte; the cells are hermetically sealed by a glass-to-metal seal and laser welding.

The coin-type Li/MnO_2 cell uses manganese dioxide as its positive

Table 12.1. $Li/SOCl_2$ wafer cells used in TPMS applications.

Cell type	**Capacity [Ah]**	**Weight [g]**	**Volume [ml]**
TL 4986	0.40	5.3	1.2
TL 2450	0.55	8.8	2.6

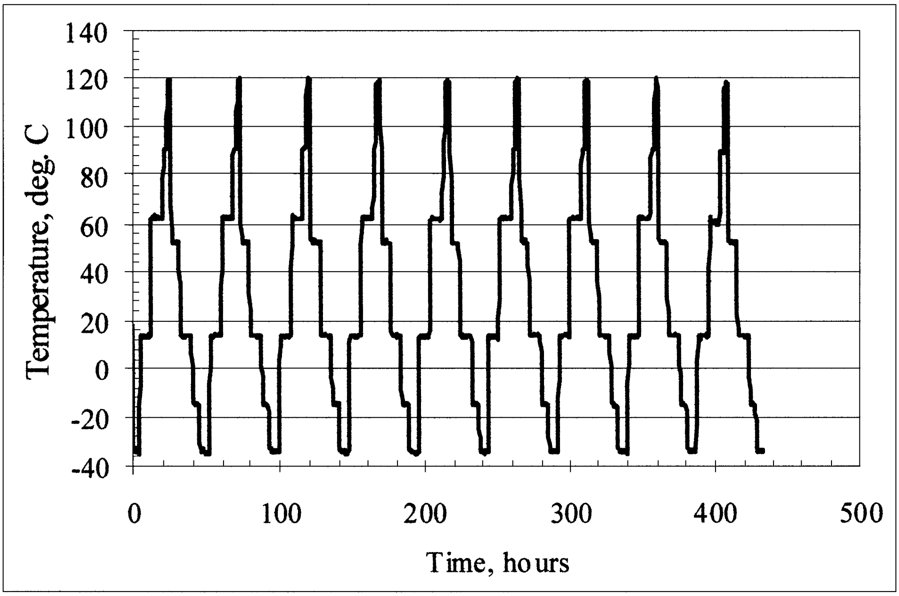

Figure 12.1. Extended temperature cycling test of a battery for TPMS applications.

active material, and organic electrolyte. The coin cell CR 2450 HR is produced by Maxell, Japan, and has a capacity of 550 mAh with an operating temperature range of –40°C to 120°C. CR 2450 EX has a capacity of 525 mAh and can operate between –40°C and 150°C. This cell is currently used for high-end TPMS systems.

12.3. Electronic Toll Collection

Several types of toll collection systems are currently used worldwide. Some of them are fully automated, others are semi automated or manually operated [1-4]. Automatic toll collection systems help to reduce traffic delay, increase toll road efficiency and provide a means to address future traffic demands. In this chapter, the various types of toll collection systems will be described with focus on the ETC methods (electronic toll collection). These systems are being more widely used for toll highways and bridges and for the most part are powered by batteries located inside the electronic device. The currents and voltages required, the environmental conditions and the most appropriate power sources will be discussed.

12.3.1. Toll Collection Systems

Electronic toll collection systems depend on Automated Vehicle Identification (AVI), which is the process of determining the identity of a vehicle subject to toll. The majority of toll facilities record the passage of the vehicle through the tollgate. Most of the AVI systems rely on radio frequency identification (RFID) where a reading device located at the tollgate, communicates with a transponder (transmitter- responder), which is commonly called tag and is located on the vehicle using an onboard battery. Such tag is known as active tag and can accept, store and transmit data. The RFID tag has been proven to have excellent accuracy, and can be read at highway speed without the need to stop the vehicle or to slow down [5-7]. A passive tag has no battery and is powered by the electromagnetic field generated by the reading device.

Another type of tag is currently used in road toll collections. A vehicle may have a bar code to be read optically or electronically. The optical systems use the reflection of light, *i.e.* a laser, from bar coded tags. Such systems are sensitive to physical location of the tag relative to the reader and to atmospheric or weather conditions (such as fog, rain, dust, snow). The optical systems are more useful in parking lots where environmental and speed constrains are of less concern than on highways.

To avoid the need for transponders, some systems use automatic number plate recognition by means of cameras capturing images of the vehicle passing through tolled areas. The image of the number plate is used to identify the vehicle. This allows the drivers to use the facility without any advanced interaction with the toll authority. The disadvantage is that fully automatic recognition requires a manual review stage to avoid billing errors.

12.3.2. Power Sources

Most of the active-tag ETC systems use an independent power source inside the electronics device. A typical load profile of active tag consists of a small stand by currents of 5 to 30 microamps coupled with very short pulses of 10 to 50 mA. Out of the tollgate area, the current drawn is mainly the standby current. While vehicle approaches the toll area, the transponder is activated and communicates with the reader. This approach consumes a higher level of (pulse) currents. Typical operating voltage of a RFID tag is 3.0 to 3.6 V with minimum cut-off voltage of 2.7 to 2.8 V. The required battery operating life is highly depending on the ETC equipments and on toll authority. Some toll authorities require 2-3 years of operation while others require 5-10 years. Battery capacity is between 1.0 and 3.0 Ah, depending on current consumption and the required operating life. Operation temperature requirements depend on the geographic location of the toll area. Typical temperature range is –40°C to 85°C, but a more limited range of -20°C to 72°C is also used.

Due to the relatively high voltage requirements under the pulse load, the most widely used system for toll collection is Li/$SOCl_2$ (bobbin or bobbin+capacitor cell type). This system can also provide the widest operating temperature range. Other systems such as Li/MnO_2 or alkaline are also used. To provide the 3.0 V level, either a single Li/MnO_2 cell is used with step up converter or two serial connected cells with step down converter. Alkaline cells are mainly used as user replaceable when two years of operation are required.

12.4. Automatic Crash Notification (ACN)

Several tens of thousands of lives could be saved and a reduction of up to 15% in the severity of injuries could be obtained annually in the U.S.A. or Europe, if emergency responders knew instantly where a vehicle crash had occurred. Members of the European Parliament's Transport and Tourism Committee recommended that the Parliament support and encourage rapid implementation of E-call, which is the pan-European in-vehicle emergency call system. It is expected to enter into force by the 2009 deadline.

ACN systems use wireless communications and GPS technologies to automatically notify the emergency medical service after an accident and give the rescue team the exact location of the incident. The system is activated when an airbag is deployed or an in-car button located on the dashboard is pressed. In its more advanced form, utilizing a group of sensors, advanced automatic crash notification (AACN) automatically calls a telematics service center if the vehicle is involved in a qualified frontal, rear or side-impact crash, regardless of air bag deployment.

Telematics is a package of automotive communications technology that combines wireless voice and data to provide location-specific security, information, and in-vehicle entertainment services to drivers and their passengers. The heart of a telematics system within the car is a Telematics Communications Unit (TCU) that is connected wirelessly to a central service center. The TCU serves as the central platform of a system, where all telematics-related technologies are integrated. It communicates location-specific information to a central service center and the center helps deliver telematics services to a driver via the cellular phone [8-11].

These services can include sending ambulance services to a driver in an emergency, or sending roadside assistance to a driver whose car has broken down. Other services include the ability of a central server to deliver navigation assistance and real-time traffic information.

12.4.1. Electrical Requirements and Power Sources

Most of the current ACN systems use the vehicle battery as the power source. However, in case of accident, the main vehicle battery can be damaged and the communication interrupted. A backup battery is essential to maintain the communication call for this life saving application. Power source requirements vary from manufacturer to manufacturer. Typical requirements of a back up battery are to provide an immediate high power of about 20 W for 5 to 15 minutes, operate in a wide temperature range of –40°C to 85°C, be safe to use within the passenger compartment, be very reliable in harsh vehicle environmental conditions, and have 5 to 10 years operating life. Currently, only a few telematics systems offer a battery backup in the event that the main battery is disconnected or damaged during the collision. It is expected that battery backups will be widely available in the next few years when the ACN systems become mandatory. Two different systems are designed for this telematics application: (a) lithium manganese dioxide batteries manufactured by Ultralife, USA; (b) Tadiran's primary high-power cells (see description in Sub-section 12.4.4) [12,13]. Figure 12.2 describes typical discharge curves of eight AA cells assembled in 4S 2P configuration (4 cells in series, 2 in parallel). The battery weighs 170 grams and has a 10-year shelf life.

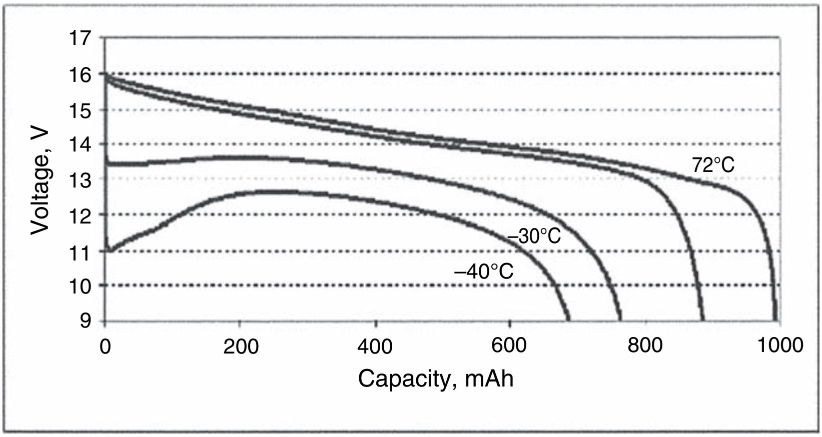

Figure 12.2. Typical discharge curves at 2 A of a Tadiran battery pack designed for telematics applications.

12.5. Tracking

In this globalization era, asset tracking has become an increasingly demanding issue. The assets can be classified according to their sizes and the distances between them and their owners: from small products in a defined limited area, such as a supermarket, through platforms in a defined deck area to large removable containers carried by ships, trains and trucks throughout the world.

Asset tracking is important from an economics, logistics or security viewpoint: it improves the distribution efficiency of stocks, provides theft protection and gives the ability to prevent the use of a portable asset for terrorist activities. For that, the asset has to be equipped with a tag/transmitter for identification and information transmittance. This equipment needs power sources to operate it, *i.e.* batteries.

Other types of tracking such as human tracking or animal's location tracking for research purposes will not be discussed in this review.

This section will mention the tracking methods and provide a description of the different electronics systems, their electrical and power characteristics and an overview of several power sources that can be useful for these applications. In particular, this section will be focused on large asset tracking systems requiring very high-power, high-energy sources. For more information on the monitoring of mobile objects or persons, see also Chapter 12.

12.5.1. Tracking Methods

There are many types of tracking systems. In general, these systems can be classified into two general categories that differ in the asset size and the distance between the assets and their owners. For small-size assets located in limited areas, the energy sources required are relatively simple and small, whereas for portable large assets, high-power energy sources are required to transmit information over long distances. These sources also have to be long lasting, as frequent battery replacement for a portable asset traveling over large areas can be problematic.

12.5.1.1. RFID (Radio Frequency Identification)

In this method, an electronic tag is attached to the asset. A radio wave detector can read this tag, which can carry such information as asset type, shelf life, storage temperature, *etc*. This system is very useful for goods in a small, defined area like supermarkets, production lines and small warehouses.

In the simple version of this method, the tag does not require an energy source and the power source is placed in the reader/detector.

An advanced RFID method requires an active tag for transmission of information and/or the location of the goods. In this case, a power source is needed to operate the tag.

Typical characteristics of active RFID tags equipped with antenna are: a) ~3 kg weight; b) transmission power of ~1W; c) storage and operation temperature range from about –20°C to 50°C; d) power source's life of ~6 months.

Under these conditions, the most useful candidate is expected to be the 2/3A Li/MnO_2 cell. The capacity of this cell is about 1.3 Ah, and it can deliver at least 13,000 transmissions of 1 W with 1-sec duration in the above temperature range during 6 months of operation. This cell is relatively cheap and readily available and therefore is expected to be widely used in these applications.

Other candidates that can also be suitable are AA-size spiral Li/$SOCl_2$, alkaline and even bobbin Li/$SOCl_2$ cells for lower power and longer operating period requirements.

12.5.1.2. GPS (Global Positioning System)

This method is very useful for tracking of large assets, such as containers and cargos carried by trucks, ships, trains and airplanes all over the globe. In this method, the transmitter sends the information to a communication satellite and the satellite logs and transmits the information to a stationary location that delivers the information to the asset owner.

The different types of transmitters for this method differ according to the satellite type with which they communicate.

LEO (Low Earth Orbit) Satellites

LEO satellites surround earth at a relatively low altitude of 160 km to 480 km. Their velocities are relatively high and they orbit the earth in about one and a half hour. Their low altitude enables them to cover only small areas at a time and, due to their high velocity, the periods of communications are short with many "dead periods" without communication ability.

The advantage of the communication of these satellites is the low power of transmission required by their transmitters.

GEO (Geo-stationary Earth Orbit) Satellites

GEO satellites orbit the earth at a high altitude of up to 36,000 km. Their position, relative to a certain point on earth, is constant and, as a result, they complete one circle every 24 hours (the natural time for rotation of the earth).

Their high altitude enables them to cover a very large communication area and therefore 3 GEO satellites can cover almost all the earth's area except for small parts at the poles.

These characteristics enable continuous communication and tracking ability without any "dead periods". However, contrary to the LEO communication, GEO transmitters require a high level of power.

MEO (Medium Earth Orbit) Satellites

MEO satellites orbit the earth at a medium altitude of up to 19,000 km. Their orbit is oval, and not circular like that of LEO and GEO satellites. As opposed to the last two satellites, their orbit also covers the poles.

The power of communications required by their transmitters is moderate (between the communication requirements of LEO and GEO).

12.5.2. GPS Transmitters

Table 12.2 summarizes the requirements of several GPS transmitters produced by leading companies of this field. The table summarizes voltage, current and operating and storage temperature as well as lifetime expectancy of the power source.

Voltage

As can be seen, the transmitters require a relatively high voltage, from 6 V to 36 V. Typical operating voltage for these applications is about 12 V.

Background currents

The background currents are relatively low, and in some cases a background current is not needed at all. Typical values are tens of microamperes. However in some cases, *e.g.* for accessory systems such as data loggers, antennas, *etc.*, several milliamperes are required

Transmission current

The transmission currents required are several tens to hundreds of milliamperes with peak currents of up to 2.5 A for short durations of up to a few milliseconds (GSM and CDMA transmission profiles). Transmission times vary between several seconds to several minutes every few hours, up to one transmission a week.

The transmission currents values, their duration and frequency are defined according to the communication satellite type: communication to LEO satellites usually requires relatively low currents with short communication times and frequency, whereas communication to GEO satellites requires higher currents for frequent long transmissions.

Temperature range

These applications require a very wide operating and storage

Table 12.2. GPS tracking application requirements.

Application #	**Operating voltage** [V]	**Background Current** [mA]	**Peak Current** [A]	**Working temperature range** [°C]	**Storage temperature range** [°C]	**Operating Life** [Years]
1	7.2	0.4	2.2 CDMA*	-40 to 85	-40 to 85	3
2	12	0	2 GSM**	-20 to 70	-20 to 70	2
3	12	15	1 GSM	-25 to 70	-25 to 70	10
4	7.2	0	2 GSM	-40 to 85	-40 to 85	2
5	8	0.05	2.5 GSM	-30 to 72	-30 to 72	100 days
6	12.4	0	2 CDMA	-20 to 60	-40 to 85	2
7	36	0.1	2.5 GSM	-40 to 85	-40 to 85	2
8	6	0.04	1 CDMA	-40 to 60	-40 to 85	3
9	7.2	0.1	2 GSM	-35 to 55	-35 to 55	3
10	14.4	0.035	0.725	-35 to 85	-35 to 85	3

* CDMA=Code Division Multiple Access ; ** GSM=Global System for Mobile Communications

temperature range. Usually the temperature range is –40°C to 85°C, but in some cases, temperatures are required beyond these limits. These severe requirements are needed for the mobility of the assets from very cold places (in the poles for instance) to very hot places such as the desert. In many cases, long operating times at the extreme temperatures are also required (*e.g.* times up to several days at temperatures above 85°C or below –40°C).

Sometimes storage is required prior to operation. A high storage temperature increases the self-discharge rate as well as the impedance of the battery. Power sources based on lithium metal have the tendency to passivate and, as a result, TMV (Transient Minimum Voltage) problems are expected at the beginning of discharge.

Operating time

The operating time required for these applications varies between a few months to several years. These periods define the time for battery replacement: longer operating life requires less battery replacements and allows saving money and resources.

Conclusions

It can be seen from Table 12.2 that these transmitters require a peak power of about 24 W (2A x 12V). For a typical average current value of 0.1 mA (including background current), during two years of operation, about 17.5 Ah will be needed over a very wide temperature range.

Therefore, energy sources required for these applications must have high energy density with high peak power capabilities over a wide temperature range for long operating periods (years). Low self-discharge will also be an advantage.

Hermetically sealed power sources will have a great advantage as gasket crimped systems are temperature-limited (up to 60°C).

These applications require high voltage, therefore power sources with high operating voltage will be preferred, as using these systems will require less serial branches.

12.5.3. Power Sources

Rechargeable systems

Table 12.3A summarizes the characteristics of three rechargeable systems taken from leading battery manufacturers: VRLA (Valve Regulated Lead Acid), Ni/MH (Nickel Metal Hydride) "D" size cells and 18650 Li-Ion cells. The operating voltage of these systems varies from 1.2 V for Ni/MH to 4 V for Li-Ion; their capacity is about 2.5 Ah for Li-Ion and VRLA, and 9 Ah for Ni/MH.

Table 12.3. Candidate power sources for GPS tracking applications.

System	**Nominal operating voltage [V]**	**Capacity [Ah]**	**Working temperature range [°C]**	**Storage temperature range [°C]**	**Max continuous current [A]**	**Self discharge rate [%/Y]**	**Type of sealing**
A Rechargeable							
VRLA	2	2.5	-40 to 65	-20 to 60	30	50	Hermetical
Ni/MH	1.2	9	-20 to 50	-20 to 30	70	100	Gasket
Li-Ion 18650	4	2.5	-30 to 60	-20 to 50	12	20	Gasket
B Primary							
Alkaline	1.5	16	-20 to 55	-20 to 55	2	3	Gasket
Li/MnO$_2$	3	10	-20 to 60	-20 to 60	2.5	1	Gasket
Li/SO$_2$	3	8	-55 to 70	-55 to 70	4	3	Hermetical
Li/TC Spiral	3.6	13	-60 to 85	-60 to 85	2	3	Hermetical
Li/TC Bobbin	3.6	19	-55 to 85	-55 to 85	0.2	1	Hermetical
Pulses Plus Li/TC "D" Bobbin + HLC1550	3.6	19	-55 to 85	-55 to 85	0.2 (5 for few min)	1	Hermetical

These systems, including Li-Ion cells of last generation, have high rate capabilities, both in continuous and pulsed discharge.

The maximum working temperature is 65°C for the VRLA system. The minimum working temperature is –40°C for the VRLA, a temperature that can be attained by Li-Ion batteries too if special electrolytes are used. The storage temperature is limited to –20°C for each of these systems and reaches a maximum of 60°C for the VRLA batteries. The upper temperature limit is set by a drastic increase in self-discharge, especially for the VRLA and the Ni/MH systems. It is to be noted that the gasket crimp sealing of the Ni/MH and Li-Ion systems is temperature-sensitive. The maximum storage temperature is limited to just 30°C for the Ni/MH system, which is the most prone to self-discharge.

All of these systems have a long cycle life (several hundreds of cycles). Their charge temperature range is limited to –20°C ÷ 40°C for the Li-Ion and 0°C ÷ 40°C for the VRLA and Ni/MH systems. The recommended charge temperature for these systems is RT. The charge time is about one hour for VRLA and the Ni/MH systems and about 2 hours for the Li-Ion system.

The operating life varies between 5 years for the Li-Ion and Ni/MH and 10 years for the VRLA system.

Primary systems

Table 12.3B summarizes the characteristics of several primary systems. The values reported are for "D" size cells from leading manufacturers.

The primary systems include alkaline and different lithium cells. Typical working voltages vary between 1.5 V for alkaline cells up to 3.6 V for $Li/SOCl_2$ (Li/TC) cells. Capacities for these primary systems vary between 8 Ah for the Li/SO_2 system up to 19 Ah for the $Li/SOCl_2$ and the PP (PulsesPlus) systems.

Operating temperature ranges for the alkaline and the Li/MnO_2 systems are –20°C ÷ 55/60°C (gasket crimp sealing). The other systems are hermetically sealed and therefore their temperature ranges are wider.

The continuous current reaches a maximum of 5 A for the PulsesPlus system for a few minutes. Continuous current for long periods ranges from 200 mA for both the $Li/SOCl_2$ bobbin and the PP batteries to 2-4 A for the other systems.

The peak currents for the bobbin systems are relatively low: about 250 mA can be delivered. Instead, the spirally wound configuration allows much higher currents: for instance, the Li/SO_2 cell can deliver pulse currents of up to 30 A. The maximum peak current for the PP system is 15 A, thanks to the presence of the hybrid layer capacitor (see next sub-section).

The self-discharge rate is relatively low: between ~1% per year for the Li/MnO_2, Li/TC bobbin type and the PP systems and ~3% per year for alkaline, Li/SO_2 and spiral $Li/SOCl_2$ systems.

12.5.4. Advantages and Disadvantages of Available Batteries

Rechargeable Systems

Advantages

The three rechargeable systems described in Table 12.3A can deliver the currents (continuous as well as peak) required for the described tracking applications. Their operating life (up to 5 years) is also in the applications range. The large number of cycles obtained from these systems allows a long life without replacement. The Li-Ion system has the additional advantage of a high voltage (~4V), this reducing the number of cells in series.

Disadvantages

Recharging these systems requires time and resources: they must be charged under controlled conditions of voltage, current and temperature, this being a burden from a logistics point of view.

To fulfill the high voltage requirements of these applications, large numbers of serial branches for the low-voltage systems, VRLA and Ni/MH, must be used. This can be a technical limitation, as each of the serial branches must be controlled separately during the charge process.

Other disadvantages of these cells include the higher self-discharge rate and limited operating and storage temperature range with respect to the majority of the primary systems. The estimation is that these systems will be only in limited use for special tracking applications requiring a short operating time in a limited area with an easy access for the charge systems.

Primary Systems

Alkaline

The alkaline cells are used widely for many applications, due to their availability, low cost and ease of use. Their capacity and power capabilities can also meet the basic tracking applications requirements. However, their low voltage, narrow practical temperature range and relatively high self-discharge rate will be critical disadvantages for many of the tracking applications.

Li/MnO_2

The capacity (10 Ah), current capability and low self-discharge of the $LiMnO_2$ cells can meet some of the tracking applications demands. Their big disadvantage is the limited operating and storage temperature range (only –20°C to 60°C). Most of the tracking applications require a wider temperature range, this representing a hurdle for a widespread use of these cells.

Li/SO_2 and spiral $Li/SOCl_2$

The Li/SO_2 system has the power, energy and operating temperature capabilities required by the tracking applications, but this cell will probably not be an optimal solution compared to the spiral $Li/SOCl_2$ cell because of the higher operating voltage and wider storage and operating temperature range of the latter. The advantage of the Li/SO_2 cell compared to the spiral Li/$SOCl_2$ cell is the ability to operate continuously at high currents under low temperatures. However, this characteristic is not critical for most tracking applications.

For tracking applications that require a short operating time (up to few months) with many (several per hour) and longer (more than several minutes) transmissions, the spiral Li/$SOCl_2$ system is expected to be the most useful candidate. The disadvantage of this system over other systems is the relatively high self-discharge rate. This disadvantage is critical for tracking applications requiring long operating life at relatively high temperatures.

Bobbin Li/$SOCl_2$

The only disadvantage of this cell is its limited current capability. Without this disadvantage, this cell could be an excellent candidate for tracking applications. It has high operating voltage (3.6 V), large capacity (19 Ah in the D size), wide storage and operating temperature range and very low self-discharge rate [14-16]. The power requirements for the tracking applications are critical and therefore this cell is not useful by itself for these applications.

PulsesPlus battery

The PulsesPlus system was developed in order to overcome the current limitation of the bobbin Li/$SOCl_2$ cell. This system, described in detail in Refs. [17-20], combines a bobbin type Li/$SOCl_2$ cell together with a special capacitor (Hybrid Layer Capacitor, HLC) in parallel. The addition of the HLC provides the advantage of a very high current capability (up to 5 A continuous and up to 15 A in one-second pulses for an AA size cell).

This combination of a high-energy bobbin type Li/$SOCl_2$ cell and high power HLC makes the PulsesPlus system useful for tracking applications requiring long operating life (years) with several short (up to a few minutes) transmissions per day.

12.6. Oil Drilling

In the oil and gas industry, the down-hole drilling process demands several types of measurements while drilling (MWD) and logging while drilling (LWD) at the remote location without interrupting the actual drilling operation. It saves time and decreases some undesirable effects like doglegs – deviations from the optimal drilling path to the target site. MWD tools supply real time data on drilling conditions and the subsurface orientation.

There are different types of remote sensors and MWD tools used to survey and transmit the acquired data to a surface operator.

Drilling orientation survey data can be transmitted by means of Mud Pulse Telemetry [21]. The information of the tool orientation and inclination, measured by the accelerometer and magnetometer, is transmitted to the digital processor as logical signals via the drilling mud circulation system. The mud pressure pulses (activated by special tools), "translated" as logical "1" (positive and negative pressure pulses) or logical "0" (medium pressure between the pulses), transfer data as binary information.

The same information can be transmitted without mud pulse telemetry by sending the data to the surface through the soil formation from an electromagnetic MWD tool. The control information can be sent back to the tool electronics from the surface operator or software.

12.6.1. Applications

The power line in most remote applications is not convenient and rather expensive. Due to the remote location of MWD sensors and some down-hole tools, they must be supplied with power by an independent battery pack placed as close to the tool as possible (Figure 12.3).

The battery pack should meet several requirements depending on the specific application. The battery must work in very harsh environmental conditions: a wide temperature range, from -40°C or -20°C to 150°C (but in some cases up to 200°C), severe mechanical shocks and vibrations, and high pressure.

The electrical requirements vary depending on the application. Low rates are typical of memory back up, when the acquired data should be stored in memory while drilling between transmission sessions and/or analyzed at the surface; high drain rates are necessary in the case of cutting tools or motors activation. Some examples of such applications will be given below.

The geometry of the down-hole drilling tool strictly limits the battery

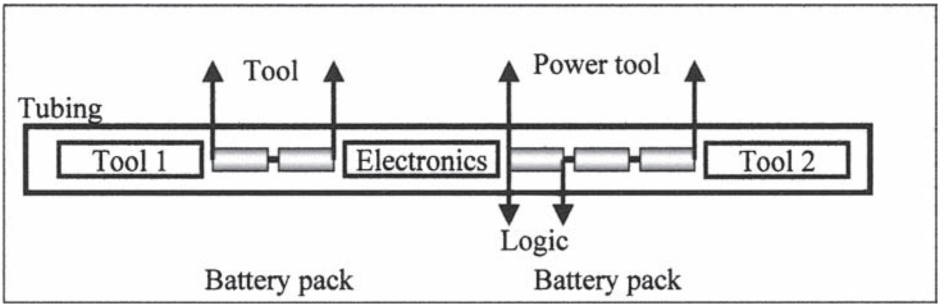

Figure 12.3. Schematic battery pack location in the drilling tool.

pack size and shape. As it is placed inside the drilling pipe, the battery pack has a cylindrical shape and comprises, besides the batteries, appropriate safety circuitry, connectors and battery-to-battery wiring, and insulating sleeve/housing.

The down-hole drilling applications regarding the battery power supply could be divided into three main groups: memory back up, sensors and power tools. All these applications are usually powered by the same battery pack, but the pack can be divided into a few sections, each being used for different applications (Figure 12.3).

Memory back up applications use battery energy to store sensors survey data while drilling and retrieve it upon finishing drilling at the surface. For energy saving reasons, the accumulated information is stored in memory allowing energy-consuming transmission operations to occur less frequently. A memory back up regime requires low to moderate power and a high capacity for longer uninterrupted operation.

MWD and LWD applications operate at moderate to high power depending on the number and type of sensors and tools and on the electronic circuitry design. MWD sensors gather, store and transmit information including drilling temperature and pressure, soil formation resistance, oil reservoir porosity, drilling three-dimensional orientations and pipeline inspection data. The transmission of accumulated data can then be accomplished by the mud pulse telemetry or by electromagnetic pulse transmitters.

The power tools applications comprise, amongst other uses, activation of sensors, shut-in tools and perforators for the formation penetration and starting oil and gas flow, shear tools for down-hole cutting procedures, spin-less flow meters, down-hole shut-off valves, and different kinds of motors.

These applications consume quite a bit of energy and need a high amount of power, but have a limited number of sessions.

In Table 12.4, a few examples of down-hole drilling applications are presented.

12.6.2. Power Requirements

The pressure and temperature sensors typically require currents of tens to hundreds of microamps in memory back up mode and up to tens of milliamps while sampling and transmitting or switching between the sensors. The sampling rate is adjustable from seconds to hours.

The operating voltage is about 3 V and the operating time varies from hundreds of hours to a few years depending on the survey and transmission protocols, electronic circuitry and battery energy.

Table 12.4. Some examples of down-hole drilling applications.

Application	**Voltage [V]**	**Background current [mA]**	**Low pulse (mA)**	**High pulse (mA)**	**Period**	**Temp. range [°C]**	**Batteries in use**
Memory gauge	3	0.05-0.3	4-5 < 1sec	10-50 < 1sec	few sec	-40 +130	AA, C Lithium, Alkaline
Pressure-temperature gauge	3	0.1-0.2	4-5 < 1sec		few sec to hours	-40 +150	C Lithium, Alkaline
Master controller (memory)	15	0.2				-40 +150	C Lithium
Sensing device	3	0.05	50 few msec		few sec	-40 +150	C Lithium
Pipe inspection gauge	7	200-400			tens of hours (total)	-40 +150	C, D Lithium
MWD tool	30	70-80	250 few sec	1200 few sec	0.5-1h	-40 +120	DD Lithium
Power MWD timer	50 / 7	10		1500 few sec	min to hours	-40 +150	DD Lithium
Shear tool	15	5	250 few min	5000 few sec	4-6 cycles	-40 +165	C Lithium

These applications are usually powered by a single primary lithium C-size, AA-size or smaller battery, and small battery packs with single battery voltage equal to or greater than 3 V. In case of alkaline battery use, the number of batteries in series should be doubled due to the lower nominal battery voltage (1.5 V); however, the high maximum application temperature limits the deployment of this type of batteries. Indeed, as already mentioned, the temperature reaches 150°C in most cases and, on occasions, even 200°C.

The battery voltage must not drop below the minimum cut-off application voltage during operation in order to maintain the memory content of hundreds of thousands of readings.

MWD and LWD usually draw from the battery tens to hundreds milliamps in stand-by and logic mode and hundreds milliamps to few amps in operating mode. Sleep mode with a few milliamps drain incorporated between operating cycles decreases the overall energy consumption and increases the battery life.

The voltage of the battery pack in some designs reaches a few tens of volts by means of several primary batteries stacked in series. A number of parallel strings may be desirable to increase battery pack capacity, power capability and operating life. C, CC and DD-size battery packs are widely used.

In addition to these requirements, in power tools operations the operating currents can be as high as several amps for hundreds of milliseconds to several seconds, as, for example, when a shearing tool is used.

The power required by these operations is a matter of concern. Due to the battery internal impedance, the current drained from the battery causes a voltage drop and the output power decreases. In case the battery cannot maintain the minimum functional power, the operation will fail. In the shearing tool example, the tool motor will stall.

In contrast to the data survey consisting of frequent functions, the power tool applications usually require only a few working cycles and could be executed during separate drilling operations. Sometimes such an application could be intermittent, with long storage periods between working sessions.

As can be seen, in all these applications the current and voltage profiles vary in a very wide range depending on the tool design and task. Therefore, nearly each battery-powered down-hole drilling application needs its own specifically designed battery pack.

Let us see what factors the tool designer should take into account while looking for the best battery pack design.

12.6.3. Criteria of Battery Choice

Electrical Requirements

Every down-hole drilling session is a complicated, expensive process, not less challenging for the drilling tool designers than is a rocket launch for NASA engineers.

The main task of MWD and LWD is to acquire maximum information and to produce maximum operations while drilling. The number of simultaneous operations dictates the appropriate power and current drain levels and minimum voltage values required for the proper functioning of the specific electronic circuitry. The load profile timing is very important as it may affect the battery performance and the application average current, ultimately limiting the battery life. All these requirements must be clear before starting the battery pack design.

Working Temperature Range

In many down-hole drilling applications, the lower temperature may reach -40°C (see Table 12.4). As the internal impedance of different types of batteries is a function of temperature and increases with temperature decrease in a different manner, the minimum possible temperature will be a factor to consider.

The maximum temperature is usually the most critical issue and significantly narrows the battery choice. High temperature batteries are available in the market with different performance characteristics and different chemistries suitable for 125°C, 150°C, 165°C, 180°C and 200°C maximum temperature. The battery hermetical seal design helps to avoid electrolyte drying out at high temperatures.

Mechanical and Environmental Conditions

The battery must withstand harsh drilling shocks and vibrations, and high pressure conditions. This is especially important for high-power spirally wound and double anode lithium batteries because in the case of an internal short circuit they may become hazardous.

Battery Pack Dimensions

Tailoring the battery pack to the existing fixed cavity does not always give the most efficient battery performance, but is practically unavoidable. In down-hole drilling applications, there are severe space limitations and the application designers are recommended to collaborate with the battery manufacturers in order to find the best solution. In some cases, the fixed cavity may even cut down the application operating life and cause frequent and costly battery replacements.

Therefore, the battery volume is an important choice factor. For example, the rated voltage of alkaline batteries (1.5 V) is less than half that of lithium thionyl chloride (3.6 V) or lithium sulfuryl chloride (3.9 V) batteries, and so require a higher number of batteries for the same voltage. The practical volumetric energy density of the battery (Watt-hours per volume unit), which is connected to its design and chemistry type, greatly influences the battery pack volume and performance.

Battery Self Discharge

This feature becomes a matter of concern if the application requires that the battery undergoes long non-operational storage or the application average current is low and comparable with the battery self discharge. Different battery designs of the same chemistry type influence the self discharge; for example, spirally wound batteries manifest higher self discharge rates than bobbin type batteries with the same chemistry and size.

Safety

Different battery designs have different safety features. Spirally wound lithium batteries, for example, have intrinsically lower safety than bobbin type batteries.

12.6.4. Battery Chemistry

The proper balance between the pack design and the individual battery performance affects the pack performance under the specific load profile and environmental conditions. The battery performance, in turn, derives from its design and chemistry.

There are three types of primary battery chemistries available in the market for high temperature applications: alkaline, lithium thionyl chloride and lithium sulfuryl chloride. Table 12.5 compares the three battery chemistries used in oil drilling applications.

Alkaline Batteries

The voltage of alkaline battery is continuously decreasing with the depth of discharge and the slope becomes steeper as the current drain increases. A larger number of batteries in the pack can compensate for this.

In comparison to lithium batteries, the energy density of alkaline batteries is three times lower, this significantly increasing their number in comparison to lithium thionyl chloride or sulfuryl chloride batteries used for the same application. The number of cells in the pack must be also doubled in order to maintain the same voltage.

The low energy available from alkaline batteries at low temperatures may affect their restart capability in cold weather conditions after partial discharge in the previous working cycles. Besides, these batteries, being crimp sealed, can be only used at a relatively low upper temperature and for only a

Table 12.5. Comparison of the main characteristics of DD-size batteries (at room temperature)*.

Battery Chemistry	**Battery Design**	**Rated Voltage (V)**	**Rated Capacity (Ah)**	**Power capability**	**Volumetric Ener. Dens. (Wh/L)**
Alkaline (2 D-size cells)	bobbin	1.5	15·2= 30	High	320
Li-thionyl chloride	bobbin	3.6	40	Low	1470
Li-thionyl chloride	dual anode	3.6	29	Moderate	1020
Li-thionyl chloride	spirally wound	3.6	27	High	900
Li-sulfuryl chloride	spirally wound	3.9	25	High	930

* The DD size is obtained by connecting in parallel two D size cells.

short duration.

Although alkaline batteries are cheaper than lithium batteries and possess a higher power capability for the same design (bobbin), all the drawbacks mentioned above make them rarely used in down-hole drilling applications.

Lithium Thionyl Chloride and Sulfuryl Chloride Batteries

Primary oxyhalide batteries with lithium anode possess the highest energy density (Table 12.5) and exist in three designs: bobbin, spirally wound and dual anode. The cover laser welding, with the positive terminal being of a glass-to-metal seal construction, hermetically seals these batteries and prevents electrolyte leaking or drying-out.

The volumetric energy density of the thionyl chloride system is very high, especially for the bobbin configuration (Table 12.5). If the spirally wound design is considered, the sulfuryl chloride system has a somewhat higher energy density.

The oxyhalide batteries manifest very low self discharge rates in bobbin type design: ~1% capacity loss per year. This feature is attributed to the passivation layer (SEI), instantly formed on the surface of the lithium anode upon its contact with the liquid cathode [22]. The layer is very thin and is a good ionic conductor; it provides long-term stability to the system and makes the battery useful even after several years of storage. At the same time, this positive feature causes an inconvenience when an immediate high current pulse is applied. A voltage drop (delay in voltage response) occurs, especially at low temperatures, and in some cases the battery may become useless if its short-term power is affected by passivation.

The reason of the voltage delay is the resistance of the SEI passivation layer, which increases with time and temperature, as does the SEI thickness. Several efforts have been done to solve this problem on a chemical basis, but it can also be tackled by an appropriate battery pack design or intelligent use of the depassivation protocol before initial usage.

Thionyl chloride and sulfuryl chloride batteries at standard conditions (room temperature and rated current) deliver all the rated capacity at a very steady voltage that drops only at the very end of the battery life. The batteries continue to keep a steady voltage under various application currents and under a high temperature environment as well, but the voltage level depends on the discharge and storage conditions.

Thionyl chloride bobbin type batteries with lithium aluminum chloride as the electrolyte salt, have good low rate performance at low and ambient to moderately high temperatures, but undergo passivation at 150°C and maintain a low voltage. The substitution of $LiAlCl_4$ with $LiGaCl_4$ is known to improve the battery performance at very low temperatures (down to -80°C) and the power capability to some extent.

The dual-anode lithium thionyl chloride batteries have a moderate power capability, while the spirally wound batteries show the best power performance. The drawbacks of high power batteries are their lower energy density (see Table 12.5) and higher self discharge rate. Furthermore, as the interior of the spiral is relatively thermally insulated from the metallic can, removal of the heat developed during current flow is less efficient. This may create concern in terms of safety.

In these down-hole drilling applications, the battery use may be interrupted from time to time, and the partially discharged (at high temperature) battery pack may need to be stored on a shelf for weeks. This makes the restart behavior a matter of concern because of the passivation effect [23]. This passivation state can be removed by performing one of these procedures prior to a working cycle: a) applying short-time high current pulses; b) briefly shortcircuiting the battery several times.

12.6.5. Future Developments

Not all down-hole drilling applications require high energy for their tasks. Some of them, like power tools, need a power burst for a short period with comparatively low energy consumption. Another application needing only a small amount of energy is the memory back up used in case of mudflow telemetry failure due to a lack of mud circulation. Future developments may include the introduction of lithium rechargeable batteries or super capacitors into use. If rechargeable batteries were to be implemented, they could also prove to be a remedy for the primary battery packs substitution. The idea is based on the mudflow-activated turbine charging a pack in the idle mode, and drawing the energy from the pack when the mudflow fails. The rechargeable batteries smaller size is an advantage in avoiding the lithium batteries transportation restrictions.

However, there are some hurdles on the way to implementing this change.

(a) Lithium rechargeable batteries cannot withstand even a temperature of 125°C for a long time and their internal resistance increases significantly at these temperatures.

(b) The energy density of these batteries is lower than that of lithium primary batteries. That means the battery pack could be rather big in comparison to the primary battery pack.

(c) Pack safety is an issue. All the rechargeable lithium batteries are jelly rolled with high power capability. The heat dissipation in high temperature environment will be less effective.

Super capacitors in comparison have a significantly narrow temperature range and high self discharge rate. Although they support high power, their energy storage capability is far below that of lithium batteries. These factors make these solutions not only cost sensitive, but also questionable as to their ability to fulfill the task at high temperature or under other non-standard conditions.

Conclusions

The best battery chemistry for use in down-hole drilling applications is still the lithium oxyhalide system where the battery anode is metallic lithium and the cathode (and solvent as well) is thionyl chloride or sulfuryl chloride.

The low and medium rate batteries possess very high energy density and low self discharge, this making them useful for long life, low power operations like memory and some MWD applications.

The high rate spirally wound lithium thionyl chloride or sulfuryl chloride batteries are the best for MWD and power tools applications, which require high current drain and power bursts. Drawbacks of these batteries, in comparison with the bobbin types, are: higher self discharge (5% per year), more evident passivation effect (voltage delay) because of the higher currents required, and less safety.

Alkaline batteries show high power capability and are cheaper that lithium oxyhalide batteries, but their voltage and energy density are significantly lower. The crimp seal construction makes them not suitable for high-temperature applications and shortens their operating life.

The development of rechargeable systems is still at the beginning and has many technological and safety hurdles on its way to a successful completion.

The use of super capacitor is limited by the application temperature range and low energy density.

12.7. Oceanography

The fast growth of modern communication technologies and infrastructures are playing a significant role in the fast development of many new conceptions and applied technologies in oceanography [24-26].

Today there are several worldwide programs running in this field. Several universities and OEM companies developed new platforms and ways to study the processes occurring under water. The net of scientific and GPS buoys cover the blue part of the world map. The global satellite systems acquire, using buoys or any other mobile object, information on: sea level, salinity, ocean currents, temperature and color changes, ocean floor profile and tectonic conditions, and so on.

12.7.1. Applications

Most oceanographic applications, being remotely located, require an independent power source (battery) working without back up or easy substitution. It could be placed far away in the ocean, in the Antarctic ices, or on a drifting iceberg, and the battery replacement would be a costly procedure. Primary batteries are used in this field and a specific design of the battery pack is necessary in most cases, as the application profile, task and life expectancy is unique for nearly every project.

In spite of the great diversity of oceanographic applications, they could be roughly divided into a few groups:

(a) Buoys of different kinds bearing oceanographic, geophysics' and GPS equipment
(b) Underwater vehicles with scientific exploration payload and industrial and military tasks
(c) Ocean floor oceanographic and geophysics' sensors
(d) Safety systems, requiring long stand-by and then a short-term high power burst.

Oceanographic application platforms frequently manage different types of operations. The ocean floor scientific equipment can transmit to the buoy the survey information, which then goes via satellite to the end user or to a web net database location [27]. A deep-water apparatus coupled with an underwater vehicle, floating up to the surface (or close to it) where the transmission will be accomplished, can fulfill the same task.

12.7.2. Power Requirements

These systems support acquisition data survey, processing and storage, requiring low to moderate power for a long time, and data transmission and powering of vehicle motors with high power demands. In the transmission stage or when changing the under water vehicle's location, the power demand can increase rapidly for a short period of time and then return back to the lower level. The battery pack performance and life is critical: it could be requested to sustain high power drains in a wide temperature range, -55°C to 85°C, and has to be long lasting.

Table 12.6 presents some examples of oceanographic applications. As can be seen from the table, most applications require high pulse loads (few amps), so that high-power cells must be used. In a few applications, only low current drains are requested: in these cases, primary lithium thionyl chloride bobbin type batteries with their high energy density are used for long operation times.

12.7.3. Criteria of Battery Choice

Several requirements should be taken into account in the battery pack design for oceanographic applications:

(a) High battery pack capacity, resulting in longer operation time between replacements; cost saving
(b) High energy density, resulting in lower pack weight and size
(c) High power capability; must support high power pulses during operation
(d) Wide operating temperature range; some battery chemistries and designs may not support the low temperature conditions or the significant derating that will increase the number of batteries in the pack
(e) Safety. Different battery types used in oceanographic applications possess different safety ratings. The application can demand high power batteries, like spirally wound batteries known as potentially hazardous, and the battery packs could consist of several tens of batteries in order to maintain the desired operation life. Therefore, safety circuitry and personnel precautions will be of great importance.

High-power oceanographic applications oblige the device designers to choose a few battery technologies (Table 12.6): alkaline batteries, spirally wound lithium batteries or PulsesPlus battery packs, the last ones described in Sub-section 12.5.4. A DD-size PulsesPlus cell, with thyonil chloride, has a capacity of 40 Ah, an energy density of 1420 Wh/L, and a very high power capability (compare these values with those of Table 12.5).

Alkaline batteries possess high power capabilities but low energy density and low working voltage in comparison to lithium batteries (see again Table 12.5). The capacity and energy density average values reported in the table are for room temperature conditions. These figures decrease at low temperatures more drastically for alkaline batteries compared to the other options.

In order to maintain the same power and energy of, for example, the PulsesPlus battery pack, the alkaline battery pack must be significantly larger

Table 12.6. Examples of oceanographic applications powered by battery packs.

Application	**Voltage [V]**	**Pulse load**	**Pack Capacity**	**Temp. [°C]**	**Life time**	**Battery in use**
Sea-floor seismometer	~15	3 A 1 sec	300 Ah 3.9 kg	About 0	62 days	Pulses Plus
Safety inflation system	6	4.5 A 20 msec	2.3 Ah 0.12 kg	-34 +54	7 years	Pulses Plus
Sea-floor seismometer	27	5 A 1 min	50 Ah	About 0	7 days	Li - spiral wound
			48 Ah 2.5 kg		10 days	Pulses Plus
GPS seismic sensor	~7	Few Watts	50 Ah	About 0	1 year	Li - spiral wound
		Few Watts	80 Ah 3.2 kg	About 0	2 years	Pulses Plus
GPS ice buoy	~15	Few Watts	54 kg	-40 +85	1 year	Alkaline
			152 Ah 3.2 kg	-40 +85	1 year	Pulses Plus
GPS buoy	~15	2 A 10 sec	960 Ah 19.4 kg	-40 +85	6 months	Pulses Plus
Glider	~15	Few Watts	30 Ah 1 kg	-40 +85	45 days	Pulses Plus
Current meter	9	1.27 A 1 sec	7.8 Ah* 70 Wh	0 +35	~1 month	Alkaline
	~12		17 Ah* 199 Wh		3 months	Pulses Plus
Sensor system	6.2	10 mA	137 Ah	20	13 months	Li bobbin

* Same battery pack volume

and heavier. This could be very important in under-water vehicle applications due to the lack of space and the mass and shape limitations.

In applications under extremely cold ambient temperatures, like in GPS/ice buoys mounted in the arctic ice, the alkaline batteries become even less efficient, this resulting in even larger battery packs to cope with these extreme conditions. In this specific example, the alkaline battery pack (380 D-size batteries, 54 kg total) was successfully substituted by the PulsesPlus pack of 3.2 kg with 32 D-size lithium thionyl chloride batteries and 4 hybrid layer capacitors (Figure 12.4) [28]. The lifetime of the pack, one year, remained unchanged.

It is difficult to imagine what size of alkaline battery pack would be needed for a performance comparable to the battery pack formed by 96 DD-size

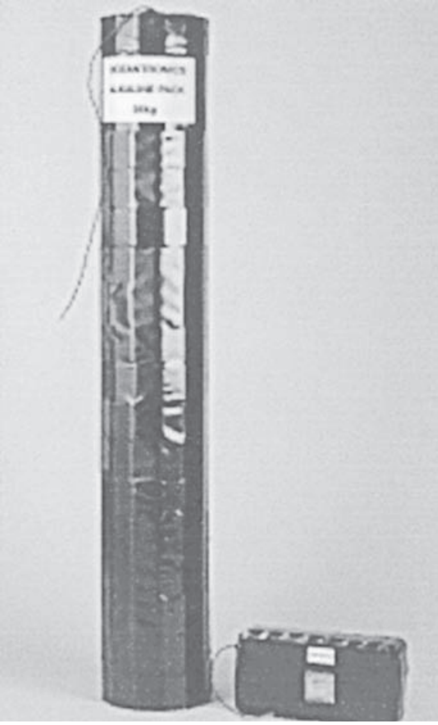

Figure 12.4. Same operating life alkaline battery pack (*left*) and PulsesPlus pack (*right*) for use in GPS/ice buoys.

lithium thionyl chloride cells and 12 hybrid layer capacitors (Figure 12.5) [16].

Lithium spirally wound batteries are capable of delivering their energy and supporting high power pulses at high discharge rates in wide temperature ranges, making this type of batteries suitable for short-term applications (see Tables 12.3 and 12.5). As already mentioned, these batteries, in comparison to lithium bobbin type and PulsesPlus hybrid lithium batteries, have higher self discharge rates, lower energy density and questionable safety; additionally, they are expensive.

The hybrid lithium battery packs possess a high energy density, unsurpassed power capability, low self discharge and high safety. They work in wide temperature ranges, in both short term and very long term applications, where high power pulse capability is required on the background of a medium to low average current drain. That makes the packs suitable not only for applications where size is the most important element, but also for those where the fixed pack cavity has been used to house other types of batteries. In one

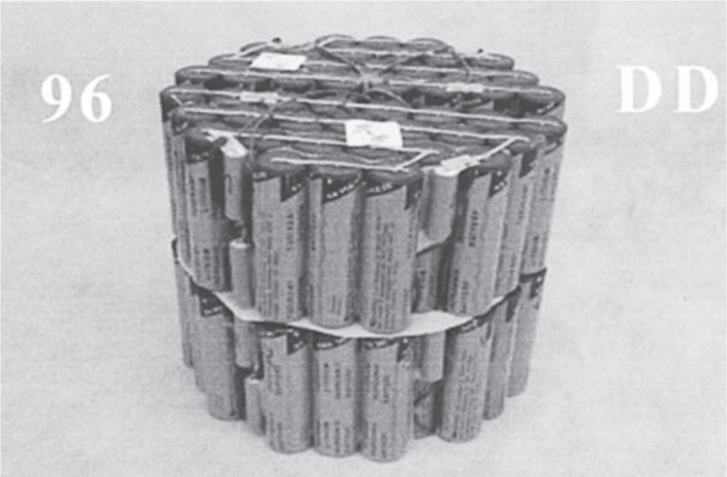

Figure 12.5. Battery pack formed by 96 DD-size lithium thionyl chloride cells and 12 hybrid layer capacitors for oceanographic applications. (*Courtesy of Tadiran*)

application of acoustic current meter and profiler, the substitution of the alkaline battery pack with the hybrid lithium battery of the same size increased the battery pack capacity about 3.5 times.

The hybrid lithium battery packs have advantages not only over alkaline batteries, but also over other lithium battery technologies. Being a comparable choice with lithium spirally wound batteries for short-term applications with high drain rates (if the price and safety of spirally wound batteries is not an issue), the PulsesPlus hybrid lithium battery packs support longer operating life. In a GPS seismic equipment deployed to survey the underwater tectonic information and currently powered by 15 DD-size spirally wound lithium batteries, the operating life is one year. The hybrid lithium battery pack of 15 DD PulsesPlus batteries can provide two years of function.

Some oceanographic applications require a very limited power pulse capability but a high energy density. In these cases, the advantage of lithium thionyl chloride bobbin type batteries is clear in that they possess the highest energy density and will work longer than any other battery type.

The safety stand-by applications are interesting in that the battery must be non-loaded, or under very low background current, for several years until it will be requested to provide high power and energy. These applications, like for example the boat safety inflation system, can use all types of lithium high power batteries, *i.e.* spirally wound Li/oxyhalide or PulsesPlus.

References

1. J.J. Hasset, "Electronic Vehicle Toll Collection System and Method" US Patent No. 7012547, March 2006.
2. E.M. Stuart *et al., IBTTA AVI Conference Proceedings,* June 1990, New York, New York.
3. J.J. Hasset *et al.,* "Electronic Vehicle Toll Collection System and Method" US Patent No. 5144553, April 1992.
4. "Toll Booth Net Automates Fare Collection, Save Cash" *Network World, Vol .5,* Issue 23, June 12, 1989.
5. *Wikipedia, http://en.wikipedia.org/wiki/Electronic_Toll_Collection_System*
6. J.C. Freeny, "Object Monitoring Method and Apparatus" US Patent No. 4217588, 1980.
7. *Encyclopedia of Computer Science and Engineering,* Van Nostrand Reinhold Company Inc, 1983, pp. 563-565.
8. A. Demmler, *Automotive Engineering* 104 (1996) 85.
9. Sang-Bin Rhee, *IEEE Trans. Vehicular Tech.* Vol. VT-27 (1978) 244.
10. C. Reuber, *Funk-Technik* 41 (1986) 275.
11. H.L. Song, "Vehicle Locating and Navigating System", US Patent No.5208756, May 1993.
12. H. Yamin and C. Menachem, *The 22th international Seminar on Primary and Secondary Batteries,* Fort Lauderdale, Florida 2005.
13. H. Yamin and C. Menachem, *The 23th international Seminar on Primary and Secondary Batteries,* Fort Lauderdale, Florida 2006.
14. H. Yamin, M. Pallivatical and U. Zak, *10th international Seminar on Lithium Technology and Applications,* Deerfield Beach, Florida, 1993.
15. H. Yamin, M. Pallivatical and E. Elster, *Proceeding of the 35th International Power Sources Symposium,* Cherry Hill, New Jersey, 1992.
16. H. Yamin, M. Shlepakov, C. Menachem and D. Bar-Tov, *The 40th International Power Sources Symposium,* Cherry Hill, New Jersey, 2002.
17. H. Yamin, S. Luski, J. Carmely, E. Elster and M. Shlepakov, *The 16th International Seminar on Primary and Secondary Batteries,* Fort Lauderdale, Florida 1999.
18. H. Yamin, E. Elster and M. Shlepakov, *The 17th international Seminar on Primary and Secondary Batteries,* Fort Lauderdale, Florida 2000.
19. C. Menachem and H. Yamin, *The 19th international Seminar on Primary and Secondary Batteries,* Fort Lauderdale, Florida 2002.
20. C. Menachem and H. Yamin, *The 23th IPSS Meeting,* Amsterdam 2003, *and J. Power Sources* 136 (2004) 268.
21. *Wikipedia, http://en.wikipedia.org/wiki/Mud_pulse_telemetry*
22. E. Peled, *in "Lithium Batteries",* J.-P. Gabano, Ed., Academic Press, New York, 1983, 211-239.
23. A. P. Johnson, *Proceeding of the 39th Power Sources Conference,* Cherry Hill, New Jersey, 2000.
24. S. Levitus, T.P. Boyer, M.E. Conkright, T. O'Brien, J. Antonov, C. Stephens, L. Stathopolis, D. Johnson, and R. Gelfeld, *World Ocean Database Volume 1: Introduction, U.S. Government Printing Office,* Washington, D.C., 1998.
25. "*Implementation Plan for the Global Observing Systems for Climate in Support of the UNFCCC*" October 2004, GCOS - 92 (WMO/TD No. 1219), World Meteorological Organization, 2004.
26. T. Garrison. *Oceanography (5th Edition)*, Thomson Brooks/Cole, 2005, p. 252.
27. M. Yilmaz, P. Migliacio and E. Bernard, *Oceans 2004 Proceedings*, Kobe, Japan.
28. S. Jacobs, *Sea Technology Magazine,* July 2001.

This page intentionally left blank

Industrial Applications of Batteries. From Cars to Aerospace and Energy Storage
M. Broussely and G. Pistoia Eds.,
© 2007 Elsevier B.V.

Chapter 13

BATTERY MANAGEMENT AND LIFE PREDICTION

Bor Yann Liaw[a] **and Daniel D. Friel**[b]

a. Hawaii Natural Energy Institute, University of Hawaii, Honolulu, HI 96822, USA
b. POWERPRECISE Solutions, Inc., 607 Herndon Parkway, Herndon, VA 02170, USA

13.1. Definitions

To establish a proper dialog of *battery management* and *life prediction*, we believe many battery terminologies need to be clarified for consistency in the discussion. A good summary of such terminologies can be found in Ref. [1], of which the readers are strongly encouraged to review then first. We will use the terminologies defined in Ref. [1] for technical discussion in this chapter.

13.1.1. Battery Management

Battery Management can be defined as the effective use and control of energy and power into and out of a string of at least one battery, either primary or secondary. Typically, a battery is a combination of series and/or parallel of cells placed into a single containment as a battery module. A battery pack usually consists of modules in series and/or parallel. The battery pack may be enclosed in the device it is powering entirely or may be removable and replaceable. The battery management includes discharge and may include charge for secondary batteries.

Battery Management is typically implemented into battery operation for two major purposes. One is to optimize the battery performance, and the other to mitigate safety hazards. A typical management system may first involve *monitoring* of basic characteristics such as pressure, temperature, voltage, or current for pre-set values in order to protect the cell from operation outside the limits set by the manufacturer.

The next level involves *measuring* of individual battery characteristics to get appropriate information on present conditions. This more detailed information may then be used for more advanced tasks such as a local display of capacity or charge status. It may also be used to directly control the power and energy into or out of the battery cells.

Battery Management beyond basic monitoring and measuring involves additional processing and perhaps communication of the measured information from the battery to the host device. This may also include calculations based on the measurements which can provide additional information, such as remaining operating time or capacity of the battery. This information can then be used by the device in order to better utilize the energy available in the battery. This communication path can also be used by a charger to determine the best method of charging the battery, thus maximizing capacity.

In general, *Battery Management* is concerned with getting the most useful energy out of the battery cells on a single discharge cycle. For secondary rechargeable batteries, this may include optimizing the charge into the battery as well, so as to get the most energy out of the battery cells on subsequent discharges. By doing so, the management system also minimizes the impact of operating conditions that could harm the battery performance, including life.

13.1.2. Battery Life Prediction

Battery Life Prediction is often used as an estimate of the *service life*, which may include *calendar life* and/or *cycle life* (for secondary batteries) of either a battery or a battery pack. Often, the life of a battery pack will differ from that of an individual battery due to multiple factors that influence the pack.

The calendar life is usually the "*shelf life*" of the chemistry which is frequently defined as the point at which the battery or pack can no longer be expected to deliver more than 80% of its original capacity. Although the battery can still deliver useful energy, the industry uses this 20% decline in capacity as a reference point for *End-of-Life* (EOL). The shelf life of a battery or battery pack is determined by its charge retention characteristics, or the self-discharge rate.

In a secondary rechargeable battery or pack, the battery service life is often referred to as the *cycle life* of the battery: The amount of full charge/discharge cycles that can be expected before the battery can no longer deliver 80% of its original capacity when charged the first time is typically used as the EOL point.

Battery Life Prediction therefore involves determining how the battery is aging and degrading toward the EOL point. It can also be used to indicate how soon a battery is degrading to the EOL point in the near future. The *State-of-Health* (SOH) is often used to indicate the progression of battery or pack to EOL.

Performance, Function, and Life: A battery can be characterized by its chemistry with specific characteristics, such as the nominal voltage, capacity, specific energy and power, energy/power density, peak power, or maximum current that it can sustain without causing any serious damages to its life. The *performance* of a battery is therefore regarded as an assessment of its characteristics toward a certain set of criteria that can be measured using a scalar index, usually as percentage, as compared to a desired goal to carry out a *function*. A *function* is defined often in a duty cycle, which can be either fulfilled or not, as depicted by *State-of-Function* (SOF) to specify its validity between 1 and 0 for pass and fail. In other words, the battery has reached the EOL, if the SOF is 0. This definition is applied for mission critical pass-or-fail tests; even though in many cases the battery after recharging or a regenerative regime, sometimes under different operating conditions, may be able to fulfill the required function again.

Operating Conditions: The service life of a battery or pack largely depends on *operating conditions*. Three basic parameters, current, voltage, and temperature, are typically used to represent the battery performance under an operating condition. Battery current and voltage might often be affected by temperature fluctuations due to heat generation within the battery and heat transfer to or from the battery as a result of duty cycles and operating conditions, which often complicate the assessment of the battery's service life.

Aging Mechanisms: Degradation of a battery results in fading in performance and shortened service life. Degradation can be reversible or irreversible, depending on the nature of the process. *Aging* refers to the degradation in the property of a component or material used in the battery, which leads to changes in the characteristics of the battery performance. For instance, in lead-acid batteries, acid stratification and sulfation can cause performance degradation. Acid stratification can usually be reversed at any point in time, whereas sulfation accumulated over a long period of time usually cannot be reversed. Aging can come from chemical or physical origin, or via a coupled mechanism. *Aging mechanisms* are mechanistic understanding of the aging processes, which can be categorized into thermodynamic or kinetic origins, or in a coupled manner. The aging mechanisms in the nickel metal hydride (Ni-MH) or Li-ion battery systems are often complicated to identify and characterize.

Stress factors: Stress factors are variables, most within the *operating conditions*, that affect battery performance and life. They are the results of user requirements, duty cycles, ambient conditions, operating regimen, and battery design. They induce aging and/or alter its rate. We should be mindful that aging could take place with several mechanisms at work simultaneously. These aging mechanisms might be coupled or independent, depending on the nature of the processes under the specific operating condition.

Design, *planning*, and *selection* of a battery system for specific operation conditions: It is important to evaluate the impact of the operating conditions to the battery life, so a proper *design*, *planning* and *selection* of the most suitable system can be identified. Although certain operating conditions can be abusive to the selected chemistry under consideration, a well-planned and executed battery operation with good design principles can lead to the best solution to meet overall technical and economical goals. An interesting example is the use of lead-acid batteries for renewable energy storage systems. Due to the sporadic power generation of the renewable energy systems, battery storage often encounters abusive operating conditions in such applications. However, if the battery system can be fully recharged periodically after a certain duty period, it may perform its function with a prolonged life without the concern of sulfation fouling. A well-thought through operation planning can therefore alleviate abuse and result in optimal use of the battery system.

13.2. Monitoring & Measuring

Battery management first involves monitoring and measuring the various physical characteristics of the battery to determine the present conditions of the battery itself.

Monitoring involves a single characteristic or parameter, such as pressure, and a single action or trip-point, such as interrupting current. In contrast, measurement can resolve multiple characteristics, such as voltage and temperature, over a pre-defined range. An example of how a safe operating area is defined for a typical Li-ion cell is shown in Figure 13.1.

Both monitoring and measurement are used to maintain the cells, modules, and the battery pack within the desired safe operational limits set by the manufacturer. Typically, battery measurements are used at the battery pack level as a first stage for maintaining operational limits. Cell monitoring is then used at the cell level to prevent extreme abuse conditions which could cause cell destruction.

Additionally, cell measurements and battery measurements provide the foundation for advanced battery management features such as *State-of-Charge* (SOC) calculation and display, 'smart' battery functions, intelligent charging, and battery life prediction.

13.2.1. Cell Monitoring

Each cell within the battery can be monitored internally and externally. This is particularly important for Li-ion battery, in which the tolerance to abuse

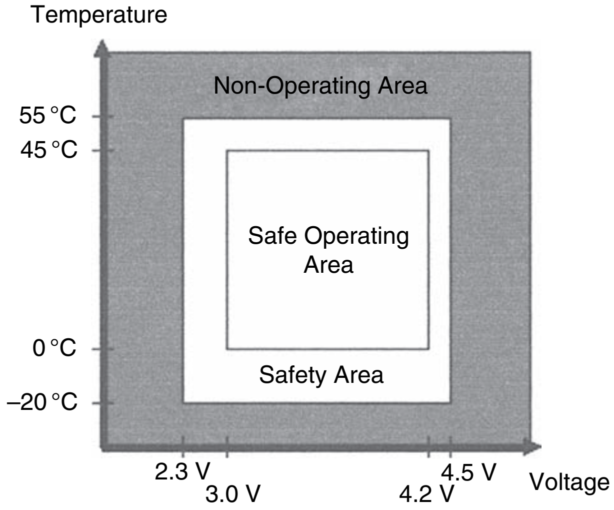

Figure 13.1. Example of safe operating area for a typical Li-ion cell (Temperature & Voltage).

and concern of safety is very sensitive and critical. Internally, the cell manufacturer may include one or more of the following monitoring devices:

- Pressure sensitive current interrupt device (CID), which stops current flow at high internal cell pressures.
- Melting separator, which prevents further operation of the cell.
- Thermal fuse, which opens at a set temperature and prevents current flow.
- Flame arresting vents to prevent explosive electrolyte venting.
- Positive temperature coefficient (PTC) resistor, which significantly increases its resistance when self-heated due to high current flow.

These devices monitor a single parameter (pressure, temperature, *etc.*) for a single condition or trip-point. Often these are safety related and used to protect the cell from severe abuse. Typically they disable the cell from further use [2,3]. Schematics of typical Li-ion cells with some of these internal safety monitoring devices are shown in Figures 13.2 and 13.3.

External monitoring may include similar single point monitors for characteristics such as temperature, voltage, or current. Each would have a corresponding activation to prevent further abuse to the cell, such as interrupting current flow. Examples of such devices, which may be one-time only or can be reset, include:

- PTC resistor, which interrupts high currents [4,5].

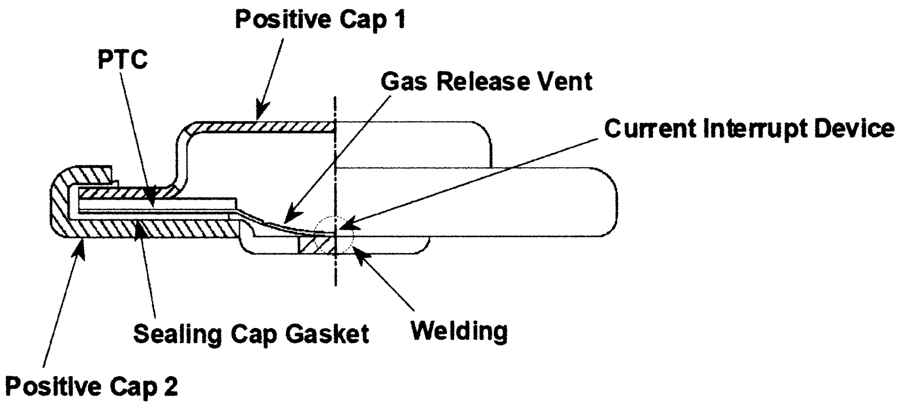

Figure 13.2. Example of internal cell monitor devices: PTC, Current Interrupt Device & Gas Release Vent.(*Courtesy SANYO Energy, Ref.* [2])

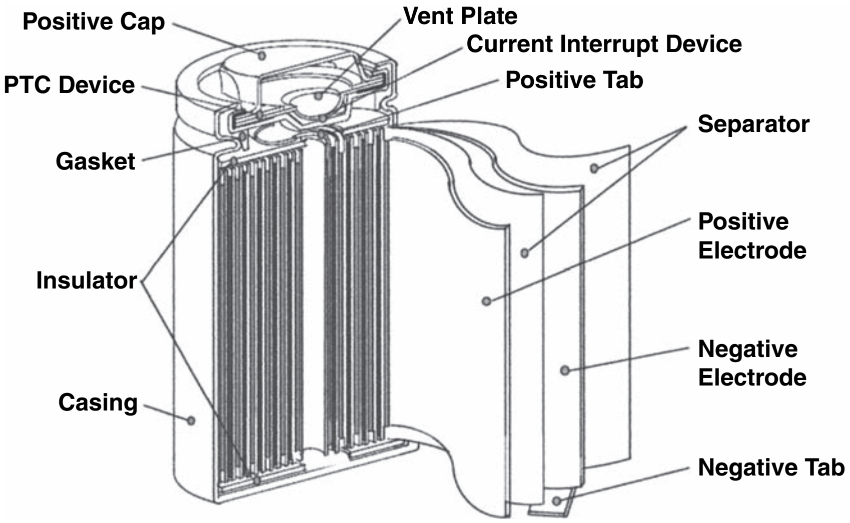

Figure 13.3. Example of internal cell monitor devices: PTC Device, Current Interrupt Device & Vent Plate. (*Courtesy SANYO Energy, Ref.* [2])

- Thermal fuse, which opens at a set temperature, usually one-time only.
- Bi-metal protector, which interrupts current at a set temperature and reconnects at a lower temperature [6].

Note that the above mentioned monitoring devices can be both internal and external to the cells, depending on the chemistry, the cell manufacturer, and the anticipated application. For example, PTCs and thermal fuses can often be found in both inside individual cells and a battery pack or device.

Most monitoring functions are passive, non-electronic, and consume minimal, if any, power during operation.

13.2.2. Cell Measurement

Measuring a cell's characteristics is more complex than the monitoring devices previously discussed. Measurement of cell parameters requires devices that can translate the physical characteristics of the cell to a meaningful and accurate representation. This must also be done without adding a significant power consuming drain on the cells being monitored. Various types of analog-to-digital (A/D) converters can be used to make these measurements.

Cell temperature measurements can be determined using a resistor that varies with temperature, called a thermistor or negative temperature coefficient (NTC) resistor. These devices vary their resistance greatly when exposed to a changing temperature. The resulting resistance change can be easily translated to a corresponding temperature change by a simple electronic circuit [7].

A cell's voltage is also easily measured by an electronic circuit, often after being reduced to a range that can be handled by the electronics. (Simple resistive voltage divider circuits consume some current from the cells being measured and thus can create a cell imbalance issue and degrade the capacity if not properly designed.)

Cell measurement differs from cell monitoring in that the result is a value that can be used to prevent operation of the cell outside a desired range. For example, at elevated temperatures a circuit can be activated to interrupt current flow. Unlike a monitor function which may not re-activate, or which may only re-activate at the same trip-point, thus causing potential oscillations, a measurement can be used to re-enable the current flow at a lower temperature than the trip-point.

Some cell characteristics, such as pressure, although useful, are sometimes difficult to measure in a cost effective manner. However, strain gauges and similar components can be used with some cell constructions to obtain pressure related information.

Note that cell measurements can be made externally from the battery pack when appropriate signal lines are available outside the battery enclosure. Such signal lines must be carefully routed and protected to prevent inadvertent short circuits. This arrangement can be used when measuring primary cells inserted directly into a host device, without a battery pack enclosure.

13.2.3. Battery Monitoring

In this section and on, the "battery" could mean a module or a pack. Monitoring a series/parallel string of cells in a battery typically looks at the full series string parameters such as battery voltage and/or the current (see Figure 13.4). The voltage is monitored for extreme over-voltage or under-voltage while the current is monitored for over-current conditions such as short-circuits. Additional pack temperature monitoring may be included if external temperature influences on the pack are anticipated by the application.

Monitoring of the pack-level characteristics can use all of the previously discussed devices, such as thermal fuses, PTCs, thermistors, *etc.* It often also utilizes simple electronic circuits, all with the goal of keeping the battery in a safe operating range and preventing destructive abusive conditions. For example, when using primary cells, a diode may be inserted in series with the battery's current path in order to prevent the cells from being charged. While often considered a protection or safety device, a diode is simply a type of current and voltage monitor – it only allows current to pass if the voltage across the diode is correct.

Although some cell monitoring devices may be duplicated at the battery module/pack level, the set points may be configured differently so as to provide a tighter operational range and redundancy.

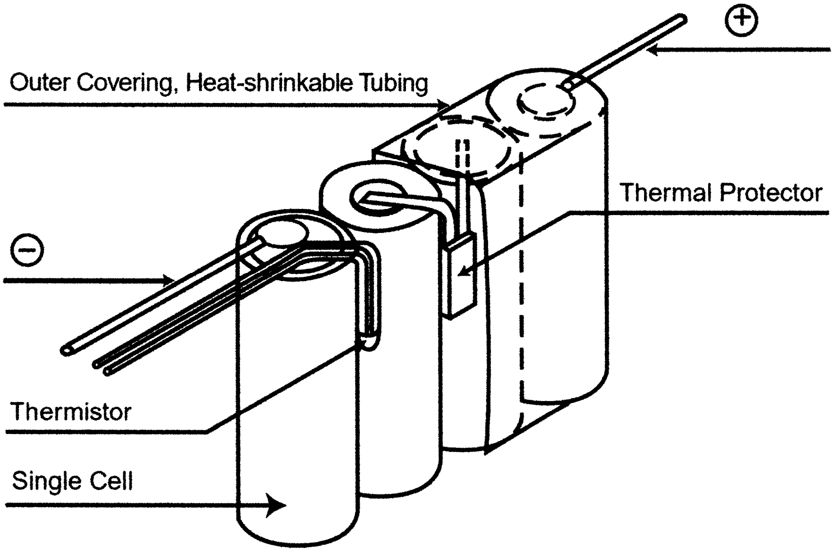

Figure 13.4. Example of external battery monitoring and management devices: Thermistor & Thermal Protector. (*Courtesy Panasonic Battery, Ref.* [3])

13.2.4. Battery Measurement

As with cell measurements, battery measurements of voltage, temperature, and current can be used to maintain the desired operational limits of the battery. Electronic circuits with various levels of accuracy and complexity can be used to make these measurements while minimizing the power drain on the battery itself.

In addition, the battery measurements can also be expanded and combined with cell measurements to provide additional information on both the battery and the cells. For example, cell voltage measurements can be synchronized with battery current measurements in order to obtain an equivalent resistance (impedance) measurement for each individual cell. This information is useful in determining battery wear and aging effects.

Battery level measurements can also be interpreted using additional information not available with cell measurements. Open-circuit voltage (OCV) can be obtained if the current measurement is monitored – although the time after the current has stopped is useful to know as well. (Alternatively, the OCV can be repeatedly measured to determine the rate of change and thus the approximate time since the load or charge current was removed.)

Similarly, the initial step-function of the voltage when a charge or discharge current is first applied can be measured if the battery current is also being measured. This specific information can often give unique insights into the performance of the battery. As with cell measurements, it is possible to perform the battery level measurements inside or outside the battery, such as by electronics located in the host device.

13.3. Battery Management Functions

Whereas monitoring of cells and the battery is designed to keep the system within a safe operating area, *battery management* uses the cell and battery measurements to fully utilize the energy delivered to the battery-powered host device.

Maximizing the delivered energy to the host device may also include managing multiple aspects of the battery system, such as:

- The discharge of a primary or secondary battery.
- The charging of a secondary battery.
- The temperature of the battery, during both discharge and charge (if rechargeable).

A *battery management system* (BMS) can be as simple or as complex as the battery chemistry and host device require. In the case of a few primary cells inserted into a small device, the management may consist of simply monitoring a voltage to detect when the cells are completely discharged and empty.

In the case of a battery pack in a hybrid electric vehicle (HEV) the control and management system may be significantly more complex, requiring sophisticated functions such as SOC and SOH estimates.

The architecture of the BMS is also battery and device specific. For small devices, sensing battery parameters outside the battery or inside the device may be preferred. The characteristics of the cells and battery can be monitored or measured by the host device. This is often the case when small primary cells are used [8].

As the battery or device gets larger, or the cell chemistry more complex, more of the monitoring and measuring functions may be directly connected with the cells and reside inside the battery. (Cell monitors may still exist inside the cells.)

Hybrid architecture is often used. Some monitoring and measurement functions reside inside the battery and some reside inside the host device. Complexity and cost are factors in such architectural decisions [9].

For example, a Li-ion battery pack may contain safety-related monitoring functions within the battery pack itself while measurement functions are performed externally for such features as SOC estimate or charge control. Alternatively, some fully self-contained batteries may place all the battery management functions internal to the pack, including charge controls.

The smart batteries found in most laptop computers use such a hybrid approach where measurement occurs inside the battery pack but a data communication channel is used to transfer the measured and calculated information to the host device and the charger.

In each case, the requirements of the host device, from a portable music player to an automotive vehicle, dictate the function, size, and complexity of the BMS. But in all cases, some basic aspects must be considered, each with an eye toward the specific requirements of the battery cell chemistry and the device's requirements.

13.3.1. Charge Management

In all secondary systems, charge management is most critical to the safe and reliable operation of the battery. Even in systems with only primary cells, prevention of charge is still a design concern. (This is an added issue when interchangeability between primary and secondary cells or battery packs is required by the device).

Charge management ranges from prevention of charge, as in a primary system; to enabling or disabling charge; to actually controlling and regulating the charging voltage and current. This is often battery and device specific – some require the ability to signal when to charge or not, others require actual control of the charge, while still others must create the exact charging voltage and current waveforms needed.

Charge management also encompasses correctly charging the battery to full capacity without overcharge or other stress on the battery cells, such as excessive heat during the charging process.

Charge management can be accomplished externally to the battery pack or completely internally, depending on the architecture desired. Often it resides outside the battery pack due to the added heat that may be generated by power conversion and regulating devices that are necessary for charging.

The phrase "charge control" is often used to indicate where the actual device resides that can enable or disable the current flowing into the battery during the charging process. This is typically the battery charger which converts line power or another power source to the voltage and current needed to charge the battery. The charger can get information from the battery that it can use to determine when and how to charge the battery but the charger itself usually contains the power control devices which can enable or disable the charge current.

In some systems, the charger is also the system power supply – the battery being charged is simply connected in parallel with the system load. This is typical of power backup systems: When the system power fails, the battery is already connected to the load. When the system power returns, there is spare power available to charge the battery while simultaneously powering the load. This type of system, common with standby backup lead-acid batteries (Pb-acid), may not have any charge control device to disable current flowing into the battery. Instead, the charge voltage is lowered such that current does not flow into the battery cells. (In a fault condition, where a battery would still pull current, the battery must be manually taken out of the system.) In such a system, the 'charger' is actually the DC rectifier which is generating the power required for the system load, as well as for charging.

The following sections illustrate specific monitoring and measurement aspects of charge management. A typical battery management system will often include multiple techniques in order to provide a robust, safe, and redundant charge management function.

13.3.1.1. Charge Management with Temperature

The temperature of the battery's cells can be used as a charge management technique, depending on the chemistry of the cells and the host device's requirements.

Regardless of specific chemistry requirements, charging is not initiated if the battery is too hot or too cold. Charging may also be stopped when the battery temperature moves out of a preset temperature range. The charge rate may be reduced due to temperature as well, not just completely stopped.

Enabling or disabling charge can be accomplished by an internal temperature sensing device, such as a NTC thermistor. A simple electronic circuit can monitor the resistance of the NTC thermistor to determine the relative temperature of the battery pack and enable or disable charging appropriately.

For more precise temperature control of charging, the NTC thermistor's resistance can be measured and used to detect the rate of change of the battery temperature. This information can be used to determine when the battery is nearly fully charged in Ni-Cd and Ni-MH chemistry systems. A temperature rate of change, dT/dt, of 1 to 2°C when the charging current is constant and above 0.5C indicates a 95% full condition. This is the dT/dt "end-of-charge" (EOC) condition used for fast charging of Ni-Cd and Ni-MH chemistries [3,7].

Similarly, in Pb-acid systems, temperature is used to adjust the charge voltage. In other chemical systems, a maximum temperature change can also be used to indicate a fully charged battery.

Temperature can also be used as part of the SOC calculations for some chemistry due to their charge acceptance characteristics which may vary with the temperature. (Nickel-based rechargeable chemistries exhibit a decreasing charge acceptance with increasing temperature). This relationship can be modeled and used to track the SOC of the battery during the charging cycle [10].

In all cases, the complexity of the temperature sensing can be matched to the requirements of the battery and device.

13.3.1.2. Charge Management with Voltage

The battery voltage is often used as a charge management technique, again depending on the cell chemistry. Simple monitoring of the voltage of the battery cells in total or individually can be used to start or stop charging when preset limits are reached: in some chemical systems, batteries with too low a voltage may have an internal cell short or other failure mechanism and should not be charged. Similarly, when the battery or cell voltages reach high levels, charging should also be interrupted.

For example, in Li-ion battery, electronic safety monitoring circuits are used to monitor the individual cell voltages and prevent both charge and discharge if any one cell voltage is too low or too high. The circuit typically consists of a set of voltage comparators with their outputs driving a current interrupting device (CID) such as a power transistor or relay [2].

Measured battery voltage is also used for charge management in some chemical systems, such as Ni-Cd and Ni-MH, to determine a fully charged state based on a change in the battery voltage. By tracking the rate of change of the battery voltage, a negative slope can be detected which indicates a full condition. (A "$-\Delta V$," negative delta-voltage, of 5 to 15 mV per cell is often used as an indication of full charge when a constant charging current greater than 0.5C is used. [3])

Both Li-ion battery and Pb-acid systems use the battery voltage as the charge management means by charging with a constant current to a fixed voltage level, which may vary with temperature. When this voltage level is reached, the charger will maintain this battery voltage indefinitely, as in a backup Pb-acid system; or for a set time; or until the current being accepted by the battery drops to a set limit. Other cell chemistries also use a fixed voltage charge management method.

Some voltage charge management techniques, such as pulse charging, rely on voltage measurements and time intervals to charge the battery. These methods may also include brief discharge periods. Often these techniques claim faster charge times but may also impact cycle life or long-term performance. Voltage measurements used in these techniques require very fast measurement sampling rates and high accuracy – both of which come with additional cost and complexity.

Charge management of the battery pack may also consider the individual cells in the battery pack. In addition to the cell safety requirements, the issue of cell voltage imbalance should also be addressed. Cell imbalance is often the result of temperature differences within the battery or device, which cause individual cells to self-discharge at different rates. Some cell chemistries can be re-equalized or balanced by overcharging the battery, so that all the cells reach a full state. However, most Li-ion rechargeable chemistries do not permit overcharging, even at low rates, so other methods must be employed [11].

As with previous considerations of measurement means, the complexity, accuracy, and associated cost of the voltage measurement can vary with the requirements of the battery and the device. In the example for Ni-Cd or Ni-MH full charge detection, the ability to detect 5 to 15 mV of voltage change over time would require a more sophisticated electronic measurement technique.

13.3.1.3. Charge Management with Other Means

Other charge management techniques include timers, often used for low-rate charging of specific chemistries. Some nickel and Pb-acid batteries are charged at low rates for set times on the order of 15 or more hours. Often this trickle charge is stopped only after a preset time duration which insures that even a completely empty battery would be fully charged in this time period. These chemistries, however, are not damaged by overcharge at this low rate and thus can tolerate the additional charge if the cells were already partially full. The added benefit of this charge management technique is that it can re-balance the cells which may have become unbalanced over time due to usage or temperature differences.

More specific duration electronic timers are also used for safety backups or to prevent false triggers by other measurements. Such timers can prevent excessive charging when one of the previously mentioned full charge conditions does not occur. For example, in Ni-MH systems, the temperature inflection point, dT/dt, may never occur due to external thermal influences or a failed cell. A charge timer that interrupts the charging current and voltage after a predetermined time, typically directly proportional to the C-rate of the charge current, would prevent excessive charging if the dT/dt signal is never detected.

Timers also assist in preventing false or early detection of EOC conditions. The same dT/dt temperature inflection point could falsely occur early in the charge process due to an initially low battery temperature. By delaying the detection of the dT/dt condition until 10 minutes after the start of charge, this potential early false positive condition can be avoided [3].

Tracking relative time requires an electronic circuit and a reasonably reliable time base, usually created from an oscillator. Since the times involved are relatively long – 10 minutes to a few hours – a digital counter is used to count the oscillations from the time base and create an output to drive the appropriate circuit.

In some cases the timer can be provided by the host device to the charger for use in these charge managements. The host device may have an available timebase and digital counter already available that can be utilized.

In more recent development, some Ni-MH systems began to adopt a sensitive pressure monitoring and termination scheme for charging control and management. Building up internal cell pressure is often a signal of reaching the EOC condition, where oxygen recombinant cycle begins to play a dominant role, generating heat and temperature rise, and reducing charging efficiency. Terminating charging of the cell at this point is quite beneficial not only to prevent overcharging, but also to avoid any significant temperature fluctuation, or even thermal run-away. Yang and Liaw [12] demonstrated this principle in Ni-MH rapid charging. Rayovac's IC^3 technology [13] takes such an approach to consumer Ni-MH batteries with its 15-min charger.

The battery's SOC is sometimes used for charge management so that techniques for detecting EOC can be applied appropriately. Similarly to the use of timers, SOC can indicate when a battery is expected to be full and that dT/dt or $-\Delta V$ EOC signals should soon be detected. This is desirable in chemistries which can be damaged by repeated overcharge or re-charging attempts. For example, attempting to detect a –ΔV or dT/dt EOC signal on an already full battery can push the battery into overcharge, which may have an adverse effect on capacity and cycle life [10].

Using SOC for charge management is also particularly useful in battery applications where full charge is not desired, such as in an HEV. A typical HEV battery must always be able to supply power as well as accept power, such as from regenerative braking. For this reason, the HEV battery is usually maintained at a SOC level between 40 and 80%. In most chemical systems, there is no specific charge management technique that can detect an 80% full condition, so accurately tracking SOC is essential.

Note that SOC calculation involves more than tracking the charge current and EOC conditions related specifically to charge management. Although charge efficiency or charge acceptance of the cell chemistry must be modeled and considered for the charge portion of SOC calculations, other factors are also involved, such as self-discharge, discharge rate efficiency, end-of-discharge (EOD) detection, and temperature impacts [2,3,9,10].

13.3.2. Discharge Management

The primary purpose of discharge management is the optimized use of the energy in the battery by its effective utilization on discharge.

This may include preventing discharge under some conditions; enabling or disabling discharge, or actually controlling and regulating the discharge output voltage and current. This is often battery and device specific – some require a signal when discharge is permitted, while others may require actual control of the discharge.

Even in primary battery systems, the ability to discharge the energy from the cells in the most effective manner, perhaps with intermediate conversion electronics, is the goal. Primary cell battery packs meant to be interchangeable with rechargeable battery packs may include additional electronics to translate the output voltage of the primary cells to better match the voltage of a particular rechargeable chemistry. Thus, the host device can utilize the energy from the primary battery pack as if it were a rechargeable battery pack, at least for discharge [14].

Discharge management includes properly limiting the discharge to safe levels, such as avoiding short-circuit discharges, as well as terminating the discharge when the battery cells are empty.

In simple systems, discharge management may only consist of a fuse to prevent the discharge current from exceeding a dangerous threshold such as during a short circuit. The cell chemistry or host device may not require any further level of discharge management since the device will simply stop functioning and cease draining the battery at some low voltage.

However, not all host devices will stop draining the battery even after the device has stopped functioning due to a low battery voltage. Some devices can have measurable current draw even in their off state. A few mA of current can still damage battery cells if left unchecked.

Some chemical systems require the interruption of current in order to prevent the discharge from continuing beyond a preset threshold and potentially damaging the cells. This may be based on some monitored or measured cell or battery characteristic such as voltage or temperature.

For example, when the battery output is applied to a constant power DC converter, such as those found in laptop computers, the DC converter could rapidly deplete the battery and possibly cause a cell voltage reversal within the battery. This is due to the constant power load that the DC converter creates – as the battery voltage drops, the current draw must increase in order to maintain constant total power (current times voltage). For high power discharges, the current load at the low end of the battery's voltage curve can drive the voltage much lower than the recommended value set by the manufacturer.

The phrase "discharge control" is used to indicate where the actual device resides that can enable or disable the current flowing out of the battery during discharge. This is typically the DC converter inside the host device which translates the battery's output voltage to lower voltages which are used within the host device when it is operating.

In more advanced discharge management systems, such as smart batteries, the host device can get information from the battery that it can use to determine how best to discharge the battery for maximum efficiency via the DC converter sub-system.

As with charge management, discharge management techniques can be employed internally or externally to the battery pack.

13.3.2.1. Discharge Management with Voltage

Most simplistic discharge management techniques are voltage based, since this is the easiest battery characteristic to use to determine when the battery is fully discharged. A simple electronic circuit to monitor the battery voltage and disable discharge below a preset voltage threshold is easy and inexpensive to construct.

However, many cell chemistries have flat voltage *vs.* capacity discharge profiles, making the prediction of when discharge should cease difficult, if not impossible. Primary lithium chemistries have such non-sloping discharge curves while some secondary Li-ion rechargeable chemistries have a somewhat sloping discharge curve, depending on the specific formulation. These flat voltage *vs.* capacity curves have a sharp "knee" at which point the voltage drops rapidly and the remaining useable capacity is negligible.

To improve voltage-only based discharge management, particularly in cell chemistries with a sloping voltage discharge profile, a mid-point voltage can be monitored or measured to determine a capacity point on the discharge curve prior to the fully discharged state. This can improve the performance of the remaining capacity estimation somewhat.

Discharge management with voltage should also consider the host device's discharge profile, if Ni-Cd and Ni-MH cell chemistries are employed. These chemistries can exhibit a voltage anomaly called "memory effect" if repeatedly discharged to the same voltage. This memory effect causes a voltage depression to form which can appear like the knee found at the end of the voltage curve, thus falsely indicating a fully discharged state.

The host device's discharge profile can contribute to this effect if the device continually discharges to the same point on a voltage discharge curve. This may happen if the host device uses an early end-of-discharge voltage (EODV), perhaps with the idea of reserving capacity in the battery for later use by the device at a lower discharge rate.

For example, the host device may go into a suspend or sleep state when the battery voltage reaches an equivalent to 1.05 V/cell instead of the typical 1.0 V/cell or 0.9 V/cell EODV suggested by most manufacturers. The theory in this case being that the capacity between 1.05 and 1.0 V/cell will still be available to the host device after entering a lower power operational state, and thus a lower drain on the battery. However, repeated discharges to the same voltage point may cause the formation of the memory effect knee which prevents access to the additional capacity that the host device was expecting. The capacity is still available, but it can only be obtained by discharging to a lower voltage, which may be lower than the host device's DC input section can accommodate or was designed to accommodate.

The end user of the host device can also contribute to the condition by repeatedly using the device in a similar manner each time, thus discharging the battery to the same voltage point each use.

The common remedy to the Ni-Cd and Ni-MH memory effect is to discharge the battery completely prior to charging. This is often accomplished in a charger which has the appropriate circuitry to fully discharge the battery before commencing the charging process. Recent improvements in Ni-Cd and Ni-MH cell chemistries have reduced the occurrence of memory effect.

Some battery systems, including Li-ion and lead-acid, use a lower voltage cut-off or low voltage disconnect to prevent damage to the cells which can lead to capacity loss. Such a disconnect control allows the battery to interrupt the discharge current via a power transistor or relay.

In Li-ion systems, this control is based on any one cell voltage dropping below a preset threshold, usually well below the recommended EODV for the cells. Note that it is possible that the full battery voltage of all the series cells is still greater than the typical EODV of the host device. This conflicting condition occurs due to the wide voltage range of Li-ion cells, 4.2 V to 3.0 V, but is most likely to be caused by cell-to-cell imbalance [11].

Other chemical systems can also be damaged by discharge when one cell is discharged below the recommended EODV or even below zero volts. This can occur in larger series cell strings when the cells are not individually monitored, such as Ni-Cd or Ni-MH, and there are too many series cells in the battery. Since Ni-Cd or Ni-MH have nominal cell voltages of only 1.2 V each, in battery packs containing more than 12 series cells, it becomes increasing difficult to detect the drop-out of one cell by monitoring only the battery pack voltage.

For example, in power tool devices with as many as 15 series Ni-Cd cells, the discharge would range from the 1.2 V/cell nominal voltage to 1.0 V/cell EOD. This equates to an 18 V to 15 V discharge profile. However, an imbalanced, faulty, or damaged cell could rapidly drop to 0 V and the remaining cells would mask this condition from the total battery voltage, which would still be above the 15 V lower limit that would normally terminate the discharge. The 0.0 V cell would be driven into reversal and potentially damaged further.

Although simple and easy to implement, voltage-only discharge management has drawbacks for most high performance battery management systems when temperatures and discharge rates vary.

13.3.2.2. Discharge Management with Temperature & Current

The primary temperature and current discharge management techniques are utilized to prevent abusive discharge conditions that may result from high currents or high temperatures.

Short-circuit overloads are commonly prevented by PTC CID similar to those found in some cell constructions. Fast acting electronic circuits can also continuously monitor the discharge current and activate a power transistor or relay to interrupt the discharge path if a high current is detected. Such circuits are common in Li-ion battery packs. Power fuses of various types that react to high current conditions are also available [4,5].

Thermal fuses and other devices may also be utilized to prevent discharge above preset temperature limits that may damage the battery cells. Electronic circuits can monitor temperature and activate a power transistor or relay to interrupt the discharge current to prevent further temperature increases. Although less commonly used for discharge management, these temperature techniques may be employed due to the requirements of the cell chemistries or the host device.

The battery temperature and discharge current may be used for discharge management directly in some cases.

When a host device requires constant power from the battery, the resulting increase in current as the battery voltage declines can be used as a method to detect the fully discharged condition of the battery. This assumes that measuring the current accurately enough to detect the resulting increase near the EOD is cost effective for the host device. In addition, the host device's power load on the battery must be characterized and consistent.

Similarly, the increase in current from the battery will also cause an increase in battery temperature, although this increase will be delayed due to the thermal response time of the cells. The increase in temperature, due to the increase in current with constant power loads can also be used as an indication that the battery is nearing full discharge.

Temperature and discharge current can also be used to augment previously mentioned voltage-based discharge management.

In most chemical battery systems, the ideal voltage to terminate the discharge can vary with temperature and the magnitude of the discharge current. Higher discharge currents are less likely to fully utilize the available energy in a battery, whereas lower discharge rates can more efficiently drain the battery completely. Most devices, however, have a wide range of discharge currents due to their operational requirements. Additionally, temperatures of operation can also vary with a similarly wide effect on the ability of the cell chemistry to deliver its full capacity.

Thus, a more advanced discharge management technique should attempt to change the desired EODV, or the effective empty point of the battery, based on the measured temperature and the measured discharge current.

Some chemistry's discharge efficiencies are well modeled and understood for both temperature and discharge rate dependencies and thus the DC converter's input section on the host device can be adjusted to appropriately utilize the battery down to the most optimal voltage based on the measured temperature and discharge rate. As the battery ages these models must accurately track the changes in the efficiencies and the associated voltage response due to age, most of which is altered by a change in the cell's impedance.

Adjusting the host device's power input stage to accept a wider range of input voltages adds cost and complexity to the host device. Additionally, the efficiency of the power converter in the host device will be altered due to the larger input voltage range. An alternative approach is to utilize a fixed EODV, but indicate the capacity or power that can be delivered based on measured and calculated values.

13.3.2.3. Discharge Management with State-of-Charge

A more robust discharge management technique utilizes a representation of the battery's SOC calculated using measured characteristics such as voltage, temperature, current, time, and perhaps impedance or others parameters. Depending on the cell chemistry and the requirements of the host device, the determination of SOC can vary widely in complexity. Approximate values may be obtained using one or two measured characteristics of the battery while sophisticated systems may utilize five or more measured or calculated characteristics.

SOC in absolute terms is defined as the capacity available for discharge represented as a percent of the original rated capacity of the battery. In some cases, a relative SOC is calculated as a percent of the last full charge capacity, thus it does not represent any aging of the battery.

As with temperature and current discharge management, SOC can be used to help predict when a voltage threshold will be reached so as to limit the chance of discharge below the recommended minimum voltage of the battery cells.

SOC often uses temperature and discharge current compensation not to adjust the EODV, but to compensate the resulting SOC value when an appropriate voltage is actually reached.

By compensating the SOC value, instead of adjusting the voltage, this method can represent the capacity that still remains in the battery, but which may be drained out only at a lower discharge rate or a different temperature. Thus at high discharge rates, the battery may reach an EODV but still have some capacity available if the discharge rate is reduced.

In contrast, the previously mentioned voltage technique that alters the EODV based on current and temperature will discharge all the capacity that is available at the present temperature and discharge current. This may be acceptable for fixed discharge currents, but is less useful for varying discharge loads.

SOC techniques such as this will often represent the remaining capacity in percent as well as in other units in order to simplify the host device's use of the information. Remaining capacity in mAh or mWh may be used, but normalized to a C/5 or other standardized discharge rates. This allows the host device to be able to correctly interpret and utilize the SOC information.

Such information provides enhanced power management features to the host device by giving it the information on the battery's ability to deliver energy and/or power. This is particularly useful for host devices that need to manage a limited battery capacity with widely varying discharge loads, such as in a laptop computer.

Laptop computers may have peak discharge currents of 5 A or more while also having the potential to discharge at rates less than 10 mA for long periods of time, such as when in a suspend state. Similarly, the requirements of the laptop computer's processor may change the discharge current between these extremes very rapidly. In addition, as more peripheral components are added to the laptop computer, such as DVD drives, wireless connectivity, and widescreen displays, the power consumption demands on the battery can increase significantly.

Enhanced SOC information from the battery allows the laptop computer's power management system to better utilize the available energy from the battery. The laptop computer's internal systems can limit power consumption by decreasing screen brightness, reducing the processor's clock speed, turning off the hard disk drive, and similar methods. These techniques can be employed more aggressively as the battery's SOC decreases, thus optimizing the useful discharge energy from the battery.

In some devices, discharge management must utilize other methods according to the requirements of host device, a good example being an HEV.

A typical HEV does not require significant capacity, but instead the power of the battery is utilized in short bursts for acceleration or low-speed operation. Therefore, the most useful information is State-of-Power (SOP) or power capability which represents the ability of the battery to deliver discharge power or accept charge power, such as from regenerative braking.

In this case, the battery's ability to deliver power is the more important aspect of discharge management. Such SOP information is calculated much like SOC for enhancing the operation of the HEV's utilization of the battery. Although similar, the SOP calculation is often more complex than SOC and requires accurate cell models, multiple measurements, and significant understanding of the requirements of the device.

SOC and SOP are predictive calculations that require accurate measurements of the battery and cell characteristics, as well as significant processing power to continually update the calculations. The measurements must be of high resolution and made frequently enough to provide useful information. Additionally, the cells used in the battery must be well characterized over a large operating range of expected temperatures and rates of charge and discharge. This characterization includes parameters such as charge acceptance, discharge efficiency, and self-discharge correlated with time, temperature, and perhaps SOC as well.

Finally, information on how these characteristics change over time and with the age or abuse of the battery must also be understood and coded for use by the processor performing these predictive calculations.

Cell chemistry also impacts the calculation of SOC for a particular battery. For example, SOC for Pb-acid can often be obtained by measuring the specific gravity of the electrolyte via an electronic sensor in the battery cells.

Variants of SOC information can be found in modern laptop computer systems which utilize the Smart Battery Systems (SBS) set of standards for battery management. Such SBS implementations often utilize information similar to SOC which can better assist the utilization of the battery's available capacity. Examples include the ability to interrogate the battery to determine the ability to deliver capacity at higher or lower discharge currents than what the battery is presently supplying. (See Sub-section 13.3.4 for a more complete discussion.)

13.3.3. Safety Management

The safe operation of the battery and the host device is a requirement in any BMS. Some cell chemistries are more volatile that others while some host devices and operating environments are harsher on the battery cells.

Electrolyte leaking, venting, cell swelling, and thermal run-away are just some of the cell failure mechanisms that can occur when abusive conditions are not constrained.

Proper battery pack construction is a requirement for safe operation in the event of a failure. Battery packs should be built with non-flammable materials, use careful layout to avoid inadvertent cell shorting, include protection against leaking electrolyte (such as coating components that could be short circuited by electrolyte) and adhere to manufacturer's recommendations.

As previously listed in both charge and discharge management, devices are often included in cells and battery packs in an attempt to limit abusive conditions. These may include current, voltage, temperature, and pressure monitoring or measuring of the battery cells independently or in small groups. Flame arresting vents, pressure sensitive seals, thermally responsive separators and similar features may be added to cells or batteries to increase their operational safety regardless of the charge or discharge management of the battery.

Additionally, modern electronic circuits are employed to monitor the battery cells, battery pack characteristics, and other electronic circuits within a battery pack.

For example, when CID such as power transistors or relays are used in a battery system, electronic monitors are often placed on these devices to insure fail-safe operation. It is possible for a power transistor to overheat and fail in a closed, current conducting state. Thus, a thermal power fuse is often mounted close to the power transistors such that if these devices overheat the thermal fuse will open and prevent further current flow. Similarly, electronic devices controlling power transistors or relays can monitor the result when the transistor or relay has been activated. If current continues to flow even after the transistor or relay should have interrupted current, then a secondary safety fuse is activated to permanently stop current flow.

Some chemical systems can also be damaged by abusive discharge such that one cell is discharged below zero volts and into reversal. This can occur in larger series cell strings when the cells are not individually monitored. Similarly, over voltage or over charge can cause excessive heating and induce thermal runaway, venting, or perhaps explosions in some chemical systems.

In all cases, it is the responsibility of the BMS designer to also consider the safety limitations of the battery and host device environment beyond the normal operational limits [15].

13.3.4. "Smart Battery System" – A Specific Battery Management Example

An example of a common battery management system can be found in today's laptop computers. The Smart Battery System (SBS) is a group of specifications for batteries, chargers, and host devices that was originally developed by Duracell Inc. and Intel Corp. in 1995 for use with rechargeable batteries in laptop computers. This system is an example of a complex but complete battery management system which utilizes many of the features previously discussed.

Although safety is a factor in the SBS standards, the specifications were written to be chemistry independent, thus the specific safety requirements of each cell chemistry are left up to the system designer to consider, although most laptop battery systems use Li-ion cells.

The SBS specifications detail the measured, calculated, and communicated information that is passed between a smart battery, a smart charger, and a smart system host device. These components communicate to allow charge management (battery and charger) and discharge management (battery and system host) [16-18].

Although a specific architecture is not explicitly required, a typical laptop system employs a smart battery which contains all of the appropriate electronics needed to measure the cell and battery characteristics necessary to calculate over 30 data values similar to SOC. These data values are communicated via a standardized communication interface – the System Management Bus (SMBus) – which is based on the two-wire Philips Corporation's inter-integrated circuit (I^2C) bus. This data path allows the three components (or more if additional smart batteries are used) to communicate together to optimize the battery management for the benefit of the host device [19].

Some SBS implementations are architected such that the measurement electronics may not be internal to the battery. No restriction on the architecture is implied as long as the appropriate information can be obtained via a data path to the system host device. Similarly, the smart charger may share functions with the system host device's power control electronics and not be a completely separate device [8,20].

The SBS system includes charge management by communication between the smart battery and the smart charger. The smart battery indicates via the data interface both how and when it should be charged by sending specific charging voltage and charging current requests to the smart charger. The smart charger obliges by providing the requested voltage and current. The smart battery must continually request the desired charge voltage and current appropriate to the best method to be charged based on the present conditions of the battery, which it is continually measuring during the charge process.

The smart charger provides the requested current and voltage within the limits of its design but also contains timers and failsafe mechanisms to prevent abusive conditions. (The smart charger must receive updated information from the smart battery every two minutes or otherwise stop charging.)

The smart battery itself determines when charging is complete and similarly signals the smart charger to stop charging. If the charging is stopped before the battery is full, perhaps due to an internally high temperature measurement, the smart battery can similarly halt charging via the data interface to the smart charger. When conditions permit charging to resume, the smart battery again requests an appropriate charging current and charging voltage from the smart charger.

Discharge management follows in a similar manner using the communication between the smart battery and the system host device, usually a processor in the laptop computer, typically the keyboard controller or embedded controller. The smart battery provides historical, static, and dynamic data that can be utilized by the system host device for discharge management. This information includes both relative and absolute SOC data, last full charge capacity data, cycle count data, and calculated run time to empty and run time to full values. In addition, the smart battery provides continuously updated measurement data for voltage, current, and temperature.

Of particular use in discharge management with the SBS system is the capability of the system host device in the laptop to query the smart battery as to its ability to deliver energy at discharge currents above or below the present rate. This feature is useful to the laptop computer's power management policy since it can be used to indicate to the end user how much additional run time is available if the laptop's processor changes to a slower clock speed. Similarly, the laptop could query the smart battery to determine if enough capacity is available to run the hard disk drive for a save-to-disk shutdown function or if a low-power suspend state should be utilized instead.

BMS with similar requirements can be constructed using the properties of the SBS system but with other communication interfaces and data values. For example, some HEV BMS uses a more robust communication interface such as CANBus and data which includes SOP information.

13.4. Life Prediction

As we hardly can live without batteries in our life, battery's reliability is of great concern to many users who rely heavily upon them. Portable devices such as cellular phones, music players, PDA's, digital cameras, notebook computers, HEVs, autonomous sensor systems, security and safety systems, *etc.*, all need reliable batteries with long operating life. Premature failure or shortened life in the battery than the expected could be costly, sometimes, if not just inconvenient, in some of these applications. To no surprise, new SOC meters, SOH gauges, and SBS are therefore being developed for the professional and consumer marketplace.

There are many aspects in battery life prediction that are desirable by the users for various specific applications. One of them, for example, is the prediction of immediate performance characteristics of a battery to meet certain criteria for a function. In this case, it is critical for one to predict if a battery can deliver a specific power to achieve an acceleration of an HEV or to wake up a device (*e.g.* camera or cellular phone) to function. This is usually observed in the arena of estimating SOC or SOP, so one can predict the remaining capacity or power capability of the battery for immediate use. Another common objective of life prediction is to estimate the long term life of a battery regarding its EOL criteria, so one can decide if the battery should be replaced to regain a good confidence of reliability for an operation system to perform certain functions. This aspect is commonly known as the calendar and cycle life, or in general, the service life of a battery.

It is important to point out that battery life depends on the criteria for EOL, therefore is dependent on the nature of application. One needs to have a thorough understanding of aging mechanisms when discussing life prediction, where considerable differences among cell designs and operating conditions in applications could lead to very different results. First of all, life prediction is used for making technical or commercial decisions, and thus has to be based on clear criteria which determine the EOL of a battery in a given application. Secondly, life prediction has to combine all aging mechanisms that are likely to occur in any given application, preferably into one figure of merit, regardless of the severity of the individual aging mechanisms. For instance, postmortem analyses of lead-acid batteries may have shown very severe corrosion with some parts of the grid while the battery itself may still be able to deliver adequate capacity.

Life prediction is a projection of possibility or probability, best in a single figure of merit, which describes whether a particular function, *e.g.* starting a motor or operation of a safety system for a certain duration is possible or not at the desired moment. In addition to the effects of all aging mechanisms, life prediction has to take into account all stress factors at the point of making the prediction and take the specific design features of a battery into consideration.

The real challenge of life prediction, therefore, is predicting the life of a battery under operating conditions for which there are no life tests with a similar combination of stress factors. Two often-asked questions are:

- How long will this battery last under these operating conditions and how will the life change if the operating conditions were changed?
- How long will a new design of battery or a battery with new material compositions last in a well known type of operation?

More than often, before all life tests have been carried out, an answer is needed for battery design, planning, and selection for a specific application.

When discussing life prediction, we also should be mindful that, at least, two different categories of performance prediction of battery have to be distinguished. The first type is a "performance prediction" or a prediction on immediate battery performance characteristics (discharge/charge curves, power capability, capacity, *etc.*) under a specific set of operating conditions. The second type is a "life prediction" or a prediction on the average, long-term prospect in performance of a battery, particularly focused on the EOL criteria, which is of primary interest for planning purpose or cost analysis in selecting a battery chemistry and design.

For practical battery life prediction, particularly the goal is a realistic prediction of battery life in real-life situations; in general, we can perceive that at least four stages of development in modeling and simulation need to be realized:

1. Stage one is to deduce a precise performance prediction model for the cell chemistry. The model needs to be scaled to a module level to have useful practicality.
2. In Stage two, one needs to derive a life prediction model based on laboratory evaluations. The degradation processes and mechanism need to be identified and incorporated into the model to allow prediction of battery performance with a degradation rate estimated from the (predominant) aging mechanism.
3. In Stage three, one needs to accomplish a few steps in real-life evaluation to learn:
   a. how to collect battery performance data in real-life situations;

b. how to analyze the data to derive useful information for model prediction; most importantly to derive reliable methodology to decipher aging mechanism and the associated aging rate;

c. how to incorporate the above information into the model for real-life prediction.

4. In Stage four, one needs to develop validation protocols to certify the model prediction capability and to permit deduction of data for training adaptive models to allow battery life prediction according to the use and operating conditions.

With these four steps implemented, we can then expect a more reliable battery life prediction for practical applications. The following sections will follow this pathway of model evolution to describe and assess the maturity of each stage of development.

13.4.1. Performance Prediction: Stage One Developments

Performance prediction of a battery is now accomplished often by computer modeling and simulation either analytically or numerically; and, most of the time, using the combination of both analytical and numerical techniques to achieve the goal. A typical result is to model the charge and discharge curves to predict the capacity of the battery for a certain duty cycle. This type of prediction is useful, for instance, for battery design or for optimization to achieve safe operation of the battery.

With today's powerful computation capability, growing at a rapid pace in hardware or software developments, one can expect that the modeling and simulation capabilities will emerge from various aspects, from "first-principle" materials property prediction, processing, to device design. In the near future, we almost can anticipate that various macroscopic and microscopic modeling and simulation approaches will be integrated into a powerful set of tools for system design and processing. Thus, from first principles, and from molecular scales, to macroscopic dimensions, materials' property can be predicted in conjunction with devices' performance characteristics to give us very insightful understanding and control of how things work.

At least, there are four major approaches that are being taken to predict battery performance:

- Empirical methods,
- First-principle-based electrochemical models,
- Equivalent circuit techniques,
- Artificial intelligence-based techniques.

Each of them can also incorporate stochastic techniques to yield predictions with statistically meaningful analyses.

The ultimate goal of any modeling and simulation is to achieve a reliable prediction of battery performance for a specific application within the constraint of resources, while minimizing the cost, time, and errors. Therefore, it is important to choose the most effective and suitable approach and technique. For simple performance forecasts, interpolation or extrapolation from test results, via empirical data curve fitting, to derive necessary information by "analytical" models, may serve the purpose quite well [*e.g.* 21,22]. For battery design or rapid prototyping, models based on "first principles" would be a good choice [*e.g.* 23-30]. These "first-principle" electrochemical models might be too complicated to use, since they do incorporate many factors including: geometric configuration, kinetic/transport properties, and the thermodynamic properties of the materials and/or cell components to give close-to-reality simulations. On the other hand, these models can simulate battery behavior in response to variations in designs or operating conditions, therefore be of great value to derive insightful detailed performance characteristics and understanding of limiting processes.

Another method of predicting battery behavior with limited empirical data uses so-called "equivalent-circuit" models [*e.g.* 31-34] that emulate battery behavior by mimicking its physical processes and electrochemical reactions by a series of electrical components in a circuitry. This method, which is simpler in model construction and requires less parameterization than those based on the "first-principle" electrochemical models, has the ability to accurately predict the battery in many conditions, suitable for system-focused simulations.

More recently, "artificial intelligence"-based ("inductive") models [*e.g.* 35-38], primarily using neural network techniques, have become promising. These models tend to be more adaptive, due to the nature of their "black-box" approach. This approach disregards the mechanism, which, in turn, disregards any changes in the mechanism, thus making it more adaptive than the former models. These models can be trained to provide explicit battery information from test data, or data collected instantly in the loop during battery operation.

The purposes for making performance predictions can range from design feasibility study, optimization of design for performance, forecasting performance envelope, performance validation, safety limitations in operation, maintenance planning, warranty assessment, to cost analysis, *etc.*

When real-time monitoring and measuring of the battery is coupled with model prediction, one can employ concurrent developments with virtual bench testing, or hardware-in-the-loop concept and techniques to conduct advanced component and system developments. Some of these approaches are currently being considered for more complicated applications such as in HEV powertrain developments.

Earlier work on the battery modeling has been focused on Pb-acid systems [23-30] using "first-principle" electrochemical models. Efforts were

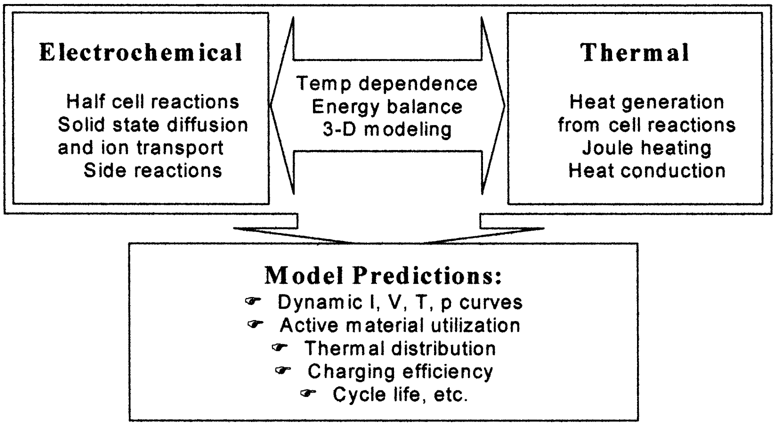

Figure 13.5. A schematic diagram showing a "first-principle" electrochemical model that combines reactions and transport kinetics, coupled with thermal phenomena in an electrochemical cell, to predict battery performance [30].

attempted to create more realistic models to accurately predict battery cell behavior. Figure 13.5 shows a schematic of a "first-principle" electrochemical model [30] that combines electrochemical phenomena (charge transfer reactions and mass transport) and thermal processes (heat generation and dissipation) into a unified framework. This model can produce detailed temporal and spatial information (such as potential, chemical concentration, current density, temperature profile, and internal pressure change) during a battery's operation. This framework can actually be applied to various chemistries as long as the necessary input parameters (cell characteristics and operating conditions) are known.

Figure 13.6 illustrates a simulation of the acid stratification phenomenon in a flooded Pb-acid cell with information derived from a report by Alavyoon *et al* [39]. The y-axis in the figure is the height of the electrode plate in mm. The x-axis is the acid concentration in molarity (M). Even though the experimental data are often difficult to obtain, the detailed temporal and spatial information derived from this "first-principle" electrochemical model is very useful to help us understand the nature of this phenomenon. Once the model is carefully validated, the simulation can be used to evaluate various "what-if" scenarios for different cell designs or various extremes in operating conditions to yield guidance for consistent and safe operation of the battery. Gu *et al* [40] further applied the modeling capability from cell to battery module.

As more advanced Ni-MH and Li-ion battery systems are being considered and employed in electric and hybrid vehicles (EHVs), battery modeling and simulation can be used to predict dynamic performance

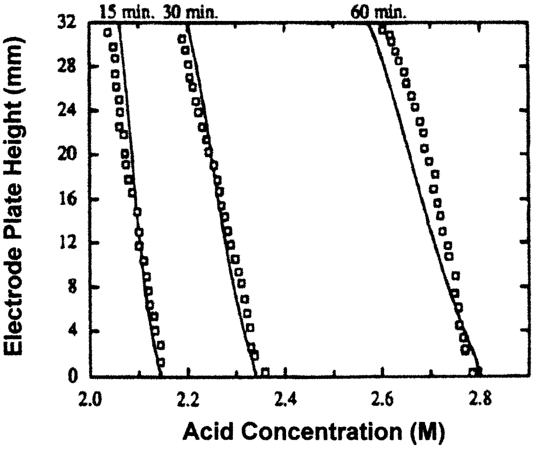

Figure 13.6. Simulation results of a flooded lead-acid cell showing the acid stratification during a recharge. The squared data points are extracted from the report by Alavyoon *et al* [39], while the lines are simulated results based on the parameters derived from the same paper.

characteristics [30]. Figure 13.7 is an example showing the simulation of a nominal 7.2 V, 6.5 Ah Ni-MH battery module going through a discharge, charge, and dynamic stress test (DST) cycle and the comparison with the test data. The battery model can predict behavior not only in the laboratory tests but also in real-world operating conditions. Thus, high fidelity simulation can be feasible and practical.

Although "first-principle" electrochemical models can provide detailed performance prediction, the model construction and validation, as well as the computation requirements, are often complicated and demanding. For other applications that need high fidelity of performance prediction, but can only afford limited resources for computation, techniques using "equivalent-circuit" or "artificial-intelligence" models may become more attractive. For example, Verbrugge and Conell [32] used an equivalent circuit model that incorporated self-discharge and thermal behavior to simulate GM-Ovonic (now Cobasys) Ni-MH battery performance for EHV applications. Liaw *et al* [33,34] have applied similar approaches to other chemistries in Pb-acid and Li-ion battery. Urbina *et al* [37] and Yap *et al* [38] have been trying to use artificial neural network (ANN) to train a stochastic recurrent ANN model and predict battery capacity and power capability for Li-ion battery in hybrid vehicle operation.

These and many other successful demonstrations of battery simulation capabilities indeed illustrate the improvements made in short-term prediction of battery's performance, mainly in capacity and power capability. The long-term prediction of battery's service life remains, nonetheless, still a challenge.

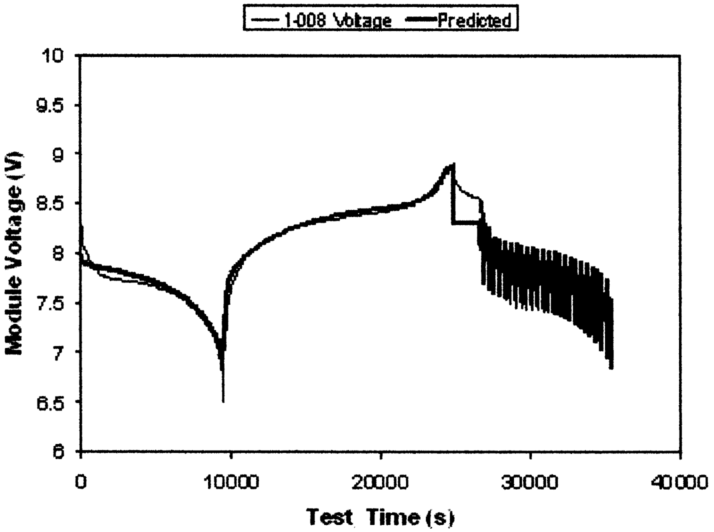

Figure 13.7. Simulation (in the heavier line) of the performance of a nominal 7.2 V, 6.5 Ah Ni-MH battery module going through a discharge, charge and dynamic stress test (DST) cycle, compared with test data (in a thin solid line).

13.4.2. Life Prediction with Laboratory Evaluations: Stage Two Developments

Although these advanced modeling and simulation tools are very useful in predicting battery performance, the most ailing point that prevents their practical use is their inability to predict battery behavior with aging, which changes the battery performance characteristics. Therefore, a successful battery life prediction hinges upon the development of a reliable model that can accommodate these changes in performance characteristics due to aging.

In addition, the sporadic nature of the duty cycles in the EHV and renewable energy system (RES) applications make battery modeling and simulation more challenging. Laboratory testing and empirical predictions can hardly produce satisfactory results. Innovative approaches that utilize integrated laboratory testing and computer modeling and simulation [30] seem to be a more viable solution to address the challenges raised by these unique applications.

The degradation mechanism of a battery often depends on the history of exposure to stress factors such as temperature fluctuations, depth of discharge (DOD), degree of overcharging, discharging and charging rates, and/or self-discharge. It is also very dependent on the operating conditions, including parameters such as operating temperature, and the frequency and amplitude of the stress imposed by the duty cycle.

It is useful to point out that, although the principles for life prediction described herein are general, we will use the case for EHV as an example, because for such an application the demand on the battery management and life prediction is more strenuous than for other applications. It is also useful to note that the discussion will be dependent on the size of the battery, which certainly will lead to some differences in some of the issues in the discussion. We will put our discussions on a broader basis; therefore tend to ignore those effects.

Batteries used in the EHV applications are often called "traction" batteries. The most commonly available are either flooded Pb-acid or sealed (either "maintenance-free" or "valve-regulated") lead-acid (VRLA) battery modules. Ni-MH batteries are now used in hybrids, such as Toyota Prius and Honda Insight and Civic, because of their higher specific energy, improved power capability, and life. Li-ion batteries, and, more recently, lithium polymer batteries, are being seriously considered as an alternative, if the safety, cost, and life issues can be properly addressed. Currently, several large format prismatic Li-ion or Li-polymer cells are being commercialized and under testing and evaluation of their applicability in EHV applications.

To take battery performance model to life prediction model, we need to incorporate degradation processes into battery model to evaluate their impacts on battery performance, such as loss of capacity or power capability. Figure 13.8 is an example based on a "first-principle" electrochemical model that was used to simulate the loss of capacity in a nominal VRLA cell that experienced repetitive gas venting, resulting in dry-out, in a series of hypothetical overcharging deep-cycle testing. In this case, the "first-principle" model

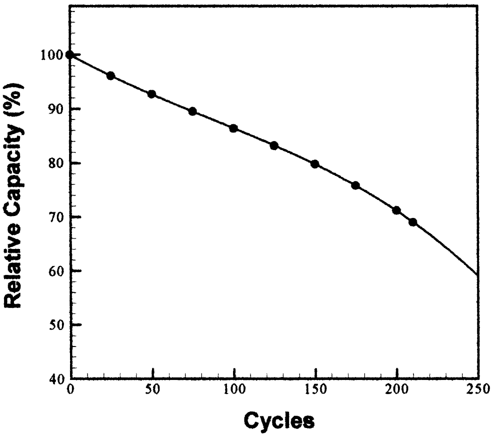

Figure 13.8. Simulation of capacity fading in a nominal VRLA cell due to excessive gas venting and dry-out.

incorporated the condition of excessive gassing due to overcharging in each cycle. The pressure setting of the valve and the amount of gas generated by the cell reaction led to the loss of water in the electrolyte in each cycle, which in turn changed the acid concentration and distribution. The change of acid concentration from cycle to cycle also affected the reaction rate and mass transport; thus, the gas recombinant rate and pressure build-up were altered. The changing cell characteristics and conditions accelerated the water loss and the dry-out process, thereby aggravating the capacity loss.

Figure 13.9 is an example showing how an "equivalent-circuit" model was used to simulate capacity loss due to the changes in resistance of a nominal VRLA cell during a deep-cycle life testing. The VRLA cell was subjected to an over 40% overcharge in a deep-cycle (100% DOD) test and became dysfunctional after 375 cycles. Although the amount of gas vented and water loss were monitored, the capacity of the cell remained nearly constant during the first 250 cycles. From post-mortem analysis, we found that the degradation comes from (1) overcharging that led to gas venting and water loss and (2) positive electrode plate expansion (as a result of excessive outgassing) and grid corrosion. The "equivalent-circuit" model effectively simulated the interplay of these two phenomena over cycles. It also accurately predicted the capacity loss behavior as the major role of the underlying mechanisms change. The dry-out process did not show any impact to the cell capacity until the cell experienced more than 250 cycles. In addition, the plate expansion due to outgassing and grid corrosion did not play a major role in affecting the capacity until about 320 cycles. In the equivalent circuit model, the changes in resistance with cycles were attributed to either faradic or ohmic contributions. The faradic contribution is primarily related to process (1), while the ohmic contribution is predominantly attributed to conditions associated with (2). The progression of the change in resistance in the cell affects the resulting capacity over cycles. This equivalent circuit model correctly captured the phenomena observed by the experimental evidence [41] and exhibited the capacity fade behavior in the corresponding simulation in Figure 13.9(a).

The above illustrations using both "first-principle" and "equivalent-circuit" models have demonstrated some interesting capabilities in battery life prediction. They, however, only show the potential of battery life prediction under well-defined regimes in laboratory tests. The next critical step is to demonstrate the capability of simulating battery performance during actual use, where degradation would be taken into account. This is where models such as ANN can prevail over the "first-principle" or "equivalent-circuit" models.

Initial trials have shown that it is feasible, in principle, to take adaptive approaches [38] to deal with this challenge. The "artificial-intelligence" model, complemented by the "first-principle" and "equivalent-circuit" models, can

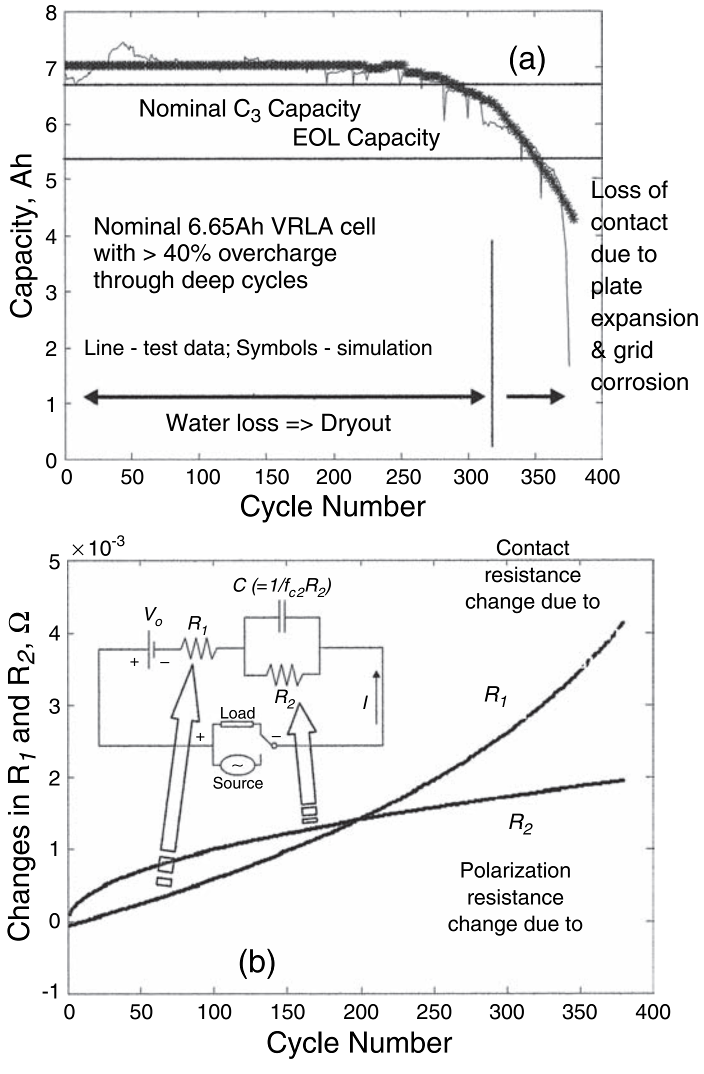

Figure 13.9. (a) Capacity change over a deep cycling test of a nominal VRLA cell subjected to more than 40% overcharge in each cycle. Contributions from gas vent and water loss and from plate expansion and grid corrosion, as explained in (b), are shown to indicate how they affect the cell capacity. The symbols are the simulation results for each cycle as derived from the model used in (b), and the solid line is the experimental data. (b) An "equivalent-circuit" model that incorporates the degradation of a VRLA cell due to (1) gas vent and water loss, and (2) plate expansion and grid corrosion.

assess the degree of stress (in stress factors) imposed on the cell during use. The corresponding impact on the cell performance and the degree of degradation can thus be estimated, and incorporated into the model, to simulate and predict battery behavior. This approach, although promising, needs to be developed in the future.

13.4.3. Life Prediction in Practical Use: Stage Three Developments

One must realize that, along with operation, battery degradation occurs during storage and stand-by modes. A successful prediction of actual battery life needs to incorporate degradation from all events. Conventional laboratory tests on calendar, and cycle, life are typically performed under strict, benchmark conditions. However, this does not accurately reflect real-life situations where the operating conditions are often changing and uncontrolled. Therefore, to predict battery life in practical real-life situations, one has to continuously monitor and measure the stress that the battery experiences and conduct a comprehensive analysis of the impact on battery performance and life. This issue is particularly complicated in situations where the loads are sporadic, such as in EHV and RES applications. Predicting battery life over these conditions is very difficult and problematic at the present time. Through the following discussions, we shall address these challenges and situations and find feasible solutions to overcome them.

Predicting the battery life may be possible with a simple extrapolation, if the operating conditions of the battery in a working environment are very similar to life tests which have been carried out in the laboratory. However, successful cases are rare; so far, probably only float operation of batteries in uninterruptible power supplies (UPS) and systems with a battery stabilized DC intermediary circuit would be able to allow accurate prediction with the results of life tests to be applied to field installations. Another more likely case that would allow a straightforward use of life tests is cyclic operation of batteries with frequent full recharges, such as those found in forklifts. However, upon a close look, one may soon find out that operating conditions, such as DOD, charging conditions as a function of temperature and DOD, average discharge current, and variations of discharge current, vary greatly in the operation of forklifts. It is by no means clear if these operating conditions have various degrees of impact on the life of the battery.

In advanced UPS, the system provides an estimate of the remaining backup time in case of a power failure. A common feature is a comparison of the discharge curve with previous curves and, as a result, an indication of the actual capacity of the battery is assessed. The operation of the battery in the next few weeks can be accurately predicted unless certain failure modes occur.

These empirical approaches, although practical, are not generic enough for advanced computer modeling and simulation for life prediction. One of the obstacles is the lack of reliable analytical tools to allow determination of the capacity fade mechanisms. Recently, an in-situ, non-invasive incremental capacity analysis (ICA) technique [42] has been reported to allow one to correlate capacity fade with several fading mechanisms, some intrinsic and others extrinsic, in a quantitative manner. This technique can be used to separate both negative and positive electrode contributions in capacity fade in a timely evolution over the testing cycles.

Such an analysis is based on the interpretation of the incremental capacity (IC) ($\Delta Q/\Delta V$ *vs.* V) curves. Such representation transforms either voltage plateaus (related to first-order phase transformations) or inflection points (related to solid state solutions) into clearly identifiable $\Delta Q/\Delta V$ peaks, leading to a specific signature for any negative or positive electrode reaction. A schematic illustration is shown in Figure 13.10, in which a eutectic binary system is used as an example to depict the relationship between phase diagram, equilibrium

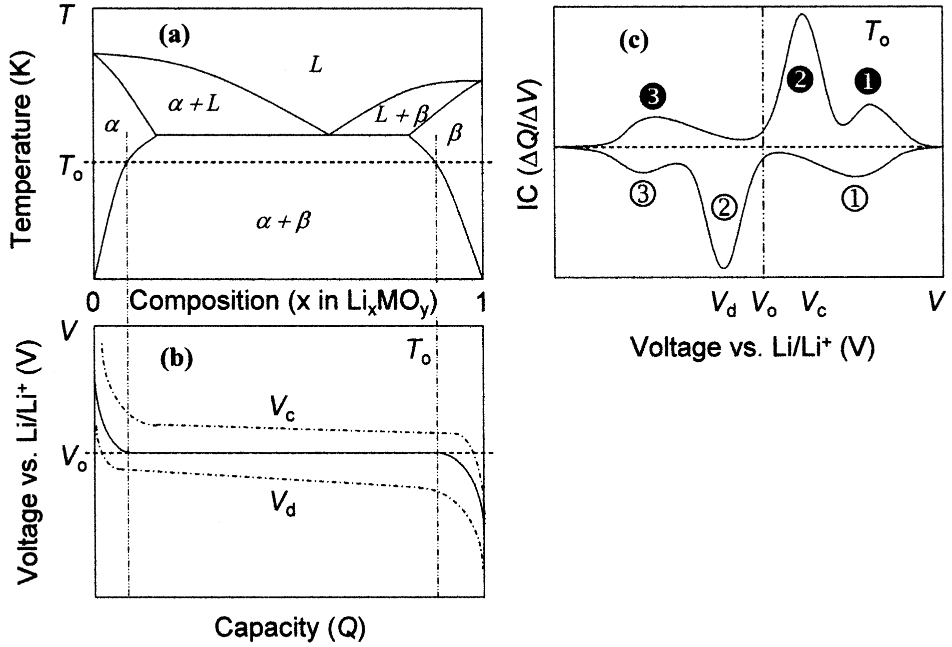

Figure 13.10. Schematic illustration of a eutectic system as an electrode material in the battery application. (a) The binary phase diagram, (b) the equilibrium potential curve and the charge and discharge curves, and (c) the corresponding IC curves, showing characteristic IC peaks related to phase transformation and solid solution regimes.

potential curve, the charge and discharge curves, and the corresponding IC curves, delineating that the IC peaks will exhibit specific characteristics in relation to the phase transformation and the solid solution regimes.

Most of the ICA is performed on cells using Li metal reference in order to observe only the signatures from the working electrode active material. Performing ICA on commercial cells is usually not preferred, because the interpretation of the IC data could be complicated and difficult. Nevertheless, to investigate capacity fade it is often necessary to conduct the evaluation in a full cell configuration with both positive and negative electrodes present, since degradation might be initiated from one electrode but lead to a subsequent adverse effect on the other via the interaction with the electrolyte.

Through aging, the IC curves will exhibit changes in their characteristic peaks according to the aging mechanism. Two intrinsic primary mechanisms that contribute to capacity or power capability fading can be used to categorize the changes in the system due to aging. One of them is simply *loss of active materials*, through processes such as loss of electrical contact or disintegration of the electrode active matrix from volume expansion and accumulated strain. The other is the *change in chemistry*, usually due to side reactions that caused active materials degradation, such as a surface layer formation at the interface between the electrode and the electrolyte, *e.g.* solid electrolyte interphase (SEI) formation in Li-ion batteries. These degradations often result in permanent, irreversible loss in capacity or power capability.

These intrinsic degradation mechanisms can lead to higher polarization in charging and discharging, inducing subsequent extrinsic degradation from *underdischarge* or *undercharge*, which might be temporary and recoverable, thus reversible. Figure 13.11 illustrates these phenomena in the schematics.

Analyzing IC curves on a full cell configuration can also provide useful information on a number of aspects of the cell performance. For example, the kinetics of the reactions involved in negative or positive electrode can be revealed by the ICA. The degradation of the kinetics can also be analyzed through cycling. Loss of active material, change of chemistry, *etc*., can also possibly be determined by this technique. The sensitivity of this analysis can be quite profound than other techniques to derive a more detailed comparison among various materials, processing or aging conditions.

The application of ICA is just one of the examples of enabling techniques that need to be developed and utilized to quantify degradation with specific mechanisms. Through this exercise, validation of the model for prediction of battery life in real-life situations can be analyzed and refined.

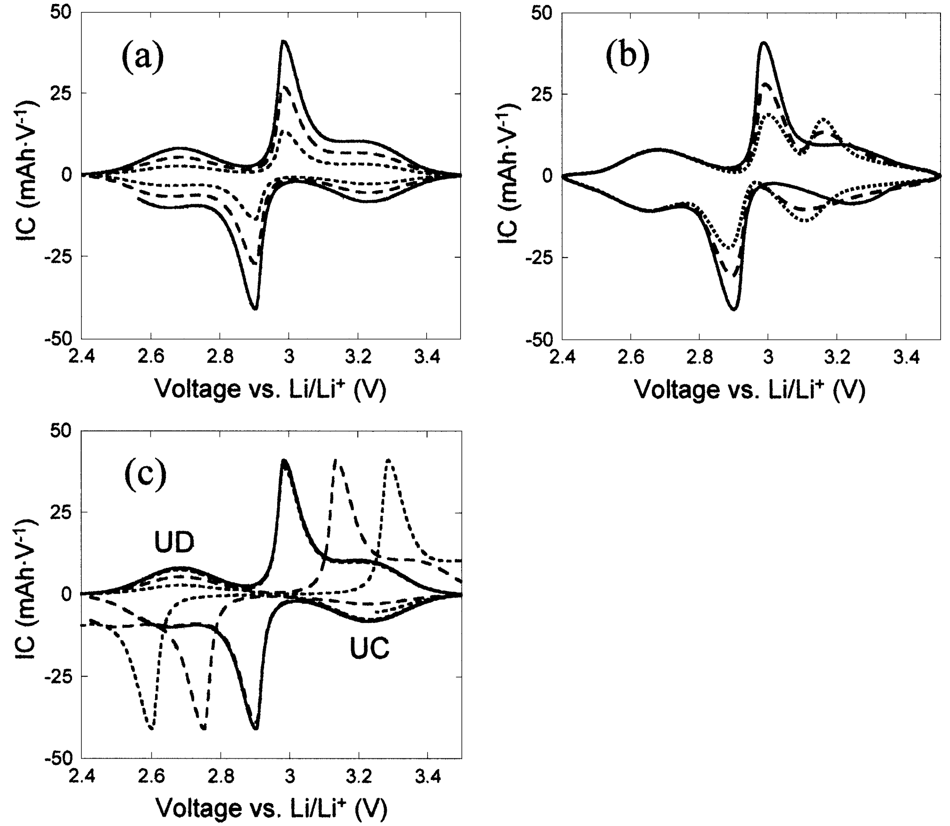

Figure 13.11. Schematic illustrations of IC curve changes due to different mechanisms such as (a) loss of active material, (b) change in chemistry, and (c) underdischarge and undercharge.

13.4.4. Future Directions

The stage one and stage two developments of predictive battery models are maturing and may have high fidelity toward real-life applications. Future work for stage three and stage four remain challenging. Not much guidance is available, though, nor can be derived from any prior experiences. One of the most critical tasks is to categorize and quantify "usage" of battery for real-life applications. The term "usage" is quite abstract and amorphous at the present time. The quest to quantify "usage" is to allow better characterization of duty cycles in terms of "usage patterns" which will allow us to infer the battery use in a mathematically manageable way and thus analysis of irregular or sporadic duty cycles will become meaningful.

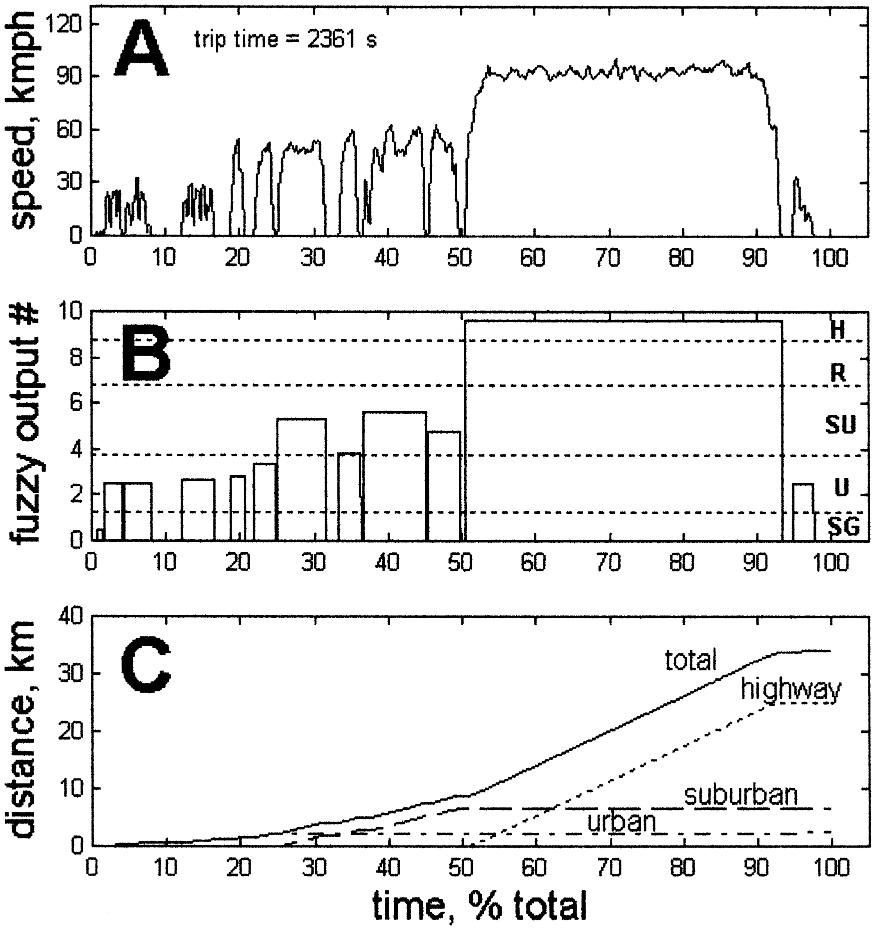

Figure 13.12. Driving cycle analysis using fuzzy logic driving pattern recognition technique to compose any driving cycle into sequential driving patterns (H: highway, R: rural, SU: suburban, U: urban, SG: stop-and-go) deciphered by the fuzzy logic rules and represented by the percentage of time driven or distance. Using this approach, any driving cycles can be analyzed consistently and compared side-by-side among one another.

One example is the driving cycle analysis for EHV application. Driving cycle analysis is a very challenging subject in real life situations. There is no systematic approach that can be used to date to analyze any driving cycles recorded in the field consistently for comparison. Therefore, standard driving schedules, such as federal urban driving schedule (FUDS), are used for analysis, comparison and validation, including collecting data with dynamometer testing and simulation. This traditional approach, although adopted by the industry for comparison of vehicle performance on a common basis, provides little guidance for real-life prediction.

To enable any useful driving cycle analysis in real-life situations, a fuzzy-logic driving pattern recognition technique was proposed recently [43,44] to recognize driving patterns in any driving cycles for analysis and comparison.

This simple and intuitive approach normalizes driving cycles into percentage of time and distance of driving, as shown in Figure 13.12, therefore allows any real-life driving cycles be compared side by side among one another. The fuzzy-logic pattern recognition technique allows one to compose a driving cycle with specific driving patterns assigned to periods of time where the vehicle was actively being driven. Using this method, one can begin to analyze driving cycles with more quantitative description and comprehensive analysis.

This type of approach may find some values in the analysis of battery duty cycles, where one can begin to label the consumption of power and capacity in the "usage patterns," so the impact to battery life due to the characteristics of the "usage patterns" can be identified and categorized [45]. This is just an example to show how stage three development of battery life prediction can be realized in the near future. Successful characterization of duty cycles and correlation of such "usage patterns" with impacts on battery life can thus greatly enhance our capability in predicting battery life more accurately.

With similar developments of battery management systems in stage three and four, we can then anticipate a more reliable prediction of battery service life in practical applications, where irregular duty cycles that exhibit sporadic consumption of power and capacity can be analyzed and predicted.

References

1. *USABC Electric Vehicle Battery Test Procedures Manual,* Revision 2, DOE/ID-10479, January 1996, Appendix F. A Portable Document Format (PDF) copy can be found at http://www.uscar.org/consortia&teams/USABC/manualPDFs/USABC_Manual_App_F.pdf
2. *Engineering Handbook - Lithium Ion,* Sanyo Energy, Chapter 2, Section 2-2, p 4, p 16, and p 27, http://www.sanyo.com/batteries/lit.cfm
3. *Nickel Metal Hydride Handbook,* Panasonic Battery, pp 12-13, pp 36-37 (2005).
4. *Raychem Circuit Protection,* Tyco Electronics, PolySwitch™, http://www.circuitprotection.com/polyswitch.asp
5. M. Galla, in "*PowerPulse.net*", *Battery Pack Manufacturers Use PPTC Devices for Primary Overcharge Protection,* 2006.
6. Texas Instruments, *Sensors & Controls,* Klixon® snap-acting bi-metal protectors, http://www.ti.com/snc/support/klixon.htm
7. SeMitec® Ishizuka Electronics Corp., NTC thermistors, http://www.semitec.co.jp/english
8. D.F. Stolitzka and S.E. Austin, U.S. Patent 6,486,636 (2002).
9. D. Freeman and J.A.V. Formenti, U.S. Patent 6,650,089 (2003).
10. R. Casas and O. Casas, in "*IEEE Computer*", *Battery Sensing for Energy-Aware System Design,* IEEE Computer Society, 2005.

11. POWERPRECISE Solutions, Inc., http://www.powerprecise.com
12. X.G. Yang and B.Y. Liaw, *J. Power Sources* 101 (2001) 158; U.S. Patent 6,437,542 (2002).
13. W.H. Bushong *et al.*, U.S. Patent 6,878,481 (2005).
14. J. Hewes, R. Yoppolo and M.P. Hull, U.S. Patent 6,232,749 (2001).
15. IEEE Std 1625™-2004, *"IEEE Standard for Rechargeable Batteries for Portable Computer"*, IEEE Power Engineering Society, Institute of Electrical and Electronics Engineers, Inc. (2004).
16. R. Dunstan, U.S. Patents 5,565,759 and 5,572,110 (1996).
17. Smart Battery System Implementers Forum (SBS-IF), http://www.sbs-forum.org
18. System Management Interface Forum (SMIF), http://www.powersig.com
19. System Management Bus (SMBus), http://www.smbus.org
20. D. Friel, *"SBS Simplifies Portable Power System Design"*, *Electronics Engineer Asia*, Cover Story, June 1999.
21. W. Peukert, *Electrotech Z.* 18 (1897) 287.
22. C.M. Shepherd, *J. Electrochem. Soc.* 112 (1965) 657.
23. J. Newman and W. Tiedemann, *AIChE J.*, 21 (1975) 25.
24. W.G. Sunu, in *Electrochemical Cell Design*, R.E. White, Editor, p. 357, Plenum Press, New York, (1984).
25. H. Gu, T.V. Nguyen and R.E. White, *J. Electrochem. Soc.* 134 (1987) 2953.
26. T.V. Nguyen, R.E. White and H. Gu, *J. Electrochem. Soc.* 137 (1990) 2998.
27. D.M. Bernardi, H. Gu and A.Y. Schoene, *J. Electrochem. Soc.* 140 (1993) 2250.
28. J. Newman, Karen E. Thomas-Alyea, *Electrochemical Systems*, 3rd ed., Wiley Interscience, NY, 2003.
29. W.B. Gu, C.Y. Wang and B.Y. Liaw, *J. Electrochem. Soc.* 144 (1997) 2053.
30. B.Y. Liaw, K.P. Bethune and X.G. Yang, *J. Power Sources* 110 (2002) 330.
31. P. Mauracher and E. Karden, *J. Power Sources* 67 (1997) 69.
32. M.W. Verbrugge and R.S. Conell, *J. Electrochem. Soc.* 149 (2002) A45.
33. B.Y. Liaw, R.G. Jungst, A. Urbina and T.L. Paez, *Proc. of the Electrical Energy Storage – Applications and Technologies Conference 2003(EESAT 2003)*, San Francisco, CA, 27-29 October 2003.
34. B.Y. Liaw, G. Nagasubramanian, R.G. Jungst and D.H. Doughty, *Solid State Ionics* 175 (2004) 835.
35. C.C. Chan, E.W.C. Lo and W. Shen, *J. Power Sources* 87 (2000) 201.
36. A. Salkind, T. Atwater, P. Singh, S. Nelatury, S. Damodar, C. Fennie, Jr. and D. Reisner, *J. Power Sources* 96 (2001) 151.
37. A. Urbina, T.L. Paez, R.G. Jungst and B.Y. Liaw, *J. Power Sources* 110 (2002) 430.
38. K.C. Yap, A. Urbina, B.Y. Liaw and R.G. Jungst, *Proc. of the Electrical Energy Storage – Applications and Technologies Conference 2003(EESAT 2003)*, San Francisco, CA, 27-29 October 2003.
39. F. Alavyoon, A. Eklund, F.H. Bark, R.I. Karlsson and D. Simonsson, *Electrochim. Acta* 36 (1991) 2153.
40. W.B. Gu, C.Y. Wang and B.Y. Liaw, *J. Power Sources* 75 (1998) 151.
41. K. Bethune and B.Y. Liaw, presented in the 201st Electrochemical Society Meeting, Philadelphia, PA, May 2002, Abstract 147.
42. M. Dubarry, V. Svoboda, R. Hwu and B.Y. Liaw, presented in the 209th Electrochemical Society meeting, Denver, CO, May 7-11, 2006, Abstract # 101.
43. B.Y. Liaw, K.P. Bethune, C.S. Kim, *Proceedings of the 19th Electric Vehicle Symposium* (EVS-19), October 19-23, 2002, Busan, Korea, p. 348.
44. B.Y. Liaw, *J. Asian Electric Vehicles* 2 (2004) 551.
45. M. Dubarry and B.Y. Liaw, presented in the International Meetings of Lithium Batteries (IMLB) 2006, Biarritz, France, June 18-23, 2006.

This page intentionally left blank

Industrial Applications of Batteries. From Cars to Aerospace and Energy Storage
M. Broussely and G. Pistoia Eds.,
© 2007 Elsevier B.V.

Chapter 14

BATTERY COLLECTION AND RECYCLING

Daniel Cheret

Umicore Recycling Solutions, Umicore Group, 2250 Olen, Belgium

14.1. Introduction

Decreasing the consumption of non-renewable resources and the amount of waste produced is now becoming mandatory. The task of saving natural resources and keeping the environment clean can be accomplished by developing new technologies enabling a cost-effective and environmentally sound recycling of end-of-life products or equipments.

All battery types, whatever their chemistry, contain a good proportion of metals. Metals can be recycled repeatedly without loosing any of their initial properties. Furthermore, recycling is very often much less expensive and more environmentally friendly than extracting virgin ores, and generally much less critical for environment. Indeed, compared to producing metals from original ores, recycling metals enables a significant energy saving, a decrease in water use, and a drastic decrease in air emissions.

Waste management is becoming more and more a relevant issue in our developed society. Specifically for batteries, the question is: should separate collection schemes for batteries be applied, or could we simply collect them with the rest of the waste? To answer this question, one should better understand the possible routes that can be followed by the waste after being collected.

Typically, there are three possible options for the management of batteries at the end of their life: incineration, landfill or recycling. As most of the batteries do not contain many combustible materials, incineration is definitely not the preferred route.

In many countries, disposal of end-of-life batteries in landfills is still allowed. Even if there is no evidence proving that this could represent a major burden for the environment, landfilling batteries should not be considered a primary option, as this entails the extraction of new ores to produce fresh metals that could have been recovered from used materials. In that sense, landfilling can be considered as generating a burden for the environment.

Thus, the last remaining option for managing end-of-life batteries is recycling. Not only this reduces risks that may exist with batteries in terms of pollution, but it conserves valuable natural resources as well. However, there could be other environmental impacts which must be considered: the energy consumption for recycling, the amount of "elements" to be cleaned up (emissions into water, air), and the usability of the produced or recycled materials. Of course, all these points have to be balanced with economical efficiency. Trying to find the best compromise among all these parameters is the objective of the so-called "eco-efficiency" studies introduced in the following section.

It is one objective of this chapter to highlight the different collection schemes and recycling processes existing and try to point out their main advantages and drawbacks.

14.2. Eco-efficiency Study on Recycling Techniques

The eco-efficiency concept considers the relationship between environmental effectiveness and cost effectiveness of collection and recycling. Studies on eco-efficiency of environmentally sound management practices in battery recycling are still relatively rare. However, the principles applied to perform these studies on other materials are valid for batteries as well. Here, the QWERTY study performed in 2004 in Sweden by Stevels and Huisman on the issue of recovering and recycling mobile phones will be discussed.

This study, using an eco-efficiency approach, examines the environmental effectiveness of several waste management scenarios, ranging from disposal in a landfill to direct insertion into a metal smelter via a possible preliminary dismantling operation. The study considers the environmental losses/gains of each scenario, *e.g.* landfill of batteries, and takes into account the different environmental characteristics of the materials contained in the product, and assigns an "*environmental weight*" to each material, rather than just a "*physical weight*" [1].

This "Environmental Weight" approach, for example, places a high value on the recovery of gold from used mobile phones, because it avoids the significant environmental damage of gold mining and production from ore. Thus, it views recovery of a small amount of selected metals from mobile phones as carrying greater environmental benefits than recovery of, for example, a larger amount of steel or plastics. The focus of recycling should then be shifted from plastics to metals for an effective environmentally sound recycling. In Figure 14.1, the difference between weight and

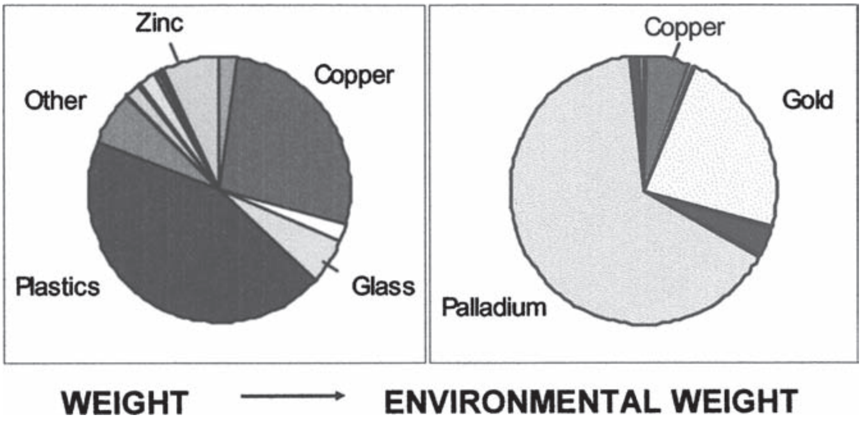

Figure 14.1. Weight *vs.* environmental composition for mobile phones.

environmental composition is illustrated for mobile phones. After applying these environmental weights, the study then compares the overall environmental losses and gains of a waste management scenario with the economic costs and benefits of that scenario.

The QWERTY study comes to the conclusion that, for the particular case of small electronic appliances like mobile phones, the direct smelter route is more eco-efficient than the other waste management scenarios that were examined. Specifically, this study concludes that manual or automatic disassembly does not return significant environmental benefit, and its costs outweigh the economic benefits that might otherwise be achieved through efficient metal recovery in a dedicated pyro process.

The QWERTY eco-efficiency study is cited here as an example of a valuable approach that can be helpful to reaching conclusions on best practices for environmentally sound and economically efficient management. This study would not necessarily reach the same conclusion for other types of waste with different disassembly costs and different types and amounts of materials recovered. Each type of waste should be examined for its unique characteristics – economic and environmental – to determine its most eco-efficient management. Furthermore, the study did not examine every waste management scenario and the results of other studies will vary according to different circumstances, including the particular recycler and smelter practices that are examined. In this study, the practices of several specific Swedish recycling and recovery facilities were examined.

However, a true parallelism can be done between the above

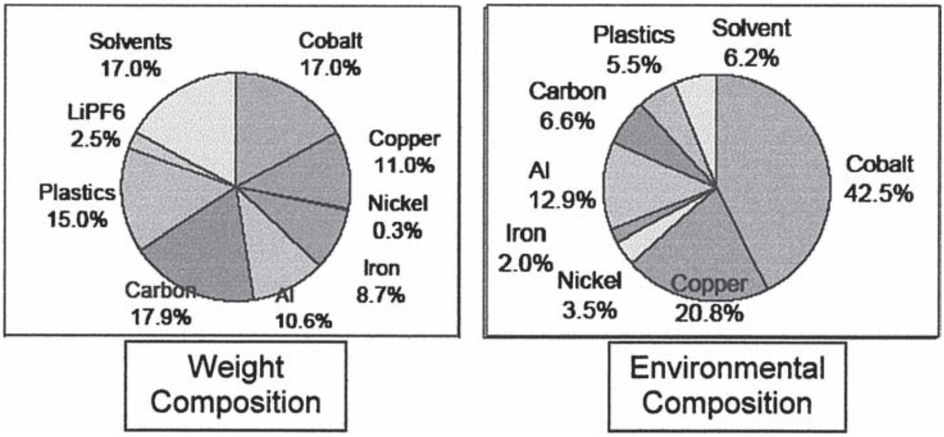

Figure 14.2. Weight composition *vs*. environmental composition for Li-ion batteries.

conclusions on mobile phones and batteries. As an example, the same methodology has been applied by Huisman for defining the environmental weight of the components of a Li-ion battery, compared to the normal weight (see Figure 14.2).

In that example, the initial weight of Cobalt + Nickel + Copper is 28.3% whereas the environmental weight for the same elements is as high as 66.8%, *i.e.* more than two times higher. This points out the environmental and costs benefit of recycling the metal content of a battery. This could be conveniently done in a direct smelting route, instead of recycling the elements separately with the remarkable risk of loosing metals in other fractions.

Starting from that, an eco-efficiency diagnose can be obtained by evaluating the cost/revenue *vs*. environmental gain/burden for the different possible scenarios. In Figure 14.3, the horizontal axis represents the absolute environmental outcomes of the Qwerty calculations (expressed in environmental millipoints based on Life Cycle Assessment outcomes) whereas the vertical axis represents the economic outcomes. The letters in the graph represent various end-of-life scenarios for the same product. The scenarios are based on different technologies for recycling, design and system organization.

If a result ends in the up-right region, this scenario should be chosen, whereas if it ends up in the low-left region, this scenario should be avoided.

This methodology has been applied to mobile phones and their batteries, for which different technologies have been tested, from all dismantling to all smelting.

Clearly, the worst scenario is municipal waste incineration. Therefore,

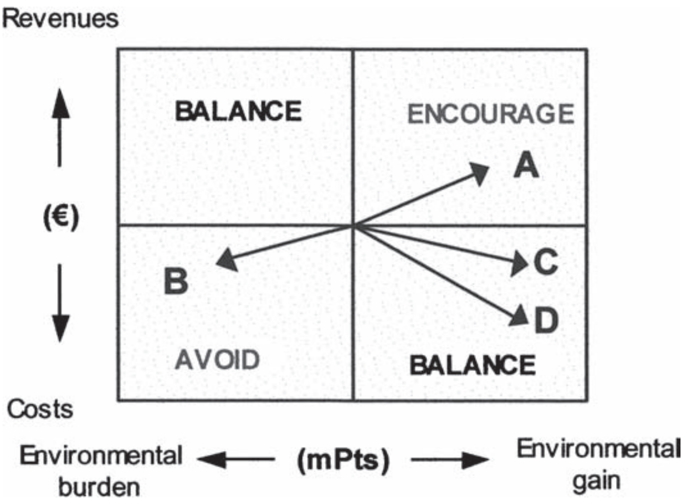

Figure 14.3. The visualization of eco-efficiency.

batteries have to be separated from the rest of the domestic and/or municipal wastes. The best scenario is when the mobile phone is directly put into a smelter for recovering all precious metals and the battery smelted in parallel in a dedicated smelter to recover the metals. An alternative that has positive outcomes for environment but much more financial negative impact is the total dismantling of mobile phones and batteries to recover all parts separately, including plastics. Figure 14.4 illustrates these concepts.

Of course, this way of thinking is not unanimously accepted. For instance, Ökopol [2], the German Institute for Environmental Strategies, has stressed the limitations of the QWERTY study, with particular reference to the fact that it examines only Swedish practices and conditions, rather than a more complete set of possible waste management scenarios. Ökopol's review also questions the lack of transparency regarding the cost data used in the QWERTY study (proprietary data for specific Swedish firms), as well as some of the economic calculations and data inputs.

Anyway, recycling in general and recycling of batteries in particular need to be looked from a new perspective to optimize the financial costs *vs.* benefits for the environment, and the way of thinking based on "Environmental Weight" can be considered as a first important step towards this direction.

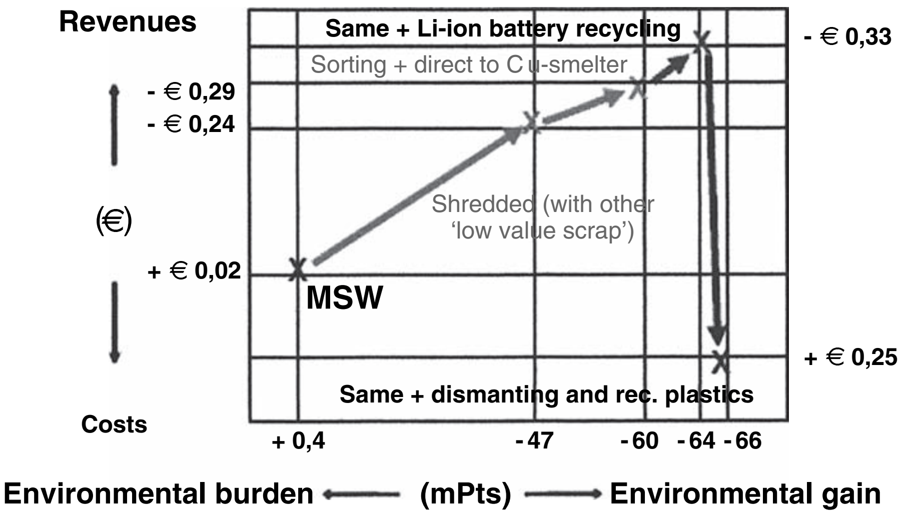

Figure 14.4. Eco-efficiency directions for a complete mobile phone with Li-ion battery (QWERTY study).

14.3. Trans-Boundary Movement of Batteries within the OECD Member States

Collecting and recycling end-of-life batteries implies many technical issues. The transport of collected, sorted or unsorted, batteries is one of them. OECD (Organization for Economic Cooperation and Development) member nations have implemented strict waste handling requirements to assure protection against dispersing hazardous substances into the environment.

As several batteries contain potentially hazardous substances, these particular OECD rules apply to batteries as well. This means, for instance, that for any trans-boundary movement of unsorted batteries a general notification has to be filed and should contain the following elements:

- the name of the supplier of batteries and their origins (from OEM, collection, scrap, *etc.*)
- the designation of the country where batteries will be recycled
- the designation of any country of transit as well as the designation of the transport company with copy of special authorizations, if needed
- the composition of the waste and the estimation of its intrinsic value
- a description of the recycling process
- a certificate proving the agreement of a contract for recycling these batteries between the supplier and the recycler
- a certificate stating that applicable insurance and guarantees are in force.

The establishment of such a notification can take several months before getting the approval for shipment. In addition, it is valid for one year and a movement tracking form disclosing all the above-mentioned information should accompany each shipment. Finally, the recycler has to process the waste within 190 days and inform its authorities after recycling the waste.

Even if all these formalities have undoubtedly a positive intention and are somehow necessary to track the exchanges of waste, they can generate some constraints and produce the opposite effect. The American story about NiCd batteries is a good illustration of that. In 1990, the US Environment Protection Agency changed its test protocol for determining which waste should be classified as hazardous or not – the TCLP test. Because this new test required that material should be crushed, end-of-life NiCd batteries failed to pass it, due to a too high leaching level of Cd. Consequently, NiCd became classified as hazardous waste requiring all the collection and recycling chain to get special permits for handling, storing, transporting and recycling.

This complexity immediately resulted in a suspension of most of the existing collection and recycling schemes of NiCd batteries due to the high administrative burdens. In addition, transporting batteries by specialized hazardous waste carriers at a cost at least two to three times higher made also the whole chain economically prohibitive. The collection rate of NiCd dramatically decreased in the following years. Finally, in 1995, the EPA allowed again any institution or company to collect and store end-of-life NiCd batteries without any special license. In addition, shipment of batteries was made easier and the collection rate grew up again reaching today more than 5 million pounds per year for the United States and Canada through the RBRC structure [3].

Clearly, by facilitating the collection and transport of batteries, the authorities did not increase the potential environmental risk but did exactly the contrary. Even with the best recycling processes in place, the protection of the natural resources and the environment will only be possible if batteries are effectively collected up to a high collection level.

So, today all used or end-of-life batteries have to be transported under a Basel Notification procedure based on the OECD Classification AA 180:

> "*Used batteries or accumulators, whole or crushed, other than lead-acid and waste & scrap from production of batteries and accumulators*".

Each chemistry has its special code for transport as illustrated with the European Waste Codes (16 06 xx), with some of them classified as hazardous wastes for transport and some even to be transported as "Class 9" waste, this being the most stringent class existing (mixed/unsorted used batteries are always classified as hazardous on class 9). The European waste codes and the transport hazards are summarized in Table 14.1. In Figure 14.5, the symbol of

Table 14.1. European waste codes for batteries.

	EW Code	Hazardous for transport
Pb batteries	16 06 01	Yes
NiCd	16 06 02	Yes
Hg-containing batteries	16 06 03	Yes
Alkaline batteries	16 06 04	No
Other batteries	16 06 05	No*
Electrolyte	16 06 06	Yes
Mixed batteries	16 06 05	Yes

*Some batteries, *e.g.* Li batteries, are classified as dangerous for transport.

Class 9 hazardous waste is presented.

This is the case for the category called "Lithium Batteries" (UN 3090). The legislator included under this name all Li-containing batteries, whatever their chemistry. In this way, primary lithium batteries (containing metallic lithium) and secondary Li-ion batteries have to be transported under the same denomination even if the potential hazards are totally different. In the case of a primary lithium battery, the main risk is the contact with external environment of the active components, mainly metallic lithium. This metal is not stable under normal circumstances and is spontaneously transformed into its oxide, this reaction being exothermic and releasing a big amount of energy. Quite often, the reaction is very violent and an explosion occurs.

Li-ion batteries do not contain any metallic lithium and do not present any explosion hazards due to oxidation. Anyway, the legislator grouped these two types into the same family, so Li-ion batteries are also considered hazardous waste for transport.

CLASS 9 HAZARD
Miscellaneous dangerous substances and articles

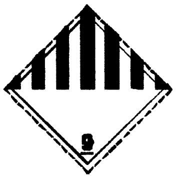

(No. 9)
Symbol (seven vertical stripes in upper half): black;
Background: white;
Figure '9' underlined in bottom corner

Figure 14.5. A class 9 symbol to be used for transporting some batteries.

14.4. Battery Collection Schemes

In some parts of the world, collection schemes for end-of-life batteries are already in place. In other parts, they are under discussion. In general, the basic "Extended Producer Responsibility" (EPR) principle is used in most countries. The OECD defines EPR as:

> "*an environmental policy approach in which a producer's responsibility for a product is extended to the end of life stage of the life cycle of the product*".

Nevertheless, the situation is not as clear as it should be and some discrepancies are visible between countries or regions. Let us review the particular case of what can probably be considered the most advanced area in that field: Europe.

14.4.1. The Particular European Situation

A new European directive on batteries is expected to be ratified by the 4th quarter of 2006. After that, some time will be needed to translate the directive into all European languages and to have enough data for a first evaluation. This means that by 2009/2010, minimum collection rates of batteries (and recycling rates) will have to be achieved.

In any case, this new directive is strongly inspired by the Waste Electric and Electronic Equipments Directive (WEEE- 2002/96/EC) entered into force in August 2005 in all European countries.

Even if all aspects are not yet fully defined, it clearly appears that the same EPR principle will be applied within all European countries, including those having recently joined the European Community (EU-25). After its reading, the Council defined in September 2005 the "producers" as follow:

> "*producer means any person in a Member State that, irrespective of the selling technique used, including by means of distance communication according to Directive 97/7/EC on the protection of consumers in respect of distance contracts places batteries or accumulators, including those incorporated into appliances or vehicles, on the market within the territory of that Member State for the first time on a professional basis*".

The Council has simplified the definition so as to ensure that, for each battery placed on the market within a member state, there is an easily identifiable producer in that state. This is necessary in order to make the principle of producer responsibility effective.

Apart from that, the new directive will impose:

- the collection of batteries in all European countries
- minimum collection rates of used batteries (from small size to big industrial batteries) based on sales volumes of previous years

- recycling targets of, probably, 75% for NiCd, 65% for Pb/Acid and at least 55% for all other batteries
- ban landfilling of any type of battery
- limit and/or ban the use of certain substances in batteries (mainly Cd, Hg, Pb).

It will also be the responsibility of the member states to ensure that:

- schemes are set up under which spent portable batteries and accumulators can be collected individually from end-users or from an accessible place in their vicinity free of charge
- end-users deliver their spent batteries and accumulators to a collection scheme
- producers of industrial batteries and accumulators, or third parties acting on their behalf, take back from end-users spent industrial batteries and accumulators.

In 2005, some European countries already had public or private collection scheme(s) in place at least for some types of batteries. Certainly, the most advanced in that field are Belgium (Bebat), the Netherlands (Stibat) and Germany (GRS) where collection rates have already reached high levels and will probably be compliant with the legislation to come. But some countries do not have anything in place yet. This is especially the case of the "new comers" to the EU-25.

14.4.2. Financing the Schemes

The main obstacle for a high collection and recycling ratio is the financing of the entire infrastructure. With the EPR, producers have to assure that a collection and recycling scheme can be put in place in all countries and have to finance it. Very often, this is accomplished – as it has been done for the WEEEs – by including a visible or non visible recycling fee on top of the normal price usually paid by any customer. However, depending on the solution developed for the scheme, fees can substantially vary from country to country as shown in Table 14.2.

In general, collection and recycling costs are correlated to the collected volumes of batteries and accumulators and to their intrinsic value, also linked to their metal content. Consequently, as metals always represent the most valuable part of batteries and their values can significantly fluctuate with time (see Figure 14.6), the intrinsic battery value can also significantly vary.

For some types of batteries and at the present level of metal price the whole scheme can generate a positive financial balance. This is for example currently the case of NiMH batteries, with the nickel price at 14,000 USD/Ton (see Figure 14.7; the abscissa reports material value/recycling cost ratios).

Table 14.2. Collection and recycling fees (in Euro cent per kg) in various European Member States and in Switzerland.

	Primary		Secondary			
Country	**ZnC (Alk)**	**Lithium**	**Ni-Cd**	**Li-Ion**	**Ni-MH**	**Small Pb-Acid**
Austria (UFB)	90	90	90	90	90	90
Belgium (Bebat)	350	350	350	350	350	350
Denmark (Gov)	–	–	1610	–	–	4
France (Screlec)	46	91	175	175	175	130
Germany (GRS)	40	78	51	34	24	27
Netherlands (Stibat)	65	65	65	65	65	65
Norway (Rebatt)	8	8	155	155	155	155
Sweden (Gov)	–	–	3320	–	–	19
Switzerland (Inobat)	320	320	320	320	320	320

However, this is not the case for most of the other systems, for which the total financial cost for collecting and recycling exceeds the single intrinsic value.

Nevertheless, as explained in the "Environmental Weight" or QWERTY study, the environmental gain of recycling these batteries always exceeds the single financial cost and there is always a benefit for the environment. From this viewpoint, recycling in dedicated and well managed and controlled processes is the solution of choice for the management of end-of-life batteries.

Battery manufacturers are continuously looking for solutions to reduce the intrinsic value of a battery to improve their competitiveness and decrease their working capital. This is particularly the case of "new technology" systems like Li-ion batteries.

A "standard" Li-ion battery contains ~14% of cobalt in weight, but due to the high cobalt price and its important fluctuations, industrials tend to develop Li-ion batteries with much less cobalt and even no cobalt at all. This will generate a battery with much lower intrinsic value, and consequently will further increase the negative impact – or costs – for recycling. This represents an important issue that should be better taken into account by industrials when developing and designing their new products, whose management at end of life will become economically non-convenient.

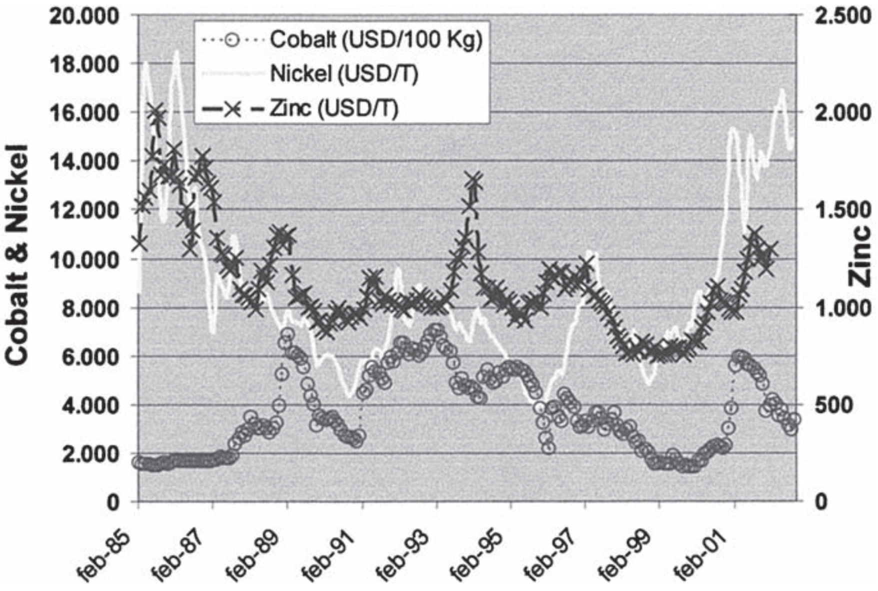

Figure 14.6. Market value *vs.* time for Cobalt, Nickel and Zinc.

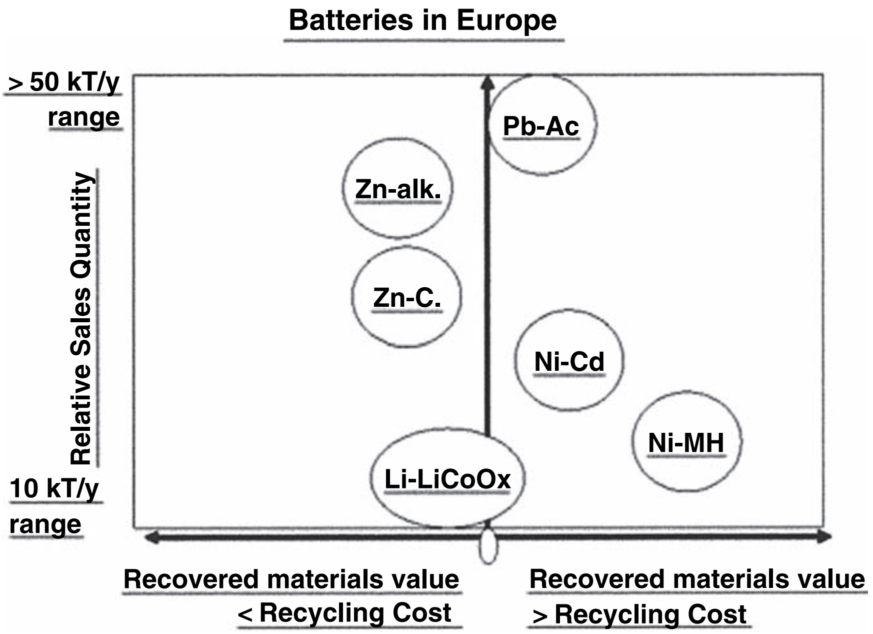

Figure 14.7. Typical intrinsic battery value *vs.* recycling costs (estimation for 2005).*(From Ref. 4)*.

14.4.3. A Closed Loop Concept to Reduce the Exposure to Metal Price Fluctuation

The Blokland's report [5] at the European Parliament working on the Battery Directive introduced the notion of "Closed Loop" for recycling:

> "*Closed loop means that the metal content of a waste battery or accumulator will be re-used in the manufacturing of new products*".

This concept has indeed some advantages. To avoid fluctuations of the value of collection and recycling, the best solution is to implement the "closed loop" philosophy whereby the materials used in the batteries are for the most part recovered and re-used in the same application (see Figure 14.8). A responsible material producer would then put in place (either by developing its own recycling system or by partnership) a recycling installation so that all used batteries can be returned to it and at least a majority of the material used can be put again into the material loop. This is especially the case for metals that are always the most costly and potentially hazardous products in a battery. By recovering, for instance, 80% of the total metal content of a battery, the manufacturer will be much less exposed to the metal value fluctuations, as producing new batteries will only demand to buy 20% of "fresh metal", the remaining 80% coming from the recycling scheme.

This closed loop approach is also supported by most of the environmental studies and tends to become more and more visible on the metal-containing product market.

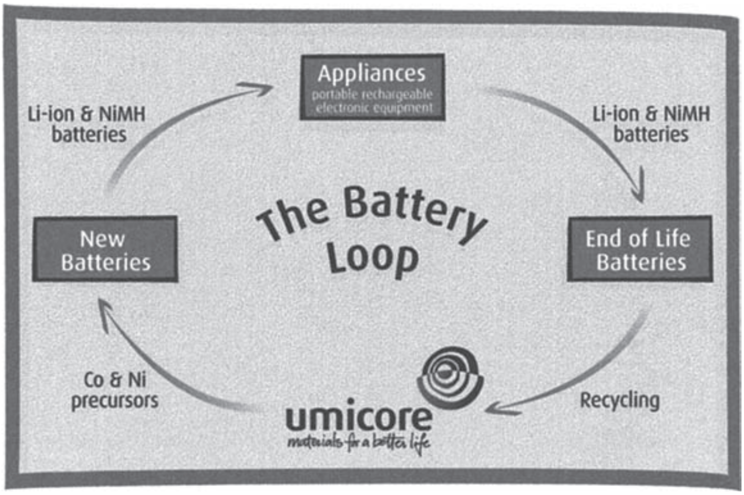

Figure 14.8. A closed loop solution for batteries.

One can even imagine one step further towards this direction to totally "liberate" the battery manufacturers from the potential metal price fluctuations, by just proposing to the material producers to lease them the necessary amount of metals. By doing so, the owner of the metals would remain the metal producer, while the manufacturer would just rent them, thus significantly reducing his working capital and exposure.

14.5. The Particular Example of a Battery Producer: SAFT

Next to the imposed national collection schemes, some battery manufacturers took the lead and decided to develop their own collection schemes to assure a perfect management of end-of-life batteries. Indeed, the manufacturers' dilemma is: just rely on other collection/recycling schemes or have an approach where the manufacturer takes an active role.

In the first type of approach, there are often some efficient waste collection companies acting as brokers between waste holders/generators and waste treatment/recycling companies. These companies are heavily regulated, controlled and monitored so that they should normally do their job properly. In a word, the market forces tend to organize themselves and take care of the problem.

In the second approach, the battery producer is directly or indirectly involved in the collection and recycling scheme. The French company Saft does this [6].

Saft is a world specialist in the design and manufacture of high-tech batteries for industrial applications. Saft's batteries are used in high performance applications such as industrial infrastructures and processes, transportation, space and defence. Saft is for example the world's leading manufacturer of NiCd batteries for industrial applications and primary Li batteries for a wide range of consumer applications.

This specialist in industrial batteries decided to implement a European-wide collection scheme for NiCd and primary lithium batteries, to be extended to the other types of batteries they are producing. Saft made this choice for financial, marketing and strategic reasons.

The financial reason was based on the fact that:

- they were already in the economic loop when purchasing metals and compounds as raw materials for their production of industrial batteries
- the know-how of recyclers for recovering the metals was existing, proven and well monitored in Europe
- a fraction of the metals for the production of new batteries were already purchased from the recycling industry

- they were experiencing the impact of raw material price changes and wanted to develop a system to immunize themselves from such swings.

In addition, some marketing factors played an important role in their decision:

- in the industrial sector, any new constraint on a product/service is an additional source of vendor differentiation. The EPR concept proposed by the European legislators can become one
- they also noticed that end users were putting pressure on equipment vendors, which in turn were putting pressure on battery manufacturers for the management of their end-of-life equipment
- in this way, battery manufacturers had no other choice than adding a new service to their portfolio – the recycling of used batteries.

Finally, the strategic aspect was also not to be forgotten. Indeed, if they had left a sizable fraction of spent batteries to end up in uncontrolled channels, they would have created the conditions for regulatory intervention in the future (this is particularly true for NiCd batteries). In addition, in some countries where regulations are not yet in place, some market players could be tempted to seeking cheap and non-environmentally sound solutions, so damaging the image of battery manufacturers.

For all these reasons, they decided to take an active participation to the collection and recycling schemes. They finally audited recycling companies and put in place a scheme of collectors where all batteries from their customers could be addressed. Contracts have been signed with collecting, transporting and recycling companies to assure a clean and controlled treatment of any end-of-life NiCd battery sent back.

In addition, even if difficult to quantify, this probably added some marketing power to the company and enabled Saft to keep its leadership positions in its markets.

Saft is just one example of battery manufacturers or original equipment manufacturers looking for developing their own collection schemes. Other examples are represented by electronic appliance manufacturers or by automotive manufacturers looking today for solutions for the recycling of their batteries used in hybrid electric vehicles (HEV).

14.6. Recycling Rate: What Does It Mean?

Some wastes generated either by consumers or industries are collected, sorted (in some cases) and landfilled. Can this be qualified as "recycling"? No, without discussion. Can dismantling a battery, and re-using all its constituents for new batteries, be qualified as "recycling"? Yes, without discussion. However, recycling is not always so simple to define. Indeed, plastics -

manually or automatically separated from batteries - are landfilled because of the lack of secondary plastic market, thus are not recycled

Many discussions are going on everywhere and particularly in the European Union with the new directive intending to impose a minimum level of "recycling efficiency" or "recycling rate". However, without clear definition of what can be qualified as "recycling", figures do not have much signification.

Generally, a first distinction is made between "Recycling" and "Recovering".

Recycling is

> "*The reprocessing in a production process of the waste materials for the original purpose or for other purposes*",

whereas recovery is defined as

> "*The use of combustible waste as a mean to generate energy through direct incineration with or without other waste but with recovery of the heat.*"

But, at which stage of the recycling process should the calculation be done for defining what is recycled, recovered or lost?

Let us imagine a company dismantling all used batteries and separating all main constituents into different fractions. At least a plastic fraction, a steel fraction, and one or several metal fractions can result. Each of these fractions is theoretically usable and could then be considered as an intermediate product for other industries. It is obvious that in that case, the recycling rate would be nearly 100%.

Let us now look closer, one step further. Let us assume that all fractions are pure and not contaminated by each other (which is never the case, due to the complexity and high interconnection between different types of materials). The steel fraction can probably be re-used and valorized in the steel industry with no major problem, especially in today's situation with high steel demand and consumption worldwide. It can be considered as recycled. As for the metal fractions, the situation becomes often critical, as the next step depends on their composition. Some processes for recovering a given metal are incompatible with the existence of other metals. This is for example the case of cobalt, whose refining cannot be performed directly in a hydro process if all traces of aluminium are not eliminated. If this is the case, a pyro process is necessary. Therefore, even if direct recovery is sometimes not easy and the chosen route can be questionable, probably most of these metal fractions could be considered as recycled.

But now, let us take a look at the most difficult fraction: plastics. There is not one single type of plastic involved in the construction of a battery – as in any other product: a mobile phone can contain more than 20 different types of plastics. Each plastic is incompatible with any other if the aim is to recycle them as a virgin "ore" in the plastic industry. So the only solution for plastics is to re-use them as a blend. But then, physical characteristics of the blend are variable and always worse than original, so that it is very difficult for a process using plastic blends as input material to be managed in a sustainable way. Therefore, only downgraded applications such as garden or urban furniture can be proposed. The simple conclusion is that the market for such plastic blends is very limited and cannot absorb the huge volumes of plastics coming from the recycling industry. This unbalanced situation has in addition recently been worsened with the imposed collection and recycling of waste from electric appliances, for which big weight fractions are made of plastics. On top of that, recycled plastics often contain some metallic parts that are totally incompatible with the extrusion technology normally used for re-melting and shaping plastics.

So, quite often the only remaining solution for the plastic fraction recovered by manual or automatic dismantling of batteries is either to landfill it, or, at the best, to send it for incineration in cement plants or metal industries. Is this recycling? According to the definition of the European legislation, incineration of plastics is not recycling, and re-using plastic as energy provider can only be considered as recovery.

Now, let us come back to our original situation with our fractions and the recycling rate. Now that the plastic fraction cannot be properly recycled, what is the "real" recycling rate? At which stage of the process should this recycling rate be calculated? After the first shredding/dismantling operation or after having found an adequate route for each fraction? Not an easy question.

In general, the owner of the waste should evaluate the planned recycling process and always take into account these questions:

- is it really recycling?
- are all fractions really recycled?
- are all the steps of the process worthwhile?
- is it environmentally well controlled?
- is it the most logical and "environmentally sound" way to do it?

14.7. Battery Recycling: the Existing Technologies

First, discussions on how batteries have to be collected and recycled have been going on for many years and are continuing today. Is there a need for a separate collection and recycling scheme per battery chemistry or can they all be recycled in the same process? To provide a reasonable answer to this question, let us simply look at the chemical composition of some typical batteries.

Each battery has its own chemistry, which is based on one or several metal(s) whose characteristics are different from those of other metals. Table 14.3 reports the chemical composition of the main commercial batteries. Simply

Table 14.3. General composition of main battery systems.

Battery chemistry	Average composition (wt%)
Lead-acid	63-67Pb – 27-23H_2SO_4
Alkaline	30Fe – 20Zn – 15Mn
Ni-Cd	30-35Fe – 15-20Ni – 20-25Cd – 2-4Co
Ni-MH	35-45Ni – 15-20Fe – 5-8Co – 12-15 Rare Earth
Li-ion	20-25Fe – 11-16Co – 5-10Al – 5-10Cu – 2Li
Li-Polymer	13-15Co – 20-30Al – 6-11Cu – 2Li

looking at the chemical variety and complexity of batteries provides the answer to the question: should they be recycled in a dedicated process or not?

The answer is normally yes. Separating all the metals contained in different batteries would require too much energy consumption and would generate high volumes of water and air to be cleaned up, so that it would never be profitable neither economically nor environmentally. The only reasonable way of recycling batteries is to keep the different chemistries separated from each other and use each of them as a real secondary source of metals to replace virgin ores. Indeed, batteries are much more concentrated than virgin metals ores and represent a non-negligible source of metals. In a few cases, however, recycling mixed batteries may be convenient (see the Citron's process and the Umicore's process in the following sub-sections).

So, it is worthwhile recycling batteries, not only for environmental reasons (decreasing the amount of waste in deposits, neutralizing potentially hazardous substances, limiting the extraction of fresh ores, using secondary materials more concentrated than ores and consequently using less energy and potentially polluting products for extraction, *etc.*) but also for financial reasons in some cases. However, to be fully efficient, recycling processes have to be well adapted and controlled.

Two major types of recycling processes exist: the “hydro” process and the “pyro” process.

Typically, hydro metallurgic processes employ a first mechanical step where batteries are crushed and sometimes their main constituents already separated (plastics, steel, *etc*). The crushing operation is followed by dissolution in different types of solutions (acids, bases or organic solvents) to dissolve some or most of the metals. The solution is then purified by selective extraction methods such as solvent extraction, ion exchange or precipitations at different pH to finally produce pure or semi-pure metals.

The economics of hydrometallurgical processes depend on the complexity of the input material, its purity and the valorization of the output products. The key issue is to determine at which step the process should be stopped and the residue sold or disposed of.

Indeed, the production of pure products needs a number of steps to eliminate or reduce the impurities that would otherwise lower the value of the products or even make them worthless. All these steps make the whole process generally very complex to manage and expensive, also in view of such necessary operations as cleaning of the polluted water, gas extraction and treatment, *etc*.

Pyrometallurgy is the second large category of recycling processes. In that case, a treatment at high temperature is applied to the waste and a molten – or non-molten, depending on the treatment temperature – metal-containing phase is produced. A clear drawback of this technology is the energy consumption for melting out the batteries, and the potential gas emissions and pollutions from metal vapors if the gas outlet is not well monitored. The battery itself due to its high plastic content generally provides part of the energy required for melting the batteries. Finally, pyro processes have the advantage of being generally much more flexible than hydro processes and can accept not-well-sorted batteries, assuming that their gas cleaning system is suitable, which is the case of most recycling plants.

Both processes can generally be used for all battery types and it is the objective of the following sub-sections to present and discuss these processes per battery chemistry.

14.7.1. The Recycling of Mixed Batteries

As mentioned earlier, everything tends to support the sorting of collected end-of-life batteries into the existing chemistries. By doing so, the recycling is highly facilitated and recovery can proceed much faster.

However, in some cases batteries are not sorted. It could be because they are too old to be recognized clearly or too dangerous to handle. In that case, they have to be recycled in a process able to accept mixed batteries.

A well-known company able to handle that type of mixed batteries is Citron in France. Citron has developed a new recycling process: the Oxyreducer™ process.

A new plant using the Oxyreducer™ process was put into operation in September 1999. The main characteristic of this process is the chemical reduction of metal oxides and hydroxides in the solid phase and the selective oxidation of metal vapors and organic components in the gas phase. The process outputs are metal concentrates that are sold to the metal industry according to their composition.

In the furnace (see Figure 14.9), the organic components are pyrolyzed. The resulting CO is oxidized to CO_2 in the gaseous phase before leaving the furnace. Because of its high CO composition, the battery bed is in a reducing

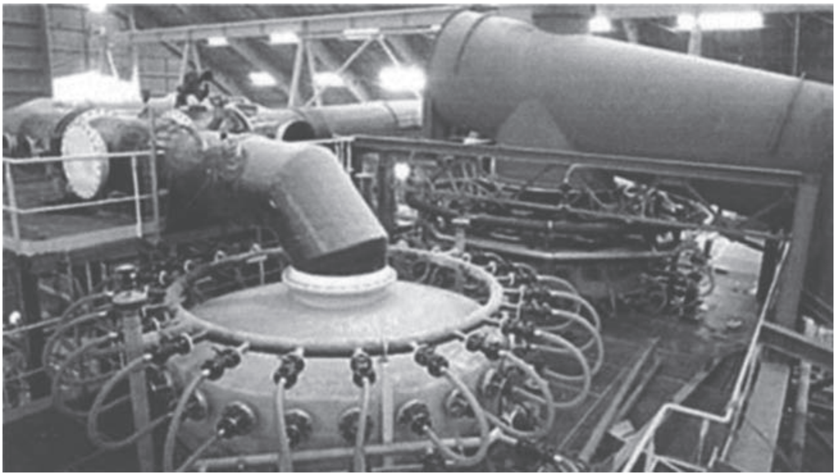

Figure 14.9. The Oxyreducer™ furnace at Citron.

atmosphere, so that the metal oxides and hydroxides can be reduced. The metals with high vapor pressure, notably zinc, lead, cadmium and mercury, are vaporized. In the gaseous phase they are re-oxydized into fine solid particles (except the mercury) before leaving the Oxyreducer™ and are collected in the gravity chamber. A large part of the salts is also vaporized.

Mercury is vaporized and separated from zinc in the gravity chamber, then is washed out in the gas cleaning system generating a mercury sludge, further treated in a mercury-distilling unit.

The exhaust gas is further cleaned in a classical gas cleaning installation including two quenchers in series and a special mercury recovery system. The wastewater is cleaned in a state-of-the-art treatment system, which allows the water to be recycled 50 times, thus significantly reducing water consumption. All sludge from the wastewater treatment system is recycled in the plant.

By this process, most of the battery components can be recycled:

- Organic materials

All organic materials are completely oxidized in the gas phase of the Oxyreducer™ at temperatures up to 1350°C, generating at the same time a significant amount of energy. The total retention time in the oxidizing atmosphere is more than 4 seconds, which guarantees a complete combustion. After passing through the dust retention system, the combustion products are cooled down to 55°C in a quencher.

- Mercury

The mercury is vaporized in the Oxyreducer™ in a metallic form and is washed out in two quenchers, electrostatic precipitator and basic scrubber. The metallic mercury is discharged directly out of the water pumps and the mercury containing sludges are treated in the mercury distillation unit. The remaining sludges are re-entered into the process. An active carbon filter takes out the final traces of mercury before the waste gas leaves the stack. The active carbon is also recycled in the Citron's plant.

- Metals with high vapor pressure: Zn, Cd, Pb

Zinc, cadmium and lead are evaporated and thereafter oxidized in the combustion area. Together with the carry over of other metals, these fine particles are settled out in the gravity chamber. The main product recovered is a zinc oxide concentrate that can be valorized in other zinc recyclers.

- Metals with low vapor pressure: Fe, Mn, Ni, Cr, Co and Cu

Due to their low vapor pressure, these metals are not easily evaporated. They are not affected by the working temperature, which remains below 1200°C and are simply discharged in their solid form. The manganese oxide contained in alkaline batteries is a very fine powder that can be separated from the other metals by screening. The remaining metals are sold as ferrous scraps to the steel industry.

- Refractory elements: Si, Al, Mg

These elements are also not affected by the treatment at this temperature and are mostly found in the ferrous scrap fraction – only a small fraction being recovered in the gas cleaning installation due to carry over. They will follow the iron scraps and will be transformed into slag in the steel works.

- Salts and electrolytes

They are evaporated during thermal treatment and washed out in the gas cleaning system. Salts are reduced mainly into NaCl and KCl and leave the plant in controlled concentrations with the cleaned wastewater.

14.7.2. The Recycling of Primary Batteries Containing Mercury

Even if phased out several years ago in most of the world, still some quantities of alkaline or button cells containing Hg are collected. These batteries have to be treated in specialized installations so that the mercury can be effectively recovered.

Generally, the process consists in heating up the batteries (often mixed with other Hg-containing wastes) so that mercury is evaporated (at a temperature typically between 350°C and 650°C, depending on the working pressure: the process may be done under vacuum). The mercury is then condensed and distilled to produce pure metal. The solid residue - generally mostly composed of stainless steel - can be further processed or directly sold to the steel industry. To avoid any release of mercury into the air, it is mandatory

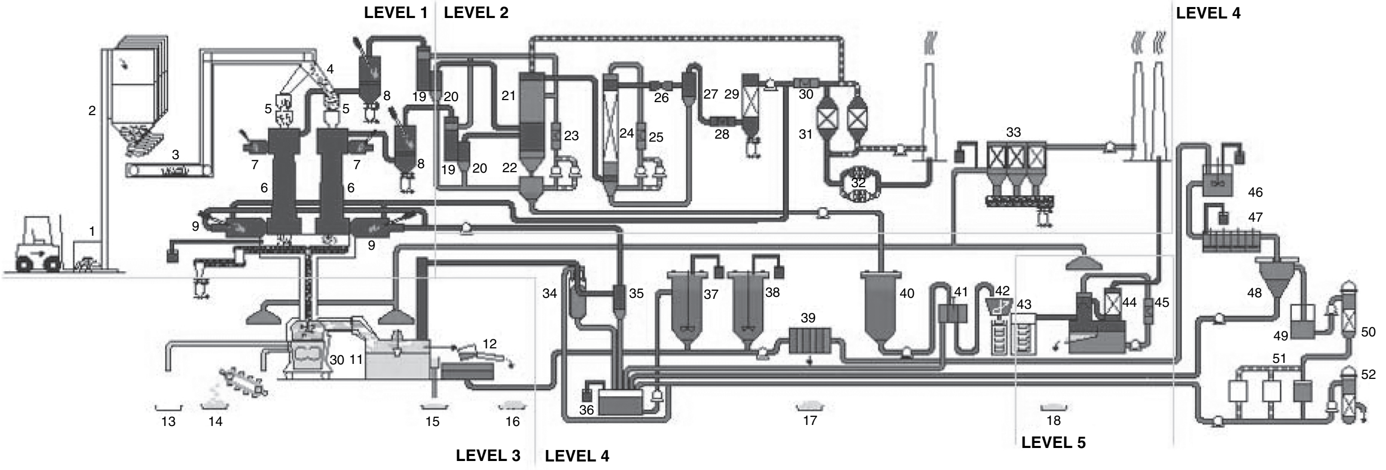

Feeder

1 Paliet Elevator
2 Battery- and Waste Bins
3 Bucket Elevator
4 Switch Point

Furnace Complex

5 Shaft Furnace Feed Valve
6 Shaft Furnace
7 Pre Heater
8 Incinerator
9 Hot Gas Generator
10 Induction Melting Furnace
11 Zinc Condenser
12 Zinc Dust Scrubber

Products

13 Slag
14 Ferromanganese
15 Zinc
16 Zinc
17 Zincoxide
18 Mercury

Exhaust Gas Treatment

19 Quencher
20 Mist Eliminator
21 Acid Scrubber
22 Acid Butter
23 Chillier
24 Packed Column
25 Chillier
26 Venturi
27 Mist Eliminator
28 Exhaust Gas Heater
29 Bag Filter
30 Chillier
31 Activated Carbon Filter
32 HEPA-Filter
33 Bag Filter

Waste Water Treatment I

34 Basic Scrubber
35 Basic Mist Eliminator
36 Zinc Dust Slurry Tank
37 Buffer Tank
38 Buffer Tank
39 Filter Press
40 Buffer Tank
41 Acidic Centrifuge
42 Slurry Collector

Mercury Recovery

43 Hg Distillation Furnace
44 Hg Condenser
45 Chillier

Waste Water Treatment II

46 Reactor
47 Reactor
48 Callow Cone
49 Waste Water Buffer Tank
50 Sand Filter
51 Waste Water Storage Tank
52 Activated Carbon Filter

adding a special active carbon filter to the exhaust gas cleaning system.

Some companies like Batrec (Switzerland), NQR (Nordische Quecksilber-Rückgewinnung GmbH, Germany) or GMR (Gesellschaft für Metallrecycling GmbH, Germany) are specialized in the treatment of Hg-containing waste and need a special authorization from the environmental authorities to continue their activity. Batrec is using a simple vertical furnace where batteries are heated above 350°C (Figure 14.10). The produced gases are collected and mercury is distilled to produce metal with a purity >99.9%.

In 2002, GMR introduced a new vacuum recycling plant for the de-mercurization of residues and naturally radioactive slurries containing mercury taken from the natural gas industry. The plant provides dust-free treatment of these waste products through the entire process and works in charging operations with a capacity of approximately 1 metric ton/day. The de-mercurization takes place in a vacuum-sealed, double-wall heated mixer, using thermal oil with a maximum temperature of 340°C as the heating medium. For dust separation, a highly efficient vapor filter is used. As the plant has been designed for mobility, clients can also operate it locally. In Figure 14.11, a view of the GMR's furnaces is presented.

Separate recovery of water and contaminated samples (hydrocarbons/mercury) is made possible by a fractional distillation. Cooling/conditioning of the de-mercurized residue then takes place in an integrated cooling mixer connected via vacuum to the heating mixer. For the withdrawal of the mineral residues, a discharge screw is used. The intensive mixing during distillation guarantees a very good energy exchange and allows energy saving.

The company Mercury Boys Manufacture (MBM, France) has also developed a process for the recycling of Hg-containing batteries and button cells. Cells and batteries are crushed under liquid nitrogen: at this low temperature, no reaction or explosion can occur. The residue is then sorted by

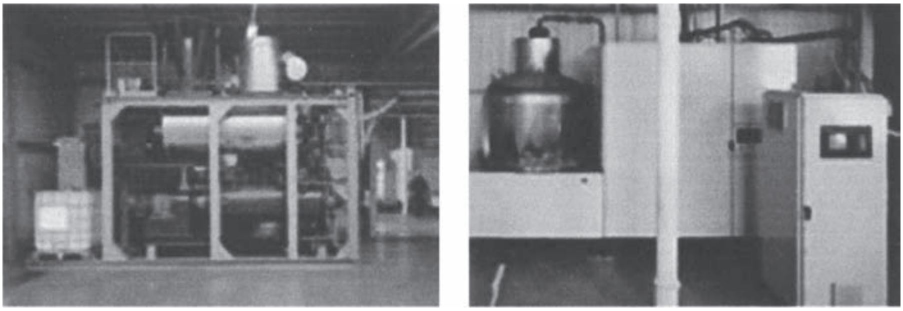

Figure 14.11. Furnaces installed at GMR in Leipzig, Germany.

particle size to produce a mercury/zinc and a mix steel/plastics fraction. The mercury/zinc fraction is then filtered and heated up to evaporate the mercury. The residual part is simply an Hg-free zinc metal scrap. In the other fraction, steel is removed by magnetic separation and can be sent to the steel makers.

14.7.3. The Recycling of Zinc-Carbon and Alkaline-Manganese Primary Batteries

The major constituents of these batteries are zinc, carbon, iron and manganese. However, it is very important to check the presence of mercury, as in the past it was added to limit zinc corrosion. In the 1990s, Hg has been phased out and today very little quantities of these Hg-containing batteries are found in the collection bins. In that case, their recycling should be performed in a dedicated recycling operation (quite often with pyrometallurgy) so that Hg can be recovered properly (see previous sub-section).

Assuming that the collected batteries are Hg-free, still many of them end up in a non-dedicated recycling industry: the steel industry. By re-melting steel scraps (automotive, construction, containers, *etc.*) in large electric arc furnaces (EAF), the steel industry is one of the largest recyclers in the world and is operating on a very large scale (typically more than 500,000 tons/y per plant).

EAF is the main furnace type for the electric production of steel. The primary application of the EAF is re-melting of steel scraps, but it can be charged with limited amounts of iron scraps, pig iron, and direct reduced iron. About 40% of the total steel produced in the U.S. comes from EAFs in operations called mini-mills. With 100% of the charge coming from scraps, it is difficult to control the purity and quality of the steel produced. Therefore, mini-mills centered on EAF steel production have concentrated on market segments where steel quality is not critical. Most of the metals present in the furnace are melted, whereas zinc is evaporated and captured in a bag house filter. A second step generally enables to fume again the EAF's dust to recover the zinc in its oxidized form and stabilize the rest of the residue. This is notably what is done at Scandust in Sweden or at ERAS in Norway with the new submerged plasma technology.

Zinc, steel, manganese and carbon represent ~65% by weight of alkaline batteries and can be successfully recovered or valorized in the steel industry. The remaining constituents (water, paper, bitumen, *etc.*) are burned in the EAF. Carbon is either directly burnt in the EAF to provide part of the necessary energy or incorporated into the steel liquid phase decreasing as such

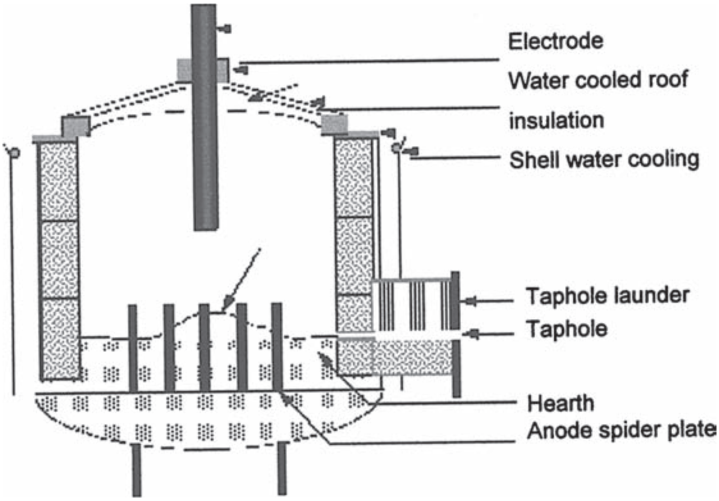

Figure 14.12. Typical Direct Current-transferred arc furnace.

Figure 14.13. Fe/Mn ingots produced at Valdi.

the melting temperature. The scheme of an EAF's furnace is shown in Figure 14.12.

Manganese dioxide is generally dissolved into the slag in the EAF operation, without any significant effect on its properties, and is used as aggregate for concrete.

Some dedicated recyclers try to cope with the increasing demand of environmentally sound solutions for waste in general and batteries in particular. They generally assure a much better control of the emissions into the air, as the batteries are not "diluted" into a bigger stream of other materials. This dilution significantly reduces the measurability of potentially hazardous substances released into the air. This cannot happen in a dedicated facility with a limited capacity, as is the case of Scandust in Sweden [7] or Valdi in France, a subsidiary of AFE Group.

VALDI is recycling various metals and by-products to produce some ferro/manganese and zinc oxides in their facility in Feurs (France). They also use an electric arc furnace and melt alkaline batteries in the presence of coke to reduce manganese oxide and recover it in the metallic phase. Batteries are charged into the furnace together with some fluxes (limestone, dolomite, sand) to produce a fluid inert slag, at the temperature of ~1500-1600°C, which can be further re-used in road construction. The other liquid phase produced, a ferro/ manganese alloy, has a purity not very high but sufficient to be valorized. It is generally cast into small (25 kg) or big (600 to 1000 kg) ingots, depending on their final destination (see Figure 14.13). The zinc is evaporated and further transformed into zinc oxide and recovered in the bag house filter. Such zinc oxide is a standard low-grade quality that can be sold to the zinc industry for

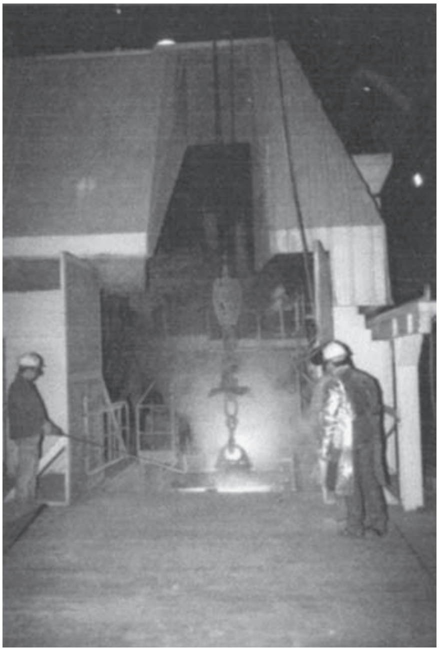

Figure 14.14. The electric arc furnace at Valdi.

further refining and transformation. The furnace used at Valdi is shown in Figure 14.14.

The Scandust process is different, as it uses a plasma gun to generate the energy for melting the metal and evaporating the zinc (Figure 14.15). The adequate mixture (containing batteries and slag formers) is injected into the furnace either directly by the plasma gun (in the powder form) or by top feeding. At regular intervals, metal and slag are tapped off and the metal (Fe/Ni/Cr) is cast into granules that are sent to the steelworks.

After the slag has been separated from the metal, it is cooled down and screened to recover the remaining small amounts of metal tapped with it. This slag can be used for road building purposes as a substitute for natural materials.

In the gas cleaning operation, the zinc-rich fraction is separated and then removed for further treatment in an external process where the zinc content is recovered. The remaining gas is re-circulated in the plasma generators via a compressor, used as a fuel for the dryer or fed into a district heating network.

Some companies, like Erachem in Belgium, use the hydrometallurgy to recycle the manganese and zinc fraction of primary batteries. Erachem is a chemical company specialized in the production of Mn-containing products. In their recycling process, batteries are shredded and milled so that a "black mass" containing most of the metals is produced. This mass contains zinc oxide

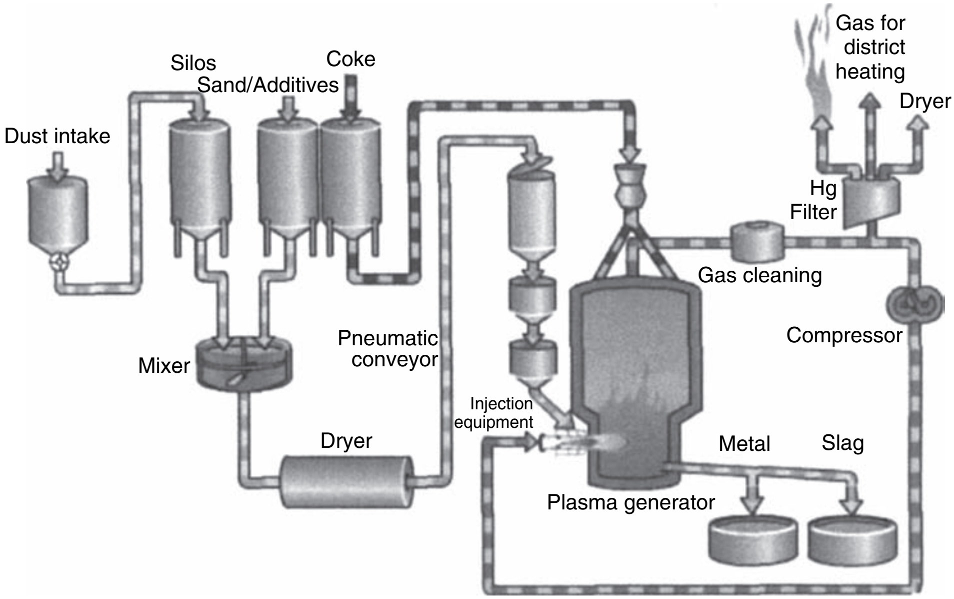

Figure 14.15. Scheme of the process of Scandust's installation.

and manganese oxides and is further purified by dissolution into sulfuric acid and selective precipitation. In this way, marketable zinc oxide and manganese oxides are produced. The negative fact is that all other fractions are not directly recovered by Erachem and have to be sent to a third party. The potential hazard connected to transporting shredded batteries from one company to another has to be taken into account.

14.7.4. The Recycling of Lithium Primary Batteries

Primary lithium batteries are probably the most potentially hazardous batteries that could be collected today if not well handled. Indeed, they contain metallic lithium, which is highly unstable in contact with moisture-containing environment or atmosphere. There have been many accidents involving these high-energy batteries during their entire life from production to recycling.

For this reason, the recycling of primary lithium batteries requires special equipments for transport, storage and final treatment. In particular, they are classified as "hazardous waste" for transport and should be transported under very strict conditions including a specific packaging.

In addition, lithium batteries do not contain many valuable products, this making their recycling not very interesting. Probably for this reason, there are very few companies able to treat lithium batteries and always at very negative values (between 1 and 4 Euro per kg, depending on the size and composition).

Lithium batteries can be categorized into several different types, this complicating their recycling. The most common and known are those having such cathodes as thionyl chloride, sulfur dioxide, sulfuryl chloride, manganese dioxide, carbon monofluoride or iron disulfide. All these products have potential hazards, so that the primary objective of recycling these batteries is clearly to control the end-of-life battery outputs from a safety point of view.

Two types of processes are possible. Citron in France applies an oxy-reduction process and can treat Li primary batteries by "diluting" them into the flow of other materials to be recycled. The oxy-reduction process is explained in details in Section 14.7.1.

The second type of process starts with battery crushing. Of course this operation should be done either under controlled atmosphere (like at Batrec, in Switzerland) or at very low temperature (at Toxco, in Canada, see recycling facility in Figure 14.16)) to avoid any uncontrolled Li oxidation.

The Toxco process is based on the principle that the kinetics of typical chemical reactions is halved when the temperature is decreased by 10 degrees.

Figure 14.16. Battery recycling facility at Toxco, Canada.

So, at the temperature of liquid nitrogen (-273°C) the oxidation reaction rate is only 1/250000th of the room temperature rate.

In their process, batteries are crushed in liquid argon or nitrogen so that the resulting materials are: the soluble components (*e.g.* Li), the combusting components that are either floating, sinking or remaining in suspension (paper, carbon, *etc.*) and the sinking heavy fraction (metals).

The dissolved components are processed to produce pure lithium carbonate. The metal fraction is washed up and sent to metal recovery installations according to its composition. The combustible fraction is filtered and sent to incineration.

In the Batrec process, illustrated in Figure 14.17, the crushing operation is performed at room temperature under inert atmosphere (*e.g.* nitrogen), so that no oxidation reaction is possible. The next operation is “neutralization” or “controlled oxidation” of metallic lithium by adding a controlled amount of an oxygen-containing reactant (*e.g.* air or a carbonate). After neutralization of lithium (transformed into lithium oxide or lithium carbonate), the batteries are further crushed and the fractions separated by granulometry. The rest of the process is similar to that of Toxco.

14.7.5. The Recycling of Lead-Acid Batteries

Lead-Acid batteries have been the first ones benefiting by collection

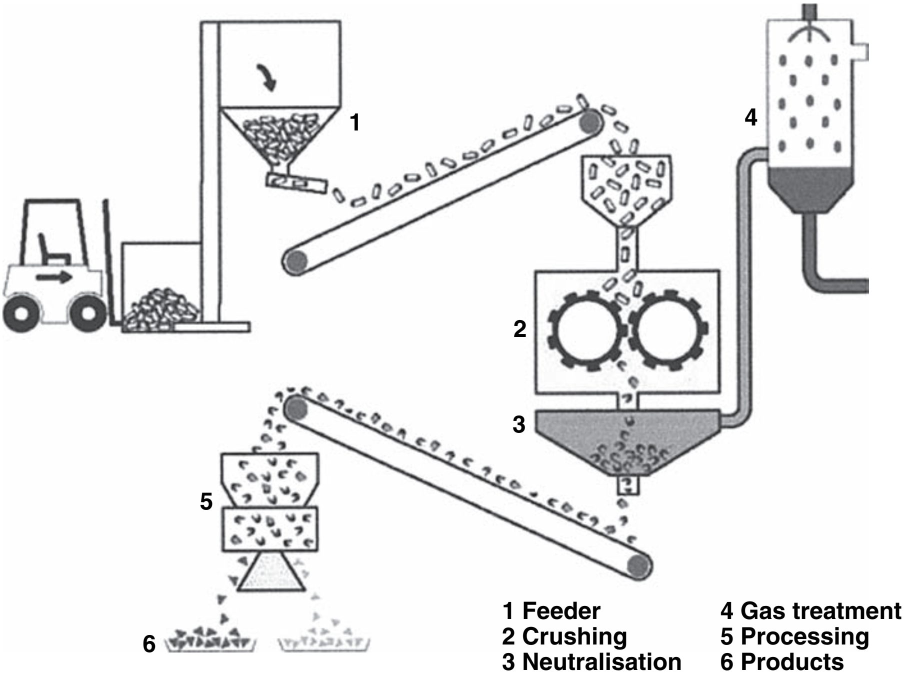

Figure 14.17. BATREC's process for recycling Li primary batteries.

and recycling schemes, mainly due to the demonstrated toxicity of lead. This is probably the reason why the legislator has allowed an exception on the use of this battery system whereas lead has been prohibited in most of the other batteries and products. Indeed, manufacturers were able to demonstrate a real closed loop solution, where 80-95% of used car batteries are collected and recycled at the end of their life (with collection figures even reaching ~100% in industrial countries). In addition, no real alternative of this chemical system exists for automotive batteries.

More than 70% of the lead produced in the world (out of ~6 billion tons) is used for battery applications and ~65% is originated from recycled lead. Today, every industrialized country has one or more systems to collect and recycle lead-acid batteries. Quite often, collection systems start at the repair shop or garage and end up at the recycling plant. After that, batteries are sent to a dedicated center where they are emptied so that sulfuric acid can be recovered; the acid is frequently further purified and re-used. The second step can be either removal of the plastic housings or direct smelting. In the first case,

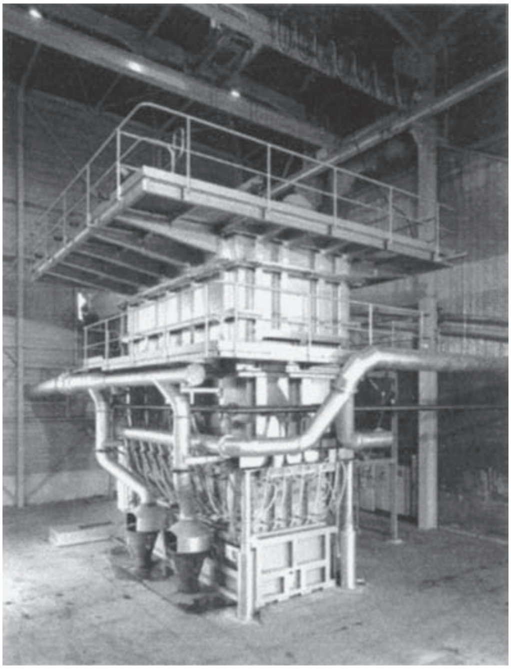

Figure 14.18. Blast furnace at Campine, Belgium.

plastic housings are removed and washed carefully to avoid any trace of Pb, so that they can be easily re-used, often for the same purpose: production of new lead-acid batteries.

In the second case, emptied batteries are melted in different types of furnaces, the most popular one being a kind of blast furnace. Treating lead in a pyrometallurgic process is advantageous, as it does not require a high amount of energy to melt (melting point: 327.5°C).

In general, each country has a sufficient capacity to recycle its own recovered batteries. This is mainly due to the high transport costs of lead-acid batteries (hazardous and very heavy) compared to the intrinsic metal value. The Belgian company Campine, for example, has a capacity of 40,000 tons per year in its blast furnace shown in Figure 14.18. The plastic provides in that case the energy necessary to melt the metal. A lead matte (PbS) is formed. Part of the matte is further treated in house to produce a Pb-rich valuable product (see Pb ingots in Figure 14.19) and part of it is sent to other smelters able to receive Pb-containing products, such as the Precious Metals recycling facility of Umicore in Hoboken (near Antwerp, Belgium). Lead is there fully recovered and sold as pure lead on the market.

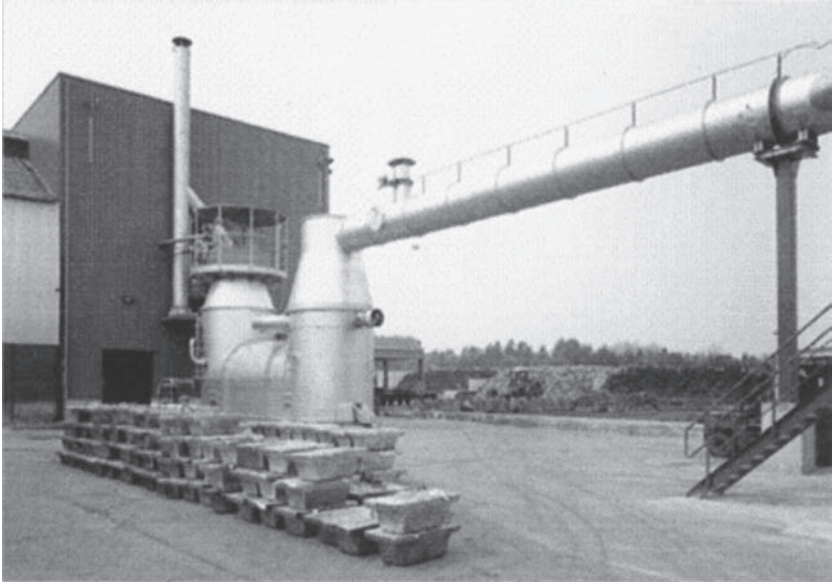

Figure 14.19. Gas cleaning installation and lead ingots at Campine, Belgium.

14.7.6. The Recycling of NiCd Batteries

Together with lead-acid batteries, NiCd batteries are those of greater concern for environment and human health, thus requiring an appropriate legislation. Indeed, they contain ~20-30% in weight of cadmium, a dangerous heavy metal, and so are under very strong pressure especially in the European Union. Indeed, in the new directive on battery recycling, Cd is banned. Industries specialized in NiCd batteries have tried for several years to establish closed loop collection and recycling systems, to prove that these batteries are not hazardous because every single battery put on the market is collected after use and properly recycled.

The new industrial market of NiCd batteries, *e.g.* the first generation of electric vehicles, ensures a complete collection of used batteries, as OEMs remain the owners of the batteries that are just leased by the consumer. With efficient collection and recycling schemes, no NiCd would end up in uncontrolled deposits or incineration plants and no damage to the environment could be produced. In addition, some OEMs are putting their own collection systems in place, so that all end-of-life batteries can be collected and recycled as an extra service provided to their customers (see the example of Saft previously detailed).

Europe will probably ban the use of Cd with a long list of exemptions, representing ~70% of the today's total market of NiCd, so that a big amount of these batteries will continue to be put on the market. Furthermore, the collection of batteries cannot reach the 100% level: even if most of the industrial companies have put in place their collection and recycling scheme, they cannot oblige each single battery user to bring back his battery to a defined and dedicated location. Industrial batteries are very well collected and recycled, recycling facilities are well established and monitored, but many portable batteries are today not yet collected, making probably a non negligible amount of NiCd batteries ending up in uncontrolled or unwished areas.

Anyway, most collection schemes existing today have started some years ago specially for the collection of NiCd batteries. This is particularly the case of countries like the USA, Japan, Sweden and France

In the today's existing collection schemes within Europe, NiCd batteries represent the second biggest volume collected after primary zinc-carbon and alkaline batteries. As an example, the GRS Batterien foundation is collecting each year in Germany ~1000 tons of NiCd batteries (*vs.* ~10000 metric tons of zinc-carbon + alkaline batteries).

Today, there are few but well established NiCd recycling facilities worldwide whose cumulative capacity is sufficient to recycle all collected volumes. All existing processes are based on pyrometallurgy and on the evaporation/distillation of Cd, which is usually evaporated in a furnace, oxidized and then captured in a bag house filter. The main difficulty is capturing Cd particles in the off-gas system without releasing any particle into the ambient.

Another slightly different pyro process consists in evaporating the cadmium, and, instead of oxidizing it in a post combustion-type chamber, keeping it out of the air (closed furnace or furnace under vacuum) so that pure Cd can be condensed. In that case, a 99%+ pure Cd metal can be produced, which is often further refined for final applications. These furnaces are operated in a closed circuit and at different vapor pressures, either atmospheric (but closed) or under low/high vacuum. The difference among all these processes is of course the heating temperature needed to evaporate Cd, but no big differences exist in terms of energetic efficiency or energy consumption.

Generally, industrial batteries have to be dismantled and/or crushed before recycling at high temperature. Some zinc-producing companies recycle NiCd batteries too or have done so in the past. Indeed, cadmium is a by-product of zinc and all companies producing zinc from ores have to cope with Cd residues in their process. So, their installations are endowed with all necessary equipments to capture Cd vapors and condense them, sometimes with a final purification step. Therefore, recycling NiCd batteries may be an important business for these companies, even if not their core business.

Today, in Europe only three companies are industrially recycling NiCd batteries, for a total recycling capacity of ~10,000 tons, the biggest being the Société Nouvelle d'Affinage des Métaux (SNAM) in France. All of them (SNAM, ACCUREC in Germany and Saft/Nife in Sweden) are using a pyro process and are dedicated to the recycling of used batteries. However, Saft has also developed a hydro process (and is probably the only one in the world using this technology) to recycle their own production scraps and sludges from the NiCd manufacturing process and end-of-life batteries. The battery recycling plant of Saft AB in Oskarsham, Sweden, has an annual capacity of 120 tons of cadmium, corresponding to 2000 tons of batteries. The flowsheet of NiCd recycling at Saft is shown in Figure 14.20.

Industrial cells (vented, prismatic cells) are dismantled manually. The negative plates with 20-25% Cd are washed and dried, charged into a crucible and heated with coke to 900°C in an electric furnace for 24 hours. Cd is distilled off and the fluid metal is dripped into water where it forms small metallic pellets.

Sealed NiCd batteries are subjected to a pyrolysis step prior to distillation, in which the polymer compounds are decomposed at 400°C. The pyrolysis gas is completely combusted, washed and filtered before being emitted to the atmosphere. The generated heat is used for another process. The recovered cadmium (purity grade >99.95%) is used for production of new industrial batteries. The plates and the distillation residues are sold to the steel industry, where the nickel-containing material is used for stainless steel production. Other battery components of dismantled cells, containers, lids and separators, are washed free of nickel and cadmium.

The process water is treated in the wastewater treatment plant, where the battery recycling contributes with 0.4 kg/year to the cadmium emission. All exhaust air passes through double filters, securing an emission of cadmium less than 0.5 kg/year.

In the rest of the world, there are very few companies recycling NiCd batteries: INMETCO in the USA, Kobar in Korea, Toho Zinc, Kansai Catalyst and Nippon Recycle Center in Japan. The recycling capacities of the major companies are presented in Table 14.4.

Let us review their processes in more detail.

Kansai and Toho Zinc treat the batteries in a rotary kiln recovering Cd in its oxidized form in the gas. The fraction remaining in the furnace is a Ni/Fe alloy residue that can be further processed in the stainless steel industry. Cd can be further purified by reduction of CdO and distillation.

At Nippon Recycle Center, NiCd batteries are first crushed and the steel and/or plastic casings are separated from the rest of the batteries. The casings are sold to the steel industry (stainless steel casing) or burnt or land-filled (plastic casing). The remaining part of the batteries is thermally treated to

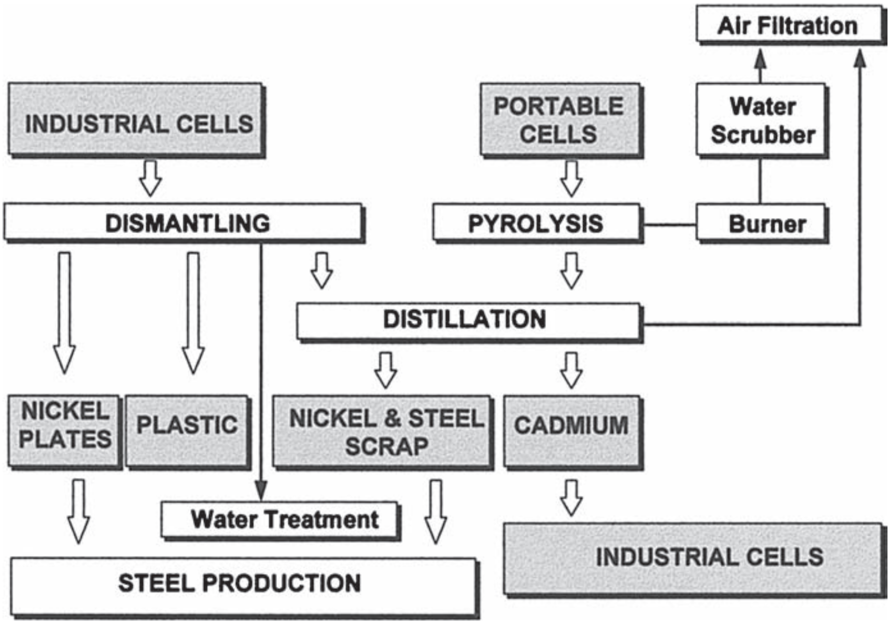

Figure 14.20. NiCd recycling flowsheet at Saft, Sweden.

evaporate Cd, which is then condensed as CdO.

At the SNAM facility, batteries are either crushed to separate the plastic casing (as done at Nippon Recycle Center) or pyrolized. In this case, plastics are simply burnt out in a rotating furnace together with the electrolyte that is evaporated. At the end of this first operation, a mixture of Ni, Fe and Cd remains. Cd is then separated from the rest by thermal treatment and is further refined to produce high purity metal, mainly used again for NiCd applications.

Table 14.4. Main NiCd recyclers and their recycling capacities.

Company	**Country**	**Capacity in Tons/year**
Inmetco	USA	3500
Snam	France	5500
Saft	Sweden	1500
Accurec	Germany	1000
Kobar	Korea	3000
Toho Zinc	Japan	1700
Mitsui Mining	Japan	1800
Total		18 000

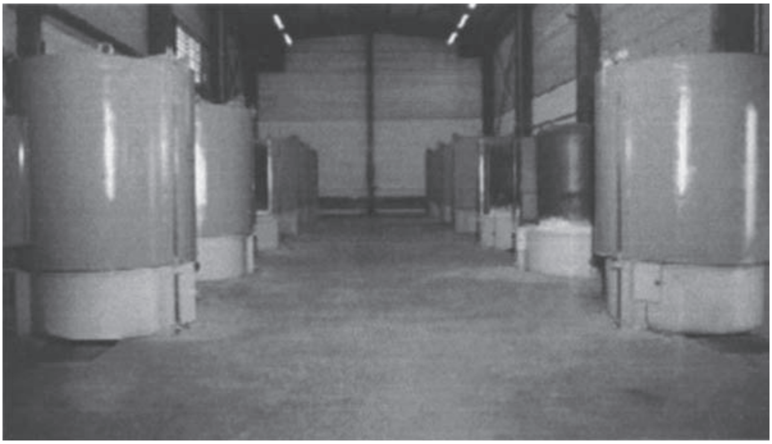

Figure 14.21. Distillation furnaces at SNAM, France.

The residual Ni/Fe part is sold to the steel industry. SNAM's furnaces are shown in Figure 14.21.

The Accurec process is based on the vacuum thermal recycling technology (recycling durch vakuumdestillation: RVD) developed together with the company ALD Vacuum Technology GmbH. Generally, industrial batteries are first manually dismantled and electrolyte removed. Next step is the treatment of all parts containing cadmium in the vacuum furnace shown in Figure 14.22. This process has the advantage of avoiding any contamination of external air with Cd, as the whole installation is working under vacuum. Leakage, if any, would bring air into the system and would never allow a gas release to the outside. This is a process very well suited for the treatment of NiCd batteries and can be qualified as "zero emission" process. Unfortunately, operational costs are somewhat higher than for conventional processes, even if it is probably worthwhile to pay some more and be sure that the environment is preserved. Based on costs, the use of this vacuum process for treating other types of battery is not recommended.

Inmetco is not what we could call a "dedicated" recycler but recycles all secondary materials containing Fe, Ni, Co, Cr and Mo. They have a very flexible process able to accept many different types of scraps. The main part of their production is done via a first reducing step where all metal oxides are reduced by cokes to their metallic phases, followed by a melting operation and production of a Fe/Ni/Co/Mo alloy. This alloy is then shipped to the stainless steel industry for special steel qualities. Apart from that, they produce a slag from their smelting operation, which often contains small quantities of metals and cannot always be sold. In this process they can treat NiCd batteries (from

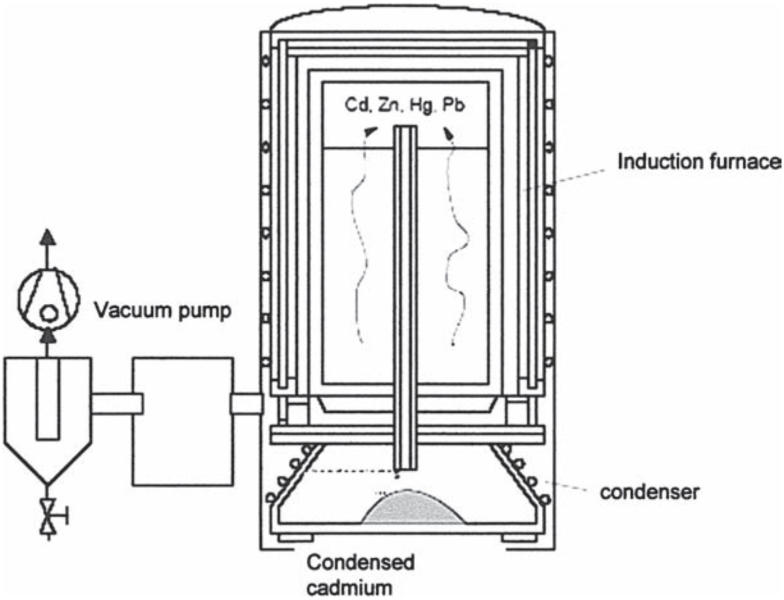

Figure 14.22. Schematic view of the RVD furnace at Accurec, Germany.

portable or industrial appliances) either first calcined (once the electrolyte is removed) or not. If no pre-calcination is performed, they have to cope with the potential production of not-fully combusted organic materials, which can generate dioxins and/or furans.

In addition, they also have a semi-dedicated installation for treating NiCd batteries and more generally Cd-containing wastes. Here again, a pre-treatment can be made for removing the plastic and electrolyte fraction. After that, Cd is evaporated and distilled. The final products are pure Cd and Fe/Ni fractions for the steel industry. Inmetco has authorization to treat up to 10,000 tons of NiCd batteries and the majority of NiCd collected on the American continent is treated there, mainly due to their close cooperation with RBRC (Rechargeable Batteries Recycling Corporation).

14.7.7. The Recycling of NiMH Batteries

Nickel Metal Hydride batteries appeared only in 1990 on the market. Their general analytical composition makes them suitable for stainless steel secondary applications and some companies are still looking for different recycling solutions. Volumes sold each year remain limited and will probably not increase much due to the competition with Li-ion and Li-polymer technologies. The only possible way to increasing the volumes is the development of hybrid electric vehicles (HEV), if Li-ion is not chosen for this application.

NiMH batteries do not contain hazardous substances and are quite easy to handle. So, just a few companies are really proposing an industrial solution for their recycling and none of them is dedicated to this type of product only.

Nickel primary smelters and producers

Apart from the stainless steel industry, some big Ni smelters are potentially interested in recycling NiMH batteries, if this does not perturb too much their process. The main problem is that these smelters normally treat ores free of organic materials, so their process is not equipped with the required gas cleaning installations for treating organic-containing (plastics) products. However, until now, no real increase in the production of volatile organic compounds (like dioxins or furans) could be detected in the off gas of these installations, as the amount of batteries or organic-bearing products is very low compared to the huge volumes of ores processed. Organic volatile products (inevitably formed during the thermal treatment of NiMH batteries) are just simply diluted into the rest of the process gas.

Another problem for these smelters not dedicated to recycling batteries is the size of industrial batteries. They generally cannot put the whole battery directly into their process and have to first dismantle it, which is definitely not their core business and even out of their scope. This makes them generally refuse industrial batteries.

In the case of Ni/Co smelters, the recycling rate can be calculated as shown in Table 14.5.

Pre-processors for steel industry

Some companies are also treating NiMH batteries for the steel industry. This is the case of Redux GmbH in Germany where a treatment facility with a capacity of 2000 tons per year is installed. Batteries are opened under controlled atmosphere to remove the potential hydrogen. Plastic is then removed from the resulting product so that a mix mainly composed of Ni and Fe can be produced and further valorized in the steel industry. This Redux process can be seen as a transition between full hydro process and full pyro process as here just plastics are removed in a first stage before smelting.

Umicore (Olen, Belgium; Hofors, Sweden)

The advantage of the pyro process developed by Umicore (Belgium) is that all potential hazards have been taken into account during the design of the

Table 14.5. Recycling rate of NiMH batteries by smelting.

Constituent	Weight %	Ending up in/as	%Recycled	%Recovered
Steel casing	20	Alloy	100	
Ni + Co	35	Alloy	100	
Plastics*	15	Reducing agent Energy provider	0 0	30 70
Electrolyte	15	Evaporated	0	0
Rare earths**	15	Slag	0	0
TOTAL	**100**		**55**	**15**

* Most of the plastics are used as energy sources, as the process is performed at high partial pressure of oxygen and consequently in a highly oxidizing ambient. They replace other energy sources as cokes, fuel or gas.

** All the rare earths end up in the slag. The slag in these processes cannot be valorized and is often landfilled in open mines from the deposit of the companies.

process in 2000-2003. At Umicore, batteries are directly introduced into a furnace (after partial dismantling, if needed, of big batteries that are divided into their modules) and all metals melted out into a single metallic phase and tapped at a temperature around 1500°C. Due to the particular smelting conditions (strong reducing atmosphere) and the type of furnace used, all plastics are used as reducing agents so that nothing is added to reduce $Ni(OH)_2$. The produced alloy is then atomized and sent to a state-of-the-art Ni/Co refining installation.

The recycling rate can be calculated as shown in Table 14.6.

This Umicore process is the only industrial pyro process dedicated to the recycling of batteries. It can also treat Li-ion batteries (see specific section for details) and creates a closed loop for Ni in rechargeable batteries. It has a total capacity of ~4000 tons of batteries per year and can treat any battery size.

Table 14.6. Recycling rate of NiMH batteries by the Umicore process.

Constituent	Weight %	Ending up in/as	%Recycled	%Recovered
Steel casing	20	Alloy	100	
Ni + Co	35	Alloy	100	
Plastics*	15	Reducing agent Energy provider	50 0	0 50
Electrolyte	15	Evaporated	0	0
Rare earths**	15	Slag	100	0
TOTAL	**100**		77	7

* In this process, the partial pressure of oxygen is very low and most of the plastics are not burnt but used as reducing agents in the heart of the furnace

** All the rare earths end up in the slag. Due to the highly reducing ambient (low oxygen partial pressure) the slag is totally free of metals and can be re-used either in the steel or in the construction industry

14.7.8. The Recycling of Li-ion and Li-Polymer Batteries

The Li-ion technology with liquid electrolyte was introduced into the market in the early 1990s, while Li-polymer batteries using a polymeric electrolyte were introduced more recently. Being the technology so young, the volumes of end-of-life Li-ion batteries available on the market are relatively low. Furthermore, at present, the main market for these batteries is the consumer market (mobile phones, laptop computers, cameras, *etc.*), even if industrial applications are increasing. Portable electronic devices are often rapidly changed, so that a second market can develop: the devices are collected by specialized companies and marketed in other parts of the world. A second life is given to the equipment, including the battery, and most of the time this occurs in countries where nothing is done for end-of-life management of equipments, so that no battery is finally collected. As an example, the European Battery Recycling Association (EBRA) reported a total collection in Europe of less than 200 tons for the years 2003 and 2004 [8].

Anyway, these collected batteries have to be recycled in an environmentally sound manner, and this is done today at the industrial scale by just two companies: one Ni/Co mining industry (Falconbridge, Canada) and one with a dedicated industrial closed loop process for batteries (Umicore, Belgium).

Hydro-metallurgy in laboratory or pilot scale operations

Apart from these two industrial solutions, different lab or pilot scale processes have been developed, all based on hydro-metallurgy. These processes were originally developed for the potentially dangerous primary lithium batteries, but secondary batteries are treated as well with the same processes.

In these lab-scale installations, batteries are first crushed in an inert atmosphere (CO_2 or N_2) or at low temperature (liquid N_2) and then sieved. Several fractions are produced according to the average particle size: plastics, steel casing, aluminum + copper and fines with most of the $LiCoO_2$, graphite powder and other fine materials. Theoretically, all these fractions can be valorized if pure enough, which is rarely the case (see "Recycling rate: what does it mean?"). With these technologies – only existing on a pilot scale, mainly due to their low economic efficiency – the recycling rate can be calculated as shown in Table 14.7.

Falconbridge (Sudbury, Canada)

An industrial solution is proposed by a Ni/Co/Cu primary producer. Falconbridge – recently merged with Noranda – is primarily a Ni mining

Table 14.7. Recycling rate of Li-ion batteries in hydro-metallurgical lab scale processes.

Constituent	Weight %	Ending up in/as	%Recycled	%Recovered
Steel casing	20	Steel	100	
$LiCoO_2$	20	Fine fraction*	60	
Plastics	15	Plastic fraction: land-filled or incinerated	0	100
Electrolyte	10	Lost in water, evaporated or partially lost in all fractions	0	0
Graphite**	10	Fine fraction*	0	0
Aluminum	15	Al fraction Fine fraction	98 0	0 2
Copper foil***	10	Al fraction Fine fraction	50	50
TOTAL	**100**		**51**	**23**

*The only valuable product of the fine fraction is Co. This fraction is sent to Co refiners. However, other battery constituents like Al may be present, which can harm the refining process and need a first pyrometallurgic treatment. $LiCoO_2$ contain 60 wt% Co.

** Graphite is present as a very fine powder, mixed with $LiCoO_2$ at the cathode. This powder ends up in the fine fraction, and perturbs Co refining, so imposing a pyrometallurgic step. In any case, graphite is not valorized as such and cannot be considered as recycled.

*** The copper foil is partially crushed and ends up partly in the Al fraction and partly in the fine fraction. In the first case, Al goes to the Al industry, but Cu is lost. In the second case, it is recovered in the Co refining process. It is assumed that 50% of Cu goes to the Al fraction.

industry and is the fourth largest Ni producer in the world. It has several Ni and Cu mines where Ni and Cu concentrates are produced, as is done in Sudbury (Canada): the concentrates are then smelted.

It should be noted that only small rechargeable batteries (from portable devices) are recycled by Falconbridge, not industrial or large-size batteries. Indeed, such batteries should be dismantled prior to smelting and this is not feasible at Falconbridge.

The Sudbury smelter, shown in Figure 14.23, treats Ni-Cu concentrates from the Sudbury and Raglan mines and processes custom-feed materials. It is capable of producing 130,000 metric tonnes of Ni-Cu matte annually. The smelter's electric furnace converts the mineral concentrate into a high-grade matte containing Ni, Cu and Co. The smelted and granulated matte is sent to Quebec City, then shipped overseas to Nikkelverk, in Norway, for refining into pure metals.

In the particular case of batteries, Li-ion are incorporated either into the smelter or the converter. Parts of the plastics and carbon are used for providing the necessary energy to the process (and some as reducing agent, even if the process is more oxidizing than reducing). The organic volatile compounds inevitably formed during the thermal step are just diluted into the huge flow of

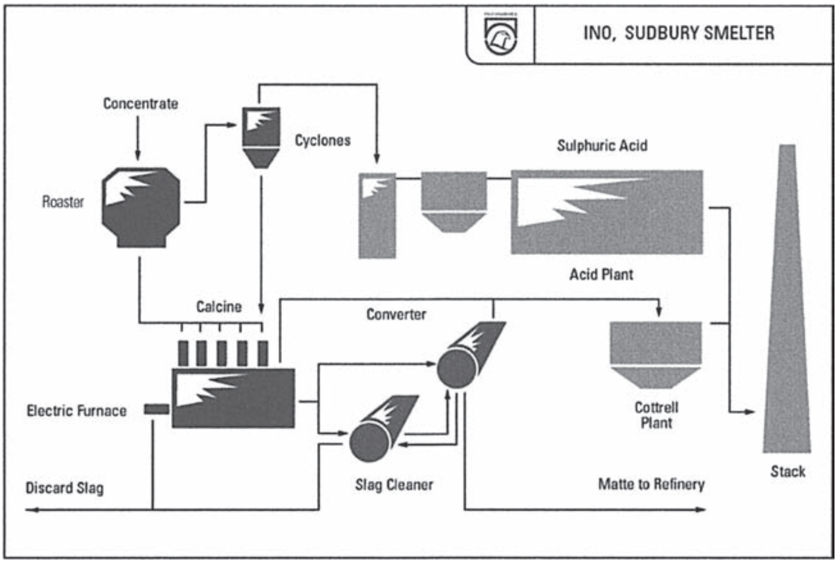

Figure 14.23. Falconbridge metallurgical operations in Sudbury.

exhaust gas and are not taken into account as their relative volume is negligible (they remain under the legal limit).

The converter gives rise to two products: a Ni/Co matte that is further granulated and a Ni/Co-rich slag that is further retreated in the first smelter, which is producing a purer slag, but still containing some potentially leachable amounts of Co and Ni. The management of this slag is performed internally and the slag is used to partially refill the mining areas under strict and special conditions, but cannot be sold as a product. This represents the main disadvantage of this process, especially when looking at the recycling efficiency.

The recycling rate can be calculated as shown in Table 14.8.

Umicore Val'Eas dedicated process (Olen, Belgium; Hofors, Sweden)

The second company recycling Li-ion and Li-polymer batteries is Umicore. They developed in 2000-2003 a new recycling concept, called Val'Eas®, proposing a really closed loop solution for rechargeable NiMH and Li-ion batteries, as well as a full service package comprising for instance the logistics support to the customer. The Umicore Val'Eas® process is the only industrial process really dedicated to these batteries and is not derived from processes previously used for other products. In addition, it can treat portable batteries as well as industrial batteries as such.

Table 14.8. Recycling rate of Li-ion batteries at Falconbridge.

Constituent	**Weight %**	**Ending up in/as**	**%Recycled**	**%Recovered**
Steel casing	20	Alloy	100	
$LiCoO_2$	20	Co in alloy Li in slag*	80	
Plastics**	15	Reducing agent Energy provider		30 70
Electrolyte	10	Evaporated	0	0
Graphite**	10	Reducing agent Energy provider	0	50 50
Aluminum	15	Slag	0	0
Copper foil***	10	Alloy	100	
TOTAL	**100**		**46**	**25**

*Lithium is easily oxidized and ends up in the slag, which is landfilled.

** The plastics are partly (30%) used as reducing agents in the pyro process to reduce the Co oxide into metallic Co, and partly (70%) as energy sources. The graphite powder is mixed with $LiCoO_2$ and less exposed to oxygen at the beginning of the process, so that it reacts differently from plastics and remains longer in the form of carbon. It can be assumed that is more used as reducing agent in the liquid bath itself than as energy provider above the bath. For the easiness of calculation (and corresponding on what is currently stated by the European legislation), it is assumed that all plastics are "recovered" and not "recycled"

*** All the copper foil ends up in the alloy and is recycled in the Co refining process.

Umicore has been able to develop a process that can cope with any evolution of future materials and designs of batteries. Umicore is also one of the two major players in the production of materials for Li-ion positive electrodes ($LiCoO_2$ or other mixed-metal materials).

The aim of the Val'Eas® closed-loop process, shown in Figure 14.24, is to provide a simple and flexible solution for treating end-of-life batteries and production scraps. Batteries are directly introduced into a furnace without any hazardous pre-processing, *e.g.* crushing or dismantling. The increase in temperature and reducing conditions are closely managed so that no explosion can occur and the totality of Co, Ni and steel is recovered in the metallic phase. This metallic phase is then atomized into a very fine powder with an average particle size of 200 μm and further refined in the Co/Ni refinery already managed by Umicore for several decades in one of its Belgian sites.

Pure Co and Ni compounds are thus produced and further transformed into hydroxide or carbonate for new battery applications (see Figure 14.24). In short, end-of-life batteries are transformed into new batteries.

The other product formed during the first smelting step is a pure inert slag. By managing the smelting conditions, no metal can be found in the slag, which can be re-used in construction, concrete or even as raw material in replacement of pure limestone and silica in the special steel industry.

Umicore has also developed a new gas cleaning system to cope with

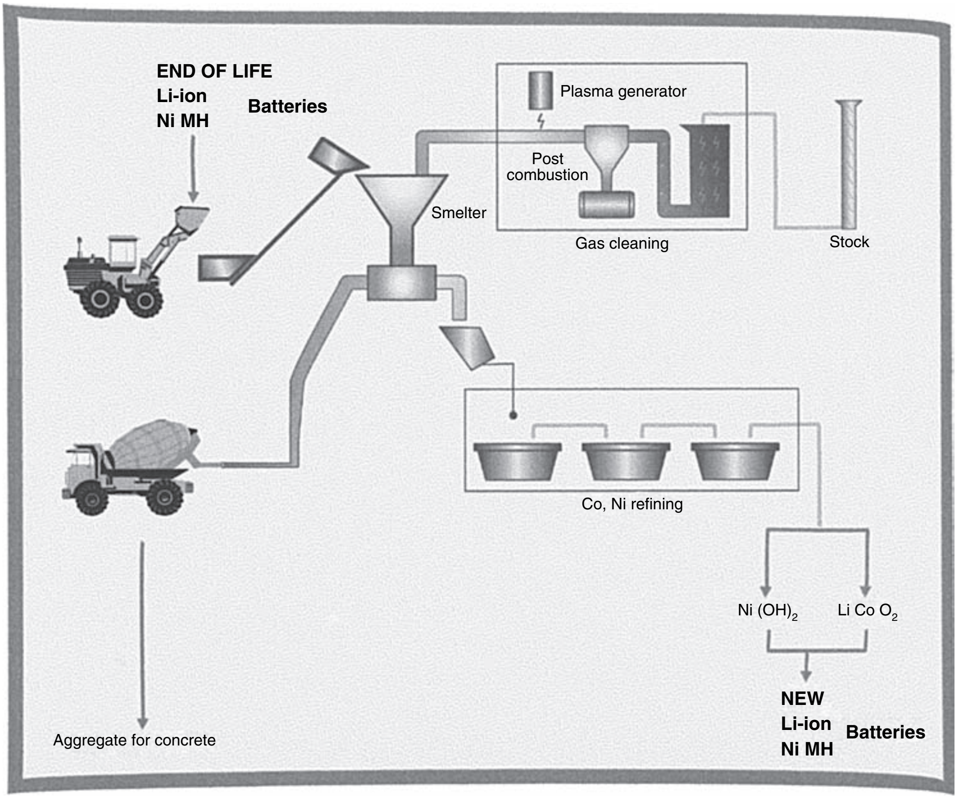

Figure 14.24. Pictorial view of Val'Eas® process for battery recycling at Umicore.

any hazardous gas. Indeed, one particular point often forgotten is that when receiving sorted end-of-life batteries in a recycling facility, there are always undesired types of batteries with them. Indeed, battery sorting– either manual or automatic – can never be perfect and there are always other battery types in a majority of well-sorted batteries.

This represents a potential big trouble for the recycler, mainly if a hydro process specially calibrated for a given type and chemistry is being used. Pyro metallurgy is less sensitive to that; however, pyro recyclers have to be aware of this situation and develop the adequate processes to cope with it. As an example, sorted Li-ion batteries often contain some NiCd, NiMH and/or primary zinc batteries. Ni is not a problem, but metals like Cd or Zn with a high partial pressure will evaporate during the process and can be found in the stack if nothing is installed to catch them.

That is the main reason why Umicore developed a gas cleaning installation where all potentially contaminating metals, like Cd or Zn, can be caught before releasing. Li-ion batteries also contain plastics and halogens: a perfect mixture for producing dioxins and furans. As already mentioned, these volatile organic compounds are normally released into the air as diluted into bigger gas flows and not measured. However, Umicore decided to develop a dedicated process in which dioxins and furans are not formed.

This new process uses the technology of the plasma generator (see again Figure 14.24). The gas coming from the furnace has a temperature of approximately 400°C; by heating at high temperature in the plasma generator, its properties change and at about 2000°C the gas molecules start to dissociate into atoms. At 3000°C, the atoms lose some of their electrons: the gas is ionized. After this step, a rapid quenching of the gas is applied so that the residential time is so low that no dioxins – that are very complex molecules needing certain conditions and long time to be formed – can be produced. In this way, the gas is 100% composed of carbon monoxide and hydrogen/water and no system for capturing dioxins before release into the air is necessary.

The recycling rate can be calculated as shown in Table 14.9.

For these characteristics of the Val'Eas® process, the European Environmental Press Association assigned to Umicore its Gold Award in 2004. The primary objective of this association is to recognize the efforts of European companies that are improving the environment with their innovative technologies.

Table 14.9. Recycling rate of Li-ion batteries by the Umicore's Val'Eas process.

Constituent	Weight %	Ending up in/as	%Recycled	%Recovered
Steel casing	20	Alloy	100	
$LiCoO_2$	20	Co in alloy Li in slag*	80 5	
Plastics**	15	Reducing agent Energy provider**	50	0 50
Electrolyte	10	Evaporated	0	0
Graphite**	10	Reducing agent	100	0
Aluminum	15	Slag*	100	0
Copper foil***	10	Alloy	100	
TOTAL	**100**		**81**	**8**

*Li is easily oxidized and ends up in the slag, which is used in the construction industry as free from any leacheable metal.

**Half of the plastic is used as reducing agent in the pyro process, to reduce Co oxide into metallic Co; the other half is used as energy provider. For the graphite powder, see footnote of Table 14.8.

***See footnote of Table 14.8.

14.8. Conclusion

Many innovative and diverse processes have been developed over the years to tackle the problem of battery recycling. However, some of them have simply been proposed to solve a local issue, while others are clearly looking to the future and treat much larger battery volumes. As with any competitive market, the processes that will prove sustainable in the end will be those able to adapt to changes in battery composition and remain economically viable, while providing a true benefit for the environment.

The management of all resources of our planet is a key issue all of us have to address now. No doubt, recycling is one of the main pillars of sustainability and batteries are one of the products to be recycled. Of course, the legislator can and should push each of us towards this direction, but he should also help us making the right choices and force us to take care of our wastes.

Europe is undoubtedly at the leading edge of used battery management. The European Union is working on the expansion of battery collection and recycling and will shortly propose a new legislation in an attempt to harmonize efforts across Europe and oblige the collection and recycling of all kinds of batteries.

However, even with the right legislation in place, the success of waste collection is only granted if the waste generator himself is a responsible person. Moreover, it is the responsibility of everyone collecting/recycling waste to look for the best available technology that can cope with the real financial and environmental cost of a process, as for example proposed by the theory of the "Environmental Weight" developed in the Qwerty study.

References

1. For details see: J. Huisman, The QWERTY/EE Concept, Quantifying Recyclability and Eco-Efficiency for End-of-Life Treatment of Consumer Electronic Products, Ph.D. Thesis, *ISBN 90-5155-017-0*, Delft university of Technology, May 2003, Delft, The Netherlands.
2. K. Sander, Qwerty and Eco-Efficiency Analysis on Cellular Phone Treatment in Sweden, September 2004, *Ökopol GmbH, Institute for Environmental Strategies*, Nernstweg, Hamburg, Germany.
3. www.RBRC.com
4. J.P. Wiaux, *Batteries 2005*, Paris, www.rechargebatteries.com
5. Draft Recommendation for Second Reading, 8 September 2005, 579597EN.doc - *Directive 91/157/EEC*(5694/5/2005 – C6-0268/2005 – 2003/0282(COD).
6. www.saftbatteries.com
7. Scandust Technology, www.scandust.se
8. *10th International Battery Recycling Congress*, Sitges, Spain, 2005, www.ebrarecycling.org

Industrial Applications of Batteries. From Cars to Aerospace and Energy Storage
M. Broussely and G. Pistoia Eds.,
© 2007 Elsevier B.V.

Chapter 15

WORLD MARKET FOR INDUSTRIAL BATTERIES

Donald Saxman

BCC Research, 15402 Winterhaven, Tomball, TX 77377, USA

15.1. Scope & Analysis Assumptions

15.1.1. Definition of Industrial Battery

The fundamental question when characterizing the world market for industrial batteries is to establish the scope of the market. The fundamental component of this market scope is the definition of an "industrial battery." A literature search does not establish a consensus. In fact, the term is fraught with technological, marketing and even legislative implications.

For instance, there are dozens of significant industrial battery manufacturers, but each tends to define industrial batteries in a manner that reflects positively on their product lines. Two examples are Exide (GNB Industrial Power) and Panasonic (Matsushita). Exide takes a market-driven approach and defines industrial battery markets to include network power applications such as telecommunications systems, electric utilities, railroads, photovoltaic (solar-power related) and uninterruptible power supply (UPS), and motive power applications including lift trucks, mining and other commercial vehicles [1]. Panasonic takes a technology-driven approach and describes the company's industrial battery product line as including lithium-ion, nickel-metal hydride, lithium, nickel-cadmium, valve regulated lead-acid, alkaline and zinc-carbon [2].

Starting in 2003 and accelerating in 2004 and 2005, the definition of industrial batteries became a pivotal stumbling block in the European Union. The European Parliament's Environment, Public Health and Food Safety Committee released a "Common Position" on a battery management and recycling directive that included a definition of industrial batteries. Almost immediately corporate, political and environmental groups objected and suggested revisions. For instance, Eurobat objected to the definition of "portable" for some industrial batteries used in an industrial/professional setting [3]. Many environmental groups objected to any definition that allowed the use of cadmium or mercury in industrial batteries. To put this in perspective, according to the Environment, Public Health and Food Safety Committee, the EU market for batteries amounts to about 800,000 tonnes of automotive batteries, 190,000 tonnes of industrial batteries and 160,000 tonnes of consumer batteries every year [4].

Other sources of definitions are the many market research firms that produce commercially available and confidential single-client market studies. Frost & Sullivan, Freedonia, and ICON Group International are just a few of the many analyst groups that have defined industrial batteries to reflect each entities' view on what their customers will find most useful. [5-7].

15.1.2. Definitions of Industrial Battery Market Sectors

BCC Research has also produced a number of technical marketing reports that discuss industrial batteries. This analysis draws heavily on the author's definition of "large and advanced" batteries, which broadly includes industrial batteries, non-automotive transportation batteries, and many consumer batteries, especially if they are portable product batteries. The following kinds of large-and-advanced batteries were discussed [8].

Widely used large battery systems:

- non-automotive lead-acid batteries
- nickel-cadmium batteries

Recently commercialized large battery systems:

- nickel-metal hydride batteries
- lithium-ion and lithium-polymer batteries

Developmental large battery systems:

- high temperature batteries
- redox and flow batteries
- metal-air batteries
- nickel-iron batteries
- other lithium rechargeable batteries
- exploratory batteries

This establishes a technological definition. As discussed below, this analysis primarily takes an inclusive market-driven approach. Readers are encouraged to take the data provided and apply whatever definition they find useful.

The following lists define the assumptions in this analysis, including market sectors considered, definitions of regions tracked, analysis duration, and monetary unit conventions.

Candidate market sectors include the following:

- Computing - This is the large and well-established market for portable computer batteries, as well as Personal Digital Assistant (PDA) and calculator power supplies. Originally mainly commercial, the market sector for portable computing devices is approximately 30% non-commercial and 70% industrial, commercial, and governmental.
- Communications - This includes the well-established and very large market cell phone batteries. This market sector also includes a steadily shrinking market for pagers (mainly powered by replaceable primary batteries) and portable transceivers (powered by everything from lead-acid to lithium-ion). As with portable computing devices, this market was originally mainly commercial; the market sector for portable communications devices is approximately 90% non-commercial and 10% industrial, commercial, and governmental.
- Tools - This is a well-established niche market for portable personal grooming, hand tools, lawn tools, and kitchen tools. This market sector is approximately 30% industrial.
- Other portable - This is the market for other portable battery-powered products, including lighting, toys (especially large toys like ride-ons and robots), scientific instruments, photographic devices, smart cards, timepieces, *etc*. This market sector is approximately 15% industrial.
- Medical - This is a well-established niche market for primary and secondary power supplies used in portable medical devices like hearing aids, heart pacemakers, defibrillators, sensor and test equipment, and various therapeutic devices. Although not a large market in terms of numbers, there is also a well-developed market for artificial organ power supplies.
- Computer memory - This is the relatively small but well-established niche market for small cells used to energize various types of computer memory chips and protect data during power outages or when the overall product is deactivated. The market is shrinking as computers employ non-battery approaches to memory preservation.
- UPS/Stationary - This is the well-established niche market for uninterruptible power supplies and emergency power supplies that are activated when utility power is interdicted. Large units are used to provide standby power to telecommunications arrays. This market sector is approximately 90% industrial.
- Military/aerospace - This is the industrial market for a wide variety of portable product, stationary, remote power, aircraft power, and munitions power supplies.
- Industrial EV - This is the well-established market for large battery stacks to

power industrial vehicles like forklifts and burden carriers.

- HEV/EV - This is the relatively small, but growing market for large battery stacks to power street-ready automobiles and trucks. This includes a limited number of "plug in" EV (electric vehicle) battery stacks that are recharged from the utility power grid as well as HEVs (hybrid EV) stacks where an internal combustion engine (or potentially a fuel cell) charges the battery.
- Auto SLI - This is the giant, well-established market for the "starting, lighting, ignition" batteries used by most internal combustion vehicles. It is considered outside the scope of industrial batteries.

15.1.3. Other Analysis Assumptions

Definitions of Regions

- North American - Includes Canada and U.S.
- Far East - Includes all of Far East, including Japan, China, India, Indonesia, *etc.*
- Europe - Includes Western Europe
- Rest of World (ROW) - All South America, Mexico, Central America, Africa, Middle East, Australia, New Zealand, other Pacific nations, Russia, Eastern Europe, Turkey

Analysis Duration

- This discussion's consensus scenario is based on a Year 2006 actuals, and 2006 through 2016 market value predictions based on the indicated driving forces.

Monetary Conventions

- The projected "market value" represents wholesale sales (manufacturer level) during each calendar year.
- U.S. dollars are used throughout this analysis.
- Detailed market value prediction units are in million U.S.
- All market predictions are in constant Year 2006 dollars not adjusted for inflation.
- All pre-2006 values are in current actual dollars.

15.2. Driving Forces Used to Predict World Market Value

Over the next ten years, the market for industrial batteries will include some sectors that grow and some that shrink. At the same time, as prices per unit increase or decrease, the overall value of each sector can shrink even as the number of units consuming the new technology grows.

With this in mind, the following driving forces comprise a simple market value model:

- Overall Value of all Batteries Consumed - which consists of two components:
    - The overall value of all batteries sold with battery-consuming products - How large is the OEM portion of the target market?
    - The overall value of all batteries sold separately from battery-consuming products - How large is the "aftermarket/accessory/ removable" portion of the target market?
- Anticipated growth for the battery-consuming product - How much will the number of battery-consuming products increase?
- Competitiveness factor - To what extent can the new technology displace the existing technology?
- Competition from new technologies - To what extent can other new technologies displace the existing and the new technology?
- Marketing & strategic factors - Are there non-market driven factors that influence the value?
- The cost per unit - What is the cost for the battery?

The "old technology" portion of the "Overall Value of all Batteries Consumed" is determined as follows:

- The "Overall Value of all Batteries Consumed" establishes the target's market value - that is, the value of all the old technology batteries sold each year (new and replacement).
- The "Overall Value of all Batteries Consumed" will grow or shrink with time based on the fortunes of the battery-consuming products.
- The "Overall Value of all Batteries Consumed" will also grow or shrink with time based on the cost per unit.
- The "Overall Value of all Batteries Consumed" will also grow or shrink with time if large numbers of OEM batteries fail and must be replaced by "aftermarket/ accessory/ removable" batteries.

This model is valid if there is no "new technology" introduced and if there are no non-market-driven factors (like predatory pricing, legislation, non-market shortages, *etc.*)

"New technology," much as a new battery system, can take over a portion of the previously described "Overall Value of all Batteries Consumed." When it does so, it grows or shrinks based on the same previously described factors. Three additional factors are involved:

- The "Competitiveness Factor" will allow the value of the new technology to grow or shrink (starting from "zero". Note that the new battery technology could be displacing wither OEM or aftermarket/ accessory/ removable "old technology" or both).
- At the same time, "competition from new technologies" will be reducing the

new battery system's value by "beating it to market" or even by eroding the recently gained market value.

- Finally, if the new technology is more or less expensive than the old technology, the market value will also be increased or decreased.

15.3. Industrial Energy Storage Systems

This section describes industrial energy storage technology, including batteries as well as competing non-battery energy storage systems that could potentially impact the world market.

Widely used rechargeable or secondary battery systems include:

- Nickel-cadmium ("nicad") batteries
- Nickel-metal hydride batteries
- Lead-acid batteries
- Secondary alkaline batteries
- Secondary lithium batteries (including lithium-ion and lithium polymer)
- Zinc-air batteries

In addition, specialty secondary batteries with established but limited commercial application include aluminum-sulfur, nickel-zinc, silver-zinc, and nickel-hydrogen.

Developmental industrial battery stacks include Zebra (sodium-metal chloride), zinc-bromine, vanadium redox, iron-air, and sodium-sulfur.

Widely used primary, nonrechargeable batteries include:

- Zinc-carbon batteries
- Primary alkaline batteries
- Primary lithium batteries
- Primary zinc-air batteries

Specialty primary silver oxide and magnesium cells are used to a much lesser extent. Mercury batteries are no longer widely used because of environmental consequences.

Conventional electrochemical batteries will compete with several non-conventional battery energy storage systems, including:

- Proton Exchange Membrane (PEM) fuel cells
- Aluminum-air fuel cells
- Alkaline fuel cells
- Phosphoric acid fuel cells
- Solid oxide fuel cells
- Molten carbonate fuel cells
- Ultracapacitors
- Flywheels

15.3.1. Battery Characteristics by Type

The following tables describe commercial battery characteristics.

Table 15.1. Commercial secondary battery types.

Lead-Acid	
Advantages	Variety of design options; mature technology; low cost; availability of sealed versions.
Limitations	Safety and environmental problems with lead and sulfuric acid; high weight; explosive gas generation; relatively low energy density.
Applications	• Motive power: industrial trucks, materials handling and mining vehicles, electrical vehicles (EV) and hybrid electrical vehicles (HEV), specialty power for military applications (submarine), railroads, signaling, car power systems, diesel locomotive and rapid-transit batteries. • Automobile: SLI (Starting-Lighting-Ignition), golf carts, lawn mowers, tractors, aircraft, marine. • Stationary: emergency and stand-by power, utilities (power distribution controls), telecommunication back-up power, UPS (uninterruptible power source), load leveling, energy storage, lighting. • Portable (*now decreasing*): portable tools, small appliances and devices, TV and portable electronic equipment.
Types of Chargers	Charging stations, OEM, automotive/traction/industrial, developmental.
Lithium-Ion (conventional)	
Advantages	Long retention time; direct state-of-charge indicator; relatively high energy density.
Limitations	Need of electronic control for charge and discharge, safety.
Applications	Portable products, military equipment, potentially EVs.
Types of Chargers	OEM.
Lithium-Ion polymer	
Advantages	Long retention time; direct state-of-charge indicator; relatively high energy density, can be configured in a variety of shapes
Limitations	Cost. Electronic controls. Moderate power.
Applications	Portable products, military equipment, potentially EVs.
Types of Chargers	OEM.
Manganese Zinc "Alkaline"	
Advantages	Moderate retention time; direct state-of-charge indicator; low cost.
Limitations	Limited configurations currently available; new commercialization.
Applications	Radios, clocks, flashlights, toys, tape recorders, electronic equipment.

Types of Chargers	Custom designed.
Nickel-Cadmium	
Advantages	High life cycle; high current at stable voltage; robustness; cyclability at high DOD and low/high temperatures.
Limitations	Cost *vs*. Pb-Acid; low energy vs. NiMH, Li Ion and alkaline; memory effect in sealed cells; environmental problems.
Applications	• Stationary: stand-by power, utilities (power distribution controls), telecommunication back-up power, UPS, load leveling, energy storage. • Emergency lighting. • Aircraft (*main application*). • Portable (*now decreasing, mainly used in power tools*)
Types of Chargers	Charging stations, OEM, developmental.
Nickel Metal Hydride	
Advantages	Relatively high cycle life; higher energy density than Ni-Cd; tolerant to over-charge and –discharge; good power.
Limitations	Higher cost *vs*. Pb-Acid and NiMH; high self discharge.
Applications	• Motive power: industrial trucks, materials handling and mining vehicles, hybrid cars and trucks (HEV), specialty power for military applications, transit buses. • Stationary: railroad signaling, UPS, lighting; in utilities, up to know, only used in a microgrid demonstration site (see Chapter 8). • Portable (*now decreasing, except tools*): portable tools, small appliances and devices, TV and portable electronic equipment.
Types of Chargers	Charging stations, OEM, developmental. Regenerative braking systems in vehicles
Nickel-Zinc	
Advantages	Very high specific energy; good capacity retention; good temperature stability.
Limitations	Cycle life too low for many uses; relatively high cost; commercial versions not sealed; excessive heat generation in some applications.
Applications	Existing commercial versions compete with secondary silver systems at reduced cost. • Float charge and standby applications such as emergency lighting, power back-up systems, and UPS. • Military applications such as torpedoes, swimmer delivery vehicles, and other submersibles.
Types of Chargers	OEM, developmental.
Silver-Zinc	
Advantages	High constant discharge voltage; high watt-hour capacity; mechanical ruggedness; availability in high- or low-rate versions; good volumetric and gravimetric energy density.
Limitations	High cost; sensitivity to overcharge; relatively low cycle life in many versions.
Applications	High-intensity lighting high-power portable equipment, military sensors, aerospace and space power supply, underwater power supply.

Types of Chargers	OEM, developmental.
Zinc-Air	
Advantages	High energy density; no environmental hazard.
Limitations	High cost; relatively low cycle life.
Applications	Traction (*developmental*); military.
Types of Chargers	OEM.

Table 15.2. Commercial primary battery types.

Zinc-Carbon	
Advantages	Best performance with low-drain-rate uses; most watt-hours per dollar; gradually tapering discharge curves; variety of shapes and sizes.
Limitations	Poor low-temperature performance; sharp discharge voltage drop; inefficiency at high current drains.
Applications	Portable low end: radios, clocks, flashlights, pagers, toys, tape recorders.
Alkaline Manganese	
Advantages	Best performance for heavy continuous drains; low cost for high-drain use; good low-temperature stability.
Limitations	High cost for low-drain use; poor high-temperature stability and low-temperature performance.
Applications	As with zinc-carbon, and especially with higher-performance applications.
Mercury Oxide (Now phased out and banned in many countries)	
Advantages	Best performance for good voltage regulation; long shelf life; good high-temperature stability.
Limitations	Poor low-temperature stability; heaviness; high cost; Environmental risks.
Applications	Originally televisions, radios, hearing aids, calculators, security systems, watches, scientific instruments. This technology has practically disappeared due to environmental concerns.
Silver Oxide	
Advantages	High power density; long shelf life; flat discharge curve; good low-temperature stability.
Limitations	High cost of silver; silver supply's unreliability and subjectivity to investor speculation; low service life versus shelf life of silver oxide.
Applications	Hearing aids, scientific instruments, photographic equipment, reference voltage sources, moderate power applications.
Lithium	
Advantages	High power density; long shelf life; adjustable discharge curve; good temperature stability.
Limitations	Price; possible safety problems with some designs.
Applications	Watches, calculators, televisions, photographic equipment, military equipment, scientific equipment, other higher-voltage systems. Any other 9-volt application.

Zinc-Air	
Advantages	High energy density; flat discharge curve; very long shelf life; best performance for high drain, short life, or low drain.
Limitations	Sensitivity to water; short service life; no intermittent drain; must be used in the atmosphere.
Applications	Hearing aids, watches, communications equipment. Military.

15.3.2. Competing Fuel Cell Systems

Fuel cells include both large, stationary arrays and small portable configurations. High-temperature fuel cells require heat management equipment and insulation, not components that contribute to "smallness". Recently, smaller sealed, low-temperature, and truly portable fuel cell power sources have been developed and commercialized. The type of electrolyte usually defines the fuel cell (battery-like metal-air fuel cells are an exception). The following types of fuel cells have been commercialized:

- Alkaline
- Phosphoric acid
- Solid oxide
- Molten carbonate
- Proton exchange membrane
- Metal-air (aluminum-air; zinc-air)

Fuel cells also can be classified by operating temperature or stack size.

Alkaline Fuel Cells - Alkaline fuel cells originally used molten potassium hydroxide as the electrolyte, but now they usually are based on an alkaline aqueous potassium hydroxide solution electrolyte. A wide range of electrocatalysts have been demonstrated, including platinum group metals, as well as nickel, silver, various metal oxides and spinel. Structural support and fillers typically are provided by stainless steel, carbon or nickel. Because the alkaline fuel cell reaction uses potassium hydroxide electrolyte to react with CO_2 to form potassium carbonate, a stream of pure oxygen typically is used in addition to the hydrogen fuel.

Phosphoric Acid Fuel Cells - Phosphoric acid fuel cells are the best developed of the large fuel cells for commercial applications and are accepted for stationary 250-kW applications. No future development is contemplated: what is on the market now is on the market. They have a wide range of power outputs (1 kW to 5 MW) and are relatively easy to upgrade to increase capacity by adding additional modules. Typical operating temperatures range from 150°C to 220°C. Phosphoric acid fuel cells use an aqueous phosphoric acid as an electrolyte, a platinum or platinum alloy electrocatalyst, and graphite current collectors and gas separators. These fuel cells run on hydrogen and are relatively tolerant of fuels containing contaminants like carbon monoxide.

Solid Oxide Fuel Cells - Solid oxide fuel cells (SOFCs) use a solid nonporous metal oxide like yttria-stabilized zirconia as an electrolyte. Cathodes are a different metal oxide, for instance praseodymium oxide or indium oxide. Typically, anodes are nickel or a nickel alloy like cermet. Structural stability and fillers typically are provided by ceramics or metal oxide components. Operating temperatures generally are between 900°C and 1000°C. Most applicable for large stationary applications.

Molten Carbonate Fuel Cells - The molten carbonate fuel cell uses an electrolyte of lithium and potassium carbonate. The fuel cell anode generally is porous nickel that is stabilized using chromia or alumina to inhibit sintering. Most cathodes are porous nickel that oxidizes during the initial stack start-up and then becomes a semiconductor that it is doped by lithium electrolyte. Molten carbonate fuel cells require relatively high temperatures for conductivity, around 650°C, and run on hydrogen.

Proton Exchange Membrane Fuel Cells - A proton exchange membrane (PEM) fuel cell consists of two electrodes separated by an ion conductive polymer electrolyte. Each of the electrodes is coated on one side with a platinum containing catalyst. Hydrogen fuel dissociates into free electrons and protons in the presence of the platinum catalyst at the anode. The free electrons are conducted in the form of usable electric current through the external circuit. The protons migrate through the membrane electrolyte to the cathode. At the cathode, oxygen from the air, electrons from the external circuit and protons combine to form pure water and heat. Increasing the number of cells in a stack increases the voltage, while increasing the surface area of the cells increases the current. Because of the need for a water-charged electrolyte, PEM fuel cells are limited to relatively low temperatures (60°C to 120°C).

Metal-Air Fuel Cells - Metal-air fuel cells include aluminum-air and zinc-air. Lithium-air and several other designs have been fabricated, but are not likely to be commercialized. In a metal-air cell, the metal (fuel) anodes react with an atmospheric air cathode to produce electricity. The metal (aluminum or zinc) is consumed as fuel and converted into a hydroxide. A sealed unit is especially a primary battery (called a power cell) that is discarded when all the fuel is consumed. A non-sealed design is more like a traditional fuel cell in that the metallic hydroxide can be removed and replaced with fresh fuel ingots. Applications include portable product power, small vehicles like scooters, and even large stationary UPS stacks. The portable power cells can be coupled with lithium ion batteries to recharge the battery.

15.3.3. Competing Exotic Energy Storage Systems

Capacitive Energy Storage - A capacitor is an electronic component that stores an electric charge using two conductors separated by an insulator. Capacitors are used in most high voltage appliances, including televisions. Capacitive energy storage includes supercapacitors and ultracapacitors (essentially very large electronic capacitors), as well as aerocapacitors (which combine electronic capacitors and electrochemical cells). There is a significant overlap between ultracapacitor and supercapacitor form and function. In common usage, the terms are essentially used interchangeably. A supercapacitor is essentially a large capacitor configured as a non-electrochemical power storage device. Aerocapacitors are a specific kind of supercapacitor/ultracapacitor based on aerogel materials. The aerocapacitor is an electrochemical, double-layer capacitor that uses thin-film carbon aerogel paper, developed at Lawrence Livermore Laboratory, as both the positive and negative electrodes. An aerocapacitor combines elements of electronic energy storage (capacitor) and electrochemical energy storage (battery).

Flywheel Energy Storage - Steam engine inventor James Watt originally developed the flywheel over 200 years ago. This early flywheel was a heavy metal wheel attached to a steam engine's drive shaft. Flywheel energy storage has been proposed for near fifty years for vehicles, remote power, satellite power, and uninterruptible power supplies. In a typical advanced flywheel, kinetic energy storage is achieved by adding energy (plugging the flywheel into an electric socket), causing the rim mass to rotate like an electric motor, but at a very high velocity in a frictionless environment. The flywheel spins at its steady state speed on frictionless magnetic bearings drawing a minimal load from the bus. The external energy supply is removed (unplugged), the rim mass continues to rotate. Energy is withdrawn in the form of electricity by reversing the process so that the rotating rim mass becomes the energy supply for the motor/generator. When providing standby power, a flywheel transitions from a motor into a generator to draw the kinetically stored energy from the flywheel to deliver uninhibited power. Ideally the flywheel is installed in a vault to insure safe operation and is connected via an underground cable to a flywheel electronics module that can interface directly to a battery terminal. The amount of energy stored in a flywheel is determined by measuring the rotational flywheel speed.

15.4. Industrial Battery Configurations

The following lists define the marketing and technical battery configurations tracked in this analysis. Marketing configurations control how the battery is sold, while technical configurations control a battery's size and shape.

15.4.1. Lifecycle Configurations

Marketing configurations are based on when in the battery-using product's lifecycle the battery is purchased.

- OEM - Original equipment manufacturer (OEM) batteries are shipped with the product that uses them. They are often uniquely shaped to interface with each individual product and are usually secondary. In most cases they can be easily removed and replaced by an accessory or aftermarket battery.
- Accessory - Accessory batteries replace OEM or aftermarket batteries by providing improved performance or lower price.
- Aftermarket - Aftermarket batteries replace OEM or accessory batteries after those batteries are retired.
- Removable/multipurpose - Removable multipurpose batteries include button cells, AA, C, D, and 9-volt consumer batteries. Although they may be "bundled" with consumer products, they are not installed in the product so they are not considered OEM. They may be primary or secondary. The niche consumer rechargeable market similar to that presently occupied by RAM (rechargeable alkaline manganese) is promising once manufacturability and price issues are resolved.

15.4.2. Technical Configurations

Technical configurations are based on size, shape, and packaging. There are a variety of possible battery configurations, but the following six represent the bulk of the market. Other configurations tend to be optimized for a particular unique application.

- Button cells - Disk-shaped cells generally smaller in diameter than a coin. Both primary and secondary designs are used. Button cells are usually removable/multipurpose.
- Consumer-sized (AA, C, D, 9-volt, *etc.*) - Various cylindrical and rectangular cells that are used in both portable and stationary products. These cells are almost always removable/multipurpose. As previously discussed, the niche consumer rechargeable market similar to that presently occupied by RAM (rechargeable alkaline manganese) is promising once manufacturability and price issues are resolved.
- Cellphone/laptop sized - Most cellphone and laptop batteries are uniquely shaped to interface with each individual product. Most are also smart secondary batteries that incorporate charging control circuits. Most laptops and cellphones are shipped with an OEM battery, and in most cases, an accessory and aftermarket equivalent is also available.

- UPS/stationary-sized - UPS and other stationary configurations consist of a single large battery or in some cases, a closely integrated battery stack. They are invariably secondary systems.
- Automotive-sized - Automotive-sized batteries are a well-established 6, 12, 22, or (more recently) 42-volt battery configuration. Although most are used for vehicle SLI, they can also be used for industrial vehicle traction, very large stationary UPS stacks, and marine power. Technical design options include multi-battery stacks, smart charging options, and enhanced electrode plates to allow "deep cycle" charging.
- HEV/EV Stacks - Electric vehicle and hybrid electric vehicle power storage systems consist of a series of batteries combined into a stack. Early EV battery stacks consisted of dozens of deep cycle lead-acid batteries. State-of-the-art purpose-built HEV/EV batteries are more closely integrated batteries stacks and developmental systems can consist of a single (or just a few) large batteries.

15.5. Driving Forces by Market Sector

15.5.1. Computing Batteries

This is the large and well-established market for portable computer batteries, as well as Personal Digital Assistant (PDA) and calculator power supplies. Portable computer batteries are typically lithium-ion and less frequently, nickel metal hydride. PDAs typically use lithium-ion batteries, and to a lesser extent nickel metal hydride, primary alkaline, and a variety of other advanced systems. Calculators use a variety of lower-performance alkaline, nickel-based systems, including removable primary batteries.

As with portable communications, trends include an increasing convergence between cell phones and other portable products like PDAs and cameras. At the same time, developmental and even exotic power options are appearing.

Driving forces and market developments include the following:

- Explosive growth has ended, and consumers are scaling back top-of-the-line laptop purchases. Slow but steady sales until the next tech market upturn.
- Tablet computers are becoming more important (mainly for commercial users). Tablet computers are a viable alternative for many applications, and this could eventually grow from a niche market to a significant commercial hardware market sector.

Table 15.3. Total world computing battery market value prediction (million dollars & average annual growth rate).

Region	**'02**	**AAGR '02 - '06**	**'06**	**AAGR '06 - '011**	**'11**	**AAGR '11 - '16**	**'16**
N. America	1,400	2.2%	1,560	0.5%	1,600	2.0%	1,770
Far East	900	3.1%	1,050	0.0%	1,050	0.0%	1,050
Europe	510	1.1%	540	0.7%	560	0.0%	560
ROW	220	0.0%	220	3.4%	260	0.0%	260
Total	**3,030**	**2.1%**	**3,370**	**0.6%**	**3,470**	**1.0%**	**3,640**

- Wearable computers are still an idea whose time has yet to come. Technical issues are being solved, but creative marketing approaches are needed.
- Convergence between cell phones, PDAs, digital cameras, GPS, *etc.* Eventual blurring between market sectors. Is it a PDA or a cell phone? Need for higher-performance batteries and chargers.
- Consumers anticipate high-performance broadband wireless for data services, e-mail, e-commerce, *etc.* Consumers delay purchase of high-end hardware because they are waiting for even higher-performance units. In the long run, cell phones may cut into the PDA or laptop markets (but consider the convergence issues).
- Lower prices for PDA hardware and services. Higher unit sales but proportionally lower market value. At a certain point, portable phones will clearly be a valid alternative to residential and business landlines. This could spark even higher unit sales. Meanwhile, the pager market is shrinking.
- Competing full-featured operating systems. Polarization between consumer and business operating systems.

As shown in Table 15.3, in 2002, over $3 billion worth of computing batteries were shipped. By 2016, this will grow to $3.64 billion. North America represents about 45% of the market, followed by 30% for the Far East and 18% for Europe. The rest of the word (ROW) splits the remaining 7%, including about 3% for Latin America (especially Brazil, Mexico, and until recently Argentina). A recovery in sales began in 2005 and will accelerate through 2011 (starting in North America, and then moving to the Far East and then to Europe). A spike in ROW sales will not occur until 2011.

15.5.2. Communications Batteries

This includes the well-established and very large market of cellular phone batteries. Lithium-ion batteries predominate, but nickel metal hydride, primary alkaline, and a variety of other advanced systems are used. This market sector also includes pagers (mainly powered by replaceable primary batteries) and portable transceivers (powered by everything from lead-acid to lithium-ion). Cellphones are increasingly being used throughout the world, including developing countries. Early innovators are concentrated in the Far East.

Trends include an increasing convergence between cell phones and other portable products like PDAs and cameras. At the same time, developmental and even exotic power options are appearing. Pagers use is declining as pager functionality and pricing converges with cellphone pricing and functionality.

Driving forces and market developments in the portable communications industry include the following:

- Possibility that lawsuits will help open the U.S. cell phone outside the 'big four'. More imports and the possibility that more cell phones will be made in the U.S. Possibly lower prices.
- The requirement that cell phone numbers be 'portable' makes it easier for consumers to switch service providers. More 'churning' by consumers, possibly more inclination to upgrade hardware when a new service provider is selected. Lower prices.
- Convergence between cell phones, PDAs, digital cameras, GPS, and so forth – see previous section.
- Consumers anticipate high-performance broadband wireless for data services, etc - see previous section.
- Lower prices for cell-phone hardware and services – see previous section.
- Cordless phones adopt cell-phone look and feel. Relatively lower prices and higher performance.

As shown in the following table, in 2002, nearly $2.3 billion worth of communications batteries were shipped. By 2016, this will grow to $3.13 billion. The Far East represents about 36% of the market, followed by 28% for North America and 22% for Europe. The rest of the word splits the remaining

Table 15.4. Total world communications battery market value prediction (million dollars & average annual growth rate).

Region	**'02**	**AAGR '02 - '06**	**'06**	**AAGR '06 - '011**	**'11**	**AAGR '11 - '16**	**'16**
N. America	700	2.7%	800	2.4%	900	2.1%	1,000
Far East	920	1.3%	980	2.0%	1,080	1.8%	1,180
Europe	430	2.2%	480	1.6%	520	0.0%	520
ROW	240	0.8%	250	11.4%	430	0.0%	430
Total	**2,290**	**1.9%**	**2,510**	**3.1%**	**2,930**	**1.3%**	**3,130**

14%. A modest recovery in sales started in 2004 and will accelerate through 2010, starting in the Far East, then moving to North America and then Europe and finally the ROW.

15.5.3. Portable Tools Batteries

This is a well-established niche market for portable personal grooming, hand tools, lawn tools, and kitchen tools. This is one of the largest remaining nickel-cadmium battery markets. Lead-acid, lithium, and alkaline primary batteries are also commonly used.

Driving forces and market developments include the following:

- A wide variety of battery types compete for the same portable tool applications. Nickel-cadmium batteries will continue to be used for low-end applications, but will lose ground to nickel-metal hydride for medium-performance systems and to lithium for high-end systems.
- Shift from removable consumer batteries to higher-performance OEM lithium and nickel-metal hydride batteries. If this trend solidifies, there could be a decrease in unit sales and an increase in overall battery market value.

As shown in the following table, in 2002, nearly $250 million worth of portable tools batteries were shipped. By 2016, this will grow to $400 million. North America represents about 56% of the market, followed by 28% for the Far East and 12% for Europe. The rest of the word splits the remaining 4%. Although some recovery in the Far East should begin by 2007, North America should continue to dominate the portable tools market through 2016.

Table 15.5. Total world portable tools battery market value prediction (million dollars & average annual growth rate).

Region	**'02**	**AAGR '02 - '06**	**'06**	**AAGR '06 - '011**	**'11**	**AAGR '11 - '16**	**'16**
N. America	140	4.0%	170	3.3%	200	0.0%	200
Far East	70	0.0%	70	9.5%	110	7.8%	160
Europe	30	0.0%	30	0.0%	30	0.0%	30
ROW	10	0.0%	10	0.0%	10	0.0%	10
Total	**250**	**2.3%**	**280**	**4.6%**	**350**	**2.7%**	**400**

15.5.4. Other Portable Product Batteries

This is the market for other portable battery-powered products, including lighting, toys (especially large toys like ride-ons and robots), scientific instruments, photographic devices, smart cards, timepieces, *etc*. A wide variety of primary and secondary systems are used, including button cells and much of the removable rechargeable battery market.

Driving forces and market developments include the following:

- Increased demand for portable video games. Growing unit and market value from an already large base.
- Increased demand for wireless game products. Growing unit and market value from a relatively small base.
- Increased interest in all kinds of toy robots. The birth of a better-defined market niche with increased sales in low-end, medium-end, and high-end products.
- Shift from removable consumer batteries to higher-performance OEM lithium and nickel-metal hydride batteries. If this trend solidifies, there could be a decrease in unit sales and an increase in overall battery market value.
- Continued demand for GPS systems, including units incorporated in cell phones. Steadily growing GPS sales, with some decrease in unit price.
- Slow and steady growth in consumer weather instruments.
- Competition from capacitive energy storage devices.

As shown in the following table, in 2002, over $12 billion worth of "other portable product" batteries were shipped. By 2016, this will grow to over $15 billion. These figures represent a large portion of the giant market for alkaline and zinc-carbon "dry cell" consumer batteries. North America and the Far East both represent about 43% of the market, followed by about 11% Europe. The rest of the word splits the remaining 3%.

Table 15.6. Total world other portable product battery market value prediction (million dollars & average annual growth rate).

Region	**'02**	**AAGR '02 - '06**	**'06**	**AAGR '06 - '011**	**'11**	**AAGR '11 - '16**	**'16**
N. America	5,360	2.0%	5,920	1.8%	6,460	1.0%	6,800
Far East	5,400	1.8%	5,900	1.1%	6,240	0.9%	6,540
Europe	1,400	1.4%	1,500	1.3%	1,600	1.2%	1,700
ROW	340	0.0%	340	3.3%	400	0.0%	400
Total	**12,500**	**1.8%**	**13,660**	**1.5%**	**1,4700**	**1.0%**	**15,440**

Table 15.7. Total world medical battery market value prediction (million dollars & average annual growth rate).

Region	**'02**	**AAGR '02 - '06**	**'06**	**AAGR '06 - '011**	**'11**	**AAGR '11 - '16**	**'16**
N. America	350	2.7%	400	1.9%	440	2.2%	490
Far East	150	2.5%	170	5.3%	220	1.8%	240
Europe	70	0.0%	70	5.1%	90	2.1%	100
ROW	30	0.0%	30	5.9%	40	4.6%	50
Total	**600**	**2.2%**	**670**	**3.3%**	**790**	**2.2%**	**880**

15.5.5. Medical Batteries

This is a well-established niche market for primary and secondary power supplies used in portable medical devices like hearing aids, heart pacemakers, defibrillators, sensor and test equipment, and various therapeutic devices. Although not a large market in terms of numbers, there is also a well-developed market for artificial organ power supplies. A variety of different battery types are used, including zinc-air (mainly for hearing aids), lead-acid, removable alkaline, nickel-based, and lithium primary and lithium-ion.

Driving forces and market developments include the following:

- Increasing number of affluent seniors, disabled vets. Continued sales growth for a variety of medical products.
- Possibility for increased subsidies for portable medical products. Continued sales growth for a variety of medical products.
- Lower prices for established medical product lines, like hearing aids. Increased unit sales for medium- and high-end hearing aids.
- Steadily improving heart disease treatment products and new guidelines that increase the number of potential implantable defibrillator patients. Continued sales growth for heart disease treatment products, including developmental systems.

High volume, low price markets like hearing aid power tend to be dominated by well-entrenched button cell systems like zinc-air. Small volume, high price markets like implantable devices tend to be dominated by systems with very specific, demanding performance requirements (like lithium-iodine systems). As shown in Table 15.7, in 2002, over $350 million worth of medical batteries were shipped. By 2016, this will grow to approximately $880 million.

Table 15.8. Total world computer memory battery market value prediction (million dollars & average annual growth rate).

Region	**'02**	**AAGR '02 - '06**	**'06**	**AAGR '06 - '011**	**'11**	**AAGR '11 - '16**	**'16**
N. America	110	-6.2%	80	-9.0%	50	0.0%	50
Far East	90	-4.9%	70	-10.6%	40	0.0%	40
Europe	30	-7.8%	20	0.0%	20	0.0%	20
ROW	10	0.0%	10	0.0%	10	0.0%	10
Total	**240**	**-5.6%**	**180**	**-7.8%**	**120**	**0.0%**	**120**

15.5.6. Computer Memory Batteries

This is the relatively small but well-established niche market for small cells used to energize various types of computer memory chips and protect data during power outages or when the overall product is deactivated. Small primary battery button cells predominate. They include a variety of lithium, alkaline, and other types. Lithium-based memory preservation solutions should hold their own, but use of other battery systems will decline, mainly due to competition from non-battery systems like ultracapacitors.

As shown in Table 15.8, in 2002, approximately $240 million worth of computer memory preservation batteries were shipped. By 2016, this will shrink to approximately $120 million.

15.5.7. UPS/Stationary Batteries

This is the well-established niche market for uninterruptible and emergency power supplies that are activated when utility power is interdicted. Large units are used to provide standby power to telecommunications arrays.

Table 15.9. Total world UPS/stationary battery market value prediction (million dollars & average annual growth rate).

Region	**'02**	**AAGR '02 - '06**	**'06**	**AAGR '06 - '011**	**'11**	**AAGR '11 - '16**	**'16**
N. America	870	5.9%	1,160	3.7%	1,390	1.4%	1,490
Far East	570	4.8%	720	2.9%	830	2.3%	930
Europe	250	3.7%	300	3.1%	350	2.7%	400
ROW	130	0.0%	130	1.5%	140	1.4%	150
Total	**1,820**	**4.9%**	**2,310**	**3.2%**	**2,710**	**1.8%**	**2,970**

Lead-acid and nickel-cadmium batteries predominate, but higher-performance systems, including non-battery systems are beginning to make in-roads.

As shown in Table 15.9, in 2002, over $1.8 billion worth of UPS/stationary batteries were shipped. By 2016, this will grow to nearly $3 billion. North America represents approximately 48% of this market, followed by the Far East with 31% and Europe with nearly 14%. The rest of the word splits the remaining 7%.

15.5.8. Military/Aerospace Batteries

This is the market for a wide variety of portable products, stationary, remote power, aircraft power, and munitions power supplies. Virtually all battery types are used, including large numbers of nickel-based, lithium primary and secondary, alkaline, and even lead-acid. Many types of specialty batteries are used to meet unique performance requirements. There is a continuing trend toward lithium-based systems. There is also a trend toward increased use of developmental specialty battery systems. Although there is no expectation that a significant military HEV/EV market will develop within the next fifteen years, there is a potential for a few high profile exceptions, for instance for military robots and especially unmanned aircraft like third generation predators and perfected Helios drones.

Driving forces include the following:

- Transition from garrison to combat deployments for U.S. military forces.
- Increased number of combat deployment of U.S. forces.
- Improved advanced battery-powered combat devices.

All these factors tend to increase usage of a variety of portable military products.

Advanced military and aerospace systems that could dramatically affect the battery technology market include:

- EV fleets for non-combat missions
- Adoption of battery-powered fighting vehicles
- Robots and automated flexible manufacturing
- Strategic Defence Initiative.

Each possible market should be considered as a separate developmental battery scenario.

Military Electric Vehicles Scenario - The U.S. Armed Forces, especially the Army, have long been intrigued by the possibility of replacing internal combustion vehicles with EVs or HEVs. The Army is the free world's largest "fleet" operator, with more than a million vehicles in use. It continues to fund vehicle battery research. Most realistically, HEVs would be battery-powered

Hummers configured for support roles, *e.g.*, ambulances, ground support vehicles and ammunition carriers.

Battery-Powered Fighting Vehicle Scenario - If military EVs are problematical, battery-powered combat vehicles remain theoretical. There are significant logistical problems associated with recharging combat EVs on the front lines, perhaps under fire. Electricity supplies may be easier to interdict than supplies of conventional fuel. On the other hand, developmental EV batteries could potentially reduce the mass and weight of a combat vehicle power plant. This would translate directly into increased room for protective armor or weapon systems and ammunition. A battery-powered motor will run quieter and cooler than an internal combustion engine. This makes it harder to detect and destroy. Heat-seeking missiles will not easily find an EV motor, compared to a hot, internal combustion engine. In addition, fighting vehicles are using increasingly sophisticated electrical equipment. It is easier to anticipate hybrid battery/internal combustion or battery/fuel cell systems with batteries powering electrical equipment and perhaps supplying traction when under fire by heat seeking missiles. Further in the realm of science fiction are battery-powered, armored "Pitman Suits" (exoskeletons) under development at Los Alamos National Laboratory, and elsewhere. Essentially, these are combat space suits that incorporate strength-amplifying servomechanisms. Individual combat soldiers could potentially use these suits. More likely, despite science fiction, they would be used in ad hoc situations, such as operation in chemical warfare zones or unloading supplies while under fire. Battery-powered unmanned aircraft are another possibility. Existing drones, which were wildly successful in Afghanistan and Iraq, are not battery-powered, but future units (fielded beyond the five year scope of this report) may include smaller battery-powered units. The military also conducts research into robot support and weapons systems. The most advanced are battery-powered, remote controlled fire fighting and rescue robots. Remote controlled security robots also are used.

Military Automated Factory Scenario - The military also has long been interested in automated, flexible manufacturing. Everyone is aware of the military's difficulties with obtaining specialized, combat-durable equipment. All too often, it ends up paying thousands of dollars for equipment only marginally more durable than the same product in a consumer version. With this in mind, it would like to have access to a "flexible factory" that could be quickly and inexpensively reconfigured to make small runs of a variety of different products. Such flexible factories would be highly automated and use electrically-powered, automatic guided vehicles and robots wherever possible.

Strategic Defense Initiative (SDI) Revival Scenario - It is difficult to imagine a revival of the SDI considering the current global geopolitical and domestic budgetary situation. On the other hand, the break-up of the Soviet Union did not

Table 15.10. Total world military/aerospace battery market value prediction (million dollars & average annual growth rate).

Region	**'02**	**AAGR '02 - '06**	**'06**	**AAGR '06 - '011**	**'11**	**AAGR '11 - '16**	**'16**
N. America	120	3.1%	140	0.0%	140	0.0%	140
Far East	40	0.0%	40	0.0%	40	0.0%	40
Europe	40	0.0%	40	0.0%	40	0.0%	40
ROW	20	0.0%	20	0.0%	20	0.0%	20
Total	**220**	**1.8%**	**240**	**0.0%**	**240**	**0.0%**	**240**

result in the removal of all of Russia's nuclear warheads. Indeed, the break-up appears to have created several new nuclear superpowers. Nuclear proliferation in Iran, North Korea, India, and Pakistan are all concerns. It is not unthinkable that SDI could be dusted off and the concept re-examined sometime before 2009. It just is unlikely given the current situation in Congress.

As shown in Table 15.10, in 2002, approximately $220 million worth of military/aerospace batteries were shipped. By 2016, this will grow to $240 million. North America represents approximately 54% of this market, followed by the Far East and Europe with 18% each. The rest of the word splits the remaining 10%.

15.5.9. Industrial EV Batteries

This is the well-established market for large "traction" battery stacks to power industrial vehicles like forklifts and burden carriers. Lead-acid batteries are invariably used. Despite promising non-lead alternatives, there has been little motivation to switch from lead-acid.

For EV and HEV commercialization to continue, these market-related problems must be addressed:

- Promotional marketing problems (the inevitable expenses associated with introducing a new product, especially a product trying to displace existing, mature technology); legislative mandates can require the use of a product (like HEVs or EVs), but they usually do not require that a particular company's product fulfill that legislative mandate.
- Cost effectiveness, especially compared to gasoline or diesel fuel (but also alternative fuels like natural gas, fuel cells or ethanol).
- Technical marketing problems (optimization of performance, comfort, cycle life, safety, *etc.*, to the extent that the market will support).

Table 15.11. Total world industrial EV battery market value prediction (million dollars & average annual growth rate).

Region	'02	AAGR '02 - '06	'06	AAGR '06 - '011	'11	AAGR '11 - '16	'16
N. America	500	6.3%	680	0.0%	680	0.0%	680
Far East	300	0.0%	300	0.0%	300	0.0%	300
Europe	300	0.0%	300	0.0%	300	0.0%	300
ROW	40	0.0%	40	0.0%	40	0.0%	40
Total	**1,140**	**3.0%**	**1,320**	**0.0%**	**1,320**	**0.0%**	**1,320**

- Financial marketing problems (the need for capital to complete the commercialization process, including manufacture, promotion, distribution, *etc.*).
- Safety issues, such as revisions of rescue protocols for HEVs that contain high voltage power conduits.

As shown in Table 15.11, in 2002, approximately $1.1 billion worth of industrial EV batteries were shipped. By 2016, this will grow to about $1.3 billion. North America represents approximately 44% of this market, followed by the Far East and Europe with 26% each. The rest of the word splits the remaining 4%.

15.5.10. HEV/EV Batteries

This is the relatively small, but potentially attractive market for large battery stacks to power street-ready automobiles and trucks. This includes some "plug in" EV battery stacks that are recharged from the utility power grid and HEVs stacks where an internal combustion engine (or potentially a fuel cell) charges the battery. "Regenerative braking" stores kinetic energy generated when a driver applies a vehicle's break.

Lead-acid and nickel metal hydride systems are used in most commercial vehicles. Lithium-ion is another promising option. There is intense and well-funded research to establish and evaluate a variety of other developmental battery systems.

Especially in the U.S., the trend is toward HEV systems and pure-battery powered vehicle use is quickly declining. At the same time, there is the potential for competition from other alternative power sources, especially fuel cells. Outside the U.S., especially in Western Europe and the Far East, EVs are still used - albeit at declining levels. There is controversy whether a revival of plug in EVs is possible during the ten year time frame of this analysis. Our consensus

Table 15.12. Total world HEV/EV battery market value prediction (million dollars & average annual growth rate).

Region	**'02**	**AAGR '02 - '06**	**'06**	**AAGR '06 - '011**	**'11**	**AAGR '11 - '16**	**'16**
N. America	30	52.8%	250	0.0%	205	0.0%	250
Far East	50	32.0%	200	0.0%	200	0.0%	200
Europe	60	20.1%	150	0.0%	150	0.0%	150
ROW	<1	15.0%	20	0.0%	20	0.0%	20
Total	**140**	**34.7%**	**620**	**0.0%**	**620**	**0.0%**	**620**

scenario assumes no significant revival; on the other hand, it predicts wider adoption of hybrid internal combustion/battery HEVs and significantly, fuel cell/battery HEVs.

As we move out of the traditional ICE vehicle to the hybrid and beyond, SLI automotive batteries will change into the assist and max power battery working in tandem with the vehicles. Even diesels may go to hybrids as they are converted to lead-acid diesel hybrids.

As shown in Table 15.12, in 2002, only about $30 million worth of HEV/EV batteries were shipped in North America. By 2016, this will grow to $250 million. North America currently represents about 21% of the 2002 market, but by 2016 the share will grow to over 40%. Europe, which has long maintained a fleet of relatively low performance EVs, was the leading region in 2002, with 43% of the market. Europe's share will drop to 24% by 2016. The Far East's share will shrink from 35% in 2002 to 24% by 2016.

15.5.11. Auto SLI Batteries

Starting, lighting, and ignition (SLI) batteries are a giant, well-established market for the lead-acid batteries used by most internal combustion vehicles. There are no significant regional constraints. All areas of the globe that use automobiles consume SLI batteries. However, developing countries tend to use less expensive units. Not unexpectedly, Japanese, American, and Western European consumers tend to be the early innovators who employ new technology as it is introduced.

OEM and aftermarket, and to a much lesser extent accessory products are used worldwide. Accessory batteries include dual batteries that are essentially two separate batteries fabricated into a single package. If one battery in the set is inadvertently discharged, the other auxiliary battery can provide cranking power.

Trends include use of "smart" technology, 36- and 42-volt systems, and

Table 15.13. Total world auto SLI battery market value prediction (million dollars & average annual growth rate).

Region	'02	AAGR '02 - '06	'06	AAGR '06 - '011	'11	AAGR '11 - '16	'16
N. America	3,100	0.3%	3,150	0.6%	3,250	0.1%	3,260
Far East	2,100	-0.2%	2,080	0.2%	2,100	0.0%	2,100
Europe	1,700	-0.4%	1,670	0.1%	1,680	0.0%	1,680
ROW	500	0.0%	500	0.0%	500	0.0%	500
Total	**7,400**	**0.0%**	**7,400**	**0.3%**	**7,530**	**0.0%**	**7,540**

mandatory recycling legislation. There is a small niche market for portable jump-start batteries, including lithium-ion jump-start products.

As shown in Table 15.13, in 2002, over $7.40 billion worth of Auto SLI batteries were shipped. By 2016, this will grow to nearly $7.54 billion. North America represents approximately 42% of this market, followed by the Far East with 28% and Europe with nearly 23%. The rest of the word splits the remaining 7%.

15.6. Historic and Predicted World Market Summary for Industrial Batteries

The following table summarizes the current and predicted value of the world battery market. Historic actual values are in Year 2002 current dollars. Year 2006 and predicted values are in constant Year 2006 million dollars (no correction for inflation). Value is manufacturer's wholesale. Please refer to Section 15.1 for definitions of market sectors and regions.

To put the approximately $32 billion wholesale market value in perspective, the corresponding retail battery market value for Year 2006 should be on the order of $55-$60 billion (based on how exchange rates and non-market pricing situations are factored).

Table 15.14. Total historic & predicted world battery market value (million dollars).

Market Sector/ Year	Region	'02	'05	'06	'11	'16
Computing	N. America	1,400	1,470	1,510	1,600	1,750
	Far East	900	1,010	1,050	1,050	1,050
	Europe	510	520	520	540	560
	ROW	220	220	220	240	260
	Total	**3,030**	**3,220**	**3,300**	**3,430**	**3,620**

Market Sector/ Year	**Region**	**'02**	**'05**	**'06**	**'11**	**'16**
Communications	N. America	700	740	780	880	980
	Far East	920	940	960	1,060	1,160
	Europe	430	460	470	520	520
	ROW	204	240	250	430	430
	Total	**2,290**	**2,380**	**2,460**	**2,890**	**3,090**
Tools	N. America	140	140	170	200	200
	Far East	70	70	70	70	140
	Europe	30	30	30	30	30
	ROW	10	10	10	10	10
	Total	**250**	**250**	**280**	**310**	**380**
Other portable	N. America	5,360	5,680	5,800	6,400	6,720
	Far East	5,400	5,700	5,800	6,180	6,480
	Europe	1,400	1,460	1,480	1,580	1,680
	ROW	340	340	340	400	400
	Total	**12,500**	**13,180**	**13,420**	**14,560**	**15,280**
Medical	N. America	350	380	390	430	480
	Far East	150	160	160	210	250
	Europe	70	70	70	90	100
	ROW	30	30	30	40	50
	Total	**600**	**640**	**650**	**770**	**880**
Computer memory	N. America	110	90	80	60	50
	Far East	90	80	70	50	40
	Europe	30	20	20	20	20
	ROW	10	10	10	10	10
	Total	**240**	**200**	**180**	**140**	**120**
UPS/Stationary	N. America	870	1,040	1,100	1,370	1,470
	Far East	570	660	690	810	910
	Europe	250	280	290	340	390
	ROW	130	130	130	140	150
	Total	**1,820**	**2,110**	**2,210**	**2,660**	**2,920**
Military/ aerospace	N. America	120	130	140	140	140
	Far East	40	40	40	40	40
	Europe	40	40	0	40	40
	ROW	20	20	20	20	20
	Total	**220**	**230**	**240**	**240**	**240**
Industrial EV	N. America	500	630	680	680	680
	Far East	300	300	300	300	300
	Europe	300	300	300	300	300
	ROW	40	40	40	40	40
	Total	**1,140**	**1,270**	**1,320**	**1,320**	**1,320**
HEV/EV	N. America	30	150	200	250	250
	Far East	50	160	180	200	200
	Europe	60	110	130	150	150
	ROW	<10	10	10	20	20
	Total	**140**	**430**	**520**	**620**	**620**
Auto SLI	N. America	3,100	3,050	3,100	3,250	3,260
	Far East	2,100	2,040	2,060	2,100	2,100

Market Sector/ Year	Region	'02	'05	'06	'11	'16
	Europe	1,700	1,630	1,650	1,680	1,680
	ROW	500	500	500	500	500
	Total	**7,400**	**7,220**	**7,310**	**7,530**	**7,540**
Total	N. America	12,680	13,500	13,950	15,260	15,980
	Far East	10,590	11,160	11,380	12,070	12,670
	Europe	4,820	4,920	5,000	5,290	5,470
	ROW	1,540	1,550	1,560	1,850	1,890
	Total	**29,630**	**31,130**	**31,890**	**34,470**	**36,010**

The following table summarizes the current and predicted value of the world lithium battery market. Historic actual values are in Year 2002 current dollars. Year 2006 and predicted values are in constant Year 2006 million dollars (no correction for inflation). Value is manufacturer's wholesale.

Table 15.15. Total historic & predicted world lithium battery market value (million dollars). Both primary and secondary batteries are included.

Market Sector/ Year	Region	'02	'05	'06	'11	'16
Computing	N. America	900	970	1,010	1,100	1,250
	Far East	600	610	660	660	710
	Europe	360	360	360	380	400
	ROW	140	120	120	130	140
	Total	**2,000**	**2,060**	**2,150**	**2,280**	**2,500**
Communications	N. America	450	480	500	590	620
	Far East	550	570	590	660	680
	Europe	350	350	360	420	420
	ROW	220	220	230	420	420
	Total	**1,570**	**1,620**	**1,690**	**2,090**	**2,140**
Tools	N. America	20	20	30	40	60
	Far East	10	10	10	10	20
	Europe	<10	<10	10	10	10
	ROW	<10	<10	<10	<10	<10
	Total	**30**	**30**	**40**	**60**	**90**
Other portable	N. America	150	160	170	190	210
	Far East	150	160	170	190	210
	Europe	40	40	40	50	50
	ROW	10	10	10	10	10
	Total	**350**	**380**	**390**	**440**	**480**
Medical	N. America	50	50	50	60	80
	Far East	20	20	20	30	40
	Europe	10	10	10	10	20
	ROW	<10	<10	<10	10	10
	Total	**80**	**80**	**80**	**110**	**150**

Market Sector/ Year	**Region**	**'02**	**'05**	**'06**	**'11**	**'16**
Computer memory	N. America	50	50	50	50	50
	Far East	40	40	40	40	40
	Europe	10	10	10	10	10
	ROW	<10	<10	<10	<10	<10
	Total	**100**	**100**	**100**	**100**	**100**
UPS/Stationary	N. America	0	20	30	100	140
	Far East	0	10	10	30	40
	Europe	0	10	10	10	10
	ROW	0	<10	<10	<10	10
	Total	**0**	**40**	**50**	**140**	**200**
Military/ aerospace	N. America	80	90	100	100	100
	Far East	10	10	10	10	10
	Europe	10	10	10	10	10
	ROW	<10	<10	<10	<10	<10
	Total	**100**	**110**	**120**	**120**	**120**
Industrial EV	N. America	0	<10	<10	<10	<10
	Far East	0	<10	<10	<10	<10
	Europe	0	<10	<10	<10	<10
	ROW	0	<10	<10	<10	<10
	Total	**0**	<10	<10	**10**	**10**
HEV/EV	N. America	<10	10	10	20	40
	Far East	<10	10	10	20	40
	Europe	0	<10	<10	10	10
	ROW	0	0	0	<10	<10
	Total	**10**	**20**	**20**	**50**	**70**
Auto SLI	N. America	10	10	10	30	50
	Far East	<10	<10	<10	<10	10
	Europe	<10	<10	<10	<10	<10
	ROW	<10	<10	<10	<10	<10
	Total	**10**	**10**	**10**	**30**	**50**
Total	N. America	1,710	1,860	1,960	2,290	2,600
	Far East	1,380	1,440	1,520	1,650	1,790
	Europe	780	790	810	910	940
	ROW	370	350	360	570	590
	Total	**4,250**	**4,450**	**4,650**	**5,430**	**5,840**

References

1. Exide Technologies, GNB Industrial Power, www.exide.com.
2. Panasonic (Matsushita), www.panasonic-industrial.com/1000.htm?flash=true.
3. Eurobat, "Eurobat position paper on amendments tabled in the Committee on Environment, Public Health and Food Safety," http://www.eurobat.org/pdf/pr_pp_amen-35-96.pdf. (11/03/2005)
4. "Batteries Directive," http://www.euractiv.com/Article?tcmuri=tcm:29-117445-16 &type=Links Dossier. (2005).
5. Frost & Sullivan, "*World Industrial Secondary Lithium Battery Markets*" (04/2005).

6. Freedonia, "*World Batteries*" (09/2004).
7. ICON Group International, "*The 2002 World Forecasts of Batteries and Electric Accumulators Export Supplies*" (2002).
8. D. Saxman, S. Colson-Inam "*Large and Advanced Battery Technology and Markets*" 2004.

Subject Index

Aerospace battery technology 357-80
  primary batteries 357-363
  secondary batteries 365-387
Aircraft batteries 316-25
  Lead-Acid 319-325
  NiCd 319-25
Alkaline batteries
  basic characteristics 108-14
  practical characteristics 7-9
  miscellaneous application, Chapters 11 and 12
Automatic crash notification 620-2

Batteries
  characterization
    stages and levels in 129-32
  characterization techniques
    electrochemical 155-60, 169-71, 175-84, 187-91
    non-electrochemical 132-55, 160-66, 171-73
  charge management 658-63
  collection and recycling 691-736
    collection schemes 699-704
    existing technologies 707-735
    recycling rate 705-707
    trans-boundary movement of spent batteries 696-8
  discharge management 663-70
  electrode materials 120-125
  electrolyte systems 126-7
  general composition of main systems 707
  industrial 742-6
    configurations 748-50
    definition 737-8
    market sectors 738-40
  life prediction 673-85
  management 648-73
  monitoring and measuring 652-7
  performance prediction 675-88
  safety management 670-1
  stationary applications 395-451, 455-94
  technologies for traction 214-268
  world market 737-766
    value prediction 740-2
    sectors 750-762
BESS in Alaska (Ni-Cd) 558-62

Electric vehicles 204-8
  different technologies 207
Electrical energy storage
  by batteries 460-78, 497-542, 558-62
  by other systems 478-86
  comparison of systems 486-94

Flow batteries
  basics 103-8
  electrodes for 103-8, 176-7
  in load levelling 467-73, 486

Genesis mission 356
GEO satellites 274-7

HEO satellites 279-80
Hubble Space Telescope 354
Human exploration missions 336-9
Hybrid electric vehicles 208-13
  comparison of different types 209
  fuel cells for 213-4
  commercial cars 232-8

International Space Station 354-5

Kari launcher battery 312

Launcher batteries 308-316
  Lithium 313-15
  Li-ion 311-2
  NiCd 309-11
  primary, comparison 314-5
  Silver-Zinc 313

Lead/Acid batteries
  AGM batteries 435-42
    spiral type 446

- for aircraft 319-325
- basics 53-66
- charge/discharge reactions 57-9
- charging methods 65-6
- gel batteries 431-6
  - for solar energy storage 524-37
- large batteries 402-9,
  - for solar energy storage 505-12
- for load levelling 475
- plate designs 55-6
- power performance improvement 409-17
- practical characteristics 743
- self-discharge 64-5
- SLI batteries 59-60
- for solar (and wind) energy storage 497-543
- stationary batteries 61-3, Chapters 7 and 9, 475
- technology 53-63, Chapters 7 and 9
- for telecommunications and UPS 395-451
- traction batteries 60-1, 215-21
- VRLA
  - comparison with flooded batteries 64
  - for solar energy storage 512-24
  - technology 417-30
  - for tracking systems 627-9

LEO satellites 277-9

Li-Al/Iron sulfide batteries 38-42, 363-5

Lithium-ion batteries
- for aerospace 297-308, 374-87
- basics 17-32
- for load levelling 477-8
- practical characteristics 743
- for traction 242-62

Li-metal-polymer batteries
- basics 32-8
- for traction 262-5

Lithium primary batteries
- miscellaneous applications 619-47
- practical characteristics 745

Lithium/Carbon monofluoride batteries
- for aerospace 361-2
- basics 14-6

Lithium/Manganese dioxide batteries
- basics 10-4
- for tracking systems 629-31

Lithium/Sulfur batteries 32-3

Lithium/Sulfur dioxide batteries
- for aerospace 359-61
- basics 2-5
- for tracking systems 629-31

Lithium/Thionyl chloride batteries
- for aerospace 361
- basics 5-10
- for oceanography 643-7
- for oil drilling 637-9
- for tracking systems 629-31
- for tyre pressure monitoring 619

Load levelling 455-94

Melco battery for satellites 307

MEO satellites 279-80

Missions to Mars and Other Planets 339-356
- Galileo 344
- Mars Exploration Rovers 349-54
- Mars Express and Beagle-2 Lander 343
- Mars Global Surveyor 341
- Mars Microprobe-Deep Space 2 347-9
- Mars Observer 340-1
- Mars Odissey 342
- Mars Pathfinder Lander and Sojourner Rover 345-7
- Mars Reconnaisssance Orbiter 343-4
- Mars Science Laboratory 357
- Mars Surveyor Program 341-2
- MSP1 Lander 349
- Viking Program 340

Nickel/Cadmium batteries
- for aerospace 365-8
- for aircraft 319-325
- applications summary 566-71
- basics 68-76, 548-56
- cost and reliability 556-8
- large battery in an energy storage applications 558-62

- memory effect 71-73, 549
- plate types 66-9, 550-1
- practical characteristics 744
- for satellites 281-88
- in stationary applications 546-71
- in telecommunications applications 562-5

Nickel/Hydrogen batteries
- for aerospace 368-73
- basics 89-91
- for satellites 288-97

Nickel/Iron batteries 91-4

Nickel/Metal hydride batteries
- for aerospace 373-4
- basics 77-88
- for load levelling 475-7
- practical characteristics 744
- for tracking systems 629-9

Nickel/Zinc batteries
- basics 94-7
- practical characteristics 744

Oceanography 641-7

Oil drilling 631-41

Phoenix Lander 356

Planetary and space exploration missions 329-57

Primary Li batteries 1-17
- basic parameters 17
- in miscellaneous applications, Chapters 11 and 12

PulsesPlus™ batteries 621-31, 643-7

Recycling
- eco-efficiency study 692-6
- existing technologies 707-52
- Hg-containing batteries 711-14
- Lead/Acid batteries 719-22
- Li primary batteries 718-9
- Li-ion and Li-polymer batteries 730-5
- metal price fluctuation 703-4
- mixed batteries 709-11
- NiCd batteries 722-27
- NiMH batteries 727-9
- Zn/C and alkaline batteries 714-8

Rechargeable Batteries
- aqueous 53-112
  - basic parameters 113-14
- non-aqueous 17-50
  - basic parameters 49
- pseudo-Ragone plot of main systems 244
- for satellites 280-308

Robotic space exploration 330-6

Satellite batteries 273-308
- comparison of 298-300
- Li-ion 297-308
- NiCd 281-8
- NiH_2 288-97

Silver/Zinc batteries
- basics 101-3
- practical characteristics 744-5
- for aerospace 357-9, 365

Smart battery system 673-5

Sodium/Nickel Chloride batteries
- basics 46-8
- for traction 265-8

Sodium/Sulfur batteries
- basics 41-6
- for load levelling 461-9

Space batteries
- general characteristics 328-9

Stardust mission 355

Stentor battery for satellites 307

Telecommunications batteries
- lead-acid, Chapter 7
- NiCd 562-4

Thermal batteries 38-50, 265-8, 314, 363-5

Toyota Prius hybrid car 232-4

Tracking 696-706

Traction
- battery technology 214-68
  - Lead/Acid 215-22
  - Lithium-ion 242-62
  - Lithium-Polymer 262-5
  - Nickel/Cadmium 222-7
  - Nickel/Metal hydride 228-42
  - Sodium/Nickel Chloride 265-8

Tyre pressure monitoring systems 616-20

Umicore's Val'Eas® Process 732-5
UPS batteries
  lead-acid, Chapter 7
  NiCd 566-8

Vanadium Redox-flow batteries
  basics 106-8
  for load levelling 468-74

World market 737-66
    batteries for
      auto SLI 761-2
      communications 751-3
      computer memory 756
      computing 750-1
      HEV/EV 760-1
      industrial EV 759-60
      medical applications 755
      military/aerospace 757-9
      portable products other than tools 754
      portable tools 753
      UPS/stationary applications 756-7
  summary (tables) 762-5

Zinc/Air batteries
  basics 97-101
  practical characteristics 745
Zinc/Bromine batteries 103-5, 176-7